NUCLEAR PHYSICS

JOURNAL DEVOTED TO THE EXPERIMENTAL AND THEORETICAL STUDY OF THE FUNDAMENTAL CONSTITUENTS OF MATTER AND THEIR INTERACTIONS

EDITOR: L. ROSENFELD - COPENHAGEN
ASSOCIATE EDITOR: O. NATHAN - COPENHAGEN

VOLUME V

NORTH-HOLLAND PUBLISHING COMPANY - AMSTERDAM

NUCLEAR PHYSICS A

ADVISORY BOARD

AUSTRALIA & NEW ZEALAND:	H. Messel (Sydney), M. L. Oliphant (Canberra)
AUSTRIA:	B. Karlik (Vienna), W. Thirring (Vienna)
BELGIUM:	M. de Hemptinne (Louvain), J. Verhaeghe (Ghent)
CANADA:	A. E. Litherland (Toronto)
CZECHOSLOVAKIA:	L. Trlifaj (Řež)
DENMARK:	G. E. Brown (Copenhagen), C. Møller (Copenhagen), S. Rozental (Copenhagen)
U.A.R. & ARAB COUNTRIES:	F. El Bedewi (Cairo)
FINLAND:	L. Simons (Helsinki)
FRANCE:	A. Berthelot (Saclay), S. Gorodetzky (Strasbourg)
GERMANY (DEM. REP.):	F. Kaschluhn (Berlin)
GERMANY (FED. REP.):	W. Gentner (Heidelberg), J. H. D. Jensen (Heidelberg)
GREAT BRITAIN:	W. E. Burcham (Birmingham) R. J. Blin-Stoyle (Brighton), T. H. R. Skyrme (Birmingham)
HUNGARY:	L. Janossy (Budapest)
INDIA:	M. G. K. Menon (Bombay), R. Ramanna (Trombay)
IRISH REPUBLIC:	L. McConnell (Maynooth)
ISRAEL:	I. Talmi (Rehovoth)
ITALY:	E. Amaldi (Rome)
JAPAN:	I. Nonaka (Tokyo), S. Tomonaga (Tokyo)
MEXICO:	M. Moshinsky (Mexico)
NETHERLANDS:	H. Brinkman (Groningen), S. R. de Groot (Amsterdam)
NORWAY:	A. Lundby (Oslo), H. Wergeland (Trondheim)
POLAND:	L. Infeld (Warsaw), J. Werle (Warsaw)
PORTUGAL:	J. M. Araújo (Porto), J. R. de Almeida Santos (Coimbra)
SOUTH AMERICA:	G. Beck (Bariloche)
SPAIN:	J. M. Otero (Madrid), C. Sanchez del Rio (Madrid)
SWEDEN:	O. Klein (Stockholm), K. Siegbahn (Uppsala), I. Waller (Uppsala)
SWITZERLAND:	P. Huber (Basel), P. Scherrer (Zürich), V. F. Weisskopf (CERN)
U.S.A.:	S. Devons (New York), D. Kurath (Argonne), V. F. Weisskopf (MIT)
U.S.S.R.:	M. A. Markov (Moscow), I. S. Shapiro (Moscow)
YUGOSLAVIA:	I. Supek (Zagreb)

NUCLEAR PHYSICS

Journal devoted to the experimental and theoretical study of the fundamental constituents of matter and their interactions

***Editor*: L. Rosenfeld - Copenhagen**

Associate editors: H. H. Barschall, Madison; D. M. Brink, Oxford; T. E. O. Ericson, Cern; M. Gourdin, Orsay; G. Källén, Lund; Z. Koba, Copenhagen; H. J. Lipkin, Rehovoth; D. R. O. Morrison, Cern; O. Nathan, Copenhagen; J. Reignier, Brussels; J. Rollnik, Bonn; H. P. C. Rood, Groningen; W. Rühl, Cern; J. Sacton, Brussels; H. Schopper, Karlsruhe; B. Stech, Heidelberg; C. van der Leun, Utrecht; A. Winther, Copenhagen

***Technical Editor*: W. Hass, Copenhagen**

VOLUME V

JANUARY 1958 – MARCH 1958

NORTH HOLLAND

PRINTED IN THE NETHERLANDS

Nuclear Physics **5** (1958) 1—10; © *North-Holland Publishing Co., Amsterdam*
Not to be reproduced by photoprint or microfilm without written permission from the publisher

SCATTERING FUNCTIONS WITH CROSSING SYMMETRY AND THEIR APPLICATIONS TO THE PROBLEMS OF MESON-NUCLEON SCATTERING

NING HU

Joint Institute of Nuclear Research, Dubna, USSR

Received 11 June 1957

Abstract: It is shown that the general form of scattering functions satisfying appropriate crossing conditions are general solutions of the equations of Chew and Low. These scattering functions fall into two classes. In one class they are analytic functions (usually double valued) of the momentum variable k with only simple poles and zeros, while in the other class they have a line of discontinuity on the imaginary k-axis between $k = -i$ and $k = -i\,\infty$.

1. Introduction

Recently it has been shown by many authors [1]) that the principle of causality leads to restrictions on the analytic behaviour of Heisenberg's scattering functions $S(\omega, k)$; ω, k being, respectively, energy and momentum variables of the scattered particle. In the case of meson-nucleon collision, broadly speaking, these restrictions amount to the requirement that $S(\omega, k)$ should have no poles above the real axis in the complex ω-plane. Alternatively, Chew and Low obtained a set of equations for the phase shifts which require also that $S(\omega, k)$ should have no poles in the complex ω-plane except on the real axis between $\omega = -1$ and $\omega = +1$ (here and in the following we shall use the natural units $\mu = c = h = 1$). Both developments bring out an interpretation of the scattering functions when the energy variable is negative. It is the aim of the present paper to investigate the general analytic properties of the scattering functions which satisfy certain crossing conditions.

Our starting point is the theory of the S-matrix as formulated by Heisenberg. Doubt as to the usefulness of this formulation was raised after it was discovered that the S-matrix as an analytic function may possess redundant poles. However, it was shown that these poles will not appear when the interaction is cut off at great distances. This means that we can always choose an S-matrix which represents the scattering phenomena quite accurately and at the same time is free from redundant poles. This representation of the S-matrix will be used in the present theory.

2. Analytic Properties of S (ω, k) when ω is positive on the Effective Range Approximation

The asymptotic "radial" wave function of a scattered particle when it is very far from the scatterer may be written as

$$\psi(r) \sim \frac{1}{r}[e^{-ikr}+S(\omega,\ k)e^{ikr}],\ \omega = \sqrt{1+k^2}, \tag{1}$$

where we have suppressed the indices representing angular momentum states as well as total spin and total isobaric spin states if they exist. We shall now make the ansatz that S should be an analytic function of k in the whole complex k-plane. In doing this, however, we must introduce one further requirement that all results which are obtained from (1) by analytic continuation and which satisfy the physical boundary conditions at infinity must represent a true solution of the system. Thus, if we replace k by $-k$ in (1) we obtain

$$\begin{aligned}\psi(r) &\sim \frac{1}{r}[e^{ikr}+S(\omega,\ -k)e^{-ikr}] \\ &= \frac{1}{r}S(\omega,\ -k)\left[e^{-ikr}+\frac{1}{S(\omega,\ -k)}e^{ikr}\right].\end{aligned} \tag{2}$$

Now the function (2) satisfies the same boundary condition at infinity as (1), therefore it must represent a true solution according to our requirement. But (1) and (2) must also be the same solution; consequently

$$S(\omega,\ k) = \frac{1}{S(\omega,-k)}. \tag{3}$$

The unitary condition for $S(\omega,\ k)$ is

$$S(\omega,\ k)S^*(\omega,\ k) = 1$$

or

$$S(\omega,\ k) = \frac{1}{S^*(\omega,\ k)}, \tag{4}$$

where $S^*(\omega,\ k)$ denotes the complex conjugate of $S(\omega,\ k)$ when ω and k are both considered as real. Since ω is a double valued function of k, $S(\omega,\ k)$ is therefore a double valued function of k or ω. In order to confine ourselves only to the region where the real part of ω is always positive, cuts must be introduced in the complex k-plane along the imaginary axis from $k = -i\infty$ to $k = -i$ and from $k = +i$ to $k = +i\ \infty$. In the following we shall call the cut plane the upper Riemann sheet and the other plane connected to it through the cut-lines the lower Riemann sheet. After the introduction of the cuts, $S(\omega,\ k)$ in the upper Riemann sheet may simply be written as $S(k)$. $S(k)$ is in general discontinuous across the cuts. From (3) and (4)

we see that whenever $S(k)$ has a pole at $k = k_n$, it must also have a pole at $k = -k_n^*$ and two zeros at $k = -k_n$ and $k = k_n^*$. The general form of $S(k)$ may therefore be written as

$$S(k) = S_1(k) \prod_\lambda \frac{(k_\lambda - ik)}{(k_\lambda + ik)} \prod_n \frac{(k^* - k)(k_n + k)}{(k_n - k)(k_n^* + k)} \qquad (0 < k < 1); \tag{5}$$

k_λ represents a bound state and k_n represents a metastable state of the system, whereas $S_1(k)$ is a function of k which is unitary on the real k-axis and may become discontinuous along the two cuts introduced above.

According to results obtained from causality considerations and from the theory of Chew and Low, $S(k)$ should have no poles or any other kind of singularity above the real k-axis (except, of course, the cut on the positive imaginary axis introduced above).

The cut is introduced only as a consequence of the fact that ω is a double valued function of k. One would expect that if $S(k)$ is continued analytically across the cut to the lower Riemann sheet, a function of similiar analytic properties would be obtained. Before the crossing condition was known, the physical meaning of the analytic continuation was not quite clear, and consideration was confined to those cases in which $S(\omega, k)$ was of the same type of function in the lower Riemann sheet as it was in the upper Riemann sheet [3]). In the following section we shall show that there also exist important cases in which the crossing condition requires the properties of $S(\omega, k)$ in the lower Riemann sheet to be quite different from those in the upper sheet.

In the non-relativistic limit, the cut in (5) will go to infinity and we obtain [3])†

$$S(k) = e^{ick} \prod_\lambda \frac{(k_\lambda - ik)}{(k_\lambda + ik)} \prod_n \frac{(k_n^* - k)(k_n + k)}{(k_n - k)(k_n^* + k)}. \tag{6}$$

The formula for $S(k)$ given above and also for $S(\omega, k)$ obtained in the following section would be of little practical value if the poles were numerous and clustered together in such a way that it would be difficult to determine them from experiments. The question may then arise whether each pole possesses an unequivocal meaning as a metastable state. In the case of nuclear interaction in which the range of force is very small, however, the

† The possible appearance of the exponential factor exp (ick) (which equals unity if $c = 0$) follows from the condition for $S(k)$ at infinity, derived from the completeness condition (cf. ref. [3])):

$$\int_\Gamma S(k)\, e^{ik(r+r')}\, dk = 0,$$

which holds for large values of $r+r'$. The path of integration is an infinite semi-circle above the real k-axis. It is seen that if the above condition is satisfied by an $S(k)$ without the exponential factor exp (ick), it will also be satisfied if $S(k)$ is multiplied by this factor since the effect of introducing this factor is equivalent to replacing $r+r'$ by $r+r'+c$.

poles are found to be far apart. This is due to the fact that with decreasing range of force, the energy intervals between successive metastable levels increase. Hence when k is very small, we may introduce in (6) the following substitution

$$\frac{(k_n^*-k)(k_n+k)}{(k_n-k)(k_n^*+k)} \to 1$$

for all n. Furthermore, we know that for the proton-neutron system there is only one bound state near $k = 0$; therefore we have

$$S(k) = e^{ick} \frac{K-ik}{K+ik}. \tag{7}$$

Since c can only be of the order of a small length representing the range of force, we may write approximately

$$e^{ick} \approx \frac{1+\frac{1}{2}ick}{1-\frac{1}{2}ick} = \frac{L-ik}{L+ik} \tag{8}$$

where $L = 2/c$. Eq. (7) then becomes

$$S(k) = \frac{L-ik}{L+ik} \frac{K-ik}{K+ik}. \tag{9}$$

Inserting this in

$$\cot\delta(k) = i\frac{S(k)+1}{S(k)-1},$$

where $\delta(k)$ denotes the phase shift, we obtain immediately

$$k \cot \delta(k) = -\frac{KL}{K+L} + \frac{1}{K+L}k^2. \tag{10}$$

This is just the usual effective range formula in which k^2 is the value of the deuteron binding energy. The same expression (9) has been given by Jost and Kohn [4]). These authors consider $k = iL$ as a redundant pole of $S(k)$. From our derivation we see that this is actually a false pole introduced by the approximation (8).

3. The Case of Meson-Nucleon Scattering

The crossing condition may be stated as follows:

$$t_{\mathbf{qp}}(\omega) = t_{\mathbf{pq}}(-\omega), \quad \omega = \sqrt{p^2+1} = \sqrt{q^2+1} \tag{11}$$

where $\mathbf{q}$, $\mathbf{p}$ represent momenta of the scattered particle in the initial and final states respectively, and $t_{\mathbf{qp}}(\omega)$ is connected to the complete S-matrix by the following relation:

$$\langle \mathbf{p}|S|\mathbf{q}\rangle = \delta_{\mathbf{pq}} - 2\pi i\delta(E_{\mathbf{q}}-E_{\mathbf{p}})t_{\mathbf{qp}}(\omega). \tag{12}$$

On the one-meson approximation, the complete S-matrix simply becomes the scattering function considered in the last section with $p = q = k$.

We shall first consider the case of a neutral scalar meson. In this case $\langle \mathbf{p}|S|\mathbf{q}\rangle$ becomes just $S(\omega, k)$ and (11) becomes

$$S(\omega, k) = S(-\omega, k) = S(k). \tag{13}$$

The general form of $S(\omega, k)$ satisfying the above condition has been derived in ref. [3]); it is

$$S(k) = e^{2ick} \prod_{\lambda} \frac{K_\lambda - ik}{K_\lambda + ik} \prod_{n} \frac{(k_n^* - k)(k_n + k)}{(k_n - k)(k_n^* + k)} \tag{14}$$

where K_λ represents the energy value of a bound state and k_n represents a metastable state.

Next we consider the case of a charged scalar meson. We may put

$$t_{pq}(\omega) = \sum_{\alpha=1}^{2} \Lambda_\alpha(\mathbf{p}, \mathbf{q}) h_\alpha(\omega, k) \tag{15}$$

where

$$\begin{aligned} \Lambda_1(\mathbf{p}, \mathbf{q}) &= \tau_p^{\,1}\tau_q^{\,1} + \tau_p^{\,2}\tau_q^{\,2} \\ \Lambda_2(\mathbf{p}, \mathbf{q}) &= \delta_{pq} - \tfrac{1}{2}(\tau_p^{\,1}\tau_q^{\,1} + \tau_p^{\,2}\tau_q^{\,2}). \end{aligned} \tag{16}$$

The S functions for the states $\alpha = 1, 2$, are given by

$$S_\alpha(\omega, k) = 1 - 2\pi i h_\alpha(\omega, k)\omega k. \tag{17}$$

Application of the condition (11) leads immediately to the following result:

$$\begin{aligned} S_1(-\omega) &= S_2(\omega), \\ S_2(-\omega) &= S_1(\omega). \end{aligned} \tag{18}$$

This means that the two scattering functions corresponding to two different isobaric states together form a single analytic function of ω and k defined in both Riemann sheets of the complex k-plane. It was shown in ref. [3]) that the general form of this function is

$$\begin{aligned} S_1(\omega, k) &= S_2(-\omega, k) \\ &= e^{2ick} \prod_{s} \frac{\omega - 1 - ib_s k}{\omega - 1 + ib_s k} \prod_{n} \frac{(k_n + k_n^*)(\omega - \omega_n^*) - (\omega_n^* - \omega_n)(k - k_n^*)}{(k_n + k_n^*)(\omega - \omega_n) - (\omega_n - \omega_n^*)(k - k_n)} \\ &\quad (\omega_n^{\,2} = k_n^{\,2} + 1, \quad b_s = \text{real}) \end{aligned} \tag{19}$$

where b_s, k_n are arbitrary constants to be determined by the detailed structure of the system. Each b_s will give rise to a bound state, and each pair of ω_n and k_n determines a metastable state of the system.

If the imaginary parts of the k_n's in (15) and (20) are all negative, then these two functions will have no pole above the real k-axis except on the imaginary axis between $k = 0$ and $k = i$. It can easily be seen that they are the general solutions of the equations of Chew and Low for the cor-

responding cases †. Our results agree with the conclusion obtained by Castillejo, Dalitz and Dyson that the general solutions of the Chew and Low equations in the two preceding cases contain an infinite number of adjustable constants.

We now come to the case of S-wave scattering for an interaction "symmetrical" with respect to charged and neutral mesons. The following investigation will show that the scattering functions for this case are essentially of a new type.

The matrix element $t_{pq}(\omega)$ may be written as

$$t_{qp}(\omega, k) = \sum_{\alpha=1}^{2} A_\alpha(\mathbf{p}, \mathbf{q}) h_\alpha(\omega, k) \tag{20}$$

where

$$\begin{aligned} A_1(\mathbf{p}, \mathbf{q}) &= \tau_p \cdot \tau_q = \tau_p{}^1\tau_q{}^1+\tau_p{}^2\tau_q{}^2+\tau_p{}^3\tau_q{}^3, \\ A_2(\mathbf{p}, \mathbf{q}) &= \delta_{pq}-\tfrac{1}{3}\tau_p \cdot \tau_q. \end{aligned} \tag{21}$$

The crossing condition (11) leads immediately to the following conditions for S_1 and S_2 corresponding respectively to the singlet and triplet states:

$$\begin{aligned} S_1(-\omega, k)+2S_2(-\omega, k) &= S_1(\omega, k)+2S_2(\omega, k), \\ S_1(-\omega, k)-S_2(-\omega, k) &= -S_1(\omega, k)+S_2(\omega, k). \end{aligned} \tag{22}$$

According to the requirement expressed by the dispersion relation as well as by the equation of Chew and Low, $S(\omega, k)$ and $S_2(\omega, k)$ should be continuous as k passes from one Riemann sheet of the complex k-plane to the other through the cut between $k = i$ and $k = i\infty$. Let $k = iK-\varepsilon$, where K is real and positive and greater than unity; eqs. (22) then become

$$\begin{aligned} S_1(iK-\varepsilon)+2S_2(iK-\varepsilon) &= S_1(iK+\varepsilon)+2S_2(iK+\varepsilon) \\ S_1(iK-\varepsilon)-S_2(iK-\varepsilon) &= -S_1(iK+\varepsilon)+S_2(iK+\varepsilon) \\ (1 \leqq K < \infty) & \end{aligned} \tag{23}$$

where we have omitted the variable $\omega = \sqrt{1+k^2}$ since all functions in (23) are given in the upper Riemann sheet of the complex k-plane. Our problem now reduces to finding two functions $S_1(k)$ and $S_2(k)$ defined in the upper Riemann sheet of the complex k-plane and satisfying the conditions (3) and (4), and whose boundary values along the cut on the positive imaginary axis satisfy (23). After such $S_1(k)$ and $S_2(k)$ are obtained, they can immediately be continued analytically to the lower Riemann sheet of the complex k-plane through the cut between $k = i$ and $k = i\infty$ to get the complete functions $S_1(\omega, k)$ and $S_2(\omega, k)$. We can easily see that the last two functions satisfy (22). If $S(k)$ have no poles above the real axis except on the imaginary axis, then $S_1(\omega, k)$ and $S_2(\omega, k)$ will have the same

† It will be noted that in order to satisfy the equation of Chew and Low, $S(\omega, k)$ must satisfy certain conditions at $\omega = 0$ and $\omega = \infty$. However, these conditions only give rise to two relations among the infinite number of adjustable constants.

property in the lower Riemann sheet. In other words $S_1(\omega, k)$ and $S_2(\omega, k)$ satisfy Chew and Low's equation.

It should be pointed out, however, that except for the trivial and unphysical case $S_1(\omega, k) \equiv S_2(\omega, k)$, the condition (23) cannot be satisfied also by values of k on the lower cut between $k = -i$ and $k = -i\,\infty$. This can be seen by noticing that

$$S_\alpha(-iK-\varepsilon) = \frac{1}{S_\alpha(iK+\varepsilon)}.$$

Eqs. (23) would then become, for $k = iK-\varepsilon$,

$$\begin{aligned} \frac{1}{S_1(iK-\varepsilon)} + \frac{2}{S_2(iK-\varepsilon)} &= \frac{1}{S_1(iK+\varepsilon)} + \frac{2}{S_2(iK+\varepsilon)} \\ \frac{1}{S_1(iK-\varepsilon)} - \frac{1}{S_2(iK-\varepsilon)} &= \frac{-1}{S_1(iK+\varepsilon)} + \frac{1}{S_2(iK+\varepsilon)} \end{aligned} \qquad (24)$$

$$(1 \leqq K < \infty).$$

The above relations cannot be satisfied simultaneously with (23) except in the unphysical case $S_1(\omega, k) \equiv S_2(\omega, k)$. This means that $S_\alpha(\omega, k)$ must change discontinuously as k passes through the cut on the negative imaginary axis from one Riemann sheet to the other. We see further that $S_\alpha(\omega, k)$ are unitary only on the real axis in the upper Riemann sheet. In the lower Riemann sheet, as can be seen from (22), they become linear combinations of two unitary functions (see (24) below) and therefore cannot be unitary themselves. This may be understood as a consequence of the presence of the line of discontinuity.

The non-unitarity of $S(\omega, k)$ for negative values of ω can also be seen physically from the following consideration. From (22) we obtain

$$S_2(-\omega, k) = \tfrac{2}{3}S_1(\omega, k) + \tfrac{1}{3}S_2(\omega, k).$$

The right-hand side of (24) is just the scattering function of direct scattering of a negative meson by a proton. This scattering function is obviously not unitary since the same collision also leads to charge-exchange scattering with a neutral meson as an outgoing particle. This consideration together with (18) also brings out a connection between negative values of ω and charge conjugation.

We have also considered the case of F-wave meson-nucleon scattering under symmetrical pseudo-vector coupling. There the crossing relations may be written

$$\begin{aligned} &S_1(iK-\varepsilon) + 2S_3(iK-\varepsilon) = S_1(iK+\varepsilon) + 2S_3(iK+\varepsilon) \\ &S_2(iK-\varepsilon) + \tfrac{1}{2}S_3(iK-\varepsilon) = S_2(iK+\varepsilon) + \tfrac{1}{2}S_3(iK+\varepsilon) \\ &S_1(iK-\varepsilon) + S_2(iK-\varepsilon) - 2S_3(iK-\varepsilon) = -S_1(iK+\varepsilon) - S_2(iK+\varepsilon) + 2S_3(iK+\varepsilon) \end{aligned}$$

$$(1 \leqq K < \infty).$$

We found that the scattering functions are of the same type as those in the last case.

4. Effective Range Expansion of Phase Shifts

From the results of the last section we see that it will be convenient to expand $S_\alpha(\omega, k)$ into a power series with respect to the branch point $k = i$ in the following form:

$$S_\alpha(\omega, k) = \sum_{n=0}^{\infty} A_n^{(\alpha)} \xi^n + \xi^{\frac{1}{2}} \sum_{n=0}^{\infty} B_n^{(\alpha)} \xi^n, \quad \xi = k - i; \tag{26}$$

or, alternatively, we may use one of the following series †:

$$\delta_\alpha(\omega, k)/k^{2l+1} = \sum_{n=0}^{\infty} a_n^{(\alpha)} \xi^n + \xi^{\frac{1}{2}} \sum_{n=0}^{\infty} b_n^{(\alpha)} \xi^n, \tag{27}$$

$$k^{2l+1} \cot \delta_\alpha(\omega, k) = \sum_{n=0}^{\infty} \lambda_n^{(\alpha)} \xi^n + \xi^{\frac{1}{2}} \sum_{n=0}^{\infty} \mu_n^{(\alpha)} \xi_n \tag{28}$$

(l = angular momentum variable),

where $A_n^{(\alpha)}$, $B_n^{(\alpha)}$, $a_n^{(\alpha)}$, $b_n^{(\alpha)}$, $\lambda_n^{(\alpha)}$ and $\mu_n^{(\alpha)}$ are complex constants.

Owing to the presence of the line of discontinuity from $k = -i$ to $k = -i\,\infty$, the circle of convergence of the above series will be $|\xi| = 2$, if preceding functions contain no poles inside this circle. In the case when there are poles, the same circle of convergence may still be obtained by a suitable choice among (27) and (28), since $k^{2l+1} \cot \delta$ and δ/k^{2l+1} do not have poles at the same position. We notice that the circle of convergence includes a portion of the real k-axis from $k = -\sqrt{3}$ to $k = +\sqrt{3}$. The corresponding energy interval is $-2 < \omega < +2$ which just corresponds to the lower limit where the effect of meson production would set in. Therefore the circle of convergence actually includes the whole interval of the real k-axis in which the one-meson approximation is strictly valid.

From results of last section, we see that the expressions (27) and (28) must satisfy the following requirements:

i) they must be real only on the real axis in the upper Riemann sheet of the complex k-plane, but *not* on the real axis in the lower Riemann sheet;

ii) they must satisfy boundary conditions such as (24) and (25) along the cut on positive imaginary axis from $\xi = 0$ to $\xi = 2i$ (i.e., from $k = i$ to $k = 3i$);

iii) they must be odd functions of k on the real axis in the upper Riemann sheet of the complex k-plane (this is a consequence of (3));

† The connection between S and δ is $S = \exp 2i\delta = (\cot \delta + i)/(\cot \delta - i)$. The unitary condition for S requires that δ and $\cot \delta$ must be real on the real k-axis in the upper Riemann sheet.

iv) their values in the interval $1 \leqq |\omega| \leqq 2$ must agree with their observed values from the scattering experiments.

Our expansion may be considered as an improvement over the usual effective range expansion

$$k^3 \cot \delta(\omega, k) = a+b\omega+c\omega^2+ \cdots \tag{29}$$

which also uses $k = i$ as the centre of expansion. However(29) inevitably leads to the result that $S_a(\omega, k)$ must be unitary on the real axes of both Riemann sheets of the complex k-plane, which is in contradiction with the crossing condition.

We believe that our series (27) or (28) form a better basis for extrapolating the experimental values for $\omega > 1$ to $\omega = 0$ to obtain the value of the interaction constant g.

5. Metastable States of the K-Capture Type

As we have stated in the introduction, the dispersion relation requires that $S(\omega, k)$ should have no poles above the real axis in the upper Riemann sheet of complex ω-plane in which the imaginary part of k is positive, or in other words, $S(\omega, k)$ should have no poles above the real axis in both Riemann sheets of the complex k-plane except on the imaginary axis between $k = 0$ and $k = i$. In this section we shall show that this requirement is violated by the very existence of π-mesic atoms. For the sake of simplicity, we shall first assume that the meson interacts with the proton only through a Coulomb field. Then there will exist a series of bound states between the negative meson and the proton. These bound atomic states will be represented by poles of $S(\omega, k)$ on the real axis between $\omega = -1$ and $\omega = +1$ in the upper Riemann sheet of the complex ω-plane. Now let us switch on the nuclear interaction between the meson and the proton. It has been shown by Deser *et al.* [7]) that the effect of the nuclear interaction is to displace these poles by complex values $\Delta\omega = \alpha+i\beta$. From conditions (3) and (4) it can easily be seen that the complex conjugate displacement $\Delta\omega^* = \alpha-i\beta$ must give rise to another pole. These two poles will correspond respectively to metastable states of K-capture and K-emission types [8]). This means that the requirement imposed by the dispersion relation as stated above is now violated.

If we look into the cause of the failure of the dispersion relation, we shall find that it is closely connected with the fact that in the derivation of this relation, the interaction of meson and nucleon with other fields was neglected. Indeed, the proton could never capture a meson from the K-orbit if it were not allowed to emit γ-rays or other lighter particles, and in the above example the atomic orbits of mesons would not be there at all if the Coulomb field were neglected.

From the above consideration we may conclude that in order to decide whether $S(\omega, k)$ has poles above the real axis in the upper sheet of the complex ω-plane, one must take into account interactions of mesons and nucleons with other fields. As the usual dispersion relation was derived by considerations which only take into account the interaction between mesons and nucleons, it cannot say anything about poles which represent metastable states of the K-capture type.

The displacements of levels $\Delta\omega$, mentioned above, are actually very small quantities. One may think, perhaps not without justification, that the dispersion relation is after all still correct when these displacements can be neglected. To this we wish only to add that our main objection is to the implication that poles representing metastable states of the K-capture type violate the causality principle.

References

1) M. L. Goldberger, Phys. Rev. **97** (1955) 508; **99** (1955) 979; F. J. Dyson, Phys. Rev. **100** (1955) 344; A. Klein, Phys. Rev. **104** (1956) 1131; R. Oehme, Phys. Rev. **100** (1955) 1503; **102** (1956) 1174
2) G. F. Chew and F. E. Low, Phys. Rev. **101** (1956) 1570
3) N. Hu, Phys. Rev. **74** (1948) 131
4) R. Jost and W. Kohn, Phys. Rev. **87** (1952) 977; Mat. Fys. Medd. Dan. Vid. Selsk. **27** (1953) no. 9
5) L. Castillejo, R. H. Dalitz and F. J. Dyson, Phys. Rev. **101** (1956) 453
6) G. Feldman and P. T. Matthews, Phys. Rev. **101** (1956) 1212
7) S. Deser, M. L. Goldberger, K. Baumann and W. Thirring, Phys. Rev. **96** (1954) 774
8) W. Heitler and N. Hu, Nature **159** (1947) 776

Nuclear Physics **5** (1958) 11—16; © *North-Holland Publishing Co., Amsterda*
Not to be reproduced by photoprint or microfilm without written permission from the publish

A FOUR-STATE THEORY OF THE NEUTRINO

P. E. CAVANAGH, C. F. COLEMAN, B. W. RIDLEY and J. F. TURNER
Atomic Energy Research Establishment, Harwell, Didcot, Berks

Received 29 August 1957

Abstract: A scheme of coupling constants for the beta-decay interaction is proposed explain a wide range of experimental results. The scheme assumes a four-state neutrin It implies that all electron polarization measurements will yield one or the other of t values $\pm v/c$, whatever the values of the ratios C_T/C_A and C_S/C_V.

1. Introduction

It appears that the two component theory of the neutrino of Lee an Yang may be incapable of explaining some of the phenomena of β-decay Unfortunately the issue is still obscured by uncertainties in the experiment data, particularly in regard to the experiments on electron polarizatio This situation is hardly surprising, since a variety of new experiment techniques have had to be developed, and it takes time to evaluate t possible causes of inaccuracy. It is still too early to come to any defini conclusion about the validity of any of the results. One major discrepan appears in Au^{198}, for which Frauenfelder *et al.* [1]) and de Waard *et al.* obtain a small or zero polarization, while Wu *et al.* [3]) and Cavanagh *et al.* obtain a full $(-v/c)$ polarization. In the case of Ga^{66} a value for the electr polarization of $\approx(+v/c)$ obtained by Deutsch *et al.* [5]) disagrees w that of Frauenfelder *et al.* [6]), which is given as $(0.1\pm0.3)v/c$. In what follo we will assume that the $\pm(v/c)$ values of the polarization are correct The data on which we will base the theory will be derived from th sources, primarily. These are (i) electron polarization (ii) electron-neutr correlation (iii) Fierz terms.

(i) ELECTRON POLARIZATION

The polarization of negatons from a pure G.T. emitter is $-v/c$. Th is a large measure of agreement on this particular point, though none of

† Supporting this choice are the measurements of H. Langevin-Joliot and N. M (Comptes Rendus **245** (1957) 670) on 128 keV electrons from S^{35} $(3/2 \rightarrow 3/2)$, who ob a polarization $-(0.4\pm0.14)$ by Mott scattering from a 260 μ gm/cm² gold foil, an F. Boehm, T. B. Novey, C. A. Barnes and B. Stech (preprint) on positons from mirror transition $N^{13} \rightarrow C^{13}$. They obtain a polarization $+(0.93\pm0.20)$ v/c from the circ polarization of the high-energy quanta formed by annihilation in flight of N^{13} posit

experiments are accurate and only a few transitions have been studied. The polarization of positrons from a pure Fermi emitter is $+v/c$. This is based on the results of Deutsch *et al.* for Ga^{66}. If these results are interpreted in terms of the two component theory it implies that $T \gg A$ and $S \gg V$.

(ii) ELECTRON-NEUTRINO CORRELATION

Here again it appears that all the experimental results cannot be made compatible. This matter will be treated fully by Ridley in a separate paper. Here we will say merely that the He^6 result of Rustad and Ruby [7]) is difficult to reconcile with those for the neutron (Robson[8])), Ne^{19} and A^{35} (Allen *et al.* [9])). Moreover Ridley's measurement on another (essentially) pure G.T. emitter, Ne^{23}, shows that T is not the dominant term, as indicated by the He^6 measurement, but that T and A are present in roughly equal amounts. The limits quoted are $0.9 < |C_A|/|C_T| < 1.4$. The A^{35} measurement shows that the Fermi interaction is predominantly vector, $|C_V|/|C_S| \geqq 1.8$.

These two results taken in conjunction with those from electron polarization present a major difficulty for the two component theory.

(iii) FIERZ TERMS

Any theory must be compatible with the Fierz terms in both allowed and first forbidden decays being small. We shall take them to be zero. For a theory in which invariance under the parity and time reversal operators may be violated, they are

$$\left.\begin{aligned} &\mathrm{Re}\,(C_T C_A^* + C'_T C'^*_A) = 0 \\ &\mathrm{Re}\,(C_S C_V^* + C'_S C'^*_V) = 0 \end{aligned}\right\} \text{allowed}$$

$$\left.\begin{aligned} &\mathrm{Re}\,(C_S C_A^* + C'_S C'^*_A) = 0 \\ &\mathrm{Re}\,(C_T C_V^* + C'_T C'^*_V) = 0 \end{aligned}\right\} \text{first forbidden}$$

in the notation of Jackson *et al.*[10]).

2. Electron Polarization

Let us turn now to the expression derived by Jackson *et al.* [10]) for the electron polarization for allowed transitions (but neglect for the moment Coulomb terms) viz.

$$P = \pm 2\frac{v}{c}\frac{|M_{GT}|^2\,\mathrm{Re}\,(C_T C'^*_T - C_A C'^*_A) + |M_F|^2\,\mathrm{Re}\,(C_S C'^*_S - C_V C'^*_V)}{|M_{GT}|^2(|C_T|^2+|C'_T|^2+|C_A|^2+|C'_A|^2)+|M_F|^2(|C_S|^2+|C'_S|^2+|C_V|^2+|C'_V|^2)}.$$

The two component theory requires that neutrinos arising from T and A interactions and also S and V interactions should all have the same spin direction, either parallel or antiparallel to the direction of motion, depending on the sign of the emitted electron.

This is expressed by

$$C_T = -C'_T, \quad C_A = -C'_A, \quad C_S = -C'_S, \quad C_V = -C'_V.$$

However the above formula for the electron polarization shows that if electrons emitted in T interactions have the same sign of spin as the neutrino, those emitted in A interactions will have the opposite sign of spin. So electrons emitted in an interaction in which $C_T = C_A$ would be essentially unpolarized, contrary to the assumed data. A way out of this difficulty is to require that neutrinos emitted in a T interaction have the opposite sign of spin to those emitted in an A interaction. This is expressed by

$$C_T = -C'_T, \quad C_A = C'_A,$$

and for the Fermi interaction

$$C_S = -C'_S, \quad C_V = C'_V.$$

With this assumption the electron polarization $= \pm v/c$ irrespective of the ratio of T to A, or S to V. This enables one to reconcile the electron-polarization and electron-neutrino correlation data. Moreover it is at once seen that the Fierz terms for both allowed and first forbidden decays become identically zero. It will be of interest to examine some of the further consequences of this theory.

3. Time Reversal Terms

In what follows we shall again make extensive reference to the paper by Jackson *et al.* [10]). Their expression (A.10) includes the Coulomb terms in the electron polarization. These are of the form αZ Im $(C_S C'^*_V + C'_S C^*_V)$, and become identically zero on the basis of the new theory. Similarly the time reversal terms in every one of the expressions derived by these authors, except that for $D\xi$, become identically zero. The expression for $D\xi$ reduces to

$$D\xi = \delta_{J,J} |M_F| |M_{GT}| \sqrt{\frac{J}{J+1}} \, 4 \text{ Im } (C_S C_T^* - C_V C_A^*).$$

This only vanishes for certain special relations between the amplitudes and phases of the various coupling constants. From this it follows that no experiment which involves the measurement of the electron spin can succeed in detecting time reversal terms. The one experiment which can do this is a recoil experiment with oriented nuclei emitting β-particles in a mixed transition. In this case also the issue would not be clouded by the presence of Coulomb terms, since these vanish identically. The recoil experiment with polarized neutrons, of course, falls into this class.

4. ST and VA Interference Terms

In the expression for $A\xi$ (A.7), which gives the parity violating terms determined by Wu *et al.* [11]) in their orientation experiment, the first term is the same as the G.T. part of the expression for the electron polarization, while the second appears only for a mixed transition, and contains inter-

ference terms between S and T and between V and A. For the present theory

$$A\xi = |M_{GT}|^2 \lambda_{JJ'}[\mp 2\{|C_T|^2+|C_A|^2\}]$$
$$-\delta_{JJ'}|M_F|\,|M_{GT}|\sqrt{\frac{J}{J+1}}\,[4\ \mathrm{Re}\ (C_S C_T^*+C_V C_A^*)].$$

A similar interference term appears in the expression for the circular polarization of γ-rays, first investigated by Schopper [12]). The first orientation measurements made on a mixed transition viz. Co^{58} (Wu *et al.*[13]), Postma *et al.*[14])) were compatible with a zero value for the interference term. However the measurements on γ-ray circular polarization by Schopper [15]) on Na^{24}, Zr^{95}, and Sb^{124}, and by Boehm and Wapstra [16]) on Sc^{46} and Au^{198}, appear to require the presence of large interference terms. The failure to observe such terms in Co^{58} may be due to the Fermi part of the matrix element being very small (Grace, private communication). The smallness of the interference terms in this case is confirmed by the measurements of Boehm and Wapstra [17]). Both the present theory and the two component theory predict the presence of these terms.

5. Inverse β-Decay

Lee and Yang have pointed out that a consequence of the two component theory, on the assumption that the β-disintegrations in a nuclear reactor are predominantly G.T., is that the antineutrinos emitted should be largely polarized, and that if this were so the cross-section for inverse β-decay measured by Reines and Cowan [18]) should be twice the value they actually observed. It was suggested then that there is an incompatibility between the parity measurements on Co^{60} and Reines and Cowan's measurement, independent of any detailed theory. We would like to suggest, instead, that the result of the Reines and Cowan experiment indicates that the neutrinos from a reactor are largely unpolarized. If we also make the reasonable assumption that Fermi transitions are unimportant, this conclusion is in agreement with the theory we have put forward here and suggests, in agreement with Ridley's electron-neutrino correlation measurement, that the T and A interactions are roughly equal.

6. Double β-Decay

The two component theory of the neutrino could still be made compatible with the relations between the coupling constants suggested here, provided that lepton conservation is dropped; i.e. it is suggested that in β^-decay antineutrinos are emitted in T interactions and neutrinos in A interactions. It can however be shown that this would lead to neutrinoless β-emission in

double β-decay, since antineutrinos emitted in the T part of the interaction in the first decay could be absorbed in the A part of the interactions in the second. Although in recent years the theoretical estimates of half life of double β-decay for Majorana and for Dirac neutrinos have become much closer it still appears that the results of Awschalom on Ca^{48} [19]) and Reines and Cowan on Nd^{150} [20]) exclude the possibility of neutrinoless decay.

7. π-μ-e Decay

The relations between the parity conserving and parity violating coupling constants in the scheme put forward here are formally the same as those derived by Feynman [21]) from a two component theory of the electron. As he points out, this theory and the two component theory give opposite predictions concerning the spins of the muons and electrons in the $\pi-\mu-e$ decay. Here again the preliminary experimental results differ, that of Lederman *et al.* being in qualitative agreement with the two component theory, while the value reported by the Liverpool group [22]) for the electron polarization is of the opposite sign.

8. The Twin Neutrino Theory

This third scheme of coupling constants has been associated with the name of M. Meyer, and was also put forward at the Harwell Parity Conference by M. A. Preston. It is assumed that in β^-decay antineutrinos are emitted in G.T. transitions, and neutrinos in Fermi transitions, and vice versa for β^+ decay i.e. $C_T = -C'_T$, $C_A = -C'_A$, $C_S = C'_S$, $C_V = C'_V$. In this form lepton non-conservation is compatible with the double β-decay experiments. This follows from an argument due to Preston: in all practical cases the initial and final states in double β-decay are both 0^+, hence a G.T. transition to an intermediate 1^+ state must be followed by a further G.T. transition. The same argument may be used for Fermi transitions. If the positive result obtained by Davis on inverse β-decay in A^{37} [23]) is substantiated this would provide powerful support for the twin neutrino theory, since it requires both antineutrinos and neutrinos to be emitted from a nuclear reactor. However to reconcile the theory with full v/c electron polarization we must have $C_A = -C'_A = 0$, $C_S = +C_S' = 0$, in disagreement with the electron neutrino correlation measurements. Moreover the interference terms which appear in the γ-ray circular polarization measurements are required to vanish, as well as the Fierz terms.

9. Conclusion

We have seen that three alternative schemes of coupling constants have been advanced, each of which explains some of the features of the experimental results. The four state neutrino theory put forward here appears to be in

agreement with a wider range of experiments than the other two. This scheme implies that all electron polarization measurements, at least for allowed transitions, will give one or the other of the values $\pm v/c$, whatever the values of the ratios C_T/C_A and C_S/C_V, and that only one kind of measurement, suggested by Jackson *et al.* [10]), can reveal breakdown of time reversal invariance, a recoil measurement using oriented nuclei.

Many people must be thinking along similar lines at present, and the combination $C_T = -C'_T$, $C_A = +C'_A$ has been specifically mentioned by Schopper, and by Wapstra (private communication).

It is a pleasure to acknowledge the useful discussions we have had with Dr. T. H. R. Skyrme and Prof. M. A. Preston.

References

1) Frauenfelder, Bobone, V. Goeler, Levine, Lewis, Peacock, Rossi and De Pasquali, Phys. Rev. **107** (1957) 909
2) H. de Waard and O. J. Poppema, Physica **23** (1957) 597
3) C. S. Wu, private communication
4) Cavanagh, Turner, Coleman, Gard and Ridley, Phil. Mag. **21** (1957) 1105, footnote
5) Deutsch, Gittelman, Bauer, Grodzins and Sunyar, Phys. Rev. (submitted)
6) Frauenfelder, Hanson, Levine, Rossi and de Pasquali, Phys. Rev. **107** (1957) 910
7) B. M. Rustad and S. L. Ruby, Phys. Rev. **97** (1955) 991
8) J. M. Robson, Phys. Rev. **100** (1955) 933
9) Maxson, Allen and Jentschke, Phys. Rev. **97** (1955) 109;
W. P. Alford and D. R. Hamilton, Phys. Rev. **105** (1957) 673; } Ne^{19}
M. L. Good and E. J. Laner, Phys. Rev. **105** (1957) 213;
Herrmannsfeldt, Maxson, Stähelin and Allen, Phys. Rev. **107** (1957) 641 } A^{35}
10) Jackson, Treiman and Wyld, Nuclear Physics **4** (1957) 206
11) Wu, Ambler, Hayward, Hoppes and Hudson, Phys. Rev. **105** (1957) 1413
12) H. Schopper, Phil Mag. **2** (1957) 710
13) Ambler, Hayward, Hoppes, Hudson and Wu, Phys. Rev. **106** (1957) 1361
14) Postma, Huiskamp, Miedma, Steenland, Tolhoek and Gorter, Physica **23** (1957) 259
15) H. Appel and H. Schopper, Zeits. für Phys. **149** (1957) 103
16) F. Boehm and A. H. Wapstra. Phys. Rev. (in press)
17) F. Boehm and A. H. Wapstra, private communication
18) Cowan, Reines, Harrison, Kruse and McGuire, Science **124** (1956) 103
19) M. Awschalom, Phys. Rev. **101** (1956) 1041
20) Cowan, Harrison, Langer and Reines, Nuovo Cimento **3** (1956) 649
21) R. P. Feynman, Rochester Conference (1957)
22) J. M. Cassels *et al.*, Physical Society Meeting (Manchester, 1957)
23) R. Davis, abstract of paper, Unesco Conference (Paris, 1957)

Note added in proof: Since writing this paper we have received reprints of a series of notes by R. Nataf, in one of which the same scheme of coupling constants is put forward as presented here (Comptes Rendus **244** (1957) 1187).

Nuclear Physics **5** (1958) 17—22; © *North-Holland Publishing Co., Amsterdam*

Not to be reproduced by photoprint or microfilm without written permission from the publisher

MULTIPLE PRODUCTION OF HEAVY PARTICLES IN TWO NUCLEON COLLISIONS

V. S. BARASHENKOV, B. M. BARBASHEV and E. G. BUBELOV
Joint Institute of Nuclear Research, Theoretical Physics Laboratory, Dubna, USSR

V. M. MAKSIMENKO
P. N. Lebedev Physical Institute, USSR Academy of Sciences, Moscow

Received 27 May 1957

Abstract: The probabilities of particle production in nucleon-nucleon collisions at an energy of $E = 5$ GeV have been calculated using Fermi's statistical theory and by taking into account the conservation of baryon number, strangeness, isobaric spin as well as strong resonance pion-nucleon interaction in the $T = 3/2$, $P = 3/2$ state. Various effective space volumes in which secondary particles are produced are considered.

With the advent of giant accelerators considerable interest is being attached at present to investigation of multiple production of elementary particles in nucleon-nucleon collisions, in the GeV range.

Theoretical investigation of similar processes may yield new data on the internal structure of elementary particles and the laws of their interaction at high energies [1]) and also provide the substantial information required for planning experiments on the big accelerators.

Results of the calculations of multiple production of pions, nucleons and heavy particles in the high energy region are given in ref. [2]). However, in these papers the conservation of strangeness and baryon number was not taken into account, the calculation of phase volumes was not sufficiently rigorous and strong resonance pion-nucleon interaction in the $T = 3/2$, $P = 3/2$ [3]) state was not taken into account.

In the present paper the distribution of secondary particles produced in nucleon-nucleon collision at $E = 5$ GeV was computed by using the Fermi statistical theory [4]) and taking into account nucleon and pion resonance interaction [3]). On the assumption that baryons and K-mesons are non-relativistic particles and pions are extremely relativistic ones, the volumes in phase space have been calculated using the formulas obtained in paper [5]). Exact formulas from ref. [6]) were used for the case of two or three particles. Numerical calculations show that such a division of four or more particles into extreme relativistic and non-relativistic ones at $\lesssim 5$ GeV yields a negligible error compared with the exact calculation.

Statistical weights connected with the isobaric spin were calculated by the method described in ref. [7]). In these calculations the conservation of isobaric spin, baryon number and strangeness as well as identity of the particles were taken into account.

We neglected the conservation of angular momentum, but assumed that the statistical weight of the particles produced in the collisions with angular spin $S_1, S_2, \ldots S_k$ is proportional to the product $\prod_{i=1}^{k}(2S_i+1)$†. At present the spins of strange particles are not exactly known and the lowest possible spin value, which is $S = 0$ for K-mesons and $S = 1/2$ for the remaining strange particles, was accepted in the estimation. The calculations were made for three choices of the effective space volumes in which the production of secondary particles occurs.

1. All secondary particles were assumed to be produced in a volume V_π whose radius is equal to the pion Compton wave length.

2. K-mesons are produced in a volume V_K whose radius is equal to the K-meson Compton wave length, other particles being produced in V_π. The statistical weight factor V in this case has the form

$$V \equiv V_2 = \frac{(k+l\xi)\xi^{l-1}}{NG}\left[\frac{1}{3\pi^2}\left(\frac{1}{m_\pi c}\right)^3 \frac{Mc^2}{E_c}\right]^{N-1}$$

where

$$\xi = \left(\frac{m_\pi}{m_K}\right)^3;$$

m_π; m_K; M are the pion, K-meson and nucleon masses respectively.

E_c is the total energy in the centre of mass system,

G is a factor which takes into account identity of the particles,

K is the number of K-mesons,

$l = N-k$ is the number of other particles.

3. Pions, nucleons and isobars are produced in V_π, the other (strange) particles being produced in V_K. In this case the weight factor is

$$V \equiv V_3 = \frac{(j+i\xi)\xi^{j-1}}{NG}\left[\frac{1}{3\pi^2}\left(\frac{1}{m_\pi c}\right)^3 \frac{Mc^2}{E_c}\right]^{N-1}$$

where j is the number of strange particles and $i = N-j$ the number of pions, nucleons and isobars.

It is evident that for $k \to 0$ and $j \to 0$ the factors V_2 and V_3 transform into the weight factor V_1 which corresponds to the case of choosing the pion volume for all secondary particles.

The results of the calculations are given in table 1. It follows from the table that if one chooses the effective volume to be $V = V_1$, then the number

† An analogous assumption was used by Sandweiss and Goldhaber for the determination of multiple production of K-meson angular spin [8]) using statistical theory.

TABLE 1 †

Secondary particles	Statistical weight (%)					
	(p, p)-collision			(p, n)-collision		
	V_1	V_2	V_3	V_1	V_2	V_3
2N	0.272	0.362	0.414	0.433	0.588	0.676
2Nπ	6.20	8.25	9.42	5.92	8.00	9.20
2N2π	20.10	26.75	30.54	21.50	29.10	33.50
2N3π	27.00	36.00	41.10	24.76	33.47	38.45
2N4π	10.80	14.25	16.30	10.29	13.92	16.00
2N5π	1.00	1.32	1.51	0.92	1.24	1.42
NΛK	3.00	1.394	0.0712	4.78	2.27	0.1166
NΣK	5.10	2.37	0.1212	5.32	2.52	0.1295
N$\pi\Lambda$K	6.52	2.66	0.1350	5.15	2.01	0.1034
N$\pi\Sigma$K	10.50	4.27	0.201	11.00	4.53	0.224
2N$\bar{\text{K}}$K	1.70	0.0268	0.0307	2.10	0.0335	0.0386
NΞ2K	0.109	$0.0^{(2)}171$	$0.0^{(4)}674$	0.134	$0.0^{(2)}215$	$0.0^{(4)}847$
2Λ2K	0.0243	$0.0^{(3)}383$	$0.0^{(6)}463$	0.0390	$0.0^{(3)}625$	$0.0^{(6)}757$
$\Lambda\Sigma$2K	0.0472	$0.0^{(3)}744$	$0.0^{(6)}900$	0.0500	$0.0^{(3)}792$	$0.0^{(6)}959$
2Σ2K	0.0183	$0.0^{(3)}285$	$0.0^{(6)}348$	0.0192	$0.0^{(3)}307$	$0.0^{(6)}372$
N2$\pi\Lambda$K	2.60	0.881	0.0446	2.72	0.935	0.0476
N2$\pi\Sigma$K	4.01	1.377	0.0696	3.94	1.350	0.0687
2N$\pi\bar{\text{K}}$K	0.905	0.01424	0.01628	0.785	0.0125	0.01437

† Figures in parenthesis denote the number of zeros.

of produced strange particles will turn out to be so large relative to the number of produced pions and nucleons as to be incompatible with the experimental data [9]). On the other hand the assumption that the particles are produced in the volume $V \approx V_K$ also cannot be brought into agreement with experiment. The best agreement with the experimental evidence can be obtained by putting $V = V_2$ and $V = V_3$.

We have also obtained the charge sign distribution of strange particles produced in (p, p) and (p, n) collisions. For the sake of simplicity pions, nucleons and isobars have not been distinguished with respect to charge (see table 3). The results of the calculations for the case of weight factors $V = V_2$ and $V = V_3$ are given in table 2. Statistical weights of particles and antiparticles and charge factors which are important for statistical theory are also included in the table. The charge factor is

$$T(I, I_z) = K^2(I; I_z; i^{(j)}, i_z^{(j)})P(I-\sum_j i^{(j)}, I_z-\sum_j i_z^{(j)}),$$

where K is the Clebsch-Gordan coefficient,

P the isobaric weight of the corresponding pion, nucleon and isobar group [7]),

TABLE 2 †

Charge states	Charge factor			Statistical weight (%)			
				(p, p)-collisions		(n, p)-collisions	
	$T(0, 0)$	$T(1, 0)$	$T(1, 1)$	V_2	V_3	V_2	V_3
$N\Lambda K^+$	1/2	1/2	1	1.39	0.0712	1.13	0.0583
K^0	1/2	1/2	0	0	0	1.13	0.0583
$N\Sigma^+K^+$	0	0	3/4	0.889	0.0455	0	0
Σ^+K^0	1/3	1/2	3/4	0.889	0.0455	0.741	0.0382
Σ^0K^+	1/6	1/2	1/2	0.593	0.0303	0.518	0.0266
Σ^0K^0	1/6	1/2	0	0	0	0.518	0.0266
Σ^-K^+	1/3	1/2	0	0	0	0.741	0.0382
Σ^-K^0	0	0	0	0	0	0	0
$N'\Lambda K^+$	0	1/2	1/4	0.354	0.0180	0.353	0.0181
K^0	0	1/2	3/4	1.061	0.0541	0.353	0.0181
$N'\Sigma^+K^+$	1/4	9/20	3/10	0.333	0.0146	0.561	0.0271
Σ^+K^0	1/12	7/20	3/10	0.333	0.0146	0.298	0.0139
Σ^0K^+	1/6	1/5	7/20	0.389	0.0170	0.318	0.0156
Σ^0K^0	1/6	1/5	9/20	0.500	0.0219	0.318	0.0156
Σ^-K^+	1/12	7/20	3/5	0.667	0.0292	0.298	0.0139
Σ^-K^0	1/4	9/20	0	0	0	0.561	0.0271
$N\pi\Lambda K^+$	1/2	1	5/4	0.776	0.0394	0.659	0.0336
K^0	1/2	1	3/4	0.466	0.0236	0.659	0.0336
$N\pi\Sigma^+K^+$	1/4	9/20	21/20	0.538	0.0272	0.259	0.0132
Σ^+K^0	5/12	17/20	31/20	0.538	0.0272	0.457	0.0233
Σ^0K^+	1/3	7/10	17/20	0.436	0.0220	0.370	0.0190
Σ^0K^0	1/3	7/10	9/20	0.230	0.0117	0.370	0.0190
Σ^-K^+	5/12	17/20	3/5	0.307	0.0156	0.457	0.0233
Σ^-K^0	1/4	9/20	0	0	0	0.259	0.0132
$N'\pi\Lambda K^+$	1/2	1	5/4	0.427	0.0217	0.363	0.0185
K^0	1/2	1	3/4	0.256	0.0129	0.363	0.0185
$2NK^0K^+$	1/3	1/2	3/2	0.0135	0.0154	$0.0^{(2)}559$	$0.0^{(2)}643$

K^0	1/2	1	3/4	0.256	0.0129	0.363	0.0185
$2NK^0K^+$	1/3	1/2	3/2	0.0135	0.0154	$0.0^{(2)}559$	$0.0^{(2)}643$
$\tilde{K}^0K^0$	2/3	1	3/4	$0.0^{(2)}673$	$0.0^{(2)}767$	0.0112	0.0129
K^-K^+	2/3	1	3/4	$0.0^{(2)}673$	$0.0^{(2)}767$	0.0112	0.0129
K^-K^0	1/3	1/2	0	0	0	$0.0^{(2)}559$	$0.0^{(2)}643$
$N'\pi\Sigma^+K^+$	1/4	13/20	11/10	0.216	0.01093	0.118	$0.0^{(2)}606$
Σ^+K^0	5/12	19/20	11/10	0.216	0.01093	0.185	$0.0^{(2)}943$
Σ^0K^+	1/3	9/10	19/20	0.186	$0.0^{(2)}944$	0.161	$0.0^{(2)}824$
Σ^0K^0	1/3	9/10	13/20	0.128	$0.0^{(2)}646$	0.161	$0.0^{(2)}824$
Σ^-K^+	5/12	19/20	7/10	0.137	$0.0^{(2)}696$	0.185	$0.0^{(2)}943$
Σ^-K^0	1/4	13/20	1/2	0.0980	$0.0^{(2)}497$	0.118	$0.0^{(2)}606$
$NN'\tilde{K}^0K^+$	1/3	4/5	3/5	$0.0^{(2)}279$	$0.0^{(2)}319$	$0.0^{(2)}360$	$0.0^{(2)}827$
$\tilde{K}^0K^0$	1/6	7/10	9/10	$0.0^{(2)}418$	$0.0^{(2)}478$	$0.0^{(2)}250$	$0.0^{(2)}573$
K^-K^+	1/6	7/10	9/10	$0.0^{(2)}418$	$0.0^{(2)}478$	$0.0^{(2)}250$	$0.0^{(2)}573$
K^-K^0	1/3	4/5	3/5	$0.0^{(2)}279$	$0.0^{(2)}319$	$0.0^{(2)}360$	$0.0^{(2)}827$
$2N'\tilde{K}^0K^+$	1/3	4/5	8/5	$0.0^{(3)}147$	$0.0^{(3)}168$	$0.0^{(4)}714$	$0.0^{(4)}822$
$\tilde{K}^0K^0$	2/3	6/5	9/10	$0.0^{(4)}830$	$0.0^{(4)}948$	$0.0^{(3)}124$	$0.0^{(3)}143$
K^-K^+	2/3	6/5	9/10	$0.0^{(4)}830$	$0.0^{(4)}948$	$0.0^{(3)}124$	$0.0^{(3)}143$
K^-K^0	1/3	4/5	3/5	$0.0^{(4)}554$	$0.0^{(4)}633$	$0.0^{(4)}714$	$0.0^{(4)}822$
$N2\pi\Lambda K^+$	1	2	5/2	0.124	$0.0^{(2)}622$	0.105	$0.0^{(2)}529$
K^0	1	2	3/2	0.0743	$0.0^{(2)}373$	0.105	$0.0^{(2)}529$
$N2\pi\Sigma^+K^+$	1/2	11/10	43/20	0.0948	$0.0^{(2)}476$	0.0520	$0.0^{(2)}264$
Σ^+K^0	5/6	9/5	43/20	0.0948	$0.0^{(2)}476$	0.0860	$0.0^{(2)}436$
Σ^0K^+	2/3	8/5	9/5	0.0793	$0.0^{(2)}398$	0.0723	$0.0^{(2)}366$
Σ^0K^0	2/3	8/5	11/10	0.0485	$0.0^{(2)}243$	0.0723	$0.0^{(2)}366$
Σ^-K^+	5/6	9/5	13/10	0.0573	$0.0^{(2)}288$	0.0860	$0.0^{(2)}436$
Σ^-K^0	1/2	11/10	1/2	0.0221	$0.0^{(2)}1105$	0.0520	$0.0^{(2)}264$
$N\Xi^0K^+K^+$	0	0	3/4	$0.0^{(3)}429$	$0.0^{(4)}168$	0	0
$\Xi^0K^+K^0$	2/3	1	3/2	$0.0^{(3)}859$	$0.0^{(4)}336$	$0.0^{(3)}714$	$0.0^{(4)}282$
$\Xi^-K^+K^+$	1/3	1/2	3/4	$0.0^{(3)}429$	$0.0^{(4)}168$	$0.0^{(3)}357$	$0.0^{(4)}141$
$\Xi^0K^0K^0$	1/3	1/2	0	0	0	$0.0^{(3)}357$	$0.0^{(4)}141$
$\Xi^-K^+K^0$	2/3	1	0	0	0	$0.0^{(3)}714$	$0.0^{(4)}282$
$\Xi^-K^0K^0$	0	0	0	0	0	0	0

† Figures in parenthesis denote the number of zeros.

TABLE 3

Secondary particles	Statistical weight (%)			
	(p, p)-collision		(p, n)-collision	
	V_2	V_3	V_2	V_3
2N	0.356	0.415	0.588	0.678
NN′	1.343	1.534	0.670	0.767
2N′	1.230	1.405	2.00	2.30
2Nπ	6.91	7.89	7.33	8.44
NN′π	16.42	18.77	17.44	20.07
2N′π	12.09	13.81	10.61	12.21
2N2π	9.11	10.40	9.66	11.09
NN′2π	19.59	22.36	18.56	21.40
2N′2π	8.79	10.04	8.62	9.92
2N3π	4.32	4.94	4.31	4.97
NN′3π	5.47	6.24	5.29	6.09
2N′3π	1.325	1.513	1.244	1.431

I and I_z the isobaric spin and isobaric spin projection of all the particles produced in the nucleon-nucleon collision,

$\sum_j i^{(j)}$ and $\sum_j i_z^{(j)}$ the sum of isobaric spins and their projections of strange particles created in the collision.

Calculation of the coefficients $T(I, I_z)$ is a simple but cumbersome task.

In conclusion the authors take the pleasure in thanking Professor D. I. Blokhintsev and I. L. Rozental for discussions and valuable advice. We are also grateful to L. G. Zastavenko for discussions and assistance.

References

1) D. I. Blokhintsev, CERN Symposium (Geneva, 1956) JETP (in press)
2) L. S. Kothari, Jr., Nature **171** (1953) 309;
I. S. Kovacs, Phys. Rev. **101** (1956) 357;
G. V. Lepore and R. N. Stuart, Phys. Rev. **94** (1954) 1754;
U. Haber-Schain and G. Yekutieli, Phil. Mag. **43** (1952) 997; Phys. Rev. **94** (1953) 184;
P. Brovetto and S. Ferroni, Nuovo Cimento **3** (1956) 1387
3) S. Z. Belenky and A. L. Nikishov, JETP **28** (1955) 744;
S. Z. Belenky, Nuclear Physics **2** (1956) 259;
V. M. Maksimenko and A. I. Nikishov, JETP **31** (1956) 727
4) E. Fermi, Progr. Theor. Phys. **5** (1950) 570; Phys. Rev. **81** (1951) 683
5) V. M. Maksimenko and I. L. Rozental, JETP (in press);
I. L. Rozental, JETP **28** (1955) 118
6) M. M. Block, Phys. Rev. **101** (1956) 796
7) V. S. Barashenkov, and B. M. Barbashev, Nuovo Cimento (in press)
8) J. Sandweiss and M. Goldhaber, Bull. Am. Phys. Soc. **1**, No. 8 (1956) 385
9) W. W. Chupp *et al.*, Nuovo Cimento Suppl. **4** (1956) 358;
R. W. Birge *et al.*, Nuovo Cimento Suppl. **4** (1956) 351

Nuclear Physics **5** (1958) 23—32; © *North-Holland Publishing Co., Amsterdam*
Not to be reproduced by photoprint or microfilm without written permission from the publisher

ON THE LONG-RANGE CORRELATION MODEL OF THE PHOTONUCLEAR EFFECT

M. DANOS

National Bureau of Standards, Washington, D.C.

Received 11 June 1957

Abstract: The long-range correlation model, i.e. the hydrodynamic "second-sound" model, of the photonuclear effect predicts a splitting of the giant resonance in deformed nuclei. As a result of this, the width and the shape of the observed resonance will be different in different nuclei. The hydrodynamic model further predicts the existence of a second-sound monopole mode at roughly twice the energy of the dipole mode. However, the resonance energy is so high that this mode may be damped completely except, perhaps, in the heaviest nuclei. Observation of this mode could yield information about the energy dependence of the friction coefficient Γ of second sound in nuclear matter.

1. Introduction

The general features of the giant resonance of nuclear X-ray absorption have been explained with roughly equal success using either the assumption of strong long-range correlations in the excited state [1–5]), or the assumption of no correlations in the excited state [6–10]). The first is usually called the hydrodynamic model, the latter the shell-model approach. A connection between these opposite starting points has been pointed out by Brink [11]) who showed that in an independent-particle harmonic-oscillator potential model, the state reached after absorption of a photon actually corresponds to a motion of all protons against all neutrons in a way postulated by Goldhaber and Teller [2]) in their third model. This state clearly contains correlations. Further, the single-particle states constituting the excited state will interact and, as a result, the energy of the excited state will be changed. Thus, a reanalysis into single particle states in general will not be possible, except for kinematic features (e.g. angular distributions of fast secondaries[8]). An analogous case has been treated by Visscher and Ferrell [12,13])† who investigated the collective monopole state in O^{16} and C^{12} starting from the independent-particle model. They constructed the excited state as a linear combination of independent particle states where only one nucleon is excited at a time. Taking into account the interaction of the participating states, they found an energy shift of the order of the single-particle excitation energy. One may conclude, therefore, that there will be strong correlations in the excited state even when no correlations are

† *Editor's Note.* See also a forthcoming paper by Berenbaum [34]).

assumed in the ground state. It is now of interest to know how closely the model of extreme correlations, the hydrodynomic model, describes the behaviour of "nuclear matter." For this purpose one has to investigate the more detailed features of the model and try to compare them with experiment, since the main features are rather insensitive to the chosen model [14]).

Two of the detailed features will be discussed in the present paper. The first, the photoeffect in deformed nuclei [15, 16]), will be treated in section 2, and the other, a collective monopole mode of "second sound" [17]) will be treated in section 3. We shall restrict ourselves in this paper to the simple point of view of Steinwedel and Jensen [4]), and we shall neglect the compressibility of nuclear matter [5]) and the Coulomb repulsion of the protons [5, 18]). The surface can be assumed to be rigid, since surface oscillations do not couple to the monopole and dipole modes [5]), although they couple strongly to the quadrupole and higher modes †. The errors introduced by the above simplifications are small. By normalizing the results with respect to the dipole mode in spherical nuclei the errors will be cancelled to a large extent.

2. Photoeffect in Deformed Nuclei

In the second-sound hydrodynamic model, the resonance energy, $\hbar\omega$, is obtained by solving the eigenvalue equations [4])

$$\Delta\varrho_p + k^2\varrho_p = 0, \tag{1}$$

$$(\mathbf{n}\cdot\operatorname{grad}\varrho_p)_{\text{surface}} = 0. \tag{2}$$

Here

$$k^2 = \frac{u^2}{\omega^2}\left(1 - i\frac{\Gamma}{\omega}\right), \tag{3}$$

$$u^2 = \frac{8K}{M}\frac{\varrho_p\varrho_n}{\varrho_0^2} = \frac{8K}{M}\frac{NZ}{A^2}, \tag{4}$$

where ϱ_p, ϱ_n, and $\varrho_0 = \varrho_p + \varrho_n$ are the proton, neutron and total density respectively; k is the (real) eigenvalue, $\mathbf{n}$ is a unit vector normal to the surface, M is the nucleon mass, and K is the energy associated with the symmetry energy term $K(N-Z)^2/A$ in the Weizsäcker-Bethe nuclear binding energy formula. The finite width of the resonance is taken into account by Γ in eq. (3); if $\Gamma \neq 0$, ω is complex.

The eigenvalue equation has been solved for the spherical case by Lord Rayleigh [19]). He obtained as the eigenvalue for the lowest dipole mode $kR = 2.08$, where R is the radius of the sphere. In the case of a spheroidal nucleus, the eigenvalues depend on the deformation and are different for different m. The case $m = 0$ has been treated by McLaurin [20]). His results

† In ref. [18]) a rigid surface was assumed throughout. The results for the higher multipole modes therefore do not apply to nuclei and they are superseded by the work of Araùjo, ref. [5]).

are shown in fig. 1 where the eigenvalues are plotted as a function of a deformation parameter ε. The eigenvalues for $m = \pm 1$ are shown in fig. 2. They have been computed using tables of spheroidal wave functions [21]).

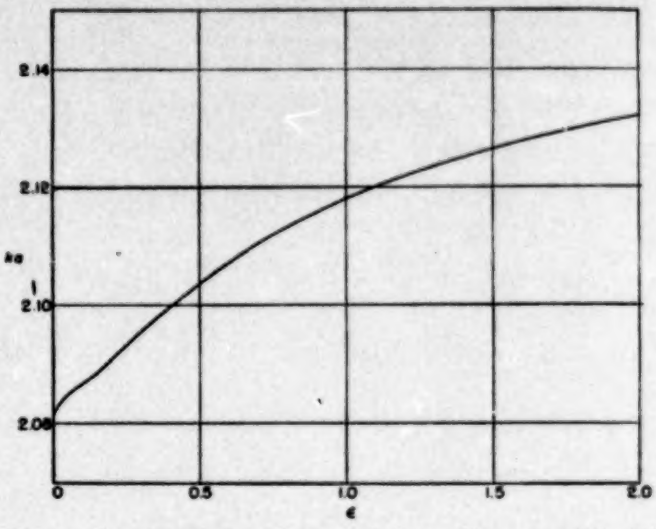

Fig. 1. Eigenvalue ka as function of deformation $\varepsilon = (a^2-b^2)/R^2$.

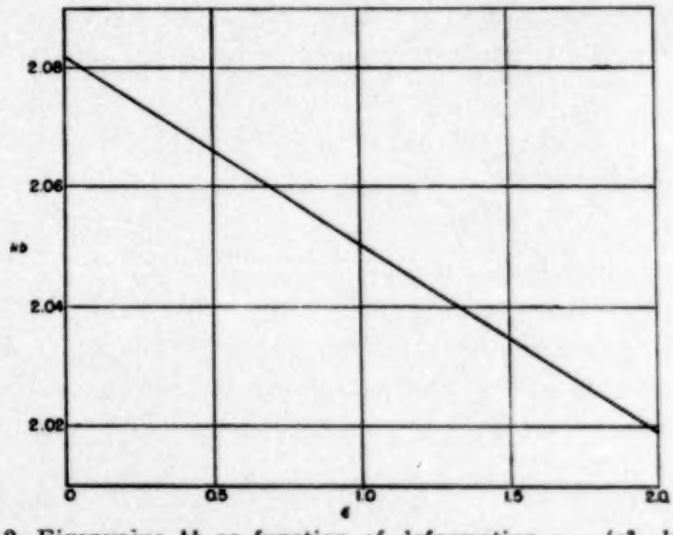

Fig. 2. Eigenvalue kb as function of deformation $\varepsilon = (a^2-b^2)/R^2$.

The deformation parameter ε has been chosen because the quadrupole moment is exactly proportional to it. This can be seen as follows. The quadrupole moment Q_0 of a spheroid with half axes a and b with uniform distribution of a charge Z is given by

$$Q_0 = \tfrac{2}{5}Z(a^2-b^2). \tag{5}$$

Here a is the axis of rotational symmetry. Defining $R^3 = R_0{}^3A = ab^2$ (R is the radius of a sphere of equal volume) and writing $a^2-b^2 = \varepsilon R^2$ for the eccentricity, (5) becomes

$$Q_0 = \tfrac{2}{5}R_0{}^2\varepsilon ZA^{2/3}. \tag{6}$$

The value of the spectroscopic quadrupole moment Q_s can be obtained from Q_0 by use of appropriate projection factors [22]). However, for the present purpose, the relevant quantity is the intrinsic deformation connected with Q_0: the value Q_s results from averaging the quadrupole moment in a time determined by the rotational energy which for deformed nuclei is of the order $\hbar/(100\ \text{keV})$. The order of magnitude of the relevant time in the case of photonuclear reactions is determined by the damping Γ and is $\hbar/(5\ \text{MeV})$. Therefore, the nucleus effectively sits still for the duration of the process. The parameter ε is connected with the constant β of Bohr and Mottelson [22]) by

$$\beta \approx \tfrac{2}{3}\sqrt{\frac{\pi}{5}}\,\varepsilon = 0.53\varepsilon \tag{7}$$

up to the first order in ε and with the constant δ of Nilsson [23]) by

$$\delta \approx \tfrac{1}{2}\varepsilon \tag{8}$$

also to first order. The quadrupole moment is not exactly linear in these parameters.

As shown in fig. 1 and 2, the eigenvalues ka and kb change very little from the value 2.08 valid for $\varepsilon = 0$. Over the range of nuclear deformations, the splitting of the eigenvalues is very accurately given by

$$\frac{\omega_b}{\omega_a} = 0.911\,\frac{a}{b} + 0.089\,. \tag{9}$$

The cross-section for absorption of γ-rays of polarization parallel to the a-axis will have the usual resonance shape [4]) located at ω_a. The integrated cross-section exhausts essentially the same fraction of the dipole sum as in the case of a spherical nucleus [4])†. The same is true for a nucleus with the b-axis parallel to the polarization vector. For a randomly oriented nucleus we have

$$\begin{aligned}\langle\sigma(E)\rangle &= \frac{1}{4\pi}\int \mathrm{d}\Omega[\sigma_a(E)\cos^2\vartheta + \sigma_b(E)\sin^2\vartheta] \\ &= \tfrac{1}{3}\sigma_a(E) + \tfrac{2}{3}\sigma_b(E).\end{aligned} \tag{10}$$

For a splitting $\omega_a - \omega_b$ less than $\frac{1}{2}\Gamma$ the cross-section essentially consists of one broadened peak [15,16]); if the splitting is greater than Γ two peaks appear. In a nucleus with positive quadrupole moment, $a > b$ and so the higher peak occurs at a higher energy. Conversely, in a nucleus with negative quadrupole moment, the higher peak occurs at a lower energy [16]).

If Γ depends on the resonance energy [24, 25]), the ratio of the heights of the disentangled peaks will be

† In ref. [4]) there is an error in the expression for the peak cross-section; a factor 2 has been omitted. Independently, a similar factor of 2 is missing in ref. [18]).

$$\frac{(\sigma_a)_{\max}}{(\sigma_b)_{\max}} = \frac{\Gamma_b}{2\Gamma_a}. \tag{11}$$

It may be possible to experimentally distinguish (11) from the value $\frac{1}{2}$ which this ratio would have if Γ were independent of the energy.

3. Collective Monopole Mode

In the past, only those multipole moments of the hydrodynamic model have been studied that can be excited by γ-radiation [2, 4, 5, 18]). However, in the case of electron bombardment, in addition to these a monopole mode [17]) can be excited. This mode is given by the spherically symmetric solution of eq. (1) and (2).

The lowest monopole eigenvalue [19]) is given by $k_M R = 4.49$. Since the lowest dipole eigenvalue is $k_D R = 2.08$, the monopole occurs at an energy

$$E_M = 2.16\ E_D \tag{12}$$

where E_D is the dipole resonance energy. The use of the experimental rather than the theoretical value for E_D will tend to eliminate most of the errors due to neglect of Coulomb forces and of compressibility of nuclear matter. The resonance energy E_M is practically independent of the deformation of the nucleus. In fact, at the largest observed deformations the energy is increased only by roughly 5 %.

The wavelength of the monopole mode is shorter than that of the dipole mode, and, in fact, is comparable to the average spacing of the nucleons ($R_0 A^{1/3} \approx 4.5\ R_0$ for $A = 90$). One may, therefore, expect that for light nuclei the monopole mode will be considerably more damped, i.e. have a considerably larger width than the dipole mode [24, 25])† while in heavy nuclei the widths in both modes can be expected to be of the same order of magnitude. The width in the monopole mode could perhaps be larger by a factor of two [24, 25]). Since the width of the dipole mode is around 5 MeV, the monopole mode in heavy nuclei ($A > 100$) could be as wide as 10 MeV.

The monopole mode can be excited by electron scattering. We shall restrict ourselves to the case of high electron energies and shall use Schiff's Born approximation formulae [26]). We shall refer the cross-sections to the elastic scattering cross-section, and for the sake of completeness give also the cross-section for excitation of the dipole mode by high energy electrons. We shall restrict ourselves furthermore to the case of spherical nuclei. As is known, the only essential difference between spherical and spheroidal nuclei is that the diffraction minima for the latter are more filled in [27]).

† The damping in light nuclei may be expected to exceed the value which one would obtain using the estimates in refs. [24]) and [25]), since in these papers the smallness of the wavelength has not been taken into account.

The relevant matrix element in Schiff's notation is

$$H'_{l,0} = -(4\pi i^l e a_0/q^2)[4\pi(2l+1)]^{\frac{1}{2}} \int j_l(qr) Y_{l,0} \varrho \mathrm{d}\tau, \tag{13}$$

which is eq. (15) of ref. [31]). The other matrix elements, eq. (16) and (17) of ref. [31]), vanish in the present case because only potential flow exists in this model [18]), and there is no magnetization present. In eq. (13), a_0 is the matrix element of the Dirac unit operator between initial and final electron states, q is the momentum transfer to the scattering electron, and ϱ is a classical charge density. For simplicity we shall use square densities throughout:

for elastic scattering

$$\varrho = \varrho_0 (Z/A) S(r); \tag{14}$$

for excitation of the monopole mode

$$\varrho = a_M \varrho_0 j_0(k_M r) S(r); \tag{15}$$

for excitation of the dipole mode

$$\varrho = a_D \varrho_0 j_1(k_D r) \cos\vartheta S(r). \tag{16}$$

In these equations, $S(r)$ is defined by

$$S(r) = \begin{cases} 1 \text{ for } r < R \\ 0 \text{ for } r > R. \end{cases} \tag{17}$$

The amplitudes a_M and a_D are discussed in the appendix. Scattering cross-sections obtained with eq. (14) give quite reliable results, except for the diffraction minima, which are too deep [28]).

No attempts have been made so far to deal with a rounded-off model because of the theoretical uncertainties involved. This question could be dealt with only in a much more sophisticated theory. In principle, a rounding off of the densities in eq. (15) and (16) could be detected experimentally.

The monopole and dipole cross-sections for $A = 150$ have been plotted in fig. 3 and 4, curve I, as a function of the momentum transfer in the form of the ratio to the elastic cross-section. For not very high primary energies, one would have to multiply this ratio by a ratio of the densities of the final electron states to obtain the actual cross-section ratio, i.e. essentially by the factor $(p_f/p_0)^2$. For low primary energies still more factors would appear [29, 30, 31]).

The cross-section for the excitation of the excited states is distributed over their width. Therefore, the calculated cross-section ratios have to be interpreted as: total number of electrons in the inelastic bump divided by total number of electrons in the elastic peak. There is a slight ambiguity in the above statement because even for a particular scattering angle the momentum transfer changes over the width of the resonance. However, the

error is very small if one takes for the momentum transfer the value valid for the center of the line.

Curve II of fig. 3 and 4 is obtained by assuming that at the diffraction minima both the elastic and the inelastic cross-sections are smoothed such that the cross-section is down by a factor of 4 from the neighbouring values,

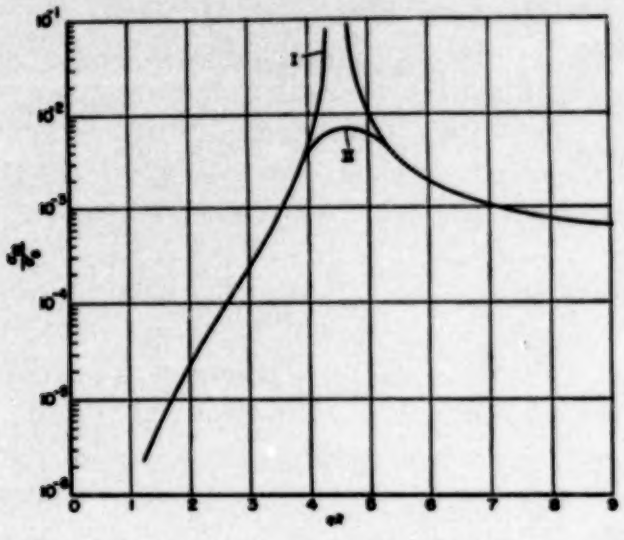

Fig. 3. Ratio of inelastic monopole to elastic high-energy electron-scattering cross-section for $A = 150$ as a function of qR.

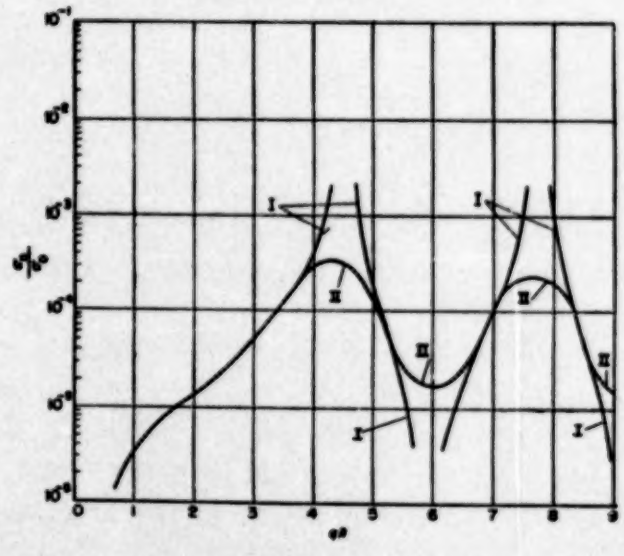

Fig. 4. Ratio of inelastic dipole to elastic high-energy electron-scattering cross-section for $A = 150$ as a function of qR.

corresponding roughly to experimental observations on the elastic cross-sections in spherical nuclei [27]). This has been done simply by rounding off by hand the cross-section curves obtained with eq. (14), (15), and (16) respectively.

In the case of excitation of the monopole mode (fig. 3), the diffraction minima coincide with those of the elastic scattering, except for the first minimum, which is missing in the inelastic monopole cross-section. If the monopole density, eq. (15), were rounded off in a different fashion than the ground-state density, eq. (14), a bump or a dip would appear at the place of the second elastic minimum depending on whether eq. (15) rounds off smoother or sharper than eq. (14).

The cross-section for excitation of the dipole mode (fig. 4) is generally lower by a factor of about 10 to 50 than the monopole cross-section and is correspondingly more difficult to detect. The diffraction minima here are located between the elastic minima. A rounding off of eq. (16) differently from eq. (14) would show up in the usual way as filling in or deepening of the diffraction minima.

In order to estimate the size of the inelastic bump we shall assume [27]) that the width of the elastic peak is 1 MeV, the ratio (peak)/(tail at 30 MeV below peak) $\approx$ 50, and the width of monopole resonance $\approx$ 10 MeV. Then, the height of the inelastic bump would be roughly 1 to 5 % of the tail. Since the cross-section for the dipole mode is around ten times smaller, but its width is about 5 MeV, the corresponding bump height would be 0.1 to 1 % of the tail.

4. Conclusions

According to section 2 one has to expect a correlation between the width of the giant dipole resonance and the quadrupole moment. A comparison of these quantities has been made by Okamoto [32])† who obtained a rather good over-all agreement. Indications of the splitting of the resonance for very large deformations have been observed by Petree, Weiss and Fuller [33]), although further experiments are needed before definite conclusions can be drawn.

Experiments of this kind as well as experiments on the monopole resonance of section 3 could be useful in the determination of the energy dependence of the damping constant Γ. Furthermore, experiments on the monopole mode would permit a differentiation between the Goldhaber and Teller models 2 and 3, since the latter does not allow for a monopole mode.

I would like to thank H. W. Koch for encouragement and him and the other members of this laboratory for constructive criticisms. I am further indebted to D. M. Brink, R. A. Ferrell, R. Hofstadter and K. Okamoto for helpful and informative discussions.

† I am grateful to Dr. Okamoto for informing me about his work prior to publication.

Appendix

The charge densities ϱ in eq. (13) can be considered either to be classical quantities, or to be quantal operators. In the latter case, one would obtain the amplitudes a_M, a_D, from quantization of eq. (1) and (2). Since this approach does not constitute an improvement of the theory (it does not, for example, explain the existence of the collective oscillation), and because it gives the same results as the simpler, classical approach, it will not be pursued here.

Classically, the amplitude is obtained from the requirement that the energy of the oscillation be $\hbar\omega$. Most conveniently this is done by considering the potential energy term [4])

$$V = \int d\tau K \frac{(\varrho_n - \varrho_p)^2}{\varrho_0} = \int d\tau \frac{K}{\varrho_0} (2\varrho_p - \varrho_0)^2 .$$

Writing

$$\varrho_l = \varrho_{p0} + a_l \varrho_0 j_l(k_l r) P_l (\cos\vartheta)$$

where $l = 0$ for the monopole and $l = 1$ for the dipole mode, one obtains

$$V = V_0 + V_1 a_l + V_2 a_l^2 .$$

Here V_0 is the ground-state potential. The term linear in a_l will cancel against other terms in the complete Hamiltonian. The term of interest is

$$\hbar\omega_l = V_2 a_l^2 = a_l^2 4K\varrho_0 \int d\tau [j_l(k_l r) P_l (\cos\vartheta)]^2 .$$

Using $K = 20$ MeV, $R = R_0 A^{1/3}$; $R_0 = 1.2 \times 10^{-13}$ cm, one obtains

$$a_M^2 = 25.4\, A^{-4/3};\ a_D^2 = 7.75\, A^{-4/3}. \qquad (18)$$

These values probably are good to 30 %.

Since the inelastic cross-sections are proportional to a_l^2, the cross-section ratios of fig. 3 and 4 can be converted to arbitrary A by multiplication with the factor $(150/A)^{4/3}$.

References

1) A. Migdal, Journ. Exp. Theor. Phys. USSR **15** (1945) 81
2) M. Goldhaber and E. Teller, Phys. Rev. **74** (1948) 1046
3) J. H. D. Jensen and P. Jensen, Z. Naturf. **5a** (1950) 343
4) J. H. D. Jensen and H. Steinwedel, Z. Naturf. **5a** (1950) 413
5) J. M. Araújo, Nuovo Cimento **12** (1954) 780
6) J. L. Burkhardt, Phys. Rev. **91** (1953) 420
7) A. Reifman, Z. Naturf. **8a** (1953) 502
8) D. H. Wilkinson, Proceedings of the 1954 Glasgow Conference on Nuclear and Meson Physics (Pergamon Press, 1955) p. 161
9) Y. K. Khokhlow, Dokl. Akad. Nauk USSR **97** (1954) 239
10) J. S. Levinger and D. C. Kent, Phys. Rev. **95** (1954) 418
11) D. M. Brink, Nuclear Physics **4** (1957) 215
12) R. A. Ferrell and W. M. Visscher, Phys. Rev. **102** (1956) 450

13) R. A. Ferrell and W. M. Visscher, Phys. Rev. **104** (1956) 475
14) J. S. Levinger and H. A. Bethe, Phys. Rev. **78** (1950) 115
15) K. Okamoto, Progr. Theor. Phys. **15** (1956) 75
16) M. Danos, Bull. Am. Phys. Soc. **1** (1956) 135
17) M. Danos, Bull. Am. Phys. Soc. **1** (1956) 246
18) M. Danos, Ann. d. Phys. **10** (1952) 265
19) Lord Rayleigh, The Theory of Sound, second edition (MacMillan Co., London, 1896) Chapter XVII
20) R. MacLaurin, Trans. Cambr. Phil. Soc. **17** (1898) 41
21) Stratton, Morse, Chu, Little and Corbato, Spheroidal Wave Functions (The Technology Press of MIT and John Wiley & Sons, New York. 1956)
22) A. Bohr and B. Mottelson, Mat. Fys. Medd. Dan. Vid. Selsk. **27** (1953) no. 16
23) S. G. Nilsson, Mat. Fys. Medd. Dan. Vid. Selsk. **29** (1955) no. 16
24) K. Wildermuth, Z. Naturf. **10***a* (1955) 447
25) K. Wildermuth and H. Wittern, Z. Naturf. **12***a* (1957) 39
26) L. I. Schiff, Phys. Rev. **96** (1954) 765
27) Hahn, Ravenhall, and Hofstadter, Phys. Rev. **101** (1956) 1131
28) Yennie, Ravenhall, and Wilson, Phys. Rev. **95** (1954) 500
29) J. S. Blair, Phys. Rev. **75** (1949) 907
30) Thie, Mullin, and Guth, Phys. Rev. **87** (1952) 962
31) H. R. Robl, Nuclear Physics **2** (1956/57) 641
32) K. Okamoto, to be published
33) Petree, Weiss, and Fuller, Bull. Am. Phys. Soc. **2** (1957) 16, and private communication
34) Berenbaum, Nuclear Physics

Nuclear Physics **5** (1958) 33—40; © *North-Holland Publishing Co., Amsterdam*
Not to be reproduced by photoprint or microfilm without written permission from the publisher

INVESTIGATION OF ASYMMETRY OF $\pi^+ \to \mu^+ \to e^+$ DECAYS IN PHOTOGRAPHIC EMULSIONS

A. O. WEISSENBERG and V. A. SMIRNITSKY
USSR Academy of Sciences, Moscow

Received 20 June 1957

Abstract: The energy dependence of the angular distribution of positons relative to the direction of emission of μ^+ mesons produced in $\pi^+ \to \mu^+ \to e^+$ decays is studied in photographic emulsions.

The correlation between the direction of emission of μ^+ mesons and positons in $\pi^+ \to \mu^+ \to e^+$ decays in emulsions and also the energy dependence of this correlation are investigated in the present paper. For this purpose the positon energy and angle between the directions of the positon and μ^+ meson in Ilford G5 and NIKFI—R emulsions were measured. The Ilford G5 emulsion layers were 600 μm thick and were part of a stack exposed at an altitude of $\approx$ 28 km. They were presented to us by C. Powell for investigation of high energy events. An analysis of the data obtained by measuring the first 120 $\pi \to \mu \to e$ decays in the emulsion was reported in ref.[1]).

The NIKFI—R emulsions, which were 10 cm in diameter and 400μm thick, were placed in a double magnetic shield which reduced the external field to less than 0.04 gauss. The emulsions were irradiated by a monochromatic beam of π^+ mesons from the synchrocyclotron of the Joint Institute of Nuclear Research. The mesons were slowed down in such a way that the π^+ mesons stopped within the emulsion. Altogether we measured 580 $\pi^+ \to \mu^+ \to e^+$ decays: 132 in the Ilford G5 emulsion and 448 in the NIKFI-R emulsion. We shall consider all 580 decay events.

The following criteria were used in choosing from a large number of $\pi^+ \to \mu^+ \to e^+$ decays those events which were to be measured:

1. Both stages of the $\pi \to \mu \to e$ decay occurred in a single emulsion layer.
2. The apex of the $\mu \to e$ decay was at a distance of more than 100 μm from any of the two emulsion surfaces.
3. The length of the positon track in the layer was not smaller than 1 mm.

The positon energies were measured by the multiple scattering method. The analysis indicated that in the NIKFI—R as well as Ilford G5 emulsions distortions were quite appreciable. Their influence decreased on changing from second to third or fourth differences. The spectra presented below were

constructed on the basis of the fourth differences. Depending on the track length and signal-to-noise ratio the scattering measurements were performed with cells of either 50, 100 or 200 μm. The track length distribution was the following:

Track length in mm	1—2	2—3	3—4	4—5	5—6	6
Number of tracks	313	126	78	34	23	6

The statistical error of the energy determination (dispersion) in 100 μm cells was between 28 % and 10 % (corresponding to the beginning and end of the table).

Besides positon energy the angle ϑ between the directions of meson and positon emission in the emulsion plane was also measured for each decay. It should be noted that a consequence of using the selection criteria mentioned above was that the angles between the positon or meson tracks and emulsion plane were not large; the halfwidths of the respective distributions were smaller than 7° for the positon and 10° for the meson tracks. Thus without introducing a considerable error we may 1) measure the projection of the volume angle ϑ on the emulsion surface instead of measuring the angle itself and 2) consider that correlation is being studied for particles whose tracks lie in the emulsion plane ("plane event").

The measured decay positon spectra are presented in fig. 1 (positons emitted in the forward direction, $0 \leqq \vartheta \leqq 90°$) and fig. 2 (positons emitted in the backward direction, $90° < \vartheta \leqq 180°$); the energy ε expressed as a fraction of the total energy $E \approx 53$ MeV is plotted along the abscissa axis and the number of particles per energy interval $\Delta\varepsilon = 0.1$ is plotted along the ordinate axis.

These two spectra are distinctly different. The spectrum for particles emitted in the forward direction sharply rises at low energy values and after passing through a maximum at $\varepsilon = 0.4—0.6$ gradually decreases; the spectrum for particles emitted in the backward direction, on the other hand, rises at an appreciably slower rate, passes through a maximum at $\varepsilon = 0.7—1.0$ and sharply drops off at higher energies. An appreciable excess of positons ejected backwards is observed beginning at $\varepsilon = 0.6$ and the relative magnitude of this excess increases with increasing energy. Thus, for example, the ratio of backward to forward particles is 219 : 163 for $\varepsilon > 0.6$, 146 : 97 for $\varepsilon > 0.8$ and 70 : 44 for $\varepsilon > 1.0$.

The two-component neutrino theory yields the following formula [2]) for the $\pi \to \mu \to$ e decay asymmetry:

$$\begin{aligned} dN &= N(a+b\alpha\lambda \cos\vartheta)d\varepsilon d\cos\vartheta, \\ a &= 2\varepsilon^2(3-2\varepsilon), \\ b &= 2\varepsilon^2(2\varepsilon-1), \end{aligned} \qquad (1)$$

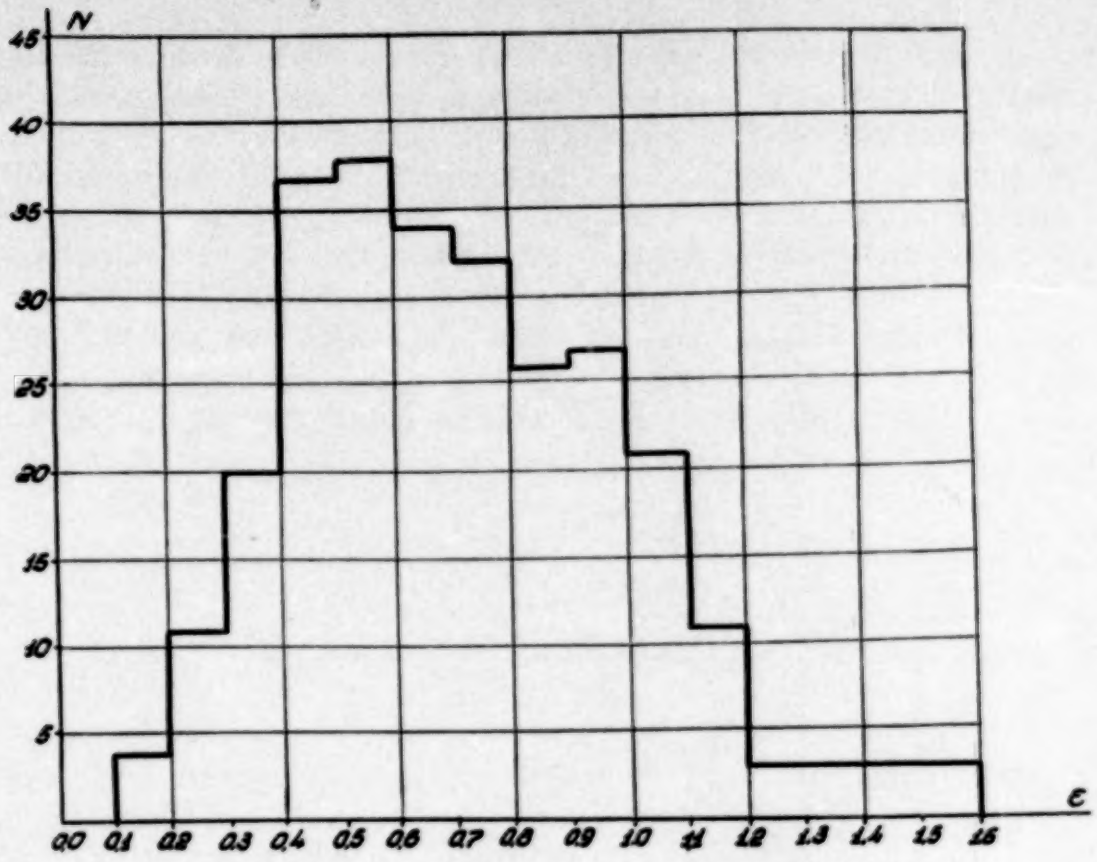

Fig. 1. Spectrum of positons emitted forward ($0° < \vartheta \leqq 90°$).

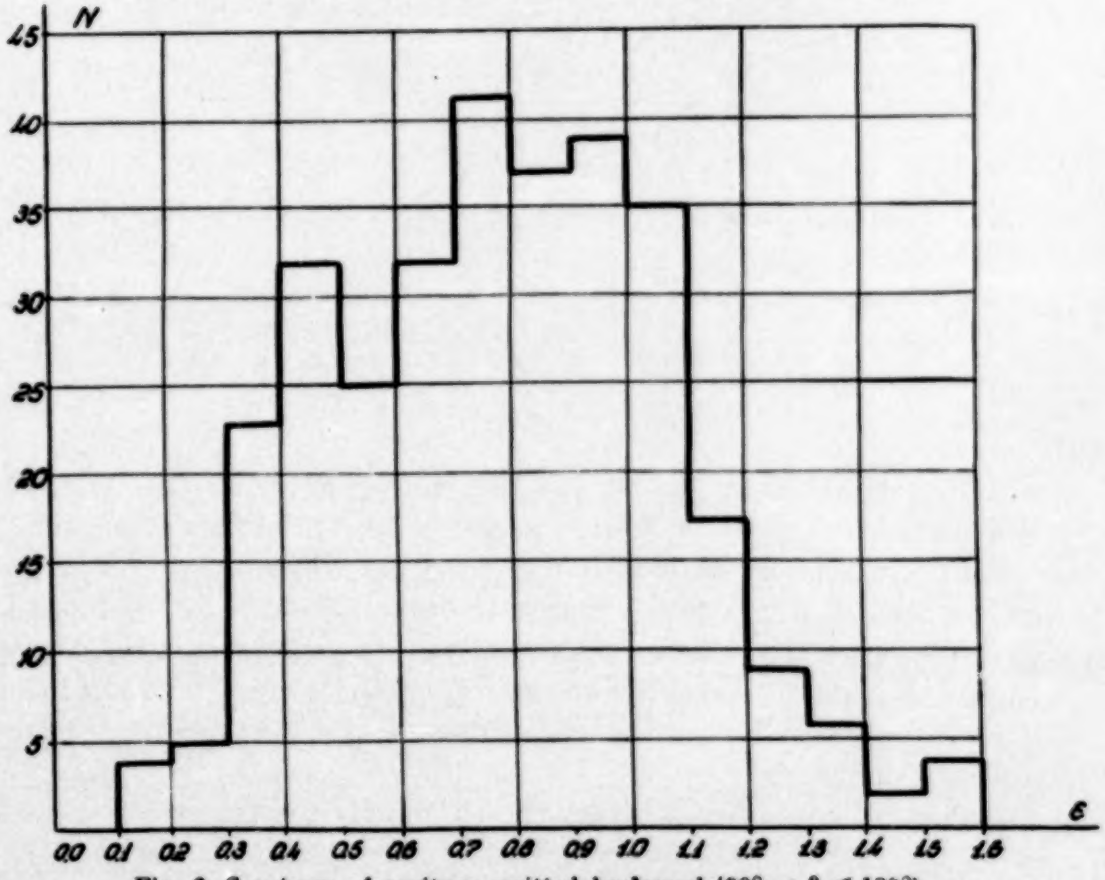

Fig. 2. Spectrum of positons emitted backward ($90° < \vartheta \leqq 180°$).

where λ is a parameter of the theory whose magnitude characterizes the fraction of vector and axial-vector variants in the $\mu \to e$ interaction; α is equal to the fraction of mesons which retain at the moment of $\mu \to e$ decay the initial spin direction acquired during the $\pi \to \mu$ decay. Comparison of our data with formula (1) is shown in fig. 3, 4 and 5. The solid lines refer to the integral energy spectra for the forward and backward directions; they were obtained by integrating (1) for plane angles (0—20° and 160°—180°, fig. 3, 0—45° and 135°—180°, fig. 4 and 0—90° and 90—180°, fig. 5). The theoretical curves were plotted on the assumption that $\alpha = 1$, $\lambda = -1$. The upper curves are the integral spectra for particles emitted

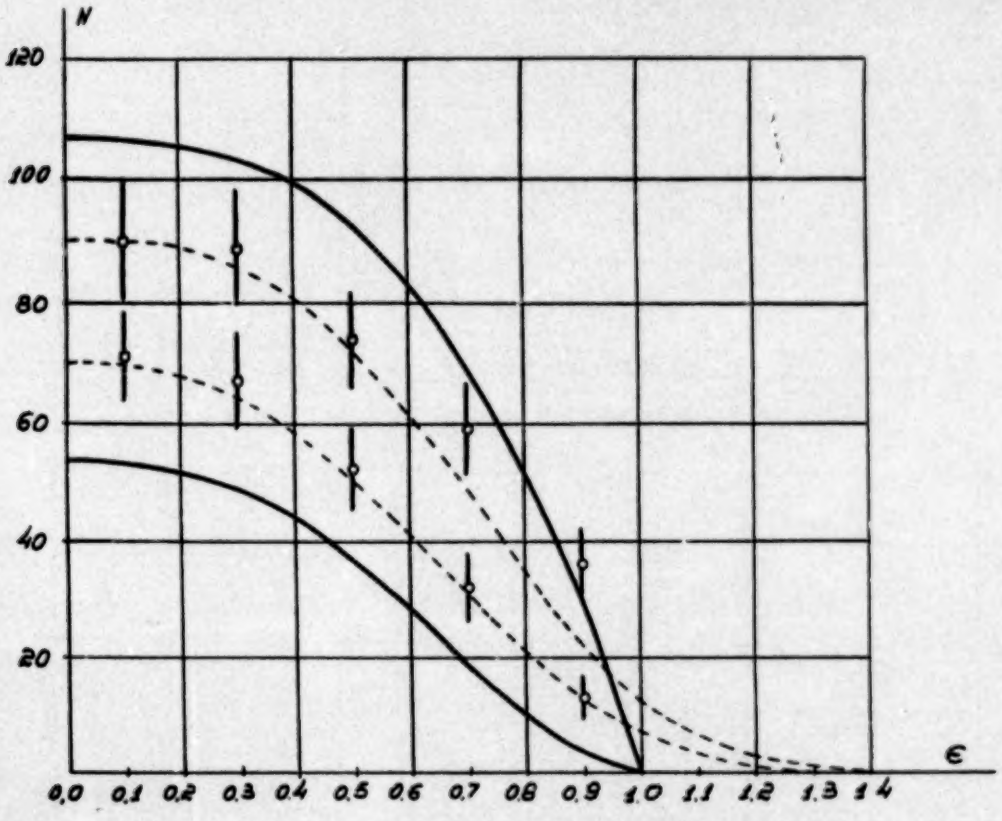

Fig. 3

backwards and the lower ones for particles emitted in the forward direction. The experimental points in figs. 3, 4 and 5 exhibit a forward-backward asymmetry which increases with the energy and with decreasing angle. However for particles emitted backward these points lie below the corresponding theoretical curve, whereas those for particles emitted in the forward direction lie above the theoretical curve; the explanation of this is that the coefficient $-\alpha\lambda$ is much smaller than 1, mainly as a result of depolarization.

The dotted lines in figs. 3—5 are the theoretical spectra for $\alpha\lambda = -0.4$

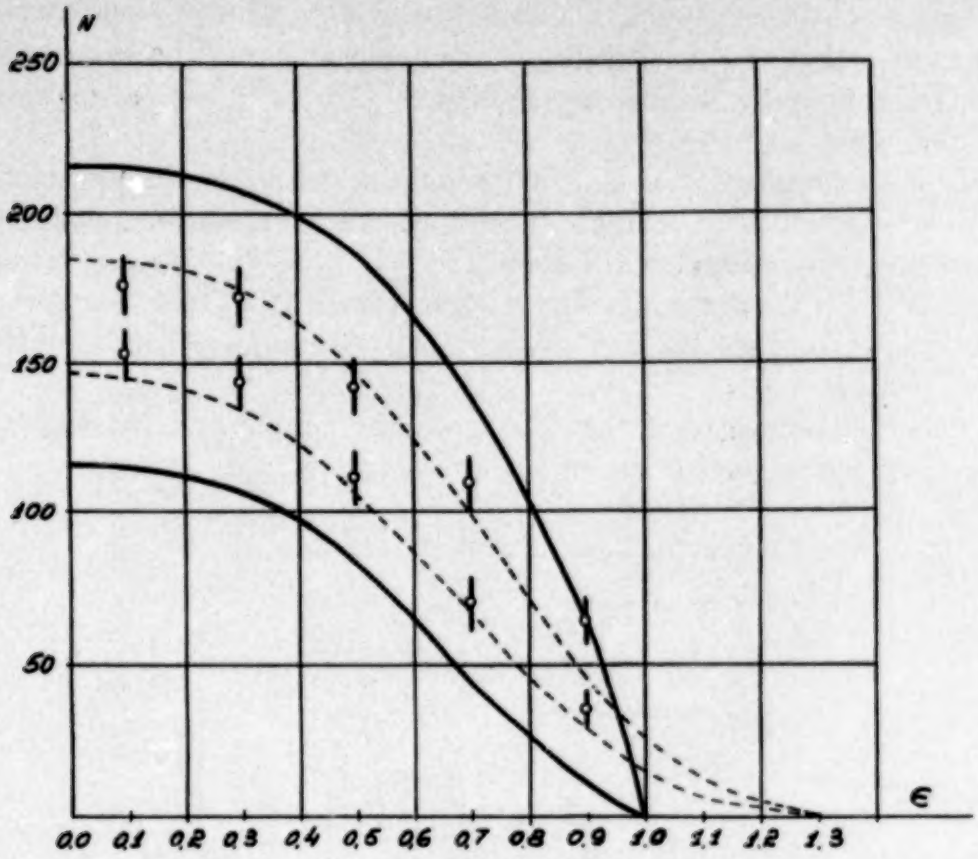
N
250
200
150
100
50
ϵ
0.0 0.1 0.2 0.3 0.4 0.5 0.6 0.7 0.8 0.9 1.0 1.1 1.2 1.3

Fig. 4

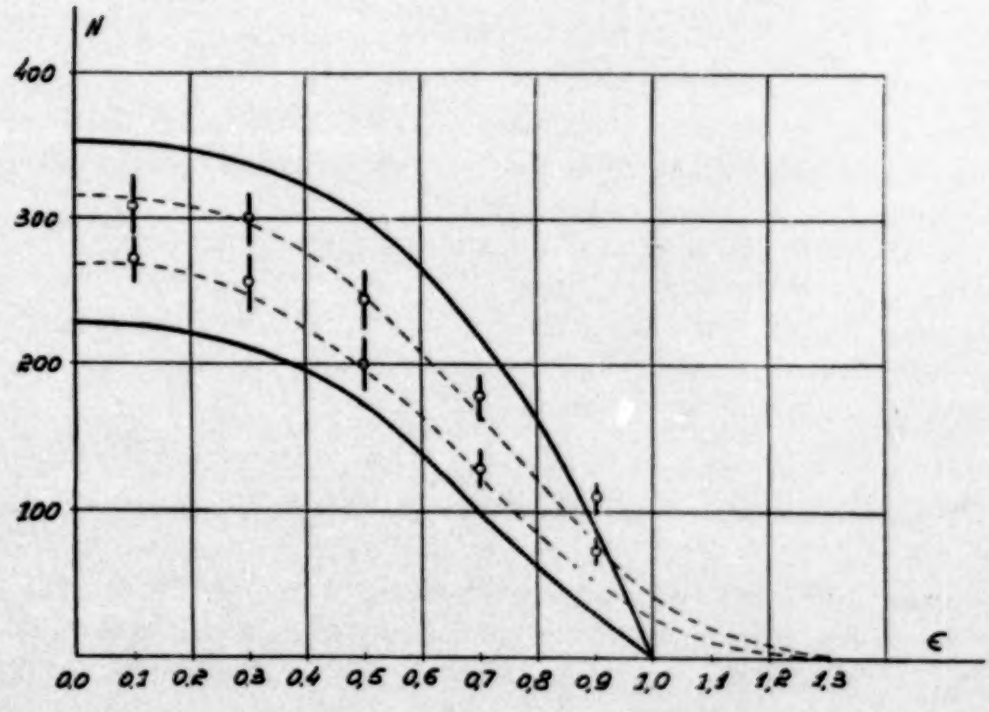
N
400
300
200
100
ϵ
0.0 0.1 0.2 0.3 0.4 0.5 0.6 0.7 0.8 0.9 1.0 1.1 1.2 1.3

Fig. 5

with a spread corresponding to a dispersion of 20 % which is approximately the mean value of the dispersion in our experiments. The experimental points are in quite satisfactory agreement with these curves; exceptions are the points at $\varepsilon = 0.9$.

For a qualitative analysis of our results we computed the mean values of $\overline{\cos\vartheta} = \sum_i \cos\vartheta_i/n$ (n is the number of particles per given energy interval) for each energy interval in the spectra of figs. 1 and 2. For a correlation of the type $1+A\cos\vartheta$ measured in a plane (which is what we have in our case) the theoretical value of $\overline{\cos\vartheta}$ is half the value of the correlation coefficient A.

The experimental values of $\overline{\cos\vartheta}$ obtained for particles possessing an energy exceeding a given value are presented in table 1.

TABLE 1

Energy	$\overline{\cos\vartheta}_{>\varepsilon} = \frac{1}{2}A$
0	$-(0.053\pm0.033)$
0.1	$-(0.053\pm0.033)$
0.2	$-(0.052\pm0.033)$
0.3	$-(0.064\pm0.034)$
0.4	$-(0.060\pm0.035)$
0.5	$-(0.083\pm0.037)$
0.6	$-(0.118\pm0.040)$
0.7	$-(0.148\pm0.045)$
0.8	$-(0.156\pm0.051)$
0.9	$-(0.192\pm0.059)$
1.0	$-(0.200\pm0.074)$
1.1	$-(0.206\pm0.104)$

The statistical errors in the table for $\overline{\cos\vartheta}_{>\varepsilon}$ were computed from the formula $0.79/\sqrt{N}$, where N is the number of particles with an energy exceeding that indicated in the table.

The data in the table exhibit a monotonic increase from $\overline{\cos\vartheta}_{>\varepsilon} \approx 0.05$ up to values about 4 times larger.

In order to compare our data with the two-component neutrino theory the theoretical value of $\overline{\cos\vartheta}_{>\varepsilon}$ for particles with an energy exceeding ε should be computed from formula (1). It equals

$$\overline{\cos\vartheta}_{>\varepsilon} = \frac{\alpha\lambda}{2}\frac{\int_\varepsilon^1 b\,d\varepsilon}{\int_\varepsilon^1 a\,d\varepsilon}.$$

The quantity $\alpha\lambda$ can be determined from our data (figs. 3—5). However, a more precise determination can be made by using emulsion data on the angular correlation averaged over the energy [3-8]). In this case the coefficient A in the correlation formula $1+A\cos\vartheta$ is equal to $\frac{1}{2}\alpha\lambda$. Data which have been available to us are presented in the following table:

Author	Number of particles	A
Chadwick, Durrani *et al.* [3])	3021	$-(0.149 \pm 0.033)$
Bhowlik *et al.* [4])	1562	$-(0.080 \pm 0.044)$
Biswas *et al.* [5])	2003	$-(0.095 \pm 0.039)$
Castagnoli *et al.* [6])	1028	$-(0.222 \pm 0.054)$
Friedman and Telegdi [7])	1300	$-(0.120 \pm 0.048)$
Gurevich *et al.* [8])	2000	$-(0.120 \pm 0.039)$

The statistical errors in the table are computed from the formula $1.73/\sqrt{N}$ where N is the total number of particles.

According to these data the mean weighted value of the coefficient A is $-A = 0.127 \pm 0.017$ which corresponds to $-\alpha\lambda = 0.380 \pm 0.050$. This value for $\alpha\lambda$ was used by us to compare the experimental values of $\overline{\cos\vartheta}_{>\varepsilon}$ taken from table 1 with the theory.

The theoretical values of $(1/\alpha\lambda)\,\overline{\cos\vartheta}_{>\varepsilon}$ are given by curve 1 in fig. 6: they vary from 0.167 for $\varepsilon = 0$ up to 0.500 for $\varepsilon = 1$. A direct comparison

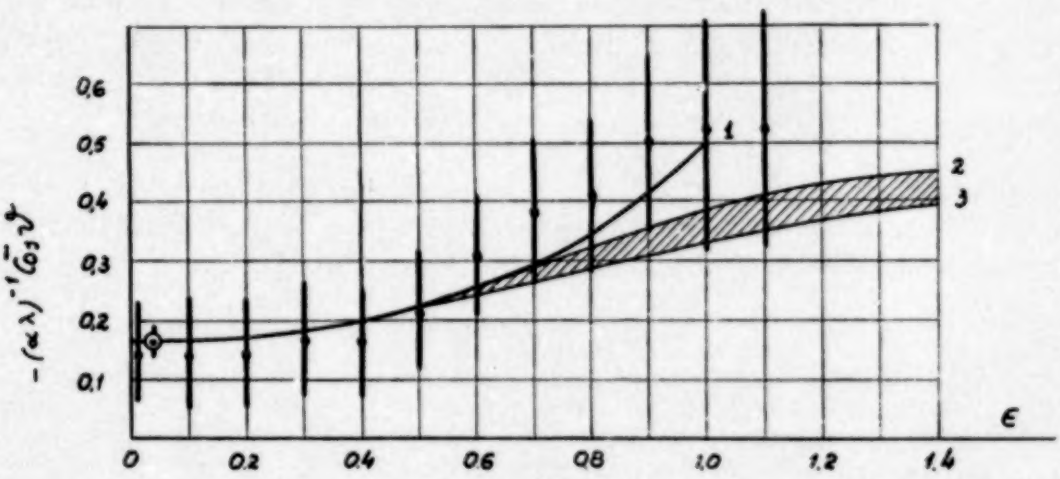

Fig. 6

of the experimental data with this curve is difficult as dispersion in the energy measurements and bremsstrahlung produce a spread in our spectrum (see figs. 1 and 2). Neglecting bremsstrahlung we computed the spread in curve 1 produced by a dispersion of 15 and 30 % in the energy measurements, almost all of our measurements being confined between these dispersion values. The results are represented by curves 2 and 3 which only slightly differ from each other. The experimental data should be compared with just these curves. The experimental points in fig. 3 correspond to the values $\overline{\cos\vartheta}_{>\varepsilon}$ from table 1 divided by $\alpha\lambda = -0.38$. The point enclosed by a circle (plotted at the beginning of the curve) corresponds to the normalized value $\alpha\lambda = -0.380 \pm 0.050$. The experimental data exhibit the sharp rise

with energy of the mean value of $\overline{\cos\theta}$ which is predicted by the two-component neutrino theory. Fig. 6 shows that the observed increase is somewhat larger than the theoretical. However the accuracy of the experiments is not sufficient to consider this point definitely established.

We shall separately consider the data referring to the low energy region. Owing to dispersion in the energy measurements the change of the correlation sign which the theory predicts to be at $\varepsilon = 0.5$ moves towards values of ε lying in the region 0.3—0.4 depending on the magnitude of the dispersion. In the range $\varepsilon < 0.4$ we recorded 34 positons emitted in the forward direction and 32 emitted backward; this result agrees with the strong decrease of the correlation and change of its sign predicted by theory.

A detailed description of the work and a thorough statistical analysis will be published in the near future.

The authors wish to thank A. I. Alikhanov for interest in this work and help and to D. M. Samoilovich in whose laboratory the NIKFI—R emulsions were processed. Most of the difficult scattering measurements and emulsion inspection were performed by E. D. Kalganova, N. V. Rabin, Z. V. Minervina, E. A. Pesotskaya, V. F. Kuzichev, A. G. Avalishvili, V. V. Titova, V. N. Kuznetsova and V. A. Savelyev to whom the authors express their appreciation.

The authors are also thankful to I. L. Ilyina for calculating the spread of the theoretical spectra due to dispersion and to I. S. Bruk for permission to use the LUMS computer to carry out the calculations.

References

1) A. O. Weissenberg and V. A. Smirnitsky, JETP **32** (1957) 1340
2) L. Landau, Nuclear Physics **3** (1957) 127
3) G. B. Chadwick, S. A. Durrani *et al.* (preprint)
4) B. Bhowlik, D. Evans, D. Browse *et al.* (preprint)
5) N. Biswas, M. Ceccarelli and J. Crussard, Nuovo Cimento **5** (1957) 756
6) C. Castagnoli, C. Franzinetti and A. Manfredini, Nuovo Cimento **5** (1957) 684
7) J. Friedman and B. Telegdi, Phys. Rev. **105** (1957) 1687
8) I. I. Gurevich *et al.*, JETP (1957) (in print)

Nuclear Physics **5** (1958) 41—46; © *North-Holland Publishing Co., Amsterdam*
Not to be reproduced by photoprint or microfilm without written permission from the publisher

THE SPECTRUM OF NEUTRONS FROM THE REACTION $p+d \rightarrow p+p+n$

A. T. G. FERGUSON and G. C. MORRISON

Atomic Energy Research Establishment, Harwell, Nr. Didcot, Berks.

Received 12 July 1957

Abstract: The continuous neutron spectrum from the disintegration of deuterium by protons has been measured for proton energies of 3.52, 3.72, and 3.92 MeV. These results are compared with the predictions of the theory of Frank and Gammel.

1. Introduction

The elastic interaction of nucleons with deuterons has been extensively studied, but much less work has been carried out on the disintegration of the deuteron by nucleon bombardment. Barkas and White [1]) have studied the cross section for disintegration by 5.1 MeV protons. Henkel *et al.* [2]) have measured, using a "long-counter" [3]), the neutron yield at 0° from the bombardment of deuterium by protons from 3.4 MeV up to 5.5 MeV. Using 14 MeV neutrons as bombarding particles Seagrave [4]) studied the spectrum of protons from the disintegration of the deuteron at a number of angles relative to the direction of the incident neutrons. The spectra determined by Seagrave were compared with the calculations of Frank and Gammel [5]). A comparison of the experimental and theoretical angular distributions showed a slight but significant disagreement.

This paper reports measurements of the spectrum of neutrons at 0° when deuterium is bombarded with protons of energies 3.52 MeV, 3.72 MeV, and 3.92 MeV. The observed spectra are compared with the predictions of the theory of Frank and Gammel.

2. Experimental Method

The resolved proton beam was provided by the Harwell Electrostatic Generator. The beam was monitored by a standard current integrator.

The deuterium was in the form of zirconium deuteride, 0.29 ± 0.06 ml of deuterium being absorbed in 3.2 mg of zirconium. The zirconium was deposited on a 0.005 inch gold backing soldered to a target can whose wall was 0.010 inch thick. The target can was rotated, and cooled by an air blast.

A "long-counter" was used as a neutron monitor, and showed that the ratio of neutron counts to integrated proton current was constant. The neutron spectrum was determined using a proportional counter containing

Helium-3[6]). The counter was set up so that the direction of the proton beam was the perpendicular bisector of the axis of the counter. The distance from the target to the counter was 15 inches and the angle subtended by the sensitive length of the counter was $\pm 9°$. The counter was surrounded by a 0.015 inch cadmium sheath.

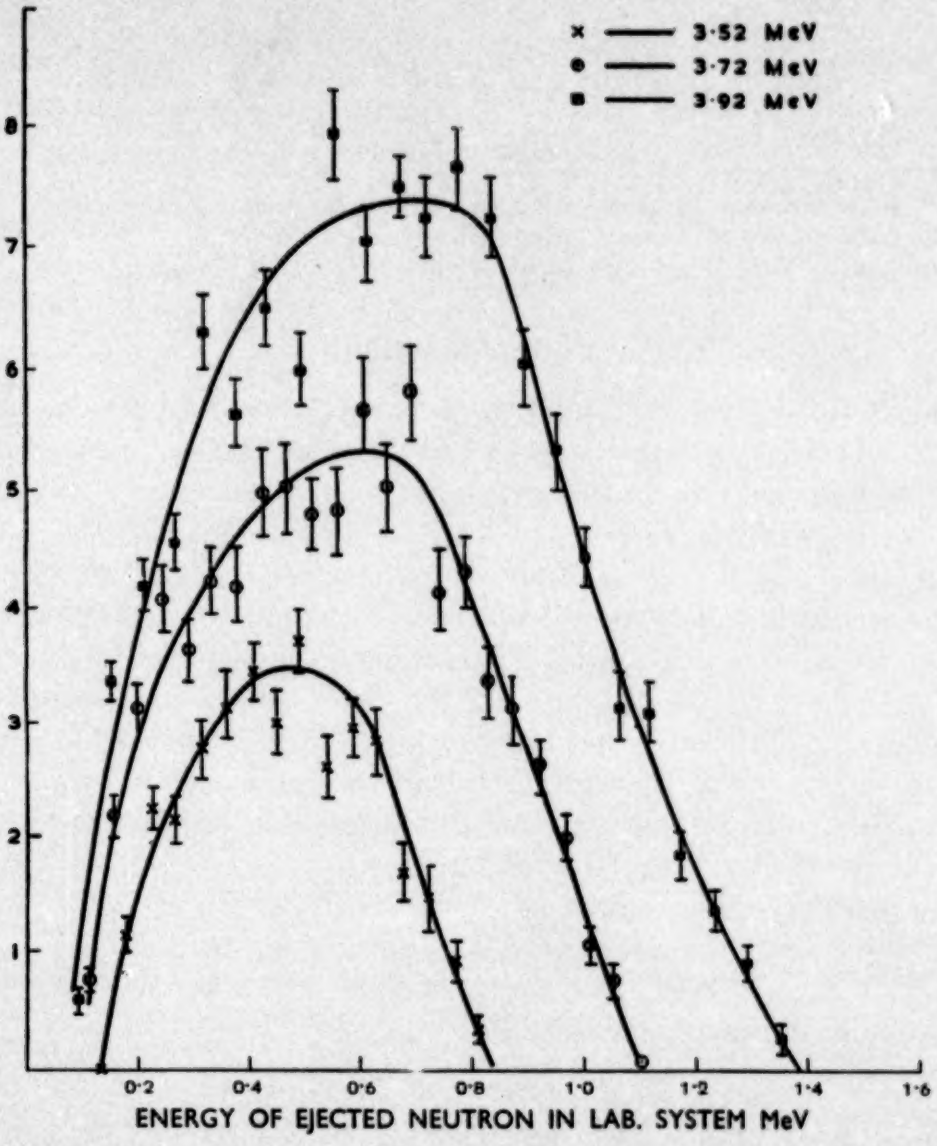

Fig. 1. Spectra of neutrons determined experimentally. The errors shown are relative only. The absolute values of the cross section may have an error of about 25 %. The line is a smooth curve through the points.

All metal surfaces with which the proton beam might come in contact were covered with 0.005 inch tantalum. Nevertheless, there were several sources of unwanted counts. Some neutrons produced in the reaction studied could reach the detector after scattering in the walls of the room; others produced in sources other than the target could reach the detector directly

or after scattering in the walls. These sources of background were determined by replacing the zirconium deuteride by an equivalent layer of zirconium and also by inserting a shadow wedge of paraffin between the targets and the counter. Combining this data, the pulse height spectrum due to neutrons from the disintegration of the deuteron was obtained.

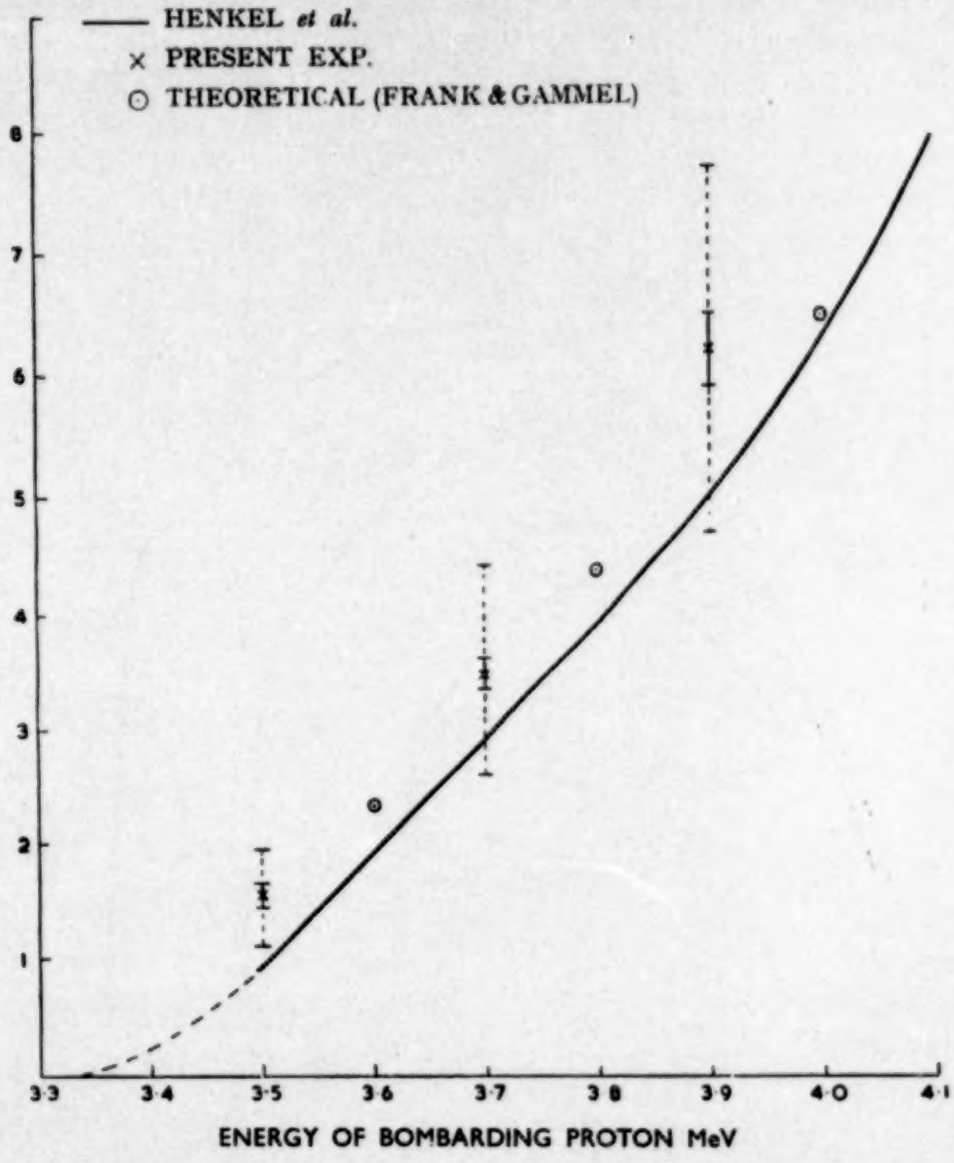

Fig. 2. The variation with proton bombarding energy of the differential cross section at 0° for the disintegration of deuterons by protons. The larger errors are in the absolute values, the smaller in their relative values.

3. Results

The observed pulse height distribution at each incident energy was converted to a neutron spectrum as follows. The low energy end of the distribution was successively corrected for the helium-3 recoils and counter wall effect produced by neutrons of higher energy. The corrections to be applied

were derived from the shape of the distribution obtained when monoergic neutrons were incident on the counter. Additional corrections were made for the variation of the (np) cross section in He^3 and the counter wall effect with energy.

The neutron spectra derived in this way are shown in fig. 1, smooth lines being drawn through the experimental points. The errors indicated are relative errors which are due to counting statistics and uncertainties in the counter wall effect and in the cross section of the He^3 reaction. The absolute

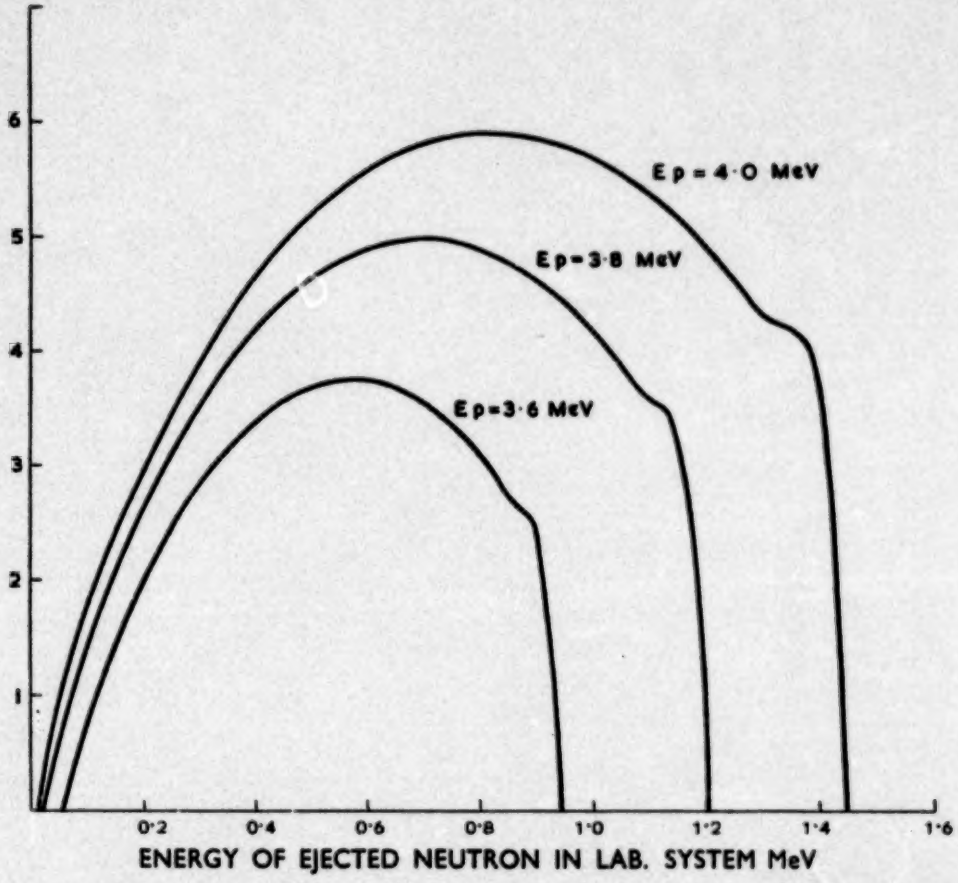

Fig. 3. The energy spectrum of neutrons ejected in the forward direction as calculated on the theory of Frank and Gammel.

values of the cross section may have additional errors due to uncertainty in the quantity of helium-3 in the counter (± 3 %) and the quantity of deuterium. The latter uncertainty may be as high as ± 20 %. The area under the curves of fig. 1 gives the differential cross section at 0° to the proton beam. This is plotted as a function of energy in fig. 2. The results of Henkel *et al.* are also shown. The absolute values are in good agreement within the errors and the variation as a function of energy is similar.

4. Comparison with Theory

The neutron spectra predicted by the theory of Frank and Gammel are shown in fig. 3. The areas under these curves are plotted in fig. 2 and they agree well with the experimental results.

In order to compare the theoretical and observed spectra, the theoretical spectra have been modified to take account of target thickness (about 40 keV)

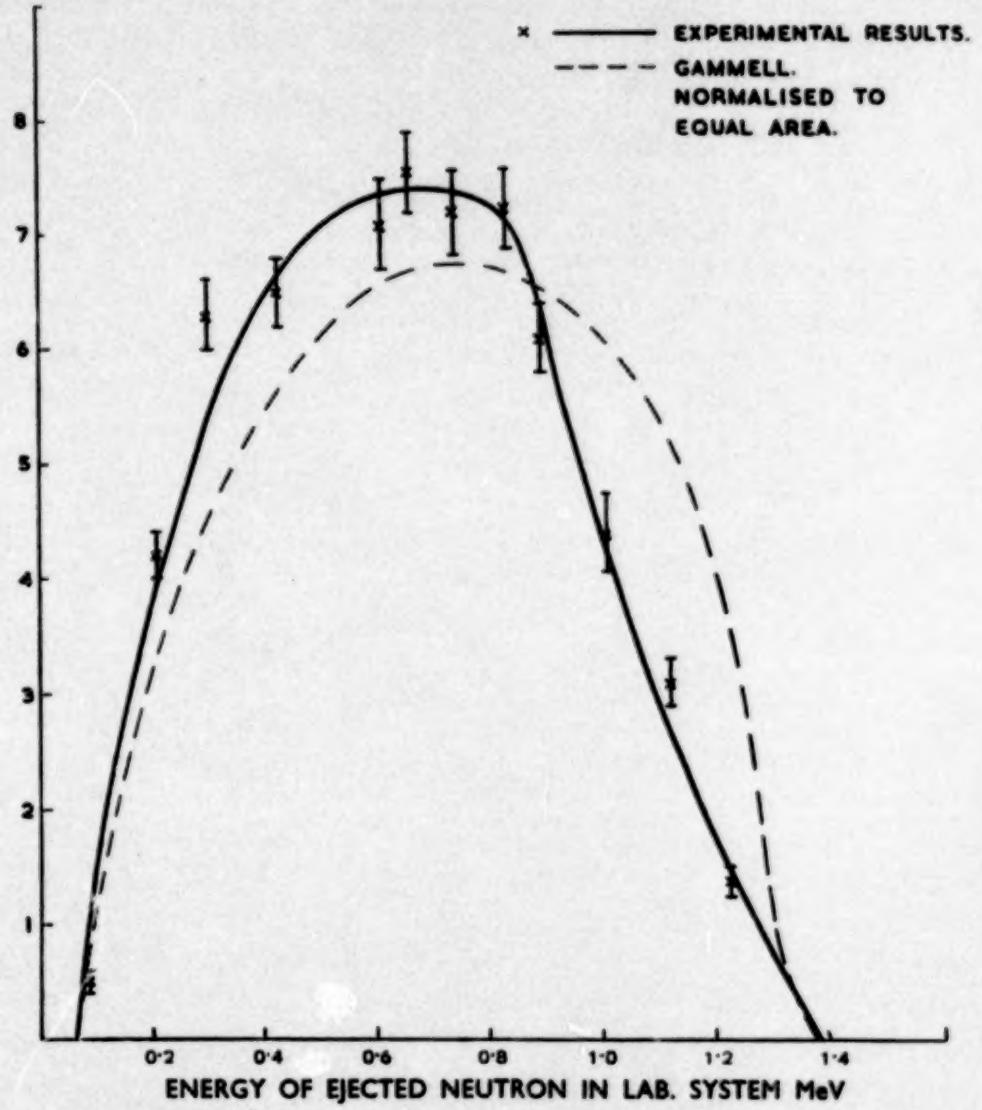

Fig. 4. Comparison of observed spectrum at proton bombarding energy of 3.92 MeV with calculated spectrum, the spectra being normalized to equal area.

and finite angle subtended by the counter (± 9°), by interpolating between the curves of fig. 3. Since the integrals of the experimental and theoretical spectra agreed within the errors, the modified theoretical curve was normalized to the area under the experimental curve. The two curves cor-

responding to an incident proton energy of 3.92 MeV are shown in fig. 4. The experimentally determined neutron spectrum would appear to fall off more rapidly at high energies than the theoretical predictions. A similar effect appears in comparisons at lower energy.

When the extreme simplifying assumptions of the theory are taken into account, the extent of the agreement with our results is surprising.

The writers are indebted to Dr. A. M. Lane, and Dr. T. H. R. Skyrme for discussions and to Dr. J. L. Gammel for having computed theoretical spectra at our bombarding energies. We should also like to thank Dr. W. D. Allen for his encouragement of this work.

References

1) W. H. Barkas and M. G. White, Phys. Rev. **56** (1939) 288
2) R. L. Henkel, J. E. Perry and R. K. Smith, Phys. Rev. **99** (1955) 1050
3) A. O. Hanson and J. L. McKibben, Phys. Rev. **72** (1947) 673
4) J. D. Seagrave, Phys. Rev. **97** (1955) 757
5) R. M. Frank and J. L. Gammel, Phys. Rev. **93** (1954) 463
6) R. Batchelor, R. Aves and T. H. R. Skyrme, Rev. Sci. Instr. **26** (1955) 1037

Nuclear Physics **5** (1958) 47—57; © *North-Holland Publishing Co., Amsterdam*

Not to be reproduced by photoprint or microfilm without written permission from the publisher

THE INTERNAL COMPTON EFFECT

A DETERMINATION OF CROSS SECTION AND ANGULAR CORRELATION

TORSTEN LINDQVIST, BO-GÖRAN PETTERSSON AND KAI SIEGBAHN
Institute of Physics, Uppsala

Received 10 July 1957

Abstract: The internal Compton effect, a nuclear transition in which there is a simultaneous ejection of a bound electron and emission of a gamma ray, has been unambiguously demonstrated. The experiment concerned the 662 keV transition in Ba^{137m} and was carried out with a gamma scintillation spectrometer and a beta-ray spectrometer in coincidence. The presence of other effects was carefully considered. The experimental cross section was found to be 1.86×10^{-5} photons in the energy region 97 keV—120 keV per conversion electron at 90° between the electron and photon directions. Angular correlation experiments were carried out. Comparison with various theories shows that the theory by Spruch and Goertzel does fit the experimental results excellently both regarding absolute cross section and angular correlation.

1. Introduction

It is well known that there exist some fundamental effects where energy is transferred from a photon or an excited nucleus to an electron. One usually discriminates between internal and external effects, respectively. Thus, internal and external photo- and pair-effects are easily observable. So far the internal counterpart of the classical Compton effect has not been unambiguously demonstrated. Brown and Stump [1]) looked for the internal Compton effect but neither their cross section nor the general shape of the angular correlation agreed with theory. Their experiment cannot therefore be considered as a full verification of the effect.

The internal Compton effect (ICE) is a nuclear transition in which there is a simultaneous ejection of a bound electron and emission of a gamma ray. The process can be looked upon as an electron and a nucleus exchanging a virtual photon and the electron emitting a real gamma ray. In all three effects, the photo-, pair- and Compton effects, the essential distinction between the internal and the external process is in the presence of a virtual rather than a real photon.

The ICE is quite small. Among competing processes the emission of a gamma ray is of course the most probable. The probability of internal conversion, which has been referred to as internal photoeffect, is also much larger. Thus the ICE has the character of a third order process, which explains why the effect is so difficult to prove experimentally.

Though the cross section is very small indeed the angular correlation is a rather strong function of the multipole order and it might therefore be useful in some cases for assigning multipole orders.

2. General Experimental Procedure

Let us consider a decay process, in which a beta group is followed by a converted gamma ray. The beta spectrum (fig. 1a) then consists of a continuous group and a line. The scattered electrons from the ICE are distributed as a long low-energy tail to the line. The intensity of this effect

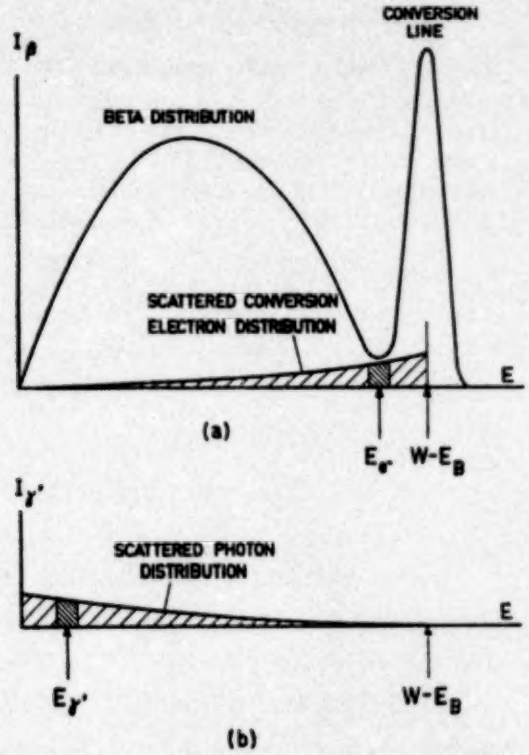

Fig. 1. Principal sketch of the internal Compton effect. a. Beta spectrum of a beta group followed by a converted gamma ray. The scattered conversion electrons from the ICE are distributed as a long low-energy tail to the conversion line. b. Gamma spectrum of the corresponding scattered photons.

is of course greatly exaggerated in the figure. The corresponding photons give rise to a "mirror" distribution (fig. 1b). The sum of the energy of a scattered electron, E_{e^-}, and the energy of the corresponding photon, $E_{\gamma'}$, is constant:

$$E_{e^-}+E_{\gamma'}=W-E_B, \tag{1}$$

where W is the total energy given up by the nucleus in this transition and E_B is the binding energy of the electron.

The experimental procedure would then be to measure coincidences between the scattered electron and the corresponding photon. In order to discriminate against other effects present one can choose a certain electron

energy E_{e^-} and keep this channel fixed. The other channel should then scan over the actual energy region in order to find the effect. At the energy $E_{\gamma'}$, determined by eq. (1), a coincidence "line" should show up. The choice of E_{e^-} is subject to two main restrictions. The upper limit of E_{e^-} is

$$E_{e^-} = W - E_B - E_x \tag{2}$$

where E_x is the energy of the corresponding x-ray. At this limit one gets coincidences between x-rays and conversion electrons. The lower limit of E_{e^-} is

$$E_{e^-} = 2W^2[mc^2 + 2W]^{-1} \tag{3}$$

where mc^2 is the electron rest mass. Eq. (3) comes from the fact that the external Compton effect appears at this energy. As a matter of fact, this is one of the main differences between internal and external Compton effects. In the ICE the nucleus itself can take care of momentum, and thus give electrons any energy up to the maximum energy $W - E_B$. In the external Compton effect, however, the momentum is shared between the scattered photon and the electron and the maximum electron energy is given by eq. (3).

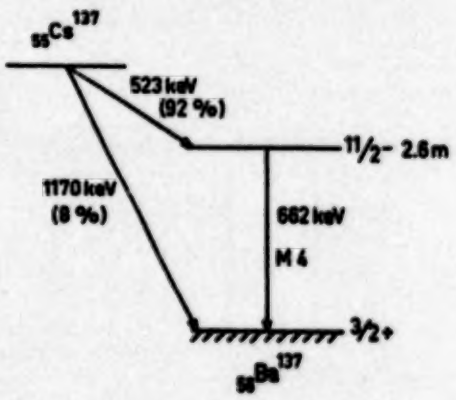

Fig. 2. Decay scheme of Cs^{137}.

It was decided to look for the ICE in the case of Ba^{137m}, which isomeric state is reached by beta decay from Cs^{137} (fig. 2). This case has many advantages. The decay of Cs^{137} ($T_{\frac{1}{2}} = 33$y) is well known. There is only one gamma transition and it is highly converted. The presence of beta groups however, makes some corrections necessary.

3. Apparatus

A newly designed beta-gamma coincidence spectrometer (fig. 3) was used for the measurements. The beta spectrometer was of long lens type with a scintillation detector. The anthracene crystal was 1/16 in. thick. The transmission of the beta-spectrometer was 3 %, and the momentum resolution was chosen to be 6 % in order to detect a large part of the scattered electron distribution. The gamma detector was a scintillation spectrometer

with a NaI(Tl) crystal, 1 in. diam. and 1/4 in. thick. After each detector followed linear amplifiers and differential discriminators. The coincidence circuit was of fast-slow type [2]) with a resolving time of $2\tau = 50$ mμs.

The gamma detector could be moved around the source in order to measure the angular correlation (fig. 3). Because of the lens geometry the angular region was limited to 90°—270°. The source was located in the centre of a thin aluminium cup, which made the absorption from source to gamma detector isotropic in the actual angle region.

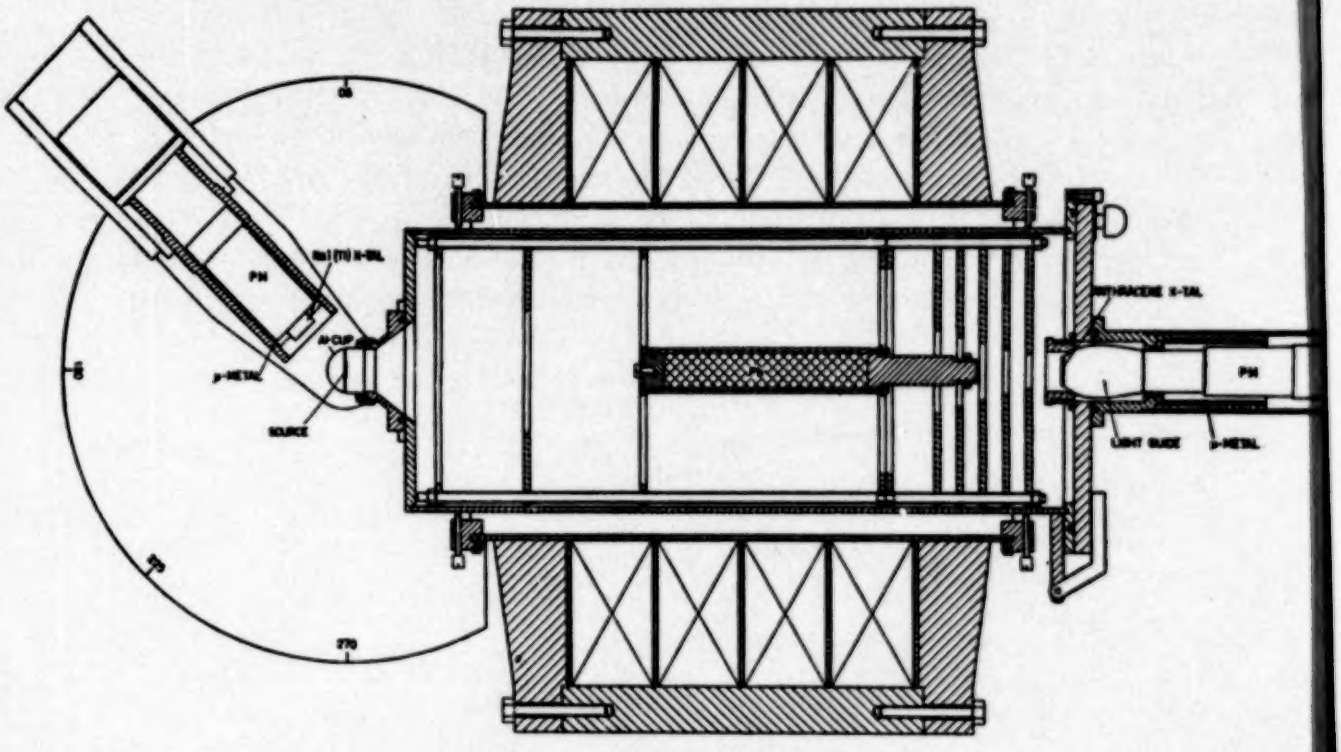

Fig. 3. Beta-gamma coincidence spectrometer.

4. Experiment

The source was prepared by evaporating the active caesium solution onto a thin aluminum backing. The source thickness was estimated to be 27 μg/cm^2. The caesium activity was about two years old, which was of some importance because of the presence of Cs^{134} ($T_{\frac{1}{2}} = 2.3$y). A fresh caesium activity † contains less than 4 % Cs^{134}. The total source strength was 18 μC.

The total energy given up by the nucleus in the isomeric transition, an M4 transition, in Ba^{137} is $W = 661.6$ keV. The binding energy of the K-electron is 37.4 keV and the energy of the K-conversion line is 624 keV. Eqs. (2) and and (3) imply that

† The caesium activity was obtained from the Radiochemical Centre, Amersham, Bucks., England.

$$(E_{e^-})_{max} = 600 \text{ keV} \qquad (E_{e^-})_{min} = 475 \text{ keV}.$$

The finite resolutions of both detectors must of course be considered for these maximum and minimum values. The choice of the energy E_{e^-} is governed by two other facts. Since the scattered electron intensity increases towards the full conversion energy (fig. 1a) it is desirable to have E_{e^-} as close as possible to the maximum value. In order to get a favorable ratio between true and accidental coincidences it is desirable to have a low single channel counting rate.

After all these considerations E_{e^-} was chosen to be 516 keV. According to eq. (1) the corresponding scattered photon energy was 108 keV. The momentum resolution of the beta spectrometer was set to be 6 %, which means that electrons in the energy band 501—531 keV were accepted.

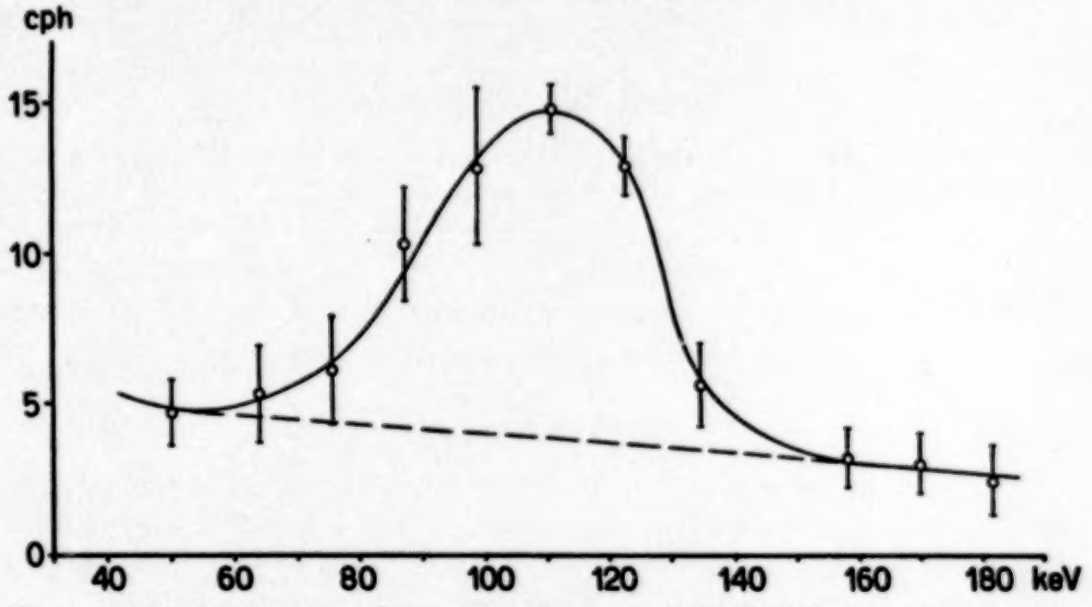

Fig. 4. Coincidence spectrum of the scattered photons in Ba^{137}. Beta-channel fixed at 516 keV. The peak at 110 keV corresponds to internal Compton scattered photons (108 keV).

Accordingly, the corresponding photon energy band was 93—123 keV. The channel width of the differential discriminator of the gamma detector was 23 keV, which means that the gamma channel did not accept all photons belonging to the electron energy band. The gamma detector was calibrated with Ba^{137} x-ray (32 keV), Pb^{207} x-ray (70 keV) and Co^{57} (123 keV).

5. Cross Section Determination

The first part of the experiments was a determination of the ICE cross section at 90° between electron and photon directions. The beta channel was fixed at 516 keV and the gamma channel was moved over the energy region 50 keV—180 keV. After a very tedious run, a spectrum, consisting of a background and an ICE "line", was obtained (fig. 4). The points are corrected for accidental coincidences .The peak of the line agrees very well

with the expected value, 108 keV. The background is due to various other effects, which will be discussed in detail below. However, with the experimental method used, it is possible to extrapolate the background to the energy of interest with high accuracy. The accuracy thus obtained is far higher than if the background should be estimated [1]).

The total coincidence rate on the peak at 108 keV is

$$C_{\mathrm{TOT}} = 14.8 \pm 0.8 \text{ cph.}$$

The background, extrapolated to the same energy is

$$C_{\mathrm{BG}} = 3.8 \pm 0.8 \text{ cph.}$$

The remaining coincidence rate, due to the ICE at 90° between electron and photon directions, is then

$$C_{\mathrm{ICE}} = 11.0 \pm 1.2 \text{ cph.}$$

6. Angular Correlation

The second part of the experiments was to investigate the angular correlation between the electron and the photon. The beta channel was kept on the same value as before and the gamma channel on the peak at 108 keV. The coincidence rates at the angles 90°, 120°, 150°, 180°, 210°, 240°, and 270° were recorded. The results, after correcting for accidental coincidences and absorption in the aluminum cup, are shown in fig. 5.

7. Background

Before going into the analysis of the results obtained, it is necessary to consider the origin of the background and its possible angular correlation. The various effects which have a theoretical chance to contribute to the background, are the following:

(a) Internal bremsstrahlung (IB). The high energy beta group of Cs^{137} (fig. 2) gives rise to a continuous gamma spectrum, i.e. internal bremsstrahlung. The probability S for the emission of a gamma-quantum with energy q can be expressed as [3])

$$S(q) = \int_{1+q}^{W_{\max}} \mathrm{d}W_e \, P(W_e) \phi(W_e, q) \qquad (4)$$

where $P(W_e)$ is the distribution of the beta spectrum. The function $\phi(W_e, q)$ is the probability of an electron coming from the nucleus with energy W_e emitting a quantum of energy q. The upper limit of the integrand, $W_{\max}$, is the maximum energy of the beta spectrum. In our experiments, the integration limits of eq. (4) are determined by the energy band accepted by the beta spectrometer because of the coincidence arrangement. Therefore the effect of inner bremsstrahlung is considerably decreased. The Cs^{137} 1.2 MeV beta-spectrum determined

by Langer and Moffat [4]) was used for the calculation of $S(q)$. The function $\phi(W_e, q)$ is given in ref. [3]). Considering also the angular correlation of the IB the following coincidence rates were obtained:

$$C_{IB}\ (90°) = 1.3 \pm 0.5 \text{ cph},$$
$$C_{IB}\ (180°) = 0.$$

(b) External bremsstrahlung (EB). The source thickness was 27 $\mu g/cm^2$. It is therefore very unlikely that the EB should appear. In order to check this point the source was covered with a thin foil. The coincidence rate did not increase.

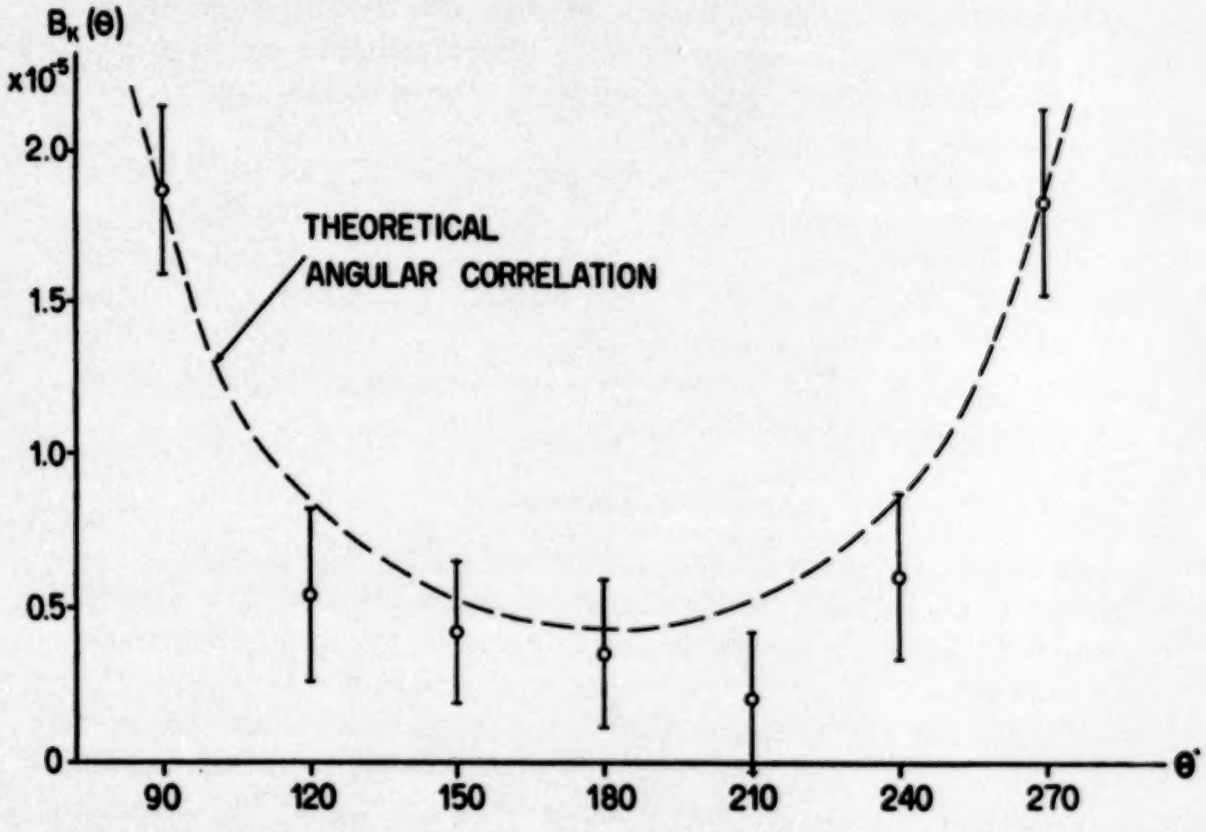

Fig. 5. Angular correlation of the internal Compton effect in Ba^{137}. $E_\gamma = 108$ keV. $E_{e-} = 516$ keV. Dashed line is theoretical distribution (ref. [5])).

(c) External Compton effect. It has already been pointed out that this effect is excluded by the choice of E_{e-}.

(d) Conversion-electron-x-ray coincidences. Also in this case the choice of E_{e-} excludes the effect.

(e) Beta-gamma coincidences from Cs^{134}. With less than 2 % Cs^{134} in the source it was estimated that the coincidence rate due to Cs^{134} was less than 0.02 cph, which is negligible.

(f) ICE from L-conversion. This effect should give coincidences when the gamma channel accepts

$$E_\gamma = W - E_L - E_{e^-} = 140 \text{ keV}.$$

Because of the resolution of the gamma detector it might appear also at 108 keV. The ICE from L-conversion has not so far been treated in detail but it is estimated to be small [5]).

The estimate of the background does not agree with the experimental result. This can be due to approximations in the internal bremsstrahlung theory or other causes. It is therefore obvious that it is necessary to determine the background experimentally.

8. Corrections

(a) Accidental coincidences have been subtracted in all the given coincidence rates. The numbers of accidental coincidences have been measured for each point by inserting a delay of 90 mμs in the gamma channel.

(b) The background without source was measured during 12 h and no coincidence appeared.

(c) The absorption in the aluminum cup around the source was calculated. The result of the angular correlation experiment (fig. 5) has been corrected for this absorption. The NaI(Tl) crystal was covered with a 1 mil Al-foil. The absorption in this foil is negligible for the gamma energy considered.

9. Theory

The probability of an internal Compton transition was considered previously by Cooper and Morrison [6]) who refer to the process as internal scattering. The calculation was limited to high-energy electric dipole transitions and is not valid over the entire range of permissible electron energies. Angular correlation between the electron and the photon was not considered.

A similar process, inner bremsstrahlung, i.e. photon production accompanying charged particle transformation has been studied in connection with nuclear beta-decay by Chang and Falkoff [7]). They found full agreement between the quantum mechanical calculations and the semi-classical theory, assuming small photon energies. The theory of Chang and Falkoff was applied in the experiment by Brown and Stump [1]).

A very general theory, giving both absolute and relative probabilities of the ICE, has been worked out recently by Spruch and Goertzel [5]). The Born approximation was used and hence the calculation was expected to be valid only if the nuclear charge Z is small, and the nuclear energy level separation large. According to the theory by Spruch and Goertzel the relative probability of the internal Compton effect, $B_K(L, q_1 q_2, \theta)$, also defined as the differential magnetic K-shell internal Compton coefficient per unit

solid angle for a multipole of order L, is the ratio of the absolute internal Compton transition rate to the absolute internal conversion rate:

$$B_K(L, q_1 q_2, \theta) = \frac{e^2 m^2}{\pi^2 W^{L-\frac{1}{2}}(W+2m)^{L+\frac{1}{2}}} \int_{q_1}^{q_2} dq \frac{P}{q} Q^{2L} H \cdot F, \qquad (5)$$

where

$$H = (E')^{-2}\,[WP^2(1-\mu^2)+q^2E'] - (mE')^{-1}[qP^2(1-\mu^2)(mq+P^2+Pq\mu)Q^{-2}] + (q/m^2)[qE'-P^2q^2(1-\mu^2)Q^{-2}];$$

$E = W+m-q$,
$F = [(Q^2-W^2)^2+(2mW\alpha Z)^2]^{-1}$;
W = energy given up by the nucleus,
E = energy of scattered electron,
P = momentum of scattered electron,
q = energy and momentum of scattered photon ($c = 1$),
θ = angle between electron and photon directions,
$\mu = \cos\theta$,
$E' = E-P\mu$,
α = fine structure constant,
Z = nuclear charge,
$Q = P+q$,
$e^2 = \alpha$ [8]),
L = order of multipole of the nuclear transition,
$m = 1$,
q_1 and q_2 = lower and upper limit of scattered photon energy.

At small photon energies, i.e. $q \to 0$ it was found that

$$B_K(L, q_1 q_2, \theta) \to \frac{e^2}{4\pi^2} \int_{q_1}^{q_2} \frac{\beta^2(1-\mu^2)}{(1-\beta\mu)^2} \cdot \frac{dq}{q}, \qquad (6)$$

where $\beta = P/E$.

This is the same result as Chang and Falkoff derived for the case of the inner bremsstrahlung associated with beta decay, where it was shown to arise from the instantaneous acceleration of the electron.

Another recent theoretical investigation on the ICE has been carried out by Iakobson [9]). This theory was restricted to non-relativistic energies. The angular correlation between electron and photon was not treated. The following analytic expression for the differential ICE coefficient per unit solid angle was obtained:

$$B_K(q_1 q_2) = \frac{\alpha}{3\pi^2} W \int_{q_1}^{q_2} \frac{dq}{q}. \qquad (7)$$

It was found that in the overlap region between the theories by Spruch-Goertzel and Iakobson the two results were identical.

It should be pointed out that only in the theory by Spruch-Goertzel is

there dependence on the multipole order L and nuclear charge Z. Further, eq. (5) includes only magnetic transitions, whereas eqs. (6) and (7) are identical for magnetic and electric transitions.

10. Comparison between Experiment and Theory

In order to compare the experimental results with theory the relative probability coefficients $B_K(L, q_1q_2, \theta)$ have to be calculated from the coincidence rates

$$C_{ICE}(\theta) = N_0\delta(\beta_1)\cdot\alpha_K\cdot\omega_\beta\cdot\varepsilon_\beta\cdot\omega_\gamma\cdot\varepsilon_\gamma\cdot\varepsilon_c\cdot B_K(L, q_1q_2, \theta)\cdot 4\pi, \quad (8)$$

where

$C_{ICE}(\theta)$ = coincidence rate due to ICE,
N_0 = disintegrations per unit time,
$\delta(\beta_1)$ = branching ratio for the low energy beta group,
α_K = internal conversion coefficient,
ω_β = solid angle of beta-spectrometer,
ε_β = efficiency of beta-detector,
ω_γ = solid angle of gamma-detector,
ε_γ = efficiency of gamma-detector,
ε_c = efficiency of coincidence circuit.

After correction for absorption the following result was obtained:

$$C_{ICE}(90°) = 11.9\pm1.2 \text{ cph.}$$

The gamma channel width was 23 keV. From eq. (8) one thus obtains

$$\text{(Exp.) } B_K(\text{M4, 97—120 keV, 90°}) = (1.86\pm0.27)\cdot10^{-5}.$$

The corresponding theoretical value according to Spruch and Goertzel, eq. (5), is

$$\text{(Theor.) } B_K(\text{M4, 97—120 keV, 90°}) = (1.88\pm0.18)\cdot10^{-5}.$$

The error in the theoretical value comes from the uncertainty of the gamma channel width.

The theoretical angular correlation, B_K(M4, 97—120 keV, θ) is drawn in fig. 5.

In Table 1 are given the different theoretical values together with the

TABLE 1
Comparison between experiment and theory

Z	$B_K(q_1q_2, 90°)$ Chang-Falkoff	$B_K(q_1q_2)$ Iakobson	B_K(M4, q_1q_2, 90°) Spruch-Goertzel	B_K(M4, q_1q_2, 90°) Exp.
0	$3.04\cdot10^{-5}$	$5.25\cdot10^{-5}$	$2.22\cdot10^{-5}$	
20			$2.17\cdot10^{-5}$	
56			$1.88\cdot10^{-5}$	$1.86\cdot10^{-5}$
$q_1 = 0.190$ $q_2 = 0.235$				

experimental value of the cross section. In the case of Spruch-Goertzel theory different Z-values have been treated in order to show the atomic number dependence.

11. Conclusion

The agreement between our experiments and the Spruch-Goertzel theory is excellent, both regarding the cross section and the angular correlation. It should be pointed out that in comparing the experimental points with the theoretical curve for the angular correlation we have not normalized the theoretical curve to fit our experimental points. The fact that the experimental values follow the theoretical curve very closely over the entire interval of angles investigated, indicates that theory is able to give a good account for the ICE, even in spite of the fairly high Z value [10]).

The authors are indebted to Professor Konrad Bleuler, Switzerland, for interesting theoretical discussions. We are also thankful to Dr. T. R. Gerholm for the construction of the beta-spectrometer. Support from the Swedish Atomic Committee and the U.S. Air Force Research and Development Command is acknowledged.

References

1) H. B. Brown and R. Stump, Phys. Rev. **90** (1953) 1061
2) B. Johansson, Nuclear Instruments **1** (1957) (in press)
3) C. S. Wu, in Beta and Gamma Ray Spectroscopy, Editor Kai Siegbahn (North-Holland Publishing Company, Amsterdam, 1955) Ch. XX, p. 652
4) L. M. Langer and R. J. D. Moffat, Phys. Rev. **82** (1951) 635
5) L. Spruch and G. Goertzel, Phys. Rev. **94** (1954) 1671
6) E. P. Cooper and P. Morrison, Phys. Rev. **57** (1940) 862
7) C. S. W. Chang and D. L. Falkoff, Phys. Rev. **76** (1949) 365
8) Baranger, Bethe and Feynman, Phys. Rev. **92** (1953) 482
9) A. M. Iakobson, Soviet Physics (JETP) **2** (1956) 751
10) L. Spruch and G. Goertzel, Phys. Rev. **93** (1954) 642

Nuclear Physics **5** (1958) 58—88; © *North-Holland Publishing Co., Amsterdam*
Not to be reproduced by photoprint or microfilm without written permission from the publisher

ANGULAR DISTRIBUTION AND LINEAR POLARIZATION OF THE GAMMA RAYS FROM ORIENTED ^{56}Co NUCLEI

A. N. DIDDENS

Natuurkundig Laboratorium, Rijksuniversiteit, Groningen

W. J. HUISKAMP, J. C. SEVERIENS†, A. R. MIEDEMA and M. J. STEENLAND

Kamerlingh Onnes Laboratorium, Leiden

Communication No. 308c from the Kamerlingh Onnes Laboratorium, Leiden, Nederland

Received 19 June 1957

Abstract: Measurements are reported on the beta-gamma and gamma-gamma coincident radiation observed in the decay of ^{56}Co and on the angular distribution and linear polarization of the gamma rays emitted by oriented ^{56}Co nuclei. Discrepancies between various proposed decay schemes have been removed by means of coincidence measurements (performed at room temperature). Experiments with oriented nuclei (using low temperature techniques) gave information about the multipole order of the gamma rays, the mixing ratio of two multipoles and the electric or magnetic character of the transitions. As a result, evidence is presented for a decay scheme of ^{56}Co and for spin and parity assignments to the excited levels in ^{56}Fe (see fig. 10). A possible theoretical interpretation of some of these levels is discussed. A review is given of the data available from other experiments.

1. Introduction

The nucleus ^{56}Fe is an interesting one to study because both its neutron and proton numbers lie close to the magic number 28. Therefore, a change from the rotational aspect of the low lying levels to one of core vibrations can be expected. Hence it is important that a thorough identification be made of the various energy levels and the gamma ray transitions amongst them.

The present studies were therefore undertaken employing beta-gamma and gamma-gamma coincidence techniques and low temperature orientation methods. ^{56}Fe is particularly easy to study by means of nuclear orientation because it can be produced through the positon and electron capture decay of ^{56}Co. The cobalt nuclei, occurring in paramagnetic ions, can be oriented by the magnetic hyperfine structure polarization method in cerium magnesium nitrate crystals.

The radiations in the decay of ^{56}Co (77 days) have been the subject of several investigations since the early work of Elliott and Deutsch [1]). Sakai *et al.* [2,3]) constructed a decay scheme based on coincidence studies and

† Present address: Universitetets Institut for Teoretisk Fysik, Copenhagen.

deduced the spins of the excited states in ^{56}Fe from angular correlation measurements. Also in an earlier contribution by our group [4, 5]), based on the information obtained from measurements of the angular distribution of the gamma rays emitted by oriented ^{56}Co nuclei, spins were assigned to the excited levels.

Several other experiments have been reported since. A short account of these is given in section 3. The work of Jones *et al.* [6]) and Baker *et al.* [7]) on the paramagnetic resonance hyperfine structure showed the spin of ^{56}Co to be $I_0 = 4$. This result provides thus a convenient starting point for the analysis of the levels in ^{56}Fe. Howard *et al.* [9]) found some additional beta and gamma transitions which led to a revised decay scheme, differing from the earlier one. The revised scheme can be found in "Nuclear Level Schemes" [9]).

New gamma-gamma and beta-gamma coincidence experiments are described in section 4, all measured with scintillation counters except for one case where a beta spectrometer was used. These new measurements agree with the old decay scheme of Sakai *et al.* (extended to include some weak gamma transitions and shown in fig. 10) and are in disagreement with the one proposed in "Nuclear Level Schemes". In section 4 also a comparison is made with the data available from the (p, p′) and (n, n′) reactions on ^{56}Fe.

The following two sections (5 and 6) deal with measurements made with oriented nuclei. The results obtained from the gamma ray angular distribution measurements are found in section 5, while section 6 gives the result of the linear polarization measurements made on five of the gamma rays. The polarimeter used is briefly described.

The conclusions that can be drawn from these data with regard to the spins and parities of the excited levels are presented in section 7 and the final result is shown in fig. 10. The simultaneous use of the data from angular correlation measurements [3]) and those reported here from oriented nuclei proved to be very helpful.

A possible vibrational character of some of the levels in ^{56}Fe is discussed in section 8.

2. Instrumentation

2.1. SOURCE AND CRYOGENICS

The ^{56}Co sources were prepared in the cyclotron of the I.K.O. at Amsterdam through the (d, 2n) reaction on natural (91 % ^{56}Fe) iron. These sources also contained some ^{57}Co; however, this isotope decays by electron capture and gamma radiations of about 100 keV and therefore did not interfere with any of the present measurements dealing with higher energy radiations. A total amount of about 75 μC of ^{56}Co was used for all the

experiments with oriented nuclei. This activity was grown into several single crystals of $2Ce(NO_3)_3 \cdot 3Mg(NO_3)_2 \cdot 24H_2O$ having a total weight of about 20 g, the Co^{++}-ions replacing some of the Mg^{++}-ions. These crystals were mounted with their axes parallel [11, 31]).

At 1°K a demagnetizing field of 22 kOe was applied in the direction of the large g-value, which produced a temperature of about 0.003 °K after demagnetization to zero field. The cryostat containing the crystals was thereafter removed from the demagnetizing magnet and the detection apparatus raised around it by means of a hydraulic lift. A magnetic field of 300 Oe for polarizing the nuclei was then applied in the direction of the small g-value (c-axis). This polarizing magnetic field was produced by a Helmholtz coil in the case of angular distribution measurements, whilst for the gamma ray linear polarization measurements space requirements necessitated the use of a slightly less homogeneous field generated by a small iron electro magnet. The polarizing magnetic field caused the initial temperature to increase to about 0.005 °K. There upon it took 30 minutes before the temperature had risen to the region of 0.01 °K where the orientation effects become small and at which point the measurements were stopped. All measurements were thereafter normalized at 1 °K. The susceptibility measurements were performed in the usual way. The quoted magnetic temperatures T^* have been corrected neither for the demagnetizing factor nor for the influence of the polarizing field on the susceptibility because these do not affect the type of experiments reported here [29]).

2.2. DETECTION APPARATUS

The gamma rays were detected in NaI(Tl) crystals, $1\frac{3}{4}''$ diameter and $2''$ long, mounted on E.M.I. 6260 photomultipliers, carefully shielded to make the influences of magnetic fields negligible. Where angular distribution measurements were made, the gamma rays were detected in the direction parallel ($\vartheta = 0°$) and perpendicular ($\vartheta = 90°$) to the applied polarizing field.

The counters used in the $\gamma-\gamma$ coincidence measurements were also NaI(Tl) scintillation crystals, of the same dimensions. A coincidence resolving time $2\tau = 2\times10^{-8}$ s was used, giving a 100 % coincidence detection efficiency for gamma rays of energy of 0.5 MeV and higher. The fast-slow coincidence technique was employed.

A block diagram of the electronics of the polarimeter used for the measurement of the gamma ray linear polarization (described in section 6) is given in fig. 1. Again use is made of the fast-slow coincidence technique. The gamma radiation, emitted in the direction $\vartheta = 90°$ falls on the central scintillator, which is a plastic in the shape of a $2''\times2''$ cylinder, and is Compton scattered over about 75° into NaI(Tl) crystals. Fast coincidences are required between the central scatterer and one of the two NaI(Tl) crystals. The fast coincidence

circuit was of the shorted stub type of Bell, Graham and Petch [12]) and the coincidence resolving time was chosen at $2\tau = 2\times10^{-8}$ s. The slow triple coincidence circuit had a resolving time of $2\tau = 0.4\times10^{-6}$ s.

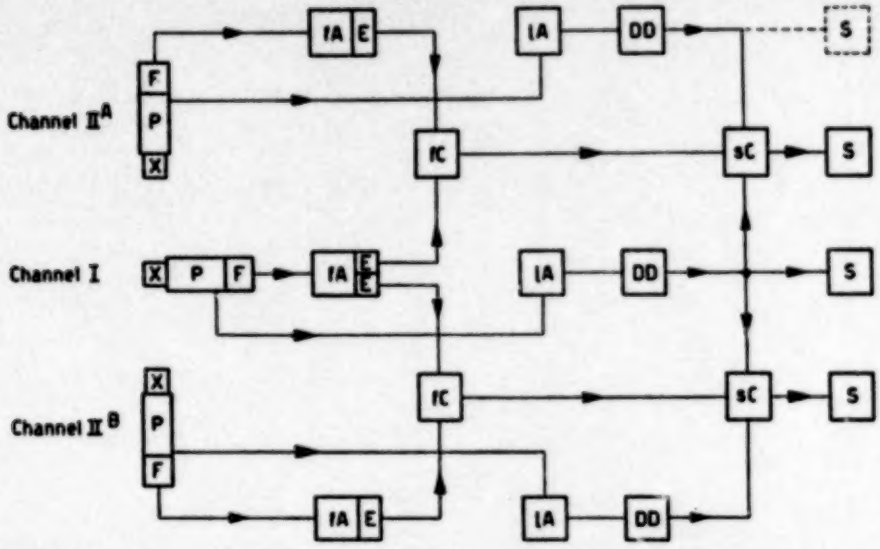

Fig. 1. Block diagram of the polarimeter (Channel I, II^A and II^B) and the gamma-gamma coincidence spectrometer (Channel I and II^A, including the dotted part). X = scintillator; P = photomultiplier; F = coincidence output; A = amplifier; E = equalizer; C = coincidence unit; DD = pulse height selector; S = scaler; f = fast; s = slow; l = linear.

3. The Radiations Present in the Decay of ^{56}Co

3.1. THE BETA RADIATION

It is generally agreed that ^{56}Co mainly decays by positons with maximum energy of 1.50 MeV. Sakai, Kurbatov *et al.* first observed a weaker branch with maximum energy of 0.995 MeV [13]), later on changed it to 0.44 MeV [2]) (intensity 4 % of the total positon spectrum) and finally deleted it, allowing an upper limit of 2 % for possible weaker transitions: with sources as thin as 6 μg/cm^2 they found the Kuri plot linear down to 320 keV [14]). Howard, Pond and Jastram [9]) found besides the main branch (75 %) weaker beta components with end points of 0.98 MeV (13 %), 0.32 MeV (8 %) and 0.19 MeV (4 %).

3.2. THE GAMMA RADIATION

Table 1 lists the energy (MeV) of the gamma rays as reported by different investigators. Column 2 gives the original values of Elliott and Deutsch, column 3 and 4 the data of Kurbatov, Sakai *et al.* (an originally reported 2.30 MeV gamma has been proved erroneous by these authors themselves [3])). In column 5 the measurements of Sharp Cook and Tomnovec, performed with a 4″×4″ NaI(Tl) crystal, are shown. The construction of a decay

TABLE 1

Energies (MeV) and relative intensities of the gamma rays from ^{56}Co, as found by different authors

Gamma no	Reference and method						accepted	uncertain
	[1] spe	[2] spe; scin	[6] scin	[15] scin	[9] spe; scin	[3] spe; scin		
1	2	3	4	5	6	7	8	9
0	0.51 (2×25 %)	0.51 (2×23 %)	0.51	0.51 (2×19 %)	0.51	0.51	0.51 (2×20 %)	
1	0.845 (100 %)	0.845 (100 %)	0.845 (100 %)	0.845 (100 %)	0.845 (100 %)	0.845	0.845 (100 %)	
2				0.975 (2 %)	0.935			0.95 (2 %)
3			1.03 ?(10 %)	1.025 (16 %)	1.085 (25 %)	1.028	1.028 (16 %)	
					1.18 (8 %)			
4	1.26 (50 %)	1.24 (55 %)	1.24 (65 %)	1.22 (70 %)	1.238 (74 %)	1.238	1.238 (70 %)	
5				1.35 (6 %)	1.30 (14 %)			1.33 (6 %)
6					1.50 (25 %)	1.500		1.50 (≦1 %)
7	1.74 (20 %)	1.75 (24 %)	1.75 (20 %)	1.76 (17 %)	1.749 (16 %)	1.749	1.75 (17 %)	
					1.762 (17 %)	1.762		1.75 ?
8	2.01 (10 %)	2.03 (≈10 %)	2.02 (15 %)	2.02 (11.5 %)	2.022 (11 %)	2.020	2.020 (12 %)	
9			2.06		2.17 (7 %)			2.1
10	2.55 (20 %)	2.60 (14 %)	2.6 (20 %)	2.56 (15.5 %)	2.609 (15 %)	2.609	2.609 (16 %)	
11					2.674 (6 %)	2.674		2.674
12					2.87 (7 %)	2.730		2.730
13			2.99 (2 %)	2.98 (2 %)	3.0	×	2.99 (2 %)	
14	3.25 (20 %)	3.25 (24 %)	3.25 (15 %)	3.25 (11.5 %)	3.25	×	3.25 (12 %)	
15				3.47 (1.1 %)				3.47 (1 %)

spe: spectrometer study of photoelectrons.

scin: scintillation spectrometry.

× not looked for owing to instrumental limitations.

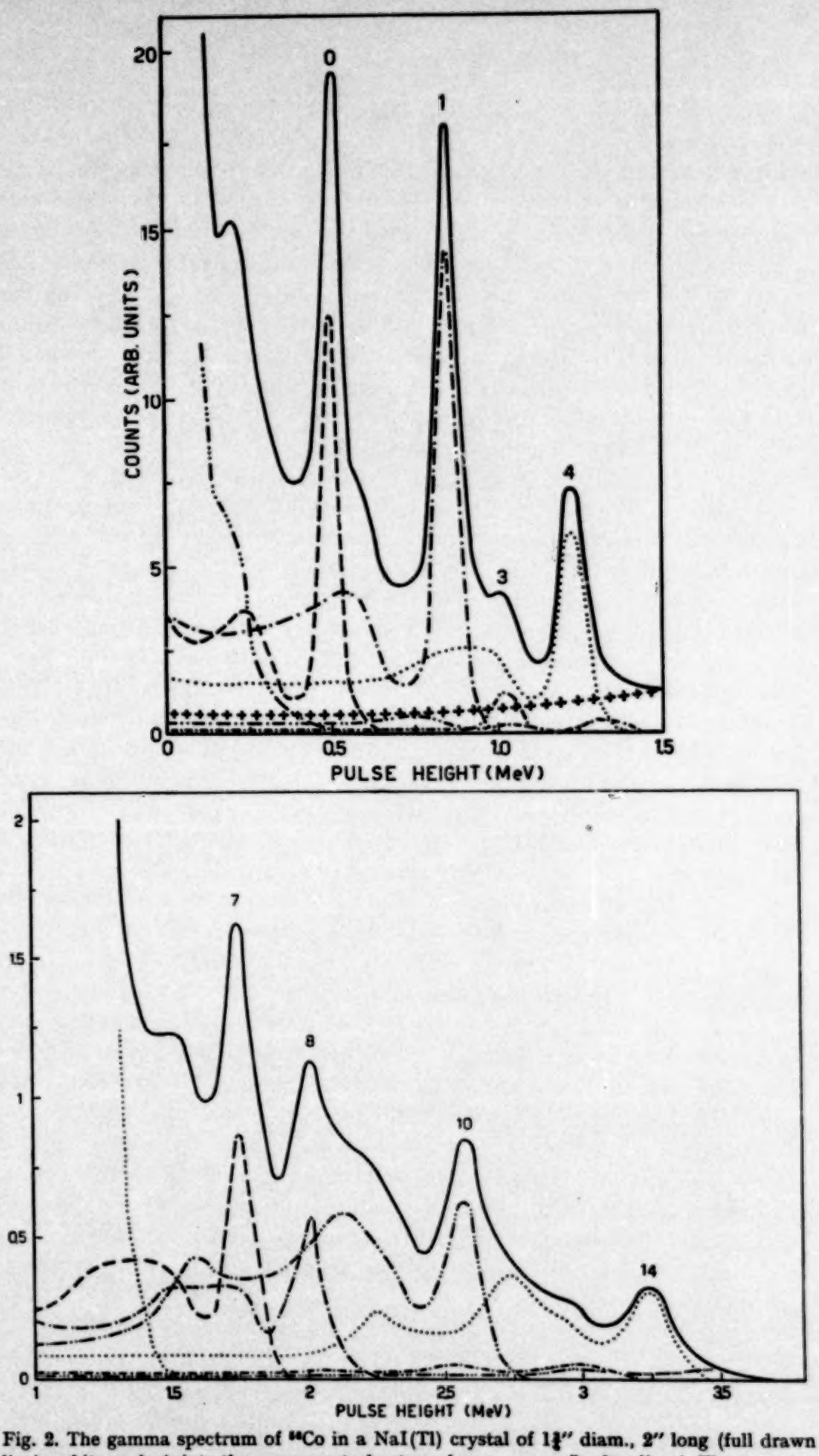

Fig. 2. The gamma spectrum of ^{56}Co in a NaI(Tl) crystal of 1¾" diam., 2" long (full drawn line) and its analysis into the components due to each gamma ray (broken lines). The ++++ line in the upper figure denotes the sum of the contributions of all gamma rays with an energy higher than 1.5 MeV. The numbers of the photopeaks correspond with the numbers of the

scheme is much facilitated by a precision determination of the gamma ray energies from the photoelectron spectrum. Howard *et al.* performed such measurements, the results of which are given in column 6. Column 7 shows a revised interpretation of the data with some uncertain gamma rays discarded (private communication from C. Dulgeroff). The last columns show the values accepted by us in the analysis of the measured spectrum; as for the energies, preference has been given to ref. [9]), for intensities to ref. [15]). The question about the existence of one or two gamma rays of 1.75 MeV is left open. It was likewise impossible to resolve the gamma rays at 2.609 MeV, 2.674 MeV and 2.730 MeV.

Fig. 2 represents the pulse height spectrum of the gamma rays present in the decay of ^{56}Co in a $1\frac{3}{4}''$ diameter, 2'' long NaI(Tl) crystal. This spectrum was analyzed into its components because it was necessary for the measurements to be described in the following sections to know the relative contributions of each gamma ray to the counting rate in a certain energy interval. For this analysis use was made of the shape of the pulse height spectra of the well known gamma rays of ^{24}Na (2.76 MeV and 1.38 MeV), ^{56}Mn (2.13 MeV, 1.81 MeV and 0.85 MeV), ^{22}Na (1.28 MeV and 0.51 MeV) and ^{137}Cs (0.66 MeV) in the scintillators used, of the photofraction of these gamma rays in the experimental arrangement (the photofraction of a collimated beam from a point source has been calculated by Berger and Doggett [16]); but in our case the whole scintillator was exposed to the radiation, resulting in a smaller photofraction) and of the energy resolution of the apparatus. The pulse height distribution due to each gamma ray separately is drawn in fig. 2. The photopeaks of the gamma rays are denoted by a number, corresponding to the numbers given in column 1, table 1.

In fig. 2 the existence of the 3.47 MeV, 2.99 MeV and 1.33 MeV gamma rays was taken from table 1, although only the 2.99 MeV gamma seems to be certain. Their presence affects the overall spectrum but slightly because of their low intensities. Arriving at the 1.50 MeV region from the high energy side in the analysis of the spectrum, the upper limit for a possible gamma of this energy appears to be 5 % (relative to 100 % for the 0.845 MeV gamma) instead of 25 % as found in ref. [9]). In ref. [15]) an upper limit of 1 % is given. In the next section more will be said about the 1.03 MeV gamma.

From the area under the photopeaks the relative intensities of the gamma rays can be calculated. But preference is to be given to the values of Sharp Cook and Tomnovec [15]), who were able to obtain more accurate results with larger crystals.

4. Coincidence Measurements

Because of the existence of two proposals for the decay scheme of ^{56}Co it was necessary to perform further investigations in order to ascertain the

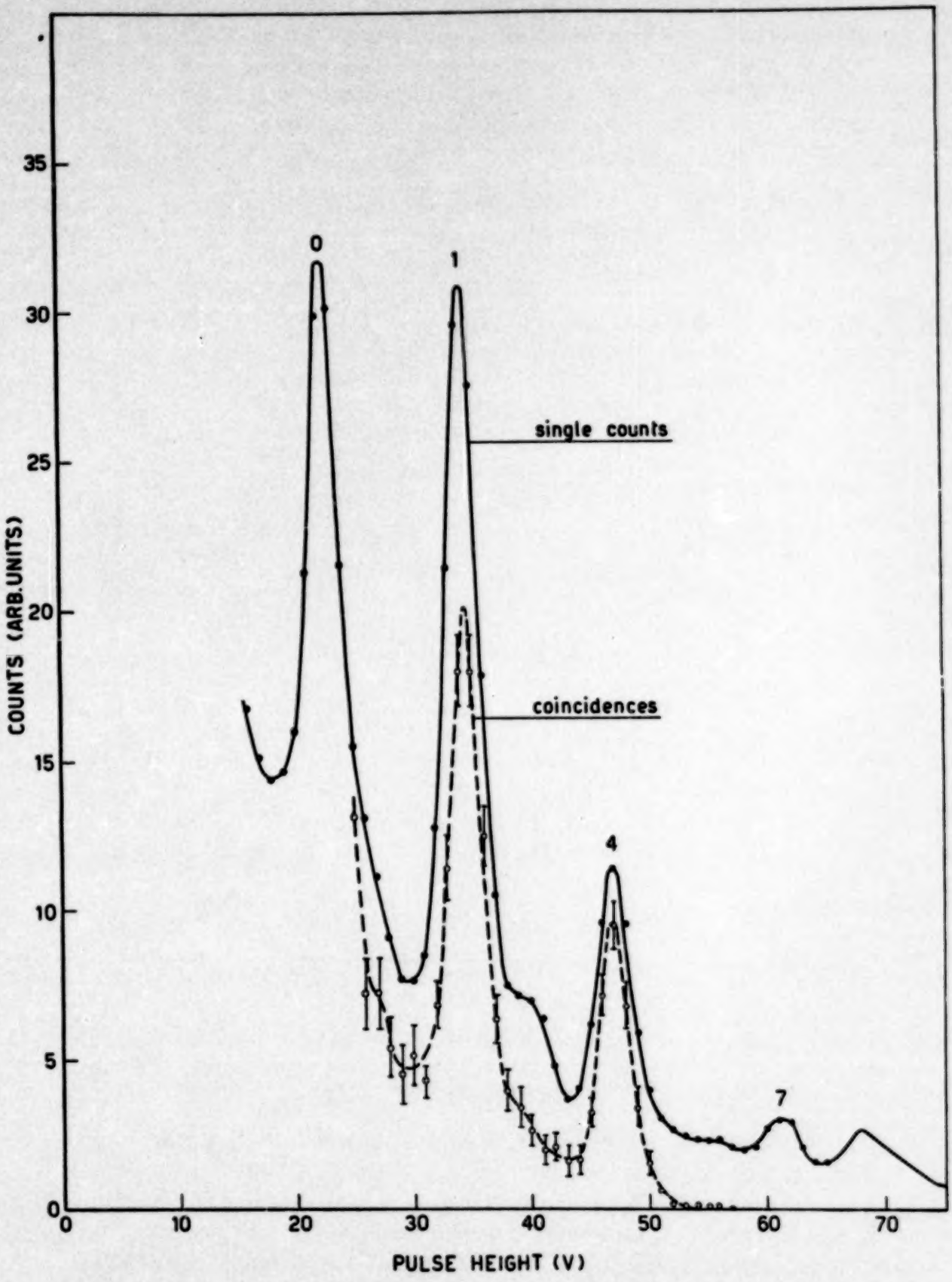

Fig. 3. The gamma spectrum of ^{56}Co in coincidence with positons and the single count gamma spectrum. The coincidences between the annihilation radiation (no. 0) and the positons are not shown in the figure. The numbers of the photopeaks correspond to those in table 1.

actual decay scheme, needed for the interpretation of the experiments with oriented nuclei. Coincidence measurements had been made earlier by Sakai *et al.*[2,3]; their results were confirmed and extended by the $\beta-\gamma$ and $\gamma-\gamma$ coincidence measurements described below.

4.1. $\beta-\gamma$ COINCIDENCES

Fig. 3 compares the overall gamma spectrum with the spectrum of the gamma rays in coincidence with positons having an energy between 700

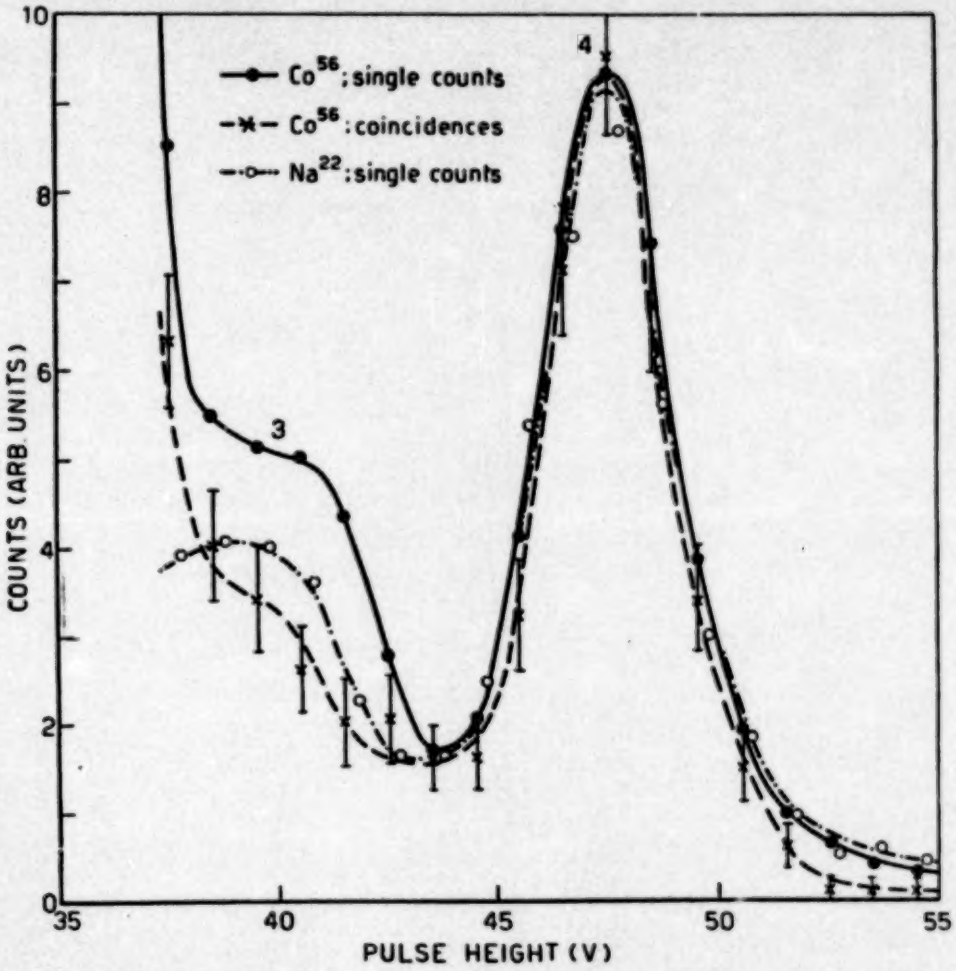

Fig. 4. Comparison of the single count gamma spectrum in the 1 MeV region with the gamma spectrum in coincidence with positons and the single count gamma spectrum of ^{22}Na (horizontally transposed).

and 900 keV. The source, 4 μC, was about 1 mg/cm^2 thick on formvar backing. The positons were detected in a 5 mm thick anthracene crystal. The contribution due to $\gamma-\gamma$ coincidences was determined experimentally, using absorbers, and subtracted from the total coincidence spectrum. Fig. 3 thus reconfirms the well-established fact that the gammas of 0.845 MeV and 1.238 MeV are in coincidence with the main positon branch.

Fig. 4 shows the 1 MeV region of fig. 3 on an enlarged scale in order to establish the existence of a 1.03 MeV gamma. The ^{56}Co spectrum has been corrected now for the contributions due to Compton scattering of gamma rays with an energy higher than 1.5 MeV. The photopeak of the 1.28 MeV gamma from ^{22}Na, horizontally transposed to coincide with the 1.238 MeV gamma from ^{56}Co, is also shown in this figure in order to compare its line shape with that of the 1.238 MeV ^{56}Co gamma. A small part of the excess pulses in the single count spectrum at 1 MeV is due to the high energy tail of the photopeak of the 0.845 MeV gamma but the main part is attributed to the reported 1.03 MeV gamma; furthermore, fig. 4 shows that this gamma is not coincident with the main positon branch.

According to the decay scheme of Howard *et al.* [9]), $\beta-\gamma$ coincidences should be expected between gammas of 1.8 MeV and 2.6 MeV and betas in the energy interval between 200 keV and 400 keV. These coincidences were not detected, however, since the same results as displayed in fig. 3 were obtained when the positon energy is taken between 200 keV and 400 keV. But the accuracy was not very high due to the correction that had to be applied and due to the abundance of low energy pulses coming from scattered high energy positons. This last experiment has therefore been repeated in a lens-type beta spectrometer [17]). Positons of 230 keV were focussed on an anthracene crystal and brought into coincidence ($2\tau = 0.3\times10^{-6}$ s) with the output of a pulse height selector accepting pulses from a NaI(Tl) scintillator in the interval of 1.65 MeV to 1.90 MeV. From the known number of coincidences of the positons with the 1.24 MeV gamma ray, it was possible to set an upper limit to the 0.9 MeV positon branch intensity of 1 % of the total positon intensity. An upper limit of 0.6 % could be deduced from the same experiment for a possible 0.6 MeV or 0.45 MeV positon component followed by a 2.1 MeV or 2.3 MeV gamma, respectively. From the experimental ratio of the number of positons to the number of disintegrations and from the theoretical value for the ratio of K-capture to positon emission in an allowed transition [18]) an upper limit can be calculated for the presence of these gamma rays. The upper limits found are 0.3 % for the 1.8 MeV and 2.6 MeV gamma together, 0.4 % for the 2.1 MeV and 0.6 % for the 2.3 MeV gamma (relative to 100 % for the 0.845 MeV gamma), as far as they are excited directly by positons and K-capture. Most of these results are in contradiction with the decay scheme based on the data of Howard *et al.* [9]).

4.2. $\gamma-\gamma$ COINCIDENCES

The two counters, separated by 5 cm of lead, received the radiation in two directions making an angle of about 120° with each other so that $P_2(\cos\vartheta)$ is about zero, resulting in only a small, negligible, anisotropy

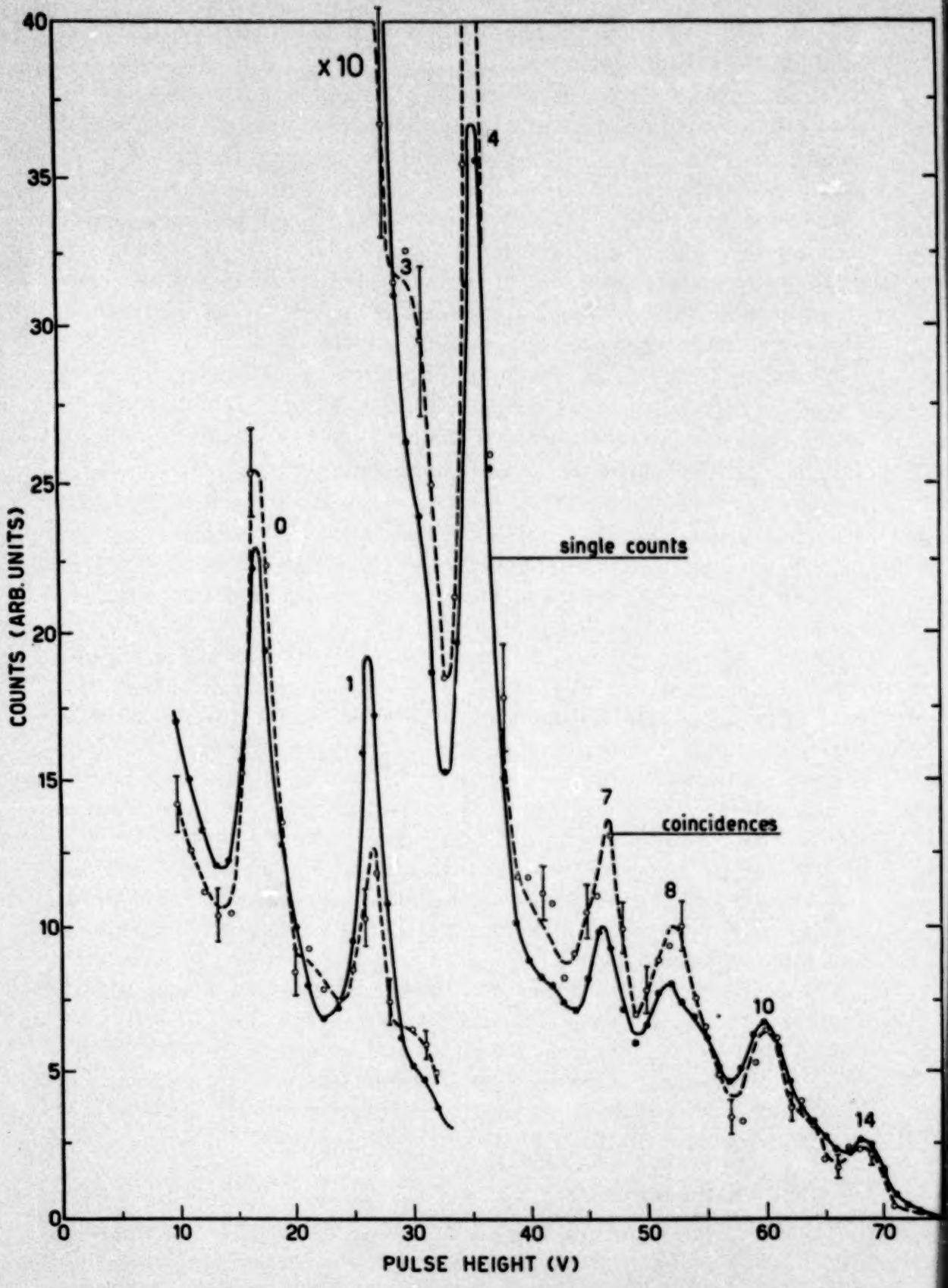

Fig. 5. The gamma spectrum of ^{56}Co in coincidence with the 0.845 MeV gamma and the single count gamma spectrum. The numbers of the photopeaks correspond to those in table 1.

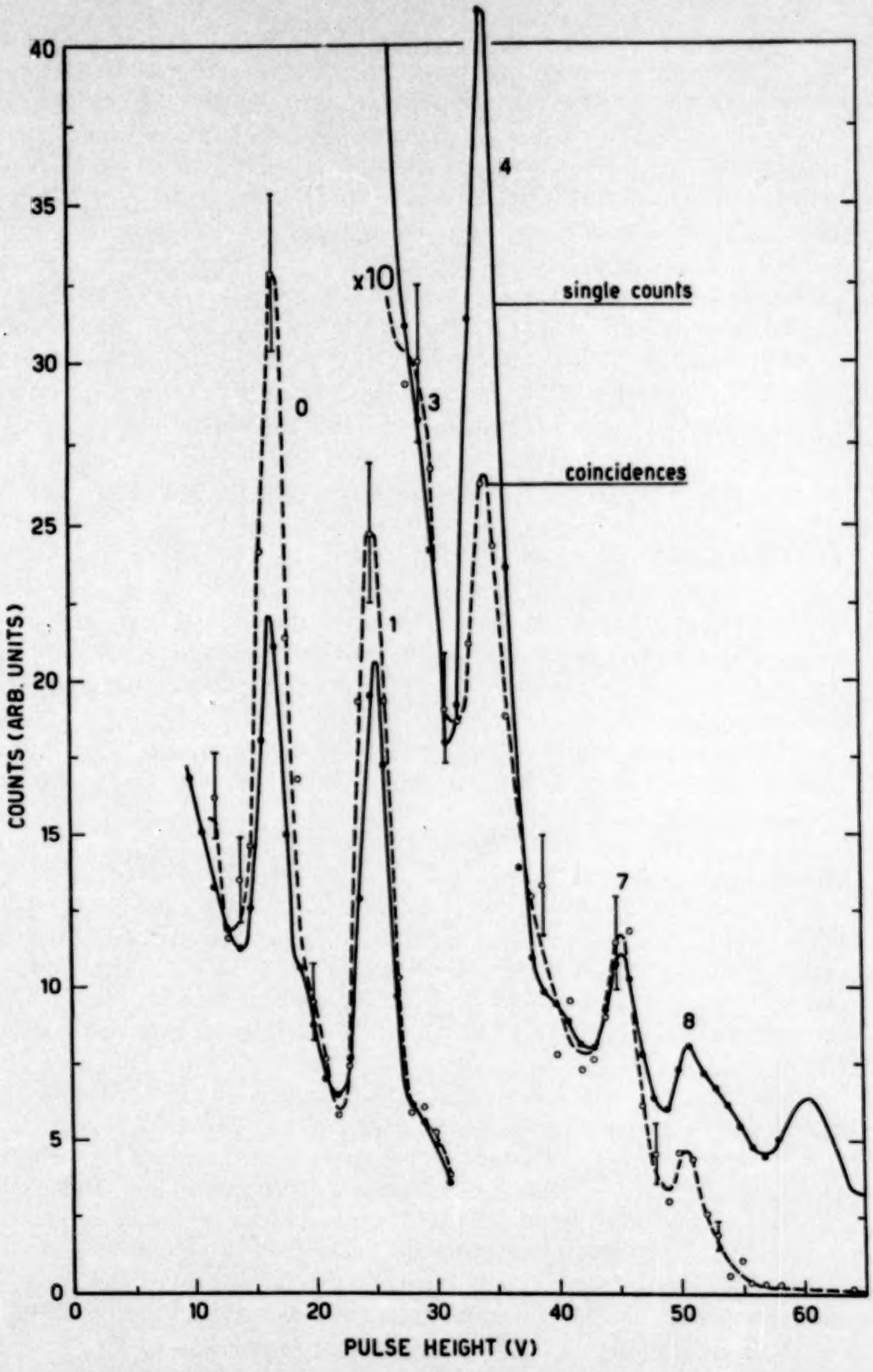

Fig. 6. The gamma spectrum of ^{56}Co in coincidence with the 1.24 MeV gamma and the single count gamma spectrum. The numbers of the photopeaks correspond to those in table 1.

correction — due to the angular correlation between the gamma rays — on the number of coincidences. The activity of the source was about 15 μC. The gamma ray spectra in coincidence with the 0.845 MeV and 1.238 MeV gamma are shown in fig. 5 and 6, respectively. It can be concluded that (0.845) is in coincidence with (1.028), (1.238), (1.75), (2.02), (2.61) and (3.25); and that (1.238) is in coincidence with (0.845), (1.028), (1.75) and (2.02). This is in accordance with the measurements of Sakai *et al.* [2, 3]), but not with the decay scheme in ref. [9]). Moreover, the coincidences were measured between the gamma rays in the 2 MeV region ((1.75) and (2.02)) and those in the 1 MeV region ((1.028) and (1.238)), giving the same result as shown in fig. 4. This can be interpreted as (1.028) not being coincident with (1.75), (2.02) and (2.61). It can be deduced from a careful comparison between the number of coincidences and the single counts that at most 20 % of the gamma rays in the 1.8 MeV region and 30 % of the gamma rays in the 2.0 MeV region are not in coincidence with the (1.238) gamma.

4.3. CONCLUSIONS

These data lead to the decay scheme shown in fig. 10. It is in agreement with and extends that of Sakai *et al.* [2, 3]) and Sharp Cook and Tomnovec [15]); however, it differs much from the one based on the data of Howard *et al.* [9]). The following points can be stressed in connection with the presently proposed decay scheme:

1. The intensities of the various beta and gamma components are internally consistent. The ratio of the intensities of the positons to the 0.845 MeV gamma is about 0.20 [1, 2, 15]).

2. The energies (in MeV) and relative intensities of the gamma rays observed in the decay of ^{56}Mn are known to be [19, 20]): 0.845 ± 0.006 (100%); 1.809 ± 0.009 (29 %); 2.134 ± 0.011 (15 %); 2.65 (1.8 %) and 2.98 (0.4 %). Elliott and Deutsch [1]) showed in their early work on ^{56}Mn that the 1.81 MeV and 2.13 MeV gammas are different from the 1.75 MeV and 2.02 MeV gammas observed in the decay of ^{56}Co. We confirmed this in measuring the energies of the radiations emitted by both isobars by means of scintillation counters.

3. The reported 2.67 MeV and 2.99 MeV gammas from ^{56}Co cannot be identified with the weak gammas of 2.65 MeV and 2.98 MeV from ^{56}Mn, usually interpreted as crossovers to the groundstate, because this would necessitate in ^{56}Co the existence of intense gamma rays of 1.81 MeV and 2.13 MeV, whereas arguments based on the last sentence of part 4.2 above (γ—γ coincidences) and table 1 give an upper limit of only 4 % for each gamma. It should be remarked, however, that according to the (p, p') data (see below) there are two close-lying levels at 2.95 MeV, thus making the argument for the 2.98 MeV gamma not conclusive.

4. It is difficult to make a choice between the decay scheme of fig. 10 and that of Howard *et al.* on the basis of the gamma rays observed from the (n, n') reaction on natural Fe (91 % ^{56}Fe), because the energy spread in the measurements is too large. One of the most accurate measurements probably has been made by Rothman *et al.* [21]). (incident neutron energy 3.7 MeV) who observed gamma rays of 0.845 ± 0.010; 1.23 ± 0.01; 1.80 ± 0.02; and 2.10 ± 0.03 MeV and higher. More support comes from the (p, p') data on enriched ^{56}Fe by Buechner and Sperduto [22]), who found 10 levels in ^{56}Fe from the energy analysis of the scattered protons. These levels are shown at the left side in fig. 10. The fair agreement between the energies is much in support of the decay scheme of fig. 10.

5. Concerning the gamma rays of weak intensity (see table 1), only the existence of the 2.99 MeV gamma is thought to be certain. It might de-excite one of the two levels at about 2.95 MeV (viz. the one that is not populated in the decay of ^{56}Mn) or the level at 3.84 MeV. Some of the other reported weak gamma rays can also be fitted into the decay scheme [15]). They are not shown in fig. 10 since their existence has not yet been definitely established. Since it was found in the $\gamma-\gamma$ coincidence measurements that at least 80 % of the gamma rays in the photopeak at 1.75 MeV (no. 7) are coincident with the 1.238 MeV gamma, the existence of only one such gamma of 1.75 MeV was accepted, instead of the two about equally intense ones reported by Howard *et al.* [9]).

5. The Gamma Ray Angular Distribution

The angular distribution of the gamma rays from ^{56}Co nuclei oriented by the magnetic hyperfine structure alignment method in a Tutton salt crystal had been studied earlier [4]). However, because of the properties of the crystal, the angular distribution could only be measured between the angles $\vartheta = 34^0$ and $\vartheta = 90°$. In the experiments described in this section, ^{56}Co nuclei were polarized in a crystal of cerium-magnesium nitrate by the magnetic hyperfine structure polarization method. With this set-up the whole angular range between $\vartheta = 0°$ and $\vartheta = 90°$ was available for measurements, resulting in a much larger anisotropy although the degree of orientation of the nuclei was about the same in both cases. It was therefore thought worthwhile to survey the gamma ray angular distribution once again.

Columns 3, 4, 5 and 6 of table 2 show the results of the measurements at two different temperatures, $W_m(\vartheta)$ being the counting rate at the indicated temperature at an angle ϑ with respect to the axis of polarization of the nuclei, normalized to the counting rate at 1 °K. $W_m(\vartheta)$ is measured on the photopeaks of the gamma rays; $W_m(\vartheta)$ is corrected for the contributions due to other gammas, using fig. 2, and the result, called $W(\vartheta)$, is shown in

TABLE 2

Anisotropies of the gamma rays emitted by oriented ^{56}Co nuclei

Gamma ray		$W_m(\vartheta)$ (measured)				$W(\vartheta)$ and ε (corrected)						Source of error
		$1/T^* = 250$		$1/T^* = 125$		$1/T^* = 250$			$1/T^* = 125$			
no	MeV	$\vartheta=0°$	$\vartheta=90°$	$\vartheta=0°$	$\vartheta=90°$	$W(\vartheta=0°)$	$W(\vartheta=90°)$	ε	$W(\vartheta=0°)$	$W(\vartheta=90°)$	ε	
1	0.845	0.765 ±0.006	1.102 ±0.005	0.872 ±0.006	1.045 ±0.005	$0.755^{.765}_{.745}$	$1.105^{.115}_{.095}$	+0.32	$0.865^{.875}_{.855}$	$1.045^{.055}_{.035}$	+0.17	s, c
4	1.24	0.800 ±0.006	1.088 ±0.005	0.905 ±0.006	1.042 ±0.005	$0.73^{.76}_{.705}$	$1.12^{.10}_{.14}$	+0.35	$0.875^{.895}_{.855}$	$1.055^{.045}_{.07}$	+0.17	c
7	1.75	1.12 ±0.015	0.94 ±0.015	1.06 ±0.01	0.97 ±0.01	$1.12^{.17}_{.07}$	$0.94^{.99}_{.89}$	−0.19	$1.07^{.10}_{.04}$	$0.98^{.01}_{.95}$	−0.09	s
8	2.02	1.14 ±0.02	0.93 ±0.02	1.06 ±0.01	0.95 ±0.01	$1.18^{.09}_{.29}$	$0.93^{.86}_{.04}$	−0.27	$1.06^{.99}_{.12}$	$0.95^{.89}_{.02}$	−0.11	c
10	2.61	1.02 ±0.02	0.96 ±0.02	1.04 ±0.02	0.98 ±0.02	$1.15^{.09}_{.22}$	$0.88^{.93}_{.82}$	−0.30	$1.11^{.07}_{.16}$	$0.93^{.97}_{.89}$	−0.19	c
14	3.25	0.71 ±0.015	1.145 ±0.015	0.87 ±0.015	1.09 ±0.015	$0.71^{.73}_{.65}$	$1.14^{.125}_{.205}$	+0.38	$0.87^{.89}_{.84}$	$1.09^{.07}_{.12}$	+0.20	s, c

For $W_m(\vartheta)$ the standard deviation is given, for $W(\vartheta)$ the upper and lower limit compatible with the measurements

the further columns of the table, together with the value of the anisotropy $\varepsilon = 1-[W(\vartheta = 0°)/W(\vartheta = 90°)]$. The standard deviation in $W_m(\vartheta)$ is given in small print. The errors in $W(\vartheta)$ are due partly to the standard deviations in $W_m(\vartheta)$ (therefore being of statistical nature) and partly to the uncertainty in the corrections for the higher energy gamma ray contributions; the most important of these two sources of error has been designated by s and c, respectively, in the last column. The quoted errors do not include those incurred in the spread in the temperature measurements between various runs, which can amount to at most 5 % in T^* and produce an effect of about 0.5 % in $W(\vartheta)$. Corrections for the angular resolution of the system and for scattering in the source, cryostat and polarizing magnet could be neglected. The results are in agreement with the earlier measurements; they will be discussed in section 7 in connection with spin and parity assignments.

6. Linear Polarization of the Gamma Rays

6.1. GENERAL

The gamma radiation emitted by oriented nuclei in the direction $\vartheta = 90°$ is linearly polarized; the degree of linear polarization, P_1, is determined by the degree of orientation of the nuclei and by the gamma transition involved and therefore shows a relation with the anisotropy ε of the gamma ray; for all gamma transitions that do not involve mixtures of different multipole orders this relation is given by $|P_1| = |\varepsilon|$ [23]). P_1 is taken positive when the electric vector of the radiation lies preponderantly in the plane of the direction of propagation, **k**, and the axis of orientation of the nuclei, $\boldsymbol{\eta}$, whereas P_1 is negative when the electric vector is perpendicular to this plane. (P_1 corresponds to $P\xi_1$ ($\vartheta = \pi/2$) in the notation of ref. [32]) and to $-P_1(\pi/2)$ in the notation of ref. [23])). The sign in the relation between P_1 and ε is determined by the electric or magnetic character of the gamma radiation and therefore gives information about the parities involved (see section 7). The magnitude of P_1 relative to ε is of importance when mixtures of two different multipole contributions are taken into consideration (see section 7).

The Compton scattering process can be used to analyze the state of linear polarization, because the radiation is preferentially scattered in a direction perpendicular to the electric vector [10]). The cross section for this process can be written as [24, 25, 26])

$$d\sigma/d\omega = f(\chi, k)\{1-P_1Q(\chi, k)\cos 2\varphi\}; \qquad (1)$$

k is the energy of the incident gamma ray (in units of mc^2), χ is the scattering angle and φ is the azimuth of the scattering direction, $\varphi = 0$ being in the plane through $\boldsymbol{\eta}$ and **k**. The symbols are explained in fig. 7. $f(\chi, k)$ is

the ordinary Klein-Nishina cross section for Compton scattering. $Q(\chi, k)$ is given by

$$Q(\chi, k) = \frac{\{1+k(1-\cos\chi)\}\sin^2\chi}{1+\cos^2\chi+k(1-\cos\chi)(1+\cos^2\chi)+k^2(1-\cos\chi)^2}. \qquad (2)$$

For zero gamma energy $Q(\chi, k)$ has a maximum at $\chi = 90°$, for an energy of 3 MeV at about $\chi = 60°$.

P_1 can now be determined from

$$\zeta = \frac{N_\perp}{N_\parallel} = \frac{1+P_1 Q(\chi, k)}{1-P_1 Q(\chi, k)} \qquad (3)$$

in which $N_\perp$ and $N_\parallel$ are the number of coincidences between the scatterer (a plastic scintillator) and the detector (a NaI(Tl) crystal) at $\varphi = \pi/2$ and $\varphi = \pi$, respectively.

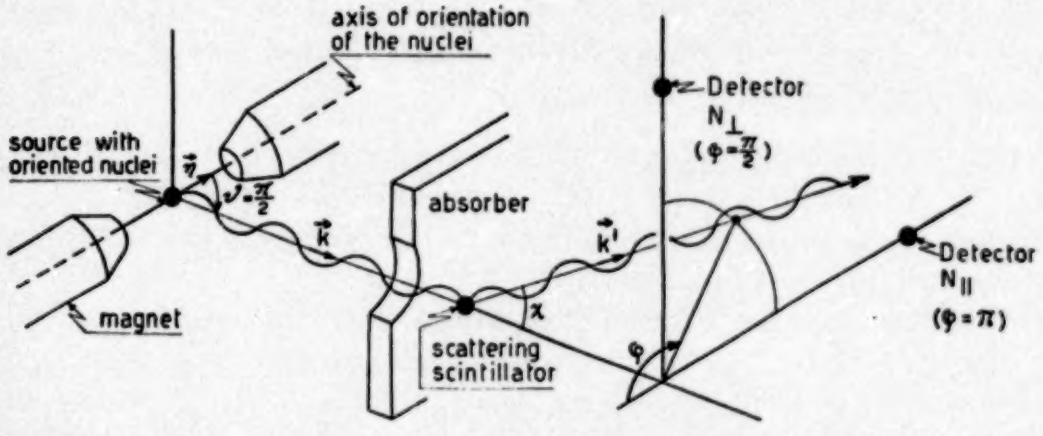

Fig. 7. Scheme of the experimental arrangement for the measurement of the linear polarization of the gamma radiation emitted by oriented nuclei. The scattering scintillator is a plastic, the detectors are NaI(Tl) crystals.

An important factor with this polarimeter is its energy resolution, especially in the case of ^{56}Co with its many gamma rays. The resolution is determined partly by the statistics in the number of photoelectrons released in the photomultiplier, partly by the spread in scattering angle allowed by the geometrical arrangement of the scintillators. It would have been best for achieving good statistics if NaI(Tl) could have been used as the central scattering scintillator. But this turned out to be impossible since in the coincidence pulse spectrum of the 2.76 MeV gamma from ^{24}Na a spurious peak at 1.74 MeV appeared as large as the Compton peak. This spurious peak is due to pair production in the NaI(Tl) scatterer with the annihilation radiation, which has about the same energy as the Compton scattered gamma rays, being detected in the detectors. Therefore, a plastic scintillator was chosen as scatterer; indeed, no pulses due to pair production were found in the coincidence pulse spectrum.

The condition of sufficient detection efficiency could be fulfilled by giving the cylindrically shaped plastic scintillator the dimensions of 2″ diameter, 2″ long, and by using NaI(Tl) detectors of $1\frac{3}{4}$″ diameter, 2″ long, placed with their centers at 12 cm from the center of the plastic. This allows an angular spread in χ of $\pm\Delta\chi = \pm 15°$. An average scattering angle of $\chi = 75°$ was chosen because at this angle $Q(\chi, k)$ reaches its maximum in the energy range of interest to us, whereas the loss of energy resolution due to the geometrical effect does not exceed the contribution due to the scintillator-photomultiplier combination. The detectors were shielded from the direct radiation by 8 cm of lead; the plastic scintillator was placed 12 cm from the source. The halfwidth (full width at half height) of the coincidence peak thus found is: 14 % for a gamma ray of 2.76 MeV; 25 % for 1.2 MeV and 40 % for 0.66 MeV.

The efficiency, defined as the probability for a gamma ray to be counted by the polarimeter when it falls into the solid angle subtended by the plastic scintillator at the source, is found to be 0.02 %, 0.05 % and 0.09 % respectively for the above mentioned energies, in agreement with a rough calculation. It should be remarked that only pulses corresponding to the full energy of the scattered radiation were accepted from the NaI(Tl) detector. Some information about the electronics of the polarimeter can be found in subsection 2.2 and fig. 1. A description of other Compton polarimeters can be found in ref. [10, 27, 28]).

6.2. MEASUREMENTS

Fig. 8 shows the single count spectrum of the gamma rays of ^{56}Co in the plastic scintillator and the spectrum that is in coincidence with pulses in a NaI(Tl) detector due to gamma rays scattered over $\chi = 75°$. While the pulse height selector took this spectrum in the plastic (channel I, fig. 1), the pulse height selector following the NaI(Tl) detector (channels II, fig. 1) was moved in a few steps from the 250—350 keV region, corresponding to the energy of the scattered 0.51 MeV gamma, to the 500—700 keV region, corresponding to the energy of the scattered 3.25 MeV gamma. The counting rate was 13 c/s for the 0.845 MeV gamma, 0.5 c/s for the 3.25 MeV gamma.

The linear polarization was measured for the gamma rays of energy 0.845 MeV, 1.24 MeV, 1.75 MeV, 2.61 MeV and 3.25 MeV. The various discriminator settings for these gammas used in the channel of the scattering scintillator are indicated in fig. 8. After each demagnetization, about half an hour was available before the temperature arrived in the 0.01 °K region; during this time the values of ζ as a function of the temperature were taken for each selected gamma ray; we write them as $\zeta_{low}(T^*)$. Immediately afterwards, when the source was brought to 1 °K, normalization points

were taken under the same conditions, giving ζ_{norm} (1 °K), from which $\zeta(T^*)$ was determined, being $\zeta(T^*) = \zeta_{low}(T^*)/\zeta_{norm}$ (1 °K). From $\bar{Q}(\chi, k)$, being the value of $|\cos 2\varphi| \cdot Q(\chi, k)$ averaged over the accepted χ and φ interval, and from $\zeta(T^*)$ the degree of linear polarization P_1 is calculated then as a function of T^*. From the measurements in section 5, ε is known as a function of T^*; this allows the comparison of $P_1(T^*)$ and $\varepsilon(T^*)$.

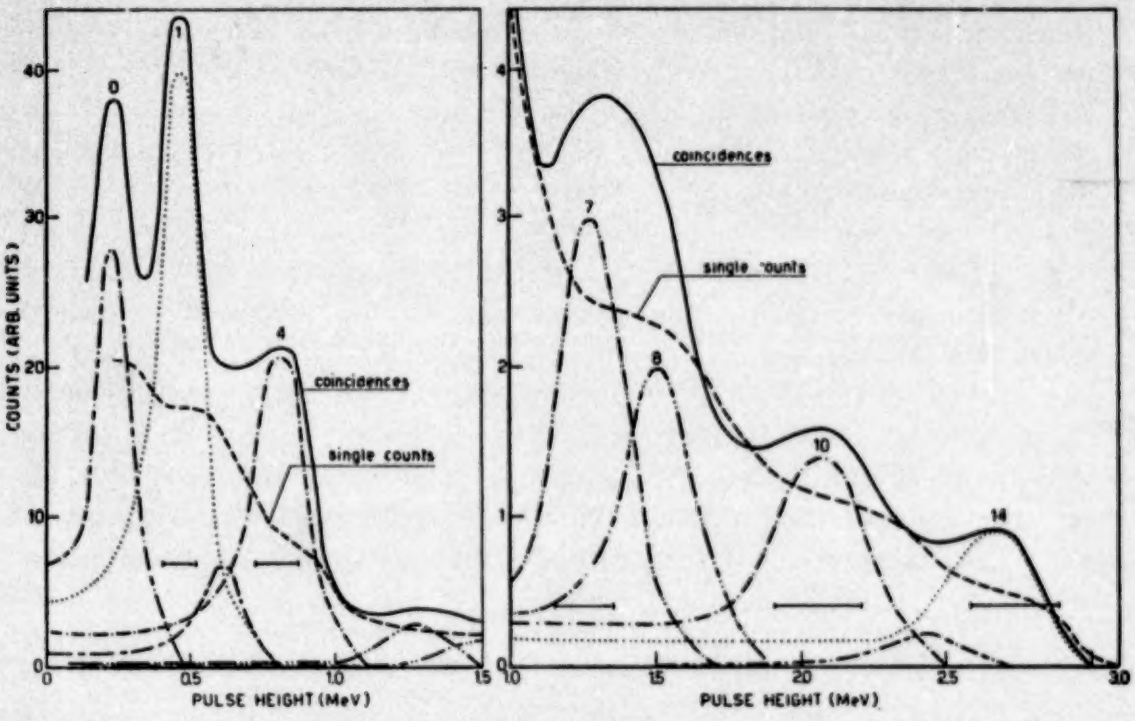

Fig. 8. The coincidence spectrum of the gamma rays of ^{56}Co in the polarimeter (full drawn line) and the analysis of this spectrum into the components due to each gamma ray (broken lines); $\chi = 75°$. The single count spectrum is also shown. The numbers of the Compton peaks correspond to the numbers of the gamma rays in table 1. The vertical scales of the left and the right figure differ by a factor of 10.

A check on the values of $\bar{Q}(\chi, k)$ used is given by the result of the measurement of the linear polarization in the simpler case of the three gamma rays of ^{52}Mn, all three of which are expected to be pure electric quadrupoles [29]). Indeed $P_1(T^*) = -\varepsilon(T^*)$ was found there within the statistical accuracy, thus giving confidence in the performance of the polarimeter and the calculated value of $\bar{Q}(\chi, k)$.

It was observed for the 0.845 MeV and the 1.24 MeV gamma ray that $P_1(T^*) = -\varepsilon(T^*)$ between $1/T^* = 250$ and $1/T^* = 100$. In table 3 two values of P_1 and two values of ε are given, each averaged over a region near the indicated T^*. In the case of the 1.75 MeV, 2.61 MeV and 3.25 MeV gammas the statistics were too poor to measure P_1 as a function of the temperature. For these gammas the average of many series, 9, 9 and 16

respectively, is given in the table and compared to the value of ε at the mean temperature.

TABLE 3

The degree of linear polarization of the gamma rays emitted by oriented ^{56}Co nuclei

Gamma		$1/T^*$	ε	$Q(\chi=75°, k)$	$\overline{Q}(\chi=75°, k)$	P_1	ε
no.	MeV						
1	0.845	250	0.73 ±0.01	0.540	0.49	−0.32 ±0.015	+0.32±0.01
		125	0.82 ±0.01	0.540	0.49	−0.20 ±0.015	+0.17±0.01
4	1.24	200	0.82 ±0.015	0.425	0.39	−0.25 ±0.02	+0.28±0.02
		125	0.90 ±0.015	0.425	0.39	−0.135±0.02	+0.17±0.02
7	1.75	≈ 125	1.047±0.017	0.325	0.305	+0.075±0.027	−0.09±0.04
10	2.61	≈ 125	1.071±0.020	0.235	0.23	+0.15 ±0.04	−0.19±0.07
14	3.25	≈ 125	0.977±0.016	0.187	0.18	−0.065±0.045	+0.20±0.025

Some measurements with a broader channel for the gammas of 1.75 MeV and 2.02 MeV together gave about the same value for ζ as the 1.75 MeV alone; therefore it is thought, that the sign in the relation between P_1 and ε for the 2.02 MeV gamma is negative.

The errors quoted in P_1 are standard deviations; those in ε are equal to 2/3 the value deduced from the upper and lower limit of ε given in table 2. An error for the T^* measurements is not included, but might be estimated as 5 % in T^*, equivalent to 5 % in P_1 in case of the gammas of 0.845 MeV and 1.24 MeV and 10 % for the gammas of 1.75 MeV, 2.61 MeV and 3.25 MeV. Corrections for the finite energy resolution were not made for P_1. A chi-square test was applied to the ζ-data of the gammas of 1.75 MeV, 2.61 MeV and 3.25 MeV, which showed that the spread in the various points was in accordance with Poisson statistics. It can be concluded from table 3, that for all radiations $P_1 \approx -\varepsilon$, except for the 3.25 MeV gamma.

7. Spin and Parity Assignments

7.1. INTRODUCTION

If nuclei with spin I_0 are oriented with one of the usual methods, in which an axis of rotational symmetry exists, then the angular distribution of the gamma radiation emitted from a level with spin I_1 is given by [32, 33])

$$W(\vartheta) = 1 + \sum_{k=2,4,\ldots} b_k(I_1, \Delta I, L, \delta) \cdot f_k(I_1, \beta_0) \cdot P_k(\cos\vartheta) \qquad (4)$$

where ϑ is the angle between the emitted radiation and the orientation axis. b_k is a parameter depending on I_1, ΔI, L and δ. δ is the mixing ratio in a transition involving two different multipoles of order L and L' ($L' = L+1$) and is defined as $\delta^2 =$ (intensity $2^{L'}$-pole)/(intensity 2^L-pole). ΔI is the spin difference between the initial and the final level of the gamma

transition, $\Delta I = I_f - I_i$. k is restricted to $k \leqq (2I_0, 2I_i, 2I_x)$ and to $k \leqq 2L$ for $\delta = 0$, $k \leqq 2L'$ for $\delta \neq 0$; I_x stands for the spins of the intermediate levels populated in the decay between the level I_0 and the level I_i.

$f_k(I_i, \beta_0)$ are the orientation parameters introduced by Tolhoek and Cox [32]; $\beta_0 = (\mu H)/(I_0 kT)$, μ being the magnetic moment of the nucleus in the state I_0 and H the magnetic field acting on the nucleus. The relation between the orientation parameters $f_k(I_i, \beta_0)$ of the level I_i and those of the original level I_0 in which the nuclei were oriented, $f_k(I_0, \beta_0)$, is given in ref. [33, 34]) and is written by us as

$$f_k(I_i, \beta_0) = V_k^{0-i} f_k(I_0, \beta_0); \tag{5}$$

V_k^{0-i} depends on the spins of all the intermediate levels populated in the decay between the level I_0 and the level I_i, as well as on the angular momentum of the radiation connecting the various levels (thus, for instance, on L and δ of a preceding gamma transition or on the ratio of the matrix elements for the Fermi interaction and Gamow-Teller interaction, $\lambda/(1-\lambda)$, of a preceding beta transition with $\Delta I = 0$, no parity change).

It is clear from the relation (5) that a quantitative comparison of the measured angular distribution with theory cannot be made without a knowledge of the properties of the preceding beta and gamma transitions. The same applies for an evaluation of β_0 at a certain temperature in order to deduce the value of μ [4, 35, 6, 7]). In a few cases it is even possible that the anisotropy, ε, changes sign for a certain transition, due to a change in f_k because of a preceding transition.

Formulae for the degree of polarization of the gamma radiation can be found in ref. [32, 33]). When $\delta = 0$ or $|\delta| = \infty$, then the degree of linear polarization P_1 in the direction $\vartheta = \pi/2$ is given by $P_1 = -\varepsilon$ if the parity is not changed in the gamma transition (M1, E2) and by $P_1 = +\varepsilon$, if it does change (E1, M2) [23, 32, 33]). For the other values of δ there is an extra term, that is dependent on I_i, ΔI, L, δ and $f_k(I_i, \beta_0)$. As an example fig. 9 shows $W(\vartheta = 0)$, $W(\vartheta = \pi/2)$, ε and P_1 for a gamma transition consisting of a mixture of M1 and E2 in the decay sequence mentioned in the caption of the figure ($\beta_0 = 0.60$). The 2.61 MeV gamma in the decay of ^{56}Co is of this kind.

In this paper no assumptions have been made about the details of the orientation mechanism, neither about the values of μ, H and T occurring in the parameter β_0. Only ε and P_1, either for the same gamma ray or for different gamma rays, are to be compared at a certain magnetic temperature T^*. If merely terms with $k = 2$ would be present in (4) ε and P_1 of all gammas could be expressed in the orientation parameter $f_2(I_0, \beta_0)$ by means of (5). But table 2 shows (by comparing $W(\vartheta = 0)$ and $W(\vartheta = \pi/2)$) that also contributions of terms in $f_4(I_0, \beta_0)$ are present, although small —

at least in the more accurate measurements. The relative magnitude of f_2 and f_4 for the level I_0 depends on details of the orientation mechanism. Therefore, in order to include also terms in f_4 in the calculated angular

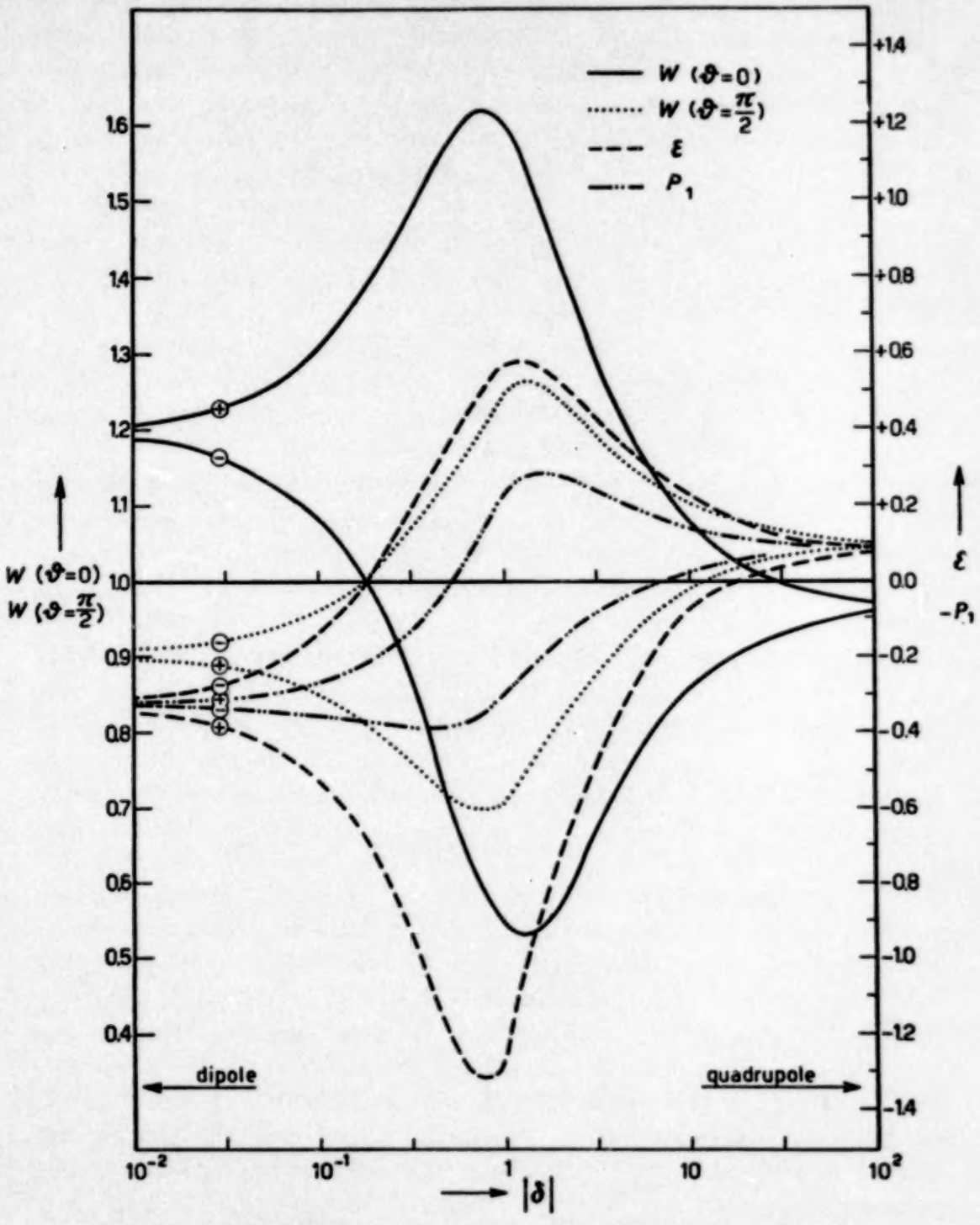

Fig. 9. $W(\theta = 0)$, $W(\theta = \pi/2)$, ε and P_1 as a function of the mixing ratio δ for a M1+E2 gamma transition in the decay sequence $I_0 = 4 \xrightarrow[\text{allowed}]{\beta} I_1 = 3 \xrightarrow[\delta]{\gamma} I_f = 2$ at the degree of nuclear orientation $\beta_0 = 0.60$. The sign of δ is shown in the curves.

distribution and degree of linear polarization, with which the measurements are to be compared, $W(\vartheta = 0)$, $W(\vartheta = \pi/2)$, ε and P_1 were calculated for various gamma transitions, possibly present in the decay of ^{56}Co, as a function of β_0 under the assumption that the magnetic sublevels are equally spaced with a spacing $(\mu H)/I_0$. This condition is certainly not fulfilled for the Co^{++}-ions in Ce—Mg-nitrate crystals [31]), but the result is accurate enough for our purpose since at the degree of orientation reached the contribution of f_4 is still found to be small, as stated above. As a consequence, β_0 only serves as a reference parameter in this paper.

Effects of reorientation or disturbance of the orientation parameters, for instance due to changes in the electron shell after an electron-capture transition, are thought to be negligible because the lifetimes of the excited states are too short.

7.2. ASSIGNMENTS

An interpretation of the earlier anisotropy measurements [4]) into spin assignments to the excited levels in ^{56}Fe was given by Poppema, Siekman, Van Wageningen and Tolhoek [5]). Mixtures of different multipoles were not taken into account in that paper. The additional information given by the linear polarization measurements (section 6) not only allows conclusions about the parity of the excited levels but also gives the possibility of taking mixtures properly into account.

Before starting with the considerations about the spins and parities of all the excited levels, successively, some initial remarks are made. A level that is deexcited by a gamma showing an anisotropy cannot have spin zero. Multipole orders higher than octupole can be rejected because the lifetime of the level would then be too long. The log *ft* values of the positon and K-capture branch to the 2.08 MeV level and of the K-capture branches to the 3.11, 3.45, 3.84 and 4.10 MeV levels are respectively 8.6, 7.3, 7.1, 6.6 and 6.2. This rules out the possibility of second and higher forbidden beta-transitions. Since ^{56}Co has spin $I_0 = 4$, as measured by paramagnetic resonance [6, 7]), and positive parity according to the shell-model (the configuration should be $(f_{7/2}, p_{3/2})$, perhaps $(f_{7/2}, p_{1/2})$ or $(f_{7/2}, f_{5/2})$) the levels in ^{56}Fe that are fed by positon emission or K-capture from ^{56}Co can thus only have spin values 2^-, $3^\pm$, $4^\pm$, $5^\pm$, 6^-. At this moment, the magnitude of β_0 at a certain temperature is still unknown, but it will appear in the course of the discussion that its value can be specified. The gamma rays are denoted by γ_0, γ_1, γ_2, $\cdots$ in this section, the numbers corresponding with those of table 1.

Ground state of ^{56}Fe: $I = 0^+$, ^{56}Fe being even.

0.845 MeV *level*: Since γ_1 goes to a level with spin zero, it must have $\delta = 0$; from the sign of ε (all cases, in which ε should change sign due to

preceding transitions, can be rejected) it follows, that γ_1 can be only quadrupole or octupole; but for an octupole radiation the transition probability is much too high [36]). From the polarization measurements it follows then, that γ_1 is E2, in accordance with Coulomb excitation data [37]); thus the 0.845 MeV level has $I = 2^+$.

2.08 MeV *level*: Spin 6^- can be excluded because of the upper limit set to the lifetime by Coleman [36]) ($t_{1/2} \leqq 2 \times 10^{-10}$ sec). Spin $5^\pm$ can be excluded for the same reason and also because of the anisotropies of γ_1 and γ_4 are nearly the same. Spin 2^-, thereby making γ_4 a mixture of E1 and M2, can be excluded by the following arguments: the anisotropies for both γ_1 and γ_4 can be written as a function of the orientation parameter f_2 for the 2.08 MeV level and of the mixing ratio δ of the E1 and M2 in γ_4 (the temperature is taken high enough to neglect the term in f_4). It can be concluded from a comparison of the anisotropies that δ then must have the limits $+0.1 \leqq \delta \leqq +0.2$, the fact that only 70 % of γ_1 is fed by γ_4 being taken into account. This value of δ leads to a value for P_1 of $P_1 \approx +2\varepsilon$. The measurements gave, however, $P_1 = -\varepsilon$. Hence spin 2^- can be excluded. The angular correlation data of Sakai [3]) can, furthermore, only be brought into accord with $I = 2^-$ if $\delta \approx -0.17$. It may be remarked that no conclusions can be made from the sign and magnitude of the contribution of f_4 relative to f_2 at low temperatures since these depend largely on the character of the preceding transitions γ_3, γ_7 and γ_8.

The same argument can be applied to the case of $I = 3^\pm$ and leads to limits on δ of $-0.45 \leqq \delta \leqq -0.30$. The measurement of P_1 limits δ to -0.45 and together with the sign of P_1, necessitates γ_4 to be the improbable mixture of E1 and M2. The assignment of $I = 3^\pm$ can be rejected more positively, however, by taking into account the angular correlation measurements of Sakai [3]); these do not fit very well to a spin $3^\pm$ and certainly limits δ to $-0.30 \leqq \delta \leqq -0.22$.

Thus $I = 4^+$ is left, the polarization measurement indicating positive parity since γ_4 is E2. It might be remarked, that, whereas our difficulty lies in the rejection of $I = 3$ for this level, the bottleneck for the angular correlation measurements is the rejection of $I = 2$: Sakai [3]) finally accepts $I = 4$ from the fact that γ_7 has the same angular correlation with respect to γ_4 as to γ_1.

Also in several other papers it was found that the angular correlation of γ_1 and γ_4 is in agreement with the sequence 4(2) 2(2)0 [39, 47]) and that the parity of the 0.845 MeV level is positive [40]), but it was not shown that this assignment is unique.

As the $\beta^+ - \gamma_4 - \gamma_1$ cascade is fixed now with respect to spins and parities and this cascade comprises 1/3 of the γ_4 intensity, the value of β_0 can be estimated to be in the region of 0.5.

4.10 MeV *level*: $I = 6^-$ can be excluded because of the presence and intensity of γ_{14}; $I = 5^+$ can be excluded because this would lead to a branching ratio of 10^6 for γ_8 relative to γ_{14}, according to the Moszkowski-Weisskopf estimate, instead of the measured ratio 1. The same can be said against $I = 5^-$ as well as the fact that the sign in the relation between P_1 and ε for γ_{14} does not fit with this supposition; moreover, $I = 5$ does not agree very well with the angular correlation data on the γ_8–γ_4 cascade obtained by Sakai [3]). The anisotropy and polarization data on γ_{14} can be reconciled with $I = 2^-$, γ_{14} being then a mixture of E1 and M2 with $\delta \approx -2$, but this requires γ_8 to be a quadrupole which disagrees with the sign of ε. $I = 3^-$ can be fitted for γ_{14} by a mixture of E1 and M2 with δ about -1; $I = 3$ is also allowed as far as the anisotropy of γ_8 is concerned if $\delta \approx -0.1$ or $|\delta| \geqq 10$. But because the sign in the relation between P_1 and ε is probably negative, γ_8 would need $I = 3^+$. A stronger argument comes from the angular correlation measurements that cannot be fitted by $I = 3$ at all. Thus $I = 4$ is left as the only possibility. The sign of P_1 of γ_{14} makes this gamma an E2 and the parity of the level positive. The only difficulty comes from the fact that the linear polarization measurements gave $P_1 = -(0.35 \pm 0.25)\varepsilon$ instead of $P_1 = -\varepsilon$.

The anisotropy of γ_{14} at $1/T^* = 250$ fixes β_0 to 0.62 ± 0.07 at this temperature, the uncertainty due to the unknown value of λ being included in the limit. ($\lambda/(1-\lambda)$ is the ratio of the matrix elements for the Fermi interaction and the Gamow-Teller interaction in the beta decay.) Such a value of β_0 can also be expected from the orientation experiments of ^{60}Co in this crystal. Therefore, we are now able to compare quantitatively the measured anisotropy of a gamma at $1/T^* = 250$ with the theoretical prediction at $\beta_0 = 0.62$. The anisotropy of γ_8, now being a mixture of M1 and E2, requires then $\delta = +1.0 \pm 0.3$ (for which P_1 should be about $+\varepsilon$!), $\delta \geqq +5$, or $\delta \leqq -30$ (the last two cases yielding $P_1 \approx -\varepsilon$). The angular correlation measurements [3]) are fitted very well by $+5 \leqq \delta \leqq +15$; $\delta \geqq +15$ and $\delta \leqq -30$ are just outside the errors quoted and $\delta = +1$ does not fit at all, whereas $\delta = -0.7$ might be just possible. It is concluded that γ_8 is M1+E2, having probably $+5 \leqq \delta \leqq +15$, although $\delta \geqq +15$ and $\delta \leqq -30$ cannot be excluded.

3.45 MeV *level*: The anisotropy and polarization of γ_{10} agree with the assignments $I = 3^+$ for $|\delta| < 0.04$, $I = 2^-$ for $\delta = +0.8 \pm 0.1$ and $I = 3^-$ for $\delta = +4.5 \pm 0.5$, the fit in the last case being poor. In case of $I = 2^-$ or $I = 3^-$ the part of γ_1 that is in cascade with γ_{10} should have a rather small anisotropy but this cannot be excluded because only 16 % of γ_1 is fed in this way. The reported γ_5 and γ_{15} (see table 1) can be fitted into the accepted level scheme when they deexcite this level †; if their existence

† But it should be remarked, that the (p, p') data [22]) revealed also two other levels in the very neighbourhood, from which these two gamma rays could proceed.

could be confirmed, $I = 3^+$ would be highly improbable because the intensity ratio of γ_{15} to γ_{10} should be then $\approx 10^{-6}$ according to the Moszkowski-Weisskopf estimate. However, we prefer $I = 3^+$ since $I = 2^-$ and $I = 3^-$ both involve the improbable case of an appreciable mixture of E1 and M2.

3.84 MeV *level*: $I = 2^-$ and $I = 6^-$ can be rejected because of the anisotropy measurements on γ_7. $I = 4$ can be rejected because the angular correlation data allow only $\delta \approx -1$ whereas $|\delta| \geqq 10$ or $\delta \approx +1.0$ are needed to fit our angular distribution and polarization data. A similar argument shows that $I = 5^+$ might just be possible, giving a $\delta = +0.04$ which is just at the edge of the experimental limits (see also ref. [3,38])). The data are best satisfied with $I = 3^+$ for $|\delta| \leqq 0.05$, especially for $\delta \approx -0.03$. The reported presence of a 2.99 MeV gamma (γ_{13}) fitting nicely between the 3.84 MeV and 0.845 levels highly favors $I = 3^+$ instead of $I = 5^+$ because with the former spin it should be about 50 times weaker than γ_7 whereas with the latter it should be 2×10^5 times stronger, according to the Moszkowski-Weisskopf estimate. It should be remembered that the 1.75 MeV gamma has been reported to have two close lying components [9]).

3.11 MeV *level*: $I = 4^\pm$, $5^\pm$, or 6^- are possible.

7.3. CHECK

After making the above assignments the anisotropies were calculated on the basis of the decay scheme of fig. 10 with the values of the mixing ratio δ as shown in table 5, $\beta_0 = 0.60$, $\lambda_1 = 0.5$ and $\lambda_2 = 1$, λ_1 and λ_2 belonging to the positon plus K-capture branch to the 2.08 MeV level and to the K-capture branch to the 4.10 MeV level, respectively. The intensity of γ_3 has been added to that of γ_7 in the calculation. The results are shown in table 4 and can be compared with the measured values for $1/T^* = 250$,

TABLE 4

The calculated angular distribution of the gamma rays from ^{56}Co in the decay sequence of fig. 10 for $\beta_0 = 0.60$, corresponding to about $1/T^* = 250$, and with $\lambda_1 = 0.5$ and $\lambda_2 = 1$. The mixing ratios δ used for the 1.75 MeV, 2.02 MeV and 2.61 MeV gammas can be found in table 5. The errors quoted in ε (last column) are equal to 2/3 of the value deduced from the upper and lower limit of ε as given in table 2.

Gamma		$W(\theta = 0°)$ (calculated)	$W(\theta = 90°)$ (calculated)	ε (calculated)	ε (measured; see table 2)
no.	MeV				
1	0.845	0.744	1.117	+0.334	+0.32±0.01
4	1.24	0.764	1.110	+0.312	+0.35±0.03
7	1.75	1.114	0.943	−0.181	−0.19±0.08
8	2.02	1.168	0.887	−0.317	−0.27±0.13
10	2.61	1.195	0.903	−0.324	−0.30±0.11
14	3.25	0.701	1.131	+0.380	+0.38±0.035

to be found in table 2, from which ε is reproduced in table 4. For $1/T^* = 125$, $\beta_0 \approx 0.40$.

As may be seen in table 4, fair agreement can be reached for a proper choice of β_0, λ_1 and λ_2. Since the calculated angular distributions are not too sensitive for variations in λ_1 and λ_2 and because the measurements of the angular distribution of some of the gamma rays are rather inaccurate, it should not be inferred from this agreement that the chosen values for λ_1 and λ_2 also represent the actual ones (see also ref. [46])).

8. Conclusions and Discussion

Fig. 10 shows the decay scheme and the assigned spins and parities; the uncertain gamma rays (see table 1) are not drawn. The multipole order

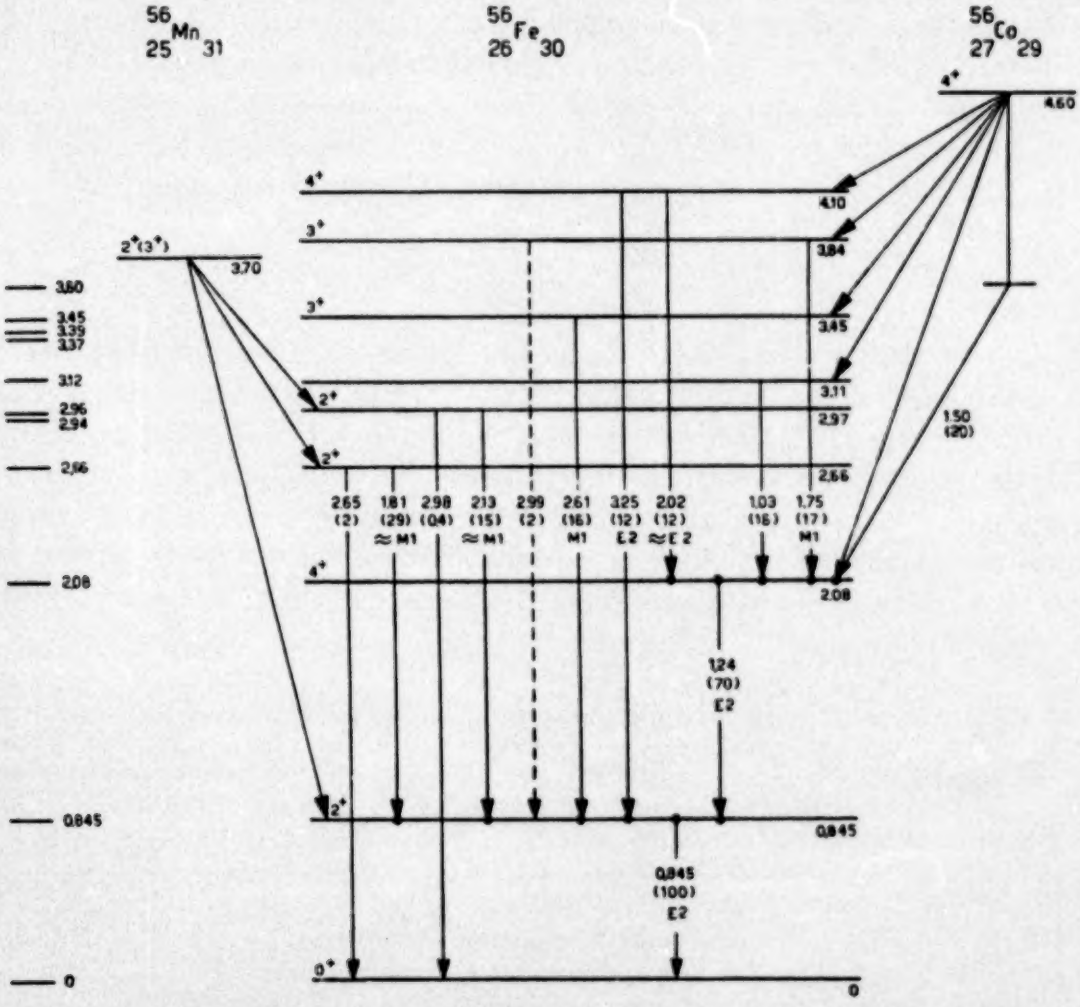

Fig. 10. Decay scheme of ^{56}Co and ^{56}Mn [30]). The energy (in MeV), the relative intensity (between brackets) and the order of the multipole that gives the main contribution to the gamma transition are denoted. Only those gamma rays are shown of which the existence is thought to be certain. Some remarks on less probable assignments and the values of the mixing ratio δ can be found in section 8. On the left are shown the levels found by (p, p') scattering on ^{56}Fe [22]).

of the gamma rays is indicated in the figure; for the transitions between levels with $\Delta I = 0$ or $|\Delta I = 1|$ only the one giving the main contribution is denoted. The mixing ratios δ for this category of transitions are collected in table 5. For the gamma rays in the decay of ^{56}Co possible values and limits of δ can be found in the preceding section, for the gammas from ^{56}Mn the data have been taken from Metzger and Todd [30]). For the 3.45 MeV level the assignments $I = 2^-$ and $I = 3^-$ are also compatible with the measurements if the improbable mixture of E1+M2 with $\delta = +0.8 \pm 0.1$ or

TABLE 5.

The mixing ratio δ of different multipoles for gamma rays between levels in ^{56}Fe with $\Delta I = 0$ or $|\Delta I| = 1$.
For details see section 7 (^{56}Co) and ref. [30]) (^{56}Mn).

Gamma (MeV)	ΔI	δ (approximately)
1.75	+1	−0.03
2.02	0	+10
2.61	−1	0
1.81	0	+0.15
2.13	0	−0.3

$\delta = +4.5 \pm 0.5$, respectively, is accepted for the 2.61 MeV gamma; if the existence of the once reported 3.47 MeV gamma could be verified, this would favour $I = 2^-$. For the 3.84 MeV level $I = 5^+$, requiring $\delta = +0.04$ for the M1+E2 mixture of the 1.75 MeV gamma, cannot be rejected entirely on the basis of the measurements but the 2.99 MeV gamma, fitting nicely between this level and the 0.845 MeV level, testifies against it. Also the fact that two gamma rays were reported at about 1.75 MeV [9]) should be remembered in a criticism of the results concerning this level (see at the end of subsection 4.3, point 5).

The spin and parity of the 2.66 MeV and 2.97 MeV level have been taken from Metzger and Todd [30]) and are consistent with assignments to the levels excited by ^{56}Co [5]).

It has been observed in those even nuclei whose nucleon numbers are or lie close to magic numbers, that the collective rotational character of the low lying energy levels is replaced by a vibrational one, due to core vibrations [41]). In the approximation of zero coupling between the particles and the core and assuming harmonic vibrations these excitations are at energies of $\hbar\omega$, $2\hbar\omega$, $3\hbar\omega$, etc. above the ground state. The first excited level has spin 2^+, the second 0^+, 2^+, 4^+ (3 fold degenerate) the third 0^+, 2^+, 3^+, 4^+, 6^+ (5 fold degenerate). The transitions between them should be of pure E2 nature and, since only one phonon jumps are allowed, crossover transitions

are prohibited. Because of their collective nature these E2 transitions should be faster than the Moszkowski-Weisskopf single particle estimate [41]).

Many medium weight even nuclei exhibit these characteristics [41, 42, 44]), although some rules are somewhat relaxed, as can be explained by assuming a weak [42]) or a strong [43]) coupling between core and particles. The ratio of the energies of the second excited state (having spin 4^+ or 2^+ mostly) to that of the first (spin 2^+ with very few exceptions) is found to fluctuate around 2.2. The gamma transition between the two 2^+ levels in nuclei having the spin sequence 0^+, 2^+, 2^+ for the groundstate, the first and the second excited state is predominantly E2 with some M1 admixed and is much stronger than the crossover transition to the ground state (an example is for instance ^{58}Fe [45])). Another common feature of these nuclei, revealed by Coulomb excitation [37]), is the reduction of the lifetime of the first excited state by a factor between about 10 and 40 compared to the single particle estimate.

For ^{56}Fe the ratio between the energy of second and first excited state is 2.46 and the transition probability of the 0.845 MeV gamma is increased by a factor 15 [37]). It is therefore tempting to assign some vibrational characteristics to this nucleus, also because both neutron and proton numbers lie close to the magic number of 28. The 0.845 MeV level is taken to be the first excited vibrational state, decaying only by E2. The 2.08 MeV level is considered to be the 4^+ member of the 3-fold degenerate second excited state. The 4.10 MeV level is taken to represent the 4^+ member of the 5-fold degenerate third excited state. The latter identification is made on the basis of the almost total E2 character of the 2.02 MeV gamma ($|\delta| \geqq 5$, probably ≈ 10) and the fact that the transition matrix element for the 3.25 MeV crossover gamma is 0.09 times smaller than that for the 2.02 MeV gamma. The 2.02 MeV gamma thus would connect the $3\hbar\omega$ vibrational band with the $2\hbar\omega$. The identification of both 2^+ levels at 2.66 MeV and 2.97 MeV as vibrational levels (one of the $2\hbar\omega$, the other of the $3\hbar\omega$ band?) is less convincing: the E2 contribution is rather low in the 1.81 MeV and 2.13 MeV gamma; but the crossover transitions are weak, indeed.

We are indebted to Prof. C. J. Gorter and Prof. H. Brinkman for their interest, to Dr. H. de Waard for advise on many subjects. We gratefully acknowledge the technical assistance of Messrs. J. van Weesel, A. R. B. Gerritse and B. J. Rigterink. Messrs. P. J. Pasma and J. G. Siekman are gratefully thanked for their help in the irradiation of Mn^{55} and the β-spectrometer experiment. Acknowledgements are also due to Drs. C. Sharp Cook and C. Dulgeroff for communicating their results to us prior to publication. The sources were kindly prepared by Prof. A. H. W. Aten and his staff at the I. K. O., Amsterdam. One of us (J. C. S.) wishes to thank

Prof. C. J. Gorter for the hospitality extended to him while he was at the Kamerlingh Onnes Laboratorium.

This investigation is part of the research program of the "Stichting voor Fundamenteel Onderzoek der Materie (F.O.M.)", which is financially supported by the "Nederlandse Organisatie voor Zuiver Wetenschappelijk Onderzoek (Z.W.O.)". Three of the authors (A.N.D., W.J.H., J.C.S.) took part in this research as members of the scientific staff of the F.O.M.

References

1) L. G. Elliott and M. Deutsch, Phys. Rev. **64** (1943) 321
2) M. Sakai, J. L. Dick, W. S. Anderson and J. D. Kurbatov, Phys. Rev. **95** (1954) 101
3) M. Sakai, Journ. Phys. Soc. Japan **10** (1955) 729
4) L. J. Gallaher, C. E. Whittle, J. A. Beun, A. N. Diddens, C. J. Gorter and M. J. Steenland, Physica **21** (1955) 117; Commun. Kamerlingh Onnes Lab. Leiden No. 298*c*.
5) O. J. Poppema, J. G. Siekman, R. van Wageningen and H. A. Tolhoek, Physica **21** (1955) 223; Commun. Leiden, Suppl. No. 109*b*.
6) R. V. Jones, W. Dobrowolski, and C. D. Jeffries, Phys. Rev. **102** (1956) 738
7) J. M. Baker, B. Bleaney, P. M. Llewellyn and P. F. D. Shaw, Proc. Phys. Soc. A**69** (1956) 353
8) J. D. Kurbatov, H. J. Sathoff, K. Hisatake and M. Sakai, Nuclear Data Cards
9) K. P. Howard, T. A. Pond and P. S. Jastram, private communication to K. Way, R. W. King, C. L. McGinnis and R. van Lieshout, Nuclear Level Schemes $A = 40$ to $A = 92$ (U. S. Government Printing Office, Washington 25, D. C., 1955)
10) F. Metzger and M. Deutsch, Phys. Rev. **78** (1950) 551
11) O. J. Poppema, M. J. Steenland, J. A. Beun and C. J. Gorter, Physica **21** (1955) 233; Commun. Leiden No. 298*b*.
12) R. E. Bell, R. L. Graham and H. E. Petch, Can. J. Phys. **30** (1952) 35
13) L. S. Cheng, J. L. Dick and J. D. Kurbatov, Phys. Rev. **88** (1952) 887
14) J. D. Kurbatov, H. J. Sathoff, K. Hisatake and M. Sakai, Bull. Am. Phys. Soc. **1** (1956) 163
15) C. Sharp Cook and F. M. Tomnovec, Phys. Rev. **104** (1956) 1407
16) M. J. Berger and J. Doggett, J. Res. Nat. Bur. Stand., Wash. **56** (1956) 355
17) H. de Waard, Thesis Groningen University (1954)
18) F. Feenberg and G. Trigg, Rev. Mod. Phys. **22** (1950) 399
19) M. G. Muñoz and D. Maeder, Helv. Phys. Acta **28** (1955) 359
20) C. Sharp Cook and F. M. Tommovec, Bull. Am. Phys. Soc **2** (1957) 24
21) M. A. Rothman, H. S. Hans and C. E. Mandeville, Phys. Rev. **100** (1955) 83
22) W. W. Buechner and A. Sperduto, M. I. T. Annual Progress Report (June 1, 1955 to May 31, 1956)
23) N. R. Steenberg, Proc. Phys. Soc. A **66** (1953) 391
24) U. Fano, Journ. Opt. Soc. Amer. **39** (1949) 859
25) F. W. Lipps and H. A. Tolhoek, Physica **20** (1954) 85, 395
26) N. R. Steenberg, Can. Journ. Phys. **31** (1953) 204
27) G. R. Bishop and J. P. Perez y Jorba, Phys. Rev. **98** (1955) 89
28) C. F. Coleman, Phil. Mag. 1 (1956) 166; Phys. Rev. **103** (1956) 647
29) W. J. Huiskamp, A. N. Diddens, J. C. Severiens, A. R. Miedema and M. J. Steenland, Physica **23** (1957); Commun. Leiden No. 306*e*
30) F. R. Metzger, and W. B. Todd, Phys. Rev. **92** (1953) 904
31) J. C. Wheatley, W. J. Huiskamp, A. N. Diddens, M. J. Steenland and H. A. Tolhoek, Physica **21** (1955) 841; Commun. Leiden No. 301*b*
32) H. A. Tolhoek and J. A. M. Cox, Physica **19** (1953) 101
33) C. D. Hartogh, H. A. Tolhoek and S. R. de Groot, Physica **20** (1954) 1310

34) J. A. M. Cox and H. A. Tolhoek, Physica **19** (1953) 673
35) R. C. Sapp and C. M. Schroeder, Bull. Am. Phys. Soc. **1** (1956) 91
36) C. F. Coleman, Phil. Mag. **46** (1955) 1135
37) G. M. Temmer and N. P. Heydenburg, Phys. Rev. **104** (1956) 967
38) M. Morita, H. Ogata and M. Sakai, Physica **22** (1956) 915
39) J. P. Hurley, S. W. Rudman and P. S. Jastram, Phys. Rev. **98** (1955) 1187
40) G. T. Wood and P. S. Jastram, Phys. Rev. **98** (1955) 1187
41) K. Alder, A. Bohr, T. Huus, B. R. Mottelson and A. Winther, Rev. Mod. Phys. **28** (1956) 432
42) G. Scharff-Goldhaber and J. Weneser, Phys. Rev. **98** (1955) 212
43) L. Wilets and M. Jean, Phys. Rev. **102** (1956) 788
44) J. J. Kraushaar and M. Goldhaber, Phys. Rev. **89** (1953) 1081
45) H. Frauenfelder, N. Levine, A. Rossi and S. Singer, Phys. Rev. **103** (1956) 352
46) P. S. Jastram, C. M. Schroeder and R. C. Sapp, Bull. Am. Phys. Soc. **1** (1956) 172
47) G. Bertolini, E. Lazzarini and M. Mandelli Bettoni, Nuovo Cimento **5** (1957) 356

Nuclear Physics **5** (1958) 89—121; © *North-Holland Publishing Co., Amsterdam*
Not to be reproduced by photoprint or microfilm without written permission from the publisher

AN ANALYSIS OF SLOW NEUTRON RESONANCES IN SILVER

E. R. RAE, E. R. COLLINS, B. B. KINSEY, J. E. LYNN and E. R. WIBLIN
Atomic Energy Research Establishment, Harwell, Didcot, Berks

Received 27 May 1957

Abstract: The spins, radiation widths and neutron widths of ten levels in Ag^{109} and Ag^{110} have been determined from the measurement of total, elastic scattering and radiative capture cross sections for slow neutron resonances with silver, in the range of neutron energy from 1 eV to 135 eV. The experimental measurements are described. The results of these measurements are combined by a least squares method of analysis to obtain an unambiguous assignment of level spin (J) and to derive values for the radiation and neutron widths. Seven levels are found to have $J = 1$ and three to have $J = 0$. The radiation widths appear to be approximately equal in both isotopes and to be independent of the level spins, $J = 0$ or 1. The theoretical implications of these results are briefly discussed.

1. Introduction

In recent years considerable efforts have been directed to the study of the properties of slow neutron resonances. The experimental results, in general, have been analysed on the basis of the Breit-Wigner formula, on the assumption that such levels are caused by s-wave neutrons, are well separated, and do not interfere with one another. These analyses have yielded a large amount of information concerning the resonance parameters in many elements other than those at the lower end of the periodic table. The maxima in the strength function for elements in the region of mass numbers 55 and 160, predicted by the complex potential model of the nucleus, have been observed [1]) and information has been obtained about the distribution of neutron widths and level spacings in several elements. The general variation of the radiation width (observed in slow neutron resonances) with mass number, excitation energy, level density and spin has also been studied (Hughes and Harvey [2]), Landon [3]), Levin and Hughes [4])), but most estimates of this quantity have been made with poor accuracy. Few measurements have been made with accuracy better than about 10 %; most have been for only one resonance in a particular isotope. The only exceptions are the crystal spectrometer studies of In^{115} and Eu^{151} of Landon and Sailor [5]). In these cases two and three resonances, respectively, were measured. The spin of the compound nucleus has been determined for a few isolated resonances (Sailor [6])) but in no case has a spin determination been accompanied by a good measurement of the radiation width for more

than one level in any isotope. There is, as yet, no direct knowledge of the distribution in spin of the levels excited by s-wave neutrons in a single isotope.

This paper describes the investigation, using the Linear Accelerator time-of-flight spectrometer at Harwell, of neutron resonances in silver up to a neutron energy of about 135 eV. Observations of transmission, scattering and capture have been made, and the combined results, including transmission measurements made at Brookhaven [7]) and M.T.R. [8]), have been used to determine the resonance parameters for ten of the first eleven resonances, seven of which belong to the isotope of mass number 109, and four to that of mass number 107. This number of resonances is too small to give statistically sound evidence about the dependence of the level density on spin; it does, however, make possible a comparison between the radiation widths corresponding to levels of the two spin states in either isotope.

2. General Remarks and Notation

The total cross section for neutrons incident with energy E on non-fissile nuclei at rest is the sum of the partial cross sections for elastic scattering and radiative capture:

$$\sigma_t(E) = \sigma_n(E)+\sigma_\gamma(E). \tag{1}$$

The partial cross sections close to a resonance (with spin J) at E_R may be expressed in terms of the Breit-Wigner single-level formulae for s-*wave* collisions with nuclei having spin I:

$$\sigma_n(E) = \pi\lambda\!\!\!^{-}_R{}^2 g \frac{\Gamma_n{}^2}{(E-E_R)^2+(\frac{1}{2}\Gamma)^2} + \frac{4\pi\lambda\!\!\!^{-}_R g\Gamma_n a_J(E-E_R)}{(E-E_R)^2+(\frac{1}{2}\Gamma)^2} +\sigma_p, \tag{2}$$

$$\sigma_\gamma(E) = \pi\lambda\!\!\!^{-}\lambda\!\!\!^{-}_R \frac{\Gamma_n\Gamma_\gamma}{(E-E_R)^2+(\frac{1}{2}\Gamma)^2}, \tag{3}$$

$$g = \frac{2J+1}{2(2I+1)} \qquad (J = I\pm\tfrac{1}{2}). \tag{4}$$

In the above $\lambda\!\!\!^{-}$ is the de Broglie wavelength, divided by 2π, of the relative motion ($\lambda\!\!\!^{-}_R$ at resonance); Γ_n is the neutron width at resonance, Γ_γ the radiation width at resonance, and

$$\Gamma = (\lambda\!\!\!^{-}_R/\lambda\!\!\!^{-})\Gamma_n+\Gamma_\gamma \approx \Gamma_n+\Gamma_\gamma,$$

since, in the cases to be discussed, $\Gamma_\gamma > \Gamma_n$ and the variation of $(\lambda\!\!\!^{-}_R/\lambda\!\!\!^{-})$ is small. Finally,

$$\sigma_p = 4\pi \sum_J g a_J{}^2$$

is the effective potential scattering cross section.

In the following discussion it is assumed that this single level formula is an adequate description. It is convenient to write σ_0, $\sigma_{0\gamma}$, σ_{0n} for the most important contributions to the total, capture and scattering cross sections, respectively, at exact resonance. These quantities are defined by

$$\sigma_0 = 4\pi\lambda_R^2 g\Gamma_n/\Gamma = \sigma_t(E_R) - \sigma_p, \tag{5}$$

$$\sigma_{0\gamma} = \sigma_0\Gamma_\gamma/\Gamma = \sigma_\gamma(E_R), \tag{6}$$

$$\sigma_{0n} = \sigma_0\Gamma_n/\Gamma = \sigma_n(E_R) - \sigma_p. \tag{7}$$

The practical problem of evaluating the above resonance parameters experimentally is complicated by the thermal motion of the target nuclei in the sample (Bethe [9]) and by the finite energy resolution of the neutron spectrometer. These effects, when combined with self-screening and self-absorption in samples of finite thickness, are in general too great to allow the nuclear cross sections to be measured directly. With a sufficiently thin sample, however, the experimental yields of elastically scattered neutrons and of capture radiation, integrated over a resonance, can be shown to be simply related to the product of the total width Γ of the resonance and the peak values of the respective partial cross sections (equations (6) and (7)). This "area" technique is now well known. It has been most thoroughly investigated for the interpretation of transmission measurements, and is discussed in detail by, for example, Hughes [10]) and Lynn and Rae [11]). Stated very briefly, transmission measurements give σ_0 as a function of Γ. From a very thick sample measurement $\sigma_0\Gamma^2$ may be evaluated whilst a very thin sample yields a value for $\sigma_0\Gamma$. In general, therefore, numerical values appropriate to a particular resonance can be obtained for the quantities

$$\sigma_0\Gamma^2 = 4\pi\lambda_R^2 g\Gamma_n\Gamma \quad (T(E_R) \approx 0) \tag{8}$$

and

$$\sigma_0\Gamma = 4\pi\lambda_R^2 g\Gamma_n \quad (T(E_R) \approx 1), \tag{9}$$

where $T(E_R)$ is the sample transmission for neutrons with the resonant energy. Radiative capture measurements with thin samples ($T(E_R) \approx 1$) give the value of $\sigma_{0\gamma}\Gamma$ and scattering measurements with vanishingly thin samples yield $\sigma_{0n}\Gamma$. There are, therefore, at least three, possibly four, experimental quantities from which to derive three parameters, g, Γ_n and Γ_γ. Not all these experimental quantities need be measured with equal accuracy. From (5), (6) and (7),

$$\frac{\sigma_{0\gamma}\Gamma}{\sigma_0\Gamma} = \frac{\Gamma_\gamma}{\Gamma} = 1 - \frac{\Gamma_n}{\Gamma}, \tag{10}$$

$$\frac{\sigma_{0n}\Gamma}{\sigma_0\Gamma} = \frac{\Gamma_n}{\Gamma}. \tag{11}$$

TABLE 1
Transmission measurements on samples of natural silver

E_R (eV)	Isotope	Area of transmission dip in electron-volts						
16.3	107	0.130±0.013	0.369±0.037	0.991±0.042				
30.7	109	0.147±0.022		1.10 ±0.045		1.10±0.035		
41	109			Total = 1.50±0.075	Areas equal within 10 % error			
42	107							
45	107			0.267±0.035				1.17±0.07
52	107	0.230±0.033	0.708±0.085	1.54 ±0.09		1.60±0.05		
56	109		0.438±0.053	1.20 ±0.066		1.22±0.04		3.40±0.19
71	109	0.259±0.041		1.60 ±0.088		1.56±0.08		4.26±0.28
88	109			0.666±0.096		0.57±0.13		1.17±0.16
134	109						4.09±0.16	
140							0.5	
144							1.34±0.08	
Sample Thickness (No. of atoms per cm² normal to beam)		4.17×10^{20}	1.49×10^{21}	8.42×10^{21}	8.84×10^{21}	1.18×10^{22}	3.74×10^{22}	7.43×10^{22}
Length of Flight Path (Metres)		11.48	20.86	11.48	55.6	20.74	55.6	20.86
Resolution (μsec per metre)		0.175	0.096	0.175	0.018	0.096	0.018	0.096
Reference in table 4		A_1	A_2	A_3	A_4	A_5	A_6	A_7

In principle (and in practice) transmission measurements will give $g\Gamma_n$ and Γ, but at least one of the other measurements is required to evaluate explicitly g, Γ_n and Γ_γ. If $\Gamma_\gamma \gg \Gamma_n$ equation (10) shows that a relatively inaccurate measurement of Γ_n/Γ (equation 11) gives a better determination of Γ_γ/Γ than the direct capture experiment, equation (10). If $\Gamma_n \gg \Gamma_\gamma$ then $\Gamma_n/\Gamma \approx 1$ and the correct choice of g can be inferred from (8) or (9), but the capture measurement is needed to determine Γ_γ accurately. In section 6 of this paper a method of combining the observations of $\sigma_0\Gamma^2$, $\sigma_0\Gamma$, $\sigma_{0\gamma}\Gamma$ and $\sigma_{0n}\Gamma$ to yield the best set of self consistent values for g, Γ_n and Γ_γ is described. For silver the values of $\sigma_{0n}\Gamma$ for the resonance scattering are crucial, but they are the most troublesome to measure.

3. Transmission Measurements

The linear accelerator (Wiblin [12])) provides a neutron pulse of about 0.6 μsec duration (Lynn, Firk and Moxon [13])) at the source with a repetition frequency of 400 pulses per second. Neutron flight path lengths vary from 11 to 56 metres. Timing channels for sorting the detected neutrons into velocity groups are of either one or two μsec duration.

Details of the measurement of the neutron transmission, $T(E)$, through natural silver are shown in table 1. The nominal resolution is the full width of the resolution function at half maximum. Typical experimental transmission curves are shown in figures 1 and 2.

Area analyses were made of the dips in these curves. They were carried out with the aid of theoretical curves given by Hughes [10]). The method of analysis may be described briefly. First, points between the resonances were averaged to give a "normalisation level" of transmission which was assumed, as a first approximation, to be attributed to the potential scattering cross section, σ_p. The whole transmission curve was divided by the value of the "normalisation level". The area of a dip was found by summing the experimental values of $(1-T(E))$ over the dip between two cut-off points (chosen at positions where the normalised transmission was greater than 0.9). The value of the Doppler coefficient (Lamb [14])) was calculated, a value of Γ was assumed, and a first approximation to the value of $\sigma_0\Gamma^2$ was found for the resonance from the curves of Hughes. This value of $\sigma_0\Gamma^2$ was used to calculate the "wing correction" (i.e. the area of the transmission dip included in the wings of the resonance beyond the arbitrary cut-off points) and also to correct the "normalisation level" for resonance contributions. Successive approximations to $\sigma_0\Gamma^2$ were made in this way for a number of different values of Γ. Further details of the method are given by Lynn and Rae [11]).

The two resonances at about 41 eV were incompletely resolved in the measurements on the 11 and 20 metre flight paths. Thin sample measure-

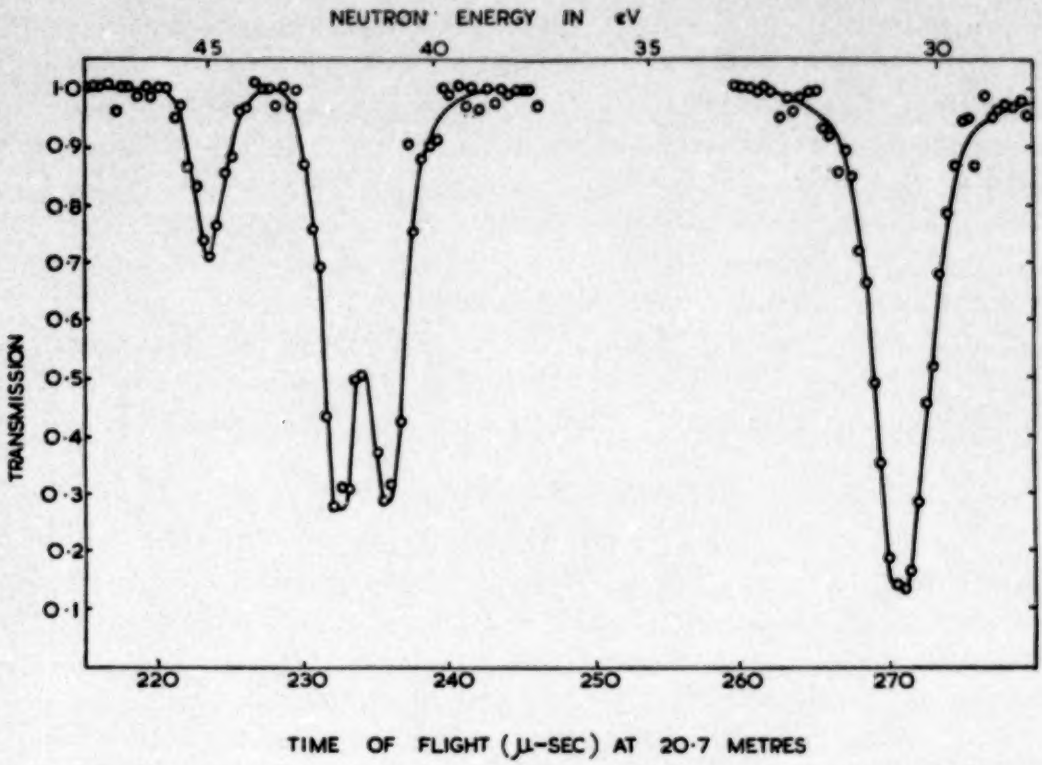

Fig. 1. Transmission of a natural silver sample (1.18×10^{22}) atoms/cm^2) measured at 20.7 metres. The 41 and 42 eV resonances are evidently of similar strength.

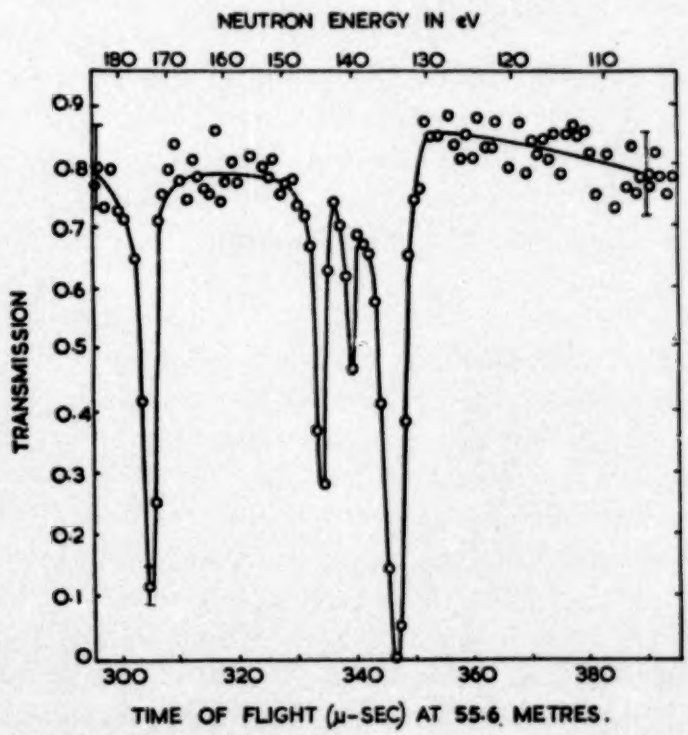

Fig. 2. Transmission of a natural silver sample (3.74×10^{22} atoms cm^2/measured at 55.6 metres. The resonances at 134, 140 and 144 eV are well resolved.

ments made by Grimm [15]), with a resolution of the order of 0.02 μsec per metre, show that these resonances have values of $\sigma_0\Gamma$ which are very nearly equal. The present measurements made on a thicker sample with a resolution of 0.018 μsec per metre, show that, in addition, the values of $\sigma_0\Gamma^2$ are approximately equal. The more accurate measurements of the combined transmission dip using the shorter flight paths were then used with the information on the relative values to obtain absolute values of the parameters $\sigma_0\Gamma^2$ and $\sigma_0\Gamma$ for these two resonances.

The isotopic assignment of the resonances was fixed by observing radiative capture from samples of the separated isotopes (Rae and Bowey [16])) supplied by the Electromagnetic Separator group at A.E.R.E.

4. Scattering Measurements

The resonance scattering was measured by comparing the number of neutrons counted in an annular detector surrounding a thin silver sample with the number counted from a sample of pure lead (which has a known and constant cross section). Provided that precautions are taken to ensure that the scattering geometry is the same in both cases the absolute values of the incident neutron intensity and of the detector efficiency do not need to be known. The detected scattering events were recorded in a multi-channel time-of-flight analyser so as to give the yield of scattered neutrons as a function of the incident neutron energy.

Doppler and resolution effects were eliminated by evaluating the area under the resonance yield (see § 2, above). Complications introduced by the necessity for measuring the scattering from samples of finite thickness were eliminated by extrapolating the observed areas, measured as a function of sample thickness, to zero sample thickness.

4.1. THE DETECTOR

The detector consisted of eighteen boron trifluoride proportional counters containing approximately 45 g of boron-10. These have the advantage of giving perfect discrimination between scattered neutrons and capture gamma-rays. They were arranged to form an annular detecting volume effectively 38 cm long by 30 cm outside diameter and 13 cm inside diameter. The detector assembly was mounted in an aluminium chamber which, together with the neutron collimators, was evacuated by a diffusion pump. The axis of the detector was accurately aligned with the axis of the collimated neutron beam, and the samples, in the form of flat foils normal to the neutron beam, were placed at the centre of the detector. The complete assembly (figure 3) was heavily shielded with 1½ tons of boric oxide. The background, measured with no sample in the chamber, was closely proportional to the total machine output during a run and was less than 0.5 % of the total

flux from the collimated beam incident on the scattering sample.

The overall detector efficiency for an isotropic point source of 1 eV neutrons at the centre of the detector was calculated to be approximately $12\frac{1}{2}\%$ and for neutron energies greater than 1 eV the efficiency varied

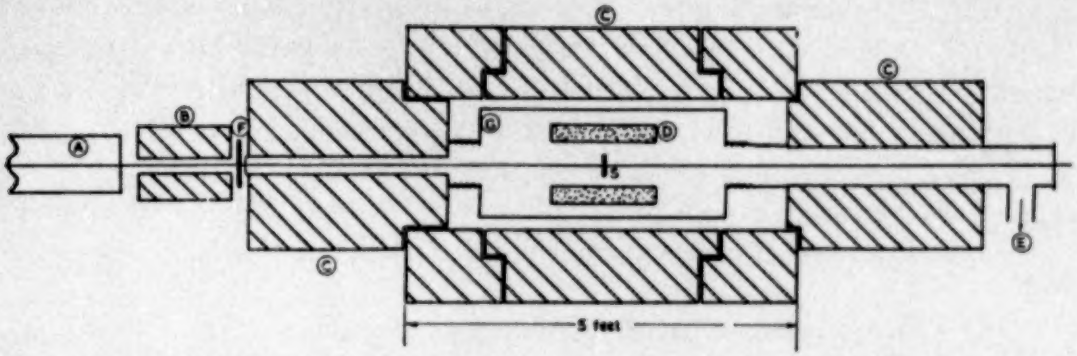

Fig. 3. General arrangement of the scattering apparatus. A, evacuated flight path; B, final collimator, C, boric oxide shielding; D, active volume of neutron detector; E, diffusion pump; F, boron or cadmium filter; G, vacuum chamber; S, scattering sample.

approximately as $E^{-\frac{1}{2}}$. A neutron incident on the sample with energy E will enter the detector with an energy $E' < E$ after scattering. The consequent increase in detector efficiency, after averaging over all angles of scattering, is just $(A+1)/A$ per collision, where A is the mass number of the scattering nucleus. This effect is sufficiently small to be neglected when comparing the scattering from silver with that from lead.

The counts recorded in the time-of-flight channels were normalised to the neutron output of the machine by comparison with the counts recorded from beam monitor BF_3 counters. These were placed inside a well shielded enclosure surrounding one of the four collimating apertures disposed along the flight path. The monitor counts were shown to be proportional to the neutron beam entering the scattering chamber. Efficient monitoring of this neutron flux was most important, particularly since many runs took several days to complete. Three independent monitor circuits were used and the overall stability of the electronics was checked by observing the constancy from run to run of the ratios of the counts observed in each of the three monitor systems.

4.2. METHOD OF MEASUREMENT

Typical portions of yield curves for single foil samples are shown in figure 4. Channel widths were nominally 2 μsec and the runs were interlaced to give points 1 μsec apart. In curves (b) and (c) the resonance contributions to the total scattering from natural silver are visible above the general level caused by the sum of the effective potential scattering(σ_p) and the background (curve b) observed with no sample in the chamber. It is evident that the resonance scattering yields are not linear functions of sample

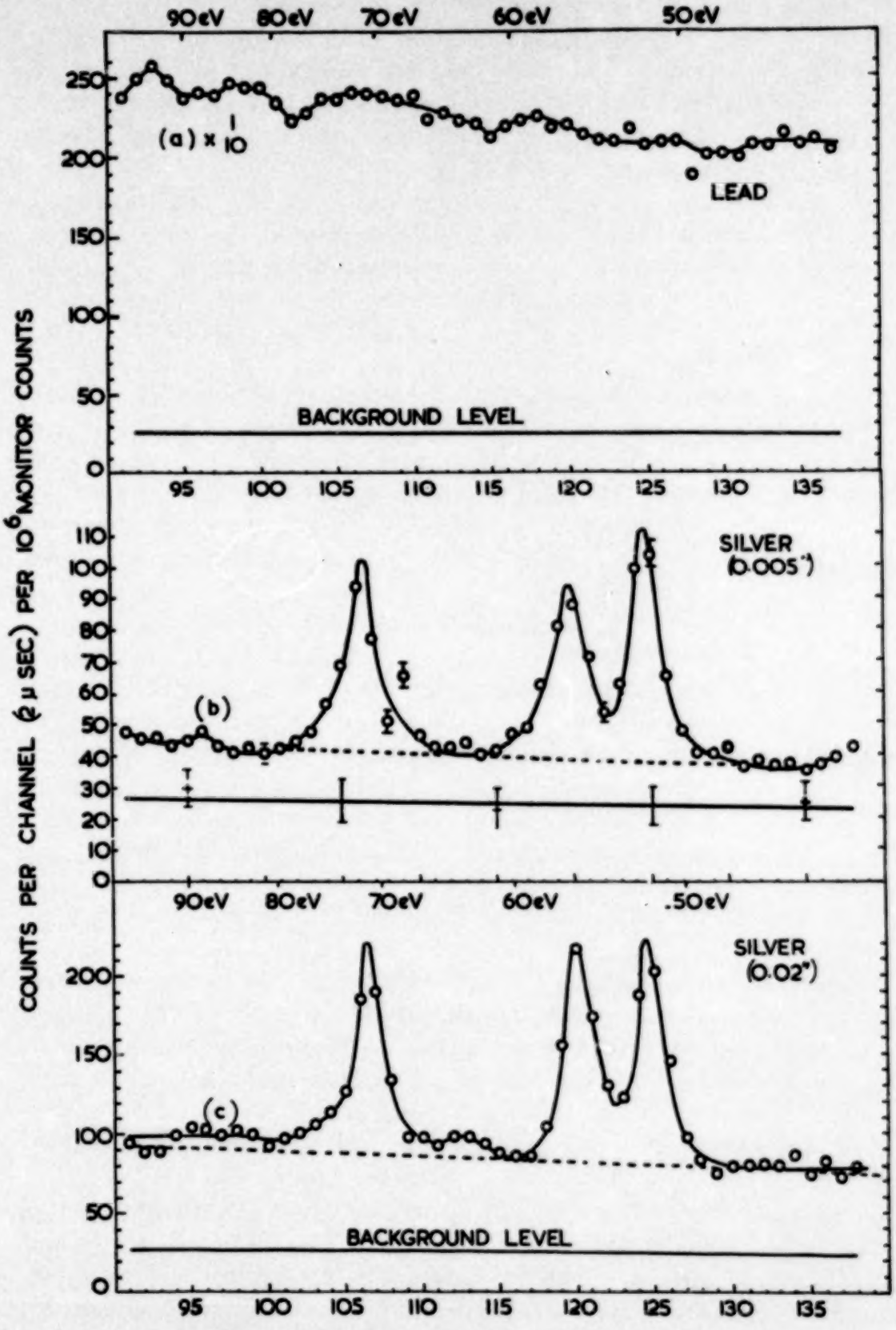

Fig. 4. Typical scattering results. Yields obtained from (a), lead sample of 7.815×10^{22} atom/cm^2 (b), natural silver sample of 8.02×10^{20} atom/cm^2; (c) natural silver sample of 2.99×10^{21} atom/cm^2.

The solid lines sketched through the experimental points have no quantitative significance. The statistical S.D. on the experimental points in (a) and (c) is approximately equal to the diameter of the circles as plotted.

thickness. This is to be expected because the attenuation of the beam by the sample depends exponentially on the thickness and, more important, the loss of scattered neutrons through multiple collisions is proportionally larger in the thicker samples. (Radiative capture is the predominant process in resonances below 100 eV in silver).

Quantitative analysis of the measurements is based on the theoretical yield of a very thin sample in which self absorption is negligible. If $T(E)$ is the transmission of a sample (of N nuclei/cm^2) for incident neutrons of energy E, then the fraction scattered elastically is $\{1-T(E)\}\sigma_n(E)/\sigma_t(E)$ per incident neutron of energy E. This reduces to $N\sigma_n(E)$ per incident neutron for sufficiently thin samples; that is when $T(E) \approx 1$. The resonant scattering cross section $\sigma_n(E) - \sigma_p$ (see equations (2) and (7) above), when integrated between limits E_1 and E_2 ($E_1 = E_R - \frac{1}{2}\Gamma x$ and $E_2 = E_R + \frac{1}{2}\Gamma x$) symmetrical about the resonance energy, E_R, is equal to $\sigma_{0n}\Gamma \tan^{-1} x$. It is shown in appendix 1 that this quantity is obtained from the experimentally measured areas in the limit of vanishingly thin samples independently of instrumental resolution, of Doppler effect and of radiative capture in the sample.

4.3. AREA MEASUREMENT

In order to evaluate the resonant scattering it is necessary to subtract from the total yield the slowly varying contributions from potential scattering and background. This requires some care, since an incorrect estimate of this *"zero level"* (broken lines, fig. 4) can lead to a large systematic error in the evaluation of the resonance area, particularly if the resonance is weak. The zero level was determined from the counts recorded between well resolved resonances, where the samples were always extremely thin. The shape of the zero level and its value at intermediate points was determined by interpolation in comparison with the observed dependence of the lead scattering on time-of-flight. An objective test of the zero levels so estimated was made for each sequence of experimental runs by plotting the estimated zero level count, averaged over several adjacent channels, against the sample thickness; N atoms/cm^2. A consistent set of zero level estimates fitted a straight line which passed through the background point at $N = 0$. The slope of the line determines the effective potential scattering cross section and values consistent with $\sigma_p = 5.2 \pm 0.3$ barn were obtained.

The choice of the limits E_1, E_2 (corresponding times-of-flight τ_1, τ_2), between which the area under a resonance is evaluated, is to some extent arbitrary, provided that the interval $|E_2 - E_1|$ is greater than the resolution width and much greater than the width of the Doppler broadened resonance. In practice the limits were determined by the extent to which resonances were resolved and by the counting statistics.

4.4. CALIBRATION MEASUREMENTS

The channel counts obtained with a lead scattering sample, give, when plotted against time-of-flight, a curve in which the ordinates are everywhere proportional to the product of the neutron spectrum, detector efficiency and the individual channel widths.

If N' be the number of lead nuclei per cm^2 and σ' cm^2 be the cross section, then the fraction scattered by the lead is equal to $1-\exp(-N'\sigma') = f_{\mathrm{Pb}}$. This fraction is constant since the lead cross section is independent of energy and radiative capture may be neglected [17]). Subsidiary experiments showed that the observed yield was a linear function of f_{Pb} in the range of thicknesses used for calibrating the scattering chamber.

Ideally, the ratio of the *resonance* count (c), in a given channel, to that produced by a lead scatterer (c') in the same channel is equal to the ratio of the respective fractions scattered from the incident beam. In general the width of a timing channel in energy units (ΔE) is comparable with or greater than the resonance width Γ. The fraction scattered from the resonance, therefore, by a very thin sample into a channel of width ΔE is $\int_E^{E+\Delta E} N\{\sigma_{\mathrm{n}}(E)-\sigma_{\mathrm{p}}\}\mathrm{d}E$. Thus for a thin sample, $c/c' = N\int_E^{E+\Delta E}\{\sigma_{\mathrm{n}}(E)-\sigma_{\mathrm{p}}\}\,\mathrm{d}E/(f_{\mathrm{Pb}}\cdot\Delta E)$. The quantity determined experimentally was the sum $\sum_{\tau_1}^{\tau_2}(c/c')\Delta\tau$. This is the area under the resonance peak between times-of-flight τ_1 and τ_2, corresponding respectively to the limits E_1 and E_2 previously discussed. $\Delta\tau$ is the interval between the experimental points. In the ideal case of vanishingly small thickness ($N \to 0$) this area is equal to

$$N\sigma_{0\mathrm{n}}\Gamma\tan^{-1}x(\tau_{\mathrm{R}}/2E_{\mathrm{R}})/f_{\mathrm{Pb}}. \tag{12}$$

Scattering samples of finite thickness were necessary to obtain a measurable yield, therefore the area under the resonance curve multiplied by f_{Pb}/N ($= A_N$ say) was plotted against N and extrapolated to zero thickness to find the value (A_0) of A_N corresponding to $N = 0$. Fig. 5 shows some typical examples of this empirical extrapolation. The values for $\sigma_{0\mathrm{n}}\Gamma$ in table 2 were then calculated from the thin sample formula (12):

$$\sigma_{0\mathrm{n}}\Gamma = \frac{2E_{\mathrm{R}}}{\tau_{\mathrm{R}}}\cdot\frac{A_0}{\tan^{-1}x}\ \mathrm{cm^2\ eV/nucleus}.$$

4.5. EFFECTS OF SELF ABSORPTION

In the geometry described, neutrons scattered in the sample may suffer one or more additional collisions before they escape to the detector. In the silver resonances below 130 eV capture is more probable than scattering ($\Gamma_\gamma > \Gamma_{\mathrm{n}}$) and a sample thick enough to scatter a measurable fraction of the incident neutrons may, therefore, absorb many of the scattered neutrons before they can escape to the detector. An exact calculation of this self absorption effect is complicated, because at energies near a narrow resonance

the collision mean free path is very sensitive to small changes in the neutron energy. The small energy loss per collision in laboratory space depends on the thermal motion of the target nucleus and is, therefore, not a simple

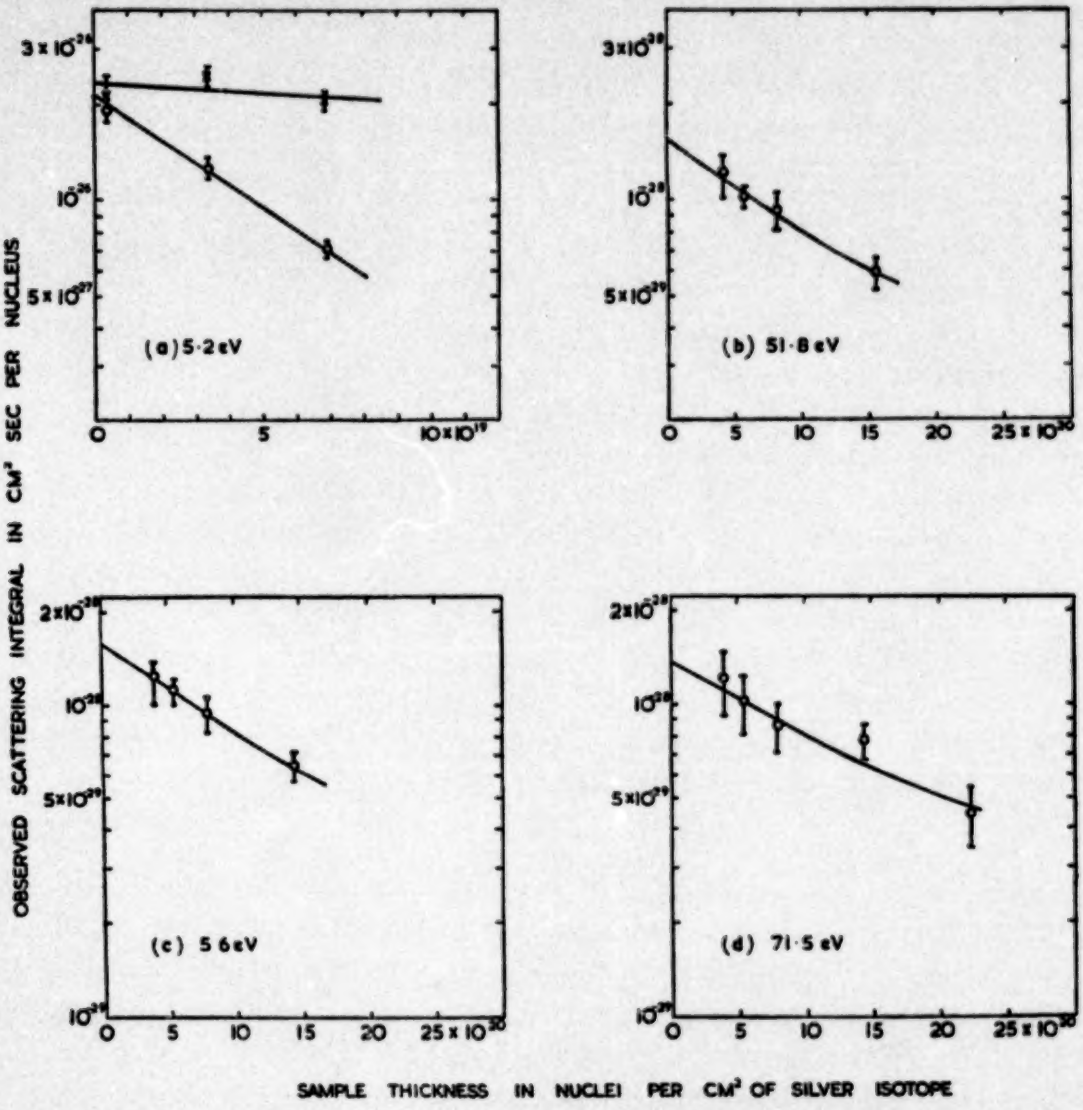
OBSERVED SCATTERING INTEGRAL IN CM² SEC PER NUCLEUS
(a) 5·2 eV
(b) 51·8 eV
(c) 5·6 eV
(d) 71·5 eV
SAMPLE THICKNESS IN NUCLEI PER CM² OF SILVER ISOTOPE

Fig. 5. Typical extrapolations, to zero thickness, of the resonance scattering integral. The semi-log plot is used for convenience in displaying the results. The points, shown as crosses, in diagram (a) show the result of applying the corrections, calculated by the Monte Carlo method, for finite sample thickness.

function of the angle of scattering. An approximate first order calculation of the self absorption is, however, given in appendix 1. The average energy shift is approximately 2 % per collision in silver and it is, therefore, even for the 5.2 eV resonance, comparable with the resonance width Γ. This means that a large proportion of the neutrons, scattered from collisions in which $E \leqq E_R$, has a longer collision mean-free-path after the collisions than before it. This effect has a practical advantage in that the self ab-

sorption near a resonance is much less than it would be if there were no energy shift. The effect is clearly shown in the scattering curve (fig. 6) for a sample which is thick enough to give "line reversal" at the 5.2 eV resonance.

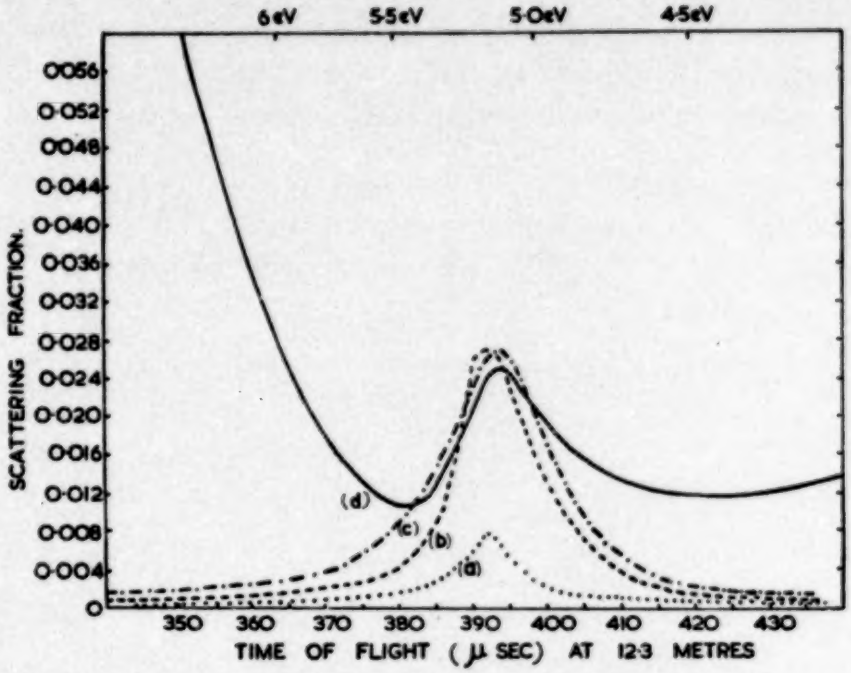

Fig. 6. Scattering from natural silver samples in the region of the 5.2 eV resonance. Smooth curves, sketched through the experimental points, are shown to illustrate the effects of self absorption in samples of finite thickness. The solid curve (d) illustrates "line reversal" from a very thick sample and the rise in yield caused by the "energy-shift" effect on neutrons incident close to the resonant energy. (a), 7.48×10^{18} atom/cm^2; (b), 6.86×10^{19} atom/cm^2; (c), 1.40×10^{20} atom/cm^2; (d), 3.73×10^{22} atom/cm^2.

To check the reliability of the empirical extrapolation to zero thickness the scattering yield from the 5.2 eV resonance for thin and moderately thick samples was treated by a Monte-Carlo analysis (Morton [18])). The 5.2 eV resonance was chosen for this study since the resonance parameters were already well established and the self absorption is large. Doppler broadened resonance parameters were used but thermal motion was neglected in computing the energy shifts following collisions. The variation of detector efficiency with angle of escape from the sample was included. The results of this analysis were used to correct the experimental points shown in figure (5a). The least-squares fitted straight line drawn through the three corrected experimental points (crosses) is not quite horizontal but it is in good agreement, within the estimated standard errors, with the value of the area previously found by empirical extrapolation of the uncorrected points. Calculated first order correction for both the 5.2 eV and the 16 eV resonances also indicated that the empirical extrapolation

procedure could be used with confidence. The method was, therefore considered sufficiently reliable to use in deriving $\sigma_{0m}\Gamma$ for other resonances.

An attempt was made to minimize the effect of self absorption by disposing very thin foils spaced equidistantly along the detector axis, instead of using a single foil at the centre. The counting rate observed from such multiple samples was, however, not significantly different from that observed from single foil samples of the same equivalent thickness. Results from the two sample arrangements were in good agreement.

4.6. RESULTS

The results from the scattering measurements are summarized in table 2. The numerical value of $\sigma_{0n}\Gamma$ quoted for the 16.3 eV resonance is derived

TABLE 2

Scattering measurements on natural silver

Resonant Energy (eV)	Target Isotope	Number of Sample Thicknesses	$\sigma_{0n}\Gamma$ (barn-eV)
5.2	109	3	419±41
16.3	107	1	32±6
30.7	109	5	18±2
41	109	5	7.8±1.3
42	107	5	7.8±1.3
45	107	—	No result
52	107	5	100±8
56	109	5	87±6
71	109	5	120±9
88	109	1	≈18
134	109	5	620±56

from one good measurement on a 0.005″ sample. The correction factor for finite thickness and self absorption applied to the observed area was 1.96, computed numerically to first order (see appendix 1). This exception to the general procedure was adopted because during a sequence of later runs on this resonance an intermittent fault in the time-of-flight spectrometer was suspected. The 41 eV and 42 eV resonances were not resolved, but it was assumed (see § 3) that their scattering contributions were equal. Similarly the strong 134 eV resonance in Ag^{110} could not be separated from the weak resonances at about 140 eV and 144 eV. The transmission measurements showed, however, that these could not contribute more than 3 % to the total scattering when combined with the 134 eV resonance (see table 1). The 45 eV resonance scattering yield was too weak to measure. The 88 eV resonance scattering was also very weak and the value quoted cannot be claimed to be more than a rough estimate. It was derived by comparing the observed yields in the 88 eV and 71.5 eV resonance peaks during a long run on a 0.005″ sample. The absolute values quoted for $\sigma_{0n}\Gamma$ depend

on the cross section of 11.4 barn assumed for lead and the assigned errors are statistical standard errors.

5. Capture Measurements

The neutron capture data was obtained from measurements of capture gamma-ray yields by the method described by Rae and Bowey [16]). The gamma-rays were detected in sodium iodide crystals placed round the sample and all pulses above a certain bias were counted. The yield, obtained as a function of neutron time-of-flight, was corrected for the known shape of the neutron spectrum and calibrated against the yield at the 5.2 eV resonance from a thick sample; that is, from one in which radiative capture results from nearly 100 % of the neutrons incident near this resonant energy. The details of the calibration, the reduction of results and the variation in detector efficiency for the gamma-rays from different resonances is discussed elsewhere [16]).

Three sample thicknesses of natural silver (0.001, 0.002 and 0.020 inch) were examined at a flight path distance of 11.48 metre. The yields from the two thinner samples were used to determine $\sigma_{0\gamma}\Gamma$ for all of the resonances in the range 12 eV to 135 eV. The thickest sample was used for the very weak resonances at 45 eV and 88 eV. The levels at 41 eV and 42 eV were not resolved but were assumed to be of equal strength. In all cases the samples were thin at the resonance energies and corrections for self-screening were applied by using the curves prepared by Roe [19]). The results, summarized in table 3, differ from those previously published [16]) in that the value for $\sigma_{0\gamma}\Gamma$ for the 56 eV resonance has been revised and a result for the 134 eV resonance is included.

TABLE 3

Capture measurements on natural silver

Resonance Energy (eV)	Target Isotope	$\sigma_{0\gamma}\Gamma$ (barn-eV)
16.3	107	498±30
30.7	109	485±34
41	109	281±28
42	107	281±28
45	107	51±7
52	107	882±62
56	109	284±34
71	109	684±49
88	109	131±9
134	109	720±108

6. Analysis of Results

The method of combining the results of experiments of the type mentioned above has already been described (Rae [20]), Lynn and Rae [11])). Briefly, each of the combinations of parameters obtained for a given resonance $\sigma_0\Gamma$, $\sigma_{0n}\Gamma$, $\sigma_0\Gamma^2$, etc., defines a relationship between Γ_n and Γ for that resonance. If one of the two possible values of the statistical weight factor (g) be selected, then these relationships can be represented by curves in the Γ_n, Γ plane. For the correct value of g, these curves should be concurrent. In practice, exact concurrence is very improbable, but in the case of a target nucleus of spin $\frac{1}{2}$, such as silver, the "degree of concurrence" obtained with one g-value is generally markedly better than that obtained with the other, and the correct solution can be obtained by inspection. To place the selection of the correct g-value on a more quantitative basis, a least-squares method of comparison has been used. This indicates which

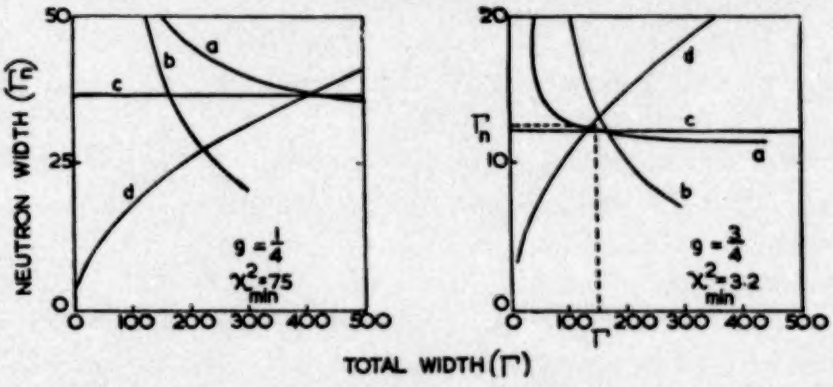

Fig. 7. Combination of the experimental data to determine Γ_n and Γ for the 5.2 eV resonance in Ag^{110} and the appropriate statistical weight factor, g. Ordinate and abscissa scales are in milli-electron-volts. Curves show the variation of Γ_n with Γ as determined by: (a), radiative capture in a thin sample; (b), thick sample transmission; (c), thin sample transmission; (d), elastic scattering. (See § 2, equations (5), (6), (7), (8), (9)).

result is more probable, and also determines the most probable values of Γ and Γ_n.

Each of the curves referred to above determines Γ_n as a function of Γ. An error, which is taken to be a standard deviation, is associated with each curve such that for any chosen value of Γ, it indicates the standard deviation in Γ_n. Consider the point (Γ'_n, Γ') in the Γ_n, Γ plane and define the quantity

$$\chi^2(\Gamma'_n, \Gamma') = \frac{(\Gamma'_n - {}_1\Gamma_n)^2}{{\delta_1}^2} + \frac{(\Gamma'_n - {}_2\Gamma_n)^2}{{\delta_2}^2} + \cdots$$

where δ_1, δ_2, etc. are the standard deviations in the values $({}_1\Gamma_n, {}_2\Gamma_n$, etc.) of Γ_n determined by each of the experimental curves. The function $\chi^2(\Gamma'_n, \Gamma')$ is calculated for chosen values of Γ' with Γ'_n as variable, and a family of curves plotted for different values of Γ' as parameter. One family is obtained

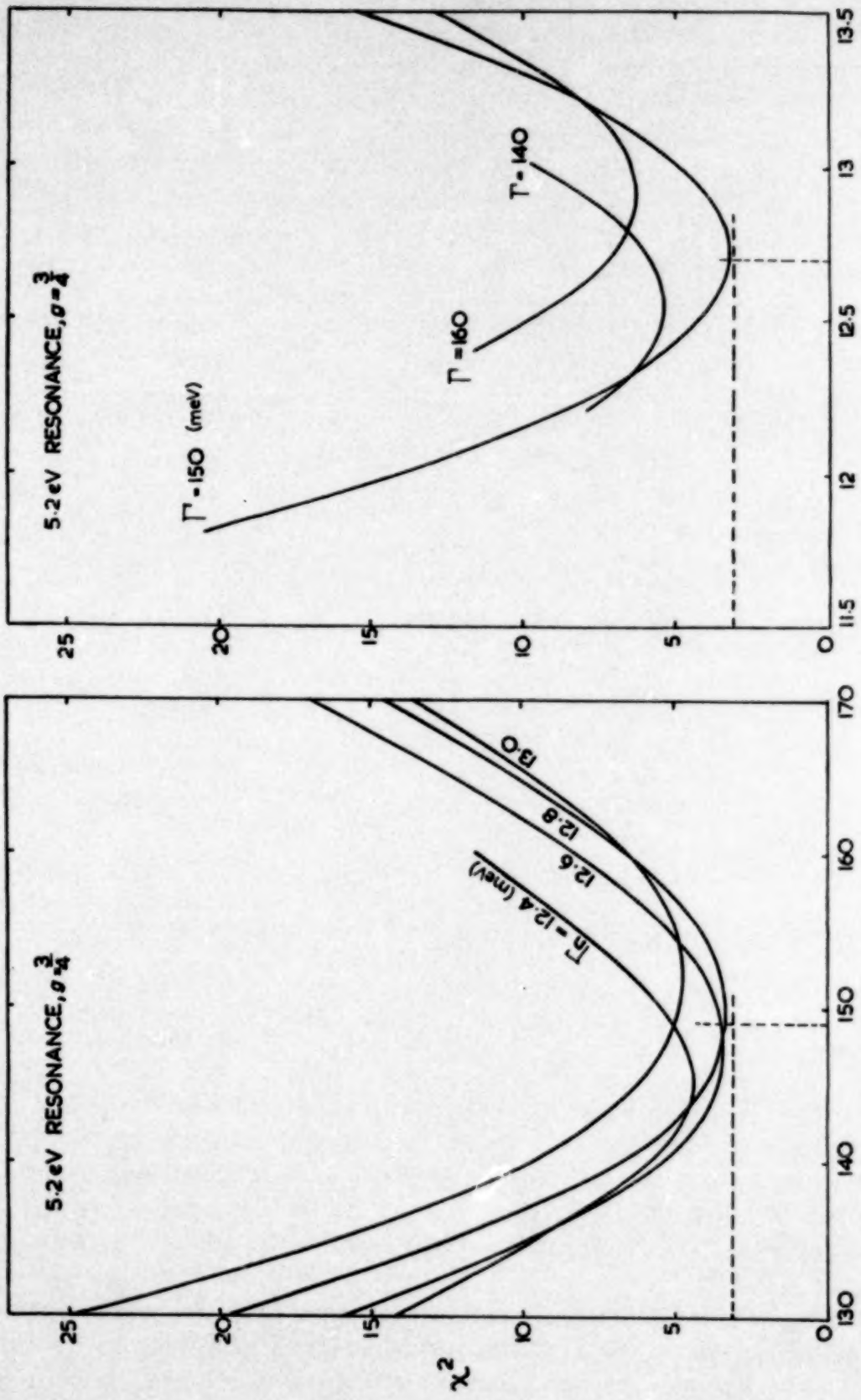

Fig. 8. The function $\chi^2(\Gamma''_n, \Gamma'')$ of § 6 plotted against Γ''_n (for different Γ'') and against Γ'' (for different Γ''_n). χ^2 was calculated from the experimental data on the assumption that $g = \frac{3}{4}$.

for each g-value and in each such diagram there is a pair (Γ''_n, Γ'') which makes $\chi^2(\Gamma''_n, \Gamma'')$ an absolute minimum, χ^2_{min}. There are, thus two such absolute minima; the diagram with the lower value of χ^2_{min} indicates the more likely g-value and the corresponding values of Γ''_n, Γ'' are the most probable values of Γ_n and Γ. The standard deviations in Γ_n and Γ can be estimated from the curvature of the χ^2 surface in the appropriate plane.

Consider for example the 5.2 eV resonance. The experimental data are shown in figure 7. The scattering and capture curves are based on the Harwell results, but in this case the transmission results are taken from

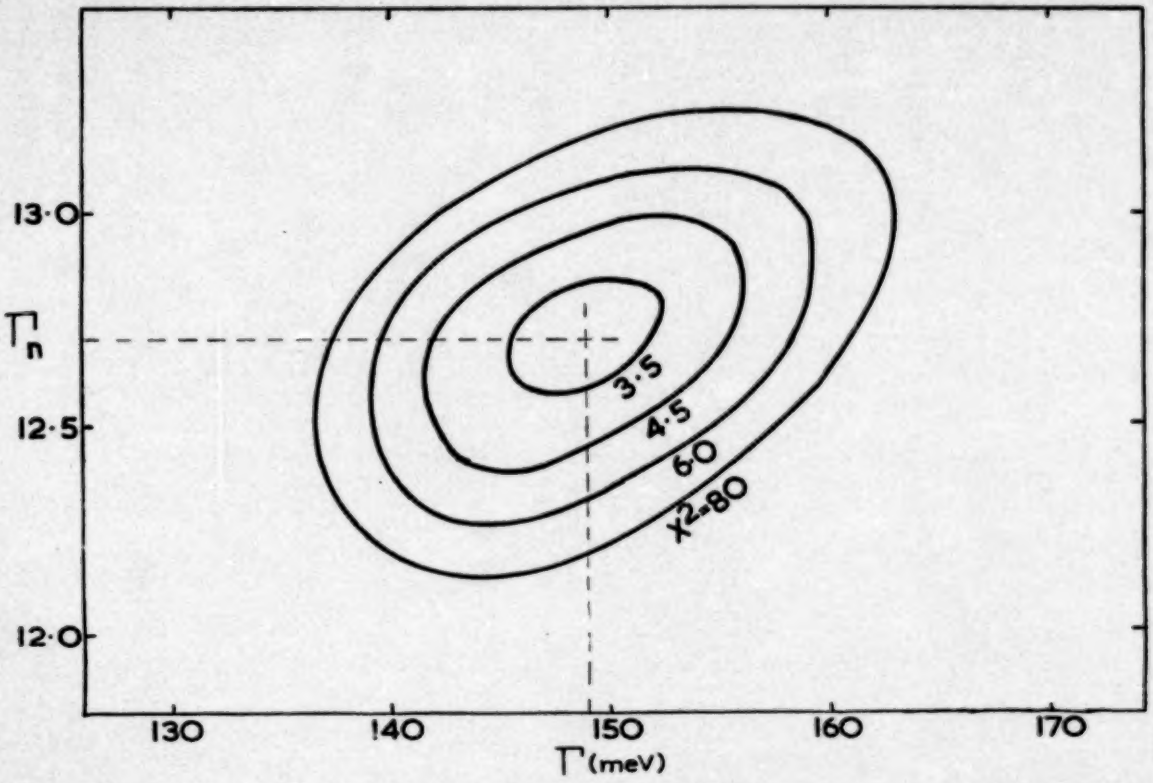

Fig. 9. Contours of χ^2 = constant plotted in the Γ, Γ_n plane for the 5.2 eV resonance ($g = \frac{3}{4}$). The best values of Γ_n and Γ are obtained from the estimated centre of these contours.

Seidl *et al.* [7]). It will be seen that the correct g-value is clearly $g = \frac{3}{4}$ since for this value of g the curves intersect in a small area, while for $g = \frac{1}{4}$ the spread is much larger than is consistent with the standard deviations on the curves. The value of χ^2_{min} for $g = \frac{3}{4}$ is 3.2, while that for $g = \frac{1}{4}$ is 75. The probability of obtaining a value of χ^2_{min} greater than 75 is extremely small.

Fig. 8 shows X^2, for $g = \frac{3}{4}$, plotted as a function of Γ_n for a range of values of Γ and vice versa. The best values of Γ_n, Γ are obtained from the estimated centre of the set of contours of equal χ^2 (see fig. 9) derived

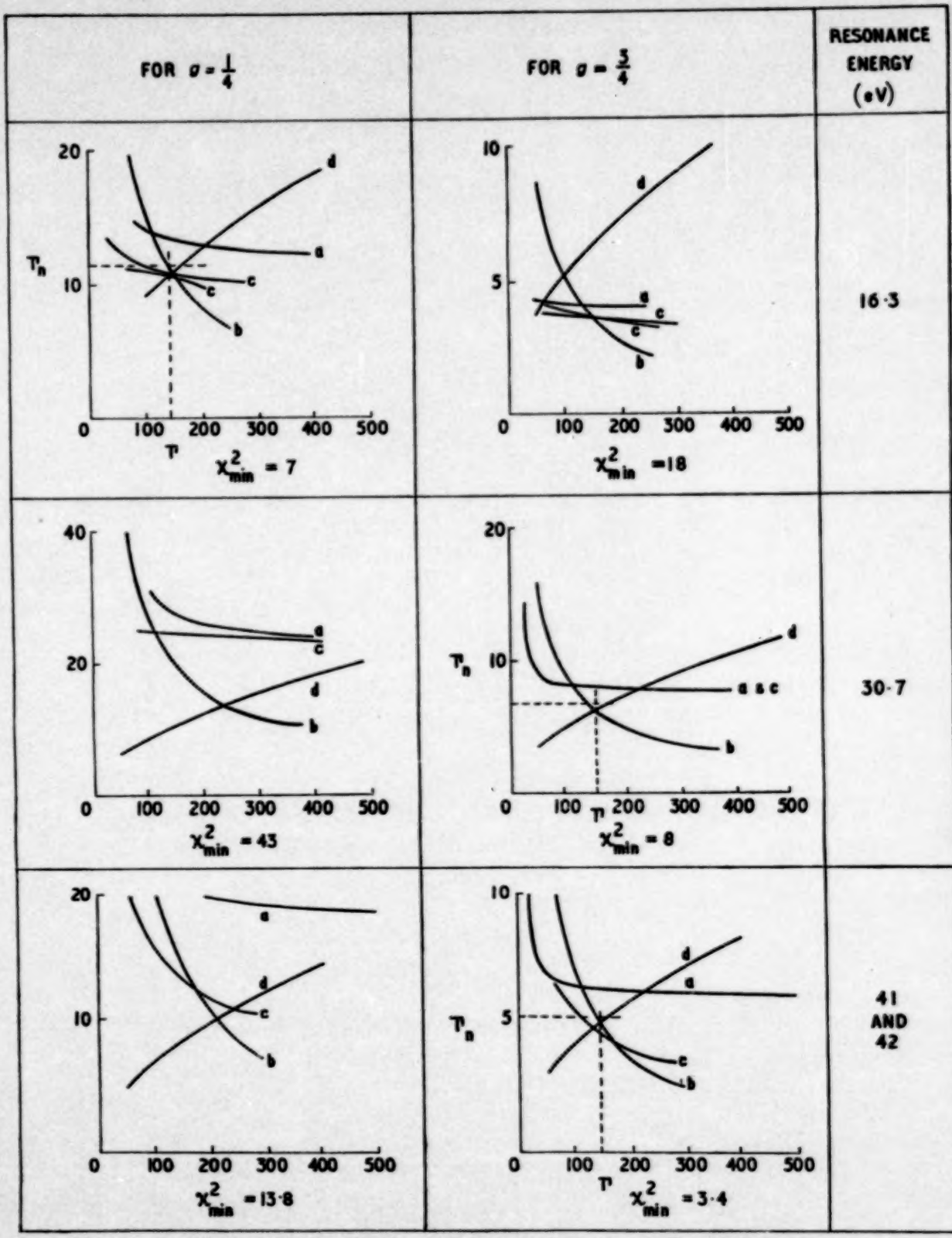

Fig. 10. Combination of the experimental data to determine g, Γ_n and Γ for resonance at 16.3, 30.7, 41 and 42 eV. Ordinates, Γ_n in meV; abscissae, Γ, in meV.
The curves are derived from measurements of: (a) radiative capture; (b), thick sample transmission; (c), thin sample transmission; (d), elastic scattering.

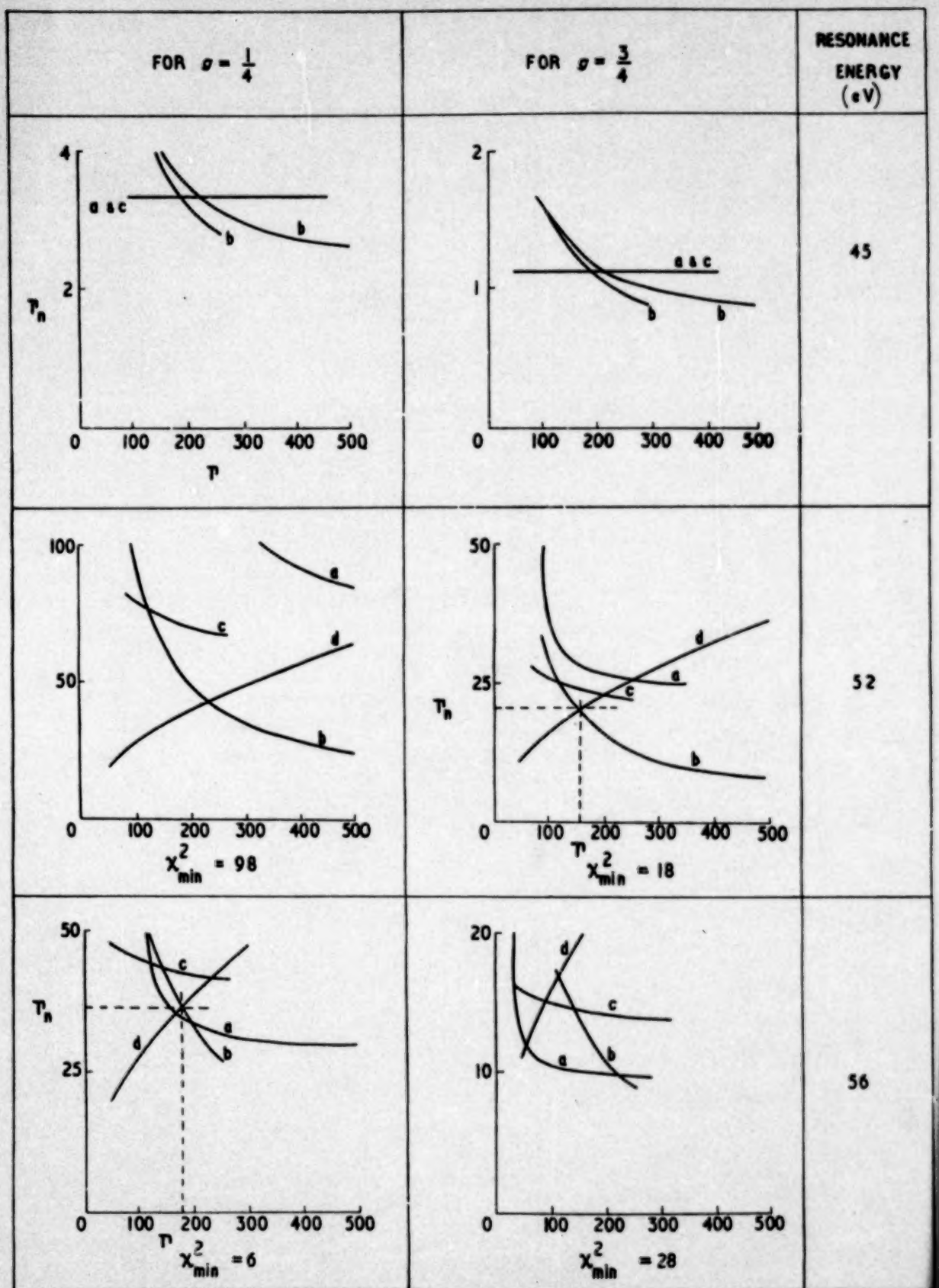

Fig. 11. Combination of the experimental data to determine g, Γ_n and Γ for resonances at 45, 52 and 56 eV. Ordinates, Γ_n, in meV; abscissae, Γ, in meV.
The curves are derived from measurements of: (a), radiative capture; (b), thick sample transmission; (c), thin sample transmission; (f), elastic scattering.

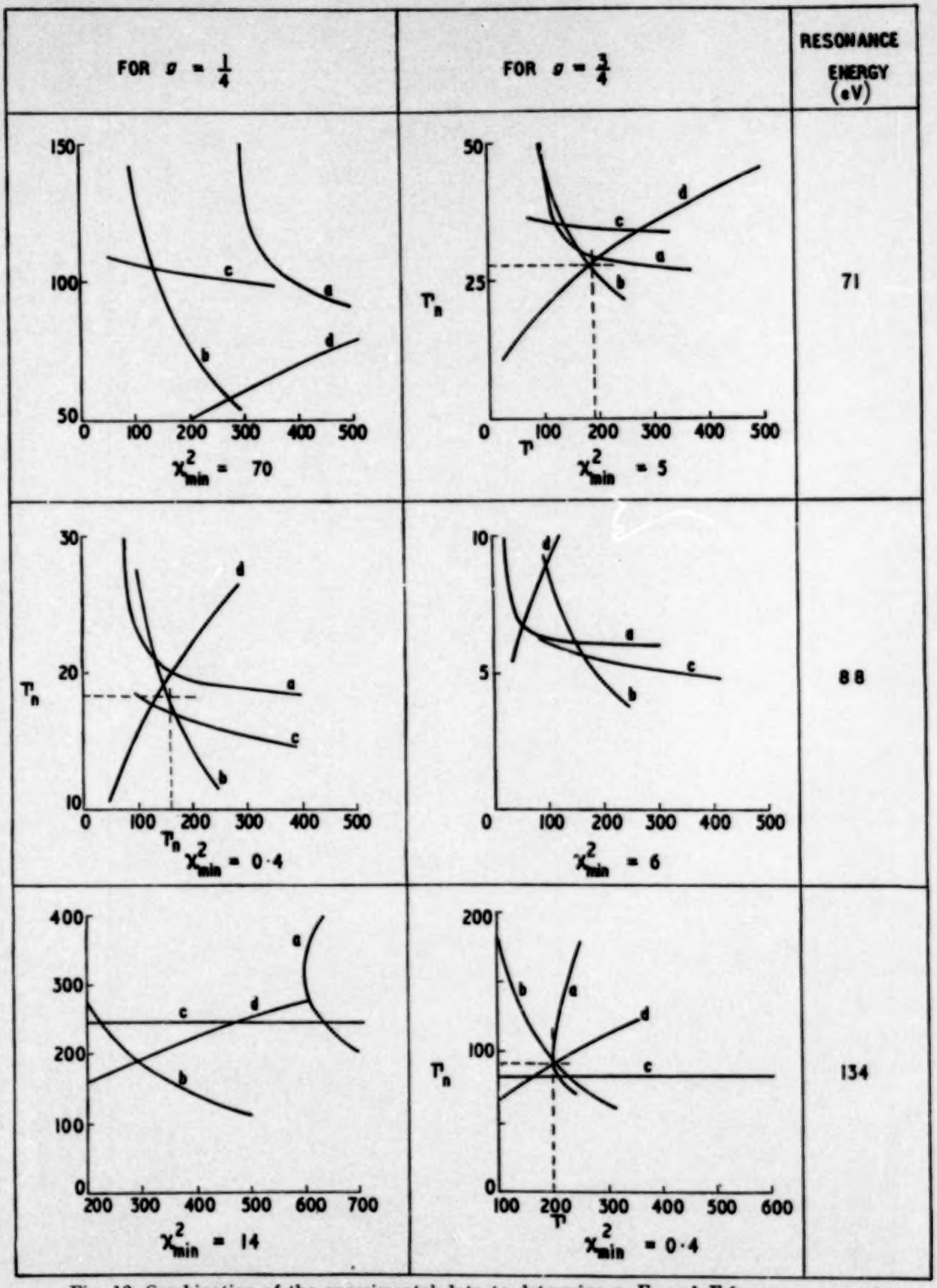

Fig. 12. Combination of the experimental data to determine g, Γ_n and Γ for resonances at 71, 88 and 134 eV. Ordinates, Γ_n, in meV; abscissae, Γ, in meV.
The curves are derived from measurements of: (a), radiative capture; (b), thick sample transmission; (c), thin sample transmission; (d), elastic scattering.

TABLE 4

Information obtained from experimental data

E_R (eV)	Isotope	χ^2_{min} $g = \frac{1}{2}$	χ^2_{min} $g = \frac{3}{2}$	Degrees of Freedom	Preferred g-value	Γ (meV)	Γ_n (meV)	Γ_γ (meV)	Reference to Data †			
									Transmission (thick)	Transmission (thin)	Scattering	Capture
5.2	109	75	3.2	2	$\frac{1}{2}$	149±7.8	12.7±0.23	136±7.8	B 6.4 %	B 4.3 %	A 10 %	A 4.3 %
16.3	107	7	18	3	$\frac{1}{2}$	143±9	11.4±0.41	132±9	A_3, B 8.4 % 11.7 %	A_1, A_2 10 % 10 %	A 7 %	A 6 %
30.7	109	43	8	2	$\frac{3}{2}$	149±13	6.7±0.43	142±13	A_3 + A_5 + B 82 % 6.4 % 11.5 %	A 15 %	A 5.6 %	A 7 %
41 42	109 107	13.8	3.4	2	$\frac{3}{2}$	142±19	5.0±0.40	137±19	A_3, B 12 % 25 %	—	A 10 %	A 10 %
						for each resonance						
45	107	—	—	—	—	≈ 200	—	≈ 200	A_7 + B 12 % 20 %	A_3 13 %	—	A 14 %
52	107	98	18	3	$\frac{3}{2}$	157±16	20.8±9.4	136±16	A_3 + A_5 + B 12 % 6 % 20 %	A_1, A_2 15 % 12 %	A 3 %	A 7 %
56	109	6	28	3	$\frac{1}{2}$	180±11	36.3±1.4	144±11	A_3 + A_5 + B 11 % 6.8 % 26 % + A_7 11 %	A_2 12 %	A 3.4 %	A 12 %
71	109	70	5	3	$\frac{3}{2}$	190±6	27.8±6.5	162±6	A_3 + A_5 + B 11 % 10.4 % 20 % + A_7 12 %	A_1 16 %	A 3.1 %	A 7 %
88	109	0.4	6	3	$\frac{1}{2}$	158±21	18.3±1.4	140±21	A_7, B 18 % 24 %	A_3, A_5 20 % 23 %	A 15 %	A 7 %
134	109	14	0.4	2	$\frac{3}{2}$	199±12	93 ±7	106±14	A_6 8 %	C 18 %	A 9 %	A 15 %

† (1) "A„ indicates authors' work and A_1, A_2 etc. refer to the transmission measurements specifed in table 1.
(2) "B" indicates Brookhaven data[7]).
(3) "C" indicates M.T.R. data[8]).
(4) The standard errors assigned to the respective values of $\sigma_0 \Gamma^2$, $\sigma_0 \Gamma$, $\sigma_{0n} \Gamma$ and $\sigma_{0\gamma} \Gamma$ used in computing the tabulated values of Γ, Γ_n and χ^2_{min} are indicated by the percentages below the reference symbol.

from the curves of fig. 8. The errors were estimated from the curvature of the envelope of the sections of the χ^2 surface by planes normal to the Γ_n and Γ axes using the formula: var $x = 2/(\partial^2\chi^2/\partial x^2)$. The results are

$$\Gamma = 149 \pm 7.8 \text{ meV},$$

$$\Gamma_n = 12.7 \pm 0.23 \text{ meV}.$$

The experimental data for the remaining ten resonances examined are shown in figures 10, 11 and 12. The information obtained from the diagrams for all the resonances is given in table 4.

In most cases several thick sample transmission measurements have been combined to give a single curve, while in a few cases two thin sample measurements have been combined. (To give an impression of the degree of consistency of the transmission data, values of $\sigma_0\Gamma^2$ and $\sigma_0\Gamma$ have been calculated and are listed in appendix 2).

Column 5 of table 4 lists the number of degrees of freedom — the number of curves in the diagram more than is required for a theoretical solution of Γ_n and Γ for *given* g. It will be noted that χ^2_{min} has been obtained in some cases for a distribution with two degrees of freedom and in others for three degrees of freedom. These cases correspond to four and five curves in the Γ_n, Γ diagrams.

The standard errors on Γ and Γ_n (Column 7, 8) have been calculated, as mentioned above, from the curvature of the χ^2 surface near the minimum. In those cases where χ^2_{min} was rather high (presumably because of a systematic error in an experimental measurement) and corresponded to a probability less than 0.05 of obtaining a higher value of χ^2_{min}, then the standard error estimated from the curvature was increased by the factor $\{\chi^2_{min}(\text{observed})/\chi^2_{min}(0.05)\}^{\frac{1}{2}}$.

The two levels at 41 and 42 eV have been assumed to be equal in all respects. As mentioned in Section 3 the values of $\sigma_0\Gamma^2$ and $\sigma_0\Gamma$ are known to be very nearly equal for the two resonances. In addition the scattering yield observed is less than that predicted from the measured transmission and capture results for either possible g-value. (The theoretical scattering yield $\sigma_{n0}\Gamma$ is greater if $g = \frac{1}{4}$ than if $g = \frac{3}{4}$). Had the spins been different one would have expected a scattering yield lying between those predicted by $g = \frac{3}{4}$ and $g = \frac{1}{4}$ respectively. The experimental results therefore indicate that $g = \frac{3}{4}$ for both levels.

7. Discussion

Evidence on the spin dependence of the level density and any correlation of radiation widths with level spin or neutron number in adjacent isotopes is of particular interest in the development of a satisfactory statistical

Γ_n and χ^2_{min} are indicated by the percentages below the reference symbol.

description of the highly excited nucleus. The radiation widths (Γ_γ) are grouped with respect to spin and isotope in table 5.

TABLE 5

Radiation widths, level spin and isotope

Isotope	$J=0$	$J=1$
Ag^{108}	132 ± 9 meV	137 ± 19 meV 136 ± 16
Ag^{110}	144 ± 11 140 ± 21	162 ± 6 142 ± 13 137 ± 19 136 ± 8 106 ± 14 (Mean = 137 meV)

The evidence, meagre though it is, does indicate that there are more levels with $J = 1$ than $J = 0$, that there is no marked isotope effect on the radiation width and that the radiation widths are independent of spin. That the widths should be independent of the spin is not unexpected; that they should appear to be the same in each isotope is more surprising. It is worth while discussing the implications of the above tentative conclusions to emphasize, if for no other reason, the importance of collecting more systematic data on radiation widths.

The total radiation width must be compounded out of the numerous partial radiation widths corresponding to individual transitions. If $\langle\Gamma_{\gamma p}(E)\rangle$ is the average *partial* radiation width for a transition with energy E, from an initial state with spin J to a final state with spin J' and if the density of final states (with spin J') is $\varrho_{J'}(B-E)$, where B is the neutron binding energy, the total radiation width must be

$$\Gamma_\gamma = \int_0^B \sum_{J'} \varrho_{J'}(B-E)\langle\Gamma_{\gamma p}(E)\rangle \mathrm{d}E \tag{13}$$

summed over all possible values of J' which will combine with the initial state. There is experimental evidence [21]) that, at least for thermal neutrons and for the higher energy γ-rays, dipole radiation is more probable than quadrupole radiation, that E1 radiation is more probable than M1 radiation and that the partial widths of individual γ-rays are proportional to the level spacing in the vicinity of the initial state, as predicted by Blatt and Weisskopf [22]). Thus (13) can be written

$$\Gamma_\gamma = C\int_0^B \sum_{J'} \varrho_{J'}(B-E)E^3/\varrho_J(B)\mathrm{d}E \tag{14}$$

where C is a constant.

Brink [23]) has pointed out that, if the densities of levels with spin J are

proportional to $(2J+1)$, as would be expected from elementary theories of level densities, the expression (14) is independent of J. This may be easily verified, by evaluation of the sum: $\sum_J \varrho_J(E)$, which, for dipole radiation, gives

$$\sum_J \varrho_J(E) = 3(2J+1)\varrho_0(E).$$

Thus

$$\Gamma_\gamma = 3C \int_0^B \varrho_0(B-E)/\sigma_0(B)E^3 \mathrm{d}E \tag{15}$$

and is independent of J. Thus the observed constancy of the radiation widths in the silver isotopes suggests that the level densities are indeed proportional to $(2J+1)$. This conclusion assumes, however, that the average partial width can be written

$$\langle \Gamma_{\gamma p}(E) \rangle = CE^3/\varrho(B) \tag{16}$$

with the constant C independent of J. There is no experimental evidence which permits one to conclude that the average partial radiation widths are independent of J; moreover, Lane [24]) has questioned the theoretical basis of this assumption. The proportionality of the level density with the factor $(2J+1)$ is, however, well founded theoretically, at least for small values of J ($J < 3$ or 4). The present results therefore suggest that (16) is indeed independent of J.

The fact that the widths are the same for the two isotopes is more difficult to understand. If the radiation width given by (15) is calculated on the basis of the theoretical level density formula [25]),

$$\varrho(E) \propto \exp\,[-(aE)^{\frac{1}{2}}]/(E+\theta)^2 \tag{17}$$

(where a and θ are constants), the radiation width is sensitive to the neutron binding energy B. This formula is known from other evidence to give a fairly good account of the energy dependence [25]). For silver, a numerical computation (with $a = 50$ MeV^{-1} and $\theta = 0.5$ MeV) shows that the radiation width should increase at approximately 30 percent per MeV of binding energy when $B \approx 7$ MeV. We should expect, therefore, that the widths for the heavier isotope (Ag^{109}) should be smaller than those of the lighter isotope (Ag^{107}). The difference between the neutron binding energies of the two product nuclei is not known from direct measurement, but appears to be about 0.5 MeV [26]); this should lead to a difference of about 15 percent between the widths for the two isotopes. The radiation width, if given by a formula of the type (15), remains indepedent of the level density if the latter is changed by a simple multiplicative factor. To account for the equality of the radiation widths in the two different isotopes it is necessary to assume that the energy variation of level density is different in the two isotopes, and that the density in Ag^{110} increases with energy

less rapidly then in Ag^{108}. If true this difference must be ascribed to a difference in the argument of the exponential term in (17); such differences might be anticipated, for Newton [27]) has shown that the influence of shell structure on level density can be accounted for by making the constant a in (17) proportional to the product of the statistical weights of the spins of the unpaired protons and neutrons remaining in an unclosed shell. Differences in the rate of increase of level density of the silver isotopes, therefore, might be ascribed to differences in the neutron configurations.

If the level density in Ag^{110} increases less rapidly than in Ag^{108}, one would expect the level density in Ag^{110} at the neutron binding energy to be less than that of Ag^{108}. In fact, the opposite is true. This is indicated by the larger number of levels which have been ascribed to Ag^{109} targets (see table 4); it is confirmed by the higher capture cross sections of Ag^{109} compared with Ag^{107} [17]). If this difference in level density were caused by a simple multiplicative factor in (17) it would be possible to reconcile the differences in level densities at the binding energy with the equality of the radiation widths. It would, then, be necessary to find an explanation of the difference in level densities in the two nuclei, which, at low energies, have an almost identical structure.

It seems more likely that radiation widths cannot be represented by a formula as simple as (15). When the constant C is derived from the data of thermal neutron capture radiation, this formula, as shown elsewhere [28]), gives values which are consistently too high. In deriving this formula it is assumed that partial radiation widths, when corrected by the cube of the energy, can be averaged as if all could be treated on an equal footing. The present results indicate that this assumption may not be well founded.

In the extensive programme of experimental work described the authors acknowledge much direct assistance from their immediate colleagues as well as most helpful discussions from workers in other laboratories. In the former category are Messrs. R. W. Ford, S. A. Ferris, J. E. Evans, F. W. K. Firk, M. C. Moxon, J. W. Jagger, J. F. Gallagher and Miss E. M. Bowey, together with Miss P. A. Browne who did much of the computation.

Special help has been given by Prof. W. W. Havens of Columbia University, New York and by Dr. D. J. Hughes of Brookhaven National Laboratory, in providing advance information of their experimental results, and by Drs. J. V. Jelley and E. B. Paul in criticism of the manuscript.

Finally, the authors would wish to express their appreciation of the continued support of Dr. E. Bretscher as Head of the Nuclear Physics Division, AERE.

Appendix 1

THE APPLICATION OF AREA ANALYSIS TO SCATTERING MEASUREMENTS

1) *The effect of instrumental resolution*

If $Y(x)$ be the true yield, which would be obtained by scanning the neutron resonance spectrum with an apparatus of perfect resolution, then the actual spectrometer produces an observed yield given by

$$Y_{\text{obs}}(x) = \int_{x-a}^{x+b} Y(x')R(x'-x)\mathrm{d}x'$$

where $R(x)$ is the instrumental resolution function of total width $a+b$ and normalized so that $\int_a^b R(x)\mathrm{d}x = 1$. The measured area under a resonance peak between limits x_1 and x_2 is

$$\int_{x_1}^{x_2} Y_{\text{obs}}(x)\mathrm{d}x = \int_{x_1}^{x_2} \mathrm{d}x \int_{x-a}^{x+b} Y(x')R(x'-x)\mathrm{d}x'.$$

Writing $y = x'-x$, $Y(x')$ can be expanded in a Taylor series about x to give

$$\int_{x_1}^{x_2} Y_{\text{obs}}(x)\mathrm{d}x = \int_{x_1}^{x_2} Y(x)\mathrm{d}x + C_1\{Y(x_2)-Y(x_1)\} + C_2\{Y'(x_2)-Y'(x_1)\}+\cdots \quad \text{(A)}$$

provided that the functional form of $R(x'-x)$ is idependent of x. Since the resolution function, $R(x)$, is, to a good approximation, of a symmetrical gaussian or triangular shape, the odd coefficients $C_1 \approx C_3 \approx \cdots \approx 0$, and (A) becomes

$$\int_{x_1}^{x_2} Y_{\text{obs}}(x)\mathrm{d}x \approx \int_{x_1}^{x_2} Y(x)\mathrm{d}x \quad \text{(B)}$$

if the limits x_1 and x_2 are chosen so that the slopes at x_1 and x_2 (i.e. $Y'(x_1)$ or $Y'_{\text{obs}}(x_1)$ etc.) are small.

2) *The Doppler Effect and extrapolation to zero thickness*

The incident neutron energy (E) is measured in laboratory co-ordinates and the effective nuclear cross sections are not given exactly by equations (2) and (3) of § 2 because the thermal motions of the nuclei in the sample cannot be neglected when the cross section is a rapidly varying function of the relative collision energy (i.e. near the peak of a sharp resonance). If the target nuclei were at rest the transmission of a sample N nuclei/cm^2 thick is

$$T(E) = \exp\{-N\sigma_t(E)\}, \text{ or } T(x) = \exp\{-N\sigma_t(x)\}$$

in terms of the variable $x = 2(E-E_R)/\Gamma$. The true sample transmission near an isolated resonance is

$$T(x) = \exp\left[-N\left\{\sigma_0\psi(x,\eta) + \frac{2a_J\sigma_0}{\lambda_R}\cdot\frac{x}{1+x^2} + \sigma_p\right\}\right] \quad \text{(C)}$$

where $\psi(x, \eta)$ is the well known Doppler integral [9, 29]).

Equation (C) gives $T(x)$ with good accuracy provided that the contributions from other resonances can be included in the constant term σ_p. The fraction scattered from the incident beam in primary collisions is

$$F(E, N) = \{1-T(E)\}\sigma_n(E)/\sigma_t(E).$$

The fraction observed, $f(E, N)$, is less than this because of self absorption in escaping from the sample, but the integral of the observed scattering fraction taken over a sufficiently wide range $E_1 < E_R < E_2$ may be written as

$$\int_{E_1}^{E_2} f(E, N)\mathrm{d}E = \Phi(N)\int_{E_1}^{E_2} F(E, N)\mathrm{d}E \qquad \text{(D)}$$

where $\Phi(N)$ is a correction factor which, for a *particular* resonance, scattering geometry and range of integration, depends only on the sample thickness N. In § 3 of this appendix it is demonstrated that $\Phi(N) \to 1$ as $N \to 0$.

The empirical extrapolation to zero thickness, discussed in §§ 4.3 and 4.4, is equivalent to finding the limit as $N \to 0$ of $(1/N)\int_{E_1}^{E_2}\{f(E, N)-N\sigma_p\}\mathrm{d}E$. But from (D)

$$\begin{aligned} A_0 = \lim_{N\to 0}\frac{1}{N}\int_{E_1}^{E_2}\{f(E, N)-N\sigma_p\}\mathrm{d}E &= \lim_{N\to 0}\frac{\Phi(N)}{N}\int_{E_1}^{E_2}\{F(E, N)-N\sigma_p\}\mathrm{d}E \\ &= \int_{E_1}^{E_2}\left[\lim_{N\to 0}\frac{1}{N}\{1-T(E, N)\}\frac{\sigma_n(E)}{\sigma_t(E)}-\sigma_p\right]\mathrm{d}E \\ &= \frac{\Gamma}{2}\int_{-x}^{x}[\sigma_{0n}\psi(y, \eta)+\{(1+y^2)\psi(y, \eta)-1\}\sigma_p]\mathrm{d}y \end{aligned}$$

using equations (1), (2), (C), the fact that $\psi(x, \eta) = \psi(-x, \eta)$ and on choosing the limits, E_1, E_2 symmetrically about E_R so that $E_1 = E_R-\frac{1}{2}\Gamma x$ and $E_2 = E_R+\frac{1}{2}\Gamma x$. Since $(1+y^2)\psi(y, \eta)$ is of order unity and $\sigma_{0n} \gg \sigma_p$, the second term in the integrand is very small compared with the first term. The extrapolated area, measured in energy units, is, thus, to a good approximation

$$A_0 = \sigma_{0n}\Gamma\int_0^x \psi(y, \eta)\mathrm{d}y \sim \sigma_{0n}\Gamma\tan^{-1}x$$

for sufficiently large x (> 10).

3) *First order scattering*

Consider a sample in the form of a thin flat disc of area greater than the collimated neutron beam incident perpendicularly on it. Consider monoenergetic neutrons with energy E and having a collision mean free path l. The number making nuclear collisions at a depth between z and $z+\mathrm{d}z$ (fig. 13) is $(\mathrm{d}z/l)\exp(-z/l)$ per incident neutron. The fraction which is scattered elastically is, therefore,

$$\frac{\sigma_n(E)}{\sigma_t(E)}\frac{dz}{l}\exp\left(-\frac{z}{l}\right) \qquad \text{(E)}$$

and from equations (1) and (2) of § 2, $\mu = \sigma_n(E)/\sigma_t(E) \approx \Gamma_n/\Gamma =$ constant. The differential cross section in c. of m. co-ordinates is isotropic but in laboratory space it is approximately proportional to $(1+(2/A)\cos\theta)$ for target

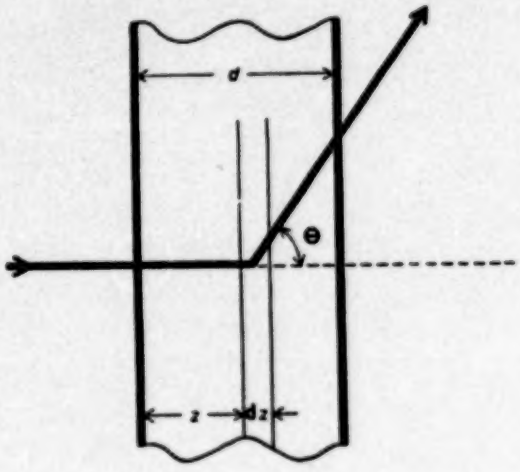

Fig. 13. The scattering geometry for primary collisions.

nuclei of mass number $A \gg 1$ or $(1+0.02\cos\theta)$ in a silver sample. This degree of anisotropy will be neglected. The fraction scattered into θ to $\theta+d\theta$ is, therefore,

$$\mu \exp(-z/l)(dz/l)\tfrac{1}{2}\sin\theta d\theta. \qquad \text{(F)}$$

After scattering from a nucleus of mass number A the neutron has energy E' given by

$$E'/E \approx 1-(2/A)(1-\cos\theta) \quad \text{to } O(A^{-2}) \qquad \text{(G)}$$

if the thermal motions of the target nuclei are ignored. (The analysis is much more complicated if the thermal motion is included in the calculation of the energy shift). The mean free path l' after scattering through the angle θ is not, in general, the same as that (l) before collision. The probability that the scattered neutron will escape without making another collision is

$$\begin{aligned} &\exp\{-(d-z)\sec\theta/l'\} \quad &&\text{for } 0 \leqq \theta \leqq \pi/2, \\ &\exp\{-z\sec(\pi-\theta)/l'\} \quad &&\text{for } \pi/2 \leqq \theta \leqq \pi. \end{aligned} \qquad \text{(H)}$$

The number of once-scattered neutrons which escape from the sample between θ and $\theta+d\theta$ is therefore the product of expressions (F) and (H) integrated between $z = 0$ and $z = d$. This integral is

$$\mu \cdot \nu(E,\theta)\mathrm{d}\theta = \frac{\mu}{2}\sin\theta\mathrm{d}\theta \frac{\exp\left(-\frac{d}{l}\right) - \exp\left(-\frac{d}{l'}\sec\theta\right)}{(l/l')\sec\theta - 1} \quad (0 \leqq \theta \leqq \pi/2)$$
$$= \frac{\mu}{2}\sin\theta\mathrm{d}\theta \frac{1 - \exp\left\{-\frac{d}{l} - \frac{d}{l'}\sec(\pi-\theta)\right\}}{(l/l')\sec(\pi-\theta)+1} \quad (\pi/2 \leqq \theta \leqq \pi) \qquad \text{(I)}$$

giving the number of these neutrons per neutron incident on the sample with energy E. Near a resonance at energy E_R of width Γ, total resonant cross section σ_0 and Doppler coefficient η in a sample of thickness N nuclei/cm^2,

$$l/l' = \psi(x', \eta)/\psi(x, \eta),$$
$$d/l = N\sigma_0 \cdot \psi(x, \eta)$$

and

$$d/l' = N\sigma_0\psi(x', \eta),$$

where

$$x = 2(E - E_R)/\Gamma \quad (= 0 \text{ at resonance})$$

and from equation (G)

$$x' = 2(E' - E_R)/\Gamma$$
$$\approx x - (4E_R/\Gamma A)(1 - \cos\theta).$$

4) *Self absorption loss of neutrons*

The fraction of the incident beam scattered in primary collisions is, from equation (F),

$$F(E) = \int_0^\pi \mathrm{d}\theta \int_0^d (\mu/l)\exp(-z/l)\,\tfrac{1}{2}\sin\theta\mathrm{d}z$$
$$= \mu\{1 - \exp(-d/l)\}. \qquad \text{(J)}$$

The fraction which actually escapes from the sample is

$$f(E) \geqq \mu\int_0^\pi \nu(E, \theta)\mathrm{d}\theta \qquad \text{(K)}$$

and, from relations (I), (J) and (K), $\lim_{d\to 0} f(E)/F(E) = 1$ independently of the energy E. The self absorption correction factor, $\Phi(N)$ in equation (D), therefore, also goes to unity as $N\sigma_0 \to 0$.

The number of neutrons which survive a second collision in the sample is proportional to μ^2 and, if radiative capture is more probable than scattering ($\mu \approx \Gamma_n/\Gamma \ll 1$), then the first order (using the equality sign in (K) above) will be a good approximation. The analytical calculation of the fraction surviving after second and higher order collisions in a sample of finite thickness, when the average energy shift at a collision ($\langle \Delta E \rangle \approx -2E/A$) is comparable with Γ, leads to very heavy numerical computation. It is

more economical to carry out a Monte Carlo experiment if higher order corrections are desired.

5) *Calculation of the first order correction to the resonance area*

The detector collects neutrons between $\theta = \theta_0$ and $\theta = \pi - \theta_0$ with relative efficiency $\varepsilon(\theta)$. The variation in detector efficiency with neutron energy ($\propto E^{-\frac{1}{2}}$) is negligibly small in an interval sufficient to span the resonance and the number which is detected is therefore (equation (K))

$$\mu I(x) = \mu \int_{\theta_0}^{\pi-\theta_0} \varepsilon(\theta) \nu(x, \theta) \mathrm{d}\theta \Big/ \int_{\theta_0}^{\pi-\theta_0} \varepsilon(\theta) \tfrac{1}{2} \sin\theta \mathrm{d}\theta$$

per neutron incident with energy corresponding to x. If $I(x)$ is evaluated

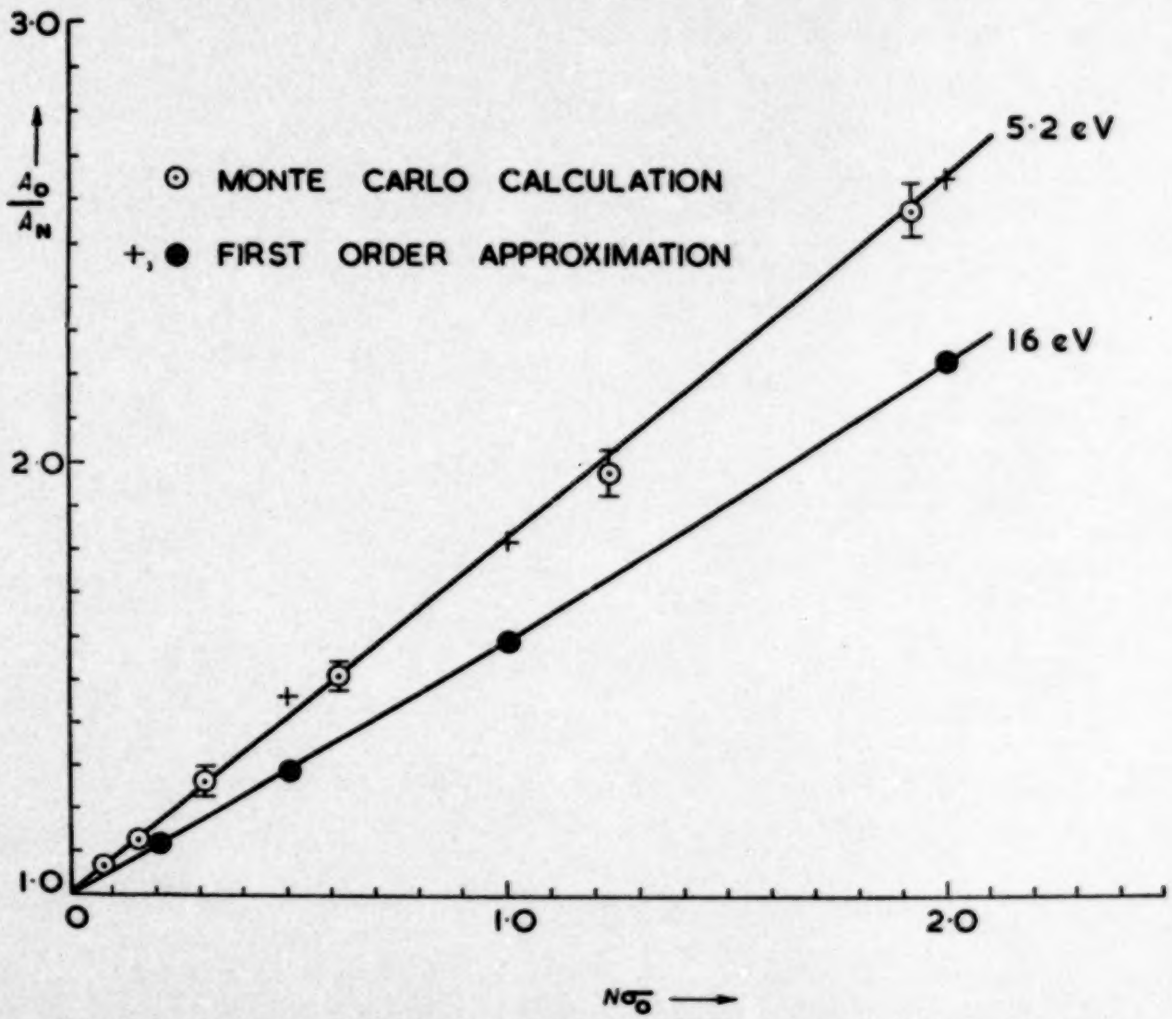

Fig. 14. The correction factor A_0/A_N plotted as a function of sample thickness ($N\sigma_0$ mean free paths at exact resonance) for the 5.2 eV and 16 eV resonances.

numerically as a function of x, for a sample of thickness $N\sigma_0\psi(0, \eta)$ mean free paths at exact resonance, then the theoretical estimate of the resonance

integral which should be observed experimentally is $\mu \int I(x)\mathrm{d}x$ in units of $\frac{1}{2}\Gamma$. Strictly speaking, μ is also a function of x but the error introduced by assuming $\mu = \Gamma_n/\Gamma = \sigma_{0n}/\sigma_0$ is in practice negligible. The procedure, discussed in § 4.4, for reducing the experimental results is equivalent to evaluating $(\mu/N)\int I(x)\mathrm{d}x$ at $N = 0$. This is, from equation (*J*), $\mu\sigma_0 \int \psi(x, \eta)\mathrm{d}x$ and, therefore, the correction factor to be applied to measurement of A_N, from a sample of finite thickness, to give the area A_0 is

$$N\sigma_0 \int \psi(x, \eta)\mathrm{d}x / \int I(x)\mathrm{d}x.$$

Fig. 14 shows the results of this first order calculation carried out for the 5.2 eV and 16 eV silver resonances, using the $\varepsilon(\theta)$ calculated for the detector arrangement in fig. 3.

Appendix 2

Values of $\sigma_0\Gamma^2$ and $\sigma_0\Gamma$, calculated from the transmissions data used in obtaining the resonance parameters listed in table 4

E_R (eV)	$\sigma_0\Gamma^2$ (barn · eV²)					$\sigma_0\Gamma$ (barn · eV)			
16.3	60± 7	64 ± 5				419± 42	428± 43		
30.7	52± 6	79 ± 6	55± 4						
41	34±10	31 ± 4							
42	45±15	31 ± 4							
45	8± 2	8.3± 1			8.3± 1				
52	150±30	143 ±17	110± 7			782±113	974±117		
56	95±25	87 ±10	65±4.5		99 ±11				
71	150±30	160 ±18	107±11		159 ±19				
88	21± 5				21 ± 4			156±31	89±20
134				270±22					
Reference	B	A_3	A_5	A_6	A_7	A_1	A_2	A_3	A_5

The Harwell figures were from the transmission areas listed in table 1 and the values of Γ listed in table 4. The danger of accepting a single experimental determination is obvious.

References

1) H. Feshbach *et al.*, Phys. Rev. **96** (1954) 448;
J. A. Harvey *et al.*, Phys. Rev. **99** (1955) 10;
L. M. Bollinger *et al.*, Phys. Rev. **100** (1955) 126;
D. B. Gayther and K. P. Nicholson, Proc. Phys. Soc. A **70** (1957) 51
2) D. J. Hughes and J. A. Harvey, Nature, London **173** (1954) 942
3) H. H. Landon, Phys. Rev. **100** (1955) 1414
4) J. S. Levin and D. J. Hughes, Phys. Rev. **101** (1956) 1328
5) H. H. Landon and V. L. Sailor, Phys. Rev. **98** (1955) 1267

6) V. L. Sailor, Phys. Rev. **104** (1956) 736
7) F. G. P. Seidl *et al.*, Phys. Rev. **95** (1954) 476
8) R. G. Fluharty, F. B. Simpson and O. D. Simpson, Phys. Rev. **103** (1956) 1778
9) H. A. Bethe, Rev. Mod. Physics **9** (1937) 649; see page 140
10) D. J. Hughes, Journal of Nuclear Energy **1** (1955) 237
11) J. E. Lynn and E. R. Rae, Journal of Nuclear Energy **4** (1957) 418
12) E. R. Wiblin, Proc. Int. Conference on Peaceful Uses of Atomic Energy **4** (1955) 35
13) J. E. Lynn, F. W. K. Firk and M. C. Moxon (to be published)
14) W. E. Lamb, Phys. Rev. **55** (1939) 190
15) G. W. Grimm, Columbia University Report C.U.-155 (1956)
16) E. R. Rae and E. M. Bowey, Journal of Nuclear Energy **4** (1957) 179
17) Neutron Cross Sections, BNL-325 (1955) 12
18) K. W. Morton, Journal of Nuclear Energy (In press)
19) G. M. Roe, Knolls Atomic Power Laboratory Report, KAPL-1241 (1954)
20) E. R. Rae, Proc. Int. Conference on Peaceful Uses of Atomic Energy **4** (1955) 110
21) B. B. Kinsey and G. A. Bartholomew, Phys. Rev. **93** (1954) 1260
22) J. M. Blatt and V. F. Weisskopf, Theoretical Nuclear Physics, (John Wiley and Co., New York, 1952)
23) D. Brink, Thesis (Oxford, 1956)
24) A. M. Lane, Proc. of the Conference on Time-of-Flight Neutron Physics (Gatlinburg, Tennessee, 1956)
25) J. M. B. Lang and K. J. Le Couteur, Proc. Phys. Soc. A **67** (1954) 586
26) G. A. Bartholemew and B. B. Kinsey, Can. J. Phys. **31** (1953) 1025
27) T. D. Newton, Can. J. Phys. **34** (1956) 804
28) Handbuch der Physik **50** (Springer-Verlag, Berlin, 1957) p. 367
29) M. E. Rose, W. Miranker and P. Leak, BNL 257 (1953)

Nuclear Physics **5** (1958) 122—140; © *North-Holland Publishing Co., Amsterdam*

Not to be reproduced by photoprint or microfilm without written permission from the publisher

BETA AND GAMMA RAY SPECTROSCOPY OF Cs^{137}

YASUKAZU YOSHIZAWA

Department of Physics, Faculty of Science, Osaka University, Osaka, Japan

Received 22 June 1957

Abstract: Beta rays and internal conversion electrons from Cs^{137} have been studied using a two directional focusing beta ray spectrometer ($\varrho = 40$ cm). The K shell conversion coefficient α_K of 661 keV gamma transition has been determined to be 0.0976 ± 0.0055, and K/L/M to be $(5.66 \pm 0.04)/1/(0.260 \pm 0.003)$, which are in good agreement with Rose's calculated values for the M4 transition. The maximum energy of the lower component of the beta rays has been found to be 514 ± 2 keV. The Kurie plot, corrected by the factor of the unique first forbidden transition, shows a straight line. The spectrum of the higher component was interpreted by the second forbidden correction factor with a linear combination of scalar and tensor interactions. In an attempt to determine the sign of the ratio of scalar to tensor interaction constants, G_S/G_T, the spectrum could be only explained by the negative sign, assuming that the single particle model is a good approximation for the nuclear matrix elements.

1. Introduction

The beta and gamma rays of Cs^{137} have been measured by many groups and the decay scheme is well known. The half-life has been reported to be 33 years [1]) or 26 years [2]). The energy of the 661.6 keV gamma ray has been accurately measured [3, 4]), and this level is a 158 sec isomeric state [1, 5]). The K shell conversion coefficient and the ratios K/L or K/(L+M) were reported by Waggoner [6]), Kelley [7]), Bendel, Shore, Brown and Becker [8]) and Graves, Langer and Moffat [9]), as shown in table 1, and these values were interpreted as the M4 transition. According to the observed values [10]) of the spins of Cs^{137} and Ba^{137} ground states, and considering the following experimental results as well as the shell theory, spins and parities of the ground state of Cs^{137}, the first excited and the ground states of Ba^{137} were assigned as 7/2+, 11/2− and 3/2+, respectively.

The beta ray has two components and the intensity of the higher component is about 8 percent [11]). The lower and the higher components have been found by Peacock and Mitchell [12]), Agnew [13]), and Langer and Moffat [11]) to have 510 keV and 1170 keV for maximum energies, a unique first forbidden shape and a non-unique second forbidden shape for the spectra, and 9.2 and 11.6 for log *ft* values, respectively.

In order to measure K/L/M and to compare it with Rose's calculated values without nuclear finite size correction, a high resolution beta ray spectrometer was used, with which the L and M conversion lines can be

resolved. In addition we tried to measure them by means of the flat topped method similar to that used in mass spectroscopy. As it is rather easier to measure the maximum energy of the unique forbidden spectrum than that of non-unique one, the maximum energy of the lower component was accurately measured with the high resolution spectrometer and its value is useful for the analysis of the higher component.

Many beta ray spectra which belong to the unique and the non-unique forbidden transition types have been found, since the forbidden shape spectrum of Y^{91} was discovered in 1949 by Langer and Price [14]). Now one knows that the spectra of Cl^{36}, Tc^{99} and higher components of Sc^{46}, Fe^{59} Co^{60} and Cs^{137} are classified as non-unique second forbidden transitions[15, 16, 17]). To account for the beta transitions a linear combination of five forms of interactions, scalar, vector, tensor, axial vector and pseudoscalar, must be used. Many kinds of analysis and experiments [18]), however, involve a linear combination of only scalar and tensor interactions, and even if vector and axial vector interactions exist, they may be much smaller than the others. Especially, straightforward evidence has been provided by directional angular correlation measurements of electrons and nuclear recoils on He^6 [19, 20]) and Ne^{19} [21, 22]). Positive evidence for the existence of the pseudoscalar interaction is only shown by the analysis of the beta spectrum of Pr^{144} [23]). For the second forbidden transition, a linear combination of only scalar and tensor interactions is used, as a pseudoscalar transition of this type vanishes by a selection rule. The correction factor contains some nuclear matrix elements which are difficult to estimate and are almost always treated as parameters. It also depends on the maximum energy, but it is very difficult to determine directly the accurate maximum energy for such a second forbidden transition as the higher component of Cs^{137}. Therefore, we used for it the sum of the maximum energy of the lower component and the energy of the gamma ray. For the comparison between the experimental and the theoretical correction factor not only the interference term but also the effect of the finite nuclear size and the finite de Broglie wave-length correction should be taken into consideration. Fortunately, we could utilize the theoretical correction factor calculated by Matsumoto and Yamada [24]).

The ratio of the coupling constants G_S, G_T of the scalar and tensor interactions has been investigated [15, 25]) and is given as

$$0.75 \leqq |G_S/G_T|^2 \leqq 1.15.$$

It seems that $|G_S| \approx |G_T|$, but it was not know whether G_S/G_T is positive or negative. Morita, Fujita and Yamada [16]) estimated $G_S/G_T < 0$ from the analysis of the beta ray spectra of Rb^{77} and Cs^{137}. Recently, $G_S/G_T > 0$ was derived from the beta ray spectra and the beta-gamma angular cor-

relation experiment of Re^{186} by Porter *et al.* [26]). In order to determine the sign of G_S/G_T, we attempted to measure and analyse the second forbidden spectrum of Cs^{137}.

2. Instrument and Sources

A two-directional focusing beta ray spectrometer of a mushroom type with the mean radius of 40 cm was used for the measurements of beta rays and internal conversion electrons. The radioactive cesium was obtained from Oak Ridge.

2.1. SPECTROMETER

The spectrometer is similar to that reported by Hedgran, Siegbahn and Svartholm [27, 28]) and Hinman [29]). The characteristics are as follows:

magnet diameter			1240 mm
pole gap at the mean radius			220 mm
weight of the iron			2.2 tons
resolutions	0.17	to	0.50 %
solid angle	0.07	to	0.25 %
luminosity	0.14	to	2.5×10^{-3} cm^2

There are defining and exit slits made of brass and three aluminium baffles in the spectrometer. When no aluminium baffle was set, a small number of scattered electrons were observed in the low and high energy parts, but scattered electrons have much decreased after setting up the baffles. The upper limit of this effect in the high energy part was estimated as 1/5000 from measurements of Sr^{90} and Y^{90} spectra. In order to verify the linearity of the magnetic field to the magnet current, the field was measured by a fluxmeter, but it was not accurate enough. Therefore, by observing the internal conversion lines of the various kinds of Ir^{192} gamma rays precisely measured by DuMond *et al.* [3, 30]), it was shown that the linearity of the field was within 1/1000 in this gamma ray energy region. Moreover, it was concluded from the measurements of well known beta ray spectra of P^{32} and Y^{90} that the distortion due to the spectrometer is negligible in the energy region lower than 2.2 MeV.

End window G—M counters filled with argon and alcohol were used. The windows were made of 1.8 and 2.5 mg/cm^2 thickness mica covered with the evaporated aluminium of 0.05 mg/cm^2 thickness. Absorption of electrons by the counter windows began below 200 keV. Rotating coil magnetic field measuring apparatus is now being constructed. More details of this spectrometer will be published in the near future.

2.2. SOURCE

Cs^{137} as CsCl was deposited on an aluminium foil of 1.8 mg/cm^2 thickness.

The average thickness of the sample was about 0.2 mg/cm², and an acetic acid solution of insuline was used to make the source uniform.

3. Results

3.1. INTERNAL CONVERSION ELECTRONS

The beta ray and internal conversion spectra are shown in fig. 1, where a strong conversion line is exhibited. It may be seen that K and L con-

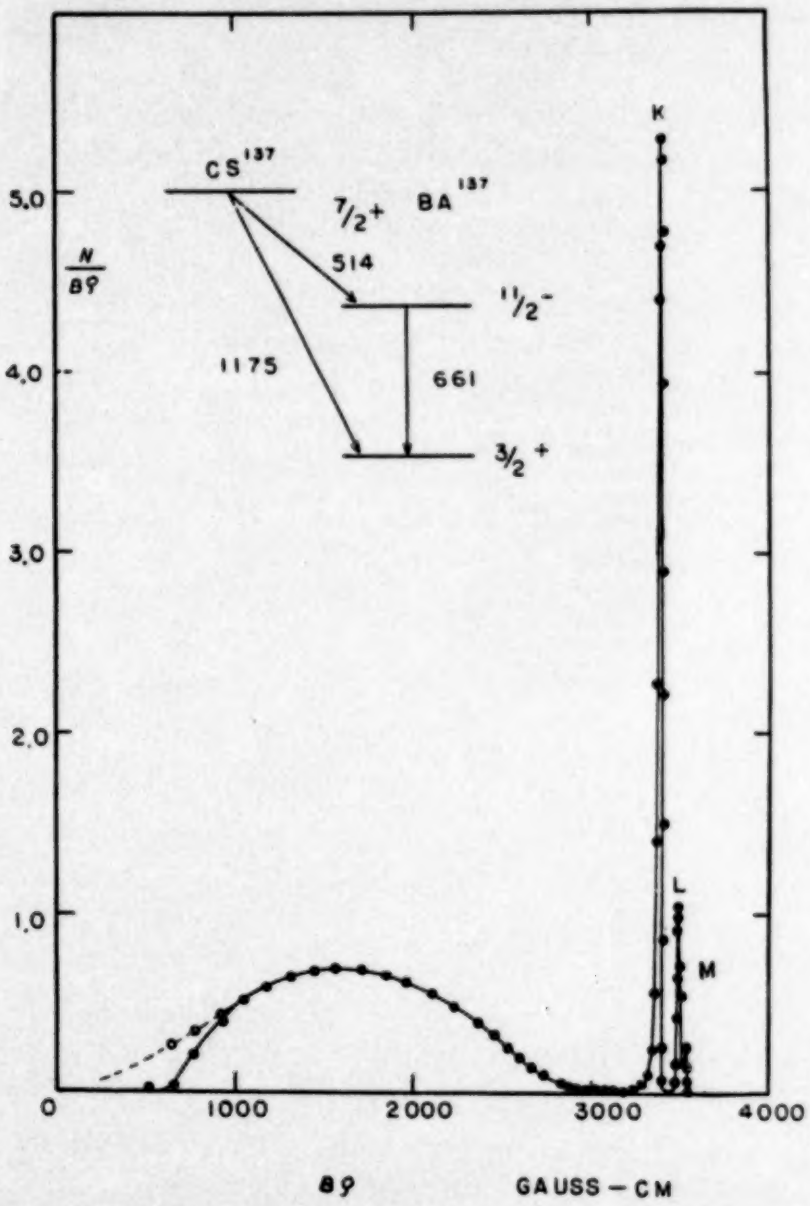

Fig. 1. Momentum spectrum of beta rays of Cs^{137}.

version lines are completely separated and L and M lines are also separated. Fig. 2. shows K, L and M lines in three cases of different resolution 0.17,

0.33 and 1.0 percent. The last one, called the flat topped method, was obtained with the exit slit opened widely in comparison with the source width. In this case the ratio of K to L line heights gives K/L, but as L

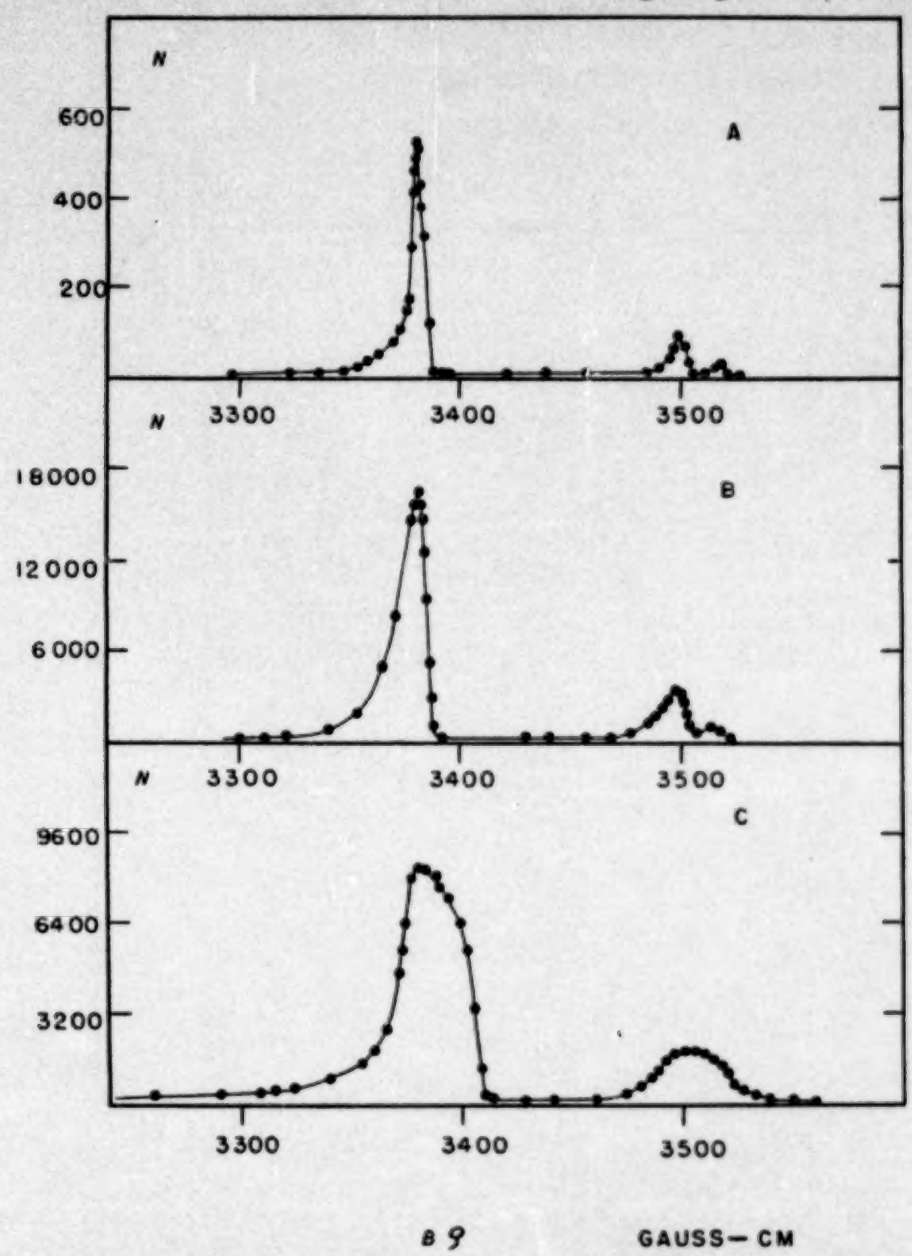

Fig. 2. Momentum spectra of internal conversion lines of 661 keV gamma ray. Curves A, B and C are plotted in the condition of resolution 0.17, 0.44 and 1.0 percent, respectively.

and M lines could not be separated, the ratio K/(L+M) was obtained. The intensity measurement of the gamma radiation was so difficult that the intensity ratio of K electrons to the lower component of beta rays was used to determine the K conversion coefficient α_K. The counter window absorption of low energy beta rays was corrected by the extrapolation of the first forbidden Kurie plot. The values of α_K and K/L/M are indicated in table 1.

TABLE 1

Internal conversion coefficients and beta rays of Cs^{137}

	Preceding	Ref.	Present
γ ray energy in keV	661.60±0.14	3)	
	661.65±0.15	4)	
K conversion coefficient, α_K	0.097±0.005	6)	0.0976±0.0055
K/L	5.5	8)	5.66±0.04
M/L	0.27	8)	0.260±0.002
K/(L+M)	4.57±0.05	7)	
	4.64±0.23	9)	
Maximum energy of lower component (keV)	510	11)	514±2
	523	13)	
	518	6)	
Maximum energy of higher component (keV)	1170	11)	1176±3
Relative intensity lower comp./higher comp.	92/8	11)	(92.4±0.8)/(7.6∓0.8)

3.2. THE LOWER COMPONENT BETA RAY

In figs. 3 and 4 are illustrated allowed and corrected Kurie plots of the

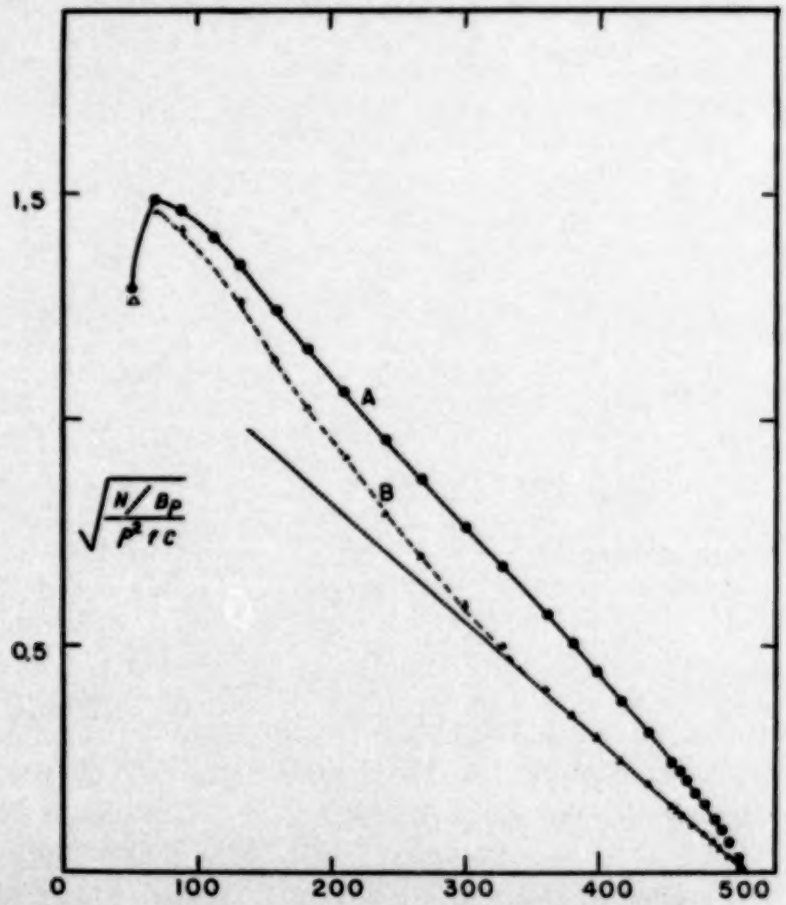

Fig. 3. Kurie plots of lower component beta ray. (A) uncorrected plot, $C = 1$; and (B) corrected plot, $C = p^2+q^2$, where p and q are momenta of electrons and neutrinos, respectively. In both curves the higher component with the allowed shape approximation is subtracted.

lower component. Since the spectrum of the higher component which has a non-unique forbidden shape contains a few parameters, as mentioned in the next section, there remain some ambiguities in the spectrum of the low energy component. Therefore, the spectrum of the high energy component in two extreme approximations was used. An allowed Kurie plot (A) and

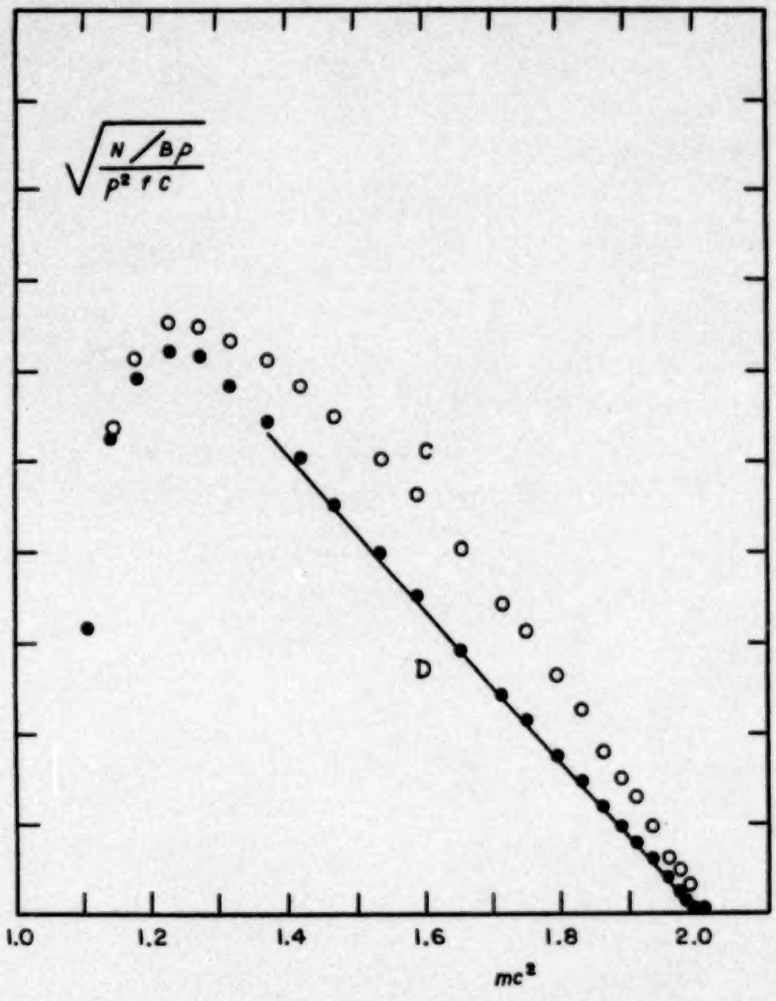

Fig. 4. Kurie plots of lower component beta ray. (C) uncorrected plot, $C = 1$, and (D) corrected plots, $C = p^2+q^2$, but the higher component with the approximate second forbidden correction factor, $C = q^2$, is subtracted.

a corrected plot (B) in fig. 3 were obtained from the subtraction of the higher component of the allowed shape approximation, $C = 1$, where no aluminium baffle was inserted in the spectrometer. An allowed plot (C) and a corrected plot (D) in fig. 4 were obtained from a second forbidden shape, $C = q^2$, which was estimated to be a good approximation within 10 percent, as detailed in the next section; in this case as three aluminium baffles were inserted, the effect of the scattering was quite decreased.

The correction factor for the so-called unique first forbidden shape [31, 32]),

$C = p^2+q^2$, was used, where p and q are the momenta of electrons and neutrinos, respectively. A deviation from a straight line appears at a region below 350 keV in the plot (B), but not in the plot (A). This difference must be the effect due to the subtracted spectrum shape and the aluminium baffles. The Kurie plots in fig. 3 was measured in the condition of no aluminium baffle.

The maximum energy was accurately determined as in table 1 in reference to the conversion lines by means of the high resolution condition. This is important for the determination of the maximum energy of the higher component.

3.3. THE HIGHER COMPONENT BETA RAY

The low energy part of the higher component is screened by the strong lower component and conversion electrons. Therefore, it is impossible to measure the spectrum lower than 510 keV. We tried to measure not only the high energy part but also points between lower component and K electrons, and between K and L electrons by using the high resolution condition. Actually, however, a long tail of the L line, which covered the higher component existed between the K and L lines.

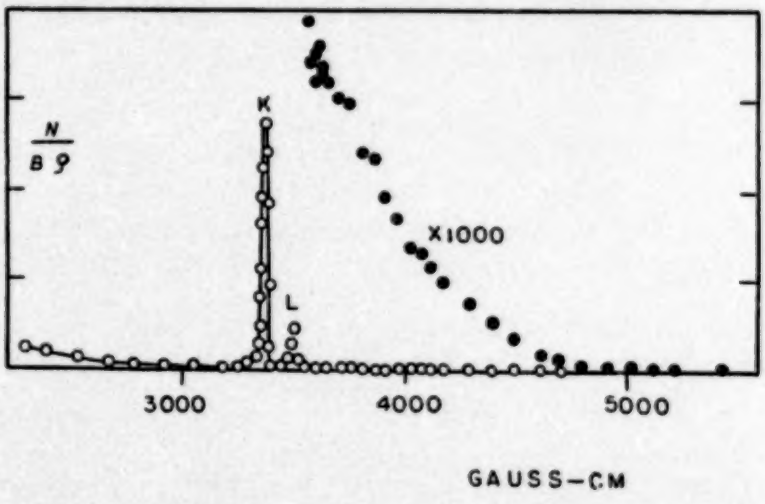

Fig. 5. Momentum spectrum of high energy part. Enlarged scale shows spectrum of higher component.

In fig. 5 the momentum spectrum of the higher component is shown. Electrons having energy near the maximum were so few that one could not determine the value of the maximum energy. Fig. 6 illustrates the uncorrected Kurie plot of the higher component which clearly deviates from the allowed type. In this figure the plot of Langer and Moffat [11]) is compared with the present experiment. The agreement of the plots is fairly good, but a slight deviation in the vicinity of the maximum energy is recognized.

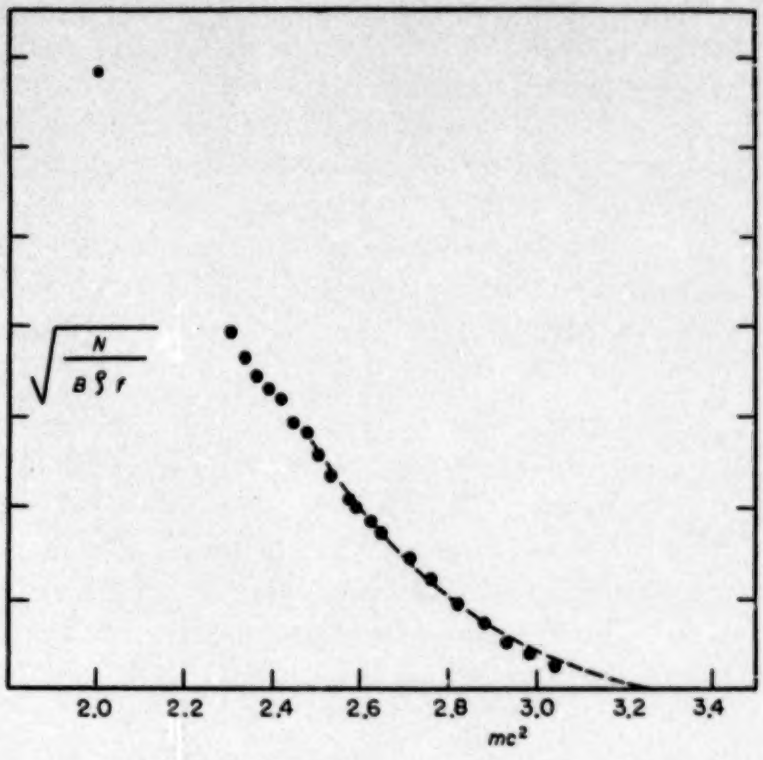

Fig. 6. Kurie plot of higher component beta ray. Broken curve gives the result of Langer and Moffat [11]).

4. Discussions

The K/L ratio is in good agreement with Rose's calculation [33]) of the magnetic 2^4-pole with the screening effect shown in table 2. This means that

TABLE 2

Theoretical K conversion coefficients and K/L ratios for 661 keV gamma ray with the screening effect and without the finite nuclear size effect

	E3	E4	E5	M3	M4	M5
α_K	0.0092	0.028	0.042	0.040	0.0918	0.22
K/L	5.9	4.5	3.4	6.7	5.66	5.1

the finite nuclear size effect is negligible and this transition does not contain other multipoles. The K conversion coefficient is expected to have a rather large uncertainty and has some deviation from Rose's value, but agrees with the other experimental value. The correction of the counter window absorption may not be accurate, though the subtraction of the higher component decrease this uncertainty.

In figs. 3 and 4 it is again verified that the spectrum of the lower component agrees with the unique first forbidden transition, $\Delta I = 2$, yes, as well as the results given by many authors.

The problem of the higher component is not simple; we tried to analyse it by many methods under the following conditions. First, the measured values of spins and the estimated parities of the ground states of Cs^{137} and Ba^{137} are reliable, i.e., the analysis is based on the second forbidden transition, $\Delta I = 2$, no. Second, a linear combination of the scalar and tensor interactions is assumed. Third, the sum, 1175 keV, of the maximum energy of the lower component and the accurately measured gamma ray corresponds to this maximum energy, as mentioned earlier. Because fewer electrons near the maximum energy are ejected in such a forbidden spectrum as Cs^{137}, it is difficult to determine the maximum energy directly, while the correction factor near maximum energy strongly depends on this value.

Recent investigation of the beta decay has shown that the finite nuclear size correction [34]), the finite de Broglie wave length correction [35]), and the screening effect [36, 37]) cannot be neglected in heavy nuclei. Other corrections, for example, the radiative correction [38]) and the effect of the beta decay in nucleus [39]) etc., have been discussed, but sometimes these corrections are too complicated. Fortunately, we could use calculated formulae of Matsumoto and Yamada [24]). Their formulae contain all the corrections except that for the radiative effect. However, this formula for the second forbidden transition contains four parameters, whereas that of Konopinski and Uhlenbeck's ordinary theory has three parameters.

First, because of the simplicity of the analysis we use the approximate formula in the ordinary theory which neglects the finite nuclear size and the finite de Broglie wavelength, as it is a fairly good approximation for such a nucleus as Cs [137]. The correction factor obtained is

$$C_{2ST} = G_T^2 \sum |T_{ij}|^2 (a_1 X_1^2 + a_2 X_2^2 + a_3 X_1 Y + a_4 X_2 Y + a_5 Y^2 + a_6 X_1 + a_7 X_2 + a_8 + a_9 T^2), \tag{1}$$

$$X_1 = \frac{G_T A_{ij} - (\alpha Z/2\varrho) G_T T_{ij} - 2i(\alpha Z/2\varrho) G_S R_{ij}}{G_T T_{ij}} = \frac{A_{ij}}{T_{ij}} - \frac{\alpha Z}{2\varrho}(1+2Y),$$

$$X_2 = \frac{G_T A_{ij} - \frac{1}{2}(\alpha Z/2\varrho) G_T T_{ij} - i(\alpha Z/2\varrho) G_S R_{ij}}{G_T T_{ij}} = \frac{A_{ij}}{T_{ij}} - \frac{1}{2}\frac{\alpha Z}{2\varrho}(1+2Y), \tag{2}$$

$$Y = i\frac{G_S R_{ij}}{G_T T_{ij}}, \qquad T = \frac{S_{ijk}}{T_{ij}},$$

where a_i's $(i = 1, 2, \cdots, 9)$ are functions of energies and momenta of electrons and neutrinos, as given in the appendix, and R_{ij}, A_{ij}, T_{ij} and S_{ijk} are given by Konopinski and Uhlenbeck [31, 40, 41, 42]). It is estimated from the empirical ft-values of unique second forbidden transitions that the value of T is small, i.e., $-1 \lessapprox T \lessapprox 1$. Therefore, the last term of eq. (1) can be neglected, considering $a_9 \ll 1$. Only two independent parameters remain in eq. (1).

A remarkable point of the experimental results is that the correction factor is in good agreement with $C = q^2$ within the experimental error. This means that the term of X_1^2 in eq. (1) is predominant and all other terms are small or cancel each other, though usually X_1 and X_2 are the same order and much larger than Y. The experimental spectrum was analysed in the region $-2 \leqq Y \leqq 2$, because the term in Y^2 becomes predominant

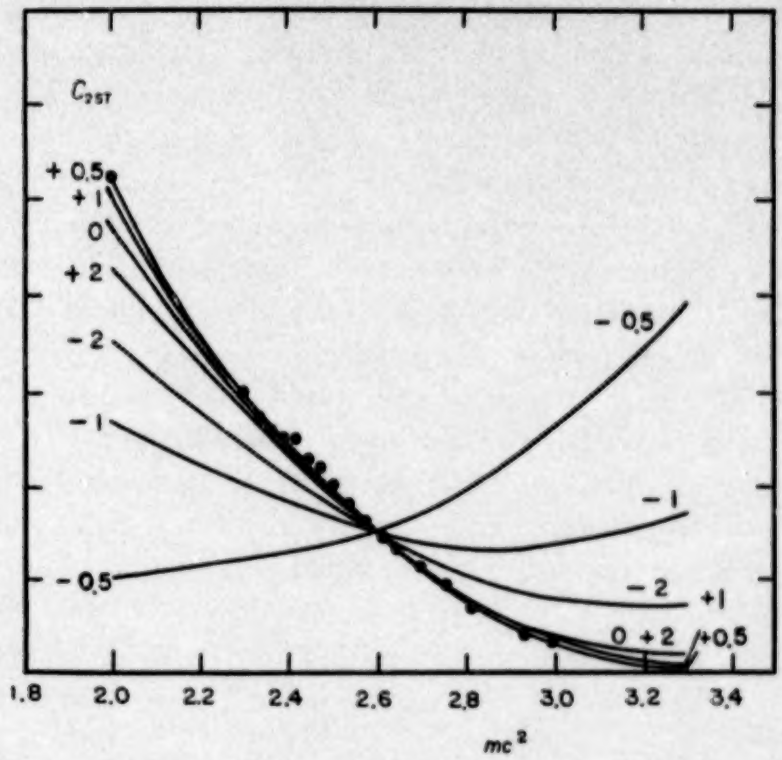

Fig. 7. Experimental and theoretical correction factors of higher component. Points indicate the experimental values. Numbers in figure are the values of Y. Curves show theoretical values which are given by the parameters:

Y	2	1	0.5	0	−0.5	−1	−2
X_1	−28.6	−17.1	−11.3	−5.6	0.20	6.0	17.5
X_2	2.37	1.50	1.07	0.63	0.20	−0.23	−1.10

where X_1 and X_2 are selected to make the theoretical curves approach the experimental points for each Y.

in the region near the maximum energy if Y takes a large value. By varying X_1 and X_2, a theoretical curve which most nearly fits the experimental data was obtained for each value of Y, where only one but not both of the parameters X_1 and X_2 are independent. The results are shown in fig.7. When X_2 is small, i.e., $-1 \lessapprox X_2 \lessapprox 1$, the correction factors are not so sensitive for X_2. In the region $-2 \leqq Y < 0$ no value of the parameter X_1 or X_2 led to a theoretical correction factor consistent with the experimental

result, but in the region $0 < Y \leqq 2$ it was in good agreement with the ex-

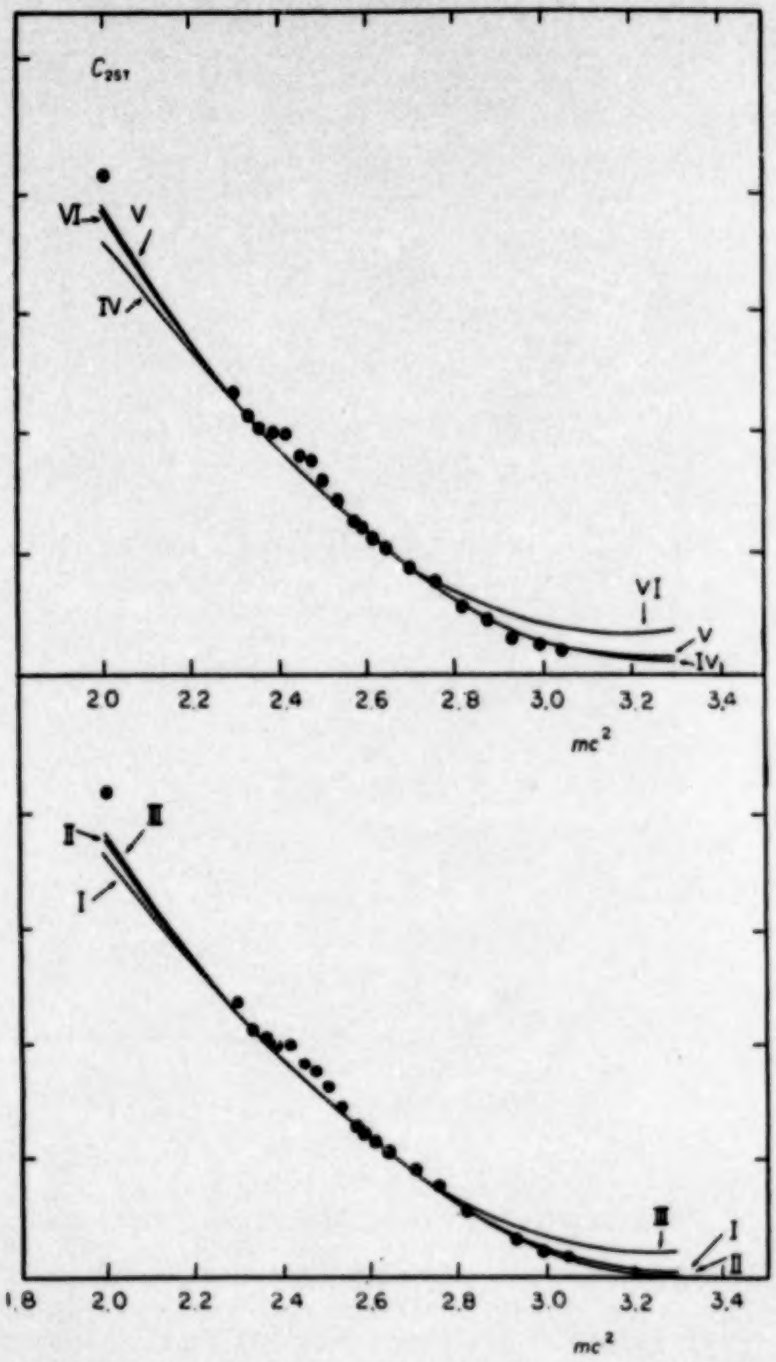

Fig. 8. Experimental and theoretical correction factors of higher component. Solid points are experimental results, the ratios of experimental values to allowed theoretical spectrum. Curves show theoretical correction factors, C_{2ST}, with different parameters, i.e. different values of nuclear matrix elements in the linear combination of scalar and tensor interactions.

Curve I	$x_1 = -10,$	$x_2 = 1,$	$y = 0.5,$	$t = 0,$
Curve II	$x_1 = -10,$	$x_2 = 1,$	$y = 0.2,$	$t = 0,$
Curve III	$x_1 = -10,$	$x_2 = 1,$	$y = -0.2,$	$t = 0$
Curve IV	$x_1 = -10,$	$x_2 = 0.5,$	$y = 0.5,$	$t = 0,$
Curve V	$x_1 = -10,$	$x_2 = 0.5,$	$y = -0.2,$	$t = 0,$
Curve VI	$x_1 = -10,$	$x_2 = 0.5,$	$y = -0.5,$	$t = 0.$

perimental result, as shown in fig. 7. In consideration of the finite nuclear size effect [34]) the correction factors in fig. 7 are given values of Y that

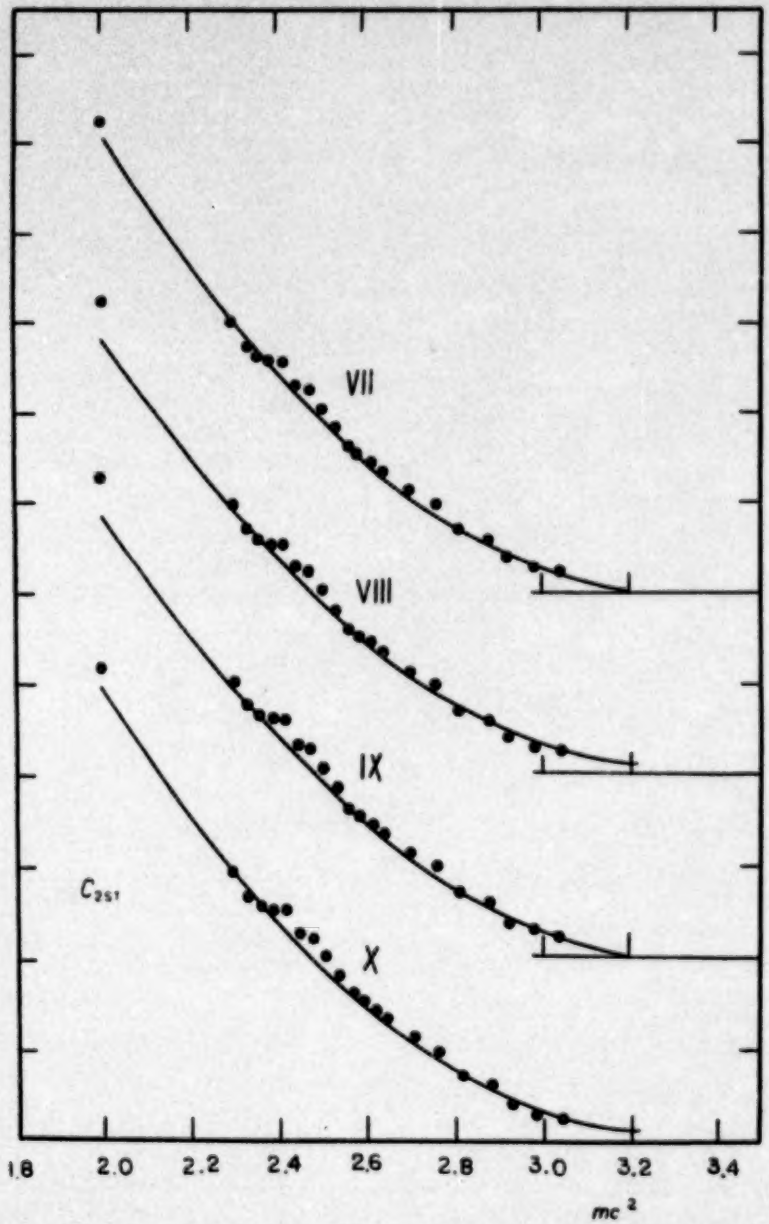

Fig. 9. Experimental and theoretical correction factors of higher component. Points and curves show experimental and theoretical values, as shown in fig. 8:

Curve VII	$x_1 = +50$,	$x_2 = +1$,	$y = +1$,	$t = 0$,
Curve VIII	$x_1 = +50$,	$x_2 = +1$,	$y = -1$,	$t = 0$,
Curve IX	$x_1 = -50$,	$x_2 = +1$,	$y = +1$,	$t = 0$,
Curve X	$x_1 = -50$,	$x_2 = +1$,	$y = -1$,	$t = 0$.

differ by 10 to 30 percent and this conclusion about the sign of Y does not change.

The scattering in the spectrometer is important for the measurement

of such a weak higher component. This effect is estimated to be small and the upper limit is about five percent of the higher component, as

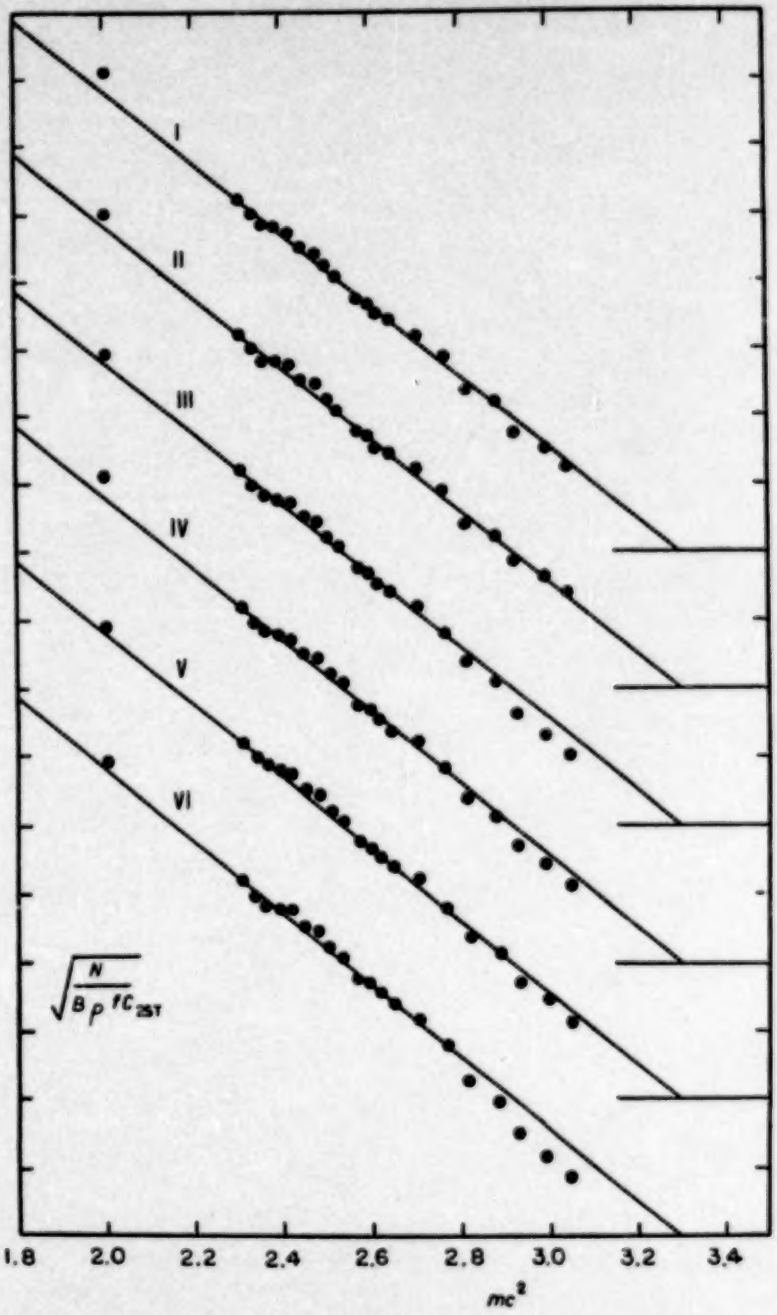

Fig. 10. Corrected Kurie plots of higher component. Second forbidden correction factors shown in fig. 8 are used.

mentioned in section 2. Even if 5 to 10 percent scattered electrons are contained in the spectrum, the result of this analysis does not change.

If the matrix elements R_{ij} and T_{ij} follow the time reversal property and the single particle model, it is found that $R_{ij}/T_{ij} = i/2$ [16, 43]), when

the configurations of the ground states of Cs^{137} and Ba^{137} are assumed to be $g_{7/2}$ and $d_{3/2}$, respectively. Therefore, Y becomes $-G_S/G_T$ and the

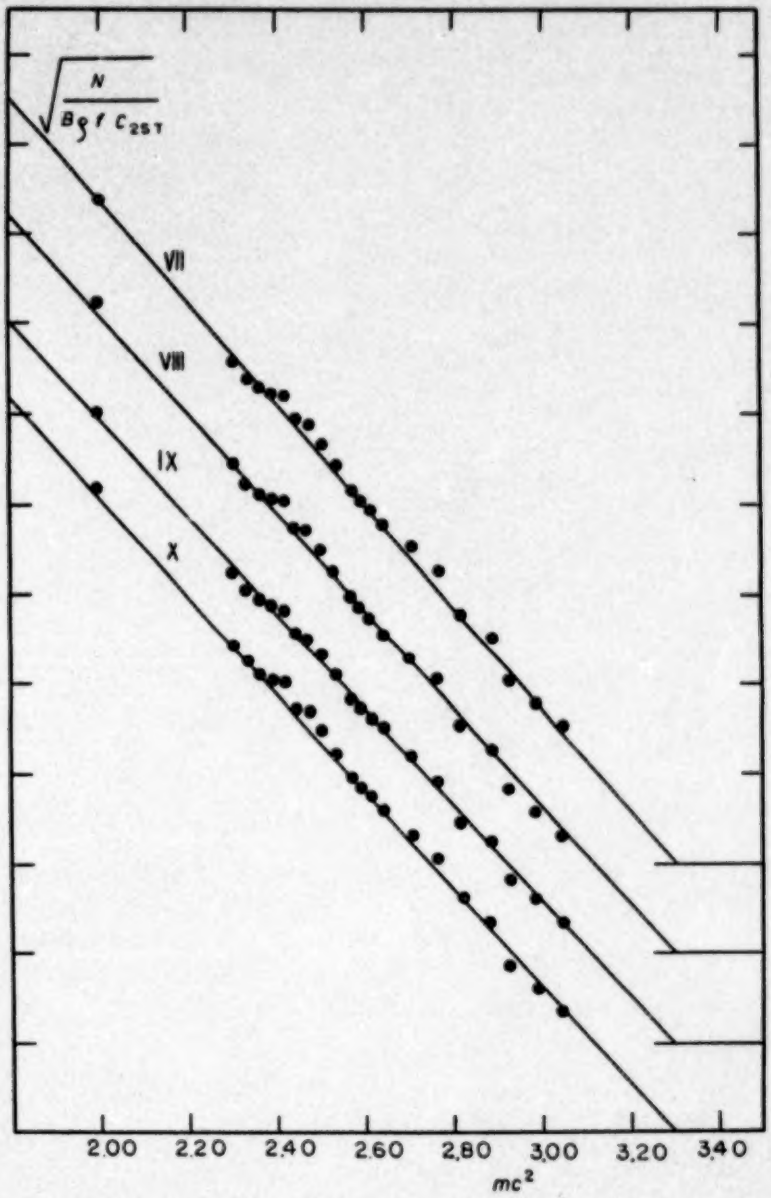

Fig. 11. Corrected Kurie plots of higher component. Second forbidden correction factors shown in fig. 9 are used.

sign of Y depends on that of G_S/G_T. As the single particle model is expected to be a good approximation for such an odd mass nucleus as Cs^{137} near a magic number, it may be thought that $iR_{ij}/T_{ij} \approx -\frac{1}{2}$ is reliable. Considering $|G_S/G_T| \approx 1$, it is concluded that the sign of G_S/G_T is negative, as Morita, Fujita and Yamada [16]) pointed out.

Next, the experimental result was analysed using the formula of Matsu-

moto and Yamada, given in the Appendix. They denoted the matrix elements by $\int A^{\beta}_{ij} I'_1(r)$, $\int A^{\beta}_{ij} I'_2(r)$, $\int T^{\beta}_{ij} I'_1(r)$, $\int T^{\beta}_{ij} I'_2(r)$, $\int R^{\beta}_{ijk} I'_1(r)$, $\int R^{\beta}_{ij} I'_2(r)$ and $\int S^{\beta}_{ijk} I'_1(r)$, instead of A_{ij}, T_{ij}, R_{ij} and S_{ijk}, where $I'_k(r)$ is an energy-independent function indicated in eq. (A5). They used "effective nuclear radius" instead of the ordinary nuclear radius. Their approximate formula is similar to eq. (1), but all four ratios of the matrix elements are treated as independent parameters. The term in q^2, i.e., $a_1 x_1^2$ in eq. (A1), is estimated to be predominant, according to the experimental result. The correction factors are shown in figs. 8 and 9, and the Kurie plots are shown in figs. 10 and 11, where $x_1 = 10$ or ± 50, $-1 \leqq x_2 \leqq 1$, $-1 \leqq y \leqq 1$, and $t = 0$. If the parameters take values $|x_1| \gtrsim 50$, $|x_2| \approx 1$, and $|y| \approx 1$, many correction factors are found to agree with the experimental result, whether y is positive or negative. It is estimated that $y \approx Y$. The sign of G_S/G_T does not seem to be determined from this analysis. The parameter x_1 cannot, however, take such a large value as ± 50 in curves VII, VIII, IX and X, when $-1 \lesssim x_2 \lesssim 1$ and $-1 \lesssim y \lesssim 1$, because parameters x_1, x_2 and y can be treated as independent parameters only under some restrictive conditions [44]). Curves I, II, IV, and V are in agreement with experimental points, but the value of x_1 in curve V is not appropriate, as $|x_1|$ is much smaller than 10 from the conditions when $x_2 = 0.5$ and $y = -0.2$. Theoretical curves with other values of these parameters lead to similar results. Therefore, only positive values of y remain and the result of this analysis is not essentially different from the former conclusion about the sign of G_S/G_T.

Recently the beta ray angular distributions in the polarized cobalt nuclei were investigated by Wu *et al.* [45]). It is impossible to explain that experiment by the ordinary theory existing hitherto; rather it demands a new theory [46]). In this paper, the higher component was analysed by the ordinary theory, but the present analysis may be applied to the new theory.

The author wishes to express his gratitude to Dr. Nakamura for his helpful discussions, to Mr. Z. Matsumoto for his valuable calculations, and to Mr. Y. Koh, Mr. M. Nozawa and Mr. T. Katoh for their help in this work. Also the author is greatly indebted to Dr. M. E. Rose for sending him the calculated tables of internal conversion coefficients.

Appendix

The second forbidden correction factor [24]) mentioned in section 4 is

$$C_{2ST} = \sum |\int T^{\beta}_{ij} I'_1(r)|^2 (a_1 x_1^2 + a_2 x_2^2 + a_3 x_1 y + a_4 x_2 y + a_5 y^2 + a_6 x_1 + a_7 x_2 + a_8 + a_9 t^2), \quad \text{(A1)}$$

where parameters including the finite nuclear size and the finite de Broglie

wavelength effect become

$$x_1 = \frac{G_T\int A^\beta_{ij} I'_1(r) - \frac{\alpha Z}{2\varrho_T^{(1)}} G_T\int T^\beta_{ij} I'_1(r) - 2i\frac{\alpha Z}{2\varrho_R^{(1)}} G_S\int R^\beta_{ij} I'_1(r)}{G_T\int T^\beta_{ij} I'_1(r)},$$

$$x_2 = \frac{G_T\int A^\beta_{ij} I'_2(r) - \frac{1}{2}\frac{\alpha Z}{2\varrho_T^{(2)}} G_T\int T^\beta_{ij} I'_2(r) - i\frac{\alpha Z}{2\varrho_R^{(2)}} G_S\int R^\beta_{ij} I'_2(r)}{G_T\int T^\beta_{ij} I'_1(r)}, \tag{A2}$$

$$y = i\frac{G_S\int R^\beta_{ij} I'_1(r)}{G_T\int T_{ij} I'_1(r)},$$

$$t = \frac{\int S^\beta_{ijk} I'_1(r)}{\int T^\beta_{ij} I'_1(r)}.$$

When the screening effect is neglected, one obtains

$$\begin{aligned}
a_1 &= \frac{q^2}{12},\\
a_2 &= \frac{p^2}{12},\\
a_3 &= \frac{q^2}{3}\left(\frac{q}{5} - \frac{p^2}{3w}\right),\\
a_4 &= \frac{p^2}{3}\left(\frac{q}{3} - \frac{p^2}{5w}\right),\\
a_5 &= \frac{1}{30}(q^4+p^4) + \frac{q^2p^2}{9} - \frac{2}{45}\frac{qp^2}{w}(q^2+p^2),\\
a_6 &= -\frac{q^2}{6}\left(\frac{q}{5} + \frac{p^2}{3w}\right),\\
a_7 &= -\frac{p^2}{6}\left(\frac{q}{3} + \frac{p^2}{5w}\right),\\
a_8 &= \frac{1}{180}(q^4+p^4) + \frac{p^2q^2}{54} + \frac{qp^2}{90w}(q^2+p^2),\\
a_9 &= \frac{1}{1080}(q^4+p^4) + \frac{p^2q^2}{324},
\end{aligned} \tag{A3}$$

where w is the energy of electron.

If the potential for electrons is denoted by $V(r')$, $\varrho_R^{(k)}$ and $\varrho_T^{(k)}$ $(k = 1, 2)$ which are called "effective nuclear radii" are given by the equations

$$\int R^{\beta}_{ij} r^{-2k-1} \int_0^r dr' r'^{2k} V(r') I'_k(r') = -\frac{1}{k} \frac{\alpha Z}{2\varrho_R^{(k)}} \int R^{\beta}_{ij} I'_k(r),$$
$$\int T^{\beta}_{ij} r^{-2k-1} \int_0^r dr' r'^{2k} V(r') I'_k(r') = -\frac{1}{k} \frac{\alpha Z}{2\varrho_T^{(k)}} \int T^{\beta}_{ij} I'_k(r), \tag{A4}$$

where α is the fine structure constant. The function $I'_k(r)$ means

$$I'_k(r) = \frac{\gamma_k}{k} \left\{ \left(\frac{k+\gamma_k}{2k} \right)^{\frac{1}{2}} I_k(\varrho) + \left(\frac{k-\gamma_5}{2k} \right)^{\frac{1}{2}} \varrho^{-2k} \int_0^{\rho} dr\, r^{2k} V(r) I_k(r) \right\}^{-1} I_k(r),$$

$$I_k(r) = 1 - \int_0^r dr_1 r_1^{-2k} V(r_1) \int_0^{r_1} dr_2 r_2^{2k} V(r_2) + \int_0^r dr_1 r_1^{-2k} V(r_1) \int_0^{r_1} dr_2 r_2^{2k} V(r_2) \int_0^{r_3} dr_3 r_3^{-2k} V(r_3) \int_0^{r_3} dr_4 r_4^{2k} V(r_4), \tag{A5}$$

$$\gamma_k = (k^2 - \alpha^2 Z^2)^{\frac{1}{2}}.$$

When $I'_k(r) = 1$ and $\varrho_R^{(k)} = \varrho_T^{(k)} = \varrho$ where ϱ is the nuclear radius, eq. (A1) is equivalent to the Konopinski and Uhlenbeck's $\alpha Z \ll 1$ approximation. However, there are four independent parameters in eq. (A1), instead of three parameters as in Konopinski and Uhlenbeck.

In the formula of Konopinski and Uhlenbeck, and Smith, $\alpha Z/2\varrho = 1.17 Z A^{-1/3} = 12.4$ for Cs^{137}, where $\varrho = 1.2 \times 10^{-13} A^{1/3}$ cm. If the terms except the highest order ones in $\alpha Z/2\varrho$ in the coefficient of each matrix element are neglected [47]),

$$C_{2ST} = G_T^2 \sum |T_{ij}|^2 \tfrac{1}{12} (X_1^2 q^2 + X_2^2 p^2). \tag{A6}$$

This corresponds to the first two terms in eq. (1). X_1 and X_2 cannot be treated as independent parameters, though x_1 and x_2 in eqs. (A1) and (A2) are regarded as independent parameters, and are not expected to make a large difference from X_1 and X_2, respectively. The higher order approximation of Konopinski and Uhlenbeck is expressed by eq. (1) in which the parameters x_1, x_2, y and t in eq. (A1) are exchanged for X_1, X_2, Y and T. In comparison with the experimental result, it is estimated that $|X_1| \gg 1$ and $|X_2| \lesssim 1$ in eq. (A6). When $|X_1| \approx 10$ and $|X_2| \lesssim 1$, the neglected terms in eq. (A6) are effective in the vicinity of the maximum energy. Then the higher order approximation is used for the analysis in fig. 7. The ratio of matrix elements A_{ij}/T_{ij} is obtained from the parameter X_1 or X_2 used in fig. 7, and is determined for each value of Y, $A_{ij}/T_{ij} = 33.4$, 20.1 and 13.7 for $Y = 2$, 1 and 0.5, respectively.

References

1) Hollander, Perlman and Seaborg, Rev. Mod. Phys. **25** (1953) 469
2) D. M. Wiles and R. H. Tomlinson, Phys. Rev. **99** (1955) 188
3) Muller, Hoyt, Klein and DuMond, Phys. Rev. **88** (1952) 775

4) Lindström, Siegbahn and Wapstra, Proc. Phys. Soc. B **66** (1953) 54
5) Townsend, Cleland and Hughes, Phys. Rev. **74** (1948) 499
6) M. A. Waggoner, Phys. Rev. **80** (1950) 489 and **82** (1951) 906
7) W. C. Kelley, Phys. Rev. **85** (1952) 101
8) Bendel, Shore, Brown and Becker, Phys. Rev. **87** (1952) 195
9) Graves, Langer and Moffat, Phys. Rev. **88** (1952) 344
10) J. E. Mack, Rev. Mod. Phys. **22** (1950) 64
11) L. M. Langer and R. D. Moffat, Phys. Rev. **82** (1951) 635
12) C. L. Peacock and A. C. G. Mitchell, Phys. Rev. **75** (1949) 1273
13) H. M. Agnew, Phys. Rev. **77** (1950) 655
14) L. M. Langer and H. C. Price, Jr., Phys. Rev. **75** (1949) 1109
15) E. J. Konopinski and L. M. Langer, An. Rev. Nuc. Sci. **2** (1953) 261
16) Morita, Fujita and Yamada, Prog. Theor. Phys. **10** (1953) 630
17) G. L. Keister and F. H. Schmidt, Phys. Rev. **93** (1954) 140
18) H. Mahmond and E. Konopinski, Phys. Rev. **88** (1952) 1266
19) B. M. Rastad and S. L. Ruby, Phys. Rev. **89** (1953) 880
20) J. S. Allen and W. K. Jentschke, Phys. Rev. **89** (1953) 902
21) W. P. Alford and D. R. Hamilton, Phys. Rev. **95** (1954) 1351
22) Maxson, Allen and Jentschke, Phys. Rev. **97** (1955) 109
23) M. J. Laubitz, Proc. Phys. Soc. A **69** (1956) 789
24) Z. Matsumoto and M. Yamada, Soryusiron Kenkyu **12** (1956) 139 (Japanese)
25) E. J. Konopinski, Rev. Mod. Phys. **27** (1955) 254
26) Porter, Freedman, Novey and Wagner, Phys. Rev. **103** (1956) 921 and 942
27) Hedgran, Siegbahn and Svartholm, Proc. Phys. Soc. A **63** (1950) 960
28) A. Hedgran, Ark. f. Fys. **5** (1952) 1
29) G. W. Hinman, private communication
30) Baggerly, Marmier, Boehm and DuMond, Phys. Rev. **100** (1955) 1364
31) E. J. Konopinski and G. E. Uhlenbeck, Phys. Rev. **60** (1941) 308
32) C. S. Wu, Rev. Mod. Phys. **22** (1950) 386
33) M. E. Rose, Beta and Gamma Ray Spectroscopy, Ed. K. Siegbahn (North-Holland Publishing Co., Amsterdam, 1955) p. 396, and privately circulated tables
34) M. E. Rose and D. K. Holmes, Phys. Rev. **83** (1951) 190
35) M. E. Rose and C. L. Perry, Phys. Rev. **90** (1953) 479
36) C. Longmire and H. Brown, Phys. Rev. **75** (1949) 264 and 1102
37) J. R. Reitz, Phys. Rev. **77** (1950) 10
38) E. Merzbacher, Phys. Rev. **81** (1951) 942
39) M. Yamada, Prog. Theor. Phys. **10** (1953) 245
40) A. M. Smith, Phys. Rev. **82** (1951) 955
41) E. Greuling, Phys. Rev. **61** (1942) 568
42) D. L. Pursey, Phil. Mag. **42** (1951) 1193
43) M. Yamada and M. Morita, Prog. Theor. Phys. **8** (1952) 431
44) M. Yamada, private communication
45) Wu, Ambler, Hayward, Hoppes and Hudson, Phys. Rev. **105** (1956) 1413
46) T. D. Lee and C. N. Yang, Phys. Rev. **104** (1956) 254 and **105** (1957) 1671
47) E. J. Konopinski, Beta and Gamma Ray Spectroscopy, Ed. K. Siegbahn (North-Holland Publishing Co., Amsterdam, 1955) p. 292

Nuclear Physics **5** (1958) 141—149; © *North-Holland Publishing Co., Amsterdam*
Not to be reproduced by photoprint or microfilm without written permission from the publisher

THE NUCLEAR REACTION He^4 (α, p) Li^7 AND ITS INVERSE

I. THE REACTION He^4 (α, p) Li^7

W. E. BURCHAM and G. P. McCAULEY
University of Birmingham

D. BREDIN and W. M. GIBSON
Queen's University of Belfast

D. J. PROWSE
University of Bristol

and

J. ROTBLAT
Medical College of St. Bartholomew's Hospital, London

Received 12 July 1957

Abstract: Differential cross sections for the reaction He^4 (α, p) Li^7 leaving Li^7 in its ground and first excited state have been measured for an alpha particle energy of 38.5 MeV. The cross sections are in fair agreement with those predicted from the yield of the inverse reaction Li^7 (p, α) He^4. Under certain simplifying assumptions the partial inelastic cross sections for s and d waves in the reaction He^4 (α, p) Li^7 are 11 ± 1 mb and 33 ± 3 mb respectively for the stated incident energy.

1. Introduction

In a recent study of the elastic scattering of 30—40 MeV alpha-particles by helium, evidence for the occurrence of inelastic processes was obtained. The experimental technique and results giving the differential cross section for elastic scattering of 38.5 MeV alpha particles have already been described [1]). The elastic scattering cross section falls to the very small value of 0.5 mb/steradian at a centre-of-mass angle of 63° and a range distribution of particles observed at angles near this value clearly shows the presence of two groups of singly charged particles (fig. 1). Since the energy available in the centre-of-mass system in this experiment was less than the threshold energy for the He^4 (α, d) Li^6 reaction these groups are assigned to the reaction

$$He^4+He^4 \rightarrow Be^8 \rightarrow Li^7+H^1-17.34\ \text{MeV} \qquad (1)$$

with the Li^7 nucleus left in its ground state and first excited state of 0.478 MeV. The observed ranges are consistent with this interpretation, assuming the energy of 38.5 MeV indicated for the incident beam by the observed range of the scattered alpha particles.

The proton groups were detected over a range of angles between 30° and 120° in the centre of mass system. Some allowance for the background tracks

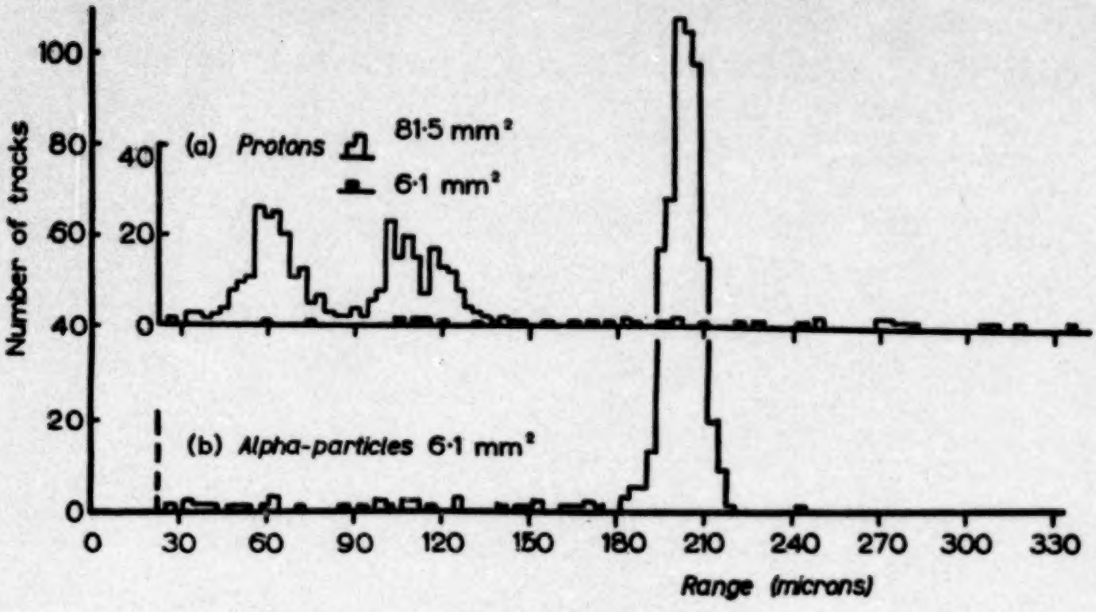

Fig. 1. Range distribution of particles observed in the bombardment of helium by 38.5 MeV alpha particles, c.m.s. angle = 40°. (a) protons observed in areas of 81.5 mm² and 6.1 mm², (b) alpha particles observed in area of 6.1 mm².

which underlie the discrete groups had to be made at each angle and this is the major cause of uncertainty in the observed cross sections. Comparison was made between two independent exposures and the plates were scanned independently in both Bristol and Belfast. The differential cross sections finally adopted for the ground and excited state transitions are plotted in fig. 2. The least squares fit to an expression of the form $a+b\cos^2\theta$ gave

$$\begin{aligned}\sigma_{\alpha p}(\theta) &= (1.53\pm0.09)+(1.93\pm0.15)\cos^2\theta \text{ mb. steradian}^{-1} \text{ for the ground state,}\\ \sigma'_{\alpha p}(\theta) &= (1.32\pm0.07)+(0.66\pm0.23)\cos^2\theta \text{ mb. steradian}^{-1} \text{ for the excited state.}\end{aligned} \quad (2)$$

2. The (p, α) reaction

Reaction (1) is the inverse of the familiar reaction

$$Li^7+H^1 \rightarrow Be^8 \rightarrow 2He^4+17.34 \text{ MeV} \quad (3)$$

discovered by Cockcroft and Walton. This reaction has been extensively studied (see ref. 2) but absolute cross sections have not so far been published for the proton energy range 1 to 2 MeV. Some such measurements are reported in Part II of this paper. The angular distribution of the alpha particles observed in reaction (3) has been discussed by Inglis [3]), whose

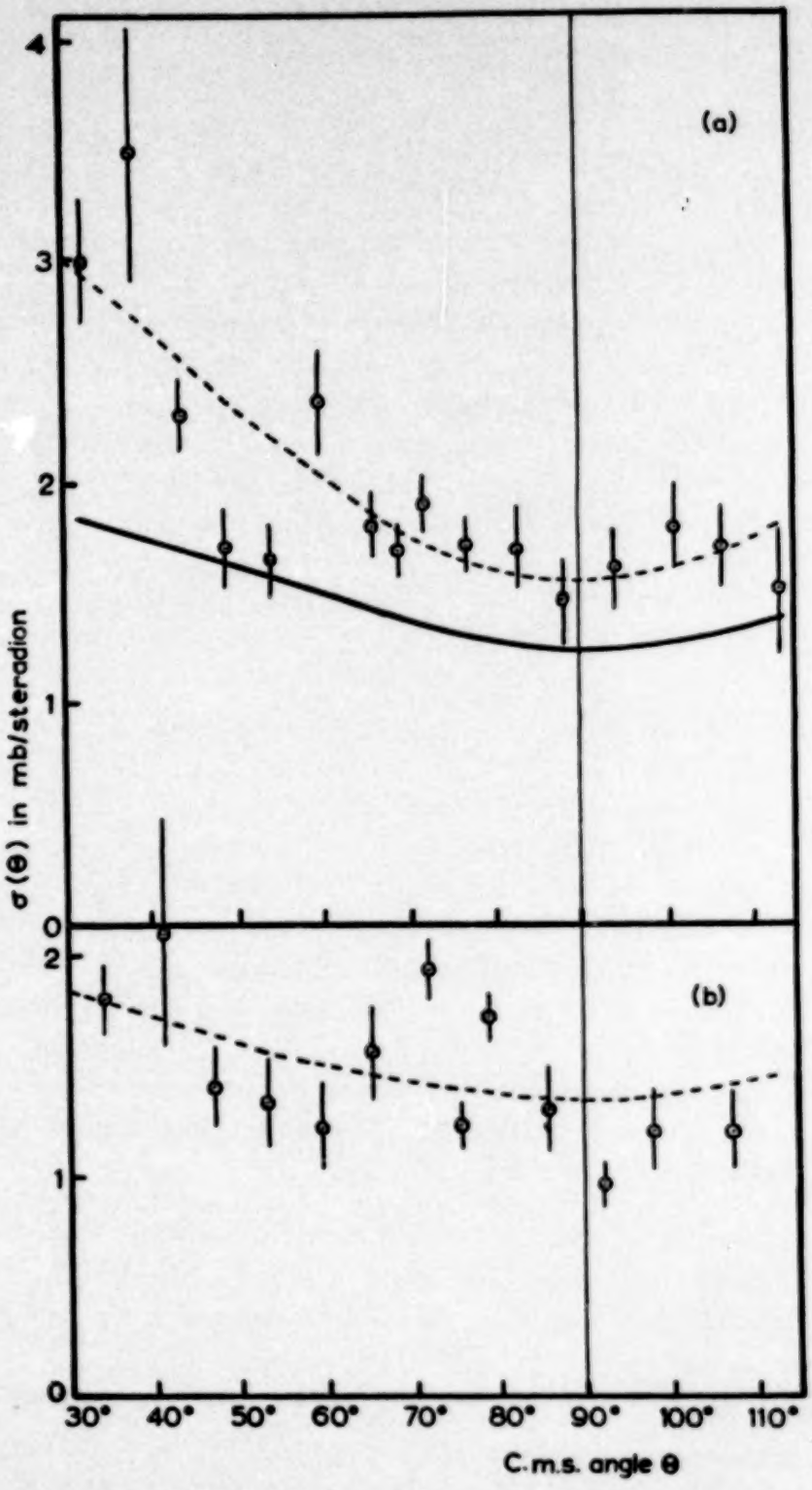

Fig. 2. Differential cross section for the reactions He^4 (α, p) Li^7, He^4 (α, p) Li^{7*}.
(a) Ground state transition. The dotted line is the least squares fit $\sigma(\theta) = 1.53+1.93\cos^2\theta$. The full line is the curve $\sigma(\theta) = 1.23+1.11\cos^2\theta-0.43\cos^4\theta$ predicted from the (p, α) reaction.
(b) Excited state transition. The dotted line is the least squares fit $\sigma(\theta) = 1.32+0.66\cos^2\theta$.

expression for the differential cross section for an incident energy E_p and centre of mass angle θ may be written

$$\sigma_{p\alpha}(E_p, \theta) = \pi\lambda\!\!\!^{-2}{}_p \frac{1}{(2s_1+1)(2s_2+1)} \sum_{S, m_s} \left| \sum_{j=0,2;\, l} \beta^l_{jS}(lS0m_s|jm_s) Y^{m_s}_j(\theta, \phi) \right|^2 \quad (4)$$

where β^l_{jS} is a matrix element, including a resonance denominator, for the transition from the initial state of a proton ($s_1 = \frac{1}{2}$) incident on a Li^7 nucleus ($s_2 = 3/2$) to a final state of two alpha particles ($s'_1 = s'_2 = 0$ and even relative orbital momentum) through an intermediate state of Be^8 with spin j, $\mathbf{S} = \mathbf{s}_1 + \mathbf{s}_2$ is the channel spin of the initial system, with quantum number S (= 1 or 2) and component m_s along the beam direction, and l is the incident orbital momentum quantum number, which must be odd because of conservation of parity. The matrix element β^l_{jS} may be written, in the notation of Inglis, as

$$\frac{\beta^l_{jS}}{4\sqrt{\pi}} = \frac{\left[\frac{lSj}{lj}\right] \phi_l(E)\alpha_l}{E - E_{res} + \frac{1}{2}i\Gamma},$$

where $\phi_l(E)$ is a penetrability factor and the quantities $[\frac{lSj}{lj}]$ and α_l, which are not required explicitly in the present work, are discussed by Inglis; β^l_{jS} is independent of m_s. The Clebsch-Gordan coefficient $(lS0m_s|jm_s)$ transforms from the (lS) representation to the j-scheme for the compound state, and j gives also the orbital momentum removed by the outgoing alpha particles; λ_p is the channel wave length (see ref. [4])) for the initial system. Inglis finds that the main features of the observed angular distribution for reaction (3) can be accounted for in terms of a narrow resonance with $j = 2^+$, a broad resonance with $j = 0^+$ and incident p-waves ($l = 1$). The addition of f-waves improves the agreement with experiment, but introduces extra parameters. The angular distribution obtained from (4) may be expressed, if f-waves are included, as

$$\sigma_{p\alpha}(E_p, \theta) = \sigma_{p\alpha}(90°)(1 + A(E)\cos^2\theta + B(E)\cos^4\theta) \quad (5)$$

where $A(E)$ and $B(E)$ may be obtained directly from the experimental results of Heydenburg, Hudson, Inglis and Whitehead [5]).

3. The (α, p) reaction leading to the ground state of Li^7

For reaction (1) forming Li^7 in the ground state the arguments of Inglis [3]) may be reversed to give

$$\sigma_{\alpha p}(E_\alpha, \theta) = \pi\lambda\!\!\!^{-2}_\alpha \frac{1}{(2s'_1+1)(2s'_2+1)} \sum_{S, m_s} \left| \sum_{j=0,2;\, l} \beta^l_{jS}(j0|lSm_s - m_s) Y^{m_s}_l(\theta, \phi) \right|^2 \quad (6)$$

where S is now the channel spin quantum number of the final system

Li^7+H^1, s'_1 $(= 0)$ and s'_2 $(= 0)$ are the spins of the two reacting particles, λ_α is the wavelength for the incident channel and it is assumed that the matrix elements β^l_{jS} have the same value as those for reaction (3) for the same energy of the compound system. The incident alpha particles thus interact through the s- and d-waves forming intermediate states of $j = 0^+$ and 2^+ which break up into Li^7+H^1 with odd relative orbital momentum. Comparison of equations (4) and (6) gives the result (which is familiar from the principle of detailed balancing)

$$\frac{\sigma_{p\alpha}(E_p, \theta)}{\sigma_{\alpha p}(E_\alpha, \theta)} = \frac{\lambda_p^2}{\lambda_\alpha^2} \frac{(2s'_1+1)(2s'_2+1)}{(2s_1+1)(2s_2+1)} \tag{7}$$

where E_α and E_p are the laboratory energies in reactions (1) and (3) which give the same excitation of the compound nucleus Be^8.

Experimental values of the quantities in this equation are given in table 1.

TABLE 1.

Comparison of Reactions $Li^7+H^1 \rightleftarrows He^4+He^4+17.34$ MeV

Reaction	E (Lab) MeV	Centre of mass energy MeV	Excitation energy of Be^8 MeV	$\lambda^2 \times 10^{-26}$ cm^2	$(2s_1+1) \times (2s_2+1)$	$\sigma(90°)$ cm · mb · ster^{-1}	$(2s_1+1) \times (2s_2+1) \times \frac{\sigma(90°)}{\lambda^2}$
He^4+He^4	38.5 ±0.2	19.25	19.15	0.543 ±0.003	1	1.53 ±0.09	2.81 ±0.20
Li^7+H^1	2.18 ±0.1	1.91	19.15	12.50 ±0.05	8	3.52 ±0.25	2.25 ±0.16

The cross section $\sigma_{p\alpha}(90°)$ for a proton energy of 2.2 MeV in the laboratory system was obtained from the data of Part II of this paper together with the excitation function and angular distribution for this reaction [5]). The figures in the last column are in fairly satisfactory agreement in view of the possible difference in the systematic errors of the two experiments.

The angular distribution predicted by (7) for the (α, p) reaction is obtained by substituting for $\sigma_{p\alpha}(E_p, \theta)$ from (5), taking $\sigma_{p\alpha}(90°)$ from table 1 and the coefficients $A(E)$ $(= 0.9)$ and $B(E) = (-0.35)$ from the results of Heydenburg, Hudson, Inglis and Whitehead [5]) for a proton energy of 2.2 MeV. This gives

$$\sigma_{\alpha p}(\theta) = 1.23+1.11 \cos^2\theta - 0.43 \cos^4\theta \text{ mb steradian}^{-1} \tag{8}$$

and this distribution is compared with the experimentally observed distribution in fig. 2a. The experimental results follow roughly the calculated curve with a slight change of scale; the points at 32° and 35°, for which the deviation is most marked, are the least accurate.

4. The (α, p) reaction leading to Li^{7*}

In the excited state transition observed in reaction (1) the channel spins of the final state (Li^7, $s_2 = \frac{1}{2}$; H^1, $s_1 = \frac{1}{2}$) are 0 and 1, of which only the latter can be formed by the emission of p or f waves from the intermediate state with $j = 0$ or 2. The relation between the ground state and excited state transitions may be seen by expanding equation (6) for the two cases, with the assumption, as a first approximation, that only outgoing p-waves are effective. This gives, for the ground state

$$\sigma_{\alpha p}(\theta) = \frac{\lambda_\alpha^2}{4}\left\{ 2\left|\frac{1}{\sqrt{2}}\beta_{01}+\tfrac{1}{2}\beta_{21}\right|^2+\tfrac{3}{2}|\beta_{22}|^2 + \cos^2\theta\left(|-\beta_{01}+\sqrt{2}\,\beta_{21}|^2 -2\left|\frac{1}{\sqrt{2}}\beta_{01}+\tfrac{1}{2}\beta_{21}\right|^2-\tfrac{3}{2}|\beta_{22}|^2\right)\right\} \quad (9)$$

and for the excited state

$$\sigma'_{\alpha p}(\theta) = \frac{\lambda_\alpha^2}{4}\left\{ 2\left|\frac{1}{\sqrt{2}}\beta'_{01}+\tfrac{1}{2}\beta'_{21}\right|^2 + \cos^2\theta\left(|-\beta'_{01}+\sqrt{2}\,\beta'_{21}|^2-2\left|\frac{1}{\sqrt{2}}\beta'_{01}+\tfrac{1}{2}\beta'_{21}\right|^2\right)\right\}. \quad (10)$$

The ground and the first excited states of Li^7 are usually described as a ^2P doublet, and have then the same spatial wave function. The β values for the two transitions should therefore differ mainly because of the penetrability factor $\phi_l(E)$ included in β. The term $|\beta_{22}|^2$ which occurs in (9) but not in (10) decreases the anisotropy of the ground state transition relative to that of the excited state transition. The observed distributions (2) show the opposite effect, so that $|\beta_{22}|^2$ is probably small in comparison with either $|\beta_{01}|^2$ or $|\beta_{21}|^2$ or both, as would be expected if LS coupling and an intermediate state of character $^1D_2$ were assumed. If $|\beta_{22}|^2$ is neglected the ratios $|\beta'_{01}/\beta_{01}|^2$ and $|\beta'_{21}/\beta_{21}|^2$ may be obtained by assuming that $\sigma'_{\alpha p}$ is proportional to $\sigma_{\alpha p}$ and by using the observed cross sections given in (2). It follows that

$$\frac{\sigma'_{\alpha p}}{\sigma_{\alpha p}}\frac{(90°)}{(90°)} = \left|\frac{\beta'_{01}}{\beta_{01}}\right|^2 = \left|\frac{\beta'_{21}}{\beta_{21}}\right|^2 = 0.86\pm0.09. \quad (11)$$

The value for this ratio predicted from the p-wave penetrabilities for the system Li^7+H^1 given by Christy and Latter [6]) is 0.66.

5. The total inelastic α—α cross-section

The total inelastic cross section σ_{tot} for the He^4+He^4 reaction at 38.5 MeV differs little from $\sigma_{\alpha p}+\sigma'_{\alpha p}$. This is because the energy is insufficient to induce (α, d), (α, t) or (α, He^3) reactions or to excite known levels in Li^7 above the 0.478 MeV state. The threshold energy for the He^4 (α, n) reaction

is 37.96 MeV and as this reaction and the (α, p) reaction are mirror processes they should have the same intrinsic probability. The energy of the present experiment is however much closer to threshold for the (α, n) reaction than for the mirror process, and a rough estimate of the barrier penetrabilities for p-waves suggests that the (α, n) yield would be less than 10 % of the (α, p) yield for an incident alpha particle energy of 38.5 MeV. This is consistent with the results of Walker, Link and Smith [7]) who found that the cross section for the (α, n) reaction at 39 MeV was less than 0.7 mb. The (α, n) reaction has therefore been disregarded. From (11) it then follows that $\sigma_{tot} = 1.86 \times 2\pi \int_0^\pi \sigma_{\alpha p}(\theta) \sin\theta \, d\theta$ and using the observed value of $\sigma_{\alpha p}(90°)$ from (2) and the angular distribution given by (8) we find that $\sigma_{tot} = 44 \pm 3$ mb.

In the approximation which neglects outgoing f-waves the total inelastic cross section may also be expressed, by integration of (9) and (10), as

$$\sigma_{tot} = \sigma_{\alpha p} + \sigma'_{\alpha p} = \pi \lambda_\alpha^2 (|\beta_{01}|^2 + |\beta'_{01}|^2 + |\beta_{21}|^2 + |\beta'_{21}|^2 + |\beta'_{22}|^2) = \sigma_0 + \sigma_2 \quad (12)$$

where

$$\sigma_0 = \pi \lambda_\alpha^2 (|\beta_{01}|^2 + |\beta'_{01}|^2), \quad \sigma_2 = \pi \lambda_\alpha^2 (|\beta_{21}|^2 + |\beta'_{21}|^2 + |\beta_{22}|^2) \quad (13)$$

are the partial inelastic cross sections for s and d waves. Values of σ_0 and σ_2 can then be obtained if the ratio $|\beta_{21}/\beta_{01}|^2$ is known.

This ratio has been estimated in two ways:

(a) by using the preliminary analysis given by Inglis [3]) for the (p, α) reaction. A typical set of resonance parameters used in this analysis assumes a d-wave level of width 0.1 MeV at a proton energy of 0.6 MeV. This leads to a value of $|\beta_{21}/\beta_{01}|^2 = 0.15$ and the s-wave cross section is found to be $2.3\pi\lambda_\alpha^2$ which is larger than the theoretical maximum.

(b) by assuming that the d-wave level concerned in the reactions is that found near 3 MeV, with a width of about 1 MeV, by Heydenburg *et al.* [5]). In this case the d-wave term makes the main contribution to the cross section and $|\beta_{21}/\beta_{01}|^2 = 2.85 \pm 0.4$. The partial cross sections in this case are found to be

$$\begin{aligned} \sigma_0 &= (0.66 \pm 0.06)\pi\lambda_\alpha^2 = 11 \pm 1 \text{ mb}, \\ \sigma_2 &= (1.92 \pm 0.2)\pi\lambda_\alpha^2 = 33 \pm 3 \text{ mb}. \end{aligned} \quad (14)$$

These cross sections will help in the analysis of the angular distributions of the elastic scattering of alpha particles by helium, which have now been obtained for the energy range 30—38.5 MeV.

We are grateful to Professor R. E. Peierls and to Dr. G. E. Brown for their interest in this work and particularly for suggesting a search for the inelastic processes in the α—α reaction.

References

1) W. E. Burcham, W. M. Gibson, D. J. Prowse and J. Rotblat, Nuclear Physics **3** (1957) 217
2) F. Ajzenberg and T. Lauritsen, Rev. Mod. Phys. **27** (1955) 77
3) D. R. Inglis, Phys. Rev. **74** (1948) 21
4) J. B. Blatt and V. F. Weisskopf, Theoretical Nuclear Physics (John Wiley, New York, 1953) pp. 315, 320, 377
5) N. P. Heydenburg, C. M. Hudson, D. R. Inglis and W. D. Whitehead, Phys. Rev. **73** (1948) 241; **74** (1948) 405
6) R. F. Christy and R. Latter, Rev. Mod. Phys. **20** (1948) 185
7) D. Walker, W. T. Link and W. I. B. Smith, Proc. Phys. Soc. A **65** (1952) 861

II. THE REACTION Li^7 (p, α)He^4

JOAN M. FREEMAN, R. C. HANNA and J. H. MONTAGUE
Atomic Energy Research Establishment, Harwell

Received 12 July 1957

Abstract: The absolute differential cross section for the Li^7 (p, α) He^4 reaction at 90° has been measured for a number of proton energies between 1 and 1.5 MeV for comparison with results on the inverse reaction He^4 (α, p) Li^7.

Although a number of measurements have been made of the excitation function and angular distributions of the α-particles emitted in the Li^7 (p, α) He^4 reaction [1]), no precise data on absolute yields are available. We have made some absolute measurements of the cross section at 90°, in the proton energy range 1.0 to 1.5 MeV, in order to provide data required for use in connection with experiments on the inverse reaction He^4(α, p)Li^7 (described in Part I of this paper).

Thin targets of lithium fluoride (2 to 3 keV thick for 1.5 MeV protons) were prepared by evaporation on to 0.005 mm thick aluminium backings, the mass of LiF per unit area being determined by weighing. These were bombarded by a collimated beam of protons from the Harwell Van de Graaff machine and the reaction products emitted at an angle of 90° to the beam direction were detected by a 2.5 mm thick CsI(Tl) crystal mounted on an E.M.I. photomultiplier, the crystal being shielded from light by a thin aluminium foil. The solid angle subtended by the crystal at the beam spot on the target was estimated (i) from the geometry, (ii) by counting the α-particles from calibrated Am^{241} sources placed at the position occupied by the target spot. The direction of the target normal was set to an angle of 45° with respect to the proton beam. The number of protons bombarding the target was measured by collecting the beam on a tantalum plate mounted behind the target and connecting the target and collector to a current

integrator; secondary emission was suppressed by applying suitable potentials to the target and a grid placed in front of the target. The spectra of pulses obtained in the CsI (Tl) crystal were displayed on a hundred-channel pulse-height analyser. Alpha-particle groups due to the reactions Li^7 (p, α) He^4 and F^{19} (p, α_0) O^{16} (ground-state transitions) were completely resolved provided the beam intensity was kept low enough to prevent build-up on the small pulses due to scattered protons. With the beam intensities used, not more than 3 % of the fluorine α-pulses were displaced into the peak of lithium α-pulses; a correction was applied by assuming the peak shapes of the two α-particle groups to be the same. The number of α-particles from each reaction was measured for a given proton charge as a function of proton energy at small intervals in the range 1.3 to 1.5 MeV. In this way a measurement of the α-particle yield from the F^{19}(p, α_0) reaction at the peak of the 1.36 MeV resonance was obtained simultaneously with the yield from the lithium reaction. A value for the cross-section of the fluorine reaction has already been obtained by Clarke and Paul [2]), so this procedure provided a check on our absolute measurements. Our estimate of the fluorine cross-section at 90° at the 1.36 MeV resonance is 2.71 ± 0.27 millibarns per steradian. The value calculated from Clarke and Paul's results is 2.16 ± 0.32 millibarns per steradian, which is in fair agreement with our value.

The cross-section for the Li^7 (p, α) He^4 reaction was calculated for four proton energies (i) from our absolute measurements and (ii) by comparison with the F^{19}(p, α_0) cross-section at the 1.36 MeV resonance, for which the value of Clarke and Paul was assumed (account was taken of the fact that in the lithium reaction two α-particles are emitted per disintegration). The means of these two sets of results are given in table 1. The errors shown refer to the absolute values; the errors on the relative values at ditferent proton energies are about ± 4 %.

TABLE 1.

Proton energy (MeV)	1.01	1.28	1.36	1.47
Cross-section of Li (p, α) at 90° (lab. system) mb · sterad^{-1}	0.67 ± 0.06	0.79 ± 0.07	0.94 ± 0.08	1.16 ± 0.10

Values of the absolute cross-section can be obtained over a wider range of energy and at angles other than 90° by combining the results given in table 1 with the relative cross-section values of Heydenburg, Hudson, Inglis and Whitehead [3]).

References

1) F. Ajzenberg and T. Lauritsen, Rev. Mod. Phys. **27** (1955) 77
2) R. L. Clarke and E. B. Paul, Canad. J. Phys. **35** (1957) 155
3) N. P. Heydenburg, C. M. Hudson, D. R. Inglis and W. D. Whitehead, Phys. Rev. **73** (1948) 241

Nuclear Physics **5** (1958) 150—166; © *North-Holland Publishing Co., Amsterdam*
Not to be reproduced by photoprint or microfilm without written permission from the publisher

LA DIFFUSION D'UN PROJECTILE PAR UN SYSTÈME COMPLEXE LIÉ

J. YVON

Centre d'Études Nucléaires de Saclay, Gif-sur-Yvette (S & O)

Reçu le 1er juin 1957

Abstract: In the calculation of coherent scattering, the perturbation method is replaced by the search for an equation of propagation which would allow the progress of the diffusion to be followed from point to point. The method consists, after the traditional perturbation calculation, in eliminating the incident radiation by expressing it as a function of the scattered coherent radiation. In the case of a system originally in a well defined quantum state, the coherent wave is propagated according to an optical type equation. In the case of a system in thermodynamic equilibrium, this property also belongs to the optical wave, which is a certain average of the elementary coherent waves. An analogous method, when applied to the mixture which represents the overall scattering, allows the origin and propagation of this scattering to be followed at the same time. In the case of light scattering, more detailed deductions relative to Rayleigh scattering may be expected-intensity and fine structure. Considered from a more general viewpoint, the theory proposed is a theory of the brownian motion of a microscopic particle. The fundamental equation which summarises this theory is a generalized form of the Boltzmann equation.

1. Introduction

Des études sur la diffusion de la lumière dans un milieu transparent [1]). d'autres études analogues sur la diffusion des neutrons, m'ont montré l'utilité de développer une théorie formelle mais générale de ces phénomènes. L'avantage d'attaquer un tel problème avec une grande généralité est d'estomper certains détails et de mettre en évidence seulement les difficultés fondamentales — ou du moins certaines d'entre elles.

Dans le cas des neutrons, l'intérêt du sujet est surtout de bien poser le problème. Dans le cas de la lumière, l'ambition est plus grande. En effet les opinions les plus diverses règnent sur l'importance de l'intensité diffusée, autrement dit sur la valeur du rapport de Rayleigh. Récemment Fixman [2]) reprenant les méthodes mêmes de l'auteur, parvient à un résultat différent et revient à l'ancienne formule d'Einstein. Ce n'est pas l'expérience qui départagera, pour le moment, les théoriciens; Rousset [3]) a en effet dénoncé l'inconsistance qui règne quant aux valeurs expérimentales du rapport de Rayleigh. Cabannes [4]) est également revenu récemment sur le sujet. L'étude de la diffusion Rayleigh appelle de nouveaux efforts.

Le diffuseur est lié. Ses états quantiques sont discrets. C'est un système complexe, c'est à dire constitué de nombreuses particules: l'acte de diffusion

résulte d'une interaction relativement élémentaire entre la particule incidente (le projectile) et l'une des particules du diffuseur. L'effet moyen de ces actes innombrables qui se produisent au hasard présente une certaine organisation qui se manifeste particulièrement dans l'onde cohérente. C'est cette organisation qu'on cherchera à mettre en évidence.

Nous étudierons successivement le cas d'un diffuseur initialement dans un état bien déterminé, puis le cas d'un diffuseur en équilibre thermodynamique.

2. Onde Incidente et Onde Réelle

Des parois entourent le diffuseur. Elles sont imperméables aux particules qui constituent ce dernier. Les particules ne peuvent s'échapper. Les parois du diffuseur sont par contre traversées librement par le projectile incident. De telles parois sont évidemment schématiques, mais elles ne gênent pas le traitement des phénomènes physiques auxquels nous entendons nous limiter.

Le diffuseur a un hamiltonien H, des états propres discrets n, p, . . ., des fonctions propres $\phi_n, \phi_p, \ldots$, auxquels correspondent les valeurs propres de l'énergie E_n, E_p. Les fonctions ϕ_n forment un système orthonormé complet à l'intérieur du volume offert au diffuseur.

Le projectile a un hamiltonien K. A cet hamiltonien correspond un spectre continu. Une fonction d'onde du diffuseur sera représentée par la lettre χ munie d'indices appropriés le cas échéant.

L'hamiltonien d'interaction entre le diffuseur et le projectile sera représenté par V, une fonction d'onde du système global par Ψ. L'interaction V s'annule dès que le projectile est tant soit peu éloigné du diffuseur.

Nous supposerons, pour simplifier l'écriture, que la constante de Planck est égale à l'unité.

L'équation de propagation de Ψ est l'équation de Schrödinger

$$i\frac{\partial}{\partial t}\Psi = (H+K+V)\Psi. \tag{1}$$

Cette équation définit la fonction Ψ à tout instant si celle-ci est définie à l'instant initial. L'instant initial est rejeté à un instant très reculé. Les conditions initiales sont donc définies par $\Psi(-\infty)$.

Nous supposons que pendant la phase initiale le projectile, qui se rapproche peu à peu du diffuseur, en reste néanmoins assez éloigné pour que l'interaction reste nulle. L'état du système évolue donc alors d'après l'équation

$$i\frac{\partial}{\partial t}\Psi = (H+K)\Psi. \tag{2}$$

Nous utiliserons comme référence, non seulement pendant la période initiale, mais même à tout instant, l'état décrit par l'équation précédente. Nous le qualifierons d'état „incident". Pour distinguer la fonction d'onde

incidente de la fonction d'onde réelle, nous désignerons la première par Ψ_0. Nous écrirons donc

$$i\frac{\partial}{\partial t}\Psi_0 = (H+K)\Psi_0, \tag{3}$$

en même temps que, bien entendu,

$$\Psi_0(-\infty) = \Psi(-\infty). \tag{4}$$

Un premier point de la méthode que nous suivrons consiste à exprimer $\Psi(t)$ en fonction de $\Psi_0(t)$. Les équations (1), (3) et (4) permettent d'écrire

$$\Psi(t) = \lim_{\theta\to\infty} e^{-i(H+K+V)\theta} \cdot e^{i(H+K)\theta} \cdot \Psi_0(t). \tag{5}$$

Nous poserons

$$\Omega = \lim_{\theta\to\infty} e^{-i(H+K+V)\theta} \cdot e^{i(H+K)\theta}. \tag{6}$$

L'opérateur Ω est unitaire.

3. Hypothèse sur l'état Initial. Cohérence et Incohérence

Nous énonçons maintenant une nouvelle hypothèse: c'est l'absence avant l'interaction de toute corrélation entre le projectile et le diffuseur. Cette hypothèse se traduit par le fait que l'état initial est le produit d'un état du projectile par un état du diffuseur. Cette propriété reste vraie à tout instant pour l'état incident:

$$\Psi_0 = \chi_0\phi. \tag{1}$$

Cette hypothèse est tellement naturelle qu'on omet généralement de l'énoncer explicitement. Mais elle est trop fondamentale dans notre étude pour que nous puissions l'utiliser sans la mettre en valeur. Il convient d'en préciser une limitation: une relation telle que (1) n'est possible que si le diffuseur ne contient pas de particules de même nature que le projectile. Dans ce cas il pourrait se produire des phénomènes d'échange: des opérateurs de permutation devraient alors compléter la formule (1).

Nous supposons de plus que l'état initial du diffuseur est un état propre soit l'état n. Nous poserons donc en définitive

$$\Psi_0 = \chi_0\phi_n. \tag{2}$$

Il est clair que χ_0 vérifie l'équation

$$i\frac{\partial}{\partial t}\chi_0 = K\chi_0. \tag{3}$$

Nous représenterons la fonction d'onde réelle à l'aide des fonctions propres du diffuseur et de fonctions à déterminer du projectile:

$$\psi = \sum \chi_p \phi_p; \tag{4}$$

χ_n représente l'onde cohérente — qui se confond avant l'interaction avec l'onde χ_0.

Il y a de plus une infinité d'ondes incohérentes dont l'une est représentée par χ_p. La diffusion amène le projectile à l'état de mélange, ce mélange étant représenté par l'expression suivante:

$$\sum_p |\chi_p\rangle\langle\chi_p| . \tag{5}$$

La théorie de la diffusion porte essentiellement sur l'étude de ce mélange, car dans les expériences de diffusion les mesures concernent seulement le projectile.

4. Propagation des Ondes Diffusées

Introduisons l'expression § 3 (2) dans § 2 (5) et projetons membre à membre sur l'état n. Il vient

$$\chi_n = \langle n|\Omega|n\rangle\chi_0 . \tag{1}$$

Nous désignerons l'élément de matrice $\langle n|\Omega|n\rangle$ tantôt par Ω_{nn}, quand nous l'envisagerons comme l'une des composantes de la matrice $\langle p|\Omega|q\rangle$, tantôt, plus simplement, par Ω_n, quand nous l'envisagerons à part comme un opérateur qui ne concerne que le projectile. L'opérateur en question n'est ni unitaire ni hermitique. Nous récrirons donc la formule (1):

$$\chi_n = \Omega_n\chi_0 . \tag{2}$$

Inversement

$$\chi_0 = \Omega_n^{-1}\chi_n . \tag{3}$$

Portons ce résultat dans § 3 (3). Il vient

$$i\frac{\partial}{\partial t}\chi_n = G_n\chi_n , \tag{4}$$

en posant pour abréger

$$G_n = \Omega_n K \Omega_n^{-1} . \tag{5}$$

L'opérateur G_n n'est pas hermitique. On peut le mettre sous la forme:

$$G_n = G_n^R + iG_n^I , \tag{6}$$

les opérateurs G_n^R et G_n^I étant l'un et l'autre hermitiques. Si le premier existait seul, l'onde cohérente se propagerait dans le diffuseur comme une onde sans diffusion, autrement dit comme une onde libre, à l'hamiltonien près. En fait l'onde s'affaiblit par suite de l'apparition progressive d'ondes incohérentes. C'est ce qu'exprime la seconde composante de G_n. Notons que la diffusion ne comporte pas seulement des effets d'affaiblissement; des effets de renforcement par diffusion des ondes incohérentes sont possibles: mais on peut prévoir qu'ils ne seront pas très importants.

L'onde incohérente p, calculée par la même procédure que l'onde cohérente, s'écrit

$$\chi_p = \langle p|\Omega|n\rangle\chi_0 = \Omega_{pn}\chi_0 . \tag{7}$$

Mais on imagine que l'onde cohérente représente beaucoup mieux que l'onde incidente le passage du projectile à travers le diffuseur. Dans l'expression précédente, on élimine comme ci-dessus l'onde incidente en faveur de l'onde cohérente:

$$\chi_p = \Omega_{pn}\Omega_n^{-1}\chi_n. \tag{8}$$

L'onde incohérente, une fois créée, se propage dans un diffuseur qui se trouve dans l'état p. Si on néglige les phénomènes de diffusion qu'elle peut subir à son tour, sa propagation s'effectue suivant l'équation sans diffusion

$$\left(i\frac{\partial}{\partial t} - G_p^R\right)\chi_p = 0. \tag{9}$$

Appliquons l'opérateur $i(\partial/\partial t) - G_p^R$ aux deux membres de l'équation (7). Nous obtiendrons cette fois une équation rigoureuse

$$\left(i\frac{\partial}{\partial t} - G_p^R\right)\chi_p = \{\Omega_{pn}K - G_p^R\Omega_{pn}\}\Omega_n^{-1}\chi_n. \tag{10}$$

C'est l'équation de propagation de l'onde incohérente, compte tenu des actes créateurs ou destructeurs qui modifient son intensité. Ces actes ont été rattachés, un peu artificiellement, à l'onde cohérente. Dans la réalité physique ce sont toutes les ondes n, p, ... qui réagissent les unes sur les autres. L'équation (10) est néanmoins un moyen passable de résumer ces actes divers. Nous n'approfondirons pas cette question.

Il serait d'autre part intéressant d'examiner si les opérateurs G_n^R, G_p^R peuvent avoir des valeurs propres discrètes: il leur correspondrait des résonances du projectile au sein du diffuseur. Cette question se pose notamment dans la théorie des réactions nucléaires (C. Bloch [5]).

Nous laisserons ce point de côté, l'effort portera maintenant sur une méthode d'approximation.

5. Développement des Opérateurs

En négligeant de spécifier qu'il s'agit d'une expression limite pour θ infiniment grand, nous récrivons l'opérateur Ω

$$\Omega = e^{-i(H+K+V)\theta} \cdot e^{i(H+K)\theta}. \tag{1}$$

Une autre écriture est commode:

$$\Omega = e^{-i(H+K+V|-H-K)\theta}; \tag{2}$$

ici la ligne verticale ponctuée indique dans quel ordre doivent être appliqués les opérateurs.

Une limite comme la précédente peut s'écrire de diverses manières. Le lecteur se reportera à l'ouvrage de Heitler [6]). Nous écrirons maintenant

$$\Omega = \frac{i\sigma}{-(H+K+V)|+H+K+i\sigma}, \tag{3}$$

σ étant un nombre positif infiniment petit. On lit sur cette formule, comme d'ailleurs évidemment sur la formule (1), que l'opérateur Ω se réduit à l'opérateur identique si l'interaction V est nulle.

Compte tenu de cette remarque, la formule (3) est équivalente à la suivante:

$$\Omega(H+K+i\sigma)-(H+K+V)\Omega = i\sigma, \tag{4}$$

ou encore, en faisant apparaître l'interaction comme une perturbation,

$$\Omega(H+K+i\sigma)-(H+K)\Omega = i\sigma+V\Omega. \tag{5}$$

Cette équation peut être résolue par approximations successives, V étant traité comme une quantité du premier ordre. L'opérateur cherché est représenté par l'expression suivante:

$$\Omega = 1-\zeta_1+\zeta_2-\zeta_3+\ldots, \tag{6}$$

avec

$$\zeta_1 = \frac{|V|}{|H+K|\ |-(H+K+i\sigma)|}, \tag{7}$$

$$\zeta_2 = \frac{|V|\ \dfrac{|V|}{|H+K|\ |-(H+K+i\sigma)|}}{|H+K|\ |\ |-(H+K+i\sigma)|}, \tag{8}$$

....

Posons

$$\zeta_{1n} = \langle n|\zeta_1|n\rangle = \frac{|V|}{|K|\ |-(K+i\sigma)|} \tag{9}$$

$$\zeta_{2n} = \langle n|\zeta_2|n\rangle = \ldots\ \ \ldots. \tag{10}$$

Il vient

$$\Omega_n = 1-\zeta_{1n}+\zeta_{2n}-\zeta_{3n}+\ldots,$$

puis en inversant

$$\Omega_n^{-1} = 1+\zeta_{1n}-\zeta_{2n}+(\zeta_{1n})^2+\zeta_{3n}-\zeta_{1n}\zeta_{2n}-\zeta_{2n}\zeta_{1n}+(\zeta_{1n})^3-\ldots. \tag{11}$$

Récrivons l'opérateur de propagation de l'onde cohérente défini par § 4 (5):

$$G_n = \Omega_n K \Omega_n^{-1}. \tag{12}$$

L'équation (5) permet de commuter Ω_n et K. On en déduit en effet

$$\Omega_n K = K\Omega_n+i\sigma(1-\Omega_n)+(V\Omega)_n. \tag{13}$$

Le terme en σ, nécessaire pour la définition correcte de Ω, est négligeable ici. Il vient donc

$$G_n = K+(V\Omega)_n\Omega_n^{-1}, \tag{14}$$

soit, en se limitant au troisième ordre,

$$G_n = K+V_n-(V\zeta_1)_n+V_n\zeta_{1n}+V\zeta_{2n} \\ -(V\zeta_1)_n\zeta_{1n}-V_n\zeta_{2n}+V_n\zeta_{1n}{}^2-\ldots. \qquad (15)$$

Le terme du second ordre, par exemple — changé de signe — s'explicite:

$$\sum_{p\neq n}\langle n|V|p\rangle\langle p|\zeta_1|n\rangle.$$

Le fait que les éléments de matrice diagonaux disparaissent assure, au moins dans les circonstances favorables, une convergence plus rapide au développement de G_n qu'au développement (6) de Ω.

6. Onde Monochromatique

Lorsque l'onde incidente est monochromatique il se produit une certaine simplification. Désignons par E_0 l'énergie qui correspond à l'onde χ_0:

$$E_0\chi_0 = K\chi_0. \qquad (1)$$

La relation

$$\Psi = (1-\zeta_1+\zeta_2-\zeta_3+\ldots)\Psi \qquad (2)$$

peut s'écrire maintenant

$$\Psi = (1-ZV+(ZV)^2-(ZV)^3-\ldots)\Psi_0, \qquad (3)$$

le nouvel opérateur Z étant défini par la relation suivante:

$$Z = (H+K-E_0-E_n-i\sigma)^{-1}. \qquad (4)$$

Cet opérateur, qui gouverne la propagation de la diffusion d'une interaction élémentaire à la suivante peut être qualifié de „propagateur". Le terme complexe infiniment petit $i\sigma$ est indispensable à sa définition. Il assure que les ondes successives qui prennent naissance ne sont jamais des ondes convergentes: elles ne peuvent être que divergentes ou stationnaires (c'est à dire pour ces dernières du type e^{-kr}/r, k étant réel).

De la relation (3) on déduit

$$\chi_n = \{1-(ZV)_n+[(ZV)^2]_n-[(ZV)^3]_n+\ldots\}\chi_0. \qquad (5)$$

En résolvant par rapport à χ_0,

$$\chi_0 = \{1+(ZV)_n-[(ZV)^2]_n+[(ZV)_n]^2+[(ZV)^3]_n \\ -(ZV)_n[(ZV)^2]_n-[(ZV)^2]_n(ZV)_n+[(ZV)_n]^3-\ldots\}\chi_n. \qquad (6)$$

Le terme du second ordre, par exemple, prend une forme suggestive. Nous l'écrivons à part en le changeant de signe:

$$[(ZV)^2]_n-[(ZV)_n]^2. \qquad (7)$$

Il apparaît comme le carré moyen de la fluctuation de ZV. Comme les fluctuations sont parfois faibles, on conçoit qu'il puisse ne pas être très important. C'est une autre manière de souligner le fait déjà mentionné au paragraphe précédent que l'élimination de l'onde incidente en faveur de

l'onde réelle favorise la convergence de développements qui initialement sont surtout justifiés par la petitesse supposée de l'interaction. Comme les fluctuations sont d'autant plus faibles qu'intervient mieux la loi des grands nombres, ajoutons que nos propositions seront d'autant plus vraisemblables que le système diffusant contiendra plus de particules agissantes. Nous préciserons davantage ces idées à propos de la diffusion par un système thermodynamique.

Appliquons aux deux membres de l'équation (6) l'opérateur $K-E_0$. Compte tenu de la relation

$$\langle \mathrm{n}|Z = (K-E_0-i\sigma)^{-1}\langle \mathrm{n}| \tag{8}$$

et en négligeant σ dans le produit

$$(K-E_0)(K-E_0-i\sigma)^{-1} \tag{9}$$

ce qui est permis puisque le second facteur n'est qu'un inverse particulier du premier, on obtient l'équation suivante pour la propagation de l'onde cohérente:

$$\{K+V_\mathrm{n}-(VZV)_\mathrm{n}+V_\mathrm{n}(ZV)_\mathrm{n}+(VZVZV)_\mathrm{n}-V_\mathrm{n}(ZVZV)_\mathrm{n} -(VZV)_\mathrm{n}(ZV)_\mathrm{n}+V_\mathrm{n}(ZV)_\mathrm{n}(ZV)_\mathrm{n}-\ldots\}\chi_\mathrm{n} = E_0\chi_\mathrm{n}. \tag{10}$$

Lorsqu'on aura affaire à une onde monochromatique, cette équation sera plus commode à utiliser que l'équation générale § 4 (4). Les développements par rapport à l'interaction étant limités au même ordre, ils ne sont pas équivalents. Le propagateur Z dépend en effet de E_0 ou, si l'on préfère, de la longueur d'onde dans le vide. Dans le cas où le milieu diffusant est homogène et si l'onde cohérente est une onde plane, l'application de G_n à χ_n fera apparaître, au contraire, la longueur d'onde dans le milieu diffusant †.

7. Diffusion par un Système Thermodynamique L'Onde Optique

Maintenant le système diffuseur est un système macroscopique en équilibre thermodynamique. P_n est la probabilité pour qu'il se trouve initialement dans l'état n. Le projectile, avant l'interaction, se trouve dans l'état monocinétique χ_0. Mais nous désignerons maintenant par χ_{nn} et χ_{pn} l'onde cohérente et l'onde incohérente respectivement produites par le diffuseur initialement dans l'état n.

La diffusion amène le projectile à l'état de mélange. Ce mélange s'écrit

$$\nu = \sum_{\mathrm{n,\,p}} P_\mathrm{n}|\chi_{\mathrm{pn}}\rangle\langle\chi_{\mathrm{pn}}|. \tag{1}$$

† Un intéressant mémoire de Watson [7]) vient de paraître qui traite en principe le même sujet que le présent mémoire. On y trouve, entre autres choses, l'idée d'étudier la diffusion inélastique à partir de l'onde cohérente et aussi une formulation de l'équation de propagation de cette onde. Watson n'aborde pas systématiquement l'étude des systèmes thermodynamiques. On fera attention que l'opérateur défini ici en § 2 (6) n'est pas identique à celui que Watson définit par son équation (8).

On distinguera encore ici la diffusion cohérente, qui ne comporte pas de changement d'état du diffuseur et qui donne naissance au mélange:

$$\nu_C = \sum_n P_n |\chi_{nn}\rangle\langle\chi_{nn}|, \tag{2}$$

et la diffusion incohérente qui comprend le reste du mélange (1).

Dans le cas de la diffusion par un système thermodynamique, il est essentiel d'introduire l'onde optique, qui est la moyenne des ondes cohérentes:

$$\chi = \sum_n P_n \chi_{nn}. \tag{3}$$

Le mélange

$$\nu_C - |\chi\rangle\langle\chi| \tag{4}$$

a un caractère de fluctuation. Il faut s'attendre à ce qu'il soit petit, et, ce qui suppose aussi que la diffusion incohérente soit peu importante, à ce que le projectile se trouve essentiellement sur l'onde optique.

L'expression de l'onde optique, obtenue par la méthode de perturbation, se déduit aisément de § 6 (3). Il faut introduire ici une notation plus précise et poser

$$Z_n = (H+K-E_0-E_n-i\sigma)^{-1}. \tag{5}$$

Il vient

$$\chi = \{1 - \sum P_n\langle n|Z_nV|n\rangle + \sum P_n\langle n|(Z_nV)^2|n\rangle - \ldots\}\chi_0. \tag{6}$$

Résolvons par rapport à χ_0. Nous écrirons d'une manière générale, X_n étant un opérateur qui dépend de l'état n,

$$\sum P_n\langle n|X_n|n\rangle = \langle X_n\rangle. \tag{7}$$

Il vient

$$\chi_0 = \{1+\langle Z_nV\rangle - \langle Z_nVZ_nV\rangle + (\langle Z_nV\rangle)^2 + \ldots\}\chi. \tag{8}$$

En appliquant l'opérateur $H-E_0$ on obtient l'équation suivante:

$$\{H-E_0+\langle V\rangle - \langle VZ_nV\rangle + \langle V\rangle\langle Z_nV\rangle + \langle VZ_nVZ_nV\rangle - \langle V\rangle\langle Z_nVZ_nV\rangle - \langle VZ_nV\rangle\langle VZ_nV\rangle + \langle V\rangle(\langle Z_nV\rangle)^2 + \ldots\}\chi = 0. \tag{9}$$

Telle est l'équation fondamentale de l'optique des milieux réfringents. On comprend que cette équation puisse être maniable si les termes des premiers ordres donnent une approximation suffisante.

L'interaction entre le projectile et le diffuseur a lieu, comme nous l'avons souligné dans l'introduction, entre le projectile et les particules constituantes du diffuseur. La particule diffusée exécute un va et vient compliqué d'une particule diffusante à l'autre. C'est le rôle du propagateur Z_n de transcrire ces mouvements. Comme seuls interviennent, à partir du second ordre, des écarts de fluctuation, les trajets correspondants sont courts. Il en résulte que, dans la fonction de Green du propagateur, qui est du type e^{ikr}/r, la valeur de k n'a pas beaucoup d'importance, du moins si k^{-1} est grand devant le „grain" du milieu diffusant. Au lieu d'adopter pour k la valeur correcte, on

peut adopter une valeur standard: sa valeur dans le vide. On néglige donc dans une certaine mesure les variations d'énergie du projectile dans ses diffusions multiples.

On remplace donc le propagateur Z_n par une approximation qui est

$$Z_0 = (K - E_0 - i\sigma)^{-1}.$$

Les moyennes telles que la correction du 2nd ordre W_2 à l'énergie s'en trouvent toutes simplifiées parce que maintenant le propagateur commute avec les états du diffuseur. Par exemple maintenant W_2 est la trace du produit de l'opérateur densité du diffuseur par l'opérateur VZ_0V. Le calcul n'exige d'ailleurs pas la connaissance de l'opérateur densité complet, relatif à tous les degrés de liberté du système diffusant, mais seulement de l'opérateur densité à deux particules. Celui-ci s'obtient à partir de l'opérateur complet par voie régressive. Mais surtout ses propriétés sont assez faciles à imaginer qualitativement. De plus il existe à son sujet des théorèmes généraux. On retiendra que l'approximation proposée ici est d'autant plus justifiée que la longueur d'onde du projectile est plus grande, ou son énergie cinétique plus faible.

Les raisonnements précédents appellent une certaine réserve. L'hypothèse des „trajets courts" est parfaitement justifiée quand Z_0 a remplacé Z_n. Il n'est pas sûr qu'elle le soit auparavant et il est possible que nous ayons fait appel prématurément à cette hypothèse. C'est un point qu'il conviendrait d'approfondir. Dans la suite de cette étude, nous ferons néanmoins confiance à l'hypothèse des trajets courts.

Il en résulte que l'opérateur de propagation de l'onde optique est un opérateur local. Appliqué à la fonction d'onde optique, il ne fait intervenir les valeurs de celle-ci qu'en un point et dans son voisinage immédiat. Ceci est en définitive une conséquence de l'absence de corrélations entre des particules d'un milieu quelconque lorsque leur distance dépasse le „grain" du milieu.

Dans une région oú le milieu est homogène, l'onde optique peut être représentée par des ondes planes. L'équation (9) détermine alors la longueur d'onde de ces ondes, ou, ce qui revient au même, elle définit un indice de réfraction. En général, dès qu'on tient compte au moins des termes du second ordre, l'indice de réfraction est imaginaire. L'onde cohérente s'affaiblit au cours de sa propagation. On se représente la diffusion comme prenant naissance au sein de l'onde optique et l'affaiblissant progressivement.

Les termes du second ordre de l'équation (5) généralisent dans le cas de l'optique générale le champ de Lorentz qui est classique dans l'optique proprement dite.

On peut en induire que les termes du troisième ordre et les termes d'ordre supérieur seront négligeables lorsque l'interaction sera du type qui gouverne

la diffusion de la lumière: intense pour le projectile mais faible du point de vue du milieu diffusant.

On comprend que l'équation (5) puisse être maniable si les termes des premiers ordres donnent une approximation suffisante et si on peut se représenter a priori les opérateur-densités en question.

Si le milieu est isotrope, l'indice de réfraction sera naturellement indépendant de la direction de propagation.

Supposons qu'on puisse, schématiquement, représenter le milieu diffusant comme un milieu homogène séparé du vide par une frontière franche: l'indice de réfraction est discontinu. La propagation de l'onde optique pourra se calculer, en principe, suivant les procédés classiques de l'optique.

Le calcul de la partie réelle de l'indice de réfraction est à peu près insensible à la substitution de Z_0 à Z_n. C'est l'indice d'extinction qui s'en trouvera altéré, et probablement médiocrement lorsque la diffusion incohérente macroscopique reste au voisinage de la fréquence incidente: il y a des chances alors pour que les actes incohérents microscopiques qui obligent en toute rigueur à remplacer Z_0 par Z_n soient peu dispersifs.

Le formalisme que nous avons présenté s'applique directement aux neutrons. Dans le cas de la lumière l'exposé sort de la tradition puisque d'ordinaire ni le milieu diffusant ni la lumière ne sont quantifiés. Mais la quantification est avantageuse; elle n'apporte pas de complication sérieuse et elle procure des notations commodes. Elle permet de traiter en principe la diffusion incohérente. Les électrons optiques du milieu diffusant sont des vibrateurs harmoniques. Leur fréquence propre est très supérieure à la fréquence de la lumière incidente. Ces électrons sont traités dans l'approximation dipolaire. Avant que la lumière n'atteigne le milieu diffusant, ils sont tous dans l'état fondamental. La lumière ne provoque que des transitions virtuelles vers le premier état excité. Si on néglige de mentionner explicitement les créations ou les absorptions virtuelles de photons, c'est un unique photon que l'on suit de bout en bout. Il en résulte que les raisonnements ne diffèrent pas de ceux qu'on peut faire pour un neutron.

Dans le cas de la diffusion des neutrons par un milieu macroscopique, on représente l'interaction entre les noyaux diffuseurs et le neutron par le potentiel singulier de Fermi, amélioré pour pouvoir aller jusqu'au second ordre par les prescriptions de Blatt et Weiskopf [8]) destinées à supprimer certaines singularités. Une telle précision dans le calcul de l'indice de réfraction pourrait s'avérer utile si la détermination de l'interaction électron-neutron devait reposer en définitive sur des mesures d'indice de réfraction.

Nous sommes restés ici sur leplan des généralités, ou du moins de certaines généralités. L'effort a porté uniquement sur les problèmes statistiques. Le lecteur trouvera une mise au point récente de la question du point de vue de l'optique chez Fuller Brown [9]). Il trouvera dans les travaux de Mazur

[10]) une synthèse des problèmes statistiques et des problèmes de structure moléculaire.

8. Équation de Propagation du Mélange Diffusé

Nous avons supposé jusqu'à présent que le projectile se trouvait, avant l'impact, à l'état de cas pur. Pour étudier le mélange diffusé, il est utile de supposer désormais que le projectile est déjà à l'état de mélange avant l'impact. Et que ce mélange n'est pas monocinétique.

Nous désignerons par ξ l'opérateur densité qui représente l'état du système global. Avant que le projectile n'atteigne le thermostat diffuseur, nous désignons ce mélange par ξ_0. Le mélange incident évolue en fonction du temps suivant l'équation

$$i\frac{\partial}{\partial t}\xi_0 = [H+K, \xi_0], \tag{1}$$

le crochet désignant un commutateur, suivant la formule générale

$$[X, Y] = XY-YX.$$

Cette équation permet de calculer ξ_0 à tout instant, même après que le projectile a pénétré dans le diffuseur. Naturellement le mélange ainsi obtenu ne représente pas la réalité physique, mais il nous est utile pour la suite des calculs. C'est le mélange incident „prolongé".

D'après l'équation § 2 (5), le mélange ξ se déduit du mélange ξ_0, à chaque instant, par la formule

$$\xi = \Omega\xi_0\tilde{\Omega}. \tag{2}$$

Du mélange global on déduit, par un calcul partiel de trace, le mélange qui représente le diffuseur et celui qui représente le projectile:

$$\mu = \mathrm{T}_K\xi, \tag{3}$$

$$\nu = \mathrm{T}_H\xi; \tag{4}$$

T_K représente ici une trace prise à travers les états du projectile. De même T_H représente une trace prise seulement à travers les états du thermostat. On notera qu'en général le mélange μ n'est pas indépendant du temps: le projectile perturbe le diffuseur. Il ne le perturbe peut être pas beaucoup, mais il n'est pas nécessaire de négliger le phénomène a priori.

Le mélange global réel vérifie une équation analogue à (1), qui est

$$i\frac{\partial}{\partial t}\xi = [H+K+V, \xi], \tag{5}$$

d'où on déduit des équations pour μ et ν respectivement:

$$i\frac{\partial}{\partial t}\mu = [H, \mu]+\mathrm{T}_K[V, \xi], \tag{6}$$

$$i\frac{\partial}{\partial t}\nu = [K, \nu]+\mathrm{T}_H[V, \xi]. \tag{7}$$

Les équations (5), (6) et (7) forment un système qui se suffit à lui-même. Y ajouter l'équation (2) donne un ensemble surabondant. Mais l'équation (2) permet de tenir compte de l'hypothèse fondamentale qui est l'absence de corrélation avant l'impact entre le diffuseur et le projectile. Dans ces conditions le mélange incident est un produit

$$\xi_0 = \mu_0\nu_0. \tag{8}$$

Cette absence de corrélation avant l'impact se poursuit même après l'impact, non pas pour le mélange réel bien entendu, mais pour le mélange incident.

La procédure que nous allons suivre est alors la suivante:

1) insérer l'expression (8) dans (2).

2) insérer le résultat dans (3) et (4).

3) résoudre (3) et (4) par rapport à μ_0 et ν_0: ces opérateurs sont maintenant exprimés en fonction de μ et de ν.

4) reporter les valeurs de μ_0 et ν_0 ainsi obtenues dans (2).

5) reporter enfin l'expression obtenue de ξ dans (6) et (7).

Finalement (6) et (7) constitueront un système complet d'équations pour μ et ν. Il s'agit d'un système „instantané": toutes les grandeurs variables qui y figurent sont à prendre au même instant.

Les opérations précitées s'effectuent aisément — du moins formellement, sauf la troisième qui nécessite une méthode d'approximation. Nous obtenons tout d'abord

$$\mu = \mathrm{T}_K\Omega\mu_0\nu_0\tilde{\Omega}, \tag{9}$$

$$\nu = \mathrm{T}_H\Omega\mu_0\nu_0\tilde{\Omega}. \tag{10}$$

En posant

$$\Omega = 1+\eta,$$

et en considérant η comme un infiniment petit, on imagine en principe une méthode d'approximations successives pour résoudre les équations précédentes, l'approximation zéro étant la suivante:

$$\mu_0 \approx \mu, \qquad \nu_0 \approx \nu. \tag{11}$$

Mais le fait que le projectile est dispersé à travers un grand volume, que sa densité est faible, le fait aussi qu'il perturbe peu le thermostat, conduit à négliger les termes qui dans l'expression de ξ sont du second degré ou d'ordre supérieur en ν. Cette approximation entraîne qu'il faut prendre simplement ici

$$\mu_0 \approx \mu. \tag{12}$$

Dans ces conditions l'équation (10) se transcrit

$$\nu = \mathrm{T}_H\Omega\mu\nu_0\tilde{\Omega}. \tag{13}$$

Posons

$$\Omega_K = \mathrm{T}_H \Omega \mu, \tag{14}$$

l'indice K signifiant que le nouvel opérateur ne commute pas avec les états du projectile alors qu'il commute avec les états du thermostat. L'équation (13) est identique à la suivante:

$$\nu = \Omega_K \nu_0 \tilde{\Omega}_K + \mathrm{T}_H(\Omega - \Omega_K)\mu\nu_0(\tilde{\Omega} - \tilde{\Omega}_K). \tag{15}$$

Le second terme représente la moyenne quadratique d'une fluctuation à travers les états du thermostat. On peut procéder à une nouvelle approximation et la traiter comme un infiniment petit. On trouve donc, au premier ordre près dans la nouvelle approximation,

$$\nu_0 = \Omega_K^{-1} \nu \tilde{\Omega}_K^{-1}. \tag{16}$$

Nous avons limité nos approximations au strict minimum. Il ne serait pas impossible de les améliorer le cas échéant. On notera qu'aucune approximation n'a été effectuée sur l'opérateur Ω lui-même. Il vient maintenant:

$$\xi = \Omega \Omega_K^{-1} \mu\nu \tilde{\Omega}_K^{-1} \tilde{\Omega}. \tag{17}$$

Introduisons ce résultat d'abord dans l'équation de propagation du projectile. Généralisant la notation (14), nous poserons

$$\mathrm{T}_H V \Omega \mu = (V\Omega)_K. \tag{18}$$

Il vient

$$\begin{aligned} i\frac{\partial}{\partial t}\nu = {} & (K + (V\Omega)_K \Omega_K^{-1})\nu - \nu(K + \tilde{\Omega}_K^{-1}(\tilde{\Omega}V)_K) \\ & + \mathrm{T}_H\{[V\Omega - (V\Omega)_K]\Omega_K^{-1}\mu\nu\tilde{\Omega}_K^{-1}[\tilde{\Omega} - \tilde{\Omega}_K] \\ & - (\Omega - \Omega_K)\Omega_K^{-1}\mu\nu\tilde{\Omega}_K^{-1}[\tilde{\Omega}V - (\tilde{\Omega}V)_K]\}. \end{aligned} \tag{19}$$

On s'est arrangé pour faire apparaître à nouveau des moyennes de fluctuation. Mais cette fois-ci il s'agit de fluctuations mixtes puisque les deux facteurs qui sont nuls en moyenne sont maintenant distincts; ce sont respectivement, pour la première de ces moyennes par exemple,

$$V\Omega - (V\Omega)_K \quad \text{et} \quad \tilde{\Omega} - \tilde{\Omega}_K. \tag{20}$$

L'opérateur

$$G_K = K + (V\Omega)_K \Omega_K^{-1} \tag{21}$$

est évidemment la généralisation au cas présent de l'opérateur G_n. Ceci résulte de l'expression § 5 (14) de ce dernier. L'opérateur

$$\tilde{G}_K = K + \tilde{\Omega}_K^{-1}(\tilde{\Omega}V)_K \tag{22}$$

est l'adjoint de G_K. Nous décomposerons G_K comme autrefois G_n en une partie hermitique et une partie antihermitique. L'équation (19) s'écrit alors

$$i\frac{\partial}{\partial t}\nu = [G_K^{\mathrm{R}}, \nu] + \mathrm{T}_H\{\ldots\} + i(G_K^{\mathrm{I}}\nu + \nu G_K^{\mathrm{I}}). \tag{23}$$

Dans le second membre le commutateur représente la propagation sans diffusion. La diffusion est créée par les termes suivants qui représentent les „sources" et les „puits" de la diffusion. De son côté l'équation du diffuseur s'écrit

$$i\frac{\partial}{\partial t}\mu = [H, \mu] + \mathrm{T}_K[V, \Omega\Omega_K^{-1}\mu\nu\tilde{\Omega}_K^{-1}\tilde{\Omega}]. \tag{24}$$

Il n'y a pas intérêt à faire apparaître ici des fluctuations puisque la moyenne, représentée par la trace, porte sur les états du projectile qui est un système simple: les fluctuations n'ont pas de raison d'être petites. Par contre, sous l'effet du projectile, le thermostat ne s'écarte pas beaucoup de l'équilibre thermodynamique. On traitera l'effet du projectile comme une perturbation: ceci est conforme à l'approximation qui a consisté à négliger les termes de degré supérieur au premier degré en ν.

Il est aisé de vérifier que les équations (19) et (24) ont pour conséquence

$$\frac{\mathrm{d}}{\mathrm{d}t}\mathrm{T}_H\mu = \frac{\mathrm{d}}{\mathrm{d}t}\mathrm{T}_K\mu = 0$$

comme il convient.

9. Application aux Problémes de Diffusion

On a cherché à présenter un formalisme qui permette de traiter avec quelque sécurité les problèmes de diffusion dans le domaine optique, c'est à dire lorsque la longueur d'onde du projectile est grande devant le grain du milieu diffusant.

On a négligé des fluctuations d'ordre supérieur: fluctuations biquadratiques et fluctuations d'ordre plus élevé — ceci dans la résolution de l'équation § 8 (13), ce qui est probablement entièrement justifié, ceci dit sans preuves spéciales.

On a donné en principe le moyen de calculer au premier ordre la perturbation du diffuseur, ce qui est apparemment un luxe inutile si la radiation incidente n'a qu'une faible intensité. Notons que nous avons raisonné comme si le projectile incident était unique. Mais l'envoi d'une succession de particules de même nature sans actions appréciables entre elles se traiterait de la même manière.

L'équation § 8 (19) où on donne à l'opérateur densité du diffuseur son expression pour un système en équilibre thermodynamique couvre donc le problème. On n'y distingue pas le rayonnement incident et le rayonnement diffusé. L'équation couvre donc à la fois les phénomènes de propagation et de diffusion: elle tient compte des diffusions multiples que le rayonnement peut subir avant de quitter le diffuseur.

Il est possible qu'on veuille tenir compte seulement de la diffusion simple. On procèdera alors de la manière suivante:

1) on supposera que le rayonnement incident est un cas pur monochromatique. Il n'y a là aucune perte de généralité.

2) on traitera, dans le second membre de l'équation fondamentale, les termes en $G_K{}^R$ comme des termes d'ordre zéro et les autres termes comme des termes du premier ordre.

3) on trouvera donc en première approximation le cas pur optique.

4) à partir du cas pur optique on trouvera en seconde approximation le mélange provenant d'une diffusion simple.

Il est clair que, lorsque nous parlons ici d'une diffusion simple, il s'agit d'une diffusion macroscopique et non pas d'un acte de diffusion élémentaire.

Notons parmi les phénomènes à étudier celui de la structure fine de la raie Rayleigh.

Fabelinskii [11]) en a repris récemment la théorie phénoménologique. La théorie présentée ici permettra peut-être d'aborder cette question du point de vue microscopique ainsi que celle de l'intensité globale de la lumière diffusée, mais le travail qui reste à accomplir est certainement considérable.

10. Equation de Boltzmann

Jusqu'à présent il a été supposé que les parois qui ceinturent le diffuseur sont parfaitement perméables au projectile. Rien de fondamental n'est changé aux raisonnements précédents si on imagine que ces parois sont parfaitement réfléchissantes dans certaines régions — sur les deux faces — et parfaitement transparentes dans les autres. À la limite on peut même supposer que la région transparente est très petite: le projectile a peu de chances de pénétrer dans le diffuseur, mais, une fois qu'il y a pénétré, il a peu de chances d'en ressortir. Il a tout le temps d'y subir de nombreux chocs élastiques et inélastiques. Physiquement nous savons que le système diffuseur + projectile finira par se trouver en équilibre thermodynamique.

Les équations § 8 (19) et § 8 (24) décrivent alors — dans l'approximation où le diffuseur reste toujours très proche de son état initial — l'évolution des phénomènes et le mouvement brownien du projectile. On notera encore ici l'importance de l'hypothèse § 8 (8). Les équations (19) et (24) constituent un système d'équations qui sont l'adaptation au problème de l'équation de Boltzmann. On devrait pouvoir en déduire un théorème-H, ce à quoi l'auteur n'est pas parvenu.

Dans une application à la diffusion d'un projectile par un liquide, par exemple, on aperçoit aisément ce que la présente théorie a de schématique. Si en effet on supprime dans l'équation (24) les termes d'interaction entre diffuseur et diffusé, l'équation (24) ne peut plus traduire que des phénomènes réversibles: le liquide est sans viscosité. Le problème général de l'irréversibilité est à peine effleuré par la présente étude.

Dans une approximation moins poussée, et dans un cadre un peu différent,

l'équation (19) a déjà été obtenue par Wangness et Bloch [12]). L'auteur lui-même avait présenté les rudiments d'une telle équation au Colloque de Bruxelles sur les Phénomènes de Transport en Mécanique Statistique (1956) et avait réussi dans un cas très particulier à établir le théorème-H.

Bibliographie

1) J. Yvon, Actualités scientifiques et industrielles no. 543 (Hermann et Cie, Paris 1937)
2) M. Fixman, J. of Chem. Phys. **23** (1955) 2075
3) A. Rousset et R. Lochet, J. de Chimie Physique **51** (1954) 13
4) J. Cabannes, Ann. de Phys. **1** (1956) 857
5) C. Bloch, Nuclear Physics **4** (1957) 503
6) W. Heitler, The Quantum Theory of Radiation (Oxford 1954) p. 72
7) K. M. Watson, Phys. Rev. **105** (1957) 1388
8) J. Blatt et V. Weisskopf, Theoretical Nuclear Physics (Wiley 1952) p. 71
9) W. Fuller Brown Jr., Handbuch der Physik (Springer 1956), volume XVII (Dielectrics) p. 62
10) L. Jansen et P. Mazur, Physica **21** (1955) 193 et 209
P. Mazur et M. Mandel, Physica **22** (1956) 289
11) I. L. Fabelinskii, Soviet Physics "Doklady", traduction américaine **1** (1956) 115
12) F. Bloch, Phys. Rev. **105** (1957) 1206
U. Fano, Reviews of Modern Physics **29** (1957) 91

Nuclear Physics 5 (1958) 167—172; © *North-Holland Publishing Co., Amsterdam*
Not to be reproduced by photoprint or microfilm without written permission from the publisher

MANY BODY EFFECTS IN BETA-DECAY

J. S. BELL
Atomic Energy Research Establishment, Harwell

Received 26 August 1957

Abstract: In mirror transitions involving nuclei with doubly closed cores plus or minus one particle the Gamow-Teller contribution appears to be smaller, by from 15 % to 60 %, than that predicted by the shell model. The effect of correlation in the nuclear wave function, tentatively estimated by applying perturbation theory to a simple Fermi gas model, is found to be in the right direction but too small.

1. Introduction

An estimate is made of the importance of correlation in the nuclear wave function, represented by the model operator F of Brueckner theory, for beta-decay matrix elements. It is based on the very simple Fermi gas model used already in connection with the magnetic moment problem [1]). Only the simplest cases are considered, namely mirror transitions between nuclei with doubly closed cores (in the LS-sense) plus or minus one particle.

2. Experimental Information

The experimental information is taken from the survey by Kofoed-Hansen and Winther [2]).

According to the usual theory the ft value is given by

$$(ft)^{-1} = \alpha|M_F|^2+\beta|M_{GT}|^2, \qquad (1)$$

where the constants α and β are the same, assuming no Fierz interference, for all nuclei. They can then be determined from the data on the neutron (for which $|M_F|^2 = 1$, $|M_{GT}|^2 = 3$) and on O^{14} (for which $|M_F|^2 = 2$, $|M_{GT}|^2 = 0$, assuming only charge independence). The neutron information is rather poor, and we prefer to use that for H^3, assuming that there also $|M_{GT}|^2 = 3$ to a good approximation. With α and β so determined, the relation (1) in the form

$$\frac{|M_{GT}|^2}{|M_F|^2} = -\frac{\alpha}{\beta} + \frac{(ft)^{-1}}{\beta|M_F|^2}$$

is represented by the broken lines in the diagram, the difference between them indicating the experimental errors in the H^3 and O^{14} data. For mirror transitions between nuclei with doubly closed shell cores plus or minus one particle, assuming charge independence, $|M_F|^2 = 1$ exactly. From the ob-

served ft value we can then read off from the diagram an experimental value for $|M_{GT}|^2$. It is seen that in each case this lies below the corresponding shell model estimate of $|M_{GT}|^2$, represented (together with the experimental error in ft) by the short horizontal line. The effect is of order 15 % in O^{15}, 25 % in F^{17}, 30 % in Sc^{41}, and 60 % in Ca^{39}. According to Blatt [3] $|M_{GT}|^2 = 3$ is very probably an upper limit on the matrix element for H^3, and configuration mixing might decrease it by a few percent. The broken lines in the diagram would then lie slightly lower, and the above discrepancies would be slightly increased. These lines would also lie very slightly lower if the O^{14} result were replaced by that for Al^{26} or Cl^{34}.

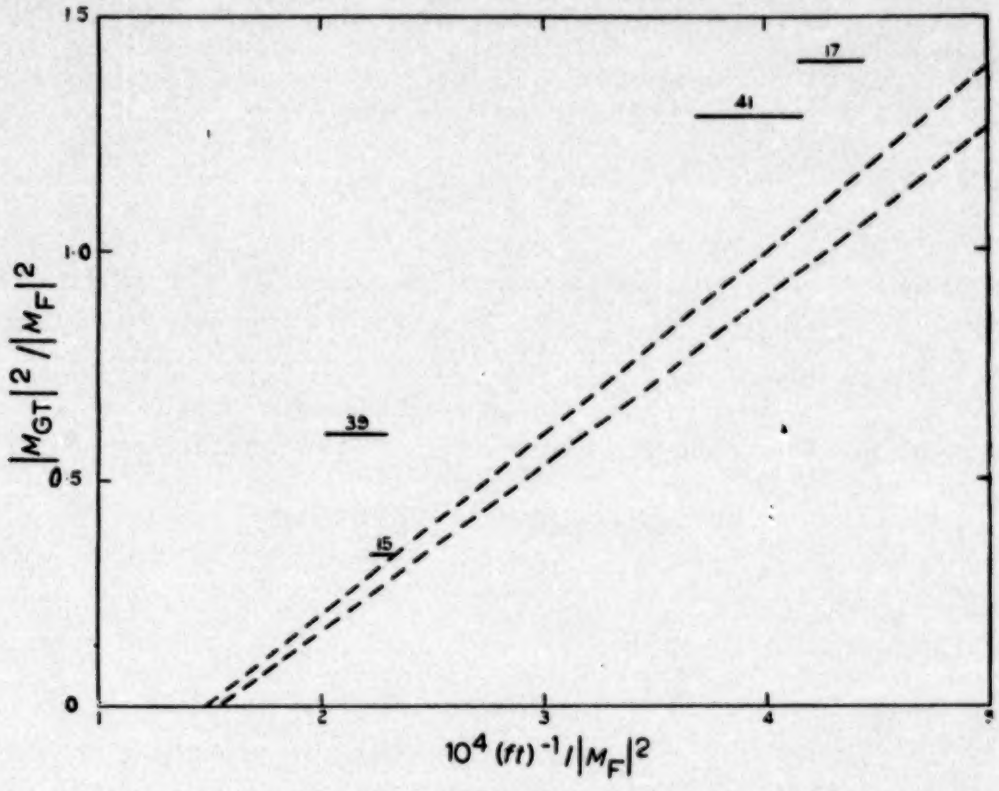

Fig. 1

In principle deviations like the above could be caused by Coulomb effects, but these are probably negligible in the nuclei considered [7].

3. Effect of the Model Operator

We consider now the effect on M_{GT} of the correlations introduced by the model operator. The method and notation are essentially those of a previous paper [1] (henceforward I). We have to evaluate

$$\langle 2|F^+ \sum_i \tau_i \sigma_i F|1\rangle / \langle 1|F^+ F|1\rangle \qquad (2)$$

where $|1\rangle$ and $|2\rangle$, the initial and final states, differ only in the isobaric and

(possibly) ordinary spin of the odd particle or hole; $\frac{1}{2}\tau_i$ is the 2-component of the isobaric spin of particle i. Denoting the denominator by N, (2) may be written

$$N^{-1}\{\langle 2|F^+ F\sum\tau\sigma|1\rangle+\langle 2|F^+[\sum\tau\sigma,\ F]|1\rangle\}. \tag{3}$$

It may then be shown (see appendix) that the first term is equal to the zero order matrix element $\langle 2|\sum\tau\sigma|1\rangle$, and by similar arguments that in the second term F^+ may be replaced by F^+-1; this gives

$$\langle 2|\sum\tau\sigma|1\rangle+N^{-1}\langle 2|(F^+-1)[\sum\tau\sigma,\ F]|1\rangle. \tag{4}$$

We now specialise to the infinite nuclear model. In first order perturbation theory

$$F = 1+\frac{Q}{\varepsilon}\{\sum_{i>j}v_{ij}-\sum_i V_i\}, \tag{5}$$

where the effective one body potential V is diagonal in momentum space and independent of spin and isobaric spin. To second order (4) becomes

$$\langle 2|\sum\tau\sigma|1\rangle+\langle 2|\sum v\frac{Q}{\varepsilon}\frac{Q}{\varepsilon}\sum v'|1\rangle, \tag{6}$$

where

$$v'_{ij} = [(\tau_i\sigma_i+\tau_j\sigma_j),\ v_{ij}]. \tag{7}$$

Note that V does not appear explicitly because on the one hand it commutes with $\sum\tau\sigma$, and on the other it has only diagonal elements so that $\langle 2|VQ = 0$. As usual the cross terms in (7) involving different pairs (i, j) vanish by conservation of momentum, so that the double summation reduces to a single one. To take care of antisymmetry we then replace v' by

$$v'' = v'(1-P^\tau P^\sigma P^\tau), \tag{8}$$

giving

$$\langle 2|\sum\tau\sigma|1\rangle+\sum_{i>j}\langle 2|v_{ij}\frac{Q}{\varepsilon}\frac{Q}{\varepsilon}v''_{ij}|1\rangle \tag{9}$$

where $|1\rangle$ and $|2\rangle$ are now just product wave functions.

The case of a hole is quite similar to that of an odd particle, and for definiteness we consider the latter. Explicitly, in terms of single particle states, (9) becomes

$$(\phi''|\tau\sigma|\phi)+\sum_{\psi,\psi',\phi'}\frac{(\phi''\psi|v|\phi'\psi')(\phi'\psi'|v''|\phi\psi)}{\{E_0(\phi)+E_0(\psi)-E_0(\phi')-E_0(\psi')\}^2} \tag{10}$$

where ϕ and ϕ'' are the initial and final states of the odd particle, the ψ are the states constituting the core, and the ϕ' and ψ' are all single particle states other than those of the core; the E_0 are the corresponding single particle energies.

For v we take the conventional central force of I:

$$v = u\{W+MP^\tau+BP^\sigma+HP^\tau P^\sigma\}. \tag{11}$$

Then

$$v'' = -u\{(B+HP^\tau)P^\sigma-(BP^\tau+H)P^\tau\}(\tau_1-\tau_2)(\sigma_1-\sigma_2). \tag{12}$$

When these are substituted in (10), the fact that in spin and isobaric spin space $\sum|\phi'\psi')(\phi'\psi'|$ is just the unit operator allows the collection together of all spin and isobaric spin operators. Terms may then be dropped whose spin dependence is in a factor $P^\sigma(\sigma_1-\sigma_2)$, for this may be written

$$P^\sigma(\sigma_1-\sigma_2) = P^\sigma\sigma_1-\sigma_1P^\sigma = \tfrac{1}{2}(\sigma_1\cdot\sigma_2\sigma_1+\sigma_1\sigma_1\cdot\sigma_2) \tag{13}$$

which will vanish on averaging over the spin of the second particle. Likewise terms with isobaric spin dependence $P^\tau(\tau_1-\tau_2)$ do not contribute, nor of course those whose isobaric spin dependence is simply through a factor τ_2. There remains

$$(\phi''|\tau\sigma|\phi)-\sum\frac{(\phi''\psi|u(B+HP^\tau)|\phi'\psi')(\phi'\psi')u(B+HP^\tau)\tau_1\sigma_1|\phi\psi)}{\{E_0(\phi)+E_0(\psi)-E_0(\phi')-E_0(\psi')\}^2}. \tag{14}$$

This may be written

$$(\phi''|\tau\sigma|\phi)(1-\alpha) \tag{15}$$

with

$$\alpha = 4\sum_{l\leq k_F,\,k'>k_F,\,l'>k_F}\frac{(\mathbf{k}_0\mathbf{l}|u(B+HP^\tau|\mathbf{k}'\mathbf{l}')(\mathbf{k}'\mathbf{l}'|u(B+HP^\tau)|\mathbf{k}_0\mathbf{l})}{\{(k_0^2+l^2-k'^2-l'^2)/2m^*\}^2} \tag{16}$$

where $\mathbf{k}_0$ is the initial momentum of the odd particle, and $\mathbf{l}$ that of the core particle with which it interacts; the factor 4 arises from spin summations, and the effective mass approximation has been used. The fractional reduction in $|M_{GT}|^2$ is 2α. That α should come entirely from the spin dependent part of the interaction was of course to be expected from the Wigner supermultiplet theory.

Replacing the sum by an integral, and introducing

$$\begin{aligned}\mathbf{a} &= \mathbf{k}_0-\mathbf{k}' = \mathbf{l}'-\mathbf{l}\\ \mathbf{b} &= \mathbf{k}'-\mathbf{l} = \mathbf{k}_0-\mathbf{l}'\end{aligned} \tag{17}$$

we have

$$\alpha = 4(2\pi)^{-6}(m^*)^2\int_{\substack{|\mathbf{k}_0-\mathbf{a}|>k_F\\ |\mathbf{k}_0-\mathbf{b}|>k_F\\ |\mathbf{k}_0-\mathbf{a}-\mathbf{b}|<k_F}}\mathrm{d}\mathbf{a}\mathrm{d}\mathbf{b}\{B\tilde{u}(a)+H\tilde{u}(b)\}^2(\mathbf{a}\cdot\mathbf{b})^{-2} \tag{18}$$

which we write as

$$\alpha = 4\left(\frac{m^*}{m}\right)^2\{(B^2+H^2)I_1+2HBI_2\}. \tag{19}$$

The integral I_1 can be reduced to

$$I_1 = (2\pi)^{-4}\int_0^\infty \mathrm{d}x[k_F m\tilde{u}(2k_F x)]^2 F(x), \tag{20}$$

where for $x < 1$

$$F(x) = (1-x^2)\log\frac{1+x}{1-x} + 2x(1+x)(2\log 2 - 1), \tag{21}$$

and contributions from $x > 1$ are negligible for the force (I, 2.14). With that force numerical integration gives

$$I_1 = 0.114. \tag{22}$$

The second integral is more difficult and has not been evaluated. However it follows from the positive character of (18) for arbitrary B and H that $|I_2| < I_1$; moreover because $\tilde{u}$ has always the same sign for the Yukawa shape, I_2 is positive; thus

$$0 < I_2 < I_1. \tag{23}$$

The shell model studies of Elliott and Flowers [4]) suggest an exchange mixture with

$$\begin{aligned} W &= 0.36 - 0.25x, \quad M = 0.49 + 0.25x, \\ B &= 0.01 + 0.25x, \quad H = 0.14 - 0.25x, \end{aligned} \tag{24}$$

where x measures the strength of the singlet-singlet interaction, which is the least known part of the force. The values (24) are obtained by reversing the signs of W, M, B, and H (for we use the opposite convention) in their equations (4) and (5) and using $W+M+B+H = 1$. Unless B and H are both very small, they are of opposite sign; we then obtain an upper limit by dropping the second term in (19):

$$2\alpha < 0.91(m^*/m)^2(B^2+H^2). \tag{25}$$

From (I, 3.9)

$$(m^*/m^2) = (1.32+0.042x)^{-2}. \tag{26}$$

According to Elliott and Flowers a reasonable value for x is -0.5; with this $2\alpha < 0.04$. That is to say that $|M_{GT}|^2$ is reduced by less than 4 %, a very small effect. To obtain from (25) an upper limit of say 25 % requires x to lie outside the interval $(-1.6, +2.3)$, which excludes the range of acceptable values.

The predicted effect is still smaller if, as in appendix B of I, the finite minimum excitation energy of real nuclei is crudely allowed for; a minimum of about 6 MeV reduces I_1 by about one third.

4. Conclusion

The effect predicted by this very simple model and the central force of shell model theory is in the right direction but too small. A better model and a more realistic treatment of the reaction operator t (which should appear instead of v in (5)) are of course desirable. But there is also the

possibility that the observed effects are in part due to deficiencies in the theory underlying (1). This theory neglects relativistic effects, which might be of order several percent (Stech, quoted by Michel [5])), and possible interaction effects arising through the meson field [6]).

I am indebted to my colleagues, and especially to Dr. B. H. Flowers, for valuable discussion of this work.

Appendix

The statement following equation (3) is to be proved. We may write

$$\langle 2|F^+ F \sum \tau\sigma|1\rangle = \sum_n \langle 2|F^+ F|n\rangle\langle n| \sum \tau\sigma|1\rangle \qquad \text{(A1)}$$

where $|n\rangle$ is a complete set of states. Clearly the only states which will contribute are those that can be obtained from $|1\rangle$ by changing the spin and isobaric spin, but not the orbital state, of the odd particle. In a finite nucleus spherical symmetry in ordinary and isobaric spin space, and the associated conservation laws, prevent any such state other than $|2\rangle$ itself from arising from $|2\rangle$ through F^+F. Thus

$$\langle 2|F^+ F \sum \tau\sigma|1\rangle = \langle 2|F^+ F|2\rangle\langle 2| \sum \tau\sigma|1\rangle = N\langle 2| \sum \tau\sigma|1\rangle, \qquad \text{(A2)}$$

which is the required result.

For the infinite nuclear model we proceed differently. In the subspace defined by the core being unexcited and the odd particle having a given momentum $\mathbf{k}_0$, F^+F must have the general form

$$A + \mathbf{B}\cdot\boldsymbol{\sigma} \qquad \text{(A3)}$$

where A and $\mathbf{B}$ may depend on the core and the orbital state of the odd particle. By charge independence A and $\mathbf{B}$ will not depend on isobaric spin. The quantity $\mathbf{B}$ would have to transform like $\boldsymbol{\sigma}$ under inversions and under those rotations permitted by the periodic boundary conditions. No such quantity exists, for one can find (in several ways) an axis a rotation about which by π followed by an inversion therein reverses the spin of the odd particle but leaves everything else, including therefore $\mathbf{B}$, unaltered. With $\mathbf{B} = 0$, (A2) again follows.

References

1) J. S. Bell, Nuclear Physics **4** (1957) 295
2) O. Kofoed-Hansen and A. Winther, Mat. Fys. Medd. Dan. Vid. Selsk. **30** (1956) no. 20
3) J. M. Blatt, Phys. Rev. **89** (1953) 86
4) J. P. Elliott and B. H. Flowers, Proc. Roy. Soc. (to be published)
5) L. Michel, Rev. Mod. Phys. **29** (1957) 223
6) M. Ross, Phys. Rev. **104** (1956) 1736
7) M. MacDonald, Princeton thesis (1954)

Nuclear Physics **5** (1958) 173—178; © *North-Holland Publishing Co., Amsterdam*
Not to be reproduced by photoprint or microfilm without written permission from the publisher

A SEMI-EMPIRICAL FORMULA FOR THE NUCLEAR RADIUS

L. R. B. ELTON

Wheatstone Laboratory, King's College, London

Received 14 August 1957

Abstract: It is shown that the experimental results on negaton and proton scattering by nuclei are in agreement with the assumptions that the central density of nuclear matter is constant for all nucleides and that the neutron and proton distributions in a nucleus are the same.

Until now it has generally been assumed that the parameters which characterize the shape and extent of nuclear matter in atomic nuclei are smoothly varying functions of the mass number A. The limits of usefulness of this approach have probably been reached, since recently very accurate experimental measurements on the proton distribution have shown up effects due to deformations from spherical shape [1]) and to the closing of shells [2]). Nevertheless, formulae which average over these effects would be useful, and we shall show that it is possible to construct such formulae, which will in general reproduce all the experimental results within the accuracy claimed for them.

To establish these formulae we make the following assumptions:

(a) The proton distribution is given by the functional form

$$\varrho(r) = \frac{Z}{A}\,\frac{\varrho_0}{1+\mathrm{e}^{(r-c)/a}}\,. \tag{1}$$

This assumption has no physical significance. Other functional forms can be made equally well to agree with the experimental results [1]).

(b) The neutron distribution is identical with the proton distribution, except that Z must be replaced by $A-Z$. There is now evidence both experimental [3]) and theoretical [4]), which indicates that neutron and proton distributions extend outwards from the centre of the nucleus to the same extent. This makes our assumption very plausible.

(c) The central density of nuclear matter

$$\varrho(0) = \frac{\varrho_0}{1+\mathrm{e}^{-c/a}} \tag{2}$$

is independent of the mass number A. This should be true except for the lightest nuclei, because of the saturation properties of nuclear forces. Negaton scattering experiments can unfortunately say almost nothing about the central density.

(d) The transition region in which the nuclear density drops from its central value to zero is independent of the mass number A, i.e. a in (1) is

constant. This assumption can certainly only be valid as a rough average, since the transition region must be strongly affected by shell structure and nuclear deformations.

In the older work the radius was usually defined through

$$R = \left\{ \frac{5}{3Z} \int_0^\infty r^2 \varrho(r) \mathrm{d}\tau \right\}^{\frac{1}{2}}. \tag{3}$$

This is the radius of the uniform charge distribution which yields the same low energy negaton scattering results as the actual distribution [5]). The not very accurate results obtained at the time could then be fitted to the formula

$$R = r_0 A^{1/3}, \tag{4}$$

where r_0 was constant. The more recent results [1]) indicate clearly that such a fit is not possible, but that a similar formula can more nearly be fitted to the so-called half-way radius c, which is the radius at which the nuclear density has dropped to half its central value. A perfect fit is still not possible, which is not surprising, since with a transition region of nearly constant thickness — and the experimental evidence [1]) clearly requires this — the fraction of the total nuclear matter that is in the transition region decreases as A increases.

Since it turns out that even for light nuclei $a < \frac{1}{5}c$, we can make some approximations (see appendix) and then obtain from (1) that

$$A = 4\pi \int_0^\infty \varrho r^2 \mathrm{d}r = \tfrac{4}{3}\pi \varrho_0 c^3 \left(1 + \frac{\pi^2 a^2}{c^2}\right), \tag{5}$$

so that

$$c = bA^{1/3} - \frac{\pi^2 a^2}{3b} A^{-1/3} \tag{6}$$

and

$$R = bA^{1/3} + \frac{5\pi^2 a^2}{6b} A^{-1/3} - \frac{7\pi^4 a^4}{8b^3} A^{-1}, \tag{7}$$

where we have put

$$b = (\tfrac{4}{3}\pi \varrho_0)^{-1/3}. \tag{8}$$

These formulae are now fitted to the Stanford negaton scattering results [2]) and a best fit is obtained with

$$b = 1.121 \pm 0.005, \quad a = 0.575 \pm 0.015. \tag{9}$$

(All distances are measured in 10^{-13} cm). Hence

$$c = 1.121A^{1/3} - 0.970A^{-1/3}, \tag{10}$$

$$R = 1.121A^{1/3} + 2.426A^{-1/3} - 6.614A^{-1}, \tag{11}$$

and the distance in which the density decreases from 90 % to 10 % of its

central value is

$$t = 2.53 \pm 0.06. \tag{12}$$

The calculated values of c and R are compared with the experimental ones in table 1 and are, with two exceptions, in excellent agreement. The excep-

TABLE 1

Nucleide	c_{exp}	c_{calc}	R_{exp}	R_{calc}
C^{12}	2.3	2.17	3.04	3.08
Mg^{24}	2.85	2.90	3.84	3.80
Si^{28}	2.95	3.05	3.93	3.93
S^{32}	3.28	3.25	4.13	4.12
Ca^{40}	3.69	3.55	4.37	4.38
V^{51}	3.98	3.90	4.65	4.68
Co^{59}	4.09	4.12	4.94	4.87
Sr^{88}	4.80	4.78	5.33	5.47
In^{115}	5.24	5.25	5.79	5.89
Sb^{122}	5.32	5.36	5.95	6.00
Ta^{181}	6.45	6.18	7.06	6.74
Au^{197}	6.38	6.36	6.88	6.91
Pb^{208}	6.5	6.46	6.98	7.00
Bi^{209}	6.47	6.49	7.13	7.03

tions are the doubly magic nucleide Ca^{40} and the strongly aspherical nucleide Ta^{181}. For Ca^{40} we obtain the correct value of R, but seriously underestimate c. This indicates an unusually narrow transition, region, as would be reasonable for such a nucleide. Similar effects are observable for C^{12} and Si^{28}. With Ta^{181} both R and c are much larger experimentally than according to the formulae. This corresponds to a very wide transition region or, more probably, a strong asphericity. The doubly magic nature of Pb^{208} does not show up, but this is hardly to be expected in such a heavy nucleide.

It would of course be rash to suggest that the agreement between the experimental results and the semi-empirical formulae shows that the assumptions on which the latter are based are justified. In particular, assumption (c) can only be an approximation to the truth as we have neglected the effects of the repulsive Coulomb forces and of the exclusion principle, both of which, would decrease the central density for large A [7]). As the Coulomb forces do not saturate, they almost certainly will have such an effect, but it is not easy to tell how big it is. The exclusion principle will have opposite effects on neutrons and protons, since for a given nucleon density the proton density decreases and the neutron density increases as A increases. The resultant effect is therefore only of second order, although it too will lead to a decrease of the central density. Recent calculations [12]) indicate that for $A \approx 200$ the net correction is at or beyond the limit of experimental accuracy, so that at present no definite conclusions can be drawn from the

experiments about a possible violation of the requirements of strict saturation of nuclear forces.

So far we have confined ourselves to the analysis of electromagnetic measurements of the nuclear radius. It will now be shown that a similar formula can be obtained for the half-way radius C of the optical model potential [8]), which is used to fit the data on the elastic scattering of nucleons by nuclei [9, 10]). Although these results are not as accurate as those obtained from negaton scattering, they too show quite un-equivocally that a fit of the type (4) is not possible. But while the value of r_0 for c increases with A, that for C decreases as A increases. If we assume, as is reasonable, that, owing to the finite range of nuclear forces, the potential half-way radius exceeds the matter half-way radius by a constant amount, then we obtain a very good fit to the experimental data with

$$C-c = 0.81\pm0.10, \tag{13}$$

i.e.

$$C = 1.121A^{1/3}-0.970A^{1/3}+0.81. \tag{14}$$

Owing to the effect of exchange forces, which are partially repulsive, $C-c$ would be expected to be somewhat smaller than the range of the nuclear two-body force [11]). Comparison between experiment and theory is made in table 2, where it should be noted that the data for carbon and silver are less reliable than those for the other nucleides.

TABLE 2

Nucleide	$C_{exp}A^{-1/3}$	C_{exp}	C_{calc}	Reference
C	1.24–1.28	2.8 –2.9	2.98	9
Al	1.29	3.87	3.85	9
Co	1.30–1.36	5.08–5.31	4.93	11
Cu	1.29	5.16	5.05	9
Ag	1.2 –1.3	5.7 –6.2	5.96	9, 11
Au	1.23	7.16	7.18	9

There has always been a rival theory to the above to account for the fact that nuclear measurements gave nuclear radii larger than electromagnetic ones, namely that our assumption (b) is wrong and the neutron distribution extends further out than the proton distribution. In a heavy nucleus this would be due to the operation of the exclusion principle, which affects the more numerous neutrons more strongly than the protons, and which on balance has a stronger effect than the electrostatic repulsion of the protons, which works in the opposite direction. But for a nucleide as light as carbon or aluminium the exclusion principle has the same effect on neutrons and protons, so that the net result, if any, would be for the protons to be spread out further than the neutrons, because of the Coulomb

repulsion. The fact that $C-c$ is the same for these light nucleides as for gold makes it very unlikely that the half-way radii of the neutron and proton distributions differ by a significant amount.

My thanks are due to Dr. A. E. Glassgold for keeping me informed of his results in advance of their publication.

Appendix

We have to evaluate the integral

$$F_n(k) = \int_0^\infty \frac{x^n \, dx}{1+e^{x-k}}. \tag{A1}$$

We expand the integrand and obtain

$$F_n(k) = \int_0^k \sum_{m=0}^{\infty} (-1)^m x^n \, e^{m(x-k)} dx + \int_k^\infty \sum_{m=0}^{\infty} (-1)^m x^n \, e^{(m+1)(k-x)} \, dx.$$

The two series can be integrated term by term, since they are boundedly convergent. Hence

$$\begin{aligned} F_n(k) &= \frac{k^{n+1}}{n+1} + \sum_{m=1}^{\infty} (-1)^m \left\{ \int_0^k x^n \, e^{m(x-k)} \, dx - \int_k^\infty x^n \, e^{m(k-x)} \, dx \right\} \\ &= \frac{k^{n+1}}{n+1} - \sum_{m=1}^{\infty} \frac{(-1)^m}{m} \left\{ \sum_{r=0}^{n} [1-(-1)^r] \frac{n!}{m^r (n-r)!} k^{n-r} + \frac{(-1)^n n!}{m^n} e^{-mk} \right\} \\ &= \frac{k^{n+1}}{n+1} + \sum_{r=0}^{n} [1-(-1)^r] \frac{n!}{(n-r)!} k^{n-r} \left(1 - \frac{1}{2^r}\right) \zeta(r+1) \\ &\qquad - \sum_{m=1}^{\infty} (-1)^{m+n} \frac{n!}{m^{n+1}} e^{-mk}. \end{aligned} \tag{A2}$$

The final re-arrangement is permissible, since the series are absolutely convergent. For large k the last sum is $O(e^{-k})$ and can be neglected.

Then

$$A = 4\pi \varrho_0 a^3 F_2\left(\frac{c}{a}\right) = \tfrac{4}{3}\pi \varrho_0 c^3 \left(1 + \frac{\pi^2 a^2}{c^2}\right), \tag{A3}$$

and

$$R^2 = \frac{20\pi}{3A} \varrho_0 a^5 F_4\left(\frac{c}{a}\right) = \tfrac{4}{3}\pi \varrho_0 c^5 A^{-1} \left(1 + \frac{10\pi^2 a^2}{3c^2} + \frac{7\pi^4 a^4}{6c^4}\right). \tag{A4}$$

We next solve (A3) for c to order $(a/c)^5$. Thus

$$\begin{aligned} c &= bA^{1/3} \left(1 - \frac{\pi^2 a^2}{3c^2} + \frac{2\pi^4 a^4}{9c^4}\right) \\ &= bA^{1/3} \left\{1 - \frac{\pi^2 a^2}{3b^2} A^{-2/3} + O\left(\frac{a}{c}\right)^6\right\}, \end{aligned} \tag{A5}$$

after a little simplification, where b is given by (8). This is now substituted in (A4) and yields (7).

References

1) B. Hahn, D. G. Ravenhall and R. Hofstadter, Phys. Rev. **101** (1956) 1131
2) O. Kofoed-Hansen, Nuclear Physics **2** (1956) 441
3) A. Abashian, R. Cool and J. W. Cronin, Phys. Rev. **104** (1956) 855
4) L. Wilets, Phys. Rev. **101** (1956) 1805
5) H. Feshbach, Phys. Rev. **84** (1951) 1206
6) J. Fregeau, R. H. Helm and R. Hofstadter, Physica **22** (1956) 1195
7) L. Rosenfeld, Nuclear Physics **2** (1956) 450
8) R. W. Woods and D. S. Saxon, Phys. Rev. **95** (1954) 577
9) A. E. Glassgold and P. J. Kellog, Bull. Amer. Phys. Soc. **2** (1957) 71 and private communication
10) M. A. Melkanoff, J. S. Nodvik, D. S. Saxon and R. D. Woods, Phys. Rev. **106** (1957) 793
11) S. D. Drell, Phys. Rev. **100** (1955) 97
12) P. Gombás, P. Szépfalusy and E. Mágori, Nuclear Physics **4** (1957) 488

Nuclear Physics **5** (1958) 179—182; © *North-Holland Publishing Co., Amsterdam*
Not to be reproduced by photoprint or microfilm without written permission from the publisher

THE TWO-BODY SPIN-ORBIT INTERACTION

S. M. VAIDYA

Tata Institute of Fundamental Research, Apollo Pier Road, Bombay, India

Received 1 August 1957

Abstract: The effect of the inclusion of a two-body spin-orbit interaction is considered for the deuteron. It is found that the change in the strengths of the central and the tensor interactions is significant and varies linearly with the strength of the spin orbit interaction.

The present investigation is carried out to find the trend of the change in the depth of the central and the tensor force components when a given spin-orbit force [1, 2, 3]) is included in the two-body interaction V_{12}, the depths being determined from the deuteron ground state. The spin orbit force and the tensor force are the only non-central interactions allowed by charge independence and general invariance considerations [4]). We shall consider the following expression for V_{12}:

$$V_{12} = V_c J_c(r) + V_t S_{12} J_t(r) + V_m M_{12} J_m(r) \tag{1}$$

where

$$S_{12} = \frac{3(\boldsymbol{\sigma}_1 \cdot \mathbf{r})(\boldsymbol{\sigma}_2 \cdot \mathbf{r})}{r^2} - \boldsymbol{\sigma}_1 \cdot \boldsymbol{\sigma}_2,$$

$$M_{12} = (\boldsymbol{\sigma}_1 + \boldsymbol{\sigma}_2) \cdot \{(\mathbf{r}_1 - \mathbf{r}_2) \times (\mathbf{p}_1 - \mathbf{p}_2)\hbar^{-1}\},$$

$$J_c(r) = \frac{e^{-\beta r}}{\beta r}, \qquad J_t(r) = \frac{e^{-\tau r}}{\tau r}, \tag{2}$$

$$\mathbf{r} = \mathbf{r}_1 - \mathbf{r}_2, \quad r = |\mathbf{r}|,$$

$$J_m(r) = -\frac{1}{\beta r}\frac{d}{d(\beta r)}\left(\frac{e^{-\beta r}}{\beta r}\right) = \frac{e^{-\beta r}}{\beta^2 r^2}\left(1 + \frac{1}{\beta r}\right). \tag{3}$$

Pease and Feshbach [5]) have calculated the parameters in (1) to fit the deuteron data in the absence of the spin-orbit interaction. Their values are

$$\begin{aligned} &\beta^{-1} = 1.18 \times 10^{-13} \text{ cm}, \quad \tau^{-1} = 1.67 \times 10^{-13} \text{ cm}, \\ &V_c = -46.1 \text{ MeV}, \quad V_t = -24.9 \text{ MeV}. \end{aligned} \tag{4}$$

We calculate the binding energy of the deuteron on the basis of equation (1) using a trial wave-function due to Feingold [4]),

$$\psi = C\left(1 + \lambda(\alpha r)^2 V_t S_{12}\frac{e^{-\tau r}}{\tau r}\right)\psi_0 \tag{5}$$

where C is the normalization constant, and ψ_0 is given by

$$\psi_0 = \sqrt{\frac{\alpha^3}{\pi}}\, e^{-\alpha r}\, \alpha(1)\alpha(2); \tag{6}$$

$\alpha(1)\alpha(2)$ is the usual triplet spin-function, α and λ are the variational parameters.

The energy E is written in the form

$$E = \frac{E_0 + A\lambda + B\lambda^2}{1 + D\lambda^2}, \tag{7}$$

where

$$E_0 = \langle \psi_0 \left| -\frac{\hbar^2}{2M}\Delta \right| \psi_0 \rangle + V_c \langle \psi_0 | J_c | \psi_0 \rangle \equiv I_1 + I_2 V_c\,, \tag{8a}$$

$$A = 16 V_t^2 \langle \psi_0 | (\alpha r)^2 J_t^2 | \psi_0 \rangle \equiv I_3 V_t^2, \tag{8b}$$

$$\begin{aligned} B = {} & 8 V_t^2 V_c \langle \psi_0 | (\alpha r)^4 J_t^2 J_c | \psi_0 \rangle + V_t^2 \langle (\alpha r)^2 J_t S_{12} \psi_0 \left| -\frac{\hbar^2}{2M}\Delta \right| (\alpha r)^2 J_t S_{12} \psi_0 \rangle \\ & - 16 V_t^3 \langle \psi_0 | (\alpha r)^4 J_t^3 | \psi_0 \rangle - 48 V_m V_t^2 \langle \psi_0 | (\alpha r)^4 J_t^2 J_m | \psi_0 \rangle \\ \equiv {} & I_4 V_t^2 V_c - I_5 V_t^3 - I_6 V_t^2 V_m + I_7 V_t^2, \end{aligned} \tag{8c}$$

$$D = 8 V_t^2 \langle \psi_0 | (\alpha r)^4 J_t^2 | \psi_0 \rangle \equiv I_8 V_t^2. \tag{8d}$$

The value of λ which makes E a minimum is obtained by differentiating equation (7). This value of λ will be denoted by λ_0:

$$\lambda_0 = \frac{(B - DE_0) - \sqrt{(B - DE_0)^2 + A^2 D}}{AD}. \tag{9}$$

The value of α which makes E a minimum is chosen by direct numerical calculation with $\lambda = \lambda_0$.

In the absence of spin-orbit interaction this procedure gives a binding energy of 1.86 MeV and a D-state admixture of 3.47 % for the deuteron. Introducing a given spin-orbit interaction we now fit the values of V_c and V_t to give us the same binding energy of 1.86 MeV and a D-state admixture of 3.37 %. The results are tabulated below. It has been found that the value of the parameter α does not change in the variational procedure of minimizing E for the different strengths of spin-orbit interaction considered.

TABLE 1

V_m (MeV)	V_c (MeV)	V_t (MeV)
−10	−37.8	−34.0
− 5	−42.0	−29.4
0	−46.1	−24.9
5	−50.2	−20.4
10	−54.4	−15.8

From the table it can be seen that the dependence of V_c and V_t on V_m is linear. This linearity can be explained in the following way. The two conditions that the D-state admixture d and the binding energy E are constants give the relations

$$\frac{D\lambda_0^2}{1+D\lambda_0^2} = d, \tag{10}$$

$$\frac{E_0+A\lambda_0+B\lambda_0^2}{1+D\lambda_0^2} = E. \tag{11}$$

Eliminating λ_0 from eqs. (10) and (11) and making use of (8) we obtain the linear relation

$$\left(I_2 + \frac{I_4}{I_8(1-d)}\right)V_c + \left(I_3\sqrt{\frac{d}{I_8(1-d)}} - \frac{I_5 d}{I_8(1-d)}\right)V_t - \frac{I_6}{I_8}\frac{d}{1-d}V_m + I_1 + \frac{I_7 d}{I_8(1-d)} - \frac{E}{1-d} = 0. \tag{12}$$

Using the values of table 1 we find

$$A^2D \ll (B-DE_0)^2 \tag{13}$$

and hence eq. (9) can be written as

$$\lambda_0 \approx -\frac{1}{2}\frac{A}{B-DE_0}. \tag{14}$$

Eliminating λ_0 from eqs. (10) and (14), we obtain the second linear equation

$$I_2 V_c + \left(\frac{1}{2}\sqrt{\frac{I_8(1-d)}{d}}\, I_3 - I_5\right)V_t - I_6 V_m + I_7 = 0. \tag{15}$$

To get a better value for the binding energy of the deuteron we modify ψ_0 to

$$\psi_0 = C'\sqrt{\frac{\alpha^3}{\pi}}\,(e^{-\alpha r}+\mu e^{-\nu r})\alpha(1)\alpha(2) \tag{16}$$

where C' is the normalization constant and μ and ν are additional variational parameters; ψ is still defined by eq. (5). For the variational calculation we take the value of α obtained with the simple form (6) of ψ_0 and then vary μ and ν. With the above modification of the wave function the binding energy of the deuteron is 1.99 MeV and the D-state admixture is 3.48 %. Keeping these values fixed, values of V_c and V_t are fitted for assumed values of V_m. It was found that the values given in table 1 do not change by more than 1 %. The simple form (6) of ψ_0 therefore seems to be adequate.

It is a great pleasure to thank Dr. G. Abraham for suggesting the problem. The author is grateful to Professor L. Rosenfeld for his advice.

References

1) E. van der Spuy, Nuclear Physics **1** (1956) 381
2) G. Abraham, Nuclear Physics **1** (1956) 415
3) G. Abraham, L. Cohen and A. S. Roberts, Proc. Phys. Soc. A **68** (1955) 256
4) L. Eisenbud and E. P. Wigner, Proc. Nat. Acad. Sc. **27** (1951) 281
5) R. L. Pease and H. Feshbach, Phys. Rev. **81** (1951) 142
6) A. M. Feingold, Phys. Rev. **101** (1956) 258

Nuclear Physics **5** (1958) 183—186; © *North-Holland Publishing Co., Amsterdam*
Not to be reproduced by photoprint or microfilm without written permission from the publisher

POSSIBLE EXPERIMENTS ON THE BEHAVIOUR OF THE WEAK HYPERON DECAY INTERACTIONS UNDER P, C, AND T

R. GATTO †

Radiation Laboratory, University of California, Berkeley, California ††

Received 15 July 1957

Abstract: Various experimental possibilities for detecting the transformation properties of the weak hyperon decay interactions under P, C, and T are discussed.

1. Introduction

The possibility of detecting parity non-conservation in hyperon decay has been discussed recently [1, 2]. In this note we treat briefly of some further experimental possibilities for detecting the transformation properties of the weak hyperon decay interactions under P, C and T. The experiments proposed here are in general more difficult than the detection of the up-down asymmetries suggested by Lee and Yang [1, 2]; however, they will give more complete information.

2. Hyperon Production from the K^- Beam

The reaction $K^- + p \rightarrow Y + \pi$ (and similar reactions on complex nuclei †††) will presumably be the most useful way of producing hyperons. If we assume spin zero for K and $\frac{1}{2}$ for Y and no change of intrinsic parity in the process, and denote the initial and final centre-of-mass momenta by $\mathbf{p}$ and $\mathbf{p}'$, the transition matrix for this reaction has the form $M = A + B\boldsymbol{\sigma} \cdot \mathbf{n}$, where A and B are functions of p and $\mathbf{p} \cdot \mathbf{p}' = pp' \cos\theta$, and $\mathbf{n}$ is a unit vector normal to the production plane. The amplitudes A and B are further restricted by the requirement of containing $\mathbf{p}$ and $\mathbf{p}'$ only up to some powers, corresponding to the maximum values of the orbital angular momenta for the initial and final state respectively. Explicit expressions

† On leave of absence from Istituto di Fisica dell' Università di Roma.

†† This work was performed under the auspices of the U.S. Atomic Energy Commission.

††† The hyperon in $K^- + p \rightarrow Y + \pi$ is polarized only if the K^- is absorbed in flight. Unfortunately only a few cases for $K^- + p \rightarrow Y + \pi$ in flight have been reported so far. On the other hand, a large number of cases of K^- absorption at rest from emulsion nuclei are now available. The absorbing nucleon has, however, a Fermi momentum inside the nucleus. By choosing only those events from which the emitted Σ and π have not suffered appreciable scattering inside the nucleus (almost all energy taken by the Σ and the π), it might be possible to detect an up-down asymmetry in the Σ decay with respect to the plane defined by the direction of emission of the Σ and of the π, if p-wave absorption is efficient at such low relative energies.

in terms of the reaction matrix elements will be given by Spitzer and Stapp in a paper in preparation. The differential cross section is given by

$$F = \tfrac{1}{2}\,\mathrm{tr}\,[MM^\dagger] = |A|^2+|B|^2$$

and the polarization of the produced Y by †

$$\langle\boldsymbol{\sigma}\rangle_Y = \frac{\mathrm{tr}\,[MM^\dagger\boldsymbol{\sigma}]}{\mathrm{tr}\,[MM^\dagger]} = \frac{2\,\mathrm{Re}\,(AB^*)}{|A|^2+|B|^2}\,\mathbf{n}. \tag{1}$$

Note that if first order perturbation theory were applicable, we would have $\langle\boldsymbol{\sigma}\rangle_Y = 0$. The transition matrix for the decay $Y \to N+\pi$ in the centre-of-mass system is $T = g+h\boldsymbol{\sigma}\cdot\mathbf{k}$ where g and h are complex numbers and $\mathbf{k}$ is a unit vector in the direction of the emitted N. The distribution of $\mathbf{k}$ is given by

$$\begin{aligned} G &= \tfrac{1}{2}\{\mathrm{tr}\,[TT^\dagger]+\langle\boldsymbol{\sigma}\rangle_Y\,\mathrm{tr}\,[T\boldsymbol{\sigma}T^\dagger]\} \\ &\propto 1 + \frac{2\,\mathrm{Re}\,(gh^*)}{|g|^2+|h|^2}\cdot\frac{2\,\mathrm{Re}\,(AB^*)}{|A|^2+|B|^2}\,(\mathbf{n}\cdot\mathbf{k}), \end{aligned} \tag{2}$$

showing the up-down asymmetry (term proportional to $\mathbf{n}\cdot\mathbf{k}$) pointed out by Lee and Yang [1, 2]). We write $g = g_3+g_1$ and $h = h_3+h_1$, where g_3 and h_3 are the amplitudes corresponding to $N+\pi$ in the s and p states respectively with $I = 3/2$, and g_1 and h_1 are corresponding amplitudes for $I = \frac{1}{2}$. If time reversal is satisfied, these amplitudes can be written in the form $\varrho e^{i\alpha}$ where the ϱ's are real numbers (positive or negative) and the α's are the relevant $N+\pi$ phase shifts taken at the hyperon decay energy [3]). If charge conjugation is satisfied, the amplitudes can still be written in the form $\varrho e^{i\alpha}$, where the α's are the phase shifts; however, the ϱ's are real for the two g amplitudes and pure imaginary for the h amplitudes (or vice versa) [2]). Because the relevant phase shifts are small for spin $\frac{1}{2}$ of Y, if C is satisfied g is essentially real and h essentially pure imaginary, and the up-down asymmetry would be small. Observation of a large $(\mathbf{n}\cdot\mathbf{k})$ term in (1) would therefore essentially imply both P and C non-conservation—but it would, of course, provide no information on T. Unfortunately, the coefficient of such a term could also be small because of $\langle\boldsymbol{\sigma}\rangle_Y$ being small. A measurement of the polarization of the emitted nucleon would provide direct information on the question of P and C non-conservation and, if $\langle\boldsymbol{\sigma}\rangle_Y$ is not very small, also on the question of T invariance. The polarization of the emitted nucleon in the hyperon decay will be given by

$$\begin{aligned} G\langle\boldsymbol{\sigma}\rangle_N &= \tfrac{1}{2}\{\mathrm{tr}\,[TT^\dagger\boldsymbol{\sigma}]+\langle\boldsymbol{\sigma}\rangle_Y\,\mathrm{tr}\,[T\boldsymbol{\sigma}\cdot T^\dagger\boldsymbol{\sigma}]\} \\ &= 2\,\mathrm{Re}\,(gh^*)\mathbf{k}+(|g|^2-|h|^2)\langle\boldsymbol{\sigma}\rangle_Y \\ &\quad +2i\,\mathrm{Im}\,(gh^*)\langle\boldsymbol{\sigma}\rangle_Y\wedge\mathbf{k}+2|h|^2\,(\langle\boldsymbol{\sigma}\rangle_Y\cdot\mathbf{k})\mathbf{k}. \end{aligned} \tag{3}$$

† If there is change of intrinsic parity in the process M has the form $M = C\boldsymbol{\sigma}\cdot\mathbf{p}+D\boldsymbol{\sigma}\cdot\mathbf{p}'$, from which one finds $F = |C|^2p^2+|D|^2p'^2+2\,\mathrm{Re}\,(CD^*)\mathbf{p}\cdot\mathbf{p}'$ and $\langle\boldsymbol{\sigma}\rangle_Y = -2F^{-1}\,\mathrm{Im}(CD^*)\,\mathbf{p}\wedge\mathbf{p}'$. All conclusions are, of course, unchanged.

Taking hyperons from any origin, independently of their production process, one is left only with a longitudinal polarization for the emitted nucleon, which is given by

$$\langle \boldsymbol{\sigma} \rangle_N = \frac{2 \text{ Re } (gh^*)}{|g|^2+|h|^2}\mathbf{k}. \tag{4}$$

Such longitudinal polarization could be detected by bending it into a transverse one with a magnetic field, or by successive scatterings, or by utilizing the transverse component that originates from the transformation from the Y rest frame to the laboratory system. The detection of a large longitudinal polarization would imply violation not only of P but also of C, and vice versa, if P is violated, such polarization must always be different from zero but very small if C is conserved. To illustrate the quantitative argument, let us consider, as Lee and Yang do, the simple case of Σ^- decay for which only the final $I = 3/2$ is possible. (A corresponding simple situation perhaps holds for the Λ^0 decay for which, according to the latest measurements, only the final $I = \frac{1}{2}$ seems to contribute.) In the case of Σ^- decay, the coefficient of $\mathbf{k}$ in (4) is $\pm \sin(\alpha_3-\alpha_{31}) \cdot 2x/(1+x^2)$, with $x = |g|/|h|$ if C is satisfied, and $\pm \cos(\alpha_3-\alpha_{31}) \cdot 2x/(1+x^2)$, if T is satisfied. If the production planes are also observed, the polarization will be given by the full expression (3), and we note that the observation of the third term proportional to Im (gh^*) may give information on T conservation by the same arguments used before.

3. Production and Decay of Ξ

In the reaction $K^-+p \to \Xi^-+K^+$ with observation of the subsequent cascade decay of Ξ^- (which will be investigated in Berkeley by Alvarez and collaborators), the decay of the emitted Λ^0 could serve as an analyzer of the possible polarization of the Λ^0 itself. If we assume spin $\frac{1}{2}$ for the hyperons, the polarization of the Ξ^- will be given by an expression like (1), where A and B refer to the above production reaction. The polarization of the Λ^0 from the decay of Ξ^- will similarly be described by (3), where g and h refer to $\Xi^- \to \Lambda^0+\pi^-$. Such polarization is directly observed in the subsequent Λ^0 decay for which the distribution of $\boldsymbol{\chi}$, the unit vector in the direction of emission of the nucleon, will be given by

$$W \propto 1+\frac{2 \text{ Re } (pq^*)}{|p|^2+|q|^2}\langle \boldsymbol{\sigma} \rangle_\Lambda \cdot \boldsymbol{\chi} \tag{5}$$

where we have written the transition matrix for $\Lambda^0 \to N+\pi$ in the form $p+q\boldsymbol{\sigma} \cdot \boldsymbol{\chi}$. If Ξ^- particles from any origin are considered independent of the production reaction, observation of a large $\boldsymbol{\chi}$ dependence (forward-backward asymmetry) in (5) would imply not only violation of P in both Ξ

and Λ decay but also violation of C, unless the relevant $\Lambda^0-\pi^-$ phase shift is large. If the production plane in $K^-+p \to \Xi^-+K^+$ is observed, observation of a large term proportional to $(\mathbf{n} \wedge \mathbf{K}) \cdot \boldsymbol{\chi}$ in (5) would imply violation of T invariance.

4. Decay of Hyperfragments

The possibility of observing P non-conservation essentially depends on the s—p interference in the final state. Especially in Λ^0 decay, p-wave emission could be rather infrequent because of the angular-momentum barrier which is more efficient due to the low Q value. We might ask whether any possibility exists of enhancing this p-wave amplitude in hope of obtaining larger interference effects. A possibility presents itself in the non-mesonic decay of hyperfragments, for which the angular momentum barrier for larger orbital angular momenta is less disfavoured with respect to the case of free Λ^0 decay because of the larger momentum transfer. If we write the transition matrix for $\Lambda^0 \to N+\pi$ as $T = g+l\boldsymbol{\sigma} \cdot \mathbf{j}$, where $\mathbf{j}$ is the momentum of π, the transition matrix for $\Lambda^0+N \to N+N$ in perturbation theory is essentially of the form $f(g+l\boldsymbol{\sigma}_1 \cdot \mathbf{p}_N)(\boldsymbol{\sigma}_2 \cdot \mathbf{p}_N)$, where f is a constant and $\mathbf{p}_N$ is the momentum of each final N in the centre-of-mass system. The p amplitude of Λ^0 decay thus appears to be enhanced by a factor $\approx p_N/p_\pi \approx 4$ with respect to the case of free Λ^0 decay if we assume, as Ruderman and Karplus do, that the energy dependence of g and l can be neglected [4]). The above factor is expected to increase if the Λ^0—N correlation and the effect of the exclusion principle for the final nucleons in heavy fragments are taken into account. For the detection of P non-conservation, a measurement of the angular correlations in the decay of simpler hyperfragments could be useful. Such correlations must not necessarily depend on the polarization of the hyperfragment. In a four-body decay with final momenta $\mathbf{p}_1$, $\mathbf{p}_2$, $\mathbf{p}_3$, and $\mathbf{p}_4$ of an unpolarized hyperfragment, $\langle(\mathbf{p}_1 \wedge \mathbf{p}_2) \cdot \mathbf{p}_3\rangle$ is a pseudoscalar, and its detection would imply parity non-conservation. Moreover, a careful examination of the decay distributions of the different decay modes of the same hyperfragment could also give information on the possible existence of final amplitudes of opposite parity. Such study would be of interest in any case for the theory of hyperfragments.

References

1) T. D. Lee and C. N. Yang, Phys. Rev. **104** (1954) 254
2) Lee, Steinberger, Feinberg, Kabir and Yang, (to be published)
3) See E. Fermi, Supplemento Nuovo Cimento **1** (1955) 62
4) M. Ruderman and R. Karplus, Phys. Rev. **102** (1956) 247

Nuclear Physics **5** (1958) 187—194; © *North-Holland Publishing Co., Amsterdam*

Not to be reproduced by photoprint or microfilm without written permission from the publisher

EXCITED STATES OF Eu^{153}

C. W. McCUTCHEN

Cavendish Laboratory, Cambridge

Received 29 August 1957

Abstract: The β^- decay of Sm^{153} and the electron capture decay of Gd^{153} have been studied with a NaI scintillation spectrometer, with a xenon proportional counter used with and without escape gating [1]), and with a conversion-electron proportional counter. The two decay schemes have been verified and, in one case, extended. From a measurement of its internal conversion coefficient the 97 keV γ in the Gd^{153} decay is shown to be E1. The decay schemes and multipolarities are shown to be inconsistent with any likely spin sequence for Eu^{153} and ground state spin of Gd^{153}.

1. Introduction

The excited states of Eu^{153} can be reached both by the β^- decay of 47 h Sm^{153} and the electron capture decay of 236 d Gd^{153}. For a summary of the situation on Sm^{153} the reader is advised to consult the recent paper by Dubey, Mandeville, and Rothman [2]). All groups agree that the first and second excited particle states are at 103 and 172 keV respectively, that the cascade transitions are M1+E2 and that the cross-over transition is very weak.

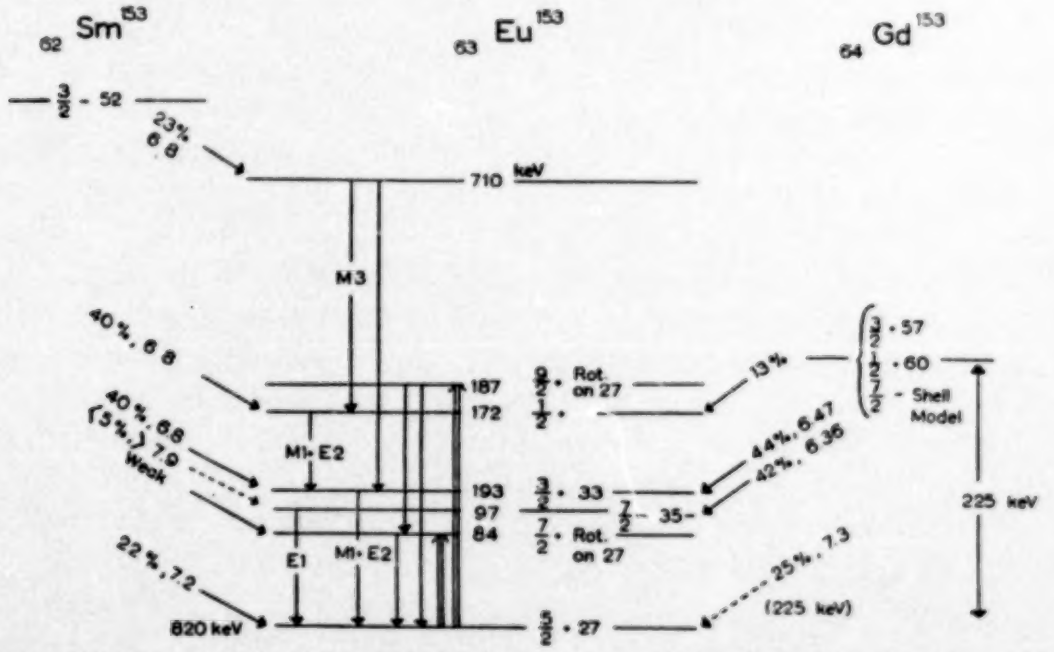

Fig. 1. Sm^{153} and Gd^{153} disintegration schemes. Level assignments show the spin parity and the Nilsson orbit number. β branches show the intensity in % and the log ft value and, in the case of ground state transitions, the energy.

There is no agreement on the place of the 540 keV γ (and the 600 keV γ) in the decay scheme. Fig. 1. shows the conclusions of Dubey *et al.* [2]). The 103 keV level has a half-life of 3.4×10^{-9} sec [6]). Mrs. Marty [3]) reports that the 84 keV rotational level (previously observed by Coulomb excitation [4])) is weakly excited.

The data on Gd^{153} are more conflicting. Conversion electron studies [5]) have found what are apparently the same 103 and 70 keV transitions as are excited in the Sm^{153} decay. However, Church and Goldhaber [7]) have also seen a 97 keV line. McGowan [6]) reports that within a few keV of the delayed 103 keV γ there is a prompt γ ($T_{\frac{1}{2}} \leqq 10^{-9}$ sec). This is presumably the 97 keV transition reported by Church and Goldhaber. He further states that in the Gd^{153} decay the 70 keV transition leads to the metastable level rather than to the short-lived one.

2. Sources

The sources were natural Sm_2O_3 and Gd_2O_3 irradiated with thermal neutrons at the A.E.R.E. at Harwell. The Gd sources were allowed to age for several weeks before use to allow the 18 h Gd^{159} and the 7 d Tb^{161} activities to die. For the conversion electron work the sources were either deposited from a water slurry of the finely divided oxide or vacuum evaporated as the chloride.

3. Experimental Procedure and Results

First the γ spectra of Sm and Gd were compared to verify which γ's were common to both decays. Two escape gated [1])† xenon counter runs were taken in quick succession to avoid possible gain shifts. These (fig. 2) show clearly that the 103 and 70 keV γ's are those common to both decays. These runs also place an upper limit of 10 % on $I_\gamma(97)/I_\gamma(103)$ in the Sm decay.

An ordinary xenon counter run, in better statistics, on Gd showed that the 97 keV γ was 1.74 times as strong as the 103 keV γ. McGowan, separating the γ's by means of time resolution, gives this same intensity ratio as 1.4.

A coincidence experiment on Gd in which receipt of a 70 keV γ by the scintillator gated xenon counter pulses to the kicksorter showed (fig. 3) that in Gd the 70 keV γ is in coincidence with the 103 keV γ and not with the 97 keV γ. This provides direct confirmation of the conclusion reached by McGowan by less direct reasoning.

An upper limit for the K conversion coefficient of the 97 keV transition was obtained by comparing $I_\gamma(97)/I_\gamma(103)$ with $I_e(97)/I_e(103)$. To find

† Escape gating suppresses all the full energy peak in the xenon counter spectrum; the resulting spectrum is made up entirely of K X ray escape peaks.

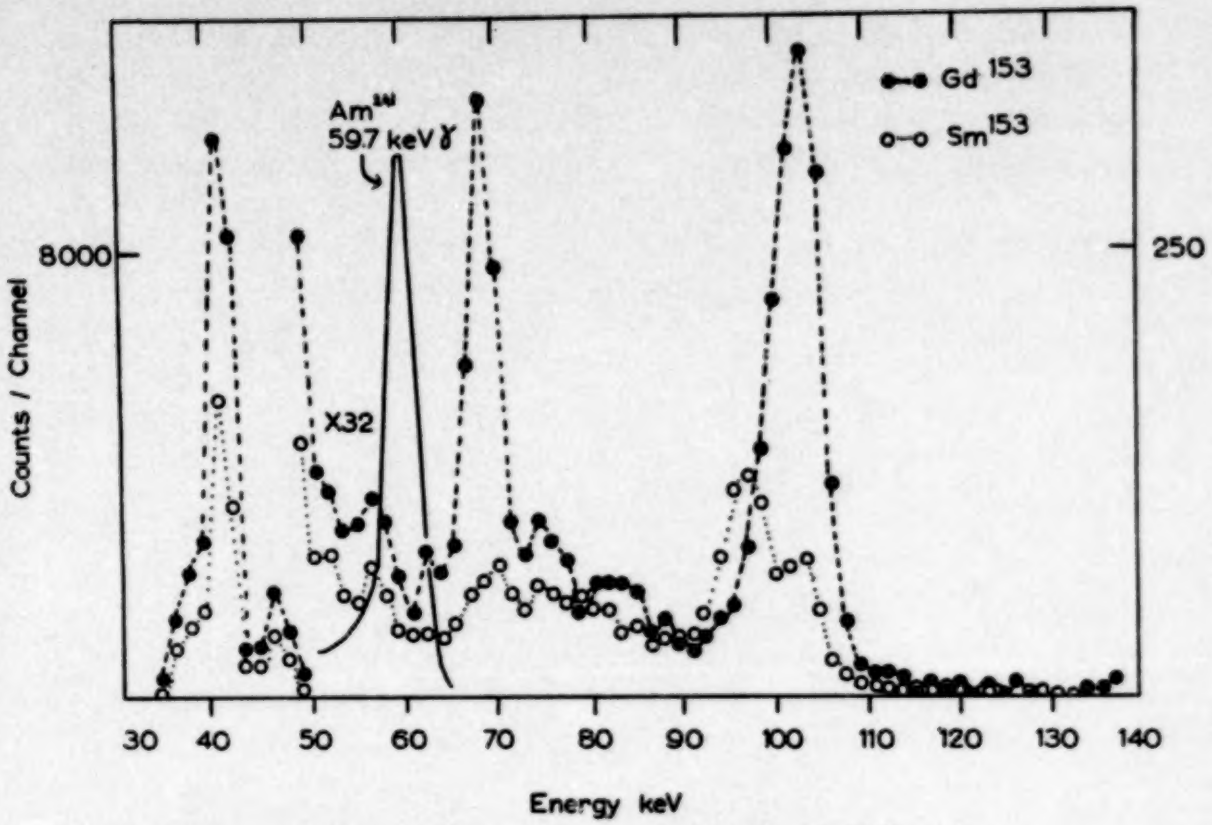

Fig. 2. Escape-gated xenon counter runs comparing Sm^{153} and Gd^{153} spectra.

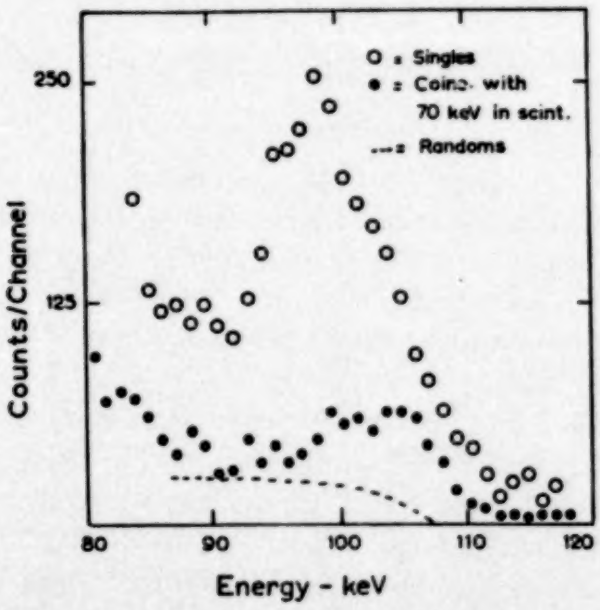

Fig. 3. The xenon counter spectrum in coincidence with the 70 keV γ is compared with the spectrum of single counts.

the latter quantity the conversion electron spectrum was examined with a proportional counter of 4 in. diameter filled with 1 to 2 atm of argon and

a few cm of ethylene. Fig. 4 shows that the highly K converted transition of the pair at about 100 keV is that at 103 keV. As the two γ's are very close in energy some care was taken to be certain of the identification. For this purpose the counter was equipped with an aluminium window near the source to let out γ's and X rays. These could then be counted by an external γ counter. That the supposed K conversion line really was a K

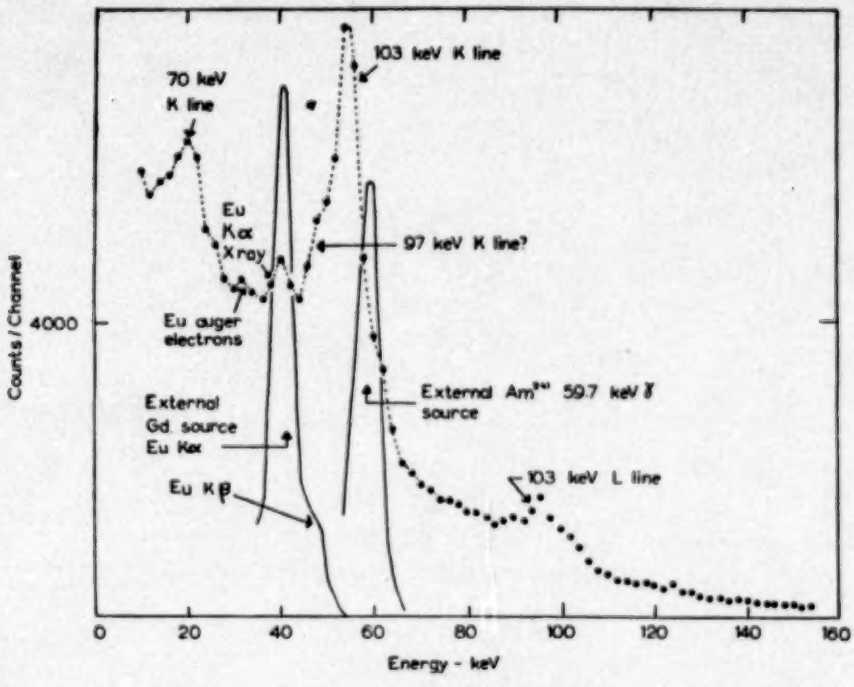

Fig. 4. Conversion electron spectrum of Gd^{153} obtained with an argon filled proportional counter.

line was shown by enhancement of the peak when the proportional counter was put in coincidence with K X rays caught by a scintillator just outside the window. The assignment to 103 rather than to 97 keV was first made on the basis of energy by calibrating the counter with an external X ray source. The assignment was verified by showing that the conversion electron line was in coincidence with 70 keV γ's.

The K conversion line, of the 97 keV transition, though not clearly resolved is certainly less than $\frac{1}{2}$ as strong as that of the 103 keV transition. The measured K conversion coefficient for the 103 keV transition is about 1.2 [7, 8]). Combining these data with my value for $I_\gamma(97)/I_\gamma(103)$ gives an upper limit of 0.37 for $\alpha_K(97)$ which definitely classifies the transition as E1. The theoretical K conversion coefficients (as given by Sliv and Band [8]) are 0.226 and 1.10 for E1 and E2 respectively. Since this work was completed Bisi, Germagnoli and Zappa [9]) have published a magnetic spectrometer spectrum of these conversion electrons. Though they appear not to notice it, their curve (and as far as I know this is the first time that the

actual spctrum has been published) clearly shows the K line of the 97 keV transition. From their data the ratio $I_e(97)/I_e(103)$ seems to be between 0.25 and 0.35. This would put the 97 keV conversion coefficient between 0.185 and 0.26 which agrees well with the theoretical value.

The escape gated runs in fig. 2 also show that, in the Gd decay, there is electron capture directly to the 103 keV state. In the Sm decay there is a β branch to the 103 keV level. Fig. 2 shows that $I_\gamma(70)/(I_\gamma(103)$ in the Gd decay is no higher than $I_\gamma(70)/I_\gamma(103)$ in the Sm decay so the 103 keV level must be fed directly in the Gd decay also.

If the necessary counter efficiency and wall effect corrections are made $I_\gamma(70)/I_\gamma(103)$ in the Sm decay is found to be 0.2. This should be compared with 0.25 found by McGowan and 0.24 found by Dubey *et al.* My value is probably poorer than theirs as the various corrections are harder to estimate for the xenon counter than for a scintillator. The agreement does, however, provide some confidence in the method. In the Gd decay the results of fig.2 must be used with care because any full energy counts from the Eu K X ray peak which manage by informal processes to get recorded despite the K escape gating will appear at 71 keV on the escape peak energy scale. Filtering out these X rays with 0.015 in. of Cd gave a value of $I_\gamma(70)/I_\gamma(103)$ of $0.11\ ^{+0.07}_{-0.05}$. The large uncertainty is because the statistics were poor and because there was some geometrical uncertainty in the effective thickness of the Cd absorber.

Searches for other low energy γ's yielded nothing. The apparent peaks at 76 keV in fig. 2 (which might have represented a transition from the 172 keV level to the 97 keV level) were apparently lead fluorescence from the lead shield used in the K escape gating apparatus. They disappeared when the plain lead shield was replaced by a lead-cadmium graded shield.

The high energy γ's in the Sm decay were verified and their intensity was measured relative to that of the 103 keV γ. Scintillator-scintillator coincidences showed that the 535 keV was in coincidence with the 103 keV γ and probably with the 70 keV γ as well. This agrees with the findings of Dubey *et al.*

The relative γ intensities found in this investigation are summarized in table 1 where they are expressed in terms of the intensity of the 103 keV γ.

TABLE 1

	605	535	170	103	97	70
Sm^{153}	0.001	0.005	not measured	1	< 0.1	0.2
Gd^{153}				1	1.74	≈ 0.11 (definitely < 0.2)

If the ratio $I_\gamma(535)/I_\gamma(103)$ is compared with $I_e(535)/I_e(103)$ from the data of Lee and Katz [10]) and the known value of the K conversion coefficient for the 103 keV transition is employed the K conversion coefficient for the 535 keV transition is found to be 0.175 which implies an M3 transition. Various groups disagree somewhat on $I_\gamma(535)/I_\gamma(103)$ but use of any γ data makes this transition at least E3. This point was first noticed by Mrs. Marty [3]).

4. Beta Branching Ratios and *ft* Values

There is reasonable agreement between the most recent workers (Dubey and Mrs. Marty) on the branching ratios in the Sm decay. The numbers in fig 1 are those of Dubey *et al.* except that the branch to the 700 keV level has been made to agree with my idea of $I_{\text{total}}(535)/I_{\text{total}}(103)$.

In the Gd decay the transition energy has been deduced by measuring the ratio of L to K capture and then using the theory of Marshak [11]). Gupta and Jha [12]) and Bisi, Germagnoli and Zappa [13]), both using simplified decay schemes, have found the energy difference between the ground states of Gd^{153} and Eu^{153} to be 225 and 183 keV respectively. Gupta and Jha find that the intensity of the electron capture branch to the ground state is 25 % while Bisi *et al.* make it to be 2 %. The simplifications in the decay scheme do not entirely vitiate these results which, roughly, state that there is much L capture and that therefore the decay energy is small.

The log *ft* values shown for the Gd decay in fig. 1 were derived assuming a total transition energy of 225 keV and splitting up the decay by means of the total (γ+conversion electron) transition intensities. To do this the measured γ intensities were combined with the total conversion coefficients assumed by Dubey *et al.* in the case of the 103 and 70 keV transitions and taking 0.4 as the total conversion coefficient for the E1 97 keV transition. No *ft* value is given for the branch to the 172 keV level because the transition energy is then uncertain by a large factor.

5. Interpretation

The ground state spin of Eu^{153} has been measured [14]) to be 5/2. From the rotational spectrum and Coulomb-excitation cross section [15]) it is known that the deformation is large so the ground state is identified with the 5/2+ Nilsson [16]) orbit 27. The ground-state spin of Sm^{153} has not been measured but that of the neighbouring nucleus Gd^{155} has spin 3/2 [17]). As Gd^{157} has the same spin and nearly the same magnetic moment it is likely that the ground states of both Gd isotopes are Nilsson orbit 52; in Gd^{155} the $h_{11/2}$ orbit 28 is empty while in Gd^{157} it is filled. Sm^{153} is there-

fore assumed to have the 3/2− Nilsson orbit 52 as its ground state since, like Gd^{155} it is a 91 neutron nucleus.

Alaga [18]) has analysed the β decay of Sm^{153} using these assignments and finds it consistent with his asymptotic quantum number selection rules. The ground state β branch is first forbidden hindered.

The β and γ selection rules require that the 103 keV and 172 keV states be 3/2+ and $\frac{1}{2}$+ respectively. In the absence of unsuspected selection rules, any other sequence which would attract first forbidden $\Delta J = 0$ or 1 branches will not account for the extreme weakness of the cross-over transition.

The 97 keV state decays to the ground state by E1 radiation so it can be 3/2−, 5/2− or 7/2−. Of these, only 7/2− will not be fed by an allowed β decay.

On present information the 700 keV state poses an insoluble problem. The strength of the β branch feeding it requires that its spin be $\frac{1}{2}$, 3/2, or 5/2 and yet it appears to decay to the 103 keV state by E3 or M3 radiation. Clearly it is important to recheck the conversion electron data to see if the conversion coefficient really is so large. Only Lee and Katz have seen the conversion line of either high energy transition. Mrs. Marty looked but found nothing detectable in the presence of the β's.

Ignoring this difficulty we move on to the Gd^{153} decay and find another. Gd^{153} decays to the 97, 103, and 172 keV levels in Eu^{153} with *ft* values which indicate spin changes of no more than 1. From the decay of Sm^{153} the spins of these states are required to be 7/2, 3/2, and $\frac{1}{2}$. No choice for the ground state spin of Gd^{153} can feed all of these levels. The situation is even more difficult if we believe that the ground state branch is very weak (as the results of Bisi *et al.* [13]) indicate) for this means that the intermediate spin value of 5/2 is for some reason not fed.

The ground state spin of Gd^{153} has not been directly measured, nor has that of any other 89 neutron nucleus. Between 88 and 90 neutrons a violent change occurs in the deformation of the even isotopes of Gd [17]) so the deformation status of 89-neutron nuclei is in doubt. The spherical shell model would predict an $f_{7/2}$− level while the Nilsson assignment is either the $\frac{1}{2}$+ orbit 60 or the 3/2+ orbit 57; the former if the $h_{11/2}$ orbit 28 is filled and the latter if it is not.

6. Possible Explanations

Perhaps Gd^{153} has an as yet undetected long lived isomeric state from which one or more of the electron capture branches originate. If the isomeric state possesses the shell model spin and parity (7/2−) and the ground state has either of the deformed model values ($\frac{1}{2}$+, 3/2+) or vice versa then all the electron capture branches can be explained.

This supposition could most easily be checked by an investigation of the ratio $I(97)/I(103)$ for sources of different ages, for it is unlikely that the initial population ratio for the isomeric and ground states would be the equilibrium values. No change in $I_\gamma(97)/I_\gamma(103)$ was noted in these experiments, but the youngest sources were about a week old so equilibrium might already have been attained.

Finally, if the E1 97 keV transition leads not to the ground state but to an as yet undetected state the level that feeds it might be of even parity in which case the β branch to it in the Sm decay would be first forbidden and could possibly be weak enough to agree with its experimental absence. Many choices of the spin of this level would then permit one of the Nilsson predictions to be used for the ground state of Gd^{153}.

References

1) C. W. McCutchen, Nuclear Physics **3** (1957) 76
2) V. S. Dubey, C. E. Mandeville and M. A. Rothman, Phys. Rev. **103** (1956) 1430
3) N. Marty, J. Phys. Rad. **16** (1955) 458
4) N. P. Heydenburg and G. M. Temmer, Phys. Rev. **100** (1955) 150
5) R. E. Hein and A. F. Voight, Phys. Rev. **79** (1950) 783
J. M. Cork, J. M. Le Blanc, W. H. Nester and F. B. Stumpf, Phys. Rev. **88** (1952) 685
6) F. K. McGowan, Phys. Rev. **93** (1954) 163
7) E. L. Church and M. Goldhaber, Phys. Rev. **95** (1954) 626
8) L. A. Sliv and I. M. Band, (Academy of Sciences of the U.S.S.R. Moscow, Leningrad; issued in U.S.A. as Report 57 ICC K1, Physics Dept., Univ. of Illinois, Urbana, Illinois)
9) A. Bisi, E. Germagnoli and L. Zappa, Nuclear Physics **3** (1957) 670
10) M. R. Lee and R. Katz, Phys. Rev. **93** (1954) 155
11) R. E. Marshak, Phys. Rev. **61** (1942) 431
12) R. K. Gupta and S. Jha, Nuovo Cimento **4** (1956) 88
13) A. Bisi, E. Germagnoli and L. Zappa, Nuclear Physics **1** (1956) 593
14) B. Bleaney and W. Low, Proc. Phys. Soc. A **68** (1955) 551
15) N. P. Heydenburg and G. M. Temmer, Phys. Rev. **104** (1956) 981
16) S. G. Nilsson, Mat. Fys. Medd. Dan. Vid. Selsk., **29** (1955) no. 16;
B. R. Mottelson and S. G. Nilsson, Phys. Rev. **99** (1955) 1615L
17) D. R. Speck, Phys. Rev. **101** (1956) 1725
18) G. Alaga, Phys. Rev. **100** (1955) 432

Nuclear Physics **5** (1958) 195—201; © *North-Holland Publishing Co., Amsterdam*

Not to be reproduced by photoprint or microfilm without written permission from the publisher

APPLICATION OF THE TAMM-DANCOFF-METHOD TO THE LEE-MODEL

W. HEISENBERG

Max-Planck-Institut für Physik, Göttingen

Received 20 September 1957

Abstract: The new Tamm-Dancoff-method is applied to the Lee-model, after the renormalization for the special case of the 'dipole-ghost' had been carried out. The Tamm-Dancoff-method leads to the exact solutions. Contravariant representations of the state vectors by means of the renormalized operators can be found only if these operators are spread out over finite time intervals, i.e. if integrals of the operators over finite time intervals are applied to the state vector of the vacuum.

The new method of quantisation which had been used for a non linear spinor equation [1]) has recently been analyzed in connection with the Lee-model [2]). The actual calculation of the stationary states and the S-matrix has in the case of the non linear spinor equation been carried out in a first approximation by means of the new Tamm-Dancoff method, while the ordinary Schrödinger formalism has been used for the Lee-model. In order to get a close connection between the two mathematical schemes it seems instructive to repeat the calculations for the Lee-model by means of the Tamm-Dancoff method, i.e. just by that method which had been used for the non linear spinor equation, and to compare the results with those obtained from the Schrödinger equation. The notation will be taken from the paper on the Lee-model [2]).

Just as in the case of the spinor equation the calculation shall be performed without using any process of renormalization. Therefore we have to start with the renormalized wave equations which contain only finite constants and are the analogues of the non linear spinor equation. The wave equations [ref. [2]), eq. (62 a—d)] are written by means of the field operators $\psi_{\mathrm{Vr}}(\mathbf{x}, t)$, $\psi_{\mathrm{N}}(\mathbf{x}, t)$ and $a(\mathbf{x}, t)$, referring to the V, N and θ-particles, and by the quantities $\varphi(\mathbf{x}, t)$ and $\Pi(\mathbf{x}, t)$ related to $a(\mathbf{x}, t)$:

$$g\int_{-\infty}^{t} \mathrm{d}t'\,\chi(t-t')\psi_{\mathrm{Vr}}(\mathbf{x}, t') = -2i\pi^2 g\int_{-\infty}^{t} [a(\mathbf{x}, t)a^*(\mathbf{x}, t') - s(t-t')]\psi_{\mathrm{Vr}}(\mathbf{x}, t')\mathrm{d}t' - \pi\sqrt{2}\, a(\mathbf{x}, t)\psi_{\mathrm{N}}(\mathbf{x}, -\infty); \quad \text{(1a)}$$

$$i\frac{\partial\psi_{\mathrm{N}}(\mathbf{x})}{\partial t} = -\pi g\sqrt{2}\, a^*(\mathbf{x})\psi_{\mathrm{Vr}}(\mathbf{x}); \quad \text{(1b)}$$

$$\frac{\partial\Pi(\mathbf{x})}{\partial t} = \Delta\varphi(\mathbf{x}) - m_\theta^2\varphi(\mathbf{x}) + \frac{\pi g}{\sqrt{2}}[\psi_{\mathrm{Vr}}^*(\mathbf{x})\psi_{\mathrm{N}}(\mathbf{x}) + \psi_{\mathrm{N}}^*(\mathbf{x})\psi_{\mathrm{Vr}}(\mathbf{x})]; \quad \text{(1c)}$$

$$\frac{\partial\varphi(\mathbf{x})}{\partial t} = \Pi(\mathbf{x}) - \frac{i\pi g}{\sqrt{2}}\int \mathrm{d}^3x'\,\frac{\mathrm{e}^{-m_\theta|\mathbf{x}-\mathbf{x}'|}}{|\mathbf{x}-\mathbf{x}'|}[\psi_{\mathrm{Vr}}^*(\mathbf{x}')\psi_{\mathrm{N}}(\mathbf{x}') - \psi_{\mathrm{N}}^*(\mathbf{x}')\psi_{\mathrm{Vr}}(\mathbf{x}')]. \quad \text{(1d)}$$

$s(t-t')$ and $\chi(t-t')$ are defined by ($\omega = \sqrt{m_0^2+k^2}$)

$$s(t-t') = \langle 0|a(\mathbf{x}t)a^*(\mathbf{x}t')|0\rangle = \frac{1}{4\pi^2}\int_0^\infty \frac{k^2 \mathrm{d}k}{\omega} \mathrm{e}^{i\omega(t'-t)};$$
$$\chi(t-t') = \frac{1}{2\pi}\int_{-\infty}^{+\infty} h^+(z)\mathrm{e}^{iz(t'-t)}\,\mathrm{d}z, \tag{2}$$

where $h^+(z)$ is a function characteristic for the Lee-model [ref. [2]), eqs. (15), (16) and (29)].

The following calculations will be confined to the sector $\binom{N+s\vartheta}{V+(s-1)\vartheta}$.

Let $\Phi\rangle$ be a state vector in this sector. Then we can define the τ-functions

$$\tau_N(\mathbf{x}_1 t_1, \cdots, \mathbf{x}_s t_s;\ t_N) = \langle 0|Ta(\mathbf{x}_1 t_1)\cdots a(\mathbf{x}_s t_s)\psi_N(t_N)|\Phi\rangle,$$
$$\tau_V(\mathbf{x}_1 t_1, \cdots, \mathbf{x}_{s-1} t_{s-1};\ t_V) = \langle 0|Ta(\mathbf{x}_1 t_1)\cdots a(\mathbf{x}_{s-1} t_{s-1})\psi_{Vr}(t_V)|\Phi\rangle, \tag{3}$$

or in momentum space:

$$\tau_N(\mathbf{k}_1 t_1, \cdots, \mathbf{k}_s t_s;\ t_N) = \langle 0|Ta(\mathbf{k}_1 t_1)\cdots a(\mathbf{k}_s t_s)\psi_N(t_N)|\Phi\rangle,$$
$$\tau_V(\mathbf{k}_1 t_1, \cdots, \mathbf{k}_{s-1} t_{s-1};\ t_V) = \langle 0|Ta(\mathbf{k}_1 t_1)\cdots a(\mathbf{k}_{s-1} t_{s-1})\psi_{Vr}(t_V)|\Phi\rangle. \tag{4}$$

(The letter T denotes the time-ordered product.)

Integrating eq. (1a) over $\mathbf{x}$ gives (the N or V-particle is at $\mathbf{x} = 0$):

$$g\int_{-\infty}^{t} \mathrm{d}t'\,\chi(t-t')\psi_{Vr}(t') = -2\pi^2 ig\int_{-\infty}^{t} \mathrm{d}t'\,[a(0,\ t)a^*(0,\ t') - s(t-t')]\psi_{Vr}(t')$$
$$-\pi\sqrt{2}\,a(0,\ t)\psi_N(-\infty). \tag{5}$$

If one multiplies (5) from the left by $a(\mathbf{k}_1 t)\,a(\mathbf{k}_2 t)\cdots a(\mathbf{k}_{s-1} t)$ and considers the matrix element of this operator between the states $\langle 0$ and $\Phi\rangle$, one gets an equation between the two τ-functions (4). $a(0,\ t)$ is to be replaced by

$$a(0,\ t) = (2\pi)^{-3/2}\int \frac{a(\mathbf{k}t)}{\sqrt{2\omega}}\,\mathrm{d}^3 k. \tag{6}$$

In this way one derives from (5)

$$g\int_{-\infty}^{t} dt'\,\chi(t-t')\tau_V(\mathbf{k}_1 t, \mathbf{k}_2 t, \cdots, \mathbf{k}_{s-1} t; t')$$
$$= -\frac{ig}{4\pi}\int \mathrm{d}^3 k\int_{-\infty}^{t} \mathrm{d}t' \sum_{l=1}^{s-1} \frac{\mathrm{e}^{i\omega_l(t'-t)}}{2\sqrt{\omega\omega_l}}\tau_V(\mathbf{k}_1 t, \cdots, \mathbf{k}_{l-1} t, \mathbf{k}_{l+1} t, \cdots, \mathbf{k}t; t') \tag{7}$$
$$-\frac{1}{2\sqrt{\pi}}\int \frac{\mathrm{d}^3 k}{\sqrt{2\omega}}\tau_N(\mathbf{k}_1 t, \cdots, \mathbf{k}_{s-1} t, \mathbf{k}t; -\infty).$$

If one multiplies (1b) from the left by $a(\mathbf{k}_1 t)\ldots a(\mathbf{k}_s t)$ one gets

$$i\frac{\partial}{\partial t_N}\tau_N(\mathbf{k}_1 t, \cdots, \mathbf{k}_s t,\ t_N)_{t_N=t}$$
$$= -\frac{g}{2\sqrt{\pi}}\sum_{l=1}^{s} \tau_V(\mathbf{k}_1 t, \cdots, \mathbf{k}_{l-1} t, \mathbf{k}_{l+1} t, \cdots, \mathbf{k}_s t;\ t)\frac{1}{\sqrt{2\omega_l}}. \tag{8}$$

These two Tamm-Dancoff equations should be sufficient to determine the two τ-functions (4). Contrary to the case of the spinor equation [1]) it is not necessary here to introduce approximations through the process of contraction. Due to the special simplicity of the Lee model the Tamm-Dancoff formalism leads to exact solutions.

In a state in which there are several θ-particles, but no N- or V-particle, the total energy is simply the sum of the energies of the free θ-particles; there is no interaction between the θ-particles. Therefore the time dependence of the τ-functions (4) in the time interval needed for (7) can be given without difficulty: if E is the energy of the state $\Phi\rangle$, we have for $t_N \leqq t_1, t_2, \cdots, t_z$ and $t_V \leqq t_1, t_2, \cdots, t_{z-1}$:

$$\begin{aligned}\tau_N(\mathbf{k}_1 t_1, \cdots, \mathbf{k}_z t_z;\ t_N) &= \tau_N(\mathbf{k}_1, \cdots, \mathbf{k}_z)\, e^{-i\sum_1^z \omega_l t_l - i(E-\sum_1^z \omega_l)t_N},\\ \tau_V(\mathbf{k}_1 t_1, \cdots, \mathbf{k}_{z-1} t_{z-1};\ t_V) &= \tau_V(\mathbf{k}_1, \cdots, \mathbf{k}_{z-1})\, e^{-i\sum_1^{z-1} \omega_l t_l - i(E-\sum_1^{z-1} \omega_l)t_V},\end{aligned} \tag{9}$$

where the τ-functions on the right hand side depend only on the momentum variables.

Inserting (9) into (7) and (8) leads to

$$\begin{aligned}gh^+(E-\sum_1^{z-1}\omega_l)\tau_V(\mathbf{k}_1, \cdots, \mathbf{k}_{z-1}) &= \frac{g}{4\pi}\int d^3k \sum_{l=1}^{z-1} \frac{\tau_V(\mathbf{k}_1, \cdots, \mathbf{k}_{l-1}, \mathbf{k}_{l+1}, \cdots, \mathbf{k})}{2\sqrt{\omega_l \omega}(E-\sum_1^{z-1}\omega_r - \omega + i\gamma)}\\ &\quad - \frac{1}{2\sqrt{\pi}}\int \frac{d^3k}{\sqrt{2\omega}}\, \tau_N(\mathbf{k}_1, \cdots, \mathbf{k}_{z-1}, \mathbf{k})\, e^{i(E-\sum_1^{z-1}\omega_r - \omega)(t+\infty)} \qquad (\gamma \to 0)\end{aligned} \tag{10}$$

and

$$(E-\sum_1^z \omega_l)\tau_N(\mathbf{k}_1, \cdots, \mathbf{k}_z) = -\frac{g}{2\sqrt{\pi}}\sum_{l=1}^{z}\frac{1}{\sqrt{2\omega_l}}\tau_V(\mathbf{k}_1, \cdots, \mathbf{k}_{l-1}, \mathbf{k}_{l+1}, \cdots, \mathbf{k}_z). \tag{11}$$

The second line in (10) needs an explanation since the time $-\infty$ from (7) appears in the exponent. One can see from (11), that $\tau_N(\mathbf{k}_1 \cdots \mathbf{k}_z)$ can be written as

$$\tau_N(\mathbf{k}_1, \ldots, \mathbf{k}_z) = \tau_{0N}(\mathbf{k}_1, \ldots, \mathbf{k}_z) + \frac{\chi_N(\mathbf{k}_1, \ldots, \mathbf{k}_z)}{E-\sum_1^z \omega_l + i\gamma}, \tag{12}$$

where $\tau_0(\mathbf{k}_1, \cdots, \mathbf{k}_z)$ is an arbitrary solution of

$$\tau_{0N}(\mathbf{k}_1, \cdots, \mathbf{k}_z)\cdot(E-\sum_1^z \omega_r) = 0,$$

and $\chi_N(\mathbf{k}_1, \ldots, \mathbf{k}_z)$ is regular at the point $E-\sum_1^z \omega_r = 0$.

When one inserts (12) in the second line of (10), the contribution from

the term $\chi_N(\mathbf{k}_1, \ldots, \mathbf{k}_s)$ vanishes, since the correct interpretation of the exponent would be

$$e^{i(E-\sum_1^{s-1}\omega_r-\omega+i\gamma)(t+\infty)} = 0 \quad (\gamma \to 0).$$

Therefore only the contribution from $\tau_{0N}(\mathbf{k}_1, \ldots, \mathbf{k}_s)$ remains and one gets instead of (10)

$$h^+(E-\sum_1^{s-1}\omega_l)\tau_V(\mathbf{k}_1, \cdots, \mathbf{k}_{s-1}) = \frac{1}{4\pi}\int d^3k \sum_{l=1}^{s-1} \frac{\tau_V(\mathbf{k}_1, \ldots, \mathbf{k}_{l-1}, \mathbf{k}_{l+1}, \ldots, \mathbf{k})}{2\sqrt{\omega\omega_l}(E-\sum_1^{s-1}\omega_r-\omega+i\gamma)}$$

$$- \frac{1}{g\sqrt{4\pi}}\int \frac{d^3k}{\sqrt{2\omega}} \tau_{0N}(\mathbf{k}_1, \ldots, \mathbf{k}_{s-1}, \mathbf{k}). \quad (13)$$

The two equations (11) and (13) become identical with the Schrödinger equations of the sector $\binom{N+s\theta}{V+(s-1)\theta}$, namely the equations (120) and (122) of ref. [2]), if one puts (using again the notation of ref. [2]))

$$\tau_N(\mathbf{k}_1, \ldots, \mathbf{k}_s) = \varphi(\mathbf{k}_1, \ldots, \mathbf{k}_s),$$

$$\tau_V(\mathbf{k}_1, \ldots, \mathbf{k}_{s-1}) = \frac{g_0}{zg}\varphi(\mathbf{k}_1, \ldots, \mathbf{k}_{s-1}). \quad (14)$$

This result shows that the Tamm-Dancoff formalism leads to the exact solutions in the case of the Lee model and that the τ-functions are — except for constant factors — identical with the Schrödinger functions. It should be emphasized, however, that the τ-functions of the renormalized operators have finite values, while one of the Schrödinger functions becomes infinite for $g_0 \to 0$; further that the square of the single Schrödinger functions (or τ-functions) integrated over the whole space can diverge. The norm of $\Phi\rangle$, however, is finite; formally the norm appears in the Schrödinger formalism as the difference of two divergent terms. In order to derive the norm in the Tamm-Dancoff formalism it is convenient to calculate — besides the covariant representation of $\Phi\rangle$ by means of the τ-functions — a contravariant representation in terms of the renormalized operators. For the sake of simplicity we will confine the calculations to the sector $\binom{N+\theta}{V}$.

In ref. [2]), eq. (7R) the state $\Phi\rangle$ was expressed as

$$\Phi\rangle = (-c\psi_V^* + \psi_N^* \int \varphi(\mathbf{k})a^*(\mathbf{k})d^3k)|0\rangle. \quad (15)$$

In the process of renormalization $\varphi(\mathbf{k})$ turns out to be independent of $g_0 (g_0 \to 0)$, while c varies as g_0^{-1}. We define the constant b by $c = -b/g_0$. If one introduces the renormalized operator $\psi_{Vr} = (g_0/g)\psi_V$, one gets

$$\Phi\rangle = \left(\frac{bg}{|g_0^2|}\psi_{Vr}^* + \psi_N^* \int \varphi(\mathbf{k})a^*(\mathbf{k})d^3k\right)|0\rangle. \quad (16)$$

This expression cannot be used for the representation of Φ after renormalisation, since it diverges in the limit $g_0 \to 0$. It is possible, however, to represent $\Phi\rangle$ by means of the time dependent operators $\psi^*_{Vr}(t)$. $\psi_N{}^*(0)$ and $a^*(\mathbf{k}, 0)$ shall refer to the time $t = 0$. Then we try the expression

$$\Phi\rangle = \Big(\int \psi^*_{Vr}(t) f(t) \mathrm{d}t + \psi_N{}^*(0) \int \sigma(\mathbf{k}) a^*(\mathbf{k}, 0) \mathrm{d}^3 k\Big)|0\rangle, \tag{17}$$

where $f(t)$ is different from zero in a finite interval around $t = 0$. The only condition imposed on $f(t)$ is, that it must lead to the correct τ-function, i.e. to the same τ_V-function as (15). This condition gives

$$\langle 0|\psi_{Vr}(0) \frac{b}{g_0} \psi_V{}^*(0)|0\rangle = \langle 0|\psi_{Vr}(0) \int \psi^*_{Vr}(t) f(t) \mathrm{d}t|0\rangle. \tag{18}$$

The first expression is simply $-b/g$, the second can be taken from the commutation relation of ref. [2]), eqs. (52) and (49),

$$-\frac{b}{g} = \int f(t) \mathrm{d}t \frac{1}{g^2} \left[-\frac{2h'''(E_0)}{3[h''(E_0)]^2} \mathrm{e}^{iE_0 t} + \int_{m_0}^{\infty} \frac{k \mathrm{e}^{i\omega t} \mathrm{d}\omega}{2h^+(\omega) h^-(\omega)} \right]. \tag{19}$$

One can for instance assume

$$f(t) = \begin{cases} f & \text{for } -t_0 \leqq t \leqq t_0 \\ 0 & \text{otherwise.} \end{cases}$$

Then one gets from (19), using ref. [2]), eq. (48),

$$bg = 2t_0 f \left[-\frac{2h'''(E_0)}{[3h''(E_0)]^2} \left(1 - \frac{\sin E_0 t_0}{E_0 t_0}\right) + \int_{m_0}^{\infty} \frac{k \mathrm{d}\omega}{2h^+(\omega) h^-(\omega)} \left(1 - \frac{\sin \omega t_0}{\omega t_0}\right) \right]. \tag{20}$$

If $t_0 \ll 1/E_0$ and $\ll 1/m_0$, one can use the asymptotic expression for $h^{\pm}(\omega)$:

$$h^{\pm}(\omega) \sim -\frac{\omega}{2} \ln \frac{\omega C}{m_0} \quad \text{for} \quad \omega \gg m_0, \tag{21}$$

where the constant C depends on E_0 and can be calculated from ref. [2]), eq. (29). In a first approximation one gets from (20)

$$bg = \frac{4t_0 f}{\ln \dfrac{C}{t_0 m_0}} \quad \text{or} \quad f t_0 = \frac{bg}{4} \ln \frac{C}{t_0 m_0}. \tag{22}$$

This result shows that the 'area' $\int f(t) \mathrm{d}t = 2ft_0$ increases logarithmically, when t_0 goes to zero, as one could expect from eq. (16).

The function $\sigma(\mathbf{k})$ in (17) is not identical with $\varphi(\mathbf{k})$ in (15); the first term in (17) gives now after replacing (15) by (17) some contribution to the τ_N-function, which together with the contribution from $\sigma(\mathbf{k})$ must give the same result as $\varphi(\mathbf{k})$ in (15). This condition leads for $\sigma(\mathbf{k})$ to

$$\sigma(\mathbf{k}) = \varphi(\mathbf{k}) - \sum_E \int f(t) \mathrm{d}t \langle 0|\psi_N(0) a(\mathbf{k}, 0)|\Phi_E\rangle \mathrm{e}^{iEt} \langle \Phi^E|\psi^*_{Vr}(0)|0\rangle \tag{23}$$

or again for $t_0 \ll 1/E_0$ and $t_0 \ll 1/m_\theta$, using ref. [2]), eqs. (17) ,(18) and (21),

$$\sigma(\mathbf{k}) \approx \varphi(\mathbf{k}) - \int f(t)\mathrm{d}t\,(\mathrm{e}^{i\omega t}-1)\,\frac{1}{\sqrt{8\pi\omega}\,g h^-(\omega)}$$
$$-\int f(t)\mathrm{d}t \int_0^\infty k'^2\,\mathrm{d}k'\,\frac{\mathrm{e}^{i\omega' t}-1}{2\sqrt{8\pi\omega}\,\omega'\,g(\omega'-\omega+i\gamma)h^+(\omega')h^-(\omega')} \quad (\gamma \to 0) \quad (24)$$

$$\approx \varphi(\mathbf{k}) - \int f(t)\mathrm{d}t(\mathrm{e}^{i\omega t}-1)\left(g\sqrt{2\pi}\,\omega^{3/2}\ln\frac{\omega C}{m_\theta}\right)^{-1}$$
$$-\int f(t)\mathrm{d}t\int_0^\infty k'^2\,\mathrm{d}k'\,\frac{\mathrm{e}^{i\omega' t}-1}{g\sqrt{2\pi\omega}\,\omega'^3(\omega'-\omega+i\gamma)\,\ln^2\dfrac{\omega' C}{m_\theta}} \quad (\gamma \to 0). \quad (25)$$

It follows from (22) and (25) that for values of $\omega \ll 1/t_0$ the difference between $\sigma(\mathbf{k})$ and $\varphi(\mathbf{k})$ is relatively small, while for $\omega \gg 1/t_0$ the last term in (25) compensates the main part of $\varphi(\mathbf{k})$. Therefore we conclude from (25)

$$\frac{\sigma(\mathbf{k})}{\varphi(\mathbf{k})} \to \begin{cases} 1 \text{ for } \omega \ll \dfrac{1}{t_0} \\ 0 \text{ for } \omega \gg \dfrac{1}{t_0}. \end{cases} \quad (26)$$

Finally we get for the norm of $\Phi\rangle$ from (17)

$$\langle\Phi|\Phi\rangle = \langle\Phi|\int \psi_{\mathrm{Vr}}^*(t)f(t)\mathrm{d}t + \psi_{\mathrm{N}}^*(0)\int\sigma(\mathbf{k})a^*(\mathbf{k},\,0)\mathrm{d}^3k|0\rangle$$
$$= \tau_{\mathrm{V}}^*\int f(t)\mathrm{d}t\,\mathrm{e}^{tEt} + \int\sigma(\mathbf{k})\tau_{\mathrm{N}}^*(\mathbf{k})\mathrm{d}^3k, \quad (27)$$

where E is the energy of the state $\Phi\rangle$. For $Et_0 \ll 1$ eq. (27) becomes

$$\langle\Phi|\Phi\rangle \approx -\tfrac{1}{2}|b^2|\ln\frac{C}{t_0 m_\theta} + \int_0^{1/t_0} 4\pi k^2\,\mathrm{d}k|\varphi(\mathbf{k})|^2. \quad (28)$$

One sees from (28) that the expression for the norm in the Tamm-Dancoff method contains only finite terms. Both terms depend on the width t_0 of the time interval in (17) which can be chosen arbitrarily. The norm itself, however, cannot depend on t_0. Actually it follows from ref. [2]), eq. (13) and (21), that

$$\varphi(\mathbf{k}) \approx \frac{b}{\sqrt{8\pi}\,\omega^{3/2}} \quad \text{for} \quad \omega \gg |E|. \quad (29)$$

Therefore the second term in (28) varies as $\frac{1}{2}|b^2|\ln(1/t_0)$ for small values of t_0, and the norm is independent of t_0.

If one uses ordinary space instead of momentum space in the contravariant representation (17), the function $\varphi(\mathbf{x})$ varies for small radii as const. $r^{-3/2}$ (ref. [2]), eq. (45)). The function $\sigma(\mathbf{x})$, however, is rounded off at

small radii of the order l_0, it agrees only for $r \gg l_0$ with $\varphi(\mathbf{x})$, and the integral $\int \varphi^*(\mathbf{x})\sigma(\mathbf{x})\mathrm{d}^3x$ converges. One would be inclined to consider the expression $\varphi^*(\mathbf{x})\sigma(\mathbf{x})$ as the matter density of the stationary state, as has been suggested in an earlier paper [1]). But one sees here that this expression depends on the function $f(l)$ which can be arbitrarily chosen within the condition (19). The fact that a well defined state $\Phi\rangle$ can have a continuous variety of contravariant representations prevents a unique definition of a matter density for this state.

In the Lee model the Tamm-Dancoff method leads to exact solutions. This is certainly not true for the non linear spinor equation [1]), where one has to introduce approximations by the process of contraction. The difference between the two cases is caused by the fact that in the Lee model only one particle can be created or absorbed — actually this simplification can be considered as the main feature of the Lee model —, while in the spinor model many particles may be produced. Therefore the Lee model does not provide any direct argument from which one could judge the degree of approximation attainable by the Tamm-Dancoff method in the spinor model. But the following comparison may be adequate. The Lee model should be compared with the harmonic oscillator; in both cases the Tamm-Dancoff method gives exact results, since only one particle (θ-particle or photon) can ever be created or absorbed. The spinor model, on the other hand, should be compared with the strongly anharmonic oscillator; in both cases several particles can be produced and the Tamm-Dancoff method needs the process of contraction, therefore it is a method of successive approximations. It was this analogy which had been discussed extensively in the first paper [1]) on the spinor model, and it had led to the result that the first approximation in the Tamm-Dancoff method may give the eigenvalues with an inaccuracy of 10 to 20 %. The calculations of the present paper seem to support this view.

References

1) W. Heisenberg, Nachr. Gött. Akad. Wiss. (1953) 111; Zs. f. Naturf. **9a** (1954) 282; W. Heisenberg, F. Kortel u. H. Mitter, Zs. f. Naturf. **10a** (1955) 425; W. Heisenberg, Zs. f. Physik **144** (1956) 1; Nachr. Gött. Akad. Wiss. (1956) 27; R. Ascoli u. W. Heisenberg, Zs. f. Naturf. **12a** (1957) 177

2) W. Heisenberg, Nuclear Physics **4** (1957) 532

Nuclear Physics **5** (195) 202—210; © *North-Holland Publishing Co., Amsterdam*
Not to be reproduced by photoprint or microfilm without written permission from the publisher

ROTATIONAL PROPERTIES OF THE TWO-DIMENSIONAL ANISOTROPIC HARMONIC OSCILLATOR

I. EXPECTATION VALUES

H. J. LIPKIN and S. GOLDSTEIN
Department of Physics, The Weizmann Institute of Science, Rehovoth, Israel

Received 14 September 1957

Abstract: Expectation values are given for operators useful in unified model calculations with anisotropic harmonic oscillator wave functions. The operators chosen are of particular interest in regard to a description of the oscillator system in terms of collective and intrinsic coordinates.

1. Introduction

In the unified nuclear model [1]) the intrinsic motion of the particles is described as independent-particle motion in a deformed central field. The most convenient deformed potential for use in calculations is the anisotropic harmonic oscillator. The energy values and the antisymmetrized wave functions for systems of many particles moving in this potential can be calculated exactly and are well known. The anisotropic harmonic oscillator has therefore been widely used in unified model calculations [2]), particularly in calculations of the moments of inertia of rotational states [3, 5, 6, 7, 8]).

Although the oscillator system can be easily solved and the states completely specified in terms of particle oscillator quantum numbers, certain other operators are of interest when the oscillator wave functions are used in calculations of rotational states. These include powers of the total angular momentum and angles describing the fluctuations in the orientation of the system. Since these operators are not sums of single particle operators, their matrix elements are not easily calculated using antisymmetric wave functions. However, a method developed by one of us (H. J. L.) [4]) is particularly suitable for use with oscillator wave functions and has enabled the calculation of a number of interesting expressions with relative ease.

In this paper the expectation values of certain operators are presented with brief comments regarding their significance. In subsequent papers a description of the oscillator system will be given in terms of the collective and intrinsic co-ordinates of the unified model, as opposed to the usual independent particle description.

1.1. DEFINITIONS AND NOTATION

The system treated in this paper is that of A particles moving in a two dimensional anisotropic harmonic oscillator potential. The hamiltonian for this system is

$$H = \sum_{i=1}^{A} (p_{x_i}^2 + p_{y_i}^2)/2M + M \sum_{i=1}^{A} \tfrac{1}{2}(\omega_x^2 x_i^2 + \omega_y^2 y_i^2), \tag{1}$$

where x_i, y_i, p_{x_i} and p_{y_i} are the co-ordinates and momenta of the i-th particle, M is the particle mass, and ω_x and ω_y are the constants characterizing the oscillator potential. Without loss of generality it can be assumed that

$$\omega_y > \omega_x. \tag{2}$$

The symmetric potential ($\omega_y = \omega_x$) can be considered as a limiting case of the condition (2).

Although the system treated here is two-dimensional, many of the results obtained can be applied directly to the three dimensional anisotropic oscillator. This is discussed in section 2.3.

The Hamiltonian (1) is separable into $2A$ independent harmonic oscillators corresponding to the x and y co-ordinates of each particle. The eigenstates of the system can therefore be specified by the set of oscillator quantum numbers n_{x_i} and n_{y_i} for each particle, describing the states of excitation of each of the $2A$ individual oscillators. The total energy of the system is given by

$$E = \sum_{i=1}^{A} (n_{x_i} + \tfrac{1}{2})\hbar\omega_x + \sum_{i=1}^{A} (n_{y_i} + \tfrac{1}{2})\hbar\omega_y. \tag{3}$$

It is convenient to define the following quantities:

1. the total oscillator quantum numbers

$$N_x = \sum_{i=1}^{A} (n_{x_i} + \tfrac{1}{2}), \quad N_y = \sum_{i=1}^{A} (n_{y_i} + \tfrac{1}{2}); \tag{4}$$

2. the rigid moment of inertia

$$I_{\text{rig}} = \hbar \left[\frac{N_x}{\omega_x} + \frac{N_y}{\omega_y} \right] = \sum_{i=1}^{A} M \langle x_i^2 + y_i^2 \rangle; \tag{5}$$

3. the deformation

$$\delta = \frac{(N_x/\omega_x) - (N_y/\omega_y)}{(N_x/\omega_x) + (N_y/\omega_y)} = \frac{\sum_i \langle x_i^2 - y_i^2 \rangle}{\sum_i \langle x_i^2 + y_i^2 \rangle}. \tag{6}$$

In terms of the total oscillator quantum numbers (4), the energy (3) is given by

$$E = \hbar(N_x\omega_x + N_y\omega_y). \tag{7}$$

For given values of the quantum numbers and a given volume for the

system ($\omega_x\omega_y$ = constant), the energy (7) is minimized if ω_x and ω_y are chosen to satisfy the condition

$$N_x\omega_x = N_y\omega_y. \tag{8}$$

This has been called the condition of "equilibrium deformation" by Bohr and Mottelson [6]). If this condition is satisfied, then

$$\frac{N_x}{N_y} = \frac{\omega_y}{\omega_x} = \sqrt{\frac{1+\delta}{1-\delta}}. \tag{9}$$

The definition (6) of the deformation is slightly different from the conventional definition because the system is two-dimensional. Nilsson [9]) for example defines δ for the three-dimensional axially symmetric system such that

$$\frac{\omega_x}{\omega_z} = \frac{\omega_y}{\omega_x} = \sqrt{\frac{1+\frac{2}{3}\delta}{1-\frac{4}{3}\delta}}. \tag{10}$$

If δ is small, equation (10) is equivalent to equation (9).

Rotational states have been observed mainly in nuclei in the rare earth and transuranium regions of the periodic table. In these regions N_x and N_y are large, varying from 200 to 350 for the appropriate three-dimensional oscillator wave functions. Certain calculations can be simplified by the use of expansions in powers of $1/N_x$ or $1/N_y$ or some combination of the two. In this paper expansions of this general type are called expansions in powers of $1/N$. Since the deformation δ varies from 0.2 to 0.5 in the region of rotational states [6]), $N\delta$ and sometimes even $N\delta^2$ are large numbers. Expansions in powers of $1/N\delta$ or $1/N\delta^2$ can thus also be used.

2. Expectation Values

By use of the method of ref. [4]), it is possible to express the expectation values of certain operator products in terms of the expectation values of simple operators such as $\sum_i x_i^2$. A list of expectation values calculated using this method is tabulated in the appendix, along with some general rules for the approximate calculation of more complicated expectation values using a series expansion in powers of $1/\sqrt{N}$. In this section certain expectation values are given which are of particular interest to the rotational problem.

All the expectation values given in this paper are expressed in terms of the total quantum numbers N_x and N_y of the state considered and the constants ω_x and ω_y. The results are independent of the symmetry properties of the wave function. They are valid, therefore, for the particular symmetry describing nucleons in a spin-independent field; namely four independent sets of particles, each separately antisymmetrized; neutrons and protons

each having two spin states. The only restriction placed upon certain results is their validity for only the ground state of the system; i.e. for the case where the particular total quantum numbers used define the lowest state of the system having the desired symmetry property.

2.1. POWERS OF THE TOTAL ANGULAR MOMENTUM

The Hamiltonian (1) is not rotation-invariant; its eigenstates are therefore not eigenfunctions of the total angular momentum operator

$$L = \sum_i (x_i p_{y_i} - y_i p_{x_i}). \tag{11}$$

In certain methods for calculating moments of inertia of nuclei, the ground state eigenfunction of (1) is effectively expanded [7]) into a set of eigenfunctions of the operator L. It is of interest to know how many such states have an appreciable amplitude; i.e. to what extent high values of L are present. This can be estimated from the expectation value of L^2, which is given exactly for the ground state wave function by the expression [4])

$$\langle L^2 \rangle = \tfrac{1}{2}\hbar^2 \left\{ N_x \left(\frac{\omega_x}{\omega_y} + \frac{\omega_y}{\omega_x} \right) - 2N_y \right\}. \tag{12a}$$

Note that since $\omega_y > \omega_x$ by the assumption (2), then $N_x \geqq N_y$ for the ground state wave function and (12a) is always positive.

For the case when the Bohr-Mottelson condition (8) is satisfied, equation (12a) reduces to

$$\langle L^2 \rangle_{\mathrm{BM}} = \tfrac{1}{2}\hbar^2 \left[\frac{N_x}{\omega_x} - \frac{N_y}{\omega_y} \right] \omega_y = \tfrac{1}{2}\hbar\omega_y \, \delta I_{\mathrm{rig}}, \tag{12b}$$

where the subscript BM is used to denote expressions which are valid only when the condition (8) is satisfied.

In strongly deformed nuclei in the rare earth or transuranium regions, N_x and N_y are each of the order 200—350 whereas the deformations are of the order 0.2—0.5. The product $(N_x+N_y)\delta$ is therefore of the order of 100 and can be considered a large number. The result (12b) indicates that the ground state oscillator wave function has appreciable components having angular momenta greater than $10\hbar$ if the number of particles is large and the deformation not too small, as is the case in strongly deformed nuclei.

A better idea of the distribution of states of different L in the ground state wave function is obtained by examining the higher moments of L. The expectation value of L^4 is also useful in Skyrme's method for calculating moments of inertia [8]). This is given by

$$\langle L^4 \rangle = 3\langle L^2 \rangle^2 + \frac{\hbar^4 N_x}{4\omega_x^2 \omega_y^2} \{ 3(\omega_y^2 - \omega_x^2)^2 - 4\omega_x \omega_y (\omega_x^2 + \omega_y^2) \} + 2\hbar^4 N_y. \tag{13a}$$

Note that the leading term in (13a) is quadratic in N, whereas the remaining terms are linear and can be neglected if N is large and δ not too small. If these terms are neglected, the result $L^4 = 3L^2\delta^2$ is just the relation between the fourth and second moments of a Gaussian distribution curve. One can therefore expect that the expansion of the ground state oscillator wave function in eigenstates of L will result in an approximately Gaussian wave packet in L-space.

If the Bohr-Mottelson condition (8) is satisfied, (13a) reduces to

$$\langle L^4\rangle_{\mathrm{BM}} = 3\langle L^2\rangle^2\left\{1-\frac{\hbar^2}{\langle L^2\rangle}\left(\frac{2}{3}-\frac{\delta}{\sqrt{1-\delta^2}}\right)\right\}. \tag{13b}$$

Thus if $\langle L^2\rangle$ is large, the deviation of $\langle L^4\rangle$ from $3\langle L^2\rangle^2$ is small.

2.2. ANGLE OPERATORS

It is sometimes of interest to examine the fluctuations in the orientation of the system, as expressed by the mean square value of some angle defining this orientation. Consider, for example, the angle

$$\theta_1 = \tfrac{1}{2}\tan^{-1} 2\{\sum_i x_i y_i/\sum_i (x_i^2-y_i^2)\}; \tag{14}$$

θ_1 is the angle between the principal axes of inertia of the system of particles and the $x-y$ co-ordinate axes fixed in the laboratory. Let us consider the expectation value

$$\langle \tfrac{1}{4}\tan^2 2\theta_1\rangle = \langle(\sum_i x_i y_i)^2/(\sum_i \{x_i^2-y_i^2\})^2\rangle. \tag{15}$$

The exact evaluation of this expectation value (15) is difficult. However, an expansion in powers of $1/N$ can be obtained by the use of the general method discussed in the appendix. The result to the order $1/N^2$ is

$$\begin{aligned}\tfrac{1}{4}\tan^2 2\theta_1 &\approx \frac{N_x\omega_x\omega_y}{2(N_x\omega_y-N_y\omega_x)^2}\left[1-\frac{N_x\omega_y^2+N_y\omega_x^2}{(N_x\omega_y-N_y\omega_x)^2}\right]\\ &= \frac{\hbar(1+\delta)}{4\omega_y\delta^2 I_{\mathrm{rig}}}\left[1-\hbar\frac{[(1+\delta)/\omega_x]+[(1-\delta)/\omega_y]}{2\delta^2 I_{\mathrm{rig}}}\right].\end{aligned} \tag{16}$$

The expectation value $\langle\theta_1^2\rangle$ can be obtained to order $1/N^2$ directly from equation (16) by using the first two terms in the power series for the inverse tangent. The result is

$$\begin{aligned}\langle\theta_1^2\rangle &\approx \langle\tfrac{1}{4}\tan^2 2\theta_1\rangle-\tfrac{8}{3}\langle\tfrac{1}{4}\tan^2\ 2\theta_1\rangle^2\\ &= \frac{\hbar(1+\delta)}{4\omega_y\delta^2 I_{\mathrm{rig}}}\left[1-\hbar\frac{[(1+\delta)/\omega_x]+[(7+\delta)/3\omega_y]}{2\delta^2 I_{\mathrm{rig}}}\right].\end{aligned} \tag{17}$$

If the Bohr-Mottelson condition (8) is satisfied and terms of the order δ and δ^2 are neglected in the second term in the square bracket,

$$\langle\theta_1^2\rangle_{\mathrm{BM}} \approx \frac{\hbar(1+\delta)}{4\omega_y \delta^2 I_{\mathrm{rig}}}\left[1-\frac{5\hbar}{3\omega_y \delta^2 I_{\mathrm{rig}}}\right]. \tag{18}$$

The value of $\langle\theta_1^2\rangle$ characterizes the magnitude of the fluctuations of the orientation of the principal axes of inertia of the system. From equation (17) it is evident that these fluctuations will be small if $\delta^2 N$ is large.

Another angle variable which can be used to describe the orientation of the system is

$$\theta_2 = \tfrac{1}{2}\tan^{-1} 2\{[\sum_i x_i y_i + \sum_i p_{x_i} p_{y_i}/M^2\omega_y^2] \\ [\sum_i (x_i^2 - y_i^2) + \sum_i (p_{x_i}^2 - p_{y_i}^2)/M^2\omega_y^2]^{-1}\}. \tag{19}$$

The expectation value $\langle\theta_2^2\rangle$ can be calculated in the same manner as $\langle\theta_1^2\rangle$. The result to order $1/N^2$ is

$$\langle\theta_2^2\rangle \approx \frac{\hbar^2}{4\langle L^2\rangle}\left\{1+\frac{4\hbar^2}{3\langle L^2\rangle}-\frac{\hbar^4}{4\langle L^2\rangle^2}N_x\left(\frac{\omega_x}{\omega_y}-\frac{\omega_y}{\omega_x}\right)^2\right\}. \tag{20}$$

where L^2 is given by equation (12a). Since L^2 is of order $N\delta$, $\langle\theta_2^2\rangle$ is of order $1/N\delta$ instead of $1/N\delta^2$ like $\langle\theta_1^2\rangle$. The fluctuations of θ_2 are thus smaller than those of θ_1.

2.3. APPLICATION TO THE THREE DIMENSIONAL CASE

All the expectation values given in this section are valid for the three-dimensional anisotropic harmonic oscillator, since the three directions of motion are separable. The operator L defined by equation (11) is of course the z-component L_z of the total angular momentum in the three-dimensional case; therefore L must be replaced by L_z in all formulas. With this single change, all the results of this paper are valid for the three dimensional case if the states are specified by the total quantum numbers N_x, N_y, and N_z, subject to the condition (2) and the Bohr-Mottelson condition (8) when required. Additional formulas can be obtained by permutation of the indices x, y, z, provided that the same permutation is made in the conditions (2) and (8).

The three dimensional case of greatest interest is the one of axial symmetry, in which two of the three ω's are equal. In this case the most convenient representation is not the one in which N_x, N_y, and N_z are diagonal, but rather the one in which the component of the total angular momentum in the direction of the symmetry axis is diagonal. Consider, for example, the case $\omega_x = \omega_y$. Then the most convenient representation is that in which L_z, N_x, and N_y+N_z are diagonal, but N_y and N_z individually are not. For this case the results (12) and (13) are not valid as they stand, but they can be used with certain minor modifications. For example the result obtained from equation (12a),

$$\langle L_z^2+L_y^2\rangle = \hbar^2\left\{N_x\left[\frac{\omega_x}{\omega_y}+\frac{\omega_y}{\omega_x}\right]-(N_y+N_z)\right\} \quad (\omega_z=\omega_y>\omega_x), \tag{21a}$$

is valid for each of the degenerate ground state wave functions specified by N_x, N_y, and N_z; it has the same value for all of these functions, and it is also valid for any linear combination of them, including the ones in which L_z is diagonal. By permutation of the indices x, y, z, expressions similar to (12a) can be obtained for all axially symmetric cases with a prolate deformation. For the oblate case,

$$\langle L_z^2+L_y^2\rangle = \frac{\hbar^2}{2}\left\{(N_x+N_z)\left(\frac{\omega_x}{\omega_y}+\frac{\omega_y}{\omega_x}\right)-4N_y\right\} \quad (\omega_z=\omega_x<\omega_y). \tag{21b}$$

Appendix

Table of Expectation Values

Using the method of calculation of ref. [4]), it is possible to calculate directly a large number of expectation values of operators for the ground state anisotropic harmonic oscillator wave function. Some of these are tabulated below.

GROUP A. SIMPLE EXPECTATION VALUES

1. $\langle\sum_i x_i^2\rangle = \dfrac{\hbar N_x}{M\omega_x}$; $\quad \langle\sum_i y_i^2\rangle = \dfrac{\hbar N_y}{M\omega_y}$;

   $\langle\sum_i p_{x_i}^2\rangle = \hbar M N_x\omega_x$; $\quad \langle\sum_i p_{y_i}^2\rangle = \hbar M N_y\omega_y$.

2. $\langle\sum_i (x_i p_{x_i}-p_{x_i}x_i)\rangle = \langle\sum_i (y_i p_{y_i}-p_{y_i}y_i)\rangle = i\hbar A$;

   $\langle\sum_i (x_i p_{x_i}+p_{x_i}x_i)\rangle = \langle\sum_i (y_i p_{y_i}+p_{y_i}y_i)\rangle = 0$.

3. $\langle\sum_i x_i p_{y_i}\rangle = \langle\sum_i y_i p_{x_i}\rangle = \langle\sum_i x_i y_i\rangle = \langle\sum_i p_{x_i}p_{y_i}\rangle = 0$.

GROUP B. EXPECTATION VALUES OF PRODUCTS OF OPERATORS OF GROUP A1

1. $\langle(\sum_i x_i^2)^2\rangle = \dfrac{\hbar^2 N_x}{M^2\omega_x^2}(N_x+1) = \langle\sum_i x_i^2\rangle^2+\dfrac{\hbar^2}{M^2\omega_x^2}N_x$

   $\langle(\sum_i y_i^2)^2\rangle = \dfrac{\hbar^2 N_y}{M^2\omega_y^2}(N_y+1) = \langle\sum_i y_i^2\rangle^2+\dfrac{\hbar^2}{M^2\omega_y^2}N_y$

   $\langle(\sum_i p_{x_i}^2)^2\rangle = \hbar^2 M^2\omega_x^2 N_x(N_x+1) = \langle\sum_i p_{x_i}^2\rangle^2+\hbar^2 M^2\omega_x^2 N_x$

   $\langle(\sum_i p_{y_i}^2)^2\rangle = \hbar^2 M^2\omega_y^2 N_y(N_y+1) = \langle\sum_i p_{y_i}^2\rangle^2+\hbar^2 M^2\omega_y^2 N_y$

   $\langle\sum_i x_i^2\sum_i p_{x_i}^2+\sum_i p_{x_i}^2\sum_i x_i^2\rangle = 2\hbar^2 N_x(N_x-1)$

   $= 2\langle\sum_i x_i^2\rangle\langle\sum_i p_{x_i}^2\rangle-2\hbar^2 N_x$

$$\langle \sum_i y_i^2 \sum_i p_{y_i}^2 + \sum_i p_{y_i}^2 \sum_i y_i^2 \rangle = 2\hbar^2 N_y(N_y-1)$$
$$= 2\langle \sum_i y_i^2 \rangle \langle \sum_i p_{y_i}^2 \rangle - 2\hbar^2 N_y.$$

2. $\langle \sum_i x_i^2 \sum_i y_i^2 \rangle = \langle \sum_i x_i^2 \rangle \langle \sum y_i^2 \rangle = \hbar^2 N_x N_y / M^2 \omega_x \omega_y$

$\langle \sum_i p_{x_i}^2 \sum_i p_{y_i}^2 \rangle = \langle \sum_i p_{x_i}^2 \rangle \langle \sum p_{y_i}^2 \rangle = \hbar^2 M^2 N_x N_y \omega_x \omega_y$

$\langle \sum_i x_i^2 \sum_i p_{y_i}^2 \rangle = \langle \sum_i x_i^2 \rangle \langle \sum p_{y_i}^2 \rangle = \hbar^2 N_x N_y \omega_y / \omega_x$

$\langle \sum_i p_{x_i}^2 \sum_i y_i^2 \rangle = \langle \sum_i p_{x_i}^2 \rangle \langle \sum_i y_i^2 \rangle = \hbar^2 N_x N_y \omega_x / \omega_y.$

GROUP C. EXPECTATION VALUES OF PRODUCTS OF OPERATORS OF GROUP A3

$\langle (\sum_i x_i y_i)^2 \rangle = \hbar^2 N_x / 2M^2 \omega_x \omega_y$; $\langle (\sum_i p_{x_i} p_{y_i})^2 \rangle = \frac{1}{2}\hbar^2 M^2 N_x \omega_x \omega_y$

$\langle (\sum_i x_i p_{y_i})^2 \rangle = \hbar^2 N_x \omega_y / 2\omega_x$; $\langle (\sum_i y_i p_{x_i})^2 \rangle = \frac{1}{2}\hbar^2 N_x \omega_x / \omega_y.$

$\langle (\sum_i x_i y_i \sum_i p_{x_i} p_{y_i} + \sum_i p_{x_i} p_{y_i} \sum_i x_i y_i \rangle = -\hbar^2 N_y$

$\langle (\sum_i x_i p_{y_i} \sum_i y_i p_{x_i} + \sum_i y_i p_{x_i} \sum_i x_i p_{y_i} \rangle = +\hbar^2 N_y$

$$\langle L^2 \rangle = \frac{\hbar^2}{2}\left\{ N_x \left(\frac{\omega_x}{\omega_y} + \frac{\omega_y}{\omega_x} \right) - 2N_y \right\}.$$

GENERAL RULES

On the basis of the results tabulated above, the following general rules can be noted:

1. The expectation values of operators which are sums of single particle operators quadratic in the particle variables are tabulated in group A. These expectation values are all proportional to the total quantum number N. The one apparent exception to this rule, the first operator in group A2, is actually equal identically to the number $i\hbar A$ and is a function of the particle variables only in the trivial sense. A number of expectation values in this category vanish for symmetry reasons.

2. The expectation values of operators which are products of two operators of group A having non-vanishing expectation values are tabulated in group B. These expectation values are of order N^2. The expectation values of operators which are products of two operators of group A having vanishing expectation values are tabulated in group C. These expectation values are of order N.

3. For all possible products of two operators of group A, the difference between the expectation value of the product and the product of the expectation values either vanishes or is of order N.

On the basis of these rules, a general method can be developed for expanding more complicated functions of these operators in powers of $1/N$ or of $1/\sqrt{N}$.

4. Let us apply rule 3 to the square of an operator A in group A. Then $A^2-\langle A^2\rangle$ is of order N. But tnis is just the sum of the squares of the off-diagonal elements of A. Thus the off-diagonal elements of an operator in group A are of order $\sqrt{N}$.

5. The operator A can be written

$$A = \langle A\rangle + (A-\langle A\rangle).$$

The term in the parentheses is just the off-diagonal part of A which is of order $\sqrt{N}$. This therefore gives a method for separating the operator A into two parts, one of order N (if it does not vanish) which is a number, and one of order $\sqrt{N}$ which is an operator.

6. The operator A^{-1} can be expanded as follows ($\langle A\rangle \neq 0$):

$$A^{-1} = \langle A\rangle^{-1}\left(1+\frac{A-\langle A\rangle}{A}\right)^{-1}.$$

Since $(A-\langle A\rangle)/\langle A\rangle$ is of oder $1/\sqrt{N}$, the term in parentheses can be expanded by the binomial theorem. Expectation values of the resultant series can be evaluated term by term giving a series in $1/\sqrt{N}$.

7. Complicated expressions involving products and quotients of operators can be expanded in powers of $1/N$ or of $1/\sqrt{N}$ by expanding each factor in the denominator according to rule 6 and separating the resultant product into terms of different order by use of rule 5.

References

1) K. Alder, A. Bohr, T. Huus, B. Mottelson and A. Winther, Rev. Mod. Phys. **28** (1956) 432
2) S. G. Nilsson, Mat. Fys. Medd. Dan. Vid. Selsk. **29** (1955) no. 16
3) S. A. Moszkowski, Phys. Rev. **99** (1955) 803; Phys. Rev. **103** (1956) 1328
4) H. J. Lipkin, Phys. Rev. (to be published)
5) D. R. Inglis, Phys. Rev. **96** (1954) 1059
6) A. Bohr and B. Mottelson, Mat. Fys. Medd. Dan. Vid. Selsk. **30** (1955) no. 1
7) R. E. Peierls and J. Yoccoz, Proc. Phys. Soc. A **70** (1957) 381
J. Yoccoz, Proc. Phys. Soc. A **70** (1957) 388
8) T. H. R. Skyrme, Proc. Phys. Soc. A **70** (1957) 433

Nuclear Physics **5** (1958) 211—217; © *North-Holland Publishing Co., Amsterdam*
Not to be reproduced by photoprint or microfilm without written permission from the publisher

NEUTRON-INDUCED FISSION OF Ra^{226}

R. A. NOBLES† and R. B. LEACHMAN
Los Alamos Scientific Laboratory, University of California, Los Alamos, New Mexico

Received 12 August 1957

Abstract: Energy distributions of single fragments from fission of Ra^{226} by neutrons from 4 to 21 MeV have been observed. The distribution changes from a double peak for 4 MeV neutrons, through unequal double peaks for 8 MeV neutrons, to a single peak for 10 MeV neutrons. The cross section for fission was found to rise from 0.5 millibarns for 2 MeV neutrons to 37 millibarns for 23 MeV neutrons.

1. Introduction

Recent radiochemical studies by Fairhall and Jensen [1, 2]) of the mass distribution of fragments from Ra^{226} fission induced by 11 MeV protons has disclosed a hitherto unobserved combination of fission modes. Both symmetric and asymmetric fission occur with approximately equal probabilities, causing a triple-peak mass distribution. Further, the cross section for fission was observed to be small, in the order of millibarns. The only other reports of moderate-energy fission of elements below thorium are of Bi^{209} fission induced by 15 and 22 MeV deuterons [2]) and by 30 and 50 MeV protons [3]). These unexpectedly resulted in symmetric fission with single-peak mass distributions considerably narrower than those obtained by the filling of the valley between the two peaks of asymmetric fission.

To investigate further the characteristics of low-energy fission of radium, a study of neutron-induced fission of Ra^{226} has been made. The use of neutrons makes possible studies of a span of excitation energies, including particle energies below the Coulomb barrier of charged particles, and also provides observation of the fission of a different compound nucleus, Ra^{227}. A preliminary account of this work has been made by Nobles *et al.* [4]).

2. Experimental Method

Limitations of cross section and of practical masses of radium that can be handled made it impractical to measure mass yield by radiochemical methods. Instead, energies of single fragments from neutron irradiation of a thin deposit of Ra^{226} were observed. To facilitate the measurements of pulse heights of fission fragments in the alpha-particle background of the

† Work performed under the auspices of the U. S. Atomic Energy Commission.
†† Now at Radiation Laboratory, University of California, Berkeley, California.

radium sample, a scintillation counter of xenon gas was used. Its characteristic linearity of response, high speed, and large light output [5]) made possible rather simple discrimination against alpha particles.

The counter consisted of a pillbox-shaped gas cell, one wall of which was formed by the face of an RCA-6342 photomultiplier coated with 30 μg/cm^2 of quaterphenyl. The opposing wall, 6 mm away, was coated with radium, which was a 39 μg deposit of Ra^{226} in the form of $RaBr_2$ uniformly distributed on a 2.5 cm diameter circle upon platinum. With a 320 cm Hg filling of xenon, fragments were stopped in the gas between the sample and the photocathode. All surfaces inside the chamber were either gold or platinum to reduce the number of charged particles from neutron-induced reactions in the walls. A convective purifier containing a eutectic alloy of calcium and magnesium at 400° C was used to improve pulse height stability of the scintillation counter [6]).

The 39 μg mass of Ra^{226} was determined by alpha counting, but the question of the presence of the daughter activities made this determination uncertain by no more than ± 18 %. The alpha rate of this radium sample with its daughter products was about 6×10^6 alphas per second.

Output pulses from the anode of the photomultiplier were used, the pulse width at half maximum being about 15 mμsec. A crystal diode discriminator circuit biased to pass only pulses above the level of alpha particles passed the fission pulses to a conventional linear amplifier and multichannel analyzer. This scheme took advantage of the high speed of the gas scintillator to reduce pile-up in a manner making possible the use of electronics equipment of conventional design. The diode discriminator introduced some nonlinearity of response, but this was calibrated with a mercury relay pulser which formed pulses having rise times and duration times similar to the fission pulses.

Fragments from the spontaneous fission of Cf^{252} on a foil replacing the Ra^{226} foil were used to investigate the energy resolution and for energy calibration. The ionization chamber measurements of Cf^{252} fission by Smith *et al.* [7]), which have been corrected for ionization defect, were used. To determine the effect of the radium alphas on the observation of fragment energies, the Cf^{252} was combined with the Ra^{226} in a test. The distributions observed were similar to ionization chamber results [7]).

Neutron sources of the order of 10^9 neutrons/steradian · sec and higher in the forward direction were obtained from the T(p, n), D(d, n) and T(d, n) reactions. The large Van de Graaff accelerator and the Variable Energy Cyclotron were used with gas targets of up to 580 cm Hg pressure contained by cooled-foil entrance windows [8]). Neutrons of 14 MeV were obtained from the T(d, n) reaction in tritium-loaded zirconium targets at the Cockcroft-Walton accelerator. The combination of the small cross section for fission

and the requirement of a small total amount of Ra^{226} to avoid excessive alpha pile-up made these large fluxes of neutrons desirable for reasonable observation times in the experiment.

The cross-section measurements were made by observing the fission rate of the radium atoms in the calculated neutron fluxes. Fluxes were determined from reported [9]) and unpublished [10]) measurements of the differential cross sections for the source reactions used and from the distances between the neutron source and the radium foil. Distances of $\approx$ 9 cm were used to provide adequate neutron flux without incurring a large variation of flux with angle. This method of determining the neutron flux was probably no more accurate than $\pm$ 10 %. Because of the low fission rate in these fluxes, only $\approx 10^2$ fissions were observed in each measurement. The neutron flux from the Cockcroft-Walton was determined to $\pm$ 4 % by counting the associated alpha particles from the reaction.

In the measurements of the spectra of fragment energies, usually $\approx 10^3$ fissions were observed. For these measurements, the distances between the neutron source and the radium target were decreased to $\approx$ 5 cm, which resulted in appreciable spreads in neutron energy.

3. Results

The geometry of the experiment and the gas conditions of the neutron sources resulted in a span of neutron energies on the radium in each bombardment, the maximum energy being at 0° from charged particles entering the gas and the minimum at the maximum angle from the end of the gas target. Observations of the energy distribution of fragments from radium fission were made at the following neutron energies: 3.3—4.6 MeV, 5.8—8.2 MeV, and 19.6—22.2 MeV from the Van de Graaff; 6.9—8.2 MeV, 9.0—11.0 MeV, and 10.7—12.9 MeV from the cyclotron; and 14.7 MeV from the Cockcroft-Walton. Fig. 1 shows the results of these measurements for four of these energies which demonstrate the change in the energy distribution of the fragments with increasing neutron energy.

At the lowest neutron energy the fragment energy distribution is seen to be asymmetric, exhibiting the familiar double-peak distribution observed in the fission of heavier nucleides such as uranium. Bombardments with $\approx$ 8 MeV neutrons resulted in energy distributions with unequal double peaks. The larger number of pulses in the low-energy group seen in the distribution for neutrons of 6.9—8.2 MeV can be explained by a contribution of pulses from symmetric fission if these are of lower average energy than pulses from asymmetric fission. As illustrated by the other distributions of fig. 1, all the fragment energy distributions for higher neutron energies showed only one predominate peak, indicating the symmetric mode of fission was dominant.

Background studies were made to determine the contribution of alpha-particle and neutron-induced pile-up pulses to the observed fission spectra.

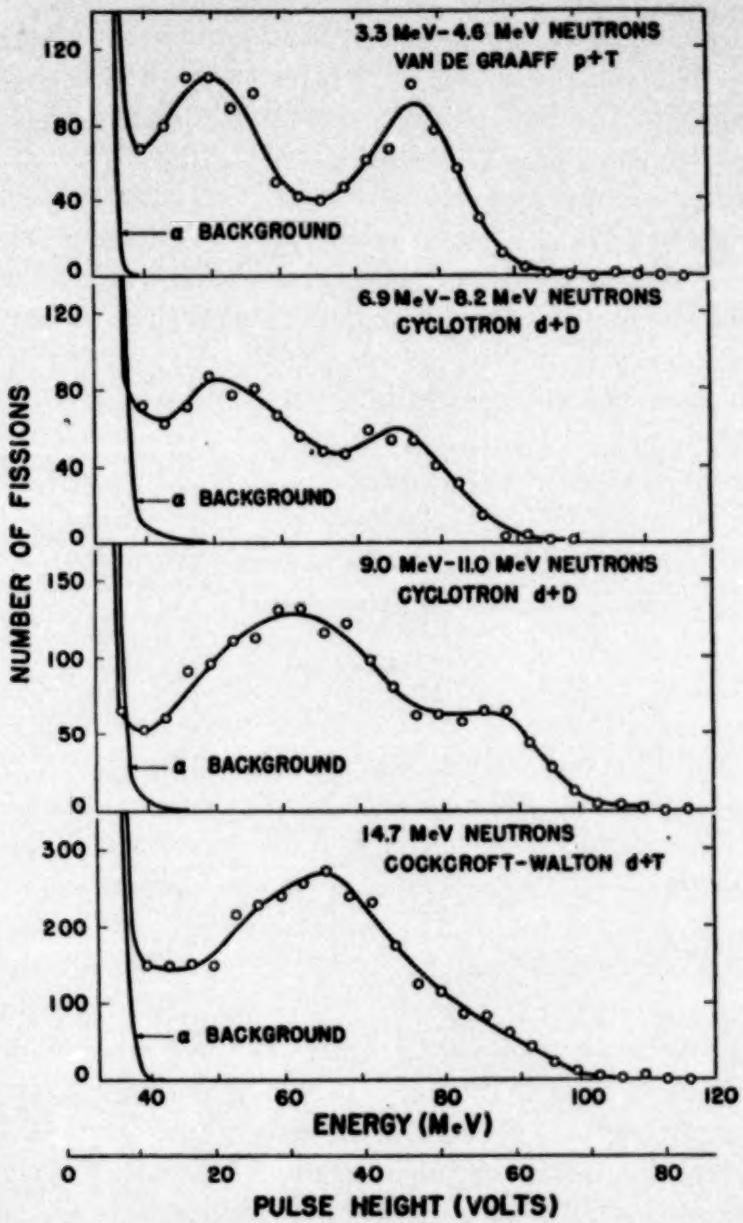

Fig. 1. The energy distribution of fragments from Ra^{226} fission for various energies of neutrons inducing fission.

The indicated spreads of neutron energies are results of particle slowing in the neutron sources and of reaction angles for the neutrons. The non-linearity of the energy scale was determined by pulser calibration. The absolute calibration of the energy scale is from Cf^{252} spontaneous fission, but is uncertain by about 5 % because of instabilities and changes of scintillator gas. The backgrounds of pile-up alpha pulses are for the same observation time as for fission.

Observations were made with neutrons incident upon bare platinum to observe reaction products from platinum, gold, and xenon. To observe

reaction products from lighter elements, 50 μg of $BaCl_2$ on platinum was bombarded. A bombardment of a Po^{210} coating of about the same alpha activity as radium was made to observe combined effects of alpha background and reaction products. In each case the rate of pulses greater than 40 MeV was negligible compared to the fission rates obtained in the experiments. Backgrounds from alpha-particle pile-up for the same observation times as the runs are shown in fig. 1.

Because the scintillator gas filling was changed between Cf^{252} calibrations and Ra^{226} measurements, and because of the instability of the detector equipment, the energy of the fission fragments is uncertain to about ± 5 %.

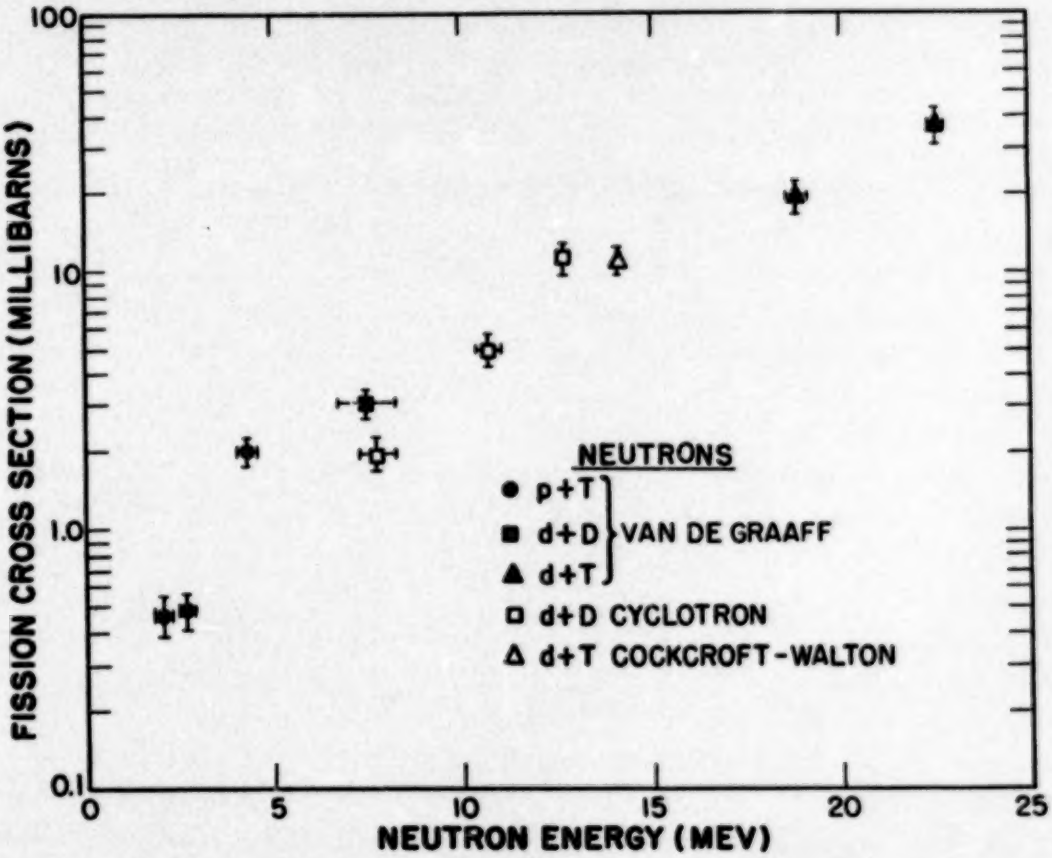

Fig. 2. Cross sections for neutron-induced fission of Ra^{226}.
Energy spreads are explained in fig. 1 caption. Cross section uncertainties include the statistics of the number of fissions of each point and an arbitrary 10 % uncertainty in neutron flux (4 % for the 14.1 MeV point). The uncertainty in the Ra^{226} mass results in ± 18 % uncertainty in the cross section scale.

This instability is demonstrated in fig. 1 by low-energy cutoffs being at larger pulse heights in background runs than in fission runs. Runs were as long as 16 hours.

In fig. 2 are shown the measured cross sections for Ra^{226} fission, which rise unusually rapidly with neutron energy. The experimental uncertainties

are sufficiently large, especially with the changes of the experimental conditions at the two accelerators, to explain the different cross sections at 7—8 MeV.

4. Discussion

The change from predominately asymmetric fission to symmetric fission in the energy region shown in fig. 1 demonstrates considerable energy sensitivity. Comparison of this sensitivity with that of fragment mass distributions [11, 12]) from heavier nucleides is difficult because these different quantities involve an indirect comparison, but the sensitivities seem to be similar. For neutron energies of ≈ 10 MeV and greater, the width of the energy peak of fragments seems narrower than the peak expected from a filling of the valley between the two peaks from 4 MeV neutron fission. This result corresponds to the narrow mass yield distributions from bismuth irradiation [2, 3]).

A possible interpretation of the change from asymmetric to symmetric fission is that the fission of the compound nucleus Ra^{227} is asymmetric, but that the fission of Ra^{226} from the (n, n'f) process is symmetric and becomes increasingly more probable above the threshold of about 6 MeV. In this interpretation, however, fission of Ra^{225} from (n, 2n'f) above the approximately 12 MeV threshold and of Ra^{224} from (n, 3n'f) above the approximately 18 MeV threshold must also be symmetric.

In terms of excitation energy of the compound nucleus, the present radium fission data from ≈ 10 MeV neutrons are comparable in excitation to the 11 MeV proton data of Fairhall and Jensen [1]) because, according to mass systematics [13]), the neutron binding energy is only 0.5 MeV less than the proton binding energy. The fact that both data indicate a transition from asymmetrical to symmetrical fission at this excitation is consistent with studies of the systematics of fission asymmetry [12, 14]).

The cross section for radium fission for a number of neutron energies is shown in fig. 2 to increase from 0.5 millibarn at 2 MeV to 37 millibarns at 23 MeV. The systematics of fission thresholds [15, 16]) based on Z^2/A, where Z and A are nuclear charge and mass number of the fissioning nucleus, give about 2.6 MeV as the "threshold" (knee) energy for neutron-induced fission of Ra^{226}. On this basis, the exponential rise of the cross section is not to be understood as penetration of the fission barrier.

The dissimilarity of the shape of this apparently continuous cross section for fission and the corresponding cross sections for thorium and heavier nucleides [17]), which increase in steps, is to be noted. The nearly constant cross section for fission of the heavier elements in these steps can be interpreted [15]) as the probability for fission increasing at nearly the same rate as for neutron emission. In terms of reaction widths Γ_f and Γ_n, where

subscripts denote fission and neutron emission, then Γ_f/Γ_n is nearly constant for these heavier elements. The exponential rise in present data of neutron-induced fission of radium is the first serious departure from this cross section pattern. This indicates that Γ_f is relatively very small and increases with neutron energy much faster than Γ_n, or else indicates that a large difference between the barriers for fission and for neutron emission plays a role in the relative level spacings for the two processes. In the latter case, fission channels and levels reached by neutron emission are considered. According to fig. 2, the increase is sufficiently great to hide, within the accuracy of the data, the rises due to the onset of the (n, xn'f) processes.

An upper limit of the contribution of impurities of heavier nucleides to the observed fissions is provided by the measurement of 0.5 millibarn fission cross sections at 2 MeV neutron energy, which is above the fission threshold for these nucleides.

The authors are indebted to Professor J. H. Manley for his initial undertaking of this experiment and for his continued interest. The radium foil was prepared by Mrs. Patricia Stein and was counted by Miss Suzanne Krainock. The polonium foil was provided by Mr. J. P. Balagna.

References

1) A. W. Fairhall and R. C. Jensen (1957) to be published
2) A. W. Fairhall, Phys. Rev. **102** (1956) 1335
3) T. T. Sugihara, Clark University Report NYO-7755 (1957) unpublished, and private communication (1957)
4) R. A. Nobles, J. H. Manley and R. B. Leachman, Bull. Am. Phys. Soc. **2** (1957) 70
5) J. A. Northrop and R. A. Nobles, Nucleonics **14** (1956) 36; R. A. Nobles, Rev. Sci. Instr. **27** (1956) 280
6) L. Colli and U. Facchini, Rev. Sci. Instr. **23** (1952) 39; C. H. Reed, private communication
7) A. B. Smith, A. M. Friedman and P. R. Fields, Phys. Rev. **102** (1956) 813
8) R. A. Nobles, to be published
9) J. L. Fowler and J. E. Brolley, Jr., Revs. Modern Phys. **28** (1956) 103
10) S. J. Bame, Eugene Haddad, J. E. Perry and R. K. Smith, private communication (1957)
11) H. G. Hicks and R. S. Gilbert, Phys. Rev. **100** (1955) 1286;
E. V. Luoma, University of California Radiation Laboratory Report UCRL-3495 (1956) (Office of Technical Services, U. S. Department of Commerce, Washington 25, D. C.);
R. A. Glass, R. J. Carr, J. W. Cobble and G. T. Seaborg, Phys. Rev. **104** (1956) 434
12) W. H. Gibson, University of California Radiation Laboratory Report UCRL-3493 (1956) (Office of Technical Services, U. S. Department of Commerce, Washington 25, D. C.)
13) R. A. Glass, S. G. Thompson and G. T. Seaborg, Journal of Inorganic and Nuclear Chemistry **1** (1955) 3
14) W. H. Jones, A. Timnick, J. H. Paehler and T. H. Handley, Phys. Rev. **99** (1955) 184
15) J. D. Jackson, Chalk River Project Report CRP-642-A (1956) (Scientific Document Distribution Office, Atomic Energy of Canada Limited, Chalk River, Ontario, Canada)
16) W. J. Swiatecki, Phys. Rev. **101** (1956) 97
17) R. K. Smith, R. L. Henkel and R. A. Nobles, Bull. Am. Phys. Soc. **2** (1957) 196

Nuclear Physics **5** (1958) 218—234; © *North-Holland Publishing Co., Amsterdam*
Not to be reproduced by photoprint or microfilm without written permission from the publisher

THE COULOMB EXCITATION OF U^{233} AND Np^{237} AND A DISCUSSION OF THE ENERGY LEVELS OF U^{233}

J. O. NEWTON †
Atomic Energy Research Establishment, Harwell

Received 12 July 1957

Abstract: Gamma rays of energy 40.4 ± 0.2, 51.5 ± 0.5, and 92.3 ± 1 keV for U^{233} and 33.24 ± 0.2 and 42.57 ± 0.3 keV for Np^{237} have been observed in the Coulomb excitation of these nuclei by helium ions; a xenon filled proportional counter was used as detector. The gamma rays are interpreted as arising from the decay of rotational states. From the absolute cross sections and from the branching ratios of the gamma rays from the second rotational states the reduced transition probabilities B_{E2} and intrinsic quadrupole moments Q_0 were estimated. Mean values for Q_0 of 13.7 and 9.0 barns were obtained for U^{233} and Np^{237} respectively. Possible assignments of single particle states in a deformed potential to the ground state of Np^{237} and to the ground and excited states of U^{233} are discussed.

1. Introduction

This paper reports on some further Coulomb excitation experiments with heavy radioactive nuclei. The experimental method and method of analysis are the same as described in a previous paper [1]) which will be denoted hereafter by (I).

Three gamma rays were definitely observed from U^{233} and two were observed from Np^{237}; as in (I) it seems reasonable to attribute these to the decay of rotational states. In the case of Np^{237}, there is a low-lying state, 60 keV in energy, which could in principle be excited by electric dipole excitation. No gamma rays were observed from this state, however, because the E1 transition has [2]) a very small reduced transition probability B_{E1}.

2. Energies, Relative Intensities and Cross Sections for Production of the Gamma Rays

2.1. EXPERIMENTAL DETAILS

The targets in oxide form and of thickness approximately 400 $\mu g\ cm^{-2}$ were on 0.005 inch nickel backings and mounted in aluminium target cans of end thickness 0.02 inch. The resolved singly charged helium beam from the Van de Graaff generator hit the centre of these targets and was of 0.6

† At present on leave of absence at the Radiation Laboratory, University of California, Berkeley, California.

cm diameter; it was collimated by nickel apertures. The gamma rays were detected by means of a proportional counter filled to 2.3 atmospheres pressure with xenon; methane, having a partial pressure of 4 cm of mercury, was also added. The counter, of diameter 5 cm and active length 9 cm, had aluminium walls of thickness 0.03 inch. It was placed in the 0^0 position with respect to the incident beam and its axis was 3.2 cm from the target. The counter was surrounded by a lead shield lined with cadmium, iron and aluminium; the lining prevented any X-rays produced in the lead from being detected in the counter.

Cross sections were measured for all the gamma rays and where possible the excitation functions were measured also. The form of the excitation function, which can be calculated, is strongly dependent on the energy of the excited state that emits the gamma ray and on the charge of the bombarded nucleus. Therefore, a measurement of the excitation function can usually show whether or not an observed gamma ray comes from excitation of the desired nucleus rather than from, say, a light element contaminant; if the radiation is not from a contaminant the energy of the excited state can also be obtained. The experimental method is given in greater detail in (I).

2.2. URANIUM-233

A pulse height spectrum showing all the gamma ray lines produced in the Coulomb excitation of U^{233} is given in fig. 1; the K-lines of uranium are

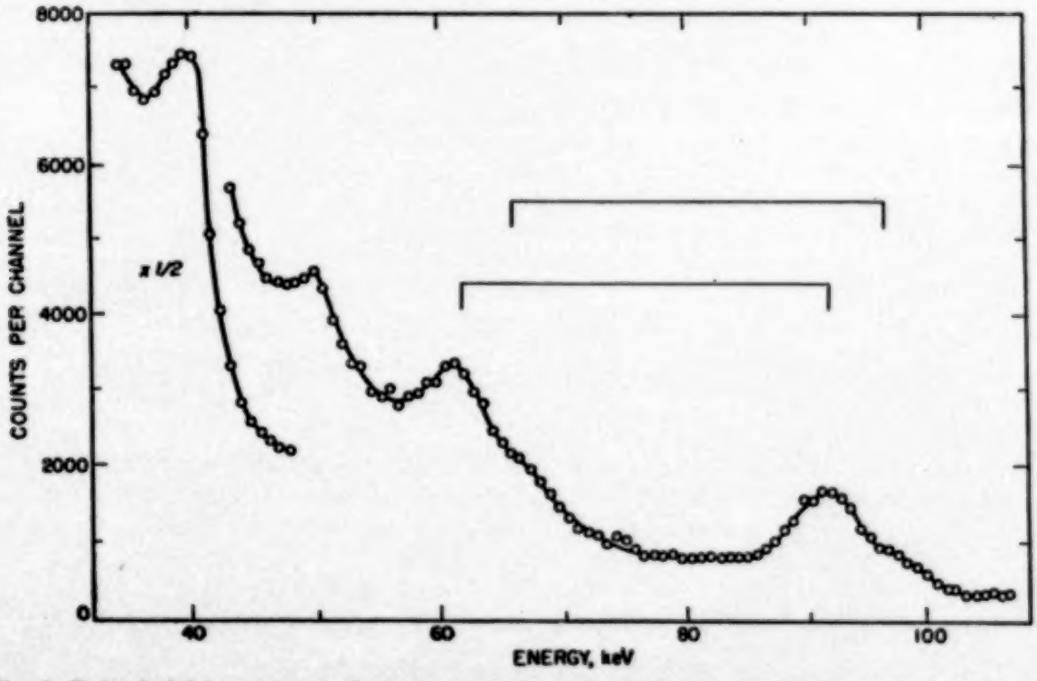

Fig. 1. Pulse height spectrum of gamma rays from the Coulomb excitation of U^{233}. Main and escape peaks are joined by bars. The source background has not been subtracted from this spectrum.

also evident. The radioactive contribution from the source was not negligible and had to be subtracted. The excitation functions for all the gamma rays were measured and are shown in fig. 2. They are consistent with these gamma rays arising from the excitation of states at 40.4 and 92.0 keV.

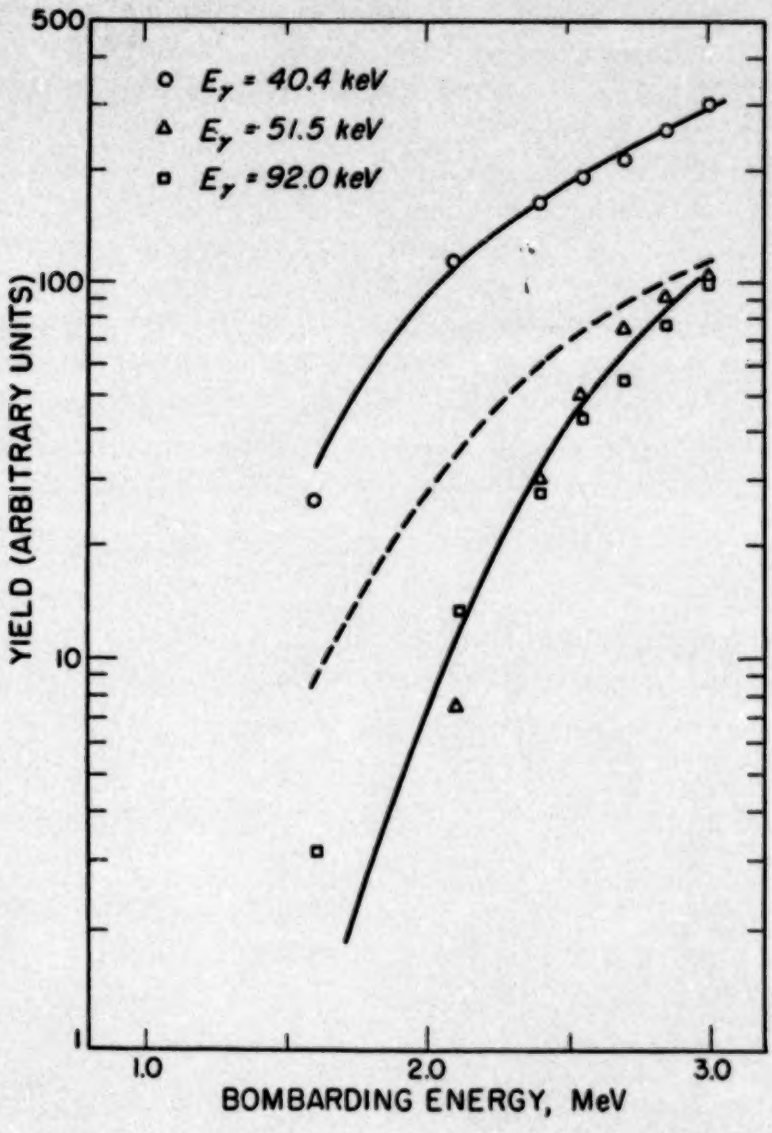

Fig. 2. Excitation functions for the 40.4, 51.5, and 92.3 keV gamma rays of U^{233}. The full lines are theoretical curves for excitation of states at 40.4 and at 92.0 keV; the broken line is the theoretical curve for excitation of a state at 51.5 keV.

The relative intensities of the gamma rays at a bombarding energy of 2.85 MeV are given in table 1; the cross section for production of the 40.4 keV gamma ray being $(5.3\pm0.7)10^{-29}$ cm^2. The target thickness was approximately 200 keV.

TABLE 1

Relative intensities of the gamma rays from the Coulomb excitation of U^{233} by 2.85 MeV helium ions

Energy in keV	40.4 ± 0.2	51.5 ± 0.5	92.3 ± 1
Relative intensity	1.00	$(1.22 \pm 0.2)10^{-1}$	$(5.7 \pm 0.5)10^{-1}$

2.3. NEPTUNIUM-237

Unfortunately, it did not prove possible to obtain a source of Np^{237} which was free from contaminants such as iron. As a consequence of this,

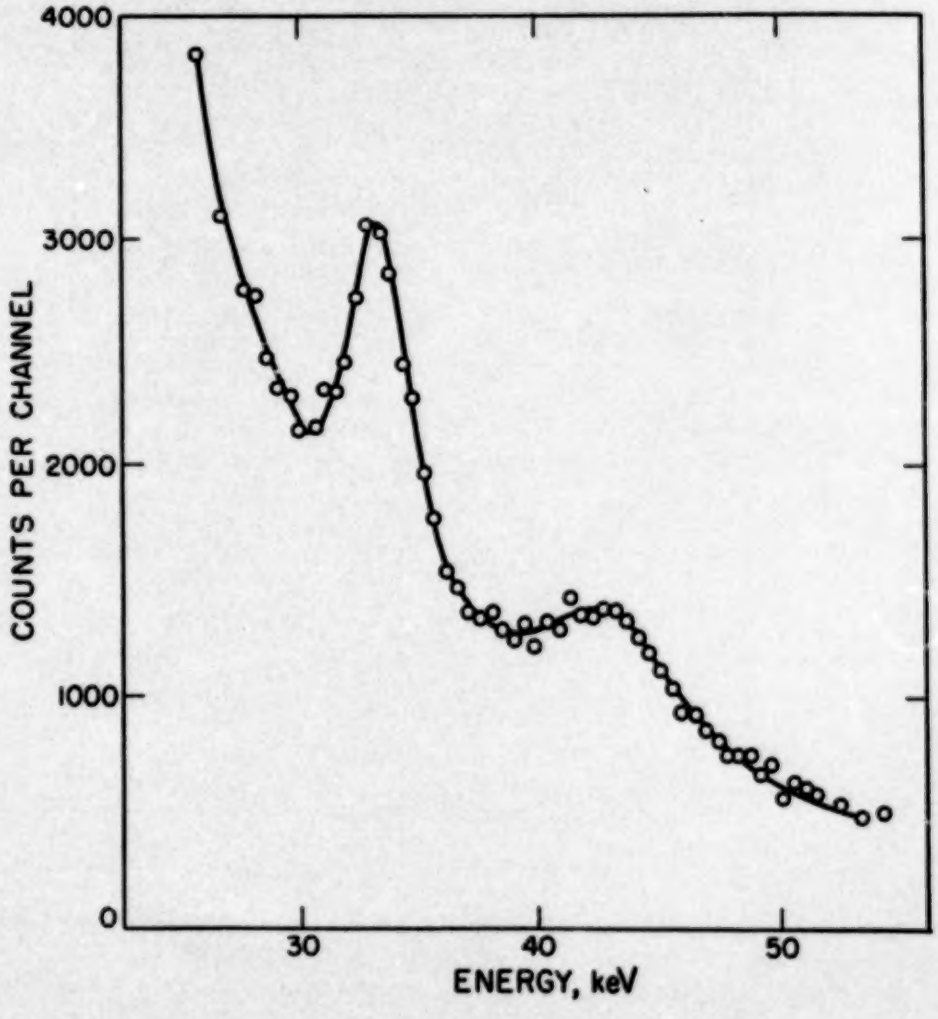

Fig. 3. Pulse height spectrum, with source background subtracted, of the 33.2 and 42.6 keV gamma rays from the Coulomb excitation of Np^{237}.

the general background, other than that from the decay of the source, was several times larger than it was when the other nuclei were bombarded. In addition to this, the source thickness was about 700 keV, much higher

than in the other cases, and the Np^{237} was not distributed uniformly through the thickness of the source material.

The latter effects were apparent when a measurement was made of the pulse height spectrum of the alpha particles from the source in a "low geometry" proportional counter. In order to use this information for the

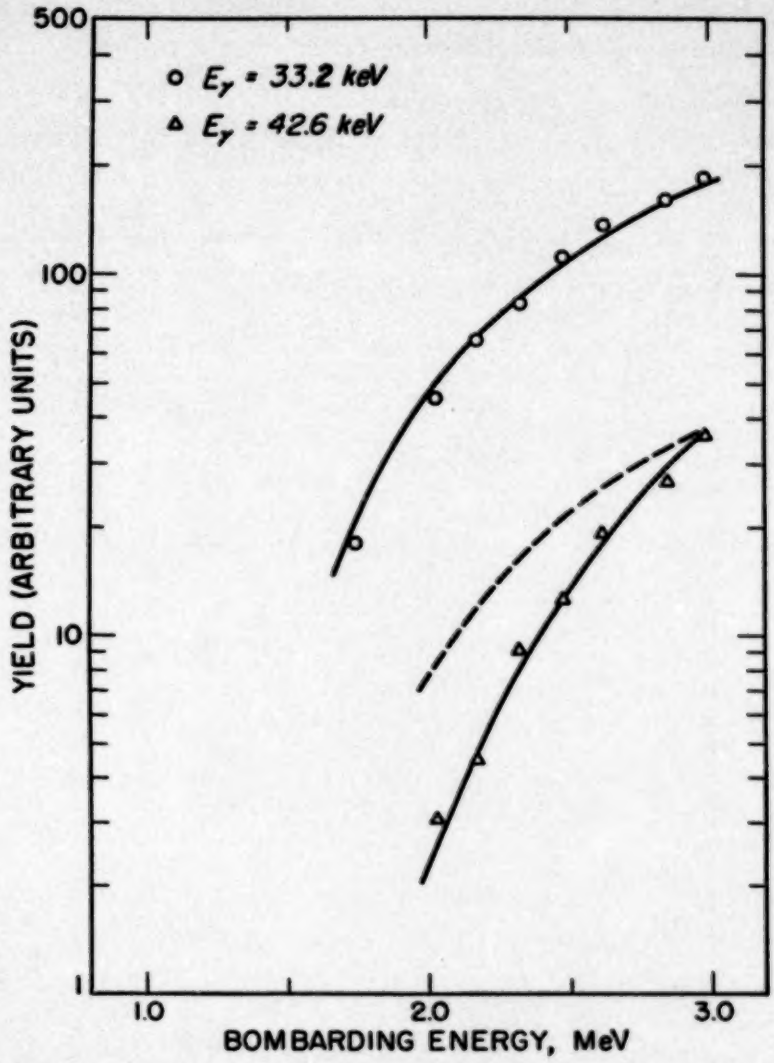

Fig. 4. Excitation functions for the 33.2 and 42.6 keV gamma rays of Np^{237}. The full lines are the theoretical curves, corrected for target thickness, for excitation of states at 33.2 and 75.8 keV; the broken line is the theoretical curve for excitation of a state at 42.6 keV.

purpose of computing cross sections it was necessary to assume a range-energy relation for alpha particles in the source material; the energies of the Np^{237} alpha particles and of the bombarding particles were widely different, implying different rates of energy loss in the source.

The choice of range energy relation is not obvious but fortunately the

results are not very sensitive to it. We chose to use that for gold as computed from the data given in the review article by Allison and Warshaw [3]). The error introduced by this assumption was taken to be half of the difference between the result obtained with this range-energy relation for gold and that with the range-energy relation for air; the latter result corresponds to an extreme case.

A pulse height spectrum of the 33 and 42 keV gamma rays is shown in fig. 3. The excitation functions are given in fig. 4 the theoretical curves being computed with the range-energy relation for gold. These are consistent with the 42 keV gamma ray arising from a state at 76 keV rather than from a state at 42 keV.

The relative intensities of the gamma rays at a bombarding energy of 2.85 MeV are given in table 2; the observation of the "76 keV gamma ray" can only be considered very doubtful. The cross section for the production of the 33 keV gamma ray at 2.85 MeV bombarding energy is $(9.2\pm1.5)10^{-29}$ cm^2. This figure is for a thin target.

TABLE 2

Relative intensities of the gamma rays from the Coulomb excitation of Np^{237} by 2.85 MeV helium ions

Energy in keV	33.24 ± 0.2	42.57 ± 0.3	(76)
Relative intensity	1.00	$(2.8\pm0.4)10^{-1}$	$\left(3^{+1}_{-2}\right)10^{-2}$

3. Interpretation

3.1. THEORETICAL CONSIDERATIONS

There is now a large body of evidence indicating that rotational states occur systematically in nuclei, well removed from closed shells. Coulomb excitation of the rotational states of the ground state bands which can be reached by E2 excitation occurs with large cross sections because of the large matrix elements for these transitions. As in (I), we therefore assume that the states excited in these experiments are rotational states. A brief résumé of the relevant theory together with references to the original papers is given in (I) and will not be repeated here. However, reference must be made to the recent paper by Alder, Bohr, Huus, Mottelson and Winther [4]), which gives a comprehensive review of the whole subject of Coulomb excitation.

3.2. THE ROTATIONAL LEVELS

The spin of U^{233} is reported to be 5/2 [5, 6, 7]). The ratio of the energy of the second to that of the first excited state is 2.277 ± 0.015 which is in

good agreement with that of 2.286 expected on the simple theory for a rotational band with $K = 5/2$.

The spin of Np^{237} is also given as 5/2 [8]) and the observed energy level ratio of 2.280 ± 0.012 is again in good agreement with the value expected from the simple theory for a $K = 5/2$ band. The energy parameter $\hbar^2/2\mathcal{I}$ for this band is abnormally low; it has a value of 4.79 keV which is to be compared with values of about 7.3 keV for the neighbouring even nuclei and about 6 keV for odd mass nuclei in this region. Previous to this experiment only the 33 keV state of this band was known and there was therefore some doubt as to whether or not it was a rotational state. The observation of the 76 keV state almost certainly removes this doubt.

3.3. QUADRUPOLE MOMENTS AND REDUCED TRANSITIONS PROBABILITIES

The total cross sections for excitation of the states were calculated as follows. The gamma ray transition γ_{20} between the second and ground states is assumed to be pure electric quadrupole. From its intensity and assuming the E2 gamma ray branching rules of the strong coupling model [9]) it is then possible to calculate the E2 component of the transition γ_{21} between the second and the first excited states. From this and the intensity of γ_{21} we obtain the M1 component of γ_{21}. A further assumption of the validity of the transition rules between rotational states in the strong coupling model gives the ratio of the M1 to the E2 component in the transition γ_{10} between the first and ground states. When the mixing ratios are known, the total cross sections can be estimated from the theoretical conversion coefficients. This method is discussed in more detail in (I).

The values of the L-conversion coefficients which were derived from the tables circulated by M. E. Rose are given in table 3. The neglect of the

TABLE 3

L-conversion coefficients used in the calculations

Nucleus	E2			M1	
	γ_{10}	γ_{21}	γ_{20}	γ_{10}	γ_{21}
U^{233}	810	252	14.5	80	39.2
Np^{237}	2380	738	44	166	79

effect of finite nuclear size in Rose's calculations is expected to produce a large error in the M1 conversion coefficients. The final results were calculated, (a) with the values in table 3 and (b) with the E2 values of table 3 and the M1 values of the table multiplied by 0.6, this factor being an estimate of the finite size correction [1]). The ratio of M+N+ . . . conversion to L conversion was taken to be 0.3 for both E2 and M1 transitions [1]).

It should be noted that the measurements were made at a fixed angle of 0^0 to the incident helium beam. The cross sections derived here therefore assume isotropy of the gamma radiation. We now consider the validity of this assumption. The theoretical angular distributions [10, 4]), with no attenuation due to precession of the nuclear moments in external fields during the lifetime of the states, were calculated for each gamma ray; it was assumed that the states excited were rotational states. After allowing for the geometry of the experiment the errors indicated below are made in the yields of the gamma rays of U^{233} if isotropy is assumed and if the theoretical angular distributions are valid. The ratio of the amplitude of the E2 to that of the M1 component in the mixed transitions is denoted by δ. In γ_{20} the error is +4.5 %; in γ_{21}, it is −6 %, −9 %, +8.5 %, and +2.4 % for $\delta = -0.2, -1.0, +1.0$ and 0.2 respectively; in γ_{10} the error is always less than 1 %. The results for Np^{237} differ only slightly. These errors lead to errors in the magnitudes and in the ratios of the total yields to the two excited states, and hence in the Q_0, calculated on the assumptions of this paper. The error in the ratio of the total excitation of the first to that of the second excited state is +6 %, +10 %, −9 % and 0 % for $\delta = -0.2, -1, +1$ and 0.2 respectively. Thus, where $|\delta|$ is of order unity the error is about the same as that of the measurement. The actual error may well be less than this since the angular distributions are likely to be attenuated; such attenuation certainly occurs in alpha-gamma angular correlations in heavy elements [11]).

In table 4 are given the values of B_{E2}, for excitation, Q_0 and $|g_Q - g_R|$. The estimated errors do not include any allowance for the possibility that the conversion coefficients used may be inaccurate, nor for the possible effects of angular distributions as discussed above. It is interesting to note the large difference

TABLE 4

Values of Q_0, B_{E2} and $|g_Q - g_R|$

Nucleus	K	Energy of state (keV)	$(1/e^2)B_{E2} \times 10^{48}$ (cm^4)	Q_0(R) $\times 10^{24}$ (cm^2)	Q_0(c) $\times 10^{24}$ (cm^2)	$\lvert g_Q - g_R \rvert$
U^{233}	5/2	40.4	$(1.2 \pm 0.2)10^1$	15.7 ± 1.6	15.6 ± 1.6	$\left(7.6^{+2.4}_{-4.4}\right)10^{-2}$
		92.0	2.38 ± 0.14	11.9 ± 0.4	11.8 ± 0.4	
Np^{237}	5/2	33.24	$4.5^{+0.6}_{-0.9}$	$9.8^{+0.7}_{-1.0}$	$8.1^{+0.6}_{-0.9}$	$\left(7.1^{+4}_{-0.8}\right)10^{-1}$
		75.8	2.4 ± 0.4	12.0 ± 1.1	9.9 ± 0.9	

The B_{E2} and Q_0(R) were obtained with Rose's conversion coefficients. For Q_0(c), Rose's M1 conversion coefficients were multiplied by 0.6. A further error of ±10 % for the B_{E2} and ±5 % for the Q_0 must be combined with those shown above to get the errors on the absolute values.

in the values of $|\delta|$ for the transition γ_{21} of these two nuclei. That for U^{233}

is $(2^{+3}_{-0.5})$ while for Np^{237}, it is $(1.4^{+0.2}_{-0.6})10^{-1}$. This last value is consistent with that reported in the paper by Hollander, Smith and Rasmussen [12]). The large value for U^{233} is due to a chance cancellation of g_Ω by g_R, since the reduced transition probability for cascade M1 radiation is proportional to $(g_\Omega - g_R)^2$; the value for Np^{237} corresponds more nearly to the average case.

The magnetic moment μ of U^{233} has been given as 0.56 nuclear magnetons [6, 13]) and from this, values of +0.25 and +0.17 or +0.20 and +0.28 are obtained for g_Ω and g_R respectively, assuming that g_R is positive.

Since (I) was written, Dorian, Hutchison and Wong [13]) have reported values for the quadrupole moments of U^{235} and U^{233}, which imply values for Q_0 of 8.6 for U^{235} and of 9.6 for U^{233}. These values are probably lower limits and are therefore not necessarily inconsistent with our mean values of 11.7 and 13.7 for these quantities. Their value for the ratio $Q_0(U^{233})/Q_0(U^{235})$, which is not subject to such large errors, is 1.12 ± 0.2. This is consistent with our mean value of 1.17.

The absolute value of the magnetic moment of Np^{237} has been given [8]) as 6 ± 2.5. This value is surprisingly large especially as the Schmidt limit for spin 5/2 is 4.79 and most nuclei of this spin have values considerably smaller than this limit [14]); another measurement of this quantity is desirable. If we use this value for the magnetic moment and the value in table 4 for $|g_\Omega - g_R|$ we obtain values of 1.9 ± 1.1 and $+2.6 \pm 1.1$ or 2.9 ± 1.1 and 2.2 ± 1.1 for g_R and g_Ω respectively, assuming that g_R is positive. These values for g_R are much higher than those usually obtained, which seem to be of the same order or less than Z/A. In order to give $g_R = Z/A$ we should require μ to have a value of 2.3.

The differences between the $Q_0(1)$ and $Q_0(2)$, $+(3.8 \pm 1.7)$ for U^{233} and $-(1.8^{+1.3}_{-1.1})$ for Np^{237}, lie outside the estimated standard errors of the measurements. The fact that the angular distributions have not been taken into account may, as indicated above, lead to fictitious differences between the $Q_0(1)$ and $Q_0(2)$ derived from the experimental data. The magnitudes of the differences from this effect are not greater than 0.7 for U^{233} and 0.3 for Np^{237}; they are therefore not sufficient to bring the deviations within the errors.

A possible explanation for the discrepancy in the case of U^{233} is that there is a higher proportion of M1 radiation in the γ_{10} transition than in the γ_{21} transition. The M1 transition probability is proportional to $(g_\Omega - g_R)^2$ hence this implies that the value of $g_\Omega - g_R$ is different for the two transitions. Since g_Ω is nearly equal to g_R for U^{233} the M1 transition probability will be very sensitive to small changes in g_Ω which can arise from admixtures with other rotational bands having K equal to 3/2 or 7/2. The first order terms of the perturbation treatment of admixtures do not show any

dependence of g_Ω on the spin of the state [12]), the second order terms do however. The results for $G_I = 2\Omega(g_{\Omega I} - g_R)$ are given below; K refers to the perturbed band, K' to the perturbing band, and for these bands $K = \Omega$:

$$K' = K+1\colon\ G_I = G^{KK} - \frac{A_K}{\Delta E}\sqrt{2}\,(K+1)G^{KK'} + \left(\frac{A_K}{\Delta E}\right)^2\{G^{KK}[I^2 - K(K+1)] + G^{K'K'}[I^2 - (K+1)^2]\}.$$

$$K' = K-1\colon\ G_I = G^{KK} + \frac{A_K}{\Delta E}\sqrt{2}\,(K-1)G^{KK'} + \left(\frac{A_K}{\Delta E}\right)^2\{G^{KK}[I^2 - K(K-1)] + G^{K'K'}[I^2 - (K-1)^2]\}.$$

The notation used is that of Kerman [15]). A value for $A_K/\Delta E$, which is related to the strength of the mixing, was estimated from a comparison of the value of $\hbar^2/2\mathcal{I}$ for the U^{233} rotational band with that for the neighbouring even nuclei U^{234} and U^{232} [16]). $G^{K'K'}$ was calculated assuming, for simplicity, that the perturbing state was the ($i_{11/2}$, 631, 3/2+) level of Nilsson [17]) (see § 5.1). Other higher lying states will also contribute but our choice should give an upper limit to the effect. It appears from this calculation that the difference between $Q_0(1)$ and $Q_0(2)$ for U^{233} can at most be reduced by 0.5 if we assume that the excitation energy of the 3/2+ level is about 300 keV. This effect, taken together with the angular distribution effect, can at most, reduce the difference to 2.6 ± 1.7. We therefore have to assume (a) that the errors in this experiment have been underestimated or (b) that the conversion coefficients used are inaccurate or (c) that the transition probability rules of the strong coupling model do not apply with high accuracy to these particular cases. Further investigations are desirable. Since the derivation of $Q_0(2)$ from the experimental data involves fewer assumptions than that of $Q_0(1)$, it seems that $Q_0(2)$ should give the more reliable value for the intrinsic quadrupole moment. Differences between the $Q_0(1)$ and $Q_0(2)$ have been observed in other experiments [4]).

It was possible to set an upper limit of 1.10^{-29} cm^2 for the cross section for production of a 59.6 keV gamma ray in Np^{237}. A level in this nucleus at 59.6 keV is known to decay to the ground state by an E1 transition having a partial photon lifetime of 1.7×10^{-7} sec [2, 33]). This is slower than the single particle estimate by a factor of about 10^5. From our cross section we can set an upper limit to $(1/e^2)B_{E1}$ for this transition of 3×10^{-29} cm^4, which is about 10^3 times smaller than the single particle estimate. Hence an improvement in signal to background ratio by a factor of one hundred would be required in order to observe the 59.6 keV transition.

3.4. INTERPRETATION IN TERMS OF NILSSON'S ENERGY LEVELS

From the wave functions given by Nilsson [17]), for energy levels in a

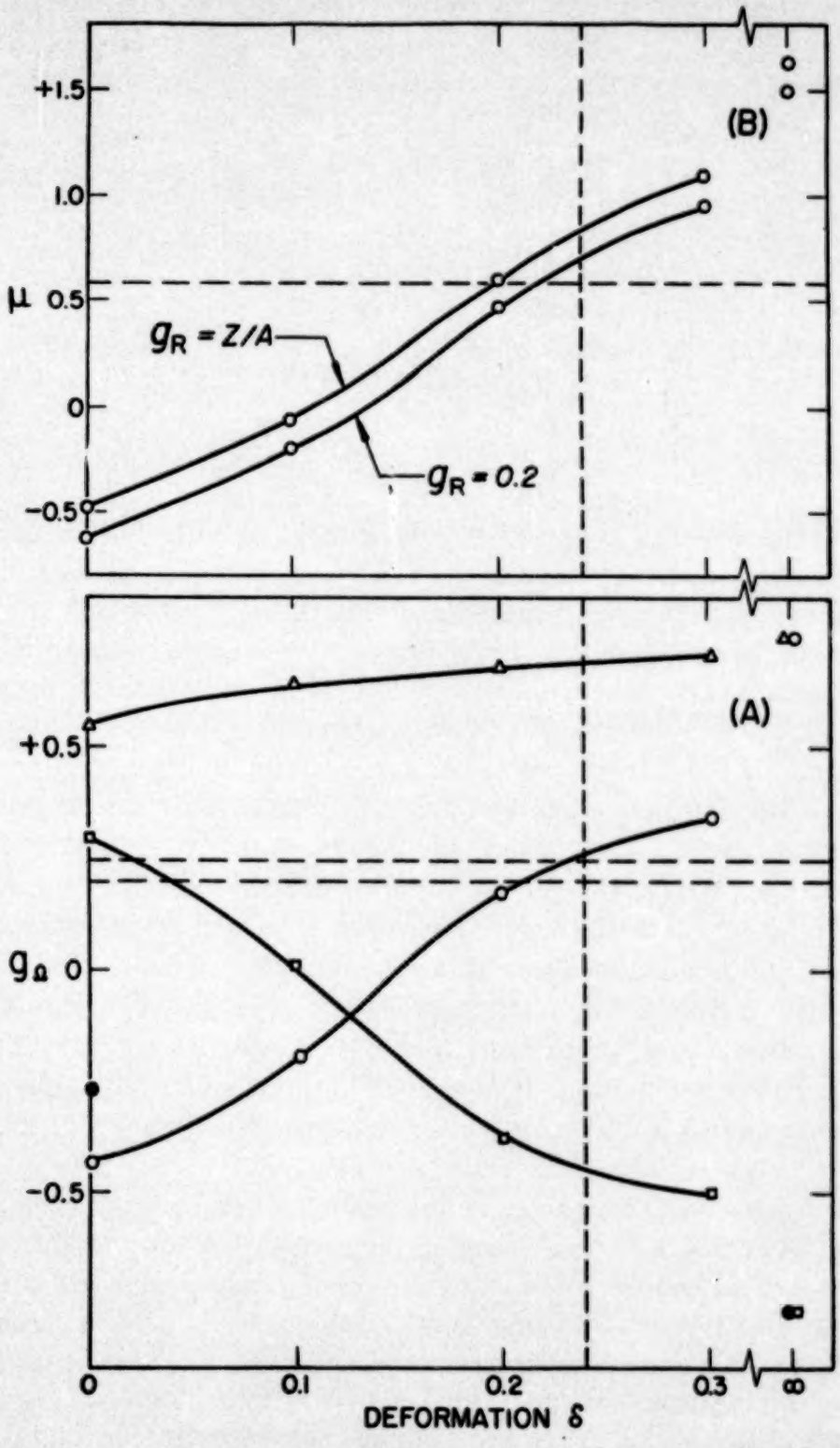

Fig. 5. Calculated values of g_Ω and μ as functions of δ for the states ($g_{9/2}$, 633, 5/2+) denoted by open circles, ($j_{15/2}$, 752, 5/2−) filled circles, ($f_{5/2}$, 503, 5/2−) triangles and ($i_{13/2}$, 622, 5/2+) squares. Experimental values are given by the broken lines.

spheroidal potential, we have calculated values for g_Ω which are compared with experiment. The notation is the same as that used in (I).

(i) *The nucleus* U^{233}. The energy levels for odd neutron nuclei in this region were given in fig. 7 of (I). The levels arising from the $j_{15/2}$ spherical states were guessed; they have now been calculated [18]) and give a more satisfactory ordering of the levels than the figure in (I).

The possible states are those denoted by ($f_{5/2}$, 503, 5/2−), ($j_{15/2}$, 752, 5/2−), ($i_{11/2}$, 622, 5/2+) and ($g_{9/2}$, 633, 5/2+). The values of g_Ω for these states are given as a function of deformation δ in fig. 5A. Only the level ($g_{9/2}$, 633, 5/2+) gives agreement with the experiment and we therefore take this to be the correct assignment. The values of the magnetic moment μ for this level are given in fig. 5B. It can be seen that the magnetic moment is predicted to be positive. This is consistent with the assignment given to U^{235} in (I), which predicted a negative μ for that nucleus, and the experimental fact that U^{235} and U^{233} have magnetic moments of oppositite sign [6]).

It is of interest to compare the value of $|g_\Omega - g_R|$ for the ground state band in U^{233} with that of the ground state band of Th^{229} which is fed by the unhindered alpha particle groups from U^{233} decay [19]). According to the selection rules for unhindered alpha decay [11, 20]) the band in Th^{229} must be based on the same single particle state as that of U^{233}. West, Dawson, and Mandleberg [21]) gave measured the gamma radiation from the decays of U^{233} and of Pu^{239}. Their relative intensities are probably correct but the absolute intensities are known to be too small [22]). The correction factor for their absolute intensities was estimated from the Pu^{239} results, assuming the strong coupling theory to give the conversion coefficients (cf. section 3.3) and using the measured intensities of the alpha particle groups populating the states [23]). Taking this factor of 2.7 to be the same for the U^{233} results, values of 0.28 for δ^2 and 0.3 for $|g_\Omega - g_R|$ were obtained.

The different value of $|g_\Omega - g_R|$ for the Th^{229} band may arise because the deformation of the Th^{229} nucleus is smaller than that of U^{233}. Such a change in deformation is indicated by the increase in the energies of the first excited states of even nuclei with decreasing mass number in this region. A change in deformation would also make reasonable the fact that the unhindered alpha particle groups from U^{233} lead to the ground state band in Th^{229}. If the deformation did not change it would be more likely that the unhindered alpha groups would lead to a rotational band of an excited state in the daughter nucleus; this is the usual case.

(ii) *The nucleus* Np^{237}. The only available levels in this region of the Nilsson scheme, having spin 5/2, are the ($f_{7/2}$, 523, 5/2−) and the ($i_{13/2}$, 642, 5/2+). The values of g_Ω and of μ calculated for these levels as a function of deformation are shown in figs. 6A and 6B. It can be seen that the level

($i_{13/2}$, 642, 5/2+) gives the best agreement with the experimental data. The level ($f_{7/2}$, 523, 5/2−) can be assigned to the 59.6 keV state of Np^{237} which is known to have opposite parity to that of the ground state and is thought to have spin 5/2 from the rotational structure. These assignments have also been suggested by Strominger and Rasmussen [21]).

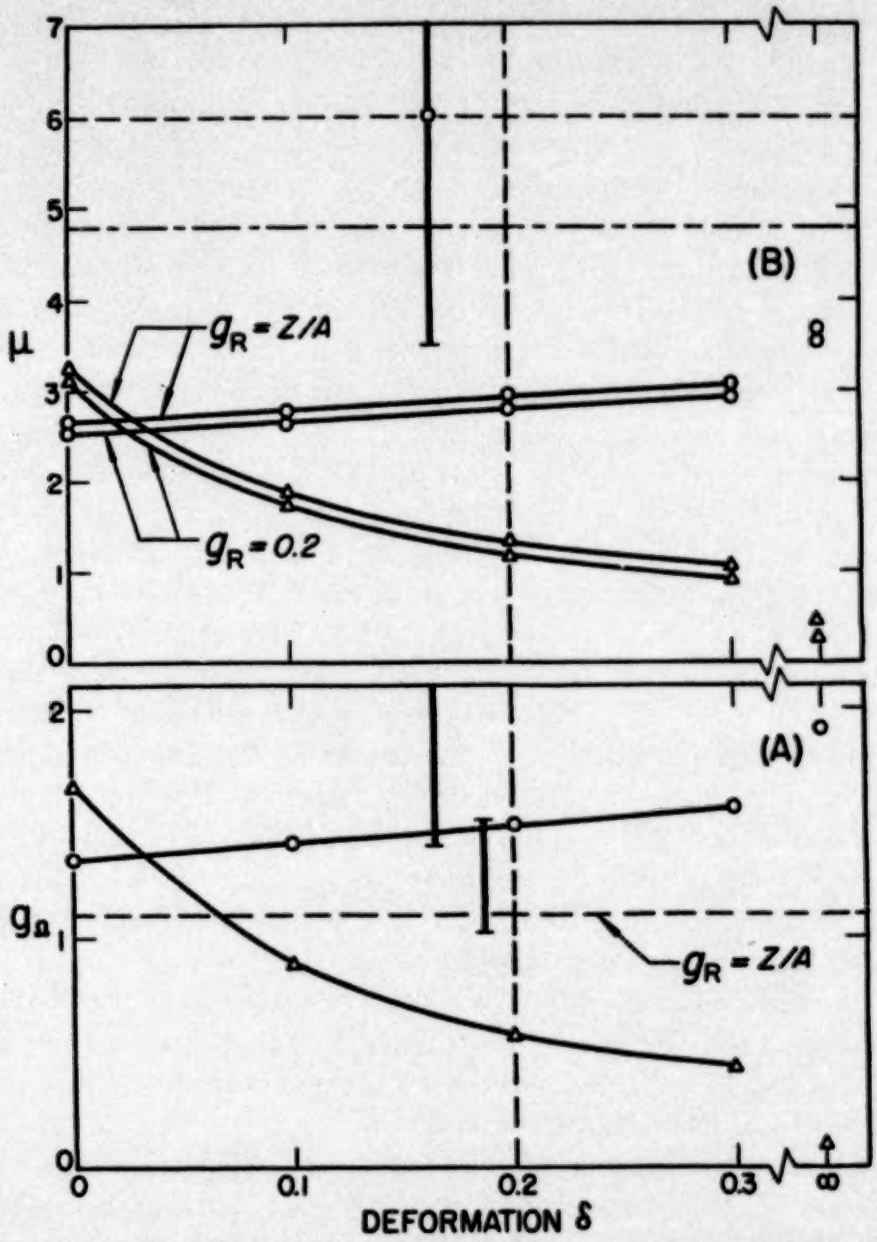

Fig. 6. Calculated values of g_Ω and μ as functions of δ for the states ($i_{13/2}$, 642, 5/2+) denoted by open circles and ($f_{7/2}$, 523, 5/2−) denoted by triangles. The regular broken lines are the experimental values the irregular broken line shows the Schmidt limit for μ.

5. Comparison with Other Data

5.1. THE NUCLEUS U^{233}

Energy levels in U^{233} have been investigated by Brodie [25]), Ong Ping

Hok and Kramer [26]), Keller and Cork [27]) and Brown [28]); they all studied the decay of Pa^{233}. The level scheme proposed by Brodie is consistent with all their data and is shown in fig. 7. The Coulomb excitation data confirm that the level at 40.4 keV is indeed the first excited state of U^{233}; our value for the energy of this state of 40.4 ± 0.2 keV is in good agreement with the other reported values of 40.7 [25]), 40.1 [26]) and 40.47 keV [28]). In addition this work indicates a previously unreported level at 92.0 keV.

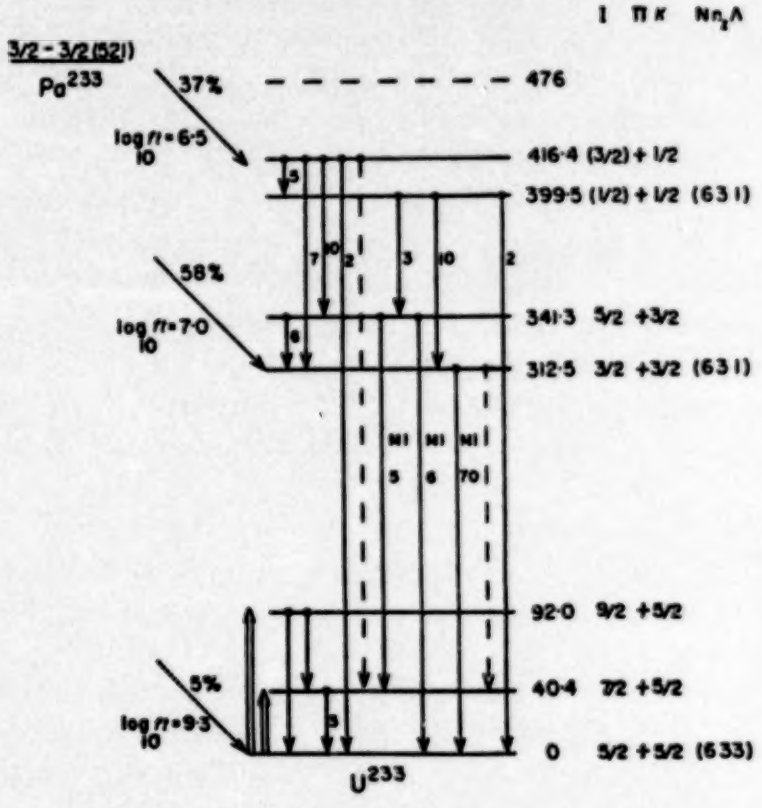

Fig. 7. Energy levels of U^{233}. Data taken from this work, from the work of Brodie [25]) and that of Ong Ping Hok and Kramer [26]). The figures to the right of the gamma transitions are the transition intensities in the Pa^{233} beta-decay.

In section 3.4 of (I), on the basis of the Coulomb excitation data, we have assigned to the ground state of U^{233} the level ($g_{9/2}$, 633, 5/2+) of Nilsson. If we use the data obtained from the decay of Pa^{233} by the authors above it is possible to make similar assignments to some of the excited states of U^{233}.

The 312 keV state decays to the ground state by a strong M1 transition [26]) but by a very weak and barely detectable transition to the 40.4 keV state. If the 312 keV state has spin 5/2 or 7/2 it can decay to the 40.4 keV state by an M1 transition. Then if the gamma ray branching rules of Alaga *et al.* [9]) are obeyed we find that the relative intensity of the 272 keV K conversion line to that of the 312 keV line should be 0.41 or 0.30 for the

313 keV level having spin 5/2 or 7/2 respectively. The fact that these branching rules might be expected to be fairly well obeyed in this region and that the 272 keV line is much weaker than expected on this basis suggests strongly that the 312 keV state must have the only other allowed spin of 3/2. It must also have even parity since it decays by an M1 transition to the 5/2+ ground state.

If the state at 341 keV were the first rotational state of the 312 keV level then it would have a value of $\hbar^2/2\mathscr{I}$ of 5.74 keV which is to be compared with that of 5.77 keV for the ground state band. The 341 keV level is observed to decay by means of M1 transitions to the ground and 40.4 keV states [26]), which means that it must have spin 5/2 or 7/2 and even parity; decay is also observed to the 312 keV state. This evidence taken together strongly suggests that the 341 keV state is indeed the first rotational state of the $K = 3/2+$ band.

The only 3/2+ state expected to lie close to the ($g_{9/2}$, 633, 5/2+) state is the ($i_{11/2}$, 631, 3/2+) state, which we therefore assign to the 312 keV level. Note that this state lies below the 5/2 state in the Nilsson scheme; its appearance as an excited state in U^{233} therefore arises from the excitation to the 5/2 state of a single neutron of the pair originally in the 3/2 state, thus making a pair in the 5/2 state.

There is much less information on the decay of the 399 and 416 keV levels. The fact that they are only 16 keV apart and that a transition between them is seen is suggestive that they may belong to a $K = 1/2$ band. The branching ratio of the transitions from the 416 keV state to the two members of the $K = 3/2$ band does not seem inconsistent with this assignment. If the assignment is correct the transition between the 399 and 341 keV states must be E2. The fact that the 58 keV gamma ray was not seen by Brown [28]) although the 75 and 86 keV gamma rays were reported as very strong suggests that the 58 keV transition has a relatively high conversion coefficient; the intensity of its conversion line is only about three times smaller than that of the 75 and 86 keV transitions. This result suggests that the 58 keV transition is of a higher multipolarity than that of the 75 and 86 keV transitions, which would be M1 on this scheme. The state ($d_{5/2}$, 631, 1/2+) might be expected to appear in the low lying excited states of U^{233} since it appears in Pu^{239} and U^{235} (see (I)). We therefore very tentatively assign this state to the 399 keV level. This assignment explains the weakness of the transitions to the ground state band. M1 transitions to this band will be K forbidden whilst both M1 and E2 transitions are forbidden on the asymptotic selection rules for infinitely deformed nuclei [29]); on the other hand, M1 transitions to the $K = 3/2$ band should be unhindered since the asymptotic quantum numbers differ only in the quantum number Σ (component of spin along the symmetry axis).

The nucleus Np^{237} decays by alpha particle emission to Pa^{233}. The "unhindered alpha group" leads to a level which decays by E1 radiation to the ground state of Pa^{233} [30]). If we assume the rules for unhindered alpha decay and the result of section 3.4, that Np^{237} is 5/2+ then it follows that the ground state of Pa^{233} has odd parity. From Nilsson's diagram [17]) it appears that the ground state of Pa^{233} is likely to be the state ($h_{9/2}$, 521, 3/2−); note that the neighbouring nucleus Pa^{231} which is likely to have the same configuration has measured spin 3/2.

If our various assignments are correct the beta decays to base states of the three rotational bands in U^{233} will be first forbidden. According to the asymptotic selection rules for beta decay given by Alaga [31]) the decays to the two excited bands should be unhindered. That to the ground state should however be hindered because it involves a change in the Λ quantum number or two units. This may explain why the $\log_{10} ft$ value for the ground state transition has the high value of 9.3, suggesting a unique first forbidden transition, and yet the spectrum has an allowed shape, whilst the transitions to the excited states have "normal" $\log_{10} ft$ values for first forbidden transitions.

It appears therefore that our assignments are qualitatively consistent with the experimental data. More precise data on the decay of Pa^{233} seem required before it is worth while to make a quantitative comparison of experiment and theory.

5.2. THE NUCLEUS Np^{237}

The energy of 33.24 ± 0.2 keV obtained for that of the first excited state is in good agreement with that of 33.20 keV reported by Day [32]) from measurements with a bent crystal spectrometer. The level at 75.8 keV has not previously been reported. Several papers discussing the levels of Np^{237} in detail have appeared [29, 33]) and we shall not give any further discussion here.

I should like to thank Mr. J. Waldron and Mr. F. Hudswell of the Chemistry division at Harwell for preparing the targets.

References

1) J. O. Newton, Nuclear Physics **3** (1957) 345
2) J. K. Beling, J. O. Newton and B. Rose, Phys. Rev. **87** (1952) 670
3) S. K. Allison and S. D. Warshaw, Rev. Mod. Phys. **25** (1953) 779
4) K. Alder, A. Bohr, T. Huus, B. Mottelson and A. Winther, Rev. Mod. Phys. **28** (1956) 432
5) K. L. van der Sluis and J. R. McNally, J. Opt. Soc. Amer. **44** (1954) 87; **45** (1955) 65
6) N. I. Kaliteeskii and M. P. Chaika, Dok. Ak. Nauk SSSR **103** (1955) 49
7) L. A. Korostyleva, A. R. Striganov and N. M. Iaskin, Zhur. Eksp. Teor. Fiz. **28** (1955) 471; Soviet Physics JETP **1** (1955) 310
8) B. Bleaney, P. M. Llewellyn, M. H. L. Pryce and G. R. Hall, Phil. Mag. **45** (1954) 992

9) G. Alaga, K. Alder, A. Bohr and B. R. Mottelson, Mat. Fys. Medd. Dan. Vid. Selsk. **29** (1955) no. 9
10) L. C. Biedenharn, M. Goldstein, J. L. McHale and R. M. Thaler, Phys. Rev. **101** (1956) 662
11) J. O. Newton, Progress in Nuclear Physics **4** (1955) 234
12) J. M. Hollander, W. G. Smith and J. O. Rasmussen, Phys. Rev. **102** (1956) 1372
13) P. B. Dorian, C. A. Hutchison and E. Wong, Phys. Rev. **105** (1957) 1307
14) R. J. Blin-Stoyle, Rev. Mod. Phys. **28** (1956) 75
15) A. K. Kerman, Mat. Fys. Medd. Dan. Vid. Selsk. **30** (1956) no. 15
16) J. M. Hollander, Phys. Rev. **103** (1956) 1590
17) S. G. Nilsson, Mat. Fys. Medd. Dan. Vid. Selsk. **29** (1955) no. 16
18) B. R. Mottelson and S. G. Nilsson, Mat. Fys. Medd. Dan. Vid. Selsk. to be published
19) L. L. Goldin, G. I. Novikova and E. F. Tretyakov, Phys. Rev. **103** (1956) 1004.
20) A. Bohr, P. O. Fröman and B. R. Mottelson, Mat. Fys. Medd. Dan. Vid. Selsk. **29** (1955) no. 10
21) D. West, J. K. Dawson and C. J. M. Mandleberg, Phil. Mag. **43** (1952) 875
22) D. West, private communication
23) L. L. Goldin, E. Tretyakov and G. I. Novakova, Conf. Acad. Sci. USSR on Peaceful Uses of Atomic Energy, Phys. Math. Sci. (1955) 226
24) D. Strominger and J. O. Rasmussen, Nuclear Physics **3** (1957) 197
25) W. D. Brodie, Proc. Phys. Soc. A **67** (1954) 397
26) Ong Ping Hok and P. Kramer, Physica **21** (1955) 676
27) H. B. Keller and J. M. Cork, Phys. Rev. **79** (1950) 1030
28) C. I. Brown, University of California report UCRL-1764 (1952) unpublished
29) J. O. Rasmussen, F. L. Canavan and J. M. Hollander (1957) submitted to Phys. Rev.
30) L. B. Magnussen, Bull Am. Phys. Soc. **30** (1955) No. 7, unpublished
31) G. Alaga, Phys. Rev. **100** (1955) 432
32) P. P. Day, Phys. Rev. **97** (1955) 689
33) J. M. Hollander, W. G. Smith and J. O. Rasmussen, Phys. Rev. **102** (1956) 1372

Nuclear Physics **5** (1958) 235—255; © *North-Holland Publishing Co. Amsterdam*
Not to be reproduced by photoprint or microfilm without written permission from the publisher

PARITY NON-CONSERVATION IN NEUTRINO INTERACTIONS AND THE τ—θ PROBLEM

R. GATTO†

Radiation Laboratory, University of California, Berkeley, California††

Received 19 August 1957

Abstract: Solutions of the τ—θ problem are sought whereby one could avoid the conclusion that parity is violated also in weak interactions not involving neutrinos. It is shown that no such solutions can be constructed that are theoretically acceptable, and experimental tests are indicated for a definite disproof of such models. The discussion is limited to the usual description of neutrino interactions such that the known neutrino processes occur at first order in the neutrino coupling constants.

1. Introduction

It was pointed out by Dalitz that, in the absence of parity-non-conserving interactions, the $K^+_{2\pi}$ and the $K^+_{3\pi}$ decays could not be attributed to the same particle [1]) —this conclusion is rigorous for spin zero. On the other hand, if two different K mesons were assumed, it was difficult to understand, in the absence of parity-non-conserving interactions, the apparent equality of the masses, cross sections, and lifetimes for such two particles. Recently, experimental evidence has been reported for parity non-conservation in β decay [2]), in $\pi \to \mu + \nu$ decay [3]), and in $\mu \to e + \nu + \nu$ decay [3]). Moreover, a theory of the neutrino has been proposed which provides a simple model for parity non-conservation in neutrino interactions [4]). Such a theory describes the physical neutrino as a 'screwon'. This description is possible only if the physical neutrino has mass zero: for a particle of finite mass, in the centre-of-mass system, there would be no way of defining a screw sense. No models for parity non-conservation in interactions not involving neutrinos have been proposed so far; however, the absence of simple models does not, of course, imply a difficulty. It is the purpose of this paper to examine the possible role in the τ—θ problem of the established parity non-conservation in neutrino interactions, under the conservative assumption that the other interactions do not violate parity. We shall show that it is difficult to account for all the present evidence on strange-particle decays and interactions on this basis. We shall, however, explicitly restrict our discussion to the assumption that the

† On leave of absence from Istituto di Fisica dell' Università di Roma.

†† This work was done under the auspices of the U. S. Atomic Energy Commission.

neutrinos are coupled only by weak interactions, such that, for instance, β decay or μ decay occurs at first order in the neutrino interactions. The possibility that the known weak interactions are effectively second-order processes in the neutrino interactions is now being investigated by Lee and Yang.

If the strong parity-conserving Hamiltonian has only one eigenstate describing a K meson (at rest), such a state can decay according to one of the two decay modes, $K^+_{2\pi}$ and $K^+_{3\pi}$, by a parity-conserving interaction, and according to the other mode through virtual neutrino states. The probability for the latter transition, however, — involving two virtual steps due to weak interactions — would be extremely small. Therefore a solution of the τ—θ problem with only one K meson and with parity non-conservation only for neutrino interactions does not appear to be possible, at least under the restriction imposed in our discussion to the neutrino interactions. If the strong Hamiltonian has two independent eigenstates describing a K meson, these two states must have opposite parity and the same mass in order that, after the degeneracy has been removed by turning on weak interactions, the resulting physical states contain appreciable amplitudes for both parities. The relevant difference between the case with only one K eigenstate and this case with two eigenstates is that, whereas in the former case only the first-order perturbed state could have amplitudes for both parities, in the latter case the zero-order perturbed state contains amplitudes for both parities, as soon as some of the perturbing weak interactions do not conserve parity. The possibility of such a solution for the τ—θ problem has been pointed out by Treiman and Wyld [5]). The required equality of mass for the two independent K-meson states almost necessarily leads to parity-doublet structures. The strong argument against non-parity-doublet theories for such models would be the impossibility of having two different K mesons with same mass (in the absence of weak interactions) without a symmetry principle responsible for the degeneracy; of course there would be essentially no parity mixing at all if an original mass difference, much larger than the decay rates, were already present when weak interactions are turned off.

Assuming the validity of present experimental evidence — which clearly indicates that only single particles are observed with single lifetimes and fixed branching ratios, and not doublets — we shall see that essentially only one solution can be constructed that is able to simulate such evidence. A detailed discussion of this solution shows, however, that its consistency would require rather unphysical conditions for the weak interactions, and moreover it would lead to specific difficulties for the neutral K^0, which would fit the scheme only accidentally. The model would lead to up-down asymmetries in a way qualitatively similar to that for parity non-conserva-

tion. It would lead, however, to the associated production in nuclear interactions, with a cross section equal to that for production of the observed strange particles, of hyperons and K mesons which rapidly decay into leptons; evidence against such processes would constitute a direct disproof.

2. Parity-Mixing Theory

2.1. DECAY OF PARITY DOUBLET

We discuss here the decay of particles that exist in parity doublets. In order to be definite we limit the discussion to K^+ mesons. The treatment is similar to that given by Lee, Oehme, and Yang for K^0 decay [6]). We derive both the decay matrix and the mass matrix from the Schrödinger equation at lowest order in the weak interactions. The weak decay interactions produce at the same time a level width (finite lifetime) and a level shift (mass difference) for the states of a K^+ particle. The total Hamiltonian is $H+h$, where h contains only the weak interactions. The states $|K^+\rangle$ of a K^+ particle in the absence of weak interactions satisfy the equation $H|K^+\rangle = \mu|K^+\rangle$, where μ is the mass eigenvalue. After h is turned on, a state $|K^+\rangle$ goes into a time-dependent state $|t\rangle$, which satisfies

$$(H+h)\,|t\rangle = i(\mathrm{d}/\mathrm{d}t)|t\rangle \tag{1}$$

and the initial condition $|0\rangle = |K^+\rangle$. We solve eq. (1) to lowest order in h with the ansatz [6])

$$|t\rangle = [c_1|K_1{}^+\rangle\, e^{-\frac{1}{2}\lambda_1 t} + c_2|K_2{}^+\rangle\, e^{-\frac{1}{2}\lambda_2 t}]\, e^{-i\mu t} + \sum_{f\varepsilon} v_{f\varepsilon}(t)\, e^{-i\varepsilon t}|f,\ \varepsilon\rangle, \tag{2}$$

where $|f, \varepsilon\rangle$ satisfy $H|f, \varepsilon\rangle = \varepsilon|f, \varepsilon\rangle$, and $|K_1{}^+\rangle$, $|K_2{}^+\rangle$, λ_1 and λ_2 are determined from eq. (1) and from the initial conditions. If eq. (2) is substituted into eq. (1) the states $|K_1{}^+\rangle$ and $|K_2{}^+\rangle$ and the amplitudes $v_{f\varepsilon}$ are found to satisfy

$$-i\lambda|K^+\rangle\, e^{-\frac{1}{2}\lambda_1 t} = 2\sum_{f\varepsilon} v_{f\varepsilon}(t)\, e^{-i(\varepsilon-\mu)t}\, h|f,\ \epsilon\rangle, \tag{3}$$

$$i\dot{v}_{f\varepsilon}(t) = \langle f\varepsilon|h|K^+\rangle\, e^{-\frac{1}{2}\lambda_1 t + i(\varepsilon-\mu)t}. \tag{3'}$$

Integrating eq. (3') and substituting in eq. (3), one finds that the states $|K_1{}^+\rangle$, $|K_2{}^+\rangle$ must satisfy the non-Hermitian eigenvalue problem

$$\Lambda|K^+\rangle = \lambda|K^+\rangle, \tag{4}$$

where $\Lambda = hTh$ and

$$T = -2i\sum_{f\varepsilon}|f\varepsilon\rangle\frac{1-e^{-i(\varepsilon-\mu+\frac{1}{2}i\lambda)t}}{\varepsilon-\mu+\frac{1}{2}i\lambda}\langle f\varepsilon|$$

$$= 2\sum_{f}\left\{\pi|f\mu\rangle\varrho_f(\mu)\langle f\mu| - iP\int \mathrm{d}\varepsilon|f\varepsilon\rangle\varrho_f(\varepsilon)\frac{1}{\varepsilon-\mu}\langle f\varepsilon|\right\}. \tag{5}$$

The last equality holds provided the variation of the matrix elements in an energy interval on the order of the energy uncertainty of the initial state can be neglected [6]); $\varrho_f(\varepsilon)$ is the density of states f, and P denotes the principal part. Inserting eq. (5) into eq. (4) and putting $\Lambda = \Gamma + i\Delta$, we find

$$\Gamma = 2\pi h\Big(\sum_f |f\mu\rangle\, \varrho_f(\mu)\, \langle f\mu|\Big)h, \tag{6}$$

$$\Delta = 2h\left(\sum_f \mathrm{P}\int \mathrm{d}\varepsilon |f\varepsilon\rangle\, \varrho_f(\varepsilon)\, \frac{1}{\mu-\varepsilon}\, \langle f\varepsilon|\right)h. \tag{6'}$$

Both Γ and Δ are Hermitian; Γ is the decay matrix (contributions from the energy shell) and Δ is the mass matrix (off energy-shell contributions). In the representation with basic vectors $|\mathrm{K}_+{}^+\rangle$ and $|\mathrm{K}_-{}^+\rangle$ ($P|\mathrm{K}_+{}^+\rangle = |\mathrm{K}_+{}^+\rangle$, $P|\mathrm{K}_-{}^+\rangle = -|\mathrm{K}_-{}^+\rangle$, in which P is the parity operator) we shall write:

$$\langle \mathrm{K}_+{}^+|\Lambda|\mathrm{K}_+{}^+\rangle = \Gamma_+ + i\Delta_+ = c_+,$$
$$\langle \mathrm{K}_-{}^+|\Lambda|\mathrm{K}_-{}^+\rangle = \Gamma_- + i\Delta_- = c_-,$$
$$\langle \mathrm{K}_+{}^+|\Lambda|\mathrm{K}_-{}^+\rangle = \Gamma_\times + i\Delta_\times = c.$$

In this representation the states $|f\varepsilon\rangle$ contributing to Λ_+ and Λ_- are those which can be reached from $\mathrm{K}_+{}^+$ and $\mathrm{K}_-{}^+$ respectively by the weak interaction; the states contributing to $\Lambda_\times$ are those which can be reached from both $\mathrm{K}_+{}^+$ and $\mathrm{K}_-{}^+$. If parity is assumed to be violated only by neutrino interactions, the states $|f\varepsilon\rangle$ contributing to $\Lambda_\times$ must contain neutrinos, while the states contributing to Λ_+ and to Λ_- are the states with neutrinos and the states without neutrinos having parity + and − respectively. If time reversal is satisfied, the matrix elements can essentially be taken as real, and the matrix is symmetric in such a case. Such a symmetry also follows independently of time reversal if it is assumed that the amplitudes for a final state with neutrinos from $\mathrm{K}_+{}^+$ and $\mathrm{K}_-{}^+$ are the same — such an assumption will appear in the following to be the most consistent one. From eq. (4) it follows that for a normalized $|\mathrm{K}^+\rangle$ satisfying eq. (4) the corresponding λ satisfies

$$\langle \mathrm{K}^+|\Gamma|\mathrm{K}^+\rangle = \mathrm{Re}\,(\lambda), \quad \langle \mathrm{K}^+|\Delta|\mathrm{K}^+\rangle = \mathrm{Im}\,(\lambda), \tag{7}$$

where Re and Im denote real and imaginary parts respectively. Comparing with eqs. (6) and (6'), we find that Re (λ) is the inverse lifetime and $\mu + \frac{1}{2}\,\mathrm{Im}\,(\lambda)$ is the mass of $|\mathrm{K}^+\rangle$. The scalar product of two eigensolutions $|\mathrm{K}_1{}^+\rangle$ and $|\mathrm{K}_2{}^+\rangle$ satisfies

$$(\lambda_1 + \lambda_2{}^*)\, \langle \mathrm{K}_2{}^+|\mathrm{K}_1{}^+\rangle = 2\langle \mathrm{K}_2{}^+|\Gamma|\mathrm{K}_1{}^+\rangle. \tag{8}$$

Since Γ must be positive definite, from eq. (8) we obtain the inequality

$$|\langle \mathrm{K}_1{}^+|\mathrm{K}_2{}^+\rangle|^2 < 4\,\mathrm{Re}(\lambda_1)\,\mathrm{Re}(\lambda_2)/[(\mathrm{Re}\,(\lambda_1+\lambda_2))^2 + (\mathrm{Im}(\lambda_1-\lambda_2))^2]. \tag{9}$$

In the following we shall write simply K^+ for a state $|\mathrm{K}^+\rangle$. From the assumed

symmetry of Λ, the normalized solutions of eq. (5) are of the form

$$K_1^+ = \frac{1}{\sqrt{N}}(qK_+^+ + K_-^+), \quad K_2^+ = \frac{1}{\sqrt{N}}(K_+^+ - qK_-^+), \tag{10}$$

where $N = |q|^2+1$, and q is a complex number,

$$q = \frac{c_+ - c_- + \sqrt{(c_+-c_-)^2+4c^2}}{2c}. \tag{11}$$

The eigenvalues corresponding to K_1^+ and K_2^+ are

$$\lambda_{1,2} = \tfrac{1}{2}[(c_+ + c_-) \pm \sqrt{(c_+-c_-)^2+4c^2}]. \tag{12}$$

The two solutions are not, in general, orthogonal:

$$\langle K_1^+ | K_2^+ \rangle = 2iN^{-1} \operatorname{Im}(q). \tag{13}$$

In eq. (12) Im (q) is zero if Δ is negligible in comparison with Γ. The states that at $t = 0$ represent a K_+^+ and a K_-^+ respectively are

$$\phi_+(t) = \frac{1}{q^2+1}[(q^2 e^{-\frac{1}{2}\lambda_1 t} + e^{-\frac{1}{2}\lambda_2 t})K_+^+ + q(e^{-\frac{1}{2}\lambda_1 t} - e^{-\frac{1}{2}\lambda_2 t})K_-^+]e^{-i\mu t}, \tag{14}$$

$$\phi_-(t) = \frac{1}{q^2+1}[q(e^{-\frac{1}{2}\lambda_1 t} - e^{-\frac{1}{2}\lambda_2 t})K_+^+ + (e^{-\frac{1}{2}\lambda_1 t} + q^2 e^{-\frac{1}{2}\lambda_2 t})K_-^+]e^{-i\mu t}. \tag{14'}$$

If K_+^+ and K_-^+ are produced incoherently, the rate of decay into a final state f is given by

$$\begin{aligned} R_f(t) = \frac{2\pi\varrho_f(\mu)}{|q^2+1|^2}[&N_+|(q^2 e^{-\frac{1}{2}\lambda_1 t} + e^{-\frac{1}{2}\lambda_2 t})\langle f|h|K_+^+\rangle \\ &+ q(e^{-\frac{1}{2}\lambda_1 t} - e^{-\frac{1}{2}\lambda_2 t})\langle f|h|K_-^+\rangle|^2 + N_-|q(e^{-\frac{1}{2}\lambda_1 t} - e^{-\frac{1}{2}\lambda_2 t})\langle f|h|K_+^+\rangle \\ &+ (e^{-\frac{1}{2}\lambda_1 t} + q^2 e^{-\frac{1}{2}\lambda_2 t})\langle f|h|K_-^+\rangle|^2, \end{aligned} \tag{15}$$

where N_+ and N_- are the numbers of K_+^+ and K_-^+ respectively that are originally produced. For the 2π and the 3π decays we find from eq. (14) for $N_+ = N_-$ (parity-conjugation theory [7]),

$$\begin{aligned} R_{2\pi}(t) = w(K_+^+|2\pi)[&(1+|q|^2)(|q|^2 e^{-\gamma_1 t} + e^{-\gamma_2 t}) \\ &+ 2e^{-\frac{1}{2}(\gamma_1+\gamma_2)t} \operatorname{Re}[(q^2-|q|^2)e^{i\delta t}], \end{aligned} \tag{16}$$

$$\begin{aligned} R_{3\pi}(t) = w(K_-^+|3\pi)[&(1+|q|^2)(e^{-\gamma_1 t} + |q|^2 e^{-\gamma_2 t}) \\ &+ 2e^{-\frac{1}{2}(\gamma_1+\gamma_2)t} \operatorname{Re}[(q^2-|q|^2)e^{-i\delta t}]. \end{aligned} \tag{16'}$$

We have put $\lambda_i = \gamma_i + i\delta_i$ and introduced $\delta = \frac{1}{2}(\delta_2 - \delta_1)$, and we denote with w the transition probabilities; it is assumed in this model that only K_+^+ contributes to the 2π mode and only K_-^+ to the 3π mode. The relevant feature is the appearance of the oscillating interference term (last term in eqs. (16) and (16'))[5]. This term comes from the interference between the

K_1^+ and the K_2^+ amplitudes. This term is small, however, if the lifetimes are widely different. We can find a limitation for the interference term by using the condition in eq. (9) that follows from the requirement that Γ be positive definite:

$$|\text{interference term}| \leqq 2\sqrt{\frac{\tau_S}{\tau_L}}\ (\text{direct term}). \tag{17}$$

We see from eqs. (14) and (14′) that after a time t from its production, an original K_+^+ becomes a coherent superposition of K_+^+ and K_-^+. In the parity-doublet model, for production processes in which no pseudoscalars are observed, the K^+ beam originally produced is an incoherent superposition of K_+^+ and K_-^+. Parity non-conservation in neutrino processes transforms each of the incoherent amplitudes into a coherent superposition of K_+^+ and K_-^+ after a time comparable to the lifetimes. However, in a process such as (for instance) $K^- + p \to \Sigma + \pi$ occurring at rest, the beam again behaves as an incoherent mixture of K_+^- and K_-^-. In the Lee-Yang parity-conjugation model, the predicted forward-backward asymmetry in the angular distribution of the pions from Σ decay is still expected to occur essentially in the same way as for absolute parity conservation.

2.2. K-COMPONENTS WITH VERY DIFFERENT LIFETIMES

Present evidence clearly indicates only single particles with definite lifetimes and definite branching ratios. We shall now examine, using the results derived in subsection 2.1, whether a solution can be constructed that can simulate a situation in which only single particles instead of doublets are observed. In particular, a necessary requirement will be that the two K lifetimes be widely different, so that in most experiments only the long-lived component is observed. In experiments in which only the long-lived component is observed the decay rates would exhibit a single exponential time dependence consistent with the same lifetime—that of the long-lived component—and the relative abundances of the various decay modes would always be the same. Both the 2π and the 3π decay modes would be permitted for this component. In general, however, the long-lived K, after scattering, would also generate short-lived K. The short-lived K that is produced would be easily detected, for instance, in K^+-scattering experiments in nuclear emulsion—if the lifetime is very short, so that the produced short-lived K decays before being observed, the process would appear in most cases to violate strangeness if the energy of the incident K^+ is known; moreover, associated production experiments such as $\pi^+ + p \to \Sigma^+ + K^+$ would also appear in some cases to violate strangeness. To be definite let us assume that K_1 is the short-lived component and K_2 the long-lived. In the parity-doublet model we find, for the scattered am-

plitude from an initial K^+ beam that has lived enough so that the short-lived component is already extinguished,

$$\text{(scattered amplitude)} \approx (1-q^2)f_- K_1^+ + [(1+q^2)f_+ - 2qf_-]K_2^+, \quad (18)$$

where f_+ and f_- are the two independent scattering amplitudes (energy- and angle-dependent) in the parity-conjugation model. It is seen from eq. (18) that only if q is close to ± 1 the scattered amplitude never contains a short-lived component. From eq. (11), $q = \pm 1$ is possible only if $c_+ = c_-$, in which case $q = +1$. However c_+ contains the parity-conserving amplitudes with $P = +1$ (such as those for $K_+ \to 2\pi$) and c_- the $P = -1$ parity-conserving amplitudes (such as for $K_- \to 3\pi$). These amplitudes are completely unrelated, and, further, there is no general way of relating them to the amplitudes for the neutrino decay modes. Therefore the only non-accidental explanation of $c_+ \approx c_-$ would be the predominance of the neutrino contributions in both c_+ and c_-, since such contributions could be related one to the other. The simplest way of relating the neutrino amplitudes so that, in the absence of non-neutrino interactions we have $c_+ = c_-$, is to require the invariance of the Hamiltonian under the composite transformation (the signs are not necessarily related),

$$\psi_+ \to \pm\psi_-, \quad \psi_\nu \to \pm\gamma_5 \psi_\nu, \quad (19)$$

where ψ_+, ψ_- are the field operators for the two components of a parity doublet, ψ_ν is the neutrino field, and the first transformation is carried out for each particle existing in parity doublet (particles of odd strangeness in the parity-conjugation model). The $K \to \mu + \nu$ decay interaction, for instance, would possibly be written as

$$g_S K_S \bar{\psi}_\mu (1 \pm \gamma_5)\psi_\nu + g_A K_A \bar{\psi}_\mu (1 \mp \gamma_5)\psi_\nu,$$

giving equal total decay rates from K_+ and from K_-. A further requirement of separate invariance under $\psi_\nu \to \gamma_5 \psi_\nu$ (or $\psi_\nu \to -\gamma_5 \psi_\nu$) would be equivalent to postulating equal or opposite amplitudes for the neutrino modes, and in this case all elements of the Λ matrix would be equal in the absence of non-neutrino interactions. We shall not use this particular assumption; however, we shall be led in the following to adopt it for the consistency of the model. In any case, it follows from the more general assumption eq. (19), and from the assumption of the preponderance of the contributions from neutrino interactions that the physical particles in a parity doublet (i.e., the eigensolutions of the equations of the form of eq. (4)) are approximately described by states of the form (eqs. 10)

$$s_S = \frac{1}{\sqrt{2}}(s_+ + s_-), \quad s_A = \frac{1}{\sqrt{2}}(s_+ - s_-), \quad (20)$$

where s_S and s_A are the two states of opposite parity for a particle of odd

strangeness in the parity-conjugation theory. (The case of the neutral K mesons is more complicated and is discussed later.) The states (20) are eigenstates of the parity-conjugation operator c_P with eigenvalue $+1$ and -1 respectively, therefore these states are conserved in scattering processes. The corresponding eigenvalues λ are $\lambda_S = c_+ + c$ and $\lambda_A = c_+ - c$. If the real part of c is positive, s_S is short-lived and s_A long-lived, and the opposite holds if the real part of c is negative. It can be seen that, if the sign for each s in the first of the two relations (19) is chosen appropriately, it is possible to construct a situation such that, for instance, s_S is always short-lived and s_A always long-lived. In particular, if the more stringent assumption is adopted of separate invariance under $\psi_\nu \to \pm\gamma_5\psi_\nu$, the choice of the sign in the first of eq. (20) would be the same for all s. If so, for each doublet the short-lived component would have, for instance, $c_P = +1$ and the long-lived $c_P = -1$. Let us now consider a production experiment, to be definite $\Sigma + K^+$ production from ordinary particles. Conservation of c_P restricts the final amplitude to the form

$$c_S(\Sigma_S K_S^+) + c_A(\Sigma_A K_A^+), \tag{21}$$

where c_S and c_A are complex amplitudes. This final amplitude gives zero probability for the production of a short-lived Σ with a long-lived K^+, and for the production of a long-lived Σ with a short-lived K^+. Therefore, if only the long-lived particles are observed, no apparent violation of the strangeness selection rule will be noticed. Moreover, a beam of long-lived K^+ or K^- in subsequent strong interactions with ordinary nuclear matter will always produce long-lived particles (the case in which K^0 are produced will be examined later). Therefore experiments such as (N stands for nucleon), $K^+ + N \to K^+ + N$, $K^- + N \to \Sigma^{\pm,0} + \pi$ (including the subsequent Σ^0 decay and possible subsequent interactions of the $\Sigma^\pm$) will fail to reveal a short-lived component. This conclusion does not hold at higher energies if more than one strange particle is produced by the long-lived K. Production of more than one strange particle from the K^- beam can occur, for instance, in the reaction $K^- + p \to \Xi^- + K^+$, and in various other reactions at still higher energies. The Ξ^- has a given c_P ($= \pm 1$) and exhibits only one lifetime, namely the observed one. If c_P of Ξ^- is -1, the emitted K^+ is short-lived. In this case the reaction would appear to violate strangeness. If c_P of Ξ^- is $+1$ the emitted K^+ is long-lived. In this case the final K amplitude in the production process

$$(\text{ordinary particles}) \to \Xi^- + K^+ + K^+$$

has the form $c_S(K_S^+ K_S^+) + c_A(K_A^+ K_A^+)$, and it would sometimes lead to apparent violation of the strangeness rule. If c_P of Ξ^- is -1 the final K amplitude has the form $c_{SA}(K_S^+ K_A^+)$, and it would practically always lead to apparent violation of the strangeness. From present evidence [8]) we would

be led to assume $c_P = +1$ for Ξ^-. In the decay of Ξ^- the produced Λ^0 could be sometimes long-lived and sometimes short-lived. If the shorter lifetime were such as to give no visible track the event would simulate

$$\Xi^- \to \pi^- + (\Lambda^0 \text{ decay products}).$$

The experimental upper limits on the shorter K^+ lifetime will depend of course on the assumed abundance of short-lived K^+. However, in this theory short-lived and long-lived particles are produced in the same abundance. To see this point in a simple way, consider the production of K^+ without observing the Σ. The $K_+{}^+$ and the $K_-{}^+$ are produced incoherently. Therefore there are two amplitudes, one for $K_+{}^+$ and one for $K_-{}^+$, which are incoherent. Both amplitudes contain the same number of $K_S{}^+$ and $K_A{}^+$. From present data it would seem that the theory could be made consistent with a K lifetime $\leqq 10^{-14}$ to 10^{-13} sec, but it is difficult to obtain reliable estimates. The couplings responsible for such decays would therefore be rather larger than generally assumed for the weak decay interactions, and this could constitute a theoretical difficulty. Moreover, we must discuss the mathematical conditions for the consistency of the solution. We shall see that in order for the solution to be consistent the weak interactions must satisfy rather stringent conditions, and we shall derive the relevant result that the short-lived particles must always decay into neutrino modes.

We decompose the diagonal matrix elements of Λ into two parts, separating the contributions due to neutrino interactions from the remaining contributions due to the parity-conserving interactions. We thus write

$$\Gamma_+ + i\Delta_+ = (V + W_+) + i(M + N_+),$$
$$\Gamma_- + i\Delta_- = (V + W_-) + i(M + N_-),$$

where V and M are the contributions from neutrino interactions. The non-diagonal matrix element $\Gamma_\times + i\Delta_\times$ is entirely due to neutrino interactions; it must be noted that $V \geqq \Gamma_\times$. For the two physical states, $s_1 = N^{-\frac{1}{2}}(qs_+ + s_-)$ and $s_2 = N^{-\frac{1}{2}}(s_+ - qs_-)$, we can calculate the total rate for decay into non-neutrino final states with parity $+$, which we call $w(s|+)$, and the total rate for decay into non-neutrino final states with parity $-$, $w(s|-)$. These rates are given by

$$w(s|+) = N^{-1}|q|^2 W_+,$$
$$w(s|-) = N^{-1} W_-,$$
$$w(s|\nu) = N^{-1}[(1+|q|^2)V + 2\mathrm{Re}\,(q)\Gamma_\times],$$

and by

$$w(s_2|+) = N^{-1} W_+$$
$$w(s_2|-) = N^{-1}|q|^2 W_-$$
$$W(s_2|\nu) = N^{-1}[(1+|q|^2)V - 2\mathrm{Re}\,(q)\Gamma_\times].$$

From these quantities we can obtain the quantities that are relevant for our discussion, namely the branching ratios between neutrino modes and parity-conserving modes for s_1 and s_2, B_1 and B_2 respectively, and the lifetime ratio τ_2/τ_1:

$$B_1 = \frac{(1+|q|^2)V+2\,\mathrm{Re}\,(q)\Gamma_\times}{|q|^2W_+ + W_-}, \tag{22}$$

$$B_2 = \frac{(1+|q|^2)V-2\,\mathrm{Re}\,(q)\Gamma_\times}{W_+ + |q|^2 W_-}, \tag{22'}$$

$$\frac{\tau_2}{\tau_1} = \frac{\mathrm{Re}\,(\lambda_1)}{\mathrm{Re}\,(\lambda_2)} = \frac{W_+ + |q|^2 W_- + (1+|q|^2)V - 2\,\mathrm{Re}\,(q)\Gamma_\times}{|q|^2W_+ + W_- + (1+|q|^2)V + 2\,\mathrm{Re}\,(q)\Gamma_\times}. \tag{23}$$

The mixing parameter q can be expanded as

$$q = 1 + \frac{c_+ - c_-}{2c} + \mathrm{O}\left(\left(\frac{c_+ - c_-}{2c}\right)^2\right), \tag{24}$$

and the condition $q \approx 1$ thus means $|(c_+ - c_-)/2c|^2 \ll 1$. To be definite we assume s_2 long-lived and s_1 short-lived.

Let us first discuss the solution for the hyperons (Λ, Σ). We must simultaneously satisfy

$$\left|\frac{c_+ - c_-}{2c}\right| \ll 1, \tag{25}$$

which guarantees $q \approx 1$, and

$$\frac{\tau_2}{\tau_1} = \frac{W_+ + W_- + 2(V+\Gamma_\times)}{W_+ + W_- + 2(V-\Gamma_\times)} \gg 1, \tag{25'}$$

$$B_2 = \frac{2(V-\Gamma)}{W_+ + W_-} \ll 1. \tag{25''}$$

The last condition ensures that the branching ratio for neutrino modes of the observed component is small, as known experimentally. After eq. (25'') has been substituted into (25'), (25') can be written as

$$\frac{\tau_2}{\tau_1} = \frac{2(V+\Gamma_\times)}{W_+ + W_-} \gg 1, \tag{26}$$

and, comparing with (22), we find the important result

$$B_1 = \frac{\tau_2}{\tau_1} \gg 1, \tag{27}$$

which shows that the short-lived component essentially decays into neutrino modes. However, from eqs. (25'') and (26) we find

$$\frac{V-\Gamma}{V+\Gamma} = B_2 \frac{\tau_1}{\tau_2},$$

which would strongly suggest $V = \Gamma$ (or $V = -\Gamma$ if the long-lived is s_1). This equality, as shown by eq. (6), would strongly suggest the equality of the neutrino-mode amplitudes from s_+ and from s_-; we have already discussed this possible symmetry requirement. The conditions to be satisfied are now the inequality (26), in the form

$$\frac{\tau_2}{\tau_1} = \frac{4V}{W_+ + W_-} \gg 1, \tag{28}$$

and (25), which can be written as

$$\left| \frac{c_+ - c_-}{2c} \right| = \left| \frac{(W_+ - W_-) + i(N_+ - N_-)}{2(V + i\Delta)} \right| \ll 1. \tag{29}$$

These conditions are consistent, and by taking for instance $V \approx \Delta$, $W_+ \approx W_- \approx N_+ \approx N_-$, we find $|(c_+ - c_-)/2c| \approx \tau_2/\tau_1$, which would mean that the physical particles are very closely eigenstates of c_P, in agreement with the experimental conditions, as already discussed. We then find that for $V = \Gamma$ the branching ratio in neutrino modes for the long-lived component would be, from eq. (22′) and (24) and the last result on $|(c_+ - c_-)/2c|$,

$$B_2 \approx \frac{\tau_1}{\tau_2},$$

which would agree very well with the experimental results. We therefore see that for hyperons a rather consistent scheme can be constructed — at the following price, however: first we must admit an inequality like (28), which is not easy to understand theoretically and sounds rather unphysical; second, the short-lived component, according to (27), would mostly decay into neutrino modes, a situation that could give rise to peculiar observational consequences — because of conservation of nucleons another lepton (μ, e or ν) must be emitted in these decay modes.

For $K^{\pm}$ mesons we want again to satisfy conditions (25) and (25′); however, condition (25″) must be substituted by

$$B_2 \approx 1, \tag{30}$$

as known experimentally. From (30) and (25′) we are led to

$$\frac{V - \Gamma}{V + \Gamma} = \frac{1}{2} \frac{\tau_1}{\tau_2},$$

which again strongly indicates $V = \Gamma$. We therefore write for this case the conditions corresponding to (25′) and (25″) in the hyperon case in the form

$$\frac{\tau_2}{\tau_1} = \frac{W_+ + W_- + 4\Gamma}{W_+ + W_- + \left| \frac{c_+ - c_-}{2c} \right|^2 \Gamma} \gg 1, \tag{31}$$

$$B_2 = \frac{\left|\frac{c_+ - c_-}{2c}\right|^2 \Gamma}{W_+ + W_-} \approx 1. \tag{31'}$$

If eq. (31') is substituted into (31), (31) can be written as

$$\frac{\tau_2}{\tau_1} = \frac{2\Gamma}{W_+ + W_-} \gg 1. \tag{32}$$

Again, comparing with (22), we have

$$B_1 = 2\frac{\tau_2}{\tau_1} \gg 1,$$

which implies that the short-lived component must practically always decay into neutrino modes — this result follows in any case even if we do not assume $V = \Gamma$. The independent conditions to be satisfied are now the conditions similar to (29), (31'), and (32). The last two give

$$\left|\frac{c_+ - c_-}{2c}\right| = \sqrt{2\frac{\tau_1}{\tau_2}}, \tag{33}$$

which is sufficient to guarantee that K_1 and K_2 are close to eigenstates of c_P. Equation (32), like (28), seems very unphysical. Moreover, we note that (33) if different from the corresponding condition for the hyperons, essentially because of the square root in (33) — this difference is because we have assumed for the K mesons $B_2 \approx 1$ instead of $B_2 \ll 1$ as for the hyperons. This means that eq. (33) cannot be satisfied with the same choice $W \approx N$ as for the hyperons — in which case, using eq. (34) one obtains $|(c_+ - c_-)/2c| \leqq (\tau_1/\tau_2)$. It can be shown from eq. (34) that (33) can be satisfied only provided we have

$$\frac{|N_+| + |N_-|}{W_+ + W_-} > 2\frac{\tau_2}{\tau_1},$$

a condition which again is rather unphysical. An alternate possibility could be to assume that only some neutrino decay interactions, not observed for the long-lived K, are predominant. In any case, according to conservation of statistics and conservation of heavy particles, the predominantly neutrino decay modes of the short-lived particles must lead to at least two final leptons. One of these leptons would be expected to be a muon or an electron, at least in some cases. No cases of μ mesons or electrons coming out from stars have been reported. Direct mass measurements on the secondary tracks emerging from high-energy stars would generally fail to indentify μ mesons and electrons [9]). A systematic investigation carried out at Bristol on the nature of the particles emerging from stars [10]) was not in an ap-

propriate condition for identifying such mesons or electrons because of the low limit imposed on the velocity of the particles examined.

2.3. NEUTRAL K-MESONS

Other difficulties for this solution occur in connection with neutral K mesons. A parity-doublet theory would lead in general to four different states with four different lifetimes for the neutral K mesons. In the representation in which the strangeness S and the parity P are diagonal K_+^0, K_-^0, $\overline{K}_+^0$, $\overline{K}_-^0$ are the four basic states — these states do not in general have a definite lifetime. Since weak interactions do not conserve strangeness, the physical particles are linear combinations of K^0 and $\overline{K}^0$ states. States of both parities are present in these combinations because of the mixing produced by neutrino interactions. It will be convenient to use the representation with basic vectors

$$\begin{aligned} K_{++}^0 &= \frac{1}{\sqrt{2}}(K_+^0+\overline{K}_+^0), \quad K_{+-}^0 = \frac{1}{\sqrt{2}}(K_+^0-\overline{K}_+^0), \\ K_{-+}^0 &= \frac{1}{\sqrt{2}}(K_-^0+\overline{K}_-^0), \quad K_{--}^0 = \frac{1}{\sqrt{2}}(K_-^0-\overline{K}_-^0). \end{aligned} \tag{34}$$

On the basis of Lüders theorem, the assumption of time-reversal invariance is equivalent to the assumption of conservation of the quantum number $L = CP$. If a single K^0 is assumed, L conservation alone uniquely determines the physical particles in terms of K^0 and $\overline{K}^0$. The physical particles are in this case the two eigenstates of L,

$$\frac{1}{\sqrt{2}}(K^0+\overline{K}^0), \quad \frac{1}{\sqrt{2}}(K^0-\overline{K}^0).$$

These states are the eigenstates of L, with eigenvalue $+1$ and -1 respectively. In fact these states are eigenstates of L when there are no weak interactions, and as long as weak interactions are assumed to conserve L, they remain eigenstates of L, with eigenvalues $+1$ and -1 respectively, also after turning on the weak interactions. A system of two pions has $L = +1$, and therefore only the state with $L = +1$ can decay into two pions. By the same argument it follows that of the states (34), K_{++}^0 and K_{--}^0 are eigenstates of L with $L = +1$, and K_{+-}^0 and K_{-+}^0 are eigenstates of L with eigenvalue $L = -1$. Of the states (34) only K_{++}^0 and K_{--}^0 can decay into two pions. Conservation of L requires the physical states to be of the form

$$u_{++}K_{++}^0+u_{--}K_{--}^0 \qquad \text{with } L = 1, \tag{35}$$

$$u_{-+}K_{-+}^0+u_{+-}K_{+-}^0 \qquad \text{with } L = -1. \tag{35'}$$

There is no choice of the coefficients u which makes the states (35) and

(35′) eigenstates of c_P. The eigenstates of c_P can be expressed in terms of the basic vectors

$$K_S^0 = \frac{1}{\sqrt{2}}(K_+^0+K_-^0),\ K_A^0 = \frac{1}{\sqrt{2}}(K_+^0-K_-^0),\ \overline{K}_S^0 = \frac{1}{\sqrt{2}}(\overline{K}_+^0+\overline{K}_-^0),$$

$$\overline{K}_A = \frac{1}{\sqrt{2}}(\overline{K}_+^0-\overline{K}_-^0) \qquad (36)$$

as

$$c_S K_S^0+\bar{c}_S \overline{K}_S^0, \qquad \text{with } c_P = +1, \qquad (37)$$

$$c_A K_A^0+\bar{c}_A \overline{K}_A^0, \qquad \text{with } c_P = -1. \qquad (37')$$

A superposition of the form (35) or (35′) cannot be expressed in the form (37) or (37′), unless all the coefficients are zero. This result merely reflects the circumstance that L and c_P anticommute for strangeness odd. In fact, from the definition of the parity conjugation operator c_P, it follows that $c_P L-(-)^S L c_P = 0$.

In a Wigner-Weisskopf treatment the physical states (35) and (35′) are determined as eigensolutions of a non-Hermitian matrix $\Lambda = \Gamma+i\Delta$, where Γ is the contribution from the energy shell and Δ the contribution from outside the energy shell. In the representation with basic vectors (34) there are no matrix elements of Λ connecting the two subspaces with $L = +1$ and with $L = -1$. This follows from the assumed L conservation for the total Hamiltonian (which is equivalent, according to Lüders theorem, to time-reversal invariance). Therefore the eigenvalue problem is split into two separate eigenvalue problems, one in the $L = +1$ subspace (solutions of the form (35)) and one in the $L = -1$ subspace (solutions of the form (35′)). Moreover, the assumption of time-reversal invariance allows one to take all the matrix elements real, so that the matrix elements symmetric with respect to the first diagonal are equal. The solutions are thus of the form

$$K_1^0 = \frac{1}{\sqrt{F}}[fK_{++}^0+K_{--}^0], \qquad (38)$$

$$K_2^0 = \frac{1}{\sqrt{F}}[K_{++}^0-fK_{--}^0], \qquad (38')$$

$$K_3^0 = \frac{1}{\sqrt{G}}[gK_{-+}^0+K_{+-}^0], \qquad (38'')$$

$$K_4^0 = \frac{1}{\sqrt{G}}[K_{-+}^0-gK_{+-}^0], \qquad (38''')$$

where f and g are in general complex numbers, and $F = |f|^2+1$, $G = |g|^2+1$. The solutions K_1^0 and K_2^0 pertain to the eigenvalues $L = +1$, K_3^0 and

K_4^0 to $L = -1$. The states K_1^0 and K_2^0 can decay into two pions, while the states K_3^0 and K_4^0 cannot.

The states which at $t = 0$ represent a K_+^0 and a K_-^0 are respectively

$$K_+^0 \to \frac{1}{\sqrt{2}}\left[\frac{\sqrt{F}}{f^2+1}\,(fK_1^0\,e^{-\frac{1}{2}\lambda_1 t}+K_2^0\,e^{-\frac{1}{2}\lambda_2 t}) + \frac{\sqrt{G}}{g^2+1}\,(K_3^0\,e^{-\frac{1}{2}\lambda_3 t}-gK_4^0\,e^{-\frac{1}{2}\lambda_4 t})\right] e^{-i\mu t}, \qquad (39)$$

$$K_-^0 \to \frac{1}{\sqrt{2}}\left[\frac{\sqrt{F}}{f^2+1}\,(K_1^0\,e^{-\frac{1}{2}\lambda_1 t}-fK_2^0\,e^{-\frac{1}{2}\lambda_2 t}) + \frac{\sqrt{G}}{g^2+1}\,(gK_3^0\,e^{-\frac{1}{2}\lambda_3 t}+K_4^0\,e^{-\frac{1}{2}\lambda_4 t})\right] e^{-i\mu t}. \qquad (39')$$

The λ are the complex eigenvalues of the matrix Λ. The resulting decay curves are very complicate, containing exponential terms and oscillating terms. The behaviour of the solutions in the limiting case of predominant neutrino interactions is quite different from the behaviour for charged K. We have already remarked that, in contrast to the case of charged K, the eigensolutions (38)—(38‴) cannot be eigenstates of c_p (this holds in general). We must assume, as a result of the foregoing discussion, that the matrix elements from K_+ are the same, apart from sign, as those K_- for processes involving neutrinos. To be definite let us assume that the amplitudes from K_+ are equal to those from K_-. The eigenvalue problem in the $L = +1$ subspace is then the same as for the $L = -1$ subspace in this limit of predominant neutrino interactions. Therefore, we have $\lambda_1 = \lambda_3$, $\lambda_2 = \lambda_4$, and $f = g$ in the above eq. (40)—(40‴). Since two different lifetimes have already been observed in the K^0 beams we would be led to identify the two different lifetimes with those which are observed. We can show, however, that this solution is not in agreement with experiment, since it would lead to a large fraction of non- 2π decays of the short-lived component. The fraction of decay into 2π of the short-lived component can be calculated by considering that K_+^0 and K_-^0 are produced incoherently and noting that the solutions K_1^0 and K_2^0 are orthogonal and normalized to unity. We see from eqs. (39) and (39′) that, in the limiting case considered, at least one-half of the short-lived component does not decay into two pions. This is in apparent disagreement with experiment, considering that no confirmed evidence exists for the 2π decay of the long-lived component — the anomalous decay modes at times comparable to the shorter lifetimes are no more than about 10 %.

A general argument shows that the distortion of the solutions due to non-neutrino interactions cannot modify this condition, at least as long as

one wants to maintain the feature of approximate coincidence of the four lifetimes into two distinct lifetimes. From eqs. (39) and (39′) we see that the fraction of the short-lived K^0's in the incoherent K_+^0, K_-^0 beam that can decay into two pions is given by

$$\frac{1}{2}\frac{(|f|^2+1)^2}{|f^2+1|^2}, \tag{40}$$

and the fraction that cannot decay into two pions is given by

$$\frac{1}{2}\frac{(|g|^2+1)^2}{|g^2+1|^2}. \tag{41}$$

The condition on the Hermitian matrix Γ of being positive definite leads to the inequality

$$\frac{|f-f^*|^2}{(|f|^2+1)^2} < \frac{4\,\mathrm{Re}\,(\lambda_1)\,\mathrm{Re}\,(\lambda_2)}{[\mathrm{Re}\,(\lambda_1+\lambda_2)]^2+4[\mathrm{Im}(\lambda_1-\lambda_2)]^2}. \tag{42}$$

The right-hand side in (42) is less than $4(\tau_S/\tau_L)$, where τ_S is the shorter lifetime and τ_L the longer. According to present data τ_S/τ_L is less than 1/100. An inequality similar to (42) holds for g if one substitutes λ_3 and λ_4 for λ_1 and λ_2. If now we use the identity

$$\frac{1}{2}\frac{(|f|^2+1)^2}{|f^2+1|^2} = \frac{1}{2}\frac{(|f|^2+1)^2}{(|f|^2+1)^2-|f-f^*|^2}$$

and the similar indentity for (41), comparing with (42) and with the corresponding inequality for g, we find that both (40) and (41) are approximately equal to $\frac{1}{2}$ apart from terms smaller than $4(\tau_S/\tau_L) \approx 4/100$. Another difficulty in reconciling with a solution with essentially two lifetimes would occur if, in the associated production of Λ^0 with K^0 (not eigenstate of c_P in this theory) a high frequency of visible Λ^0 were found in association with the K^0 with shorter lifetime. Recent results at Columbia point in this direction.

3. Up-Down Asymmetries in Hyperon Decays

We now discuss the decay distribution in this theory, in particular the question of up-down asymmetries in hyperon decay. We shall see that a parity-doublet model with parity non-conservation in neutrino interactions and with parity conservation in other interactions leads to up-down asymmetries for hyperon decays, at least as long as there is sufficient parity mixing in the states representing the physical particles. The problem of the polarization of particles with parity-doublet structure has been discussed by Lee and Yang assuming parity conservation [11]). If parity is not conserved the density matrix has a more complicated structure because of

the parity mixing due to the weak interactions. Following Lee and Yang, we describe a particle with parity-doublet structure by a 4-component wave function

$$\psi(t) = \begin{bmatrix} \psi_+(t) \\ \psi_-(t) \end{bmatrix},$$

where ψ_+ and ψ_- refer to the even-parity and odd-parity states respectively, and each of them has two components describing spin up and spin down. The density matrix is given by

$$D(t) = \sum \psi(t)\psi^\dagger(t),$$

and it is written in the form

$$D(t) = \begin{bmatrix} D_+(t) & D_\times(t) \\ D_\times(t)^\dagger & D_-(t) \end{bmatrix}. \tag{43}$$

Under space inversion, $D_+(t)$ and $D_-(t)$ are invariant while $D_\times(t)$ and $D_\times(t)^\dagger$ change sign. Lee and Yang introduce the pseudovectors $\mathbf{P}_+(t)$ and $\mathbf{P}_-(t)$, the vectors $\mathbf{P}_r(t)$ and $\mathbf{P}_i(t)$, the scalars $I_+(t)$ and $I(t)$, and the pseudoscalars $I_r(t)$ and $I_i(t)$, defined by the relations

$$D_+(t) = \mathbf{P}_+(t) \cdot \boldsymbol{\sigma} + I_+(t), \tag{44}$$

$$D_-(t) = \mathbf{P}_-(t) \cdot \boldsymbol{\sigma} + I_-(t), \tag{44'}$$

$$D_\times(t) = D_r(t) + iD_i(t)$$
$$= (\mathbf{P}_r(t) + i\mathbf{P}_i(t)) \cdot \boldsymbol{\sigma} + (I_r(t) + I_i(t)). \tag{45}$$

The quantities $I_+(t)$ and $I_-(t)$ are the intensities, and $\mathbf{P}_+(t)/I_+(t)$ and $\mathbf{P}_-(t)/I_-(t)$ the polarization vectors for the particles with parity + and − respectively. The limitations that follow from the condition that $D(t)$ be positive definite are reported in the Lee-Yang paper. If the value of the density matrix at the instant of production, $D(0)$, is known, its values at times t later can be obtained by the Wigner-Weisskopf treatment of the decay interactions. In contrast to the case of parity conservation, $D_+(t)$ and $D_-(t)$ have a non-exponential time dependence, and they contain two exponential terms and an oscillating exponential term. We find

$$D_+(t) = \frac{1}{|q^2+1|^2}\left[|q|^2 E_1 \, e^{-\gamma_1 t} + 2 \, \mathrm{Re}(qE e^{i\delta t}) e^{-\frac{1}{2}(\gamma_1+\gamma_2)t} + E_2 \, e^{-\gamma_2 t}\right], \tag{46}$$

$$D_-(t) = \frac{1}{|q^2+1|^2}\left[E_1 e^{-\gamma_1 t} - 2 \, \mathrm{Re}\,(q^* E \, e^{i\delta t}) \, e^{-\frac{1}{2}(\gamma_1+\gamma_2)t} + |q|^2 E_2 \, e^{-\gamma_2 t}\right], \tag{46'}$$

$$D_\times(t) = \frac{1}{|q^2+1|^2}\left[qE_1 \, e^{-\gamma_1 t} - |q|^2 E e^{-\frac{1}{2}(\gamma_1+\gamma_2)t} \, e^{i\delta t} + E^\dagger \, e^{-\frac{1}{2}(\gamma_1+\gamma_2)t} \, e^{-i\delta t} - q^* E_2 \, e^{-\gamma_2 t}\right] \tag{46''}$$

with

$$E_1 = |q_2|^2 D_+(0)+qD_\times(0)+q^* D_\times(0)^\dagger+D_-(0), \tag{47}$$

$$E_2 = D_+(0)-q^* D_\times(0)-qD_\times(0)^\dagger+|q|^2 D_-(0), \tag{47'}$$

$$E = qD_+(0)-|q|^2 D_\times(0)+D_\times(0)^\dagger-q^* D_-(0). \tag{47''}$$

Equations (46) to (47'') completely specify the density matrix at time t once the two lifetimes, the mass difference, and the parity-mixing parameter q are known. From the density matrix each measurable probability can be derived. In particular, considering the decay of hyperons, the momentum distribution of the decay pion in the hyperon rest system can be written as

$$W(\mathbf{k}) = \xi+\boldsymbol{\eta}\cdot\mathbf{k}, \tag{48}$$

where ξ and $\boldsymbol{\eta}$ are expressed linearly through the elements of $D(t)$ [10].

For the hyperons emitted in the capture of K^- at rest, $\boldsymbol{\eta}$ is parallel to the hyperon momentum, thus giving a forward-backward asymmetry. However, in a production process from particles with kinetic energy, $\boldsymbol{\eta}$ has in general a component normal to the plane of production. Therefore both forward-backward asymmetries and up-down asymmetries are expected — even after the states of the other produced particles are summed over. Let us discuss in particular the case in which only the long-lived component (of Λ or of Σ) is observed. In this case, from eqs. (46'') and (47') (to be definite we take particle 2 as the long-lived), we have

$$D_\times(t) \to -\frac{q^*}{|q^2+1|^2}\, e^{-\gamma_2 t}[D_+(0)-q^* D_\times(0)-qD_\times{}^\dagger(0)+|q|^2 D_-(0)]. \tag{49}$$

The vector $\boldsymbol{\eta}$ expressing the average direction of $\mathbf{k}$ is of the form (constant) $\times$ $\mathbf{P}_r(t)+$(constant) $\times\mathbf{P}_i(t)$ [10]. The vectors $\mathbf{P}_r(t)$ and $\mathbf{P}_i(t)$ can be obtained from eqs. (48) and (49). From the invariance under rotations and reflections in the production process and from the invariance of the density matrix under c_p (we assume that the states of the other particles produced are not observed), $\boldsymbol{\eta}$ is found to have the form

$$\boldsymbol{\eta}=[\mathbf{P}(0)\ (1+|q|^2)-2\,\mathrm{Re}\ (q)\mathbf{P}_r(0)]\times[(\text{constant})\ \mathrm{Re}\ (q)+(\text{constant})\ \mathrm{Im}(q)], \tag{50}$$

where $\mathbf{P}(0) = \mathbf{P}_+(0) = \mathbf{P}_-(0)$ is a pseudovector normal to the production plane and the vector $\mathbf{P}_r(0)$ lies in the production plane. Equation (50) shows that both up-down asymmetries (except for forward direction) and forward-backward asymmetries occur. The only exceptional case would be $q = 0$, which corresponds to observing only one particle with definite parity.

4. Strangeness Duplication and Parity Doublets

If K_+ and K_- have all quantum numbers equal and differ only in the parity assignment, the minimum symmetry required for accounting of the

equality of their masses would be the invariance under parity conjugation [7]). Our discussion so far applies to the parity-conjugation model. One can note, however, that in Gell-Mann's theory I_3 conservation is equivalent to S conservation and therefore, as long as the I_3 assignment is maintained, one can very well reverse the S value for each particle (and accordingly modify the relation between Q and I_3) without introducing any forbidden reaction (single production, etc.). This freedom allows for a duplication of the number of strange particles — by introducing for each strange particle a particle with opposite S and the same I_3. In a recent paper Pais points out that by taking S pseudoscalar one can use this freedom for generating parity doublets [12]). Because P and S anticommute, the parity operator reverses the strangeness (however, it leaves I_3 unchanged), therefore invariance of the theory under P is sufficient for obtaining the equality of the masses. However, again owing to the anticommutation between P and S, the particles with definite strangeness have no definite parity. This theory is in some sense more economical than the parity-conjugation theory; in fact, no c_p invariance is needed. No forward-backward asymmetries are expected in this theory. Most of the discussion carried out so far for parity-conjugation invariance applies in a similar form to Pais' theory. The K^+ beam at time t after the production is a superposition of K_+^+ and K_-^+, or (changing the representation) of K^+ with $S = +1$ and of K^+ with $S = -1$. These latter, however, still cannot generate hyperons because of I_3 conservation. The only possibility allowed is again that with two very different lifetimes. Moreover, the long-lived particles must not generate short-lived particles in interaction, and the only way of obtaining such a situation is assuming that they are close to eigenstates of the strangeness, in which case the short-lived are also, corresponding to the opposite eigenvalue. This again means $q = +1$, and the physical realization would again be of the same kind as discussed for the parity-conjugation model.

The following differences must be noted however. First, in Pais' theory also the Ξ particles are doublets. Therefore there would be short-lived and long-lived Ξ. Short-lived are produced with short-lived, and long-lived with long-lived. Moreover, the Λ^0 emitted from the decay of the long-lived Ξ^- must again be long-lived if $\Delta S = \pm 1$ holds. Therefore the difficulties concerning Ξ-particles would be in part removed by acceptance of the Pais' formulation of parity-doublet theory. Second, since $L = CP$ and S commute in Pais' theory (they anticommute in the ordinary theory) it would not be impossible for the K^0 with definite L to have also definite S. However, we cannot give any argument showing that this occurs; it would in fact be quite accidental. Moreover, the limit of strong neutrino interactions would essentially lead to the same difficulties as for the Lee-Yang

parity-doublet theory. In particular, the present scheme for associated production of Λ^0+K^0 with one observed Λ^0 lifetime and two observed K^0 lifetimes occurring with about the same relative frequencies would not in general be fitted in this model. The arguments discussed in section 2 concerning the conditions imposed for the consistency of the solution would, moreover, still apply in exactly the same form.

5. Conclusion

We have examined in this discussion what modifications in the original $\tau-\theta$ problem are brought about by the recent discovery of parity non-conservation in neutrino interactions, and whether such modifications could permit avoidance of the conclusion that parity must be violated also in other weak interactions not involving neutrinos. We have, however, restricted our discussion to the usual description of neutrino interactions such that the observed neutrino processes occur as direct processes at first order in the weak neutrino coupling. Under this restriction our conclusion is negative. In fact, the only possible solutions would require at least two K mesons, and hence almost unavoidably general parity-doublet structures. Such models would appear in any case more complicated than models with parity non-conservation in weak non-neutrino interactions also. A detailed discussion of the possible cases shows that one solution could be constructed that can simulate the present experimental evidence strongly indicating single particles and single lifetimes [13]). According to this solution there would be short-lived and long-lived particles, which are described by states that very approximately are eigenstates of the parity conjugation operator in the Lee-Yang parity-doublet theory, or eigenstates of the strangeness in the parity-doublet theory recently suggested by Pais. Short-lived particles would be produced in association with short-lived, and long-lived with long-lived. Moreover, long-lived particles would for most experiments originate only long-lived particles after nuclear interaction. This solution can be constructed consistently if a (rather unphysical) predominance of the neutrino interactions is assumed with respect to the parity-conserving weak interactions, and the neutrino interactions are further assumed to satisfy some symmetry requirement with respect to exchange of the two parity states in the parity doublet. However, it is shown that the consistency of the solution requires very unphysical conditions on the decay interactions (large differences in the magnitudes of various matrix elements, strong energy dependences or different behaviour of various classes of neutrino interactions). It is shown that the decay of the short-lived particles would practically always occur into neutrino modes. A particular difficulty occurs in connection with the neutral K mesons, which do not fit the scheme properly. In the Lee-Yang form of parity doublets, the presence of the non-

observed forward-backward asymmetries and the non-doublet structure of the Ξ particle would constitute further difficulties. The model would lead to up-down asymmetries even if the interaction directly responsible for the observed hyperon decay conserved parity.

In conclusion, we feel that the unavoidable complication of the scheme, the unphysical conditions on the weak interactions required for its consistency, and some of the specific difficulties encountered — in particular the difficulty found in connection with neutral K mesons — already constitute a disproof of this model. Unfortunately the mere qualitative discovery of up-down asymmetries in hyperon decays would not directly exclude the model. Since a definite quantitative prediction of the model is that short-lived particles that decay rapidly into leptons must be produced with the same cross section as for production of the observed strange particles, any evidence against such processes would constitute a direct experimental disproof.

The author would like to acknowledge the useful discussions with Doctors F. Crawford, Jr., K. Gottstein, A. Rosenfeld, F. Solmitz, H. Ticho, and in particular, with Dr. M. Good. Moreover, he takes the opportunity for expressing his appreciation to Dr. D. Judd for the hospitality at the Theoretical Group of the Radiation Laboratory.

References

1) R. H. Dalitz, Proc. Rochester Conf. **8** (1956) 19
2) Wu, Ambler, Hayward, Hoppes, and Hudson, Phys. Rev. **105** (1957) 1413
3) Garwin, Lederman, and Weinrich, Phys. Rev. **105** (1957) 1415; Friedman and Telegdi, Phys. Rev. **105** (1957) 1681
4) T. D. Lee and C. N. Yang, Phys. Rev. **105** (1957) 1671; A. Salam, Nuovo Cimento **5** (1957) 299; L. Landau, Nuclear Physics **3** (1957) 127
5) S. B. Treiman and H. W. Wyld, Phys. Rev. (to be published)
6) T. D. Lee, R. Oehme, and C. N. Yang, Phys. Rev. **106** (1957) 340
7) T. D. Lee and C. N. Yang, Phys. Rev. **102** (1956) 290
8) G. H. Trilling and A. Neugenbauer, Phys. Rev. **104** (1956) 1688
9) Daniel, Davies, Mulvey and Perkins, Phil. Mag. **43** (1952) 753
10) Dahanake, François, Fujimoto, Iredale, Waddington and Yasin, Phil. Mag. **45** (1954) 885
11) T. D. Lee and C. N. Yang, Phys. Rev. **104** (1956) 822
12) A. Pais, A suggestion concerning the reflection properties of hyperons and K-mesons (unpublished manuscript)
13) Eisler, Plano, Samios, Schwartz and Steinberger, Phys. Rev. **107** (1957) 324

Nuclear Physics **5** (1958) 256—270; © *North-Holland Publishing Co., Amsterdam*
Not to be reproduced by photoprint or microfilm without written permission from the publisher

PHOTOPRODUCTION OF MESONS ON NUCLEONS: PHASE SHIFT ANALYSIS AND DISPERSION RELATIONS

L. D. SOLOVYOV
Moscow State University, U.S.S.R.

Received 14 June 1957

Abstract: A phase shift analysis of the dispersion relations obtained in ref. [1]) for photoproduction of mesons is carried out. It is assumed that the integrals in the dispersion relations converge with sufficient rapidity.

The dependence of the photoproduction amplitude on the spin and isobaric variables and also the relation between the photoproduction and scattering amplitudes which follows from the unitary condition are considered. The range of unobservable angles, $\cos\theta < -1$, in the dispersion relations is examined in the c.m.s.

Phase shift analysis of the photoproduction amplitude is investigated and dispersion relations for partial waves have been obtained on the assumption of rapid convergence of the integrals. In this case the equations for S and P waves have been completely determined in the first approximation differing from the static one (that is, to terms of the order of μ/m).

1. Spin Structure of the Photoproduction Amplitude

The matrix element of the transition R-matrix corresponding to photoproduction of a meson on a nucleon can be written, on the basis of translational invariance considerations, in the following form [1]):

$$\langle\pi|R|\gamma\rangle = \frac{i(2\pi)^4}{\sqrt{4k^0q^0}}\delta(p_1+q-p-k)M. \tag{1}$$

Here k, q, p and p_1 are respectively the 4-momenta of the photon, meson and initial and final nucleons. The dependence of M on the spin variables of the final and initial nucleons can also be obtained from general considerations. In fact, the conditions of relativistic and gradient invariance yield 4 independent spin operators η_i, in terms of which M can be expanded [2]):

$$M = \sum_{i=1}^{4} A_i\eta_i. \tag{2}$$

In the c.m.s. ($\mathbf{p}+\mathbf{k} = \mathbf{p}_1+\mathbf{q} = 0$) we have in this case [1])

$$\begin{aligned}\eta_1 &= i(\boldsymbol{\sigma}\cdot\boldsymbol{\pi}'), \quad \eta_2(\theta) = |\mathbf{k}|^{-1}|\mathbf{q}|^{-1}(\boldsymbol{\sigma}\cdot\mathbf{q})(\boldsymbol{\sigma}\cdot[\mathbf{k}\wedge\boldsymbol{\pi}']),\\ \eta_3(\theta) &= i|\mathbf{k}|^{-1}|\mathbf{q}|^{-1}(\boldsymbol{\sigma}\cdot\mathbf{k})(\mathbf{q}\cdot\boldsymbol{\pi}'); \quad \eta_4(\theta) = i|\mathbf{q}|^{-2}(\boldsymbol{\sigma}\cdot\mathbf{q})(\mathbf{q}\cdot\boldsymbol{\pi}').\end{aligned} \tag{2a}$$

$\boldsymbol{\pi}'$ is the photon polarization vector. A_i depends on the meson and nucleon

isobaric variables, cosine of the scattering angle, $|\mathbf{k}|^{-1}|\mathbf{q}|^{-1}(\mathbf{k}\cdot\mathbf{q}) = \cos\theta = x$ and energy of the system, $w = p^0+k^0 = p_1{}^0+q^0$.

2. Isobaric Structure

Since it is the isobaric matrix combinations τ_ϱ, $\frac{1}{2}(1+\tau_3)$, which enter the photon-nucleon-meson interaction, the dependence of A_i on the charge variables can be represented in the form

$$A_i = \delta_{\varrho 3} A_i^{(1)} + \tau_\varrho A_i^{(2)} + \tfrac{1}{2}[\tau_\varrho, \tau_3] A_i^{(3)}. \tag{3}$$

Here ϱ is the meson production charge variable; $\varrho = 1, 2, 3$. The final and initial nucleon charge states are characterized by the τ-matrix subscripts. For this choice of the charge variables the π^+, π^0 and π^- meson isobaric functions will have the form

$$\pi^+ = -\frac{1}{\sqrt{2}}(\delta_{\varrho 1}+i\delta_{\varrho 2});\ \pi^0 = \delta_{\varrho 3};\ \pi^- = \frac{1}{\sqrt{2}}(\delta_{\varrho 1}-i\delta_{\varrho 2}) \tag{4}$$

and for a proton and a neutron

$$\mathrm{p} = \begin{pmatrix}1\\0\end{pmatrix};\qquad \mathrm{n} = \begin{pmatrix}0\\1\end{pmatrix}. \tag{4a}$$

In order to change from $A_i^{(\lambda)}$ to quantities which describe photoproduction processes:

$$A_i(\pi^0):\ \gamma+\mathrm{p}\to\mathrm{p}+\pi^0;\quad A_i(\mathrm{n}\pi^0):\ \gamma+\mathrm{n}\to\mathrm{n}+\pi^0;$$
$$A_i(\pi^+):\ \gamma+\mathrm{p}\to\mathrm{n}+\pi^+;\quad A_i(\pi^-):\ \gamma+\mathrm{n}\to\mathrm{p}+\pi^-,$$

it is sufficient to multiply (3) from the left and right by the isobaric functions of the respective states. Thus multiplying (3) from the left by $(\mathrm{p}\pi^0)^*$ and from the right by p we get

$$A_i(\pi^0) = A_i^{(1)}+A_i^{(2)}.$$

Similarly

$$A_i(\mathrm{n}\pi^0) = A_i^{(1)}-A_i^{(2)},\quad A_i(\pi^+) = -\sqrt{2}\,(A_i^{(2)}+A_i^{(3)}),$$
$$A_i(\pi^-) = \sqrt{2}\,(A_i^{(2)}-A_i^{(3)}). \tag{5}$$

The final states can be classified by assuming a total isobaric spin I. Then [3]), $A_i^{(\lambda)}$ $(\lambda = 1, 2, 3)$ are related to $A_i^{(I)}(I = \frac{1}{2}, \mathrm{S}, \frac{3}{2})(A_i^{(\frac{1}{2})}$ and $A_i^{(\mathrm{S})}$ correspondingly describe "vector" and "scalar" transitions to a state with $I = \frac{1}{2}$ and $A_i^{(3/2)}$ pertains to a "vector" transition to a state with $I = \frac{3}{2}$) in the following way:

$$A_i^{(\frac{1}{2})} = A_i^{(1)}+2A_i^{(3)},\quad A_i^{(\mathrm{S})} = A_i^{(2)},\quad A_i^{(3/2)} = A_i^{(1)}-A_i^{(3)}. \tag{6}$$

Thus instead of (3) one may also write

$$A_i = \sum_{I=\frac{1}{2},\,\mathrm{S},\,3/2} A_i^{(I)}\,P_\gamma^{(I)} \tag{7}$$

where the projection operators $P_\gamma^{(I)}$ are

$$P_\gamma^{(\frac{1}{2})} = \tfrac{1}{3}\tau_\varrho\tau_3; \quad P_\gamma^{(S)} = \tau_\varrho; \quad P_\gamma^{(3/2)} = \delta_{\varrho 3} - \tfrac{1}{3}\tau_\varrho\tau_3. \tag{7a}$$

3. Dispersion Relations and Unitarity Condition

The quantities $A_i^{(\lambda)}$ as functions of energy satisfy the dispersion relations. In ref. [1]) disperion relations were derived form quantities $\mathcal{M}_\lambda^i$ which were proportional to the $A_i^{(\lambda)}$:

$$\begin{aligned}
\mathcal{M}_\lambda^1 &= \frac{1}{w-m}\left[\frac{4E_kE_q}{(E_k+m)(E_q+m)}\right]^{\frac{1}{2}} A_1^{(\lambda)},\\
\mathcal{M}_\lambda^2 &= \frac{1}{q(w-m)}\left[\frac{4E_kE_q(E_q+m)}{E_k+m}\right]^{\frac{1}{2}} A_2^{(\lambda)},\\
\mathcal{M}_\lambda^3 &= \frac{1}{q(w-m)}\left[\frac{4E_kE_q}{(E_k+m)(E_q+m)}\right]^{\frac{1}{2}} A_3^{(\lambda)},\\
\mathcal{M}_\lambda^4 &= \frac{1}{q^2(w-m)}\left[\frac{4E_kE_q(E_q+m)}{E_k+m}\right]^{\frac{1}{2}} A_4^{(\lambda)}.
\end{aligned} \tag{8}$$

Here and further m designates the nucleon mass and μ the meson mass,

$$q = |\mathbf{q}| = \frac{1}{2w}[(w^2-m^2-\mu^2)^2-4m^2\mu^2]^{\frac{1}{2}}, \quad k = |\mathbf{k}| = \frac{1}{2w}(w^2-m^2),$$
$$E_q = (q^2+m^2)^{\frac{1}{2}}, \quad \omega = (q^2+\mu^2)^{\frac{1}{2}}. \tag{9}$$

In the c.m.s. the dispersion relations have the form

$$\operatorname{Re} A_i^{(\lambda)}(w, \nu_1) = \mathring{A}_i^{(\lambda)}(w, \nu_1) + \frac{1}{\pi}\mathrm{P}\int_{m+\mu}^{\infty} \mathrm{d}w' \sum_{i'=1}^{4} f_{ii'}^{(\lambda)}(w, w', \nu_1) \operatorname{Im} A_{i'}^{(\lambda)}(w,' \nu_1) \tag{10}$$

if the integrals in the right hand side converge for large w'. Here ν_1 is an invariant parameter related to x and ω by the equation

$$2m\nu_1 = k(\omega - qx); \tag{11}$$

$f_{ii'}^{(\lambda)}$ and $\mathring{A}_i^{(\lambda)}$ are known functions: they can easily be obtained from the corresponding functions for $\mathcal{M}_\lambda^i$ (eqs. (2.8)—(2.15) of ref. [1]), by employing eq. (8). They are presented in appendix B with an accuracy to $1/m$.

Relations (10) were obtained under the condition that

$$2m\nu_1 = k(\omega - qx) < m\mu + \tfrac{1}{2}\mu^2 \tag{12}$$

or, with account of (9),

$$x > \frac{(w^2-m^2)(w^2-m^2+\mu^2) - 4w^2(m\mu+\frac{1}{2}\mu^2)}{(w^2-m^2)[(w^2-m^2-\mu^2)^2-4m^2\mu^2]^{\frac{1}{2}}}; \tag{12a}$$

thus, only those values of x in (10) are permissible which lie above the

curve shown in fig. 1. We see that every possible value of x is permissible only if

$$m+\mu \leqq w \lesssim m+3\mu.$$

The twelve relations in (10) relate 24 real functions. Twelve other relations which are corollaries of the unitarity condition should be added. In the

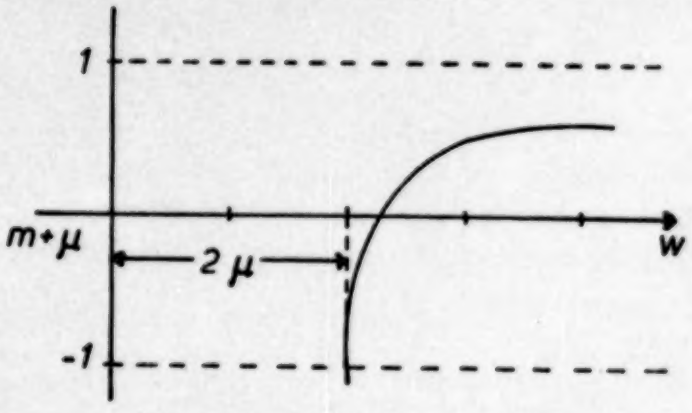

Fig. 1. (Explanation in the text).

lowest electron charge and single-meson approximation the unitarity condition yields a relation between $A_i^{(I)}$ and the $B_i^{(I)}$ which describe elastic scattering of mesons on nucleons. It is shown in appendix A that these relations have the form

$$\begin{aligned}
\text{Im } A_1^{(I)}(x) &= \frac{qE_q}{(4\pi)^2 w}\int d\Omega'\{[B_1^{(I)}(z)+f_1 x B_2^{(I)}(z)]\dot{A}_1^{(I)}(y) \\
&\quad + [B_1^{(I)}(z)-zB_2^{(I)}(z)][f_1\dot{A}_2^{(I)}(y)+b^2\sin^2\theta\dot{A}_4^{(I)}(y)]\}, \\
\text{Im } A_2^{(I)}(x) &= \frac{qE_q}{(4\pi)^2 w}\int d\Omega'\{f_1 B_2^{(I)}(z)\dot{A}_1^{(I)}(y)+[aB_1^{(I)}(z)+f_2 B_2^{(I)}(z)]\dot{A}_2^{(I)}(y) \\
&\quad + b^2\sin^2\theta\, B_2^{(I)}(z)\dot{A}_3^{(I)}(y)\}, \\
\text{Im } A_3^{(I)}(x) &= \frac{qE_q}{(4\pi)^2 w}\int d\Omega'\{[aB_1^{(I)}(z)+(af_1 x-b^2)B_2^{(I)}(z)]\dot{A}_3^{(I)}(y) \\
&\quad + (b^2 x-af_1)[B_1^{(I)}(z)-zB_2^{(I)}(z)]\dot{A}_4^{(I)}(y)\}, \\
\text{Im } A_4^{(I)}(x) &= \frac{qE_q}{(4\pi)^2 w}\int d\Omega'\{(b^2 x-af_1)B_2^{(I)}(z)\dot{A}_3^{(I)}(y) \\
&\quad + [(a^2-b^2)B_1^{(I)}(z)+(b^2 z+af_2)B_2^{(I)}(z)]\dot{A}_4^{(I)}(y)\}.
\end{aligned} \tag{13}$$

Here

$$I = \tfrac{1}{2},\ \mathrm{S},\ \tfrac{3}{2}; \qquad B_i^{(\mathrm{S})} \equiv B_i^{(\frac{1}{2})};$$
$$x = \cos\theta, \quad y = \cos\theta', \quad z = \cos\alpha;$$

θ is the angle between the momenta of the photon and final meson, θ' the angle between the momenta of the photon and intermediate meson and

α is the angle between the momenta of the intermediate and final mesons. Integration is carried out with respect to the directions of the intermediate meson momentum. Moreover,

$$a = \frac{\sin\theta'}{\sin\theta}\cos\varphi', \quad b = \frac{\sin\theta'}{\sin\theta}\sin\varphi',$$
$$f_1 = a\cos\theta - \cos\theta', \quad f_2 = 1 - a\cos\alpha, \tag{13a}$$
$$\cos\alpha = \cos\theta\cos\theta' + \sin\theta\sin\theta'\cos\varphi'.$$

The single-meson approximation employed in the deduction of (13) implies that the energies are smaller than the energies at which appreciable meson pair formation occurs; in other words these energies should not significantly contribute to the integrals in (10) or the integrals should converge with sufficient rapidity.

4. Unobservable Region

Consider the relations (10). They can be conveniently rewritten as follows:

$$\operatorname{Re} A_i^{(\lambda)}(w, x) = \overset{\circ}{A}{}_i^{(\lambda)}(w, x) + \frac{1}{\pi}\,\mathrm{P}\int_{m+\mu}^{\infty} dw' \sum_{i'=1}^{4} f_{ii'}^{(\lambda)}(w, w', x)\operatorname{Im} A_{i'}^{(\lambda)}(w', x'), \tag{14}$$

where the cosine of the new angle x' is related to x by the condition of constancy of ν_1:

$$2m\nu_1 = k(\omega - qx) = k'(\omega' - q'x'). \tag{15}$$

Thus for a fixed ν_1, x' is a function of w'. We shall consider its behaviour. It will be convenient to relate w' to the energy E' in a system in which $\mathbf{p}+\mathbf{p}_1 = 0$ (p-system). Writing the invariant $k(p+p_1)$ in the c.m.s. and p-system we get

$$w'^2 = 2E'E_p + 2|\mathbf{p}|E_n + m^2 \tag{16}$$

where $E_n = (\mathbf{p}^2 + \frac{1}{4}\mu^2)/|\mathbf{p}|$ is the boundary of the region of observable energies in the p-system, $E_p = (\mathbf{p}^2 + m^2)^{\frac{1}{2}}$, $\mathbf{p}$ is the nucleon momentum in the p-system and is related to ν_1 by the equation

$$2m\nu_1 = 2\mathbf{p}^2 + \tfrac{1}{2}\mu^2. \tag{17}$$

We now have, for $w' \to \infty$,

$$x' = \frac{1}{q'}\left(\omega' - \frac{2m\nu_1}{k'}\right) \to 1. \tag{18}$$

For $E' = E_n$,

$$w'^2 = 2E_n(E_p + |\mathbf{p}|) + m^2,$$

and hence with account of (9) we obtain

$$x' = -1. \tag{19}$$

The latter result can readily be illustrated as follows (see fig. 2):

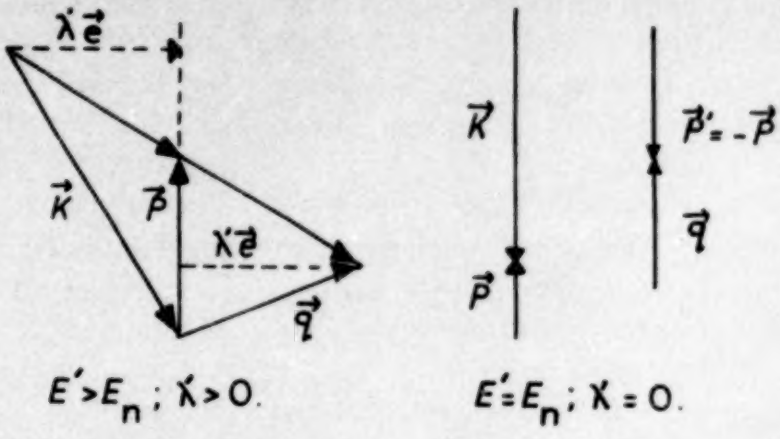

Fig. 2. Particle momenta in p-system.

For $E' = E_n$,

$$\lambda' = \sqrt{E'^2 - E_n^2} = 0$$

and the momenta of all particles in the p-system are directed along a straight line. In order to change to the c.m.s. it is sufficient to move along this straight line. This movement will not change the mutual orientation of **k** and **q**. Thus for fixed values of ν_1 and $E' = E_n$ the angle between **k** and **q** will equal π in the p-system as well as in the c.m.s., and $x' = -1$.

For $E' = E_1$ (integration boundary in p-system),

$$w' = m + \mu, \; q' = 0 \text{ and } x' = -\infty.$$

Thus a region of unobservable angles

$$-\infty < x' < -1 \tag{20}$$

in the c.m.s corresponds to a region of unobservable energies in the p-system, $E_1 < E' < E_n$ (just as in the case of scattering of mesons [5])).

In order to assess this region, the analytical properties of $A_i^{(\lambda)}(w, x')$ with respect to x' should be known.

5. Expansion in Partial Waves

By using the usual quantal procedure of phase shift analysis the dependence of $A_i^{(\lambda)}(w, x)$ on x can be represented as a series in Legendre polynomials. This method yields the following expression for the spin matrix elements of the photoproduction amplitude:

$$M_{s's} = \sum_{\mathcal{J}, L, l} \sum_{p=0,1} i^{L-l+p} (\pi/2)^{\frac{1}{2}} (2L+1)^{\frac{1}{2}} \nu^p$$
$$\times C_{L,\frac{1}{2}}(\mathcal{J}, M; \nu, s) C_{l,\frac{1}{2}}(\mathcal{J}, M; M-s', s') Y_{l,M-s'}(\Omega) R_{\mathcal{J}}(l; L, p). \tag{21}$$

Here $\mathcal{J}$ is the total angular momentum of the system, M is its projection,

L and l are the photon and meson angular momenta respectively; $p = 0(1)$ corresponds to a magnetic (electric)photon; $\nu = \pm 1$ is the photon circular polarization; C are Clebsch-Gordan coefficients.

The physical meaning of formula (21) is very simple. The first coefficient $C_{L,\frac{1}{2}}(\mathcal{J}, M; \nu, s)$ determines the probability that two particles with angular momenta L and $\frac{1}{2}$ and their projections ν and s combine to form a system with a total momentum $\mathcal{J}$ and its projection M. The second coefficient $C_{l,\frac{1}{2}}(\mathcal{J}, M; M-s', s')$ determines the probability of decay of the system into two particles with angular momenta l, $\frac{1}{2}$ and their projections $M-s$ and s' respectively. $Y_{l,M-s'}(\Omega)$ determines the probability that one of the particles (possessing an angular momentum l) will be emitted at an angle Ω with respect to the direction of motion of one of the initial particles. These probabilities are purely kinematic. The probability that a given photon, nucleon and meson were involved in the described processes are determined by the coefficient $R_{\mathcal{J}}(l; L, p)$.

We are considering a purely inelastic process and therefore the $R_{\mathcal{J}}$ should obey a definite selection rule with respect to parity.

Indeed, a Feynman diagram with a single photon line corresponds to this process. This is a process of lowest order with respect to the fine structure constant. In this case the transition amplitude is proportional to $\int \psi_f^* (\mathbf{j} \cdot \mathbf{A}) \psi_i \, d\tau$ where ψ_f is the nucleon + meson wave function, ψ_i is the wave function of the initial nucleon, $\mathbf{A}$ is the vector potential of the electromagnetic field; its parity is $(-1)^{L+p}$ and hence the parity of $\mathbf{j} \cdot \mathbf{A}$ ($\mathbf{j}$ is the nucleon current) is $-(-1)^{L+p}$.

By definition, the nucleon is even, that is, ψ_i is even and the parity of ψ_f equals that of a meson of angular momentum l that is, $-(-1)^l$.

Thus the transition amplitude does not vanish only if $(-1)^l = (-1)^{L+p}$, that is,

$$R_{\mathcal{J}}(l; l \pm 1, 0) = 0 \text{ and } R_{\mathcal{J}}(l; l, 1) = 0.$$

For non-vanishing coefficients $R_{\mathcal{J}}$ we introduce the notations

$$\begin{aligned} M_{l,\pm} &= -i[4l(l+1)]^{-\frac{1}{2}} R_{l\pm\frac{1}{2}}(l; l, 0); \quad l = 1, 2, 3, \ldots \\ E_{l,+} &= i[4(l+1)(l+2)]^{-\frac{1}{2}} R_{l+\frac{1}{2}}(l; l+1, 1); \quad l = 0, 1, 2, \ldots \\ E_{l,-} &= i[4(l-1)l]^{-\frac{1}{2}} R_{l-\frac{1}{2}}(l; l-1, 1); \quad l = 2, 3, \ldots \end{aligned} \tag{22}$$

The isobaric structure of $M_{l,\pm}$, $E_{l,\pm}$ is, of course, the same as that of A_i. Relations (1), (5) and (6) remain valid if A_i in them are replaced by $M_{l,\pm}$ or $E_{l,\pm}$.

Comparing the expressions of $M_{s's}$ in (21) and (2), (2a) we find

$$
\begin{aligned}
&M_{\frac{1}{2},\frac{1}{2}}\colon\ A_3+A_4x=-\sum_{l=1}^{\infty}\{(l+2)[M_{l,+}-E_{l,+}]+(l-1)[M_{l,-}+E_{l,-}]\}P_l'(x);\\
&M_{\frac{1}{2},-\frac{1}{2}}\colon\ 2A_1-2A_2x+A_4(1-x^2)\\
&\quad=\sum_{l=0}^{\infty}\{(l+1)[lM_{l,+}+(l+2)E_{l,+}]-l[(l+1)M_{l,-}-(l-1)E_{l,-}]\}P_l(x);\\
&M_{-\frac{1}{2},\frac{1}{2}}\colon\ A_4=\sum_{l=2}^{\infty}[M_{l,+}-E_{l,+}-M_{l,-}-E_{l,-}]P_l''(x);\\
&M_{-\frac{1}{2},-\frac{1}{2}}\colon\ 2A_2+A_3+A_4x=\sum_{l=1}^{\infty}[lM_{l,+}+(l+2)E_{l,+}\\
&\qquad\qquad+(l+1)M_{l,-}-(l-1)E_{l,-}]P_l'(x).
\end{aligned}
\tag{23}
$$

Here P_l, P_l' and P_l'' are a Legendre polynomial and its derivatives which satisfy the following orthogonality conditions:

$$
\int_{-1}^{1}\frac{\mathrm{d}^m P_l(x)}{\mathrm{d}x^m}\frac{\mathrm{d}^m P_{l'}(x)}{\mathrm{d}x^m}(1-x^2)^m\,\mathrm{d}x=\frac{2}{2l+1}\frac{(l+m)!}{(l-m)!}\delta_{l,l'};\ m=0,\,1,\,2,\ldots \tag{24}
$$

which permit one to express $M_{l,\pm}$ and $E_{l,\pm}$ in terms of A_i. It is convenient to introduce the notations

$$
\begin{gathered}
M_{l,1}\equiv M_{l,-}-M_{l,+},\quad M_{l,2}\equiv(l+1)M_{l,+}+lM_{l,-},\\
M_{l,3}\equiv E_{l,+},\quad M_{l,4}\equiv E_{l,-}.
\end{gathered}
\tag{25}
$$

Then

$$
M_{l,i}=\int_{-1}^{1}\mathscr{P}_{l,i}[A_j]\mathrm{d}x;\quad i=1,\,2,\,3,\,4 \tag{26}
$$

where the linear operators $\mathscr{P}_{l,i}[A_j]$ have the form

$$
\begin{aligned}
&\mathscr{P}_{l,1}[A_j]=\frac{2l+1}{2l(l+1)}\left[-P_l(x)A_1+\frac{lxP_l(x)+P_{l-1}(x)}{l+1}A_2+\frac{(1-x^2)P'_l(x)}{l(l+1)}A_3\right],\\
&\mathscr{P}_{l,2}[A_j]=\frac{2l+1}{2l(l+1)}(1-x^2)P_l'(x)A_2,\\
&\mathscr{P}_{l,3}[A_j]=\frac{1}{2(l+1)}\left\{P_l(x)A_1-P_{l+1}(x)A_2+(1-x^2)\left[\frac{P'_l(x)}{l+1}A_3+\frac{P'_{l+1}(x)}{l+2}A_4\right]\right\},\\
&\mathscr{P}_{l,4}[A_j]=\frac{1}{2l}\left\{P_l(x)A_1-P_{l-1}(x)A_2-(1-x^2)\left[\frac{P'_l(x)}{l}A_3+\frac{P'_{l-1}(x)}{l-1}A_4\right]\right\}.
\end{aligned}
\tag{26a}
$$

Finally, solving equations (23) with respect to A_i we find

$$
\begin{aligned}
&A_1=\sum_{l=0}^{\infty}\{-[l^2P_l(x)-P'_{l-1}(x)]M_{l,1}+xP'_l(x)M_{l,2}+P'_{l+1}(x)M_{l,3}+P'_{l-1}(x)M_{l,4}\},\\
&A_2=\sum_{l=1}^{\infty}P'_l(x)M_{l,2},\\
&A_3=\sum_{l=1}^{\infty}\{[lP'_l(x)+P''_{l-1}(x)]M_{l,1}-P'_l(x)M_{l,2}+P''_{l+1}(x)M_{l,3}+P''_{l-1}(x)M_{l,4}\},\\
&A_4=-\sum_{l=2}^{\infty}[M_{l,1}+M_{l,3}+M_{l,4}]P''_l(x).
\end{aligned}
\tag{27}
$$

6. Dispersion Relations for Partial Waves

Assume now that the infinite series in (27) can be broken off. The higher harmonics are relatively effective only for high energies and if the integrals in the dispersion relations converge with sufficient rapidity finite sums can be considered instead of the series (27). But then $A_i(w', x')$ is simply a polynomial in x', defined for all x' including those in the unobservable region (20). Furthermore, the restriction (12a) is also invalid now since the left and right hand sides of the dispersion relations contain analytical functions of x.

For sufficiently rapid convergence of the integrals in (14) the angles can be excluded and dispersion relations for $M_{l,i}(w)$ can be written. From (26) we have

$$\operatorname{Re} M^{(\lambda)}_{l;i}(w) = \int_{-1}^{1} \mathscr{P}_{l,i}[\operatorname{Re} A_j^{(\lambda)}]\mathrm{d}x = \int_{-1}^{1} \mathscr{P}_{l,i}[\mathring{A}_j^{(\lambda)}]\mathrm{d}x + \frac{\mathrm{P}}{\pi}\int_{m+\mu}^{\infty}\mathrm{d}w' \int \mathscr{P}_{l,i}[\sum_{i'} f^{(\lambda)}_{ji'} \operatorname{Im} A^{(\lambda)}_{i'}(w', x')]\mathrm{d}x.$$

Expressing $A^{(\lambda)}_{i'}(w', x')$ through $M^{(\lambda)}_{l',i'}(w')$ with the aid of (27) we obtain

$$\operatorname{Re} M^{(\lambda)}_{l,i}(w) = \mathring{M}^{(\lambda)}_{l,i}(w) + \frac{1}{\pi}\,\mathrm{P}\int_{m+\mu}^{\infty}\mathrm{d}w' \sum_{l',i'} \xi^{(\lambda)}_{l,i;\,l',i'}(w, w')\operatorname{Im} M^{(\lambda)}_{l',i'}(w') \quad (28)$$

where

$$\mathring{M}^{(\lambda)}_{l,i} = \int_{-1}^{1} \mathscr{P}_{l,i}[\mathring{A}_j^{(\lambda)}]\mathrm{d}x,$$

$$\xi^{(\lambda)}_{li;\,l'1} = \int_{-1}^{1} \mathrm{d}x \mathscr{P}_{l,i}[(-l'^2 P_{l'}(x') + P'_{l'-1}(x'))f^{(\lambda)}_{j1} + (l'\,P'_{l'}(x') + P''_{l'-1}(x'))f^{(\lambda)}_{j3} - P''_{l'}(x')f^{(\lambda)}_{j4}], \quad (28a)$$

$$\xi^{(\lambda)}_{li;\,l'2} = \int_{-1}^{1} \mathrm{d}x \mathscr{P}_{l,i}[P'_{l'}(x')(x' f^{(\lambda)}_{j1} + f^{(\lambda)}_{j2} - f^{(\lambda)}_{j3})],$$

$$\xi^{(\lambda)}_{li;\,l'3} = \int_{-1}^{1} \mathrm{d}x \mathscr{P}_{l,i}[P'_{l'+1}(x')f^{(\lambda)}_{j1} + P''_{l'+1}(x')f^{(\lambda)}_{j3} - P''_{l'}(x')f^{(\lambda)}_{j4}], \quad (28b)$$

$$\xi^{(\lambda)}_{li;\,l'4} = \int_{-1}^{1} \mathrm{d}x \mathscr{P}_{l,i}[P'_{l'-1}(x')f^{(\lambda)}_{j1} + P''_{l'-1}(x')f^{(\lambda)}_{j3} - P''_{l'}(x')f^{(\lambda)}_{j4}].$$

The operators $P_{li}[a_j]$ are defined by formulae (26a); x' is a function of x, w and w'; in accord with (15)

$$x' = \frac{1}{k'q'}[k'\omega' - k(\omega - qx)].$$

Relation (28) should be supplemented by the unitarity condition which, for partial waves, has the form (appendix A)

$$M^{(I)}_{l,\pm} = |M^{(I)}_{l,\pm}| \exp\{i\delta^{(I)}_{l,\pm}\}; \quad E^{(I)}_{l,\pm} = |E^{(I)}_{l,\pm}| \exp\{i\delta^{(I)}_{l,\pm}\}. \quad (29)$$

7. Dispersion Relations for S and P Waves with an Accuracy to $1/m$

We shall restrict ourselves in (28) to S and P waves. Then from formulae (28a) and (28b) the quantities $\mathring{M}^{(\lambda)}_{l,i}$ and $\xi^{(\lambda)}_{l,i;\,l'\,i'}$ should be computed for l, i and l', i' to 1, 1; 1, 2; 0, 3 and 1,3.

We shall compute these functions in the simplest approximation differing from the static one, in the $1/m$ approximation. We introduce a new variable $\varepsilon = w-m$ $(\varepsilon' = w'-m)$, and neglect $(\varepsilon/m)^2$, $(\varepsilon'/m)^2$ and higher terms. In this approximation the calculations are not complicated but quite cumbersome. Inserting eq. (B1) of Appendix B in (28a) we obtain the free terms

$$\begin{aligned}
&\mathring{M}^{(\lambda)}_{l,i} = \mathring{M}^{(\lambda)}_{l,ie} + \mathring{M}^{(\lambda)}_{l,i\mu},\\
&\mathring{M}^{(\lambda)}_{0,3e} = -\frac{ef}{\mu}\frac{1}{2}\left[(1\mp 1)\mathscr{F}_s - \frac{\omega}{2m}(1\pm 1) \pm \frac{q^2}{3m\omega}\right],\\
&\mathring{M}^{(\lambda)}_{1,1e} = -\frac{ef}{\mu}\frac{1}{2}\left[(1\mp 1)\mathscr{F}_M - \frac{q}{2m}(1\pm 1)\right],
\end{aligned} \tag{30}$$

$$\begin{aligned}
&\mathring{M}^{(\lambda)}_{1,2e} = \frac{ef}{\mu}\frac{1}{2}(1\mp 1)\frac{q}{2m},\\
&\mathring{M}^{(\lambda)}_{1,3e} = -\frac{1}{3}\frac{ef}{\mu}\frac{1}{2}(1\mp 1)\mathscr{F}_Q.
\end{aligned} \tag{31}$$

For $\lambda = 1, 2$ the upper sign should be taken, for $\lambda = 3$ the lower one. The $\mathscr{F}$'s have the following meanings:

$$\begin{aligned}
&\mathscr{F}_s = 1-\frac{\omega}{2k}\mathscr{F},\quad \mathscr{F}_M = \frac{4\omega}{3q}\mathscr{F},\quad \mathscr{F}_Q = \frac{q}{k}\left[1-\frac{3\omega}{4q^2}(2\omega-k)\mathscr{F}\right],\\
&\mathscr{F} = 1+\frac{\mu^2}{2\omega q}\ln\frac{\omega-q}{\omega+q}.
\end{aligned} \tag{32}$$

Further,

$$\begin{aligned}
&\mathring{M}^{(\lambda)}_{0,3\mu} = \frac{f(\mu'_p \mp \mu_n)}{\mu}\left(\omega - \frac{3\omega^2-2q^2}{6m}\right),\quad \mathring{M}^{(3)}_{0,3\mu} = \frac{f(\mu'_p-\mu_n)}{\mu}\frac{q^2}{6m},\\
&\mathring{M}^{(\lambda)}_{1,1\mu} = \frac{f(\mu'_p\mp\mu_n)}{\mu}q,\quad \mathring{M}^{(3)}_{1,1\mu} = 0,\\
&\mathring{M}^{(\lambda)}_{1,2\mu} = -\frac{f(\mu'_p\mp\mu_n)}{\mu}q\frac{\omega}{2m},\quad \mathring{M}^{(3)}_{1,2\mu} = \frac{f(\mu'_p-\mu_n)}{\mu}q\left(1+\frac{\omega}{2m}\right).
\end{aligned} \tag{33}$$

Here $\lambda = 1, 2$; $\lambda = 1$ corresponds to the upper sign, $\lambda = 2$ to lower sign. Finally,

$$\mathring{M}^{(\lambda)}_{1,3\mu} = 0 \quad (\lambda = 1,\ 2,\ 3).$$

Substituting (B2) and (B3) into (28b) we obtain the functions $\xi^{(\lambda)}_{li;\,l'\,i'}$.

Rewriting (28) with account of (25) we get an equation for S and P waves which is correct to an accuracy of $1/m$ (for $\lambda = 1, 2$, to be the upper sign, for $\lambda = 3$ the lower):

$$\operatorname{Re} E^{(\lambda)}_{0,+}(\varepsilon) = \mathring{M}^{(\lambda)}_{0,3} + \frac{\varepsilon}{\pi} \mathrm{P}\int_{\mu}^{\infty} \mathrm{d}\varepsilon' \left\{ \left(\frac{1}{\varepsilon'-\varepsilon} \pm \frac{1}{\varepsilon'+\varepsilon} \right) \frac{1}{\varepsilon'} \operatorname{Im} E^{(\lambda)}_{0,+}(\varepsilon') \right.$$
$$- \left[1 \pm 1 - \frac{1}{2m} \left[\varepsilon' + \varepsilon \pm \left(\varepsilon' - \varepsilon + \frac{2(3\varepsilon^2+2q^2)}{3(\varepsilon'+\varepsilon)} - \frac{2\varepsilon q^2}{3(\varepsilon'+\varepsilon)^2} \right) \right] \right]$$
$$\cdot \frac{1}{\varepsilon' q'} \operatorname{Im} [M^{(\lambda)}_{1,-}(\varepsilon') - M^{(\lambda)}_{1,+}(\varepsilon')] \quad \text{(34a)}$$
$$+ 3 \left[\varepsilon' + 2\varepsilon \pm (\varepsilon' - 2\varepsilon) - \frac{1}{2m} \left[\varepsilon'(\varepsilon'+\varepsilon) \right.\right.$$
$$\left.\left. + 2(\varepsilon^2+q^2) \pm \left(\varepsilon'(\varepsilon'-\varepsilon) - \frac{2\varepsilon(\varepsilon^2+q^2)}{\varepsilon'+\varepsilon} + \frac{2\varepsilon'^2 q^2}{3(\varepsilon'+\varepsilon)^2} \right) \right] \right] \frac{1}{\varepsilon'^2 q'} \operatorname{Im} E^{(\lambda)}_{1,+}(\varepsilon') \left. \right\},$$

$$\operatorname{Re} [M^{(\lambda)}_{1,-}(\varepsilon) - M^{(\lambda)}_{1,+}(\varepsilon)] = \mathring{M}^{(\lambda)}_{1,1} + \frac{\varepsilon q}{\pi} \mathrm{P}\int_{\mu}^{\infty} \mathrm{d}\varepsilon' \left\{ \mp \frac{2\varepsilon'+\varepsilon}{2m(\varepsilon'+\varepsilon)^2} \frac{1}{\varepsilon'} \operatorname{Im} E^{(\lambda)}_{0,+}(\varepsilon') \right.$$
$$+ \left[\frac{1}{\varepsilon'-\varepsilon} \mp \frac{1}{\varepsilon'+\varepsilon} \left(1 - \frac{\varepsilon'}{m} \right) \right] \frac{1}{\varepsilon' q'} \operatorname{Im} [M^{(\lambda)}_{1,-}(\varepsilon') - M^{(\lambda)}_{1,+}(\varepsilon')] \quad \text{(34b)}$$
$$\left. + 3 \left[1 \mp 1 - \frac{\varepsilon \pm (2\varepsilon'-3\varepsilon)}{2m} \right] \frac{1}{\varepsilon'^2 q'} \operatorname{Im} E^{(\lambda)}_{1,+}(\varepsilon') \right\},$$

$$\operatorname{Re} [2M^{(\lambda)}_{1,+}(\varepsilon) + M^{(\lambda)}_{1,-}(\varepsilon)] \quad \text{(34c)}$$
$$= \mathring{M}^{(\lambda)}_{1,2} + \frac{\varepsilon q}{\pi} \mathrm{P}\int_{\mu}^{\infty} \mathrm{d}\varepsilon' \left[\frac{1}{\varepsilon'-\varepsilon} \pm \frac{1}{\varepsilon'+\varepsilon} \left(1 + \frac{\varepsilon}{m} \right) \right] \frac{1}{\varepsilon' q'} \operatorname{Im} [2M^{(\lambda)}_{1,+}(\varepsilon') + M^{(\lambda)}_{1,-}(\varepsilon')],$$

$$\operatorname{Re} E^{(\lambda)}_{1,+}(\varepsilon) = \mathring{M}^{(\lambda)}_{1,3} + \frac{\varepsilon^2 q}{\pi} \mathrm{P}\int_{\mu}^{\infty} \mathrm{d}\varepsilon' \left\{ \mp \frac{q}{6m(\varepsilon'+\varepsilon)^2} \frac{1}{\varepsilon'} \operatorname{Im} E^{(\lambda)}_{0,+}(\varepsilon') \right.$$
$$\left. + \left[\frac{1}{\varepsilon'-\varepsilon} \pm \frac{1}{\varepsilon'+\varepsilon} + \frac{1}{2m} \left(1 \mp \frac{\varepsilon'-\varepsilon}{\varepsilon'+\varepsilon} \right) \right] \frac{1}{\varepsilon'^2 q'} \operatorname{Im} E^{(\lambda)}_{1,+}(\varepsilon') \right\}. \quad \text{(34d)}$$

In accord with (6) and (29)

$$E^{(1)}_{l,\pm} = \tfrac{1}{3}(E^{(\frac{1}{2})}_{l,\pm} + 2E^{(\frac{3}{2})}_{l,\pm}). \quad E^{(2)}_{l,\pm} = E^{(\frac{3}{2})}_{l,\pm}, \quad E^{(3)}_{l,\pm} = \tfrac{1}{3}(E^{(\frac{1}{2})}_{l,\pm} - E^{(\frac{3}{2})}_{l,\pm}),$$
$$E^{(I)}_{l,\pm} = |E^{(I)}_{l,\pm}| \exp\{i\delta^{(I)}_{l,\pm}\} \ (I = \tfrac{1}{2}, \tfrac{3}{2}), \quad E^{(\frac{3}{2})}_{l,\pm} = |E^{(\frac{3}{2})}_{l,\pm}| \exp\{i\delta^{(\frac{1}{2})}_{l,\pm}\},$$

and analogous formulae are valid for $M^{(\lambda)}_{l,\pm}$.

Equations (34b, c, d) are essentially similar to the corresponding equations of Chew and Low [5]), differing from them in the choice of the integration variable (which is the total energy here), by some mixing of the M and E terms and corrections of the order of $1/m$, which are small within the resonance region (3.3). Among equations (34a) (S-wave) the equation

for $E_{0,+}^{(3)}$ ($-2\sqrt{2}\,E_{0,+}^{(3)} = E_{0,+}(\pi^+)+E_{0,+}(\pi^-)$) in which the integral converges with sufficient rapidity for large ε' is the one that is important for comparison with experiment.

In conclusion I take the opportunity to express my appreciation to A. A. Logunov for attention to this work and to D. V. Shirkov for a number of valuable remarks.

Appendix A

The S matrix unitarity condition $SS^+ = S^+S = 1$ permits one to connect the meson photoproduction amplitude with the scattering amplitude. For the transition matrix R which is related to S by the equation

$$S = 1+R \tag{A1}$$

the unitarity condition has the form [2])

$$R+R^+ + RR^+ = 0. \tag{A2}$$

Consider the matrix element of this equation which corresponds to transition from a state $|\gamma\rangle$ (photon + nucleon) to a state $|\pi\rangle$ (π-meson and nucleon). In the single meson approximation lowest with respect to electron charge,

$$\langle\pi|RR^+|\gamma\rangle = \sum_{\pi'}\langle\pi|R|\pi'\rangle\langle\pi'|R^+|\gamma\rangle \tag{A3}$$

where $\sum_{\pi'}$ denotes a sum over all indices of the intermediate nucleon and single π-meson state, i.e.

$$\langle\pi|R|\gamma\rangle+\langle\pi|R^+|\gamma\rangle+ \sum_{\pi'}\langle\pi|R|\pi'\rangle\langle\pi'|R^+|\gamma\rangle = 0. \tag{A4}$$

The expression for $\langle\pi|R|\gamma\rangle$ is given by eqs. (1), (2) and (7) and

$$\langle\pi|R^+|\gamma\rangle = \langle\gamma|R|\pi\rangle^* = \frac{-i(2\pi)^4}{\sqrt{4k^0q^0}}\delta(p_1+q-p-k)M^+ \tag{A5}$$

where, as can be shown [2]),

$$M^+ = \sum_{i,I}\dot{A}_i^{(I)}P_\gamma^{(I)}\eta_i(\theta). \tag{A6}$$

Analogous formulae for the scattering matrix element have the form [5])

$$\langle\pi|R|\pi'\rangle = \frac{i(2\pi)^4}{\sqrt{4q^0q'^0}}\delta(p_1+q-p'-q')T,\quad T = \sum_{i=1,2}\sum_{I=\frac{1}{2},\frac{3}{2}}B_i^{(I)}(w,\cos\alpha)P_\pi^{(I)}\zeta_i(\alpha).$$

Here α is the angle between the momenta of the final and initial mesons,

$$P_\pi^{(\frac{1}{2})} = \tfrac{1}{3}\tau_\varrho\tau_\varrho,\quad P_\pi^{(3/2)} = \delta_{\varrho\varrho'}-\tfrac{1}{3}\tau_\varrho\tau_{\varrho'}, \tag{A8}$$

$$\zeta_1 = 1,\quad \zeta_2 = (qq')^{-1}i\boldsymbol{\sigma}\cdot[\mathbf{q}\wedge\mathbf{q}']. \tag{A9}$$

Consider now $\mathcal{I} = \sum_{\pi'} \langle \pi|R|\pi'\rangle\langle\pi'|R^+|\gamma\rangle$,

$$\mathcal{I} = \frac{1}{(2\pi)^6}\int \mathrm{d}\mathbf{p}'\,\mathrm{d}\mathbf{q}'\,\frac{i(2\pi)^4}{\sqrt{4q^0q'^0}}\,\delta(p_1+q-p'-q')\,\frac{-i(2\pi)^4}{\sqrt{4q'^0k^0}}\,\delta(p'+q'-p-k)\,TM^+ \tag{A10}$$

where TM^+ denotes a matrix product.

Integrating in (A10) with respect to $\mathbf{p}'$ and $|\mathbf{q}'|$ and changing to the c.m.s. we get

$$\mathcal{I} = \frac{(2\pi)^4}{\sqrt{4q^0k^0}}\,\delta(p_1+q-p-k)\,\frac{qE_q}{2(2\pi)^2 w} \int \mathrm{d}\Omega' \sum_{i,I;i'I'} B_i^{(I)}(\cos\alpha)\dot{A}_{i'}^{(I')}(\cos\theta')\zeta_i(\alpha)\eta_{i'}(\theta')P_\pi^{(I)}P_\gamma^{(I')} \tag{A11}$$

where θ' is the angle between $\mathbf{k}$ and $\mathbf{q}'$. Inserting (1), (2), (7), (A5)–(A8) and (A11) in (A4) and taking into account that

$$P_\pi^{(I)}P_\gamma^{(I')} = \delta_{I,I'}P_\gamma^{(I)},\quad P_\pi^{(I)}P_\gamma^{(s)} = \delta_{I,\frac{1}{2}}P_\gamma^{(s)} \quad (I,\ I' = \tfrac{1}{2},\ \tfrac{3}{2}), \tag{A12}$$

we obtain

$$\sum_i (\mathrm{Im}\,A_i^{(I)})\eta_i(\theta) = \frac{qE_q}{(4\pi)^2 w}\int \mathrm{d}\Omega' \sum_{i,i'} B_i^{(I)}(\cos\alpha)\dot{A}_{i'}^{(I)}(\cos\theta')\zeta_i(\alpha)\eta_{i'}(\theta'), \tag{A13}$$

$$I = \tfrac{1}{2},\ \mathrm{S},\ \tfrac{3}{2};\qquad B_i^{(S)} \equiv B_i^{(\frac{1}{2})}.$$

We shall now separate the spin operators. We introduce a coordinate system with the z axis along $\mathbf{k}$ and the x, z plane passing through $\mathbf{q}$, $\mathbf{k}$ and take the trace of both sides of (A13), multiplying them beforehand by 1, $(\boldsymbol{\sigma}\cdot\mathbf{e}_x)$, $(\boldsymbol{\sigma}\cdot\mathbf{e}_y)$, $(\boldsymbol{\sigma}\cdot\mathbf{e}_z)$. For the polarization vector $\boldsymbol{\pi}'$ it will be convenient to take the values $\mathbf{e}_y$, $\mathbf{e}_x$, $\mathbf{e}_y$, $\mathbf{e}_x$ correspondingly. The traces are computed from the formulae

$$\begin{aligned}
&\mathrm{tr}\,(\boldsymbol{\sigma}\cdot\mathbf{a}) = 0,\quad \mathrm{tr}\,(\boldsymbol{\sigma}\cdot\mathbf{a})(\boldsymbol{\sigma}\cdot\mathbf{b}) = \mathbf{a}\cdot\mathbf{b},\\
&\mathrm{tr}\,(\boldsymbol{\sigma}\cdot\mathbf{a})(\boldsymbol{\sigma}\cdot\mathbf{b})(\boldsymbol{\sigma}\cdot\mathbf{c}) = i(\mathbf{a}\wedge\mathbf{b})\cdot\mathbf{c},\\
&\mathrm{tr}\,(\boldsymbol{\sigma}\cdot\mathbf{a})(\boldsymbol{\sigma}\cdot\mathbf{b})(\boldsymbol{\sigma}\cdot\mathbf{c})(\boldsymbol{\sigma}\cdot\mathbf{d}) = 2(\mathbf{a}\cdot\mathbf{b})(\mathbf{c}\cdot\mathbf{d})-(\mathbf{a}\wedge\mathbf{b})\cdot(\mathbf{c}\wedge\mathbf{d}).
\end{aligned} \tag{A14}$$

As a result, we obtain relations (13).

In order to obtain from them the conditions for the partial waves the expressions from (27) for $A_1^{(I)}$ in terms of $M_{l,\pm}^{(I)}$, $E_{l,\pm}^{(I)}$ should be inserted in (13) and analogous expressions for $B_i^{(I)}$ [5]):

$$\begin{aligned}
B_1^{(I)}(\cos\alpha) &= \frac{4\pi w}{qE_q}\sum_l [(l+1)f_{l,+}^{(I)}+lf_{l,-}^{(I)}]P_l(\cos\alpha),\\
B_2^{(I)}(\cos\alpha) &= \frac{4\pi w}{qE_q}\sum_l [f_{l,-}^{(I)}-f_{l,+}^{(I)}]P'_l(\cos\alpha).
\end{aligned} \tag{A15}$$

Integrating now with respect to Ω' we obtain

$$\begin{aligned}
&\text{Im}\,[lM_{l,+}+E_{l,+}+(l+3)M_{l+2,-}+E_{l+2,-}] = (l\dot{M}_{l,+}+\dot{E}_{l,+})f_{l,+}\\
&\qquad +[(l+3)\dot{M}_{l+2,-}+\dot{E}_{l+2,-}]f_{l+2,-};\quad l=0,1,2,\ldots\\
&\text{Im}\,[(l+1)M_{l,+}+lM_{l,-}] = (l+1)\dot{M}_{l,+}f_{l,+}+l\dot{M}_{l,-}f_{l,-};\quad l=1,2,\ldots\\
&\text{Im}\,(E_{l,+}-M_{l,+}+E_{l+2,-}+M_{l+2,-}) = (\dot{E}_{l,+}-\dot{M}_{l,+})f_{l,+}\\
&\qquad +(\dot{E}_{l+2,-}+\dot{M}_{l+2,-})f_{l+2,-};\quad l=1,2,\ldots\\
&\text{Im}\,(E_{l,+}-M_{l,+}+M_{l,-}+E_{l,-}) = (\dot{E}_{l,+}-\dot{M}_{l,+})f_{l,+}\\
&\qquad +(\dot{M}_{l,-}+\dot{E}_{l,-})f_{l,-};\quad l=2,3,\ldots.
\end{aligned} \tag{A16}$$

Since $f_{l,\pm} = e^{i\delta_{l,\pm}} \sin\delta_{l,\pm}$ eq. (A16) will be satisfied if

$$M_{l,\pm} = \mathcal{M}_{l,\pm}\, e^{i\delta_{l,\pm}};\quad E_{l,\pm} = \mathcal{E}_{l,\pm}\, e^{i\delta_{l,\pm}} \tag{A17}$$

where $\mathcal{M}_{l,\pm}$ and $\mathcal{E}_{l,\pm}$ are real quantities (for simplicity the superscript (I) has been omitted).

Appendix B

We shall write the functions $\mathring{A}_i^{(\lambda)}$ and $f_{ii'}^{(\lambda)}$ with an accuracy to $1/m$. We get $\varepsilon = w - m$, $\mathring{A}_i^{(\lambda)} = \mathring{A}_{i,e}^{(\lambda)} + \mathring{A}_{i,\mu}^{(\lambda)}$, with

$$\mathring{A}_{1,e}^{(\lambda)} = -\frac{ef}{2\mu}\left[1\mp 1-\frac{\varepsilon\pm(\varepsilon-2qx)}{2m}\right],\quad \mathring{A}_{2,e}^{(\lambda)} = \frac{ef}{2\mu}\,\frac{q(1\mp 1)}{2m},$$

$$\mathring{A}_{3,e}^{(\lambda)} = -\frac{ef}{2\mu}\,q\left[\frac{1\mp 1}{\omega-qx}\mp\frac{1}{m}\right],\quad \mathring{A}_{4,e}^{(\lambda)} = -\frac{q}{k}\,A_{3,e}^{(\lambda)}$$

(here $\lambda = 1, 2$ corresponds to the upper sign and $\lambda = 3$ to the lower),

$$\mathring{A}_{1,\mu}^{(\lambda)} = \frac{f(\mu'_p\mp\mu_n)}{\mu}(\omega-qx)\left(1+\frac{\varepsilon+2qx}{2m}\right),\quad \mathring{A}_{2,\mu}^{(\lambda)} = -\frac{f(\mu'_p\mp\mu_n)}{\mu}\,\frac{q(\omega-qx)}{2m} \tag{B1}$$

($\lambda = 1, 2$; $\lambda = 1 \to$ upper sign, $\lambda = 2 \to$ lower sign),

$$\mathring{A}_{1,\mu}^{(3)} = \frac{f(\mu'_p-\mu_n)}{\mu}\,q\left(x+\frac{q+x(\varepsilon-2qx)}{2m}\right),\quad \mathring{A}_{2,\mu}^{(3)} = \frac{f(\mu'_p-\mu_n)}{\mu}\,q\left(1+\frac{\omega-qx}{2m}\right),$$

$$\mathring{A}_{3,\mu}^{(\lambda)} = \pm\frac{f(\mu'_p-\mu_n)}{\mu}\,q\left(1+\frac{\varepsilon-2qx}{2m}\right),\quad \mathring{A}_{4,\mu}^{(\lambda)} = \pm\frac{f(\mu'_p-\mu_n)}{\mu}\,\frac{q^2}{2m}$$

($\lambda = 1, 3$; $\lambda = 1 \to$ upper sign, $\lambda = 3 \to$ lower sign),

$$\mathring{A}_{3,\mu}^{(2)} = \frac{f(\mu'_p+\mu_n)}{\mu}\,q\left(1+\frac{\varepsilon-2qx}{2m}\right),\quad \mathring{A}_{4,\mu}^{(2)} = \frac{f(\mu'_p+\mu_n)}{\mu}\,\frac{q^2}{2m}.$$

With an accuracy to $1/m$ the functions $f_{ii'}^{(\lambda)}$ are equal to

$$f_{11}^{(\lambda)} = \frac{\varepsilon}{\varepsilon'}\left[\frac{1}{\varepsilon'-\varepsilon} \pm \frac{1}{\varepsilon'+\varepsilon}\left(1+\frac{\varepsilon' qx}{m(\varepsilon'+\varepsilon)}\right)\right],$$

$$f_{12}^{(\lambda)} = -\frac{\varepsilon}{\varepsilon' q'}\left\{1 \pm \left(1-\frac{2qx}{\varepsilon'+\varepsilon}\right) - \frac{1}{2m}\left[\varepsilon'+\varepsilon \pm \left(\varepsilon'-\varepsilon+\frac{2(\varepsilon^2+q^2)-2qx(\varepsilon'-\varepsilon)}{\varepsilon'+\varepsilon}-\frac{4\varepsilon q^2 x^2}{(\varepsilon'+\varepsilon)^2}\right)\right]\right\},$$

$$f_{13}^{(\lambda)} = \frac{\varepsilon(1\mp 1)}{\varepsilon'^2 q'}\left(\varepsilon - qx - \frac{\varepsilon^2+q^2-\varepsilon qx}{2m}\right),$$

$$f_{14}^{(\lambda)} = \frac{\varepsilon(1\mp 1)}{\varepsilon' q'^2}\left(\varepsilon - qx - \frac{q^2+(\varepsilon'+\varepsilon)(\varepsilon-qx)}{2m}\right),$$

$$f_{21}^{(\lambda)} = f_{23}^{(\lambda)} = f_{24}^{(\lambda)} = 0, \quad f_{22}^{(\lambda)} = \frac{\varepsilon q}{\varepsilon' q'}\left\{\frac{1}{\varepsilon'-\varepsilon} \pm \frac{1}{\varepsilon'+\varepsilon}\left[1+\frac{\varepsilon}{m}\left(1-\frac{qx}{\varepsilon'+\varepsilon}\right)\right]\right\}, \quad \text{(B2)}$$

$$f_{31}^{(\lambda)} = \mp\frac{\varepsilon q}{m\varepsilon'(\varepsilon'+\varepsilon)}, \quad f_{32}^{(\lambda)} = \mp\frac{2\varepsilon q}{\varepsilon' q'(\varepsilon'+\varepsilon)}\left[1-\frac{1}{2m}\left(\varepsilon'-\varepsilon+\frac{2\varepsilon qx}{\varepsilon'+\varepsilon}\right)\right],$$

$$f_{33}^{(\lambda)} = \frac{\varepsilon q}{\varepsilon' q'}\left\{\frac{1}{\varepsilon'-\varepsilon} \mp \frac{1}{\varepsilon'+\varepsilon}\left[1-\frac{\varepsilon^2}{m\varepsilon'}\left(1-\frac{qx}{\varepsilon'+\varepsilon}\right)\right]\right\},$$

$$f_{34}^{(\lambda)} = \frac{\varepsilon q}{\varepsilon' q'^2}\left[1\mp 1-\frac{(\varepsilon'+\varepsilon)^2 \mp (\varepsilon'^2+\varepsilon^2)}{2m(\varepsilon'+\varepsilon)}\right],$$

$$f_{41}^{(\lambda)} = 0, \quad f_{42}^{(\lambda)} = f_{43}^{(\lambda)} = \mp\frac{\varepsilon q^2}{m\varepsilon' q'(\varepsilon'+\varepsilon)},$$

$$f_{44}^{(\lambda)} = \frac{\varepsilon q^2}{\varepsilon' q'^2}\left\{\frac{1}{\varepsilon'-\varepsilon} \pm \frac{1}{\varepsilon'+\varepsilon}\left[1-\frac{1}{m}\left(\varepsilon'-\varepsilon+\frac{\varepsilon qx}{\varepsilon'+\varepsilon}\right)\right]\right\}.$$

Here $\lambda = 1, 2$ corresponds to the upper sign and $\lambda = 3$ to the lower. With an accuracy to $1/m$

$$x' = \frac{\varepsilon'-\varepsilon}{\varepsilon' q'}\left[\varepsilon'+\varepsilon-\frac{\varepsilon'(\varepsilon'+\varepsilon)+\varepsilon^2+q^2}{2m}\right]+\frac{\varepsilon qx}{\varepsilon' q'}\left(1+\frac{\varepsilon'-\varepsilon}{2m}\right). \quad \text{(B3)}$$

References

1) A. A. Logunov, A. P. Tavkhelidze and L. D. Solovyov, Nuclear Physics **4**(1957) 427
2) T. Nakano and K. Nishijima, Prog. Theor. Phys. **8** (1952) 53
3) K. M. Watson, Phys. Rev. **85** (1952) 852
4) G. F. Chew and F. E. Low, Phys. Rev. **101** (1956) 1759
5) R. H. Capps and G. Takeda, Phys. Rev. **103** (1956) 1877

Nuclear Physics **5** (1958) 271—273; © *North-Holland Publishing Co., Amsterdam*
Not to be reproduced by photoprint or microfilm without written permission from the publisher

GAMMA RADIATION FROM ^{141}Nd

H. L. POLAK, W. SCHOO, B. L. SCHRAM, R. K. GIRGIS† and R. VAN LIESHOUT
Institute for Nuclear Physics Research, Amsterdam, the Netherlands

Received 7 August 1957

Abstract: A scintillation spectrometer study of the disintegration of ^{141}Nd produced by a (d, 2n) reaction on ^{141}Pr, shows that it decays mainly by electron capture, accompanied by a weak positon group (1.9 %); two weak gamma rays with energies of 1.14 MeV (0.50 %) and 1.30 MeV (0.26 %) have been found. The results are given in table 2; a decay scheme is proposed (fig. 1).

1. Introduction

Kurbatov *et al.* [1]) reported the nucleide ^{141}Nd to decay with a half-life of 2.5 h, emitting positons of 0.78 MeV. Wilkinson and Hicks [2]) studied the radiations in greater detail and found weak gamma radiation of $\approx$ 1.2 MeV and a weak ($\approx$ 2 %) positon group of 0.7 MeV in addition to K capture; these measurements were made by absorption methods.

We have undertaken a study of the decay of ^{141}Nd, using scintillation techniques, employing a kicksorter of the Hutchinson-Scarrott type, built at this Institute by Mr. F. E. L. ten Haaf.

2. Experimental

Praseodymium oxide was bombarded with 21-MeV deuterons in the cyclotron (2 to 10 μAh). The target was dissolved in a small quantity of nitric acid; some Al, Mg and La were added as holdback carriers. After adding boric acid and sodium fluoride, the rare earths fraction, containing Pr and Nd, was precipitated by sodium oxalate. In this way the 1.9-h ^{18}F, formed from the oxygen, which emits positons that would interfere with those of the 2.5-h ^{141}Nd, was eliminated.

The source was sandwiched between absorbers to ensure complete annihilation of the positons.

The gamma ray peaks found are shown in table 1, together with their

TABLE 1

Gamma rays in the decay of ^{141}Nd

Energy (keV)	38	511	1140±10	1300±10
Relative intensity	100	4.7±0.3	0.63±0.06	0.33±0.02

† On leave of absence from the Faculty of Science, University of Cairo, Cairo, Egypt.

relative intensities. They all decayed with a half-life of ≈ 145 minutes. In calculating the intensity of the K X-ray peak at 38 keV a correction was applied for absorption in the shielding of the scintillation counter. A weak residual activity was found in the K X-ray peak, decaying with a half-life of ≈ 3.5 days, which we assign to ^{140}Nd formed by a (d, 3n) reaction on ^{141}Pr. A peak at 1.60 MeV decaying with a half-life of ≈ 19 h is assigned to ^{142}Pr formed by a (d, p) reaction.

3. Discussion

Our measurements strongly suggest the decay scheme presented in fig. 1. The level at 145 keV in ^{141}Pr (well known from the decay of ^{141}Ce) is not expected to be fed by positons or by capture, since the spin of ^{141}Nd is predicted to be $3/2^+$. The weak 0.145 MeV gamma ray following the 1.14 MeV transition disappears completely into the Compton distribution of the higher energy gamma rays. The possibility that there are two separate levels at 1.14 and 1.30 MeV cannot be excluded; it does, however, not influence the conclusions to be mentioned below.

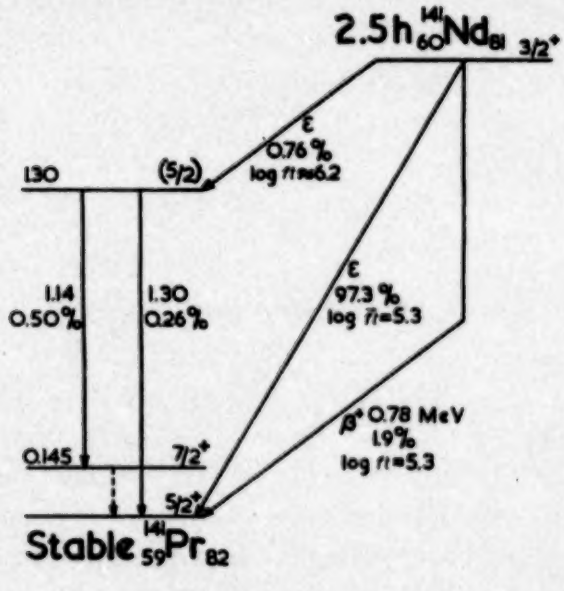

Fig. 1. Proposed decay scheme of 2.5 h ^{141}Nd.

Assuming a Pr K-fluorescence yield[3]) of 0.90 one finds $\beta^+/\varepsilon_K = 0.021 \pm 0.004$ agreeing very well with the value quoted by Wilkinson *et al.* [2]). Using the tables by E. Feenberg and G. Trigg [4]) one finds an energy of 0.78 ± 0.02 MeV for the ground state positon transition, again in agreement with the directly measured values quoted in the introduction.

To obtain the total fraction of electron capture one has to know the ratio $(\varepsilon_L + \varepsilon_M + \cdots)/\varepsilon_K$, in which ε_Y denotes capture from the Y shell. We have not measured this quantity, but have estimated ε_Y (Y = L, M, $\cdots$)

from the approximate formula

$$\varepsilon_Y/\varepsilon_K = n^{-3}(Z-\sigma_Y)^3(Z-\sigma_K)^{-3}(E-B_Y)^2(E-B_K)^{-2}$$

in which n is the principal quantum number, σ_Y the appropriate Slater screening constant and B_Y the electron binding energy in the Y shell. We find $\varepsilon_{total} = 1.12\ \varepsilon_K$. It is now possible to calculate the absolute intensities of the various radiations of ^{141}Nd from the relative intensities given in table 1; they are listed in table 2.

TABLE 2

^{141}Nd produced by ^{141}Pr (21-MeV d, 2n)

	Energy (MeV)	Branching ratio
β^+		1.9±0.4 %
ε		98.1 %
$\gamma(^{141}Pr)$	0.038 (K X-ray) scin	
	1.14±0.01	0.50±0.05 %
	1.30±0.01	0.26±0.03 %
No 0.145 γ (< 2 %) found above Compton background		

For the ground state transition, $\log_{10} ft = 5.3$ for a total disintegration energy of 1.80 MeV.

Assuming the decay scheme of fig. 1, the capture branch to the 1.30 level has an intensity of 0.70±0.07 %, yielding $\log_{10} ft \approx 6.2$; this indicates a spin change of 0 or ±1. A spin of 5/2 is preferred for the 1.30 level on account of the relative intensities of the two high energy gamma rays.

The authors wish to thank Prof. Dr. P. C. Gugelot and Prof. Dr. A. H. W. Aten Jr. for their interest in this work, Mrs A. Funke-Klopper and Miss G. Wolzak for performing the chemical separations and the cyclotron crew for the irradiations. This work was performed as part of the research program of the "Stichting voor Fundamenteel Onderzoek der Materie" (F.O.M.), which is financially supported by the "Nederlandse Organisatie voor Zuiver Wetenschappelijk Onderzoek" (Z.W.O.). One of the authors (R.K.G.) is indebted to the Egyptian Atomic Energy Commission for a grant.

References

1) J. D. Kurbatov, D. C. McDonald, M. L. Pool and L. L. Quill, Phys. Rev. **61** (1942) 106 A
2) G. Wilkinson and H. G. Hicks, Phys. Rev. **75** (1949) 1687
3) E. H. S. Burhop, The Auger Effect (Cambridge University Press, 1952)
4) E. Feenberg and G. Trigg, Revs. Mod. Phys. **22** (1950) 399

Nuclear Physics **4** (1957) 274—287; © *North-Holland Publishing Co., Amsterdam*

Not to be reproduced by photoprint or microfilm without written permission from the publisher

PROTON POTENTIAL ANOMALY AND NUCLEAR RADIUS CONSTANT FOR MIRROR NUCLEI

P. C. SOOD † and A. E. S. GREEN

Florida State University, Tallahassee ††

Received 28 June 1957

Abstract: The static diffuse boundary potential well is adjusted to reproduce the binding energies of the last neutrons and protons in mirror nuclei. The corresponding realistic wave functions, including the effects of reduced mass, spin orbit interaction and Coulomb perturbation, are used to calculate the Coulomb energy differences for these nuclei. The exchange effect is taken into account by introducing an exchange correction factor based on a study with harmonic oscillator wave functions. The theoretical results are compared with the experimental values obtained from the atomic mass data and the agreement is found to be quite good. It is concluded that no appreciable proton potential anomaly exists in this region i.e. the proton and neutron nuclear potentials are the same. The nuclear radii, as predicted by this model, are found to be in very good agreement with the results of Stanford electron-scattering experiments on five even-nuclei in this region. The calculations are carried out for the mirror nuclei, and a least square fit for the equivalent uniform radius R gives the value 1.31×10^{-13} cm for the nuclear radius constant $r_0 = RA^{-1/3}$ for these nuclei; this is compared with the results of earlier studies. The possible systematics of the variation of the radius constant with mass number are described and the significance of a larger radius constant for light nuclei is discussed.

1. Introduction

In some recent studies it has been concluded that the potential well for protons differs from that for the neutrons not only by the Coulomb potential, but by an additional attractive potential. The evidence has come from the analysis of bound states [1])††† and positive energy states [2]) in static and velocity dependent [3]) diffuse boundary potentials. In medium and heavy nuclei, this additional potential which has been referred to as the 'proton potential anomaly' cancels about one-half the Coulomb contribution, and an attempt [1]) has been made to characterize it as a function of the Coulomb interaction. Since in the case of a pair of mirror nuclei the β^+-decay changes a proton into a neutron (reverse for β^--decay), a realistic model should be able to give reliable information about this energy difference.

Previous attempts to calculate the Coulomb energy differences for mirror nuclei have been carried out using harmonic oscillator [4, 5]), infinite [5, 6])

† On leave of absence from Panjab University College, Hoshiarpur (India).

†† Supported by a grant from the Research Corporation.

††† Referred to as G.I.

or finite square well [7]) wave functions. Though the exchange effect is generally included, in many cases the reduced mass effect, the effects of Coulomb perturbation on the wave functions and also the spin orbit splitting factors have been ignored. Analytical wave functions [8])† based upon diffuse boundary independent particle model appropriately corrected for these effects form the basis of this study. A slight readjustment of well depth is made to get the predicted last neutron and proton binding energies in agreement with the experimental values. The corresponding wave functions are used to get the expectation value of the Coulomb energy of the last proton. To take the exchange effect into account, harmonic oscillator wave functions are used to calculate the direct and the exchange terms separately. The exchange correction factor, which is defined as the ratio of the exchange corrected term to the direct term and which is independent of the unknown oscillator parameter is applied to the value calculated. These theoretical results are compared with the experimental values inferred from the atomic mass data under the assumption of the charge independence of the nuclear forces. This comparison is applied in an effort to arrive at the origin and the characteristics of the proton potential anomaly.

The radii for mirror nuclei have been the subject of a number of recent studies. Attempts [6, 7]) have been made to relate them to μ-mesonic X-ray determination $R_M = 1.2\,A^{1/3}$ and as such a discrepancy is pointed out. In another study Vachaspati and Shah [9]) assume an arbitrary unrealistic charge distribution and adjust some parameters to conclude that the Coulomb energy radius is 1.43 times larger than the electron scattering radius. Some recent Stanford electron scattering experiments provide an experimental basis for the discussion of nuclear radii in this region. In this work the rms radii for mirror nuclei are calculated on the diffuse boundary model, and the equivalent uniform distribution radii thus obtained are analyzed and compared with other theoretical studies.

2. Neutron and Proton Binding Energies

In previous works [1, 8])†† a diffuse boundary model is used which is based upon a potential well characterized by

$$\begin{aligned} V &= -V_0 && (r < a) \\ &= -V_0 \exp\left(-\frac{r-a}{d}\right) && (r > a) \end{aligned} \tag{1}$$

where $V_0 = 40$ MeV, $a = 1.32\,A^{1/3} - 0.8$ and the diffuseness parameter defined as the distance to the e^{-1} value $d = 1$. (All distances are in 10^{-13} cm.) A spin orbit term of the Thomas form but 45 times larger is used.

† Referred to as G.II.

†† Unless otherwise noted the notation is that of G.I. and G.II.

In the current investigation which deals with light nuclei, it was found after some experimentation that a well depth of 45 MeV seemed more appropriate. This is in agreement with the analyses of neutron scattering for C^{13} and O^{17} by Fowler and Cohn [10]). A part of the additional well depth is necessitated because of the inclusion here of the reduced mass effect which becomes appreciable in very light nuclei.

To take care of small departures of the well from the one previously used for a given A, the method of A-shift has been employed. This method entails shifting to the value of A which leads to an equivalent dimensionless well strength

$$S = 2\frac{2m}{\hbar^2}\int_0^\infty V(r) r \mathrm{d}r. \tag{2}$$

The A shift is actually calculated using

$$\Delta A = \frac{\mathrm{d}A}{\mathrm{d}S}\Delta S \tag{3}$$

where $\mathrm{d}A/\mathrm{d}S$ is obtained from the previously used family of wells. The extra well depth used here requires an A-shift given by

$$\Delta A_{V_0} = \left[\frac{S}{8}\right]\frac{\mathrm{d}A}{\mathrm{d}S} \tag{4}$$

and the reduced mass effect, which is important in this region, leads to an A-shift

$$\Delta A_{\mathrm{m}} = -\frac{S}{A}\frac{\mathrm{d}A}{\mathrm{d}S}. \tag{5}$$

The corresponding neutron binding energies are then given by

$$W = W(A+\Delta A_{\mathrm{net}})\left[1+2a^{-1}\frac{\mathrm{d}a}{\mathrm{d}A}\Delta A_{\mathrm{net}}\right]. \tag{6}$$

The binding energies for the last neutron as calculated on this model using fig. 6 of G.II, and the experimental values obtained from the mass data through the relation

$$B_{\mathrm{n}}(Z,\ A) = M(A-1,\ Z)-M(A,\ Z)+M_{\mathrm{n}} \tag{7}$$

are given in table 1.

For the case of protons the effect of the Coulomb perturbation on the wave function is included as in G.I through an additional A shift

$$\Delta A_{\mathrm{C}} = -0.01736\ (Z-1)a(1+2.5\delta(\mathrm{d}A/\mathrm{d}S). \tag{8}$$

The proton energies are then given by

$$W = W(A+\Delta A_{\mathrm{net}})\left[1+2a^{-1}\frac{\mathrm{d}a}{\mathrm{d}A}\Delta A_{\mathrm{net}}\right]+\frac{(Z-1)e^2}{a+d}. \tag{9}$$

The binding energies for the last proton as obtained from the model along with the experimental values obtained from the mass data through the relation

$$B_p(Z, A) = M(A-1, Z-1) - M(A, Z) + M_H \qquad (10)$$

are also listed in table 1. It is seen that the same potential well gives good

TABLE 1

Experimental and predicted binding energies for the last neutron and the last proton in mirror nuclei

B_p in MeV				B_n in MeV			
	Experimental	Theoretical	Diff.		Experimental	Theoretical	Diff.
C^{11}	8.70	8.66	−0.04	B^{11}	11.46	11.61	−0.15
O^{15}	7.35	6.55	+0.80	N^{15}	10.84	10.68	+0.16
Ne^{19}	6.37	5.25	+1.12	F^{19}	10.40	9.50	+0.90
Mg^{23}	7.54	6.90	+0.64	Na^{23}	12.42	12.16	+0.26
Si^{27}	7.45	8.79	−1.34	Al^{27}	13.06	14.59	−1.53
S^{31}	6.34	4.14	+2.10	P^{31}	12.40	10.36	+2.04
A^{35}	6.52	4.87	+1.65	Cl^{35}	12.71	12.20	+0.51
Ca^{39}	5.48	6.47	−1.01	K^{39}	13.08	14.26	−1.18

agreement with the experimental binding energies for the neutrons as well as the protons in this region. The deviations, which are quite small, change sign a number of times for the nuclei considered so that from the binding energy standpoint this model is satisfactory for the whole region and to cover the slight differences, one would have to choose special potential wells for each nucleus and invoke interparticle couplings. The fact that the deviations bear the same sign and are quite comparable for the proton and the neutron energies for any mirror pair suggests that any adjustment of potential well in any individual case will be similar for the neutrons and the protons. Thus for study of bound states in these nuclei the proton potential differing from the neutron potential by full Coulomb contribution is in approximate accord with the experiment. Since the Coulomb energy values are relatively small for these nuclei, a small modification of it might not show up prominently in binding energy problems. On the other hand the experimental Coulomb energy differences for mirror nuclei should agree with the theoretical expectation values from the effective proton potential with the realistic wave functions. Thus the agreement or otherwise of the theoretical predictions with the experimental results can suggest whether the effective proton potential is the same as the Coulomb potential or some functional modification of the latter.

3. Coulomb Energy Differences

3.1. AVERAGE COULOMB POTENTIAL

In order to arrive at an expression for the Coulomb potential of the last proton, it is assumed here that the $(Z-1)$ protons acting on the last proton are distributed according to the charge density distribution

$$\begin{aligned} \varrho(r) &= \varrho_0 && (r < a_c) \\ &= \varrho_0 \exp\left[-\frac{r-a_c}{d_c}\right] && (r > a_c) \end{aligned} \tag{11}$$

where a_c and d_c are the constant part and the decay lengths for the charge distribution. The mean square radius for this charge distribution for the convenient choice $d_c = 0.5$ and $a_c = a$ are in reasonable agreement with detailed calculations of individual particle densities by Green *et al.* [11]) and with the analysis of Stanford electron scattering experiments [12]). On the basis of a classical calculation this distribution yields for the Coulomb potential of the last proton

$$\begin{aligned} V_C &= \frac{(Z-1)e^2}{a\lambda}\left[\mu-\tfrac{1}{3}\varrho^2\right] && (\varrho \leqq 1) \\ &= \frac{(Z-1)e^2}{a}\left[\frac{1}{\varrho}-\frac{\delta^2}{2\lambda}\left(1+\frac{\delta}{\varrho}\right)\exp\left(2\,\frac{1-\varrho}{\delta}\right)\right] && (\varrho \geqq 1) \end{aligned} \tag{12}$$

where

$$\mu = 1+\delta+\tfrac{1}{2}\delta^2, \tag{13}$$

$$\lambda = \tfrac{2}{3}+\delta+\delta^2+\tfrac{1}{2}\delta^3 \tag{14}$$

and ϱ and δ are the dimensionless parameters r/a and d/a respectively. Granting the charge independence of the nuclear forces, the only difference in the Hamiltonian for the mirror nuclei pair is due to the Coulomb potential of the last proton and it can be shown [7]) that

$$\langle\psi_{Z+1}|V_C|\psi_{Z+1}\rangle < \Delta E_C < \langle\psi_Z|V_C|\psi_Z\rangle. \tag{15}$$

Since the two side terms differ but slightly, to a good approximation, we have

$$\Delta E_C \approx \langle\psi_{Z+1}|V_C|\psi_{Z+1}\rangle. \tag{16}$$

To be able to handle the calculations analytically the expression for V_C for $\varrho > 1$ can be approximated quite accurately by

$$V_C = \frac{(Z-1)e^2}{a}\left[c_0+c_1x^2+c_2x^4\right] \tag{17}$$

where

$$\exp\ 2\delta\ \left(\frac{1-\varrho}{x=}\right). \tag{18}$$

Then, in the notation of G.II,

$$\langle V_C \rangle = \frac{(Z-1)e^2}{a}\left\{(1-P_e)\left[\frac{u}{\lambda}-\frac{1}{3\lambda}R_{l+\frac{1}{2}}(\varepsilon)\right]+P_e[c_0+c_1S_n(k)+c_2T_n(k)]\right\}. \tag{19}$$

The values are obtained for equivalent wells which include the effects of the extra well depth, reduced mass, Coulomb perturbation and the spin orbit interaction terms. The calculated values are listed in column 3 of table 2. In the next section we make use of harmonic oscillator wave functions to calculate the effect of exchange.

TABLE 2

Experimental and predicted Coulomb energy differences, and radii of mirror nuclei of smaller Z.

Mirror Pair $_{Z+1}N\ A\ _{Z}N$	ΔE_C Exp.	$\langle V_C \rangle$	Exchange Factor	ΔE_C Theor.	R	r_0
$_2$He $\underline{3}$ $_1$H	0.765					
$_3$Li $\underline{5}$ $_2$He	0.813	0.870	0.900	0.783		
$_4$Be $\underline{7}$ $_3$Li	1.647	1.753	0.920††	1.613	2.97	1.55
$_5$B $\underline{9}$ $_4$Be	1.854	2.303	0.920††	2.119	3.021	1.452
$_6$C $\underline{11}$ $_5$B	2.766	2.825	0.936	2.644	3.036	1.365
$_7$N $\underline{13}$ $_6$C	3.004	2.777	0.929	2.580	3.124	1.329
$_8$O $\underline{15}$ $_7$N	3.489	3.276	0.938	3.073	3.310	1.342
$_9$F $\underline{17}$ $_8$O	3.552	3.828	0.944	3.614	3.428	1.333
$_{10}$Ne $\underline{19}$ $_9$F	4.039	4.223	0.950††	4.012	3.588	1.345
$_{11}$Na $\underline{21}$ $_{10}$Ne	4.305	4.597	0.950††	4.367	3.604	1.306
$_{12}$Mg $\underline{23}$ $_{11}$Na	4.885	4.956	0.950††	4.708	3.683	1.295
$_{13}$Al $\underline{25}$ $_{12}$Mg	5.075	5.304	0.950††	5.039	3.759	1.286
$_{14}$Si $\underline{27}$ $_{13}$Al	5.608	5.639	0.952	5.368	3.829	1.276
$_{15}$P $\underline{29}$ $_{14}$Si	5.746	5.729	0.959	5.494	3.903	1.270
$_{16}$S $\underline{31}$ $_{15}$P	6.046	6.105	0.962	5.873	4.000	1.273
$_{17}$Cl $\underline{33}$ $_{16}$S	6.187	6.052	0.957	5.792	4.073	1.270
$_{18}$A $\underline{35}$ $_{17}$Cl	6.138	6.381	0.960††	6.126	4.166	1.274
$_{19}$K $\underline{37}$ $_{18}$A	6.75† 6.825 ±0.28	6.699	0.960††	6.431	4.245	1.274
$_{20}$Ca $\underline{39}$ $_{19}$K	7.605 ±0.37	7.010	0.957	6.709	4.319	1.274
$_{21}$Sc $\underline{41}$ $_{20}$Ca	6.701	7.439	0.963	7.164	4.388	1.273

† Given in ref. [6]).

†† In these cases of incomplete shells, the exchange factor is approximated between the two limits. The actual value depends on the coupling assumptions and lies within 1 to 2 per cent of the given value.

3.2. EXCHANGE CORRECTION FACTOR

If we consider an isotropic harmonic oscillator characterized by the potential function $V = \frac{1}{2}m\omega^2 r^2$ the wave functions for the states of interest in mirror nuclei are given by

$$G_{1l} = \left[\frac{2\alpha}{\Gamma(l+\frac{3}{2})}\right]^{\frac{1}{2}} (\alpha r)^{l+1}\, e^{-\frac{1}{2}\alpha^2 r^2}, \tag{20}$$

$$G_{2s} = \left[\frac{6\alpha}{\sqrt{\pi}}\right]^{\frac{1}{2}} (\alpha r)\, e^{-\frac{1}{2}\alpha^2 r^2}\, [1-\tfrac{2}{3}\alpha^2 r^2], \tag{21}$$

$$\alpha = [m\omega/\hbar]^{\frac{1}{2}}.$$

The electrostatic interaction is evaluated in terms of Slater integrals [13] $F^0(nl : n'l')$ for the direct terms and $G^k(nl : n'l')$ for the exchange terms. Using the wave functions given above we have

$$F^0(1l,\ 1l') = e^2\alpha \frac{\Gamma(\sigma)}{2^\sigma \Gamma(l+\frac{3}{2})\Gamma(l'+\frac{3}{2})}\left[\frac{2F_1(1,\sigma;\sigma-l;\frac{1}{2})}{l'+\frac{3}{2}} + \frac{2F_1(1,\sigma;\sigma-l';\frac{1}{2})}{l+\frac{3}{2}}\right] \tag{22}$$

$$G^k(1l,\ 1l') = \frac{e^2\alpha\ \Gamma(\sigma)}{n\cdot 2^{\sigma-2}\Gamma(l+\frac{3}{2})\Gamma(l'+\frac{3}{2})}\, 2F_1(1,\ \sigma;\ n+\tfrac{1}{2};\ \tfrac{1}{2}) \tag{23}$$

where

$$\sigma = l+l'+\tfrac{5}{2} \quad \text{and} \quad n = l+l'+k+3 \tag{24}$$

and ${}_2F_1(a,\ b;\ c;\ x)$ denotes Gauss' hypergeometric series. Similar, but somewhat more complicated, expressions are obtained for interaction between 2s and 1l states. On substituting for l and l' we get the value of these integrals in multiples of $e^2\alpha$ and a linear combination of such terms gives the Coulom energy in units of $e^2\alpha$ †. It is evident that a ratio of the exchange corrected Coulomb energy to the direct term energy is independent of α and this ratio we term as the exchange correction factor. For instance in the case of the O^{15}—N^{15} pair, we have

$$\text{Direct term} = 2F^0(1\text{p},\ 1\text{s}) + 5F^0(1\text{p},\ 1\text{p}) = \frac{65}{6}\,\frac{e^2\alpha}{\sqrt{2\pi}},$$

$$\text{Exchange term} = -\tfrac{1}{3}G'(1\text{p},\ 1\text{s}) - \tfrac{2}{5}G^2(1\text{p},\ 1\text{p}) = -\frac{2}{3}\,\frac{e^2\alpha}{\sqrt{2\pi}},$$

$$\text{Exchange correction factor} = \frac{\text{(Direct + Exchange) Terms}}{\text{Direct term}} = 0.938.$$

It is of interest to note that Jancovici's calculations [7]) with square well

† α can be evaluated from experimental Coulomb energy difference to give the oscillator wave functions for these nuclei as in ref. [7]). On the other hand a previous study [14]) enables us to fix α corresponding to the diffuse boundary wave functions.

wave functions yield exactly the same result. The values of exchange factor thus obtained are listed in table 2, column 4. For a complete shell, or one proton outside a closed shell, the coefficients of the Slater integrals are independent of m_l but in case of incomplete shells the exact evaluation requires specific coupling assumptions. However the values for former cases are so close that we can choose an intermediate value arbitrarily for the incomplete shell cases and still be correct within one to two percent.

Applying the exchange correction factor to $\langle V_C \rangle$, the theoretical values for the Coulomb energy differences are listed in table 2, column 5, and are shown by open circles in fig. 1.

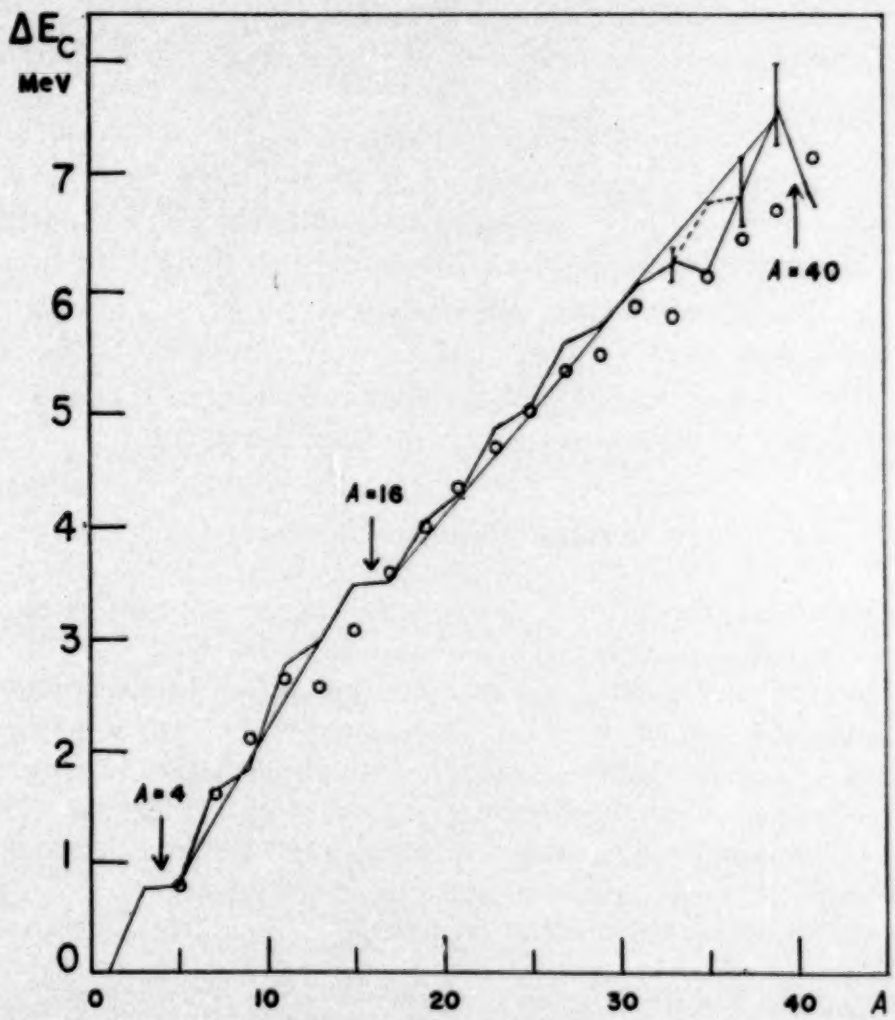

Fig. 1. ΔE_c vs A. The experimental points are joined by short lines. The vertical lines give the uncertainty of the value. The long straight lines are drawn through points in a major shell. The point joined by dotted lines ($A = 35$) corresponds to value given by β^+-decay [5]). Open circles denote the predicted values.

3.3. EXPERIMENTAL COULOMB ENERGY DIFFERENCES

In the case of a mirror nuclei pair with $(Z+1)$ and Z protons and a mass number $A = 2Z+1$, the atomic masses are given by

$$
\begin{aligned}
{}_{Z+1}M^A_Z &= [ZM_p + ZM_n + M_p] - [E_N - E_C] \\
{}_ZM^A_{Z+1} &= [ZM_p + ZM_n + M_n] - [E'_N - E'_C]
\end{aligned} \tag{25}
$$

where E_N and E_C represent the nuclear binding energy and the total Coulomb energy respectively. If the protons and the neutrons are assumed to be bound by the same nuclear energy, the number of nucleons remaining constant, we have $E_N = E'_N$ and

$$\Delta E_C = [{}_{Z+1}M^A - {}_ZM^A] + [M_n - M_p]. \tag{26}$$

The mass data tabulated by Wapstra [15]) and Mattauch *et al.* [16], incorporating more recent values where available [17,18]), are used here. The results obtained are listed in table 2 and are plotted in fig. 1 (points joined by short lines). In cases where uncertainty seemed appreciable, it is shown by vertical lines.

It is noticed that these differences exhibit pairing effects which have been studied in detail by Carlson and Talmi [4]). Moreover the figure also brings out the shell structure corresponding to $A = 4, 16$ and 40 (nucleon numbers 2, 8 and 20) as shown by the long straight lines in between these mass numbers. From the general systematics and the pairing energy considerations, it would seem that the value obtained from Wapstra's tables for $A = 35$ is too small and that the higher value, quoted by Kofoed-Hansen [5]) (joined by dotted lines in the figure) seems to fit in better.

4. Proton Potential Anomaly

A comparison of the theoretical values and the experimental results shows that there is excellent agreement between the two although the theoretical values are generally slightly smaller than those given by experiment. This small difference may be attributed to the use of eq. (16) which provides us with a lower limit for the result. A similar calculation with the use of the wave functions for the daughter nucleus would bring the agreement even closer. A smaller spin orbit interaction term would also appear to be more suitable from the point of view of shell systematics.

Let us now assume the proton perturbation is modified by an anomalous potential

$$
\begin{aligned}
V_a &= -kV_C \qquad (\varrho < 1) \\
&= -k \exp\left(\frac{1-\varrho}{\delta}\right) V_C \qquad (\varrho > 1).
\end{aligned} \tag{27}
$$

This characterization of the anomaly proved to be quite satisfactory in accounting for the line of beta-stability in heavier nuclei.

The calculations for the total proton perturbation were carried out, using a formula similar to one used in eq. (19), for a typical nucleus $A = 25$.

The effect of the anomaly on the wave functions was taken into account through A-shifts given in G.I. For a value of $k = 0.4$ the value of ΔE_C is calculated to be 3.34 and for $k = 0.7$ it drops to 2.01 as compared to the experimental value of 5.07 and the theoretical value 5.04 without the anomaly. Similar results are obtained at other mass numbers. Thus the inclusion of an additional attractive anomaly proportional to the Coulomb term is not compatible with the experiment in the region of the mirror nuclei. It will be shown in the following section that even the determination of the nuclear radii based on the assumption of full Coulomb perturbation is in very good agreement with the experiment. It may be remarked that the reduced mass and the exchange effects act to cancel a part of the Coulomb contribution which is thus effectively less than its full value. Thus the realistic wave functions for a static diffuse boundary well of proper depth adjusted according to binding energy considerations and including the various perturbation effects reproduce satisfactorily the experimental Coulomb energy differences for mirror nuclei under the assumption of full Coulomb perturbation added on to the neutron potential well.

5. Nuclear Radii

The expectation value for nuclear radii was calculated in G.II as

$$\left\langle \frac{r^2}{a^2} \right\rangle = (1-P_e)R_{l+\frac{1}{2}}(\varepsilon') + P_e[f_0 + f_1 S_n(k) + f_2 T_n(k)]. \tag{28}$$

The values obtained for our range of interest, after including all the correction factors discussed in subsection 3.1, are shown in fig. 2. The equivalent uniform distribution is given by

$$R = [\tfrac{5}{3}\langle r^2 \rangle_{av}]^{\frac{1}{2}} \tag{29}$$

and the nuclear radius constant is defined by

$$R = r_0 A^{1/3}. \tag{30}$$

To test the validity of the model, radius evaluations were carried out for the nuclei C^{12}, Mg^{24}, Si^{28}, S^{32} and Ca^{40} which have been experimentally investigated by electron scattering experiments at Stanford [12, 19]). The predicted values along with the experimental results are shown in table 3. It may be observed that the agreement is good enough to justify detailed study for the nuclei in this mass range. The values so obtained for R and r_0 are shown in the last columns of table 2. The values of r_0 are plotted as a function of A in fig. 3. The values for experimentally studied nuclei are also shown, as also are the results of some other investigators.

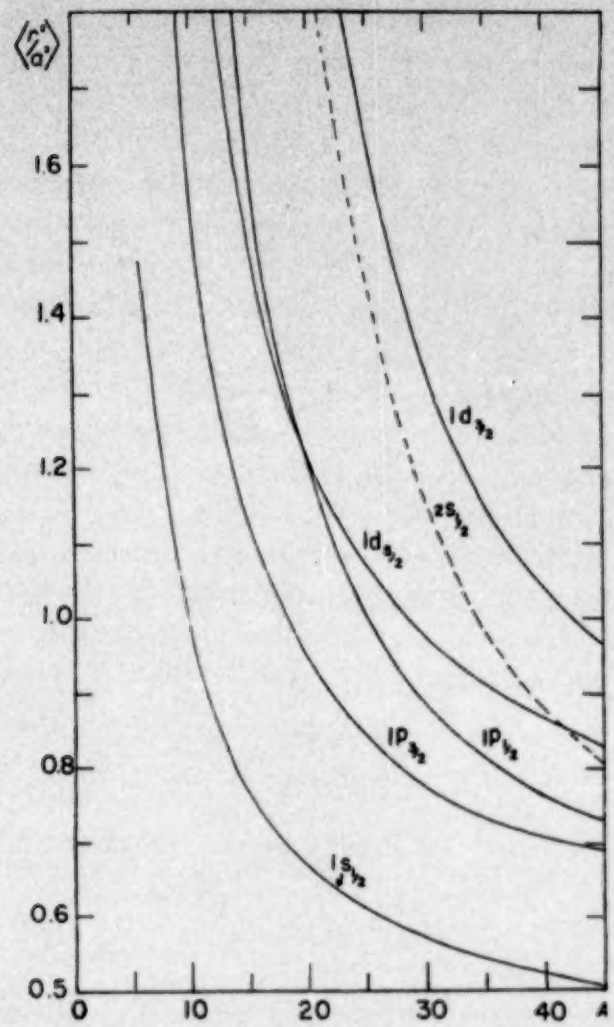

Fig. 2. Nuclear radii (i.e. expectation of r^2/a^2) for various proton orbitals.

TABLE 3

Experimental and predicted nuclear radius constants for experimentally investigated light nuclei.

Nucleus	Exp. r_0	Theor. r_0	Percentage Deviation (100 × (Th.-Exp.)/Exp.)
C^{12}	1.35	1.36	0.74
Mg^{24}	1.33	1.30	−2.31
Si^{28}	1.29	1.28	−0.78
S^{32}	1.30	1.28	−1.54
Ca^{40}	1.28	1.28	0

6. Discussion and Conclusions

The equivalent uniform distribution radii R have been fitted by the method of least squares to an equation of the type $R = aA^{1/3}+b$ to give

$$R = 0.992A^{1/3} + 0.904 \approx 1.31A^{1/3}. \quad (32)$$

The last expression is obtained by fitting to the simple form $R = r_0 A^{1/3}$. Thus the model predicts a radius constant $r_0 = 1.31$ for this region. Hofstadter [20]) reported the experimental value for the light elements to be close to $r_0 = 1.32$. Ford and Hill [21]) mention $r_0 = 1.3 \pm 0.1$ for mirror nuclei. It may be mentioned that Kofoed-Hansen [5]) arrived at the theoretical

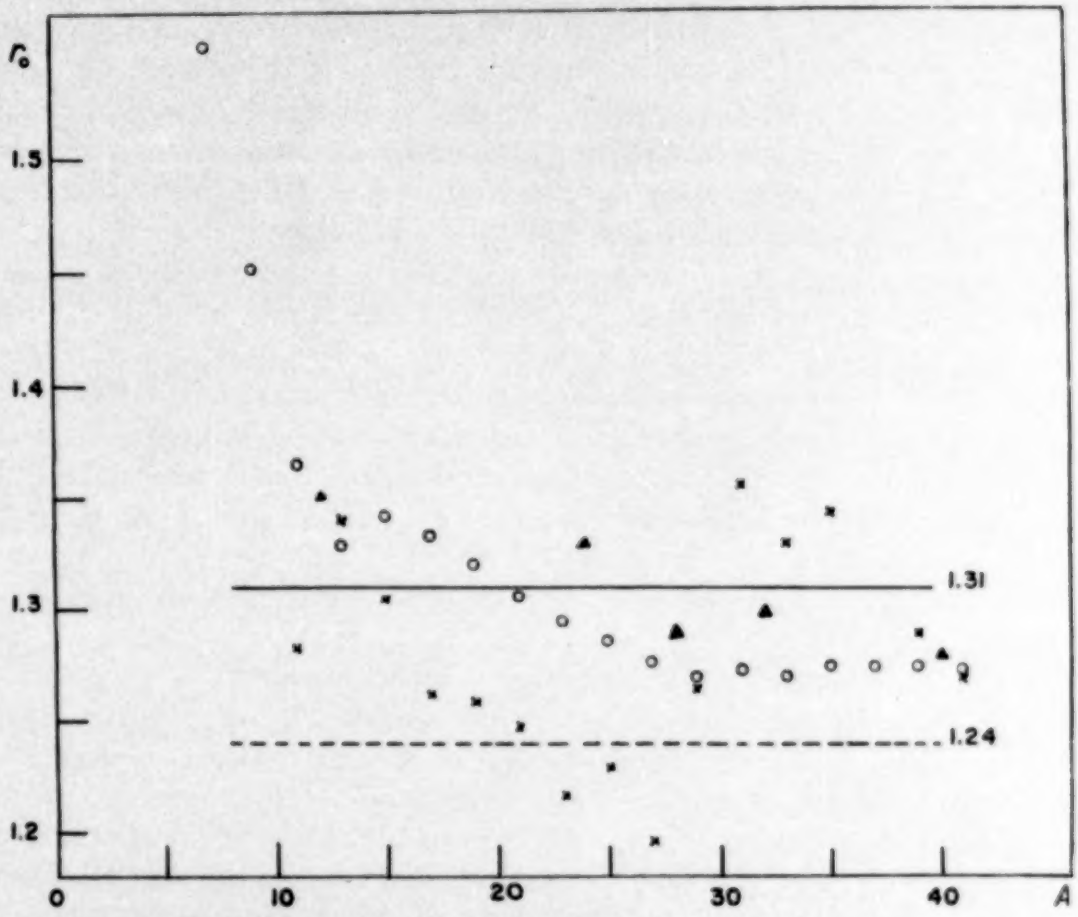

Fig. 3. r_0 vs A. Open circles denote the predicted values. Solid triangles represent the experimental results. The crosses show the results of Carlson and Talmi [4]). The lower broken line corresponds to the value given by Kofoed-Hansen [5]).

value $r_0 = 1.24$, but his results are based on a study of 'rather extreme models . . . neglecting the effects of spin orbit forces and Coulomb forces on the wave functions.'

A study of fig. 3 shows that r_0 decreases quite slowly with A for lighter nuclei and attains a fairly constant value for $23 < A < 41$. This is in agreement with the available experimental information. The decrease appears to be much slower than predicted by Carlson and Talmi [4]). On the basis of the calculations here it is clear that the so-called discrepancy of the theoretical results with the experiments, based on comparison with the

rather unrealistic value $r_0 = 1.20$ extrapolated from μ-mesonic X-ray studies, does not exist.

In the optical model analysis of low energy proton-nucleus scattering it has been observed [22]) that a number of equivalent fits may be obtained by various choices for r_0 and V if Vr_0^2 is kept nearly the same. Kellogg and Glassgold find that for silver $r_0 = 1.20$ and $V = 56.3$ MeV gives nearly as good a fit as $r_0 = 1.10$ and $V = 70.7$ MeV. This $V-r_0$ ambiguity has also been pointed out by Melkanoff *et al.*[23]) and Emmerich [24]). If the radius parameter varies in the manner found in this study, the potential well for heavier nuclei can be deeper by 15—20 MeV than that for the light nuclei yet still account for proton scattering phenomena. Accordingly, the vanishing of the proton potential anomaly in the mirror nuclei region is compatible with its existence in the heavy mass number region.

This study has led to a number of by-products which might be of general interest. These calculations suggest that differences in individual particle wave functions for the various states have a rather substantial effect upon the Coulomb energy shifts. Hence the usual procedure for matching levels of a mirror nucleus pair by shifting all the levels of one isobar by a constant amount to correct for the Coulomb effect and proton-neutron mass difference is quite open to question. The fact that the wave function changes appreciably from state to state also suggests that the spin orbit shifts may not go simply as $\frac{1}{2}(l+1)$ and $-\frac{1}{2}l$ since the spin orbit 'constant' may differ appreciably in the upper and lower states.

Summarizing a static individual particle model has been constructed for mirror nuclei in which the proton sees the same well as the neutron apart from the Coulomb barrier. The model is in general accord with experimental results on Coulomb energy differences, proton and neutron binding energies, and proton radii. The exact origin of the proton potential anomaly observed in heavier nuclei is a matter of considerable importance to the understanding of nuclear structure. An earlier study [25]) of the gross nature of the anomaly throughout the entire mass range has indicated a number of possible origins for this anomaly. This study of mirror nuclei delimits somewhat the possibilities. Particularly the fact that the anomaly does not appear to bear a simple relationship to the Coulomb potential suggests that it does not arise from the breakdown of electrostatic laws. It can be shown [26, 27]) that in a velocity dependent potential a term arises which is proportional to V_C but of opposite sign. For a velocity dependence corresponding to $m^*/m = \frac{1}{2}$ the factor of proportionality is $\frac{1}{2}$. Such a large anomaly, while appropriate in the heavy mass region, would appear to be ruled out in the mirror nuclei region. A more detailed study of the effect of velocity dependence of the nucleon-nucleus potential is under way. At this time, one thing can be said with certainty on the basis of this study with mirror nuclei,

namely that the characterization of the proton well as having a fixed depth of about 55 MeV for all nuclei as contrasted with a fixed neutron well depth of about 42 MeV is untenable.

One of us (P. C. Sood) wishes to acknowledge the helpfulness of discussions with N. V. V. J. Swamy on hypergeometric series.

References

1) A. E. S. Green, Phys. Rev. **102** (156) 1325
2) M. A. Melkanoff, S. A. Moszkowski, J. Nodvik and D. S. Saxon, Phys. Rev. **101** (1956) 507
3) A. A. Ross, R. D. Lawson and H. Mark, Phys. Rev. **104** (1956) 401
4) B. C. Carlson and I. Talmi, Phys. Rev. **96** (1956) 436
5) O. Kofoed-Hansen, Nuclear Physics **2** (1956/57) 441
6) L. M. Cooper and E. M. Henley, Phys. Rev. **92** (1953) 801
7) B. C. Jancovici, Phys. Rev. **95** (1954) 389
8) A. E. S. Green, Phys. Rev. **104** (1956) 1617
9) Vachaspati and S. M. Shah, Proc. Phys. Soc. A **67** (1954) 950
10) J. L. Fowler and N. O. Cohn, Bull. Amer. Phys. Soc. **2** (1957) 32; private communication
11) A. E. S. Green, K. Lee and R. J. Berkley, Phys. Rev. **104** (1956) 1625
12) B. Hahn, D. G. Ravenhall and R. Hofstadter, Phys. Rev. **101** (1956) 1131
13) E. U. Condon and G. H. Shortley, The Theory of Atomic Spectra (Cambridge University Press, 1953) pp. 175–178
14) P. C. Sood and A. E. S. Green, Bull. Amer. Phys. Soc. **1** (1956) 269
15) A. H. Wapstra, Physica **21** (1955) 367; **21** (1955) 385
16) J. Mattauch, L. Waldmann, R. Bieri and F. Everling, Ann. Revs. Nuclear Sci. **6** (1956) 179
17) A. G. Rubin, G. D. Johnson and J. B. Reynolds, Phys. Rev. **104** (1956) 1444
18) P. M. Endt, W. W. Bueckner, C. M. Braams, C. H. Paris and A. Sperduto, Phys. Rev. **105** (1957) 1002
19) J. H. Fregeau, R. H. Helm and R. Hofstadter, Physica **22** (1956) 1195
20) R. Hofstadter, Revs. Modern Phys. **28** (1956) 249
21) K. W. Ford and D. L. Hill, Ann. Revs. Nuclear Sci. **5** (1955) 46
22) P. C. Kellogg and A. E. Glassgold, Univ. of Minnesota AEC Report (1957) unpublished
23) M. A. Melkanoff, J. Nodvik, D. S. Saxon and R. D. Woods, Phys. Rev. **106** (1957) 793
24) W. S. Emmerich, Research Report (1957) unpublished
25) A. E. S. Green, Bull. Amer. Phys. Soc. **1** (1956) 269
26) A. M. Lane, Revs. Mod. Phys. **29** (1957) 191
27) M. H. Johnson and E. Teller, Phys. Rev. **98** (1955) 783

Nuclear Physics **5** (1958) 288—293; © *North-Holland Publishing Co., Amsterdam*
Not to be reproduced by photoprint or microfilm without written permission from the publisher

A THEORETICAL BASIS FOR A POSSIBLE THEORY OF β-DECAY

J. C. POLKINGHORNE
Tait Institute of Mathematical Physics, University of Edinburgh, Scotland

Received 5 October 1957

Abstract: A theoretical basis is proposed for a β-decay interaction similar to that suggested by Arnowitt and Feldman. The theory would account for a zero mass neutrino (though it is not a two-component theory) and negaton emission through S and T together with positon emission through A and V. It is based on a possible theory of the source of the masses of the elementary particles. An explanation is offered of the anomalous muon mass.

1. Introduction

$\beta-\nu$ angular correlation measurements on A^{35} [1]) and Ne^{19} [2]) seem to indicate that positon emissions take place through vector and axial vector couplings, in contrast to negaton emissions which are thought to take place through scalar and tensor couplings. Such an interaction cannot be expressed in terms of conventional β-decay field theory.

The most direct way in field theory of producing an expression for such an interaction would be to decompose the interaction representation electron field into its positive and negative frequency parts,

$$\psi_e(x) = \psi_e^{(+)}(x)+\psi_e^{(-)}(x), \tag{1}$$

where $\psi_e^{(+)}(x)$ annihilates a negaton and $\psi_e^{(-)}(x)$ creates a positon. Each part would then be coupled in a different way to the nucleon and neutrino fields. Such an interaction is essentially non-local because of the non-local commutation relations between $\psi_e^{(+)}(x)$ and $\psi_e^{(-)}(x)$. However, unless some numerical relationship between the coupling constants intervened, this theory would produce a different interaction-mass for the positon and the negaton.

It was presumably this consideration that led Arnowitt and Feldman [3]) to point out that if leptons are conserved it is equally possible to fit the experiments by decomposing the neutrino field into its positive and negative frequency parts,

$$\psi_\nu(x) = \psi_\nu^{(+)}(x)+\psi_\nu^{(-)}(x), \tag{2}$$

and coupling them in different ways to the nucleon and electron fields. The difference between a theory based on the decomposition (1) and a theory

based on the decomposition (2) is that the first links the reactions

$$\begin{aligned} &p \to n + e^+ + \nu, \\ &p + \bar{\nu} \to n + e^+, \end{aligned} \tag{3}$$

while the second links the reactions

$$\begin{aligned} &p \to n + e^+ + \nu, \\ &p + e^- \to n + \nu. \end{aligned} \tag{4}$$

Not enough is known at present about the lepton-absorption experiments to discriminate between the two theories.

The second scheme presents an advantage over the first only if the neutrino is guaranteed to have zero mass. One way of imposing this condition is the use of the two-component theory of Salam [4]), Lee and Yang [5]), and Landau [6]). This theory implies no restriction on the types of coupling chosen for the positive and negative frequency fields respectively.

However, as Arnowitt and Feldman [3]) point out, the present experimental data do not unambiguously confirm the two-component theory. The purpose of this paper is to present another theory which would guarantee zero mass for the neutrino and which would require that $\psi_\nu^{(+)}(x)$ is coupled through A and V, and $\psi_\nu^{(-)}(x)$ through S, P, and T, or *vice versa*. A possible β-decay Hamiltonian would be

$$\begin{aligned} H = \int \mathrm{d}^3\mathbf{x} \{ &\bar{\psi}_\mathrm{P}\, \psi_\mathrm{N}\, \bar{\psi}_\mathrm{e} (c_\mathrm{S} + c'_\mathrm{S}\, \gamma_5) \psi_\nu^{(-)} \\ &+ \tfrac{1}{2} \bar{\psi}_\mathrm{P}\, \sigma_{\mu\nu}\, \psi_\mathrm{N}\, \bar{\psi}_\mathrm{e}\, \sigma_{\mu\nu} (c_\mathrm{T} + c'_\mathrm{T}\, \gamma_5) \psi_\nu^{(-)} \\ &+ \bar{\psi}_\mathrm{P}\, \gamma_5\, \psi_\mathrm{N}\, \bar{\psi}_\mathrm{e}\, \gamma_5 (c_\mathrm{P} + c'_\mathrm{P}\, \gamma_5) \psi_\nu^{(-)} \\ &+ \bar{\psi}_\mathrm{P}\, \gamma_\mu\, \psi_\mathrm{N}\, \bar{\psi}_\mathrm{e}\, \gamma_\mu (c_\mathrm{V} + c'_\mathrm{V}\, \gamma_5) \psi_\nu^{(+)} \\ &+ \bar{\psi}_\mathrm{P}\, i\gamma_\mu \gamma_5\, \psi_\mathrm{N}\, \bar{\psi}_\mathrm{e}\, i\gamma_\mu \gamma_5 (c_\mathrm{A} + c'_\mathrm{A}\, \gamma_5) \psi_\nu^{(+)} \\ &+ \mathrm{h.c.} \}, \end{aligned} \tag{5}$$

with which it is possible to fit all the experimental data known at present. This theory is based on certain assumptions about the origin of the masses of the elementary particles. This is a subject shrouded in mystery and so the theory presented here is necessarily speculative.

In section 2 we discuss the possible theories of the origin of the masses of the elementary particles and choose one that is to be the basis of the discussion. In section 3 it is shown that the neutrino will have zero mass provided a certain scheme of couplings is adopted for the weak interactions. This scheme leads to a β-decay Hamiltonian of the type (5).

2. The Masses of the Elementary Particles

For simplicity we shall consider only the system of nucleons, pions, photons, and leptons, in mutual interaction. The extension of the theory to the strange particles will be obvious.

Many people have considered the attractive notion that the masses of the elementary particles arise solely from their interactions and that they all have zero bare mass. Such a theory would have to incorporate a cut-off, Λ, which would appear only in the form Λ^2. As Feynman has pointed out [7]), the principal difficulty encountered by this idea is that of explaining the mass of the muon. So far as we know this particle has no strong interactions but it has a considerable mass.

In such a theory it is easy to show that the bosons will acquire a mass from their interactions. However for fermions, if the interactions are all simple (i.e. the nucleon-pion interaction is either pseudoscalar or pseudovector but not a mixture of the two, etc.) the theory is invariant under the transformations

$$\psi(x) \to \gamma_5 \psi(x), \tag{6}$$

simultaneously for all fermion fields, together with

$$g_{\pi,N} \to -g_{\pi,N}, \tag{7}$$

if the pion-nucleon interaction is pseudoscalar, or

$$g_{\pi,N} \to g_{\pi,N}, \tag{7'}$$

if the pion-nucleon interaction is pseudovector. Since the interaction masses depend on the squares of the coupling constants the invariance of the theory under (6) and (7) or (7') implies that all interaction-masses vanish for the fermions. This is confirmed by perturbation theory calculations which give mass corrections $\propto m_0 \log \Lambda^2/m_0^2 \to 0$ as $m_0 \to 0$.

One way of building fermion masses would be to introduce a mixed pion nucleon interaction

$$ig_1 \bar{\psi}\tau\gamma_5 \psi \cdot \varphi + g_2 \bar{\psi}\tau\gamma_5 \gamma_\mu \psi \cdot \partial_\mu \varphi. \tag{8}$$

The theory then gives masses $\propto g_1 g_2 \Lambda^2$, since g_1 is dimensionless and g_2 has the dimensions of m^{-1}. An alternative procedure would be to keep the simple interactions and to introduce a non-zero bare mass for one of the fermions. This is the procedure we shall follow. We shall assume that the muon has non-zero bare mass and use this to explain its anomalous mass. Of course, even if this point of view is correct, the muon still remains a mysterious particle because of its otherwise great similarity to the electron.

Accordingly we assume:

(i) that all elementary particle interactions are simple in the sense used above;

(ii) that all elementary particles other than the muon have bare mass zero. Under these two assumptions we shall show in the next section how to construct a scheme of interactions that guarantees a zero mass for a four-component neutrino.

3. The Interaction Scheme

If a massless fermion field is decomposed into its positive and negative frequency parts they satisfy

$$\int d^3\,\mathbf{x}\bar{\psi}_\nu(x)\gamma_\alpha\partial_\alpha\psi_\nu(x) = \int d^3\,\mathbf{x}\{\overline{\psi_\nu^{(+)}}(x)\gamma_\alpha\partial_\alpha\psi_\nu^{(+)}(x) + \overline{\psi_\nu^{(-)}}(x)\gamma_\alpha\partial_\alpha\psi_\nu^{(-)}(x)\}, \quad (9)$$

and

$$\int d^3\,\mathbf{x}\bar{\psi}_\nu(x)\psi_\nu(x) = \int d^3\,\mathbf{x}\{\overline{\psi_\nu^{(+)}}(x)\psi_\nu^{(-)}(x) + \overline{\psi_\nu^{(-)}}(x)\psi_\nu^{(+)}(x). \quad (10)$$

Equation (10) is particularly important and constrasts with the corresponding relation for a massive fermion field

$$\int d^3\,\mathbf{x}\overline{\psi_\mu}(x)\psi_\mu(x) = \int d^3\,\mathbf{x}\{\overline{\psi_\mu^{(+)}}(x)\psi_\mu^{(+)}(x) + \overline{\psi_\mu^{(-)}}(x)\psi_\mu^{(-)}(x)\}. \quad (11)$$

The difference between (10) and (11) arises from the difference between the way in which the positive and negative energy solutions of the Dirac equation are constructed for a massless and a massive particle. Physically equation (10) is easily understood. The operator on the left-hand side conserves spatial momentum and angular momentum, and couples opposite screw-sense two-component solutions of the neutrino equations. These conditions can all be satisfied by the two terms on the right-hand side representing the creation or annihilation of a neutrino pair but not by the omitted terms representing the absorption and re-emission of a neutrino or antineutrino.

Under the assumptions discussed in section 2 an interaction-mass term in the Hamiltonian † must have the form

$$\int d^3\,\mathbf{x} m_0^\mu f(g_i^2, \Lambda^2, m_0^{\mu 2})\bar{\psi}_\nu(x)\psi_\nu(x), \quad (12)$$

where $f(g_i^2, \Lambda^2, m_0^{\mu 2})$ is a dimensionless function of its arguments. If the β-decay interaction has the form given by (5) and the μ-capture interaction a similar form, then the theory is invariant under the transformations

$$\begin{aligned} \psi_e(x) &\to \gamma_5\psi_e(x), \\ \psi_\mu(x) &\to -\gamma_5\psi_\mu(x), \\ \psi_\nu^{(+)}(x) &\to \gamma_5\psi_\nu^{(+)}(x), \\ \psi_\nu^{(-)}(x) &\to -\gamma_5\psi_\nu^{(-)}(x), \\ m_0^\mu &\to -m_0^\mu. \end{aligned} \quad (13)$$

The transformations (13) impose no restrictions on the interactions producing

† In this theory we can only prove that no mass terms appear in the Hamiltonian, not in the Hamiltonian density. This appears to be sufficient. The reason is the essential part played by the three-dimensional integral in equation (10).

$$\mu^{\pm} \to e^{\pm} + \nu + \bar{\nu}. \tag{14}$$

However the term (12) changes sign under these transformations and so there can be no neutrino interaction mass. Since the neutrino is assumed to have zero bare mass it is absolutely massless.

Alternatively we may consider the Hamiltonian obtained from (5) by interchanging $\psi_\nu^{(+)}(x)$ and $\psi_\nu^{(-)}(x)$ and obtain a similar result.

The interaction (5) together with the μ-capture interaction will provide a non-zero mass for the proton and the neutron (which is shown in the appendix to be the same for both) and for the electron. These then provide the germs from which their observed masses may grow from their other interactions. Because of the essential part played by the Fermi interaction the cut-off required in this theory would probably be higher than that usually considered.

The general argument of this section can easily be illustrated by a perturbation theory calculation. In second order equation (10) requires a neutrino self-energy graph with a positive frequency interaction at one vertex and a negative frequency interaction at the other. This graph vanishes for (5) because the closed nucleon loop (with zero mass nucleons) contains the trace of an odd number of γ matrices.

The most difficult phenomenon to understand in terms of this theory is the equality of the π^+ and π^- lifetimes. This is a feature that must be common to all theories that break the principle of charge conjugation to explain differences between positon and negaton emission. (The only exception would be a theory that split the electron field into positive and negative frequencies and forbad $\pi \to e + \nu$.) If the π-$\mu\nu$ decays take place principally through an intermediate virtual interaction with the nucleon field then the π^+ decay occurs through A in the μ-capture and the π^- decay through P, or *vice versa*. The equality of lifetimes would require a special relation to be satisfied by the relevant coupling constants.

4. Conclusion

Clearly the foregoing discussion is speculative in its assumptions. However if the experimental results continue to point to a difference in the emission of positons and negatons it may be of some interest to have a theory which will:

(i) require positon emission to be through A and V and negaton emission through S and T, or *vice versa*;

(ii) give the neutrino a zero mass;

(iii) offer some slight clue to the mystery of the muon.

With regard to the point (ii) it seems to be difficult to find a theory,

other than the present one and the two-component theory, which gives the neutrino zero mass.

Appendix

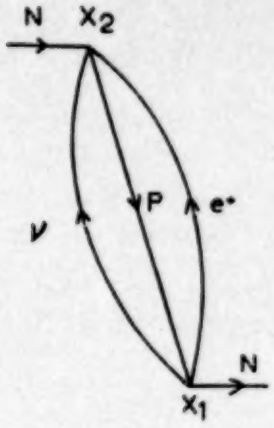

Fig. 1

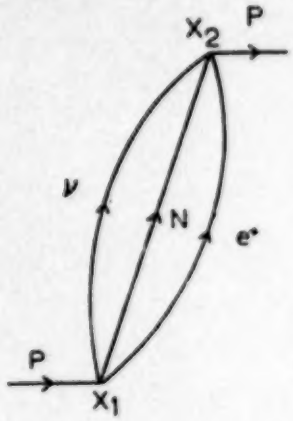

Fig. 2

Here we outline a proof of the fact that the chosen scheme for the weak interactions gives an equal mass to the proton and the neutron. Proton and neutron time-ordered self-energy graphs can be put in correspondence in pairs of which the graphs in figs. 1 and 2 are examples. The contributions to the self-energy from these two graphs are the same except that in fig. 1 the proton line has a term $S^{(-)}(x_1-x_2)$ associated with it and in fig. 2 the neutron line has a term $S^{(+)}(x_2-x_1)$ associated with it. For massless fields these two terms are equal. Therefore we conclude that

$$\sum_{\mathrm{N}} (x_1,\ x_2) = \sum_{\mathrm{P}} (x_2,\ x_1). \tag{A1}$$

The mass correction is obtained by applying a covariant procedure, identical in form for each graph, to extract a term

$$\delta m\, \delta(x_1-x_2). \tag{A2}$$

From (A1) we conclude that

$$\delta m_{\mathrm{N}} = \delta m_{\mathrm{P}}. \tag{A3}$$

References

1) Herrmannsfeldt, Maxson, Stähelin and Allen, Phys. Rev., in the press
2) W. P. Alford and D. R. Hamilton, Phys. Rev. **105** (1957) 673
3) R. Arnowitt and G. Feldman, to be published
4) A. Salam, Nuovo Cimento **5** (1957) 299
5) T. D. Lee and C. N. Yang, Phys. Rev. **105** (1957) 1671
6) L. Landau, Nuclear Physics **3** (1957) 127
7) Cf. the appendix to J. Mathews, Phys. Rev. **102** (1956) 270

Nuclear Physics **5** (1957) 294—296; © *North-Holland Publishing Co., Amsterdam*
Not to be reproduced by photoprint or microfilm without written permission from the publisher

A NOTE ON THE ISOTOPIC ASSIGNMENT OF SLOW NEUTRON RESONANCES IN SAMARIUM, IRIDIUM AND GADOLINIUM

E. M. BOWEY and J. R. BIRD
Atomic Energy Research Establishment, Harwell

Received 17 October 1957

Abstract: Some further isotopic assignments of slow neutron resonances have been made with the elements Samarium, Iridium and Gadolinium, using the Harwell 15 MeV linear accelerator and capture gamma ray scintillation detectors.

Using the apparatus described in earlier papers [1, 2]) measurements have been made of the slow neutron resonances in the separated isotopes of samarium, iridium, and gadolinium, using samples obtained from the Oak Ridge National Laboratory under an arrangement made by the Tripartite Nuclear Cross Section Committee. By detecting both capture gamma rays and scattered neutrons and comparing the yield curves with the known percentage of each isotope in the various samples, the assignment of resonances to their appropriate isotope was made.

Timing channels, 2 μsec wide, were used in the measurements of neutron time-of-flight. For each sample, two sets of runs were done, in one of which the signals were delayed by 1 μsec. A comparison of runs made it possible to determine the time-of-flight to the nearest microsecond and the errors in neutron energy include a possible error in timing of 1 μsec (0.11 μsec/m) together with a very small uncertainty in flight path length.

SAMARIUM

Oxide samples enriched to about 90 % abundance of a particular samarium isotope were used (170 mg/cm^2 of samarium) and the results are given in table 1. The assignment of resonances is straightforward up to an energy of 60 eV, and the results are in agreement with measurements made by S. J. Cocking using the Harwell fast chopper. Above 60 eV the individual resonances are not always clearly resolved.

Near 40 eV, two resonances have been found with the MTR fast chopper [3]). One of these is caused by Sm^{147} and the other by Sm^{149}. In the doublet at 45 eV, only one resonance (in Sm^{149}) is resolved.

TABLE 1
SAMARIUM

Observed Energy in eV	Mass of Isotope
3.4 ±0.03	147†
4.96±0.05	149†
6.46±0.07	149
8.05±0.09	152†
8.95±0.10	149
12.08±0.15	149
14.97±0.20	149
15.92±0.22	149
17.22±0.24	149
18.40±0.26	147
20.69±0.31	150
23.3 ±0.4	149
25.4 ±0.4	149
26.3 ±0.4	149
27.3 ±0.5	147
30.0 ±0.5	147
30.8 ±0.5	149
32.1 ±0.6	147
33.9 ±0.6	149
39.8 ±0.8	147
40.5 ±0.8	149
44.6 ±0.9	149
47.5 ±1.0	150
49.5 ±1.1	147
51.6 ±1.1	149
58.5 ±1.3	147
59.9 ±1.4	149
65.6 ±1.6	147
72.5 ±1.8	149
75.5 ±1.9	147
84.1 ±2.2	147
86.5 ±2.3	152
90.0 ±2.4	154
94.3 ±2.6	148
96.5 ±2.7	149
101.3 ±2.9	147
108.0 ±3	149
124 ±4	147
131 ±4	149
141 ±5	147
147 ±5	149
149 ±5	152
161 ±6	147
174 ±6	152
182 ±7	149

† Already assigned [3]).

TABLE 2
IRIDIUM

Observed Energy in eV	Mass No. of Isotope
5.35±0.05	191 †
9.04±0.10	193
9.88±0.11	191
19.08±0.28	191
20.46±0.31	191
24.7 ±0.4	193
25.9 ±0.4	193
30.0 ±0.5	191
32.0 ±0.6	191
36.2 ±0.7	191
42.4 ±0.8	193
52.2 ±1.1	191
52.6 ±1.1	193
64.9 ±1.5	191
68.0 ±1.6	193
77.2 ±2.0	193

† Already assigned [3]).

TABLE 3
GADOLINIUM

Observed Energy in eV	Mass No. of Isotope
6.40±0.06	155
7.81±0.09	155
10.12±0.12	155
11.57±0.14	155
12.06±0.14	155
14.64±0.19	155
16.88±0.24	157
17.57±0.25	155
19.70±0.3	155
20.8 ±0.3	155 and 157
22.24±0.33	158 and 154
23.29±0.37	155
25.6 ±0.4	157
29.5 ±0.5	155
32.5 ±0.6	155 and 156
36.4 ±0.7	155
42.7 ±0.9	155
44.8 ±0.9	157
45.5 ±0.9	155
49.5 ±1.0	157
50.8 ±1.1	155
59.1 ±1.4	157
63.7 ±1.5	154
66.9 ±1.6	155
78.0 ±1.9	155
79.7 ±2.1	156
81.4 ±2.1	157

IRIDIUM

The results obtained using 50 mg/cm² of iridium metal enriched to 90 % in Ir^{193} were compared with those for a sample of natural iridium containing a similar amount of the 193 isotope. Table 2 gives the assignment for resonances up to 80 eV, a number of which have not been reported previously. There is some evidence that the grouping of resonances in pairs at energies up to 30 eV, may also continue above this energy.

GADOLINIUM

Oxide samples containing approximately 100 mg/cm² of gadolinium were used, with enrichments varying from 33 % to 95 %. Due to the dense nature of the level structure, particularly in the 155 isotope, and the considerable mixing of isotopes in some samples, only the more prominent resonances above 25 eV could be assigned, and the results are given in table 3.

References

1) E. R. Rae and E. M. Bowey, Journal of Nuclear Energy **4** (1957) 179
2) E. M. Bowey, Nuclear Physics **3** (1957) 553
3) D. J. Hughes and J. A. Harvey, Neutron Cross sections (BNL 325)

AWARD OF THE NOBEL PRIZE FOR PHYSICS

TO

T. D. LEE AND C. N. YANG

The decision of the Swedish Academy of Sciences to award the Nobel Prize to the discoverers of the non-conservation of parity in weak interactions so soon after the event most happily expresses the general consensus of opinion concerning the fundamental importance of the discovery. All those who made the personal acquaintance of the young laureates have been impressed by the charm of their personality no less than by the versatility and profundity of their genius. The following article, racily sketching their brilliant career, will give the reader as apt a picture of their thought as the accompanying photograph of their features — brightened by the perfect Nobel laureate grin. The Editor is grateful to his old pupil and friend A. Pais for his prompt response to a request to write this article. It is fitting to remember that it was Pais' pioneering endeavour to analyze the invariance properties of elementary particles which gave the initial impetus to the theoretical developments culminating in Lee and Yang's discovery.

Nuclear Physics **5** (1958) 297—300; © *North-Holland Publishing Co., Amsterdam*
Not to be reproduced by photoprint or microfilm without written permission from the publisher

THE SCIENTIFIC WORK OF T. D. LEE AND C. N. YANG

A. PAIS
Institute for Advanced Study, Princeton

Received 15 November 1957

> Un physicien éminent me disait un jour à propos de la loi des erreurs: „Tout le monde y croit fermement parce que les mathématiciens s'imaginent que c'est un fait d'observation, et les observateurs que c'est un théorème de mathématiques." Il en a été longtemps ainsi pour le principe de la conservation de l'énergie. Il n'en est plus de même aujourd'hui; personne n'ignore que c'est un fait expérimental.
>
> H. POINCARÉ.

It seems fair to say that two years ago (to fix a reasonable point in time) nearly all theoretical physicists believed that the general validity of space reflexion invariance had firmly been established by observation †. It seems fair to say that at that time few experimentalists thought of devising experiments which might challenge the universal validity of parity conservation ††. It seems fair to say that the main contribution to physics which Lee and Yang have made so far has been to point out that parity conservation had never been checked in a domain of physics of which much, but not enough, was known two years ago (β-decay, π-decay, μ-decay); and to discuss a series of experimental conditions under which such checks could be made [3]).

The incentive to these investigations came from the puzzling properties of the K-mesons. Various participants of the Sixth Rochester Conference (April 1956) felt and expressed doubts about the universal validity of parity conservation in view of the experimentally found near equality in mass and, above all, in life time of the charged θ- and τ-mesons. Whatever might be the answer to this $\theta-\tau$ puzzle, it was clear that "the τ-meson will have either domestic or foreign complications," as Oppenheimer put it then †††. Lee and Yang faced the challenge. Immediately after the Conference they started a systematic investigation on the then status of experimental knowledge concerning the verification of space reflexion in-

† For a notable case of misgivings, see ref. [1])

†† For a notable exception, see ref. [2]).

††† Be it recorded here that on the train back from Rochester to New York, Professor Yang and the writer each bet Professor J. A. Wheeler one dollar that the θ- and the τ-meson were distinct particles; and that Professor Wheeler has since collected two dollars.

January (2) 1958

variance and charge conjugation invariance. Their conclusion was that ior one group of interactions neither invariance had so tar been established. These reactions are all characterized by their weakness and to these belong the three types of decay processes mentioned above, as well as K-particle and hyperon disintegration. Thus the attention became focused on a whole class of phenomena instead of on an exciting but rather isolated puzzle. Soon a theoretical investigation followed [4]), together with Oehme, on the question of time reversal invariance and on the interrelations between possible violations of "C-, P- and T-invariance" with the help of the CPT theorem. And then came the great news: Neither P- nor C-invariance holds true in β-decay, nor in π-, nor in μ-decay. It will be remembered how the Co^{60}-experiment of Chien Shung Wu (Mrs. Yuan) and co-workers [5]) provided the first evidence. More recently it has been established that parity is not conserved in Λ^0-decay either, and so, via only a slight theoretical detour, the $\theta-\tau$ puzzle may be considered to be solved.

Thus Lee and Yang's suggestions have led to a great liberation in our thinking on the very structure of physical theory. Once again principle has turned out to be prejudice. The quotation from Poincaré (taken from the preface of his *Thermodynamique* [6])) may be a timely reminder of not too dissimilar struggles of other generations.

Chen Ning Yang was born in 1922 in Hofei, in the province of Anhwei. He is the oldest of the five children of the mathematician Professor K. C. Yang who now teaches in Shanghai. Tsung Dao Lee was born in 1926 in Shanghai. He is the third of six children; his father was an agriculturalist. Both men studied at the Southwest Associated University at Kumming. Later Yang went to Tsinghua University in the same city where he got an M. Sc. in 1944. Their first acquaintance dates from 1945 when Lee was a student and Yang was teaching high school in Kumming. (One of his pupils was Miss Chih-Li Tu, now Mrs. Yang.) Their close friendship starts in 1946 when both are studying in Chicago. Yang gets his Ph. D. in 1948 under Professor Teller, with a thesis on angular distributions in nuclear reactions [7]). Lee gets his degree in 1950 under Professor Fermi for his work on the hydrogen content of white dwarfs [8]). His first papers [9]) deal with astrophysical problems and with the theory of turbulence. Soon after getting his doctorate Yang joins the Institute for Advanced Study in Princeton, at first as a temporary member, eventually (1956) as a full professor. In 1950 Lee goes to Berkeley as a lecturer. Here he meets Miss Janet Chin, now Mrs. Lee. In the Fall of 1951 Lee starts a two year period of membership at the Institute. From that time on the two men have collaborated intimately and steadily. (Incidentally, their first joint paper, together with Rosenbluth, deals with weak interactions [10]).) In 1953 Lee went to Columbia, where he has been a full professor since 1956.

In collaboration with others, Lee has worked on such subjects as π-nucleon scattering [11]) and multiple meson production [12]), studied by means of variational methods; and related approaches to the ground state and effective mass of the polaron [13]). Of particular interest is his work on a rigorously solvable renormalizable model of a field theory [14]). It is a model in the sense that one has to do with a problem which is not as rich in physical features as for example electrodynamics; at the same time the model is non-trivial. It enables one to treat renormalizations explicitly without the use of power-series expansions and it leads to new insights on the relation between unrenormalized and renormalized coupling constants. The interesting and spiritual consequences of the model are still under study.

Already in his thesis we find Yang engaged on a program of obtaining physical information which is largely independent of a detailed dynamical description but where extensive use is made of the invariance properties of the problem in hand. In a similar vein are his investigations on the parity [15]) of the π^0 meson and on the reflection properties of fermion fields [16]). Further we mention a not too successful attempt to consider π-mesons as nucleon derivates [17]); and an approach to field theory [18]) where one deals directly with the equations of motion for the various fields and sources. In 1952 Yang contracted the celebrated Ising disease, but unlike many of his fellow patients he pulled through by being able to compute the spontaneous magnetization of the two-dimensional lattice [19]). This in turn led to the Yang-Lee theory of phase transitions [20]), a subject to which Yang had been attracted earlier [21]). More recently and in collaboration with others, new results have been obtained on the many body problem in quantum theory [22]), some of which will help to put the theory of superfluidity on a more rigorous mathematical basis.

Many of the papers by Lee and Yang on fundamental particles carry a marked element of speculation, such as for example their suggestions on the conservation law of heavy fermions [23]), or on parity conjugation [24]). But invariably they propose experiments to test their conjectures and so, where they have been wrong at times, they have erred in good taste. And they have had the courage to try again.

Their more recent work deals with the two-component formulation of neutrino theory [25]), a topic to which independent contributions had been made by Salam [26]) and by Landau [27]); and with the concept of lepton conservation [28]). At the time of writing the experimental situation in β-decay, after having gone through a phase of utter confusion last summer, is still too unclear to enable one to judge the tenability of these appealing ideas. Most recently they have been analyzing the information obtainable from hyperon decay [29]).

The work of T. D. and of Frank, as they are affectionately called, is

characterized by taste and ingenuity, by physical insight and formal power. Their counsel is sought by theorist and experimentalist alike. In this they have more than a touch of the late Fermi. Their friends wish them many happy and creative years to come.

References

1) Wick, Wightman and Wigner, Phys. Rev. **88** (1952) 101, footnote 9
2) Purcell and Ramsey, Phys. Rev. **78** (1950) 807
3) Lee and Yang, Phys. Rev. **104** (1956) 254
4) Lee, Oehme and Yang, Phys. Rev. **106** (1957) 340
5) C. S. Wu *et al.*, Phys. Rev. **105** (1957) 1413
6) H. Poincaré, Thermodynamique (Paris, Gauthier-Villars); also in La Science et l'Hypothèse (Paris, Flammarion) p. 155
7) Yang, Phys. Rev. **74** (1948) 764
8) Lee, Astrophys. Journal **111** (1950) 625
9) Lee, Phys. Rev. **77** (1950) 842; Astrophys. Journal **112** (1950) 561; J. App. Phys. **22** (1957) 524; Quart. App. Math. **10** (1952) 69
10) Lee, Rosenbluth and Yang, Phys. Rev. **75** (1949) 905
11) Lee and Christian, Phys. Rev. **94** (1954) 1760; Friedman, Lee and Christian, Phys. Rev. **100** (1955) 1494
12) Henley and Lee, Phys. Rev. **101** (1956) 1536
13) Lee, Low and Pines, Phys. Rev. **90** (1953) 297; Lee and Pines, Phys. Rev. **92** (1953) 883
14) Lee, Phys. Rev. **95** (1954) 1329
15) Yang, Phys. Rev. **77** (1950) 242, 722
16) Yang and Tiomno, Phys. Rev. **79** (1950) 495
17) Yang and Fermi, Phys. Rev. **76** (1949) 1739
18) Yang and Feldman, Phys. Rev. **79** (1950) 792
19) Yang, Phys. Rev. **85** (1952) 808
20) Yang and Lee, Phys. Rev. **87** (1952) 404, 410
21) Yang, Chinese J. Phys. **5** (1944) 138; **6** (1945) 59; (with Y. Y. Li) **7** (1947) 59; J. Chem. Phys. **13** (1945) 66
22) Huang and Yang, Phys. Rev. **105** (1957) 767; the same and Luttinger, Phys. Rev. **105** (1957) 776; Lee and Yang, Phys. Rev. **105** (1957) 1119; the same and Huang, Phys. Rev. **106** (1957) 1135
23) Lee and Yang, Phys. Rev. **98** (1955) 1501
24) Lee and Yang, Phys. Rev. **102** (1956) 290; **104** (1956) 822
25) Lee and Yang, Phys. Rev. **105** (1957) 1671
26) Salam, Nuovo Cimento **5** (1957) 299
27) Landau, Nuclear Physics **3** (1957) 127
28) Lee, Proc. Seventh Rochester Conference 1957
29) Lee *et al.*, Phys. Rev. **106** (1957) 3367; Lee and Yang, A general partial wave analysis of the decay of a hyperon of spin $\frac{1}{2}$; Possible determination of the spin of Λ^0 from its large decay angular symmetry (Phys. Rev. in the press)

Contributions not referred to in the text: Bull. Am. Math. Soc. **50** (1944) 373; Phys. Rev. **72** (1947) 874; **84** (1951) 581; **84** (1951) 599; **96** (1954) 191; **99** (1955) 337; **100** (1955) 932; Nuovo Cimento **3** (1956) 749; Revs. Mod. Phys. **29** (1957) 231

Nuclear Physics **5** (1958) 301—318; © *North-Holland Publishing Co., Amsterdam*

Not to be reproduced by photoprint or microfilm without written permission from the publisher

SOME REMARKS ON K-MESON DECAYS

S. ONEDA †

Department of Theoretical Physics, University of Manchester

and

S. KAMEFUCHI ††

Institute for Theoretical Physics, University of Copenhagen

Received 31 August 1957

Abstract: The standpoint that the $K \to \mu(e)+\nu$ and the $K^0 \to \pi+\pi$ interactions are the primary weak interactions responsible for all K-meson decays is investigated in detail. The significance of this standpoint is discussed in connection with the true elementarity of the so called elementary particles (§ 1). It is shown that this model necessarily requires the existence of two spin zero K-mesons which are degenerate in parity (§ 2). The direct experimental tests of the primarity of $K \to \mu(e)+\nu$ interactions in the $K_{\mu 3}$ and K_{e3} decays are mentioned in § 3. The evaluation of the branching ratios of K-meson decays in this model and the estimate of the magnitude of the strength of the $KK\pi$-interaction are made in § 4. The comparison with the standpoint that the weak Fermi interaction is primary is discussed and it is inferred that the latter is more promising (§ 5).

1. Introduction

It is certainly one of the remarkable aspects of weak baryon-meson-lepton interactions observed so far that they are, irrespective of their vast varieties of coupling schemes, characterized by very weak coupling strength of a nearly unique order of magnitude. That is, *in a suitable unit* [1, 2, 3]), the effective coupling constants g of weak interactions known so far seem to lie in the range $g^2/4\pi \approx 10^{-14}-10^{-15}$ compared with those of strong baryon-meson interactions $G^2/4\pi \approx 1$ and with electromagnetic interactions $e^2/4\pi = 1/137$. Consequently, it would not be meaningless to ask whether this fact does come from the existence of some simple source, i.e., of some sorts of weak *primary interactions*. Here we should like to use the terminology "*primary interaction*" in the sense that it would be an *elementary interaction* between *truly elementary particles*, though we do not know, at present, which particles are really elementary. There is also no convincing *a priori* criterion regarding the interaction forms of these possible primary interactions. In this respect, to attack these problems, it would be a possible approach that we first assume the simplest forms of primary interactions between particles supposed to be elementary and then ask whether they are consistent with other more complicated phenomena.

† On leave of absence from the Institute of Theoretical Physics, Kanazawa University.
†† On leave of absence from the Institute of Theoretical Physics, Nagoya University.

In this paper, we investigate in detail the standpoint in which the $K \to \mu+\nu$ and $K^0 \to \pi+\pi$ interactions are taken to be primary. Apart from the fact that this standpoint, compared with other models, is easier to yield experimental tests, we pursue such a possibility, since we believe that this study would also throw light on the problem whether the K-mesons are elementary or compound states of other elementary particles.

Before going into details we make some retrospect on the *simplest* forms of weak interactions and their examples realized in nature:

(I) Weak Fermi interactions between four fermions:
β-decay, μ-decay, $\mu^- + P \to N + \nu$.

(II) Weak Yukawa type interactions †:
$\pi \to \mu+\nu$, $K \to \mu+\nu$, hyperon decays.

(III) Weak boson-boson interactions:
$K \to \pi+\pi$.

As long as we stick to the phenomenological facts that there are only three different orders of magnitude of the coupling strength—strong (G), electromagnetic (e), and weak (g) — we are forced to conclude that the $\mu \to e+\nu+\nu$ is a direct primary interaction (category (I)), because none of the constituents of this interaction has strong interactions and so we cannot derive this interaction from (II)††.

The very scarcity of the $\pi \to e+\nu$ mode demonstrates that the β-decay cannot be intermediated by the π-meson and the β-decay couplings are regarded, at present, as the direct Fermi interactions. These arguments seem to favour the following simplest [2, 3, 7, 8, 9]) standpoint:

Standpoint (A): the weak Fermi interactions (I) are the sole source of weak interactions and all other weak interactions, including (II) and (III), are derived from (I).

However, although the rate of the process $\mu^- + P \to N + \nu$ is compatible with the idea of the so-called universal Fermi interaction, the primarity of this direct four-fermion interaction has not yet had such a strong argument as that of the μ-decay and β-decay couplings. Moreover, the striking asymmetries between the $\pi \to \mu+\nu$ and $\pi \to e+\nu$ modes would exclude the simplest possibility of having the complete symmetries between (μ, ν) and (e, ν) pairs in the weak Fermi interactions. That is, if the Fermi interactions

† The form $(g/m_i)\,\bar{\psi}_j \gamma_\mu \psi_k \partial_\mu \varphi_i$ (j, k = fermions. i = spin 0 boson with mass m_i) can best explain all these weak boson-fermion reactions in terms of g of nearly unique order of magnitude [4, 5, 6]).

†† There remains a slightly more academic question [1]). There might exist, though so far unknown, source particles of weak interactions which always mediate the weak interactions by coupling with known particles with coupling constants g' of intermediate strength, $g'^2 \approx g^2$. Then, the interactions (I), (II) and (III) would be the results of this intermediation of order g'^2. In contrast to the known particles, this source particle is very unstable against decays into lighter particles. The life-times would be less than 10^{-15} sec. Even viewed from such a standpoint, however, our analysis would have a phenomenological value.

are the sole source of weak interactions, the couplings containing the (μ, ν) and (e, ν) pairs must have, in effect, different properties, i.e., different † covariant characters or different coupling combinations. (As regards details, see for instance, ref. [2]).) The efforts to derive these *phenomenologically* process-dependent forms of interactions from more profound symmetry nature of physical laws seem to be worthwhile. In these connections it seems to be necessary to investigate the following alternative standpoint:

Standpoint (B): in addition to the weak Fermi interaction (I), there also exist certain kinds of primary interactions of the type (II) and (III).

In this standpoint (B), as stressed by Schwinger recently [10]), it is quite interesting to investigate the possibility that the (μ, ν) and (e, ν) fields are associated with different types of primary interactions, the muon being coupled to bosons (such as the $\pi \to \mu + \nu$ and $K \to \mu + \nu$ interaction) and the electron to fermions (such as the β-decay and possibly $\Lambda^0 \to P + e^- + \nu$ etc.).

The study of primary interactions has also interesting relations to the models of elementary particles, because the primarity of interactions will be inseparably related to the problem of *true elementarity* of so-called elementary particles. In the baryon-meson system, owing to the existence of strong interactions, it may not be so difficult to imagine that some baryons and bosons would be the composite states of truly elementary entities due to strong primary interactions. On the other hand, none of the leptons, having no strong interactions, could be regarded as the compound system in the same sense. Thus, in the composite particle theory of baryon-meson system, the weak lepton processes will perhaps be useful in discriminating what particles are truly elementary. In constructing a composite particle model of the baryon-meson system, two standpoints may be taken according as we regard the Λ or the K-mesons as the source of strangeness quantum number:

(a) Markov-Sakata model [11]):

The nucleon and the Λ are elementary and other baryons and mesons are composite states (with suitable isobaric spin and strangeness quantum number) of these particles.

(b) Goldhaber's model [12]):

The nucleon and the K-meson are elementary. The pion may be either an elementary or a compound particle (nucleon-anti-nucleon system).

Suppose we take a *naive* view-point that all interactions between particles stem from the *primary* interactions between the constituent *truly elementary*

† *Note added in proof:* This conclusion depends on the conjecture that the β-decay coupling is consistent with the S and T combination and particularly on the fact that the frequency ratio $\pi \to e + \nu$ to $\pi \to \mu + \nu$ decay is smaller than 1.3×10^{-4}. However, recently some evidence on the existence of A and V coupling in β-decay has been reported [22]).

particles. Then, for the Markov-Sakata model, the Fermi type weak interactions (I) would be primary and the $\pi \to \mu+\nu$ and $K \to \mu+\nu$ decays should be derived, for instance, from the primary interaction, such as $\mu^-+P \to N+\nu$ and $\mu^-+P \to \Lambda^0+\nu$ respectively. On the other hand, for the standpoint (b), the $\pi \to \mu+\nu$, $K \to \pi+\pi$ and, especially, $K \to \mu+\nu$ interaction would claim a title to be one of the primary interactions. So the study of the primarity of these interactions would offer a good test of the model (b).

There is also another interesting point. It is well known that the $\theta-\tau$ puzzle (same life-times, same masses, and same excitation functions of the θ- and τ-meson) would force us to have two kinds of K-mesons, if space parity is conserved. It has already been confirmed that the weak interactions do not conserve parity [13]), at least for neutrino processes [14]). We do not know as yet whether the same conclusion also holds for the weak interactions between baryons and mesons in spite of the fact that the doubt about the conservation of parity in weak interactions did indeed arise from the $\theta-\tau$ puzzle†. If parity is conserved in the weak baryon-meson interactions contrary to the case of neutrino interactions, it would be necessary to have two K-mesons in the model (b) and also to have two Λ's in the model (a) which are both degenerate in parity space. This problem has also quite a close connection with our following arguments on the nature of primary weak interactions.

2. The Kinematics of the Interactions when the $K \to \mu(e)+\nu$ are Primary Interactions

Before going into the specific problem, we summarize our assumptions and their direct consequences.

We avoid making specific assumptions and making perturbation expansions as much as possible with respect to the strong interactions. We take it as granted that strong baryon-meson interactions are charge independent and invariant under space and time reflections and charge conjugation. As stated in § 1, the coupling strengths of the weak interactions (I), (II), and (III) are so small that their higher order corrections are completely negligible. So we use first order perturbation theory as regards weak interactions. Except for this weak vertex, other vertices in the main contributions must be either strong or electromagnetic interactions which conserve the strangeness quantum number. This fact restricts the character of weak vertex under discussion to a considerable extent [15]). In all K-meson decay modes, only such weak couplings which are consistent with the change

† *Note added in proof:* Recent experiments [23]) on the Λ-decay seem to suggest the parity non-conservation is not peculiar to neutrino processes. This is quite in favour of our arguments in § 5.

of strangeness quantum number S by one, $|\Delta S| = 1$, (assigning, for convenience, $S = 0$ for all leptons) would be entitled to give essential contributions. Therefore, if we stick to the weak interactions of the form (I), (II), and (III), the following interactions (assumed to be elementary) would only contribute to the K-meson decays.

In standpoint (A) (adequate to model (a)),

$$\Lambda \to \mathcal{N} + \mathrm{e}(\mu) + \nu \tag{1}$$

$$\Lambda \to \mathcal{N} + \mathcal{N} + \overline{\mathcal{N}} \tag{1'}$$

(essentially equivalent to taking the $\Lambda \to \mathcal{N} + \pi$ as primary).

If baryons other than the Λ were also elementary, the interaction such as $\Sigma \to \mathcal{N} + \mathrm{e}(\mu) + \nu$ and $\Sigma \to \mathcal{N} + \pi$ etc. would also claim the same position.

In standpoint (B) (adequate to model (b)),

$$\mathrm{K} \to \mu(\mathrm{e}) + \nu \tag{2}$$

$$\mathrm{K} \to \pi + \pi. \tag{2'}$$

As our main concern in this paper is to test the standpoint (B), we assume that the K-particle is *truly elementary* and that the interactions (2) and (2′) are primary. Indeed, particularly in model (b), such interactions as (1) and (1′) could not claim to be primary interactions, since the hyperons are not taken to be elementary. The spin of K-meson is assumed to be zero, since experiments indicate this to be the best choice.

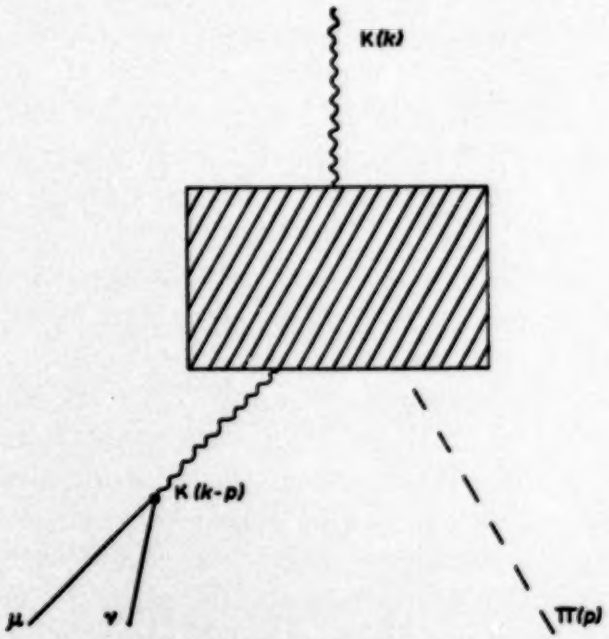

Fig. 1

First we must note that we are forced to admit the following important facts in the standpoint (B) if we assume that the $\mathrm{K}_{\mu 3}$ mode is derived from the primary $\mathrm{K} \to \mu + \nu$ coupling:

There must exist two K*-mesons of opposite parity (θ and τ) which have strong interaction (direct or indirect) of the form* $\theta \rightleftarrows \tau+\pi$.

This is because, in the present model, the $K \to \mu+\nu+\pi$ could only be derived by a mechanism such as shown in fig. 1. Namely, we first need to construct effective $KK\pi$-interaction of the form

$$F(k, p)\varphi_K(k)\varphi_K(k-p)\varphi_\pi(p), \tag{3}$$

where $\varphi_K(k-p)$ denotes the amplitude of the virtual K-meson which finally annihilates into leptons. $F(k, p)$ represents the contributions of the black box and is a scalar function of $k_\mu^2 = -M_K^2$, $p_\mu^2 = -m_\pi^2$, $(k, p) \equiv k_\mu p_\mu$, and the masses of intermediate particles. The expression (3) must be true scalar because the contributions of weak interactions (which may not conserve parity) would be completely negligible. As the pion is pseudoscalar and only two four-vectors, k_μ and p_μ, are available, the $K(k)$ and $K(k-p)$ are inevitably required to have opposite parity † from (3). This statement is only invalidated when we insert photon lines between the μ-meson and charged particles other than its parent K-meson. These corrections, however, would decrease the probability by a factor, at least, $\alpha^2 = (1/137)^2$. So in order to explain the appreciable frequency of the $K \to \mu(e)+\nu+\pi$ mode compared with the $K \to \mu+\nu$ decay, two types of K-mesons are required in the present model. If the K-meson has spin greater than zero, this would not be necessary.

Now, parity is not conserved in the neutrino processes. If this is also the case with weak baryon-meson interactions, we need not have two K-mesons and the $K_{\pi 2}$ and $K_{\pi 3}$ decays could be regarded as the alternative decay modes of the same K-meson. In this case, as was shown above, the primary $K \to \mu(e)+\nu$ interaction could not explain the occurrence of the $K \to \mu(e)+\nu+\pi$ mode.

Thus, if (i) only one K-meson does exist or if (ii) there were no strong $KK\pi$-interaction †† (direct or indirect) in spite of the existence of two K-mesons, the standpoint (A) would be favoured. That is, the weak Fermi interaction such as (1) might explain all K-meson decays comprising leptons. For the Goldhaber model, if (i) or (ii) is true, we shall perhaps be forced to take the $K \to \mu(e)+\nu+\pi$ interactions as the direct primary interaction in addition to the primary $K \to \mu+\nu$ interaction. In this sense, if non-conservation of parity is the feature of all weak interactions, the compound particle model (a) is preferable to the model (b), since, for the former model, such a complication may not be necessary. However, the possibility that parity is still conserved for the weak baryon-meson interactions (non-neutrino processes) might not, at present, be excluded. So we continue our

† This was also noted recently by d'Espagnat *et al.* [16]).

†† The existence of two K-mesons need not necessarily imply the existence of this interaction.

discussions on the applicability of the primary $K \to \mu(e)+\nu$ interactions, admitting that both (i) and (ii) are not the case.

3. Direct Tests of the Primarity of the $K \to \mu(e)+\nu$ Interaction

The equality of the life-times of $K^{\pm}$-meson decays would require that the dominant decay mode $K \to \mu+\nu$ maintain the parity reflection symmetry. The conventional forms of interactions for the $K \to \mu+\nu$ without the derivatives of the spinor wave functions are

Direct interaction: $g(K)\varphi_K \bar{\psi}_\mu \psi_\nu + \text{c.c.}$ (4)

Gradient interaction: $g'(K)\partial_\alpha \varphi_K \bar{\psi}_\mu \gamma_\alpha \psi_\nu + \text{c.c.};$ (5)

K stands for θ or τ-meson. Most probably, $g(\theta) = g(\tau)$ and $g'(\theta) = g'(\tau)$. As we are not concerned with pseudoscalar quantities, parity problems do not play any role in these interactions, since the neutrino has vanishingly small mass. So we need not distinguish reflection properties in (4) and (5). Of course, the most general form, for instance, of (4) is $g(K)\varphi_K \bar{\psi}_\mu(1+a\gamma_5)\psi_\nu +$ c. c., where a is a mixing ratio of the parity non-conserving term. The probability per unit time for the $K^+ \to \mu+\nu$, $W_{\mu 2}(K^+)$, due to the linear combination of the interactions (4) and (5), is given by [2, 4])

$$W_{\mu 2}(K^+) = \frac{1}{4\pi}\{g(K)+m_\mu g'(K)\}^2 \frac{M_K}{2}\left\{1-\left(\frac{m_\mu}{M_K}\right)^2\right\}^2. \tag{6}$$

3.1. ENERGY SPECTRUM OR ANGULAR CORRELATIONS OF THE SECONDARY PARTICLES

As is briefly referred to in the preceding paper [15]), the following test would be very powerful. As long as we neglect the electromagnetic corrections, the S-matrix of the $K \to \mu(e)+\nu+\pi$ decay through the intermediary of the primary $K \to \mu(e)+\nu$ interactions (4) or (5) shown in fig. 1 is given by the following simple form

$$F_S(k, p)\left(\frac{1}{-2(k, p)+m_\pi^2}\right)\bar{\psi}_\mu \psi_\nu \varphi_K(k)\varphi_\pi(p), \tag{7}$$

where $F_S(k, p)$ is a scalar function of (k, p) similar to $F(k, p)$ in (3). Note that both primary interactions (4) and (5) give the same expression (7), since we can use the equation of motion of the external leptons.

On the other hand, as is the case with the model (a), if the Fermi interactions are primary, we would have, in addition to (7) without a factor $[-2(k, p)+m_\pi^2]^{-1}$ (which, in this case, originates from the Fermi interaction of Scalar type with respect to rotation), other contributions [17]). That is, from Fermi interactions of Vector and Tensor type with respect to rotation, we have (see fig. 2)

$$\{F_V(k, p)\bar{\psi}_\mu(k, \gamma)\psi_\nu + F_{V'}(k, p)\bar{\psi}_\mu(p, \gamma)\psi_\nu\}\varphi_K(k)\varphi_\pi(p) + \text{c.c.} \tag{8}$$

and

$$F_{\mathrm{T}}(k,\ p)\bar{\psi}_{\mu}(\gamma_{\alpha}\gamma_{\beta}-\gamma_{\beta}\gamma_{\alpha})k_{\alpha}p_{\beta}\psi_{\nu}\varphi_{\mathrm{K}}(k)\varphi_{\pi}(p)+\mathrm{c.c.}. \qquad (9)$$

If the experiments on the $\mathrm{K}\to\mu(\mathrm{e})+\nu+\pi$ happened to show real deviations from the theoretical predictions based on the S-matrix (7), we could conclude that the postulate of the primary $\mathrm{K}\to\mu(\mathrm{e})+\nu$ interaction is not at all sufficient to explain the occurrence of the $\mathrm{K}\to\mu(\mathrm{e})+\nu+\pi$ mode.

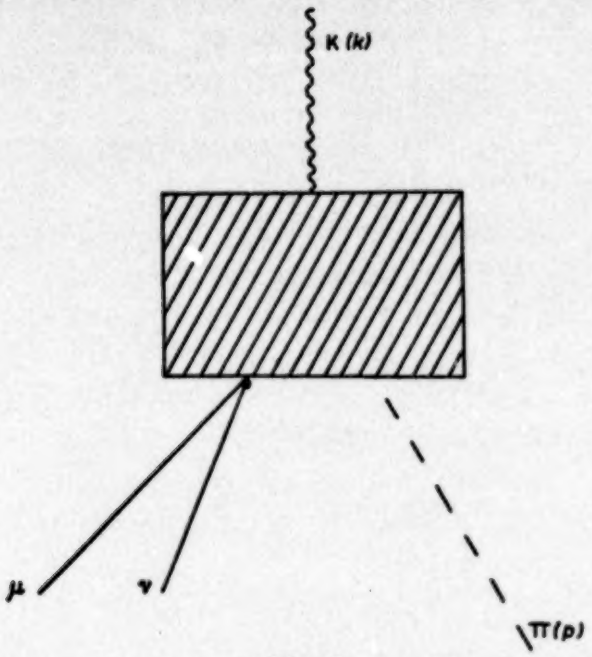

Fig. 2

The energy spectrum of the pion and muon (electron) in the $\mathrm{K}_{\mu 3}$ and K_{e3} decays would give good information, provided that the dependence of $F_i(k,p)$ ($i=\mathrm{S},\mathrm{V},\mathrm{V}'$ and T) on the $(k,p)=-M_{\mathrm{K}}E_{\pi}(p)$ ($E_{\pi}(p)=\sqrt{p^2+m_{\pi}^2}$ being the energy of the secondary pion in the rest system of the K-meson) is not so steep. This assumption seems to be rather reasonable. The S-matrix (7) gives the following pion energy spectrum $P(E)\mathrm{d}E$ (see eq. (13)):

$$P(E)\propto(M_{\mathrm{K}}^2+m_{\pi}^2-m_{\mu}^2-2M_{\mathrm{K}}E)^2(M_{\mathrm{K}}^2+m_{\pi}^2-2M_{\mathrm{K}}E)^{-1}$$
$$\times(2M_{\mathrm{K}}E-m_{\pi}^2)^{-2}(E^2-m_{\pi}^2)^{\frac{1}{2}}. \qquad (10)$$

Putting $m_{\mu}\to m_{\mathrm{e}}$ we get the pion energy spectrum of the K_{e3} decay due to (7). Observation of the deviation of the energy spectrum from the expression (10) could, at least, make it possible to check whether the $\mathrm{K}_{\mu 3}$ and K_{e3} decays could be explained in terms of the sole primary interactions $\mathrm{K}\to\mu+\nu$ and $\mathrm{K}\to\mathrm{e}+\nu$ respectively. The preliminary analysis of K_{e3}^{+} data [17]) seems to indicate the necessity of having the contributions from (9). If this turned out to be true, it would be a strong indication that the weak Fermi interactions such as $\Lambda\to N+\mathrm{e}+\nu$ having at least Tensor type are contributing.

If, in the $\mathrm{K}^0\to\pi^{\pm}+\mu^{\mp}(\mathrm{e}^{\mp})+\nu$ events, we could fix the energy of secondary pion and investigate the angular correlations [18]) or energy correlations

between the $\pi^{\mp}$ and $\mu^{\pm}(e^{\pm})$, we could avoid the approximation $F_i(k,p)=$ constant and so the results become more convincing. We hope that these studies could, at least, clarify the problem of the primarity of the K-decay interactions.

3.2. THE PARTIAL DECAY RATES OF THE $K_{\mu 3}$ AND K_{e3} DECAYS

In fig. 1, for the $K^+ \to \pi^0+\mu^+(e^+)+\nu$, $K(k) = K^+$, $K(k-p) = K^+$, $\pi(p) = \pi^0$, and $F(k, p) = F^+(k, p)$. For the $K^0 \to \pi^{\pm} + \mu^{\mp}(e^{\mp})+\nu$, $K(k) = K^0$, $K(k-p) = K^+$, $\pi(p) = \pi^{\pm}$, and $F(k, p) = F^0(k, p)$. From the charge independent properties of the strong baryon-meson interactions whicn contribute to $F(k, p)$

$$|\sqrt{2}F^+(k, p)|^2 = |F^0(k, p)|^2.$$

The K^0-decays are best discussed, not in terms of K^0 and $\overline{K}^0$, but rather in terms of K_1^0 and K_2^0, where

$$K^0 = 2^{-\frac{1}{2}}(K_1^0+iK_2^0), \quad \overline{K}^0 = 2^{-\frac{1}{2}}(K_1^0-iK_2^0);$$

then if we neglect the mass difference between pions, the following simple relations between partial decay rates would exist

$$\begin{aligned} W_{\mu 3}(K_1^0) &= W_{\mu 3}(K_2^0) = 2W_{\mu 3}(K^+), \\ W_{e3}(K_1^0) &= W_{e3}(K_2^0) = 2W_{e3}(K^+). \end{aligned} \quad (K = \theta \text{ or } \tau)$$

In the present model, these statements are quite general and are free from the detailed properties of the strong interactions. Note that if (4) and (5) maintain parity reflection symmetry,

$$W_{\mu 3}(\theta_1^0) = W_{\mu 3}(\tau_1^0), \quad W_{\mu 3}(\theta_2^0) = W_{\mu 3}(\tau_2^0), \text{ and } W_{\mu 3}(\theta^+) = W_{\mu 3}(\tau^+).$$

4. Relations between the $K_{\mu 3}$ and $K_{\pi 3}$ Decays

4.1. THE PRIMARY $K \to \pi+\pi$ INTERACTION

The primary $K \to \pi+\pi$ interaction may explain the $K_{\pi 3}$ decays and hyperon decays [10, 19]. This is especially desirable in the model (b). However, this interaction has striking asymmetry between the $\theta^0 \to 2\pi$ and $\theta^+ \to 2\pi$ modes. The former mode seems to be about 200 times more probable than the latter. In isobaric space, the $\theta \to \pi+\pi$ interaction is resolved into three parts, $\Delta I = \pm\frac{1}{2}$, $\pm\frac{3}{2}$, and $\pm\frac{5}{2}$. For the part $\Delta I = \pm\frac{1}{2}$, $\theta^+ \to \pi^+ + \pi^0$ is forbidden, provided the θ-meson has spin zero and the mass difference between pions (electromagnetic effects) is neglected. Therefore, one tentative way [10, 3]) is to postulate the selection rule $\Delta I = \pm\frac{1}{2}$ and add smaller components (about 10 %) of $\Delta I = \pm\frac{3}{2}$ or $\pm\frac{5}{2}$. It may be desirable to ascribe the latter parts entirely to the electromagnetic effects. However, these corrections might be too small, since $\alpha^2 = (1/137)^2 \approx 10^{-4}$. At any rate, for the following discussions where $\theta \to 2\pi$ is taken as primary, we shall neglect the contribution from the $\theta^+ \to \pi^+ + \pi^0$ when compared with those

from $\theta^0 \to \pi^+ + \pi^-$ and $\theta^0 \to \pi^0 + \pi^0$ interactions. The interaction forms are in the momentum space given by

$$hm_\pi \varphi_{\theta^0}(p+q)\varphi^*_{\pi^+}(p)\varphi^*_{\pi^-}(q) + h' m_\pi \varphi_{\theta^0}(p+q)\varphi^*_{\pi^0}(p)\varphi^*_{\pi^0}(q) + \text{c.c.}, \qquad (11)$$

where h and h' are dimensionless coupling constants. In general, they are scalar functions of p^2, q^2, and (p, q). The decay rate of the $\theta_1^0 \to \pi^+ + \pi^-$ due to (11) is given by [2])

$$W(\theta_1^0 \to \pi^+ + \pi^-) = \frac{(hm_\pi)^2}{4\pi} \frac{1}{8M_K} \left\{1 - 4\left(\frac{m_\pi}{M_K}\right)^2\right\}^{\frac{1}{2}}. \qquad (12)$$

$W(\theta_2 \to \pi^0 + \pi^0)$ is obtained by putting $h = h'$.

4.2. COMPARISON OF THE $K^0_{\mu 3}$ AND $K^0_{\pi 3}$ DECAYS

The τ-decays would occur through the intermediary of the primary $\theta^0 \to \pi + \pi$ interactions shown in fig. 3. In order to maintain the correspondence to the $K_{\mu 3}$ decays shown in fig. 1, we make the following simplifying approximation †:

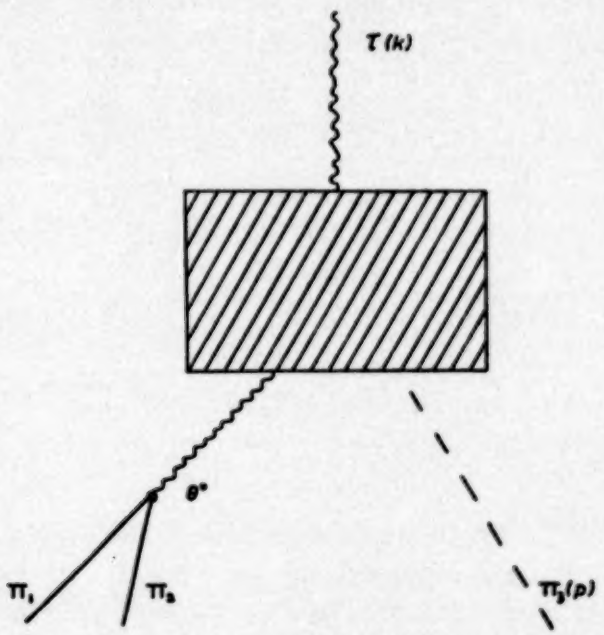

Fig. 3

Freezing approximation: As is the case with the leptons in fig. 1, the interactions of the pions, π_1 and π_2, of fig. 3 with other particles are neglected.

Though there is no strict argument for it, it is rather unlikely that this approximation affects the main points of our discussion. The relatively low available energies in $K_{\pi 3}$ decays would favour this argument.

Let us first investigate the $\theta_1^0 \to \mu^+(e^+) + \nu + \pi^-$ through the intermediary of the primary $\tau^+ \to \mu^+ + \nu$ interaction shown in fig. 1. Using

† Under this approximation, the existence of two K-mesons, θ and τ, is also required.

the result (6), the transition probability per unit time, $W_{\mu 3}(\theta_1^0; E)$ with fixed energy E of the secondary π^--meson is expressed by

$$W_{\mu 3}(\theta_1^0; E) = W_{\mu 2}(\tau^+) \left(\frac{1}{2\pi}\right)^2 \left(\frac{1}{M_K}\right)^2 \left\{1 - \left(\frac{m_\mu}{M_K}\right)^2\right\}^{-2} \frac{|F(k, p)|^2}{4\pi} I_{\mu 3}(E),$$
$$I_{\mu 3}(E) = 4\pi\sqrt{E^2 - m_\pi^2} \frac{(M_K^2 - 2M_K E + m_\pi^2 - m_\mu^2)^2}{(2M_K E - m_\pi^2)^2 (M_K^2 - 2M_K E + m_\pi^2)}. \quad (13)$$

$F(k, p)$ denotes the black box of fig. 1 (effective $\theta_1^0 \to \tau^+ + \pi^-$ interaction). The assumption of parity reflection symmetry of the primary $K^+ \to \mu^+ + \nu$ interaction,

$$W_{\mu 2}(\theta^\pm) = W_{\mu 2}(\tau^\pm) \equiv W_{\mu 2}(K^\pm), \quad (14)$$

necessarily means, in our model (fig. 1),

$$W_{\mu 3}(\theta_1^0) = W_{\mu 3}(\theta_2^0) = W_{\mu 3}(\tau_1^0) = W_{\mu 3}(\tau_2^0) \equiv W_{\mu 3}(K^0), \quad (15)$$

$W_{\mu 3}(\theta_1^0)$ denotes the total decay rate of the channel $\theta_1^0 \to \mu^+ + \nu + \pi^-$ and $W_{\mu 3}(\theta_1^0) = \int dE W_{\mu 3}(\theta_1^0; E)$. Of course, for the partial decay rates $W_{\mu 3}(\theta_1^0; E)$ etc., relations like (15) also hold.

Replacing m_μ by m_e, we get $W_{e3}(\theta_1^0; E)$ of $\theta_1^0 \to e^+ + \nu + \pi^-$.

On the other hand, the probability per unit time, $W_{\pi 3}(\tau_1^0; E)$, for the decay $\tau_1^0 \to \pi^+ + \pi^- + \pi^0$ with given energy E of the secondary π^0-meson is expressed as follows. In this case, $\tau = \tau_1^0$, $\pi_1 = \pi^+$, $\pi_2 = \pi^-$, and $\pi_3 = \pi^0$ in fig. 3.

$$W_{\pi 3}(\tau_1^0; E) = W(\theta_1^0 \to \pi^+ + \pi^-) \left(\frac{1}{2\pi}\right)^2 \left\{1 - 4\left(\frac{m_{\pi^+}}{M_K}\right)^2\right\}^{-\frac{1}{2}} \frac{|F'(k, p)|^2}{4\pi m_\pi^2} I_{\pi 3}(E), \quad (16)$$

$$I_{\pi 3}(E) = \frac{4\pi m_\pi^2 \sqrt{E^2 - m_{\pi^0}^2}\sqrt{M_K^2 - 2M_K E + m_{\pi^0}^2 - 4m_\pi^2}}{(2M_K E - m_{\pi^0}^2)^2 \sqrt{M_K^2 - 2M_K E + m_{\pi^0}^2}}. \quad (16')$$

$F'(k, p)$ represents the effective $\tau_1^0 \to \theta_1^0 + \pi^0$ interaction. The mass difference of pions is taken into account in the final density. Note that $\tau_2^0 \to \pi + \pi + \pi$ would not take place in the present model (at least under freezing approximation), since the $\tau^0 \to \theta^0 + \pi^0$ interaction (black box) is invariant under charge conjugation and the $\theta_2^0 \to \pi + \pi$ does not exist. The charge independence of the effective $KK\pi$-interaction would require

$$|F(k, p)|^2 = 4|F'(k, p)|^2. \quad (17)$$

The frequency ratio, $R_\mu(E)$ (measured at an appropriate place) of the $\tau^0 \to \pi^+ + \pi^- + \pi^0$ events with fixed energy E of the π^0-meson to the $K^0 \to \mu^+ + \nu + \pi^-$ events with the same energy E of the π^--meson turns out, due to the relation (15), to be always proportional to $W_{\pi 3}(\tau_1^0; E)/W_{\mu 3}(K^0)$. Owing to the relation (17), the $R_\mu(E)$ is free from the knowledge about the contributions from the black boxes. The dependence R_μ on E is evaluated from (13) and (16),

$$R_\mu(E) \propto \frac{m_\pi^2\sqrt{(M_K^2-2M_KE+m_{\pi^0}^2-4m_\pi^2)(M_K^2-2M_KE+m_\pi^2)}}{(M_K^2-2M_KE+m_\pi^2-m_\mu^2)^2}. \quad (18)$$

The proportionality coefficient would depend on the amplitudes of each meson (θ_1^0, θ_2^0, τ_1^0 and τ_2^0) and in general contain the interference terms between them †.

If relations similar to (14) and (15) hold for the the $W_{e2}(K)$ and $W_{e3}(K)$, we can get $R_e(E)$, replacing m_μ by m_e in (18).

In this case, it is interesting to investigate further the frequency ratio $R_{\mu-e}(E)$ of the $K^0 \to \mu^+ + \nu + \pi^-$ events to the $K^0 \to e^+ + \nu + \pi^-$ events with fixed energy E of the π^--meson. $R_{\mu-e}(E)$ is very simple:

$$R_{\mu-e}(E) \propto \left\{\frac{M_K^2-2M_KE+m_\pi^2-m_\mu^2}{M_K^2-2M_KE+m_\pi^2-m_e^2}\right\}^2. \quad (19)$$

This relation also holds even if one of the K-mesons has no (e, ν) mode at all. The $R_\mu(E)$ and $R_e(E)$ would give a rather unambiguous test whether the $K_{\mu3}$, K_{e3}, and $K_{\pi3}$ modes are simultaneously consistent with the primary interactions, $K \to \mu+\nu$, $K \to e+\nu$, and $K^0 \to \pi+\pi$, respectively. Deviations from the $R_{\mu-e}(E)$ would also suggest that primary weak interactions other than the $K \to \mu+\nu$ and $K \to e+\nu$ do exist. The same $R_{\mu-e}(E)$ is also obtained when the Fermi interaction of Scalar type with respect to rotation (the S-matrix is given by (7)) is the sole contribution. These $R_\mu(E)$ and $R_{\mu-e}(E)$ are shown in fig. 4 and fig. 5 respectively, in an arbitrary scale; T is the kinetic energy of the pion.

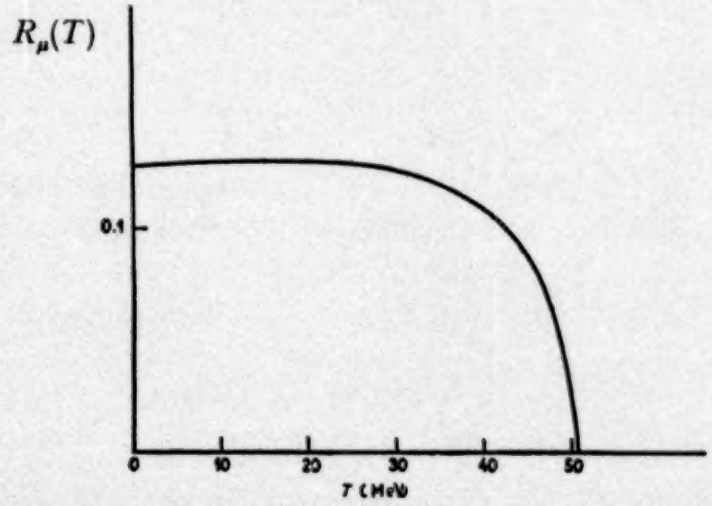

Fig. 4

4.3. THE MAGNITUDE OF THE EFFECTIVE KKπ-INTERACTION

If we assume that the dependence of $F(k, p)$ on the pion energy E is not so steep (E varies from 139 to 254 MeV for the $K_{\mu3}$ and from 139 to

† If the energy of π^0-meson in the $K^+ \to \mu^+(e^+)+\nu+\pi^0$ decay could be measured, (18) could also be applied to the $\tau^+ \to \pi^+ + \pi^0 + \pi^0$ decay with fixed energy of π^+-meson.

266 MeV for the K_{e3} decay), we could infer the strength of the effective $KK\pi$-coupling from the branching ratio Q_μ (or Q_e) of the $K^+_{\mu 3}$ (or K^+_{e3}) mode to the $K^+_{\mu 2}$(or K^+_{e2}) mode. We can use the results (13) by making a slight modification. Now, in (13), we take $F(k, p)$ as constant and put

$$F(k, p) = Gm_\pi. \tag{20}$$

Then, the constant G could be regarded as the dimensionless effective coupling constant of the $KK\pi$-coupling of the form

$$Gm_\pi \varphi_\theta \boldsymbol{\tau} \varphi_\tau \cdot \boldsymbol{\varphi}_\pi + \text{c.c.}.. \quad \varphi_\theta = \begin{pmatrix} \varphi_{\theta^+} \\ \varphi_{\theta^0} \end{pmatrix}, \quad \varphi_\tau = \begin{pmatrix} \varphi_{\tau^+} \\ \varphi_{\tau^0} \end{pmatrix}. \tag{21}$$

$\boldsymbol{\tau}$ is an isobaric spin vector and $\boldsymbol{\varphi}_\pi$ denotes the iso-vector. Thanks to the relations (14) and (15), we get from (13) and (20)

$$Q_\mu = \frac{W_{\mu 3}(K^+)}{W_{\mu 2}(K^+)} = \frac{G^2}{4\pi}\left(\frac{1}{2\pi}\right)^2\left(\frac{m_\pi}{M_K}\right)^2\left\{1-\left(\frac{m_\mu}{M_K}\right)^2\right\}^{-2} I_{\mu 3}, \tag{22}$$

$$I_{\mu 3} = \int \mathrm{d}E I_{\mu 3}(E).$$

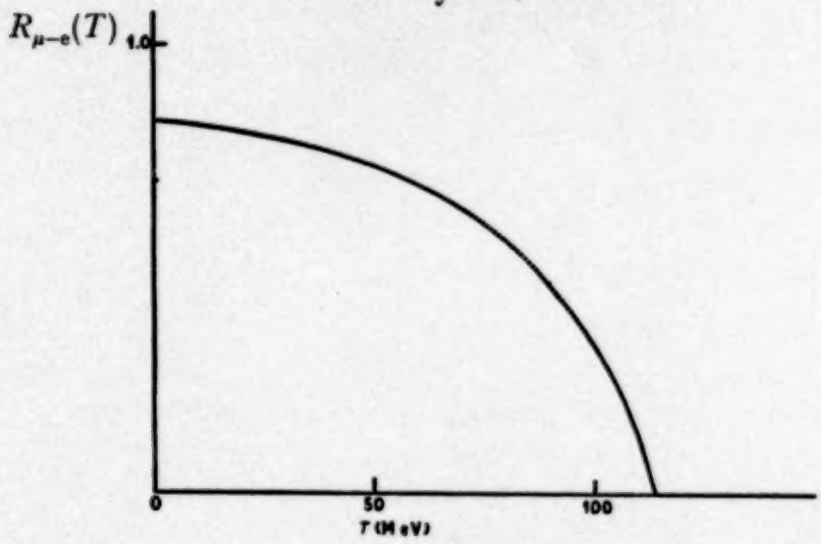

Fig. 5

Taking $M_K = 965\ m_e$, $m_{\pi^+} = 273\ m_e$, $m_{\pi^0} = 265\ m_e$, and $m_\mu = 207\ m_e$, $I_{\mu 3} = 0.28$ ($I_{e3} = 0.40$), and so

$$Q_\mu = \frac{G^2}{4\pi} \times 6.1 \times 10^{-4}. \tag{23}$$

Assuming $W_{e2}(\theta^+) = W_{e2}(\tau^+)$ we get, putting $m_\mu \to m_e$ in (22),

$$Q_e = \frac{G^2}{4\pi} \times 8.1 \times 10^{-4}. \tag{24}$$

The experimental values of Q_μ and Q_e seem to lie [21]) between 5 % to 10 %. Then, the value of the effective coupling constant, $G^2/4\pi$, must be as large as 100, so far as we admit the approximation $F(k, p) =$ constant. The

value obtained seems to be rather unnatural. (24) is entirely inconsistent with the predominance of the K_{e3}^+ decay over the K_{e2}^+ mode.

Now we turn to the $K_{\pi 3}^+$ decays. In fig. 3, we put $\tau = \tau^+$, $\pi_1 = \pi^+$, $\pi_2 = \pi^-$, and $\pi_3 = \pi^+$ for the $\tau^+ \to \pi^+ + \pi^- + \pi^+$ decays. The approximation $F'(k, p) =$ constant seems more harmless in this case than the $K_{\mu 3}$ (K_{e3}) decays, since the pion energy only changes in the range between 139 and 190 MeV. Putting

$$F'(k, p) = \sqrt{2} G m_\pi, \tag{25}$$

we can again evaluate the coupling constant G of (21). In contrast to the case (16), we must make a symmetrization as regards the final two π^+-mesons. In this procedure, we keep $F(k, p)$ (that is, G) as an absolute constant. Using the symmetrized expression of (16) we get

$$\frac{W(\tau^+ \to \pi^+ + \pi^- + \pi^+)}{W(\theta_1^0 \to \pi^+ + \pi^-)} = \frac{(\sqrt{2}G)^2}{4\pi} \left(\frac{1}{2\pi}\right)^2 \left\{1 - 4\left(\frac{m_\pi}{M_K}\right)^2\right\}^{-\frac{1}{2}} I'_{\pi 3}. \tag{26}$$

By integrating (16) over dE

$$I_{\pi 3} = \int I_{\pi 3}(E) dE \approx 1.8 \times 10^{-2}. \tag{27}$$

$I'_{\pi 3}$ in (26) includes the effect of symmetrization and turns out to be

$$I'_{\pi 3} \approx 3.6 \times 10^{-2} \approx 2 I_{\pi 3}. \tag{28}$$

Thus,

$$\frac{W(\tau^+ \to \pi^+ + \pi^- + \pi^+)}{W(\theta_1^0 \to \pi^+ + \pi^-)} \approx \frac{(\sqrt{2}G)^2}{4\pi} \times 1.1 \times 10^{-3}. \tag{29}$$

Let us assume $W(\theta_1^0 \to \pi^+ + \pi^-) \approx 10^{10}$ sec^{-1}. The life-time of the K^+-decay is about 10^{-8} sec and the frequency of τ^+-decay [21]) seems to be about 5 %. Then, we infer that $W(\tau^+ \to \pi^+ + \pi^- + \pi^+) \approx 5 \times 10^6$ sec^{-1}. Thus, from (29), we get

$$\frac{G^2}{4\pi} \approx 2.5 \times 10^{-1}. \tag{30}$$

This value is quite different from that deduced from the $K_{\mu 3}^+$ decay (see (23)). Unless in the $K_{\mu 3}$ (of K_{e3}) decay the $F(k, p)$ reveals an extraordinary steep variation, the above results will be taken as an indication that the $K_{\mu 3}$ and $K_{\pi 3}$ decays could not be explained at the same time in terms of primary $K \to \mu + \nu$ and $K^0 \to \pi + \pi$ interaction, respectively.

Finally, we add a few results on the branching ratio of the τ-decays which are strict as long as the freezing approximation is valid.

For the $\tau^+ \to \pi^+ + \pi^0 + \pi^0$ decay we get

$$\frac{W(\tau^+ \to \pi^+ + \pi^0 + \pi^0)}{W(\theta_1^0 \to \pi^0 + \pi^0)} = \frac{(\sqrt{2}G)^2}{4\pi} \left(\frac{1}{2\pi}\right)^2 \left\{1 - 4\left(\frac{m_{\pi^+}}{M_K}\right)\right\}^2 I_{\pi 3}. \tag{31}$$

Thus, the branching ratio of τ^+-decays

$$R(\tau^+) = \frac{W(\tau^+ \to \pi^+ + \pi^0 + \pi^0)}{W(\tau^+ \to \pi^+ + \pi^- + \pi^+)} = \frac{W(\theta_1^0 \to \pi^0 + \pi^0)}{W(\theta_1^0 \to \pi^+ + \pi^-)} \frac{I_{\pi 3}}{I'_{\pi 3}} \approx \tfrac{1}{2} \frac{W(\theta_1^0 \to \pi^0 + \pi^0)}{W(\theta_1^0 \to \pi^+ + \pi^-)}. \tag{32}$$

For $\Delta I = \pm \frac{1}{2}$,

$$\frac{W(\theta_1^0 \to \pi^0 + \pi^0)}{W(\theta_1^0 \to \pi^+ + \pi^-)} = \tfrac{1}{2} \tag{33}$$

neglecting final state interactions and so

$$R(\tau^+) = \tfrac{1}{4}. \tag{34}$$

Further, the ratio $R(\tau^0)$

$$R(\tau^0) = \frac{W(\tau_1^0 \to \pi^0 + \pi^0 + \pi^0)}{W(\tau_1^0 \to \pi^+ + \pi^- + \pi^0)} = \frac{W(\theta^0 \to \pi^0 + \pi^0)}{W(\theta^0 \to \pi^+ + \pi^-)} \times 3. \tag{35}$$

For $\Delta I = \pm \frac{1}{2}$,

$$R(\tau^0) = \tfrac{3}{2} \tag{36}$$

Also the ratio of the decay rates, $\tau_1^0 \to \pi^+ + \pi^- + \pi^0$ and $\tau^+ \to \pi^+ + \pi^- + \pi^+$ is given by

$$\frac{W(\tau_1^0 \to \pi^+ + \pi^- + \pi^0)}{W(\tau^+ \to \pi^+ + \pi^- + \pi^+)} = \tfrac{1}{8}. \tag{37}$$

In these formulae the mass difference between pions was neglected. In (32) and (35), it increases the ratio by about 10 %.

5. Concluding Remarks

5.1. THE PROBLEM OF THE EXISTENCE OF TWO K-MESONS

In order that the assumed primary weak interactions, $K \to \mu(e) + \nu$ and $K^0 \to \pi + \pi$, may explain the $K_{\mu 3}$, K_{e3}, and $K_{\pi 3}$ decays, the existence of two K-mesons, θ and τ, is, first of all, necessary for the spin zero K-meson. Moreover, in this model, there should exist a (direct or indirect) strong KKπ-interaction. Schwinger [10]) stressed the fact that the introduction of KKπ-coupling is quite convenient in explaining the fact that the K^0-particle in the reaction $\pi^- + P \to K^0 + \Lambda^0$, Σ^0 exhibits a pronounced forward asymmetry in the centre-of-mass system, while the angular distribution of K^+-particle, produced by $\pi^- + P \to K^+ + \Sigma^-$, is comparatively isotropic and favours the backward direction. The effects of this interaction on the K—N scattering have also been discussed. From the perturbation theoretical argument [10]), the value of the coupling constant G is inferred to be of the order $G^2/4\pi \approx 0.1$. Although this value seems to be compatible with the value (30) derived from the frequency ratio of $K_{\pi 3}(\tau^+)$ to $K_{\pi 2}(\theta_1^0)$ decay, it would be too small to explain the branching ratio of $K^+_{\mu 3}$ to $K^+_{\mu 2}$ mode

(see (23) and (24)). Thus we feel that the primary $K \to \mu(e)+\nu$ interaction is not sufficient to explain the $K_{\mu 3}$ and K_{e3} phenomena. The direct tests discussed in § 3 would be useful and most unambiguous.

If the violation of parity conservation is indeed confirmed also for the weak baryon-meson interactions, we need not have two K-mesons and therefore there would be no strong KKπ-interaction. (We should perhaps have had some substitute for Schwinger's arguments based on the KKπ-interaction.) In this case, it is quite clear that we need, at least, other sorts of primary interactions. In Goldhaber's model, where the construction of primary interaction such as (1) and (1′) which include the hyperon is not possible, we are, most probably, forced to admit the direct $K \to \mu+\nu+\pi$, $e+\nu+\pi$, and $\pi+\pi+\pi$ interactions in addition to the $K \to \mu+\nu$ and $K \to \pi+\pi$ interactions.

It might be worthwhile remembering that the existence of a strong KKπ-interaction has a defect that, from the occurrence of $K \to \pi+e+\nu$ decay, the unwanted process $K \to e+\nu$ (K and K′ have opposite parity) inevitably follows and makes the explanation of the very scarcity of the latter mode quite difficult.

5.2. THE PRIMARY WEAK FERMI INTERACTION MODEL

The primary weak Fermi interaction is certainly the simplest model and from the discussion of 5.1 this standpoint would gain more importance if there exists only one K-meson. If this, indeed, turns out to be true, it should perhaps be stressed that, in this model, there is a room to explain the scarcity of the $K \to e+\nu$ mode. Now, the primary weak interactions responsible for K-meson decays are (1) and (1′). For (1) we write, for instance, $\Lambda \to N+e+\nu$:

$$\bar{\psi}_\Lambda O_j \psi_N \bar{\psi}_e O_j(1+a\gamma_5)\psi_\nu + \text{c.c.}, \tag{38}$$

where

$$O_j = 1(S),\ \gamma_\alpha(V),\ \gamma_\alpha\gamma_\beta-\gamma_\beta\gamma_\alpha(T),\ \gamma_5\gamma_\alpha(A) \text{ and } \gamma_5(P).$$

The $K_{\mu 3}$ and K_{e3} occur through the mechanism shown in fig. 2. There are selection rules which are only invalidated by the inclusion of electromagnetic (order $\alpha^2 \approx 10^{-4}$) corrections. (See ref. [2]) appendix II or ref. [7]).) Suppose that the K-meson is pseudoscalar. Then the $K \to \mu(e)+\nu$ decays due to the interaction (38) are forbidden for S, V and T couplings and are only allowed for P and A. On the other hand, the $K \to \mu(e)+\nu+\pi$ decays are forbidden for P and A, and are allowed for S, V, and T. Thus, if the (e, ν) coupling did not contain P and A whereas some combinations of the S, V, and T couplings did exist, the scarcity of the $K \to e+\nu$ mode and the occurrence of the $K \to e+\nu+\pi$ would find their explanations. Note that the existence of A would be harmless because, for the A coupling,

the $K \to e+\nu$ mode is about 10^5 times less probable than the $K \to \mu+\nu$ mode. On the other hand, for the (μ, ν) coupling the existence of A or P or both and of some combination of S, V, and T is required in order to explain the simultaneous occurrence of the $K \to \mu+\nu$ and $K \to \mu+\nu+\pi$, respectively. For the scalar K-meson, we only need to exchange the roles of S and P, and also of V and A. The fact that in this model different coupling types must always contribute to the $K_{\mu 2}$ and $K_{\mu 3}$ decay would perhaps be important since, the abundance of the $K_{\mu 3}$ mode compared with the $K_{\mu 2}$ mode (order of 10 %) is larger than the value obtained from the simple phase space volume argument. This seems to be the reason why we get such a large value of the coupling constant G of the $KK\pi$-interaction from (23). The striking resemblance between the lepton modes of the K-meson and the pion decays ($\pi \to \mu+\nu$, $e+\nu$, $\mu+\nu+\gamma$, and $e+\nu+\gamma$) will be noted. In the present model it is certainly interesting to look for the regularity between the $N \to P+e(\mu)+\nu$ and the $\Lambda \to \mathcal{N}+e(\mu)+\nu$ type interactions. From the present standpoint, the primary interaction (1′) is responsible for the $K_{\pi 3}$ decays. The preliminary quantitative analysis is not in contradiction with the experimental results [3]).

The crucial test of the present model would be the detection of the modes $\Lambda \to \mathcal{N}+e(\mu)+\nu$, etc. which will have the decay rates of order 10^{-8} sec.

We wish to express our gratitude to Professor N. Bohr and the Institute for Theoretical Physics, Copenhagen, for the hospitality which has been extended to us. One of us (S.O.) would like to thank Professor L. Rosenfeld for giving him a chance to stay at the Institute where this work has been completed.

References

1) S. Ogawa, Prog. Theor. Phys. **13** (1955) 1387; **15** (1956) 487
2) S. Oneda and A. Wakasa, Nuclear Physics **1** (1956) 125
3) S. Oneda, Nuclear Physics **3** (1957) 97
4) K. Iwata, S. Ogawa, H. Okonogi, B. Sakita and S. Oneda, Prog. Theor. Phys. **13** (1955) 19
5) S. A. Bludman, Phys. Rev. **102** (1956) 1422
6) S. A. Bludman and M. A. Ruderman, Phys. Rev. **101** (1956) 910
7) N. Dallaporta, Nuovo Cimento **1** (1955) 962; G. Costa and N. Dallaporta, Nuovo Cimento **2** (1955) 519
8) F. Duimio, Nuovo Cimento **2** (1955) 1308
9) M. Gell-Mann, Proceedings of the 6th Rochester Conference (1956)
10) J. Schwinger, Phys. Rev. **104** (1956) 1164
11) S. Sakata, Prog. Theor. Phys. **16** (1956) 686; M. A. Markov, Proceedings of the 6th Rochester Conference (1956)
12) M. G. Goldhaber, Phys. Rev. **101** (1956) 433
13) T. D. Lee and C. N. Yang, Phys. Rev. **104** (1956) 254
14) C. S. Wu, E. Ambler, R. W. Hayward, D. D. Hoppes and R. P. Hudson, Phys. Rev. **105** (1957) 1413; R. L. Garwin, L. M. Lederman and M. Weinrich, Phys. Rev. **105** (1957) 1415
15) S. Oneda, Nuclear Physics **3** (1957) 598 and 835
16) B. d'Espagnat, R. Omnes and J. Prentki, Nuclear Physics **3** (1957) 471

17) S. Furuichi, T. Kodama, S. Ogawa, Y. Sugawara, A. Wakasa and M. Yonezawa, Prog. Theor. Phys. **17** (1957) 89; S. Furuichi, Y. Sugawara, A. Wakasa and M. Yonezawa, Nuovo Cimento **5** (1957) 285
18) A. Pais and S. B. Treiman, Phys. Rev. **105** (1957) 1616
19) G. Wentzel, Phys. Rev. **101** (1956) 505; G. Takeda, Phys. Rev. **101** (1956) 1547
20) M. Kawagachi and K. Nishijima, Prog. Theor. Phys. **15** (1956) 180; R. Gatto, Nuovo Cimento **10** (1955) 318; G. Wentzel, Phys. Rev. **101** (1956) 1215; B. d'Espagnat and J. Prentki, Nuovo Cimento **3** (1956) 1045; Iso and Kawaguchi, Prog. Theor. Phys. **16** (1956) 177; R. H. Dalitz, Proc. Phys. Soc. A **69** (1956) 527
21) Proceedings of the 6th Rochester Conference (1956) and 7th Rochester Conference (1957)
22) W. B. Herrmannsfeldt, D. R. Maxson, P. Stähelin and T. S. Allen, Phys. Rev. (in the press)
23) Proceedings of the Venice-Padova Conference (1957)

Nuclear Physics **5** (1958) 319—330; © *North-Holland Publishing Co., Amsterdam*
Not to be reproduced by photoprint or microfilm without written permission from the publisher

MEASUREMENTS ON ISOTOPE SEPARATED β-RAY SOURCES OF Re^{186} AND Re^{188}

K. O. NIELSEN and O. B. NIELSEN
Institute for Theoretical Physics, University of Copenhagen

Received 1 August 1957

Abstract: Isotopically pure β-ray sources of Re^{186} and Re^{188} were prepared from pile irradiated natural Re in an isotope separator.

The spectrum of the β-rays from Re^{188} to the ground state of Os^{188} was found not to have the allowed shape. The deviations are of the type earlier observed in the decay $Re^{186} \rightarrow Os^{186}$. Both transitions probably proceed from a 1^- to a 0^+ state.

The K-conversion lines for the transitions from the 633 keV level in Os^{188} to the ground state and to the 155 keV 2^+ level were observed. The conversion coefficients indicate E2 nature for these transitions in agreement with an angular correlation experiment.

The level schemes of Os^{186} and Os^{188} indicate that these nuclei lie in the transitional region between the strongly deformed nuclei and those of spherical equilibrium shape.

1. Introduction

In the bombardment of natural Re with slow neutrons, the 90 hour Re^{186} and the 17 hour Re^{188} are produced. The study of the radiation from Re^{188} is thus complicated by the presence of Re^{186}, whereas Re^{186} can be studied under pure conditions when the short lived activity has died.

It has been demonstrated by Porter *et al.* [1]) that the β-ray groups to the ground state ($I = 0$) and to the first excited 137 keV level ($I = 2$) in Os^{186} show deviations from allowed shape. The deviations are not of the unique type associated with $\Delta I = 2$, yes, transitions, and it is thus probable that the ground state of Re^{186} has $I = 1^-$.

The decay scheme of Re^{188} has been investigated by Johns *et al.* [2]) and by Potnis [3]). The β-ray spectrum is very similar to that of Re^{186}, with strong branches to the ground level and to a 155 keV 2^+ level in Os^{188}. The ground state spin of Re^{188} is probably 1^-, and the possibility of deviations from allowed shape has been suggested [1, 2]), but until now not verified experimentally.

The low energy of the first excited level in Os^{188} indicates ellipsoidal shape of the nucleus, and the level scheme must thus be viewed in the light of the systematics which have been observed in deformed even nuclei [4, 5]). Johns *et al.* [2]) have established a number of levels from γ-ray measurements. The study of the conversion lines for the weak transitions from the high energy levels is much hindered by the strong β-ray background. The spin

of the 633 keV level has been established as 2^+ by means of an angular correlation measurement [6]). For the other levels the spin assignments are still rather uncertain.

The method of preparing β-ray sources in an isotope separator effectively overcomes the difficulties arising from the presence of Re^{186} in the Re^{188} sources. In addition, the high quality of these isotopically pure sources makes possible an accurate determination of internal conversion lines.

2. Source Preparation

The sources were prepared in an electromagnetic isotope separator [7, 8]). The ion source is of the magnetic type and is constructed with special reference to the separation of radioactive isotopes [9, 10]). A vacuum valve connected to the ion source makes it possible to introduce the charging material without breaking the main vacuum in the separator. The separation can thus start immediately after arrival of the activity.

The charging compound was Re_2O_7. A suitable pressure could be obtained in the discharge chamber of the ion source at an oven temperature of about 170° C. To avoid the necessity of preparing the oxide from radioactive Re, Re_2O_7 was produced before irradiation. Since this compound is strongly hygroscopic, it was kept in an air-tight aluminium container during irradiation in the JENER reactor.

When the activity had arrived, the container was opened and placed in the evaporation oven, which was then immediately introduced into the ion source. This was in advance adjusted to optimum working conditions.

In addition to the beams of Re^+ ions, also the sidebands corresponding to ReO^+, ReO_2^+, ReO_3^+, and ReO_4^+ were formed in the ion source. The relative intensities of these sidebands depend on the discharge conditions. Normally, the current of ReO_2^+ was twice that of Re^+. Nevertheless, Re^{186} and Re^{188} were collected as Re^+ ions, since the ReO_2^+ sideband contained two beams of stable atoms of the same mass as $Re^{186}O_2$ and $Re^{188}O_2$, probably due to $(Re^{185}O_2H)^+$ and $(Re^{187}O_2H)^+$. Weak currents of stable ions give rise to loss of activity through sputtering, and can even destroy the 150 $\mu g/cm^2$ aluminium foil which was used as source backing.

The temperature of the discharge chamber was kept at about 700° C, and thus no condensation of Re_2O_7 could take place here. But Re and ReO formed by neutralization of ions on the top and bottom plates of the discharge chamber did not re-evaporate and were lost †. This effect together with the formation of the sidebands reduced the efficiency to about 0.01 %, or 100 times lower than obtainable in more favourable cases [9]).

The collector arrangement is shown in fig. 1. In the initial stage of separa-

† Later experience indicates that this reduction in efficiency can be overcome by increasing the discharge current in the ion source [16]).

tion, the screen (6) is in position 1, shielding the collector foils (5). When optimum working conditions are obtained, the screen is turned in position 2, and the beams of Re^{185} and Re^{188} can now strike the foils. The feeler pins (1) intercepts the Re^{188} ray, and the position of the beams is then regulated by feedback to a set of deflecting plates at the entrance of the magnetic field [8]).

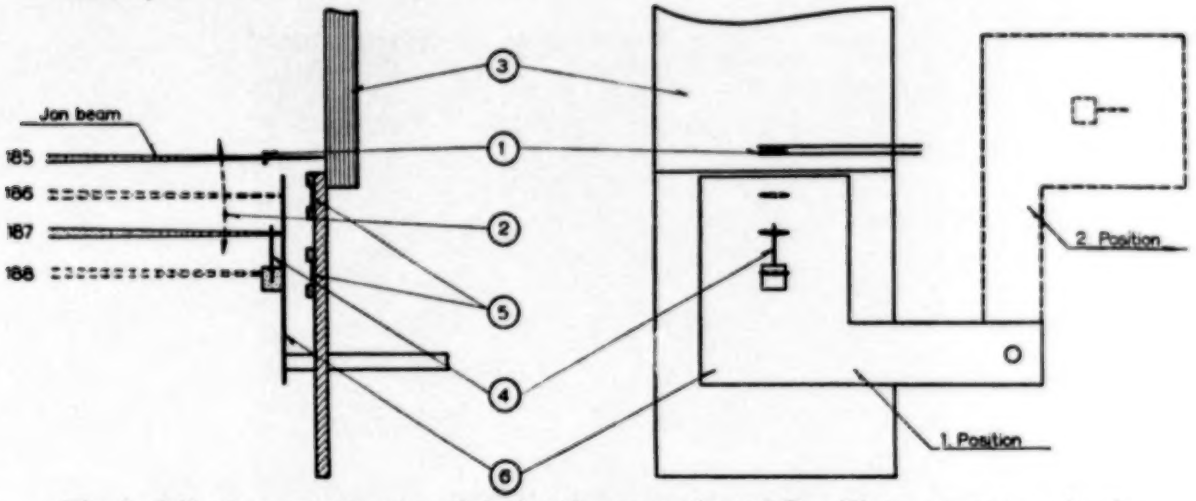

Fig. 1. Collector arrangement used during the separation of Re. (1) two tungsten pins for position regulation, (2) the horizontal scanning needle (fig. 2), (3) fluorescent glass plate, (4) vertical scanning needle (fig. 3), (5) aluminium foils, (6) shield for the foils.

Since the active foil is used directly as source in the β-ray spectrometer, it is of extreme importance that the extension of the beam at the collector is so small that the whole active area can be utilized. For this reason, the focusing was controlled continuously by a scanning device, which was based on a thin horizontal needle vibrating through the beam. A mass spectrum obtained in this way is shown in fig. 2.

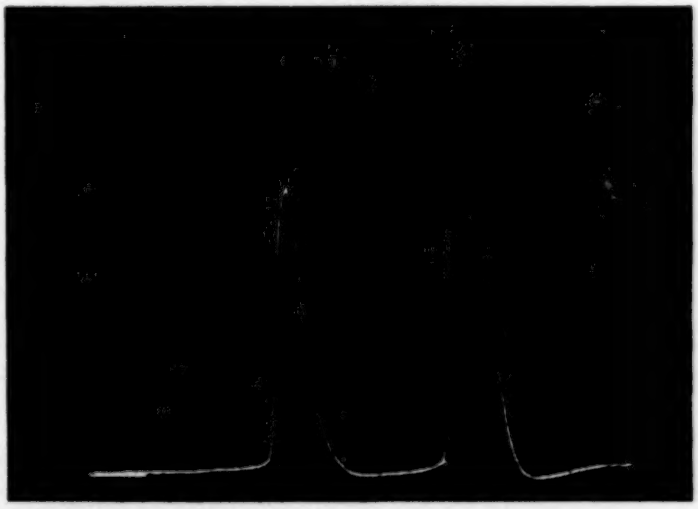

Fig. 2. Oscilloscope tracing of the mass spectrum of Re. The distance between the two stable beams of Re^{185} and Re^{187} is 9 mm. The full width at half maximum is about 1.5 mm.

The structure of the beam in the horizontal direction was controlled in a somewhat different way. The beam was swept over a vertical needle fixed on the screen (6) by means of the electric field between a pair of deflecting plates placed at the entrance of the magnetic field. This control could only be carried out when the screen was in position 1 and the collection stopped †. The current distribution found in this way is shown in fig. 3.

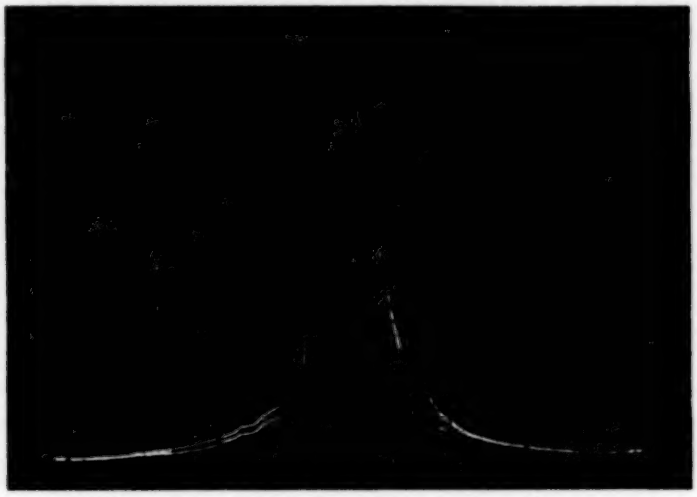

Fig. 3. The distribution in the beam in the horizontal direction. The full width at half maximum is about 5 mm.

Figs. 2 and 3 give the distribution of activity on the collector foil. The reduction of the extension of the beam in the horizontal direction (see fig. 3) is obtained at the expense of a reduced resolving power [8]). The source area used was about 2×6 mm^2, corresponding to about 60 % of the activity collected, or of the order of 20 μC. The effective source thickness is 5—10 μg/cm^2, which is the penetration depth in aluminium of Re atoms impinging with about 50 keV [12]).

3. The β-Ray Spectrometer

For the β-ray measurements, a six gap β-ray spectrometer [13]) was used. $\beta-\gamma$ coincidences were recorded with a 1.5″ dia × 1.5″ NaI crystal placed behind the source. In order to measure the shape of the continuous β-ray spectra with high accuracy, scattering of β-particles from the crystal has to be minimized. In these experiments, the distance from source to crystal was chosen as 25 mm, whereas it is kept as low as 5—10 mm in cases when the coincidence efficiency is of primary importance.

We have not investigated our β- and γ-recording channels as thoroughly as described by Porter *et al.* [1]). As a main test on the performance of the equipment, we repeated the measurements of these authors on the spectral

† An improved scanning device, which was not yet constructed when the Re separations were carried out, has been described by K. O. Nielsen and O. Skilbreid [11]).

shape of the β-ray groups from Au^{198} and Re^{186}. Good agreement was obtained in both cases (section 5).

The main β-group from Au^{198}, which accounts for about 98 % of all decays, is 100 % coincident with a 412 keV γ-ray and is thus suited for checking the coincidence equipment. It was found that the coincidences were recorded with an efficiency which was independent of the β-ray energy within the statistical accuracy, or better than 1 %. Small variations in time of this efficiency, of the order of 1 %, could be accounted for by the variation in dead time in the γ-ray counter due to the decay of the source.

4. Conversion Line Measurements and Branching Ratios

4.1. THE 137 keV TRANSITION IN Os^{186}

TABLE 1

	Porter *et al.* [1])	Johns *et al.* [2])	This investigation	Theoretical E2
I_K (%)	4.28	4.65	4.15∓0.30	
K/L	0.65	0.61∓0.07	0.68∓0.03	0.69
α_K	0.36	0.45∓0.03	—	0.42
β_{934} (%)	24.0∓1.5	24 ∓4	22 ∓2	

The theoretical K-conversion coefficients are from the tables of Sliv and Band[14]). The K/L ratios are from those of Rose *et al.* [15, 16]).

Our values for the intensity of the K-line and the K/L ratio for this transition (table 1) are in excellent agreement with the two previous determinations. The E2 nature, which is expected for a ground state transition from a low energy first excited level in an even nucleus, is confirmed by the K-conversion coefficient, the K/L ratio and the $(L_I+L_{II})/L_{III}$ ratio [2]).

Our intensity for the 934 keV β-ray, corresponding to the total intensity of the 137 keV transition (decay scheme in fig. 6), is based on the conversion line measurements and a γ-ray intensity calculated by dividing the K-line intensity with the theoretical E2 conversion coefficient of Sliv and Band [14]). This method probably represents the most accurate way of determining the γ-ray intensities, as these finite size corrected conversion coefficients must be considered accurate to within a few pct. for fast E2 transitions.

The intensity calculated in this way agrees well with the results of Porter *et al.* [1]) obtained in a coincidence experiment from the known efficiency of their coincidence counter, and independently by Fermi analysis. Also the agreement with Johns *et al.* is satisfactory. They determined the branching ratio in two ways, by Fermi analysis and by dividing the K-line intensity with the experimental conversion coefficient, which was based on the ratio between the X-ray and the γ-ray in a scintillation spectrum.

4.2. THE 155 keV TRANSITION IN Re^{188}

TABLE 2

	Johns *et al.*[1])	Potnis [3])	This investigation	Theoretical E2
I_K (%)	3.0 ∓0.4		4.4 ∓0.4	
K/L	0.79∓0.15	0.70∓0.05	0.92∓0.05	0.93
α_K	0.40∓0.05	0.29∓0.03 0.37∓0.05		0.32
β_{1975} (%)	18 ∓3		24 ∓2	

Also for this transition, the E2 nature is obvious. The experimental values in the first two columns are found by the methods applied to the 137 keV transition in Re^{186}. The value for the β-group β_{1975} is based on the total intensity of the 155 keV transition corrected for the excitations due to the weak high energy γ-rays (decay scheme fig. 7). We believe that the discrepancies in the two measurements may be due to experimental difficulties in connection with the presence of Re^{186} in the Canadian sources.

The intensity of the 1975 keV β-group obtained by Potnis is based on Fermi analysis. The first of the two experimental conversion coefficients was calculated from the corresponding excitation of the 155 keV level and the conversion line intensities. The second value was found by the scintillation method.

The ratio of ft-values for the two β-groups to the ground state and to the first rotational level is 2.3, in good agreement with the theoretical value of 2 [17]) for transitions from a state with $(K, I)=(1, 1)$ to states with $(K, I) = (0, 0)$ and $(0, 2)$.

4.3. THE 478 AND 633 keV TRANSITIONS IN Os^{188}

The numerous transitions to high energy levels in Os^{188} are all weak compared to the transitions to the ground state band. They amount together only to about 3 % of all decays, and only the two conversion lines for transitions from the 633 keV level could be observed on the high β-background (fig. 4). Table 3 contains the data on these two transitions.

TABLE 3

keV	$I_K \times 10^4$	γ_{rel}	α_K	α_K Theoretical E2	γ (%)
155	440	9		0.32	
478	2.3	0.63	0.023	0.020	1.1
633	1.8	1	0.011	0.012	1.5

The relative γ-ray intensities in column 3 are measured by means of external conversion by Johns *et al.* We have confirmed these intensity ratios by a scintillation spectrometer, but this method has lower resolution and is probably less accurate. The conversion coefficients in column 4 are found

by assuming the theoretical α_K for the 155 keV transition. The γ-ray intensities in the last column are the conversion line intensities divided by the theoretical conversion coefficients.

The experimental conversion coefficients classify both transitions as E2, in agreement with angular correlation measurements of Potnis *et al.* [6]), which indicated 633 keV as a 2^+ state decaying by an almost pure E2 γ-ray to the 155 keV 2^+ level.

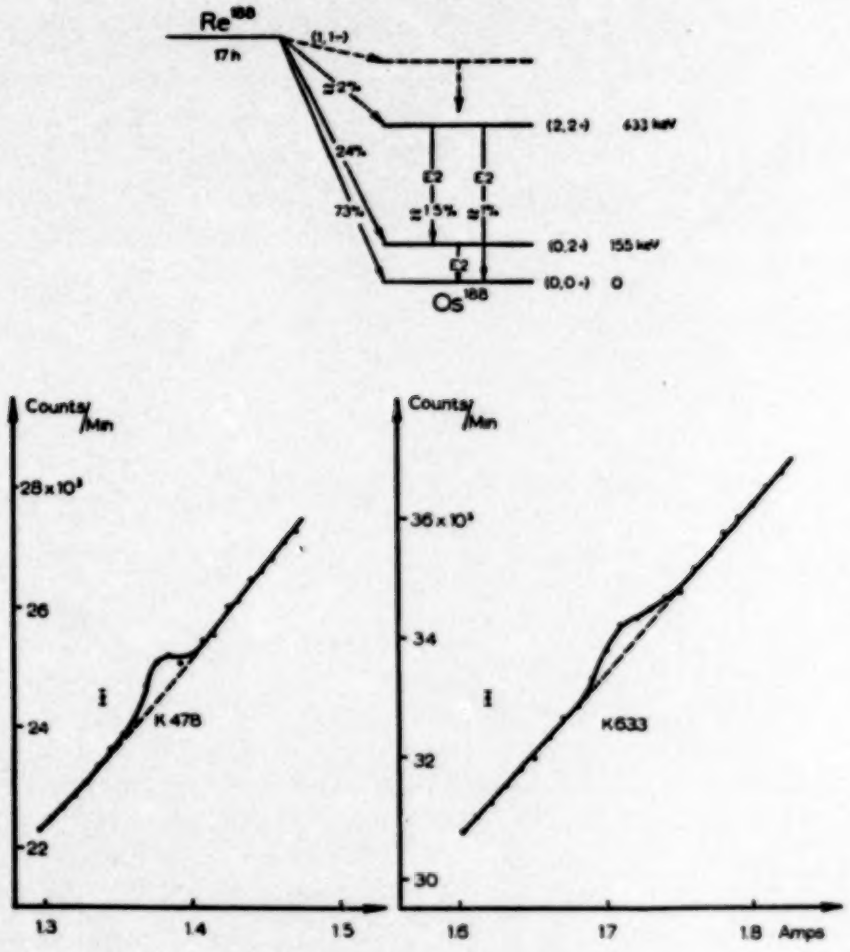

Fig. 4. K conversion lines of the 478 keV and 633 keV transitions. Resolution $\approx$ 1.8 %.

The 633 keV level is likely to be the lowest member of a rotational band, as a state with $I = 0$ or 1 probably would be excited by a β-transition. The K quantum is then 2, and a branching ratio for E2 transitions to the ground state band of $\gamma_{633}/\gamma_{478}(478/633)^5 = 0.7$ would be expected theoretically. The experimental value, based on the γ-intensities in the last column of table 3, is 0.3.

5. β-Ray Measurements

5.1. THE NUCLEUS Au^{198}

The source was prepared by evaporation in vacuum of about 100 $\mu g/cm^2$ gold on a 150 $\mu g/cm^2$ aluminium foil. The foil was then activated in the JENER reactor.

The conventional Kurie plot (fig. 5) is straight from the maximum energy to about 250 keV. At lower energies, the plot turns upwards, and the deviation is about 6 % in counting rate at 180 keV, in agreement with Porter *et al.*, who found 5.5 %. Only about half of this effect is accounted for by the low energy β-group (fig. 5). It is not clear whether the remaining

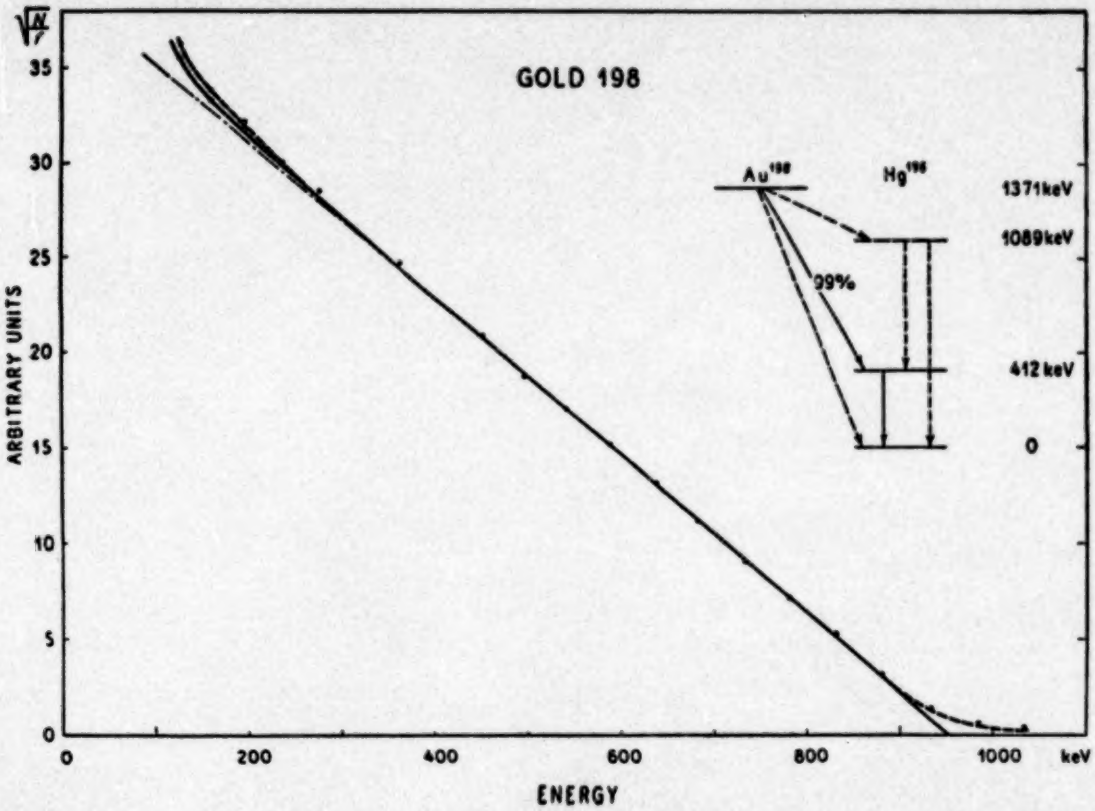

Fig. 5. Kurie plot for Au^{198}. The dotted line corresponds to the spectrum before correction for the low energy group.

part is a real deviation from allowed shape, or whether it is instrumental and due to scattering in the spectrometer and the γ-ray crystal.

5.2. THE NUCLEUS Re^{186}

The total singles spectrum as well as the part coincident with the 137 keV γ-ray were recorded. The spectrum of the ground state β-ray was obtained from the total singles spectrum after subtraction of the coincident group which was weighted according to the assumed intensity of 22 %. Our determination of the maximum energy of the ground state transition was in agreement

with, but probably less accurate than the 1071.5 ± 1.5 keV found by Porter *et al.*

The spectrum of the 1071 keV β-ray group exhibits a shape similar to that found by Porter *et al.* The deviation from linearity is evident from fig. 6, where the Kurie plot is compared to a straight reference line which was chosen so as to fit the experimental plot from the maximum energy down to about 900 keV. The downward deviation from the straight line at 250 keV corresponds in counting rate to about 10 %. Under similar conditions, the deviation found by Porter *et al.* amounts to 14 %. The difference is of the order of our assumed experimental uncertainty.

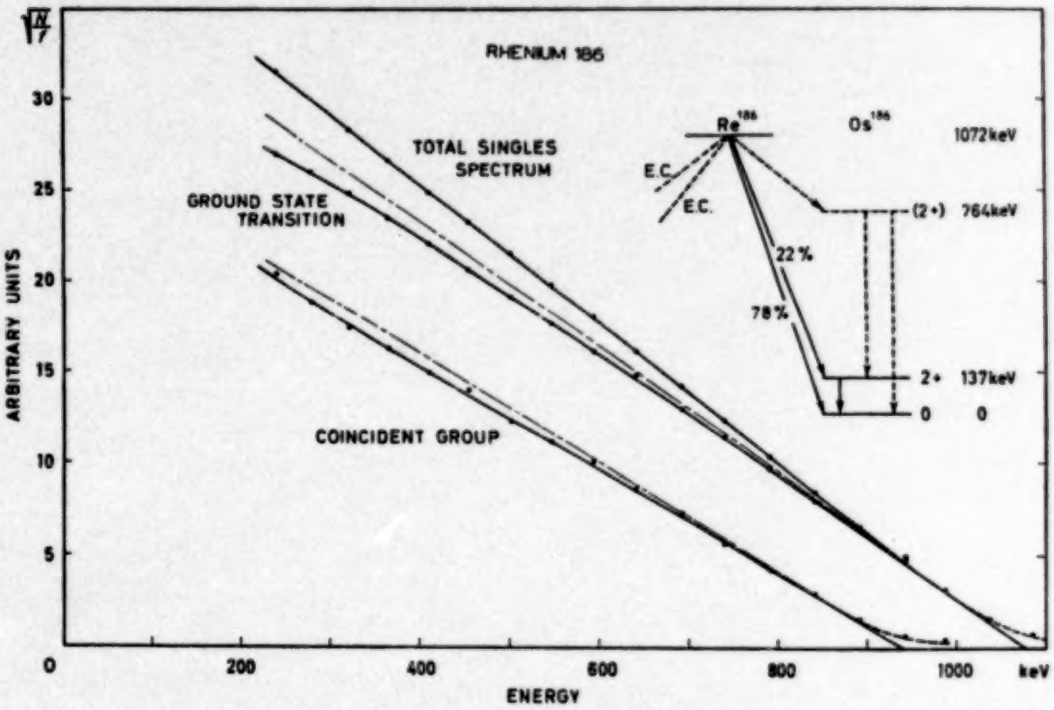

Fig. 6. Kurie plot for Re^{186}.

The deviation of the experimental points near the maximum energy from the extrapolated plot (fig. 6) cannot be completely explained by the 3 % line width of the spectrometer. The effect is probably due to scattering in the spectrometer, amounting to a few parts in ten thousand of the counting rate at the highest part of the spectrum.

The measurements on Re^{186} were performed mainly as a check on the experimental methods to be applied to Re^{188}. Since the presence of low energy β-groups in the decay of Re^{188} obscured the shape of the strong β-group to the 155 keV level in Os^{188}, a major effort to study the shape of the coincident group of Re^{186} was not justified. The Kurie plot (fig. 6) showed some tendency towards concavity against the energy axis, in agreement with the more accurate results of Porter *et al.* [1]).

5.3. THE NUCLEUS Re^{188}

The Kurie plots of the total singles spectrum and the coincident part appear in fig. 7. The ground state spectrum was found after subtraction of the contribution from the 24 % group to 155 keV. In addition, a correction due to the β-rays to high energy levels had to be applied. The intensities of these weak β-transitions were chosen according to the decay scheme of Johns *et al.*

The maximum energy 2130±20 keV is in good agreement with earlier

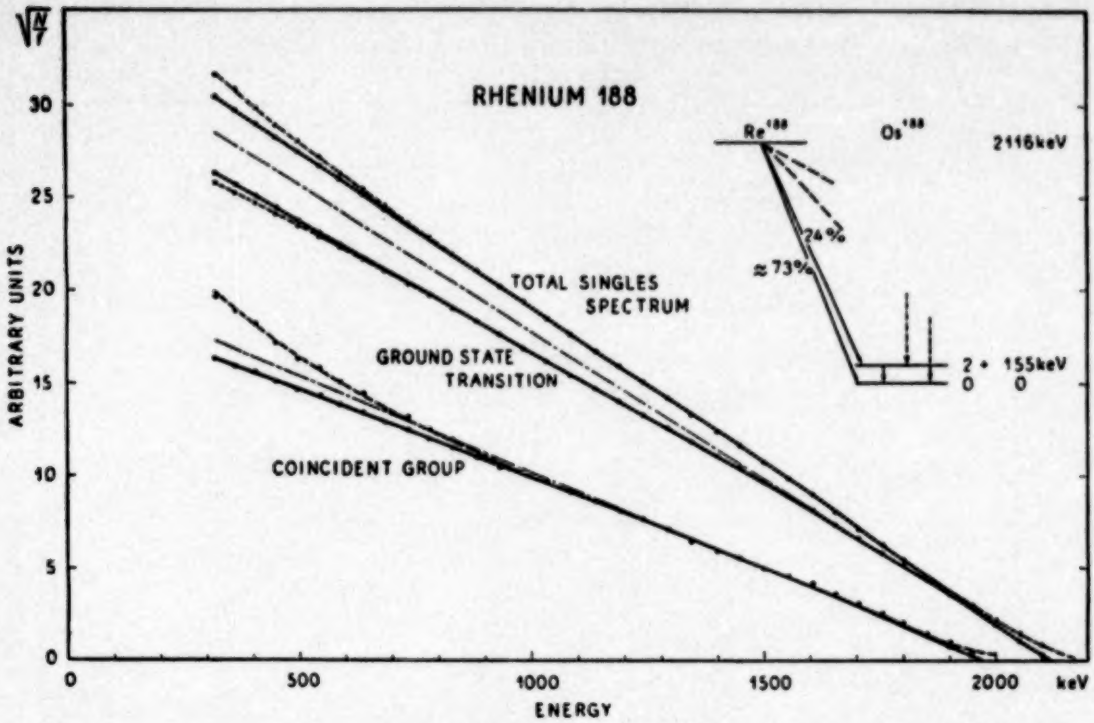

Fig. 7. Kurie plot for Re^{188}. The dotted lines correspond to the spectrum before correction for the low energy groups.

values [2, 2]). Also in this case, the experimental points near the maximum energy were shifted more than had to be expected from the line width.

The spectral shape is similar to Re^{186}. The downward shift from a reference line fitting the Kurie plot from the maximum energy to about 1700 keV amounts to 15 % in counting rate at 300 keV. The deviation from allowed shape is thus somewhat greater than for Re^{186}.

Also the β-ray to the 155 keV level probably exhibits a non-allowed shape (fig. 7). Unfortunately, the somewhat uncertain correction due to the high energy γ-rays is of the same order as the effect in question.

6. Discussion

The existence of non-unique deviations in the β-spectra of Re^{188} as well as Re^{186} can only be the result of a cancellation in the large energy in-

dependent terms and points to a striking similarity in the two transitions. It is not surprising that the effect is larger in Re^{188}, since this spectrum ranges over twice the energy interval.

The level structure of Os^{188} is of some interest, since this nucleus lies in the transition region between the deformed nuclei ($150 < A < 190$) possessing rotational spectra and the nuclei ($190 < A < 220$) exhibiting vibrations about an approximately spherical equilibrium shape.

The energy of the first excited level ($E_1 = 155$ keV) is somewhat larger than for the deformed even nuclei of lower mass, but considerably smaller than for the vibrative nuclei ($E_1 > 300$ keV). This suggests that Os^{188} may to a first approximation be considered in terms of the rotational model. On the other hand, the properties of the 633 keV level indicates significant departures from this model, corresponding to a transition towards a vibrational type of spectrum.

Thus, the energy of the 633 keV level, interpreted as a γ-vibration ($(K, I, \pi)=(2, 2, +)$), is considerably lower than the energies of about 1 MeV for the corresponding state in the region of the strongly deformed nuclei.

Also the decay of the 633 keV state seems to indicate intermediate properties. The observed branching ratio, corrected for the energy dependence, for the γ-rays to the ground state and to 155 keV is 0.3. This ratio would be 0.7 for γ-rays to pure rotational states in a deformed nucleus, while it would tend to vanish for transitions from a 2-phonon state in a spherical nucleus.

The energies of the first and second 2^+ state in Re^{186} are 137 and 764, thus indicating a similar, but less pronounced trend. The ratio of reduced transition probabilities for the transitions from 764 keV to the ground state and to 137 keV is ≈ 0.3 [1, 2]).

We wish to express our gratitude to Professor Niels Bohr for the excellent working conditions in his Institute. We are indebted to Professor A. Bohr, Dr. O. Kofoed-Hansen, and Dr. B. R. Mottelson for valuable suggestions. Mr. O. Skilbreid has contributed significantly to the operation of the isotope separator and the β-ray spectrometer.

References

1) F. F. Porter, M. S. Freedman, T. B. Novey and F. Wagner, Phys. Rev. **103** (1956) 921
2) M. W. Johns, C. C. McMullen, I. R. Williams and S. V. Nablo, Can. Jour. of Phys. **34** (1956) 69
3) V. R. Potnis, Phys. Rev. **104** (1956) 722
4) I. Perlman and J. Rasmussen, α-radioactivity in Handbuch der Physik
5) K. Alder, A. Bohr, T. Huus, B. R. Mottelson and A. Winther, Revs. Mod. Phys. **28** (1956) 432
6) V. R. Potnis, V. S. Dubey and C. F. Mandeville, Phys. Revs. **102** (1956) 459
7) J. Koch, Cir. U. S. Nat. Bur. Stand. No. 522 (1953)

8) K. O. Nielsen and O. Skilbreid, Nuclear Instruments (in print)
9) O. Almen and K. O. Nielsen, Nuclear Instruments **1** (1957) 302
10) K. O. Nielsen, Nuclear Instruments **1** (1957) 289
11) K. O. Nielsen and O. Skilbreid, Nuclear Instruments **1** (1957)
12) K. O. Nielsen, Proc. 1955 Harwell Isotope Conf. (1956) Ch. 9
13) O. B. Nielsen and O. Kofoed-Hansen, Mat. Fys. Medd. Dan. Vid. Selsk. **29** (1955) no. 6
14) L. Sliv and J. Band, K conversion coefficients
15) M. E. Rose, G. H. Goertzel and C. L. Perry, ORNL-1923 (1953)
16) M. E. Rose, G. H. Goertzel and C. Swift, L-shell internal conversion coefficients, privately distributed
17) G. Alaga, K. Alder, A. Bohr and B. R. Mottelson, Mat. Fys. Medd. Dan. Vid. Selsk. **29** (1955) no. 9

Nuclear Physics **5** (1957) 331—345; © *North-Holland Publishing Co., Amsterdam*
Not to be reproduced by photoprint or microfilm without written permission from the publisher

THE ENERGY LEVELS OF Dy^{160}

S. OFER

Department of Physics, Hebrew University, Jerusalem †

Received 14 September 1957

Abstract: A study of the γ-ray transitions between levels of Dy^{160} resulting from the decay of Tb^{160} has been made using fast slow coincidence technique. The angular correlations of six γ-ray cascades were measured. A decay scheme is suggested and assignments for the spins of excited levels and the multipolarities of the γ-radiations are made. The results support the suggestion that the 970 keV and 1050 keV levels should be interpreted as collective vibrational levels.

1. Introduction

Recently, some articles dealing with the decay of Tb^{160} to Dy^{160} have been published [1, 2, 3, 4, 5]). In the work of Burson and coworkers [1]), the spectrum of γ-rays accompanying the decay of Tb^{160} was measured, using a scintillation counter. The spectra of coincidences of some of the gamma lines were also measured. In addition, the energies of the internal conversion lines were determined, using a 180° photographic spectrometer. On the basis of their experimental results, these authors determined cascade relations between some of the γ-rays and suggested a decay scheme. The resolution of the counters used by these authors was not very good. The authors did not try to determine the relative intensities of the γ-rays and did not assign spins for the excited levels and multipolarities for the radiations emitted.

In the work of Keshishian and coworkers [2]), the shape of the spectrum of γ-rays emitted from Tb^{160} was determined. The energies of the internal conversion lines were also measured. From the results of their measurements these authors draw conclusions concerning the decay scheme of Tb^{160}. In this work, no attempt has been made either to determine the relative intensities of the γ-rays and no spin and multipolarity assignments were suggested.

In the first work of Bertolini and coworkers [3]), they determined the shape of the spectrum of the γ-radiations, measured coincidences of beta and gamma radiations and tried to determine the relative intensities of the γ-rays and their internal conversion coefficients from the spectrum of the photoelectrons reaching the β-spectrometer using various converters. An examination of the spectrum of γ-rays of Tb^{160}, as obtained from a scintillation

† Present address: Brookhaven National Laboratory, Long Island, U.S.A.

counter, indicates that most of the relative intensities determined by them are not correct and that the errors reach, in some cases, factors of 10. These authors suggested a scheme for the decay of Tb^{160}. They also suggested values for the spins of some of the excited levels. The only attempt to measure angular correlations of cascades of γ-rays obtained in the decay of Tb^{160} has been made in the second work of Bertolini and coworkers [4]). The coincidences between 300 keV γ-ray and all the γ-rays whose energy is higher than 700 keV were measured. In this way the angular correlation of a mixture of two cascades has been measured. Although their experimental results are correct, the conclusions drawn from them are doubtful, as will be explained in the present work.

In the work of Knowels and Clark [5]) the K-conversion coefficients of nine gamma rays following the decay of Tb^{160}, were determined.

In all the works mentioned, identical conclusions concerning the place of the strong γ-transitions in the decay scheme were drawn. These transitions are marked in fig. 4 by heavy lines. There is no agreement about the places of many of the weak γ-rays in the decay scheme.

In the present work, the spectrum of γ-rays accompanying the decay of Tb^{160}, was measured. The spectra of coincidences of some of the γ-rays were also measured. In addition, the angular correlation coefficients of six γ-ray cascades were determined. On the basis of the results of these measurements a decay scheme was suggested and assignments for the spins of excited levels and multipolarities of the γ-radiations were made.

The source used in most of the experiments of this work was a dilute aqueous solution of $Tb_2(SO_4)_3$. The radioactive material was produced by neutron bombardment in the Harwell pile. The measurements were carried out using two NaI scintillators in a fast-slow coincidence arrangement. The experimental arrangements were identical with those used in previous works and were already described [6, 7]). The experimental results lead to the conclusion that many of the levels of Dy^{160} are of the collective type. The experimental results concerning the γ-transitions from these levels are analysed in the light of the collective model.

2. Experimental Results

2.1. SPECTRUM OF GAMMA RAYS

The spectrum of γ-rays was examined using a scintillation counter whose resolution was 8 % at 661 keV. The spectrum of γ-rays whose energy is smaller than 500 keV is shown in fig. 1. In fig. 2A the shape of spectrum of γ-rays whose energy is higher than 500 keV is shown. The spectrum obtained is similar to that obtained in previous works, but because of the improved resolution of the counter in the present work, the two peaks belonging

to gamma radiations of 882 keV and 960 keV are clearly resolved. Fig. 2A also proves, in a convincing manner, the existence of a full peak belonging to a 1282 keV radiation on the background of the tail of the peak of the 1182 keV full-peak.

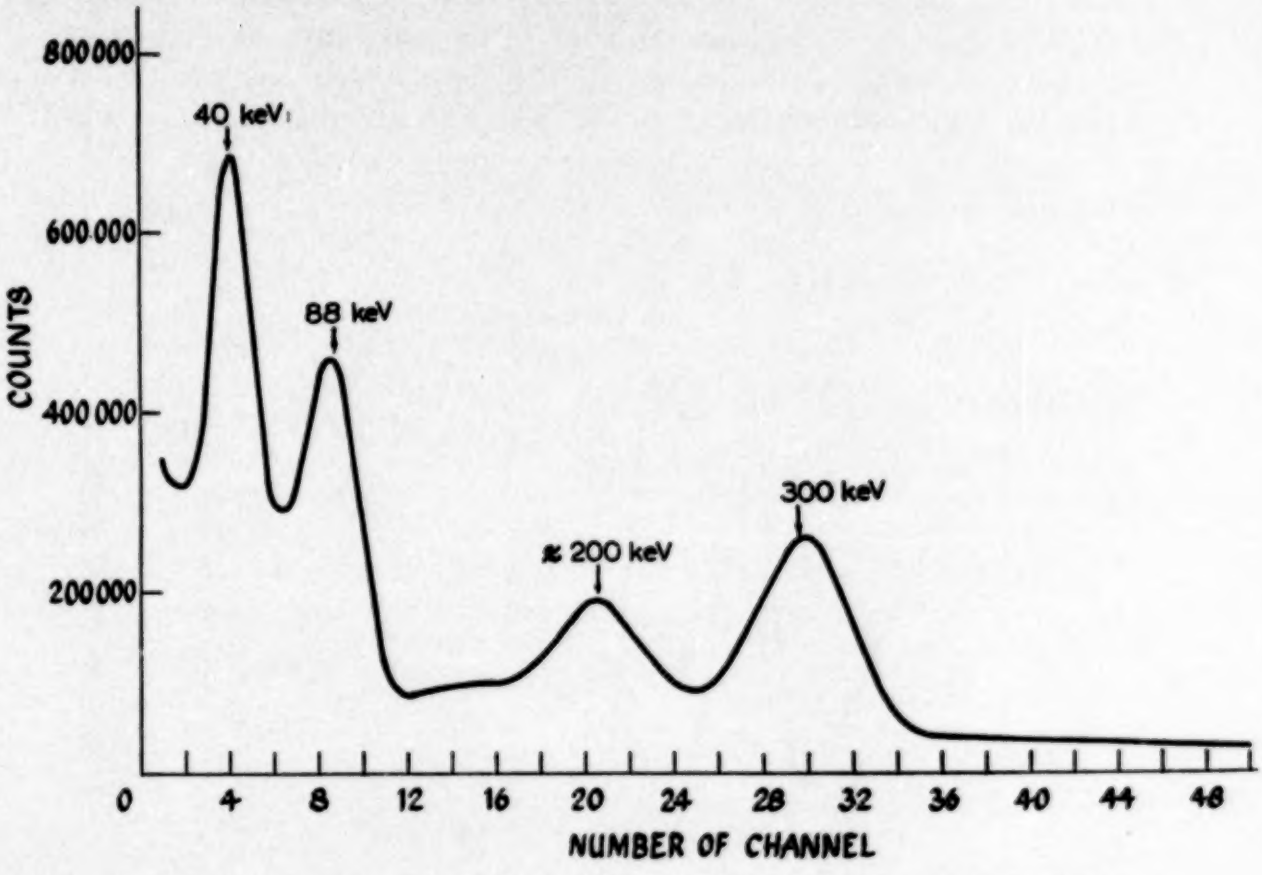

Fig. 1. Spectrum of γ-rays in the (0–500) keV region emitted in the decay of Tb^{160}.

As already pointed by Burson and coworkers the 200 keV peak is broad and it is very likely that it is obtained from two gamma lines whose energies are almost the same and with almost the same intensities. This suggestion is strongly supported by the facts that in a β-spectrometer two conversion lines corresponding to 196 keV and 214 keV radiations were obtained [2]) and that by using convertors two lines of about the same intensities corresponding to 199 keV and 218 keV lines were obtained [3]).

By an analysis of the shape of the spectrum obtained, some of the relative intensities given in table 1 were calculated.

2.2. SPECTRA OF COINCIDENCES WITH THE 88 keV, 200 keV AND 300 keV GAMMA RADIATIONS

The shape of the coincidence spectrum with the 88 keV γ-radiation is shown in fig. 2B. The shape of the spectrum shows that the 882 keV and

the 1182 keV radiations are in cascade with the 88 keV radiation and that the 970 keV radiation is not in cascade with it. The measurements prove, beyond any doubt, that the 1282 keV radiation is also in cascade with the 88 keV radiation. The last fact contradicts the assumptions made in previous works, concerning the place of the 1282 keV radiation is the decay scheme.

The shape of the coincidence spectrum of the two γ-rays whose energies are about 200 keV is shown in fig. 3A. This measurement was carried out when the angle between detectors was 180°. An absorber of 8 mm was

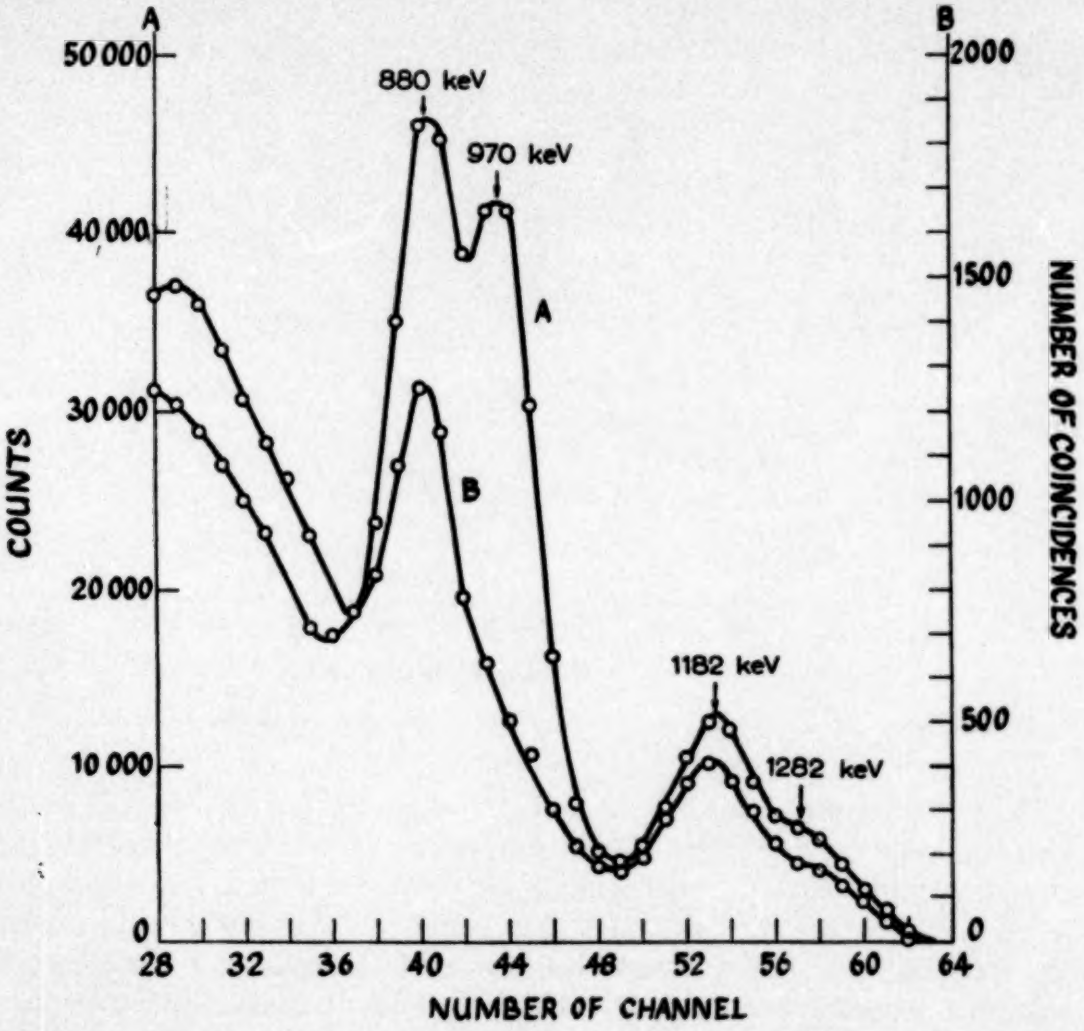

Fig. 2. A) Spectrum of γ-rays with energies higher than 500 keV emitted in the decay of Tb^{160}. B) Spectrum of γ-rays coincident with the 88 keV γ-ray.

placed between the source and the scintillator which detected the γ-rays whose energy was higher than 600 keV, in order to prevent coincidences arising from Compton scattering from one counter into the other. The lead absorbed all the secondary γ-radiations created in the other counter but allowed most of the radiations whose energy was higher than 600 keV to

enter the counter. The fixed channel of one of the pulse analysers was placed at the photo-peak of the radiations of about 200 keV.

The shape of the spectrum obtained proves the existence of γ-rays whose energies are 1082 keV, 962 keV, 762 keV and 682 keV and that these radiations are in cascade with one of the two radiations whose energies are 200 keV and 220 keV.

In order to find out with which of the two radiations of 200 keV and 220 keV are the radiations of 1082 keV, 962 keV, 762 keV and 682 keV in cascade, the channel of the fixed pulse-analyser was adjusted to select pulses belonging to the low half of the peak at 200 keV. In the spectrum of coincidence obtained in this way, the peaks corresponding to the 1082 keV and of 682 keV radiations are more intense compared to their intensities

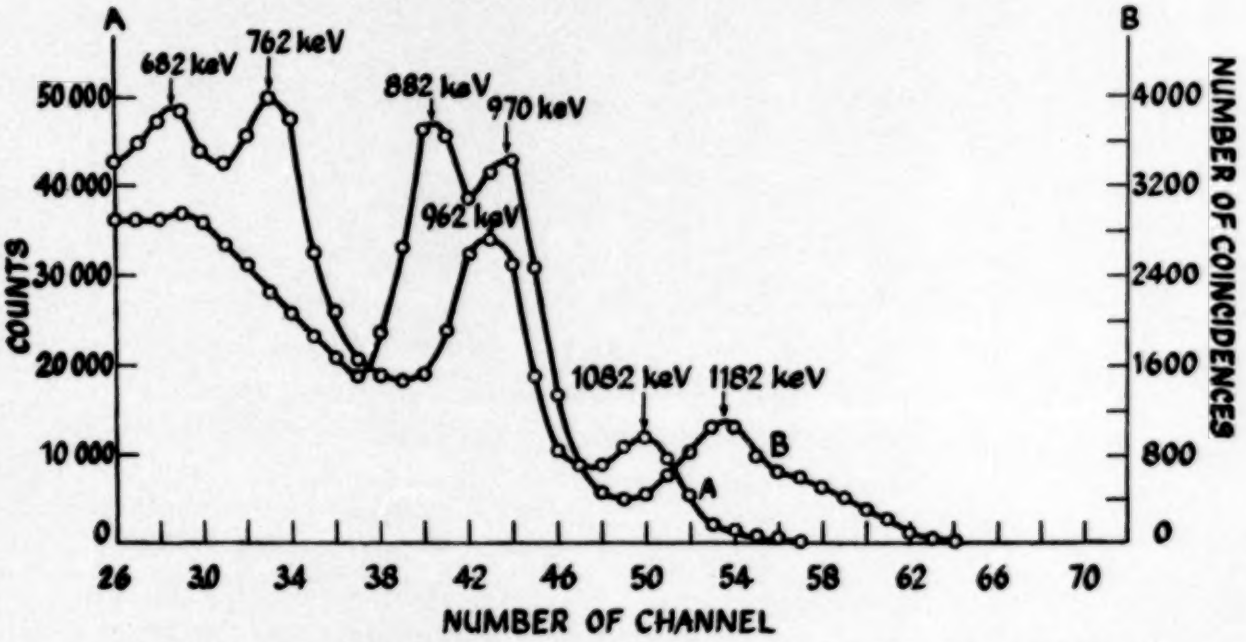

Fig. 3. A) Spectrum of γ-rays coincident with the γ-rays whose energies are about 200 keV. B) "Singles" spectrum of γ-rays.

as displayed in fig. 3A. A similar experiment performed with the channel of the analyser adjusted to select pulses of the high half of the peak at 200 keV showed that the peak at 962 became relatively higher. The conclusion is that 1082 keV and the 682 keV radiations are in cascade with the 200 keV radiation, whereas the 962 keV radiation is in cascade with the 220 keV radiation. It seems, therefore, that the 762 keV radiation is in cascade with both the radiations of 200 keV and 220 keV. A measurement of the spectrum of coincidence with the 300 keV radiation shows that the latter is in cascade with both the radiations of 972 keV and 882 keV.

The experimental results obtained concerning the energies, the relative intensities and the cascade relations of the γ-rays emitted in the decay of

Tb^{160}, are given in table 1. The values given for the energies of the γ-radiation may be in errors of about 3 % and those given for the relative intensities may be in errors of about 20 %. The values given in brackets are uncertain.

TABLE 1

Results of measurements of spectrum of γ-rays and of spectra of coincidences of various radiations

Energy of γ-radiation (keV)	Relative intensity of γ-radiation	Energy of γ-radiations in cascade with the radiation
88	36	200, 300, 882, 1182, 1282
200	(10) } 21	88, 300, 682, 762, 1082
220	(10) }	762, 962
300	42	88, 882, 970
400	(2)	
682	(2)	200
762	3	200, 220
882	100	88, 300
962	5	220
970	90	300
1082	5	200
1182	48	88
1282	22	88

2.3. ANGULAR CORRELATION OF THE 300 keV—970 keV CASCADE

All the angular correlation measurements except those described in section 2.9 were carried out with a source in the form of a dilute aqueous solution of $Tb_2(SO_4)_3$.

In the measurement of the angular correlation of the 300 keV—970 keV cascade a 4 mm lead absorber for only scattered radiations was suitably placed between the detectors to avoid the production of false coincidence pulses resulting from Compton scattering from one crystal to the other. The channel of one of the pulse analysers was adjusted to select pulses belonging to the full-peak of the 300 keV radiation and the channel of the second analyser was adjusted to select pulses belonging to the higher half of the full-peak at 970 keV, in order to avoid the counting of coincidences of pulses belonging to the 882 keV radiation. The angular correlation function obtained after correcting for the finite solid angle of the detectors was

$$P(\theta) = A[1+(0.24\pm0.02)P_2(\cos\theta)-(0.01\pm0.02)P_4(\cos\theta)]. \qquad (1)$$

2.4. ANGULAR CORRELATION OF THE 300 keV—882 keV CASCADE

The experimental arrangements were identical in this case with those of the previous case. The only difference was that the channel of the second analyser was adjusted to select only pulses belonging to the lower half of

the full-peak corresponding to the 882 keV radiation, in order to avoid the counting of coincidences of pulses belonging to the 960 keV radiation. The angular correlation function obtained, after correcting for the finite solid angle of the detectors was

$$P(\theta) = A[1-(0.045\pm0.01)P_2(\cos\theta)-(0.02\pm0.02)P_4(\cos\theta)]. \quad (2)$$

2.5. ANGULAR CORRELATION OF THE 1282 keV–88 keV CASCADE

As the 1282 keV radiation has the highest energy in the spectrum, false coincidences resulting from Compton scattering from one crystal to the other could not be produced in this case. As the full-peak corresponding to the 1282 keV radiation is relatively weak, a strong source was used in order to get good statistics and the resolving time of the fast coincidence circuit was reduced to 2.5×10^{-8} sec. The channel of one of the pulse-analysers was placed on the peak of the 88 keV radiation and the channel of the second analyser was placed on the higher half of the full peak corresponding to the 1282 keV radiation. The angular correlation function obtained after correcting for the finite solid angles of the detectors was

$$P(\theta) = A[1+(0.0115\pm0.02)P_2(\cos\theta)+(0.00\pm0.01)P_4(\cos\theta)]. \quad (3)$$

2.6. ANGULAR CORRELATION OF THE 1182 keV–88 keV CASCADE

The energies of the radiations were in this case such that there was no possibility for the production of false coincidences resulting from scattering of radiations from one counter into the other. The resolving time of the fast coincidence circuit was 7×10^{-8} sec. The channel of one of the pulse analysers was placed on the peak at 88 keV and the channel of the other was placed at the full peak corresponding to the 1182 keV radiation. The angular correlation function obtained was

$$P(\theta) = A[1+(0.08\pm0.02)P_2(\cos\theta)+(0.07\pm0.015)P_4(\cos\theta)]. \quad (4)$$

2.7. ANGULAR CORRELATION OF THE 882 keV–88 keV CASCADE

The channel of one of the analysers was placed on the peak at 88 keV and the channel of the other analyser was placed on the full peak belonging to the 882 keV radiation. An absorber of 3 mm lead was placed between the source and the scintillator which detected the 882 keV radiation and a 10 mm lead absorber for only scattered radiation was suitably placed between the detectors, to avoid the production of false coincidence pulses. False coincidence pulses could be formed by Compton scattering of 1182 keV γ-rays in one crystal and absorption of the secondary γ-ray emitted from this crystal by the second crystal. A pulse whose height corresponds to about 88 keV radiation can be obtained in the second crystal if the secondary γ-ray is absorbed in the second crystal by the Compton effect. The experimental results were corrected for the existence of true coincidences

arising from coincidences of the Compton pulses belonging to the 1182 keV and the 1282 keV radiations in the full peak of the 882 keV γ-rays with the 88 keV γ-rays. By an analysis of the 88 keV γ-rays coincidence spectrum it was found that the number of the Compton coincidences belonging to the 1182 keV radiation was 18 % and the number of those belonging to the 1282 keV radiation was 9 % of the total number of coincidences which entered the channel chosen at 882 keV, when the angle between the detectors was 180°. In order to correct properly for other angles it was necessary to use the correlation functions obtained in the two previous sections. The correlation function obtained after all the corrections was

$$P(\theta) = A[1-(0.03\pm0.01)P_2(\cos\theta)+(0.140\pm0.015)P_4(\cos\theta)]. \quad (5)$$

2.8. ANGULAR CORRELATION OF THE 1082 keV–200 keV CASCADE

Because of the relatively small intensity of the 1082 keV radiation a strong source was used and the resolving time of the fast coincidence circuit was reduced to 2.5×10^{-8} sec. An absorber of 7 mm lead was placed between the source and the scintillator which detected the 1082 keV radiation and a 10 mm lead absorber for only scattered radiation was suitably placed between the detectors to avoid the production of false coincidence pulses. The measurements showed that the correlation is isotropic to within 2 %.

2.9. ANGULAR CORRELATIONS FOR A VISCOUS LIQUID SOURCE

All the angular correlation measurements which were described were carried out with a source in the form of a dilute aqueous solution of $Tb_2(SO_4)_3$. The angular correlations of cascades whose intermediate state is the 88 keV level were also measured for a liquid source, of viscosity equal to 2 poise, which was obtained by mixing the aqueous solution of $Tb_2(SO_4)_3$ with glycerine. The correlation functions obtained in this case were identical with those obtained for the pure aqueous solution.

3. The Decay-Scheme of Tb^{160} and Spin Assignments for the Excited Levels of Tb^{160}

3.1. THE DECAY SCHEME OF Tb^{160}

A decay scheme consistent with all the experimental results is given in fig. 4. There is a full agreement between all the works published hitherto concerning the existence and the place of the 88 keV, 288 keV, 970 keV and 1270 keV in the decay scheme levels. The existence of the 1370 keV level is proved in the present work in a convincing manner from the coincidence spectra which shows the existence of the 1282 keV–88 keV and the 1082 keV–200 keV cascades. An analysis of the β-spectrum obtained by Keshishian and coworkers [2]) also shows that the existence of the 1370 keV

level is very probable. The existence of the 762 keV—200 keV, 200 keV—962 keV and the 220 keV—762 keV cascades strongly support the assumption of the existence of a 1050 keV level. In the work of Bertolini and coworkers [3]), the existence of a level with energy near 1050 keV was also suggested.

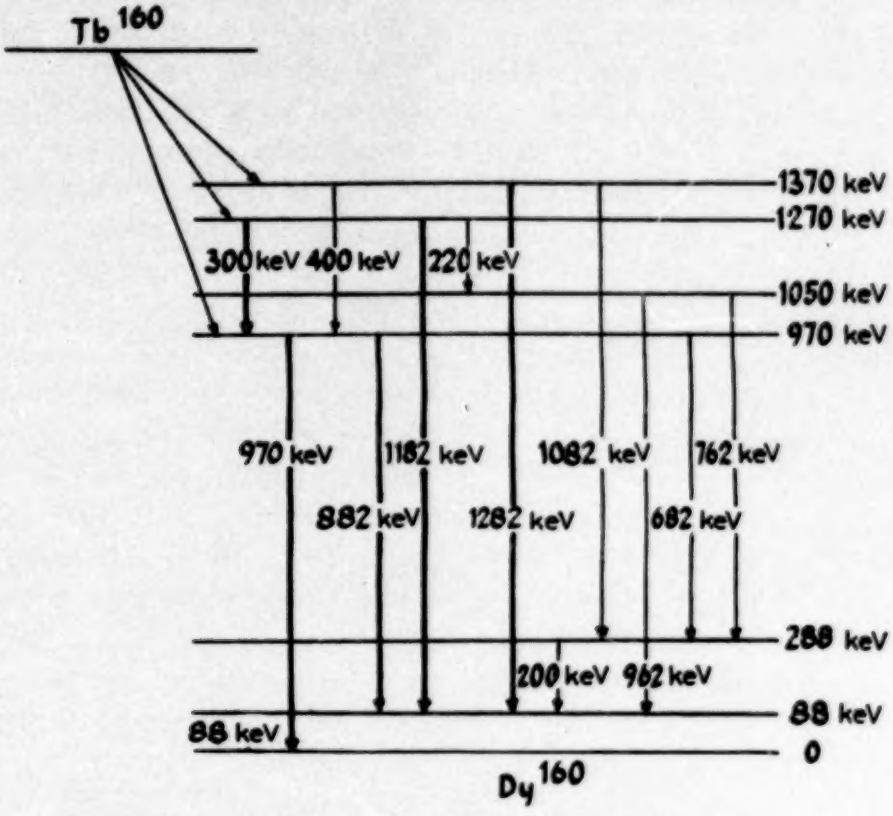

Fig. 4. Decay scheme of Tb^{160}.

3.2. THE SPINS OF THE EXCITED LEVELS OF Dy^{160}

The experimental spin and parity of the first excited state of even nuclei in the region of the rare earths is always 2+ and it is to be assumed that in our case too, the spin and parity of the 88 keV level is 2+. This assignment is supported by the values of the conversion coefficients of the 88 keV line ($K/L = 0.9 \pm 0.3$, $\alpha_K \approx 4$) [1]).

The ratio between the energies of the two first excited levels of Dy^{160} is exactly equal to the theoretical ratio between the energies of the two first rotational levels of an even nucleus. It can, therefore, be concluded that the spin and parity of the 288 keV level are 4+. This assumption is in agreement with the experimental internal conversion coefficients. ($\alpha_K = 0.18$, $K/L \approx 3$) [1, 5]) which fit an E2 transition. The fact that there is no transition from the 288 keV level to the ground level is also consistent with the assignment of spin 4 for this level.

The positive sign obtained experimentally for the coefficient of $P_4(\cos\theta)$ in the angular correlation function of the 882 keV—88 keV cascade, fits the theoretical functions if and only if the spin of the 970 keV level is 2. This value for the spin is also in agreement with the fact that there are transitions from the 970 keV level to the first three levels of Dy^{160} whose spins are 0, 2 and 4. The experimental internal conversion coefficients of the 970 keV radiation ($\alpha_K = 2.5\times10^{-3}$, K/L $\approx$ 5) [1, 5] fit an E2 transition and support the assignment of spin 2 for the 970 keV level.

The magnitude of the coefficient of $P_4(\cos\theta)$ in the experimental angular correlation function of the 1182 keV—88 keV cascade is consistent with the theoretical coefficients if and only if the spin of the 1270 keV level is 2. The experimental internal conversion coefficients of the 300 keV radiation ($\alpha_K = 0.013$, K/L $\approx$ 4) [5] are consistent with the theoretical values for an E1 transition and are in agreement with the assignment of spin 2 for the 1270 keV level. This assignment does not agree with the suggestions of Bertolini [4] and coworkers which was based on a measurement of the angular correlation of a mixture of 2 cascades. The experimental results of Bertolini and coworkers were correct but the interpretation of the results is ambiguous. The coefficients obtained by them are in full agreement with the assignment of spin 2 for the 1270 keV level. The existence of transitions from the 1370 keV level to the 288 keV and 88 keV levels whose spins are 4 and 2 respectively proves that the spin of this level is 2, 3 or 4. The value 4 must be rejected because of the value obtained for the coefficient of $P_4(\cos\theta)$ in the correlation function of the 1082 keV—200 keV cascade. As explained later the experimental correlation functions can be fitted to the theoretical ones only if a spin 3 is assigned for this level.

Conclusions concerning the character of the 1050 keV level cannot be drawn from the measurements of the present work. The character of this level will be discussed in the last section of the present work.

4. Analysis of the Results of Angular Correlation Measurements and Multipolarity Assignments for the Radiations

4.1. THE 300 keV—970 keV CASCADE

The high energies of the transitions from the 970 keV level together with their E2 character lead to the conclusion that the lifetime of this level is short (about 10^{-12} sec) and that, therefore, the angular correlations of cascades whose intermediate state in this level are not perturbed by extra-nuclear fields. The experimental correlation function obtained for the 300 keV—970 keV cascade is consistent with the theoretical function for a cascade of the 2(1,2)2(2)0 type if $\delta^2 < 0.001$ where δ^2 is the ratio between the quadrupole transition probability to the dipole transition probability

in the first component of the cascade. The conclusion is that for the 300 keV transition, the quadrupole transition probability is less than 1/1000 of the dipole transition.

The experimental value of the K-conversion coefficient of the 970 keV radiation is about 3×10^{-3} [1, 3, 5]. This value is consistent with the theoretical value for an E2 transition but is about 4 times smaller than the theoretical value for a M2 transition. Hence, the spin and parity of the 970 keV level are 2+ and the 970 keV transition is of the E2 type.

The experimental value of the K-conversion coefficient of the 300 keV radiation ($\alpha_K = 0.013$) fits the theoretical value for an E1 transition but is less than a third of the theoretical value for a M1 transition. The conclusion is, therefore, that the spin and parity of the 1270 keV level is 2− and that the 300 keV transition is predominantly of the E1 type.

4.2. THE 300 keV−882 keV CASCADE

From the previous discussions it follows that this cascade is of the 2(1)2(1,2)2 type. The theoretical angular correlation function for such a cascade is

$$P(\theta) = A\left[1+\frac{0.175+0.51\delta-0.053\delta^2}{1+\delta^2}P_2(\cos\theta)\right], \qquad (6)$$

where δ^2 denotes the E2/M1 ratio in the second component of the cascade. The experimental correlation function obtained for the 300 keV−882 keV cascade fits the theoretical function if $\delta > 60$ or if $\delta = -0.44\pm0.02$. According to the second possibility $\delta^2 = 0.19\pm0.02$ and the dipole transition is about 5 times stronger than the quadrupole transition. This possibility is rejected because of the following reasons: It is impossible to find agreement between the experimental and theoretical values for the coefficient of $P_4(\cos\theta)$ in the correlation function of the 882 keV−88 keV cascade if $\delta^2 = 0.19$ in the first component of this cascade. The experimental value obtained for the K-conversion coefficient of the 882 keV radiation ($\alpha_K \approx 2\times10^{-3}$) [1, 2, 3, 5] is in fair agreement with the theoretical value if E2 multipolarity is assigned to the 882 keV radiation but is rather different from the value expected for a M1 transition. We are, therefore, left with the first possibility that $\delta > 60$ or that $\delta^2 > 3600$. This means that for the 882 keV radiation the quadrupole transition probability is much larger than the dipole transition probability, although $\Delta I = 0$.

4.3. THE 882 keV−88 keV CASCADE

From the previous discussions it follows that this cascade is of the 2(1,2)2(2)0 type and that $\delta > 60$ in the first component of the cascade. The theoretical angular correlation function for such a cascade is

$$P(\theta) = A[1-(0.070\pm0.006)P_2(\cos\theta)+0.33P_4(\cos\theta)]. \qquad (7)$$

A comparison between this function and the experimental function (5) shows that the coefficients of the correlation function are strongly attenuated. The values of the attenuation factors are

$$G_2 = 0.40 \pm 0.15, \qquad G_4 = 0.42 \pm 0.04. \tag{8}$$

As the angular correlation is in this case, insensitive to the viscosity of the liquid source, it seems unlikely that the attenuations are due to quadrupole interactions. On the other hand the magnetic moment of the ion of Dy is very large (10 μ_B [8])) and it is possible that the attenuation is caused by the magnetic hyperfine interaction. This possibility is discussed further in an article in preparation dealing with some problems of attenuations of angular correlations in rare earth nuclei [10]).

4.4. THE 1182 keV–88 keV CASCADE

The previous discussions show that this cascade is of the 2(1,2)2(2)0 type. The angular correlation function for the 1182 keV–88 keV cascade, when the nuclei are free of perturbations as calculated from formulae (4) and (8) is

$$P(\theta) = A[1 + (0.20 \pm 0.10) P_2(\cos\theta) \pm (0.17 \pm 0.04) P_4(\cos\theta)]. \tag{9}$$

The experimental function agrees with the theoretical one, if $\delta = 1.5 \pm 0.5$. The conclusion is that for the 1182 keV transition the mixing ratio M2/E1 is equal to 2.2 ± 1.5.

4.5. THE 1282 keV–88 keV CASCADE

The angular correlation function for the 1282 keV–88 keV cascade, when the nuclei are free from perturbations, as calculated from formulae (3) and (8) is

$$P(\theta) = A[1 + (0.29 \pm 0.10) P_2(\cos\theta) + (0.00 \pm 0.25) P_4(\cos\theta)]. \tag{10}$$

As mentioned in section 3.2 the possible spin values for the 1370 keV level are 3 and 4. The experimental function (10) cannot be reconciled with the theoretical function for a cascade of 4(2)2(2)0 type. The conclusion is that the spin of the 1370 keV level is 3. The theoretical function for the angular correlation of a 3(1,2)2(2)0 type is

$$P(\theta) = A\left[1 + \frac{-0.07 - 0.78\,\delta - 0.20\,\delta^2}{1+\delta^2} P_2(\cos\theta) - \frac{0.08\,\delta^2}{1+\delta^2} P_4(\cos\theta)\right].$$

An agreement between the theoretical and experimental function is obtained if $\delta = -0.8 \pm 0.2$. This means, that for the 1282 keV radiation the probability of the quadrupole transition is about half of the dipole transition probability. There are no sufficient experimental data to determine the parity of the 1370 keV level. The experimental value of the K-conversion coefficient of the 1282 keV radiation [5]) seems to be in a better agreement with the theoretical value for a transition which is mainly of the E1 type

than with the theoretical value for a transition which is mainly of the M1 type, but from this, one cannot draw a decisive conclusion concerning the parity of the 1370 keV level.

4.6. THE 1082–200 keV CASCADE

The previous discussions show that the 1082 keV–200 keV cascade is of the 3(1,2)2(2)0 type. The theoretical angular correlation function for such a cascade is

$$P(\theta) = A\left[1 + \frac{-0.14 + 0.84\,\delta + 0.02\,\delta^2}{1+\delta^2} P_2(\cos\theta) - \frac{0.18\,\delta^2}{1+\delta^2} P_4(\cos\theta)\right], \quad (11)$$

where δ^2 denotes the ratio between the quadrupole transition probability to the dipole transition probability in the first component of the cascade. The results of the measurements of the angular correlation of this cascade show that it is isotropic to within 2 %. Function (12) corresponds to an isotropic correlation if $\delta \approx 1/7$ or $\delta^2 \approx 1/50$. The conclusion is, therefore, that for the 1082 keV transition the dipole transition probability is about 50 times larger than the quadrupole transition probability.

5. Conclusions

The properties of the energy levels of Dy^{160}, Gd^{154} and Sm^{152} [7]) are very similar and the spectra of gamma rays obtained by transitions between these levels have almost the same shapes. It seems that this similarity originates from the fact that many of the excited levels of these nuclei are of the collective type.

It is very reasonable to interpret the 88 keV and 288 keV levels of Dy^{160} as rotational levels. The following properties of the 970 keV level support the suggestion to interpret it as a collective vibrational level with $I = 2$ and $K = 2$ [9]). (K is the quantum number which represents the projection of the total angular momentum on the axis of symmetry of the nucleus.) The spin and parity of this level is 2+, its excitation energy is about 1 MeV, the gamma transition from this level to the 88 keV level is of the E2 type although $\Delta I = 0$ and the branching ratios of the γ-transitions from this level are in agreement with the theoretical ratios if it is assumed that $K = 2$ for this level. These are the properties predicted by the unified model for gamma vibrational levels [9]). The inexistence of a M1 transition between the 970 keV and 88 keV levels is explained by the K-forbiddeness of such a transition. The theoretical branching ratios according to the unified model for the transitions from the 970 keV level to the ground level, the 88 keV level and the 288 keV level, assuming that $I = 2$ and $K = 2$ for the 970 keV level, are

$$I_{970\text{ keV}} : I_{882\text{ keV}} : I_{682\text{ keV}} = 110 : 100 : 1; \quad (12)$$

the experimentally obtained values are

$$I_{970\ \mathrm{keV}} : I_{882\ \mathrm{keV}} : I_{682\ \mathrm{keV}} = 90 : 100 : 2. \qquad (13)$$

Taking into account, the errors possible in the experimental values, the agreement is good.

The experimental data are not sufficient for a certain assignment of the spin and parity of the 1050 keV level. But the following facts suggest that this level is a collective vibrational level with $I = 3$ and $K = 2$:

1) The energy separation between this level and the 970 keV is almost equal to the energy separation between the rotational level of 88 keV and the ground level.

2) This level decays by transitions to levels whose spins are 2 and 4.

3) The experimental value of the K-conversion coefficient of the 220 keV level [5]) is consistent with the theoretical value for a transition which is mainly of the E1 type. This leads to the suggestion to assign spin and parity 3+ to the 1050 keV level.

4) In Sm^{152} and Gd^{154} there is a level whose place in the decay-scheme corresponds to the place of the 1050 keV level in the decay scheme of Tb^{160}. It was proved that for these levels in Gd^{154} and in Sm^{152} $I = 3$ and $K = 2$ and one may guess that the 1050 keV level of Dy^{160} has similar properties.

The proposed scheme for the spins, parities and K-values of the states obtained in the decay of Tb^{160} and the proposed multipolarity assignments for the radiations emitted are given in fig. 5.

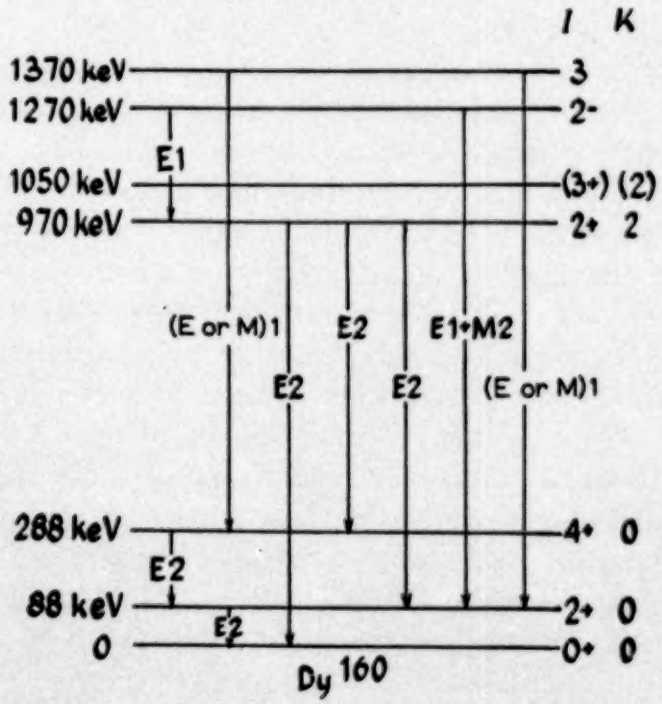

Fig. 5. Spin, parity and multipolarity assignments in Tb^{160}.

The author would like to thank Prof. S. G. Cohen for his continued interest and guidance.

Note added in proof: A recent investigation of the disintegration scheme of Dy^{160} by Nathan[11]) has come to our attention, in which the properties of the levels and the multipolarity assignments were fixed largely by measurement of internal conversion coefficients and ratios. The general conclusions are essentially identical with those obtained in the present work.

References

1) S. B. Burson, W. C. Jordan and L. M. LeBlanc, Phys. Rev. **94** (1954) 103
2) V. Keshishian, H. W. Kruse, R. J. Klotz and C. M. Fowler, Phys. Rev. **96** (1954) 1050
3) G. Bertolini, M. Bettoni and E. Lazzarini, Nuovo Cimento **3** (1956) 754
4) G. Bertolini, M. Bettoni and E. Lazzarini, Nuovo Cimento **3** (1956) 1162
5) M. A. Clark and J. W. Knowels, Bull of Am. Phys. Soc. (April 1951)
6) S. Ofer, Nuclear Physics **3** (1957) 479
7) S. Ofer, Nuclear Physics **4** (1957) 477
8) Van Vleck, Electric and Magnetic Susceptibility (Oxford, 1932)
9) K. Alder, A. Bohr, T. Huus, B. Mottelson and A. Winther, Revs. Mod. Phys. **28** (1956) 432
10) S. Ofer and S. G. Cohen (in preparation); short report in Proc. of the Conference on Nuclear Structure at Rehovoth (North Holland Publishing Co., in press)
11) O. Nathan, Nuclear Physics **4** (1957) 125

Nuclear Physics **5** (1958) 346—350; © *North-Holland Publishing Co., Amsterdam*
Not to be reproduced by photoprint or microfilm without written permission from the publisher

(n, α) AND (n, p) REACTIONS IN FLUORINE

E. KONDAIAH, K. V. K. IYENGAR and C. BADRINATHAN
Tata Institute of Fundamental Research, Apollo Pier Road, Bombay

Received 2 September 1957

Abstract: The ratio of the (n, α) to (n, p) cross-section in F^{19} has been experimentally measured for 14.5 MeV neutrons as 1.2; this ratio has been calculated, on the basis of compound nucleus formation, to be 3.5. Comparing the calculated value with the experimentally observed value, it has been concluded that either the continuum assumption is not valid in this particular case or direct interactions are playing significant part specially in the (n, p) reaction.

1. Experimental Determination

The cascade accelerator of this Institute has been used as a neutron source; 14.5 MeV neutrons were produced by T(d, n)He^4 reaction. At this neutron energy both F^{19}(n, α)N^{16} (7.5 sec half-life) as well as F^{19}(n, p)O^{19} (29.5 sec half-life) reactions occur. Thus, by comparing the saturation activities induced in F^{19} by 14.5 MeV neutrons, one can obtain the ratio of the (n, α) to (n, p) reaction cross-sections. A CaF_2 crystal (1″ diameter, 1″ long) has been used both as the target as well as the detector. The CaF_2 crystal was optically mounted on a photomultiplier window using silicone fluid. The whole assembly was covered by a cadmium sheet to avoid thermal neutrons. The pulses from the photo-multiplier were taken through a cathode follower, a linear amplifier and a discriminator to an integrator. The integrator [1]) is essentially a univibrator which takes the output pulse of the discriminator and impresses a square wave of definite width and height across a condenser and resistor in parallel. The current flowing through this resistance was recorded on an Esterline Angus pen recorder milliammeter. The deflection of the pen recorder stylus is proportional to the current flowing in the integrator circuit, which is proportional to the number of pulses at the output of the univibrator, which in its turn is proportional to the number of disintegrations occurring at any time. The current reading as recorded by the pen recorder at any instant after stopping the irradiation is thus proportional to the number of disintegrations occurring at that instant. Hence, the current decay as recorded by the pen recorder is a true representation of the composite decay curve of the induced activities.

CaF_2 was irradiated for 5 minutes and the pen recorder was started exactly 10 seconds after stopping the irradiation. Under these experimental

conditions, apart from N^{16} and O^{19} activities, only $Si^{28}(n, p)Al^{28}$ (2.5 min half-life) activity is of importance. After taking into account this long period activity, the ratio of N^{16} to O^{19} activities at the time of stopping irradiation was obtained from an analysis of the observed decay curve. The ratio of N^{16} to O^{19} formations thus observed is 1.2 ± 0.4.

2. Calculation using Compound Nucleus Theory

According to Bohr's theory of compound nucleus formation [2]), the reaction cross-section $\sigma(a, b)$ for any reaction

$$X + a \rightarrow C \rightarrow Y + b,$$

where X and Y are target and final nuclei, a and b are incident and emitted particles, is given by

$$\sigma(a, b) = \sigma_c(a) \cdot [F_b / \sum_c F_c]$$

where the F's refer to the branching probabilities in the decay of the compound nucleus.

Thus, for this particular case,

$$\sigma(n, \alpha)/\sigma(n, p) = F_\alpha / F_p = \frac{\sum_\alpha k_\alpha^2 \cdot \sigma_c(\alpha)}{\sum_p k_p^2 \cdot \sigma_c(p)} \qquad (1)$$

where the k's are the channel wave numbers, the σ_c denote the capture cross-sections, α and p refer to the different channel energies that will arise from (n, α) and (n, p) reactions respectively (in effect they refer to α groups or proton groups leading to different excited states of the residual nuclei N^{16} or O^{19} respectively).

If we examine the level schemes [3]) of N^{16} and O^{19}, we see that there exist only a few excited levels and they are close to the ground levels of these nuclei. Thus, we may assume that all the transitions in these two reactions go to the ground level of the concerned residual nucleus only; the channel energies will not be much different even if some of them go to the nearby excited states. Unless an alpha or proton group of substantial intensity going to an excited state far removed from the ground level is found to exist, we can drop off the summation signs in eq. (1)†.

According to the nuclear reaction theory given by Blatt and Weisskopf [1]), the cross-sections for compound nucleus formation σ_c are given by

† It may be argued that N^{16} being an odd nucleus, it should have higher level density than O^{19} and that, therefore, the number of channels open for decay of the compound nucleus by emitting alphas is larger than by emitting protons. This statistical factor, which may be of the order of 2, would make the calculation values given in table 2 much larger still than the experimental ones.

$$\sigma_c(\alpha) = \pi\lambda_\alpha^2 \sum_{l=0}^{\infty} [(2l+1)T_l]_\alpha,$$

$$\sigma_c(\mathrm{p}) = \pi\lambda_\mathrm{p}^2 \sum_{l=0}^{\infty} [(2l+1)T_l]_\mathrm{p}$$

where l denotes the angular momentum of the emitted particle and the T's are the transmission coefficients. Therefore,

$$\frac{\sigma(\mathrm{n},\ \alpha)}{\sigma(\mathrm{n},\ \mathrm{p})} = \frac{\sum_{l=0}^{\infty} [(2l+1)T_l]_\alpha}{\sum_{l=0}^{\infty} [(2l+1)T_l]_\mathrm{p}}. \tag{2}$$

We have calculated the transmission coefficients for alphas and protons corresponding to incident neutron energies of 8 MeV and 14.5 MeV; the expression for T_l is based on the continuum theory of nuclear reactions; the Coulomb wave functions were calculated using published tables and graphs [4, 5, 6]). In evaluating these, we have taken the channel radius R as

$$R = 1.2\times 10^{-13}\ \mathrm{cm}\times A^{1/3} + r' \tag{3}$$

where $r' = 1.2\times 10^{-13}$ cm for alpha particles and zero for protons.

TABLE 1

Reaction	E_n	$\nu^2 = (K/k)^2$	$\varrho = kR$	$\frac{E}{B}$	l	T_l
(n, p)	8 MeV	$(2.6667)^2 = 7.1113$	1.3179	0.88	0	0.566
					1	0.205
						0.057
(n, α)	8 MeV	$(1.4394)^2 = 2.0719$	4.3052	1.03	0	0.815
					1	0.766
					2	0.644
					3	0.375
					4	0.144
					5	0.015†
(n, p)	14.5 MeV	$(1.8036)^2 = 3.2530$	2.1706	2.38	0	0.861
					1	0.772
					2	0.497
					3	0.120
(n, α)	14.5 MeV	$(1.2373)^2 = 1.5309$	6.1176	2.01	0	0.899
					1	0.875
					2	0.814
					3	0.696
					4	0.536
					5	0.4†
					6	0.1†

E_n = incident neutron energy; $K^2 = K_0^2 + k^2$ where $K_0 = 10^{13}$ cm^{-1} and k is the channel wave number; R is the channel radius; E = energy of the emitted particle; B = barrier energy for the emitted particle.

† These values are estimated from ref. [6]) where R is taken as $1.5\times A^{1/3}\times 10^{-13}$ cm instead of eq. (3).

The results are given in table 1. Using the T_l values shown in table 1 and applying equation (2), the ratios of the (n, α) to (n, p) cross-sections have been calculated. These calculated values together with the experimentally observed values are given in table 2 for comparison.

TABLE 2

E_n	$\frac{\sigma(n,\alpha)}{\sigma(n,p)}$ Calculated	$\frac{\sigma(n,\alpha)}{\sigma(n,p)}$ Expt.	Reference for the experiment
8 MeV	7.1	3.2	Marion and Brugger, Phys. Rev. **100** (1955) 69
14.5 MeV	3.5	1.2 ± 0.4	Present experiment

3. Discussion

The calculated values in table 2 are derived on the continuum theory assumption; this assumption is involved in the expression for T_l. For the neutron energies considered here, the compound nucleus, F^{20}, is in an excited state of the order of 14 to 21 MeV and no resonances are reported above $E_n = 6$ MeV.

The (n, α) threshold (1.5 MeV) is lower than the (n, p) threshold (4 MeV). As such, the alpha particle has higher energy than the proton. Therefore, it is expected that the alpha particle has a greater chance of penetration through the potential barrier than the proton and as a result the (n, α) to (n, p) cross-section can be quite large below $E_n = 8$ MeV. But for $E_n = 14.5$ MeV, the ratio of the energy of the emitted particle to the corresponding barrier energy given in column 5 of table 1 is $\gtrsim 2$ for both reactions.

The experimental ratio of the cross-sections is 1.2 at $E_n = 14.5$ MeV whereas the calculated value is larger by a factor of at least 3. It is unlikely that the discrepancy between the calculated and observed values could be due to a failure of the continuum theory assumption. If we assume that the continuum assumption is valid, we should invoke "direct interactions" to explain the discrepancy. As F^{19} has a single proton in excess of the closed shell at the proton number 8, it is quite plausible that direct interactions contribute significantly to (n, p) cross-section whereas for the (n, α) cross-section, direct interactions may not be of so much significance. If this is true, we can write

$$\sigma_{\text{obs.}}(n, \alpha) = \sigma_{\text{c. n.}}(n, \alpha)$$

$$\sigma_{\text{obs.}}(n, p) = \sigma_{\text{c. n.}}(n, p) + \sigma_{\text{d. i.}}(n, p)$$

where obs. = observed; c.n. = compound nucleus; d.i. = direct interactions. Thus, we find that the direct interaction contribution to the (n, p)

cross-section at $E_n = 14.5$ MeV in this particular reaction should be twice as important as compound nucleus formation. This may be taken as a lower limit, as the calculated ratio of cross-sections may be larger than 3.5, when the appropriate factor for the difference in level densities of N^{16} and O^{19} is taken into account.

We wish to thank Dr. R. Ramanna for having taken interest in this work.

References

1) R. N. Thorn and R. W. Warick, Rev. Sci. Inst. **24** (1953) 391
2) J. M. Blatt and V. F. Weisskopf, Theoretical Nuclear Physics (John Wiley and Sons, New York)
3) F. Ajzenberg and T. Lauritsen, Revs. Mod. Phys. **27** (1955) 77
4) I. Bloch *et al.*, Revs. Mod. Phys. **23** (1951) 147
5) W. T. Sharp *et al.*, A.E.C.L. No. 268 (1955)
6) H. Feshbach *et al.*, NYO–3077 (1953)

Nuclear Physics **5** (1958) 351—357; © *North-Holland Publishing Co., Amsterdam*
Not to be reproduced by photoprint or microfilm without written permission from the publisher

SCATTERING OF FAST NEUTRONS BY NEON-22

C. P. SIKKEMA, P. J. PASMA and H. H. VAN BARNEVELD
Natuurkundig Laboratorium der Rijks Universiteit, Groningen

Received 10 September

Abstract: The scattering of monoenergetic neutrons by ^{22}Ne has been studied in the neutron energy range 1.9 to 3.5 MeV, following a similar experiment carried out recently with natural neon (ref. [1])). The total cross section of ^{22}Ne shows 10 resonance maxima in this region, viz. at neutron energies of 2.01, 2.14, 2.19, 2.32, 2.53, 2.72, 2.87, 3.10, 3.20 and 3.43 MeV. Determination of resonance parameters with the help of energy distributions of recoil nuclei appeared to be difficult in most cases. The peak at 2.32 MeV is most probably due to a superposition of a $P_{3/2}$ and a $D_{3/2}$ resonance.

1. Introduction

Fast neutron scattering experiments with ^{22}Ne may provide information about levels in the ^{23}Ne compound nucleus having an excitation energy of more than 5.189 MeV, which is the neutron binding energy in ^{23}Ne [2]). No such experiments have been reported up to the present time. The neutron source used in our experiments is the D+D reaction, the neutron energy being variable between 1.9 and 3.5 MeV. Apart from elastic scattering, inelastic scattering may be expected throughout this region, leading to the first excited state of the ^{22}Ne nucleus at 1.275 MeV. Reactions, such as (nα) or (np), however, are energetically impossible. The measurements to be described include determination of the total cross section and differential elastic scattering cross sections for scattering angles larger than about 120°.

2. Experimental Method

For a description of the method of measurement we may refer to a previous paper dealing with a similar experiment carried out with natural neon [1]). In this case the multiple-wire proportional counter used for the measurement of neon recoils had a total volume of 1.25 l. The sensitive part had a diameter of 4.8 cm and a length of 12 cm. The counter was filled with 45.5 cm of neon, containing 98.1 % of ^{22}Ne, the residual part being mainly ^{20}Ne. For the stabilization of the discharge 2.1 cm of CO_2 had been added. With a wire diameter of 0.15 mm the operating voltage was 1125 volts. The neon had been enriched with ^{22}Ne by the method of thermal diffusion in the Laboratory for Mass Spectrography at Amsterdam, under the direction of Prof. J. Kistemaker.

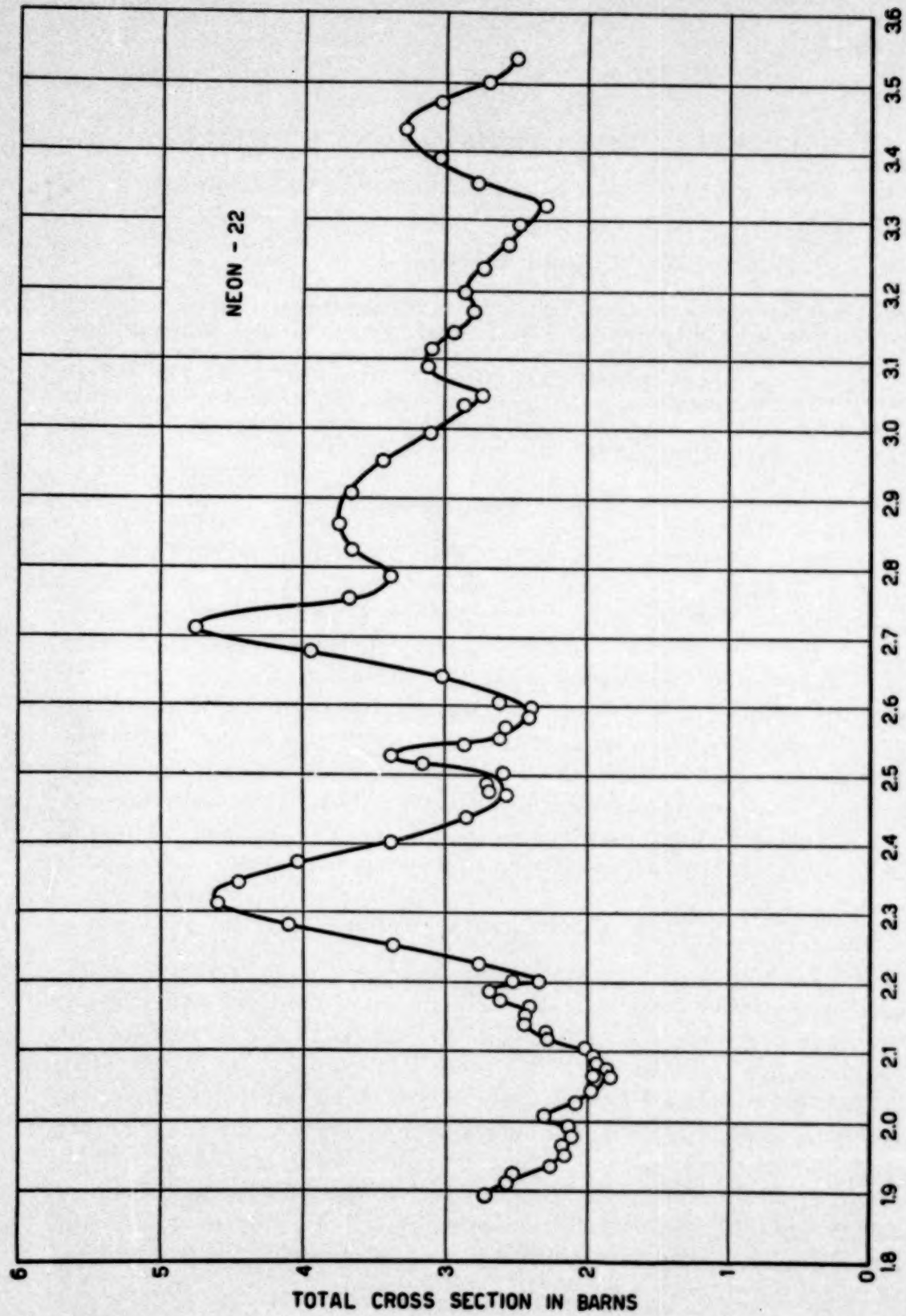

Fig. 1. Total cross section of ^{22}Ne as a function of neutron energy.

3. Results

Fig. 1 shows the total cross section of ^{22}Ne measured by integral counting of recoil pulses from the proportional counter. Corrections have been applied for the contributions of the CO_2 and the small amount of ^{20}Ne, the total cross sections of which were taken from [3]) and [1]) respectively. 10 Resonance maxima appear in σ_T, at neutron energies listed in table 1. The neutron

TABLE 1

Resonances in the scattering of neutrons by ^{22}Ne

Neutron energy (MeV)	Excitation energy of ^{23}Ne (MeV)	Assignment of levels	Width (keV)
2.01	7.11		< 20
2.14	7.24		
2.19	7.28		
2.32	7.41	$3/2^-$	160
		$3/2^+$	160
2.53	7.61		≦ 30
2.72	7.79		90
2.87	7.94		
3.10	8.16		
3.20	8.25		
3.43	8.47		

energy spread may be estimated to about 25 keV below 2.6 MeV and about 50 keV above this energy. The possible error in σ_T may be about 15 %, without taking into account the influence of the finite energy spread of the neutrons on the cross sections measured in the neighbourhood of sharp peaks. If such peaks have a natural width smaller than this energy spread, the error may be considerably larger.

Fig. 2 gives the results of some of the pulse size distribution measurements. The curves are plotted in the well-known way, representing the differential elastic scattering cross section as a function of the cosine of the scattering angle in the centre-of-mass system. In most cases, however, the observed distributions are superpositions of two pulse spectra, due to recoils of elastically and inelastically scattered neutrons respectively. The above representation is therefore valid for the sections of the curve which are due to elastic recoils only, being those laying above the upper limit of the inelastic spectra indicated by the arrows. These parts have been indicated by full lines, the other parts are shown dotted in fig. 2, except in fig. 2B, in which case inelastic scattering will probably be of minor importance. Thus the differential elastic scattering cross section has, in general, been determined only for scattering angles of the neutrons larger than about 120°.

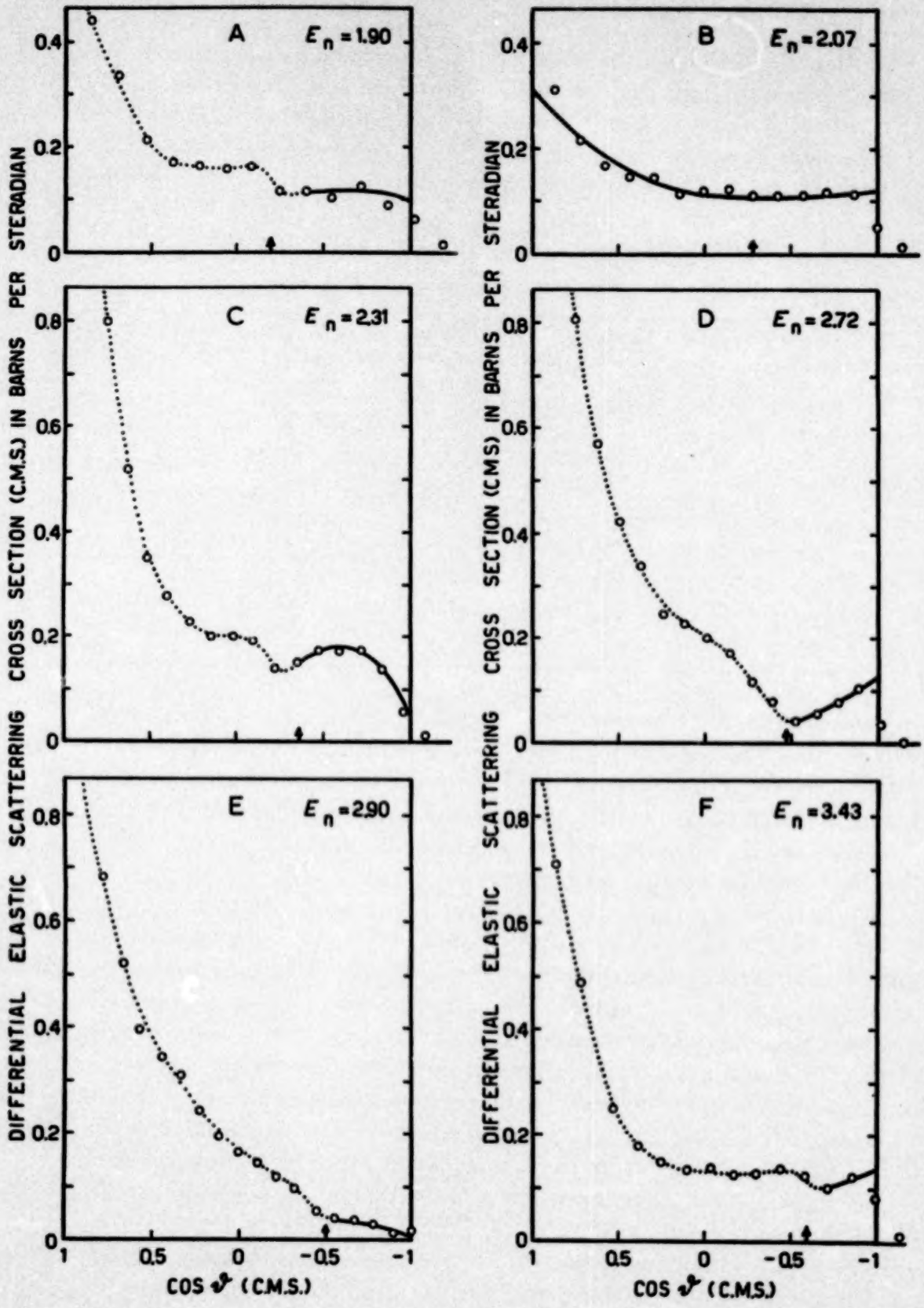

Fig. 2. Circles connected by full lines: differential elastic scattering cross section as a function of the cosine of the scattering angle, both in the centre-of-mass system, at various neutron energies (experimental). Circles connected by dotted lines: the same, increased by an unknown contribution of inelastic scattering.

4. Discussion of the Results

By an analysis of the scattering results it should be possible to determine the energies and quantum numbers of levels in the compound nucleus ^{23}Ne. There are, however, three factors in our case, which, in combination, make such an analysis very difficult. Firstly, some resonance peaks will probably not have been completely resolved due to the finite energy spread of the neutrons used (see section 3). This may apply to the peaks at 2.01, 2.14, 2.19 and probably 2.53 MeV. The second factor is the overlapping of resonances. The complexity of resonance peaks became most obvious in the analysis of the three largest ones at 2.32, 2.72 and 2.87 MeV (see below). Thirdly, the presence of inelastic scattering introduces more unknown parameters and makes energy distribution measurements of recoil nuclei less valuable for the determination of differential elastic scattering cross sections (see section 3).

The peak at 2.32 MeV can be well represented by a theoretical resonance curve of the Breit-Wigner type. One may therefore assume at first, that this resonance is single and try to fit the observed angular distribution for elastic scattering (fig. 2C) by choosing suitable parameters.

The height of a resonance peak above the background of potential scattering and neighbouring resonances is in our case (initial nucleus spin 0)

$$\sigma_r = 4\pi\lambda\!\!\!^{-2}(J+\tfrac{1}{2})\,\frac{\Gamma_{el}}{\Gamma}. \qquad (1)$$

Here $\lambda\!\!\!^{-}$ is the reduced wavelength of the neutron, divided by 2π; J the spin of the compound state, Γ_{el} the partial width for elastic scattering and Γ the total width. If we assume for the background at 2.32 MeV chiefly s-wave potential scattering with a phase shift of nearly 90°, we have $\sigma_r = 3.3$ barn. For each possible J-value, Γ_{el}/Γ can be deduced from equation (1). The angular distribution for elastic scattering can then be calculated with the Bloch formula (see for instance ref. [1])), in which the resonance part of the complex scattering amplitude has to be multiplied by Γ_{el}/Γ. In no case however, agreement was found with the measurement. Thus it had to be assumed that the resonance is complex, being a superposition of two different resonances occurring at almost the same energy. The analysis may then be carried on as follows:

The peak height in this case is given by

$$\sigma_r = 4\pi\lambda\!\!\!^{-2}\left\{(J_1+\tfrac{1}{2})\left(\frac{\Gamma_{el}}{\Gamma}\right)_1+(J_2+\tfrac{1}{2})\left(\frac{\Gamma_{el}}{\Gamma}\right)_2\right\} \qquad (2)$$

with the same notation as in eq. (1), the indices 1 and 2 referring to the two resonances. Various combinations may now be investigated. For each

set of values J_1 and J_2, there is still one parameter left free by equation (2), for instance $(\Gamma_{el}/\Gamma)_1$.

A set of curves for the differential elastic scattering cross section may now be calculated, assuming various values for this parameter. Such a set is given in fig. 3 for the combination of a $P_{3/2}$ and a $D_{3/2}$ resonance.

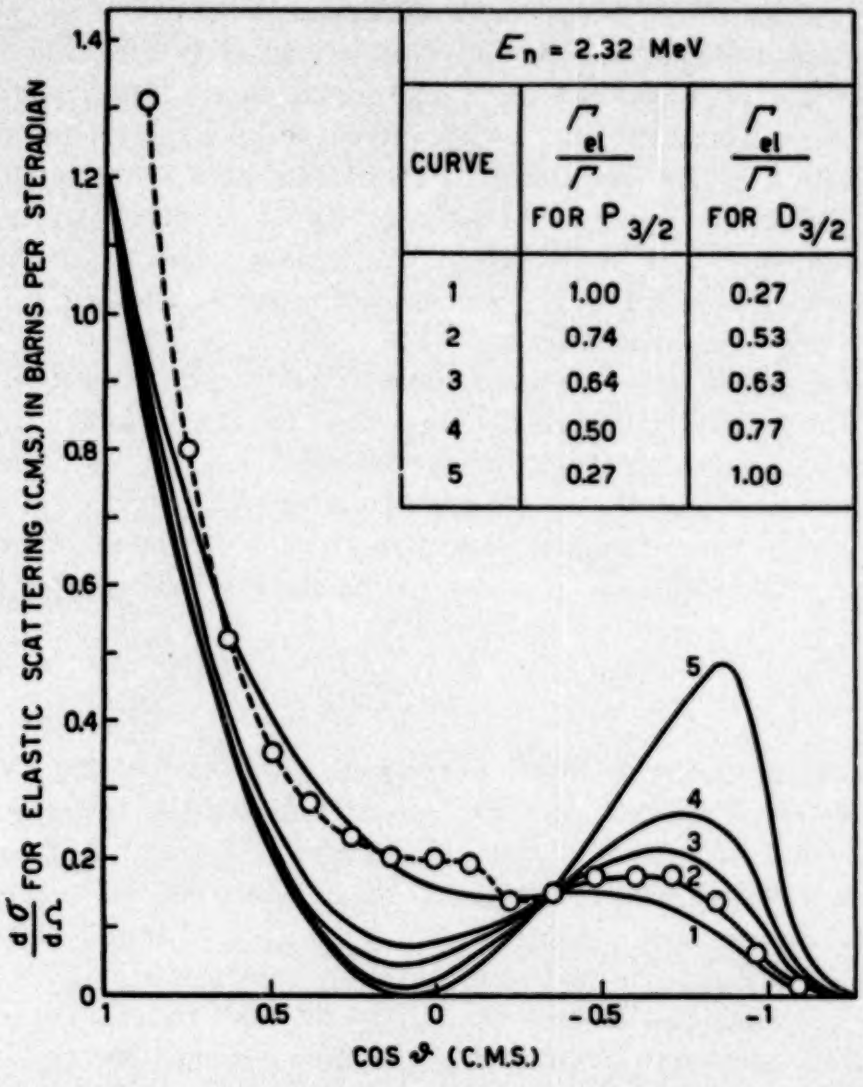

Fig. 3. Circles and dotted line: the same as fig. 2C (experimental, $E_n = 2.32$ MeV). Full lines: theoretical curves, assuming a $P_{3/2}$ and a $D_{3/2}$ resonance at this energy, for various sets of values for the parameters Γ_{el}/Γ. These curves have been corrected for the apparent recoil energy spread introduced by the counter, to fit the experimental data.

It can be seen that curve 2 fits well to the experimental points. The corresponding values for Γ_{el}/Γ are 0.74 for the $P_{3/2}$ and 0.53 for the $D_{3/2}$ resonance. In all other combinations examined (up to and including $l = 3$ and $J = 7/2$) not nearly so good a fit was obtained. The assumption of a $P_{3/2}$ and a $D_{3/2}$ resonance therefore seems to be the most probable one.

A similar analysis was tried for the resonance peaks at 2.72 and 2.87 MeV.

It appeared to be impossible to account for the observed recoil energy distributions (fig. 2D and E) assuming only two resonances in this region. A further analysis of the results at these and higher energies was not attempted due to the complexity of the phenomena.

Table 1 summarizes the information obtained in the present work. Excitation energies of the ^{23}Ne compound nucleus corresponding to peaks in the total cross section of ^{22}Ne (second column) have been calculated using a value of 5.189 MeV for the neutron binding energy in ^{23}Ne [2]).

The authors wish to thank Professor H. Brinkman, the Director of this Laboratory for his stimulating support of this work. They are also much indebted to Professor J. Kistemaker and his collaborators, especially Mr. A. Haring and Mr. F. van der Valk for preparing the ^{22}Ne and filling our counter with this gas. The work was part of the research program of the "Stichting voor Fundamenteel Onderzoek der Materie", financially supported by the Netherlands Organization for Pure Scientific Research (Z.W.O.).

References

1) C. P. Sikkema, Nuclear Physics **3** (1957) 375
2) F. Ajzenberg and T. Lauritsen, Revs. Mod. Phys. **27** (1955) 77
3) D. J. Hughes and J. A. Harvey, Neutron cross sections (Brookhaven National Laboratory, New York, 1955)

Nuclear Physics **5** (1958) 358—382; © *North-Holland Publishing Co., Amsterdam*
Not to be reproduced by photoprint or microfilm without written permission from the publisher

A CONTRIBUTION TO THE ESTABLISHMENT OF THE LEVEL SCHEME OF RADIUM C'

G. R. BISHOP

Laboratoire de Physique, Ecole Normale Supérieure, Paris

Received 7 August 1957

Abstract: The gamma-rays of radium C' and beta-rays of radium C have been studied by scintillator techniques. A decay scheme is proposed which is based on internal conversion coefficients, angular correlations between cascade gamma-rays, and transition probabilities derived from the alpha-particle fine structure. There is some evidence that collective effects occur in this nucleus.

1. Introduction

The spectrum of γ-rays emitted by excited states of Po^{214}_{84} (radium C') has been the subject of several investigations [1–9]). Of these the most precise and concordant experiments involved the measurement of the spectrum of internal conversion electrons from the active deposit of radium [1, 5]). Further precise measurements of the energy of excitation of the excited states have been obtained from the spectrum of the fine structure α-particle groups [10]). Both types of experiment indicate a complicated system of levels. Some of these levels are fed by the β-decay of Bi^{214}_{83}. Studies of the continuous β-spectrum give further indications of the positions of the levels, as well as the relative intensities in which they are populated by β-decay [7, 11]). Attempts to construct the decay scheme of Po^{214}_{84} have been based on this information and on measurements of coincidences between γ-rays.

We have used scintillation counters to study both the γ-rays and the β-rays so as to establish the decay scheme, at least for the most intense γ-ray transitions. We have estimated, relative to the ground state, the intensities of the γ-rays, and have measured the angular correlations between members of some of the cascades.

The measured relative intensities of the γ-rays are combined with measurements of the relative intensities of internal conversion electrons, so as to estimate the internal conversion coefficients of the γ-rays. In some cases this estimate allows the assignment of the multipolarity to the γ-ray transition; in combination with the angular correlation data we can then find the spin and parity of the level concerned. Another indication of the spin and parity of a level is given by the existence or non-existence of an α-

particle group of the fine structure. Since the α-particles lead to the ground state of the daughter nucleus RaD, which is assumed to be 0^+, the possible combinations of spin and parity for those levels of Po^{214}_{84} which emit α-particles are limited to $(2n)^+$ or $(2n+1)^-$.

The converse argument that levels not emitting α-particles must have the combinations $(2n)^-$ and $(2n+1)^+$ is not necessarily true, because it is conceivable that the γ-ray transition probability may be so large as to make the competing α-particle transition too feeble to be detected from the background. From the lifetime τ_α against α-decay of the ground state of Po^{214}_{84} we have estimated the lifetimes τ_α corresponding to the excited states and have then calculated τ_γ. This again is an indication of the γ-ray multipolarity but is not trustworthy. For some γ-ray cascades there are cross-over transitions to the ground state. Here again the relative intensities must be consistent with the assigned spin and parity of the level.

2. Experimental Apparatus

The spectrum of γ-rays was examined with a calibrated crystal of NaI(Tl), 8 cm in diameter and 8 cm high, coupled to a Dumont photomultiplier type 6292. This crystal was shielded on the sides with 2 cm of lead and collimating shields of lead 2 cm thickness, with central holes 4, 5 and 6 cm in diameter, could be placed in front of the crystal. Calibration of the energy scale was made with standard sources of Na^{22}, Cs^{137}, Mn^{54}, Co^{60} and RdTh. A resolution of 7.3 % was found for the 835 keV γ-ray of Mn^{54}. This crystal was calibrated in order to estimate the relative intensities of the γ-rays from the number of counts under their full energy peaks. The observed counting rate under the peak must be multiplied by the efficiency ε_p of the crystal for giving a count in the photopeak, but ε_p cannot be calculated owing to the complicated way in which multiple Compton scattering of the incident γ-ray contributes to the photopeak. However, we can calculate ε_T, the total probability that an incident γ-ray will produce a secondary electron in the crystal, from the source to crystal geometry and the absorption coefficient of NaI. Then a measurement of R, the ratio of counts under the photopeak to total counts in the whole secondary electron spectrum, leads to ε_p from the relation $\varepsilon_p = R\varepsilon_T$. Using standard sources of Na^{22}, Cs^{137}, Mn^{54}, Co^{60} and RdTh the dependence of ε_p on γ-ray energy for a given geometry was found. A log-log plot of ε_p against γ-ray energy leads to a straight line (fig. 1), so that ε_p can be found by interpolation for other γ-ray energies. The standard geometry used was with the source at 100 cm or 50 cm from the front face of the counter, and a 6 cm diameter lead collimator. As verification of the value of ε_p thus found we calibrated a source of Co^{60} (27.2 microcuries) by $\gamma-\gamma$ coincidences, and used it in the standard geometry. The

composite curve obtained due to the γ-rays of 1.17 MeV and 1.33 MeV energy, is easily decomposed by comparison with the single line at 1.28 MeV of Na^{22}. A value of the source intensity was found within 3 % of that from the coincidence calibration.

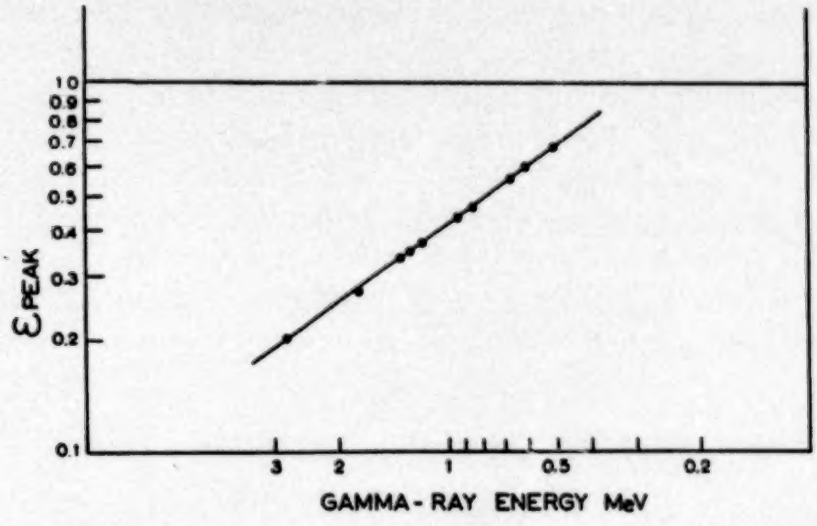

Fig. 1. The detection efficiency in the full energy peak ε_p as a function of the γ-gamma-ray energy for an 8 cm by 8 cm Harshaw NaI(Tl) crystal.

This result strengthens our confidence in the method. For the complex γ-ray spectrum of radium the decomposition of the total pulse spectrum into the contributions from the various γ-rays detected introduces further errors to the values of the relative intensities.

To establish the nature of the γ-ray-cascades occurring in the decay scheme we used a crystal NaI (Tl), 4 cm in diameter, 4 cm high, coupled to a Dumont 6292 photomultiplier, in coincidence with either the 8 cm $\times$ 8 cm crystal, or a similar 4 cm $\times$ 4 cm crystal. In each case the pulses from the photomultipliers were amplified linearly by Harwell type 1049 amplifiers, and then applied to a coincidence unit Harwell type 1036 with a minimum resolving time of 0.1 μ sec. The coincidence pulse was used to open a linear gate circuit, and the pulses thus selected were analysed with a Sunvic kicksorter (Hutchinson-Scarrot circuit). For these coincidence measurements the source strength was chosen to give 10 % of random coincidences. Selected crystals of 4 cm $\times$ 4 cm gave a resolution of 6.7 % for the 669 keV γ-ray of Cs^{137}.

For $\beta-\gamma$ coincidence measurements we used either a stilbene crystal (1.5 cm diameter and 1 cm high) for the low energy spectrum, or a plastic phosphor 5 cm diameter 4.5 cm high into which a conical hole was cut, 1 cm in depth. Collimators of plastic or aluminium were used between counter and source. The β-detectors were calibrated with the conversion

electrons of Cs^{137}, the continuous β-spectrum of P^{32}, and Compton edges of known γ-rays. For the measurements of angular correlation a fast-slow coincidence system was used of a type previously described. This consists of a fast coincidence circuit (Garwin circuit $\tau_R = 1.2\times 10^{-8}$ sec) triggered by negative pulses taken from the collectors of the photomultipliers and amplified in each channel by two Hewlett-Packard 200 Mc band-with amplifiers in cascade. Pulses proportional to the incident γ-ray energy were taken from the 7th dynodes of each photomultiplier, amplified linearly, and applied one to a gate circuit and the other to a single channel kicksorter. The out-put pulse of the kicksorter was put in coincidence (0.3 μsec) with the output pulse of the fast coincidence circuit. Thus the output pulses of the slow coincidence circuit correspond to pulses which had given a fast coincidence and also a pulse in the single channel kicksorter. They were used to open the gate circuit so that all pulses in the second counter corresponding to a selected coincident pulse in the first counter were passed for examination to the Sunvic kicksorter.

One further application of the fast-slow coincidence system was to place an upper limit to the lifetime of the excited states against γ-ray decay by measurements of $\beta-\gamma$ coincidences. A stilbene crystal was used for the β-particles in coincidence with a sodium-iodide crystal for the γ-rays. Coincident pulses in the γ-ray detector were selected with the gate circuit and the complete spectrum examined with the Sunvic kicksorter, as a function of a variable delay inserted between the two counters.

3. Results

3.1. SIMPLE γ-SPECTRA

Photopeaks were observed in the 8 cm$\times$8 cm crystal corresponding to γ-rays of energies given in table 1. To facilitate the decomposition of the pulse height spectrum into the contribution of the various γ-rays, portions of it were selected with the biased amplifier of the Sunvic kicksorter for detailed examination. Observed counting rates in each photopeak must be corrected for the contribution from the Compton spectrum of the higher energy γ-rays. This correction was estimated from the shape of the pulse height spectrum of single monocinetic γ-ray lines. Thus the region of the 609, 768 and 935 keV lines was decomposed with the aid of the 510 (Na^{22}), 669 (Cs^{137}) and 835 keV (Mn^{54}) lines; the region from 1120 to 1510 keV was similarly decomposed with the aid of the pulse height spectra given by the γ-rays of Co^{60} and Na^{22}. To control the precision of this process of decomposition the photopeaks obtained were fitted with Gaussian distributions and the moduli of these distributions compared to the square root of the γ-ray energy. It was then apparent that the peaks at 1120 and 1350

TABLE 1

The data used to construct the figures 5 and 6.

Excitation energy (keV)	α-particle intensity	γ-ray energy (keV)	Intensity ratio $I(x)/I(609)$						e_K (conversion intensity)		K/L ratio		K/L ratio (theor.)	
			K.	L.	E.A.	M.H.		B.	M.S.	E.A.	M.S.	E.A.	M1	E2
609.3	0.43	609.3	1	1	1	1	1	1	30	40	5.0	4.5		6.1
821.3	—	821.3	—	—	—	—	—	0.04	1.3	—	—	—	—	—
1281.3	0.45	1281.3	—	—	—	—	—	0.03	1.4	0.86	3.5	—	5.8	
1378.0	—	1378.0	0.10	0.15	0.10	0.32	0.22	0.14	1.3	0.90	3.25	2.25	—	4.5
		768.7	0.14	—	0.10	0.21	0.15	0.11	5.1	3.2	3.9	1.5	5.8	3.9
1415.9	22.0	—	—	—	—	—	—	—	25	25	5.1	6.7	—	—
		806.3	—	—	—	—	—	0.03	2.3	—	—	—	5.8	4.1
1544.1	—	934.8	0.12	—	0.10	0.10	0.07	0.08	4.5	5.0	3.2	1.9	5.8	4.3
1668.1	0.38	1668.1	—	—	—	—	—	0.02	0.8	0.25	—	—	—	—
1729.7	—	1729.7	—	—	—	—	—	0.04	0.9	0.7	—	—	—	—
		1120.4	0.29	0.30	0.31	0.76	0.52	0.52	12.6	13.0	4.2	6.2	5.8	—
1764.4	—	1764.4	0.36	0.30	0.39	0.61	0.42	0.40	4.6	4.2	4.2	4.4	—	—
		1155.1	—	—	—	—	—	0.06	2.6	1.0	5.2	—	5.8	—
1847.6	1.35	1847.6	0.03	0.05	—	0.06	0.04	0.04	0.6	—	—	—	—	—
		1238.3	0.11	0.07	0.10	0.27	0.19	0.15	5.0	3.6	3.3	4.2	5.8	—
2016.7	0.35	2016.7	—	—	—	—	—	0.015	0.4	0.4	—	—	—	—
		1407.4	—	—	—	—	—	0.18	1.1	—	—	—	—	—
2118.6	—	2118.6	—	—	—	—	—	0.01	0.4	0.4	—	—	—	—
		1509.3	0.08	0.09	—	0.11	0.07	0.07	1.5	—	—	—	—	—
—	1.06	—	—	—	—	—	—	—	—	—	—	—	—	—
2204.3	—	2204.3	0.11	0.12	0.11	0.19	0.13	0.12	1.1	0.95	7.8	2.4	—	—
2270.2	0.36	1661.0	—	—	—	—	—	—	0.8	0.2	—	—	—	—
2440.8	1.67	2440.8	0.06	0.06	—	0.07	0.05	0.05	—	0.2	—	—	—	—
2508.5	0.38	2508.5	—	—	—	—	—	0.005	—	0.3	—	—	—	—
2697+4 2880+10														

The intensity of α-particles in column 2 is per 10^6 α-particles from the ground state. The intensity ratios $I(x)/I(609)$ are those given by Kageyama [7]), Latyshev [8]), Ellis and Aston [1]), Mladjenovic and Hedgran [4]), and finally the present measurements. The conversion electron intensities are those of Mladjenovic and Slätis [5]) and of Ellis and Aston [1]).

keV were broader than expected for a single line of these energies. Relative intensities of the γ-rays found were then estimated from the total counting rate under the photopeaks as described above.

The spectrum was divided into three portions for this purpose, but with greater dispension (2 keV per channel), obtained by varying the con-

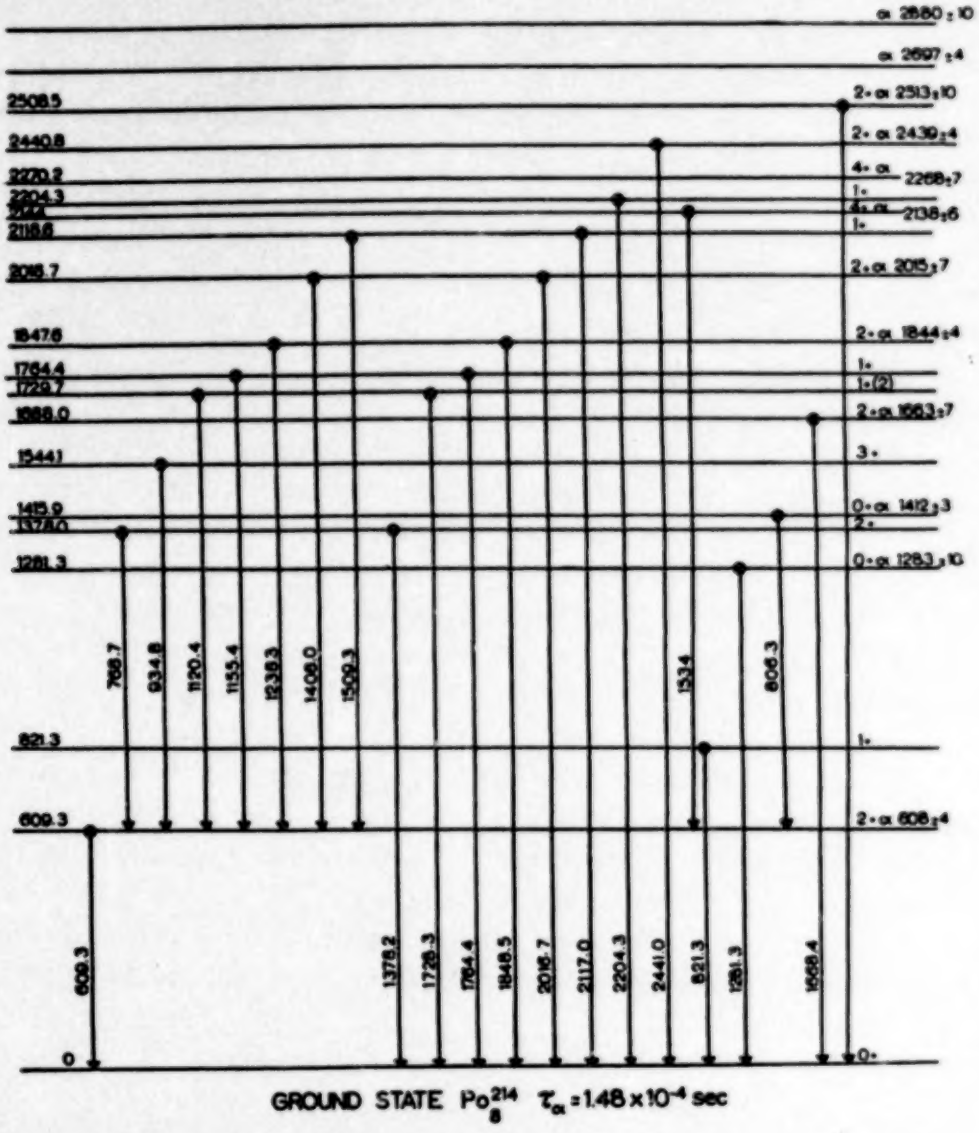

Fig. 2. The Decay Scheme of Po^{214}_{84} resulting from the present measurements. On the left are given the exact energies of the levels derived from the precise internal conversion data; on the right are the energies of the α-particle groups of the fine structure. All energies are in keV.

ditions of amplification preceding the Sunvic kicksorter, it was seen that some of the photopeaks were composite, having contributions from weaker γ-ray lines superimposed on the intense lines. It was not possible generally to separate these γ-rays so that the relative intensities are not considered

more accurate than 10 %. However, this precision is often sufficient for our purpose. The individual cases are discussed later.

For comparison with our results we give in table 1 the relative intensities found by other authors. With the results of Mladjenovic and Hedgran [4]), which have a similar precision to ours, there is definite disagreement between values at the lower and upper ends of the energy scale. This is more apparent if we add the intensities of those γ-ray lines which have been shown to give coincidences with the ground state γ-ray 609 keV. The discrepancy is removed if we adjust the M. H. results to coincide with ours for the prominent 1120 keV line as shown in the last column of table 1.

3.2. COINCIDENCE γ-RAY SPECTRA

With two NaI(Tl) crystals in coincidence cascades were found between the ground state γ-ray of 609 keV and the γ-rays of 768, 935, 1120, 1155, 1240, 1408, 1510 and 1850 keV energy, generally confirming the results of Rowlands [9]). Of the main transitions indicated in table 1, therefore, the γ-rays of 830, 1760, 2200 and 2430 keV, are not in coincidence with the first excited state of 609 keV. They are taken to be ground-state transitions. Our measurements of β-γ coincidence spectra confirm this assumption. With these results we can construct a decay scheme for Po^{214}_{84}, given in fig. 2, where we use the precise measurements of γ-ray energies from the conversion electron spectra. For comparison we give on this decay scheme the positions of levels derived from the α-particle fine structure. As can be seen, remarkably good agreement for the energies of certain levels results. These are for levels at 609, 1281, 1416, 1847, 2016, 2430 keV. The agreement is better than 4 keV and well within the errors quoted for the α-particle energies. For some of the levels whose energies are given by the addition of the energies of γ-rays thus shown to be in cascade, there exists close correspondence with a γ-ray energy corresponding to certain conversion electrons. We identify these with crossover transitions from the level to the ground state.

These are
1729.7 keV crossover 1728.3 keV
1764.7 keV crossover 1764.4 keV
1847.6 keV crossover 1848.5 keV
2118.6 keV crossover 2117.0 keV.

3.3. COINCIDENCES $\beta-\gamma$

A recent study [11]) of the β-spectrum of radium C gave several groups of transitions having end points at 3.17 MeV, 2.56 MeV, 1.72 MeV, 1.44 MeV and 1.03 MeV. Of these the first is a transition to the ground state of Po^{214}_{84} and the second to the first excited state at 609 keV [16]). The other transitions lead to groups of levels at approximately 1.4, 1.7 and 2 MeV.

So as to verify the main features of the proposed decay scheme a study of the coincidence spectrum of β and γ-rays was made. All pulses in a calibrated β-counter coincident with pulses in γ-ray counter were analysed with the kicksorter and the spectra corrected for γ-γ coincidences and random coincidences. A Kurie plot of the β-spectra showed definite changes of slope at β-ray energies of 1.7 MeV, 1.4 MeV and 1 MeV agreeing with the more precise analysis of Ricci and Trivero [11]). The source was about 1 microcurie of radium sulphate in equilibrium, sealed between sheets of aluminium of mass 2 mg/cm^2. Next the coincident γ-ray spectra were examined as the polarization of the β-counter was increased.

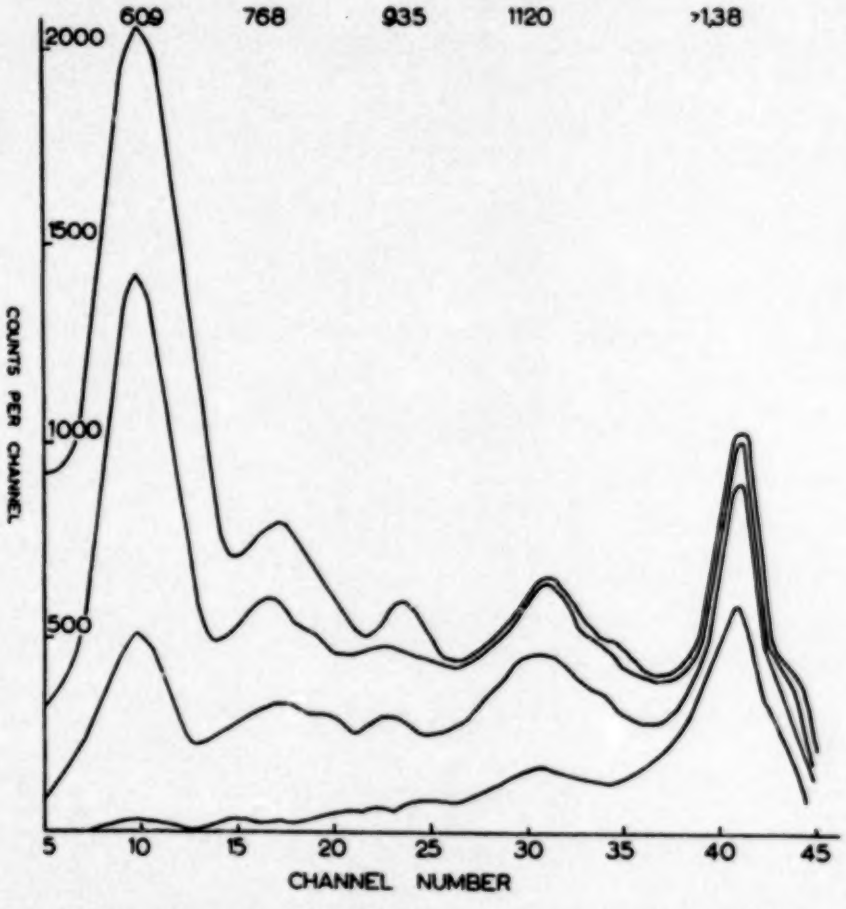

Fig. 3. The spectrum of gamma-rays in coincidence with β-particles, with a resolving time of 7×10^{-9} sec, for different delays inserted between the counters.

With increasing bias on the β-counter, the γ-ray photopeaks gradually disappear one after the other. The first peaks eliminated were due to the 2.4, 2.2 and 1.5 MeV γ-rays; the next γ-rays to become weak were the 1.85, 1.76, 1.24, 1.12 MeV ones, disappearing for a polarization corresponding to 1.5 MeV β-ray energy. The remaining peaks were at 609, 769 and 1378 keV and a weak bump at about 830 keV.

The 769 and 1380 peaks next disappeared for β-energies between 1.7 and 1.9 MeV leaving the 609 keV peak and a persistent bump at 830 keV. A γ-ray of 850 keV has been reported previously by Rowlands [9]), also found by β-γ coincidences. Finally for polarization between 2.2 and 2.6 MeV only the 609 keV peak was found. A careful search for a crossover transition from the level at 1544 keV showed very few pulses above the random counting rate. Those pulses that were found seemed to correspond to a weak

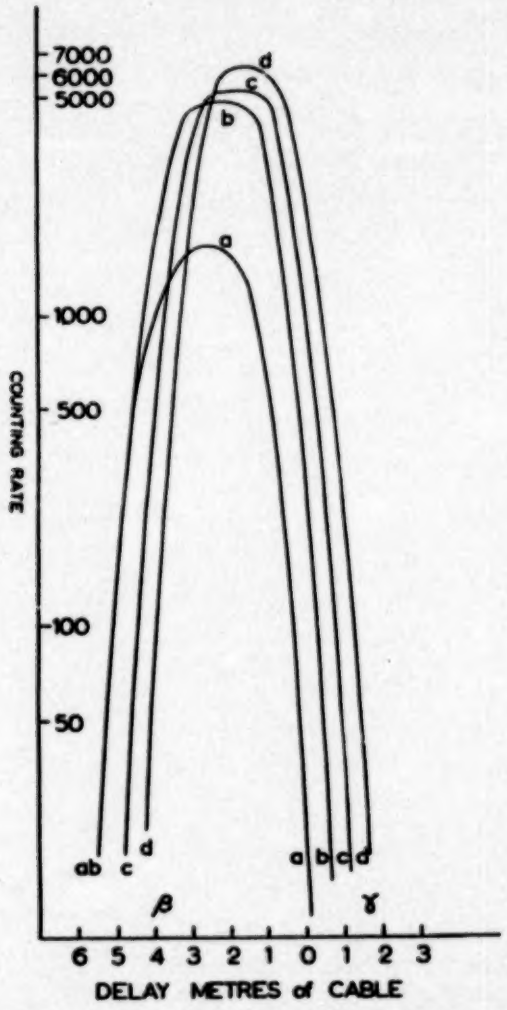

Fig. 4. Delay curves for β-γ coincidences resulting from the decomposition of the spectra of fig. 3. Curve a corresponds to 609 keV γ-rays, curve b to 768 keV γ-rays, curve c to 1120 keV γ-rays, curve d to higher energy γ-rays taken together.

γ-ray de-exciting the 1660 keV level. Owing to the complexity of the β-ray transitions it was not possible to verify quantitatively for each individual level the correspondence with the proposed decay scheme, but the relative intensities of the main coincident groups were in general agreement with the results of Ricci and Trivero.

Finally the spectrum of γ-rays above and including the 609 keV γ-ray

in coincidence with β-rays was examined as a function of delay time inserted between the counters and the fast coincidence unit, with the object of placing an upper limit on the lifetime of the levels against γ-ray emission. The dependence of the various photopeaks on delay time is very different between the lower and upper ends of the γ-ray spectrum, fig. 3. This effect can be explained if we recall that the fluorescent decay times of stilbene and sodium iodide crystals are respectively 5×10^{-9} sec and 2.5×10^{-7} sec. Pulses corresponding to β-rays of different energies detected in the stilbene crystal are all relatively prompt, whereas pulses in the sodium iodide crystal corresponding to γ-rays of different energies are delayed by a variable time depending on the γ-ray energy. This is clearly seen by decomposing the γ-ray spectra into regions corresponding to each γ-ray photopeak, and plotting the resulting delay curves separately for the intense γ-ray transitions, fig. 4. Thus, the β-pulses must be delayed longer to give full coincidence with 609 keV γ-rays than for coincidence with 1.120 keV γ-rays, and so on. A resolving time of 7×10^{-9} sec was used; the slope of the delay curves leads to an upper limit of 2×10^{-9} sec for the lifetime of the levels concerned.

3.4. $\gamma-\gamma$ CORRELATIONS

These were measured with two 4 cm$\times$4 cm cylindrical sodium iodide crystals covered with 5 mm of lead on the sides and 2 mm of lead on the front faces. One counter was held fixed with respect to the source at a distance of 12 cm, and the second counter could be rotated through 300° of arc at an equal distance from the source. The correlation apparatus was controlled by measuring the angular correlation between the γ-rays of a source of Co^{60}. The radium source was 30 μC of radium sulphate, in equilibrium with its decay products, contained in a cylindrical capsule of alluminium 5 mm$\times$5 mm with walls 1.5 mm thick. A resolving time of 1.8×10^{-8} sec was used, which gave 10 % random coincidences. Correlations were measured with a window of 60 keV width placed on the photopeak of the 609 keV γ-ray in one counter and all pulses in the second counter in coincidence with these selected pulses were sent to the Sunvic kicksorter. The resulting coincidence γ-ray spectra were decomposed into photopeaks and Compton spectra of the various γ-rays, after correction for random coincidences. Only the counts under the photopeaks were used in calculating the correlation functions by the least squares method. The process of decomposition was controlled against the spectrum of Co^{60} and by constructing dummy spectra with various sources of single γ-ray lines added together. Fortunately for the 1510, 1408 and 1238 keV γ-ray lines, the photopeaks of these lines fall on the trough between photopeak and Compton spectra of higher energy lines. These can be separated with reasonable

certainty and the results of various experimental runs agree within statistics. During the course of the correlation measurements it was obvious that the 1120 keV photopeak was composite as is shown by its different shape at different angles. The two γ-ray lines involved are 1120 and 1155 keV and must give very different correlations with the 609 keV γ-ray. It was not possible to separate these two lines unambiguously. The detailed results are discussed in the following summary. Table 2 gives the observed angular correlations and the proposed interpretation in terms of spin and parity of the levels.

TABLE 2

The measured coefficients A_2 and A_4 in the correlation formula
$W(\theta) = 1 + A_2 P_2(\cos\theta) + A_4 P_4(\cos\theta)$

Cascade (keV)	$W(\theta)$ observed		$W(\theta)$ theoretical		Correlation	Mixture
	A_2	A_4	A_2	A_4		
806–609	+(0.39 ±0.07)	+(0.91 ±0.09)	+0.357	+1.143	0(2)2(2)0	
935–609	−(0.07 ±0.03)		−0.071		3(1)2(2)0	
1238–609	+(0.165±0.031)	+(0.024±0.037)	+0.25		2(½)2(2)0	$\delta = +0.116$
1408–609	−(0.003±0.010)	+(0.325±0.02)	−0.076	+0.326	2(2)2(2)0	$\delta > 60$
1509–609	−(0.102±0.020)	+(0.004±0.015)	−0.25		1(½)2(2)0	$\delta = +0.132$
1120–609 1155–609	+(0.101±0.015)	+(0.019±0.020)				
1120–609	+(0.21± 0.04)	−(0.002±0.046)				

4. Discussion

4.1. GENERAL METHOD

There follows a discussion of the evidence leading to a spin and parity assignment to each individual level. Such an assignment in general depends on the following factors:

1. *Multipolarity of de-exciting γ-ray*, which is estimated from the *internal conversion coefficient*. This is calculated from the relation

$$\alpha_K^x = \alpha_K^{609} \times \frac{e_K^x}{e_K^{609}} \times \frac{I_{609}}{I_x} \qquad (1)$$

where e_K^x/e_K^{609} is the ratio of conversion electron intensities, and I_{609}/I_x is the ratio of γ-ray intensities, an average of the values of table 1. The 609 keV γ-ray is chosen for these calculations because it is the ground state γ-ray and its E2 character is well established by K/L ratio and L_I/L_{II} ratio. Similar ratios are known for some of the other γ-rays and also

indicate their multipolarity. The values are compared with the theoretical ones of Rose *et al.* [12]).

2. *Lifetime of state against γ-ray emission.* For those levels which emit α-particles we calculate τ_γ from the formula

$$\tau_\gamma = \tau_\alpha(I_\alpha/I_\gamma). \tag{2}$$

Here τ_α the lifetime against α-particle emission is calculated by extrapolation from the well-known lifetime $\tau_\alpha = 1.48\times10^{-4}$ sec of the ground state of Po^{214}_{84} by spin independent theory, I_α is the measured intensity of the α-particle fine structure and I_γ the absolute intensity per disintegration of γ-rays from the level concerned. τ_γ is then compared with theoretical values and general properties obtained from experimental data.

3. *Existence or non existence of a crossover transition* and its intensity relative to the stopover transition.

4. *Angular correlation between γ-rays in cascades.*

5. *Feeding of level by β-transitions.* In this connection we note that the spin and parity of the Bi^{214}_{83} ground state have been determined as 2^- by a measurement of the β-γ correlation between the 2.56 MeV β-ray and the 609 keV γ-ray [13]).

Each of these criteria taken by itself is subject to experimental and theoretical uncertainty. Taken together, however, where the data permit, they can lead to an almost unambiguous assignment of spin and parity.

The experimental data regarding α_K and τ_γ are presented, for easy comparison with theoretical values, in figs. 5 and 6. For the internal conversion coefficients the crosses correspond to the conversion electron intensities given by Mladjenovic and Slätis [5])†, and the circles to those of Ellis and Aston [1]). These points are joined by a line merely to avoid confusion; this is not intended as an indication of the errors. Theoretical values of τ_γ for various multipoles are calculated from the single particle estimates of Moszkowski [14]) as a function of the γ-ray transition energy. Also plotted is the α-particle decay lifetime τ_α of those excited states emitting α-particles, for which case the abscissa is the excitation energy and not always the energy of a γ-ray transition from such a state. As mentioned earlier, competition between γ-ray and α-particle emission may be such that α-particle transitions from a level with otherwise suitable properties as regards spin and parity, are lost in the counter background. A conservative upper limit to the detectable intensity appears to be 1 in 10^7, so, in fig. 6, the dotted line represents the previous τ_α curve divided by 10^7 (see eq. (2)). It is well-known that the single particle estimates of γ-ray transition probability often differ by orders of magnitude from established experimental values. In this connection it is worth noting here the following generalizations: M1 transi-

† This paper will be referred to as M.S.

tions are generally 100 times less probable than given by the single-particle formula; E3 transitions 500 times less probable and E2 transitions in even nuclei from 10 to 100 times more probable. Both M1 and E3 transitions approach more closely the single particle value in the region of the double closed shell represented by the isotopes of lead.

4.2. SPIN AND PARITY ASSIGNMENTS OF INDIVIDUAL LEVELS

609.3 keV. This is the first excited state since no β-γ coincidences are observed above 2.7 MeV β-energy. For an even nucleus we expect 2^+ for

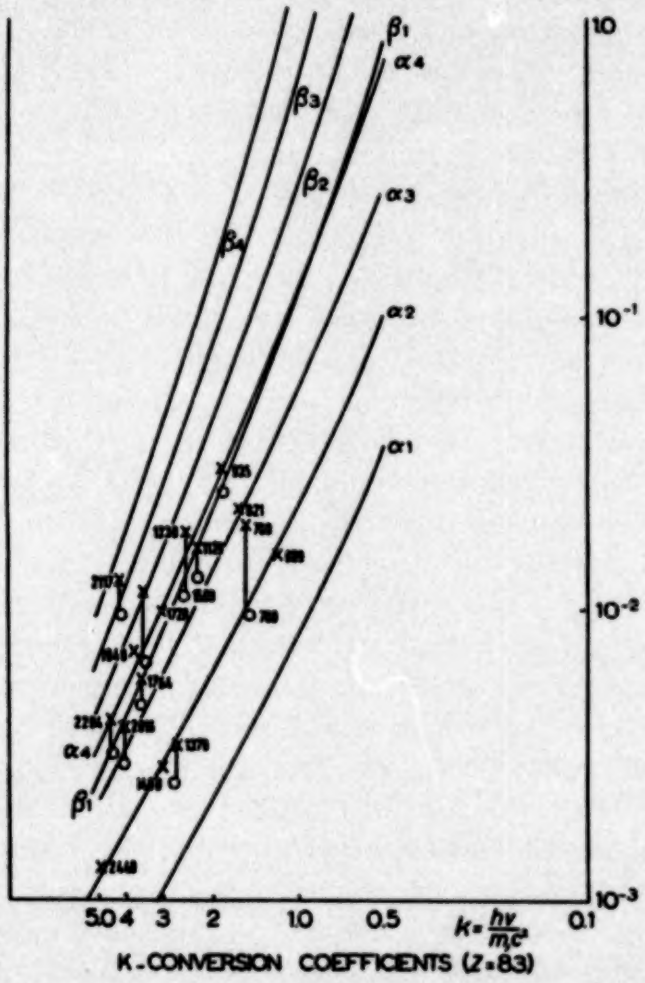

Fig. 5. The internal conversion coefficients α_K, calculated as described in the text, compared with the theoretical values of Rose *et al.*[13]).

the level and an E2 transition. The observed ratios $K/L = 5$, $L_I/L_{II} = 1.5$ and $L_{III}/L_I = 0.33$ are all compatible with an E2 transition [14]), the last two especially disagreeing with any magnetic multipolarity. Finally, the level emits α-particles leading to a lifetime $\tau_\gamma = 1.5 \times 10^{-12}$ sec, about three times faster than the theoretical value of 5.8×10^{-11} sec.

830 keV. A level at this energy is indicated by two separate observations

of β-γ coincidences. In our experiments, the coincidences were found using a resolving time of 1.1×10^{-7} sec, so the lifetime cannot be much longer than this. M. S. give a conversion line of 728.13 keV which might be the K conversion electron of a γ-ray of 821.3 keV. All other conversion lines in this region can be accounted for in the decay scheme. Using this information we find an α_K close to M1 or E3. However, no α-particles are observed, although the authors place an upper limit of 1 in 10^7 as the minimum

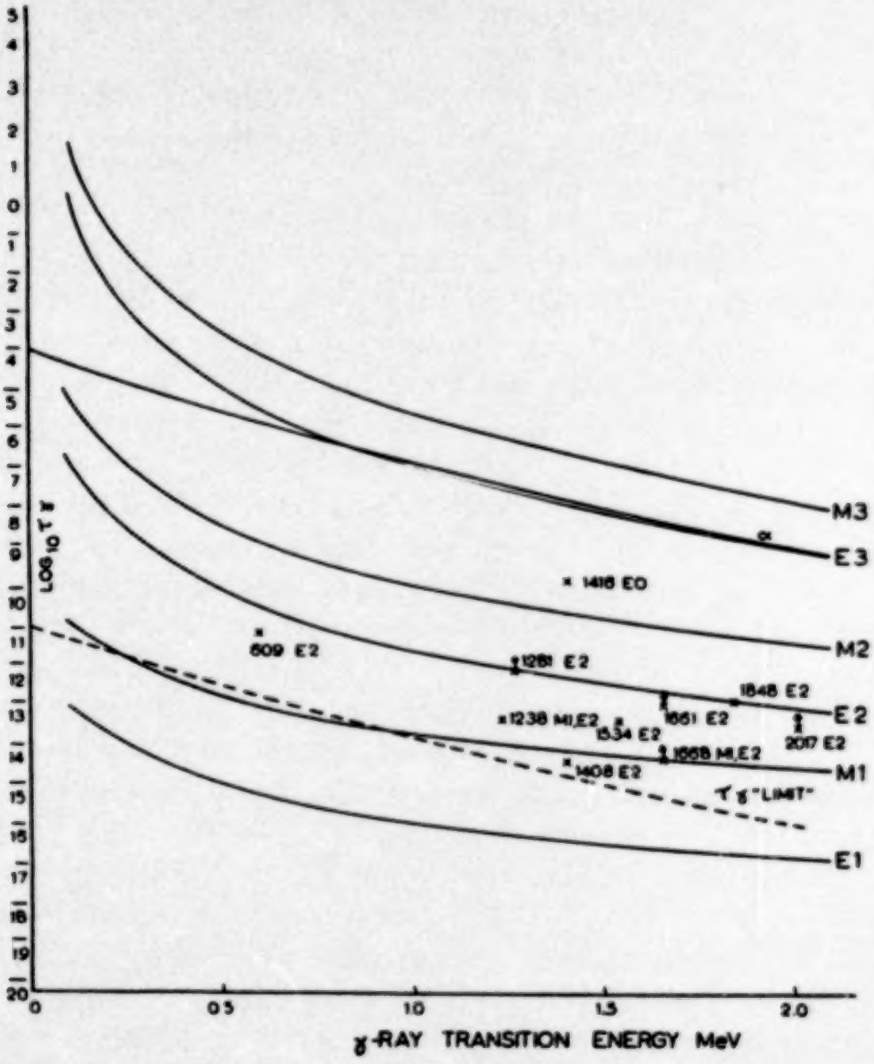

Fig. 6. The lifetimes τ_γ for γ-ray transitions in Po^{214}_{84} calculated from the lifetimes τ_α, plotted against the theoretical values derived from the single particle formulae of Moszkowski [14].

intensity they could detect. Using this limit, we can calculate the maximum lifetime that the γ-ray transition can have in order to compete successfully with α-particle emission. This is 3.9×10^{-16} sec, and as is seen from fig. 6, is at least 10^9 times too fast to be E3. Also, an E3 transition would need 3^- for the level which should therefore be strongly excited by an allowed

β-transition. Thus, the most likely values for the spin and parity are 1^+.

1281.3 keV. This level is suggested by an α-particle group and K and L conversion lines. The α-particle group was difficult to separate from the tail of the intense group corresponding to the well-known level at 1416 keV, and the authors [10]) hesitate to identify it with certainty. Further, the γ-ray line might well be a transition from a level at 2697 keV, indicated by an α-particle group, to the 1416 keV level. Thus the correspondence in energy is not sufficient to enable us to fix a level with certainty. Unfortunately, the γ-ray energy is too close to the 1238 keV line to be separated in simple spectra, although our measurements do show that it must be at least 5 times less intense than this γ-ray line. Also, a line at 1281 keV did not appear in β-γ coincidence spectra with the bias on the β-counter at 1.5 MeV. In the level exists it must therefore be 0^+.

1387 keV. Both crossover and stopover γ-ray transitions agree with 2^+ for this level, although the conversion coefficient for the stopover γ-ray of 768 keV might indicate a mixture of M1 and E2. The level should therefore emit α-particles, but if their intensity is weakened by competition with γ-ray emission, they are easily lost in the tail of the group from the 1416 level. Reference to fig. 6, shows that E2 transitions must be speeded up by about 100 times to compete successfully with α-particle emission. This supports the suggestion [17]) that this level is formed by a collective vibration of the nucleus, although we estimate crossover and stopover to have a very similar intensity. Special care was taken to establish this crossover γ-ray by β-γ coincidences. Since the probability of summation of the full energy peaks of the cascade γ-rays is large, thus simulating a crossover γ-ray, we verified that the intensity under the 1380 keV photopeak varied proportionally to the solid angle and not to its square. This was done for both large and small NaI crystals. Apart from the interest of identifying the crossover γ-ray from the 1378 keV level this caution was further justified since we observed a γ-ray of very similar energy also in coincidence with the 609 keV ground state γ-ray. This transition is discussed later. Our angular correlation measurements are not considered reliable for the 768—609 keV cascade owing to the corrections necessary for the Compton distributions of higher energy γ-rays and interference from another cascade very close to it in energy. This situation will be improved by further measurements now in progress with two 8 cm × 8 cm NaI spectrometers in coincidence.

1415.9 keV. This level has been assigned 0^+ because it decays by α-particle emission and internal conversion electrons only. The K/L ratio of 5.1 agrees well with the calculated value of 5.4 ($Z = 85$) for an electric monopole transition. Latyshev [2]) gives its intensity as 3.5×10^{-3} per disintegration which combined with the α-particle intensity leads to a life-

time of 3.5×10^{-10} sec against E0 internal conversion. Church and Weneser[15]) calculate the transition probability of E0 internal conversion $(W/\varrho^2)_K$ to be 3.17×10^9 sec^{-1} where ϱ^2, the strength parameter, is a measure of the overlap of initial and final nuclear wave functions. Thus ϱ is equal to 1.58×10^{-3}. We note here that M. S. give a conversion electron of energy 713.11 keV which might be considered as the K-electron of a γ-ray of energy 806.27 keV. This corresponds very closely to the difference 1415.9—609.3 = 806.6 keV, and thus suggests a cascade transition of the form 0(2)2(2)0. A search was made for this γ-ray, which coincides closely in energy with the 768 keV γ-ray, by examining the spectrum in a large crystal under high dispersion. The spectrum (fig. 7) shows clearly a repro-

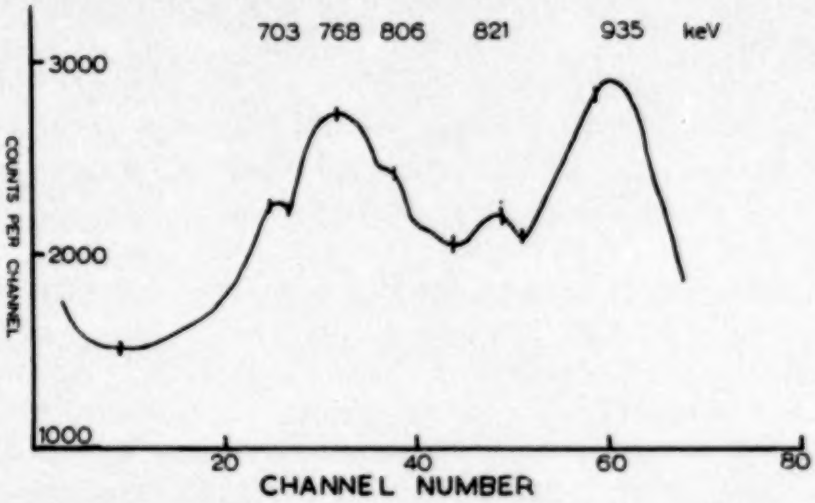

Fig. 7. A spectrum taken with a dispersion of about 2 keV per channel which shows the presence of the 806 keV γ-ray superimposed on the 768 keV γ-ray.

ducible lump on the high energy side of the 768 keV photopeak. Further the coincidence spectra taken during the correlation measurements show a small peak in the region between the 768 keV and 933 keV photopeaks which changes in magnitude considerably with the angle between the counters. An E2 transition of 806 keV has a single particle lifetime of 1.4×10^{-11} sec and could therefore compete easily with E0 internal conversion.

1544.1 keV. The M1 nature of the stopover 933 keV γ-ray, the absence of a crossover γ-ray, and the absence of α-particles suggest 3^+ for this level. Reference to fig. 6, shows that if the level were 2^+ the M1 lifetime would need to be speeded up by 25 times to compete with α-particle emission, whereas most M1 transitions are at least 100 times slower than the single particle estimate. We measured a weak correlation for the 933—609 keV cascade consistent with this assignment.

1668 keV. This level is indicated by α-particles whose energy is given as 1663 ± 7 keV. There are two conversion lines in M. S. corresponding

to 1661.0 keV and 1668.4 keV consistent with this interval, and having equal electron intensities. Our simple spectra show that the line is at most 2 % of disintegrations, thus 1^- and 3^- are unlikely. From fig. 6 we see that τ_γ calculated from this intensity limit lies close to the E2 curve. Thus 2^+ is assigned to this level. If the energy is 1668.4 keV there should be stopover γ-rays to the lower levels. As discussed later, there are three possible cascades. Also, the 1661.0 keV γ-ray can be fitted into the scheme.

1729.7 keV. From this level both stopover and crossover are consistent with M1 multipolarity, although for the crossover the experimental conversion coefficient depends on an estimate of the intensity of the 1728.3 keV γ-ray, which is uncertain owing to its proximity to the 1764.4 keV γ-ray. M. H. say it cannot be more intense than 10 % of the 1764.4 keV transition. The 1120.4 keV stopover γ-ray is most certainly mainly M1 and based on it alone the level must be one of 1^+, 2^+ or 3^+. Of these, 2^+ is improbable since no α-particles are observed, and an M1 transition would have to be faster by 10 times to compete. Also, the observed conversion electron intensity of the 1728.3 keV γ-ray implies a ratio $I(1728)/I(609) = 0.21$ for E2, obtained by rearranging eq. (1), which is five times greater than the intensity limit mentioned earlier. For 3^+, the crossover should be less intense than the stopover by a factor of nearly 10^7, which is clearly incompatible with the data. Thus 1^+ is the best choice for this level. Our correlations are difficult to interpret owing to the neighbouring cascade discussed next.

1764.4 keV. Since the crossover transition is clearly M1 the level must be 1^+. Evidence for the stopover is twofold, the close agreement in energy for a γ-ray of 1155.35 keV identified by its K and L conversion electrons, and the cascade of γ-rays put in evidence by our correlation spectra which alter perceptibly with angle (fig. 8a, b). For the stopover the K/L ratio is 5.2, agreeing very well with the theoretical value of 5.8 for an M1 γ-ray. This agreement, however, may be fortuitous since the other K/L ratios available, generally do not agree with theoretical values. The observed conversion electron intensity implies $I(1155)/I(609) = 0.084$, that is about 16 % of the 1120.4 keV γ-ray, which is a reasonable figure.

1847.6 keV. The stopover γ-ray is clearly M1 and since the level emits α-particles, it is 2^+. Our angular correlation measurement also confirms this spin and parity assignment. Based on the single-particle formula for τ_γ the crossover should be 10 times less intense than the stopover. The internal conversion coefficient for the 1848.5 keV γ-ray is close to the M1 curve, but a γ-ray of energy 1850 ± 50 keV is observed in coincidence with the 609 keV γ-ray, so it seems probable that the crossover from the 1847.6 keV level is confused with this cascade γ-ray.

2016.7 keV. We observe a γ-ray of energy 1410 ± 30 keV in cascade with the 609 keV γ-ray. M. S. give a conversion electron which corresponds to

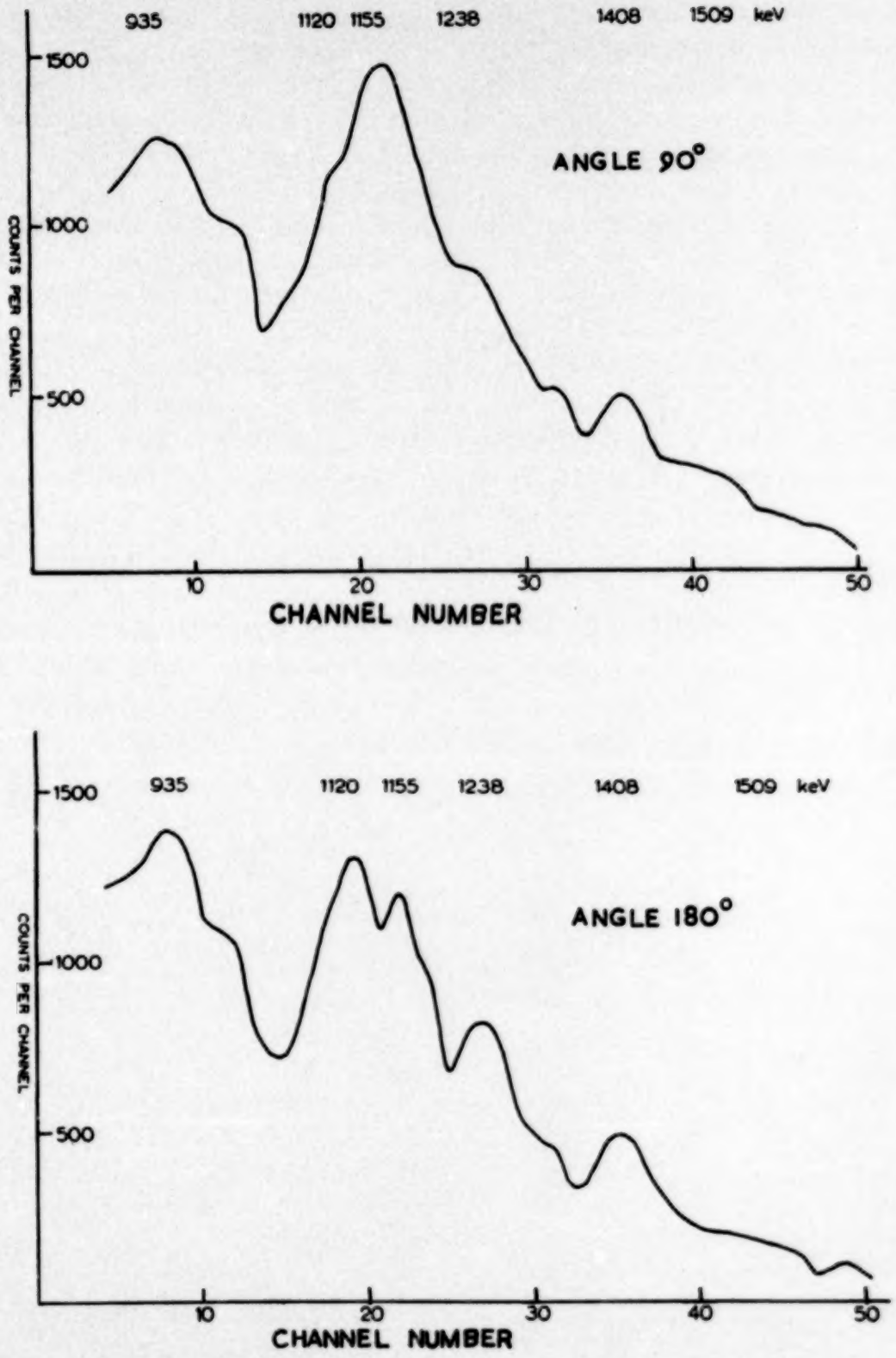

Fig. 8. Coincidence spectra of γ-rays in coincidence with the 609 keV γ-ray, taken at 0° and 90°. The change in shape of the photopeak at 1120 keV with angle, shows the presence of the 1155 keV γ-ray.

a γ-ray energy of 1408.0 keV, thus both stopover and crossover γ-rays are identified for this level which also emits α-particles. The angular correlation corresponds to the cascade 2(1,2)2(2)0 with the 1408 keV γ-ray almost pure quadrupole. The level is thus 2^+. As confirmation of the E2 character for this stopover γ-ray, we estimate the relative intensities of the 1408 keV γ-ray to the 1120 keV γ-ray from our coincidence spectra at 90° where the difference between the angular correlations of these two cascades has no influence on the estimates. This gave the ratio $I(1408)/I(609) = 0.17$, and $\alpha^K_{1408} = 3.4\times10^{-3}$, very close to the E2 curve. For the crossover γ-ray the conversion coefficient is rather large, but this may be due to an overestimation of the conversion electron intensity.

2118.6 keV. The stopover γ-ray is M1 and since there are no α-particles there remain 1^+ or 3^+ as possibilities for this level. The angular correlation could be fitted to either assignment with different values of (M1, E2) mixture. However, for 3^+ the crossover γ-ray should have only 4.6×10^{-7} of the intensity of the stopover, based on the single particle transition probability formula. This is clearly incompatible so 1^+ is the most reasonable assignment.

2204.3 keV. This level is identified by the γ-ray to the ground state. Its α_K falls well on the M1 curve but might be considered compatible with E3 or E4. However, in this case, α-particles should be observed; since they are not found, we assign 1^+ to the level.

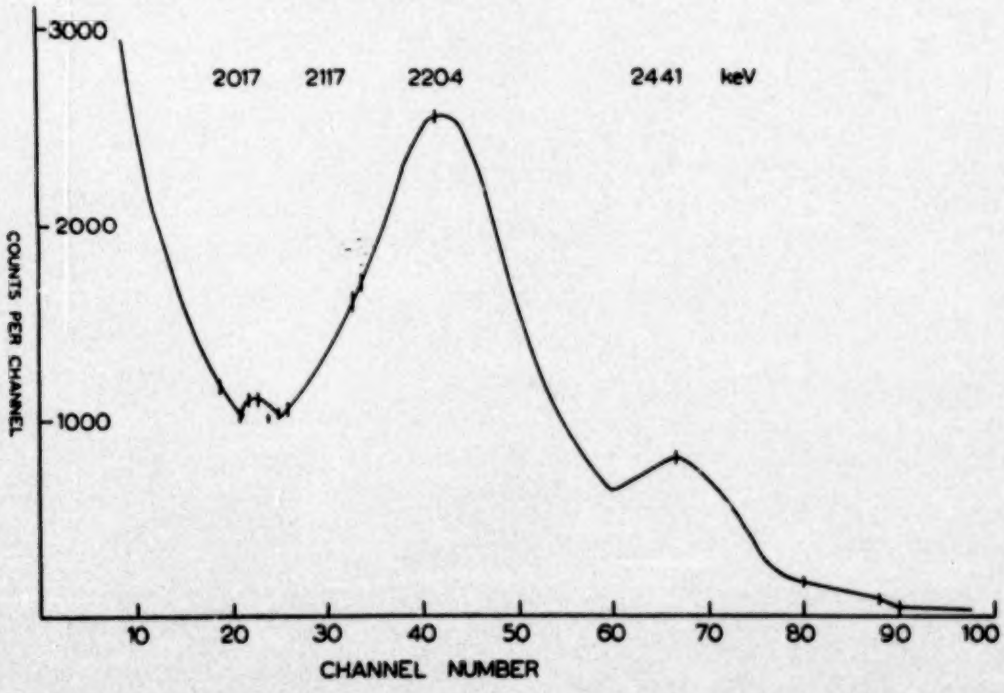

Fig. 9. Spectrum of the high energy γ-rays of radium which shows a weak peak corresponding to the 2016.7 keV γ-ray, a small boss on the low energy side of the 2204 keV peak which corresponds to the 2117 keV γ-ray, and also a poorly resolved peak for the 2513 keV γ-ray.

2440.8 keV. The α-particles from this level determine the energy as 2439±4 keV. M. H. identify a peak in their Compton recoil spectrum with a γ-ray of energy 2432 keV. Ellis gives an energy of 2432.4 keV whilst Wolfson [18]) finds a line at 2452±12 keV. Comparison of the energies given by Ellis with the more accurate values of M. S. show that the former in this region are on average 9 keV too small. Taken together this data indicates a level de-exciting by a ground state transition at 2440 keV. This gives a total of 2440.8 keV. From the conversion coefficient the crossover is E2 and the level thus 2^+. We determine the energy as (2440±20) keV (fig. 9). The lifetime τ_γ, calculated from τ_α, is 1.6×10^{-14} sec, which compares well with the single particle $\tau_\gamma = 5.7\times10^{-14}$ sec.

4.3. WEAK TRANSITIONS

The levels discussed above are well established by α-particle fine structure or observed γ-ray energies. There remain some levels indicated by the fine structure from which no γ-ray transitions are yet assigned. There are also many conversion lines [5]) belonging presumably to γ-rays as yet not identified. Perhaps the most interesting levels in this connection are those indicated by α-particle groups but not yet identified by γ-ray transitions.

2513±10 keV. We first note three possible cascades to well established levels:

$$2204.3+304.0 = 2508.3 \text{ keV, final level } 1^+$$
$$2118.6+388.9 = 2507.5 \text{ keV, final level } 1^+$$
$$1847.6+660.9 = 2508.5 \text{ keV, final level } 2^+.$$

Now, Ellis [1]) gives a conversion line (Wa5) corresponding to an energy of 2499.8 keV. As previously noted his values are too small by an average of 9 keV in this region, thus this line probably corresponds to a ground state transition with energy 2508 keV. From the conversion electron intensity of 0.2 given by Ellis we calculate the ratio $I(2508)/I(609)$ according as the γ-ray is supposed to be E1, E2 or E3. We then use this intensity to calculate the τ_γ corresponding to each multipolarity. This leads to table 3.

TABLE 3

The intensity ratio $I(2508)/I(609)$ calculated for various assumptions regarding the multipolarity of the 2508 keV γ-ray, and the $\log_{10}\tau_\gamma$ which results from it

	E1	E2	E3
$I(2508)/I(609)$	0.162	0.065	0.035
$\log_{10}(\tau_\gamma$ sec)	$\bar{1}5.0792$	$\bar{1}5.4624$	$\bar{1}5.7404$

By comparison with fig. 6 we see at once that we can eliminate E3, but that both E1 and E2 must be considered as possible on this basis alone.

However the E1 assignment should lead to an easily observable γ-ray line. Similarly from the conversion electron intensities of the stopover transition the 1^- assignment to this level implies that these are also E1. In table 4 we present the intensities relative to the 609 keV γ-ray calculated from the conversion data.

TABLE 4

The intensity ratios $I(x)/I(609)$ for the proposed cascade γ-rays from the 2508 keV level, for various assumptions regarding their multipolarity

	E1	E2	M1
$I(660.9)/I(609)$	0.208	0.077	0.019
$I(388.9)/I(609)$	0.179	0.078	0.011
$I(304.0)/I(609)$	0.116	0.043	0.006

From our low energy spectra of Po^{214}_{84} (subsection 4.4), it is quite clear that no low energy transitions exist as intense as these corresponding to E1. Thus 2^+ is the most probable assignment for this level.

2268±7 keV. Within the error of 7 keV for this α-particle group the only cascade is

$$1660.9+609.3 = 2270.2 \text{ keV}.$$

This energy then corresponds quite well with a stopover transition from the 2508.1 keV level previously established:

$$2270.2+239.1 = 2509.3 \text{ keV}.$$

There are no other cascade relationships close enough in energy to be acceptable. The data are sparse, but probably the fact that cascades to lower states do not exist indicates that the spin is high 3^-, 4^+ or 5^-. For the stopover we calculate the following data:

TABLE 5

The intensity ratios $I(1661)/I(609)$ calculated for different multipolarities of the 1661 keV γ-ray, and the values of $\log_{10}\tau_\gamma$ deduced from them

	E1	E2	E3
$I(1661)/I(609)$	0.47	0.178	0.089
$\log_{10}(\tau_\gamma \text{ sec})$	$\overline{15}.0086$	$\overline{15}.4314$	$\overline{15}.7324$

Thus E1 or E2 are both probable, but for E1 the 1661 keV γ-ray should be very prominent in the spectrum. 4^+ is the best assignment.

2138±6 keV. The conversion electron Ua1 of Ellis corresponds to a γ-ray with energy 1534 keV. In cascade with the 609 keV level this fixes the energy of the level at 2143.3 keV. If the γ-ray is assumed to be E2 the

conversion electron intensity of 0.2 leads to $I(1534)/I(609) = 0.028$, and to $\log_{10} \tau_\gamma$ sec $= \overline{14}.96$. For E1 multipolarity the ratio $I(1534)/I(609) = 0.08$, and no γ-ray of this intensity is observed in coincidence. Since no crossover γ-ray is found we assign 4^+ to this level. It is probable that the angular correlation found for the (1509—609) keV cascade includes the (1534—609) keV cascade. This could explain why the former cascade gave a smaller A_2 coefficient than expected for a 1(1)2(2)0 correlation with pure M1 for the 1509 keV γ-ray.

There remain two more levels indicated by α-particle fine structure at 2697 ± 4 keV and 2880 ± 10 keV, to which we cannot as yet assign any γ-ray transitions. Within the error of the α-particle energy measurements a few γ-ray transitions are energetically possible, but we have not yet obtained satisfactory confirmation of any of these possibilities.

The following transitions seem highly probable on the basis of their close correspondence to the energy intervals between established levels, and also do not lead to any disagreement with the proposed scheme:

TABLE 6

Proposed γ-ray transitions which fit into the decay scheme according to their energy and to observed conversion electron lines

Interval (keV)	γ-ray energy (keV)	Electron intensity	$I(x)/I(609)$
1764.4—1378.0 = 386.4	386.9	9.9	0.019
1729.7—1378.0 = 351.7	352.0	3.0	0.0045
2204.3—1415.9 = 788.4	787.1	1.0	0.012
2118.6—1415.9 = 702.7	703.1	1.6	0.015
1764.4—1415.9 = 348.5	348.5	1.8	0.0026
1847.6—1544.1 = 303.5	304.0	5.8	0.0056
1764.4—1544.1 = 220.3	219.5	5.1	0.0025
1729.7—1544.1 = 185.6	184.1	7.3	0.0019

In each case the intensity ratio is calculated assuming that the transition is M1 from eq. (1). Since these M1 transitions compete with the main transitions from the given levels, they should be less intense by the cube of the energy ratio. Thus the 787.1 keV γ-ray should be 22 times less intense than the 2204 keV γ-ray, and according to tables 1 and 6, it is 16 times less intense.

It is worth noting that the three transitions to the 0^+ level at 1415.8 keV each begin from a level with 1^+; however the transition from the 1729.7 keV level is not found. This may be taken as a further indication that the 1729.7 and 1764.4 keV levels have different spin, which would explain

why the one gives a strong ground state transition and the other a strong crossover transition. This point is discussed later.

4.4 LOW ENERGY γ-RAYS

An attempt was made to distinguish some of the lower energy γ-rays belonging to Po^{214}_{84}, whose existence is suggested by a large number of conversion electrons [5]) corresponding to γ-rays with energies less than the 609 keV ground state transition. These measurements could not be made with a source of radium in equilibrium with all its decay products because of the γ-rays of RaB which have energies up to 352 keV. We therefore carried out a chemical separation, on a source of active deposit, of RaC, an isotope of bismuth, from RaB, an isotope of lead. The efficiency of the separation was controlled by measuring the half-life of the resulting source which for RaC is 19.7 min, and for RaB is 26.8 min. The pulse height spectrum (fig. 10) shows a number of reproducible peaks superimposed on

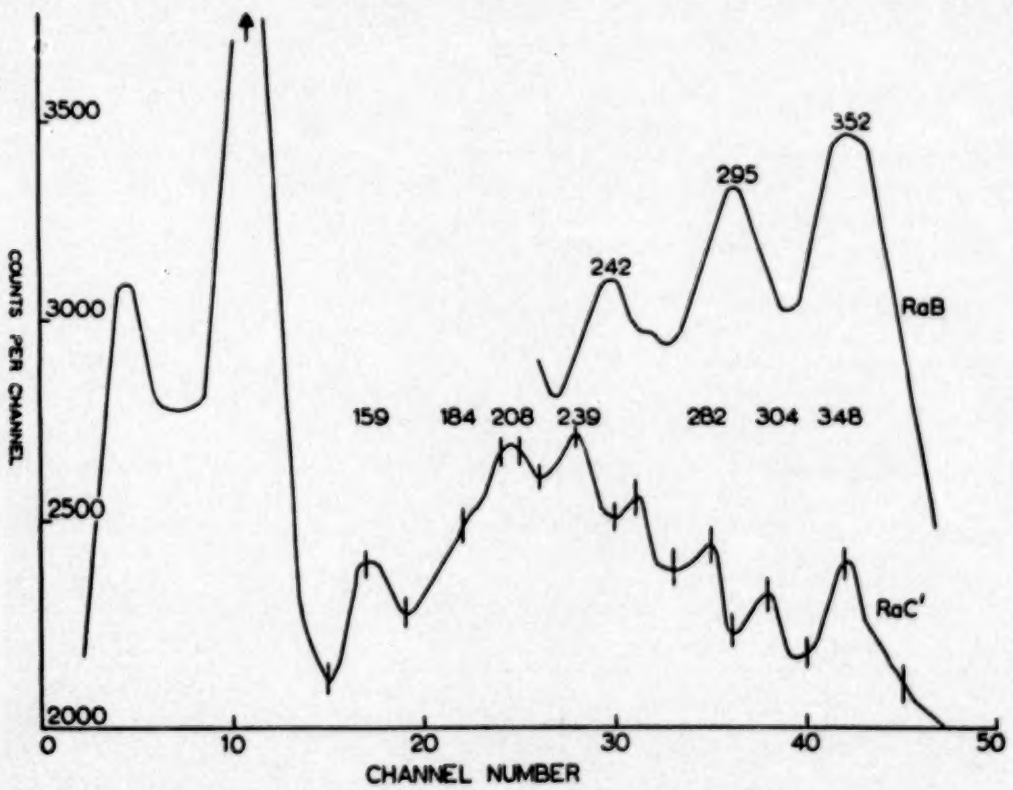

Fig. 10. Spectrum of the low energy γ-rays of Po^{214}_{84}, taken with a separated source of RaC. For comparison the spectrum obtained with a radium source in equilibrium is included in this figure, showing the γ-rays of RaB. The sharp peak to the left is given by the X-rays of lead and polonium.

the Compton distributions of higher energy γ-rays. With a stronger source than the one we have at present we hope to make β-γ coincidence measurements to establish the positions of these transitions in the decay scheme.

5. Discussion

The nucleus Po^{214}_{84} with two protons and four neutrons outside the doubly closed shell nucleus Pb^{208}_{82} occupies an interesting position midway between the region of mass numbers where shell model effects are all important, and the region of mass numbers greater than 230 where the levels are known to have a strongly collective character. There is strong evidence in the present work that collective effects occur in this nucleus: for example most of the identified E2 transitions are speeded up by factors varying from 5 to 100 over the single particle estimate of the transition probability. Such transitions can then compete with the intrinsically faster M1 transitions which are allowed by the spin and parity assignments. The most striking example of this is the 1408—609 keV cascade for which the angular correlation shows that the 1408 keV γ-ray is almost pure quadrupole. It has been suggested [17]) that the level at 1378 keV corresponds to a second vibrational excitation of the quadrupole type; however, the crossover transition should then be considerably weaker than is observed.

Although we shall not attempt a complete analysis of the level scheme in terms of a rotational-vibrational model, we point out some relationships between the experimental data here summarized, which lend support to this idea.

(a) The first 4^+ state is at 2144 keV, which might be the second rotational level of a band associated with the ground state and the 609 keV state. In this case its energy should be 3.33 times the splitting of 609 keV, whereas it is in fact 3.48. However the crossover γ-ray seems to be E2 and is faster than the single particle estimate for the transition. An alternative explanation, based on the energy difference of 600 keV, is that the level is the second member of a rotational band beginning at the 1544 keV level 3^+, which might be formed by a particle excitation. Then we should expect a γ-ray transition of this energy which is easily confused with the intense 609 keV γ-ray.

(b) It was suggested to the author by Dr. E. B. Paul of A.E.R.E., Harwell, that the 1416 keV level corresponds to a quadrupole β-vibration state with $K = 0^+$, $\lambda = 2$. The suggestion arose from trends which he has observed in the known data of such states for nuclei in this mass region. In this case we expect a 2^+ state at about 2025 keV, which might be the 2017 keV level. To support this assignment we note the following; the 2^+ state of such a band would decay to the 0^+ and 2^+ members of the ground state band with reduced transition probabilities in the ratio 1 : (10/7). The γ-rays involved are the 2017 keV crossover γ-ray and the 1407 keV stopover γ-ray, and we find the latter to be more intense by a factor of 12. To correct for the energy dependence we divide this by 6, which is the fifth power of the energy

ratio, since both γ-rays are E2. We thus arrive at a ratio of 2 for the reduced transition probabilities to compare with the 1.4 of the collective model.

This work was originally begun with the intention of measuring the angular correlation of the (1120—609) keV cascade, which is the most intense cascade. The measurement was complicated by the (1155—609) keV cascade which could not be separated. In table 2 we give the correlations observed for the whole photopeak and for the low energy side of this peak. It seems that the (1120—609) keV cascade is closer to a 2(1)2(2)0 correlation which would imply 2^+ for the 1729.7 keV level, and fit better the other data on this level. However this could also be explained by a 1(1,2)2(2) 0 correlation with a mixed M1—E2 transition for the 1120 keV γ-ray.

The author would like to thank Professor H. Halban for the interest he has shown in this work, and Professor Y. Rocard for allowing him the use of the facilities of the Laboratoire de Physique of the Ecole Normale Supérieure. His thanks are due to Mme F. Madaule for the valuable assistance she lent to these measurements; to Dr. M. Milman for performing the chemical separations on the radium sources which were supplied by the Institut du Radium, Paris. He is indebted to the Commissariat à l'Energie Atomique for a Bursary.

References

1) C. D. Ellis and G. H. Aston, Proc. Roy. Soc. A **129** (1930) 180
2) G. D. Latyshev, Revs. Mod. Phys. **19** (1947) 132
3) M. Mladjenovic and A. Hedgran, Physica **18** (1952) 1242
4) M. Mladjenovic and A. Hedgran, Arkiv för Fysik **8** (1954) no. 4, p. 49
5) M. Mladjenovic and H. Slätis, Arkiv för Fysik **8** (1954) no. 5, p. 65
6) M. Miwa and S. Kageyama, J. Phys. Soc. Japan **5** (1951) 416
7) S. Kageyama, J. Phys. Soc. Japan **7** (1952) 93
8) F. Demichelis and R. Malvano, Nuovo Cimento **10** (1953) 405
9) R. E. Rowland, Phys. Rev. **99** (1955) 757
10) Lord Rutherford, W. B. Lewis, and B. V. Bowden, Proc. Roy. Soc. A **142** (1933) 347
11) R. A. Ricci and G. Trivero, Nuovo Cimento **2** (1955) 745
12) M. E. Rose, G. H. Goertzel and B. I. Spinrad, Phys. Rev. **83** (1951) 79
13) F. Demichelis and L. A. Radicati, Nuovo Cimento **3** (1956) 152
14) Beta and Gamma Ray Spectroscopy, Ed. K. Siegbahn (North-Holland Publishing Co., Amsterdam, 1955)
15) E. L. Church and J. Weneser, Phys. Rev. **103** (1956) 1035
16) G. R. Bishop and F. Demichelis, Nuovo Cimento **4** (1956) 1599
17) K. Alder, A. Bohr, T. Huus, B. Mottelson and A. Winther, Revs. Mod. Phys. **28** (1956) 432
18) J. L. Wolfson, Phys. Rev. **78** (1950) 177

Nuclear Physics 5 (1957) 383—389; © *North-Holland Publishing Co., Amsterdam*
Not to be reproduced by photoprint or microfilm without written permission from the publisher

DISPERSION RELATIONS FOR WEAK INTERACTIONS

N. N. BOGOLUBOV, S. M. BILENKY and A. A. LOGUNOV
Joint Institute of Nuclear Research, Laboratory of Theoretical Physics, Dubna, U.S.S.R.

Received 10 July 1957

Abstract: Dispersion relations for weak interaction processes are obtained in the present paper.

It is shown that in processes which involve not only weakly interacting but strongly interacting particles as well, the dispersion relations are equivalent to the statement that the unknown amplitude functions, which are determined by strong interactions, depend only on momentum transfer between strongly interacting particles.

1. Introduction

One of the main principles of present-day local field theory is the causality principle [1]). It has been recently demonstrated that this principle underlies the deduction of the so-called dispersion relations which connect the Hermitian and anti-Hermitian parts of the process amplitudes. Consequently, an experimental check of these relations may serve to verify localizability of the theory. The dispersion relations are usually deduced for strong interactions. However it would be interesting to ascertain just what the dispersion relations yield in the case of weak interactions.

According to the general theory of dispersion relations [2]), the "Hermitian" part of the amplitude D in a special coordinate system is equal to an integral of the "anti-Hermitian" part A, taken over the energy, plus an arbitrary polynomial $P_n(E)$. The "anti-Hermitian" part of the amplitude can be expressed in terms of the product of the "meson" ("electron") current with the "neutrino" current. Because of the smallness of the weak interaction coupling constant C, only terms involving the first power of the coupling constant should be taken into account. Since the smallness of the product of the aforementioned currents is not lower than the second order the "anti-Hermitian" part will vanish in the approximation under consideration.

In the case of electromagnetic interactions, besides processes for which the "anti-Hermitian" part in the given approximation also vanishes (e.g. scattering of electrons on protons) there are some processes (photoproduction, Compton effect) for which the "anti-Hermitian" part is of the same order of magnitude as the Hermitian. Thus for all weak interactions and for those electromagnetic processes whose "anti-Hermitian" part of the am-

plitude is zero, the dispersion relations assume a particularly simple form

$$D(E) = P_n(E). \tag{1}$$

As is well known, the necessity of analyzing the analytical properties of A is the source of the main difficulties which are encountered when one attempts to prove the dispersion relations. Since in the cases under consideration A should be replaced by zero the proof is evident and can be directly obtained from general principles as well as from the usual theory.

In view of the particular simplicity of the dispersion relations (1) it would seem to be of special interest to use them to check the localizability of the theory.

2. Dispersion Relations for Weak Interactions

As an example consider the reaction †

$$\mu^- + \mathrm{p} \to \mathrm{n} + \nu. \tag{2}$$

In this reaction weakly interacting (μ, ν) as well as strongly interacting (p, n) particles are involved. We write the matrix element for process (2) in the form

$$S(p, q; p', q') = (2\pi)^3 \langle \phi^*_{p's'} a_\nu(q') S a_\mu^+(q) \phi_{ps} \rangle \tag{3}$$

where ϕ_{ps} is the state vector of the initial nucleon, a_μ^+ is the μ-meson creation operator, and a_ν is the neutrino absorption operator.

Transposing the creation operator in (3) to the position at the extreme left and the annihilation operator to the position at the extreme right we obtain

$$S(p, q; p', q') = \bar{u}_\nu(q') \int e^{i(q'x - qy)} \langle p's' | \frac{\delta^2 S}{\delta\bar{\psi}_\nu(x)\delta\psi_\mu(y)} S^+ | ps \rangle u_\mu(q) dx dy. \tag{4}$$

Introducing the "meson" and "neutrino" current operators

$$j_\mu(y) = -i \frac{\delta S}{\delta\bar{\psi}_\mu(y)} S^+, \quad j_\nu(x) = -i \frac{\delta S}{\delta\bar{\psi}_\nu(x)} S^+ \tag{5}$$

we get

$$\frac{\delta^2 S}{\delta\bar{\psi}_\nu(x)\delta\psi_\mu(y)} S^+ = \begin{cases} -i \dfrac{\delta\bar{j}_\mu(y)}{\delta\bar{\psi}_\nu(x)} - \bar{j}_\mu(y) j_\nu(x) \\ -i \dfrac{\delta j_\nu(x)}{\delta\psi_\mu(y)} + j_\nu(x)\bar{j}_\mu(y). \end{cases} \tag{6}$$

However, in virtue of the causality principle [1],

$$\frac{\delta j_\nu(x)}{\delta\psi_\mu(y)} = 0 \ (y \lesssim x), \quad \frac{\delta\bar{j}_\mu(y)}{\delta\bar{\psi}_\nu(x)} = 0 \ (x \lesssim y), \tag{7}$$

† All conclusions concerning reaction (2) are completely applicable to the reaction $e^- + p \to n + \nu$.

and therefore taking the first term in the expansion in the weak interaction constant C we get

$$\left\{\frac{\delta^2 S}{\delta\bar{\psi}_\nu(x)\delta\psi_\mu(y)}\,S^+\right\}_c = 0 \quad \text{for} \quad x \neq y. \tag{8}$$

This signifies that the given expression is a quasi-local operator and involves $\delta(x-y)$ and possibly its derivatives. The implication is that an equivalent Lagrangian exists which is local with respect to the meson-neutrino interaction and that the unknown matrix element (3) can be obtained by applying perturbation theory to the equivalent Lagrangian. If, as is customary, we assume that derivatives of the meson and neutrino fields do not enter the interaction Lagrangian we get

$$\left\{\frac{\delta^2 S}{\delta\bar{\psi}_\nu(x)\delta\psi_\mu(y)}\,S^+\right\}_c = \delta(x-y)\Lambda(x). \tag{9}$$

Taking into account (9) we obtain

$$\begin{aligned}
&\int e^{i(q'x-qy)}\langle p's'|\frac{\delta^2 S}{\delta\bar{\psi}_\nu(x)\delta\psi_\mu(y)}\,S^+|ps\rangle dx dy \\
&= \int e^{i(q'-q)x}\langle p's'|\Lambda(x)|ps\rangle dx \\
&= (2\pi)^4\delta(p'+q'-p-q)\langle p's'|\Lambda(0)|ps\rangle.
\end{aligned} \tag{10}$$

The expression (10) depends on the momenta p and $q'-q$ but not on the momentum $q+q'$. In a coordinate system in which $\mathbf{p}+\mathbf{p}' = 0$ this means that the expression (10) is a function of $\mathbf{p}$ and is independent of E.

Substituting (10) in (4) and taking into account relativistic invariance requirements we obtain

$$S(p, q; p', q') = \sum_{i,j}(\bar{u}_\nu(q')\hat{O}^i u_\mu(q))(\bar{u}_n(p')\hat{\Omega}_i^j u_p(p))F_{ij}(|p-p'|^2) \tag{11}$$

where $\hat{O}^i$ are basis Dirac matrices, and $\hat{\Omega}_i^j$ are operators consisting of matrices γ_μ and momenta p and p'.

A consequence of localizability of the meson-neutrino interaction is that the unknown functions of the amplitude, determined by strong interactions, depend only on transfer of momentum to the nucleon. It should be noted that the expression (11) was obtained without assuming localizability of strong interactions.

The independence of the functions F_{ij} on the momentum $q+q'$ established above can also be deduced from the usual theory by applying the Feynman graph technique. The most general form of diagrams contributing to the process is represented in fig. 1.

Since the meson and neutrino lines converge at a single point in the diagrams (this is a reflection of the localizability condition in the given

case), it is apparent that the strong interaction part of the graph depends only on the momenta p and $p-p'$ but not on $q+q'$, i.e., we again obtain the expression (11).

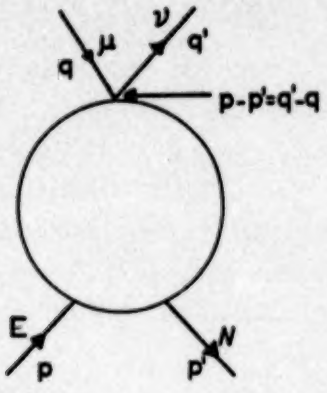

Fig. 1

It should be particularly emphasized that our main conclusion, namely, that the form factors F_{ij} depend only on momentum transfer to the nucleon, is based on the assumption of localizability of the meson-neutrino interaction but not of localizability of strong interactions.

Thus only conclusions regarding localizability of the meson-neutrino interaction can be deduced from the dispersion relations for process (2).

Indeed, if the meson-neutrino interaction is non-local (i.e., a suitable "form-factor" is introduced between appropriate lines in fig. 1), the functions F_{ij} will markedly depend on the momentum $q+q'$ †. An experimental study of this dependence should directly yield information on localizability of the meson-neutrino interaction.

A determination of the dependence of F_{ij} on momentum transfer to the nucleon should permit one to determine the "meson-neutrino" structure of the nucleon.

Comparison of the diagram in fig. 1 with diagrams for scattering of electrons on nucleons indicates that the effective dimension of the "meson-neutrino" structure of the nucleon is apparently of the same order of magnitude as that of the "electromagnetic" structure. It should also be noted that the results obtained above are completely applicable to β-decay †† and also to such hyperon and K-meson decay processes in which μ, e and ν particles participate along with strongly interacting particles †††.

† In this case, in a coordinate system in which $\mathbf{p}+\mathbf{p}' = 0$ the functions F_{ij} will depend not only on momentum transfer to the nucleon but on the energy of the incident particle as well.

†† In β-decay processes the structure functions are practically constant in virtue of the small momentum transfer to the nucleon.

††† The reaction $\mu \to e+\nu+\tilde{\nu}$ is a special case. Since only weakly interacting particles are involved here, the localizability condition is equivalent to applicability of the first approximation of perturbation theory to the usual Lagrangian.

3. K-Meson Decay

In this section we shall apply the results obtained above to K-meson decay

$$\mathrm{K} \to \pi + \mathrm{e} + \tilde{\nu}. \tag{12}$$

Assuming the K-mesons to be pseudoscalar and applying the results obtained in section 2 we arrive at the following expression for the decay amplitude

$$S(p;\ p',\ q,\ q') = G_1(|p-p'|^2)(\tilde{u}_e(q)u_\nu(q')) + \frac{G_2(|p-p'|^2)}{M}(\tilde{u}_e(q)\gamma p u_\nu(q')) + \frac{G_3(|p-p'|^2)}{M^2}(\tilde{u}_e(q)\sigma_{\mu\nu}p_\mu p'_\nu u_\nu) \tag{13}$$

where p and p' are respectively the K- and π-meson momenta, q and q' are the electron and neutrino momenta and M is the K-meson mass.

As in the foregoing it is assumed that the electron-neutrino interaction is local and does not contain derivatives. A consequence of this is that in the c.m.s. the unknown functions G_i which are determined by strong interactions, depend on the π-meson energy. Practically a verification of this fact should permit one to check the localizability of the electron-neutrino interaction. This can be done by studying the angular and energy distribution of decay products for fixed values of the π-meson energy.

The following expression for the angular distribution can readily be obtained by using formula (13) [3])

$$W(E_{p'},\ \theta) = \frac{1}{2(2\pi)^3}\{|G_1|^2(1+x\cos\theta)^2 + |G_2|^2 x^2\sin^2\theta + |G_3|^2\frac{\mathbf{p}'^2}{M^2}(x+\cos\theta)^2 - 2\,\mathrm{Im}\,G_1 G_3^*\frac{|\mathbf{p}'|}{M}(x+\cos\theta)(1+x\cos\theta)\} \times \frac{(M-E_{p'})^2(1-x^2)^2}{(1+x\cos\theta)^4}|\mathbf{p}'|E_{p'}\,dE_{p'}\sin\theta\,d\theta \tag{14}$$

where $\mathbf{p}'$ and $E_{p'}$ are respectively the π-meson momentum and energy; θ is the angle between the π-meson and electron momenta and

$$x = \frac{|\mathbf{p}'|}{M-E_{p'}};$$

the expression (14) was obtained on the assumption that the electron energy is large compared with its rest mass. The energy distribution can be written in the form

$$W(E_{p'}, E_q) = \frac{1}{(2\pi)^3}\left\{|G_1|^2(1-x^2)+|G_2|^2(x-1+2y)(x+1-2y)\right.$$
$$\left.+|G_3|^2\frac{(M-E_{p'})^2}{M^2}(1-x^2)(1-2y)^2-2\,\mathrm{Im}\,G_1 G_3^*\frac{M-E_{p'}}{M}(1-x^2)(1-2y)\right\}$$
$$\times(M-E_{p'})^2 E_{p'}\,dE_{p'}\,dE_q, \qquad (15)$$

where $\mathbf{q}$ and E_q are the electron momentum and energy and

$$y = \frac{|\mathbf{q}|}{M-E_{p'}}.$$

Comparison of formulae (14) and (15) with experimental data on the angular and energy distributions may be used to check the localizability of the electon-neutrino interaction. It should be mentioned that since the maximal decay electron energy $E_q \approx 200$ MeV, process (12) should permit one to investigate distance of the order of 10^{-13} cm. Agreement between the experimental data and formulae (15) and (16) therefore may merely indicate that the fundamental length, if it exists, does not exceed 10^{-13} cm.

4. Electromagnetic Interactions

It was mentioned in the introduction that in a number of processes involving electromagnetic interaction the "anti-Hermitian" part of the amplitude is of the same order of magnitude as the "Hermitian". The dispersion relations for these cases were derived in a number of papers [4–7]) and they will not be discussed here.

A typical process for which the "anti-Hermitian" part of the amplitude is of a higher order of smallness than the "Hermitian" is scattering of electrons on protons.

At present this process is being studied with the purpose of determining the electromagnetic structure of the nucleon [8, 9]). It is quite evident that the results obtained in section 1 are completely applicable in this case.

Summing up, it may be stated that for the processes considered above the dispersion relations are equivalent to the statement that the unknown amplitude functions, which are determined by strong interactions, depend only on momentum transfer between strongly interacting particles.

Of course, this property can be actually applied only if an analysis of radiative corrections is carried out since one must know the limits of the region in which these corrections are unimportant.

References

1) N. N. Bogolubov, Izv. Akad. Nauk, ser. fiz. **19** (1955) 237
2) N. N. Bogolubov, B. V. Medvedyev and M. K. Polivanov, Problems Related to the Theory of Dispersion Relations (in print)
3) A. Pais and S. B. Treiman, Phys. Rev. **105** (1957) 1616
4) A. A. Logunov and B. M. Stepanov, Doklady Akad. Nauk SSSR **110** (1956) 368; **112** (1957) 45
5) M. L. Goldberger, F. E. Low, G. F. Chew and Y. Nambu, Report at Seattle Conference (September 1956)
6) N. N. Bogolubov and D. V. Shirkov, Doklady Acad. Nauk (in print)
7) M. Gell-Mann, M. Goldberger and W. Thirring, Phys. Rev. **95** (1954) 1612
8) D. R. Yennie, M. M. Levy and D. G. Ravenhall, Revs. Mod. Phys. **29** (1957) 144
9) R. Hofstadter, Revs. Mod. Phys. **28** (1956) 214

Nuclear Physics **5** (1958) 390—400; © *North-Holland Publishing Co., Amsterdam*
Not to be reproduced by photoprint or microfilm without written permission from the publisher

DAMPING THEORY STUDY OF ELASTIC SCATTERING OF DIRAC PARTICLES WITH ACCOUNT OF POLARIZATION EFFECTS

A. A. SOKOLOV, B. K. KERIMOV and I. I. GUSEINOV
Physics Department, Moscow State University, Moscow, U.S.S.R.

Received 12 July 1957

Abstract: Elastic scattering of Dirac particles by a short-range force centre is considered from the standpoint of radiation damping theory. The expression for the scattering amplitude is determined. The integral equation thus obtained for the scattering amplitude permits one to investigate polarization effects.

1. Introduction

In ref. [1-4]) elastic scattering of Dirac and spinless particles by a fixed centre of force was studied by applying the damping theory. The solution for spin $\frac{1}{2}$ particles found in ref. [1, 4]) is valid only for scattering on a δ-potential. The effective cross section and phase shifts for scattering of spinless relativistic particles by a short range force centre were calculated in ref. [2, 4]).

In the present paper we extend these results to the case of elastic scattering of Dirac particles by a fixed short-range force centre with account of damping. The relation between the scattering phase shifts for Dirac and spinless particles has also been obtained by applying damping theory (see eq. (13)).

2. Free Motion of a Dirac Particle

In our investigation of elastic scattering of Dirac particles by aid of damping theory we separate the solution

$$\Psi(\mathbf{r}, t) = L^{-3/2} \sum_{\mathbf{k}, m_s=\pm\frac{1}{2}} C_{m_s} b_{m_s} \mathrm{e}^{-icKt+i\mathbf{k}\cdot\mathbf{r}} = L^{-3/2} \sum_{\mathbf{k}} \psi(\mathbf{r}, \mathbf{k}) \mathrm{e}^{-icKt} \quad (1)$$

of the free motion Dirac equation

$$\left(-\frac{\hbar}{i}\frac{\partial}{\partial t} - \frac{\hbar c}{i}(\boldsymbol{\alpha}\cdot\nabla) - \varrho_3 m_0 c^2\right)\Psi = 0 \quad (2)$$

with respect to the projection of the spin on the z-axis ($m_s = \pm\frac{1}{2}$) instead of the projection of the spin on the direction of motion, as was done in ref. [1, 4]).

Here $b_{m_s} \equiv b(\mathbf{k}, m_s, \varepsilon)$ is the Dirac spinor amplitude and the $C_{m_s} \equiv C(\mathbf{k}, m_s, \varepsilon)$ are coefficients which determine the probability that a particle will be in the state $(\mathbf{k}, m_s, \varepsilon)$, $m_s = \pm\frac{1}{2}$, $\varepsilon = \pm 1$.

Confining our attention to positive energy states ($\varepsilon = 1$) we obtain the following values for the Dirac spinor amplitude b_{m_s} which corresponds to the two values of the projection of the spin on the z-axis:

$$b_{\frac{1}{2}} = \frac{1}{\sqrt{2}} \begin{pmatrix} \sqrt{1+\frac{k_0}{K}} \\ 0 \\ \sqrt{1-\frac{k_0}{K}}\cos\theta \\ \sqrt{1-\frac{k_0}{K}}\sin\theta\, e^{i\varphi} \end{pmatrix}, \quad b_{-\frac{1}{2}} = \frac{1}{\sqrt{2}} \begin{pmatrix} 0 \\ \sqrt{1+\frac{k_0}{K}} \\ \sqrt{1-\frac{k_0}{K}}\sin\theta\, e^{-i\varphi} \\ -\sqrt{1-\frac{k_0}{K}}\cos\theta \end{pmatrix} \tag{3}$$

where θ, φ are spherical angles of wave vector $\mathbf{k}$, $E = c\hbar K = c\hbar\sqrt{k^2+k_0^2}$ is the total energy and $k_0 = m_0 c/\hbar$ is the rest mass of the particle.

Employing the familiar expansion of a plane wave in a series of spherical functions, the general solution (1) of the free motion Dirac equation which involves two types of solutions (for $j = l+\frac{1}{2}$ and $j = l-\frac{1}{2}$) can be represented in the form

$$\psi(\mathbf{r}, \mathbf{k}) = \frac{1}{\sqrt{2}} \sum_l \sum_{m=-l}^{l} g_l(kr) Y_l^{m*}\left(\frac{\mathbf{k}}{k}\right) Y_l^m\left(\frac{\mathbf{r}}{r}\right) \begin{pmatrix} \sqrt{1+\frac{k_0}{K}}\, C_{\frac{1}{2}} \\ \sqrt{1+\frac{k_0}{K}}\, C_{-\frac{1}{2}} \\ \sqrt{1-\frac{k_0}{K}}\,(C_{\frac{1}{2}}\cos\theta + C_{-\frac{1}{2}} e^{-i\varphi}\sin\theta) \\ \sqrt{1-\frac{k_0}{K}}\,(C_{\frac{1}{2}}\sin\theta\, e^{i\varphi} - C_{-\frac{1}{2}}\cos\theta) \end{pmatrix} \quad ($$

where

$$g_l(kr) = (2\pi)^{3/2} i^l (kr)^{-\frac{1}{2}} J_{l+\frac{1}{2}}(kr);$$

$J_{l+\frac{1}{2}}(kr)$ is a Bessel function and Y_l^m is an orthonormalized spherical function; l and $j = l \pm \frac{1}{2}$ are quantum numbers specifying respectively the orbital and total angular momenta and m is the quantum number of the projection of the orbital momentum on the z-axis.

3. Fundamental Integral Equation of Damping Theory and its Solution. Scattering Cross Section

Elastic scattering of Dirac particles on a fixed force centre can be described by the following damping theory integro-differential equations for the

transition coefficients C (see formulae (10) and (11) in ref. [4]); we shall employ the notations used in ref. [4])):

$$-\frac{1}{ic}\dot{C}'_{m_{s'}}=\frac{1}{c\hbar L^3}\{H^{m_{s'}m_s}_{\mathbf{k}'\mathbf{k}}\,e^{ic\Gamma' t}\,C_{m_s}+\sum_{\mathbf{k}'',\,m_{s''}}{}' H^{m_{s'}m_{s''}}_{\mathbf{k}'\mathbf{k}''}\,e^{ic(\Gamma''-\Gamma')t}\,C''_{m_{s''}}\} \tag{5}$$

$$-\frac{1}{ic}\dot{C}_{m_s}=\frac{1}{c\hbar L^3}\sum_{\mathbf{k}'',\,m_{s''}}{}' H^{m_s m_{s''}}_{\mathbf{k}\mathbf{k}''}\,e^{-ic\Gamma'' t}\,C''_{m_{s''}}+\frac{V_0}{c\hbar L^3}C_{m_s} \tag{6}$$

where

$$H^{m_{s'}m_s}_{\mathbf{k}'\mathbf{k}}=b'^{+}_{m_{s'}}V_{\mathbf{k}'\mathbf{k}}b_{m_s},\quad C_{m_s}\equiv C(\mathbf{k},\,m_s,\,t),\quad C'_{m_{s'}}\equiv C(\mathbf{k}',\,m_{s'},\,t)$$
$$b'^{+}_{m_{s'}}\equiv b^{+}(\mathbf{k}',\,m_{s'}),\quad b_{m_s}\equiv b(\mathbf{k},\,m_s),\quad \Gamma'=K'-K,\quad \Gamma''=K''-K$$
$$V_0=(V_{\mathbf{k}'\mathbf{k}})_{|\mathbf{k}-\mathbf{k}'|=0}\ \text{etc.}$$

and $V_{\mathbf{k}'\mathbf{k}}\equiv V(|\mathbf{k}-\mathbf{k}'|)$ is the Fourier component of the potential energy $V(r)$; $\hbar\mathbf{k}$, $\hbar\mathbf{k}''$ and $\hbar\mathbf{k}'$ are the particle momenta for the initial, intermediate and final states respectively.

We seek the solution of eq. (5), (6) in the form

$$C_{m_s}=e^{-c\beta_1 t+ic\beta_2 t} \tag{7}$$

$$C'_{m_{s'}}=\frac{1-e^{-c\beta_1 t+ic(\Gamma''+\beta_2)t}}{c\hbar L^3(\Gamma''+\beta_2+i\beta_1)}\sum_{l,\,n}\varepsilon_l^{(n)}H^{(n)m_{s'}m_s}_{lk'k}$$

where the index $n=1,2$ takes into account the two values of j for a given l, namely, for $n=1$, $j=l+\frac{1}{2}$ and for $n=2$, $j=l-\frac{1}{2}$.

From (5), (6) and (7) we obtain the following equations for the unknown quantities $\varepsilon_l^{(n)}$, β_1 and β_2 (see the deduction of formulae (21) and (22) in ref. [4])):

$$\begin{aligned}(\varepsilon_l^{(n)}-1)H^{(n)m_{s'}m_s}_{lk'k}&=\frac{kK}{8\pi^2 c\hbar i}\sum_{l',n',m_{s''}}\varepsilon_{l'}^{(n')}\oint d\Omega''\,H^{(n)m_{s'}m_{s''}}_{lk'k''}H^{(n')m_{s''}m_s}_{l'k''k}\\ \beta_1-i\beta_2&=\frac{kK}{8\pi^2c^2\hbar^2L^3}\sum_{l,l',n,n',m_{s''}}\varepsilon_{l'}^{(n')}\oint d\Omega''\,H^{(n)m_s m_{s''}}_{lkk''}H^{(n')m_{s''}m_s}_{l'k''k}+i\frac{V_0}{c\hbar L^3}\end{aligned} \tag{8}$$

where n and $n'=1,2$, $d\Omega''=\sin\theta''\,d\theta''\,d\varphi''$ is an element of the solid angle of vector $\mathbf{k}''$.

By expanding the Fourier component $V_{\mathbf{k}'\mathbf{k}}$ in a series in spherical functions

$$V_{\mathbf{k}'\mathbf{k}''}=\sum_{l=0}^{\infty}b_l P_l\left(\frac{\mathbf{k}'\mathbf{k}''}{k'\,k''}\right)=\sum_{l=0}^{\infty}\frac{4\pi b_l}{2l+1}\sum_{m=-l}^{l}Y_l^{\,m}\left(\frac{\mathbf{k}'}{k'}\right)Y_l^{\,m*}\left(\frac{\mathbf{k}''}{k''}\right) \tag{9}$$

we can represent the transition energy matrix element ($\mathbf{k}''\to\mathbf{k}'$) in the form

$$H^{m_{s'}m_{s''}}_{\mathbf{k}'\mathbf{k}''}=\sum_{l,\,n}H^{(n)m_{s'}m_{s''}}_{lk'k''}=\sum_{l=0}^{\infty}\frac{4\pi b_l}{2l+1}\sum_{m=-l}^{l}Y_l^{\,m}\left(\frac{\mathbf{k}'}{k'}\right)Y_l^{\,m*}\left(\frac{\mathbf{k}''}{k''}\right)b'^{+}_{m_{s'}}b''_{m_{s''}}. \tag{10}$$

With the help of formula (3) we obtain the following expression for the spin part of the transition matrix element:

$$b'^{+}_{m_s'}\, b''_{m_{s''}} = \begin{cases} \frac{1}{2}\left(1+\frac{k_0}{K}\right) + \frac{1}{2}\left(1-\frac{k_0}{K}\right)(\cos\theta'\cos\theta'' + \sin\theta'\sin\theta''\, e^{2im_{s'}(\varphi''-\varphi')}) \text{ for } m_{s''}=m_{s'} \\ m_{s'}\left(1-\frac{k_0}{K}\right)(\cos\theta'\sin\theta''\, e^{-2im_{s'}\varphi''} - \sin\theta'\cos\theta''\, e^{-2im_{s'}\varphi'}) \text{ for } m_{s''}=-m_{s'}. \end{cases} \quad (11)$$

By applying the well known recurrent relations between the functions $Y_l^m \cos\theta$, $Y_l^m \sin\theta\, e^{\pm i\varphi}$ and $Y_{l\pm1}^m$, $Y_{l\pm1}^{m\pm1}$, we may eliminate $\sin\theta\, e^{\pm i\varphi}$ and $\cos\theta$ from the matrix elements.

The matrix element component (10) which we are seeking can be transformed to

$$H^{(n)m_{s'}m_{s''}}_{\mathbf{k}'\mathbf{k}} = \frac{8\pi^2 c\hbar}{kK} c_{nl} \sum_{m_j=-j}^{j} \Omega^{(n),m_{s'}}_{l,m}\left(\frac{\mathbf{k}'}{k'}\right) \Omega^{*(n),m_{s''}}_{l,m}\left(\frac{\mathbf{k}''}{k''}\right) \quad (12)$$

where $(n = 1, 2)$

$$\begin{aligned} c_{1l} &= \tfrac{1}{2}\left(1+\frac{k_0}{K}\right) c_l + \tfrac{1}{2}\left(1-\frac{k_0}{K}\right) c_{l+1} \\ c_{2l} &= \tfrac{1}{2}\left(1+\frac{k_0}{K}\right) c_l + \tfrac{1}{2}\left(1-\frac{k_0}{K}\right) c_{l-1} \end{aligned} \quad (13)$$

and the components of the spherical spinor $\Omega^{(n)}_{l,m}$ corresponding to two values of the projection of the spin on z axis ($m_s = \pm\frac{1}{2}$) are

$$\Omega^{(n),m_s}_{l,m} = A^{(n),m_s}_{lm} Y_l^{m-m_s-\frac{1}{2}},\quad A^{(1),\frac{1}{2}}_{lm} = A^{(2),-\frac{1}{2}}_{lm} = \sqrt{\frac{l+m}{2l+1}},$$

$$-A^{(1),-\frac{1}{2}}_{lm} = A^{(2),\frac{1}{2}}_{lm} = \sqrt{\frac{l-m+1}{2l+1}},\quad m_j = m-\tfrac{1}{2}.$$

The c_l determine the scattering phase shifts for a spinless relativistic particle; according to (9) they are equal to (see also (48), (52) in ref. [4])) †

$$c_l = -\operatorname{tg}\eta_l = \frac{\pi K}{c\hbar}\int_0^\infty rV(r) J^2_{l+\frac{1}{2}}(kr)\mathrm{d}r. \quad (14)$$

The orthogonality condition of damping theory can be obtained for the matrix element components by taking into account the conditions of orthonormalization for the spherical spinors $\Omega^{(n)}_{l,m}$ (see also ref. [5]):

$$\begin{aligned} \sum_{m_{s''}} \oint \mathrm{d}\Omega''\, H^{(n)m_{s'}m_{s''}}_{\mathbf{k}'\mathbf{k}''} H^{(n')m_{s''}m_s}_{\mathbf{l}'\mathbf{k}''\mathbf{k}} &= \frac{8\pi^2 c\hbar}{kK} c_{nl}\delta_{nn'}\delta_{ll'} H^{(n)m_{s'}m_s}_{\mathbf{l}\mathbf{k}'\mathbf{k}} \\ \sum_{m_{s''}} \oint \mathrm{d}\Omega''\, H^{(n)m_s m_{s''}}_{\mathbf{l}\mathbf{k}\mathbf{k}''} H^{(n')m_{s''}m_s}_{\mathbf{l}'\mathbf{k}''\mathbf{k}} &= \frac{16\pi^3 c^2\hbar^2}{k^2K^2} c_{nl}\delta_{nn'}\delta_{ll'}(l+(2-n)). \end{aligned} \quad (15)$$

Taking into account (15) we find from equation (8) the following values for $\varepsilon_l^{(1)}$ and $\varepsilon_l^{(2)}(n = 1, 2)$:

† A minus sign should be written in front of coefficient c_l in eq. (52) of ref. [4]).

$$\varepsilon_l^{(n)} = \frac{1}{1+ic_{nl}}. \tag{16}$$

According to damping theory the differential effective cross section for elastic scattering is given by the formula (see the deduction of formula (23) in ref. [4]))

$$\mathrm{d}\sigma_{m_s' m_s} = \frac{L^3 K}{ck} \frac{\partial}{\partial t} \sum_{\mathbf{k}'} C'^{+}_{m_s'} C'_{m_s'} = |f_{m_s' m_s}(\mathbf{k}', \mathbf{k})|^2 \, \mathrm{d}\Omega' \tag{17}$$

where the scattering amplitude is

$$f_{m_s' m_s}(\mathbf{k}', \mathbf{k}) = \frac{K}{2\pi c\hbar} \sum_l \sum_{n=1,2} \varepsilon_l^{(n)} H^{(n) m_s' m_s}_{l\mathbf{k}'\mathbf{k}} \tag{18}$$

Directing the initial momentum $\mathbf{k}$ along axis z ($\theta = \varphi = 0$) we reduce the scattering amplitude (18) to the following form with aid of (12) and (16):

$$f_{m_s\, m_s}(\theta', \varphi') = -\frac{1}{k} \sum_{l=0}^{\infty} \begin{cases} \left[(l+1) \dfrac{c_{1l}}{1+ic_{1l}} + l \dfrac{c_{2l}}{1+ic_{2l}} \right] P_l(\cos\theta') & \text{for } m_{s'} = m_s \\ \left[\dfrac{c_{1l}}{1+ic_{1l}} - \dfrac{c_{2l}}{1+ic_{2l}} \right] 2m_{s'} P_l^1(\cos\theta') \mathrm{e}^{-2im_{s'}\varphi'} & \text{for } m_{s'} = -m_s. \end{cases} \tag{19}$$

Averaging over the initial spin states and summing over the final spin states we arrive at the following damping theory expressions for the total effective cross section:

$$\sigma = \frac{4\pi}{k^2} \sum_{l=0}^{\infty} [(l+1) \sin^2 \eta_l^{(1)} + l \sin^2 \eta_l^{(2)}] \tag{20}$$

where

$$\sin^2 \eta_l^{(1)} = \frac{c_{1l}^2}{1+c_{1l}^2}, \quad \sin^2 \eta_l^{(2)} = \frac{c_{2l}^2}{1+c_{2l}^2}, \tag{21}$$

and for the differential effective scattering cross section for a Dirac particle:

$$\mathrm{d}\sigma = \tfrac{1}{2} \sum_{m_s, m_s'} \mathrm{d}\sigma_{m_s, m_s'} = \{|f(\theta')|^2 + |g(\theta')|^2\} \mathrm{d}\Omega' \tag{22}$$

where

$$\begin{aligned} f(\theta') &= \frac{1}{2ik} \sum_{l=0}^{\infty} [(l+1)(\mathrm{e}^{2i\eta_l^{(1)}} - 1) + l(\mathrm{e}^{2i\eta_l^{(2)}} - 1)] P_l(\cos\theta') \\ g(\theta') &= \frac{1}{2ik} \sum_{l=0}^{\infty} [-\mathrm{e}^{2i\eta_l^{(1)}} + \mathrm{e}^{2i\eta_l^{(2)}}] P_l^1(\cos\theta'). \end{aligned} \tag{23}$$

On deducing (23) it was taken into account that

$$c_{1l} = -\operatorname{tg} \eta_l^{(1)}, \quad c_{2l} = -\operatorname{tg} \eta_l^{(2)}. \tag{24}$$

The quantities c_{1l} and c_{2l} are defined by formulae (13). For $\eta_l^{(1)} = \eta_l^{(2)}$ (i.e., $c_{1l} = c_{2l}$) formula (20) goes over to the expression for the total effective

cross section for elastic scattering of a spinless particle (see formula (50) in ref. [4])).

If, in particular, c^2_{1l} and c^2_{2l} can be neglected in comparison with unity in the denominators of formula (21) (neglection of damping effect) we obtain the following expression for the effective cross section:

$$\sigma = \frac{4\pi}{k^2} \sum_{l=0}^{\infty} (2l+1) \frac{K^2+k_0^2}{2K^2} \left\{ c_l^2 + \frac{k^2}{K^2+k_0^2} \left[\frac{l+1}{2l+1} c_l c_{l+1} + \frac{l}{2l+1} c_l c_{l-1} \right] \right\} \quad (25)$$

which can easily be obtained from perturbation theory.

In the case of a δ-like scattering potential, $V(r) = V_0 \delta(\mathbf{r})$ we get in accord with (14)

$$c_l = V_0 \frac{kK}{2\pi c\hbar} \delta_{l0}.$$

The non-vanishing phase shifts in this case will be

$$c_{1l} = \frac{V_0}{4\pi c\hbar} k(K+k_0)\delta_{l0} \equiv \delta_1 \quad \text{for } l = 0,$$

$$c_{2l} = \frac{V_0}{4\pi c\hbar} k(K-k_0)\delta_{l1} \equiv \delta_2 \quad \text{for } l = 1.$$

Hence for the total effective cross section for elastic scattering of a Dirac particle by a δ-potential we obtain the expression

$$\sigma = \frac{4\pi}{k^2} \left(\frac{\delta_1^2}{1+\delta_1^2} + \frac{\delta_2^2}{1+\delta_2^2} \right)$$

which is identical with the corresponding expression (36) in ref. [4]).

Using relations (15), (16) and (20) we obtain from the second equation in (8) for β_1 and β_2 the following expressions

$$c\beta_1 = \frac{\sigma N_0}{2}$$

$$c\beta_2 = \frac{\sigma N_0}{2} \frac{\sum_l [(l+1) \sin^2 \eta_l^{(1)} \operatorname{tg} \eta_l^{(1)} + l \sin^2 \eta_l^{(2)} \operatorname{tg} \eta_l^{(2)}]}{\sum_l [(l+1) \sin^2 \eta_l^{(1)} + l \sin^2 \eta_l^{(2)}]} - \frac{V_0}{\hbar L^3}$$

where $N_0 = ck/L^3K$. It follows from here that for $L \to \infty$, β_1 and β_2 tend to zero. It can moreover be shown with the help of the latter relation that the coefficients C will satisfy the normalization relation [5])

$$C^+_{m_s} C_{m_s} + \sum_{k', m_{s'}}{}' C'^+_{m_{s'}} C'_{m_{s'}} = 1.$$

4. Polarization of Elastically Scattered Dirac Particles

In studying polarization phenomena with the aid of damping thecry it will be convenient to use the solution of the free Dirac equation which is

separated with respect to the projection of the spin on the direction of motion ($s = \pm 1$). Strictly speaking, the projection of the spin on the direction of motion ($\mathbf{k}$), as well as that on the z axis can take the values $\pm\frac{1}{2}$ in $\hbar$ units. In order to distinguish these two possible cases we shall characterize the first projection by the doubled value $s = \pm 1$ and the second by the value $m_s = \pm\frac{1}{2}$. The relation between coefficients C_s and C_{m_s} can be easily established by equating the matrices

$$\sum_{s=\pm 1} C_s b_s = \sum_{m_s=\pm\frac{1}{2}} C_{m_s} b_{m_s}. \tag{26}$$

Here the Dirac spinor amplitude $b_s \equiv b_s(\mathbf{k})$ is defined by the formula (see (5) in ref. [4]))

$$b_s = \frac{1}{\sqrt{2}} \begin{pmatrix} \sqrt{1+\dfrac{k_0}{\varepsilon K}}\cos\theta_s \\ \sqrt{1+\dfrac{k_0}{\varepsilon K}}\sin\theta_s\, e^{i\varphi} \\ s\varepsilon\sqrt{1-\dfrac{k_0}{\varepsilon K}}\cos\theta_s \\ s\varepsilon\sqrt{1-\dfrac{k_0}{\varepsilon K}}\sin\theta_s\, e^{i\varphi} \end{pmatrix} \tag{27}$$

where $\theta_s = \frac{1}{2}\theta - \frac{1}{4}\pi\,(1-s)$; θ, φ are spherical angles of vector $\mathbf{k}$, $s = \pm 1$ and $s' = \pm 1$ should characterize the projection of the spin along or opposite the direction of motion before and after scattering.

In order to describe polarization phenomena connected with elastic scattering we shall proceed from the following integral equation of damping theory for the spin part of the scattering amplitude $f'_{s'} \equiv f_{s'}(\mathbf{k}')$ [4])

$$(f'_{s'} - b'^{+}_{s'} b_s f_s) V_{\mathbf{k}'\mathbf{k}} = \frac{kK}{8\pi^2 c\hbar i} \sum_{s''} \oint d\Omega'' V_{\mathbf{k}'\mathbf{k}''} V_{\mathbf{k}''\mathbf{k}} b'^{+}_{s'} b''_{s''} f''_{s''}. \tag{28}$$

Here $f_s \equiv f_s(\mathbf{k})$ is the amplitude pertaining to the polarization of the incident beam, $E = c\hbar K$ is the total particle energy and $V_{\mathbf{k}'\mathbf{k}}$ is the Fourier component of the potential energy $V(r)$.

Consider the polarization of a Dirac particle elastically scattered by a δ-potential

$$V(r) = V_0\,\delta(\mathbf{r}),\quad V_{\mathbf{k}'\mathbf{k}''} = V_{\mathbf{k}'\mathbf{k}} = V_{\mathbf{k}''\mathbf{k}} = V_0.$$

In this case the spin part of the matrix element should be divided into two parts:

$$b'^{+}_{s'} b''_{s''} = \sum_{j=1,2} h^{(j)}_{s's''} \tag{29}$$

where

$$h^{(1)}_{s's''} = \tfrac{1}{2}\left(1+\frac{k_0}{K}\right)[\cos\theta'_{s'}\cos\theta''_{s''}+\sin\theta'_{s'}\sin\theta''_{s''}\,e^{i(\varphi''-\varphi')}]$$

$$h^{(2)}_{s's''} = \tfrac{1}{2}\left(1-\frac{k_0}{K}\right)s's''[\cos\theta'_{s'}\cos\theta''_{s''}+\sin\theta'_{s'}\sin\theta''_{s''}\,e^{i(\varphi''-\varphi')}]$$

satisfy the orthogonality condition ($j, j' = 1, 2$)

$$\sum_{s''}\oint d\Omega''\, h^{(j)}_{s's''}h^{(j')}_{s''s} = 2\pi\left[1-(-1)^j\frac{k_0}{K}\right]h^{(j)}_{s's}\delta_{jj'}. \tag{30}$$

We seek the solution of the integral equation (28) in the form ($s' = 1, -1$)

$$f'_{s'} = \sum_{j=1,2}\varepsilon_j h^{(j)}_{s's}f_s. \tag{31}$$

Taking into account (29), (30) we find from (28), (31) the values of the unknown quantities ε_1 and ε_2:

$$\varepsilon_{1,2} = \frac{1}{1+i\delta_{1,2}}, \quad \delta_{1,2} = \frac{V_0}{4\pi c\hbar}k(K\pm k_0). \tag{32}$$

From (31), (29) we find the values for the first scattering ($s' = \pm 1$) amplitudes $f'_{s'}$:

$$\begin{aligned} f'_1 &= \frac{1}{2K}[(K+k_0)\varepsilon_1+(K-k_0)\varepsilon_2]\cos\frac{\theta'}{2}f_1-\frac{1}{2K}[(K+k_0)\varepsilon_1 \\ &\qquad -(K-k_0)\varepsilon_2]\,e^{-i\varphi'}\sin\frac{\theta'}{2}f_{-1} \\ f'_{-1} &= \frac{1}{2K}[(K+k_0)\varepsilon_1-(K-k_0)\varepsilon_2]\sin\frac{\theta'}{2}f_1+\frac{1}{2K}[(K+k_0)\varepsilon_1 \\ &\qquad +(K-k_0)\varepsilon_2]\,e^{-i\varphi'}\cos\frac{\theta'}{2}f_{-1} \end{aligned} \tag{33}$$

where θ', φ' are angles corresponding to the first scattering event ($\mathbf{k}'$).

In the case of an unpolarized incident beam,

$$f_1^*f_1+f_{-1}^*f_{-1} = 1,\ f_1^*f_1-f_{-1}^*f_{-1} = f_1^*f_{-1} = f_{-1}^*f_1 = 0,$$

we can use (33) to obtain the following expressions for the amplitude ($\mathcal{P}'_1$) and phase ($\mathcal{P}'_2, \mathcal{P}'^*_2$) polarization after the first scattering ($\mathbf{k} \parallel z$ axis):

$$\begin{aligned} \mathcal{P}'_1 &\equiv f_1'^*f'_1-f'^*_{-1}f'_{-1} = 0 \\ \mathcal{P}'_2 &\equiv f_1'^*f'_{-1} = i\frac{k^2(\delta_2-\delta_1)}{2K^2(1+\delta_1^2)(1+\delta_2^2)}\sin\frac{\theta'}{2}\cos\frac{\theta'}{2} = -\mathcal{P}'^*_2 \\ \mathcal{P}' &\equiv f_1'^*f_1'+f'^*_{-1}f'_{-1} = \tfrac{1}{4}\left[\frac{\left(1+\frac{k_0}{K}\right)^2}{1+\delta_1^2}+\frac{\left(1-\frac{k_0}{K}\right)^2}{1+\delta_2^2}+2\frac{k^2}{K^2}\frac{(1+\delta_1\delta_2)\cos\theta'}{(1+\delta_1^2)(1+\delta_2^2)}\right]. \end{aligned} \tag{34}$$

Replacing θ', φ' and f_1, f_{-1} in the right hand side of (33) by θ'', φ'' and f'_1, f'_{-1} we obtain the respective expressions for the secondary scattering amplitudes $f''_{s''} \equiv f_{s''}(\mathbf{k}'')$ ($\mathbf{k}' \parallel z'$ axis).

The differential cross section for secondary scattering is connected with $f'_{s'}$ and $f''_{s''}$ by the relation (see the deduction of (23) in ref. [4]))

$$d\sigma = \frac{1}{N}\frac{\partial}{\partial t}\sum_{\mathbf{k}'',\,s''} C''^{+}_{s''} C''_{s''} = \frac{K^2}{4\pi^2 c^2 \hbar^2}|V_{\mathbf{k}''\mathbf{k}'}|^2 \frac{\sum_{s''=\pm 1} f''^{*}_{s''} f''_{s''}}{\sum_{s'=\pm 1} f'^{*}_{s'} f'_{s'}} d\Omega'' \tag{35}$$

where $d\Omega'' = \sin\theta''\, d\theta'' d\varphi''$; θ'', φ'' are angles corresponding to secondary scattering and $k' = k'' = k$.

Hence, taking into account (32)—(34) we find the following expression from damping theory for the differential effective cross section for double scattering of an initially unpolarized beam of Dirac particles by a δ-potential

$$\sigma(\theta'', \varphi'') = \sigma_0(\theta'')[1+\varepsilon(\theta', \theta'')\cos\varphi''] \tag{36}$$

where

$$\begin{aligned} \varepsilon(\theta', \theta'') = P(\theta')P(\theta'') &= \left(\frac{V_0^2}{4\pi^2 c^2 \hbar^2}\right)^2 \frac{k^4(\delta_2-\delta_1)^2}{4(1+\delta_1^2)^2(1+\delta_2^2)^2} \cdot \frac{\sin\theta' \sin\theta''}{\sigma_0(\theta')\sigma_0(\theta'')} \\ \cos\varphi' &= \mathbf{n}' \cdot \mathbf{n}'' = \frac{(\mathbf{k}' \wedge \mathbf{k}) \cdot (\mathbf{k}'' \wedge \mathbf{k}')}{|\mathbf{k}' \wedge \mathbf{k}||\mathbf{k}'' \wedge \mathbf{k}'|}; \end{aligned} \tag{37}$$

$P(\theta')$ and $P(\theta'')$ are the polarizations acquired by the initially unpolarized beam during the first and second scattering events respectively; $\mathbf{n}'$ and $\mathbf{n}''$ are unit vectors for both polarization directions; $\sigma_0(\theta')$ is the damping theory differential effective cross section for scattering of an unpolarized beam by a δ-potential (see (35) in ref. [4])):

$$\sigma_0(\theta') = \frac{V_0^2 K^2}{16\pi^2 c^2 \hbar^2}\left[\frac{\left(1+\frac{k_0}{K}\right)^2}{1+\delta_1^2} + \frac{\left(1-\frac{k_0}{K}\right)^2}{1+\delta_2^2} + 2\frac{k^2}{K^2}\frac{(1+\delta_1\delta_2)\cos\theta'}{(1+\delta_1^2)(1+\delta_2^2)}\right].$$

It can be seen from (37) that in the first approximation of perturbation theory ($\delta_1 = \delta_2 \approx 0$) no polarization should appear as a consequence of scattering on a δ-potential.

For high energy incident particles, $k \gg (4\pi c\hbar/V_0)^{\frac{1}{2}}$ ($\delta_1^2 \gg 1$, $\delta_2^2 \gg 1$) we obtain in the case of two identical scattering events ($\theta'' = \theta'$, $P(\theta'') = P(\theta')$) the following expression for the degree of polarization

$$\varepsilon(\theta', \theta') = [P(\theta')]^2 = \left(\frac{4\pi c\hbar}{V_0}\right)^2 \frac{4k_0^2}{k^6} \operatorname{tg}^2\frac{\theta'}{2}.$$

As can be seen from (36) asymmetry of secondary scattering is yielded only by phase polarization ($f'^{*}_1 f'_{-1} \neq 0$) which appears after the first scattering.

If the incident beam possesses only amplitude polarization $f_1^* f_1 - f_{-1}^* f_{-1} \neq 0$, $f_1^* f_{-1} = f_{-1}^* f_1 = 0$, the differential effective cross section for elastic scattering of a Dirac particle by a force centre is given in the first Born approximation ($\beta_1 = \beta_2 = 0$, $\varepsilon = 1$) by the following formula:

$$d\sigma_{ss'} = \frac{L^3 K}{ck} \frac{\partial}{\partial t} \sum_{\mathbf{k}'} C'^{+}_{s'} C'_{s'}$$

$$= \frac{K^2}{4\pi^2 c^2 \hbar^2} |V_{\mathbf{k}'\mathbf{k}}|^2 \cdot \tfrac{1}{2} \sum_{s=\pm 1} \left[(1+ss') \cos^2 \frac{\theta'}{2} + (1-ss') \frac{k_0^2}{K^2} \sin^2 \frac{\theta'}{2} \right] f_s^* f_s \, d\Omega'. \tag{38}$$

Hence the ratio of the effective cross section without spin flip ($ss' = 1$) to the cross section with spin flip ($ss' = -1$) is

$$\frac{d\sigma^{\uparrow\uparrow}}{d\sigma^{\uparrow\downarrow}} = \frac{K^2}{k_0^2} \operatorname{ctg}^2 \frac{\theta'}{2}. \tag{39}$$

If only terms which are linear with respect to V_0 are retained in formulae (33) (second approximation in perturbation theory) the expression for the first scattering amplitude will have the form

$$f'_1 = (1-id) \left[(1+ia) \cos \frac{\theta'}{2} f_1 - \frac{k_0}{K} \sin \frac{\theta'}{2} e^{-i\varphi'} f_{-1} \right]$$

$$f'_{-1} = (1-id) \left[\frac{k_0}{K} \sin \frac{\theta'}{2} f_1 + (1+ia) e^{-i\varphi'} \cos \frac{\theta'}{2} f_{-1} \right] \tag{40}$$

where

$$a = \frac{V_0}{4\pi c\hbar} \frac{k^3}{K}, \quad d = \frac{V_0}{2\pi c\hbar} kK.$$

In the case of an arbitrary scattering centre, possessing spherical symmetry, the coefficients a and d will be defined by the equations [6])

$$a = \frac{k^3}{16\pi^2 c\hbar K V_{\mathbf{k}'\mathbf{k}}} \oint d\Omega'' V_{\mathbf{k}'\mathbf{k}''} V_{\mathbf{k}''\mathbf{k}} \frac{(\mathbf{k}-\mathbf{k}'') \cdot (\mathbf{k}+\mathbf{k}')}{\mathbf{k} \cdot (\mathbf{k}+\mathbf{k}')},$$

$$d = \frac{kK}{8\pi^2 c\hbar V_{\mathbf{k}'\mathbf{k}}} \oint d\Omega'' V_{\mathbf{k}'\mathbf{k}''} V_{\mathbf{k}''\mathbf{k}}. \tag{41}$$

It should be noted that the coefficient d does not influence the polarization. On the other hand the coefficient a does not diverge even in the case of a Coulomb centre and therefore these approximate formulae lead, in the case of Coulomb scattering, to the well known Mott polarization formula [7])

$$a = -\frac{Ze^2}{c\hbar} \frac{k}{K} \operatorname{tg}^2 \frac{\theta'}{2} \ln \operatorname{cosec} \frac{\theta'}{2}.$$

In conclusion it should be noted that in a first approximation perturbation theory does not predict polarization effects. Therefore, in order to describe polarization effects in a first approximation spin-orbit interaction

is introduced. As is well known, the Dirac theory automatically takes into account spin-orbit interaction in the following approximation. As a result it appears that damping theory which also takes into account the following approximations can describe polarization.

References

1) A. Sokolov and B. Kerimov, Doklady Akad. Nauk SSSR **105** (1955) 961
2) A. Sokolov and B. Kerimov, Doklady Akad. Nauk SSSR **108** (1956) 611
3) A. Sokolov and B. Kerimov, JETP **31** (1957) 1080
4) A. Sokolov and B. Kerimov, Nuovo Cimento **5** (1957) 921
5) A. Sokolov, Journ. of Phys. USSR **5** (1941) 213
6) A. Sokolov, Journ. of Phys. USSR **9** (1945) 363
7) N. Mott, Proc. Roy. Soc. A **124** (1929) 425

Nuclear Physics **5** (1958) 401—404; © *North-Holland Publishing Co., Amsterdam*
Not to be reproduced by photoprint or microfilm without written permission from the publisher

LIFETIME OF THE FIRST ROTATIONAL STATE OF Gd^{156}

OVE NATHAN
Institute for Theoretical Physics, University of Copenhagen

Received 10 October 1957

Abstract: The half-life of the 89 keV state of Gd^{156} has been measured by means of a fast-slow coincidence circuit. From the observed value $T_{\frac{1}{2}} = (1.9 \pm 0.1) \times 10^{-9}$ sec the reduced E2 transition probability can be calculated. One finds $B(E2;\ I_0 \to I_1) : e^2 = (5.1 \pm 0.3) \times 10^{-48}$ cm^4 in good agreement with the Coulomb excitation result of Ramšak *et al.* [4]).

1. Introduction

The cross section for Coulomb excitation of the first rotational state of Gd^{156} has been determined by several investigators. Heydenburg and Temmer [1]) and Mark and Paulissen [2]) measured the yield of 89 keV gamma rays following Coulomb excitation, whereas Huus *et al.* [3]) observed the L conversion electrons emitted in the decay of the first excited state. Recently, Ramšak *et al.* [4]) redetermined the cross section by the more direct measurement of the inelastically scattered protons. However, quite serious discrepancies exist in the values of $B(E2)$, the reduced transition probability, resulting from these investigations. This note describes an independent determination of $B(E2)$ from a measurement of the lifetime of the 89 keV level in Gd^{156} excited in the K capture decay of 5.6 d Tb^{156}.

2. Results and Discussion

The apparatus consists of a conventional fast-slow coincidence system utilizing RCA 6342 photomultipliers operated at about 1800 volts and a Philco IN 263 diode mixer. The detectors are plastic scintillators (Nucl. Enterpr. Ltd., NE 102), 5 cm diam. × 5 cm and 1 cm diam. × 0.2 mm, respectively. The overall fast-slow resolving time 2τ is set for $\approx 4 \times 10^{-9}$ sec. Delays into either channel could be introduced by inserting lengths of 220 Ω cable (Transradio Ltd.).

A 10 μC source of Tb^{156} was produced by the Eu^{153} (α, n) Tb^{156} reaction in the Institute's cyclotron and subsequent ion exchange. The chemical procedure is described elsewhere [5]). The resulting source was positioned on a 150 $\mu g/cm^2$ aluminium foil and had a thickness of $\approx$ 100 $\mu g/cm^2$. For optimum detection of soft conversion electrons, the source was placed

directly on the thin scintillator with the activity side facing the detector. The single channel analyser in this side was set with a broad window to accept mainly the L electrons of the 89 keV transition. The other scintillator was covered with a 3 mm lead absorber and served as a detector for the high energy γ-rays feeding the 89 keV level in Gd^{156} [5]). The analyser in this channel was used as an integral discriminator, accepting γ-rays from 300 keV and upwards. The resulting delayed coincidence curve is shown in fig. 1 together with the "prompt" curve obtained under identical

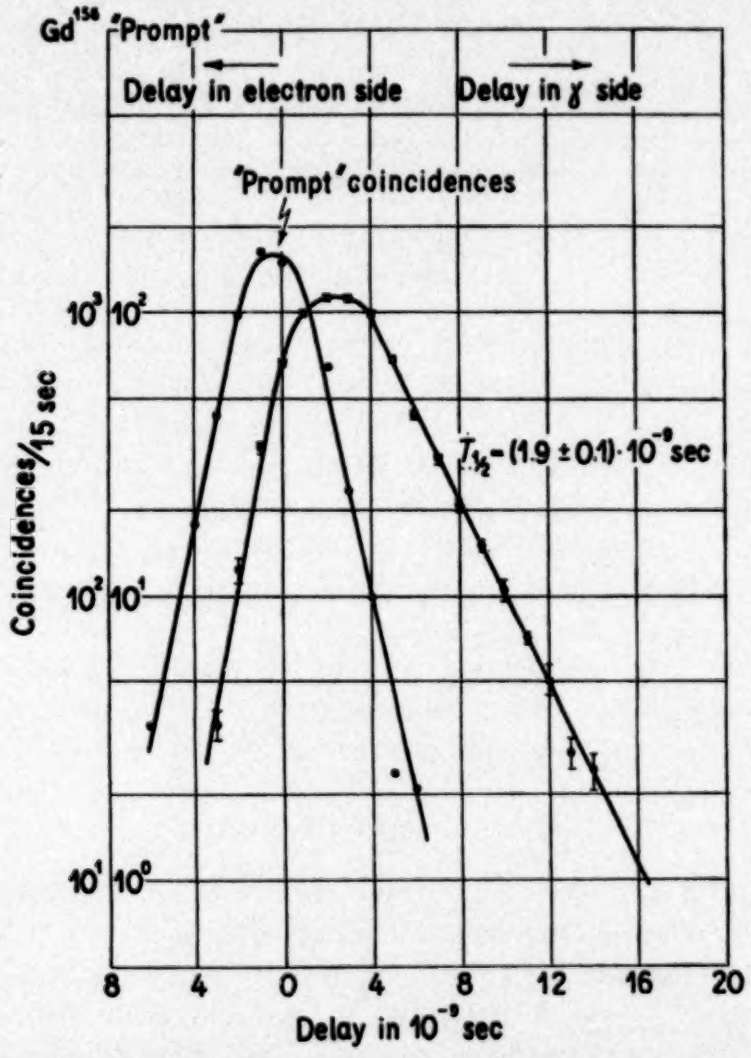

Fig. 1. Time distribution of coincidences between L conversion electrons of the 89 keV transition and high energy γ-rays of Gd^{156}. The "prompt" curve represents measurements with a Na^{22} source and unchanged channel positions. The half-life has been obtained by the "exponential tail" method rather than by centroid analysis, since the single channels, for reasons of counting rate, were operated with wide window selection and integral bias, respectively. Centroid analysis of the resolution curve [6-7]) can be performed only when the input pulse size is under rigorous control.

experimental conditions, except for the Tb^{156} source which was replaced by a source of Na^{22}. As a check on the measured half-life $T_{\frac{1}{2}} = (1.9+0.1) \times$

10^{-9} sec, the half-life of the 87 keV level in Dy^{160} was measured with the same technique, and a value of 1.8×10^{-9} sec was obtained, in perfect agreement with the experiment of Sunyar [8]).

The radiative mean life τ_γ is related to the experimental half-life $T_{\frac{1}{2}}$ by $\tau_\gamma = T_{\frac{1}{2}} \cdot (1+\alpha)/\ln 2$, where α is the total internal conversion coefficient. We have calculated α for the 89 keV E2 transition in Gd^{156} by using Sliv's K conversion coefficients [9]) and the K/L ratio which can be found by interpolation from Rose's tables of K and L conversion coefficients [10]). Conversion in the higher shells were taken as 1/3 of the total L conversion. In this way one obtains $\alpha = 4.1$ and $\tau_\gamma = (1.40\pm0.07)\times10^{-8}$ sec. For an electric quadrupole transition, the transition probability is given by [11])

$$\frac{1}{\tau_\gamma} = \frac{4\pi}{75}\cdot\frac{1}{\hbar}\left(\frac{\Delta E}{\hbar/c}\right)^5 \cdot B(\mathrm{E2}),$$

where ΔE is the γ-ray energy. By inserting the appropriate values for τ_γ and ΔE we obtain the result

$$B(\mathrm{E2}) : e^2 = (1.02\pm0.05)\times10^{-48}\ \mathrm{cm}^4,$$

where e is the electronic charge.

The reduced transition probability that enters into the expressions for the Coulomb excitation cross sections is related to the $B(\mathrm{E2})$ of the radiative decay by the formula

$$B(\mathrm{E2};\ I_0 \to I_f) = B(\mathrm{E2};\ I_f \to I_0)\cdot\frac{2I_f+1}{2I_0+1},$$

where I_0 and I_f are the spins of the ground state and the excited state, respectively. In the case of Gd^{156}, $I_0 = 0$ and $I_f = 2$, and one obtains

$$B(\mathrm{E2};\ I_0 \to I_f) : e^2 = (5.1\pm0.3)\times10^{-48}\ \mathrm{cm}^4.$$

This value is in good agreement with the most recent Coulomb excitation result

$$B(\mathrm{E2};\ I_0 \to I_f) : e^2 = (4.50\pm0.25)\times10^{-48}\ \mathrm{cm}^4,$$

given by Ramšak *et al.* [4]), whereas the earlier determinations [1–3]) of this quantity appear to deviate somewhat more from our value than expected from the reported experimental errors. It seems very likely that these discrepancies are associated with the difficulties involved in measuring absolute cross sections with the techniques presently available.

The author wishes to express his gratitude to professor Niels Bohr for the excellent working conditions offered at his Institute. He is very indebted to Mr. Gregers Hansen for having put the source of Tb^{156} at his disposal and to Mr. Ingvar Marklund, The Physical Institute Uppsala, for assistance in obtaining the data.

References

1) N. P. Heydenburg and G. M. Temmer, Phys. Rev. **100** (1955) 150, and privately circulated revisions of yield determinations
2) H. Mark and G. T. Paulissen, Phys. Rev. **100** (1955) 813
3) T. Huus, J. H. Bjerregaard and B. Elbek, Mat. Fys. Medd. Dan. Vid. Selsk. **30** (1956) no. 17
4) V. Ramšak, M. Olesen and B. Elbek, to be published in Nuclear Physics
5) P. Gregers Hansen, O. B. Nielsen and R. Sheline, to be published
6) Z. Bay, Phys. Rev. **77** (1950) 419
7) T. D. Newton, Phys. Rev. **78** (1950) 490
8) A. W. Sunyar, Phys. Rev. **98** (1955) 653
9) L. A. Sliv and J. M. Band, Tables of Gamma-Ray Internal Conversion Coefficients, Part 1 (Isdatelstvo Akademia Nauk SSSR; Moscow and Leningrad, 1956)
10) M. E. Rose, in Beta- and Gamma-Ray Spectroscopy, edited by K. Siegbahn (North Holland Publishing Company, Amsterdam, 1955); and M. E. Rose, G. H. Goertzel and C. J. Swift, privately circulated tables of K- and L-conversion coefficients
11) A. Bohr and B. R. Mottelson, Mat. Fys. Medd. Dan. Vid. Selsk. **27** (1953) no. 16

Nuclear Physics **5** (1958) 405—408; © *North-Holland Publishing Co., Amsterdam*
Not to be reproduced by photoprint or microfilm without written permission from the publisher

PARITY NON-CONSERVATION AND TRANSVERSE POLARIZATION OF β-PARTICLES

G. GYÖRGYI and H. ÜBERALL
École d'Été de Physique Théorique, Les Houches, Haute Savoie, France

Received 26 August 1957

Lee and Yang's powerful idea [1]) of parity violation in weak interactions stimulated extensive experimental research on the asymmetry of β-radiations from oriented nuclei [2]) as well as on the longitudinal polarization of the β-particles [3]). For pure Gamow-Teller transitions, the results fit within their limit of accuracy the two component neutrino theory of Landau, Lee and Yang and Salam. At present there is however no definite evidence whether Fermi transitions can be described in a consistent manner in terms of the two component theory †. At this state of affairs it seems desirable to have more independent methods available for obtaining information on the form of the β-decay Hamiltonian.

One possibility may be offered by observing the transverse polarization of β-particles which is present if the direction of the neutrino momentum is known with respect to the direction of the electron emission. In practice, a gaseous β-active substance may be brought into a cloud chamber and the decay electron and recoil of the nucleus observed ††. (Such a method was used recently [4]) to determine the electron-neutrino angular correlation in the decay of He^6.) Detection of the transverse electron polarization may proceed in a most natural way by measuring the asymmetry of Coulomb scattering of the electrons by the nuclei of the gas filling the chamber. (For this purpose a heavy gas like Xe seems to be appropriate.)

For a calculation of the electron polarization with given electron and neutrino momenta we use the general parity non-conserving Hamiltonian of Lee and Yang [1]) (in the non relativistic approximation for the nucleons):

$$H = \sum_{K} (\psi_p^+ O_K^N \psi_n) \left(\psi_e^+ O_K^L \frac{C_K + C'_K \gamma_5}{2} \psi_\nu \right) + \text{H.c.} \qquad (1)$$

K	S	V	T	A
O_K^N	1	1	σ	σ
O_K^L	γ_4	1	$\gamma_4\sigma$	σ

† C. N. Yang, private communication.
†† We are indebted to G. Hrehuss for having suggested this experimental possibility.

We calculate the squared transition matrix element from an initial neutron (proton) state to a final state containing a proton (neutron), a $\beta^{\mp}$-particle with momentum $\mathbf{p}$ and spin $\frac{1}{2}\mathbf{s}$ (in the rest system of the electron) and an antineutrino (neutrino) with momentum $\mathbf{q}$. If we choose $\mathbf{p}$ as z-axis and introduce $\mathbf{q}$ $(q\sin\vartheta,\ 0,\ q\cos\vartheta)$, $\mathbf{s}$ $(\sin\theta\cos\phi,\ \sin\theta\sin\phi,\ \cos\theta)$ the result is after the usual averaging over initial spins and summing over final nucleon and neutrino spins (assuming plane waves for the electron):

$$
\begin{aligned}
|H(\mathbf{p},\mathbf{s},\mathbf{q})|^2 &= [(a_{SS}+a_{VV})|M_F|^2+(a_{TT}+a_{AA})|M_{GT}|^2] \\
&+[(b_{SS}-b_{VV})|M_F|^2+(b_{TT}-b_{AA})|M_{GT}|^2]\frac{p}{E}\cos\theta \\
&-[(a_{SS}-a_{VV})|M_F|^2-\tfrac{1}{3}(a_{TT}-a_{AA})|M_{GT}|^2]\frac{p}{E}\cos\vartheta \\
&\mp[(b_{SS}+b_{VV})|M_F|^2-\tfrac{1}{3}(b_{TT}+b_{AA})|M_{GT}|^2]\left(\cos\vartheta\cos\theta+\frac{m}{E}\sin\vartheta\sin\theta\cos\phi\right) \\
&\pm\frac{m}{E}[(a_{SV}+a_{VS})|M_F|^2+(a_{TA}+a_{AT})|M_{GT}|^2] \\
&-i[(a_{SV}-a_{VS})|M_F|^2-\tfrac{1}{3}(a_{TA}-a_{AT})|M_{GT}|^2]\frac{p}{E}\sin\vartheta\sin\theta\sin\phi \\
&-[(b_{SV}+b_{VS})|M_F|^2-\tfrac{1}{3}(b_{TA}+b_{AT})|M_{GT}|^2]\left(\frac{m}{E}\cos\vartheta\cos\theta+\sin\vartheta\sin\theta\cos\phi\right)
\end{aligned}
\tag{2}
$$

for $\beta^{\mp}$-emission. The following notation is used:

$$
\begin{gathered}
a_{IK}=\tfrac{1}{8}(C_I C_K^*+C_I' C_K'^*)=a_{KI}^*, \\
b_{IK}=\tfrac{1}{8}(C_I C_K'^*+C_I' C_K^*)=b_{KI}^*, \\
|M_F|^2=\sum_{I_f}\left|\int\Psi_f^*\,\Psi_i\,dv\right|^2,\quad |M_{GT}|^2=\sum_{I_f}\left|\int\Psi_f^*\,\sigma\Psi_i\,dv\right|^2,
\end{gathered}
$$

$E=\sqrt{p^2+m^2}$, $m=$ electron mass.

This formula contains besides the well known terms describing angular correlation $(\cos\vartheta)$ and longitudinal polarization $(\cos\theta)$ also terms related to transverse polarisation $(\sin\theta)$. The electron spin can be found to lie in the decay plane $(\phi=0)$ and the degree of transverse polarization $(\theta=\pi/2)$ for $\beta^{\mp}$-decay is given by

$$
P_\perp{}^{(\mp)}=\frac{|H(\mathbf{p},\mathbf{s}_\perp,\mathbf{q})|^2-|H(\mathbf{p},\ -\mathbf{s}_\perp,\mathbf{q})|^2}{|H(\mathbf{p},\mathbf{s}_\perp,\mathbf{q})|^2+|H(\mathbf{p},\ -\mathbf{s}_\perp,\mathbf{q})|^2} \tag{3}
$$

$$
=\frac{\mp[(b_{SS}+b_{VV})|M_F|^2-\tfrac{1}{3}(b_{TT}+b_{AA})|M_{GT}|^2]\frac{m}{E}\sin\vartheta-[(b_{SV}+b_{VS})|M_F|^2-\tfrac{1}{3}(b_{TA}+b_{AT})|M_{GT}|^2]\sin\vartheta}{[(a_{SS}+a_{VV})|M_F|^2+(a_{TT}+a_{AA})|M_{GT}|^2]-[(a_{SS}-a_{VV})|M_F|^2-\tfrac{1}{3}(a_{TT}-a_{AA})|M_{GT}|^2]\frac{p}{E}\cos\vartheta}
$$

$$
\pm\frac{m}{E}[(a_{SV}+a_{VS})|M_F|^2+(a_{TA}+a_{AT})|M_{GT}|^2]
$$

Here $\mathbf{s}_\perp$ is (1, 0, 0). Specializing (3) for pure transitions we obtain

K	$P_\perp^{(\mp)}$	$\langle P_\perp^{(\mp)} \rangle$
S	$\mp \xi_S \frac{m}{E} \sin\vartheta \left(1 - \frac{p}{E}\cos\vartheta\right)^{-1}$	$\mp \frac{2}{\pi} \xi_S \frac{m}{E}$
V	$\mp \xi_V \frac{m}{E} \sin\vartheta \left(1 + \frac{p}{E}\cos\vartheta\right)^{-1}$	$\mp \frac{2}{\pi} \xi_V \frac{m}{E}$
T	$\pm \frac{1}{3}\xi_T \frac{m}{E} \sin\vartheta \left(1 + \frac{p}{3E}\cos\vartheta\right)^{-1}$	$\mp \frac{2}{3\pi} \xi_T \frac{m}{E}$
A	$\pm \frac{1}{3}\xi_A \frac{m}{E} \sin\vartheta \left(1 - \frac{p}{3E}\cos\vartheta\right)^{-1}$	$\pm \frac{2}{3\pi} \xi_A \frac{m}{E}$

with $\xi_K = b_{KK}/a_{KK}$. The two component theory is characterized by $C'_K = -C_K$, $\xi_K = -1$ giving a maximum value to $|P_\perp|$. $\langle P_\perp^{(\mp)} \rangle$ is the average of $P_\perp^{(\mp)}$ over ϑ for $0 \leqq \vartheta \leqq \pi$ (in the decay plane) which will be of experimental interest.

As a particularly simple example of mixed transitions the decay of a free neutron is considered. In this case $|M_F|^2 = 1$, $|M_{GT}|^2 = 3$ and experimentally $C_V = C_A$, $C_S = C_T$ is observed [5]). The two component theory would then give $P_\perp^{(n)} = 0$. Deviations from the validity of the principle of "maximum parity violation" (e.g. if the GT interaction produces two component neutrinos but the F interaction conserves parity, as the present — rather uncertain — state of experiments may indicate †) can exhibit themselves by $P_\perp^{(n)} \neq 0$.

It may be remarked — but without any hope of experimental test in the near future — that the same considerations on transverse electron polarization apply to the Cowan-Reines [6]) experiments on neutrino induced β^+-decay of free protons. In this case the direction of the neutrino is known a priori.

Let us estimate the amount of asymmetry in Coulomb scattering on the nuclei of the gas atoms filling the chamber. Consider scattering intensities in the directions $\mathbf{p} \times \mathbf{q}$, $-\mathbf{p} \times \mathbf{q}$ (scattering angle $\omega = \frac{1}{2}\pi$). Their ratio is given by [7])

$$\frac{I_1}{I_2} = \frac{1 + aP_\perp}{1 - aP_\perp}. \tag{5}$$

a is a function of the β-energy [8]) with a flat maximum of 0.25 for negatons of 0.15 MeV, 0.06 for positons of 0.9 MeV; both values hold for $Z = 80$ and have to be multiplied by $\approx Z/80$ for a gas of atomic number Z filling the chamber. Maximum β-energies lie somewhat higher than these energies: 0.78 MeV for the neutron [5]), 3.6 MeV for He^6 [9]), 2.18 MeV for Ne^{19} [10]).

† C. N. Yang, private communication.

But the spectra always contain large amounts of electrons of those energies where a is largest. Thus $|aP_\perp|$ may have values up to $0.25 \cdot Z/80$ for a β^--emitter with Fermi type coupling. In practice, this value will be reduced in consequence of the averaging over the angles ϑ (e.g. in an interval $(\frac{1}{2}\pi-\varepsilon, \frac{1}{2}\pi+\varepsilon)$ or $(0, \pi)$). If we take into account the scattering events into a finite solid angle and β-particles of energies lying in a finite interval, this will also cause a reduction. But if we select appropriate values of ϑ, ω and the β-energy, the asymmetry obtained in Coulomb scattering can be sufficiently large to be observed.

One of the authors (G. Gy.) wishes to express his deep gratitude to the "École d'Été" for a scholarship making possible his stay in Les Houches. The stimulating atmosphere of the "École d'Été" has been essential in the conception of the work.

References

1) T. D. Lee and C. N. Yang, Phys. Rev. **104** (1956) 254
2) C. S. Wu *et al.*, Phys. Rev. **105** (1957) 1413
3) H. Frauenfelder, Phys. Rev. **106** (1957) 386
4) G. Csikai, Nuovo Cimento **5** (1957) 1011
5) Robson, Phys. Rev. **100** (1955) 933
6) C. Cowan *et al.*, Science **124** (1956) 103
7) H. A. Tolhoek and S. R. de Groot, Physica **17** (1951) 1
8) H. A. Tolhoek, Revs. Mod. Phys. **28** (1956) 277
9) Rustad and Ruby, Phys. Rev. **97** (1955) 991
10) Maxon, Phys. Rev. **97** (1955) 109

Nuclear Physics **5** (1958) 409; © *North-Holland Publishing Co., Amsterdam*

NEWS ITEM

INTERNATIONAL CONFERENCE ON MESONS AND RECENTLY DISCOVERED PARTICLES

(Padua and Venice, 22-28 September 1957)

The international conference on mesons and recently discovered particles was held from 22nd to 28th September at Padua and Venice under the presidence of Professor P. M. S. Blackett. The opening meeting took place at the Fondazione G. Cini in Venice on the afternoon of the 22nd; the sessions of the 23rd, 24th and 25th were held at Padua University, while those of the 26th, 27th and 28th were again held at the Fondazione G. Cini. A large number of short communications was presented at every session. The last one, however, was devoted to a series of talks summarizing the outcome of the discussions. After the closing dinner, a boat-trip in the Laguna was arranged by the Municipality of Venice.

The conference began with a discussion of pion-phenomena, including consideration of charge independence in hyperon production by π-mesons and protons. Results were not yet conclusive. At the session on K-particles, a significant conclusion was that the best fit for the K^+-nucleus interaction is represented by a complex potential $(V+iW)$ with a repulsive real part, in contrast with the attractive interaction of the K^--particle with nuclei. At low energies, one finds $V = 27\pm 8$ MeV, $W = -5.7\pm 1.1$ MeV, while at high energies $V = 27\pm 3$ MeV, $W = -10.3\pm 1.6$ MeV.

The idea of associating left-handed neutrinos with S−T interactions and right-handed neutrinos with A−V interactions in the beta-decay coupling was put forward by Lee as a means of explaining the results of experiments including those on electron-nucleus recoil. It was pointed out by Marshak that the idea of a strictly universal Fermi-interaction could be excluded by any one of the four following experiments: (1) the He^6 recoil experiment, (2) the polarization of e^+ from $\pi-\mu$ decay (Liverpool experiment), (3) the decay ratio $(\pi \to \mu+\nu)/(\pi \to e+\nu)$ and (4) polarized neutron decay. It should be noted that some of the experiments on the $K^+ \to \mu^+ + \nu \to e^+ + \nu + \nu$ process show violation of parity, but the experiments do not all agree among themselves. Also the correlation of positive and negative values of $(\mathbf{p}_{\pi 1^-} \wedge \mathbf{p}_Y) \cdot \mathbf{p}_{\pi t^-}$ in the $\pi_1^- \to Y^- \to \pi_t^-$ process (Y represents Σ or Λ) seem to show violation of parity, but the number of events is rather small and results are not yet conclusive.

The theoretical session began with a remarkable survey by Heisenberg of his recent attempts to develop a general theory of 'matter' based on essentially non-linear spinor field equations. The mathematical problems connected with the introduction of an indefinite metric in Hilbert space have received considerable clarification from the analysis of the Lee model from this point of view. One outstanding problem stressed by Heisenberg concerns the incorporation of the isobaric spin in the fundamental equations: only when this concept is better understood can one hope to put the theory on a 'realistic' basis.

Nuclear Physics **5** (1958) 410—412; © *North-Holland Publishing Co., Amsterdam*

BOOK REVIEWS

M. HAÏSSINSKY, *La chimie nucléaire et ses applications* (Masson et Cie, Paris, 1957, 651 pages. 5000 fr. fr. sewn, 5600 fr. fr. bound)

The word "radiochemistry" was originally used to describe the chemistry of the naturally occurring radioactive elements, but since its introduction it has undergone a number of changes in connotation and more recently has tended to have different meanings in different laboratories. The broad definition suggested by Paneth, "the chemistry of bodies which are detected by means of their emitted radiations", is however too restricted in scope for the author of this comprehensive book. He prefers the title "nuclear chemistry", which he takes to be concerned with the transmutations and transformations of nuclei, by analogy with "molecular chemistry" which deals with corresponding changes in molecules. On this basis, the applications of nuclear chemistry include radiation chemistry, radiochemistry (*sic*), tracer chemistry and the use of radioactive and stable isotopes as indicators. I am not entirely happy about the derivation and significance of the title, but whatever its validity, there can be little doubt that the author has succeeded in covering practically all its possible ramifications. In a preface, Haïssinsky gives his reasons for preferring to attempt this forbidding task alone rather than as the editor of a collective work. There are, in fact, few aspects of the subject matter in which he has not taken an active interest; one is struck by the very personal nature of many of the opinions expressed.

The book opens with a brief historical review of the growth and expansion of the science of radioactivity, designed to place in perspective the detailed aspects discussed later. This chapter, incidentally, emphasises the lack of any full-scale history of the subject. A section of five chapters then deals with fundamental particles, the physics of the nucleus, and nuclear transformations and reactions; although clearly not a definitive coverage, the treatment is clear and quite adequate for an understanding of what follows. A chapter on the naturally occurring radioelements is followed by a discussion of the physical and chemical properties of the trans-uranium elements, with particular reference to the much-argued question of their position in the periodic table; Haïssinsky puts forward his arguments against the actinide theory, and in favour of a "curide" rare-earth series. Other chapters of this group deal with isotope effects, the separation of inactive isotopes and a review of the geochemical applications of nuclear chemistry.

A discussion of the physical interactions of ionising radiations with matter prefaces a series of chapters on radiation chemistry. To the reviewer's knowledge, no comparable book deals with this subject in more than perfunctory detail and its inclusion here is a further result of the author's own wide interests. The radiolysis of water and of aqueous solutions is discussed in some detail, as are the various theoretical interpretations; the large amount of experimental data on the radiation chemistry of organic compounds still appears to await some unifying theory. Chapters on radiation damage in solids and on radiation-induced fluorescence and coloration are followed by a full treatment of the chemical effects associated with nuclear transformations.

The final group of eight chapters deals in considerable detail with the applications of radioactive tracers in physical and analytical chemistry, in biology and in industry. It is evident that the intimate concern of the author with much of the subject matter has enabled him to make a critical and comprehensive survey of these topics. He has deliberately chosen to exclude any description of the experimental techniques of nuclear chemistry, nor are counting methods mentioned except inasmuch as their physical or chemical principles arise naturally in the text. This approach does not always seem satisfactory, since it results, for example, in a description of the Geiger-Muller counter at the end of a chapter on the radiation chemistry of gases. Outside these self-imposed restrictions, however, this book is an excellent and com-

prehensive coverage of the chemical aspects of radioactivity. It is difficult to think of any single volume at present available which surveys a wider field, especially since the collaborative work edited by Wahl and Bonner is now some seven years old.

It may well be that the book will prove too detailed for undergraduates, but few research workers in "nuclear chemistry" will read it without profit. The printing is reasonably good and most (but not all) of the misprints have been noted. By current costs in England, the price seems rather high. The literature references extend to 1955 and include more Russian papers than is usual in comparable British or American works.

D. G. Tuck

L. FERMI, *Atoms for the world* (The Chicago University Press, 1957. xii—227 pages. $. 3.75)

To the reader interested in the intricacies and difficulties involved in the setting up of a large conference and exhibition, Mrs Fermi's book presents a lively account of the comings and goings of the American section at the Atoms for Peace Congress which was held in Geneva in August 1955.

The first four chapters are devoted to the description of the preparation for the conference from President Eisenhower's proposals in December 1953, to the final setting up of the exhibition in Salle XV of the Palais des Nations. One chapter explains in a simple language the principles of atomic science and the uses to which atomic energy can be put in the fields of power, medicine and biology. In the second half of the book, the author describes some of the exhibits and reports on discussions concerning radiation hazards, power programmes and future advances in various countries. Throughout the book, amusing, if not wholly relevant, anecdotes remind us that scientists are, after all, human. The most illuminating chapter is the one which describes the reactions of the Americans when they discover that Russian scientists too, are after all human.

Altogether, this is a very readable book, well presented, with some interesting photographs.

J. R.

Atomo e Industria, Giornale internazionale d'informazioni nucleari (Roma, via Campo Marzio 12. Annual subscription for Europe 3200 lire, outside Europe $ 6)

A new periodical issued every fortnight, in the style of a newspaper. One page gives a summary of Italian nuclear news in English.

Atom, Monthly information bulletin of the United Kingdom Atomic Energy Authority (for distribution apply to Public Relations Branch, U.K.A.E.A., St. Giles Court, London W.C. 2)

An authoritative monthly 16-page pamphlet with news items (including Parliamentary questions and debates), patents abstracts and condensed versions of interesting lectures and articles on the industrial aspects of nuclear energy.

The Index of Technical Articles, monthly index of articles published in British technical periodicals (Iota Services Ltd., 38 Farringdon Street, London E.C.4. Annual subscription £ 6.6.0)

Section 8 covers 'Nucleonics'; judging from the sample received, rather sketchily and uncritically. Other items in section 10.1 (Electrical and Electronic Engineering; Generation, distribution etc.). Of no scientific interest.

MANSON BENEDICT and THOMAS H. PIGFORD, *Nuclear chemical engineering* (McGraw Hill Book Co., New York, Toronto, London, 1957. iv+594 pages. 71s.6d.)

Many new and interesting problems have been encountered by the chemical engineer over the past fifteen years in the field of nuclear energy. Most, if not all, of these, however, differ in degree rather than in kind from those encountered in "clasical" chemical engineering,

and in the main have been adequately solved for present purposes. The more urgent problems are now concerned rather with power reactor technology and metallurgy, and, while the chemical engineer undoubtedly has contributions to make in these fields, he will tend to do so as a member of a broadly-based development team rather than individually within his own specific field.

The appearance of a book on this subject by the present authors is therefore a matter of some note, and their selection of topics is of particular interest. These comprise, apart from two introductory chapters, discussions of reactor fuel cycles, uranium fuel production, the technology of zirconium, thorium and beryllium, the solvent extraction of metals, fuel processing, and finally, three chapters on the separation of stable isotopes with particular reference to heave water and U^{235}. Various other subjects could have been included, e.g. radioactive waste disposal, graphite, radiation shielding, and nuclear criticality as it affects the design of fuel processing equipment, and indeed it is difficult to know where to draw the line. Taken together, the contents form a somewhat heterogeneous collection of subjects, the only common feature of which is their importance in nuclear engineering, and it could hardly be expected that all could be uniformly dealt with in a single text. Indeed, it may seriously be questioned whether the title of the book is not misleading since it infers, erroneously, that the subject matter comprises a comprehensive new technology.

With the above proviso, the subjects in general are adequately dealt with and the style is lucid. Rather greater attention is paid to iostope separation, as might be expected from the known interests of the senior author. Here he has introduced Cohen's generalized method of cascade calculation [1]), and in so doing has retracted from his earlier classification of separation processes in terms of their degree of thermodynamic reversibility [2]). While admitting the merits of this treatment, and taking into account the authors' clear exposition of the subject, in the opinion of the reviewer the result is unfortunate in that the essential difference between equilibrium processes such as distillation and non-equilibrium processes such as gaseous diffusion is not clearly brought out.

To conclude, this book can be thoroughly recommended to those chemical engineers concerned with nuclear energy whose interests lie outside the field of reactor technology, and to those physicists and nuclear engineers who wish to learn something of the chemical technology associated with their subject.

H. R. C. Pratt

References

1) K. Cohen, The Theory of Isotope Separation, National Nuclear Energy Series, Division III, Vol. 1B (McGraw Hill Book Co., 1951)
2) M. Benedict, Chem. Eng. Prog. **41** (1947) 41

Nuclear Physics **5** (1958) 413—415; © *North-Holland Publishing Co., Amsterdam*
Not to be reproduced by photoprint or microfilm without written permission from the publisher

ON THE 2450-3400 keV REGION OF THE RaC GAMMA SPECTRUM

B. DZHELEPOV, S. SHESTOPALOVA and I. UCHEVATKIN
D. I. Mendeleyev Research Institute of Metrology, Leningrad

Received 23 August 1957

Abstract: Five new RaC γ-lines are reported of higher energy than those known heretofore.

In the paper by Dzhelepov and Shestopalova [1]) it was pointed out that coincidences in excess of the background which could not be attributed to the influence of the neighbouring line had been observed in the RaC spectrum beyond the γ-line 2450 keV approximately up to an energy of 2700 keV.

In the paper by Uchevatkin and Shestopalova [2]) this part of the spectrum was studied on the elotron under conditions of greater relative aperture, and it was shown that the RaC spectrum undoubtedly contains lines of higher energy than 2450 keV. However, under the experimental conditions (a beryllium target 330μ thick, and wide slits in front of the counters) the resolving power in this region was about 5 %, and hence the curve obtained could not be uniquely resolved into components. From the form of the curve it could only be concluded that there are more than two lines, and that their total intensity comprises $\approx 2\times 10^{-3}$ quantum per disintegration.

After the existence of these high energy lines had been established beyond doubt, we undertook measurements of this part of the spectrum with a beryllium target $\approx$ 150μ thick and with slits 3 mm wide and 16 and 22 mm high. In this manner we increased the resolving power by a factor of one and a half (up to 3.3 %) with a threefold loss in relative aperture. In order to study the spectral line of the apparatus under these conditions we carefully measured the 2614 keV line of ThC″.

The results of the measurements are shown in the figure. The black circles represent the spectrum of RaC; the light circles — the 2614 keV line of ThC″, which is made to coincide with the 2450 keV line of RaC. In the upper part of the figure the 2600—3400 keV region of the spectrum is drawn to a larger scale; the curve clearly exhibits four maxima (2684, 2768, 2893, 2992 keV) with a hint of a fifth (3070 keV). The background in this part of the spectrum did not comprise more than 10 % of the effect.

The relative intensities and the number of quanta per disintegration for these lines are given in the table. The third column of the table gives the energies of the three excitation levels of RaC′ known from the measurements of the long-range alpha-particle spectrum by Rutherford and co-workers [3]). We did not detect the 2514 keV γ-line [3]).

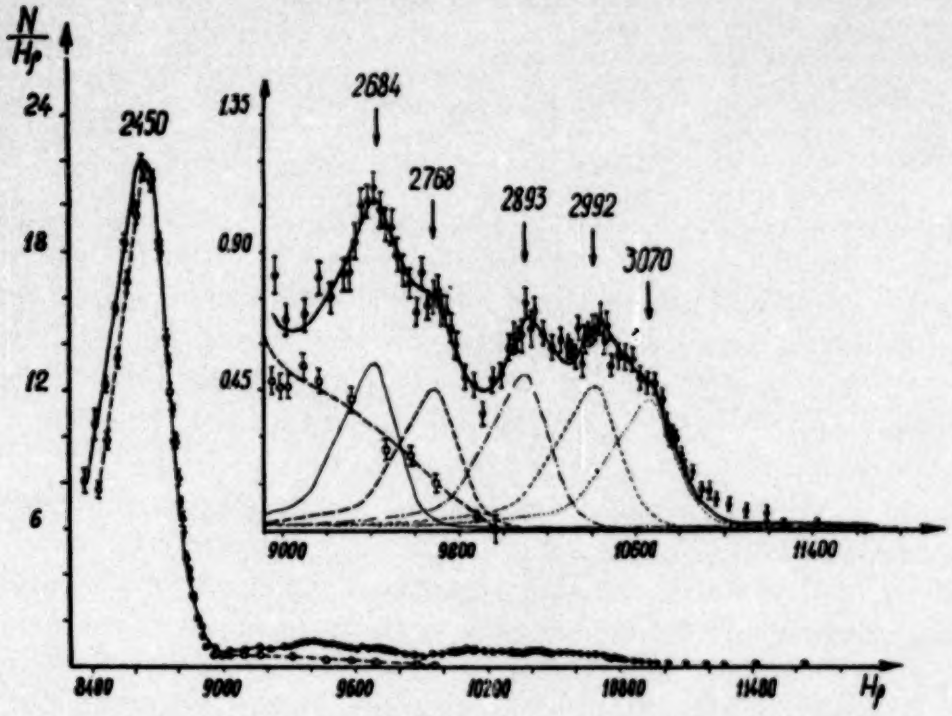

Fig .1. Region of RaC gamma-ray spectrum (2370–3400 keV). 2614 keV line of ThC″ (light circles) coincides with the 2450 keV line of RaC. In the upper part of the figure the region 2600–3400 keV of the spectrum is portrayed on a larger scale.

TABLE 1

Nos.	E_γ in keV (our data)	E in keV (Rutherford and co-workers)	$I_{rel.}$	Number of quanta per disintegration
1	2450±10	2439±5	1	2×10^{-3} †
2	2684±15	2696±5	0.024	$(5\ \pm1.2)\times10^{-4}$
3	2768±15	–	0.020	$(4\ \pm1\ )\times10^{-4}$
4	2893±15	2879±5	0.022	$(4.3\pm0.8)\times10^{-4}$
5	2992±15	–	0.020	$(3.9\pm0.7)\times10^{-4}$
6	3070±15	–	0.019	$(3.7\pm0.7)\times10^{-4}$
7	"residue"	–	0.002	$(4\ \pm2\ )\times10^{-5}$

† The number of quanta per disintegration for the 2450 keV line is taken from ref. [1]).

Upon resolving the high energy part of the spectrum into components we discovered an excess of recoil electrons in the 3120–3220 keV region. All the experimental points in this region lie above the curve obtained as

the sum of the five components mentioned. It is possible that there are one or several lines in this region with a total intensity of $\approx 4 \times 10^{-5}$ quantum per disintegration.

References

1) B. Dzhelepov and S. Shestopalova, Izvestia AN SSSR, ser. fiz. **21** (1957) No. 7
2) I. Uchevatkin and S. Shestopalova, Izvestia AN SSSR, ser. fiz. **21** (1957) No. 7
3) E. Rutherford, W. Lewis and B. Bowden, Proc. Roy. Soc. A **143** (1933) 347

Note added in proof: After the present paper was sent to press our attention was drawn to an article by H. Daniel, Zs. f. Naturforsch. **12a** (1957) 194. The author gives the relative intensities of three hard RaC lines observed by him. The agreement with our results is satisfactory.

Nuclear Physics **5** (1958) 416—434; © *North-Holland Publishing Co., Amsterdam*
Not to be reproduced by photoprint or microfilm without written permission from the publisher

MESURE DE LA POLARISATION DES ELECTRONS RELATIVISTES

CLAUDE BOUCHIAT
Laboratoire Central des Poudres, Paris †
et
LOUIS MICHEL
Faculté des Sciences, Université de Lille

Reçu le 1er juillet 1957

Abstract: We describe a covariant formalism for handling electron polarization and we show how to use it in quantum field theory calculations. We apply it to the study of polarization effects in electron-electron collisions. These effects can be used for the measurement of the transverse and longitudinal polarization of relativistic electrons.

Des expériences récentes ont brillamment confirmé l'hypothèse de la non-conservation de la parité, proposée par Yang et Lee [1]). De cette hypothèse, on peut conclure à la polarisation des particules de spin $\frac{1}{2}$, émises dans les désintégrations dues aux couplages faibles. Par exemple, les électrons de radioactivité β sont polarisés longitudinalement (lorsque les noyaux initiaux ne sont pas orientés, et que le recul ou la polarisation des noyaux finaux ne sont pas observés). L'étude de cette polarisation donnera des informations supplémentaires sur la nature de l'interaction de la radioactivité β. De même, les électrons de désintégration des mésons μ au repos sont polarisés; un travail de F. Bourdelet et L. Michel [2]) montre quelle information on peut déduire de l'étude de cette polarisation. Dans le présent travail, nous examinons de nouvelles possibilités de mesure de la polarisation des électrons relativistes, basée sur l'étude des collisions électron-électron. Cet article est divisé en deux parties. Nous décrivons d'abord avec quelque détail un formalisme relativiste, que nous avions déjà présenté [11, 14]), pour l'étude de la polarisation des particules de spin $\frac{1}{2}$, et nous passons en revue les différentes méthodes pour la mesure de cette polarisation. Puis nous étudions les collisions électron-électron de même charge ou de charge opposée, et nous appliquons ces résultats généraux à des exemples d'expériences possibles.

PREMIÈRE PARTIE

POLARISATION D'UNE PARTICULE DE SPIN $\frac{1}{2}$

1. Description Relativiste

Nous donnons ici brièvement des résultats qui seront établis dans un article à paraître, en collaboration avec A. S. Wightman (voir aussi Michel

† En stage au Palmer Physical Laboratory, Princeton University, Princeton N.J.

et Wightman [3])). Cet article sera désigné par les initiales B.M.W. dans la suite. En mécanique quantique, un système physique est représenté par un vecteur d'un espace d'Hilbert. Soit P^λ, $M^{\mu\nu} = -M^{\nu\mu}$ les dix opérateurs hermitiques infinitésimaux du groupe de Lorentz inhomogène. Ils sont interprétés physiquement comme des opérateurs d'énergie P^0, d'impulsion P^i et de moment cinétique total $M^{\mu\nu}$.

Considérons une particule de spin $\frac{1}{2}$, de masse $m \neq 0$ et d'énergie-impulsion $p^\mu = (p^0 = E, \mathbf{p})$ avec $p^\mu p_\mu = \mathfrak{p}^2 = m^2$. Les états de polarisation de cette particule sont représentés par les vecteurs d'un espace hermitique $\mathscr{E}(p^\mu)$ à deux dimensions. En suivant Bargmann et Wigner [4]) nous considérons les 4 opérateurs †

$$W^\lambda = \tfrac{1}{2}\varepsilon^{\lambda\mu\nu\varrho} p_\mu M_{\nu\varrho}. \tag{1}$$

Ces opérateurs se transforment comme les composantes d'un pseudovecteur. L'état de la particule est représenté par une fonction $u(\mathfrak{p})$, solution de l'équation de Dirac écrite, dans l'espace des moments,

$$(\overline{\not{p}}| - m)u(\mathfrak{p}) = 0 \tag{2}$$

avec $\overline{\not{p}}| = i\gamma^\mu p_\mu$. Dans cette représentation

$$M^{\mu\nu} = \frac{1}{i}\left(p^\mu \frac{\partial}{\partial p_\nu} - p^\nu \frac{\partial}{\partial p_\mu}\right) + \tfrac{1}{2}\sigma^{\mu\nu} \tag{3}$$

avec $\sigma^{\mu\nu} = (1/2i)(\gamma^\mu\gamma^\nu - \gamma^\nu\gamma^\mu)$. Seul le dernier terme de (3) contribue à W^λ dans (1). L'opérateur W^λ est donc directement lié au moment cinétique de spin de la particule. En utilisant les relations d'anticommutation des γ^μ, on trouve

$$W^\lambda W_\lambda = -\tfrac{3}{4}m^2 = -\tfrac{1}{2}(\tfrac{1}{2}+1)m^2. \tag{4}$$

Soit n^μ un quadrivecteur de genre espace tel que

$$\mathfrak{n} \cdot \mathfrak{p} = n^\mu p_\mu = 0 \quad \text{et} \quad \mathfrak{n} \cdot \mathfrak{n} = n^\mu n_\mu = -1. \tag{5}$$

L'opérateur $2W^\lambda n_\lambda/m$ agissant dans $\mathscr{E}(p^\mu)$ a pour carré l'opérateur unité, il a donc pour valeurs propres $+1$ et -1.

Nous prendrons comme vecteurs de base de $\mathscr{E}(p^\mu)$ les fonctions propres de $2W^\lambda n_\lambda/m$, solutions de (2). Nous les notons $u(\mathfrak{p}, \varepsilon\mathfrak{n})$ avec $\varepsilon = \pm 1$. Dans l'article B.M.W. il est montré que les opérateurs W^λ peuvent alors être représentés dans $\mathscr{E}(p^\mu)$ par

$$\frac{2W^\lambda}{m} = -\sum_{i=1}^{3} \tau_i n_i^\lambda, \tag{6}$$

où τ_1, τ_2, τ_3 sont les 3 matrices de Pauli, $\mathfrak{n}_3 = \mathfrak{n}$, et les vecteurs $\mathfrak{n}_1$ et $\mathfrak{n}_2$ sont définis comme suit:

† Voir l'appendice pour la définition des notations utilisées.

$$\mathfrak{n}_i \cdot \mathfrak{p} = 0, \quad \mathfrak{n}_i \cdot \mathfrak{n}_i = -\delta_{ij},$$

et (6′)

$$\varepsilon^{\lambda\mu\nu\varrho}\, p_\lambda (n_1)_\mu (n_2)_\nu (n_3)_\varrho = -m.$$

Étudions ce que donnent ces formules covariantes dans deux cas particuliers. Pour cela, nous allons exprimer $\mathfrak{W}$ au moyen des matrices $\boldsymbol{\sigma}$ et $\boldsymbol{\alpha}$ du formalisme de Dirac. On a alors

$$W^0 = -\tfrac{1}{2}\mathbf{p}\cdot\boldsymbol{\sigma}, \quad \mathbf{W} = -\tfrac{1}{2}p^0\boldsymbol{\sigma} - \frac{i}{2}\mathbf{p}\times\boldsymbol{\alpha}. \tag{7}$$

Premier cas. La particule est au repos:

$$\mathfrak{p} = (m, \mathbf{0}), \quad \mathfrak{n}_i = (0, \mathbf{n}_i), \quad W^0 = 0,$$

$$\mathbf{W} = -\tfrac{1}{2}m\boldsymbol{\sigma}, \quad \frac{2W^\mu n_\mu}{m} = \boldsymbol{\sigma}\cdot\mathbf{n},$$

ce qui est bien identique au formalisme usuel non relativiste.

Deuxième cas. Choisissons le quadrivecteur $\mathfrak{n}_3$ longitudinal, c'est à dire $\mathbf{n}_3$ parallèle à $\mathbf{p}$. Dans ces conditions,

$$\mathfrak{n} = \mathfrak{n}_3 = \left(\frac{|\mathbf{p}|}{m}, \frac{p^0}{m}\frac{\mathbf{p}}{|\mathbf{p}|}\right), \quad \mathfrak{n}_1 = (0, \mathbf{n}_1), \quad \mathfrak{n}_2 = (0, \mathbf{n}_2), \tag{8}$$

où $\mathbf{n}_1$, $\mathbf{n}_2$, $\mathbf{p}$ forment un trièdre trirectangle direct, avec le choix

$$\frac{2}{m}\mathfrak{W}\cdot\mathfrak{n} = \frac{\boldsymbol{\sigma}\cdot\mathbf{p}}{|\mathbf{p}|}. \tag{9}$$

On retrouve encore ici un résultat bien connu [5]).

Considérons un ensemble statistique d'électrons de même quantité de mouvement (par exemple les électrons d'un faisceau monocinétique). Nous appellerons pseudovecteur polarisation, le quadrivecteur $\mathfrak{s}$ obtenu en prenant la valeur moyenne sur cet ensemble des opérateurs $-2W^\lambda/m$:

$$\mathfrak{s} = -\frac{2}{m}\langle\mathfrak{W}\rangle = \sum_i \langle\tau_i\rangle\,\mathfrak{n}_i = \sum_i \zeta_i\,\mathfrak{n}_i. \tag{10}$$

Les 3 vecteurs $\mathfrak{n}_i$ ayant été choisis, la polarisation peut être également définie par les 3 pseudoscalaires ζ_1, ζ_2, ζ_3 tels que

$$-1 \leqq \zeta_i \leqq 1 \quad \text{et} \quad 0 \leqq \zeta_1^2+\zeta_2^2+\zeta_3^2 \leqq 1. \tag{11}$$

Dans un repère déterminé (le système du laboratoire par exemple), en faisant le choix particulier précédent (8) des vecteurs $\mathfrak{n}_i$, on définit un état de polarisation longitudinale par $\zeta_1 = \zeta_2 = 0$. Il est à noter que ces notions sont relatives à un repère déterminé. Une polarisation longitudinale dans un repère pourra être en partie, ou même totalement, transversale dans un autre repère.

Pour décrire un ensemble statistique d'électrons de même impulsion, il est

commode d'utiliser la notion de matrice densité. La fonction d'onde $v(\mathfrak{p})$ d'un électron peut s'écrire

$$v(\mathfrak{p}) = \sum_{\varepsilon=\pm 1} u(\mathfrak{p}, \varepsilon\mathfrak{n}) C_\varepsilon . \tag{12}$$

La matrice densité d'un ensemble statistique d'électrons de même énergie-impulsion $\mathfrak{p}$ est définie par

$$\varrho_{\varepsilon\eta} = \sum_m P^{(m)} C_\varepsilon^{(m)} C_\eta^{(m)*} \quad (\varepsilon, \eta = \pm 1). \tag{13}$$

$P^{(m)}$ est la probabilité de trouver un électron dans l'état $v^{(m)}$. Le nombre ζ_i est alors donné par

$$\zeta_i = \frac{1}{\operatorname{tr} \varrho} \operatorname{tr} (\varrho \tau_i). \tag{14}$$

La matrice ϱ peut être exprimée comme combinaison linéaire de la matrice unité et des 3 matrices τ_i ; en tenant compte de (14), ϱ peut s'écrire

$$\varrho = \tfrac{1}{2}(\operatorname{tr} \varrho)(1 + \sum_i \zeta_i \tau_i). \tag{15}$$

En résumé, pour étudier totalement la polarisation d'un ensemble monocinétique d'électrons, il faut mesurer les 3 pseudoscalaires $\zeta_1, \zeta_2, \zeta_3$, ou, ce qui revient au même, le pseudovecteur

$$\mathfrak{s} = \zeta_1 \mathfrak{n}_1 + \zeta_2 \mathfrak{n}_2 + \zeta_3 \mathfrak{n}_3 = \frac{2\langle \mathfrak{W} \rangle}{m}. \tag{16}$$

Le degré de polarisation est

$$(-\mathfrak{s} \cdot \mathfrak{s})^{\frac{1}{2}} = (\zeta_1^2 + \zeta_2^2 + \zeta_3^2)^{\frac{1}{2}}. \tag{17}$$

2. Non-conservation de la Parité et Polarisation

Observer la non-conservation de la parité, c'est observer un pseudoscalaire (par rapport aux symétries d'espace). Par exemple, on observera la probabilité de transition λ d'un système S_1 en un système S_2, et la probabilité de transition λ' de S'_1 symétrique de S_1 par rapport à un plan (ou hyperplan de genre espace) en S'_2 obtenu de S_2 par la symétrie Σ transformant S_1 en S'_1. La symétrie Σ échange donc λ et λ'. Donc $\frac{1}{2}(\lambda+\lambda')$ est un scalaire et $\frac{1}{2}(\lambda-\lambda')$ un pseudoscalaire. S'il y a conservation de la parité $\lambda = \lambda'$. Quand on observe des particules, on observe des énergies-impulsions $\mathfrak{p}$ et des polarisations $\mathfrak{s}$. Si on n'observe que des $\mathfrak{p}$, le seul pseudoscalaire que l'on peut former est le déterminant

$$\delta = -\varepsilon_{\lambda\mu\nu\varrho} p_1^\lambda p_2^\mu p_3^\nu p_4^\varrho$$

formé avec quatre impulsions-énergies. Mais si le processus ne comprend que quatre particules (radioactivité β, désintégration du méson μ) la conservation de l'impulsion-énergie annule δ, puisque les quatre $\mathfrak{p}$ sont liés par une

relation linéaire. Il faut donc observer au moins une polarisation. Dans le cas d'une désintégration d'une particule d'impulsion-énergie p_0 et non polarisée, si on observe seulement la polarisation $\hat{s}_1$ d'une particule finale (et accessoirement son énergie-impulsion p_1 avec $p_1 \cdot \hat{s}_1 = 0$), le seul pseudo-scalaire que l'on peut former est $p_0 \cdot \hat{s}_1$. Il est nul si $\hat{s}_1$ est transversal, dans le système au repos de la particule initiale. Observer la non-conservation de la parité dans une désintégration de particule non polarisée au repos exigera donc d'observer la polarisation longitudinale $\hat{s}_1$.

3. Mesure de la Polarisation des Électrons Relativistes

3.1. MÉTHODES DÉJÀ PROPOSÉES

Dans un excellent article d'ensemble [6]) H. A. Tolhoek donne la liste des différentes méthodes déjà proposées pour détecter la polarisation des électrons. Cette liste contient quatre méthodes:

1° diffusion coulombienne des électrons par des noyaux lourds,

2° diffusion des électrons par un corps ferromagnétique,

3° mesure mécanique du moment cinétique d'électrons lents polarisés longitudinalement,

4° diffusion des électrons lents par des atomes afin d'obtenir des états excités d'atomes orientés, et observation de la polarisation circulaire de la lumière émise par ces atomes.

De ces quatre méthodes, seule la première a été utilisée avec succès. Elle ne permet pas de mesurer la polarisation longitudinale (dans le système au repos des noyaux lourds). D'autre part, l'effet est maximum pour des négatons de 0.15 MeV environ d'énergie cinétique, ou des positons de 0.8 MeV et décroît assez rapidement avec l'énergie. Les méthodes 3 et 4 ne peuvent s'appliquer qu'aux électrons très lents.

Nous étudions dans cet article la deuxième méthode. Contrairement à ce qui est dit dans la réf. [6]), cette méthode peut s'appliquer aux électrons relativistes.

3.2. AUTRES MÉTHODES POUR LA MESURE DE LA POLARISATION QUELCONQUE D'ÉLECTRONS RAPIDES

Les interactions faibles de l'électron ne peuvent permettre de mesurer pratiquement sa polarisation (section efficace de l'ordre de 10^{-44} cm^2). En dehors d'une mesure mécanique (méthode 3), toute mesure sera donc basée sur l'interaction électromagnétique de l'électron. Nous avons déjà vu que la diffusion coulombienne ne permet de mesurer que la polarisation transversale (et pour une bande assez étroite de l'énergie de l'électron). En effet, le scalaire observé (les interactions électromagnétiques conservent la parité!) est proportionnel à det $(\mathfrak{P}, p_a, p_b, \hat{s})$ où $\mathfrak{P}$, p_a, p_b sont respectivement les énergies-impulsions du noyau, de l'électron initial et de l'électron final. Pour

observer la polarisation $\hat{s}$ par une autre méthode, il faudra donc faire intervenir une autre polarisation. Nous proposons dans la liste ci-dessous trois types de méthodes faisant intervenir une autre polarisation; les deux premières, a) et b), sont des mesures indirectes.

a) La polarisation $\hat{s}$ de l'électron est modifiée en $\hat{s}'$ par un phénomène qui permet de mesurer $\hat{s} \cdot \hat{s}'$, et on mesure directement $\hat{s}'$. Cette méthode a surtout l'intérêt de transformer $\hat{s}$ longitudinal en $\hat{s}'$ transversal, mesurable par diffusion coulombienne.

b) On remplace la mesure de $\hat{s}$ par la mesure de la polarisation d'une autre particule grâce à un phénomène permettant de mesurer une fonction des deux polarisations. Puisque la seule interaction que nous puissions utiliser est l'interaction électromagnétique de l'électron, cette autre particule sera un photon.

c) On mesure directement $\hat{s}$ par la diffusion sur des cibles orientées (noyaux, électrons).

3.3. MÉTHODES BASÉES SUR LA MODIFICATION DE LA POLARISATION DE L'ÉLECTRON

On se servira d'un champ électromagnétique extérieur.

a.1. *Champ magnétique*

Mentionnons ici, pour mémoire, l'expérience proposée par Louisell *et al.* [7]). Le facteur de Landé du moment magnétique de l'électron $g = 2[1+(\alpha/2\pi) + \ldots]$, étant légèrement différent de 2, la vitesse angulaire de rotation du spin, dans un champ magnétique homogène, est légèrement différente de celle de l'électron. Le but de cette expérience est de mesurer avec une grande précision le moment magnétique de l'électron. Nous la mentionnons ici puisqu'elle permet accessoirement de transformer une polarisation longitudinale en polarisation transversale.

Dans un champ électromagnétique inhomogène des expériences basées sur des phénomènes de résonance pourraient permettre la mesure de g, et accessoirement de la polarisation d'électrons de très faible énergie: voir réf. [6]).

a.2. *Champ électrique*

Il est possible de transformer la polarisation $\hat{s}$ d'un faisceau d'électrons par déviation électrostatique: voir réf. [6]).

a.3. *Diffusion coulombienne*

Une diffusion coulombienne ne permet pas d'analyser la polarisation longitudinale de l'électron. Par contre la polarisation transversale ζ'_t de l'électron après diffusion dépend de la polarisation longitudinale ζ_l initiale. Si ζ_l est nul, la polarisation ζ'_t est perpendiculaire au plan de diffusion. Si $\zeta_l \neq 0$, il apparaît une composante transversale de ζ'_t dans le plan de diffu-

sion. L'étude de ζ_1 revient à mesurer l'angle α que fait ζ'_1 avec la normale au plan de diffusion. Pour cela on fait une seconde diffusion coulombienne. La section efficace σ_2 de cette deuxième diffusion est linéaire en cos $(\varphi-\alpha)$ où φ est l'angle entre les deux normales des plans de diffusions. L'étude de la dépendance de σ_2 par rapport à φ permet donc de mesurer α. La dépendance de α par rapport à ζ_1 peut être aisément déduite des formules (3.8) de l'article de Tolhoek [6]).

Remarquons que, dans ces trois méthodes, l'énergie de l'électron n'est pas essentiellement modifiée. On est donc limité par la bande d'énergie de l'analyseur final employé (diffusion coulombienne par exemple).

a.4. *Modification de la polarisation par collision électron-électron*

Cette méthode est basée sur le sujet étudié dans cet article. En principe, elle permet de réduire l'énergie cinétique de l'électron initial par un facteur donné tout en ajoutant à sa polarisation longitudinale une partie transversale. Nous étudierons les limitations en fait de cette méthode.

3.4. MÉTHODES RAMENANT LA MESURE DE LA POLARISATION $\mathfrak{s}$ DE L'ÉLECTRON À LA MESURE DE LA POLARISATION DE RAYONS γ

On sait que la polarisation de la lumière la plus générale est elliptique. La variance relativiste [8]) des quatre éléments de la matrice densité pour cette polarisation est la suivante: †

un scalaire η (le degré de polarisation);

un pseudoscalaire ξ (qu'on peut appeler le degré de polarisation circulaire): ξ est la tangente de la demi-latitude du point représentatif sur la sphère de Poincaré;

le double d'un angle (l'azimuth du plan contenant le grand axe de l'ellipse et la direction de propagation) que l'on peut caractériser par un quadrivecteur $\mathfrak{u}$, défini au signe près et à une composante près le long de l'énergie-impulsion $\mathfrak{k}$ du photon, par les relations

$$\mathfrak{u}\cdot\mathfrak{k}=0, \quad -\mathfrak{u}^2+\xi^2=\eta^2. \tag{18}$$

Le scalaire que l'on peut donc observer pour la mesure de $\mathfrak{s}$ est $\mathfrak{s}\cdot\mathfrak{k}\xi$. Si l'on connaît la dépendance de la section efficace du premier phénomène par rapport à $\mathfrak{s}\cdot\mathfrak{k}\xi$, on est donc ramené à la mesure de ξ, degré de polarisation circulaire du photon. Celle-ci se fait par la mesure de l'absorption des γ dans un ferromagnétique saturé, la section efficace de l'effet Compton dépendant de l'orientation du champ magnétisant par rapport à la direction de propagation des photons polarisés circulairement.

Parmi les phénomènes d'émission de photons par les électrons, le rayonnement de freinage (Bremsstrahlung) semble bien convenir pour la mesure de

† Dans les notations de Jauch et Rohrlich [9]), $\eta = K$ (éq. 2—102), $\xi = \operatorname{tg}\psi$ et l'azimuth de $\mathfrak{u}$ est φ.

la polarisation des électrons rapides par la méthode indiquée dans ce paragraphe. H. Epstein et G. Flamand (à paraître) étudient ce cas du rayonnement de freinage †.

3.5. MESURE DE $\mathfrak{S}$ AU MOYEN DE CIBLES ORIENTÉES

c.1. La *diffusion des électrons par des noyaux orientés* permet en principe de mesurer la polarisation des électrons [10]).

c.2. La *diffusion d'électrons polarisés par des négatons liés et polarisés* (par exemple, dans un corps ferromagnétique aimanté à saturation) semble plus accessible à l'expérience. Nous étudions dans la deuxième partie (§ 5) les possibilités qu'elle offre pour la mesure de la polarisation d'un faisceau d'électrons.

DEUXIÈME PARTIE

PHÉNOMÈNES DE POLARISATION DANS LA COLLISION ÉLECTRON-ÉLECTRON

4. Théorie générale

On considère la collision a+b → c+d. Les impulsions-énergies $\mathfrak{p}_a$, $\mathfrak{p}_b$, $\mathfrak{p}_c$, $\mathfrak{p}_d$ des négatons a, b, c, d sont supposées déterminées. Nous donnerons l'état initial du système par une matrice densité ϱ_{in} opérant dans l'espace $\mathscr{E}(\mathfrak{p}_a) \odot \mathscr{E}(\mathfrak{p}_b)$. Les éléments de matrice de ϱ_{in} sont donnés par la formule

$$\varrho_{\varepsilon_a \eta_a \varepsilon_b \eta_b} = \sum_{m,m'} P^{(m,m')} C^{(m)}_{\varepsilon_a} C^{(m')*}_{\eta_a} C^{(m')}_{\varepsilon_b} C^{(m')*}_{\eta_b}. \tag{19}$$

Dans cette formule $P^{(m,m')}$ est la probabilité que l'électron a se trouve dans l'état

$$v^{(m)}(\mathfrak{p}_a) = \sum_{\varepsilon_a} C^{(m)} u(\mathfrak{p}_a, \varepsilon_a \mathfrak{n}_a)$$

et l'électron b dans l'état

$$v^{(m')}(\mathfrak{p}_b) = \sum_{\varepsilon_b} C^{(m')} u(\mathfrak{p}_b, \varepsilon_b \mathfrak{n}_b).$$

S'il n'existe pas de corrélation entre les électrons a et b, $P^{(m,m')}$ s'écrit sous la forme

$$P^{(m,m')} = P^{(m)} \cdot P^{(m')}.$$

Dans ce cas

$$\varrho_{in} = \tfrac{1}{4} (\mathrm{tr}\, \varrho_a)(\mathrm{tr}\, \varrho_b)[1 + {}_a\zeta_i(\tau_i \odot 1) + {}_b\zeta_j(\tau_j \odot 1) + {}_a\zeta_i\, {}_b\zeta_j(\tau_i \odot \tau_j)]. \tag{20}$$

Dans le cas général, $P^{(m,m')}$ ne peut pas se mettre sous la forme $P^{(m)} \cdot P^{(m')}$.

† Nous venons de recevoir un manuscrit de K. W. McVoy qui étudie la polarisation circulaire du rayonnement de freinage émis vers l'avant par des électrons polarisés longitudinalement, afin d'interpréter des expériences de Goldhaber, Grodzins et Sunyar. Nous remercions ces auteurs de la communication de leur travail avant publication.

Nous écrirons ϱ_{in}, qui est une matrice quatre par quatre, comme combinaison linéaire des 16 matrices $1 \odot 1$, $1 \odot \tau_j$, $\tau_i \odot 1$, $\tau_i \odot \tau_j$:

$$\varrho_{\text{in}} = \tfrac{1}{4}(\text{tr}\,\varrho_{\text{in}})[1+{}_{\text{a}}\zeta_i(\tau_i \odot 1)+{}_{\text{b}}\zeta_j(1 \odot \tau_j)+\Gamma_{ij}(\tau_i \odot \tau_j). \tag{21}$$

La quantité $C_{ij} = \Gamma_{ij} - {}_{\text{a}}\zeta_i\,{}_{\text{b}}\zeta_j$ caractérise la corrélation qui existe entre les spins des électrons a et b. M étant la matrice de collision, la matrice densité finale ϱ_f est donnée par

$$\varrho_f = \text{tr}\,(M\varrho_{\text{in}}M^\dagger). \tag{22}$$

Dans ce qui suit, nous prendrons pour M la matrice de collision calculée à partir des diagrammes de Feyman-Dyson du second ordre. Elle conduit à la formule de Moller pour la section efficace de collisions négator-négaton.

Pour alléger l'écriture, nous poserons

$$u(\varepsilon_{\text{a}}) = u(\mathfrak{p}_{\text{a}}, \varepsilon_{\text{a}}\mathfrak{n}_{\text{a}}). \tag{23}$$

L'élément de matrice de collision a pour expression [12])

$$(\varepsilon_{\text{c}}\varepsilon_{\text{d}}|M|\varepsilon_{\text{a}}\varepsilon_{\text{b}}) = \frac{e^2}{4\pi^2 i}\,\frac{1}{(E_{\text{a}}E_{\text{b}}E_{\text{c}}E_{\text{d}})^{\frac{1}{2}}}\left[\frac{\{u^+(\varepsilon_{\text{c}})i\gamma^\mu u(\varepsilon_{\text{a}})\}\{u^+(\varepsilon_{\text{d}})i\gamma_\mu u(\varepsilon_{\text{b}})\}}{(\mathfrak{p}_{\text{c}}-\mathfrak{p}_{\text{a}})^2} - \frac{\{u^+(\varepsilon_{\text{d}})i\gamma^\mu u(\varepsilon_{\text{a}})\}\{u^+(\varepsilon_{\text{c}})i\gamma_\mu u(\varepsilon_{\text{b}})\}}{(\mathfrak{p}_{\text{d}}-\mathfrak{p}_{\text{a}})^2}\right]. \tag{24}$$

Nous nous proposons d'évaluer la quantité $(\varepsilon_{\text{c}}\varepsilon_{\text{d}}|M|\varepsilon_{\text{a}}\varepsilon_{\text{b}})(\eta_{\text{a}}\eta_{\text{b}}|M^\dagger|\varepsilon_{\text{c}}\varepsilon_{\text{d}})$. Elle peut être mise sous la forme

$$(\varepsilon_{\text{c}}\varepsilon_{\text{d}}|M|\varepsilon_{\text{a}}\varepsilon_{\text{b}})(\eta_{\text{a}}\eta_{\text{b}}|M^\dagger|\eta_{\text{c}}\eta_{\text{d}}) = (\varepsilon_{\text{c}}\varepsilon_{\text{d}}|M|\varepsilon_{\text{a}}\varepsilon_{\text{b}})[(\eta_{\text{c}}\eta_{\text{d}}|M|\eta_{\text{a}}\eta_{\text{b}})]^* = \frac{e^4}{16\pi^4}\,\frac{1}{E_{\text{a}}E_{\text{b}}E_{\text{c}}E_{\text{d}}}\left[\frac{A}{\mathfrak{h}^4} - \frac{1}{\mathfrak{h}^2\mathfrak{k}^2}(C+D) + \frac{B}{\mathfrak{k}^4}\right], \tag{25}$$

où

$$A = \{u^+(\varepsilon_0)i\gamma^\mu u(\varepsilon_{\text{a}})\}\{u^+(\eta_{\text{a}})i\gamma u(\eta_{\text{c}})\}\{u^+(\varepsilon_{\text{d}})i\gamma_\mu u(\varepsilon_{\text{b}})\}\{u^+(\eta_{\text{b}})i\gamma u(\eta_{\text{d}})\},$$
$$C = \{u^+(\varepsilon_{\text{c}})i\gamma^\mu u(\varepsilon_{\text{a}})\}\{u^+(\eta_{\text{a}})i\gamma^\nu u(\eta_{\text{d}})\}\{u^+(\varepsilon_{\text{d}})i\gamma_\mu u(\varepsilon_{\text{b}})\}\{u^+(\eta_{\text{b}})i\gamma_\nu u(\eta_{\text{c}})\};$$

on obtient B à partir de A et D à partir de C, en faisant les substitutions $\text{c} \longleftrightarrow \text{d}$. On a d'autre part posé

$$\mathfrak{h} = \mathfrak{p}_{\text{c}}-\mathfrak{p}_{\text{a}} = \mathfrak{p}_{\text{b}}-\mathfrak{p}_{\text{d}}, \quad \mathfrak{k} = \mathfrak{p}_{\text{d}}-\mathfrak{p}_{\text{a}} = -\mathfrak{p}_{\text{c}}+\mathfrak{p}_{\text{b}}. \tag{26}$$

On désigne par $u \odot v$ la matrice d'élément $u_\alpha v_\beta$. En groupant convenablement les termes de A et C, on peut encore les écrire sous la forme

$$A = \text{tr}\,[\{u(\eta_{\text{c}}) \odot u^+(\varepsilon_{\text{c}})\}i\gamma^\mu\{u(\varepsilon_{\text{a}}) \odot u^+(\eta_{\text{c}})\}i\gamma^\nu] \times \text{tr}\,[\{u(\eta_{\text{a}}) \odot u^+(\varepsilon_{\text{d}})\}i\gamma_\mu\{u(\varepsilon_{\text{b}}) \odot u^+(\eta_{\text{b}})\}i\gamma_\nu], \tag{27}$$

$$C = \text{tr}\,[\{u(\eta_{\text{c}}) \odot u^+(\varepsilon_{\text{c}})\}i\gamma^\mu\{u(\varepsilon_{\text{a}}) \odot u^+(\eta_{\text{a}})\}i\gamma^\nu\{u(\eta_{\text{d}}) \odot u^+(\varepsilon_{\text{d}})\} \times i\gamma_\mu\{u(\varepsilon_{\text{b}}) \odot u^+(\eta_{\text{b}})\}i\gamma_\nu]. \tag{27'}$$

Dans B.M.W. on établit la formule

$$u(\mathfrak{p}, \varepsilon\mathfrak{n}) \odot u^{+}(\mathfrak{p}, \varepsilon'\mathfrak{n}) = \tfrac{1}{4}\left[\delta_{\varepsilon\varepsilon'} + i\gamma^{5} \sum_{i=1}^{i=3} \overline{n_i}(\tau_i)_{\varepsilon'\varepsilon}\right](\overline{p}+m). \tag{28}$$

Or la matrice densité ϱ_f décrivant l'état final est

$$(\varrho_f)_{\varepsilon_c \varepsilon_d \eta_c \eta_d} = \sum_{\varepsilon_a \varepsilon_b \eta_a \eta_b} (\varepsilon_c \varepsilon_d | M | \varepsilon_a \varepsilon_b)\,(\varrho_{in})_{\varepsilon_a \varepsilon_b \eta_a \eta_b}\,(\eta_a \eta_b | M^{\dagger} | \eta_c \eta_d). \tag{29}$$

Le calcul de ϱ_f a donc ainsi été ramené à un calcul de traces de produits de matrices de Dirac. Pour ces calculs, on peut faire usage en particulier de la formule

$$\tfrac{1}{4}\operatorname{tr} \overline{a_1}\,\overline{a_2} \ldots \overline{a_n} = \sum \delta P (a_{i_1} \cdot a_{i_2}) \ldots (a_{i_{n-1}} \cdot a_{i_n}).$$

La somme Σ est étendue à toutes les paires $(i_k,\ i_{k+1})$ avec $i_k < i_{k+1}$; δP est la signature de la permutation

$$P = \begin{pmatrix} 1 & \ldots & n \\ i_1 & \ldots & i_n \end{pmatrix}.$$

5. Diffusion d'un Faisceau d'Électrons par des Électrons Liés dont les Spins sont Orientes

Les électrons a sont des électrons d'un faisceau monocinétique polarisé. Le vecteur polarisation est noté ${}_a\mathfrak{s} = \sum_i {}_a\mathfrak{n}_i\, {}_a\zeta_i$. Les électrons b sont les électrons d'un atome d'une substance ferromagnétique aimantée à saturation. Nous supposons que les électrons a sont assez rapides pour que l'on puisse considérer les électrons b comme étant au repos dans le système du laboratoire. La polarisation des électrons b sera, dans ce repère, $\mathfrak{s}_b = (0, \zeta_b \mathbf{n})$ $\mathbf{n}$ étant un vecteur antiparallèle au champ magnétique extérieur. On pourra prendre pour $|\zeta_b|$ le rapport du nombre d'électrons magnétiques au nombre total d'électrons de l'atome, ce rapport est de l'ordre de 1/13 pour le fer. Nous allons calculer la section efficace de la diffusion a+b → c+d. Nous donnerons d'abord la formule relative à un repère quelconque. La matrice densité initiale s'écrit avec une normalisation convenable

$$\varrho_{in} = \tfrac{1}{4}\left[1 + {}_a\zeta_i(\tau_i \odot 1) + {}_b\zeta_j(1 \odot \tau_j) + {}_a\zeta_i\, {}_b\zeta_j(\tau_i \odot \tau_j)\right].$$

La section efficace de diffusion est proportionnelle à la quantité I, qui est donnée par

$$I = \frac{\operatorname{tr} \varrho_f}{\operatorname{tr} \varrho_{in}} = \operatorname{tr} \varrho_f = \operatorname{tr} M \varrho_{in} M^{\dagger}$$

$$= \operatorname{tr} M M^{\dagger} + {}_a\zeta_i \operatorname{tr} M(\tau_i \odot 1) M^{\dagger} + {}_a\zeta_j \operatorname{tr} M(1 \odot \tau_j) M^{\dagger} + {}_a\zeta_i\, {}_b\zeta_j \operatorname{tr} M(\tau_i \odot \tau_j) M^{\dagger}.$$

Examinons d'abord le cas où ${}_b\zeta_j = 0$. Ce cas correspond à une diffusion d'un faisceau d'électrons sur des électrons dont les spins ne sont pas orientés. La section efficace se réduit à

$$I_1 = \operatorname{tr} M M^\dagger + {}_a\zeta_i \operatorname{tr} M(\tau_i \odot 1)M^\dagger.$$

Nous allons montrer que $K_i = \operatorname{tr} M(\tau_i \odot 1)M^\dagger$ est une quantité nulle, ce qui entraîne que la section efficace ne dépend pas de la polarisation ζ_a. Ce résultat provient de l'approximation faite dans l'évaluation de M. Dans le cas des collisions nucléon-nucléon, où cette approximation n'est plus légitime, la quantité K_i a été trouvée expérimentalement différente de 0.

Nous avons

$$K_i = \sum (\varepsilon_c \varepsilon_d |M| \varepsilon_a \varepsilon_b)(\tau_i)_{\varepsilon_a \eta_a} \delta_{\varepsilon_b \eta_b} (\eta_a \eta_b |M^\dagger| \varepsilon_c \varepsilon_d)$$

$$= \frac{e^4}{16\pi^4} \frac{1}{E_a E_b E_c E_d} [A_i \mathfrak{h}^{-4} - \mathfrak{h}^{-2} \mathfrak{t}^{-2}(C_i + D_i) + \mathfrak{t}^{-4} B_i].$$

En tenant compte des égalités

$$\sum_\varepsilon u(\mathfrak{p}, \varepsilon \mathfrak{n}) \odot u^+(\mathfrak{p}, \varepsilon \mathfrak{n}) = \tfrac{1}{2}(\overline{p}| + m) \tag{30}$$

et

$$\sum_{\varepsilon\varepsilon'} u(\mathfrak{p}, \varepsilon \mathfrak{n}) \odot u^+(\mathfrak{p}, \varepsilon' \mathfrak{n})(\tau_i)_{\varepsilon\varepsilon'} = \tfrac{1}{2} i\gamma^5 \overline{n_i}(\overline{p}| + m), \tag{30'}$$

qui sont des conséquences immédiates de (28), on obtient pour A_i et C_i les expressions

$$A_i = \tfrac{1}{4} \operatorname{tr} [(\overline{p}|_c + m) i\gamma^\mu i\gamma^5 \overline{{}_a n_i}(\overline{p}|_a + m) i\gamma^\nu] \tfrac{1}{4} \operatorname{tr} [(\overline{p}|_d + m) i\gamma_\mu (\overline{p}|_b + m) i\gamma_\nu],$$

$$C_i = \tfrac{1}{16} \operatorname{tr} [(\overline{p}|_c + m) i\gamma^\mu i\gamma^5 \overline{{}_a n_i}(\overline{p}|_a + m) i\gamma^\nu (\overline{p}|_d + m) i\gamma_\mu (\overline{p}|_b + m) i\gamma_\nu].$$

Les quantités A_i et C_i doivent être réelles. Or avec la définition que nous avons choisie pour les matrices de Dirac, il existe une représentation dans laquelle elles sont toutes réelles (représentation de Majorana). On voit alors que les expressions donnant A_i et C_i sont imaginaires pures. On a donc

$$A_i = C_i = D_i = B_i = 0,$$

ce qui démontre le résultat annoncé.

Revenons maintenant au cas de la diffusion des faisceaux d'électrons polarisés par des électrons orientés. La section efficace de diffusion est donc de la forme

$$\sigma = \sigma_0(1 + \lambda_{ij}\, {}_a\zeta_i\, {}_b\zeta_j), \tag{31}$$

σ_0 désignant la section efficace calculée par Møller. La formule donnant λ_{ij} est

$$\lambda_{ij} = \frac{\operatorname{tr} M(\tau_i \odot \tau_j)M^\dagger}{\operatorname{tr} M M^\dagger}.$$

Nous poserons

$$\lambda_{ij} = \frac{N_{ij}}{D}$$

avec

$$D = A_0 \mathfrak{k}^4 - (C_0 + D_0)\mathfrak{h}^2 \mathfrak{k}^2 + B_0 \mathfrak{k}^4,$$
$$N_{ij} = A_{ij} \mathfrak{k}^4 - (C_{ij} + D_{ij})\mathfrak{h}^2 \mathfrak{k}^2 + B_{ij} \mathfrak{h}^4.$$

Les quantités $A_0, B_0, \ldots, A_{ij}, B_{ij}$ ont été calculées à l'aide des formules suivantes, obtenues en appliquant (30) et (30′):

$$A_0 = \tfrac{1}{4}\,\mathrm{tr}\,[(\overline{p}|_c + m)\gamma^\mu(\overline{p}|_a + m)\gamma^\nu]\,\tfrac{1}{4}\,\mathrm{tr}\,[(\overline{p}|_d + m)\gamma_\mu(\overline{p}|_b + m)\gamma_\nu],$$
$$C_0 = \tfrac{1}{4}\,\mathrm{tr}\,[(\overline{p}|_c + m)\gamma^\mu(\overline{p}|_a + m)\gamma^\nu(\overline{p}|_d + m)\gamma_\mu(\overline{p}|_b + m)\gamma_\nu],$$
$$A_{ij} = \tfrac{1}{4}\,\mathrm{tr}\,[(\overline{p}|_c + m)\gamma^\mu i\gamma^5\,\overline{{}_a n_i|}(\overline{p}|_a + m)\gamma^\nu]\,\tfrac{1}{4}\,\mathrm{tr}\,[(\overline{p}|_d + m)\gamma_\mu i\gamma^5\,\overline{{}_b n_j|}(\overline{p}|_b + m)\gamma_\nu],$$
$$C_{ij} = \tfrac{1}{16}\,\mathrm{tr}\,[(\overline{p}|_c + m)\gamma^\mu i\gamma^5\,\overline{{}_a n_i|}(\overline{p}|_a + m)\gamma^\nu(\overline{p}|_d + m)\gamma_\mu i\gamma^5\,\overline{{}_b n_j|}(\overline{p}|_b + m)\gamma_\nu].$$

Il est commode de définir les trois nombres $\varkappa, \lambda, \mu$ par

$$\mathfrak{p}_a \cdot \mathfrak{p}_b = \mathfrak{p}_c \cdot \mathfrak{p}_d = m^2\varkappa, \quad \mathfrak{p}_a \cdot \mathfrak{p}_c = \mathfrak{p}_b \cdot \mathfrak{p}_d = m^2\lambda, \quad \mathfrak{p}_a \cdot \mathfrak{p}_d = \mathfrak{p}_b \cdot \mathfrak{p}_c = m^2\mu;$$

ces trois nombres sont liés par la relation $\lambda + \mu = \varkappa + 1$. Le calcul donne †, pour N_{ij} et D,

$$\begin{aligned} N_{ij} = {} & 2({}_a\mathfrak{n}_i \cdot {}_b\mathfrak{n}_j)\,[3(\lambda+\mu) - 4 - \lambda\mu]\,(\lambda-1)(\mu-1) \\ & + m^{-2}({}_a\mathfrak{n}_i \cdot \mathfrak{p}_c)({}_b\mathfrak{n}_j \cdot \mathfrak{p}_d)(2\lambda-3)(\mu-1)^2 \\ & + m^{-2}({}_a\mathfrak{n}_i \cdot \mathfrak{p}_d)({}_b\mathfrak{n}_j \cdot \mathfrak{p}_c)(2\mu-3)(\lambda-1)^2 \\ & - m^{-2}[({}_a\mathfrak{n}_i \cdot \mathfrak{p}_c)({}_b\mathfrak{n}_j \cdot \mathfrak{p}_c) + ({}_a\mathfrak{n}_i \cdot \mathfrak{p}_d)({}_b\mathfrak{n}_j \cdot \mathfrak{p}_d)](\lambda-1)(\mu-1), \end{aligned} \tag{32}$$

$$\begin{aligned} D = {} & (\lambda^2 + 2\mu^2 + 2\lambda\mu - 4\lambda - 2\mu + 3)(\mu-1)^2 + (2\lambda^2 + \mu^2 + 2\lambda\mu \\ & - 4\mu - 2\lambda + 3)(\lambda-1)^2 + 2(\lambda+\mu-1)(\lambda+\mu-3)(\lambda-1)(\mu-1). \end{aligned} \tag{32′}$$

En vue des applications, on a intérêt à écrire ces formules dans le système du laboratoire (électrons b au repos) et à faire le choix de paramètres suivant. On pose

$$E_a = m(w+1), \quad E_c = m(wy+1), \quad \tfrac{1}{2} \leqq y \leqq 1, \tag{33}$$

en désignant par c l'électron final le plus rapide. Les vecteurs ${}_a\mathfrak{n}_i$ et ${}_b\mathfrak{n}_j$ sont pris comme suit:

$${}_a\mathfrak{n}_3 = [w(w+2)^{\frac{1}{2}},\ (1+w)\mathbf{x}_3], \qquad {}_b\mathfrak{n}_3 = (0, \mathbf{x}_3),$$
$${}_a\mathfrak{n}_1 = (0, \mathbf{x}_1), \qquad {}_b\mathfrak{n}_1 = (0, \mathbf{x}_1),$$
$${}_a\mathfrak{n}_1 = (0, \mathbf{x}_2), \qquad {}_b\mathfrak{n}_2 = (0, \mathbf{x}_2);$$

$\mathbf{x}_3$ est un vecteur unitaire parallèle à $\mathfrak{p}_a$, $\mathbf{x}_1$ est un vecteur unitaire perpendiculaire à $\mathbf{p}_a$ et situé dans le plan de diffusion, $\mathbf{x}_2 = \mathbf{x}_3 \times \mathbf{x}_1$. On trouve alors, pour les coefficients λ_{ij},

† Nous avons publié cette expression dans une note [11]) où nous proposions la mesure de la corrélation des polarisations des faisceaux d'électrons c et d, les électrons a et b n'étant pas polarisés. Malheureusement, l'expression de N_{ij} dans cette note contient des erreurs.

$$\lambda_{13} = \lambda_{31} = \lambda_{12} = \lambda_{21} = 0,$$
$$\Delta \cdot \lambda_{11} = -y(1-y)[1+w+y(1-y)w(4+w)],$$
$$\Delta \cdot \lambda_{22} = -y(1-y)[1+2w-y(1-y)w^2], \tag{34}$$
$$\Delta \cdot \lambda_{33} = -y(1-y)[(1+w)(1+2w)-y(1-y)w(4+w)],$$
$$\Delta \cdot \lambda_{13} = \Delta \cdot \lambda_{31} = -y(1-y)(1-2y)w[2y(1-y)(2+w)]^{\frac{1}{2}},$$

avec

$$\Delta = (1+w)^2-y(1-y)(3+6w+2w^2)+y^2(1-y)^2w^2.$$

On remarque sur ces formules que λ_{11}, λ_{22}, λ_{33} sont symétriques et λ_{13} est antisymétrique pour l'échange de y et $1-y$. Il est facile de voir que ces symétries sont des conséquences de l'indiscernabilité des particules finales c et d.

Les calculs précédents suggèrent une méthode de mesure de la polarisation d'un faisceau d'électrons relativistes polarisés. On fait tomber ce faisceau sur une cible formée d'une plaque d'un corps magnétique aimanté à saturation. On mesure le rapport des sections efficaces pour deux valeurs opposées du champ magnétisant.

Soient $\mathbf{n}$ et $-\mathbf{n}$ les deux directions successives du champ magnétisant, et σ_+ et σ_- les sections efficaces correspondantes. Comme nous l'avons vu, la polarisation des électrons b est respectivement ${}_b\zeta n$ et $-{}_b\zeta n$, où $n = (0, \mathbf{n})$, et ${}_b\zeta$ est de l'ordre de $-1/13$ pour le fer. En partant de (31), on trouve que la polarisation de l'électron a est alors ${}_a\zeta_i n_i$, les ${}_a\zeta_i$ satisfaisant l'équation

$${}_b\zeta \sum_{i,j} {}_a\zeta_i \lambda_{ij} \mathbf{n} \cdot \mathbf{x}_j = \frac{\sigma_+-\sigma_-}{\sigma_++\sigma_-}. \tag{35}$$

En prenant trois directions différentes pour le champ magnétisant, on mesure les trois ${}_a\zeta_i$.

En général, on observera les électrons finaux c et d lorsqu'ils partent symétriquement par rapport à $\mathbf{p}_a$, ce qui revient à faire $y = 1-y = \frac{1}{2}$ dans les formules (34). Les quantités λ_{ii} sont stationnaires pour cette valeur du paramètre y. Les formules (34) deviennent alors

$$\lambda_{11} = -\frac{4+8w+w^2}{4+8w+9w^2}, \quad \lambda_{22} = -\frac{4+8w-w^2}{4+8w+9w^2}, \quad \lambda_{33} = -\frac{4+8w+7w^2}{4+8w+9w^2}, \tag{36}$$

les autres λ_{ij} étant nuls. Dans ce cas, la polarisation du faisceau a est donnée par

$${}_a\zeta_i = \frac{1}{{}_b\zeta\, \lambda_{ii}(\mathbf{n} \cdot \mathbf{x}_i)} \frac{\sigma_+-\sigma_-}{\sigma_++\sigma_-}. \tag{37}$$

Ce résultat montre que cette méthode s'applique indifféremment à la mesure des polarisations longitudinale (${}_a\zeta_3$) ou transversales (${}_a\zeta_1$ et ${}_a\zeta_2$) d'un faisceau d'électrons. L'effet à mesurer est $(\sigma_+-\sigma_-)/(\sigma+{}_+\sigma_-)$. Sa dépendance en énergie est donnée par les λ_{ii} de la formule (36).

Nous traçons, dans la figure 1, les courbes $\lambda_{ii}(w)$. Pour la polarisation longitudinale λ_{33} varie très peu avec l'énergie, puisqu'il ne décroît que de

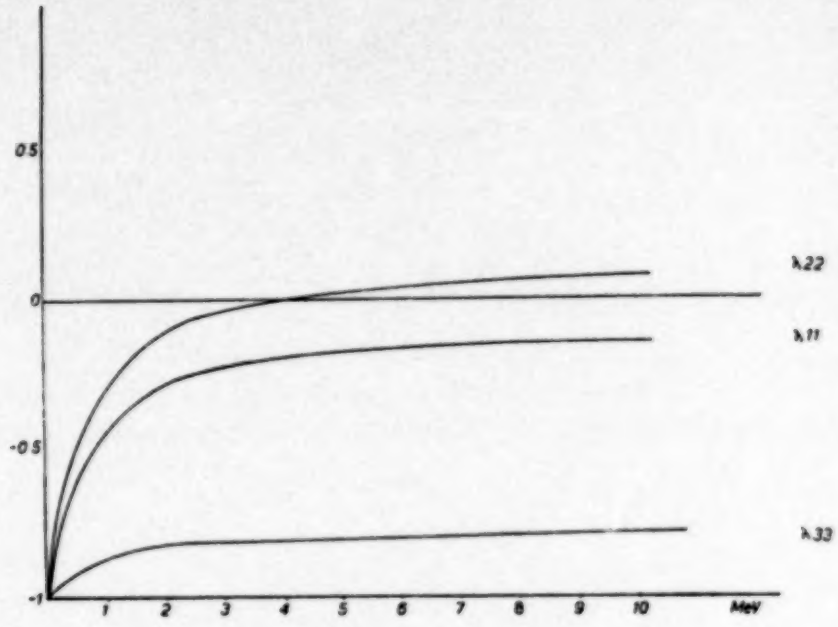

Fig. 1. Les courbes donnent les quantités $\lambda_{ii}(w)$ définies par les éqs. (36). Dans la collision négaton-négation a+b → c+d, où b est au repos, c et d se partagent également l'énergie cinétique w de l'électron a; si ${}_a\zeta_i\,\mathbf{n}_i$ et ${}_b\zeta_j\,\mathbf{n}_j$ sont les polarisations respectives de a et de b, la section efficace de la collision est $\sigma = \sigma_0\ (1+\lambda_{ij}\,{}_a\zeta_i\,{}_b\zeta_j)$. Les λ_{ij} non diagonaux sont nuls.

1 à 7/9 lorsque w varie de 0 à ∞ (l'approximation faite dans nos calculs n'est certainement plus valable pour des valeurs de $w < 0.2$). Cette mesure de la polarisation longitudinale des électrons s'applique donc dans un domaine d'énergie assez grand.

6. Modification de la Polarisation d'un Faisceau d'Électrons par Diffusion sur des Électrons non Polarisés

Les électrons a sont les électrons d'un faisceau polarisé, de vecteur polarisation $\hat{s} = \sum_i {}_a\mathbf{n}_i\,{}_a\zeta_i$. Les électrons b sont les électrons non polarisés d'un atome. On suppose encore ici que les électrons a sont assez rapides pour qu'il soit légitime de considérer les électrons b comme au repos dans le système du laboratoire. La matrice densité représentant l'état initial s'écrit avec une normalisation convenable:

$$\varrho_i = \tfrac{1}{4}[1+{}_a\zeta_i(\tau_i \odot 1)].$$

On cherche la polarisation de l'électron final c (ou d). La matrice densité finale est donnée par la formule

$$\varrho_f = M\varrho_i M^\dagger = \tfrac{1}{4}(MM^\dagger + \sum_i {}_a\zeta_i M(\tau_i \odot 1)M^\dagger).$$

La polarisation de l'électron final est obtenue en utilisant la formule (14), soit

$${}_c\zeta_j = \frac{1}{\operatorname{tr}\varrho_f} \cdot \operatorname{tr}\,[\varrho_f(\tau_j \odot 1)].$$

Or on a vu au § 5 que

$$\operatorname{tr}\varrho_f = \tfrac{1}{4}\operatorname{tr} MM^\dagger + \tfrac{1}{4}\sum_i {}_a\zeta_i \operatorname{tr} M(\tau_i \odot 1)M^\dagger = \tfrac{1}{4}\operatorname{tr} MM^\dagger.$$

D'autre part on a

$$\operatorname{tr}\,[\varrho_f(\tau_j \odot 1)] = \tfrac{1}{4}\operatorname{tr}\,[MM^\dagger(\tau_j \odot 1)] + \tfrac{1}{4}\sum_i {}_a\zeta_i \operatorname{tr}\,[M(\tau_i \odot 1)M^\dagger(\tau_j \odot 1)].$$

Par un raisonnement identique à celui déjà utilisé au § 5, on montre que $\operatorname{tr}(MM^\dagger\tau_i) = 0$; finalement on obtient pour ${}_c\zeta_j$ l'expression suivante:

$${}_c\zeta_j = \sum_i {}_a\zeta_i \frac{\operatorname{tr} M(\tau_i \odot 1)M^\dagger(\tau_j \odot 1)}{\operatorname{tr} MM^\dagger} = \sum_i {}_a\zeta_i C_{ij}. \tag{38}$$

Le calcul de

$$C_{ij} = \frac{\operatorname{tr}\,[M(\tau_i \odot 1)M^\dagger(\tau_j \odot 1)]}{\operatorname{tr} MM^\dagger}$$

a été fait par les méthodes utilisées au § 5. L'expression de C_{ij} est écrite à l'aide des nombres λ et μ introduits dans ce paragraphe (cf. éq. (32)). On a

$$C_{ij} = \frac{K_{ij}}{D}$$

avec

$$\begin{aligned} K_{ij} = {} & ({}_a\mathbf{n}_i \cdot {}_c\mathbf{n}_j)2(\mu-1)[(\lambda+\mu-2)(-\mu^2-\lambda\mu+3\lambda+\mu-3)+2(\lambda-1)] \\ & +m^{-2}({}_a\mathbf{n}_i \cdot \mathbf{p}_c)({}_c\mathbf{n}_j \cdot \mathbf{p}_a)(\mu-1)^2[2\lambda+2\mu-3] \\ & +m^{-2}[({}_a\mathbf{n}_i \cdot \mathbf{p}_c)({}_c\mathbf{n}_j \cdot \mathbf{p}_b)+({}_a\mathbf{n}_i \cdot \mathbf{p}_d)({}_c\mathbf{n}_j \cdot \mathbf{p}_a)](\mu-1)[2\mu(\mu-1) \\ & \qquad +(2\mu-1)(\lambda-1)] \\ & +m^{-2}[({}_a\mathbf{n}_i \cdot \mathbf{p}_d)({}_c\mathbf{n}_j \cdot \mathbf{p}_b)(\lambda-1)[2(\mu-1)(2-\mu-\lambda)+\lambda-1] \end{aligned} \tag{39}$$

et D donné par (32′).

Dans ce qui suit nous allons nous limiter au cas où les électrons c et d partent dans des directions symétriques par rapport à $\mathbf{p}_a$. On choisit ${}_a\mathbf{n}_i$ comme au § 5. Les vecteurs ${}_c\mathbf{n}_i$ sont pris comme suit:

$${}_c\mathbf{n}_1 = (0, \mathbf{x}'_1) \quad {}_c\mathbf{n}_2 = (0, \mathbf{x}_2) \quad {}_c\mathbf{n}_3 = [\tfrac{1}{2}(w^2+4w)^{\frac{1}{2}}, (1+\tfrac{1}{2}w)\mathbf{x}'_3];$$

le vecteur $\mathbf{x}'_3$ est un vecteur unitaire parallèle à $\mathbf{p}_c$ et $\mathbf{x}'_1$ est défini par $\mathbf{x}'_1 = \mathbf{x}_2 \times \mathbf{x}'_3$. Si l'on suppose l'électron a polarisé longitudinalement $({}_a\zeta_1 = {}_a\zeta_2 = 0)$, on a

$$_c\zeta_1 = C_{31}\zeta_3, \qquad _c\zeta_2 = 0, \qquad _c\zeta_3 = C_{33}\,_a\zeta_3.$$

On voit que l'électron c est polarisé transversalement le long de $\mathbf{x'}_1$. Posons

$$\zeta_1 = {}_a\zeta_3, \quad \zeta'_t = {}_c\zeta_1.$$

La polarisation transversale de l'électron final ζ'_t est alors donnée par

$$\zeta'_t = \zeta_1 \left(\frac{2}{w+4}\right)^{\frac{1}{2}} \frac{8w(1+w)}{9w^2+8w+4} = \zeta_1 f(w). \tag{40}$$

Dans la fig. 2 nous traçons la courbe ζ'_t/ζ_1 en fonction de l'énergie cinétique w de l'électron incident. La polarisation transversale peut alors être

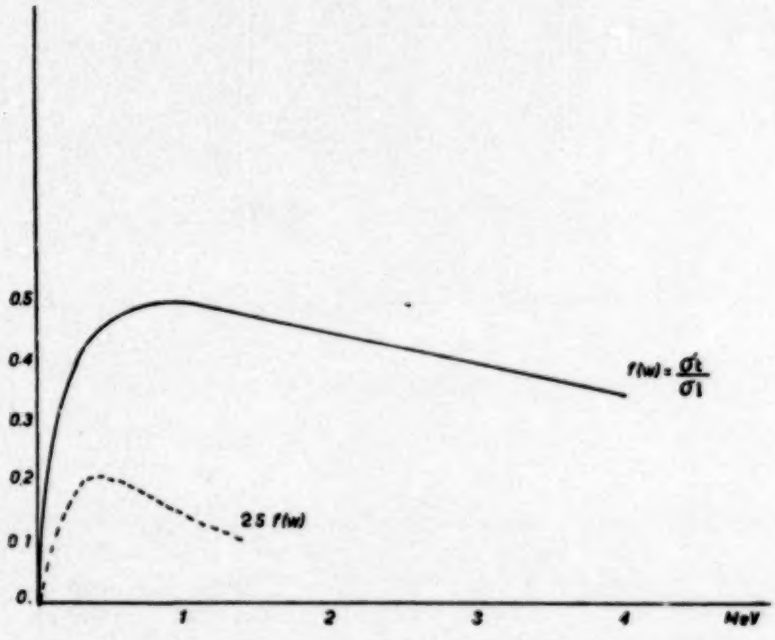

Fig. 2. Dans la collision négaton-négaton a+b → c+d, le négaton a, d'énergie cinétique w, a une polarisation longitudinale ζ_1, le négaton b est au repos. Le degré de polarisation transversale de c est $f(w)\zeta_1$. Si c subit une diffusion coulombienne perpendiculaire au plan abcd, l'asymétrie observée sera $2Sf(w)\zeta_1$.

mesurée par une diffusion coulombienne. Si cette diffusion coulombienne est dans le plan des faisceaux a, c, d, les sections efficaces $\sigma(\vartheta)$ et $\sigma(-\vartheta)$ sont égales. Si cette diffusion coulombienne est dans un plan perpendiculaire au plan a, c, d, l'asymétrie $S(\vartheta)$ entre $\sigma(\vartheta)$ et $\sigma(-\vartheta)$ est maximum.

Le schéma d'expérience de la figure 3 est tracé pour $\vartheta = \pm 90°$.

On mesurera le rapport des sections efficaces σ' et σ'', qui dépend ainsi de ζ_1:

$$\frac{\sigma''}{\sigma'} = \frac{1+\zeta_1 Sf(w)}{1-\zeta_1 Sf(w)}, \tag{41}$$

où $f(w)$ est donné par l'éq. (40) et est tracé sur la fig. 2. L'asymétrie $S(\vartheta)$ dans la diffusion coulombienne d'électrons polarisés a été récemment re-

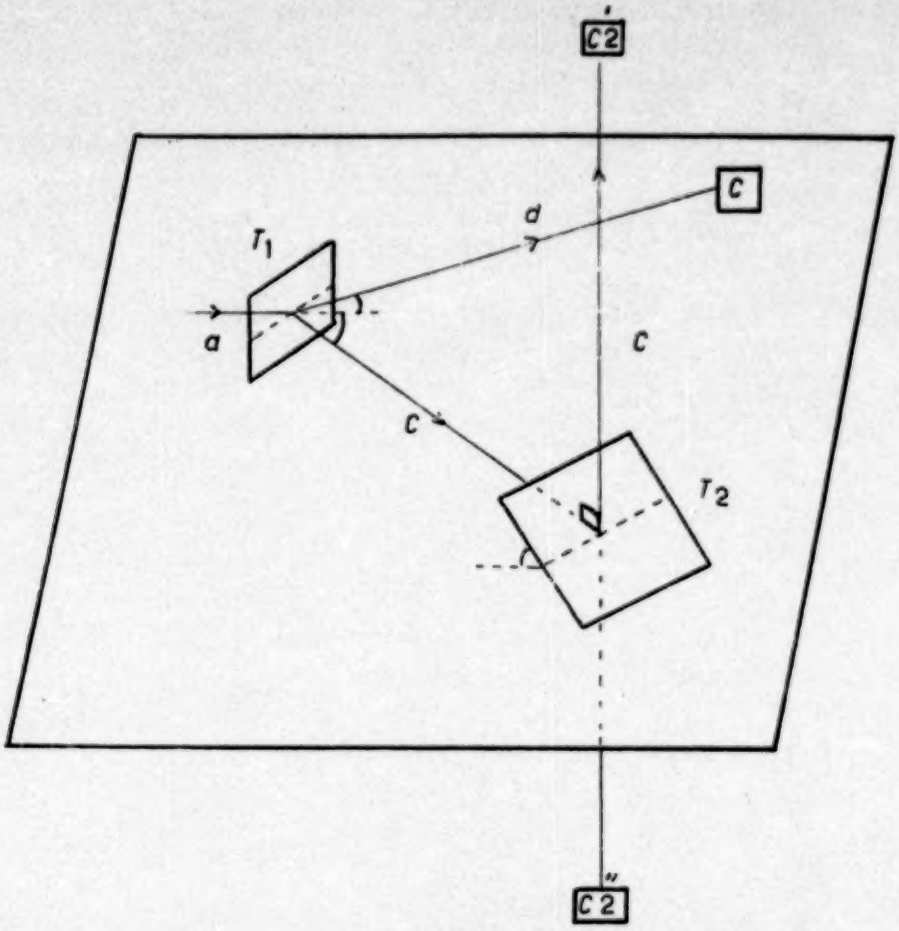

Fig. 3. Schéma d'une expérience pour mesurer la polarisation longitudinale ζ_1 du négaton a par collision avec un négaton b dans une cible T_1 (élément de faible Z). Le négaton c a une polarisation partiellement transversale. Si T_2 est une cible mince d'élément de grand Z, la diffusion coulombienne de c dans T_2 est asymétrique. La mesure du rapport $\frac{\sigma''}{\sigma'} = \frac{\text{coincidences c, c''}_2}{\text{coincidences c, c'}_2}$ permet de mesurer ζ_1 (voir éq. (41)).

calculée pour $Z = 80$ avec l'aide d'une machine électronique par Sherman [12]). En utilisant ces valeurs numériques pour la diffusion à 90° nous donnons en pointillé dans la fig. 2 le produit $Sf(w)$ qui donne directement l'asymétrie (41) qui serait observée dans l'expérience décrite sur la figure 3.

7. Effets de Polarisation dans les Collisions Positon-négaton

On peut reprendre les études faites aux §§ 5 et 6 en supposant que l'électron incident est un positon. La comparaison des diagrammes décrivant les collisions négaton-négaton et positon-positon permet d'établir une loi de correspondance simple entre les éléments de matrice des deux processus (voir par exemple réf. [9]), p. 257).

Désignons par $\mathfrak{p}'_a$ et $\mathfrak{p}'_c$ les impulsions-énergies du positon initial et du positon final et par $\mathfrak{p}'_b$ et $\mathfrak{p}'_d$ celles du négaton initial et du négaton final. La théorie générale des collisions $a'+b' \to c'+d'$ entre un positon et un négaton se déduit de celle que nous avons exposée au § 4 pour les collisions entre deux négatons par la correspondance suivante:

$$\begin{aligned}
\mathfrak{p}_a &\to -\mathfrak{p}'_c \qquad \varepsilon_a \cdot {}_a\pi_i \to \varepsilon'_c \cdot {}_c\pi'_i \\
\mathfrak{p}_b &\to +\mathfrak{p}'_b \qquad \varepsilon_b \cdot {}_b\pi_i \to \varepsilon'_b \cdot {}_b\pi'_i \\
\mathfrak{p}_c &\to -\mathfrak{p}'_a \qquad \varepsilon_c \cdot {}_c\pi_i \to \varepsilon'_a \cdot {}_a\pi'_i \\
\mathfrak{p}_d &\to +\mathfrak{p}'_d \qquad \varepsilon_d \cdot {}_d\pi_i \to \varepsilon'_d \cdot {}_d\pi'_i
\end{aligned}$$

où les $\varepsilon' \cdot \pi'$ indiquent les états de polarisation.

7.1. DIFFUSION DE POSITONS SUR DES NÉGATONS LIÉS ET ORIENTÉS

La section efficace de diffusion est de la forme

$$\sigma = \sigma_B(1+\lambda'_{ij}\,{}_a\zeta'_i\,{}_b\zeta'_j);$$

σ_B est la section efficace calculée par Bhabha. Posons $\lambda_{ij} = K_{ij}/D$. Les considérations précédentes montrent que K_{ij} et D sont les expressions données par les formules (39). Pour achever la suite du calcul il suffit, dans ces formules, de faire la substitution précédemment définie.

7.2. MODIFICATION DE LA POLARISATION D'UN POSITON PAR DIFFUSION SUR DES NÉGATONS

La polarisation ${}_c\zeta'_i$ du positon après collision est donnée par la formule ${}_c\zeta'_j = \sum C'_{ij}\,{}_a\zeta'_i$. Dans cette formule ${}_a\zeta_i$ désigne la polarisation de l'électron incident et $C'_{ij} = N_{ij}/D$. Les quantités N_{ij} et D sont données par les formules (32). Le calcul s'achève en faisant la substitution déjà indiquée.

Nous laissons au lecteur le soin d'établir des formules explicites.

Il faut noter que la diffusion coulombienne est un analyseur de polarisation (transversale) plus médiocre pour les positons que pour les négatons. Par contre, l'annihilation de positons polarisés avec des négatons orientés peut fournir la base d'une autre méthode de mesure de la polarisation des positons. Le calcul des effets de polarisation pour l'annihilation en deux photons a été faite par Page [13]).

Nous remercions M. Halban, M. Gorodetzky et ses collaborateurs pour les nombreuses discussions que nous avons eues avec eux au sujet des possibilités expérimentales des différentes méthodes que nous avons exposées.

Nous remercions le Service des Poudres et le Comité Scientifique de l'Armée pour leur aide. Nous remercions aussi M. Lévy et le Laboratoire de Physique de l'École Normale Supérieure de leur hospitalité.

Appendice

Nous utilisons comme tenseur fondamental $g^{00} = -g^{11} = -g^{22} = -g^{33} = 1$, $g^{\mu\nu} = 0$ si $\mu \neq \nu$. Les deux tenseurs $g_{\mu\nu}$ et $g^{\mu\nu}$ ont les mêmes éléments. Le produit scalaire est noté avec la convention usuelle de sommation sur les indices muets:

$$\mathfrak{a} \cdot \mathfrak{b} = a^\mu g_{\mu\nu} b^\nu = a^\mu b_\mu = a_\mu b^\mu.$$

Le tenseur complètement antisymétrique de rang 4 est noté $\varepsilon^{\mu\nu\varrho\lambda}$ avec $\varepsilon^{0123} = 1$.

Les matrices γ^μ sont définies par

$$\gamma^\mu \gamma^\nu + \gamma^\nu \gamma^\mu = -2g^{\mu\nu}.$$

On peut déplacer leur indice ainsi:

$$\gamma_\mu = g_{\mu\nu} \gamma^\nu.$$

Nous utilisons la notation $\overline{p} = i\gamma^\mu p_\mu$. Le symbole * signifie complexe conjugué, † signifie hermitique conjugué. Nous n'écrivons pas les indices spinoriels, par exemple si γ est une matrice et u un spineur, γu doit être lu $\sum_\beta \gamma_{\alpha\beta} u_\beta$ et $u\gamma$ doit être lu $\sum_\alpha u_\alpha \gamma_{\alpha\beta}$.
Si A est une matrice telle que $(Ai\gamma^\mu)^\dagger = Ai\gamma^\mu$, le spineur adjoint de u est $u^+ = u^* A$.

Nous utilisons la représentation usuelle des matrices de Pauli

$$\tau_1 = \begin{pmatrix} 0 & 1 \\ 1 & 0 \end{pmatrix}, \quad \tau_2 = \begin{pmatrix} 0 & -i \\ i & 0 \end{pmatrix}, \quad \tau_3 = \begin{pmatrix} 1 & 0 \\ 0 & -1 \end{pmatrix}.$$

Nous notons le produit tensoriel par $\odot$.

Bibliographie

1) C. N. Yang and T. D. Lee, Phys. Rev. **104** (1956) 254
2) F. Bourdelet et L. Michel, à paraître
3) L. Michel et A. S. Wightman, Phys. Rev. **98** (1955) 1190
4) V. Bargmann et E. Wigner, Proc. Nat. Acad. Sc. **34** (1948) 211
5) Voir par ex. A. Messiah, Cours de Mécanique quantique, Tome 3, XVI, 47 (Saclay 1954)
6) H. A. Tolhoek, Revs. Mod. Phys. **28** (1956) 277
7) W. H. Louisell, R. W. Pidd et H. R. Crane, Phys. Rev. **94** (1954) 7
8) Cf. réf. [3]) et notes ronéotypées de l'Université de Princeton sur la polarisation des particules de masse nulle et de spin $\frac{1}{2}$
9) Jauch and Rohrlich, Theory of photons and electrons (Cambridge, Mass., 1955)
10) R. G. Newton, Phys. Rev. **103** (1956) 385
11) C. Bouchiat et L. Michel, C. R. Ac. Sc. Paris **243** (1956) 642
12) N. Sherman, Phys. Rev. **103** (1956) 1602
13) L. A. Page, Phys. Rev. **106** (1956) 394
14) C. Bouchiat et L. Michel, Phys. Rev. **106** (1957) 170

Nuclear Physics **5** (1958) 435—446; © *North-Holland Publishing Co., Amsterdam*
Not to be reproduced by photoprint or microfilm without written permission from the publisher

K-SHELL IONIZATION BY PROTONS

S. MESSELT
Department of Physics, University of Oslo, Blindern, Norway

Received 28 September 1957

Abstract: The thick target yield of K-shell X-rays produced when protons of 0.14 to 1.3 MeV energy are stopped in Fe, Cu, Mo, Ag, Sn and Ta has been measured with a NaI scintillation spectrometer. The corresponding cross sections for K-shell ionization have been determined. The experimental values for the cross sections vary less with the atomic number and more with the energy than predicted by theory. An empirical formula, which reproduces with good approximation results reported here and by others, is given.

1. Introduction

With the development of the scintillation spectrometer technique, the absolute yield of X-rays with energies down to a few keV can be measured with better accuracy than before. Some measurements of the yield of K- and L-shell X-rays produced by protons, in which this technique has been used, have now been reported. Lewis, Simmons and Merzbacher [1]), and Bevington and Bernstein [2]), using Fe, Mo and heavier elements and 1.5 to 4 MeV protons, found good agreement with the calculations by Henneberg [3]) for the light elements and lowest proton energies. But heavier elements and higher energies gave cross sections greater than predicted by the non-relativistic formula. Calculations by Jamnik and Zupančič [4]) show that the relativistic corrections for silver are small, while they are appreciable for lead and improve the agreement with experiment.

However, no measurements were done with bombarding energies lower than 1.5 MeV. An investigation was started therefore to check the theory more carefully in this low energy region. Measurements of the ionization cross section in Cu and Mo for 0.2 to 1.6 MeV protons [5]) gave values in good agreement with theory at the highest energies, but much smaller values than the theoretical ones at proton energies below 0.5 MeV. A further investigation has now been done, using an improved scintillation spectrometer, Fe, Cu, Mo, Ag, Sn and Ta as targets and proton energies from 1.3 MeV down to 0.14 MeV for the two lightest elements. An analysis of the experimental results together with values obtained by others gives a different dependence on atomic number and energy than predicted by theoretical calculations.

2. Experimental Arrangement

The thick target was placed at an angle of 45° to the proton beam from the Van de Graaff generator. X-rays produced in the target passed through

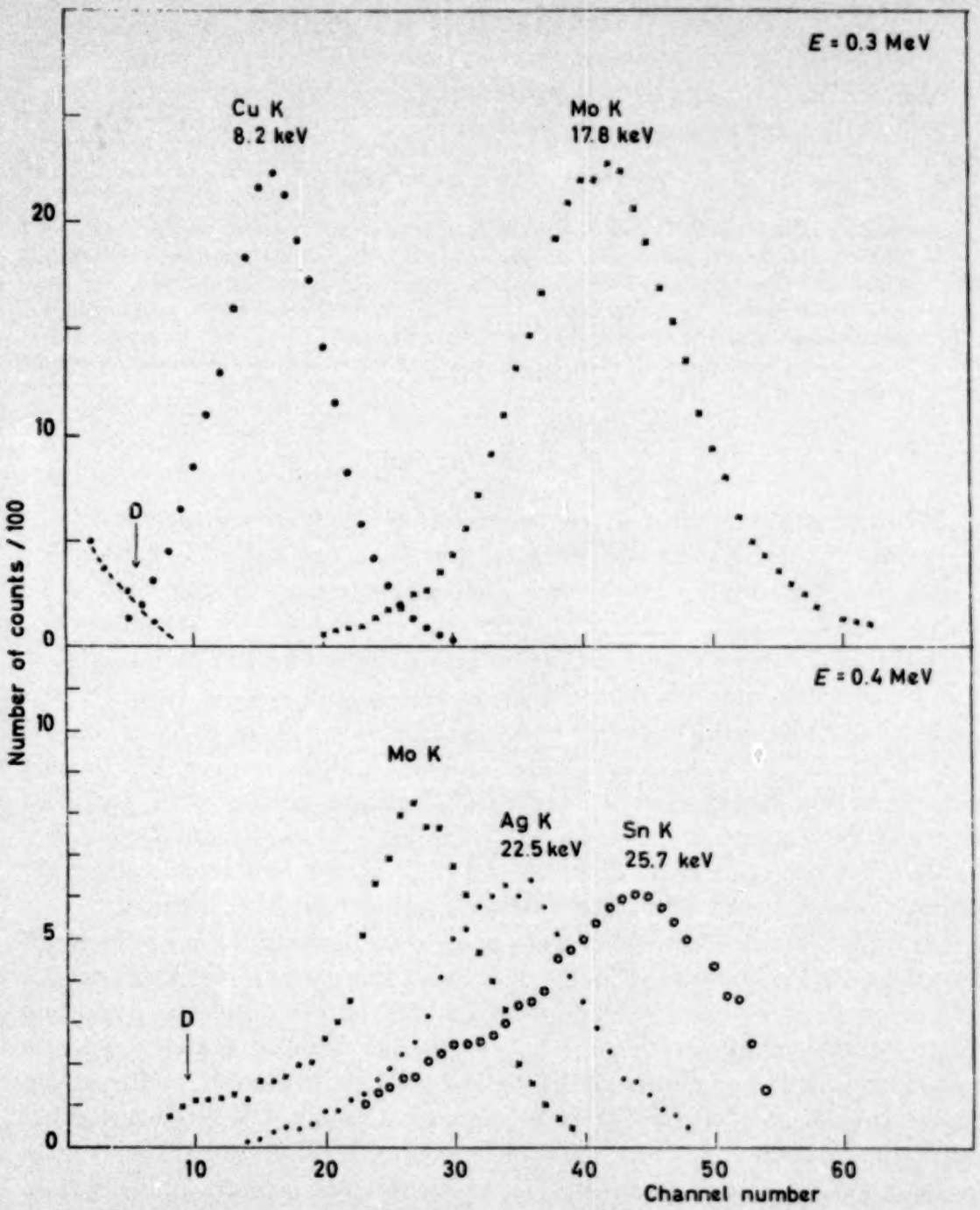

Fig. 1. Typical differential pulse-height spectra of the K-shell X-rays from Cu, Mo, Ag and Sn. The discriminator settings when measuring the total counting rate are indicated by D.

a 0.0023 cm thick aluminium window and were detected by a scintillation counter placed perpendicular to the proton beam. The distance from target

to detector was varied from 8 to 90 cm to obtain suitable counting rates at the different proton energies. The proton beam was measured with an electronic current integrator with an accuracy better than 3 %.

The NaI(Tl) scintillator, 2.5 cm in diameter and 0.1 cm thick with a 1 mil aluminium window in front, was manufactured and canned by Harshaw Chemical Company. It was mounted on a Dumont 6292 photomultiplier and shielded with lead, the hole in front of the scintillator being 2 cm in diameter.

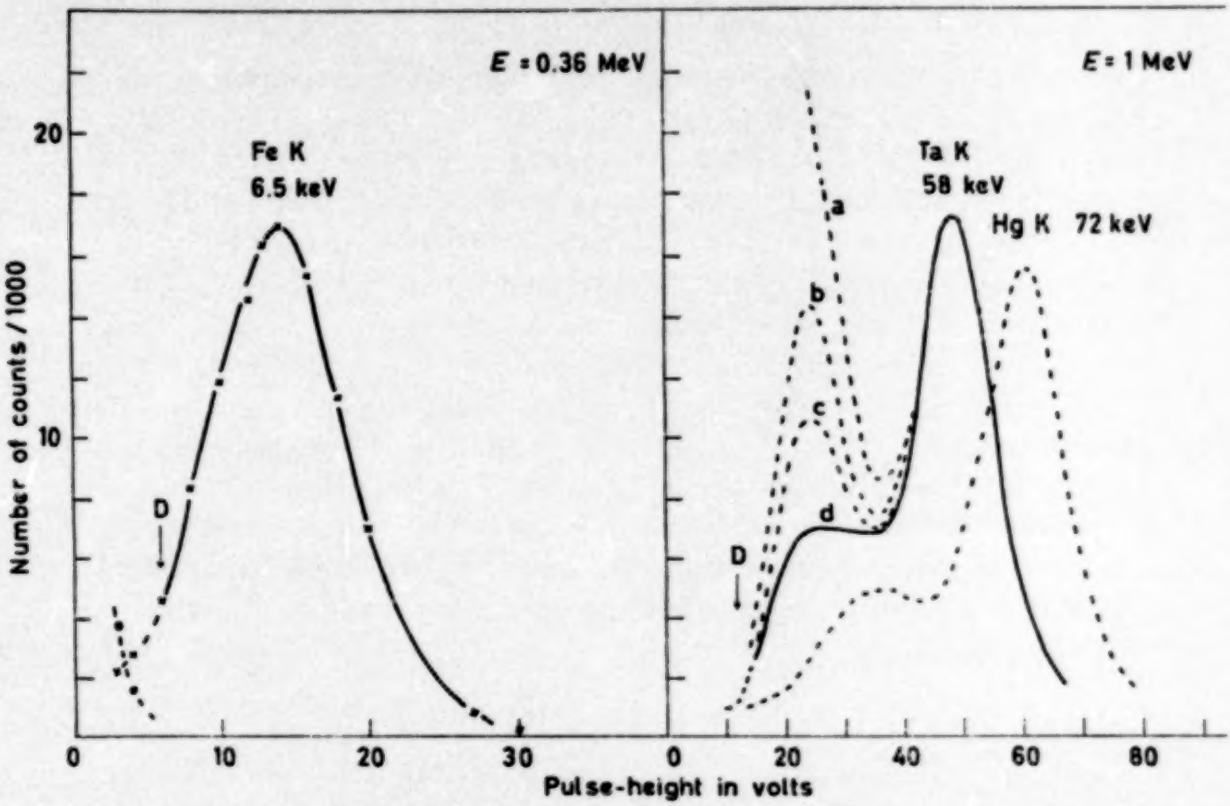

Fig. 2. Typical differential pulse-height spectra of the K-shell X-rays from Fe and Ta. In the case of Ta the changing of the spectra by using 1, 3, 5.6 and 12.5 mm Al absorbers is illustrated by the curves a, b, c and d. For convenience, the different curves are normalized at the Ta K peak. The discriminator settings when measuring the total counting rate are indicated by D.

Pulses from the photomultiplier were amplified 10 times in a preamplifier and fed through a cathode follower to an amplifier and a single-channel pulse-height analyzer. Some spectra were also recorded with an 80 channel analyzer.

The X-rays interact with the scintillator primarily by the photoelectric effect, giving pulses corresponding to the full photon energy provided the X-rays from iodine in the scintillator are also absorbed. The correction due to escape of L-shell X-rays is greatest in the case of Fe. Using the expression given by Bernstein and Lewis [6]), the ratio of the number of iodine

X-rays which leaves the scintillator to the number of incident Fe K X-rays is 0.03.

In this work only Ta K X-rays have higher energy than the K-shell binding energy of iodine. The ratio of the number of escape X-rays to the number of incident Ta K X-rays is 0.12 for a semi-infinite scintillator [7]).

Some typical pulse-height spectra of the K-shell X-rays from the various targets are shown in fig. 1 and 2. Besides the K-shell X-rays the protons also excite L-shell X-rays with an intensity several orders of magnitude greater than the former [6]). Owing to their much lower energy and stronger absorption, they may however, only influence the measurements of the K X-rays to a small extent. Using an aluminium absorber which led to a reduction of the K X-rays by a factor of 1.5 to 2.5 removed all lower energy background. The effect of this procedure was very pronounced in the case of Ta. The changing of the pulse spectra by using 1—12.5 mm aluminium absorbers is illustrated in fig. 2. 12.5 mm Al, reducing the K-shell X-rays by a factor of 2.72, was needed to make the content of lower energy radiation in the escape peak negligible. For comparison the spectra of Hg K X-rays from a small Tl^{204} source is also shown.

After recording the pulse-height spectra, all pulses greater than the discriminator values indicated by D in the figures were counted as a function of the proton energy. In the case of Ta the discriminator was set to include the escape peak to make correction for this effect unnecessary. The absorption in aluminium of the radiation detected with these discriminator settings, was also measured to assure that mixtures of lower energy radiation were negligible.

3. Experimental Results

Knowing the total number of counts per incident proton, the thick target yield of X-rays could be found after correcting for the solid angle and absorption in aluminium and air. The absorption coefficients were taken from the compilation by Allen [8]). The values of the thick target yield I_μ shown in column 3 of tables 1 and 2, and in fig. 3, are 4π times the differential yield at 90° to the proton beam.

With another target-holder the relative values of the differential yield at 90° and 150° could be directly compared. Using 0.34 MeV protons and Cu target, no differences were detected.

The relative variation in the yield of X-rays from Cu with proton energy from 0.2 to 0.44 MeV is the same as reported before [5]), but the absolute values of the new measurements are greater by a factor of 4. At higher energies the agreement is good. For Mo and proton energies from 0.25 to 0.4 MeV the new values are greater by a factor of 2.5, while the agreement is fair at the highest energies.

TABLE 1

Yield of K-shell X-rays and ionization cross sections

1 Element	2 Proton energy (MeV)	3 I_μ	4 σ_K (cm²)	5 σ_{th} (cm²)	6 Empirical formula, eq. (4) (cm²)
$_{26}$Fe	0.14	5.9×10^{-9}	2.4×10^{-26}	14.5×10^{-26}	2.4×10^{-26}
$\theta = 0.79$	0.15	9.5	3.4		
	0.16	1.45×10^{-8}	4.6	24	4.2
	0.18	3.1	8.2		
	0.20	5.2	1.3×10^{-25}	5.5×10^{-25}	1.2×10^{-25}
	0.22	9.7	1.9		
	0.24	1.55×10^{-7}	2.7	10.2	2.6
	0.26	2.4	3.6		
	0.28	3.3	5.0	18.5	5.0
	0.30	5.3	6.4		
	0.32	7.8	8.2	28	8.2
	0.34	1.05×10^{-6}	9.7		
	0.36	1.35	1.25×10^{-24}	4.1×10^{-24}	1.25×10^{-24}
	0.40	2.2	1.85	5.2	1.85
	0.44	3.6	2.6	7.4	2.7
	0.74	4.2×10^{-5}	1.17×10^{-23}	3.1×10^{-23}	1.47×10^{-23}
	0.935	1.12×10^{-4}	2.2	5.9	2.8
	1.04	2.0	3.5		
	1.20	3.2	4.5		
	1.30	4.5	5.6	12.6	6.8
$_{29}$Cu	0.14	1.3×10^{-9}	0.46×10^{-26}	4.0×10^{-26}	0.58×10^{-26}
$\theta = 0.80$	0.15	2.5	0.69		
	0.16	4.1	1.11	6.4	1.1
	0.18	9.0	2.0		
	0.20	1.9×10^{-8}	3.4	14.6	3.3
	0.22	3.6	5.3		
	0.24	6.2	7.9	28	7.7
	0.26	1.04×10^{-7}	1.13×10^{-25}		
	0.28	1.60	1.60	5.1×10^{-25}	1.5×10^{-25}
	0.30	2.4	2.2		
	0.32	3.6	2.9	8.0	2.6
	0.34	4.9	3.8		
	0.36	6.6	4.9	12.0	4.4
	0.38	8.7	6.2		
	0.40	1.17×10^{-6}	7.5	17.0	6.7
	0.44	1.93	9.4	22	9.3
	0.60	9.5	2.9×10^{-24}	5.8×10^{-24}	2.9×10^{-24}
	0.74	2.2×10^{-5}	5.3	10.2	5.5
	0.935	6.4	1.10×10^{-23}	2.05×10^{-23}	1.15×10^{-23}
	1.04	1.07×10^{-4}	1.53		
	1.135	1.46	1.90		
	1.20	2.0	2.3	4.0	2.5

TABLE 2

Yield of K-shell X-rays and ionization cross sections

1 Element	2 Proton energy (MeV)	3 I_μ	4 σ_K (cm²)	5 σ_{th} (cm²)	6 Empirical formula, eq. (4) (cm²)
$_{42}$Mo	0.24	0.61×10^{-9}	0.75×10^{-27}	2.9×10^{-27}	0.61×10^{-27}
	0.26	1.10	1.13		
$\theta = 0.83$	0.28	1.78	1.66	5.2	1.58
	0.30	3.0	2.4		
	0.32	4.2	3.4	8.5	3.2
	0.34	6.6	4.9		
	0.36	8.7	6.4		
	0.38	1.35×10^{-8}	8.6	15.7	7.5
	0.40	1.90	1.11×10^{-26}		
	0.44	3.6	1.73	2.7×10^{-26}	1.54×10^{-26}
	0.60	1.82×10^{-7}	4.7	8.2	6.3
	0.74	6.1	1.16×10^{-25}	1.70×10^{-25}	1.50×10^{-25}
	0.935	2.2×10^{-6}	2.9	3.7	3.9
	1.03	3.4	3.9		
	1.20	7.9	7.3	8.3	9.7
$_{47}$Ag	0.26	1.30×10^{-10}	1.55×10^{-28}	9.2×10^{-28}	1.64×10^{-28}
	0.28	2.5	2.5		
$\theta = 0.84$	0.30	4.1	4.0	15.4	4.0
	0.32	6.9	6.0		
	0.34	1.17×10^{-9}	9.0	25	9.0
	0.36	1.96	1.29×10^{-27}		
	0.38	2.8	1.88		
	0.40	3.9	2.6	4.5×10^{-27}	2.3×10^{-27}
	0.60	4.3×10^{-8}	1.35×10^{-26}	2.1×10^{-26}	1.61×10^{-26}
	0.74	1.60×10^{-7}	2.9	4.4	4.2
	0.935	6.2	8.0	9.8	11.5
	1.04	1.10×10^{-6}	1.21×10^{-25}		
	1.20	2.3	2.1	2.4	3.3×10^{-25}
$_{50}$Sn	0.26	0.6×10^{-10}	0.68×10^{-28}	4.9×10^{-28}	0.82×10^{-28}
	0.28	1.08	1.15		
$\theta = 0.84$	0.32	3.1	2.5	11.3	3.0
	0.36	8.3	6.2		
	0.38	1.23×10^{-9}	9.1	22	9.1
	0.40	1.71	1.26×10^{-27}		
	0.44	4.0	2.4		
	0.45	4.9	2.7	4.0×10^{-27}	2.5×10^{-27}
	0.60	2.4×10^{-8}	6.6	11.3	9.6
	0.74	1.01×10^{-7}	1.67×10^{-26}	2.5×10^{-26}	2.5×10^{-26}
	0.935	3.0	4.5		
	1.04	6.3	7.0	8.0	10.7
$_{73}$Ta	1.00	0.75×10^{-9}	0.96×10^{-27}	0.57×10^{-27}	0.69×10^{-27}
	1.12	1.5	1.57	0.86	1.33
$\theta = 0.86$	1.25	3.1	2.7	1.28	2.4

A considerable effort was made to verify the new data. At each proton energy the yield of X-rays was measured several times, and the distance between target and detector was also varied. During the measurements the electronic set-up was checked by using a pulse generator with known pulse frequency. The energy scale of the small Van de Graaff generator used for proton energies below 0.5 MeV, was checked by means of the strong resonances at 163 keV and 340 keV in the reactions B^{11} (p, γ) C^{12} and F^{19} (p, $\alpha\gamma$)O^{16} [9]).

All measurements gave values consistent with an experimental uncertainty smaller than 15 % in the average values of I_μ listed in column 3, tables 1 and 2.

In fig. 3 are also plotted the corresponding data for Mo, Ag and Ta reported by Lewis *et al.* [1]). Extrapolation of our measurements seems to give good agreement with their values. The broken curve giving some smaller values for Ta than ours, corresponds to relative values for Ta obtained by Temmer and Heydenburg [10]) normalized to the values obtained by Lewis *et al.* The discrepancy may not be too significant in view of the various experimental uncertainties.

The cross section σ for ionization with subsequent K-shell X-ray emission can be calculated from

$$\sigma = \frac{1}{n\varrho}\frac{\mathrm{d}I_\mu}{\mathrm{d}E}\frac{\mathrm{d}E}{\mathrm{d}x} + \frac{\mu}{n\varrho}I_\mu; \qquad (1)$$

n is the number of target atoms per gram, $\mathrm{d}I_\mu/\mathrm{d}E$ is the slope of the curves given in fig. 3, $(1/n\varrho)(\mathrm{d}E/\mathrm{d}x)$ is the atomic stopping cross section of the target material and μ/ϱ is the mass-absorption coefficient of the target material for its own X-rays. At the proton energies used here, the first term of eq. (1) is several times larger than the second. Values for the atomic stopping cross section were obtained directly or by interpolation and extrapolation from values given by Allison and Warshaw [11]), Green *et al.* [12]) and Bader *et al.* [13]).

The computed cross sections multiplied by the Auger factors given by Roos [14]) to give the cross sections σ_K for K-shell ionization are listed in column 4 of tables 1 and 2.

4. Discussion

Henneberg has justified the use of the Born approximation in the analysis of K-shell ionization by slow heavy particles. By using non-relativistic Coulomb wave functions he arrived at the following approximate formula ((as given in ref. [1])) for the ionization cross section by proton impact

$$\sigma_{\mathrm{th}} = \frac{3.51}{Z^4\theta}\Phi_0(\eta') \times 10^{-16}\ \mathrm{cm}^2; \qquad (2)$$

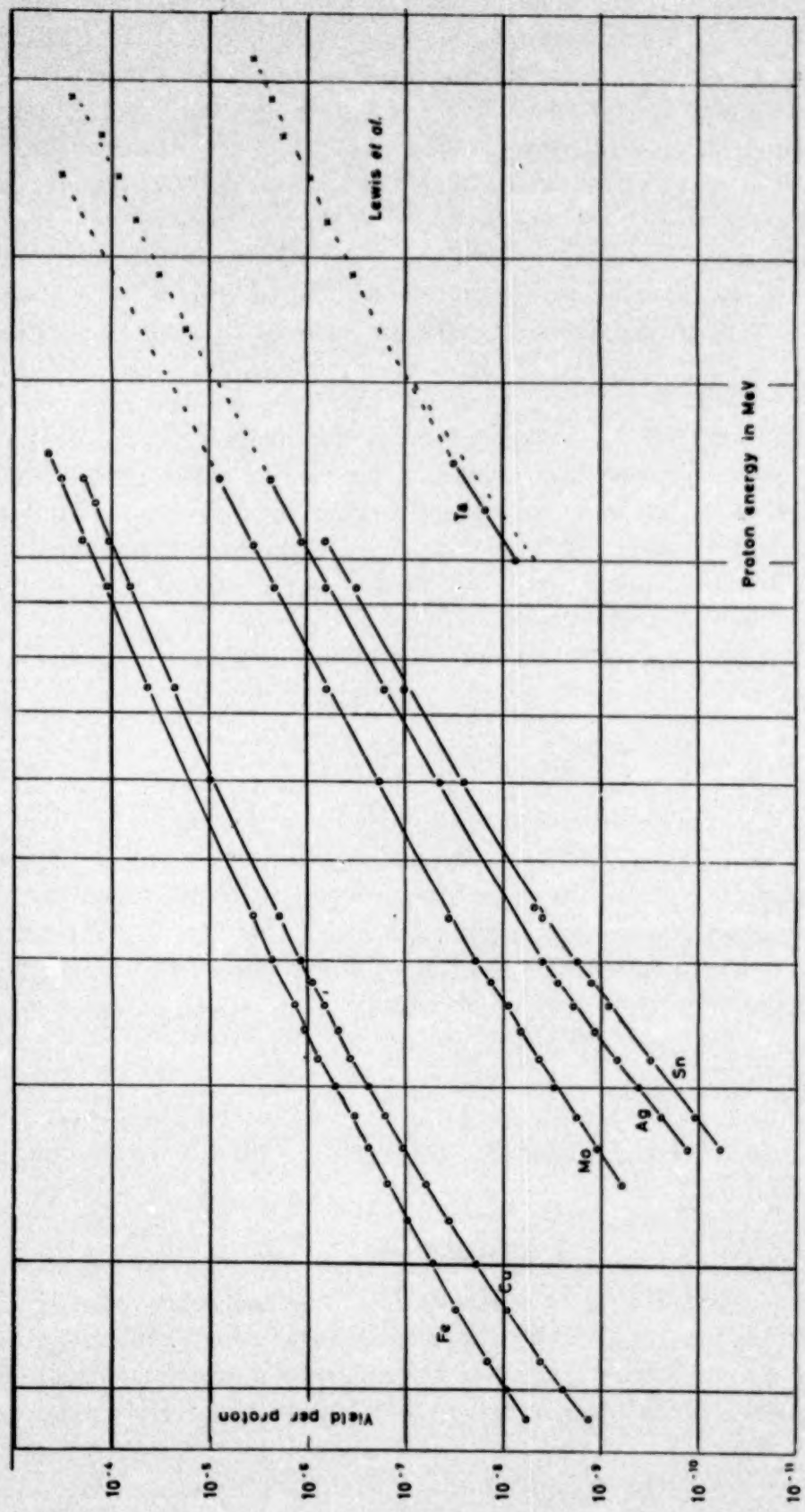

Fig. 3. Thick target yield of K-shell X-rays as a function of initial proton energy. The corresponding data from Lewis *et al.* [1]) are also shown.

Z is the charge of the nucleus, θ is the ratio of the observed K-shell ionization energy E_K to the "ideal ionization energy in the absence of outer screening",

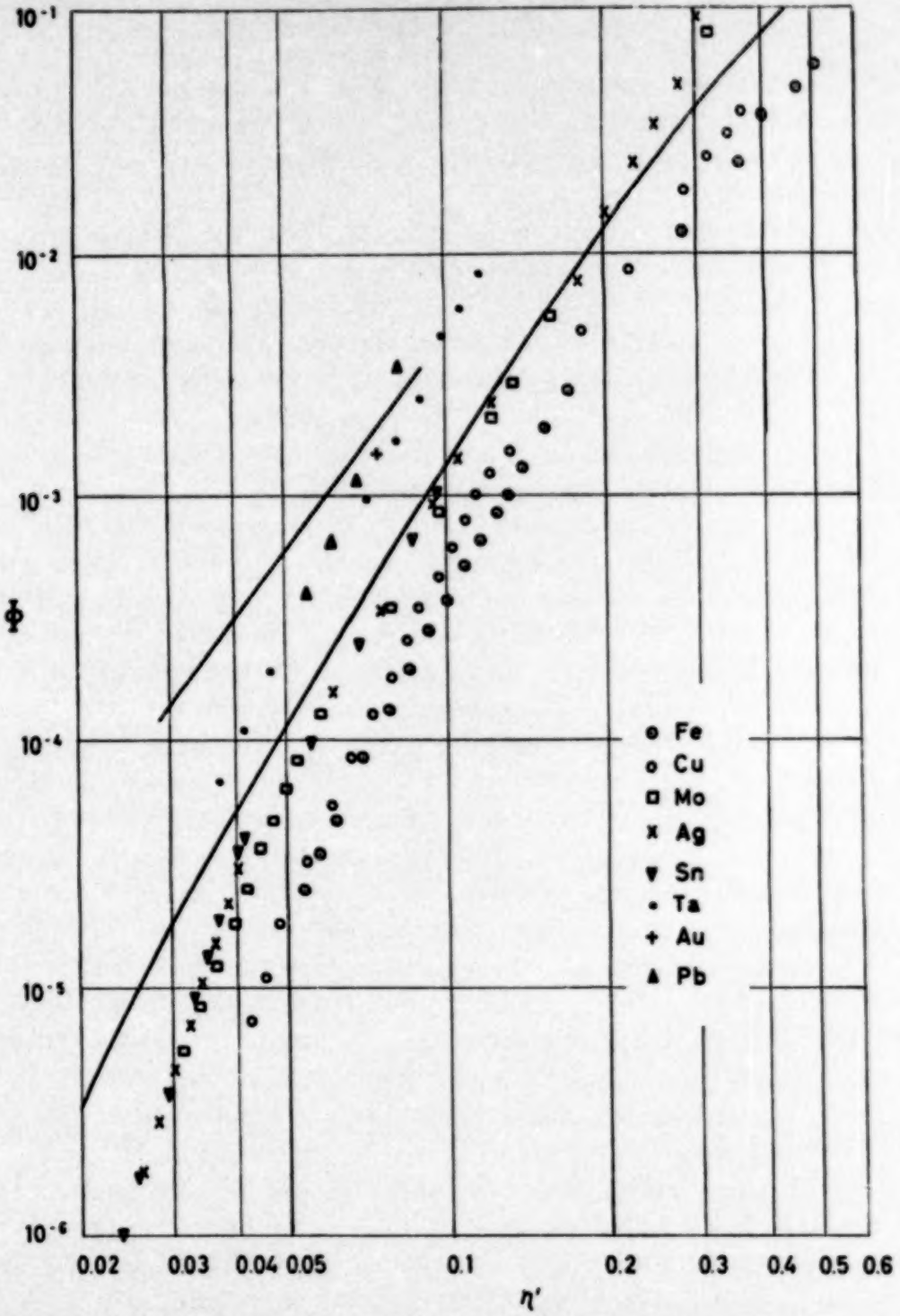

Fig. 4. This figure is taken from ref. [4]) (fig. 1) and includes our results. The points give the experimental quantity $\Phi = Z^4\theta/3.51\,\sigma_K \times 10^{18}$ together with the corresponding values from ref. [1]). The left-hand curve represents the function Φ obtained in the same way from the relativistic cross sections for lead, while the corresponding values for silver coincide with the right-hand curve, representing the function Φ_0.

and $\Phi_0(\eta')$ is defined by

$$\Phi_0(\eta') = \frac{2}{5} e^{-\frac{4\eta'}{1+\eta'}} \left(\frac{4\eta'}{1+\eta'}\right)^4 \left\{\frac{1}{4} + \frac{1}{12}\left(\frac{4\eta'}{1+\eta'}\right) + \cdots\right\} \tag{3}$$

and plotted as the right hand curve in fig. 4. The quantity η' is given by $\eta' = 4mE/M\theta E_K$ where M/m and E/E_K are the ratios of the mass and the energy of the proton, respectively, to the mass of the electron and the K-shell ionization energy.

The theoretical cross sections for some of the proton energies are given in column 5, and the values of θ used here are given in column 1 of tables 1 and 2.

Jamnik and Zupančič [4]) have repeated the calculations for lead and silver and 1—3 MeV protons using relativistic wave functions for the electron. Their results multiplied by $Z^4\theta/3.51 \times 10^{16}$ cm^{-2} are represented by the left-hand curve in fig. 4 for lead, while in the case of silver the results coincide with the curve representing the function $\Phi_0(\eta')$.

The experimental data reported here are compared with the theoretical predictions by plotting the experimental quantity $\sigma_K Z^4\theta/3.51 \times 10^{16}$ together with the corresponding values from ref. [1]) in fig. 4. The values of θ used here correspond to the relativistic values used in ref. [1]). Using higher, non-relativistic values will increase the discrepancy between the experimental data and the calculations by Henneberg for the heavy elements, but decrease it for the lightest elements and lowest energies. But even setting $\theta = 1$ would not fit the experimental points at the lowest energies with the theory. The use of relativistic electron wave functions considerably improves the agreement with the experimental data for the heavy elements. Still there remains a discrepancy, however, especially as regards the energy dependence of the cross sections. The small cross sections observed at low energies and the rapid energy dependence may be accounted for by the failure of the Born approximation, but it seems more difficult to explain the large experimental values at higher energies [4]). Calculations are now being done by means of a time-dependent perturbation method independent of the Born approximation, but quantitative results are not available [15]).

From fig. 4 it can be concluded that the experimental data vary less with the atomic number and more with the energy than predicted by Henneberg's formula. As regards the atomic number the experimental values are consistent with a dependence given by Z^{-1} to Z^{-2} instead of $1/Z^4\theta$ as given by Henneberg's formula. This is in agreement with the relativistic calculations for lead and silver which corresponds to a $Z^{-3/2}$ to Z^{-2} dependence as a function of η'. The variation with the proton energy, however, is more marked than given by both the non-relativistic and relativistic calculations in agreement with previous results.

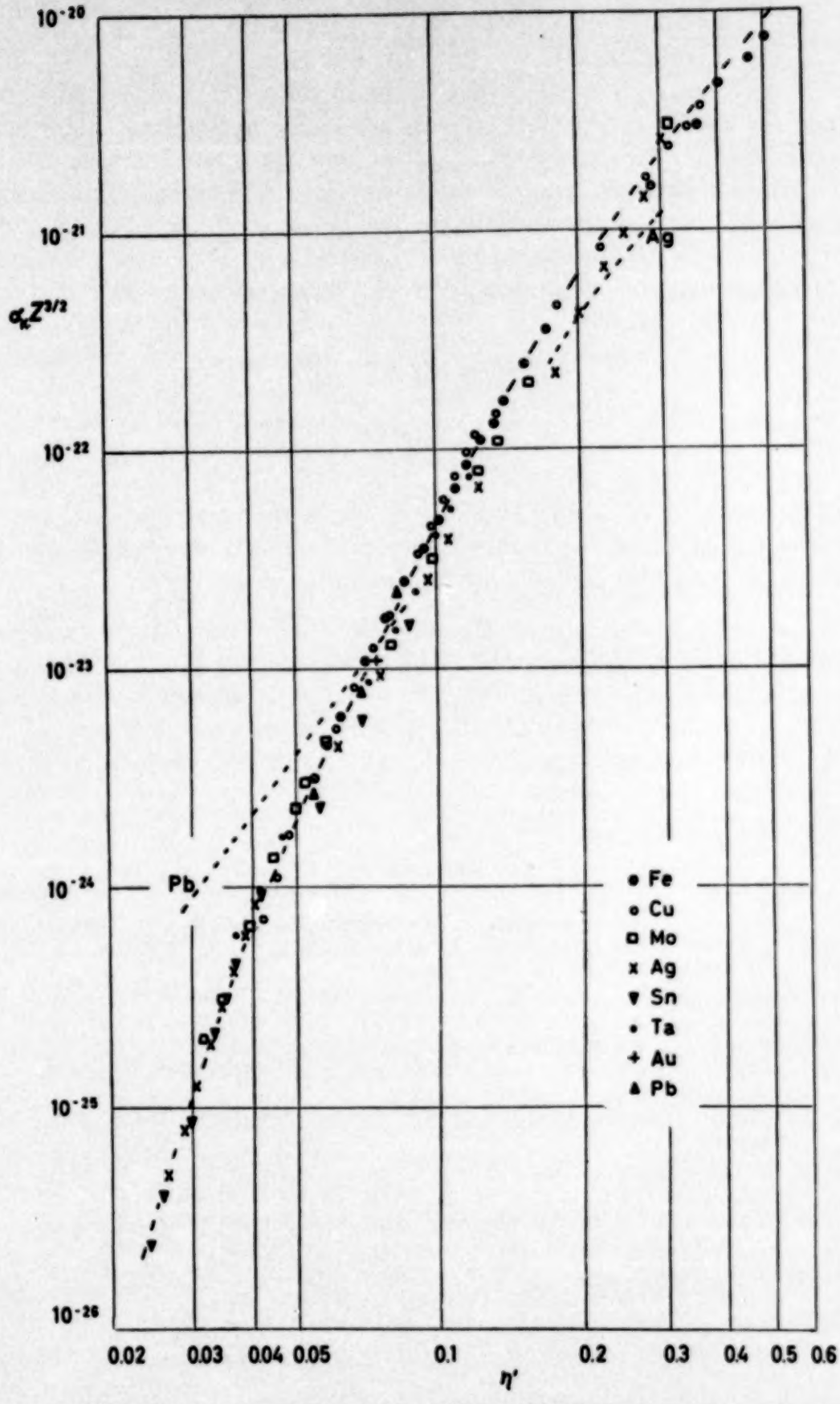

Fig. 5. The points give the experimental quantity $\sigma_K Z^{3/2}$ together with the corresponding values from ref. [1]). Some of the points coincide completely and cannot be shown. The broken curves marked Pb and Ag are the corresponding relativistic values for lead and silver. The broken curve through many of the points is $\Phi_1 \times 6.1 \times 10^{-21}$ from the empirical formula, eq. (4).

These conclusions are illustrated in fig. 5 where the same experimental data for the ionization cross sections are shown by plotting $\sigma_K Z^{3/2}$ as a function of η'. The corresponding values from the relativistic calculations for lead and silver are also shown. As seen in this figure, all experimental data with good approximation are consistent with an assumed $Z^{-3/2}$ dependence for the ionization cross sections as a function of η'. Within the experimental uncertainty all data can be reproduced by the following empirical formula:

$$Z^{3/2}\sigma_K \approx \Phi_1(\eta') \times 6.1 \times 10^{-21} \text{ cm}^2, \tag{4}$$

where

$$\Phi_1(\eta') = e^{-\frac{2\eta'}{1+\eta'}} \left(\frac{4\eta'}{1+\eta'}\right)^4 e^{-\frac{0.067}{\eta'}}. \tag{5}$$

The values of $\Phi_1(\eta') \times 6.1 \times 10^{-21}$ are shown as the broken curve in fig. 5. Cross sections calculated from this empirical formula are given in column 6 of tables 1 and 2 for some of the proton energies.

The author wishes to thank Professor R. Tangen and Dr. A. Storruste for their interest in this work, and the members of the Van de Graaff group for efficient running of the Van de Graaff generators. He is also indebted to Mr. J. Sandstad for building the electronic equipment.

This work was supported by the Royal Norwegian Council for Scientific and Industrial Research.

References

1) H. W. Lewis, B. E. Simmons and E. Merzbacher, Phys. Rev. **91** (1953) 943
2) P. R. Bevington and E. M. Bernstein, Bull. Am. Phys. Soc. **1** (1956) 198
3) W. Henneberg, Z. Physik **86** (1933) 592
4) D. Jamnik and Č. Zupančič, Mat. Fys. Medd. Dan. Vid. Selsk. **31** (1957) no. 2
5) J. M. Hansteen and S. Messelt, Nuclear Physics **2** (1956/57) 526
6) E. M. Bernstein and H. W. Lewis, Phys. Rev. **95** (1954) 83
7) P. R. Bell in Beta- and Gamma-ray Spectroscopy, Ed. Kai Siegbahn (North-Holland Publishing Co., Amsterdam, 1955) Chap. V
8) S. J. Allen in Handbook of Chem. and Phys., 34th ed. (Chemical Rubber Publishing Co.) p. 2235
9) F. Ajzenberg and T. Lauritsen, Rev. Mod. Phys. **24** (1952) 321
10) G. M. Temmer and N. P. Heydenburg, Phys. Rev. **93** (1954) 351
11) S. K. Allison and S. D. Warshaw, Rev. Mod. Phys. **25** (1953) 779
12) D. W. Green, J. N. Cooper and J. C. Harris, Phys. Rev. **98** (1955) 466
13) M. Bader, R. E. Pixley, F. S. Mozer and W. Whaling, Phys. Rev. **103** (1956) 32
14) C. E. Roos, Phys. Rev. **105** (1957) 931
15) J. Bang and J. M. Hansteen, private communication

Nuclear Physics **5** (1958) 447—454; © *North Holland Publishing Co., Amsterdam*
Not to be reproduced by photoprint or microfilm without written permission from the publisher

ON SYMMETRIES OF WEAK INTERACTIONS

B. D'ESPAGNAT and J. PRENTKI
CERN, *Geneva*
and
ABDUS SALAM
Imperial College of Science and Technology, London

Received 11 October 1957

Abstract: The $|\Delta \mathbf{I}| = \frac{1}{2}$ rule is replaced by a conservation law. This new scheme is practically equivalent to the rule just mentioned (with the possibility of introducing in a natural way some $|\Delta \mathbf{I}| = \frac{3}{2}$ admixture). Its main advantage is that it can incorporate lepton interactions.

1. Introduction

To give a quantitative description of strange-particle weak decays, several authors have suggested that the weak interaction Lagrangian L_w is an iso-spinor [1–4]). This leads to the selection rule [5]) $|\Delta \mathbf{I}| = \frac{1}{2}$, $|\Delta U| = 1$, which has been found fairly successful in various applications †.

† The rule $|\Delta \mathbf{I}| = \frac{1}{2}$ is successful in giving a correct account of τ, Λ and Σ^+ decay branching ratios as also of the ratio of Σ^+, Σ^- life-times (if parity violation is taken into account [6])). It provides the only "explanation" of the fact that K^+ has a much longer life than K^0.

The rule is not successful in the prediction of the $(K^0 \to \pi^0+\pi^0)/(K^0 \to \pi^+ + \pi^-)$ branching ratio: the theory predicts a value $\frac{1}{2}$, while the experimental ratio is at best $\approx \frac{1}{3}$. It is, of course, clear that the $|\Delta \mathbf{I}| = \frac{1}{2}$ rule is inaccurate to the extent that electromagnetic effects are to be included. It is commonly stated that electromagnetic effects should make only a difference of $\alpha^2 = (1/137)^2$, but this is not necessarily true. Electromagnetic effects appear in the $K^0 \to \pi^0+\pi^0$ and $K^0 \to \pi^+ + \pi^-$ processes through the mass difference of the π^0, $\pi^\pm$ mesons. One simple way to see the effect of this mass difference on the matrix-elements for K^0 decay is the following: Let p be the 4-momentum of K^0, $p = p_+ + p_-$ for $K^0 \to \pi^+ + \pi^-$ decay and $p = p_0 + p_0$ for $K^0 \to \pi^0 + \pi^0$ decay. The matrix elements are

$$F_1 = \sqrt{2}\, F(p^2,\ p_+^2,\ p_-^2), \qquad F_2 = F(p^2,\ p_0^2,\ p_0^2).$$

Thus,

$$F_1 = \sqrt{2}\left[F_2 + 2(p_+^2 - p_0^2)\frac{\partial F_2}{\partial p_0^2}\right];$$

assuming from dimensions $\partial F_2/\partial p_0^2 = \text{const.}\ F_2/p_0^2$,

$$F_1 = \sqrt{2}\left[1 + 2 \times \text{const.} \times \frac{p_+^2 - p_0^2}{p_0^2}\right] F_2.$$

If the const. above ≈ 1, we have

$$F_1 \approx \sqrt{2}\left[1 + 4 \cdot \frac{\Delta m}{m_0}\right] F_2 = \sqrt{2} \cdot \frac{25}{22} F_2.$$

Thus, $(F_1/F_2)^2 \approx 625/242$, giving

$$\frac{K \to \pi^0+\pi^0}{K \to \pi^+ + \pi^-} \approx \frac{3}{8}.$$

Thus, the mass-difference can have a very large effect in this problem.

From a fundamental point of view there are two objections to these suggestions. Firstly, the assumption that L_w is an iso-spinor does not correspond to the conventional procedure in which Lagrangians are normally considered as iso-scalars; secondly leptons do not find any natural place in such a scheme. We would like to suggest an alternative approach to the problem which avoids both these objections, while having the merit of giving practically † the same results as the $|\Delta \mathbf{I}| = \frac{1}{2}$ rule. In fact, we shall replace the violation of the rule $|\Delta \mathbf{I}| = \frac{1}{2}$ by a conservation rule [7]).

Briefly, we remark that the global Lagrangian (including all strong and weak interactions) is invariant for the charge-conserving transformations $\phi \to [\exp(iQ\alpha)]\phi$ (Q is the charge). Of the known particles, (π^+, π^0, π^-), $(\Sigma^+, \Sigma^0, \Sigma^-)$; (μ^+, ν, e^-) form charge triplets, while Λ^0 is a charge-singlet. If K and (N, Ξ) interactions can also be written in terms of charge triplets $(K^+, \overline{K}^0 - K^0, K^-)$ $(p, \Xi^0 - n, \Xi^-)$ and charge singlets $(\overline{K}^0 + K^0)$, $(\Xi^0 + n)$, and we shall show this, then Q can be considered as the third component of a vector and charge-conservation is the same thing as rotation invariance for rotations around a given axis in a [3]-space. To the extent that (μ^+, e^-) and (N, Ξ) mass differences can be neglected, we discover that it is possible to consider Lagrangians invariant for full rotations in this [3]-space, so that not only the charge Q (denoted by M_3 in the sequel) but also $\mathbf{M}^2$ is conserved. We find that $\mathbf{M}^2$-conservation possessed by the global Lagrangian when (N, Ξ) and (μ, e) mass-differences are neglected is practically equivalent to the $|\Delta \mathbf{I}| = \frac{1}{2}$ rule. In the paper we shall be concerned with the charge-space ($\mathbf{M}$-space) and its connection with isobaric-space theories.

The formulation can be given in two different but equivalent forms which correspond to two distinct models for strong interactions, namely the Salam-Polkinghorne [8]) [4]-dimensional theory and the d'Espagnat-Prentki [9]) [3]-dimensional theory. These two models, referred to as S.P. and E.P. theory, will be very briefly reviewed in section 2. It will be emphasized there that a very simple connection exists between them.

2. Theories of Strong Interactions

2.1. THE S.P. THEORY

The isobaric spin space is [4]-Euclidean; only rotations are considered. The different particles are attributed different irreducible representations $\mathscr{D}(I^+, I^-)$ of the rotation group as follows:

$$\begin{array}{ll} (N, \Xi) & \mathscr{D}(\frac{1}{2}\,\frac{1}{2}) \quad \begin{cases} I_3^- = +\frac{1}{2} \text{ for N} \\ I_3^- = -\frac{1}{2} \text{ for } \Xi \end{cases} \\ \Sigma & \mathscr{D}(1\ 0) \\ \Lambda & \mathscr{D}(0\ 0) \end{array} \qquad (1)$$

† *Note added in proof:* Recent experimental data increase the need for some $|\Delta \mathbf{I}| = \frac{3}{2}$ admixture. It is thus satisfactory that such an admixture can be introduced in a natural way in the present scheme (cf. footnote p. 451).

$$\begin{array}{lll} \pi & \mathscr{D}(1\ 0) & \\ \mathrm{K} & \mathscr{D}(\tfrac{1}{2}\ \tfrac{1}{2}) & \begin{cases} I_3^- = +\tfrac{1}{2} \text{ for K} \\ I_3^- = -\tfrac{1}{2} \text{ for } \overline{\mathrm{K}}. \end{cases} \end{array} \tag{1}$$

Notice that $\mathbf{I}^+$ is just the "ordinary" isobaric spin in three dimensions while $2I_3^-$ is $U = S+N$. (S denotes the strangeness, N the baryon number.) The interactions are classified in the usual way as strong ($\mathbf{I}^+$ and $\mathbf{I}^-$ conserved separately — 4-dimensional invariance) electromagnetic (I_3^+ and I_3^- conserved separately) and weak ($I_3^+ + I_3^- = Q$ conserved). The bare N and Ξ masses are of course assumed to be equal.

2.2. THE E.P. THEORY

The usual 3-dimensional isobaric spin space is considered, rotations and reflexions are taken into account, spinors of 1st and 2nd kinds are defined through $\xi \to i\xi$ $(\mathscr{D}^{(+)}(\frac{1}{2}))$ and $\eta \to -i\eta$ $(\mathscr{D}^{(-)}(\frac{1}{2}))$ in a reflexion through the origin. The attributions are as follows:

$$\begin{array}{lll} \mathrm{N} & \mathscr{D}^{(+)}(\frac{1}{2}) & (\xi) \\ \Xi & \mathscr{D}^{(-)}(\frac{1}{2}) & (\eta) \\ \Sigma & \mathscr{D}^{(-)}(1) & \text{(ps-vector)} \\ \Lambda & \mathscr{D}^{(+)}(0) & \text{(scalar)} \\ \pi & \mathscr{D}^{(-)}(1) & \text{(ps-vector)} \\ \mathrm{K} & \mathscr{D}^{(+)}(\frac{1}{2}) & (\xi). \end{array} \tag{2}$$

If p is the isoparity (reflexion through the origin) then $U = S+N$ is related to p by [10])

$$p = \mathrm{e}^{\frac{1}{2}i\pi U}. \tag{3}$$

Similarly, the reflexion A through the (1,2)-plane, is related to Q by [11])

$$A = \mathrm{e}^{i\pi Q}. \tag{4}$$

Strong interactions are invariant under rotations and reflexions, electromagnetic interactions are invariant under rotations around the 3rd axis and reflexions through the origin (therefore also under reflexions with respect to the (1,2)-plane); weak interactions conserve only $Q = I_3 + \frac{1}{2}U$.

2.3. CONNEXION BETWEEN S.P. AND E.P. THEORIES

A very simple connection exists between these two theories: in the S.P. scheme invariance with respect to rotations around the 3rd axis in $\mathbf{I}^-$-space ensures that the transformation

$$\psi \to \mathrm{e}^{iI_3^-\alpha}\psi \tag{5}$$

carried out for all fields leaves the Lagrangian invariant. For the special value $\alpha = \pi$ this gives, $\mathrm{N} \to i\mathrm{N}$, $\Xi \to -i\Xi$, $\Sigma \to \Sigma$, $\Lambda \to \Lambda$, $\pi \to \pi$, $\mathrm{K} \to i\mathrm{K}$, $\overline{\mathrm{K}} \to -i\overline{\mathrm{K}}$, i.e. just the reflexions of the E.P. theory: this is why $2I_3^-$ and U are in fact the same quantum number.

3. Invariance in Charge-Space

In the S.P. scheme the N and Ξ masses are the same. In order to reproduce the physical mass difference it is essential to break the full 4-dimensional invariance. If one believes in the conservation of ordinary isobaric spin, this should be done by introducing *intermediate* interactions that are invariant under all rotations in $\mathbf{I}^+$-space (and which moreover conserve I_3^-: conservation of strangeness). This is the same as saying that in the E.P. Lagrangian $g_1 \neq g_4$, $g_5 \neq g_7$, ... This idea has also been considered by Polkinghorne [12]).

As mentioned in section 2, $I_3^+ + I_3^-$ is nothing but the charge Q. Now it is well known that $I_3^+ + I_3^-$ is also J_{12}, one of 6 infinitesimal generators of the 4-dimensional rotation group. Among these, J_{23}, J_{31}, J_{12} form components of a vector with the usual [3] angular momentum commutation rules. Calling $J_{12} = M_3$ etc. we have here another subspace of the rotation group, the [3] **M**-space.

From the fact that Q has only integer values, it follows that the only representations of the [3] rotation group that can have physical sense are the integer ones. In fact, if multiply charged particles are excluded then the only admissible representations are scalar and vector.

Let us recall that our aim is to write down the weak interactions as invariants in a [3]-space. Now the 4-dimensional manifold furnishes three [3] dimensional spaces, namely the $\mathbf{I}^+$, $\mathbf{I}^-$ and **M**-spaces. For obvious reasons both the $\mathbf{I}^+$-space and the $\mathbf{I}^-$-space can be ruled out (as $\Delta I_3^+ = \pm\frac{1}{2}$, $\Delta I_3^- = \pm\frac{1}{2}$, $\Delta U = \pm 1$ for such interactions), thus only the **M**-space remains possible ($\Delta M_3 = 0$ because of charge conservation). *Let us therefore make the assumption that the weak interactions of bare fields are invariant under rotations in* **M***-space.*

Summarizing, the different interactions have the invariance properties given in table 1.

TABLE 1

Interactions of bare fields	Quantum numbers	Rotation-invariance properties
strong (s)	$\mathbf{I}^+$, $\mathbf{I}^-$, I_3^+, I_3^-, **M**, M_3	4-dim.
intermediate (i)	$\mathbf{I}^+$, I_3^+, I_3^-, M_3	3-dim. ($\mathbf{I}^+$ space)
electromagnetic	I_3^+, I_3^-, M_3	
weak (w)	**M**, M_3	3-dim. (**M** space)

As is well known, the $\mathscr{D}(I^+I^-)$ irreducible representation of the [4] rotation group splits into a direct sum of irreducible representations of 3-dimensional rotations through

$$\mathscr{D}(I^+I^-) = \mathscr{D}(I^+ + I^-) \otimes \ldots \otimes \mathscr{D}(|I^+ - I^-|)$$

when only rotations in **M** space are considered. This gives

$$\begin{aligned}
&(\mathrm{N},\ \Xi) \to \mathscr{D}(1) \otimes \mathscr{D}(0)\\
&\Sigma \quad\ \to \mathscr{D}(1)\\
&\Lambda \quad\ \to \mathscr{D}(0)\\
&\pi \quad\ \to \mathscr{D}(1)\\
&\mathrm{K} \quad\ \to \mathscr{D}(1) \otimes \mathscr{D}(0).
\end{aligned} \tag{6}$$

More explicitly

$$(\mathrm{N},\ \Xi) \to \begin{cases} \mathbf{B} = \left(\dfrac{\Xi^- + \mathrm{p}}{\sqrt{2}},\ \dfrac{\Xi^- - \mathrm{p}}{i\sqrt{2}},\ \dfrac{\Xi^0 - \mathrm{n}}{\sqrt{2}}\right) \\ B_s = \dfrac{\Xi^0 + \mathrm{n}}{\sqrt{2}} \end{cases} \tag{7}$$

$$(\mathrm{K},\ \overline{\mathrm{K}}) \to \begin{cases} \mathbf{K} = \left(\dfrac{\mathrm{K}^- + \mathrm{K}^+}{\sqrt{2}},\ \dfrac{\mathrm{K}^- - \mathrm{K}^+}{i\sqrt{2}},\ \dfrac{\overline{\mathrm{K}}^0 - \mathrm{K}^0}{\sqrt{2}} \equiv -\mathrm{K}_2^0\right) \\ K_s = \dfrac{\overline{\mathrm{K}}^0 + \mathrm{K}^0}{\sqrt{2}} \equiv \mathrm{K}_1^0. \end{cases} \tag{8}$$

The other particles $\mathscr{D}(10)$ and $\mathscr{D}(00)$ have of course the same representations in **M** as in $\mathbf{I}^+$ space. It may be worthwhile to point out that the neutral K's which appear here are not the K_0, $\overline{\mathrm{K}}_0$ but the K_1^0, K_2^0.

Explicit forms of L_w can now easily be obtained. As an example direct weak interactions between baryons and mesons should take the form

$$(\overline{\mathbf{B}} \times \mathbf{\Sigma}) \cdot \boldsymbol{\pi}, \qquad B_s\ \mathbf{\Sigma} \cdot \boldsymbol{\pi}; \tag{9}$$

$$\begin{aligned}
&(\overline{\mathbf{\Sigma}} \times \mathbf{\Sigma}) \cdot \mathbf{K}, \qquad &&\overline{\Lambda}\, \mathbf{\Sigma} \cdot \mathbf{K},\\
&\overline{\mathbf{\Sigma}} \cdot \mathbf{\Sigma} K_s, \qquad &&\overline{\Lambda}\ \Lambda\ K_s.
\end{aligned} \tag{10}$$

It is easily verified that these interactions satisfy the $|\Delta \mathbf{I}| = \frac{1}{2}$ rule. In fact, the Lagrangian thus obtained is just the one which follows from "spurion" theory with, however, the restriction that the N and Ξ coupling constants are equal †.

When intermediate interactions are introduced to produce the N, Ξ mass difference $\mathbf{M}^2$ is no longer conserved. (The effective N and Ξ coupling

† Strictly speaking, this is only true for interactions containing only one K and no B or conversely. Other **M**-invariant elementary interactions, such as for example the Fermi-like interactions between baryons (e.g. $\overline{\Lambda} B_s\, \overline{\mathbf{B}} \cdot \mathbf{B}$) do not satisfy the $|\Delta \mathbf{I}| = \frac{1}{2}$ rule. As far as real processes, such as Λ, Σ or K decays, are concerned, it can be shown that, as a matter of fact, such interactions lead to a violation of the $|\Delta \mathbf{I}| = \frac{1}{2}$ rule only when combined with *intermediate* (as contrasted with *strong*) interactions. On that basis it might be guessed that, even if such weak interactions are present, the violation of the $|\Delta \mathbf{I}| = \frac{1}{2}$ rule would be rather small: it should, however, be stressed that the very possibility of introducing such Fermi interactions in the present scheme is a problem in itself which requires further consideration. It may finally be noticed that weak interactions of a similar kind, namely $(\overline{\mathbf{B}} \times \mathbf{B}) \cdot \boldsymbol{\pi}$, would induce an anomalous Ξ decay ($\Xi \to \mathrm{N} + \pi$).

constants in L_w then become different). Because of the fact, however, that intermediate interactions conserve $\mathbf{I}^+$, the physical L_w still obeys the $|\Delta \mathbf{I}| = \frac{1}{2}$ rule. We come back to this question in section 5.

If μ, e, ν mass differences are forgotten, then leptons can easily be introduced into the scheme by making

$$\mathbf{L}\left(\frac{\mu^+ + e^-}{\sqrt{2}}, \frac{-\mu^+ + e^-}{i\sqrt{2}}, \nu\right)$$

the three components of a vector $\mathbf{L}$ in $\mathbf{M}$-space (with the possibility of a second neutrino as a scalar): $\pi \to \mu + \nu$ and $K \to \mu + \nu$ decays can then be accounted for simultaneously. This feature, however, needs some further comment (see section 5).

Weak interaction Lagrangians involving leptons can easily be written; we give here some examples:

$$\begin{gathered}(\bar{\mathbf{B}} \cdot \mathbf{B})(\bar{\mathbf{L}} \cdot \mathbf{L}); \qquad (\bar{\mathbf{B}} \times \mathbf{B}) \cdot (\bar{\mathbf{L}} \times \mathbf{L}) \\ (\bar{\mathbf{B}} \times \boldsymbol{\Sigma}) \cdot (\bar{\mathbf{L}} \times \mathbf{L}) \\ \boldsymbol{\pi} \cdot (\bar{\mathbf{L}} \times \mathbf{L}); \qquad \mathbf{K}(\bar{\mathbf{L}} \times \mathbf{L})\end{gathered} \tag{11}$$

4. Formulation in E.P. theory

The same results can be obtained starting directly from the 3-dimensional space of E.P. theory. The approach is then as follows. The total Lagrangian is

$$L_0 + L_r + L_w$$

where L_0, $L_r = L_s + L_1$ and L_w are the free, the E.P. and the weak interaction Lagrangians respectively: L_0 is invariant under rotations and reflexions in isospace with the E.P. attributions; the same holds for L_r. If, however, the assumption $M_N = M_\Xi$ for bare masses is made, then these are not the only attributions that make L_0 a true isoscalar. The other possibility is to take the integer representations (6) and (7) for $(N\Xi)$ and $(K\bar{K})$, with the supplementary requirement that under reflexions vectorial quantities transform as pseudo-vectors. It is assumed that with this new set of attributions L_w is a true isoscalar †. Then L_w is of course

† We also considered the possibility of taking

$$\left(\Sigma^+, \frac{\Lambda - \Sigma^0}{\sqrt{2}}\right), \left(\frac{\Lambda + \Sigma^0}{\sqrt{2}}, \Sigma^-\right)$$

as isospinors of the 1st and 2nd kind ($M_\Sigma = M_\Lambda$). As shown by Gell-Mann [13]), also the π strong interactions can be made invariant with this choice of representations; the K strong interactions, however, cannot (they should produce $M_\Sigma \neq M_\Lambda$). This choice would make it possible to write weak π interactions as invariants and is therefore a possible alternative to the choice of the present paper. Such a formalism raises, however, a difficulty concerning Σ^- decay (which becomes forbidden in lowest order). These features were considered independently by Ning- Hu [14]). The different behaviours of Σ^+ and Σ^- in this scheme make the choice of ref. [7]) and [15]) and of the present paper, in our opinion, definitely better.

the same as the one in section 3 and therefore leads to the usual $|\Delta \mathbf{I}| = \frac{1}{2}$ selection rule. The point of view chosen here is that a kind of symmetry exists between strong and weak interactions: just as L_0+L_r is a true scalar with the attributions (E.P.) adapted to strong interactions, L_0+L_w is a true scalar with the attributions adapted to weak interactions. Neither of these two sets of attributions makes of course the total Lagrangian invariant under the rotation-reflexion group. There is, however, *one* operation of that group which leaves it invariant: it is the reflexion with respect to the 1, 2 plane. If the operator corresponding to this particular reflexion is A, the general relation between A and the charge operator Q is

$$A = e^{iQ\pi}$$

valid with both sets of attributions. The invariance stated above is thus connected with charge conservation.

5. Discussion

L_w was written in terms of bare fields operators, with the essential assumption $M_N = M_\Xi$ for bare masses. $L_0+L_s+L_w$ is an invariant in **M**: this makes it possible to define a new quantum number $\mathbf{M}^2$ which is a good quantum number as long as intermediate and electromagnetic interactions are neglected. $\mathbf{M}^2$ conservation brings very strong restrictions to L_w, much stronger in fact than the usual $|\Delta \mathbf{I}| = \frac{1}{2}$ rule (it reduces the number of coupling constants by a factor 2). However, intermediate interactions should, of course, not be neglected: they are in fact of paramount importance in making the N and Ξ observed masses different and in giving a meaning to strangeness. As they are not invariant in **M**-space their introduction has the result that the effective L_w no longer has the invariance properties discussed before. The $\mathbf{M}^2$ conservation rule is thus only a poor approximation. As the net influence of intermediate interactions on the N, Ξ masses is approximately 30 %, it can be hoped, however, that the violation of $\mathbf{M}^2$ conservation produced by the introduction of N, Ξ mass differences is also of this order. It should be pointed out that, because of the fact that intermediate interactions conserve $\mathbf{I}^+$, the weak interactions derived from (9), (10) still rigorously obey the $|\Delta \mathbf{I}| = \frac{1}{2}$ rule. In some sense the present scheme is still more restrictive than the $|\Delta \mathbf{I}| = \frac{1}{2}$ selection rule because the coupling constants of the effective L_w could in principle be estimated. It should be stressed, however, that Fermi-like interactions can give a $|\Delta \mathbf{I}| = \frac{3}{2}$ admixture (see footnote p. 451).

The reason for non conservation of $\mathbf{M}^2$ is of course the fact that $\mathbf{I}^+$ does not commute with **M** (nor does $\mathbf{I}^-$) and that, for this reason, a particle cannot be attributed simultaneously I^+ and M values. As, however, the intermediate interactions are much stronger than the weak ones, the I^+,

I_3^- quantum numbers have a much more definite physical significance than the M quantum number. Quite similar remarks apply to the [3] dimensional approach †.

Finally, the present scheme is more powerful than the usual $|\Delta \mathbf{I}| = \frac{1}{2}$ rule in that it can also be applied to leptons. This, however, is only possible if the μ and e bare masses are taken equal. This, in turn, raises a difficulty which is more serious than in the nuclear particles case because no equivalent of the intermediate interactions is here at our disposal.

Of course, if [4]-representations were attributed to leptons this problem might be solved, but the danger is then that strong interactions of leptons might turn up that would contradict experiment. This raises, however, no conceptual difficulty because phenomenological mechanisms can be thought of, which would solve the dilemma: as an example consider the assumption that the only intermediate interaction is $g(\bar{\Xi}^- \Xi^- + \bar{\Xi}^0 \Xi^0)\ (\bar{\mu}\mu)$. This interaction is sufficient to account for the Ξ, N mass difference as well as for the μ, e mass difference. The suitable value for g seems to be rather small in view of the quadratic divergence involved. One would expect an anomalous μ scattering from nucleons whose magnitude is being estimated.

† It needs hardly be pointed out that the philosophy is adhered to that symmetries, invariance properties etc. which may exist in nature are intimately connected with *bare* fields and can be spoiled, or even completely hidden when *physical* particles are considered.

References

1) R. Gatto, Nuovo Cimento **2** (1956) 318
2) B. d'Espagnat and J. Prentki, Nuovo Cimento **3** (1956) 1045
3) G. Takeda, Phys. Rev. **101** (1956) 1547
4) G. Wentzel, Phys. Rev. **101** (1956) 1215
5) R. H. Dalitz, quoted by R. E. Marshak, B.A.S. **30** (1955) 25
6) B. T. Feld, Nuovo Cimento **6** (1957) 650
7) B. d'Espagnat, C. R. Acad. Sc. **245** (1957) 894
8) A. Salam and J. C. Polkinghorne, Nuovo Cimento **2** (1955) 685
9) B. d'Espagnat and J. Prentki, Nuclear Physics **1** (1956) 33
10) G. Racah, Nuclear Physics **1** (1956) 302
11) B. d'Espagnat and J. Prentki, Phys. Rev. **102** (1956) 1684
12) J. C. Polkinghorne, Nuovo Cimento **6** (1957) 864
13) M. Gell-Mann, Phys. Rev. **106** (1957) 1296
14) Ning-Hu, Padova-Venice Conference (1957)
15) B. d'Espagnat, J. Prentki and A. Salam, Padova-Venice Conference (1957)

Nuclear Physics **5** (1958) 455—463; © *North-Holland Publishing Co., Amsterdam*
Not to be reproduced by photoprint or microfilm without written permission from the publisher

ON THE POLARIZATION OF μ-MESONS IN $K_{\mu 3}$-DECAYS

L. OKUN
USSR Academy of Sciences, Moscow

Received 15 August 1957

Abstract: A calculation of the longitudinal polarization of μ-mesons in $K_{\mu 3}$-decays (and of electrons in K_{e3}-decays) is carried out under the assumption that the neutrino emitted in these processes is longitudinally polarized.

An investigation of the polarization of μ-mesons emitted in $K_{\mu 3}$-decays ($K \to \mu+\nu+\pi$) and electrons emitted in K_{e3}-decays ($K \to e+\nu+\pi$) in conjunction with a study of the energy spectra of the μ-mesons (electrons) should make it possible to elucidate the nature of non-conservation of parity in these processes. Measurement of the polarization should be especially important for the verification of longitudinality of neutrinos [1, 2, 3]) emitted in these decays and of the law of conservation of leptons (neutrino charge).

Given below is a calculation of the longitudinal polarization of μ-mesons emitted in $K_{\mu 3}$-decays. The calculation was carried out under the assumption that the neutrino is longitudinally polarized and that the direction of its polarization is the same for different types of interaction.

The matrix element for $K_{\mu 3}$ decay of a zero spin K-meson at rest, not containing derivatives of lepton functions, has the form

$$\mathfrak{M} = \left\{ g_S \bar{\psi}_\mu (1-\gamma_5)\psi_\nu + g_V \bar{\psi}_\mu \gamma_4 (1-\gamma_5)\psi_\nu + g_T \bar{\psi}_\mu i\gamma_4 \boldsymbol{\gamma}(1-\gamma_5)\psi_\nu \cdot \frac{\mathbf{k}_\pi}{m_K} \right\} \cdot \frac{1}{2m_K^{3/2} E_\pi^{\frac{1}{2}}}. \qquad (1)$$

The following notations are used: m_K, m_π, m_μ are the K, π, and μ-meson masses respectively,

$$E_\pi = \sqrt{k_\pi^2 + m_\pi^2},\ \gamma_4 = \beta,\ \boldsymbol{\gamma} = -i\beta\boldsymbol{\alpha},\ \gamma_5 = \gamma_1\gamma_2\gamma_3\gamma_4;$$

the g_S, g_V and g_T are dimensionless functions of the pion energy and are essentially form-factors of the strong interaction between a K-meson and a pion. I has been shown in refs. [4, 5, 6]) that by measuring the dependence of the probability of $K_{\mu 3}$ (K_{e3}) decay on the energy of the emerging μ-meson (electron) and pion one can determine which of these functions differs from zero and establish their dependence on E_π. At present the form of these functions cannot be calculated theoretically owing to the absence of a theory of strong interaction between the K-meson and pion. In a first approximation we assume that the g are constants. If the decay interaction

is invariant with regard to combined inversion, g_S, g_V, and g_T should be real (see ref. [6])). It should be noted that the first term in formula (1) is really the sum of two terms, one of which arises from the scalar S and the other from the vector V interaction. The form of $\mathfrak{M}$ is discussed in refs. [4,5,6]) and in the appendix.

With the help of (1) the longitudinal polarization of a μ-meson emitted in $K_{\mu 3}$-decay can easily be calculated from the expression

$$P = \frac{S_P \varrho \sigma \cdot \mu}{S_P \varrho} \tag{2}$$

where P is the degree of polarization, and the density matrix ϱ has the form

$$\begin{aligned}\varrho = {} & f_S(1-A\sigma\cdot\mu)(1+\sigma\cdot\nu)(1-A\sigma\cdot\mu)\\ & +f_V(1+A\sigma\cdot\mu)(1+\sigma\cdot\nu)(1+A\sigma\cdot\mu)\\ & +f_T(1-A\sigma\cdot\mu)\sigma\cdot\pi(1+\sigma\cdot\nu)\sigma\cdot\pi(1-A\sigma\cdot\mu)\frac{k_\pi^2}{m_K^2}\\ & +f_{SV}(1-A\sigma\cdot\mu)(1+\sigma\cdot\nu)(1+A\sigma\cdot\mu)\\ & +f_{ST}(1-A\sigma\cdot\mu)\sigma\cdot\pi(1+\sigma\cdot\nu)(1-A\sigma\cdot\mu)\frac{k_\pi}{m_K}\\ & +f_{VT}(1-A\sigma\cdot\mu)\sigma\cdot\pi(1+\sigma\cdot\nu)(1+A\sigma\cdot\mu)\frac{k_\pi}{m_K}.\end{aligned} \tag{3}$$

Here

$$A = \frac{k_\mu}{E_\mu + m_\mu} \quad \left(\frac{2A}{1+A^2} = v_\mu,\ \frac{1-A^2}{1+A^2} = \frac{m_\mu}{E_\mu}\right),$$

$$\mu = \frac{\mathbf{k}_\mu}{k_\mu}, \quad \nu = \frac{\mathbf{k}_\nu}{k_\nu}, \quad \pi = \frac{\mathbf{k}_\pi}{k_\pi},$$

σ is Pauli's matrix, and

$$f_S = |g_S|^2, \qquad f_V = |g_V|^2, \qquad f_T = |g_T|^2,$$
$$f_{SV} = \mathrm{Re}\,(g_S g_V^*), \quad f_{ST} = \mathrm{Re}\,(g_S g_T^*), \quad f_{VT} = \mathrm{Re}\,(g_V g_T^*).$$

From formulas (2) and (3) we easily get

$$\begin{aligned}P = {} & \frac{f_S(-v_\mu+\mu\cdot\nu)+f_V(v_\mu+\mu\cdot\nu)}{f_S(1-v_\mu\mu\cdot\nu)+f_V(1+v_\mu\mu\cdot\nu)}\\ & \frac{+f_T\{-v_\mu+[2(\nu\cdot\pi)(\mu\cdot\pi)-\mu\cdot\nu]\}\frac{k_\pi^2}{m_K^2}+f_{SV}\mu\cdot\nu\frac{m_\mu}{E_\mu}}{+f_T\{1-v_\mu[2(\nu\cdot\pi)(\mu\cdot\pi)-\mu\cdot\nu]\}\frac{k_\pi^2}{m_K^2}+f_{SV}\frac{m_\mu}{E_\mu}}\\ & \frac{+f_{ST}(-v_\mu\nu\cdot\pi+\mu\cdot\pi)\frac{k_\pi}{m_K}+f_{VT}\mu\cdot\pi\frac{k_\pi}{m_K}\frac{m_\mu}{E_\mu}}{+f_{ST}(\nu\cdot\pi-v_\mu\mu\cdot\pi)\frac{k_\pi}{m_K}+f_{VT}\nu\cdot\pi\frac{k_\pi}{m_K}\frac{m_\mu}{E_\mu}}.\end{aligned} \tag{4}$$

Expression (4) gives the dependence of polarization of the μ-meson on its velocity v_μ and on the cosine of the angle between μ and ν (the cosines $\nu \cdot \pi$ and $\mu \cdot \pi$ can be expressed elementarily through v_μ and $\mu \cdot \nu$ with the aid of the conservation laws. For pure S and V interactions the dependence of P on $\mu \cdot \nu$ and v_μ has the form (see also fig. 1)

$$P_S = \frac{-v_\mu + \mu \cdot \nu}{1 - v_\mu \mu \cdot \nu}, \quad P_V = \frac{v_\mu + \mu \cdot \nu}{1 + v_\mu \mu \cdot \nu}. \tag{5}$$

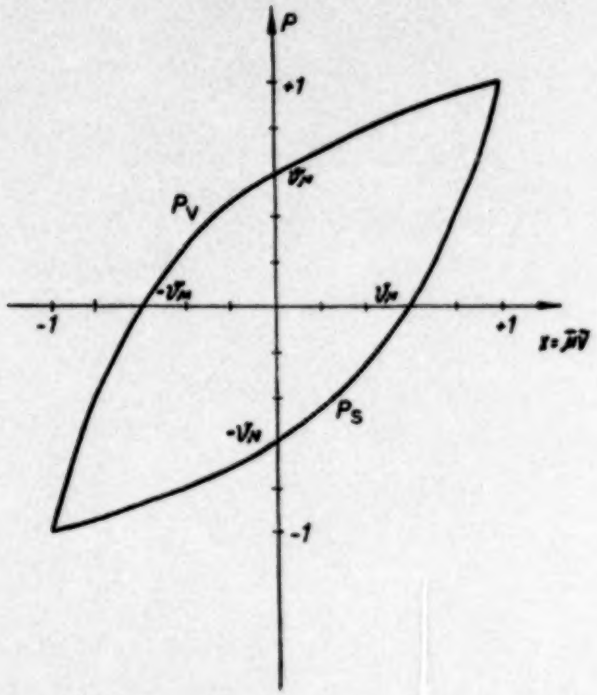

Fig. 1. Dependence of μ-meson polarization P on x (the cosine of the angle between the μ-meson and the neutrino) at a μ-meson velocity $v_\mu = 0.6$ for S- and V-interactions.

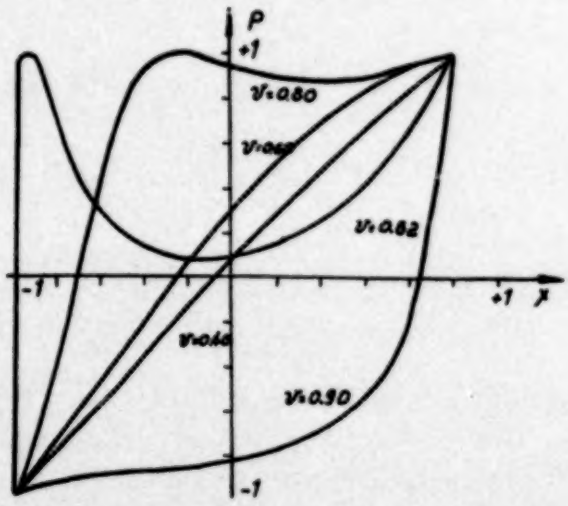

Fig. 2. Dependence of μ-meson polarization P on x (the cosine of the angle between the μ-meson and the neutrino) for T-interaction at μ-meson velocities $v_\mu = 0.4$; 0.6; 0.8; 0.82; 0.9 ($v_{\mu\,\max} = 0.896$ for $K_{\mu 3}$-decay).

For pure T-interaction the dependence is more complex (see figs. 2 and 3):

$$P_T = \frac{-vA+B}{A-vB} \tag{6}$$

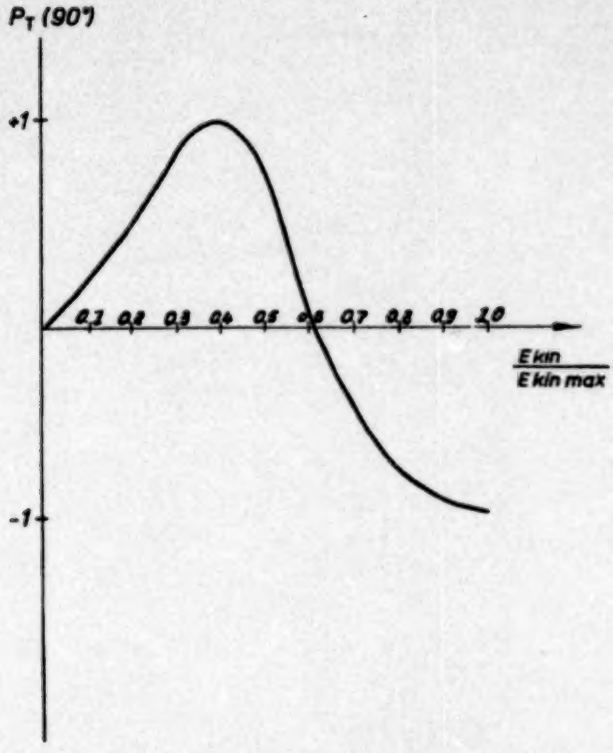

Fig. 3. Dependence of μ-meson polarization P on its velocity v_μ with the μ-meson and neutrino at right angles ($x = 0$) for T-interaction.

where

$$A = k_\mu^2+k_\nu^2+2k_\mu k_\nu x, \qquad B = k_\mu^2 x+k_\nu^2 x+2k_\mu k_\nu .$$

$$k_\nu = \frac{k_0}{1+\alpha x}, \qquad k_0 = m_K \frac{W-E_\mu}{m_K-E_\mu}, \qquad x \equiv \mu \cdot \nu, \qquad \alpha = \frac{k_\mu}{m_K-E_\mu};$$

$$W = \frac{m_K^2+m_\mu^2-m_\pi^2}{2m_K} \text{ is the maximum } \mu\text{-meson energy.}$$

It should be stressed that for all three interactions $P = +1$ if $x = +1$ and $P = -1$ if $x = -1$. This result can easily be understood by observing that in this case the spins of the μ-meson and the neutrino must compensate each other, and that the neutrino is longitudinally polarized.

From formula (6) and fig. 2 it is evident that there is an interval of velocities v_μ, determined by the conditions $k_\mu = k_\nu$, $|x| \leqq 1$, within which

polarization for the T-interaction reaches its maximum value $P = 1$ even for $x \neq 1$.

Averaging the numerator and denominator of expression (4) over the angle between the μ-meson and the neutrino, we get an expression for the longitudinal polarization of the μ-meson $\bar{P}$ as a function only of its velocity. It can easily be seen that this averaging is done by integrating over x the numerator and denominator of (4) multiplied by the weight function $(1+\alpha x)^{-3}$ arising from the phase volume. The result is

$$\bar{P} = \frac{f_S(-vI_3+L_3)+f_V(vI_3+L_3)+f_T(-v\bar{A}+\bar{B})}{f_S(I_3-vL_3)+f_V(I_3+vL_3)+f_T(\bar{A}-v\bar{B})} \qquad (7)$$
$$\frac{+f_{SV}L_3\frac{m_\mu}{E_\mu}+f_{ST}(-v\bar{C}+\bar{D})+f_{VT}\bar{D}\frac{m_\mu}{E_\mu}}{+f_{SV}I_3\frac{m_\mu}{E_\mu}+f_{ST}(\bar{C}-v\bar{D})+f_{VT}\bar{C}\frac{m_\mu}{E_\mu}}.$$

Here

$$\bar{A} = k_\mu^2 I_3+2k_\mu k_0 L_4+k_0^2 I_5,$$
$$\bar{B} = k_\mu^2 L_3+2k_\mu k_0 I_4+k_0^2 L_5,$$
$$\bar{C} = -k_0 I_4-k_\mu L_3,$$
$$\bar{D} = -k_0 L_4-k_\mu I_3,$$

$$I_n = \int_{-1}^{+1}\frac{dx}{(1+\alpha x)^n}, \qquad L_n = \int_{-1}^{+1}\frac{x\,dx}{(1+\alpha x)^n},$$

$$I_3 = \frac{2}{(1-\alpha^2)^2}, \qquad L_3 = -\frac{2\alpha}{(1-\alpha^2)^2},$$

$$I_4 = \frac{2(3+\alpha^2)}{3(1-\alpha^2)^3}, \qquad L_4 = -\frac{8\alpha}{3(1-\alpha^2)^3},$$

$$I_5 = \frac{2(1+\alpha^2)}{(1-\alpha^2)^4}, \qquad L_5 = -\frac{2\alpha(5+\alpha^2)}{3(1-\alpha^2)^4}.$$

For pure S, V and T-interactions $\bar{P}$ has the form

$$\bar{P}_S = -\frac{m_K\sqrt{E_\mu^2-m_\mu^2}}{E_\mu m_K-m_\mu^2}, \qquad (8)$$

$$\bar{P}_V = \frac{\sqrt{E_\mu^2-m_\mu^2}\,(m_K-2E_\mu)}{(m_K-2E_\mu)E_\mu+m_\mu^2}, \qquad (9)$$

$$\bar{P}_T = -v_\mu\frac{1-\beta}{1-\beta v_\mu^2}, \quad \text{where } \beta = \frac{\bar{B}}{v_\mu\bar{A}}. \qquad (10)$$

When $E_\mu/m_K \ll 1$ these formulas give expressions coinciding with the well-known results of the theory of β-decay

$$\bar{P}_S = -v, \quad \bar{P}_V = +v, \quad \bar{P}_T = -v.$$

The dependence of $\bar{P}_S$, $\bar{P}_V$ and $\bar{P}_T$ on the μ-meson energy expressed by formulas (8), (9) and (10) is represented in fig. 4.

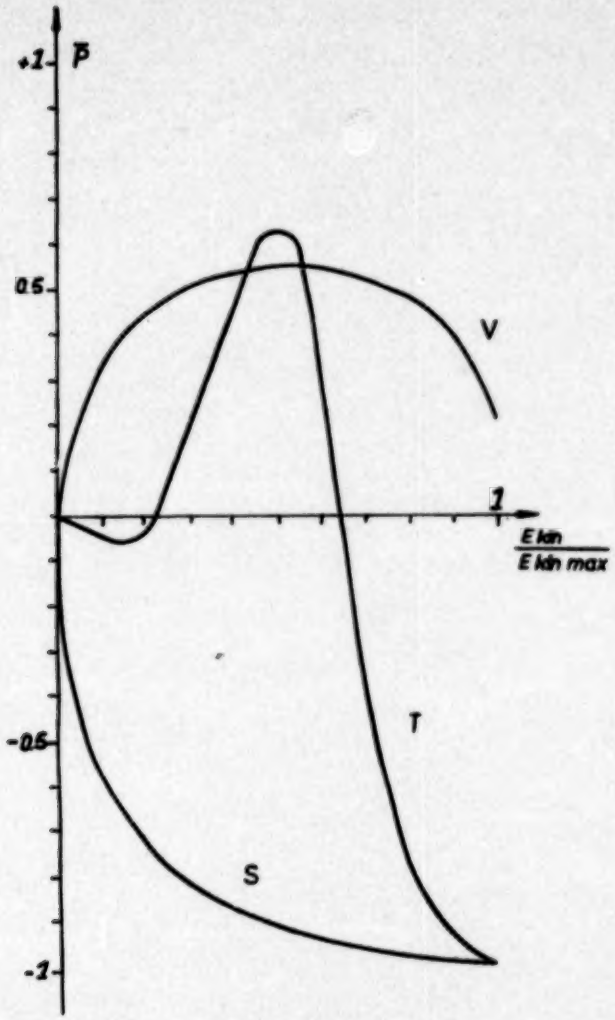

Fig. 4. Dependence of μ-meson polarization $\bar{P}$ on its energy for S, V and T-interactions.

It is noteworthy that if the $K_{\mu 3}$-decay is due only to one type of interaction, formulas (5) and (6) yield the exact polarization value independent of the assumptions concerning the form of the functions $g(E_\pi)$. This does not refer to formulas (8) to (10), which were obtained by integrating with respect to x under the assumption that $g_{S,V,T} = \text{const}$.

From formulas (4) and (7) an expression can easily be derived for electron polarization in K_{e3}-decay. In this case the mass of the electron can be neglected without perceptibly impairing the accuracy; this yields

$$\bar{P} = \frac{-f_S I_3 + f_V I_3 - f_T(\bar{A} - \bar{B}) - f_{ST}(\bar{C} - \bar{D})}{f_S I_3 + f_V I_3 + f_T(\bar{A} - \bar{B}) + f_{ST}(\bar{C} - \bar{D})}. \tag{11}$$

From (11) it can be seen that if $g_V = 0$, then $\bar{P} = -1$; but if $g_S = g_T = 0$, then $\bar{P} = +1$.

If there are two-component neutrinos and antineutrinos and if the law of conservation of the neutrino charge is valid the formulas obtained above describe the following decays:

$$\begin{aligned} &K^- \to \mu^-(e^-) + \bar{\nu} + \pi^0 \\ &K^0 \to \mu^-(e^-) + \bar{\nu} + \pi^+. \end{aligned} \tag{12}$$

The formulas for the decays

$$\begin{aligned} &K^+ \to \mu^+(e^+) + \nu + \pi^0 \\ &K^0 \to \mu^+(e^+) + \nu + \pi^- \end{aligned} \tag{13}$$

can be obtained from formulas for decays (12) by changing the polarization sign.

One of the methods of investigating polarization of μ-mesons in $K_{\mu 3}$-decay is measurement of the asymmetry of electrons produced in the decay of polarized μ-mesons. As this asymmetry is opposite in sign for identically polarized μ^+- and μ^--mesons, and in disintegrations (12) and (13) the μ^+- and μ^-- mesons are polarized oppositely, the angular distribution of secondary positons and negatons with respect to the momenta of μ^+- and μ^--mesons should be identical, in analogy to the cascade $\pi \to \mu \to e$.

The author is indebted to S. A. Nemirovskaya who kindly carried out the numerical calculations for the graphs.

Appendix

Consider the most general form of the Hamiltonian for the decay of a charged K-meson $[K^{\pm} \to \pi^0 + \mu^{\pm} + \nu(\bar{\nu})]$:

$$\begin{aligned} H = {} & \frac{g_S}{m_K} \phi \varphi \bar{\psi}_\mu (1 + \alpha_S \gamma_5) \psi_\nu + \frac{g_S^*}{m_K} \phi^+ \varphi \bar{\psi}_\nu (1 - \alpha_S^* \gamma_5) \psi_\mu \\ & + \frac{1}{m_K^2} \left(g_{V_1} \phi \frac{\partial \varphi}{\partial x_i} + g_{V_2} \frac{\partial \phi}{\partial x_i} \varphi \right) \bar{\psi}_\mu \gamma_i (1 + \alpha_V \gamma_5) \psi_\nu \\ & - \frac{1}{m_K^2} \left(g_{V_1}^* \phi^+ \frac{\partial \varphi}{\partial x_i} + g_{V_2} \frac{\partial \phi^+}{\partial x_i} \varphi \right) \bar{\psi}_\nu \gamma_i (1 + \alpha_V^* \gamma_5) \psi_\mu \\ & + \frac{g_T}{m_K^3} \frac{\partial \phi}{\partial x_i} \frac{\partial \varphi}{\partial x_k} \bar{\psi}_\mu \gamma_{ik} (1 + \alpha_T \gamma_5) \psi_\nu \\ & - \frac{g_T^*}{m_K^3} \frac{\partial \phi^+}{\partial x_i} \frac{\partial \varphi}{\partial x_k} \bar{\psi}_\nu \gamma_{ik} (1 - \alpha_T^* \gamma_5) \psi_\mu . \end{aligned} \tag{I}$$

Here ϕ and φ are the wave functions of the K and π-meson respectively;

$x_{1,2,3} = x, y, z, x_4 = it; \quad \bar{\psi} = \psi^+\gamma_4; \quad \gamma_4 = \beta, \gamma_\delta = -i\beta\alpha_\delta (\delta = 1, 2, 3);$
$\gamma_5 = \gamma_1\gamma_2\gamma_3\gamma_4; \quad \gamma_{ik} = \frac{1}{2}(\gamma_i\gamma_k - \gamma_k\gamma_i).$

It can easily be seen that $\gamma_i^+ = \gamma_i$, $\gamma_5^+ = \gamma_5$, $\gamma_{ik}^+ = -\gamma_{ik}$.

We now carry out combined inversion [1]):

$$\mathbf{x}' = -\mathbf{x}, \quad x'_4 = x_4, \quad \phi' = -\phi^+, \quad \varphi' = -\varphi,$$
$$\psi' = \beta C\bar{\psi}, \quad \bar{\psi}' = -\psi C^{-1}\beta$$

and

$$C^{-1}\gamma_i C = -\tilde{\gamma}_i, \quad C^{-1}\gamma_{ik}C = -\tilde{\gamma}_{ik}, \quad C^{-1}\gamma_5 C = \tilde{\gamma}_5.$$

Considering that the spinors corresponding to various fields anticommute, we get

$$\begin{aligned} H' = {} & \frac{g_s}{m_K}\phi^+\varphi\bar{\psi}_\nu(1-\alpha_s\gamma_5)\psi_\mu + \frac{g_s^*}{m_K}\phi\varphi\bar{\psi}_\mu(1+\alpha_s^*\gamma_5)\psi_\nu \\ & - \frac{1}{m_K^2}\left(g_{v_1}\phi^+\frac{\partial\varphi}{\partial x_i} + g_{v_2}\frac{\partial\phi^+}{\partial x_i}\varphi\right)\bar{\psi}_\nu\gamma_i(1+\alpha_v\gamma_5)\psi_\mu \\ & + \frac{1}{m_K^2}\left(g_{v_1}^*\phi\frac{\partial\varphi}{\partial x_i} + g_{v_2}^*\frac{\partial\phi}{\partial x_i}\varphi\right)\bar{\psi}_\mu\gamma_i(1+\alpha_v^*\gamma_5)\psi_\nu \qquad \text{(II)} \\ & - \frac{g_t}{m_K^3}\frac{\partial\phi^+}{\partial x_i}\frac{\partial\varphi}{\partial x_k}\bar{\psi}_\nu\gamma_{ik}(1-\alpha_t\gamma_5)\psi_\mu \\ & + \frac{g_t^*}{m_K^3}\frac{\partial\phi}{\partial x_i}\frac{\partial\varphi}{\partial x_k}\bar{\psi}_\mu\gamma_{ik}(1+\alpha_t^*\gamma_5)\psi_\nu. \end{aligned}$$

Comparing (II) with (I) and demanding invariance of H with respect to combined inversion, we get †

$$\begin{aligned} & g_s = g_s^*, \quad g_{v_1} = g_{v_1}^*, \quad g_{v_2} = g_{v_2}^*, \quad g_t = g_t^* \\ & \alpha_s = \alpha_s^*, \quad \alpha_v = \alpha_v^*, \quad \alpha_t = \alpha_t^*. \end{aligned} \qquad \text{(III)}$$

If we now carry out the following substitution in (I):

$$\frac{\partial\phi}{\partial x_l} = -ik_\pi{}^l\phi, \quad k_K = (0, im_K),$$
$$\frac{\partial\varphi}{\partial x_l} = ik_\pi{}^l\varphi, \quad k_\pi = (k_\pi, iE_\pi),$$

† If pseudoscalarity of the K-meson (condition $\phi' = -\phi^+$) or anticommutability of different spinor fields were not assumed, one would find that all α should, as before, be real but all g be imaginary. However, only the relative phases of different g are of physical interest, and they remain equal to zero as before. It should be noted that condition (III) agrees with the result obtained by Furuichi [7]), who investigated the phases of the coupling constants conditioned by invariance with respect to time reversal, and with that obtained by Pais and Treiman [4]). The footnote in ref. [6]) concerning ref. [4]) is based on a misunderstanding. See also ref. [8]).

and put $\alpha_s = \alpha_v = \alpha_t = -1$, we get the following expression for the matrix element:

$$\mathfrak{M} = \frac{1}{m_K}\phi\varphi\bar{\psi}_\mu\left[g_s+g_{v_1} i\frac{k_\pi^l}{m_K}\gamma_l+g_{v_2}\gamma_4+\frac{ig_t}{m_K}\mathbf{k}_\pi\cdot\gamma_4\boldsymbol{\Upsilon}\right](1-\gamma_5)\psi_\nu+\text{H.c.} \quad \text{(IV)}$$

Now, it can easily be proved [4]) that interaction v_1 is a linear combination of interactions v_2 and s, and that there are thus only three linearly independent types of interaction. Indeed, noting that

$$k_\pi^l = k_K^l - k_\mu^l - k_\nu^l,$$

and taking advantage of the fact that

$$\bar{\psi}_\mu(-i\gamma_l k_\mu^l + m_\mu) = 0 \quad \text{and} \quad i\gamma_l k_\nu^l \psi_\nu = 0,$$

we get easily from (IV) formula (1) of this paper, where

$$g_S = g_s - \frac{m_\mu}{m_K} g_{v_1} \quad \text{and} \quad g_V = g_{v_2} - g_{v_1}.$$

It should be noted that if $\alpha_s \neq \alpha_v$ the number of independent types of interactions should be 4 and not 3.

In his investigation of the same problem [9]), published after the present paper was written, J. Werle treats the four coupling constants of eq. (IV) as independent. Apart from this his (corrected) results are in agreement with those of this paper.

References

1) L. Landau, JETP **32** (1957) 405
2) A. Salam, Nuovo Cimento **5** (1957) 299
3) T. D. Lee and C. N. Yang, Phys. Rev. **105** (1957) 1671
4) A. Pais and S. B. Treiman, Phys. Rev. **105** (1957) 1616
5) S. Furuichi *et al.*, Progr. Theor. Phys. **17** (1957) 89
6) L. Okun, JETP **33** (1957) 525
7) S. Furuichi, On the decay interactions of neutral K_{e3} and $K_{\mu 3}$ (preprint)
8) B. L. Ioffe, JETP **32** (1957) 1246
9) J. Werle, Nuclear Physics **4** (1957) 171, (correction 693)

Nuclear Physics **5** (1958) 464—494; © *North-Holland Publishing Co., Amsterdam*
Not to be reproduced by photoprint or microfilm without written permission from the publisher

β-DECAY AND NON-CONSERVATION OF PARITY

V. B. BERESTETSKY, B. L. IOFFE, A. P. RUDIK and K. A. TER-MARTIROSYAN

U.S.S.R. Academy of Sciences, Moscow

Received 18 April 1957

Abstract: Effects due to non-conservation of parity such as longitudinal and transverse polarization of β-electrons, angular distribution of β-electrons from an oriented nucleus (including the case when the direction of the recoil nucleus momentum is fixed) are examined in the present paper for the cases of allowed β-transitions and first order forbidden transitions. It is shown that owing to the influence of the Coulomb field the magnitude of these effects for forbidden transitions in heavy and intermediate nuclei is the same as for allowed transitions. Perceptible deviations are observed in light nuclei ($Z \lesssim 20$). In the particular case of a $0-0$ transition comparison with experiment may yield important data on the contribution of pseudoscalar coupling. Unique transitions ($\Delta j = 2$, yes) for which the electron angular distribution of oriented nuclei essentially differs from that for allowed transitions are considered separately.

Introduction

The hypothesis of non-conservation of parity in β-decay proposed by Lee and Yang [1]) has been confirmed recently by Wu, Ambler, Hayward, Hoppes and Hudson [2]) who observed an asymmetry in the angular distribution of β-electrons emitted in the decay of oriented Co^{60} nuclei. The large magnitude of the observed effect agrees with the two component neutrino theory proposed by Landau [3]), Lee and Yang [4]) and Salam [5]). The β-electron polarization effect predicted by Landau has also received experimental proof [6, 7, 8]).

New experimental possibilities relating to parity non-conservation in β-decay (measurement of the angular distribution of electrons emitted by decaying oriented nuclei, of electron polarization, etc.) require theoretical investigation of these phenomena since one may hope to derive from the new experimental data additional information concerning the nature of β-interactions and the magnitudes of the nuclear matrix elements.

Allowed transitions and first order forbidden transitions are considered in the present paper. Investigation of first order forbidden transitions is of interest not only because of the purely experimental advantages it involves but also because analysis of these transitions in principle may yield an answer to the question whether β-decay interactions include pseudoscalar coupling †.

† On finishing this paper we have received preprints from K. Alder, B. Stech and A. Winter and from I. M. Shmushkevich. Their results coincide in many points with ours. Similar computations in Born approximation (including vector couplings) were done recently by J. B. Jackson, S. B. Treiman and H. W. Wyld [13]).

For the sake of brevity we shall not consider vector couplings which, apparently, are not encountered experimentally and shall restrict our considerations to three types of coupling: scalar, tensor and pseudoscalar. All calculations will be performed for the two-component neutrino. However, the results can easily be extended to the case of an arbitrary value of the coefficient λ, which determines the degree of violation of parity conservation ($\lambda = 1$ refers to a two-component neutrino) providing that one considers λ to be the same for all types of coupling.

All results obtained here can be easily extended to the most general case, which includes vector type couplings and an arbitrary degree of parity violation in each type of coupling. The formulae corresponding to this general case will be published elsewhere.

At present it is not clear whether β-decay interactions are invariant under time reversal (or, what is the same, under combined inversion), that is, if the decay interaction constants are real [9]). We shall therefore consider these constants to be complex and attempt to examine just those effects which would permit one to experimentally determine whether time parity is conserved in β-decay.

The effect of the nuclear Coulomb field is almost always a very significant factor in β-decay, especially in the case of forbidden transitions. (In first order forbidden β-transitions the Coulomb field radically changes the magnitude of the polarization and angular distribution of decay electrons from oriented nuclei and may also lead to the appearance of the same type of terms as those encountered when time parity is not conserved [10]).) All calculations will therefore be performed by using the exact relativistic electron Coulomb functions.

1. β-Decay Matrix Element and Electron Density Matrix

We shall write the matrix element of the β-interaction operator

$$H = \bar{\psi}_e [g_S(\bar{\psi}_2\psi_1)+g_P(\bar{\psi}_2\gamma_5\psi_1)\gamma_5+g_T(\bar{\psi}_2\sigma\psi_1)\cdot\sigma+g_T(\bar{\psi}_2\alpha\psi_1)\cdot\alpha] \times \frac{1+\lambda\gamma_5}{\sqrt{1+|\lambda|^2}}\psi_\nu \quad (1)$$

(ψ_1 and ψ_2 are the nucleon field operators, $\gamma_5 = \left(\begin{smallmatrix}0 & -1\\ -1 & 0\end{smallmatrix}\right)$, $\sigma = -\gamma_5\alpha$) for the case when the degree of parity non-conservation (coefficient λ) is the same for all types of coupling. It is easiest of all to perform the calculations when $\lambda = +1$ or $\lambda = -1$ which corresponds to a two component neutrino. The value $\lambda = +1$ corresponds to the formation, in β^--decay, of a neutrino, i.e., of a particle whose spin is directed along the momentum, $\lambda = -1$ implies the formation of an antineutrino, whose spin is opposite to the direction of the momentum. In the following we shall assume $\lambda = -1$ as this case

(antineutrino formation in β-decay) is apparently consistent with the experimental data [2, 6, 7, 8]).

It can readily be seen that the results obtained with the Hamiltonian (1) assuming $\lambda \neq -1$ can be directly obtained from the corresponding results for $\lambda = -1$.

Indeed, the matrix element M for the operator H corresponding to emission of an electron and antineutrino has the form

$$M_{\xi\zeta} = \left(U_\xi^* \frac{1+\lambda\gamma_5}{\sqrt{1+|\lambda|^2}} u'_{-\mathbf{q},-\zeta} \right)$$

where $u'_{-\mathbf{q},-\zeta}$ is the spinor amplitude of the neutrino wave function $u'_{-\mathbf{q},-\zeta}\, e^{-i\mathbf{q}\cdot\mathbf{r}}$ which refers to a level of negative energy $\varepsilon_\nu = -|\mathbf{q}|$, momentum $-\mathbf{q}$ and spin $-\zeta$ ($\zeta = \pm\frac{1}{2}$); the remaining part of the matrix element (corresponding to the electron spin state ξ) is denoted as a spinor U_ξ^*.

We now write down the matrix $S_{\xi\xi'} = \sum_{\zeta=\pm\frac{1}{2}} M_{\xi\zeta} M^*_{\xi'\zeta}$ which determines the total β-transition probability

$$W = \sum_{\xi=\pm\frac{1}{2}} S_{\xi\xi} = \operatorname{tr} \hat{S},$$

as well as the mean value of any component of the electron spin $\frac{1}{2}\sigma_j$ in the rest system

$$\langle \sigma_j \rangle = W^{-1} \sum_{\xi,\xi'} S_{\xi\xi'} (\sigma_j)_{\xi\xi'} = \frac{\operatorname{tr} (\hat{S}\sigma_j)}{\operatorname{tr} \hat{S}}.$$

Since

$$\sum_\zeta u'_{-\mathbf{q},-\zeta} u'^*_{-\mathbf{q},-\zeta} = \tfrac{1}{2}(1+\boldsymbol{\alpha}\cdot\boldsymbol{\nu}), \quad \boldsymbol{\nu} = \mathbf{q}/q,$$

we get

$$S_{\xi\xi'} = (1+|\lambda|^2)^{-1} (U_\xi^* (1+\lambda\gamma_5) \tfrac{1}{2}(1+\boldsymbol{\alpha}\cdot\boldsymbol{\nu})(1+\lambda\gamma_5) U_\xi)$$
$$= (U_\xi^* (1+\eta\gamma_5) \tfrac{1}{2}(1+\boldsymbol{\alpha}\cdot\boldsymbol{\nu}) U_\xi)$$

where $\eta = (\lambda+\lambda^*)/(1+|\lambda|^2)$. Thus, for an arbitrary λ the matrix $S_{\xi\xi'}$ consists of a term $S^{(0)}_{\xi\xi'} = U^*_\xi \frac{1}{2}(1+\boldsymbol{\alpha}\cdot\boldsymbol{\nu}) U_{\xi'})$ which is independent of η, and of a term $\eta S^{(1)}_{\xi\xi'} = \eta\, U^*_\xi \gamma_5 \frac{1}{2}(1+\boldsymbol{\alpha}\cdot\boldsymbol{\nu}) U_{\xi'}$, proportional to η, which is a pseudoscalar and corresponds to non-conservation of parity. It is evident that all effects involving violation of parity conservation will be simply proportional to $\eta = 2\operatorname{Re}\lambda/(1+|\lambda|^2)$ and therefore all formulae referring to the general case when λ is arbitrary can be directly derived from the formulae for $\lambda = -1$ if the pseudoscalar quantities in the latter are multiplied by $-\eta$.

This means, in particular, that all effects involving non-conservation of parity disappear† if λ is a purely imaginary quantity (for $\eta = 0$) i.e. if the theory is invariant under charge conjugation [9]).

† It being assumed, as above, that violation of parity is characterized by the same coefficient λ in the different variants of β-decay theory.

Calculation of the operator matrix element can be carried out most conveniently for $\lambda = -1$ by splitting all the quantities into two-component matrices and spinors. The final state electron wave function corresponding to a momentum $\mathbf{p}$ and the spin state ξ at infinity can be represented as

$$\psi_{\mathbf{p},\xi}(\mathbf{r}) = N \begin{pmatrix} \varphi_{\mathbf{p}} v_\xi \\ \chi_{\mathbf{p}} v_\xi \end{pmatrix}, \tag{2}$$

where v_ξ is a two-component unit spinor defining the electron polarization, N is a constant whose value is given below and $\varphi_{\mathbf{p}}$ and $\chi_{\mathbf{p}}$ are two-row matrices; $\psi_{\mathbf{p},\xi}(\mathbf{r})$ is the solution of the Dirac equation in a Coulomb field which at $r \to \infty$ can be represented as the superposition of a plane wave and spherical incoming wave. Using the spherical wave series expansion of this function given in ref. [11]) one can determine its shape within the nucleus, that is, for $pr \ll 1$. As shown in appendix 1, $\varphi_{\mathbf{p}}$ and $\chi_{\mathbf{p}}$ can be written in the following form, correct up to terms linear in pr:

$$\begin{aligned} \varphi_{\mathbf{p}} &= \alpha_0 + i\mathbf{p}\cdot\mathbf{r}\alpha_1 + i\left(\boldsymbol{\sigma}\cdot\frac{\mathbf{r}}{r}\right)(\boldsymbol{\sigma}\cdot\mathbf{n})\left(\beta_c + \frac{pr}{3}\alpha_c''\right) \\ \chi_{\mathbf{p}} &= \left[\beta_0 + i\mathbf{p}\cdot\mathbf{r}\beta_1 + i\left(\boldsymbol{\sigma}\cdot\frac{\mathbf{r}}{r}\right)(\boldsymbol{\sigma}\cdot\mathbf{n})\left(\alpha_c + \frac{pr}{3}\beta_c''\right)\right](\boldsymbol{\sigma}\cdot\mathbf{n}) \end{aligned} \tag{3}$$

where $\mathbf{n} = \mathbf{p}/p$ and constants α_i and β_i have the form † (ε is the electron energy)

$$\alpha_0 = \frac{(\gamma_1+1)\sqrt{\varepsilon+1} + i\alpha Z\sqrt{\varepsilon-1}}{2\sqrt{2\varepsilon}}; \quad \alpha_c = \frac{(\gamma_1-1)\sqrt{\varepsilon-1} + i\alpha Z\sqrt{\varepsilon+1}}{2i\sqrt{2\varepsilon}}$$

$$\beta_0 = \frac{(\gamma_1+1)\sqrt{\varepsilon-1} + i\alpha Z\sqrt{\varepsilon+1}}{2\sqrt{2\varepsilon}}; \quad \beta_c = \frac{(\gamma_1-1)\sqrt{\varepsilon+1} + i\alpha Z\sqrt{\varepsilon-1}}{2i\sqrt{2\varepsilon}}$$

$$\alpha_1 = \xi\frac{(\gamma_2+2)\sqrt{\varepsilon+1} + i\alpha Z\sqrt{\varepsilon-1}}{4\sqrt{2\varepsilon}}; \qquad \alpha_c'' = \alpha_c' - \alpha_1$$

$$\alpha'_c = \frac{3\sqrt{\varepsilon+1}}{\sqrt{2\varepsilon}(2\gamma_1+1)}\left[\frac{\gamma_1+1}{2} - \frac{\alpha^2 Z^2\varepsilon}{\varepsilon+1} + i\alpha Z\left(\frac{\gamma_1\varepsilon}{p} - \frac{1}{2}\sqrt{\frac{\varepsilon-1}{\varepsilon+1}}\right)\right]$$

$$\beta_1 = \xi\frac{(\gamma_2+2)\sqrt{\varepsilon-1} + i\alpha Z\sqrt{\varepsilon+1}}{4\sqrt{2\varepsilon}}; \qquad \beta_c'' = \beta_c' - \beta_1$$

$$\beta'_c = \frac{3\sqrt{\varepsilon-1}}{\sqrt{2\varepsilon}(2\gamma_1+1)}\left[\frac{\gamma_1+1}{2} - \frac{\alpha^2 Z^2\varepsilon}{\varepsilon-1} + i\alpha Z\left(\frac{\gamma_1\varepsilon}{p} - \frac{1}{2}\sqrt{\frac{\varepsilon+1}{\varepsilon-1}}\right)\right];$$

† The system of units in which $\hbar = c = m_e = 1$, is used, i.e. $\varepsilon = E_e/m_e c^2$ where E_e is the electron energy and m_e is its rest mass.

$$\xi = \frac{12\Gamma(2\gamma_1+1)}{\Gamma(2\gamma_2+1)} \cdot \frac{\Gamma\left(\gamma_2+i\frac{\alpha Z\varepsilon}{p}\right)}{\Gamma\left(\gamma_1+i\frac{\alpha Z\varepsilon}{p}\right)} (2ipr)^{\gamma_2-\gamma_1-1};$$

$$N = \frac{2\Gamma\left(\gamma_1+i\frac{\alpha Z\varepsilon}{p}\right)}{\Gamma(2\gamma_1+1)} e^{\frac{\pi\alpha Z\varepsilon}{2p}} (2pr)^{\gamma_1-1}.$$

Here $\alpha = 1/137$, $\gamma_1 = \sqrt{1-\alpha^2 Z^2}$, $\gamma_2 = \sqrt{4-\alpha^2 Z^2}$.

For $Z \to 0$ we get

$$\alpha_0 = \alpha_1 = \sqrt{\frac{\varepsilon+1}{2\varepsilon}}, \quad \beta_0 = \beta_1 = \sqrt{\frac{\varepsilon-1}{2\varepsilon}},$$

$\xi = N = 1$ and $\alpha_c = \alpha'_c = \beta_c = \beta'_c = 0$. In this case $\psi_{\mathbf{p},\xi}$ goes over into $u_{\mathbf{p},\xi}(1+i\mathbf{p}\cdot\mathbf{r})$, with

$$u_{\mathbf{p},\xi} = \begin{pmatrix} \sqrt{\frac{\varepsilon+1}{2\varepsilon}}\, v_\xi \\ \sqrt{\frac{\varepsilon-1}{2\varepsilon}}\, \boldsymbol{\sigma}\cdot\mathbf{n}\, v_\xi \end{pmatrix} = \sqrt{\frac{\varepsilon+1}{2\varepsilon}} \begin{pmatrix} v_\xi \\ \frac{\boldsymbol{\sigma}\cdot\mathbf{p}}{\varepsilon+1} v_\xi \end{pmatrix},$$

that is into the expansion of a plane wave in a series of powers of $\mathbf{p}\cdot\mathbf{r}$.

As will be seen below, the last term in (3), which vanishes when the Coulomb field is turned off, plays an important role in the case of first order forbidden transitions.

Writing the operator enclosed by the brackets in (1) in the form

$$\begin{pmatrix} V_1 & V_2 \\ V_2 & V_1 \end{pmatrix}$$

(the V_2 part is due to the nondiagonal terms with γ_5 and $\boldsymbol{\alpha}$ in (1)) and taking into account that †

$$\frac{1}{\sqrt{2}}(1-\gamma_5)u'_{-\mathbf{q},-\zeta} = \begin{pmatrix} w \\ w \end{pmatrix} \delta_{\zeta,\frac{1}{2}},$$

where w is a two-component spinor satisfying the condition $\boldsymbol{\sigma}\cdot\boldsymbol{\nu} w = w$, we represent the matrix element $M_{\xi\frac{1}{2}}$ of the operator H in the form

$$M_{\xi\frac{1}{2}} = (v_\xi^* V w), \tag{4}$$

where

$$V = \int (\varphi_{\mathbf{p}}^* - \chi_{\mathbf{p}}^*)(V_1+V_2)\, e^{-i\mathbf{q}\cdot\mathbf{r}}\, d\tau. \tag{5}$$

Integration is carried out over the coordinates of all the nucleons in the nucleus.

† As $u'_{-\mathbf{q},\frac{1}{2}} = \frac{1}{\sqrt{2}}\begin{pmatrix} w \\ w \end{pmatrix}$ and $u'_{-\mathbf{q},-\frac{1}{2}} = \frac{1}{\sqrt{2}}\begin{pmatrix} w' \\ -w' \end{pmatrix}$, where $\boldsymbol{\sigma}\cdot\boldsymbol{\nu} w' = -w'$.

Inserting (4) into the expression for the matrix $S_{\xi\xi'} = (\psi_\xi^* \hat{S} \psi_{\xi'})$ and noting that $w(\alpha)w^*(\beta) = \frac{1}{2}(1+\boldsymbol{\sigma}\cdot\boldsymbol{\nu})_{\alpha\beta}$ we write S in the form

$$S = V\,\tfrac{1}{2}(1+\boldsymbol{\sigma}\cdot\boldsymbol{\nu})V^+. \tag{6}$$

2. Allowed Transitions

In the case of allowed transitions it is sufficient to consider only zero approximation terms in the power expansion of the electron and neutrino wave functions in $\mathbf{p}\cdot\mathbf{r}$. The contribution of terms proportional to γ_5 and $\boldsymbol{\alpha}$ in (1) may be disregarded so that in (5) $V_2 = 0$. Denoting the nuclear matrix elements by

$$\begin{aligned} I &= g_S \int \bar{\psi}_2 \psi_1 \,\mathrm{d}\tau \\ \boldsymbol{\Lambda} &= g_T \int \bar{\psi}_2 \boldsymbol{\sigma} \psi_1 \,\mathrm{d}\tau \end{aligned} \tag{7}$$

we obtain in accord with (4), (5)

$$\begin{aligned} V_1 &= I + \boldsymbol{\sigma}\cdot\boldsymbol{\Lambda} \\ V &= N(\alpha_0^* - \beta_0^* \boldsymbol{\sigma}\cdot\mathbf{n})(I+\boldsymbol{\sigma}\cdot\boldsymbol{\Lambda}). \end{aligned} \tag{8}$$

The matrix S for allowed transitions can directly be derived from formulae (6) and (8) †:

$$S = \frac{|N|^2}{2}(\alpha_0^* - \beta_0^* \boldsymbol{\sigma}\cdot\mathbf{n})(I+\boldsymbol{\sigma}\cdot\boldsymbol{\Lambda})(1+\boldsymbol{\sigma}\cdot\boldsymbol{\nu})(I^*+\boldsymbol{\sigma}\cdot\boldsymbol{\Lambda}^*)(\alpha_0 - \beta_0 \boldsymbol{\sigma}\cdot\mathbf{n}). \tag{9}$$

It will be convenient (a similar method will also be employed in the case of forbidden transitions) to write the three middle factors in (9) as

$$(I+\boldsymbol{\sigma}\cdot\boldsymbol{\Lambda})(1+\boldsymbol{\sigma}\cdot\boldsymbol{\nu})(I^*+\boldsymbol{\sigma}\cdot\boldsymbol{\Lambda}^*) = A + \mathbf{B}\cdot\boldsymbol{\sigma} \tag{10}$$

and first compute S assuming A and $\mathbf{B}$ to be prescribed. Inserting (10) in (9) we obtain after simple calculations

$$S = \frac{1+\gamma_1}{2}\left\{A - \frac{\hat{p}}{\varepsilon}(A\boldsymbol{\sigma}\cdot\mathbf{n} + \mathbf{B}\cdot\mathbf{n}) + \left(1-\frac{\gamma_1}{\varepsilon}\right)(\boldsymbol{\sigma}\cdot\mathbf{n})(\mathbf{B}\cdot\mathbf{n}) + \frac{\gamma_1}{\varepsilon}\boldsymbol{\sigma}\cdot\mathbf{B} - \frac{\alpha Z}{\varepsilon}\boldsymbol{\sigma}\cdot(\mathbf{n}\wedge\mathbf{B})\right\}. \tag{11}$$

A and $\mathbf{B}$ are determined by the nuclear matrix elements. In computing them we shall consider several different cases separately.

† Strictly speaking the dependence of the factor N on r, $(pr)\gamma_1^{-1}$, should be included in the definition of matrix element (7) so that, for example, instead of I one should write $I' = g_S \int \bar{\psi}_2 \psi_1 (pr)\gamma_1^{-1}\,\mathrm{d}\tau$. This of course would not change anything in the subsequent results. However it should be noted that the corrections that should be introduced to take into account this circumstance are of the same order as those due to the finite size of the nucleus which we neglect. In the following exposition we shall therefore drop factors of this type.

2.1. β-ACTIVE NUCLEUS NOT ORIENTED

The first case to be considered is that in which the β-active nucleus is not oriented. Brackets (e.g. $\langle S\rangle$) will designate averaging over the initial orientation and summation over the final orientation of the nucleus (i.e. $\langle S\rangle = 1(2j+1)^{-1}\sum_{\mu,\mu'} S$ where j, μ and j', μ' are the angular momenta of the initial and final states of the nuclei).

Since

$$\begin{aligned}\langle \Lambda_i \Lambda_k^*\rangle &= \tfrac{1}{3}|C_\Lambda|^2\delta_{ik}\\ \langle II^*\rangle &= |C_I|^2,\end{aligned} \tag{12}$$

where C_Λ, C_I are constants (commonly designated as $C_I = g_S\int 1$, $C_\Lambda = g_T|\int \sigma|$), and

$$\langle I\Lambda_k^*\rangle = \langle \Lambda_k I^*\rangle = 0,$$

we easily find from (10)

$$\begin{aligned}\langle A\rangle &= |C_\Lambda|^2+|C_I|^2\delta_{j,j'},\\ \langle \mathbf{B}\rangle &= (-\tfrac{1}{3}|C_\Lambda|^2+|C_I|^2\delta_{j,j'})\boldsymbol{\nu}.\end{aligned} \tag{13}$$

Substitution of (13) in (11) yields

$$\frac{2\langle S\rangle}{W_{\text{tot}}} = 1-\frac{\mathbf{p}\cdot\boldsymbol{\nu}}{\varepsilon}\langle\beta\rangle-\frac{\boldsymbol{\sigma}\cdot\mathbf{p}}{\varepsilon}+\boldsymbol{\sigma}\cdot\left\{\left(1-\frac{\gamma_1}{\varepsilon}\right)\mathbf{n}(\mathbf{n}\cdot\boldsymbol{\nu})+\frac{\gamma_1}{\varepsilon}\boldsymbol{\nu}-\frac{\alpha Z}{\varepsilon}(\mathbf{n}\wedge\boldsymbol{\nu})\right\}\langle\beta\rangle,$$

$$W_{\text{tot}} = F(Z,\varepsilon)[|C_\Lambda|^2+|C_I|^2\delta_{j,j'}], \tag{14}$$

$$F(Z,\varepsilon) = |N|^2\frac{1+\gamma_1}{2},$$

with

$$\langle\beta\rangle = -\frac{\frac{1}{3}-|\varrho|^2\delta_{j,j'}}{1+|\varrho|^2\delta_{j,j'}};\quad \varrho = \frac{C_I}{C_\Lambda}. \tag{15}$$

From eq. (14) the following can be deduced:

a) the well known expression for electron-neutrino angular correlation

$$W_{e\nu}(\theta) = 1-\langle\beta\rangle\frac{\mathbf{p}\cdot\boldsymbol{\nu}}{\varepsilon} = 1-\langle\beta\rangle v\cos\theta; \tag{16}$$

b) the expression for longitudinal polarization of β-electrons

$$\langle\sigma_{\mathbf{p}}\rangle = [-v+\langle\beta\rangle\cos\theta][1-\langle\beta\rangle v\cos\theta]^{-1}; \tag{17}$$

c) the transverse polarization

$$\langle\boldsymbol{\sigma}_1\rangle = \langle\beta\rangle\left\{\frac{\gamma_1}{\varepsilon}(\boldsymbol{\nu}-\mathbf{n}(\mathbf{n}\cdot\boldsymbol{\nu}))-\alpha Z\frac{1}{\varepsilon}(\mathbf{n}\wedge\boldsymbol{\nu})\right\}[1-\langle\beta\rangle v\cos\theta]^{-1}. \tag{18}$$

Upon averaging over the directions of emission of the neutrino, $\langle\boldsymbol{\sigma}_\perp\rangle$ evidently vanishes and the longitudinal polarization becomes [3]) equal to v, which is the ratio of the electron velocity to that of light.

2.2. β-ACTIVE NUCLEUS ORIENTED

Assume that the nucleus is oriented along a certain direction (axis Oz), i.e., that $\langle\mu\rangle \neq 0$. We now take the average of the various quantities over the directions of neutrino emission. From (10) we then obtain

$$\begin{aligned} \bar{A} &= II^*+\boldsymbol{\Lambda}\cdot\boldsymbol{\Lambda}^*, \\ \overline{\mathbf{B}} &= I\boldsymbol{\Lambda}^*+\boldsymbol{\Lambda}I^*+i\boldsymbol{\Lambda}\wedge\boldsymbol{\Lambda}^*, \end{aligned} \tag{19}$$

where the bar denotes averaging over ν. In order to obtain convenient formula for $\bar{A}$ and $\overline{\mathbf{B}}$ the explicit dependence of the nuclear matrix elements (7) on projections μ, μ' of the nuclear moments on Oz in the initial and final states should be introduced.

Evidently,

$$\begin{aligned} \Lambda_m &= C_{\boldsymbol{\Lambda}}\sqrt{\frac{2j+1}{2j'+1}}\,C^{j'\mu'}_{j\mu,\,1m} \\ I &= C_{\mathrm{I}}\sqrt{\frac{2j+1}{2j'+1}}\,C^{j'\mu'}_{j\mu,\,00} = C_{\mathrm{I}}\delta_{j,j'}\delta_{\mu,\mu'} \end{aligned} \tag{20}$$

where $C^{j'\mu'}_{j\mu,\,1m}$ are Clebsch-Gordan coefficients, $m = 0, \pm 1$,

$$\Lambda_0 = \Lambda_z, \qquad \Lambda_1 = 2^{-\frac{1}{2}}(\Lambda_x+i\Lambda_y), \qquad \Lambda_{-1} = -2^{-\frac{1}{2}}(\Lambda_x-i\Lambda_y)$$

and $\sqrt{(2j+1)/(2j'+1)}$ is a normalization factor (which ensures as assumed above, that $\langle\Lambda_i\Lambda_k^*\rangle = \frac{1}{3}|C_{\boldsymbol{\Lambda}}|^2\delta_{ik}$). In this case summing $\bar{A}$ and $\overline{\mathbf{B}}$ over all values of μ', noting that only the projection of $\overline{\mathbf{B}}$ on axis Oz is not zero and taking into account the equalities

$$\sum_m (C^{j'\mu+m}_{j\mu,\,1m})^2 = \frac{2j'+1}{2j+1},$$

$$i(\boldsymbol{\Lambda}\wedge\boldsymbol{\Lambda}^*)_0 = |\Lambda_{-1}|^2-|\Lambda_1|^2,$$

we obtain

$$\begin{aligned} \bar{A} &= |C_{\mathrm{I}}|^2+|C_{\boldsymbol{\Lambda}}|^2, \\ \overline{\mathbf{B}} &= \left(\Delta_{j\mu}|C_{\boldsymbol{\Lambda}}|^2+\frac{\mu\delta_{jj'}}{\sqrt{j(j+1)}}\,2\,\mathrm{Re}\,C_{\mathrm{I}}C_{\boldsymbol{\Lambda}}^*\right)\mathbf{n}_j, \end{aligned} \tag{21}$$

where $\mathbf{n}_j$ denotes the unit vector along Oz.

Insertion in (11) yields the following expression for the matrix $\bar{S}$:

$$\frac{2\bar{S}}{W_{\mathrm{tot}}} = 1-\frac{\mathbf{p}\cdot\mathbf{n}_j}{\varepsilon}\bar{\beta}-\frac{\boldsymbol{\sigma}\cdot\mathbf{p}}{\varepsilon}+\boldsymbol{\sigma}\cdot\left\{\left(1-\frac{\gamma_1}{\varepsilon}\right)\mathbf{n}(\mathbf{n}\cdot\mathbf{n}_j)+\frac{\gamma_1}{\varepsilon}\mathbf{n}_j\right\}-\frac{\alpha Z}{\varepsilon}(\mathbf{n}\cdot\mathbf{n}_j)\bar{\beta} \tag{22}$$

where

$$\bar{\beta} = \frac{\Delta_{j\mu}+\dfrac{2\mu\delta_{jj'}}{\sqrt{j(j+1)}}\,\mathrm{Re}\,\varrho}{1+|\varrho|^2\delta_{jj'}}; \quad \varrho = \frac{C_{\mathrm{I}}}{C_{\boldsymbol{\Delta}}}; \tag{23}$$

$$\Delta_{j\mu}=\frac{2j+1}{2j'+1}[(C^{j'\mu-1}_{j\mu,\,1-1})^2-(C^{j'\mu+1}_{j\mu,\,1\,1})^2]=\begin{cases}\dfrac{\mu}{j} & j'=j-1\\ \dfrac{\mu}{j(j+1)} & j'=j\\ -\dfrac{\mu}{j+1} & j'=j+1.\end{cases}\tag{24}$$

Thus for the angular distribution of β-electrons relative to the nuclear orientation $\mathbf{n}_j$ and for the polarization, formulae are obtained which are similar to those written above:

$$\begin{aligned}W_{e\mathbf{n}_j}(\vartheta_{e\mathbf{n}_j})&=1-\bar{\beta}v\cos\vartheta_{e\mathbf{n}_j}\\ \langle\sigma_{\mathbf{p}}\rangle&=[-v+\bar{\beta}\cos\vartheta_{e\mathbf{n}_j}][1-v\bar{\beta}\cos\vartheta_{e\mathbf{n}_j}]^{-1}\\ \langle\boldsymbol{\sigma}_{\perp}\rangle&=\frac{1}{\varepsilon}\bar{\beta}\{\gamma_1(\mathbf{n}_j-\mathbf{n}(\mathbf{n}_j\cdot\mathbf{n}))-\alpha Z(\mathbf{n}\wedge\mathbf{n}_j)\}[1-v\bar{\beta}\cos\vartheta_{e\mathbf{n}_j}]^{-1}.\end{aligned}\tag{25}$$

Formula (25) for the angular distribution coincides with the corresponding formula derived by Lee and Yang [1]). In the case of $j\to j$ transitions, $\bar{\beta}$ depends on interference (due to Re $C_{\mathrm{I}}/C_{\mathbf{\Lambda}}$) of the scalar and tensor variants and therefore exact measurement of the electron angular distribution for an oriented nucleus or of transverse polarization should permit one (provided that the nuclear matrix elements can be estimated with sufficient accuracy) to determine the ratio of the constants $g_{\mathrm{S}}/g_{\mathrm{T}}$.

Formulae (14), (22) do not contain effects which are proportional to the imaginary part of $C_{\mathrm{I}}/C_{\mathbf{\Lambda}}$ which differ from zero only if time parity is not conserved. Observation of these effects would be of fundamental interest as their existence would directly testify to non-conservation of time parity (non-invariance of the theory with respect to combined inversion). Effects of this type arise in the electron-neutrino angular correlation of decaying oriented nuclei.

Summing (11) over the electron polarizations one gets

$$W_{e\nu,\mathbf{n}_j}=\tfrac{1}{2}(1+\gamma_1)[A-v\mathbf{B}\cdot\mathbf{n}].\tag{26}$$

Calculation of A and $\mathbf{B}$ in accord with (10) and summation over the projections of the nuclear moments in the final state can be performed in an elementary manner (see the appendix). The following expression for the angular correlation of an oriented nucleus is finally obtained:

$$\begin{aligned}W_{e\nu,\mathbf{n}_j}=1-v\mathbf{n}\cdot\boldsymbol{\nu}\left(\langle\beta\rangle-\frac{\frac{1}{3}f_{j\mu}}{1+|\varrho|^2\delta_{jj'}}\right)-v\mathbf{n}_j\cdot\mathbf{n}\bar{\beta}-\mathbf{n}_j\cdot\boldsymbol{\nu}\bar{\beta}_1\\ -\frac{1}{1+|\varrho|^2\delta_{jj'}}vf_{j\mu}(\mathbf{n}_j\cdot\boldsymbol{\nu})(\mathbf{n}_j\cdot\mathbf{n})+v\bar{\beta}_2\boldsymbol{\nu}\cdot(\mathbf{n}_j\wedge\mathbf{n}),\end{aligned}\tag{26'}$$

where, as previously, $\langle\beta\rangle$ and $\bar{\beta}$ are defined by (15) and (23),

$$\bar{\beta}_1 = \frac{\Delta_{j\mu} - \dfrac{2\mu\delta_{jj'}}{\sqrt{j(j+1)}}\operatorname{Re}\varrho}{1+|\varrho|^2\delta_{jj'}}; \quad \bar{\beta}_2 = \frac{2\mu\delta_{jj'}}{\sqrt{j(j+1)}}\frac{\operatorname{Im}\varrho}{1+|\varrho|^2\delta_{jj'}}; \tag{27}$$

$$f_{j\mu} = \begin{cases} \dfrac{-3\mu^2+j(j+1)}{j(2j-1)} & j' = j-1 \\ -\dfrac{-3\mu^2+j(j+1)}{j(j+1)} & j' = j \\ \dfrac{-3\mu^2+j(j+1)}{(j+1)(2j+3)} & j' = j+1. \end{cases} \tag{28}$$

From (27) it follows that the last term in (26) vanishes if the β-decay interaction constants are real, that is, if time parity is conserved. Indeed, since this term is due to interference of the scalar and tensor variants, it should contain only the diagonal matrix elements of operator $\boldsymbol{\sigma}$ (corresponding to $j' = j$) which in virtue of the nuclear wave functions being real should also be real. The problem of conservation of time parity in β-decay can probably be solved by studying experimentally the asymmetry of recoil nuclei relative to a plane passing through the nuclear spin and electron momentum.

If electrons whose momenta are perpendicular to the nuclear spin are considered the ratio of the number of recoil nuclei moving from the aforementioned plane in one direction to those moving in the opposite direction should be

$$\frac{W_{ev,\,n_j}^{(\text{left})}}{W_{ev,\,n_j}^{(\text{right})}} = \frac{1+\frac{1}{2}v\bar{\beta}_2}{1-\frac{1}{2}v\bar{\beta}_2}.$$

3. Transitions of First Order of Forbiddenness

In the case of first order forbidden transitions (when parity of the nuclear wave function changes and the spin changes by not more than two units, $\Delta j \leqq 2$) in the electron (3) and neutrino wave function expansions $u'_{-\mathbf{q},\frac{1}{2}} \exp(-i\mathbf{q}\cdot\mathbf{r}) \approx u'_{-\mathbf{q},\frac{1}{2}}(1-i\mathbf{q}\cdot\mathbf{r})$ one should take into account only those terms which are proportional to $\mathbf{r}$ (or $\mathbf{r}/r$). Moreover in the matrix element of Hamiltonian (1) the terms which are relativistic in heavy particles and proportional to γ_5 and $\boldsymbol{\alpha}$ should be retained.

First order forbidden transitions can thus be conditioned by terms of three types:

1) by Coulomb terms of the order of $\alpha Z = Z/137$ arising in the expansion of the electron ψ-function (the coefficients before these terms in (3) are denoted by α_c and β_c);

2) by terms containing the ratio of the nuclear dimensions to the elec-

tron wave length (terms α_1 and β_1 in (3)) or neutrino wave length (the order of magnitude of these terms is $R_0/\lambda\!\!\!^{-} \approx \sqrt{\varepsilon^2-1}A^{1/3}/270$);

3) by heavy particle relativistic terms whose order of magnitude is equal to the ratio of the velocity of the nucleons in the nucleus to the velocity of light, $v_{\text{nucl}} \approx \frac{1}{5} \div \frac{1}{10}$. For heavy and intermediate nuclei ($Z \geqq 40$) $\alpha Z \gg R_0/\lambda\!\!\!^{-}$ and $\alpha Z \gg v_{\text{nucl}}$ and hence the forbiddenness is removed, chiefly because of the presence of Coulomb terms α_c and β_c in (3). In (3) the terms $(pr/3)\,\alpha_c''$, $(pr/3)\,\beta_c''$ which contain the small factor $pr \ll 1$ can also be dropped. It may happen for light nuclei that $R_0/\lambda\!\!\!^{-}$ and v_{nucl} are comparable with αZ. In these cases however, αZ can be considered small and only terms of the order

$$(\alpha Z)^2,\ (pR_0)^2,\ (\alpha Z)(pR_0),\ v^2_{\text{nucl}},\ (\alpha Z)v_{\text{nucl}},\ (pR_0)v_{\text{nucl}}$$

should be retained, terms such as $(\alpha Z)(pR_0)^2$ or $(\alpha Z)^2(pR_0)$ being neglected. For these reasons the terms $(pr/3)\,\alpha_c''$ and $(pr/3)\,\beta_c''$ in (3) can be discarded in the case of light nuclei as well (α_c'' and β_c'' being of order of αZ).

Keeping in mind the foregoing remarks and introducing the notations

$$\begin{aligned} &P = g_P\int \bar\psi_2 i\gamma_5\psi_1\,d\tau; \qquad \mathbf{R} = g_S\int \bar\psi_2 \mathbf{r}\psi_1\,d\tau; \qquad \mathbf{m} = g_S\int \bar\psi_2 \frac{\mathbf{r}}{r}\psi_1\,d\tau \\ &\boldsymbol{\tau} = g_T\int \bar\psi_2 i\boldsymbol{\alpha}\psi_1\,d\tau; \qquad T_{ik} = g_T\int \bar\psi_2 \sigma_i x_k\psi_1\,d\tau; \quad t_{ik} = g_T\int \bar\psi_2 \frac{\sigma_i x_k}{r}\psi_1\,d\tau \end{aligned} \tag{29}$$

we can write operator $\hat V$ (5) in accord with (1), (2) and (3) as follows †:

$$\begin{aligned} \hat V = -iN[&(\alpha_0^*-\beta_0^*\boldsymbol{\sigma}\cdot\mathbf{n})(-P+\boldsymbol{\sigma}\cdot\boldsymbol{\tau}+\mathbf{q}\cdot\mathbf{R}+\sigma_j q_l T_{jl}) \\ &+(\alpha_1^*-\beta_1^*\boldsymbol{\sigma}\cdot\mathbf{n})(\mathbf{p}\cdot\mathbf{R}+\sigma_j p_l T_{jl})-(\alpha_c^*-\beta_c^*\boldsymbol{\sigma}\cdot\mathbf{n})(\boldsymbol{\sigma}\cdot\mathbf{m}+\sigma_j\sigma_l t_{jl})]. \end{aligned} \tag{30}$$

Hence, on basis of (6) one obtains

$$\hat S = \tfrac{1}{2}|N|^2 \sum_{i,k} S^{(i,k)}, \tag{31}$$

where

$$S^{(i,k)} = (\alpha_i^*-\beta_i^*\boldsymbol{\sigma}\cdot\mathbf{n})(A_{ik}+\mathbf{B}_{ik}\cdot\boldsymbol{\sigma})(\alpha_k-\beta_k\boldsymbol{\sigma}\cdot\mathbf{n}) \tag{31}$$

(i, k denote the indices 0, 1 and c) and, as in the case of allowed transitions the following notations have been introduced:

† Besides the factor $(pr)^{\gamma_1-1}$ contained in N one should introduce in the terms proportional to α_1 and β_1 in the expression for the nuclear matrix elements (29) a factor $(pr)^{\gamma_2-\gamma_1-1}$ which is due to the factor ξ in α_1 and β_1. The latter, however, can be neglected for the same reasons that the terms $\frac{1}{2}pr\alpha_c''$ and $\frac{1}{2}pr\beta_c''$ were neglected. Concerning the factor $(pr)^{\gamma_1-1}$ see the note on p. 469.

$$
\begin{aligned}
&A_{cc}+\mathbf{B}_{cc}\cdot\boldsymbol{\sigma}=(t+\boldsymbol{\sigma}\cdot\mathbf{a})(1+\boldsymbol{\sigma}\cdot\boldsymbol{\nu})(t^*+\boldsymbol{\sigma}\cdot\mathbf{a}^*);\\
&A_{1c}+\mathbf{B}_{1c}\cdot\boldsymbol{\sigma}=-(\mathbf{p}\cdot\mathbf{R}+\sigma_j\cdot p_i T_{ji})(1+\boldsymbol{\sigma}\cdot\boldsymbol{\nu})(t^*+\boldsymbol{\sigma}\cdot\mathbf{a}^*);\\
&A_{0c}+\mathbf{B}_{0c}\cdot\boldsymbol{\sigma}=-(-P+\mathbf{q}\cdot\mathbf{R}+\boldsymbol{\sigma}\cdot\boldsymbol{\tau}+\sigma_j q_i T_{ji})(1+\boldsymbol{\sigma}\cdot\boldsymbol{\nu})(t^*+\boldsymbol{\sigma}\cdot\mathbf{a}^*);\\
&A_{00}+\mathbf{B}_{00}\cdot\boldsymbol{\sigma}=(-P+\mathbf{q}\cdot\mathbf{R}+\boldsymbol{\sigma}\cdot\boldsymbol{\tau}+\sigma_j q_i T_{ji})(1+\boldsymbol{\sigma}\cdot\boldsymbol{\nu})(-P^*+\mathbf{q}\cdot\mathbf{R}^*\\
&\qquad\qquad+\boldsymbol{\sigma}\cdot\boldsymbol{\tau}^*+\sigma_j q_i T^*_{ji});\\
&A_{11}+\mathbf{B}_{11}\cdot\boldsymbol{\sigma}=(\mathbf{p}\cdot\mathbf{R}+\sigma_j p_i T_{ji})(1+\boldsymbol{\sigma}\cdot\boldsymbol{\nu})(\mathbf{p}\cdot\mathbf{R}^*+\sigma_j p_i T^*_{ji});\\
&A_{01}+\mathbf{B}_{01}\cdot\boldsymbol{\sigma}=(-P+\mathbf{q}\cdot\mathbf{R}+\boldsymbol{\sigma}\cdot\boldsymbol{\tau}+\sigma_j q_i T_{ji})(1+\boldsymbol{\sigma}\cdot\boldsymbol{\nu})(\mathbf{p}\cdot\mathbf{R}^*+\sigma_j p_i T^*_{ji});\\
&A_{ik}=A^*_{ki};\ \mathbf{B}_{ik}=\mathbf{B}^*_{ki}.
\end{aligned}
\tag{32}
$$

In (32) the tensor t_{ji} has been split into irreducible parts:

$$t_{ji}=\tilde{t}_{ji}+\tfrac{1}{2}\varepsilon_{jik}t_k+\tfrac{1}{3}\delta_{ji}t;$$

$$t=t_{jj}=g_T\int\bar{\psi}_2\frac{\boldsymbol{\sigma}\cdot\mathbf{r}}{r}\psi_1\,d\tau;\qquad t_k=g_T\int\bar{\psi}_2\frac{(\boldsymbol{\sigma}\wedge\mathbf{r})_k}{r}\psi_1\,d\tau; \tag{33}$$

$$\tilde{t}_{ji}=\tilde{t}_{ij}=g_T\int\bar{\psi}_2\left(\frac{\sigma_j x_i+\sigma_i x_j}{2r}-\frac{1}{3}\frac{\boldsymbol{\sigma}\cdot\mathbf{r}}{r}\delta_{ij}\right)\psi_1\,d\tau \tag{33'}$$

and since

$$\boldsymbol{\sigma}\wedge\boldsymbol{\sigma}=2i\boldsymbol{\sigma};\ \sigma_j\sigma_i\tilde{t}_{ji}=\tfrac{1}{2}(\sigma_j\sigma_i+\sigma_i\sigma_j)\tilde{t}_{ji}=0,$$

it follows that

$$\sigma_j\sigma_i t_{ji}+\boldsymbol{\sigma}\cdot\mathbf{m}=t+\mathbf{a}\cdot\boldsymbol{\sigma},\quad \mathbf{a}=\mathbf{m}+i\mathbf{t}.$$

In a similar way we shall also split T_{ji} into irreducible parts, writing

$$
\begin{aligned}
&T_{ji}=\tilde{T}_{ji}+\tfrac{1}{2}\varepsilon_{jik}T_k+\tfrac{1}{3}\delta_{ji}T,\\
&T=g_T\int\bar{\psi}_2\boldsymbol{\sigma}\cdot\mathbf{r}\psi_1\,d\tau,\qquad \mathbf{T}=g_T\int\bar{\psi}_2(\boldsymbol{\sigma}\wedge\mathbf{r})\psi_1\,d\tau,
\end{aligned}
\tag{34}
$$

$$\tilde{T}_{ji}=\tilde{T}_{ij}=g_T\int\bar{\psi}_2\left(\frac{\sigma_j x_i+\sigma_i x_j}{2}-\tfrac{1}{3}\boldsymbol{\sigma}\cdot\mathbf{r}\delta_{ij}\right)\psi_1\,d\tau. \tag{34'}$$

As in the case of allowed transitions we write (31) in the form

$$
\begin{aligned}
S^{(i,k)}=\lambda_{ik}A_{ik}-\chi_{ik}(A_{ik}\boldsymbol{\sigma}\cdot\mathbf{n}+\mathbf{B}_{ik}\cdot\mathbf{n})+(\lambda_{ik}-\mu_{ik})(\boldsymbol{\sigma}\cdot\mathbf{n})(\mathbf{B}_{ik}\cdot\mathbf{n})\\
+\mu_{ik}\boldsymbol{\sigma}\cdot\mathbf{B}_{ik}-\eta_{ik}\boldsymbol{\sigma}\cdot(\mathbf{n}\wedge\mathbf{B}_{ik}),
\end{aligned}
\tag{35}
$$

where

$$\lambda_{ik}=\alpha_i^*\alpha_k+\beta_i^*\beta_k;\quad \mu_{ik}=\alpha_i^*\alpha_k-\beta_i^*\beta_k;$$
$$\chi_{ik}=\alpha_i^*\beta_k+\beta_i^*\alpha_k;\quad \eta_{ik}=-i(\alpha_i^*\beta_k-\beta_i^*\alpha_k).$$

Using the values of α_i and β_i ($i=0,\ 1,\ c$) written above it is not difficult to evaluate λ_{ik}, μ_{ik}, χ_{ik} and η_{ik}. The results of the calculations are given in table 1. Values of the coefficients λ_{ik}, μ_{ik}, χ_{ik} and η_{ik} divided by the common factor K given in the last column are presented in columns 2—4 of the table.

TABLE 1

i,k	λ_{ik}/K	μ_{ik}/K	χ_{ik}/K	η_{ik}/K	Common factor K
0,0	1	$\frac{\gamma_1}{\varepsilon}$	$\frac{p}{\varepsilon}$	$\frac{\alpha Z}{\varepsilon}$	$\frac{1+\gamma_1}{2}$
0,1	$1-\frac{i\alpha Z}{\gamma_1+1}\frac{\gamma_2-\gamma_1+1}{\gamma_2-\gamma_1+3}\frac{p}{\varepsilon}$	$\frac{1}{\varepsilon}\frac{\gamma_2+\gamma_1+1}{\gamma_2-\gamma_1+3}$	$\frac{p}{\varepsilon}-\frac{i\alpha Z}{\gamma_1+1}\frac{\gamma_2-\gamma_1+1}{\gamma_2-\gamma_1+3}$	$\frac{1}{\varepsilon}\frac{\alpha Z}{1+\gamma_1}\frac{\gamma_2+\gamma_1+3}{\gamma_2-\gamma_1+3}$	$\xi(1+\gamma_1)\frac{\gamma_2-\gamma_1+3}{8}$
1,1	1	$\frac{\gamma_2}{2\varepsilon}$	$\frac{p}{\varepsilon}$	$\frac{\alpha Z}{2\varepsilon}$	$\frac{\gamma_2+2}{4}\lvert\xi\rvert^2$
1,c	1	$\frac{\gamma_1}{\varepsilon}$	$\frac{p}{\varepsilon}$	$\frac{\alpha Z}{\varepsilon}$	$\frac{1-\gamma_1}{2}\approx\frac{(\alpha Z)^2}{4}$
0,c	1	$\frac{\gamma_1}{\varepsilon}$	$\frac{p}{\varepsilon}$	$\frac{\alpha Z}{\varepsilon}$	$\frac{\alpha Z}{2}$
1,c	$1+i\frac{1-\gamma_1}{\alpha Z}\frac{\gamma_2-\gamma_1+1}{\gamma_2-\gamma_1+3}\cdot\frac{p}{\varepsilon}$	$\frac{1}{\varepsilon}\frac{\gamma_2+\gamma_1+1}{\gamma_2-\gamma_1+3}$	$\frac{p}{\varepsilon}+i\frac{1-\gamma_1}{\alpha Z}\frac{\gamma_2-\gamma_1+1}{\gamma_2-\gamma_1+3}$	$\frac{1-\gamma_1}{\alpha Z\varepsilon}\frac{\gamma_2+\gamma_1+3}{\gamma_2-\gamma_1+3}$	$\frac{\alpha Z}{2}\xi\frac{\gamma_2-\gamma_1+3}{4}$

The first row in table 1 that defines $S^{(00)}$ is evidently the expression obtained in the case of allowed transitions.

We shall consider the following types of first order forbidden β-transitions:

1) β-transitions in heavy and intermediate nuclei ($Z \gtrsim 40$);

2) β-transitions in those light nuclei ($20 \lesssim Z \lesssim 40$) for which Coulomb terms (of the order $(\alpha Z)^2$)are dominant but corrections due to terms of the order of $(\alpha Z)(pR_0)$ or $(\alpha Z)v_{\text{nucl}}$ are already appreciable and must be taken into account, although terms of the order $(pR_0)^2$ or v_{nucl}^2 may still be neglected;

3) 0—0 transitions in light nuclei; in considering 0—0 transitions we shall take into account all the types of terms—i.e., of the order

$$(\alpha Z)^2,\ (\alpha Z)(pR_0),\ (pR_0)^2,\ v_{\text{nucl}}^2,\ (\alpha Z)(v_{\text{nucl}})\ \text{and}\ (pR_0)v_{\text{nucl}};$$

4) transitions with $\Delta j = 2$. It follows from (32) that transitions involving a spin change by 2 cannot be due to Coulomb terms; the values of $S^{(c,c)}$, $S^{(0,c)}$ and $S^{(1,c)}$ for these transitions equal zero and only terms $S^{(i,k)}$ with $i,k = 0, 1$ will be of importance.

3.1. COULOMB TRANSITIONS

In the case of decay of heavy and intermediate nuclei for which $\alpha Z \gg pR_0$ only the term $S^{(c,c)}$ in (31) should be taken into account. Comparing the first row in (32) with (10) and also the rows in table 1 corresponding to allowed transitions ($S^{(0,0)}$) and to the terms in $S^{(c,c)}$ it can be seen that all the formulae in this case *are identical with those for allowed transitions* if the factor $(1+\gamma_1)/2$ in (11) which defines the total transition probability is replaced by $(1-\gamma_1)/2$ and C_I is replaced by C_t and C_Λ by $C_a = C_m + iC_t$. It is assumed that all the nuclear matrix elements of the scalar and vector

quantities in (29) are defined as in (20) but with the constants C_I and C_A replaced by suitable constants: in the case of P, T, t C_I should be replaced by C_P, C_T, C_t and in the case of τ, **R**, **m**, **T**, **t** C_A should be replaced by C_τ, C_R, C_m, C_T, C_t. These are commonly designated as $C_\tau = g_T|\int \alpha|$, $C_R = g_S|\int \mathbf{r}|$, $C_m = g_S|\int \mathbf{r}/r|$, $C_T = g_T|\int(\sigma \wedge \mathbf{r})|$, $C_t = g_T|\int(\sigma \wedge \mathbf{r}/r)|$ and $C_P = g_P \int i\gamma_5$, $C_T = g_T \int \sigma \cdot \mathbf{r}$, $C_t = g_T \int \sigma \cdot \mathbf{r}/r$.

Thus for the angular distribution and polarization we obtain formulae (16), (17), (18) and (25) in which ϱ is equal to

$$\varrho = \frac{C_t}{C_a} = \frac{C_t}{C_m + iC_t}. \tag{36}$$

As in the case of allowed transitions Re ϱ depends on the ratio g_S/g_T; however since three nuclear matrix elements instead of two enter the formula it is somewhat difficult to interpret the experimental data. Formula (26) for angular correlation of a decaying oriented nucleus will also be valid for Coulomb transitions if ϱ is expressed by formula (36).

However in this case, in contrast to that of allowed transitions, asymmetry of recoil nuclei with respect to a plane passing through the nuclear spin and electron momentum should also be observed for real constants g_S and g_T and when time parity is conserved, inasmuch as Im $\varrho \neq 0$ in virtue of (36).

3.2. LIGHT NUCLEI

We shall now consider forbidden β-transitions in light nuclei ($Z \approx 20-40$) for which $Z/137 \gtrsim pR_0 \approx v_{nucl}$. Then $\alpha Z \ll 1$ and all quantities should be expanded into a series in terms of αZ. We retain in (31) terms of the order of $(\alpha Z)^2$ (quantity $S^{(c,c)}$) and of the order of $(\alpha Z)(pR_0)$ and $(\alpha Z)v_{nucl}$ ($S^{(c\,0)} + S^{(0,c)}$ and $S^{(c,1)} + S^{(1,c)}$) and neglect all remaining terms (of the order of $(pR_0)^2$, $(\alpha Z)^n v_{nucl}$, $(\alpha Z)^n(pR_0)$ where $n > 1$). In this approximation we obtain, in accord with (31) and rows 4–6 in table 1,

$$\frac{2\hat{S}}{|N|^2} = \frac{(\alpha Z)^2}{4}\left\{A_{cc}\left(1 - \frac{p}{\varepsilon}\sigma \cdot \mathbf{n}\right) - \mathbf{B}_{cc} \cdot \mathbf{n}\left[\frac{p}{\varepsilon} - \left(1 - \frac{1}{\varepsilon}\right)\sigma \cdot \mathbf{n}\right] + \frac{1}{\varepsilon}\mathbf{B}_{cc} \cdot \sigma\right\}$$

$$+\alpha Z\left\{\mathrm{Re}(A_{0c} + A_{1c})\left(1 - \frac{p}{\varepsilon}\sigma \cdot \mathbf{n}\right) - \mathrm{Re}(\mathbf{B}_{0c} + \mathbf{B}_{1c}) \cdot \mathbf{n}\left[\frac{p}{\varepsilon} - \left(1 - \frac{1}{\varepsilon}\right)\sigma \cdot \mathbf{n}\right]\right.$$

$$\left. + \frac{1}{\varepsilon}\mathrm{Re}\,(\mathbf{B}_{0c} + \mathbf{B}_{1c}) \cdot \sigma\right\}. \tag{37}$$

A_{cc} and $\mathbf{B}_{cc}$ have been determined by considering Coulomb transitions and hence it remains to determine A_{0c}, A_{1c}, $\mathbf{B}_{0c}$ and $\mathbf{B}_{1c}$.

We shall first consider the decay of a non oriented nucleus. Averaging the matrix element products over the initial nuclear spin projections and

summing over the final nuclear spin projections with aid of (20) we obtain the following expressions for A_{0c}, A_{1c}, $\mathbf{B}_{0c}$ and $\mathbf{B}_{1c}$:

$$\begin{aligned}\langle A_{0c}\rangle &= -(-C_P+\tfrac{1}{3}qC_T)C_t^*\delta_{jj'}-\left(C_T+\tfrac{1}{3}q\mathbf{C}_R+\frac{i}{3}q\mathbf{C}_T\right)\cdot C_a^*,\\ \langle \mathbf{B}_{0c}\rangle &= -\boldsymbol{v}\left\{(-C_P+\tfrac{1}{3}qC_T)C_t^*\delta_{jj'}+\tfrac{1}{3}\left(-C_T+\tfrac{1}{3}qC_R-\frac{i}{3}qC_T\right)\cdot C_a^*\right\},\end{aligned} \tag{38}$$

$$\begin{aligned}\langle A_{1c}\rangle &= -\tfrac{1}{3}p\mathbf{n}\cdot\boldsymbol{v}\{C_TC_t^*\delta_{jj'}+(C_R+iC_T)\cdot C_a^*\},\\ \langle \mathbf{B}_{1c}\rangle &= -\tfrac{1}{3}p\{\mathbf{n}[C_TC_t^*\delta_{jj'}+(C_R-iC_T)\cdot C_a^*]\\ &\qquad +i(\boldsymbol{v}\wedge\mathbf{n})(-C_TC_t^*\delta_{jj'}+C_R C_a^*)\}.\end{aligned} \tag{39}$$

As above we have expanded tensors t_{jl} and T_{jl} into irreducible parts as in (33) and (34),.

Substitution of (38) and (39) in (37) leads to unwieldy expressions. We shall therefore give them only after averaging over the directions of the neutrino momentum has been performed, this corresponding to measurement of the longitudinal electron polarization. Then

$$\frac{2S}{W_{\text{tot}}} = 1-v\left(1+\frac{\delta}{\varepsilon}\right)\boldsymbol{\sigma}\cdot\mathbf{n} \tag{40}$$

where

$$\begin{aligned}W_{\text{tot}} &= \frac{(Z\alpha)^2}{4}(|C_a|^2+|C_t|^2\delta_{jj'})\\ &-\alpha Z\,\mathrm{Re}\left\{[-C_P+\tfrac{1}{3}(q-vp)C_T]C_t^*\delta_{jj'}+\left[C_T+\tfrac{1}{3}(q-vp)C_R+\frac{i}{3}(q+vp)C_T\right]\cdot C_a^*\right\};\end{aligned} \tag{41}$$

$$\delta = \frac{\alpha Z}{3}\frac{1}{W_{\text{tot}}}\mathrm{Re}\,[C_TC_t^*\delta_{jj'}+(C_R-iC_T)\cdot C_a^*]. \tag{42}$$

Thus in the forbidden β-decay of light nuclei the electron polarization

$$\langle\boldsymbol{\sigma}_p\rangle = -v\left(1+\frac{\delta}{\varepsilon}\right) \tag{43}$$

should differ from v. For sufficiently fast electrons ($1-v \ll 1$) this difference should be small. Indeed, according to (42) $\delta \approx R_0/Z\alpha$ and on basis of the assumption that $\varepsilon R_0/\alpha Z \ll 1$ it follows that $\varepsilon\delta \ll 1$. This signifies that the difference between the degree of polarization and v defined by the expression $v\delta/\varepsilon \approx \varepsilon\delta/\varepsilon^2 \ll 1/\varepsilon^2$ is especially small for large ε. For $\varepsilon \approx 1$ the deviation of the degree of polarization from v depends only on δ and therefore may attain several tens of per cent. However, because of the large number of different matrix elements in expressions (41) and (42) it is quite difficult to draw any reliable conclusions about the magnitude of δ excluding, possibly, the case of $0 \to 0$ transitions.

A study of the decay of oriented light nuclei leads to complex expressions which cannot be exploited to yield any interesting physical information. The relevant formulae are presented in appendix 3.

3.3. 0−0 TRANSITIONS

Of first order forbidden β-transitions the 0−0 transitions involving parity changes are especially interesting since it may be hoped that an analysis of these transitions will permit one to determine the presence of pseudoscalar coupling in β-decay interactions.

Indeed, besides the pseudoscalar nuclear matrix element P only the scalar parts of the nuclear matrix elements of tensors T_{ik} and t_{ik} will contribute in the case of 0−0 transitions involving parity changes. Thus in 0−0 transitions we are dealing with only three different nuclear matrix elements, C_P, C_T and C_t and this circumstance eases interpretation of the experimental results.

0−0 transitions in heavy nuclei will not be so interesting as the transitions will mainly be due to the Coulomb terms in the tensor interaction considered in section 1. We shall investigate here 0−0 transitions in light nuclei for which $\alpha Z \approx pR_0 \approx v_{\text{nucl}} \ll 1$. In this case we must take into account all types of terms in sum (31), that is, besides A_{cc}, A_{0c}, A_{1c}, $\mathbf{B}_{cc}$, $\mathbf{B}_{0c}$, $\mathbf{B}_{1c}$ calculated above (see (38), (39)), we must also determine A_{00}, A_{01}, A_{11}, $\mathbf{B}_{00}$, $\mathbf{B}_{01}$, $\mathbf{B}_{11}$. Simple calculations show that for 0−0 transitions

$$A_{00} = |-C_P+\tfrac{1}{3}qC_T|^2; \qquad \mathbf{B}_{00} = \boldsymbol{v}|-C_P+\tfrac{1}{3}qC_T|^2, \tag{44}$$

$$A_{11} = \tfrac{1}{9}p^2|C_T|^2; \qquad \mathbf{B}_{11} = \tfrac{1}{9}p^2|C_T|^2[2\mathbf{n}(\mathbf{n}\cdot\boldsymbol{v})-\boldsymbol{v}], \tag{45}$$

$$A_{01} = \frac{p}{3}\boldsymbol{v}\cdot\mathbf{n}(-C_T^*C_P+\tfrac{1}{3}q|C_T|^2);$$

$$\mathbf{B}_{01} = \frac{p}{3}(\mathbf{n}+i(\boldsymbol{v}\wedge\mathbf{n}))(-C_T^*C_P+\tfrac{1}{3}q|C_T|^2), \tag{46}$$

$$A_{cc} = |C_t|^2; \qquad \mathbf{B}_{cc} = |C_t|^2\boldsymbol{v} \tag{47}$$

and A_{0c}, $\mathbf{B}_{0c}$, A_{1c}, $\mathbf{B}_{1c}$ can be obtained by retaining in (38) and (39) only terms containing $C_P C_T$ and C_t. Substituting these values of A and $\mathbf{B}$ in (35) and exploiting the smallness of αZ one may expand the quantities in table 1 in powers series in αZ retaining only the zero power for 0, 0; 0, 1 and 1, 1 terms, the first power for 0, c and 1, c terms and the second power for c, c Coulomb terms.

For electron neutrino angular correlation we then obtain (after summation of (35) over the electron spins):

$$\frac{W(\theta)}{W_{\text{tot}}} = 1-v\mathbf{n}\cdot\boldsymbol{v}\left(1+\frac{h}{\varepsilon}\right) \tag{48}$$

where

$$W_{\text{tot}} = |N|^2|C_t|^2\left\{\frac{|\lambda_T|^2}{9}(p^2+q^2-2pqv)+|\lambda_P|^2\right.$$
$$\left.+\frac{(\alpha Z)^2}{4}-\tfrac{2}{3}(q-vp)\ \mathrm{Re}\ \lambda_P\lambda_T^*+\alpha Z\ \mathrm{Re}\ \lambda_P-\tfrac{1}{3}\alpha Z(q-vp)\ \mathrm{Re}\ \lambda_T\right\};\quad (49)$$

$$h = \frac{|N|^2}{3}\frac{|C_t|^2}{W_{\text{tot}}}\{-\tfrac{2}{3}q|\lambda_T|^2+2\ \mathrm{Re}\ \lambda_P\lambda_T^*+\alpha Z\ \mathrm{Re}\ \lambda_T\};$$
$$\lambda_P = C_P/C_t;\ \lambda_T = C_T/C_t. \quad (50)$$

An expression similar to (48) can be obtained for the electron polarization after averaging over the directions of emission of the neutrino. Then

$$\frac{2\hat{S}}{W_{\text{tot}}} = 1-v\mathbf{n}\cdot\boldsymbol{\sigma}\left(1+\frac{h}{\varepsilon}\right) \quad (51)$$

where as above W_{tot} and h are defined by (49) and (50). Thus the longitudinal electron polarization is

$$\langle\sigma_p\rangle = -v\left(1+\frac{h}{\varepsilon}\right). \quad (52)$$

It can be seen from (52) and (50) that deviation of the degree of electron polarization from v can, in principle, be used to determine λ_P that is, to estimate the contribution of pseudoscalar coupling. The experimental task, however, is a formidable one as two parameters, λ_P and λ_T enter function h and a knowledge of the energy dependence of the difference $|\langle\sigma_p\rangle|-v=vh/\varepsilon$ is required in order to determine them.

For intermediate nuclei ($Z \approx 50$) the magnitude of h/ε at $\lambda_P = 0$ changes from 3 to 7 %, depending on the electron energy. A small admixture of pseudoscalar coupling ($\lambda_P = 0.1$) changes the magnitude of h/ε by almost two times. A more favourable situation will hold only in the case of 0—0 transitions in very light nuclei ($Z \approx 10$) for which the role of terms containing Z is small.

A similar situation obtains in angular correlation measurements since (as can be seen from (48)) deviation from proportionality to $1-v\cos\theta_{e\nu}$ is determined by the same function of h.

3.4. TRANSITIONS WITH $\Delta j = 2$

If $j' = j\pm 2$ all nuclear matrix elements excepting $\bar{T}_{jl}$ in (32)—(34) vanish. The non-vanishing quantities in (32) then have the form

$$A_{00}+\mathbf{B}_{00}\cdot\boldsymbol{\sigma} = \sigma_j q_l \bar{T}_{jl}(1+\boldsymbol{\sigma}\cdot\boldsymbol{\nu})\bar{T}^*_{j'l'}q_{l'}\sigma_{j'},$$
$$A_{11}+\mathbf{B}_{11}\cdot\boldsymbol{\sigma} = \sigma_j p_l \bar{T}_{jl}(1+\boldsymbol{\sigma}\cdot\boldsymbol{\nu})\bar{T}^*_{j'l'}p_{l'}\sigma_{j'}, \quad (53)$$
$$A_{01}+\mathbf{B}_{01}\cdot\boldsymbol{\sigma} = \sigma_j q_l \bar{T}_{jl}(1+\boldsymbol{\sigma}\cdot\boldsymbol{\nu})\bar{T}^*_{j'l'}p_{l'}\sigma_{j'}.$$

Nucleus not oriented

If the nucleus is not oriented we obtain from (58) after simple calculations

and taking into account that†

$$\langle \tilde{T}_{jl} \tilde{T}^*_{j'l'} \rangle = \frac{|C_{\tilde{T}}|^2}{10} (\delta_{jj'}\delta_{ll'} + \delta_{jl'}\delta_{j'l} - \tfrac{2}{3}\delta_{jl}\delta_{j'l'})$$

where $|C_{\tilde{T}}|^2 = \langle \tilde{T}_{jl} \tilde{T}^*_{jl} \rangle$ the following expressions:

$$A_{00} = \frac{q^2}{3}|C_{\tilde{T}}|^2;\ \mathbf{B}_{00} = -\frac{q^2}{15}\boldsymbol{v}|C_{\tilde{T}}|^2,$$

$$A_{11} = \frac{p^2}{3}|C_{\tilde{T}}|^2;\ \mathbf{B}_{11} = \frac{p^2}{15}[\mathbf{n}(\mathbf{n}\cdot\boldsymbol{v}) - 2\boldsymbol{v}]|C_{\tilde{T}}|^2, \tag{54}$$

$$A_{01} = \frac{pq}{3}\mathbf{n}\cdot\boldsymbol{v}|C_{\tilde{T}}|^2;\ \mathbf{B}_{01} = \left\{\frac{pq}{10}\left(\frac{\mathbf{n}}{3} - (\mathbf{n}\cdot\boldsymbol{v})\boldsymbol{v}\right) + \frac{i}{6}pq(\mathbf{n}\wedge\boldsymbol{v})\right\}|C_{\tilde{T}}|^2.$$

Inserting these values in (35) and (31) and employing the values of λ_{ik}, μ_{ik}, χ_{ik} and η_{ik} $(i, k = 0, 1)$ from table 1 we find in the case of light nuclei (neglecting terms of the order of $(\alpha Z)^2$)††:

a) for electron-neutrino angular correlation

$$W_{e\nu}(\theta) = W_{\text{tot}}\{1 + 2\eta\cos\theta + \tfrac{1}{5}v[(1+2\eta\cos\theta)\cos\theta - \eta\sin^2\theta]\},$$

$$W_{\text{tot}} = F(Z,\varepsilon)|C_{\tilde{T}}|^2\frac{q^2+p^2}{3},\ \eta = \frac{qp}{q^2+p^2}; \tag{55}$$

b) for the magnitude of the longitudinal polarization

$$\langle \boldsymbol{\sigma}_{\mathbf{p}} \rangle = \frac{W_{\text{tot}}}{W_{e\nu}(\theta)}[-v(1+2\eta\cos\theta) - \tfrac{1}{5}(\cos\theta - \eta + 3\eta\cos^2\theta)]; \tag{56}$$

c) for the transverse polarization

$$\langle \boldsymbol{\sigma}_{\perp} \rangle = \frac{W_{\text{tot}}}{W_{e\nu}(\theta)}\frac{1}{5\varepsilon}\left\{[\mathbf{n}\cdot(\mathbf{n}\wedge\boldsymbol{v})]\left(1 + 3\eta\cos\theta + \frac{p^2}{p^2+q^2}\right)\right.$$
$$\left. + \alpha Z(\mathbf{n}\wedge\boldsymbol{v})\left(1 - \frac{5\eta}{v} + \tfrac{9}{4}\eta\cos\theta\right)\right\}. \tag{57}$$

As in the other cases considered above $\langle \boldsymbol{\sigma}_{\perp} \rangle$ vanishes on averaging over the directions of neutrino emission whereas the longitudinal polarization is found to equal v.

Nucleus oriented

Suppose now that the nucleus is oriented. We average all quantities over the neutrino emission direction $\boldsymbol{v}$. The last row in (53) will vanish and the first two yield

† This relation can be obtained in a straightforward manner by writing $\langle \tilde{T}_{jl}\tilde{T}^*_{j'l'} \rangle = a\delta_{jj'}\delta_{ll'} + b\delta_{jl'}\delta_{j'l} + c\delta_{jl}\delta_{j'l'}$ and determining coefficients a, b, c from symmetry conditions and from the conditions $\langle \tilde{T}_{jl}\tilde{T}^*_{jl} \rangle = |C_{\tilde{T}}|^2$, $\Sigma_j \langle \tilde{T}_{jj}\tilde{T}^*_{j'l'} \rangle = 0$. The latter condition is a corollary of (34′) since according to (34′) $\Sigma_j \tilde{T}_{jj} = 0$.

†† In the case of heavy nuclei the formulae are more complex but their structure is substantially the same and in particular on averaging over $\boldsymbol{v}$ the longitudinal polarization is found to equal v whereas the transverse polarization vanishes.

$$\overline{A_{00}+\mathbf{B}_{00}\cdot\boldsymbol{\sigma}}=\frac{q^2}{3}\sigma_i\bar{T}_{ik}\bar{T}^*_{i'k}\sigma_{i'}=\frac{q^2}{3}[(\bar{T}_{ik}\bar{T}^*_{ik})+i\sigma_l\varepsilon_{lii'}\bar{T}_{ik}\bar{T}^*_{i'k}];$$

$$\overline{A_{11}+\mathbf{B}_{11}\cdot\boldsymbol{\sigma}}=\sigma_i p_k\bar{T}_{ik}\bar{T}^*_{i'k'}p_{k'}\sigma_{i'}=p_k\bar{T}_{ik}\bar{T}^*_{ik'}p_{k'}+i\varepsilon_{lii'}\sigma_l p_k\bar{T}_{ik}\bar{T}^*_{i'k'}p_{k'}. \tag{58}$$

The quantities in the right hand part of these equations can be computed by using an expression for the tensor $\bar{T}_{jl}$ which is analogous to (20). The computation (for details see appendix 4) yields the following results:

$$\bar{A}_{00}=\frac{q^2}{3}|C_{\bar{T}}|^2;\quad \overline{\mathbf{B}}_{00}=\frac{q^2}{3}u_{j\mu}\mathbf{n}_j|C_{\bar{T}}|^2,$$

$$\bar{A}_{11}=\frac{p^2}{3}[1+a_{j\mu}(\vartheta)]|C_{\bar{T}}|^2;\quad \overline{\mathbf{B}}_{11}=\frac{p^2}{3}u_{j\mu}[\mathbf{n}b'_{j\mu}\cos\vartheta+\mathbf{n}_j b_{j\mu}(\vartheta)]|C_{\bar{T}}|^2,$$

where

$$u_{j\mu}=\begin{cases}\mu/j\\ -\mu/(j+1);\end{cases}\qquad b'_{j\mu}=\begin{cases}3\dfrac{\mu^2-j^2}{(j-1)(2j-1)}\\ 3\dfrac{\mu^2-(j+1)^2}{(j+2)(2j+3)}\end{cases};$$

$$a_{j\mu}(\vartheta)=\begin{cases}\dfrac{j(j+1)-3\mu^2}{j(2j-1)}P_2(\cos\vartheta)\\ \dfrac{j(j+1)-3\mu^2}{(j+1)(2j+3)}P_2(\cos\vartheta)\end{cases};$$

$$b_{j\mu}(\vartheta)=\begin{cases}\dfrac{3j(j-1)+1-\mu^2+[3j(j+1)-5\mu^2-1]P_2(\cos\vartheta)}{(j-1)(2j-1)}\\ \dfrac{3(j+1)(j+2)-\mu^2+1+[3j(j+1)-5\mu^2-1]P_2(\cos\vartheta)}{(j+2)(2j+3)}.\end{cases}$$

The upper values refer to the case when $j'=j-2$ and the lower to the case when $j'=j+2$.

Insertion in (35) and (31) with account of the data in table 1 yields:

a) for the electron angular distribution

$$W(\vartheta)=W_{\text{tot}}\{1+f_e a_{j\mu}(\vartheta)-u_{j\mu}v[1-f_e+f_e\bar{b}_{j\mu}]\cos\vartheta\} \tag{59}$$

where

$$W_{\text{tot}}=F(Z,\varepsilon)|C_{\bar{T}}|^2\frac{q^2+\xi' p^2}{3},$$

$$\xi'=\frac{\gamma_2+2}{2(1+\gamma_1)}|\xi|^2;\quad \bar{b}_{j\mu}=b_{j\mu}(\vartheta)+b'_{j\mu},$$

$$f_e=\frac{\xi' p^2}{q^2+\xi' p^2}=\frac{\xi'(\varepsilon^2-1)}{(\varepsilon_0-\varepsilon)^2+\xi'(\varepsilon^2-1)}$$

(ε_0 is the high energy end point of the β-spectrum);

b) for the longitudinal polarization

$$\left(\frac{W(\vartheta_{en_j})}{W_{\text{tot}}}\right)\langle\sigma_p\rangle = -v(1+f_e a_{j\mu}(\vartheta))+u_{j\mu}(1-f_e+f_e b_{j\mu}(\vartheta))\cos\vartheta; \quad (60)$$

c) for the transverse polarization

$$\left(\frac{W(\vartheta_{en_j})}{W_{\text{tot}}}\right)\langle\sigma_\perp\rangle = -\frac{\alpha Z}{\varepsilon}u_{j\mu}\{1-f_e+\tfrac{1}{2}f_e b_{j\mu}(\vartheta)\}(\mathbf{n}\wedge\mathbf{n}_j)$$

$$-\frac{1}{\varepsilon}u_{j\mu}\{\gamma_1(1-f_e)+\tfrac{1}{2}\gamma_2 f_e b_{j\mu}(\vartheta)\}[\mathbf{n}\wedge(\mathbf{n}\wedge\mathbf{n}_j)]. \quad (61)$$

As can be seen from (59)—(61) the Coulomb field leads to the appearance of a component along $\mathbf{n}\wedge\mathbf{n}_j$ in the transverse polarization and to a certain change in the coefficients before the component along $\mathbf{n}\wedge(\mathbf{n}\wedge\mathbf{n}_j)$; in all other respects the results are weakly modified by it.

4. Conclusion

Summing up we arrive at the following results.

1. *Allowed transitions.* If the direction of momentum of a recoil nucleus is fixed for decaying unpolarized nuclei, then in addition to longitudinal polarization transverse polarization of the electrons will also arise. The magnitude of the transverse polarization is determined by the same parameter $\langle\beta\rangle$ (which in the case of $j\to j$ transitions depends on the ratio of constants g_S/g_T) as does the electron-neutrino angular correlation. Longitudinal as well as transverse electron polarization takes place in the decay of oriented nuclei. Measurement of the electron-neutrino angular correlation in the decay of oriented nuclei would be of particular interest as experimental detection of asymmetry of recoil nuclei with respect to a plane passing through the nuclear spin and electron momentum would be a direct indication of nonconservation of time parity in β-decay.

2. *First order forbidden transitions.*

Due to the existence of Coulomb interaction in first order forbidden β-transitions with $\Delta j\neq 2$, the same angular distribution and same electron polarization arises in heavy and intermediate nuclei as in the case of allowed transitions. In particular the longitudinal electron polarization turns out to be equal to v, the ratio of the velocity of the electrons to that of light. The degree of polarization may differ from this value only for β-transitions in light nuclei. The case of 0—0 transitions is interesting here as for such transitions from the deviation of degree of polarization from v one may determine

whether an admixture of pseudoscalar coupling is present in the β-interactions.

In unique transitions ($\Delta j = 2$, yes) the Coulomb field does not play a significant role. The longitudinal electron polarization in this case is again equal to v but now the electron angular distribution for decaying oriented nuclei differs from that for allowed transitions.

The formulae obtained above indicate that if the nuclei are not oriented but aligned not only the angular distribution of the β-electrons but all the effects considered above related to orientation also disappear.

The formulae presented in the text correspond to the assumption of a two-component neutrino. It is shown that transition to the case of an arbitrary λ (which determines the degree of parity nonconservation) can be carried out by multiplying all pseudoscalar quantities in the transition probability (e.g. as in formulae (14), (16)—(18), (25) etc.) by

$$-\eta = -2 \operatorname{Re} (\lambda/(1+|\lambda|^2).$$

We have hitherto considered only the cases of negaton decays. It is not difficult to see, however, that all the formulae obtained above can be applied to positon decays if the signs before all the pseudoscalar quantities are changed, Z is replaced by $-Z$ and coupling constants g_S, g_P, g_T are replaced by $-g_S^*$, $-g_P^*$, g_T^*.

A few remarks concerning the role of virtual meson interactions will be made. Strictly speaking the initial formula (1) is not a correct expression for the β-decay matrix element. Indeed, nucleons possess strong meson interactions which distort the vertex part operator of the β-field-nucleon interaction matrix element. The β-decay matrix element can be represented for example for scalar coupling, in the following form:

$$M = g_S \int \bar{\psi}_2(x_2) \Gamma(x_2, x_1;\ x) \psi_1(x_1) \mathrm{d}^4 x_1 \mathrm{d}^4 x_2 (\bar{\psi}_e(x)(1+\lambda\gamma_5)\psi_\nu(x)) \mathrm{d}^4 x$$

where the vertex operator Γ is a function depending on the meson interactions. The wave functions of light particles enter this expression in the same way as in (1) because they do not contain strong interactions. The matrix elements for other types of β-interaction can be written in a similar manner.

Introducing the notation

$$\Phi^{(2,1)}(x) = \int \bar{\psi}_2(x_2) \Gamma(x_2,\ x_1;\ x) \psi_1(x_1) \mathrm{d}^4 x_1 \mathrm{d}^4 x_2,$$

we can write the matrix element for scalar interaction in the form

$$M = g_S \int \Phi^{(2,1)}(x) \bar{\psi}_e(x)(1+\lambda\gamma_5)\psi_\nu(x) \mathrm{d}^4 x.$$

Similarly, in the case of tensor interaction

$$M = \tfrac{1}{2} g_{\mathrm{T}} \int \Phi_{\mu\nu}^{(2,1)}(x) \bar{\psi}_{\mathrm{e}}(x) (\gamma_\mu \gamma_\nu - \gamma_\nu \gamma_\mu)(1+\lambda\gamma_5) \psi_\nu(x) \mathrm{d}^4 x$$

where $\Phi_{\mu\nu}^{(2,1)}(x)$ is an antisymmetric tensor of the second rank.

It can be seen that these expressions differ from (1) in that $\Phi^{(2,1)}(x)$ is substituted for $\bar{\psi}_2(x)\psi_1(x)$ and $\Phi_{\mu\nu}^{(2,1)}(x)$ for $\bar{\psi}_2\gamma_\mu\gamma_\nu\psi_1$.

If no assumptions regarding the nuclear matrix element are made excepting that concerning the nature of the selection rules (these rules follow exclusively from the transformation properties of the integrand) then all the conclusions made on basis of expression (1) for the matrix element will remain valid.

Appendix 1

RELATIVISTIC WAVE FUNCTION FOR AN ELECTRON IN A COULOMB FIELD

The β-decay matrix element contains a relativistic Coulomb function $\psi_{\mathbf{p},\xi}^{(-)}(\mathbf{r})$ of the created electrons; for $r \to \infty$ this function asymptotically approaches the sum of a plane incident wave and an incoming spherical wave

$$\psi_{\mathbf{p},\xi}^{(-)}(\mathbf{r}) \sim u_{\mathbf{p},\xi} \exp\left[i\mathbf{p}\cdot\mathbf{r} - i\frac{\alpha Z\varepsilon}{p} \ln pr(1-\cos\theta)\right] + \frac{1}{r} f^{(-)}(\theta) \exp\left(ipr - i\frac{\alpha Z\varepsilon}{p}\ln 2pr\right)$$

where $\xi = \pm\frac{1}{2}$ is the quantum number of the spin projection on the direction of the momentum $\mathbf{p}$; $\alpha = 1/137$.

$$u_{\mathbf{p},\xi} = \begin{pmatrix} \sqrt{\dfrac{\varepsilon+1}{2\varepsilon}}\, v_\xi \\ \sqrt{\dfrac{\varepsilon-1}{2\varepsilon}}\, \boldsymbol{\sigma}\cdot\mathbf{n} v_\xi \end{pmatrix}$$

is a four-component spinor $[v_{\frac{1}{2}} = \binom{1}{0},\ v_{-\frac{1}{2}} = \binom{0}{1}]$ corresponding to free motion † with an energy $E = \varepsilon mc^2$ and momentum $\mathbf{p} = \mathbf{n}p$, $p^2 = \sqrt{\varepsilon^2 - 1}$ and

$$f^{(-)}(\theta) = \begin{pmatrix} f_1(\theta) \\ f_2(\theta) \end{pmatrix};$$

($f_1(\theta)$ and $f_2(\theta)$ are two-component spinors) is a quantity which determines the spinor scattering amplitude††. In ref. [11]) $\psi_{\mathbf{p},\xi}^{(-)}(\mathbf{r})$ was represented as follows:

† In our notations the average value of the spin of a free electron in a system of rest is defined as $\frac{1}{2}(v^* \boldsymbol{\sigma} v)$.

†† To be more precise the scattering amplitude is determined by the spinor $f_\xi^{(+)}(\theta)$ in the corresponding expression for the asymptotic value of function $\psi_{\mathbf{p},\xi}^{(+)}(\mathbf{r})$ (which contains at $r \to \infty$ a spherically outgoing wave).

$$\psi^{(\pm)}_{\mathbf{p},\xi}(\mathbf{r}) = 4\pi \sum_{l,j,\mu} i^l e^{\pm i\delta_{lj}} [\Omega^{(l)}_{j\mu}(\mathbf{n})]^*_\xi \psi_{lj\mu}(\mathbf{r}) \tag{A1}$$

where

$$[\Omega^{(l)}_{j\mu}(\mathbf{n})]_\xi = C^{j\mu}_{\frac{1}{2}\xi;\, l,\mu-\xi} Y_{l,\mu-\xi}(\mathbf{n})$$

is the ξ-projection of the two-component spherical spinor † ($j = l \pm \frac{1}{2}$) and

$$\psi_{lj\mu}(\mathbf{r}) = \begin{pmatrix} \sqrt{\dfrac{\varepsilon+1}{2\varepsilon}}\, G_{lj}(r)\, \Omega^{(l)}_{j\mu}\left(\dfrac{\mathbf{r}}{r}\right) \\ \sqrt{\dfrac{\varepsilon-1}{2\varepsilon}}\, F_{lj}(r)\, i^{l'-l}\, \Omega^{(l')}_{j\mu}\left(\dfrac{\mathbf{r}}{r}\right) \end{pmatrix} \tag{A2}$$

($l' = 2j-l$) is the electron wave function in a Coulomb field corresponding to motion with prescribed angular momentum values l, j and μ. The radial parts of the Coulomb functions are denoted by G_{lj} and F_{lj} [11, 12]:

$$G_{lj}(r) = \frac{2\left|\Gamma\left(\gamma + i\dfrac{\alpha Z\varepsilon}{p}\right)\right|}{\Gamma(2\gamma+1)} e^{\frac{\pi\alpha Z\varepsilon}{2p}} (2pr)^{\gamma-1}\, 2(j-l)$$
$$\times \left[e^{i\eta_{lj} - ipr}\left(\gamma + i\frac{\alpha Z\varepsilon}{p}\right) F\left(\gamma+1+\frac{i\alpha Z\varepsilon}{p},\ 2\gamma+1,\ 2ipr\right) + \text{c.c.}\right];$$

$$F_{lj}(r) = \frac{2\left|\Gamma\left(\gamma + i\dfrac{\alpha Z\varepsilon}{p}\right)\right|}{\Gamma(2\gamma+1)} e^{\frac{\pi\alpha Z\varepsilon}{2p}} (2pr)^{\gamma-1}$$
$$\times \frac{1}{i}\left[e^{i\eta_{lj} - ipr}\left(\gamma + i\frac{\alpha Z\varepsilon}{p}\right) F\left(\gamma+1+\frac{i\alpha Z\varepsilon}{p},\ 2\gamma+1,\ 2ipr\right) - \text{c.c.}\right]$$

where $\gamma = \sqrt{(j+\frac{1}{2})^2 - Z^2\alpha^2}$ (in the text these quantities were denoted as $\gamma_{j+\frac{1}{2}}$, thus, $\gamma_1 = \sqrt{1-(\alpha Z)^2}$, $\gamma_2 = \sqrt{4-(\alpha Z)^2}$ etc.) and

$$e^{2i\eta_{lj}} = \frac{2(j-l)(j+\frac{1}{2}) + i\alpha Z(\varepsilon/p)}{\gamma + i\alpha Z(\varepsilon/p)} \quad \left(\eta_{lj} \to \frac{\pi}{2}(l-j+\tfrac{1}{2}) \text{ for } Z \to 0\right).$$

The quantities δ_{lj} which enter (A1) are equal to

$$\delta_{lj} = \eta_{lj} + \frac{\pi}{2}(l'-\gamma) - \arg\Gamma\left(\gamma + i\frac{\alpha Z\varepsilon}{p}\right).$$

For $Z \to 0$, $G_{lj}(r) \to f_l(pr)$, $F_{lj}(r) \to f_{l'}(pr)$ where $f_l(x) = \sqrt{\pi/2x}\, J^{(x)}_{l+\frac{1}{2}}$, J_l being a Bessel function. Asymptotically at $r \to \infty$

† The definition and properties of spinors $\Omega_{jm}{}^{(l)}(\mathbf{n})$ are presented in the book of Akhiezer and Berestetsky[12]) and in ref. [11]).

$$G_{lj}(r) \sim (pr)^{-1} \sin\left(pr - \frac{l\pi}{2} + \delta_{lj} + \frac{\alpha Z\varepsilon}{p} \ln 2pr\right).$$
$$F_{lj}(r) \sim (pr)^{-1} \sin\left(pr - \frac{l'\pi}{2} + \delta_{lj} + \frac{\alpha Z\varepsilon}{p} \ln 2pr\right). \tag{A3}$$

For calculation of the β-decay matrix element the function (A1) must be known in the region $pr \ll 1$; to find it we determine the first terms of the expansion of G_{lj} and F_{lj} in a series in terms of pr and substitute in (A2). Since $\Omega^{(r)}_{j\mu}(\mathbf{r}/r) = (\boldsymbol{\sigma}\cdot\mathbf{r}/r)\Omega^{(1)}_{j\mu}(\mathbf{r}/r)$ and $\Omega^{(0)}_{\frac{1}{2}\mu}(\mathbf{r}/r) = u_\mu$ $(\mu = \pm\frac{1}{2})$, we obtain

$$\varphi^{(-)}_{0,\frac{1}{2},\mu} = N\begin{pmatrix}\alpha_0\\ \left(\frac{pr}{3}\beta'_c + \alpha_c\right) i\frac{\boldsymbol{\sigma}\cdot\mathbf{r}}{r}\end{pmatrix}\frac{u_\mu}{\sqrt{4\pi}};\quad \varphi^{(-)}_{1,\frac{3}{2},\mu} = N\begin{pmatrix}\frac{ipr}{3}\alpha_1\\ 0\end{pmatrix}\Omega^{(1)}_{\frac{3}{2}\mu}\left(\frac{\mathbf{r}}{r}\right)$$

$$\varphi^{(-)}_{1,\frac{1}{2},\mu} = N\begin{pmatrix}\left(\frac{pr}{3}\alpha'_c + \beta_c\right)\frac{\boldsymbol{\sigma}\cdot\mathbf{r}}{r}\\ \beta_0\end{pmatrix}\frac{u_\mu}{\sqrt{4\pi}};\quad \varphi^{(-)}_{2,\frac{3}{2},\mu} = N\begin{pmatrix}0\\ \frac{ipr}{3}\beta_1\end{pmatrix}\Omega^{(2)}_{\frac{3}{2}\mu}\left(\frac{\mathbf{r}}{r}\right).$$

Here

$$\varphi^{(-)}_{lj\mu} = i^l e^{-i\delta_{lj}}\psi_{lj\mu}(\mathbf{r}),\quad N = \frac{2\Gamma\left(\gamma_1 + \frac{i\alpha Z\varepsilon}{p}\right)}{\Gamma(2\gamma_1+1)} e^{\frac{\pi\alpha Z\varepsilon}{2p}} (2pr)^{\gamma_1-1}, \tag{A4}$$

the coefficients α_i and β_i having the values given in the text.

Taking into account the relations

$$4\pi\sum_\mu [\Omega^{(0)}_{\frac{1}{2}\mu}(\mathbf{n})]^*_\xi \frac{u_\mu}{\sqrt{4\pi}} = u_\xi,$$

$$4\pi\sum_\mu [\Omega^{(1)}_{\frac{1}{2}\mu}(\mathbf{n})]^*_\xi \frac{u_\mu}{\sqrt{4\pi}} = \boldsymbol{\sigma}\cdot\mathbf{n}u_\xi,$$

$$4\pi\sum_\mu [\Omega^{(1)}_{\frac{3}{2}\mu}(\mathbf{n})]^*_\xi \Omega^{(1)}_{\frac{3}{2}\mu}\left(\frac{\mathbf{r}}{r}\right) = 3\frac{\mathbf{r}}{r}\cdot\left[\mathbf{n} - \frac{\boldsymbol{\sigma}}{3}(\boldsymbol{\sigma}\cdot\mathbf{n})\right]u_\xi.$$

$$4\pi\sum_\mu [\Omega^{(1)}_{\frac{3}{2}\mu}(\mathbf{n})]^*_\xi \Omega^{(2)}_{\frac{3}{2}\mu}\left(\frac{\mathbf{r}}{r}\right) = 3\left(\boldsymbol{\sigma}\cdot\frac{\mathbf{r}}{r}\right)\frac{\mathbf{r}}{r}\cdot\left[\mathbf{n} - \frac{\boldsymbol{\sigma}}{3}(\boldsymbol{\sigma}\cdot\mathbf{n})\right]u_\xi,$$

which can be verified by straightforward computation, we obtain formula (3) after simple transformations and insertion in (A1) of the values of $\varphi^{(-)}_{lj\mu}(\mathbf{r})$ presented above.

Appendix 2

QUANTITIES *A* AND **B** FOR ALLOWED TRANSITIONS

According to (10),

$$A = II^* + \boldsymbol{\Lambda}\cdot\boldsymbol{\Lambda}^* + I(\boldsymbol{\nu}\cdot\boldsymbol{\Lambda}^*) + (\boldsymbol{\Lambda}\cdot\boldsymbol{\nu})I^* - i(\boldsymbol{\Lambda}\wedge\boldsymbol{\Lambda}^*)\cdot\boldsymbol{\nu};$$

$$\mathbf{B} = i\mathbf{\Lambda}\wedge\mathbf{\Lambda}^*+I\mathbf{\Lambda}^*+I^*\mathbf{\Lambda}+(II^*-\mathbf{\Lambda}\cdot\mathbf{\Lambda}^*)\boldsymbol{\nu}$$
$$+\{\mathbf{\Lambda}(\boldsymbol{\nu}\cdot\mathbf{\Lambda}^*)+(\mathbf{\Lambda}\cdot\boldsymbol{\nu})\mathbf{\Lambda}^*+iI(\boldsymbol{\nu}\wedge\mathbf{\Lambda}^*)+i(\mathbf{\Lambda}\wedge\boldsymbol{\nu})I^*\}. \quad \text{(A5)}$$

In the case when the nucleus is oriented it is assumed that all the quantities are summed over the projections μ and μ' of the spins of the initial and final states with a weighting function w_μ which defines the degree of orientation. For a non-oriented nucleus the corresponding values are $w_\mu = 1/(2j+1)$, $\bar{\mu} = \sum_\mu \mu w_\mu = 0$. In evaluating the quantities in (A5) it is convenient to consider the spherical components of all the vectors; in terms of these components

$$\mathbf{a}\cdot\mathbf{b} = a_m b_{-m}(-1)^m = a_m(b_m^*)^*,$$

where

$$(b_m)^* = (-1)^m(\mathbf{b}^*)_{-m}, \quad b_0 = b_z, \quad b_{\pm1} = \pm\frac{1}{\sqrt{2}}(b_x \pm ib_y)$$

and

$$i(\mathbf{a}\wedge\mathbf{b})_0 = a_1b_{-1}-a_{-1}b_1;\ i(\mathbf{a}\wedge\mathbf{b})_1 = a_1b_0-a_0b_1;\ i(\mathbf{a}\wedge\mathbf{b})_{-1} = a_0b_{-1}-a_{-1}b_0 \quad \text{(A6')}$$

or

$$i(\mathbf{a}\wedge\mathbf{b}^*)_0 = a_{-1}(b_{-1})^*-a_1(b_1)^*;\quad i(\mathbf{a}\wedge\mathbf{b}^*)_1 = a_1b_0^*+a_0(b_{-1})^*;$$
$$i(\mathbf{a}\wedge\mathbf{b}^*)_{-1} = -a_0(b_1)^*-a_1(b_0)^*. \quad \text{(A6)}$$

Taking into account, in accord with (20), that

$$I(\mathbf{\Lambda}_m)^* = C_1C_{\mathbf{\Lambda}}{}^*\delta_{jj'}C^{j\bar{\mu}}_{j\bar{\mu},10}\delta_{m0} = C_1C_{\mathbf{\Lambda}}{}^*\frac{\bar{\mu}\delta_{jj'}}{\sqrt{j(j+1)}}(\mathbf{n}_j)_m \quad \text{(A7)}$$

where $\mathbf{n}_j$ is the unit vector along axis Oz (orientation direction) for which $(\mathbf{n}_j)_m = \delta_{m0}$ and also taking into account the relation

$$\sum_m (C^{j'\,\mu+m}_{j\mu\,Lm})^2 = \frac{2j'+1}{2j+1} \quad \text{(A8)}$$

given in the text we obtain

$$A = |C_1|^2\delta_{jj'}+|C_{\mathbf{\Lambda}}|^2+2\,\mathrm{Re}\,(C_1C_{\mathbf{\Lambda}}{}^*)\frac{\bar{\mu}\delta_{jj'}}{\sqrt{j(j+1)}}(\mathbf{n}_j\cdot\boldsymbol{\nu})-\Delta_{j\mu}|C_{\mathbf{\Lambda}}|^2(\mathbf{n}_j\cdot\boldsymbol{\nu}).$$

Substituting (20) in (A6) and taking into account (A7) and (A8) we also get

$$i(\mathbf{\Lambda}\wedge\mathbf{\Lambda}^*)+I\mathbf{\Lambda}^*+\mathbf{\Lambda}I^*+(II^*-\mathbf{\Lambda}\cdot\mathbf{\Lambda}^*)\boldsymbol{\nu}$$
$$= (|C_1|^2\delta_{jj'}+|C_{\mathbf{\Lambda}}|^2)\bar{\beta}\mathbf{n}_j+(|C_1|^2\delta_{jj'}-|C_{\mathbf{\Lambda}}|^2)\boldsymbol{\nu} \quad \text{(A9)}$$

where $\bar{\beta}$ is defined by (23) in the text.

Computation of the terms in the second line in (A5) enclosed in the curled brackets is somewhat more difficult. Inspection of the components of vectors

$\mathbf{\Lambda}(\boldsymbol{\nu}\cdot\mathbf{\Lambda}^*)$ and $iI(\boldsymbol{\nu}\wedge\mathbf{\Lambda}^*)$ reveals † that they are proportional to the corresponding components of $\boldsymbol{\nu}$. If the components of a vector $\mathbf{Q}$ have the form

$$Q_m = \lambda_m \nu_m, \qquad m = 0, \pm 1$$

(where, generally speaking, $\lambda_0 \neq \lambda_1 \neq \lambda_{-1}$) the vector can be represented in the form

$$\mathbf{Q} = (\lambda_0 - \tfrac{1}{2}(\lambda_1+\lambda_{-1}))\mathbf{n}_j(\mathbf{n}_j\cdot\boldsymbol{\nu}) + \tfrac{1}{2}(\lambda_{-1}+\lambda_1)\boldsymbol{\nu} + \tfrac{1}{2}(\lambda_{-1}-\lambda_1)i(\mathbf{n}_j\wedge\boldsymbol{\nu}). \quad \text{(A10)}$$

The λ_m in (A10) can be easily evaluated in the case of vectors $\mathbf{\Lambda}(\boldsymbol{\nu}\cdot\mathbf{\Lambda}^*)$ and $iI(\boldsymbol{\nu}\wedge\mathbf{\Lambda}^*)$ by applying (20) and (A6); as a result we obtain

$$\mathbf{\Lambda}(\boldsymbol{\nu}\cdot\mathbf{\Lambda}^*) = |C_{\mathbf{\Lambda}}|^2\left\{(\lambda_0 - \tfrac{1}{2}(\lambda_1+\lambda_{-1}))\mathbf{n}_j(\mathbf{n}_j\cdot\boldsymbol{\nu}) + \tfrac{1}{2}(\lambda_1+\lambda_{-1})\boldsymbol{\nu} + \frac{i}{2}\Delta_{j\mu}(\mathbf{n}_j\wedge\boldsymbol{\nu})\right\};$$

$$Ii(\boldsymbol{\nu}\wedge\mathbf{\Lambda}^*) = iC_{\mathrm{I}}C_{\mathbf{\Lambda}}^*\frac{\bar{\mu}\delta_{jj'}}{\sqrt{j(j+1)}}(\mathbf{n}_j\wedge\boldsymbol{\nu}); \quad \lambda_m = \sum_{\mu} w_\mu \frac{2j+1}{2j'+1}(C^{j',\mu+m}_{j\mu,1m})^2. \quad \text{(A11)}$$

From (A5), (A9) and (A11) it follows

$$\mathbf{B} = |C_{\mathbf{\Lambda}}|^2\left[\Delta_{j\bar{\mu}} + \frac{2\bar{\mu}\delta_{jj'}}{\sqrt{j(j+1)}}\operatorname{Re}\varrho\right]\mathbf{n}_j + (|C_{\mathrm{I}}|^2\delta_{jj'} - |C_{\mathbf{\Lambda}}|^2)\boldsymbol{\nu}$$

$$+|C_{\mathbf{\Lambda}}|^2[f_{j\bar{\mu}}\mathbf{n}_j(\mathbf{n}_j\cdot\boldsymbol{\nu}) + \varphi_{j\bar{\mu}}\boldsymbol{\nu}] + 2\operatorname{Im} C_{\mathrm{I}}C_{\mathbf{\Lambda}}^*\frac{\bar{\mu}\delta_{jj'}}{\sqrt{j(j+1)}}(\mathbf{n}_j\wedge\boldsymbol{\nu})$$

where

$$f_{j\bar{\mu}} = \lambda_0 - \tfrac{1}{2}(\lambda_1+\lambda_{-1}), \quad \varphi_{j\bar{\mu}} = \tfrac{1}{2}(\lambda_1+\lambda_{-1})$$

(the values of these quantities obtained by inserting the coefficients $C^{j',\mu+m}_{j\mu,1m}$ from (A11) (see appendix 4) in λ_m are presented in formula (28)). Substitution in (26) of the values of A and $\mathbf{B}$ thus obtained directly yields (26′).

Appendix 3

FIRST ORDER FORBIDDEN TRANSITIONS IN LIGHT ORIENTED NUCLEI

Averaging (32) over the directions of $\boldsymbol{\nu}$ we obtain

$$A_{\mathrm{cc}} = tt^* + \mathbf{a}\cdot\mathbf{a}^* \quad \mathbf{B}_{\mathrm{cc}} = i\mathbf{a}\wedge\mathbf{a}^* + t\mathbf{a}^* + \mathbf{a}t^*,$$

$$-A_{0\mathrm{c}} = \left(\frac{q}{3}T - P\right)t^* + \left(\boldsymbol{\tau} + \frac{q}{3}\left(\mathbf{R}+i\mathbf{T}\right)\right)\cdot\mathbf{a}^*,$$

$$-\mathbf{B}_{0\mathrm{c}} = i\left(\boldsymbol{\tau} + \frac{q}{3}\left(\mathbf{R}+i\mathbf{T}\right)\right)\wedge\mathbf{a}^* + \left(\frac{q}{3}T - P\right)\mathbf{a}^* + \left[\boldsymbol{\tau} + \frac{q}{3}\left(\mathbf{R}+i\mathbf{T}\right)\right]t^*,$$

$$-A_{1\mathrm{c}} = (\mathbf{p}\cdot\mathbf{R})t^* + \tfrac{1}{3}(\mathbf{p}\cdot\mathbf{a}^*)T + \tfrac{1}{2}\mathbf{p}\cdot(\mathbf{T}\wedge\mathbf{a}^*) + p_k\bar{T}_{ik}a_i^*, \quad \text{(A12)}$$

$$-\mathbf{B}_{1\mathrm{c}} = \tfrac{1}{3}Tt^*\mathbf{p} + \mathbf{\Gamma}t^* + \tfrac{1}{2}(\mathbf{p}\wedge\mathbf{T})t^* + \frac{i}{3}T(\mathbf{p}\wedge\mathbf{a}^*) + (\mathbf{p}\cdot\mathbf{R})\mathbf{a}^*$$

$$+\frac{i}{2}\mathbf{T}(\mathbf{p}\cdot\mathbf{a}^*) - \frac{i}{2}\mathbf{p}(\mathbf{T}\cdot\mathbf{a}^*) + i\mathbf{\Gamma}\wedge\mathbf{a}^*$$

† If (A6) be taken into account and also the fact that the coefficients $C^{j'\mu'}_{j\mu,1m}$ are $\neq 0$ only if $\mu' = \mu + m$.

where $\mathbf{\Gamma}$ is a vector defined in terms of its projection $\Gamma_i = p_k \bar{T}_{ik}$ ($i, k = x, y, z$; indices encountered twice imply summation). Employing the standard dependence (20) of all the vectors and scalars on μ, μ' and m (the coefficients correspondingly being C_t, C_T, C_P, C_a, C_τ, C_R etc.) and taking into account (A6'), (A6), (A7) and (A8) one may compute (in exactly the same way as in (A9) and (A10)) all terms in (A12) which do not contain the tensor $\bar{T}_{ik}$. For example, for the first four quantities in (A12) we obtain

$$
\begin{aligned}
A_{cc} &= |C_a|^2 + |C_t|^2 \delta_{jj'}, \quad \mathbf{B}_{cc} = \left\{ |C_a|^2 \Delta_{j\bar{\mu}} + 2 \operatorname{Re} C_t C_a^* \frac{\bar{\mu}\delta_{jj'}}{\sqrt{j(j+1)}} \right\} \mathbf{n}_j, \\
-A_{0c} &= \left(-C_P + \frac{q}{3} C_T \right) C_t^* \delta_{jj'} + \left[C_\tau + \frac{q}{3} (C_R + i C_T) \right] \cdot C_a^*, \\
-\mathbf{B}_{0c} &= \left\{ \left[C_\tau + \frac{q}{3} (C_R + i C_T) \right] C_a^* \Delta_{j\bar{\mu}} \right. \\
&\quad \left. + \frac{\bar{\mu}\delta_{jj'}}{\sqrt{j(j+1)}} \left[\left(-C_P + \frac{q}{3} C_T \right) C_a^* + \left(C_\tau + \frac{q}{3} (C_R + i C_T) \right) C_t^* \right] \right\} \mathbf{n}_j
\end{aligned}
\tag{A13}
$$

where $\Delta_{j\mu}$ is defined by (24).

For calculation of the terms containing tensor $\bar{T}_{ik}$ it is convenient to consider the spherical components $\bar{T}_{mn}$ ($m, n = 0, \pm 1$) where $\bar{T}_{00} = \bar{T}_{zz}$, $\bar{T}_{0,\pm 1} = \pm (\bar{T}_{zx} \pm i \bar{T}_{zy})/\sqrt{2}$ etc. Similarly to (20) we then obtain

$$
\bar{T}_{mn} = C_{\bar{T}} \sqrt{\frac{2j+1}{2j'+1}} C^{2,\, m+n}_{1m;\, 1n} C^{j'\, \mu'}_{j\mu;\, 2,\, m+n} \tag{A14}
$$

(the normalization factor $\sqrt{(2j+1)/(2j'+1)}$ being chosen so that the condition $\langle \bar{T}_{ik} \bar{T}^*_{ik} \rangle = |C_{\bar{T}}|^2$ be fulfilled).

According to (A14) in commonly used notations we shall have

$$
C_{\bar{T}} = g_T \left\{ \left[\int \left(\tfrac{1}{2} \sigma_i x_k + \tfrac{1}{2} \sigma_k x_i - \tfrac{1}{3} \boldsymbol{\sigma} \cdot \mathbf{r} \delta_{ik} \right) \right]^2 \right\}^{\frac{1}{2}}
$$

and

$$
C_t = g_T \left\{ \left[\int \left(\tfrac{1}{2} \sigma_i x_k + \tfrac{1}{2} \sigma_k x_i - \tfrac{1}{3} \boldsymbol{\sigma} \cdot \mathbf{r} \delta_{ik} \right) / r \right]^2 \right\}^{\frac{1}{2}}.
$$

The last term in the expression for A_{1c} in (A12) can be written in the form

$$
p_k \bar{T}_{ik} a_i^* = p_m^* \bar{T}_{nm} (a_n)^* \equiv p_z \bar{T}_{n0} (a_n)^* = (\mathbf{p} \cdot \mathbf{n}_j) C_{\bar{T}} C_a^* \Delta'_{j'j\bar{\mu}}
$$

where according to (A14) and (20)

$$
\begin{aligned}
\Delta'_{j'j\bar{\mu}} &= \sum_{\mu=-j}^{j} w_\mu \frac{2j+1}{2j'+1} \sum_{n=0,\pm 1} C^{2n}_{1n,\, 10} C^{j',\, \mu+n}_{j\mu,\, 2n} C^{j',\, \mu+n}_{j\mu,\, 1n} \\
&= \frac{\bar{\mu}}{2\sqrt{6}} \frac{\sqrt{(j+j'+3)(j+j'-1)(j-j'+2)(j'-j+2)}}{j(j+1)}.
\end{aligned}
$$

The right hand side has been obtained here by using the Racah formula which yields the sum of the left hand side of the equation over n. (The same

value, however, can be obtained by directly computing the three terms in the sum in the left hand part with aid of the explicit value of coefficients $C^{j'\mu'}_{j\mu,\,Lm}$.) Calculation of the remaining terms in the expression for A_{1c} is similar to that employed in determining (A13); the result is

$$-A_{1c} = p(\mathbf{n}\cdot\mathbf{n}_j)\left\{\frac{\bar{\mu}\delta_{jj'}}{\sqrt{j\,(j+1)}}(C_{\mathbf{R}}C_t^*+\tfrac{1}{3}C_{\mathbf{T}}C_a^*)-\frac{i}{2}C_{\mathbf{T}}C_a^*\Delta_{j\mu}+C_{\bar{\mathbf{T}}}C_a^*\Delta'_{j'j\mu}\right\}. \tag{A15}$$

Inspection of the components of the vectors which compose $\mathbf{B}_{1c}$ in (A12) shows (if (A6) is used) that they are proportional to the corresponding components of $\mathbf{n}$. Each of the vectors thus has the same form as (A10) where $\mathbf{n}$ has been substituted for $\boldsymbol{\nu}$ and the corresponding values of λ_m can readily be found by straightforward calculation (as that in (A9) and (A11)). As a result we obtain

$$\tfrac{1}{3}Tt^*\mathbf{p} = \frac{p}{3}C_{\mathbf{T}}C_t^*\delta_{jj'}\,\mathbf{n},$$

$$(\boldsymbol{\Gamma}t^*)_m = p_n^*\bar{T}_{nm}t^*$$

$$= \frac{p}{\sqrt{6}}C_{\bar{\mathbf{T}}}C_t^*\frac{3\bar{\mu}^2-j(j+1)}{\sqrt{j(j+1)(2j-1)(2j+3)}}\delta_{jj'}\{2\mathbf{n}_j(\mathbf{n}_j\cdot\mathbf{n})-\mathbf{n}_j\wedge(\mathbf{n}_j\wedge\mathbf{n})\}_m,$$

$$\tfrac{1}{2}(\mathbf{p}\wedge\mathbf{T})t^* = \frac{p}{2}C_{\mathbf{T}}C_t^*\delta_{jj'}\frac{\bar{\mu}}{\sqrt{j\,(j+1)}}(\mathbf{n}_j\wedge\mathbf{n}),$$

$$\frac{i}{3}T(\mathbf{p}\wedge\mathbf{a}^*) = \frac{ip}{3}C_{\mathbf{T}}C_a^*\delta_{jj'}\frac{\bar{\mu}}{\sqrt{j\,(j+1)}}(\mathbf{n}_j\wedge\mathbf{n}),$$

$$(\mathbf{p}\cdot\mathbf{R})\mathbf{a}^* = C_{\mathbf{R}}C_a^*p\{f_{j\mu}\mathbf{n}_j(\mathbf{n}\cdot\mathbf{n}_j)+\varphi_{j\mu}\mathbf{n}-\tfrac{1}{2}\Delta_{j\bar{\mu}}i(\mathbf{n}_j\wedge\mathbf{n})\},$$

$$\frac{i}{2}\mathbf{T}(\mathbf{p}\cdot\mathbf{a}^*) = \frac{i}{2}C_{\mathbf{T}}C_a^*p\{f_{j\mu}\mathbf{n}_j(\mathbf{n}\cdot\mathbf{n}_j)+\varphi_{j\mu}\mathbf{n}+\tfrac{1}{2}\Delta_{j\bar{\mu}}i(\mathbf{n}_j\wedge\mathbf{n})\},$$

$$-\frac{i}{2}\mathbf{p}(\mathbf{T}\cdot\mathbf{a}^*) = -\frac{i}{2}C_{\mathbf{T}}C_a^*p\mathbf{n},$$

$$i\boldsymbol{\Gamma}\wedge\mathbf{a}^* = -C_{\bar{\mathbf{T}}}C_a^*\{\tfrac{1}{2}[j(j+1)-3\bar{\mu}^2]F_{jj'}(3\mathbf{n}_j(\mathbf{n}_j\cdot\mathbf{n})-\mathbf{n})-\tfrac{1}{2}G_{jj'}\Delta_{j\bar{\mu}}i(\mathbf{n}_j\wedge\mathbf{n})\}.$$

The following notations have been employed:

$$p_n^*T_{nm} = (\boldsymbol{\Gamma})_m,\quad \varphi_{j\mu} = \tfrac{1}{3}(2-f_{j\mu}),$$

$$[j(j+1)-3\bar{\mu}^2]F_{jj'} = \eta_{-1}-\eta_1,\quad 2\eta_0+(\eta_1+\eta_{-1}) = \Delta_{j\bar{\mu}}G_{jj'},$$

where

$$\eta_0 = \sum_\mu w_\mu\frac{2j+1}{\sqrt{6}(2j'+1)}C^{j'\mu}_{j\mu,10}C^{j'\mu}_{j\mu,20},$$

$$\eta_{\pm1} = \sum_\mu w_\mu\frac{2j+1}{\sqrt{2}(2j'+1)}C^{j',\mu\pm1}_{j\mu,1\pm1}C^{j',\mu\pm1}_{j\mu,2\pm1}.$$

Substitution of the values of coefficients $C^{j'\mu'}_{j\mu,Lm}$ yields

$$F_{jj'}=\begin{cases}\dfrac{1}{j(2j-1)}\sqrt{\dfrac{j-1}{2(j+1)}}\\ \dfrac{\sqrt{3}}{j(j+1)\sqrt{2(2j-1)(2j+3)}};\\ -\dfrac{\sqrt{j+2}}{(j+1)(2j+3)\sqrt{2j}}\end{cases}\quad G_{jj'}=\begin{cases}\sqrt{\dfrac{j-1}{2(j+1)}} & j'=j-1\\ \sqrt{\dfrac{(2j-1)(2j+3)}{6}} & j'=j\\ -\sqrt{\dfrac{j+2}{2j}} & j'=j+1.\end{cases}$$

Hence for $\mathbf{B}_{1c}$ we obtain

$$-\mathbf{B}_{1c}=b_1\mathbf{n}_j(\mathbf{n}_j\cdot\mathbf{n})+b_2\mathbf{n}+b_3\mathbf{n}_j\wedge\mathbf{n}$$

where

$$b_1=\frac{p}{2}\left\{\left(C_{\mathrm{R}}+\frac{i}{2}C_{\mathrm{T}}\right)C_{\mathrm{a}}^{*}f_{j\bar{\mu}}+\left[3C_{\tilde{\mathrm{T}}}C_{\mathrm{a}}^{*}F_{jj'}-\frac{\sqrt{6}\delta_{jj'}C_{\tilde{\mathrm{T}}}C_{\mathrm{t}}^{*}}{\sqrt{j(j+1)(2j-1)(2j+3)}}\right][j(j+1)-3\bar{\mu}^2]\right\},$$

$$b_2=\frac{p}{2}\left\{\left[\frac{2}{3}C_{\mathrm{T}}C_{\mathrm{t}}^{*}+2C_{\tilde{\mathrm{T}}}C_{\mathrm{t}}^{*}\frac{j(j+1)-3\bar{\mu}^2}{\sqrt{6j(j+1)(2j-1)(2j+3)}}\right]\delta_{jj'}-[j(j+1)-3\bar{\mu}^2]F_{jj'}C_{\tilde{\mathrm{T}}}C_{\mathrm{a}}^{*}+C_{\mathrm{R}}C_{\mathrm{a}}^{*}\varphi_{j\mu}-\frac{i}{2}C_{\mathrm{T}}C_{\mathrm{a}}^{*}(2-\varphi_{j\mu})\right\},$$

$$b_3=\frac{p}{2}\left[-\frac{\bar{\mu}\delta_{jj'}}{\sqrt{j(j+1)}}(C_{\mathrm{T}}C_{\mathrm{t}}^{*}+\tfrac{2}{3}iC_{\mathrm{T}}C_{\mathrm{a}}^{*})+iC_{\mathrm{T}}^{\sim}C_{\mathrm{a}}^{*}G_{jj'}\Delta_{j\bar{\mu}}-i\left(C_{\mathrm{R}}-\frac{i}{2}C_{\mathrm{T}}\right)C_{\mathrm{a}}^{*}\Delta_{j\bar{\mu}}\right].$$

Insertion of these values in (35) yields the following expression for the β-electron angular distribution:

$$\begin{aligned}W_{e\mathbf{n}_j}=\frac{1}{W_{\mathrm{tot}}}\Bigg\{&\frac{\alpha^2Z^2}{4}\left[|C_{\mathrm{a}}|^2+|C_{\mathrm{t}}|^2\delta_{jj'}-v\mathbf{n}\cdot\mathbf{n}_j\left(|C_{\mathrm{a}}|^2\Delta_{j\bar{\mu}}+\frac{\bar{\mu}\delta_{jj'}}{\sqrt{j(j+1)}}2\,\mathrm{Re}\,C_{\mathrm{a}}C_{\mathrm{t}}^{*}\right)\right]\\
&-\alpha Z\left[\mathrm{Re}\left(-C_{\mathrm{P}}+\frac{q}{3}C_{\mathrm{T}}\right)C_{\mathrm{t}}^{*}\delta_{jj'}+\mathrm{Re}\left(C_{\mathrm{T}}+\frac{q}{3}C_{\mathrm{R}}+iC_{\mathrm{T}}\right)C_{\mathrm{a}}^{*}\right.\\
&-v\mathbf{n}\cdot\mathbf{n}_j\Bigg[\mathrm{Re}\,(C_{\mathrm{T}}+\tfrac{1}{3}q(C_{\mathrm{R}}+iC_{\mathrm{T}}))C_{\mathrm{a}}^{*}\Delta_{j\bar{\mu}}\\
&+\frac{\bar{\mu}\delta_{jj'}}{\sqrt{j(j+1)}}\left(\mathrm{Re}\left(-C_{\mathrm{P}}+\frac{q}{3}C_{\mathrm{T}}\right)C_{\mathrm{a}}^{*}+\mathrm{Re}\left(C_{\mathrm{T}}+\frac{q}{3}\left(C_{\mathrm{R}}+iC_{\mathrm{T}}\right)\right)C_{\mathrm{t}}^{*}\right)\Bigg]\Bigg]\\
&-\alpha Zp\left[\mathbf{n}\cdot\mathbf{n}_j\left[\frac{\bar{\mu}\delta_{jj'}}{\sqrt{j(j+1)}}\mathrm{Re}\,(C_{\mathrm{R}}C_{\mathrm{t}}^{*}+\tfrac{1}{3}C_{\mathrm{T}}C_{\mathrm{a}}^{*})+\tfrac{1}{2}\,\mathrm{Im}\,C_{\mathrm{T}}C_{\mathrm{a}}^{*}\Delta_{j\bar{\mu}}\right.\right.\\
&\left.\left.+\mathrm{Re}\,C_{\tilde{\mathrm{T}}}C_{\mathrm{a}}^{*}\Delta'_{j'j\bar{\mu}}\right]-v[\mathrm{Re}\,b_1(\mathbf{n}_j\cdot\mathbf{n})^2+\mathrm{Re}\,b_2]\right]\Bigg\};\end{aligned}$$

$$W_{\text{tot}} = \frac{\alpha^2 Z^2}{4}[|C_a|^2+|C_t|^2\delta_{jj'}] - \alpha Z\left[\text{Re}\left(-C_P+\frac{q}{3}C_T\right)C_t^*\delta_{jj'}\right.$$
$$\left.+\text{Re}\left(C_T+\frac{q}{3}C_R+iC_T\right)C_a^*\right]+Z\alpha pv[\tfrac{1}{3}\text{Re}\, b_1+\text{Re}\, b_2].$$

Appendix 4

QUANTITIES A AND $\mathbf{B}$ FOR TRANSITIONS WITH $\Delta j = 2$.

Writing the quantities of the first row in (58) in spherical coordinates, introducing (A14) and taking into account (A6) we obtain

$$\frac{q^2}{3}\bar{T}_{ik}\bar{T}_{ik}^* = \frac{q^2}{3}\bar{T}_{mn}\bar{T}_{mn}^* = \frac{q^2}{3}|C_{\bar{T}}|^2,$$
$$\frac{q^2}{3}i\sigma_l\varepsilon_{lii'}\bar{T}_{ik}\bar{T}_{i'k}^* = \frac{q^2}{3}i\sigma_0[\bar{T}_{-1n}\bar{T}_{-1n}^*-\bar{T}_{1n}\bar{T}_{1n}^*] = |C_{\bar{T}}|^2(\boldsymbol{\sigma}\cdot\mathbf{n}_j)u_{j\mu} \tag{A16}$$

where

$$u_{j\mu} = \sum_{\mu=-j}^{j} w_\mu \frac{2j+1}{2j'+1}\sum_{n=0,\pm1}\{(C^{2,\,n-1}_{1-1,\;1n})^2\,(C^{j',\,\mu+n-1}_{j\mu;\;2,\;n-1})^2-(C^{2,\,n+1}_{11,\,1n})^2\,(C^{j',\,\mu+n+1}_{j\mu;\;2,\;n+1})^2\}.$$

Since $C^{2-1}_{1-1,\,10} = C^{21}_{11,\,10} = 1/\sqrt{2}$, $C^{22}_{11,\,11} = C^{2-2}_{1-1,\,1-1} = 1$, $C^{20}_{1-1,\,11} = C^{20}_{11,\,1-1} = 1/\sqrt{2}$, $C^{20}_{10,\,10} = \sqrt{2}/3$, the quantity $u_{j\mu}$ can be expressed as

$$u_{j\mu} = \tfrac{1}{2}\delta^{(1)}_{j\mu}+\delta^{(2)}_{j\mu}$$

where

$$\delta^{(\nu)}_{j\mu} = \sum_{\mu=-j}^{j} w_\mu \frac{2j+1}{2j'+1}[(C^{j',\,\mu-\nu}_{j\mu,\;2-\nu})^2-(C^{j',\,\mu+\nu}_{j\mu,\;2\nu})^2],\quad \nu = 1,\,2.$$

Insertion of the values of $C^{j'\mu'}_{j\mu,\,L\nu}$ yields

$$\delta^{(1)}_{j\mu} = \begin{cases} 2\dfrac{j^2\bar{\mu}-\bar{\mu}^3}{j(j-1)(2j-1)} \\ -2\dfrac{(j+1)^2\bar{\mu}-\bar{\mu}^3}{(j+1)(j+2)(2j+3)} \end{cases};\quad \delta^{(2)}_{j\bar{\mu}} = \begin{cases} \dfrac{(j^2-3j+1)\bar{\mu}+\bar{\mu}^3}{j(j-1)(2j-1)} \\ -\dfrac{[(j+1)^2+3(j+1)+1]\bar{\mu}+\bar{\mu}^3}{(j+1)(j+2)(2j+3)} \end{cases} \tag{A17}$$

(the upper value everywhere refers to the case $j' = j-2$ and the lower to the case $j' = j+2$); the value for $u_{j\mu}$ given in the text directly follows from here. The values of A_{00} and $\mathbf{B}_{00}$ presented in the text follow from (A16).

A_{11} and $\mathbf{B}_{11}$ can be evaluated in a similar manner. For A_{11} we have, according to (58),

$$A_{11} = p_k\bar{T}_{ik}p_{k'}\bar{T}_{ik'}^* = p_n^*\bar{T}_{mn}p_{n'}\bar{T}_{mn'}^*$$
$$= \frac{p^2}{2}(|\bar{T}_{mn}|^2-|\bar{T}_{m0}|^2)+(\mathbf{n}_j\cdot\mathbf{p})^2(\tfrac{3}{2}|\bar{T}_{m0}|^2-\tfrac{1}{2}|\bar{T}_{mn}|^2);$$

substitution of (A14) gives $|\bar{T}_{m0}|^2 = |C_{\bar{T}}|^2\delta^{(3)}_{j\bar{\mu}}$ where

$$\delta^{(3)}_{j\bar{\mu}} = \sum_{\mu} w_{\mu}\{\tfrac{2}{3}(C^{j'\mu}_{j\mu,\,20})^2+\tfrac{1}{2}[(C^{j',\,\mu-1}_{j\mu,\,2-1})^2-(C^{j',\,\mu+1}_{j\mu,\,21})^2]\}\frac{2j+1}{2j'+1}.$$

Hence

$$A_{11} = |C_{\bar{1}}|^2(p^2/3)[1+(3\delta^{(3)}_{j\bar{\mu}}-1)P_2(\cos\vartheta)]$$

where

$$\cos\vartheta = \mathbf{n}_j\cdot\mathbf{n},\ P_2(x) = (3x^2-1)/2.$$

Substitution of the coefficients $C^{j'\mu}_{j\mu,20}$ yields for $a_{j\mu} = (3\delta^{(3)}_{j\mu}-1)P_2(\cos\vartheta)$ the value presented in the text. From (58) we have for $\boldsymbol{\sigma}\cdot\mathbf{B}_{11}$

$$\boldsymbol{\sigma}\cdot\mathbf{B}_{11} = \sigma_i i\varepsilon_{iil'}p_k\tilde{T}_{ik}p_{k'}\tilde{T}^*_{i'k'}$$

$$= \boldsymbol{\sigma}\left\{\left[\frac{p^2}{2}\delta^{(2)}_{j\bar{\mu}}+(\mathbf{p}\cdot\mathbf{n}_j)^2(\delta^{(1)}_{j\bar{\mu}}-\tfrac{1}{2}\delta^{(2)}_{j\bar{\mu}})\right]\mathbf{n}_j-\tfrac{1}{2}(\mathbf{p}\cdot\mathbf{n}_j)\delta^{(1)}_{j\bar{\mu}}\mathbf{p}\right\}|C_{\bar{1}}|^2,$$

whence

$$\mathbf{B}_{11} = \frac{p^2}{3}\{[(\delta^{(2)}_{j\bar{\mu}}+\delta^{(1)}_{j\bar{\mu}})+(2\delta^{(1)}_{j\bar{\mu}}-\delta^{(2)}_{j\bar{\mu}})P_2(\cos\vartheta)]\mathbf{n}_j-\tfrac{3}{2}\delta^{(1)}_{j\bar{\mu}}\cos\vartheta\,\mathbf{n}\}|C_{\bar{1}}|^2.$$

This is exactly the expression presented in the text, the quantity in the brackets being denoted as $b_{j\mu}(\vartheta)$ and $-\frac{3}{2}\delta^{(1)}_{j\mu}$ as $u_{j\mu}$ $b'_{j\mu}$. The values of these quantities obtained by substitution of (A17) are also presented in the text.

References

1) T. D. Lee and C. N. Yang, Phys. Rev. **104** (1956) 256
2) C. S. Wu, E. Ambler, R. H. Hayward, D. D. Hoppes and R. P. Hudson, Phys. Rev. **105** (1957) 1413
3) L. D. Landau, Nuclear Physics **3** (1957) 127
4) T. D. Lee and C. N. Yang, Phys. Rev. **105** (1957) 1671
5) A. Salam, Nuovo Cimento **5** (1957) 229
6) H. Frauenfelder *et al.*, Phys. Rev. **106** (1957) 386
7) A. I. Alikhanov, G. P. Yeliseyev, V. A. Luibimov and B. V. Ershler, JETP (in press)
8) M. E. Vishnevsky, V. K. Grigoryev, V. A. Yergakov, S. Ya. Nikitin, E. V. Pushkin and Yu. V. Trebukhovsky, Nuclear Physics **4** (1957) 271
9) B. L. Ioffe, L. B. Okun and A. P. Rudik, JETP **32** (1957) 396
10) B. L. Ioffe, JETP **32** (1957) 1246
11) V. B. Berestetsky, A. Z. Dolginov and K. A. Ter-Martirosyan, JETP **20** (1950) 527
12) A. I. Akhiezer and V. B. Berestetsky, Quantum Electrodynamics (Moscow, 1953) p. 65
13) J. B. Jackson, S. B. Treiman and H. W. Wyld, Phys. Rev. **106** (1957) 517

Note added in proof: After this paper was completed we recalculated all the formulae taking into account finiteness of the nuclear dimensions. The corrections for allowed transitions were found to be small; in the case of first order forbidden transitions the main effect is that in the matrix elements (see eq. (29))

$$\mathbf{m} = g_{\mathrm{S}}\int\bar{\psi}_2(\mathbf{r}/r)\psi_1\,d\tau,\qquad t_{ik} = g_{\mathrm{T}}\int\bar{\psi}_2(\sigma_i r_k/r)\psi_1\,d\tau$$

the quantity r is replaced by R_0, the nuclear radius. Thus in the case of 0—0 transitions only one nuclear parameter $\lambda_{\mathrm{P}} = C_{\mathrm{P}}/C_{\mathrm{T}}$ enters into the formula (50), the quantity $\lambda_{\mathrm{T}} = C_{\mathrm{T}}/C_{\mathrm{T}}$ being equal to $1/R_0$.

Nuclear Physics **5** (1958) 495—503; © *North-Holland Publishing Co., Amsterdam*

Not to be reproduced by photoprint or microfilm without written permission from the publisher

THE ANALYSIS OF ANGULAR AND DIRECTION-POLARIZATION CORRELATION MEASUREMENTS ON MIXED TRANSITIONS

C. F. COLEMAN

Atomic Energy Research Establishment, Harwell, England

Received 7 October 1957

Abstract: When two experimentally observed quantities a_{exp}, b_{exp} are given theoretically as known functions $a(t)$, $b(t)$ of a continuous variable t, a comparison between the experimental results and the theoretical predictions can be made by plotting the curve $x = a(t)$, $y = b(t)$, and noting whether the point $x = a_{exp}$, $y = b_{exp}$ lies on it. This allows a very direct comparison of the measured values of the angular correlation parameters A_2, A_4 with the theoretical predictions for any spin sequence involving a single mixed transition. Comparison between numbers of experimental and theoretical results on a single graph becomes possible, and the technique can also be used for direction-polarization correlations involving a single mixed transition.

1. Introduction

The analysis of cascade angular correlation measurements involving pure transitions only is straightforward, since each spin sequence under this restriction gives a unique angular correlation function $W(\theta)$, and in particular a unique value of the anisotropy ε defined by $\varepsilon = [W(\pi)-W(\pi/2)]/W(\pi/2)$. Once the possibility of mixed transitions is admitted the correlation becomes a continuous function of δ, the ratio of the matrix elements for the competing processes in the mixed transition. If δ is not already known the measurement of a single correlation parameter, such as ε, is of little value in distinguishing between different spin sequences. In practice angular correlation measurements seldom yield more than two independent parameters, for example the coefficients A_2 and A_4 in the expansion for the correlation function, $W(\theta) = 1+A_2P_2(\cos\theta)+A_4P_4(\cos\theta)$. At present the theoretical predictions for any particular spin sequence involving a mixed transition are usually compared with experimental results by plotting A_2 and A_4 (or ε and A_4) on a common graph as functions of $\log_{10}\delta$, or of the intensity ratio $\delta^2/(1+\delta^2)$ (fig. 1) [1, 2]. The experimental values of A_2 and A_4 then determine ranges within which δ must lie. Only those spin sequences and values of δ are admissible which are consistent with the measured values of both A_2 and A_4. A new method of presenting the theoretical results is described below, which gives a much more direct

indication of their compatibility with particular experimental measurements.

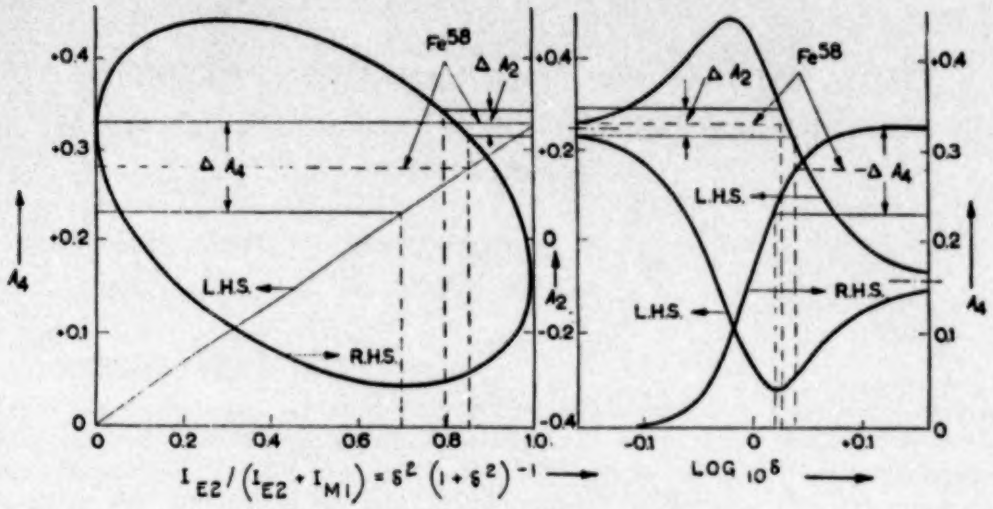

Fig. 1. Plots of A_2 and A_4 as functions of log δ and of $\delta^2/(1+\delta^2)$ for the spin sequence 2, 2, 0.

2. Parametric Plots

The new presentation can be applied to any measurement which gives values of two quantities a_{exp} and b_{exp}, the theoretically predicted values of which are known functions $a(t)$ and $b(t)$ of a continuously variable parameter t. One takes $x = a(t)$, $y = b(t)$ as the parametric equations of a curve, and the condition that the experimental results should be consistent with a particular theoretical prediction is that, within the experimental

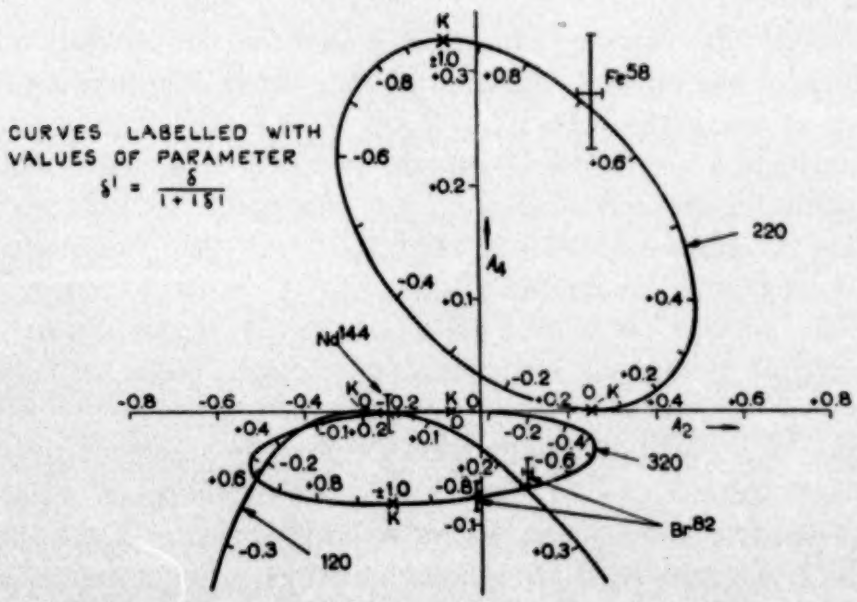

Fig. 2. Parametric plots $x = A_2(\delta')$, $y = A_4(\delta')$ for the spin sequences 1, 2, 0; 2, 2, 0; 3, 2, 0. $\delta' = \delta(1+|\delta|)^{-1}$.

uncertainties, the point given by $x = a_{exp}$, $y = b_{exp}$ should lie on the corresponding curve. Its position on the arc of the curve then determines t. Fig. 2 illustrates these points. Here $a(t)$ and $b(t)$ are the coefficients $A_2(\delta)$, $A_4(\delta)$ in the gamma-gamma angular correlation functions $W(\theta) = 1 + A_2(\delta)\, P_2(\cos\theta) + A_4(\delta)\, P_4(\cos\theta)$ for the spin sequences 3, 2, 0; 2, 2, 0; and 1, 2, 0. The first transition in each case has the mixture ratio δ. The

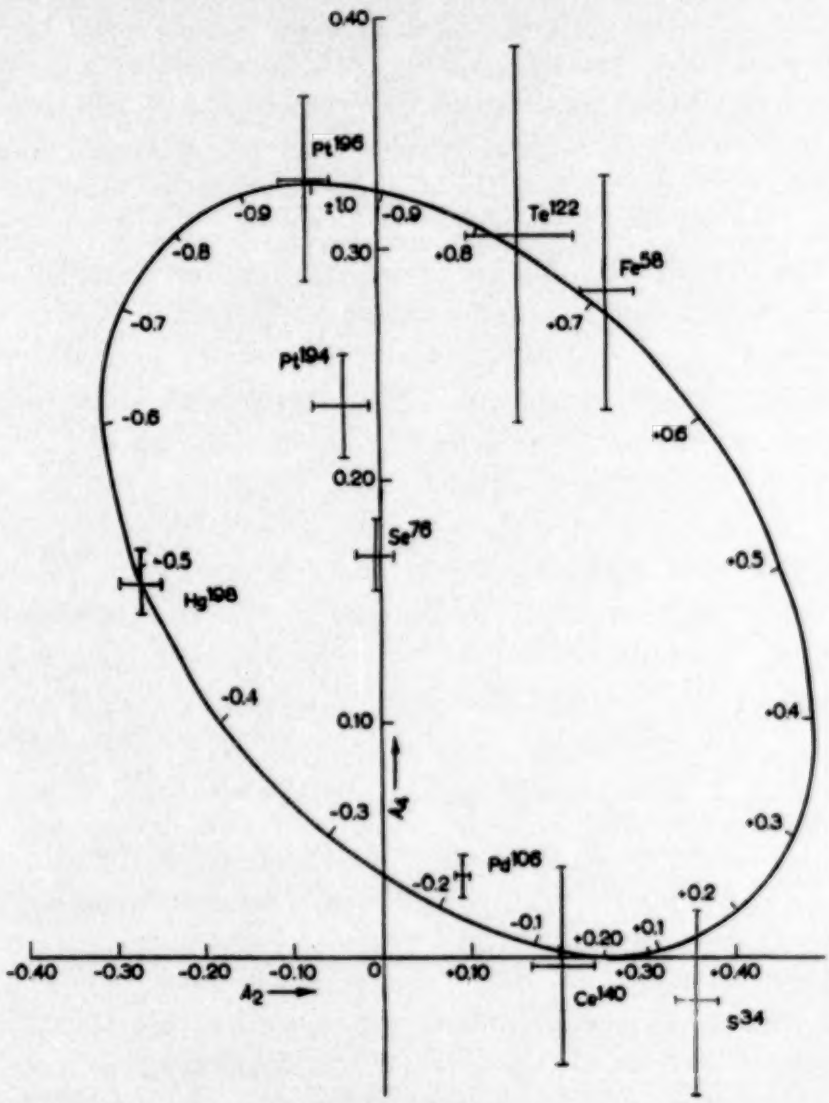

Fig. 3. Experimental results for 2,2,0 spin sequence.

S[34] H. E. Handler and J. R. Richardson, Phys. Rev. **102** (1956) 833
Fe[58] H. Frauenfelder *et al.*, Phys. Rev. **103** (1956) 352
Se[76] J. J. Kraushaar and M. Goldhaber, Phys. Rev. **89** (1953) 1081
Pd[106] E. D. Klema and F. K. McGowan, Phys. Rev. **92** (1953) 1469
Te[122] M. J. Glaubman, Phys. Rev. **98** (1955) 645
Ce[140] C. F. Coleman, Phil. Mag. **46** (1955) 1132
Pt[194] C. E. Mandeville, Jagdish Varma and Babulal Saraf, Phys. Rev. **98** (1955) 94
Pt[196] R. M. Steffen, Phys. Rev. **89** (1953) 665
Hg[198] C. D. Schrader, Phys. Rev. **92** (1953) 928.

curves are labelled with the values of the quantity $\delta' = \delta/[1+|\delta|]$, which increases rather uniformly with distance along the curve, and makes for

easier interpolation. A few experimental results [3, 4, 5]) which have been interpreted in terms of these spin sequences are plotted in the figure. The gain in clarity over the usual representations is immediately apparent (cf. fig. 1).

It can be shown (see appendix) that for all spin sequences involving a dipole-quadrupole mixture the parametric curves are ellipses touching the A_2 axis. The branches corresponding to positive and negative values of δ' link without change of slope at the points, marked by the letter K in fig. 2, corresponding to pure dipole and pure quadrupole radiation in the mixed transition. The fractional intensity of quadrupole radiation at any point on the curve is equal to the ratio of the corresponding value of A_4 to the maximum value, corresponding to $\delta' = 1$. Fig. 3 is an expanded portion of fig 2; it shows a number of experimental results which have been interpreted in terms of the spin sequence 2^+(M1+E2) 2^+(E2)0^+ plotted on the appropriate parametric curve. The results are in good agreement † with the theoretical predictions, except in a few cases where the cascades selected for measurement could not be adequately resolved from other cascades giving different correlations.

For a cascade involving two mixed transitions a set of curves $x = A_2(\delta_1, \delta_2)$; $y = A_4(\delta_1, \delta_2)$ can be plotted for a series of particular values of the second mixture ratio δ_2. Any particular experimental result may then be compatible with the given spin sequence for several paired values of the mixture ratios δ_1 and δ_2.

3. Direction-Polarization Correlations

For small values of δ', and cascades involving a dipole-quadrupole mixture, $A_4(\delta')$ is proportional to $(\delta')^2$. Under these conditions very accurate measurements of A_4 are required to distinguish between the various possible spin sequences. As an example, the result for Ce^{140} plotted in fig. 3 is also consistent with the predictions for the spin sequence 3, 2, 0 shown in fig. 2. Several authors [6, 7, 8]) have noticed that this ambiguity can be resolved by combining measurements of gamma-gamma direction-polarization correlations with measurements of the anisotropy ε. In contrast with A_4, the polarization ratio $J_{\|}(\theta_0, \delta')/J_{\perp}(\theta_0, \delta')$ for one of the cascade radiations, where θ_0 is the angle between the directions of emission of the two radiations, is of the form $a+b\delta'$ when δ' is small. The parametric plot technique can be applied here, using for preference the quantities

$$\varepsilon'(\delta') = \frac{W(\pi, \delta') - W(\pi/2, \delta')}{W(\pi, \delta') + W(\pi/2, \delta')} \text{ and } P'(\theta_0, \delta') = \frac{J_{\|}(\theta_0, \delta') - J_{\perp}(\theta_0, \delta')}{J_{\|}(\theta_0, \delta') + J_{\perp}(\theta_0, \delta')},$$

† The correlation between the uncertainties in the experimentally determined values of the quantities A_2 and A_4 is considered in the appendix.

which vary between $+1$ and -1. For a given parity sequence the plot breaks up into two branches, corresponding to the cases in which the polarisation observed is that of the mixed and of the unmixed radiation respectively. The two values of δ' corresponding to a given value of ε' give rise to rather similar values of $P'(\theta_0, \delta')$ for the pure radiation, but very different values of P' for the mixed radiation. P' for the branch corresponding to the case in which the polarization of the first radiation is observed depends on the relative parities of the initial and intermediate states, but not on that of the final state, while P' for the other branch depends on the relative parities of the intermediate and final states, but not on that of the initial state. The curves for like and unlike parities (see appendix) are just reflections of each other in the line $P'(\theta_0, \delta') = 0$. Fig. 4 shows such a plot for the

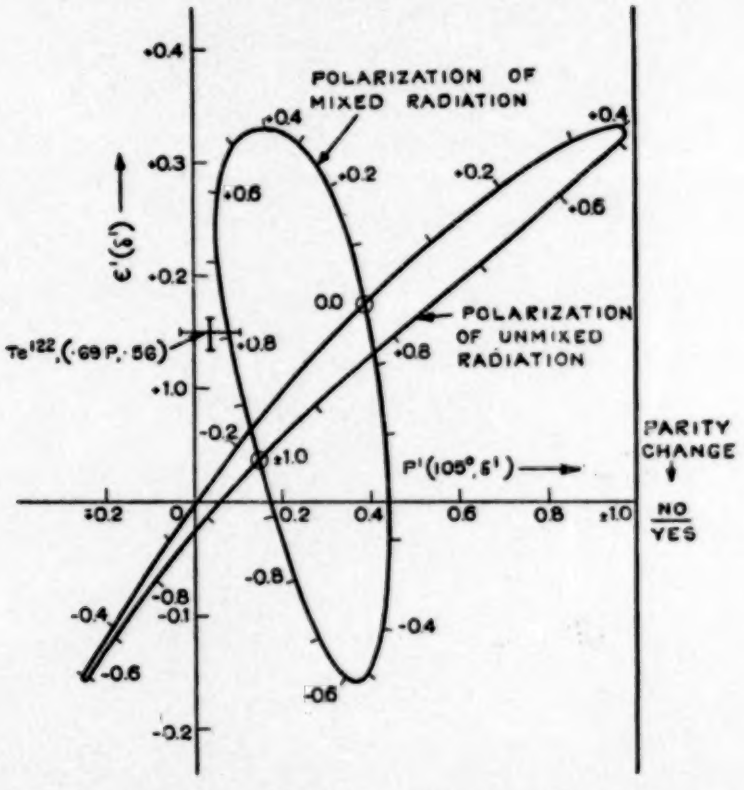

Fig. 4. Parametric plot $x=\{(U_{\|}-J_{\perp})/(U_{\|}+J_{\perp})\}$ $(105^0, \delta')$, $y=\varepsilon'(\delta')$ for the spin sequence 2,2,0.

spin sequence 2, 2, 0, with $\theta_0 = 105^0$. The scale for P' which runs from -0.2 to $+1.0$ (left to right), and is marked "NO", applies when there is no parity change in the transition of which the polarization is observed. If there is a parity change in this transition, the scale running from $+0.2$ to -1.0, and marked "YES", applies.

If the measuring equipment is not such that one of the polarization-direction correlations can be eliminated, the observed effect becomes a mixture of the two possible correlations. This mixture depends both on the

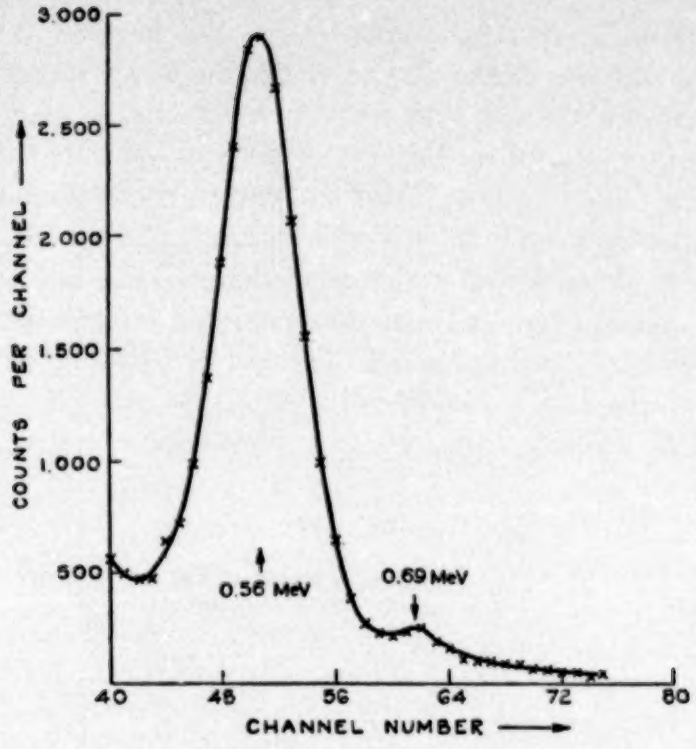

Fig. 5. Polarimeter spectrum of gamma radiation from Sb^{122}.

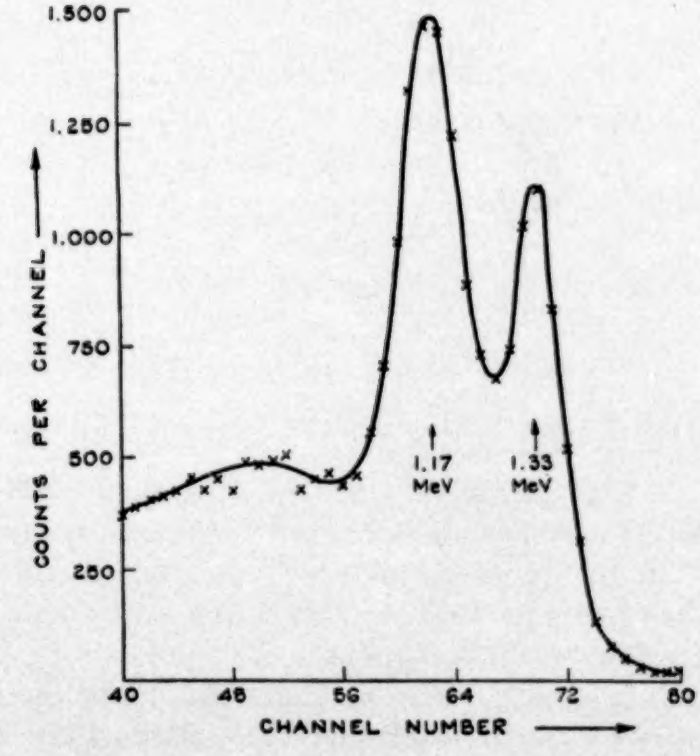

Fig. 6. Polarimeter spectrum of gamma radiation from Co^{60}.

relative counting efficiences for the two correlations, and on the variation with energy of the polarization sensitivity of the polarimeter. Thus clear cut interpretations of direction-polarization measurements are only possible with polarimeters having good energy resolution. Several energy sensitive instruments based on the two crystal Compton spectrometer have been described [9, 10, 11]). The polarimeter spectra shown in figs. 5 and 6 were obtained by using a 2" NaI-Tl cone in the scattering position, and summing the pulses from the two polarimeter detectors to improve the energy resolution, in the manner described previously [11]). The NaI-Tl scatterer gives excellent energy resolution, but produces appreciable plural scattering, and thus a diminished polarization sensitivity. The "polarimeter ratio" (the estimate of polarisation sensitivity introduced by Metzger and Deutsch[12]) for this equipment was determined from a direction-polarization measurement on the 4+(E2)2+(E2)0+ 720, 560 keV cascade [6]) in Cd^{114}, and was found to be 1.95 ± 0.3 at an energy of 720 keV. The direction-polarization correlation for the 690, 560 keV cascade in Te^{122}, with the 690 keV radiation selected in the polarimeter, was then measured. The result is plotted in fig. 4, using the "NO" scale. It shows that the 690 keV radiation is the mixed radiation, that it probably involves no change of parity, and that δ' has the value $+0.8$ rather than -0.05, in agreement with the conclusion drawn from the measured value of A_4.

4. Summary

The use of parametric plots greatly simplifies the comparison of angular correlation data with theoretical predictions involving mixed transitions. Measurements of A_2 and A_4 can be compared with the predictions for a number of spin sequences involving a single mixed transition simultaneously, or with the predictions for a single spin sequence involving two mixed transitions. Alternatively, a series of measurements on different cascades involving the same spin sequence with a single mixed transition can be compared simultaneously with the theoretical predictions. The parametric plot also provides an effective method for comparing the combined results of measurements of the angular correlation anisotropy and of the direction-polarization correlations with the predictions for a cascade involving a single mixed transition.

Appendix

The theoretical data used in calculating the parametric plots for this paper were obtained from the review article on cascade angular correlations by L. C. Biedenharn and M. E. Rose [13]). There it is shown that the gamma-gamma angular correlation for any spin sequence which allows one transi-

tion to be a mixture of dipole and quadrupole radiations with the mixture ratio δ is of the form

$$W(\theta) = 1+\frac{1}{1+\delta^2}(a_2+b_2\delta+c_2\delta^2)P_2(\cos\theta)+\frac{1}{1+\delta^2}c_4\delta^2 P_4(\cos\theta),$$

and tables are given from which the values of the coefficients a_2, b_2, c_2 and c_4 can be determined. Evidently $A_4(\delta)/A_4(\infty)$ is equal to $\delta^2/(1+\delta^2)$. Eliminating δ between the equations $A_2(\delta) = (a_2+b_2\delta+c_2\delta^2)(1+\delta^2)^{-1}$ and $A_4(\delta) = c_4\delta^2(1+\delta^2)^{-1}$ gives a biquadratic form in A_2 and A_4, which is therefore the equation of a conic. Since both A_2 and A_4 are bounded, the conic is an ellipse.

The ratio $[J_{\|}(\theta_0, \delta)-J_{\perp}(\theta_0, \delta)]/[J_{\|}(\theta_0, \delta)+J_{\perp}(\theta_0, \delta)]$ is given for the pure radiation by

$$\frac{\pm\{-(a_2+b_2\delta+c_2\delta^2)P_2^2(\cos\theta_0)+\frac{1}{6}c_4\delta^2 P_4^2(\cos\theta_0)\}}{2\{1+(a_2+b_2\delta+c_2\delta^2)P_2(\cos\theta_0)+c_4\delta^2 P_4(\cos\theta_0)\}}$$

and for the mixed radiation by

$$\frac{\pm\{-(a_2-\frac{1}{3}b_2\delta+c_2\delta^2)P_2^2(\cos\theta_0)+\frac{1}{6}c_4\delta^2 P_4^2(\cos\theta_0)\}}{2\{1+(a_2+b_2\delta+c_2\delta^2)P_2(\cos\theta_0)+c_4\delta^2 P_4(\cos\theta_0)\}}$$

where the plus and minus signs correspond to like and unlike parities for the states coupled by the gamma radiation of which the polarization is is observed.

The elliptical loci of constant probability associated with any particular experimental result in a parametric plot are not completely defined by the values of the R.M.S. deviations ΔA_2 and ΔA_4, since these are not in general statistically independent quantities. A_2 and A_4 are determined in a least squares calculation by equations of the form

$$A_k\sum_i A_{0i}W_{\exp}(\theta_i) = \sum_i A_{ki}W_{\exp}(\theta_i)$$

where the θ_i are the angles at which observations are made, the $W_{\exp}(\theta_i)$ are the observed values of $W(\theta)$ at these angles, and the A_{ki} are quantities which depend on geometrical functions of the angles θ_i, and on the weight factors associated with the various $W_{\exp}(\theta_i)$. Orthogonal combinations of A_2 and A_4 can be taken in the form $P = (1+k^2)^{-1}(A_2+kA_4)$ and $Q = (1+k^2)^{-1}(-kA_2+A_4)$. P and Q will be statistically independent if

$$\overline{[\mathrm{d}(P+Q)]^2} = \overline{[\mathrm{d}P]^2}+\overline{[\mathrm{d}Q]^2}.$$

Expressing this equation in terms of the statistically independent quantities $W_{\exp}(\theta_i)$, and taking account of this fact, one obtains the relation

$$\sum_i\{k(A_{2i}-A_2A_{0i})^2+(k^2-1)(A_{2i}-A_2A_{0i})(A_{4i}-A_4A_{0i})-k(A_{4i}-A_4A_{0i})^2\}$$
$$\times\overline{[\delta W_{\exp}(\theta_i)]^2} = 0.$$

This is a quadratic in k. From its roots the magnitudes and the directions of the major and minor semi-axes of the probability ellipse can now be determined. These directions will of course be altered in the final parametric plot, since the angular resolution correction factors applied to A_2 and A_4 are not equal.

References

1) W. H. Kelly and M. L. Wiedenbeck, Phys. Rev. **102** (1956) 1130
2) M. J. Glaubman, Phys. Rev. **98** (1955) 645
3) H. Frauenfelder, N. Levine, A. Rossi and Sidney Singer, Phys. Rev. **103** (1956) 352
4) R. C. Waddell and E. N. Jensen, Phys. Rev. **102** (1956) 816
5) R. M. Steffen, Bull. Amer. Phys. Soc. **29** (1954) 4, 26
6) J. N. Brazos and R. M. Steffen, Phys. Rev. **102** (1956) 753
7) C. F. Coleman, Phys. Rev. **103** (1956) 647
8) F. K. McGowan, Phys. Rev. **105** (1957) 1346
9) G. T. Wood and P. S. Jastram, Bull. Amer. Phys. Soc. **30** (1955) 1, 48
10) E. R. Bishop and J. P. Perez Y. Jorba, Phys. Rev. **98** (1955) 89
11) C. F. Coleman, Phil. Mag. **1** (1956) 166
12) F. Metzger and M. Deutsch, Phys. Rev. **78** (1950) 551
13) L. C. Biedenharn and M. E. Rose, Rev. Mod. Phys. **25** (1953) 729

Nuclear Physics **5** (1958) 504—511; © *North-Holland Publishing Co., Amsterdam*
Not to be reproduced by photoprint or microfilm without written permission from the publisher

ON THE CONSERVATION OF THE LEPTON NUMBER

MICHIJI KONUMA
Department of Physics, University of Tokyo

Received 23 September 1957

Abstract: The generalized conservation laws of the lepton numbers are derived from the requirement of invariance under the gauge transformation involving the γ_5 matrix. The lepton processes, especially π-μ-e decay and β decay, are systematized by means of the conservation law. For the β decay process the two component theory of the neutrino is naturally derived. However this is not so in the problem of the μ-e decay. Various characteristics of these and other lepton processes are discussed in detail.

1. Introduction

Some weak interactions associated with neutrinos are not invariant under space inversion or charge conjugation. Such a theory can be naturally formulated if we assume that the interactions are invariant under the gauge transformation involving γ_5 for the massless neutrino field together with the simultaneous gauge transformation of a suitable constant phase for the other lepton fields [1–4]). The invariance under the gauge transformation leads to the conservation law which says that the difference of numbers of particles and antiparticles is constant in time. These circumstances will be investigated in detail in section 2.

Let us first recall some known properties of the neutrino. If the neutrino is of the Majorana type [5, 6]), in which there is no distinction between neutrino and antineutrino, the lepton numbers will not be invariant in time. Recent experiments [7, 8]) on double beta decay indicate that the life times of Ca^{48}, Zr^{96} and Nd^{150} are longer than that expected from the Majorana type neutrino. This means that the following processes do not occur:

$$(Z) \rightarrow (Z \pm 2) + 2e^{\mp} \quad \text{(no)}, \tag{1}$$

where (Z) means the nucleus with the atomic number Z. Two experiments on the inverse beta reaction have also been performed by using the intense neutrino flux from the beta decay of neutrons in a large nuclear reactor:

$$n \rightarrow p + e^- + \tilde{\nu}. \tag{2}$$

First, the irradiated proton has given rise to emission of a positon [9]):

$$\tilde{\nu} + p \rightarrow n + e^+ \quad \text{(yes)}. \tag{3}$$

Secondly, the irradiated Cl^{37} has not given rise to emission of a negaton [10]):

$$\bar{\nu}+\mathrm{Cl}^{37} \to \mathrm{A}^{37}+\mathrm{e}^{-} \quad (\text{no}). \tag{4}$$

These experiments imply that the neutrino emitted with the positon is distinguishable from that emitted with the negaton.

In section 2, we shall introduce two conservation laws; one is related to the number of particles and its charge conjugate particles, and the other to the number of particles classified according to their circular polarization states. Any one of these conservation laws can forbid the processes (1) and (4) by keeping the process (3) allowed. We apply these conservation laws to systematize the lepton processes.

2. Gauge Transformation and Conservation Laws

It is well known that among the conservation laws in physics all those referring to numbers of particles are related to the invariance of the Lagrangian under gauge transformations under which the wave functions of the particles change their phases.

The free neutrino equation is invariant under the following transformations:

$$\begin{aligned}
&\psi \to \mathrm{e}^{ia\gamma_5+ib}\psi = \varrho(\alpha\Lambda_1+\alpha^*\Lambda_2)\psi \\
&\bar{\psi} \to \bar{\psi}\mathrm{e}^{ia\gamma_5-ib} = \bar{\psi}(\alpha^*\Lambda_2+\alpha\Lambda_1)\varrho^* \\
&\psi^{\mathrm{c}} \to \mathrm{e}^{ia\gamma_5-ib}\psi^{\mathrm{c}} = \varrho^*(\alpha^*\Lambda_2+\alpha\Lambda_1)\psi^{\mathrm{c}} \\
&\overline{\psi^{\mathrm{c}}} \to \overline{\psi^{\mathrm{c}}}\,\mathrm{e}^{ia\gamma_5+ib} = \overline{\psi^{\mathrm{c}}}(\alpha\Lambda_1+\alpha^*\Lambda_2)\varrho,
\end{aligned} \tag{5}$$

where $\psi^{\mathrm{c}} = C^{-1}\bar{\psi}^{\mathrm{T}}$ is the charge conjugate solution, a and b are real parameters, $\varrho \equiv \exp(ib)$ and $\alpha \equiv \exp(ia)$. The operators

$$\Lambda_1 \equiv \tfrac{1}{2}(1+\gamma_5), \qquad \Lambda_2 \equiv \tfrac{1}{2}(1-\gamma_5) \tag{6}$$

are the projection operators onto the l- and d- state, respectively [11]).

Suppose that the Lagrangian is invariant under the phase transformations (5) of the neutrino field together with the simultaneous constant phase transformation of all the other lepton fields

$$\psi_j \to \mathrm{e}^{-i\varepsilon_j a+ib}\psi_j \quad (\varepsilon_j = \pm 1). \tag{7}$$

Then eq. (5) says that the phase change of the l-state in the gauge transformation is different from that of the d-state. It will therefore be convenient to treat the d- and l-states separately. Let us introduce

$$U_i^{\pm} \equiv \Lambda_i U^{\pm}(k) \quad (i = 1, 2), \tag{8}$$

where $U^{+}(k)[U^{-}(k)]$ corresponds to the $+(-)$ frequency part of neutrino field ψ, and is the annihilation (creation) operator.

The operators U_1^{+} and U_2^{+} are the l- and d-particle annihilation operator, respectively. The state $(0|U_1^{+}$ and $U_1^{*-}|0)$ $[(0|U_2^{+}$ and $U_2^{*-}|0)]$ represent,

therefore, l- [d-]particle states, when $|0)$ and $(0|$ denote the vacuum state. The hermitian conjugates U_1^{*-} and U_2^{*-} are, thus, l- and d-particle creation operators. As U_1^{*-} corresponds to the adjoint $\bar{U}_1^{-}$, i.e. to the charge conjugate operator U_1^{c-}, U_1^{c-} [U_2^{c-}] is an l-[d-]particle creation operator. Here,

$$\begin{aligned} \bar{U}_1 &= U_1^* \gamma_4 = \bar{U} \Lambda_2 \equiv (\bar{U})_2, \\ U_1^c &= C^{-1} \bar{U}_1^{\mathrm{T}} = C^{-1} \Lambda_2^{\mathrm{T}} C C^{-1} \bar{U}^{\mathrm{T}} = \Lambda_2 U^c \equiv (U^c)_2. \end{aligned} \tag{9}$$

The states $(0|U_1^{c+}$ and $(0|U_2^{c+}$ are the charge conjugates of $(0|U_1^{+}$ and $(0|U_2^{+}$, and their polarizations are known to be d- and l-state, respectively. [cf. eqs. (5) and (9).] Let us call these states d- and l-antiparticle. Since $(0|U_1^{*+}$ is the same state as $(0|U_1^{c+}$ and is equivalent to $U_1^{-}|0)$, U_1^{-} and U_2^{-} are d- and l-antiparticle creation operators. Such a consideration leads us to table 1.

TABLE 1

l-particle l	d-antiparticle $\tilde{\mathrm{d}}$	d-particle d	l-antiparticle $\tilde{\mathrm{l}}$
U_1^{+}	U_1^{-}	U_2^{+}	U_2^{-}
U_1^{*-}	U_1^{*+}	U_2^{*-}	U_2^{*+}
$\bar{U}_1^{-}$	$\bar{U}_1^{+}$	$\bar{U}_2^{-}$	$\bar{U}_2^{+}$
U_1^{c-}	U_1^{c+}	U_2^{c-}	U_2^{c+}
U_1^{c*+}	U_1^{c*-}	U_2^{c*+}	U_2^{c*-}
$\bar{U}_1^{c+}$	$\bar{U}_1^{c-}$	$\bar{U}_2^{c+}$	$\bar{U}_2^{c-}$

In this table, + (—) frequency part corresponds to annihilation (creation) operator.

In the usual way we can define the number operators for l- and d-particle and antiparticle

$$\begin{aligned} N(\mathrm{l}) &= U_1^{*-} U_1^{+} \\ N(\tilde{\mathrm{d}}) &= U_1^{-} U_1^{*+} \\ N(\mathrm{d}) &= U_2^{*-} U_2^{+} \\ N(\tilde{\mathrm{l}}) &= U_2^{-} U_2^{*+} \end{aligned} \tag{10}$$

and their eigenvalues $n(\mathrm{l})$, $n(\tilde{\mathrm{d}})$, $n(\mathrm{d})$ and $n(\tilde{\mathrm{l}})$ respectively. Taking a and b infinitesimal in (5) and (7), one gets the conservation laws of the lepton numbers

$$n(\mathrm{l}) - n(\tilde{\mathrm{d}}) + \textstyle\sum_{(\varepsilon_j=-1)} \{n(\mathrm{L}_j) - n(\tilde{\mathrm{L}}_j)\} = \text{const.} \tag{11a}$$

and

$$n(\mathrm{d}) - n(\tilde{\mathrm{l}}) + \textstyle\sum_{(\varepsilon_j=+1)} \{n(\mathrm{L}_j) - n(\tilde{\mathrm{L}}_j)\} = \text{const.} \tag{11b}$$

where $n(\mathrm{L}_j)$ and $n(\tilde{\mathrm{L}}_j)$ denote the numbers of particles and antiparticles for the j-th lepton field. If $a \equiv 0$, we have

$$\{n(\mathrm{l}) + n(\mathrm{d})\} - \{n(\tilde{\mathrm{d}}) + n(\tilde{\mathrm{l}})\} + \textstyle\sum \{n(\mathrm{L}_j) - n(\tilde{\mathrm{L}}_j)\} = \text{const.}, \tag{12}$$

and if $b \equiv 0$, we have

$$\{n(\mathrm{d})+n(\tilde{\mathrm{d}})\}-\{n(\tilde{\mathrm{l}})+n(\mathrm{l})\}+\sum\varepsilon_j\{n(\mathrm{L}_j)-n(\tilde{\mathrm{L}}_j)\} = \text{const.} \qquad (13)$$

It is clear that in the case of $a \equiv 0$, ψ and its charge conjugate ψ^c are in the relation of particle to antiparticle, and so are the l- and d- states in the case of $b = 0$. When eqs. (11a) and (11b) hold, the antiparticle of an l- (d-) state is a $\tilde{\mathrm{d}}$- ($\tilde{\mathrm{l}}$-) state. These conclusions about the circular polarization are consistent with those of the two component neutrino theory [12]).

3. On the Processes Associated with One Neutrino

When the theory is invariant under the gauge transformation containing γ_5 for the neutrino field, l- and d- state neutrinos do not appear simultaneously in any process associated with one neutrino. This is proved as follows [1]). The interactions are built up of products of terms of the form

$$\bar{\psi}_j\gamma_A(A\Lambda_1+B\Lambda_2)\psi_\nu, \qquad (14)$$

where ψ_j is the wave function of the j-th lepton, and A and B are complex numbers. The term (14) can be invariant under the transformation (5) and (7) with $a \neq 0$, only if $A = 0$ or $B = 0$.

Therefore, even if the neutrino field itself has four components, only two components can contribute to the interaction in these processes. The j-th lepton selects to interact with two components of neutrino field according to the sign of the constant ε_j, and in this way interacts with the same two components of the neutrino field irrespective of the interaction type.

With regard to β-decay, the experiment with $Co^{60}(5+ \to 4+)$ can be interpreted by supposing that the negaton emission is associated with a l-antineutrino [13]). Therefore,

$$\varepsilon_j = +1 \qquad \text{for the electron field.} \qquad (15)$$

From the identities

$$\bar{\psi}_j\Lambda_1\gamma_A\Lambda_2\psi_\nu = 0 \quad \text{for S.T.P. interactions}$$

and (16)

$$\bar{\psi}_j\Lambda_2\gamma_A\Lambda_2\psi_\nu = 0 \quad \text{for V.A. interactions,}$$

we see that the polarization of the negaton in β-decay is a d-state if the interaction is V.A. and an l-state if the interaction is S.T.P. The situation is reversed for the polarization of the positon. Of course, both polarizations can be mixed together, if both S.T.P. and V.A. interactions exist simultaneously in nature. In the experiment with $Co^{58}(2+ \to 2+)$, the positon favours the same direction as the spin of the nucleus. This can be understood from the Gamow-Teller interaction, the positon being accompanied with the d-neutrino; this is consistent with our result.

As shown in the previous section, if $b \equiv 0$ in eq. (5), we have the conservation law (13). Then, the l-neutrino and the l-antineutrino can be emitted simultaneously with a negaton:

$$n \to \begin{cases} p+e^-+\tilde{\nu}(l) \\ p+e^-+\nu(l) \end{cases}. \tag{17}$$

However, this does not cause any double β decay process without neutrino (eq. (1)).

In the other processes associated with one neutrino, such as $\pi-\mu$ decay, internal bremsstrahlung, μ capture process and K-electron capture, it is very interesting to measure directly the sign of the polarization. This is because the conservation law of lepton number can be established only when the signs of the polarization are known to be compatible with each other.

4. On the Process Associated with Two Neutrinos

Muon decay is a process associated with two neutrinos. Let us take the interaction Lagrangian as follows:

$$L^{(A)}(\bar{e}\mu\tilde{\nu}\nu) \equiv (\bar{\psi}_e \gamma_A \psi_\mu)(\bar{\psi}_\nu(f_A+\gamma_5 f'_A)\gamma_A \psi_\nu). \tag{18}$$

Four fermions can be arranged in different orders according to the same rule as in the case of usual parity-conserving interactions. For, from the matrix relation [14])

$$\begin{aligned} \gamma_{A\rho\beta}\{(f_A+\gamma_5 f'_A)\gamma_A\}_{\alpha\sigma} &= \tfrac{1}{4}\textstyle\sum_B \gamma_{B\rho\sigma}\{(f_A+\gamma_5 f'_A)\gamma_A\gamma_B\gamma_A\}_{\alpha\beta} \\ &= \textstyle\sum_B a^{(AB)} \gamma_{B\rho\sigma}\{(f_A+\gamma_5 f'_A)\gamma_B\}_{\alpha\beta}, \end{aligned} \tag{19}$$

we have

$$L^{(A)}(\bar{e}\mu\tilde{\nu}\nu) = \textstyle\sum a^{(AB)} L^{(B)}(\bar{e}\nu\tilde{\nu}\mu), \tag{20}$$

where

$$a^{(AB)} = \begin{pmatrix} \frac{1}{4} & \frac{1}{4} & \frac{1}{4} & \frac{1}{4} & \frac{1}{4} \\ 1 & -\frac{1}{2} & 0 & \frac{1}{2} & -1 \\ \frac{3}{2} & 0 & -\frac{1}{2} & 0 & \frac{3}{2} \\ 1 & \frac{1}{2} & 0 & -\frac{1}{2} & -1 \\ \frac{1}{4} & -\frac{1}{4} & \frac{1}{4} & -\frac{1}{4} & \frac{1}{4} \end{pmatrix}. \tag{20a}$$

Considering the conservation laws (11a, b), one finds the following processes as allowed ones.

In the case of μ^- = particle,

for $\varepsilon_j = 1$ $$\pi^- \to \mu^- + \tilde{\nu}(l) \tag{21a}$$

$$\mu^- \to \begin{cases} e^- + \nu(d) + \tilde{\nu}(l) \\ e^- + \nu(l) + \tilde{\nu}(d), \end{cases} \tag{21b}$$

for $\varepsilon_j = -1$,
$$\pi^- \to \mu^- + \bar{\nu}(\mathrm{d}) \tag{22a}$$
$$\mu^- \to \mathrm{e}^- + \nu(\mathrm{l}) + \bar{\nu}(\mathrm{l}). \tag{22b}$$

In the case of μ^- = antiparticle,

for $\varepsilon_j = +1$,
$$\pi^- \to \mu^- + \nu(\mathrm{d}) \tag{23a}$$
$$\mu^- \to \mathrm{e}^- + \bar{\nu}(\mathrm{l}) + \bar{\nu}(\mathrm{l}), \tag{23b}$$

for $\varepsilon_j = -1$,
$$\pi^- \to \mu^- + \nu(\mathrm{l}) \tag{24a}$$
$$\mu^- \to \mathrm{e}^- + \bar{\nu}(\mathrm{d}) + \bar{\nu}(\mathrm{l}). \tag{24b}$$

From eqs. (16), it is clear that for the muon decay S.T.P. types of interaction give rise the same polarization of two neutrinos and V.A. types to opposite polarizations of the two neutrinos.

The Michel parameter [15]) is

$$\varrho = 3/4 \qquad \text{for (21b), (24b),}$$
$$\varrho = 0 \qquad \text{for (23b),}$$
$$\varrho = \frac{6T^2}{S^2+P^2+bT^2} \quad \text{for (22b),}$$

where $S^2 \equiv |f_s|^2 + |f'_s|^2$ etc.

This parameter ϱ is experimentally known to be somewhat smaller than 3/4. Thus, the case (23a, b) may be ruled out. As the direct measurement of μ polarization is as yet unavailable, we have no reason to choose any one of (21), (22) and (24) †.

If $a \equiv 0$, (21), (22) and
$$\mu^- \to \mathrm{e}^- + \nu(\mathrm{d}) + \bar{\nu}(\mathrm{d}) \tag{25}$$
can occur together for μ^- = particle, and (23), (24) and
$$\mu^- \to \mathrm{e}^- + \bar{\nu}(\mathrm{d}) + \bar{\nu}(\mathrm{d}) \tag{26}$$
for μ^- = antiparticle. If $b \equiv 0$, (21), (24) and
$$\mu^- \to \mathrm{e}^- + \nu(\mathrm{d}) + \nu(\mathrm{l}) \tag{27}$$
can take place together for μ^- = particle with $\varepsilon_j = 1$ and for μ^- = antiparticle with $\varepsilon_j = -1$. In this case $\varrho = 3/4$.

The invariance of eq. (18) under the gauge transformation leads to
$$\begin{aligned} f'_i/f_i &= \pm 1 \quad \text{for S.T.P. interaction} \\ &= a_i \text{ (any complex number) for V.A. interaction.} \end{aligned} \tag{28}$$

If a_i has an imaginary part, time reversal invariance is violated. Even if

† *Note added in proof:* The angular distribution of e^+ is incompatible with the cases (22) and (23).

a_i is real, if the phases of f_i and f_j are different, T invariance may be violated.

In the process (21b), the normalized electron spectrum is given by

$$dN(x, \theta) = \frac{x^2}{2\pi}[6(1-x)+\tfrac{4}{3}\varrho(4x-3)+\xi'\zeta\cos\theta(1-2x)]dxd\Omega_e \qquad (29)$$

where the mass of the electron is neglected and $\zeta(-1 \leqq \zeta \leqq 1)$ is the degree of polarization of the muon, which depends on the characteristics of the $\pi-\mu$ decay,

$$\xi' = \frac{2\,\mathrm{Re}\,(a_V f_V f_A^* + a_A f_A f_V^*)}{(1+|a_V|^2)|f_V|^2+(1+|a_A|^2)|f_A|^2} \qquad (30)$$

and other notations are the same as those of Lee and Yang [12]). The larger the imaginary part of a_i, the smaller the asymmetry part. In order to determine the value a_i, we need to measure the spectrum (29) or the degree of longitudinal polarization of the electron together with the polarization of the muon.

5. Concluding Remarks

We have classified the lepton processes, such as β and π-μ-e decay, by making use of the conservation laws of lepton numbers derived from the requirement of invariance under gauge transformation. As a result, the two component theory of the neutrino can be rather naturally derived for the β decay process. However, the situation is not so simple in the problem of μ-e decay. We want a refinement of the experimental results, especially independent measurements of the degrees of polarization of the muon and the electron.

There are still some questions left open:

(i) to extend our discussion to the other lepton processes,
(ii) to forbid, absolutely or relatively, unobserved processes,
(iii) to look for any possible treatment of the hyperon-K-meson problem by our method which succeeded in the lepton problem.

As an example of the second problem, we wish to note that the process

$$\mu^- + p \to p + e^- \qquad (31)$$

is absolutely forbidden if the muon is of the type assumed in eq. (22) or (24). Future analysis will determine whether this choice of muon types is consistent with the polarization or not. In contrast to this situation, there is no room left in the two component neutrino theory to forbid the process (31). There has been a theory of Konopinski and Mahmoud [16]), in which process (31) was forbidden. However, as this theory leads us to the conclusion that the two neutrinos in μ-decay are identical, experiments on the μ-e decay do not support this theory.

The author would like to express his sincere thanks to Professor H. Umezawa for stimulating and helpful discussions.

References

1) H. Umezawa and A. Visconti, Nuclear Physics **4** (1957) 224
2) W. Pauli, Nuovo Cimento **6** (1957) 204
3) B. F. Touschek, Nuovo Cimento **5** (1957) 754; 1281
4) K. Nishijima, Nuovo Cimento **5** (1957) 1349
5) E. Majorana, Nuovo Cimento **14** (1937) 171
6) S. Sakata, Soryushiron Kenkyu (mimeographical circular in Japanese) **7** (1955) 923
7) M. Awschalom, Bull. Amer. Phys. Soc. **1** (1956) 31
8) C. L. Cowan, Jr. and F. B. Harrison, L. M. Langer and F. Reines, Nuovo Cimento **3** (1956) 649
C. L. Cowan, Jr. and F. Reines, Phys. Rev. **106** (1957) 825
9) C. L. Cowan, Jr., F. Reines, F. B. Harrison, H. W. Kruse and A. D. McGuier, Science **124** (1956) 103
10) R. Davis, Bull. Amer. Phys. Soc. **1** (1956) 219
11) V. Bargmann and E. P. Wigner, Proceedings Nat. Acad. Sci. **34** (1948) 211
12) T. D. Lee and C. N. Yang, Phys. Rev. **105** (1957) 1671;
L. Landau, Nuclear Physics **3** (1957) 127
13) Wu, Ambler, Hayward, Hoppes and Hudson, Phys. Rev. **105** (1957) 1413;
Ambler, Hayward, Hoppes, Hudson and Wu, Phys. Rev. **106** (1957) 1361
14) K. M. Case, Phys. Rev. **97** (1955) 810
15) L. Michel, Proc. Phys. Soc. A **63** (1950) 514;
C. Bouchiat and L. Michel, Phys. Rev. **106** (1957) 170
16) E. J. Konopinski and H. M. Mahmoud, Phys. Rev. **92** (1953) 1045

Note added in proof: The conservation laws (11a) and (11b) are equivalent to the laws (12) and (13). Eq. (12) is the ordinary conservation law of the lepton number and eq. (13) is the conservation law of the neutrino charge defined in ref. [1]).

We have investigated how far these conservation laws were supported by experiments. It has been recently reported that the parity is not conserved under the hyperon decay processes. Considering these weak interactions in common with the lepton processes, we are forced to assign an intrinsic neutrino charge to heavy particles. Then, in contrast to the situation discussed in this article, we may assume that the parity is conserved in any process in which the neutrino charge is conserved, and that the neutrino charge changes by a constant in any process due to weak interactions. These two standpoints will be distinguishable e.g. by means of experiments on polarization and angular distribution in processes involving weak interactions and on the types of beta decay interactions.

See further papers by M. Konuma, S. Nakamura and H. Umezawa, to be published in Phys. Rev. and Nuclear Physics.

Nuclear Physics **5** (1958) 512—529; © *North-Holland Publishing Co., Amsterdam*
Not to be reproduced by photoprint or microfilm without written permission from the publisher

BETA-GAMMA CORRELATION AND POLARIZATION OF PARTICLES IN THE BETA DECAY OF ORIENTED NUCLEI IN CONNECTION WITH PARITY NON-CONSERVATION

A. Z. DOLGINOV
Physico-Technical Institute of the USSR Academy of Sciences, Leningrad

Received 3 June 1957

Abstract: A formula for the angular distribution and polarization of β-particles emitted by polarized or aligned nuclei is derived; the formula is valid for β-transitions of any order of forbiddenness. The investigation is carried out for β-interaction of a general form with possible parity non-conservation being taken into account. The $\beta-\gamma$ angular and polarization correlation is determined. As a way of clarifying the problem of invariance of the theory under time reversal it is suggested that $\beta-\gamma$ correlation in allowed transitions of aligned nuclei be studied. It is taken into account in the calculations that the field inside the nucleus differs from that of a point charge.

1. General Considerations

It has been suggested [1,2]) that the law of conservation of parity is violated in weak interactions and, in particular, in β interaction. Experiments have been performed [3,4]) which apparently support this hypothesis. However, the experiments are not sufficient to permit one to ascertain whether invariance of theory with respect to time reversal is also violated and this is also a problem of vital importance. Another important problem pertains to the possibility of describing the neutrino by a two-component equation [2,5]). Finally, the problem of the exact determination of the β interaction constants also remains to be solved. In connection with the foregoing it seemed desirable to carry out a general investigation of the angular and polarization distribution of particles in β decay.

Beta particles emitted by polarized nuclei should be polarized even if parity is conserved. This case has been considered in ref. [6]). Non-conservation of parity leads to an anisotropic angular distribution of β particles emitted by polarized nuclei [1]). A relevant analysis [1,6]) has been carried out only for allowed transitions. In the present paper we derive the angular distribution and polarization of β particles for transitions of an arbitrary degree of forbiddenness.

We shall also consider $\beta-\gamma$ correlation for oriented nuclei. The β interaction will be expressed as a linear combination of five invariants, and any possible parity non-conservation will be taken into account.

The nuclear Coulomb field and deviation of this field, inside the nucleus, from the field of a point charge will also be taken into account. The polarization state of the nucleus will be determined by prescribing the polarization tensors. Polarization of the dipole moment is defined by a vector, polarization of the quadrupole moment by a second rank tensor, etc.

If the β transition is immediately followed by a radiative transition of the nucleus it should be possible to determine the nuclear polarization tensor (or vector) after a β decay by observing the angular distribution (or polarization) of the gamma quanta. The tensor should depend on the initial state, nature of the β transition and, especially, on possible parity non-conservation. We shall show that in allowed transitions $\beta-\gamma$ angular correlation should be observed for oriented nuclei. Observation of $\beta-\gamma$ correlation for aligned nuclei seems to be a feasible method for obtaining direct information on invariance of the theory with respect to time reversal and for clarifying the question concerning the contribution of vector and pseudo-vector interactions.

The general form of β interaction with account of parity non-conservation will be chosen following Lee and Yang [1]). The matrix element for the β transition can be written in the form

$$H_\beta = \sum_{m,n} \int (\Psi_f^* \hat{a}_{mn} \Psi_i)(\psi_p^* \hat{a}_{mn}(g_m + G_m \gamma_5)\psi_q) d\mathbf{r}$$

$$m = 1, 2, \ldots, 5;\ n = 1, 2;\ \hat{a}_{11} = \beta,\ \hat{a}_{21} = 1,\ \hat{a}_{22} = i\boldsymbol{\alpha},$$

$$\hat{a}_{31} = \beta\boldsymbol{\sigma},\ \hat{a}_{32} = \beta\boldsymbol{\alpha},\ \hat{a}_{41} = \boldsymbol{\sigma},\ \hat{a}_{42} = i\gamma_5,$$

$$\hat{a}_{52} = \beta\gamma_5,\ \hat{a}_{12} = \hat{a}_{51} = 0,\ \gamma_4 = -\beta;$$

β, $\boldsymbol{\alpha}$, $\boldsymbol{\sigma}$ and γ_5 are Dirac matrices; $\gamma_5 = \gamma_1\gamma_2\gamma_3\gamma_4$.

If g_S, g_T etc. denote the β interaction constants for scalar, tensor, etc., theory and G_S, G_T, etc. denote the similar constants in terms encountered only in the case of parity non-conservation (that is, which contain an extra γ_5) then $g_1 = g_S$, $g_2 = g_V$, $g_3 = g_T$, $g_4 = g_A$, $g_5 = g_P$, and similarly for G_m. Ψ_i and Ψ_f are the nuclear wave functions in the initial and final states, ψ_p and ψ_q are the electron and neutrino wave functions. The wave function of an electron in the field of a nucleus which has a momentum $\mathbf{p}(p, \vartheta_e, \varphi_e)$ at infinity and has the asymptotic form of a plane and converging spherical waves can be written as

$$\psi_p^{(-)} = \sum_{j,\mu,\varrho,\lambda} i^{-l}(-1)^{j+\mu}\sqrt{(2l+1)/4\pi}\, C^{j\varrho}_{\frac{1}{2}\varrho l0} \times D^j_{-\mu\varrho}(\varphi_e, \vartheta_e, 0) v_\varrho(0) \psi_{j\mu\lambda}(\mathbf{r}) e^{-i\Delta_{jl}} \tag{2}$$

where $C^{j\varrho}_{\frac{1}{2}\varrho l0}$ are Clebsch-Gordan coefficients and $D^j_{-\mu\varrho}(\varphi_e, \vartheta_e, 0)$ is the familiar [7]) matrix of the irreducible rotation group representation. It is defined here in such a manner that

$$\psi_{j\mu}(\vartheta, \varphi) = \sum_{\mu'} D^{j}_{\mu\mu'}(\varphi, \vartheta, 0)\psi_{j\mu'}(0, 0) \tag{3}$$

and in particular $Y_{lm}(\vartheta\varphi) = \sqrt{(2l+1)/4\pi}\, D^{l}_{m0}(\varphi\vartheta 0)$. The spherical function Y_{lm} is chosen in accord with ref. [8]) and differs by $(-1)^m$ from that defined in ref. [9]). $v_\varrho(0)$ is a spinor which determines the electron polarization and is taken in a coordinate system in which the z axis is directed along $\mathbf{p}$. Its components ($\varrho = \mp\frac{1}{2}$) can be written in the form

$$v_{-\frac{1}{2}}(0) = \cos\frac{\chi}{2}\, e^{-i\frac{\omega}{2}}, \quad v_{\frac{1}{2}}(0) = \sin\frac{\chi}{2}\, e^{i\frac{\omega}{2}}. \tag{4}$$

The direction of the electron spin in a system in which the electron is at rest is given by the vector [10])

$$\zeta^0 = \left(\frac{2E}{E+1}\right)\psi^* \frac{1-\beta}{2}\,\sigma\psi, \tag{5}$$

$$\zeta_z^{\,0} = \cos\chi, \quad \zeta_x^{\,0} = \sin\chi\cos\omega, \quad \zeta_y^{\,0} = \sin\chi\sin\omega.$$

E is the electron energy, including the rest mass. The unit system employed is that in which $\hbar = c = m = 1$.

If the probability of detecting an electron in a state with a vector $\zeta^0(\chi, \omega)$ is known and equals $W(\chi, \omega)$, the mean values of the projections of this vector on the coordinate axes ($Oz||\mathbf{p}$) will be

$$\overline{\zeta_k^{\,0}} = [W_k - W_{-k}]/[W_k + W_{-k}], \tag{6}$$

with

$$k \to x, y, z; \quad W_z = W(0, 0), \quad W_{-z} = W(\pi, 0) \quad \text{etc.}$$

The polarization state of a relativistic electron is determined by the density matrix

$$\varrho = \tfrac{1}{2}(1 + i\gamma_5\hat{\zeta})\frac{1-i\hat{p}}{2E}\gamma_4 \tag{7}$$

where $\hat{p} = \gamma_\mu p_\mu$, $\hat{\zeta} = \gamma_\mu \zeta_\mu$, ζ is a four-dimensional vector which possesses the property that $\zeta_\mu p_\mu = 0$; it is uniquely defined by prescribing $\overline{\zeta_0}$:

$$\zeta = \overline{\zeta^0}_{\perp} + E\overline{\zeta^0}_{||}; \tag{8}$$

$\overline{\zeta^0}_{||}$ and $\overline{\zeta^0}_{\perp}$ are, respectively, the components of the vector $\overline{\zeta^0}$ directed along $\mathbf{p}$ and perpendicular to $\mathbf{p}$.

Let $\psi_{j\mu\lambda}(\mathbf{r})$ be a bispinor electron wave function with definite total angular momentum j, projection of the latter μ and orbital moment $l = j + \lambda$, $\lambda = \pm\frac{1}{2}$:

$$\psi_{j\mu\lambda}(\mathbf{r}) = \begin{pmatrix} -iF_{j\lambda}(r)\,\hat{Y}^{-\lambda}_{j\mu}(\vartheta\varphi) \\ G_{j\lambda}(r)\,\hat{Y}^{\lambda}_{j\mu}(\vartheta\varphi) \end{pmatrix}; \tag{9}$$

$G_{j\lambda}$ is the large and $F_{j\lambda}$ the small radial components of the electron wave

function in the field of the nucleus, $\hat{Y}^{\lambda}_{j\mu}$ is a spherical spinor whose components are those of the $(J-L)$ vector [11]) for $J=\frac{1}{2}$:

$$[Y^{J\tau}_{LA}(\vartheta,\varphi)]_{\gamma}=(-1)^{J-\gamma}C^{LA}_{L+\tau,A+\gamma;\,J,-\gamma}\,Y_{L+\tau,A+\gamma}(\vartheta\varphi). \tag{10}$$

On substitution of the wave functions of light particles in matrix element (1) quantities of the form $(\hat{Y}^{\lambda *}_{j\mu}(\vartheta\varphi)\hat{O}_{J\gamma}\hat{Y}^{\nu}_{in}(\vartheta,\varphi))$ will enter the matrix. Here

$$\hat{O}_{00}=1,\ \hat{O}_{1\gamma}=\sigma_{\gamma},\ \sigma_0=\sigma_z,\ \sigma_{\pm1}=\pm\sqrt{\tfrac{1}{2}}(\sigma_x\pm i\sigma_y);$$

$\sigma_x,\sigma_y,\sigma_z$ are Pauli matrices. The calculation yields

$$(\hat{Y}^{\lambda *}_{j\mu}\hat{O}_{J\gamma}\hat{Y}^{\nu}_{in})=\sum_{L,\tau}\beta^{jiL}_{\lambda\nu\tau}C^{j\mu}_{LAin}(-1)^{J+\tau+A}[Y^{J\tau}_{L-A}]_{\gamma}, \tag{11}$$

$$\beta^{jiL}_{\lambda\nu\tau}=\sqrt{(2J+1)(2L+1)(2f+1)(2l_1+1)(2i+1)/2\pi}\,C^{l0}_{l_1\,0/0}\,X(ll_1f,\,jiL,\,\tfrac{1}{2}\,\tfrac{1}{2}J), \tag{12}$$

where

$$l=j+\lambda,\qquad l_1=i+\nu,\qquad f=L+\tau,$$

and $X(abc,\,def,\,ghi)$ are Fano functions.

The X-function does not change on cyclic permutation of its three arguments. It has been tabulated in ref. [12, 13]). One has

$$\begin{aligned}&X(abc,\,def,\,ghi)=X(adg,\,beh,\,cfi)=X(def,\,ghi,\,abc)\\&X(abc,\,dec,\,gg0)=W(gdbc;\,ae)/\sqrt{(2g+1)(2c+1)}.\end{aligned} \tag{13}$$

Since the matrix element is only different from zero in the vicinity of the nucleus, $F^{(i)}_{j\lambda}(r)$ and $G^{(i)}_{j\lambda}(r)$ must be known in this region.

If the potential inside the nucleus is constant,

$$\begin{aligned}&F^{(i)}_{j\lambda}=n_-A_{j\lambda}f_{j-\lambda}(\varkappa r),\qquad G^{(i)}_{j\lambda}=2\lambda n+A_{j\lambda}f_{j+\lambda}(\varkappa r)\\&n_{\pm}=-\sqrt{\varkappa(W\pm1)/\pi},\qquad f_l(\varkappa r)=\sqrt{\pi/2\varkappa r}\,J_{l+\frac{1}{2}}(\varkappa r)\\&W=E+V,\quad V=\alpha Z/R,\quad \varkappa^2=W^2-1,\quad \alpha=1/137.\end{aligned} \tag{14}$$

$A_{j\lambda}$ is a coefficient which is determined from the condition of smooth fitting of the radial parts of the wave function inside and outside the nucleus.

In a Coulomb field $\Delta_{j\lambda}$ yields a phase shift. The explicit form of $\Delta_{j\lambda}$ and $A_{j\lambda}$ is presented in ref. [14, 15]) and in the tables in ref. [16]). The values of $a_{j\lambda}\equiv\sqrt{W-2\lambda}\,\varkappa^j A_{j\lambda}/(2j)!!$ are given in ref. [16]). In ref. [16]) the phase shifts $\Delta_{j\lambda}$ were denoted as $\delta_{j\lambda}$. For the case of a uniform space charge distribution the corresponding $\Delta_{j\lambda}$, $A_{j\lambda}$ and $W=E+3\alpha Z/2R$ should be taken from ref. [16]). Account of the fact that in this case $\sqrt{2\varkappa r/\pi}f_l(\varkappa r)$ is not a Bessel function yields only a small correction [15, 16]).

For the wave function of a neutrino with momentum $\mathbf{q}(q,\vartheta_{\nu},\varphi_{\nu})$ we also choose a function of the same form as (2). The neutrino angular momenta will be denoted as i and $l_1=i+\nu$, $\nu=\pm\frac{1}{2}$ and their projections by n and m_1. The radial parts of the wave function $F_{i\nu}(-qr)$ and $G_{i\nu}(-qr)$ can be

represented in a form similar to (14) by substituting $-q$ for $\varkappa$ and $q/\sqrt{\pi}$ for $n_{\pm} A_{j\lambda}$. The initial state of the nucleus will be given by the tensor $P^{j_0}_{\sigma\eta}$ which is related to the density matrix $\varrho(\mu_0, \mu'_0)$ by the equation

$$P^{j_0}_{\sigma\eta} = \frac{2g+1}{2j_0+1} \sum_{\mu_0, \mu'_0} C^{j_0 \mu'_0}_{j_0 \mu_0 \sigma\eta} \varrho(\mu_0, \mu'_0); \tag{15}$$

μ_0 is the projection of the nuclear spin j_0 on the quantization axis. If a physically preferred axis of predominant nuclear spin orientation is chosen as the quantization axis (say the direction of an external orienting field) then only the diagonal elements $\varrho(\mu_0, \mu'_0)$ will not vanish and the nuclear orientation will be given by the expression

$$P^{j_0}_{\sigma 0} = \frac{2g+1}{2j_0+1} \sum_{\mu_0} C^{j_0 \mu_0}_{j_0 \mu_0 \sigma 0} W(\mu_0); \tag{16}$$

$W(\mu_0)$ is the probability of finding a nucleus in a state with a projection μ_0 on the z axis. As wave function of the initial state of the system we take

$$\Psi_1 = \sum_{\mu_0} a^{\xi}_{\mu_0} \psi_{j_0 \mu_0},$$

where $\varrho(\mu_0, \mu'_0) = \langle a^{\xi *}_{\mu_0} a^{\xi}_{\mu'_0} \rangle_{\xi}$ and $\langle\ \rangle_{\xi}$ denotes averaging over elements of the statistical ensemble;

$$W(\mu_0) = \langle |a^{\xi}_{\mu_0}|^2 \rangle_{\xi}, \quad \sum_{\mu_0} W(\mu_0) = 1.$$

The nature of the nuclear orientation after a β transition can be determined by observing the angular distribution and polarization of the subsequent γ radiation. In order to apply (1) to the analysis of $\beta-\gamma$ correlation we insert into it $\Psi_f = \sum a_{\mu_1} \psi_{j_1 \mu_1}$, where j_1 and μ_1 are respectively the nuclear moments after β decay and its projection, and a_{μ_1} includes the radiative transition amplitude:

$$a_{\mu_1} a^*_{\mu'_1} = \sum_S C^{j_1 \mu_1}_{j_1 \mu'_1 S\sigma} P^{j_1}_{S\sigma}, \qquad P^{j_1}_{S\sigma} = \frac{2S+1}{2j_1+1} \sum_{\mu_1, \mu'_1} C^{j_1 \mu_1}_{j_1 \mu'_1 S\sigma} H_{j_1 \mu_1} H^*_{j_1 \mu'_1}; \tag{17}$$

$H_{j_1 \mu_1}$ is the γ transition matrix element. After insertion of the wave functions eq. (1) takes the form

$$H_{\beta} = \sum i^{l-l_1} (-1)^{j+\mu+i+n} \sqrt{(2l+1)(2l_1+1)}\, e^{i\Delta_{j\lambda}} v^*_{\varrho}(0) v_{\chi}(0)$$
$$\times C^{j\varrho}_{\frac{1}{2}\varrho 10} C^{i\chi}_{\frac{1}{2}\chi l_1 0} D^{j*}_{-\mu\varrho}(\varphi_e, \vartheta_e, 0) D^{i}_{-n\chi}(\varphi_\nu, \vartheta_\nu, 0) C^{j\mu}_{LA in} C^{j_0 \mu_0}_{LA j_1 \mu_1} a_{\mu_0} a^*_{\mu_1} B^{L\tau}_{\lambda\nu}, \tag{18}$$

where summation is performed over all permissible index values,

$$B^{L\tau}_{\lambda\nu} = [C^{j_0 \mu_0}_{LA j_1 \mu_1}]^{-1} \sum_{J=0}^{1} \int \psi^*_{j_1 \mu_1} S^L_{J\tau} Y^{J\tau *}_{LA}\, r^{L+\tau} \psi_{j_0 \mu_0}\, d\mathbf{r}, \tag{19}$$

$$
\begin{aligned}
S^L_{j\tau} = {} & \{[\beta(g_S R_1^- + iG_S R_2^+) + (g_V R_1^+ + iG_V R_2^-)]\delta_{j0} \\
& + [\beta\sigma(g_T R_1^- + iG_T R_2^+) + \sigma(g_A R_1^+ + iG_A R_2^-)]\delta_{j1}\} \delta_{N, L+\tau} \\
& - \{[\gamma_5(ig_A R_2^- + G_A R_1^-) - \beta\gamma_5(ig_P R_2^+ + G_P R_1^-)]\delta_{j0} \\
& + [\alpha(ig_V R_2^- + G_V R_2^+) - \beta\alpha(ig_T R_2^+ + G_T R_1^-)]\delta_{j1}\} \delta_{N-1, L+\tau},
\end{aligned} \tag{20}
$$

$$
\begin{aligned}
R_1^{\pm} &= \sum_{\omega, \chi} [\delta_{\omega, -\lambda} \delta_{\chi, -\nu} \pm 4\lambda\nu\delta_{\omega, \lambda} \delta_{\chi, \nu}] Q_{\omega\chi} \\
R_2^{\pm} &= \sum_{\omega, \chi} [2\nu\delta_{\omega, -\lambda} \delta_{\chi, \nu} \pm 2\lambda\delta_{\omega, \lambda} \delta_{\chi, -\nu}] Q_{\omega\chi},
\end{aligned} \tag{21}
$$

$$
Q_{\omega\chi} = A_{j\lambda} \beta^{jiL}_{\omega\chi\tau} \frac{\sqrt{W + 4\omega\lambda}\, \varkappa^{j+\omega} (-q)^{i+\chi}}{(2j+2\omega+1)!!\,(2i+2\chi+1)!!} \varphi_\omega \delta_{j+\omega+i+\chi, L+\tau}, \tag{22}
$$

$$
\omega = \pm\tfrac{1}{2},\ \chi = \pm\tfrac{1}{2};
$$

φ_ω with an accuracy to $\frac{1}{5}(\alpha Z)^2$ is equal to 1. Thus, for a surface nuclear charge distribution we get $\varphi_\omega = 1 + 3(\varkappa R)^2\,[10(2j+2\omega+3)]^{-1}$. For a volume distribution the deviation from unity is even smaller [15]). Formulae (18)—(22) are valid for β transitions of any order of forbiddenness. Index N in eq. (20) indicates the order of forbiddenness of the investigated transition. For allowed transitions $N = 0$ and the second braces in (20) does not make any contribution as $L + \tau \geqq 0$.

Squaring (18) and summing over the magnetic quantum numbers we obtain a general expression for angular and polarization correlation of all particles involved in a β transition (including subsequent γ quanta):

$$
\begin{aligned}
W^{j_0}_{e\nu\gamma} = {} & \sum i^{l+l'+l_1-l'_1} (-1)^{j'-j+f+\beta} \sqrt{(2l+1)(2l'+1)(2i+1)(2i'+1)} \\
& \times \sqrt{(2l_1'+1)(2f_1+1)}\,(2f+1)(2j+1)(2j'+1) \exp[i(\Delta_{j\lambda} - \Delta_{j'\lambda'})] \\
& \times W(i'\tfrac{1}{2}f_1 l_1;\ l'_1 i) X(i'if_1,\ j'jf,\ L'LN) X(ll'a,\ jj'f,\ \tfrac{1}{2}\tfrac{1}{2}b) \\
& \times C^{l_1 0}_{l'_1 0 f_1 0} C^{a0}_{b\beta f-\beta} C^{a0}_{l'0i0} C^{N\nu}_{f\varphi f_1 \varphi_1} D^{f}_{\varphi, -\beta}(\varphi_e,\ \vartheta_e,\ 0) \\
& \times P_{N\gamma} Y_{f_1\varphi_1}(\vartheta_\nu \varphi_\nu) Y_{b,-\beta}(\chi\omega) B^{L\tau}_{\lambda\nu} B^{L'\tau'*}_{\lambda'\nu}.
\end{aligned} \tag{23}
$$

Here $W(abcd;\ ef)$ are Racah functions; they have been tabulated in ref. [17]). The quantity $P_{N\gamma}$ determines the nuclear orientation before and after the β transition

$$
P_{N\gamma} = (-1)^{g+N+\gamma} X(j_1 j_1 S,\ j_0 j_0 g,\ L'LN) \sum_{\eta\sigma} C^{N-\gamma}_{g\eta S\sigma} P^{j_0}_{g\eta} P^{j_1}_{S\sigma}. \tag{24}
$$

Eq. (23) is the solution of the problem. The explicit form of the quantities in (23) is known and their numerical values can be taken from available tables. If a transition of a certain order of forbiddenness is considered, only a few terms of the sum in (23) will remain because the Clebsch-Gordan coefficients, Racah functions, Fano functions and $S^L_{j\tau}$ do not vanish only for a few values of the indices. However, the actual calculations may turn out to be simple but somewhat cumbersome. Therefore for a number of

important cases we present some simpler formulae which may be obtained from (23).

A convenient way of obtaining numerical results from (23) is the following. The value of N in (20) is assumed to equal the order of forbiddenness and permissible values of j and i are determined in a way that will make $i+\chi$ the smallest number consistent with the requirements that $j+i \geqq L \geqq |j-i|$ and $j+i+\omega+\chi = L+\tau$. For an allowed transition $L+\tau = 0$, $j = i = \frac{1}{2}$. For first order forbiddenness j and i are either $\frac{1}{2}$ or $\frac{3}{2}$. To evaluate $\beta^{jiL}_{\lambda\nu\tau}$ we use the X-function tables [13]). For various energies we find $\sqrt{W+4\omega\lambda}\, A_{j\lambda}$ and $\Delta_{j\lambda}$ from the tables of ref. [16]); inserting in (22), (21) and (20) we determine $B^{L\tau}_{\lambda\nu}$. The next step is to determine from the tables the Clebsch-Gordan, Racah and Fano coefficients for all arguments permissible in the particular case. Collecting all this together we obtained the desired expression.

If a β transition of an oriented nucleus is considered and the subsequent γ transition is disregarded we get

$$P_{N\gamma} = [(2j_1+1)(2g+1)]^{-\frac{1}{2}}(-1)^{\eta} P^{j_0}_{g\eta}\, W(j_1 L' j_0 g;\ j_0 L)\delta_{N\varrho}\,\delta_{\gamma\eta}. \quad (25)$$

For transitions in a non-oriented nucleus

$$P_{N\gamma} = [(2j_0+1)(2S+1)]^{-\frac{1}{2}}(-1)^{S+\sigma} P^{j_1}_{S\sigma}\, W(j_0 j_1 LS;\ L' j_1)\delta_{NS}\,\delta_{\gamma\sigma}. \quad (26)$$

If the γ transition is disregarded and the nucleus prior to β decay was not oriented we get

$$P_{N\gamma} = [(2j_0+1)(2j_1+1)]^{-\frac{1}{2}}\,\delta_{N0}\,\delta_{\gamma 0}. \quad (27)$$

If a knowledge of the direction of the recoil nucleus is not required we obtain

$$\begin{aligned} W^{j_0}_{e\gamma} = {} & \sum i^{l+l'}(-1)^{j'-j+f}(2j+1)(2j'+1)\sqrt{(2l+1)(2l'+1)(2f+1)} \\ & \times C^{a0}_{l'0l0}\, C^{a0}_{b\beta f-\beta}\, W(iL' jf;\ j' L) X(ll' a,\ jj' f,\ \tfrac{1}{2}\tfrac{1}{2} b) \\ & \times \exp\,[i(\Delta_{j\lambda}-\Delta_{j'\lambda'})]\, P_{f\varphi} D^{f}_{\varphi-\beta}(\varphi_e,\ \vartheta_e,\ 0) Y^{*}_{b\beta}(\chi\omega) B^{L\tau}_{\lambda\nu}\, B^{L'\tau'*}_{\lambda'\nu}. \end{aligned} \quad (28)$$

If electron polarization is not being observed we must put $b = \beta = 0$ in (23).

2. Polarization and Angular Distribution of Electrons

If parity is not conserved in β decay there should be a correlation between the directions of the spin and the β particle momentum [1]). Formula (23) can be used to find this correlation for transitions of any order of forbiddenness:

$$\begin{aligned} W(\chi) = {} & \sum i^{l+l'}(2j+1)(2L+1)^{-1}\sqrt{(2l+1)(2l'+1)} \\ & \times \exp\,[i(\Delta_{j\lambda}-\Delta_{j\lambda'})]\, C^{b0}_{l'0l0}\, W(jl\tfrac{1}{2}b;\ \tfrac{1}{2}l') B^{L\tau}_{\lambda\nu}\, B^{L\tau'}_{\lambda'\nu}\, P_b(\cos\chi). \end{aligned} \quad (29)$$

Evidently $b = 0$ or 1 and in accord with (6) the mean value of the spin, $\overline{\boldsymbol{\zeta}^0}$, is directed along the momentum $\mathbf{p}$.

For allowed transitions we obtain (with $\gamma_1 = [1-(\alpha Z)^2]^{\frac{1}{2}}$).

$$W_0(\chi) = \sum_{L=0}^{1} \{M_L - \gamma_1 E^{-1} N_L + E^{-1}(p \operatorname{Re} Q_L + \alpha Z \operatorname{Im} Q_L) \cos\chi\}, \quad (30)$$

$$\begin{aligned} M_0 &= (|g_S|^2+|G_S|^2)|K_S|^2+(|g_V|^2+|G_V|^2)|K_V|^2, \\ M_1 &= (|g_T|^2+|G_T|^2)|K_T|^2+(|g_A|^2+|G_A|^2)|K_A|^2, \end{aligned} \quad (31)$$

$$\begin{aligned} N_0 &= (g_S g_V^* + G_S G_V^*) K_S K_V^* + \text{comp. conj.}, \\ N_1 &= (g_T g_A^* + G_T G_A^*) K_T K_A^* + \text{comp. conj.}, \end{aligned} \quad (32)$$

$$\begin{aligned} Q_0 &= (G_S g_S^* + g_S G_S^*)|K_S|^2 - (G_V g_V^* + g_V G_V^*)|K_V|^2 \\ &- (G_S g_V^* + g_S G_V^*) K_S K_V^* + (G_V g_S^* + g_V G_S^*) K_V K_S^*, \\ Q_1 &= (G_T g_T^* + g_T G_T^*)|K_T|^2 - (G_A g_A^* + g_A G_A^*)|K_A|^2 \\ &- (G_T g_A^* + g_T G_A^*) K_T K_A^* + (G_A g_T^* + g_A G_T^*) K_A K_T^*. \end{aligned} \quad (33)$$

Expression (30) is accurate to terms $\approx (\alpha Z)^2/3$ and αZER compared to unity. The accuracy of formulae (35), (37)–(41) is the same.

If higher accuracy is desired $-\gamma_1 E^{-1}$ should be replaced by $b_{j_2}^{+}/b_{j_2}^{-}$, p by $b_{j_2}^{(1)}/b_{j_2}^{-}$ and αZ by $b_{j_2}^{(2)}/b_{j_2}^{-}$, where

$$\begin{aligned} b_j^{\pm} &= (W-1)A_{j\frac{1}{2}}^2 \pm (W+1)A_{j-\frac{1}{2}}^2, \\ b_j^{(1)} &= 2\varkappa A_{j\frac{1}{2}} A_{j-\frac{1}{2}} \cos(\Delta_{j-\frac{1}{2}} - \Delta_{j\frac{1}{2}}), \quad b_j^{(2)} = 2\varkappa A_{j\frac{1}{2}} A_{j-\frac{1}{2}} \sin(\Delta_{j-\frac{1}{2}} - \Delta_{j\frac{1}{2}}), \end{aligned} \quad (34)$$

$$\begin{aligned} K_S &= \int \psi^*_{j_1\mu_1} \beta \psi_{j_0\mu_0} \, d\mathbf{r}, \\ K_T &= \sqrt{4\pi}[C^{j_0\mu_0}_{1A j_1\mu_1}]^{-1} \int \psi^*_{j_1\mu_1} \beta \boldsymbol{\sigma} \cdot \mathbf{Y}^{-1}_{1A} \psi_{j_0\mu_0} \, d\mathbf{r}. \end{aligned} \quad (35)$$

The difference between K_S and K_T on the one hand and K_V and K_A on the other is that the latter do not contain matrix β. As the lower components of the wave function are large, $\beta \to -1$, that is, $K_V \approx -K_S$ and $K_A \approx -K_T$. $\mathbf{Y}^{-1}_{1A}$ is vector (10) when $J = 1$, $L = 1$, $\tau = -1$.

The angular distribution of electrons emitted by polarized nuclei in allowed β transitions is given by

$$\begin{aligned} W_0(\vartheta_e) &= \sum_{L=0}^{1} \{M_L - \gamma_1 E^{-1} N_L\} \\ &+ (2E)^{-1} \{(p \operatorname{Re} Q_1 + \alpha Z \operatorname{Im} Q_1)[2 + j_0(j_0+1) - j_1(j_1+1)] \\ &+ 4\sqrt{j_0(j_0+1)}\,(p \operatorname{Re} Q_m + \alpha Z \operatorname{Im} Q_n)\}[j_0(j_0+1)]^{-1} \sum_{\mu_0} \mu_0 W(\mu_0) \cos\vartheta_e, \end{aligned} \quad (36)$$

$$\begin{aligned} Q_m &= (G_S g_T^* + g_S G_T^*) K_S K_T^* - (G_V g_A^* + g_V G_A^*) K_V K_A^* \\ Q_n &= (G_V g_T^* + g_V G_T^*) K_V K_T^* - (G_S g_A^* + g_S G_A^*) K_S K_A^*. \end{aligned} \quad (37)$$

For a more thorough study of β interaction it would seem desirable to study the polarization of electrons emitted by polarized nuclei. In this case the formulae for $\overline{\zeta^0}$ will contain g and G in such combinations which are not encountered in (30) or (35).

Employing (23) we obtain

$$W_0(\vartheta_e,\ \chi,\ \omega) = W_0(\vartheta_e)+W_0(\chi)-\sum_{L=0}^{1}\{M_L-\gamma_1 E^{-1}N_L\}$$
$$+\{[2p\ \mathrm{Im}\ Q_n-2\alpha Z\ \mathrm{Re}\ Q_m+\sqrt{2}\,U(p\ \mathrm{Im}\ Q_1-\alpha Z\ \mathrm{Re}\ Q_1)]E^{-1}\sin\vartheta_e\sin\chi\sin\omega$$
$$+[(R-\gamma_1 E^{-1}S)+\sqrt{2}\,U(M_1-\gamma_1 E^{-1}N_1)]\cos\vartheta_e\cos\chi \qquad (38)$$
$$+[(S-\gamma_1 E^{-1}R)+\sqrt{2}\,U(N_1-\gamma_1 E^{-1}M_1)]\sin\vartheta_e\sin\chi\cos\omega\}[j_0(j_0+1)]^{-\frac{1}{2}}\sum_{\mu_0}\mu_0 W(\mu_0)$$

$$R = (g_S g_T^*+G_S G_T^*)K_S K_T^*+(g_V g_A^*+G_V G_A^*)K_V K_A^* + \text{comp. conj.}$$
$$S = (g_S g_A^*+G_S G_A^*)K_S K_A^*+(g_V g_T^*+G_V G_T^*)K_V K_T^* + \text{comp. conj.} \qquad (39)$$
$$\sqrt{2}\,U = [j_0(j_0+1)-j_1(j_1+1)+2][2\sqrt{j_0(j_0+1)}]^{-1}.$$

The angles of vector $\mathbf{p}(p\vartheta_e\varphi_e)$ are taken with respect to the z axis (axis of nuclear polarization) and angle χ with respect to the $\mathbf{p}$ axis; in this case $\omega = 0$ in the $\mathbf{pz}$ plane and axis y is directed along $\mathbf{p}\wedge\mathbf{n}_z$.

The explicit expression for the components of $\overline{\zeta^0}$ can be obtained by using (6):

$$\overline{\zeta^0}_{z_p} = [\sqrt{j_0(j_0+1)}W_0(\vartheta_e)]^{-1}\{[p\ \mathrm{Re}\ (Q_0+Q_1)+\alpha Z\ \mathrm{Im}\ (Q_0+Q_1)]E^{-1}$$
$$+[(R-\gamma_1 E^{-1}S)+\sqrt{2}\ U(M_1-\gamma_1 E^{-1}N_1)]\sum_{\mu_0}\mu_0 W(\mu_0)\cos\vartheta_e\}. \qquad (40)$$

$$\overline{\zeta^0}_{x_p} = [\sqrt{j_0(j_0+1)}\,W_0(\vartheta_e)]^{-1}\{(S-\gamma_1 E^{-1}R)$$
$$+\sqrt{2}\,U(N_1-\gamma_1 E^{-1}M_1)\}\sin\vartheta_e\sum_{\mu_0}\mu_0 W(\mu_0), \qquad (41)$$

$$\overline{\zeta^0}_{y_p} = [\sqrt{j_0(j_0+1)}\,W_0(\vartheta_e)]^{-1}E^{-1}\{2p\ \mathrm{Im}\ Q_n-2\alpha Z\ \mathrm{Re}\ Q_m$$
$$+\sqrt{2}\,U(p\ \mathrm{Im}\,Q_1-\alpha Z\,\mathrm{Re}\,Q_1)\}\sin\vartheta_e\sum_{\mu_0}\mu_0 W(\mu_0), \qquad (42)$$

$$\mathbf{n}_{z_p}\parallel\mathbf{p},\quad \mathbf{n}_{x_p}\parallel\mathbf{p}\wedge\mathbf{n}_y,\quad \mathbf{n}_{y_p}\parallel\mathbf{n}_z\wedge\mathbf{p}.$$

All the foregoing formulae pertain to β^- decay. For positon decay one should perform the substitution

$$g_S\to -g_S^*,\ g_T\to g_T^*,\ g_P\to -g_P^*,\ g_A\to -g_A^*,\ g_V\to g_V^*$$
$$G_S\to G_S^*,\ G_T\to -G_T^*,\ G_P\to G_P^*,\ G_A\to G_A^*,\ G_V\to -G_V^*$$

and change the sign before αZ. It should be noted that in those cases in

which it is difficult to determine the positon polarization from azimuthal scattering asymmetry it may be determined by observing circular polarization of the annihilation radiation. Since positon depolarization is due to relativistic effects, complete depolarization will not take place, in spite of the fact that the positons are slowed down.

It follows from (30) and (35) that for allowed transitions the angular distribution of vector $\mathbf{p}$ and $\boldsymbol{\zeta}^0$ relative to the direction of preferred nuclear spin orientation is anisotropic only for polarized nuclei. Alignment of the nuclei leads to an isotropic angular distribution.

Investigation of allowed transitions permits one to obtain the most unambiguous results regarding the nature of β interaction. In this case the theoretical formulae contain a minimum number of matrix elements whose magnitude depends on the structure of the nucleus. Investigation of forbidden transitions is useful for ascertaining the role of pseudoscalar interaction. In allowed transitions this interaction does not yield any contribution. The most unambiguous conclusions concerning the contribution of pseudo-scalar interaction can be drawn by studying the shape of the spectrum and the polarization of electrons for $0^- \to 0^+$ transitions. A transition of this type apparently occurs in Pr^{144} [18]). The expression describing the shape of the $0^- \to 0^+$ transition spectrum is known. We shall present an expression for β particle polarization derived on the assumption that pseudovector interaction is not important.

Assuming in (30) that $L = 0$, $\tau = 0$ or 1 and using (6) we obtain

$$\overline{\boldsymbol{\zeta}^0} = \frac{\mathbf{P}}{p} \{ b_{\frac{1}{2}}^{(1)} (g_P G_P^* + g_P^* G_P) |K_P|^2 + \tfrac{1}{27} b_{\frac{1}{2}}^{(1)} (G_T g_T^* + g_T G_T^*) |K_T|^2 (\varkappa^2 + q^2 - 2Wq)$$

$$- \tfrac{1}{3}\sqrt{\tfrac{1}{3}} b_{\frac{1}{2}}^{(2)} 2 \operatorname{Im} (g_P G_T^* + g_T^* G_P) K_P K_T^* + \tfrac{1}{3}\sqrt{\tfrac{1}{3}} b_{\frac{1}{2}}^{(1)} (W - q) 2 \operatorname{Re} (g_P G_T^* + g_T^* G_P) K_P K_T^* \}$$

$$\times \{ b_{\frac{1}{2}}^{\tau} (|g_P|^2 + |G_P|^2) |K_P|^2 + \tfrac{1}{27} [(A_{\frac{1}{2}\frac{1}{2}}^2 + A_{\frac{1}{2}-\frac{1}{2}}^2)(Wq^2 + W\varkappa^2 - 2q\varkappa^2) \qquad (43)$$

$$+ (A_{\frac{1}{2}\frac{1}{2}}^2 - A_{\frac{1}{2}-\frac{1}{2}}^2)(\varkappa^2 - q^2)] (|g_T|^2 + |G_T|^2) |K_T|^2$$

$$- \tfrac{1}{3}\sqrt{\tfrac{1}{3}} [(A_{\frac{1}{2}\frac{1}{2}}^2 + A_{\frac{1}{2}-\frac{1}{2}}^2)(Wq - \varkappa^2) - q(A_{\frac{1}{2}\frac{1}{2}}^2 - A_{\frac{1}{2}-\frac{1}{2}}^2)] 2 \operatorname{Re} (g_T^* g_P + G_T^* G_P) K_P K_T^* \}^{-1},$$

$$K_P = i \int \psi_{00}^* \beta \gamma_5 \psi_{00} \, d\mathbf{r}, \quad K_T = \sqrt{4\pi} \int \psi_{00}^* \beta \boldsymbol{\sigma} \cdot \mathbf{Y}_{00}^{1*} \psi_{00} \, d\mathbf{r}. \qquad (44)$$

Invariance of strong interactions with respect to time-reversal leads to the result that the phase shift between K_P and K_T should be 0 or π.

Expression (43) can be simplified by neglecting terms of order of $(\alpha Z)^2/3$ and αZER. We obtain

$$\overline{\zeta^0} = \frac{\mathbf{P}}{E}\{(g_P G_P^* + g_P^* G_P)|K_P|^2 + \tfrac{1}{27}(G_T g_T^* + g_T G_T^*)|K_T|^2(\varkappa^2+q^2-2Wq)$$

$$-\tfrac{2}{3}\sqrt{\tfrac{1}{3}}\frac{\alpha Z}{p}\,\mathrm{Im}\,(g_P G_T^* + g_T^* G_P)K_P K_T^* + \tfrac{2}{3}\sqrt{\tfrac{1}{3}}(W-q)\,\mathrm{Re}\,(g_P G_T^* + g_T^* G_P)K_P K_T^*\}$$

$$\times\{(|g_P|^2+|G_P|^2)|K_P|^2 + \tfrac{1}{27}\frac{1}{E\varkappa^2}[(WE-\gamma_1)(Wq^2+W\varkappa^2-2q\varkappa^2) \qquad (45)$$

$$+(E-\gamma_1 W)(\varkappa^2-q^2)](|g_T|^2+|G_T|^2)|K_T|^2 - \tfrac{2}{3}\sqrt{\tfrac{1}{3}}\frac{1}{E\varkappa^2}[(WE-\gamma_1)(Wq-\varkappa^2)-q(E-\gamma_1 W)]$$

$$\times\,\mathrm{Re}\,(g_T^* g_P + G_T^* G_P)K_P K_T^*\}^{-1}.$$

If, instead of fitting the electron wave function inside the nucleus onto the function outside the nucleus, we take the value of the function in the field of a point charge at the boundary of the nucleus, it will be found that the formulae for $W(\vartheta_e)$ and $\overline{\zeta^0}$ are identical with (30), (36), (38) and (45) assuming that $V = 3\alpha Z/2R$.

The general expression for $\overline{\zeta^0}$ for first order forbidden transitions contains several nuclear matrix elements. Their number is larger than in the case of allowed transitions. These matrix elements should be considered as additional unknowns to be determined experimentally or to be roughly estimated on the basis of nuclear models. Therefore an unambiguous interpretation of the experimental facts seems to be difficult. However the expression for $\overline{\zeta^0}$ can be significantly simplified for nuclei with $Z \gg A^{1/3}\,E_{\mathrm{MeV}}$, as it appears that all terms not containing $\alpha Z/R$ can be omitted. The same also holds for β neutrino angular correlation [14]). If, however, the correlation is small or vanishes in allowed transitions (e.g., if there is no angular β-γ correlation for non-oriented nuclei) all terms should be retained for first order forbidden transitions even if $Z \gg A^{1/3}\,E_{\mathrm{MeV}}$ [15]). For second and higher order forbidden transitions omission of terms which are small compared with $\alpha Z/R$ does not decrease the number of nuclear matrix elements.

The most definite results on forbidden β decay can be obtained by investigating "unique" transitions for which the nuclear momentum change exceeds the order of forbiddenness by one. However, in this case no information on the Fermi part of the β interaction will be obtained.

The expression for polarization of β particles emitted by oriented nuclei in first order forbidden unique transitions has the form

$$W(\vartheta_e,\ \varphi_e,\ \chi,\ \omega) = \sum_{j,f,b,s,} \sum_{l'\geq l} R^{W\,j}_{bsf}\, W(j_1\,2j_0 f;\ j_0\,2)\, Z^j_{lW}\, P^{j_0}_{f0}\, F_{bsf}(\vartheta_e,\ \varphi_e,\ -\chi,\ -\omega)$$

$$j = \tfrac{1}{2},\ \tfrac{3}{2};\ f = 0,\ 1,\ 2,\ 3;\ b = 0,\ 1;\ s = 0, \ldots 4;\ 2\omega_\pm = 1 \pm (-1)^{f+b+s};$$

$$Z_{01}^{\frac{1}{2}} = 2q^2[(p \operatorname{Re} Q_1 + \alpha Z \operatorname{Im} Q_1)\omega_+ - i(p \operatorname{Im} Q_1 - \alpha Z \operatorname{Re} Q_1)\omega_-],$$

$$Z_{12}^{3/2} = [p^2 + (\alpha ZE)^2][(p \operatorname{Re} Q_1 + \frac{\alpha Z}{2} \operatorname{Im} Q_1)\omega_+ - i(p \operatorname{Im} Q_1 - \frac{\alpha Z}{2} \operatorname{Re} Q_1)\omega_-],$$

$$Z_{00}^{\frac{1}{2}} = q^2(E+1)(M_1 - N_1), \quad Z_{11}^{\frac{1}{2}} = q^2(E-1)(M_1 + N_1), \tag{46}$$

$$Z_{11}^{3/2} = \frac{\varkappa^2}{2}(E+1)(M_1 - N_1), \quad Z_{22}^{3/2} = \frac{\varkappa^2}{2}(E-1)(M_1 + N_1).$$

The values of $F_{bsf}(\vartheta_e, \varphi_e, \chi, \omega)$ and $R_{bsf}^{ll'j}$ are given in the appendices I and II. $P_{f0}^{j_0}$ is defined by eq. (16).

The only difference between M_1, N_1, Q_1 and (31), (32), (33) is that for the former $K_V = K_S = 0$ and for K_T one should take

$$K_T = \sqrt{4\pi}[C_{\frac{1}{2}\lambda j_1 \mu_1}^{j_0 \mu_0}]^{-1} \int \psi_{j_1 \mu_1}^* \beta \boldsymbol{\sigma} \cdot \mathbf{Y}_{1\Lambda}^{-1*} \psi_{j_0 \mu_0} \, d\mathbf{r}$$

and the same expression but without matrix β for K_A.

3. Beta-Gamma Correlation

According to (23) the correlation between the β electron direction and γ quantum direction (or polarization) in the decay of an oriented nucleus is expressed by the following formula for transitions of any order of forbiddenness:

$$\begin{aligned} W_{\mathbf{p},\gamma}^{j_0} = \sum & i^{l+l'}(-1)^{j'-j+g} \sqrt{(2l+1)(2l'+1)/(2f+1)}\ (2j+1)(2j'+1) \\ & \times C_{l'010}^{f0} W(iL'jf;\ j'L) W(\tfrac{1}{2}jl'f;\ lj') \exp[i(\Delta_{j\lambda} - \Delta_{j'\lambda'})] \\ & \times X(j_1 j_1 S,\ j_0 j_0 g,\ L'Lf) C_{g0S\sigma}^{f\sigma} P_{S\sigma}^{j_1} Y_{f\sigma}^*(\vartheta_e \varphi_e) P_{g0}^{j_0} B_{\lambda\nu}^{L\tau} B_{\lambda'\nu}^{L'\tau'*}. \end{aligned} \tag{47}$$

For allowed transitions ($j = i = \frac{1}{2}$, $L + \tau = 0$) eq. (47) can be written in a simpler form:

$$W_{\mathbf{p},\gamma}^{j_0} = \sum \alpha_{ll'}^f \beta_{LL'}^f C_{g0S\sigma}^{f\sigma} P_{S\sigma}^{j_1} Y_{f\sigma}^*(\vartheta_e \varphi_e) P_{g0}^{j_0} B_{\lambda\nu}^{L\tau} B_{\lambda'\nu}^{L'\tau'*} \tag{48}$$

$$\begin{aligned} & \beta_{LL'}^f = (-1)^g W(\tfrac{1}{2}L'\tfrac{1}{2}f;\ \tfrac{1}{2}L) X(j_1 j_1 S,\ j_0 j_0 g,\ L'Lf)/\sqrt{2f+1}, \\ & \alpha_{00}^0 = \alpha_{11}^0 = 1, \quad \alpha_{01}^1 = \alpha_{10}^{1*} = -i \exp[i(\Delta_{\frac{1}{2}-\frac{1}{2}} - \Delta_{\frac{1}{2}\frac{1}{2}})]; \end{aligned} \tag{49}$$

$$\begin{aligned} B_{\lambda\nu}^{00} &= \sqrt{E - 2\lambda\gamma_1}\ \{2\lambda(g_S \delta_{\lambda,\nu} - 2i\lambda G_S \delta_{\lambda,-\nu}) K_S \\ &\quad + (g_V \delta_{\lambda,\nu} - 2i\lambda G_V \delta_{\lambda,-\nu}) K_V\} \\ B_{\lambda\nu}^{1-1} &= \sqrt{3(E - 2\lambda\gamma_1)}\ \{2\lambda(g_T \delta_{\lambda,\nu} - 2i\lambda G_T \delta_{\lambda,-\nu}) K_T \\ &\quad + (g_A \delta_{\lambda,\nu} - 2i\lambda G_A \delta_{\nu,-\lambda}) K_A\}. \end{aligned} \tag{50}$$

Permissible values of f, l, l', L and L' in sum (48) are 0 or 1. λ and $\nu = \pm\frac{1}{2}$. Formulae (47) and (48) are valid for polarized as well as for aligned nuclei.

The polarization tensor $P^{j_1}_{S\sigma}$ for a nucleus after β decay can be expressed in terms of observables characterizing the radiative transition. If the angular distribution of γ quanta is being studied we get

$$P^{j_1}_{S\sigma} = \sqrt{2S+1}\left[1 - \frac{S(S+1)}{2I(I+1)}\right] U(j_2 I j_1 S;\ j_1 I) C^{I0}_{I0S0}\, Y_{S\sigma}(\theta\phi) \qquad (51)$$

where I defines the multipolarity and $\mathbf{k}$ (k, θ, ϕ) the γ-quantum momentum; j_1 and j_2 are the nuclear moments before and after the radiative transition;

$$U(abcd;\ ef) = \sqrt{(2e+1)(2f+1)}\ W(abcd;\ ef). \qquad (52)$$

An additional opportunity for investigation of β transitions appears if along with the angular distribution circular polarization of γ quanta can be observed. Thus, for example, it was shown in ref. [19]), that if parity is not conserved a correlation between the direction of the β electron and circular polarization of the quantum should exist. It has been suggested [20]) that the sign of g_S/g_T can be determined by observing circular polarization of X ray quanta emitted after K-capture. A study of circular polarization of γ quanta yields information on dipole polarization of the nucleus after β decay. Observation of circular polarization of γ quanta should permit one to determine the orientation of the nuclear spin and hence to study β transitions of non-oriented nuclei. Formally, the tensor $P^{j_0}_{\sigma\eta}$ in this case is replaced by tensor $P^{j_1}_{S\sigma}$. For odd values of S the tensor $P^{j_1}_{S\sigma}$ vanishes after averaging over the γ quantum polarizations. If, on the other hand, polarization is observed $P^{j_1}_{S\sigma}$ will differ from zero for arbitrary values of S and instead of (51) we should take

$$\begin{aligned} P^{j_1}_{S\sigma} = (2S+1) \sum_{M, M_1} \xi^{\frac{M-M_1}{2}} C^{IM}_{IM_1, S, M-M_1} U(I j_2 S j_1;\ j_1 I) \\ \times e^{i(M-M_1)\alpha} D^{S}_{\sigma, M-M_1}(\phi 0 0) \end{aligned} \qquad (53)$$

The term with $M = M_1 = 1$ yields $P^{j_1}_{S\sigma}$ for quanta with right hand circular polarization and the term with $M = M_1 = -1$, $P^{j_1}_{S\sigma}$ for quanta with left hand circular polarization. The sum of terms with $M = 1$, $M_1 = -1$ and $M = -1$, $M_1 = 1$ yields $P^{j_1}_{S\sigma}$ for linearly polarized quanta. $\xi = +1$ and -1 for magnetic and electric transitions respectively. Angle α defines the linear polarization vector $\boldsymbol{\epsilon}$ in a coordinate system with the z axis directed along $\mathbf{k} \cdot \varepsilon_0 = 0$, $\varepsilon_{\pm 1} = \pm\sqrt{\frac{1}{2}}\, e^{\pm i\alpha}$.

Angle α is measured relative to the x axis in a plane $\perp \mathbf{k}$. For oriented

nuclei β-γ correlation in forbidden transitions is described by a complex expression containing several matrix elements †.

Its investigation will evidently be profitable after the main constants will be determined from allowed transition data. Investigation of "unique" transitions should furnish the most unambiguous results. In this case β-γ correlation for an oriented nucleus and first order forbidden transitions should have the form

$$W(\mathbf{p},\mathbf{k}) = \sum_{j,f,g,S} \sum_{l' \geq l} \gamma_{ll'}^{jf} Z_{ll'}^{j}(-1)^g X(j_1 j_1 S,\ j_0 j_0 g,\ 22f)$$

$$\times \sqrt{2S+1}[1-S(S+1)/2I(I+1)]C_{I0S0}^{I0} U(j_2 I j_1 S;\ j_1 I) P_{g0}^{j_0} F_{Sgf}(\vartheta_e \varphi_e \theta\phi). \quad (54)$$

$j = \frac{1}{2}, \frac{3}{2}$; $f = 0, 1, 2, 3$; l and $l' = j \pm \frac{1}{2}$, $S = 0, 2, \ldots 2I$.

The values of $\gamma_{ll'}^{jf}$ are presented in appendix III.

4. A Possible Method of Checking Time-Reversal Invariance of the Theory

A study of β-γ correlation of aligned nuclei may yield important information on the nature of parity non-conservation. We shall show that absence of this kind of correlation for allowed transitions would provide proof of time reversal invariance of the theory.

Expression (48) for aligned nuclei (polarized by the Bleaney [21]) or Pound [22]) method) can be written in the form

$$W_a(\mathbf{p},\mathbf{k}) = \sum_{g,S,\mu_0} \sqrt{2g+1}\, C_{j_0 \mu_0 g_0}^{j_0 \mu_0} W(\mu_0)$$

$$\times \Big\{ \sqrt{2S+1} \sum_{L=0}^{1} (M_L - \gamma_1 E^{-1} N_L) U(L j_0 j_1 g;\ j_1 j_0) \delta_{Sg} P_S(\cos\theta)$$

$$+ \sqrt{2g+1} \left[\frac{P}{E} \operatorname{Im} Q_m - \frac{\alpha Z}{E} \operatorname{Re} Q_n \right] U(j_0 j_0 g1;\ S j_0) \tfrac{2}{3} i F_{Sg1}(\vartheta_e, \varphi_e, \theta, \phi) \Big\} \quad (55)$$

$$\times \left[1 - \frac{S(S+1)}{2I(I+1)} \right] U(j_2 I j_1 S;\ j_1\ I) C_{I0S0}^{I0},$$

$$g = 0,\ 2,\ 4, \ldots, \qquad S = 0,\ 2,\ 4, \ldots .$$

† For those terms in the β—γ correlation formula which do not vanish when parity is conserved, one may employ the explicit expressions given in ref. [15]); in this paper values of the quantities

$$\sum_{j\lambda j'\lambda' i\nu} i^{l+l'}(-1)^{j'-j+f}(2f+1)(2j'+1)(2j+1)\sqrt{(2f+1)(2l+1)(2l'+1)(2i+1)2/(2L+1)}$$

$$\times \exp[i(\Delta_{j\lambda} - \Delta_{j'\lambda'})] C_{l'0l0}^{f0} X(j'jf,\ L'Lf,\ ii0) X(ll'f,\ jj'f,\ \tfrac{1}{2}\ \tfrac{1}{2}\ 0)\ B_{\lambda\nu}^{L\tau} B_{\lambda'\nu}^{L'\tau'*}$$

$$\equiv \sum_{i \leq k} C_{ik}^{fLL'} [\operatorname{Re} M_{iL} M_{kL}^*]$$

are presented for first order forbidden transitions. The subscript L in M_{iL} was dropped in ref. [15]).

Since invariance with respect to $t \to -t$ is not violated in strong nuclear interactions it may be asserted that the phase shift between K_V and K_A^*, K_S and K_T^* etc. is zero or π. Thus Q_m and Q_n are real or imaginary depending on g and G. If β interaction is also invariant with respect to time reversal all g and G are real and arg Q_m, arg Q_n will equal zero or π. In this case β-γ correlation will depend on the particle energy as $\alpha Z/E$ and not as p/E. Observation of p/E dependence would be a direct proof of violation of time reversal invariance. The character of the allowed β spectra apparently implies that the real parts of g_A and G_A are very small or exactly equal to zero. There are indirect indications that the real parts of g_V and G_V are also small. If this is true Q_n should be small. Thus a proof of the absence of β-γ correlation for aligned nuclei in allowed transitions should permit one, in accord with (55), to assert that 1) the theory is invariant with respect to time reversal and 2) the contribution from vector and pseudovector interaction is small.

A correlation depending on the particle energy as $\alpha Z/E$ would mean that the contribution from vector or pseudovector interaction is significant.

A number of expressions resembling (35) and (38) also contain Q_m and Q_n; however, these quantities are involved in such a manner that only very exact and thorough experiments should yield the information which can be obtained by qualitatively investigating $W_a(\mathbf{p}, \mathbf{k})$. That this case is an exclusive one can easily be understood from the following. The expression for the probability of the investigated transition should include the electron momentum $\mathbf{p}$, photon momentum $\mathbf{k}$ and the tensor $\hat{P}_g^{j_0}$ which determines orientation of the aligned nucleus †. Since the transition is allowed $\mathbf{p}$ can enter the expression only linearly. For γ transitions parity is conserved and $\mathbf{k}$ should therefore enter the expression quadratically. Under these conditions it is possible to construct only one pseudoscalar $(\mathbf{p} \wedge \mathbf{k}) \cdot \mathbf{T}$, where $\mathbf{T} = \hat{P}_2^{j_0} \cdot \mathbf{k}$, and no scalar, from $\mathbf{p}$, $\mathbf{k}$ and $\hat{P}_2^{j_0}$. This pseudoscalar changes sign under reversal of time and therefore cannot be involved in a theory which is invariant with respect to time reversal. Coulomb interaction between the electron and nucleus leads to the appearance of additional terms in the expression for angular correlation. For allowed transitions these terms should participate only in the case of vector and pseudovector interaction.

If the nuclei are polarized (e.g., by the Gorter-Rose method [24]) β-γ correlation in allowed transitions should also exist. For even and odd g we get from (46)

† All following considerations will remain valid if the $\hat{P}_g^{j_0}$ do not vanish for $g = 4,6$ etc. (only even g are possible for aligned nuclei).

$$W_p(\mathbf{p},\mathbf{k}) = W_a(\mathbf{p},\mathbf{k}) - \sum_{g=1,3,..}\sum_{S=0,2,..}\sum_{\mu_0} C^{j_0\mu_0}_{j_0\mu_0 g0}$$
$$\times W(\mu_0)\left\{\tfrac{2}{3}\sqrt{2j_0+1}\, W(j_0 j_0 g1;\ Sj_0)\left[\frac{P}{E}\operatorname{Re} Q_m + \frac{\alpha Z}{E}\operatorname{Im} Q_n\right]\right. \tag{56}$$
$$\left. -\sqrt{(2j_0+1)(2j_1+1)2/3}\, X(j_1 j_1 S,\ j_0 j_0 g,\ 111)\left[\frac{P}{E}\operatorname{Re} Q_1 + \frac{\alpha Z}{E}\operatorname{Im} Q_1\right]\right\}$$
$$\times F_{Sg1}(\vartheta_e,\ \varphi_e,\ \theta,\ \phi)(2g+1)\sqrt{2S+1}\left[1-\frac{S(S+1)}{I(I+1)}\right] C^{I0}_{I0S0}\, U(j_2 I j_1 S;\ j_1 I).$$

For $j_1 = j_0$ we obtain

$$X(j_0 j_0 S;\ j_0 j_0 g,\ 111)$$
$$= [S(S+1)-g(g+1)]W(j_0 j_0 g1;\ Sj_0)[2\sqrt{6(2j_0+1)j_0(j_0+1)}]^{-1}.$$

Observation of $W_1(\mathbf{p},\mathbf{k})$ may be a control experiment in investigations of $W_2(\mathbf{p},\mathbf{k})$ and it is of independent interest in determining g and G. Proof that all $g = -G$ would confirm the possibility of employing the two-component neutrino equation.

5. Conclusion

1. The problem of invariance of β interaction under time reversal can be clarified by investigating β-γ correlation of aligned nuclei in allowed transitions.

2. The same experiment can be used to determine the contribution of vector and pseudovector interaction.

3. The fraction of pseudoscalar interaction can be determined by studying the spectrum and polarization of particles in $0^- \to 0^+$ transitions. Investigation of β electron polarization may yield information regarding the sign of the pseudoscalar interaction constant.

4. The angular and polarization distribution of particles emitted by oriented nuclei can be studied with the aim of determining g and G. The same information on g and G can be obtained studying β-transitions in non-oriented nuclei and by determining the nuclear spin orientation by observing circular polarization of the quanta subsequently emitted.

5. As a rule it is difficult to interpret the results of forbidden transition investigations. The only exceptions are unique transitions. In many cases (e.g., for β-ν correlation, $\overline{\zeta^0}$ etc.) if we are dealing with first order forbiddenness and $Z \gg A^{1/3} E_{\text{MeV}}$ only a few terms may be retained in the formulae. This permits a more unambiguous interpretation of the experimental data to be carried out.

The author wishes to express his appreciation to Professor I. M. Shmushkevich for discussion of the results of this paper.

Appendix I

Explicit form and some particular values of $F_{abc}(\vartheta\varphi\theta\phi)$

$$F_{abc}(\vartheta\varphi\theta\phi) = 4\pi \sum_{\gamma} C^{c\gamma}_{b0a\gamma} Y_{a\gamma}(\theta\phi) Y^{*}_{c\gamma}(\vartheta\varphi);$$

$$\sqrt{2a+1}\, F_{abc}(\vartheta\varphi\theta\phi) = (-1)^{b} \sqrt{2c+1}\, F_{cba}(\theta\phi\vartheta\varphi),$$

$$F_{0bb} = \sqrt{2b+1}\, P_{b}(\cos\vartheta), \quad F_{a0a} = 4\pi \sum_{\gamma} Y_{a\gamma}(\theta\phi) Y^{*}_{a\gamma}(\vartheta\varphi);$$

$$F_{211} = -\sqrt{\tfrac{3}{2}} \{(3\cos^2\theta - 1)\cos\vartheta + 3\sin\theta\cos\theta\sin\vartheta\cos(\phi-\varphi)\},$$

$$iF_{221} = -3\sqrt{\tfrac{3}{2}}\, \sin\theta\cos\theta\sin\vartheta\sin(\phi-\varphi),$$

$$F_{231} = \tfrac{3}{2}\sqrt{\tfrac{2}{7}}\, \{(3\cos^2\theta - 1)\cos\vartheta - 2\sin\theta\cos\theta\sin\vartheta\cos(\phi-\varphi)\},$$

$$iF_{141} = -\tfrac{3}{4}\sqrt{5}\,(7\cos^2\theta - 3)\cos\theta\sin\theta\sin\vartheta\sin(\phi-\varphi).$$

Appendix II

Values of $R^{ll'j}_{bsf}$ *in eq. (46)*

$$R^{ll'j}_{bsf} = (-1)^{f+b+l}(2j+1)\sqrt{(2j+1)(2l+1)(2l'+1)(2s+1)/4}\,(2f+1)^{-1}$$
$$\times C^{s0}_{l'0l0} X(ll's,\ jjf,\ \tfrac{1}{2}\tfrac{1}{2}b) U(i2jf;\ j2).$$

$j = \frac{1}{2},\ i = \frac{3}{2}$: $\quad R^{11}_{000} = -R^{01}_{110} = \sqrt{2},$

$$R^{01}_{011} = 3R^{00}_{101} = \sqrt{\tfrac{3}{2}}\, R^{01}_{111} = -9R^{11}_{101} = \tfrac{1}{3}, \qquad R^{11}_{121} = -4\sqrt{5}/9\sqrt{6}.$$

$j = \frac{3}{2},\ i = \frac{1}{2}$: $\quad R^{11}_{000} = -R^{12}_{110} = 5\sqrt{2}\ R^{12}_{011} = \tfrac{5}{2}\sqrt{3}\ R^{12}_{111} = 2\sqrt{2},$

$$R^{22}_{121} = -3R^{11}_{121} = -\tfrac{4}{3}\sqrt{1/10},$$

$$R^{11}_{101} = -\tfrac{5}{3}\, R^{22}_{101} = \tfrac{2}{9},$$

$$R^{11}_{022} = R^{22}_{022} = \frac{5}{\sqrt{2}}\, R^{12}_{112} = -\tfrac{5}{2}\, R^{12}_{132} = -\tfrac{2}{5}\sqrt{7/5},$$

$$R^{12}_{033} = \frac{3}{\sqrt{35}}\, R^{11}_{123} = -3\sqrt{7/5}\, R^{22}_{123} = \tfrac{3}{2}\, R^{12}_{133} = -\frac{7}{4\sqrt{3}}\, R^{22}_{143} = -\tfrac{12}{35}.$$

Appendix III

Values of $\gamma^{jf}_{ll'}$ *in eq. (54)*

$$\gamma^{jf}_{ll'} = (-1)^{l}(2j+1)\sqrt{(2l'+1)/4(2f+1)}\, C^{f0}_{l'0l0} U(i2jf;\ j2) U(\tfrac{1}{2}jl'f;\ lj);$$

$$\gamma^{\frac{1}{2}0}_{ll} = -\sqrt{6}\,\gamma^{\frac{1}{2}1}_{01} = (\tfrac{1}{2})\,\gamma^{\frac{3}{2}1}_{ll} = 1,$$

$$\gamma^{\frac{3}{2}2}_{11} = \gamma^{\frac{3}{2}2}_{22} = \sqrt{\tfrac{7}{3}}\,\gamma^{\frac{3}{2}1}_{12} = -\tfrac{7}{6}\,\gamma^{\frac{3}{2}3}_{12} = -\frac{\sqrt{14}}{5}.$$

References

1) T. D. Lee and C. N. Yang, Phys. Rev. **104** (1956) 254
2) T. D. Lee and C. N. Yang, Phys. Rev. **105** (1957) 1671
3) C. S. Wu, E. Ambler, R. W. Hayward, D. D. Hoppes and R. P. Hudson, Phys. Rev. **105** (1957) 1413
4) L. M. Lederman *et al.*, Phys. Rev. **105** (1957) 1415
5) L. D. Landau, Nuclear Physics **3** (1957) 127
6) H. A. Tolhoek and S. R. de Groot, Physica **17** (1951) 81
7) E. Wigner, Gruppentheorie und ihre Anwendung auf die Quanteumechanik der Atmospektren (Braunschweig 1931)
8) H. Bethe, Quantum Mechanics of Simplest Systems (Russian Edition) (1935)
9) E. Condon and G. Shortley, Theory of Atomic Spectra (1949)
10) H. A. Tolhoek and S. R. de Groot, Physica **17** (1951) 1
11) V. Berestetsky, A. Dolginov and K. Ter-Martirosyan, JETP **20** (1950) 527
12) I. M. Kennedy, B. I. Sears and W. T. Sharp, Chalk River Report CRT-569 (1954)
13) H. Matsunobo and H. Takebe, Progr. of Theoret. Phys. **14** (1955) 589
14) A. Z. Dolginov, JETP **22** (1952) 658
15) A. Z. Dolginov and I. N. Toptigin, Nuclear Physics **2** (1956) 147
16) L. A. Sliv and B. A. Volchek, Tables of Coulomb Phase Shifts and Amplitudes with Account of Finite Nuclear Dimensions (1956)
17) K. Adler, Helv. Phys. Acta **25** (1952) 235
H. Jahn, Progr. Roy. Soc. **205** (1951) 192
18) Laubnitz, Proc. Phys. Soc. A **69** (1956) 789
19) I. S. Shapiro, Uspekhi Fiz. Nauk **61** (1957) 313
Yu. Gaponov and V. Popov, Nuclear Physics **4** (1957) 453
20) A. Z. Dolginov, Nuclear Physics **2** (1956/57) 723
21) B. Bleaney, Proc. Phys. Soc. A **64** (1951) 315
22) R. V. Pound, Phys. Rev. **76** (1949) 1410
23) A. Simon M. E. Rose and I. H. Jauch, Phys. Rev. **84** (1951) 1155

Nuclear Physics **5** (1958) 530—543; © *North-Holland Publishing Co., Amsterdam*
Not to be reproduced by photoprint or microfilm without written permission from the publisher

A POSSIBLE THEORY OF WEAK INTERACTIONS

R. GATTO †

Radiation Laboratory, University of California, Berkeley, California ††

Received 17 September 1957

Abstract: A discussion is given of some of the recent experimental results in β-decay, and a possible theory of weak interactions is presented which is able to reproduce most of the results of the two-component theory but allows for the simultaneous presence of S and V in β-interaction without violating time reversal. The theory is based on a generalization of Tiomno's mass reversal.

1. Introduction

Measurements of the angular distribution of the positons emitted in the decay of oriented Co^{58} [1, 2]) give an asymmetry coefficient opposite in sign and about one third of that of Co^{60}. Such a value would be consistent with a negligible ratio $|M_F|/|M_{GT}|$ for the transition. However, with the value for such a ratio reported previously [3]), the asymmetry would be wrongly predicted if the β-decay interaction is assumed to consist mainly of T and S. A subsequent investigation of the β^+—ν angular correlation in the decay of A^{35} — for which M_{GT} appears to be much smaller than M_F [4]) — has led the authors to the conclusion that V is the dominant Fermi coupling[5]). On the other hand, previous experiments on the β^+—ν correlation in the decay of Ne^{19} [6]) were all consistent with the absence of V but inconsistent with the absence of S. It is essential for such a conclusion to assume that T is the dominant Gamow-Teller coupling. If A were the dominant Gamow-Teller coupling, the N^{19} experiments could be interpreted as favoring V. However, the dominance of T in Gamow-Teller transitions is strongly indicated by the β^-—ν correlation in the decay of He^6 [7]). The dominance of S is also indicated from the β-decay of the neutron [8]) — again assuming the dominance of T.

In the general case of parity non-conservation, the conclusion that the assumption of time-reversal invariance, together with the absence (or smallness) of the Fierz terms, implies that either S or V is present but not both and — similarly for A and T — is no longer valid. However, such a conclusion again holds in a two-component neutrino theory ($C_j = \pm C'_j$, with the same choice of sign for all different couplings j [9])). Therefore the

† On leave of absence from Istituto di Fisica dell'Università di Roma, Italy.

†† This work was performed under the auspices of the United States Atomic Energy Commission.

two-component theory of the neutrino would be inconsistent with the presence of both S and V in appreciable quantities, and/or of both T and A, unless time reversal is violated.

No direct experimental arguments in favour of or against time-reversal invariance have been reported so far. The only indirect argument that has been presented is based on the large value found for the ratio of the lifetime of the long lived K^0 to that of the short lived K^0 [10]). The magnitude of this ratio finds a natural explanation in the assumption of time-reversal invariance. However, time-reversal invariance is not the only possible explanation of the large value of the ratio — a possible smallness of the mass difference between the two K^0 states would produce the same effect [11]). It has also been pointed out that the absence of 2π decay for the K^0 long lived and a ratio of unity between the frequencies of decay of K^0 long lived into e^+ and into e^- would both follow directly from the large ratio between the lifetimes [12]). Direct tests for testing time-reversal invariance in β-decay [13]) and in $K \to \pi+\mu(e)+\nu$ decays [14]) have been proposed.

At the present stage of experiments in β-decay, the possibility must always be left open that some of the experimental conclusions that have been drawn may be changed by later, more refined, experiments. However, if one wants to accept the present indication of the presence of both S and V, one can either conserve time-reversal and abandon the two-component theory, or conserve the two-component theory and abandon time-reversal invariance, or, of course, abandon both. We do not consider the possibility of a complicated non-local structure of the β-decay interaction essentially because it would not be expected to lead to appreciable modifications anyway since the wavelengths of the particles emitted in β-decay are large as compared to nuclear dimensions. We shall discuss here, as a possibility of retaining the hypothesis of time-reversal invariance, a four-component theory that has the advantage of preserving most of the successful predictions of the two-component theory and, at the same time, can explain most of the present data on β-decay. In this theory, parity is violated in a definite way (different from the condition $C_i = \pm C'_i$ of the two-component theory) as a result of an invariance requisite imposed on the interaction Hamiltonian. This invariance requisite has been discussed by Nishijima as a possibility of obtaining further restrictions on the possible interaction Hamiltonians of the two-component theory [15]). We use it here alone, without requiring a two-component neutrino. The theory leads in μ-decay to essentially the same conclusions of the Lee-Yand two-component theory. However, it allows for the presence in β-decay of both S and V and of A and T without violating time reversal. It can be interpreted as a theory with two two-component neutrinos, one right-handed and one left-handed, in a way rather similar to a recent proposal by Mayer and Telegdi

for β-decay [26]). However, we are concerned rather with the whole class of neutrino interactions and not with β-decay only. Specifically, in β-decay the theory comes out to be essentially different from Mayer-Telegdi's theory, in the rule by which the two neutrinos are coupled in the β-decay interaction.

2. μ-Decay

The two-component theory, with lepton conservation, leads to a μ-decay spectrum with $\varrho = 0.75$. The experiments seem to indicate a smaller value, $\varrho = 0.68 \pm 0.02$ [17]). The experiments also indicate an asymmetry parameter ξ with a magnitude $|\xi| = 0.87 \pm 0.12$ [18]), which is rather near to the maximum possible value in the two-component theory, $|\xi| = 1$. Lee and Yang have recently proposed to explain the deviation of the experimental ϱ value from the value 3/4 by assuming a non-local interaction for μ decay [19]). We shall take the viewpoint that the deviation of ϱ from 3/4 is due to non-local effects, and we shall be concerned with a local approximation of the interaction Hamiltonian, for which ϱ is exactly 3/4 and $|\xi|$ exactly 1.

Physically $|\xi| = 1$ means a definite polarization for the electron emitted in the μ-decay. We take this indication as a starting point for postulating an invariance property of the interaction Hamiltonian under a transformation of the form

$$e \to \exp(i\beta_e + i\alpha_e\gamma_5)e, \quad \bar{e} \to \exp(-i\beta_e + i\alpha_e\gamma_5)\bar{e}, \tag{1}$$

$$\mu \to \exp(i\beta_\mu + i\alpha_\mu\gamma_5)\mu, \quad \bar{\mu} \to \exp(-i\beta_\mu + i\alpha_\mu\gamma_5)\bar{\mu}. \tag{1'}$$

In (1) and (1') the factors $\exp(i\beta)$ correspond to the usual gauge transformation for charged fields, and they are introduced to compensate the phase factors arising from the factors $\exp(i\alpha\gamma_5)$.

Nishijima arrives at the invariance requirements (1) and (1') by noticing that the S-matrix of quantum electrodynamics is left invariant after such transformations †. However, if similar transformations were applied to the baryon fields, they would change the S-matrix. This happens because of the opposite commutation properties of γ_μ and γ_5 with γ_5. If we assume that weak interactions are invariant under (1) and (1'), the total S-matrix including weak interactions will be invariant under such transformations of the charged lepton fields ††.

We specify the two neutrino fields ν_1 and ν_2 by the conditions

$$\gamma_5\nu_1 = \nu_1 \tag{2}$$

$$\gamma_5\nu_2 = -\nu_2 \tag{2'}$$

and we assume lepton conservation.

† This conclusion would not hold if couplings of the form $\sigma_{\mu\nu}F_{\mu\nu}$ were present (which do not satisfy the principle of minimal electromagnetic interaction).

†† To examine the connexion with Tiomno's mass reversal we note that the transformation $\psi \to \psi \exp(i\alpha\gamma_5 + i\beta)$ is equivalent to the substitution $m \to me^{i2\alpha\gamma_5}$ in the Dirac equation, which reduces to $m \to -m$ for $\alpha = \frac{1}{2}\pi$.

Corresponding to our splitting of the neutrino field according to (2) and (2′), we write the most general Hamiltonian for a local approximation to μ-decay in the form

$$H' = H'_{22}+H'_{12}+H'_{21}+H'_{11}+\text{ Hermitian conjugate} \tag{3}$$

where

$$H'_{22} = \tfrac{1}{2}\sum_j G_j(\bar{e}\Gamma_j\mu)(\bar{\nu}_2(1+\gamma_5)\Gamma_j(1-\gamma_5)\nu_2), \tag{4}$$

$$H'_{12} = \tfrac{1}{2}\sum_j F_j(\bar{e}\Gamma_j\mu)(\bar{\nu}_1(1-\gamma_5)\Gamma_j(1-\gamma_5)\nu_2), \tag{4′}$$

$$H'_{21} = \tfrac{1}{2}\sum_j H_j(\bar{e}\Gamma_j\mu)(\bar{\nu}_2(1+\gamma_5)\Gamma_j(1+\gamma_5)\nu_1), \tag{4″}$$

$$H'_{11} = \tfrac{1}{2}\sum_j L_j(\bar{e}\Gamma_j\mu)(\bar{\nu}_1(1-\gamma_5)\Gamma_j(1+\gamma_5)\nu_1). \tag{4‴}$$

The G_j, F_j, H_j, L_j are the coupling constants for the different invariants Γ_j. The Hamiltonian H' is the most general parity-non-conserving Hamiltonian in a *four-component* theory without derivative couplings.

In H'_{22} and H'_{11}, j can take only the values A and V. In H'_{12} and H'_{22}, j can take only the values S, T, and P.

Four different classes of Hamiltonians are found to satisfy the invariance requirements (1) and (1′). These are †

$$H'_{\mathrm{I}} \text{ with } G_{\mathrm{V}} = -G_{\mathrm{A}},\ F_j = H_j = 0,\ L_{\mathrm{V}} = L_{\mathrm{A}}$$
$$H'_{\mathrm{II}} \text{ with } G_{\mathrm{V}} = G_{\mathrm{A}},\ F_j = H_j = 0,\ L_{\mathrm{V}} = -L_{\mathrm{A}}$$
$$H'_{\mathrm{III}} \text{ with } G_j = 0,\ F_{\mathrm{S}} = -F_{\mathrm{P}},\ F_{\mathrm{T}} = 0,\ H_{\mathrm{S}} = H_{\mathrm{P}},\ L_j = 0$$
$$H'_{\mathrm{IV}} \text{ with } G_j = 0,\ F_{\mathrm{S}} = F_{\mathrm{P}},\ H_{\mathrm{S}} = -H_{\mathrm{P}},\ H_{\mathrm{T}} = 0,\ L_j = 0.$$

H'_{I} is invariant under the transformations (1) if the phase factors β are chosen such †† that $\beta_e-\alpha_e = 0$, $\beta_\mu-\alpha_\mu = 0$; H'_{II} is invariant for $\beta_e+\alpha_e = 0$, $\beta_\mu+\alpha_\mu = 0$; H'_{III} for $\beta_e-\alpha_e = 0$, $\beta_\mu+\alpha_\mu = 0$; and H'_{IV} for $\beta_e+\alpha_e = 0$, $\beta_\mu-\alpha_\mu = 0$.

The distribution in energy and angle of the electron emitted in $\mu^- \to e^-+\nu+\bar{\nu}$, with μ^- completely polarized, is given, in the approximation in which the electron mass is neglected, by

$$dN \approx 9(1-x)+2\varrho(4x-3)+\cos\theta\,[-3\xi(1-x)+\eta(4x-3)] \tag{5}$$

where x is the ratio of the electron energy to its maximum value in the decay, and θ is the angle with respect to the μ spin direction. The para-

† The result is perhaps more expressive for the ordering $(\bar{\mu}\nu)(\bar{e}\nu)$. One sees immediately, either directly or by a Fierz transformation, that the four classes of Hamiltonians are $(\mathrm{STP})_{11}+(\mathrm{VA})_{22}$, $(\mathrm{STP})_{22}+(\mathrm{VA})_{11}$, $(\mathrm{STP})_{21}+(\mathrm{VA})_{12}$, $(\mathrm{STP})_{12}+(\mathrm{VA})_{21}$, where we indicate, for instance, by $(\mathrm{STP})_{11}$ an expression of the form

$$\sum_{j=\mathrm{S,T,P}} C_j(\bar{\mu}\Gamma_j(1+\gamma_5)\nu_1)(\bar{e}\Gamma_j(1+\gamma_5)\nu_1).$$

†† We are assuming that the α's for different leptons are unrelated. This assumption is equivalent to postulating invariance under separate mass reversal for each lepton field.

meters ϱ (Michel's parameter), ξ and η can be calculated for the four Hamiltonians satisfying our invariance requirement and are found to be

$$\text{for } H'_{\mathrm{I}} : \varrho = 3/4, \quad \xi = -1, \quad \eta = 3/2$$

$$\text{for } H'_{\mathrm{II}} : \varrho = 3/4, \quad \xi = 1, \quad \eta = -3/2$$

$$\text{for } H'_{\mathrm{III}} : \varrho = \frac{3|H_{\mathrm{T}}|^2}{|F_{\mathrm{S}}|^2+|H_{\mathrm{S}}|^2+3|H_{\mathrm{T}}|^2}, \quad \xi = -\frac{3(|F_{\mathrm{S}}|^2+|H_{\mathrm{S}}|^2)-7|H_{\mathrm{T}}|^2}{|F_{\mathrm{S}}|^2+|H_{\mathrm{S}}|^2+3|H_{\mathrm{T}}|^2}, \eta = -2\varrho$$

$$\text{for } H'_{\mathrm{IV}} : \varrho = \frac{3|F_{\mathrm{T}}|^2}{|F_{\mathrm{S}}|^2+|H_{\mathrm{S}}|^2+3|F_{\mathrm{T}}|^2}, \quad \xi = \frac{3(|F_{\mathrm{S}}|^2+|H_{\mathrm{S}}|^2)-7|F_{\mathrm{T}}|^2}{|F_{\mathrm{S}}|^2+|H_{\mathrm{S}}|^2+3|F_{\mathrm{T}}|^2}, \quad \eta = 2\varrho.$$

The two-component theory with nonderivative coupling gives $\varrho = 3/4$ and $\eta = -3/2\xi$. Therefore the distributions obtained from H'_{I} and H'_{II} are two particular cases of the distributions given by the two-component theory: the distribution obtained from H'_{I} is the same as that obtained from the two-component theory with the vector coupling constant equal but opposite in sign to the axial coupling constant; that obtained from H'_{II} is the same as that obtained from the two-component theory with the vector coupling constant equal to the axial coupling constant. The distributions obtained from H'_{III} and H'_{IV} become those of the two-component theory if the single condition $|F_{\mathrm{S}}|^2+|H_{\mathrm{S}}|^2 = |F_{\mathrm{T}}|^2$, or $= |H_{\mathrm{T}}|^2$, respectively, is satisfied, in which case both $\varrho = 3/4$ and $\eta = -3/2\ \xi$. For a proper choice of the parameters, H'_{III} and H'_{IV} can be made consistent with the experimental data. However, we prefer to consider the correct Hamiltonian to be either H'_{I} or H'_{II}, because they both predict, without any further assumption, both ϱ and $|\xi|$ near to their experimental values. From the discussion of β-decay experiments, we shall derive that H'_{II} is the correct Hamiltonian.

For each of the Hamiltonians H'_{I} to H'_{IV}, the electron emitted in μ^--decay is completely polarized longitudinally — we are always using the approximation $m_{\mathrm{e}} = 0$. In fact the electron is coupled in the combination $(1-\gamma_5)\mathrm{e}$ in H'_{I} and H'_{III}, and with $(1+\gamma_5)\mathrm{e}$ in H'_{II} and H'_{IV}. The polarization is independent from the μ polarization and has positive sign (spin parallel to the momentum, right-handed electron) for H'_{I} and H'_{III}, negative sign for H'_{II} and H'_{IV}.

As to the relation of the Hamiltonians H'_{I} and H'_{II} to the Lee-Yang Hamiltonians, it should be remarked that H'_{I} and H'_{II} are not equivalent to Lee-Yang Hamiltonians in the sense of the equivalence recently discussed by Pauli [20, 21, 22]). Moreover, a generalization of the Pursey-Pauli approach leads one to consider a transformation of the form (1), which also gives equivalent Hamiltonians for effects that do not depend on transverse polarization of the electron [22]) as long as the electron mass is neglected.

Again, even in this sense, H'_{I} and H'_{II} are non-equivalent to Lee-Yang Hamiltonians.

3. β-Decay

Imposing the invariance requirement (1) to the most general local β-decay Hamiltonians, one finds that the following two classes of Hamiltonians are admissible:

$$H''_{\mathrm{I}} = \sum_{\mathrm{S,T,P}} C_j(\bar{\mathrm{p}}\Gamma_j\mathrm{n})(\bar{\mathrm{e}}\Gamma_j(1+\gamma_5)\nu_1)+\sum_{\mathrm{V,A}} C_j(\bar{\mathrm{p}}\Gamma_j\mathrm{n})(\bar{\mathrm{e}}\Gamma_j(1-\gamma_5)\nu_2)$$

$$H''_{\mathrm{II}} = \sum_{\mathrm{S,T,P,}} C_j(\bar{\mathrm{p}}\Gamma_j\mathrm{n})(\bar{\mathrm{e}}\Gamma_j(1-\gamma_5)\nu_2)+\sum_{\mathrm{V,A}} C_j(\bar{\mathrm{p}}\Gamma_j\mathrm{n})(\bar{\mathrm{e}}\Gamma_j(1+\gamma_5)\nu_1).$$

H''_{I} is invariant if β_{e} is chosen such that $\beta_{\mathrm{e}}-\alpha_{\mathrm{e}}=0$, and H''_{II} is invariant for $\beta_{\mathrm{e}}+\alpha_{\mathrm{e}}=0$.

The first important point is that for both H''_{I} and H''_{II} the Fierz interference terms are always exactly zero. This can be easily derived from the observation that the Fierz terms are interference terms between S and V, and between T and A. Summing over neutrino spins, one finds such interference terms contain factors of the form $(1\pm\gamma_5)\Lambda_\nu(1\pm\gamma_5)$ (where Λ_ν is the projection operator for the ν) which give zero †. This mechanism for the disappearance of the Fierz terms permits the existence in the β-decay interaction of both S and V and of both A and T.

The asymmetry parameter α for the angular distribution (written as $1+\alpha\cos\theta$) of the electrons emitted from oriented nuclei in G.T. transitions is, in the usual notations,

$$\alpha = \pm\frac{\langle J_z\rangle}{J}\left(\frac{v}{c}\right)_{\mathrm{e}}\lambda_{J',J} \quad \text{for} \quad H''_{\mathrm{I}} \tag{5}$$

and opposite for H''_{II}. The upper sign always refers to e^-, the lower to e^+. This result is independent from the values of the coupling constants C_{T} and C_{A} (both T and A may be present). The factor $\lambda_{J',J}$ only depends on the initial and final nuclear spins, J and J', and it is equal to one for the β^--decay of Co^{60} [23]). The result of this experiment is in agreement with the prediction from H''_{II}. This excludes H''_{I} as a possible Hamiltonian, and, as a consequence, H'_{I} is excluded for μ-decay, for which case the only possible Hamiltonian is now H'_{II}. We shall return later to a discussion of the $\pi\to\mu\to\mathrm{e}$ cascade.

We note that, due to the automatic absence of the Fierz term in the present theory, the Rustad-Ruby experiment on He^6 [7]) can still be consistent with some fraction of A. The Co^{58} experiment [1, 2]) would require in our

† Mayer and Telegdi express this circumstance by saying that there can be no interference between left- and right-handed neutrinos.

theory the smallness of a term

$$\propto \mathrm{Re}\,(C_S C_T^* + C_V C_A^*)/(|C_T|^2 + |C_A|^2).$$

This can be obtained if there is an appreciable contribution from V and also a small contribution from A. The dominance of V over S, as indicated by the A^{35} experiment [5]), and the presence of a small A, would not be inconsistent with time-reversal invariance.

For both H''_{I} and H''_{II} the emitted electrons are polarized longitudinally. The polarization is, however, not complete, but of a magnitude (v/c), due to the mass term in the free-particle equation. Since the coupling is with $(1-\gamma_5)$e in H''_{I} and with $(1+\gamma_5)$e in H''_{II}, the emitted e^- is right-handed for H''_{I} and left-handed for H''_{II}. Therefore, for H''_{II} the theory predicts a longitudinal polarization $= -(v/c)$ for e^- and $+(v/c)$ for e^+, independent of the particular transition or of the values of the coupling constants. This is exactly the result that would hold in the usual two-component theory with a right-handed neutrino if V and A are absent. This result is consistent with all the results reported so far on G.T. transitions. It is consistent with the recent results on the polarization of the positrons from Ga^{66} and Cl^{34} [24]). It is, however, inconsistent with the results reported previously on the longitudinal polarization of the electrons emitted from Ga^{66} [25]) and from Sc^{46} and Au^{198} [26]). If these last results were confirmed, they would constitute a direct disproof of this theory.

4. $\pi \to \mu$ Decay

In dealing with $\pi \to \mu + \nu$ decay, we use a phenomenological local Hamiltonian including first-order derivatives of the pion field. If the decay occurs through virtual baryon-antibaryon states coupled to the leptons by a Fermi-type interaction, one would expect non-local effects to be less important because the virtual intermediate states are very far from the energy shell. Two classes of Hamiltonians are invariant under (1'):

$$H'''_{\mathrm{I}} = g(\bar{\mu}(1-\gamma_5)\nu_2)\phi + i\frac{f}{m_\pi}(\bar{\mu}\gamma_\lambda(1+\gamma_5)\nu_1)\frac{\partial\phi}{\partial x_\lambda},$$

$$H'''_{\mathrm{II}} = g(\bar{\mu}(1+\gamma_5)\nu_1)\phi + i\frac{f}{m_\pi}(\bar{\mu}\gamma_\lambda(1-\gamma_5)\nu_2)\frac{\partial\phi}{\partial x_\lambda}.$$

H'''_{I} is invariant for $\beta_\mu + \alpha_\mu = 0$, and H'''_{II} for $\beta_\mu - \alpha_\mu = 0$. The latter possibility would, however, be inconsistent with our result for μ-decay, for which the only possible Hamiltonian was H_{II}'. Therefore, we are left with H'''_{I}.

In H'''_{I} the μ is coupled through $(1+\gamma_5)\mu$; however, we cannot conclude from this that the μ^- in π^- decay is emitted left-handed, because of its low

kinetic energy. Its longitudinal polarization is, rather, given by

$$P_L = \frac{-|g|^2+|f|^2}{|g|^2+|f|^2}, \tag{6}$$

and it reaches the values ± 1 only if one of the two couplings is absent. We shall now show that the results on μ-decay imply that essentially only the derivative coupling exists. In the $\pi \to \mu \to e$ cascade, the measured value of ξ in the electron angular distribution is the product $P_L \xi$, where P_L is given by (6). The measured value of ξ is, however, very near to unity after accounting for depolarization effects in the medium, so that we are led to assume $|P_L| = 1$ in $\pi-\mu$ decay. On the other hand, the e^- from μ^--decay is known to be preferentially emitted backward with respect to the μ^- momentum. With our Hamiltonian H'_{II} the electron angular distribution with respect to the μ-spin direction is given by $1-\frac{1}{3}\cos\theta$, which implies that electrons are preferentially emitted backward with respect to the μ-spin. Therefore the μ-spin is parallel to the momentum, which according to (6) implies derivative coupling. In the two-component theory with right-handed neutrinos and with lepton conservation the μ^- emitted in π^- decay must be left-handed, whereas in the present theory it must be right-handed. Moreover, the e^- emitted in μ^--decay is right-handed in the two-component theory with lepton conservation, but it is left-handed in the present theory. All these polarizations are reversed for opposite charge, as follows directly from the TCP theorem. A *direct* measurement of such polarizations would permit us to decide between the present theory and the two-component theory with right-handed neutrinos.

A last remark concerns the absence of $\pi \to e+\nu$. It is gratifying at first sight to be able to conclude that the derivative coupling only is presumably effective in π-decay, because, as it is well known, if one likes to assume that the coupling for $\pi-e$ decay is the same as for $\pi-\mu$ decay, one finds a ratio of $\propto 10^{-4}$ for $\pi-e$ decay to $\pi-\mu$ decay. The present upper limit for this ratio is, however, still smaller, $\propto 5\times 10^{-5}$ [27]). It might be that such a reduction is due to the other small effects that we have deliberately neglected — although such a possibility seems to us artificial. Moreover, it must be remarked that we have not been able to derive directly from the theory the conclusion that the coupling must be derivative, but we have only shown that this possibility is the most consistent with the $\pi \to \mu \to e$ experiments, if they are interpreted according to the theory here discussed.

Nishijima gives a theorem stating that weak interactions involving only a $\mu-e$ pair cannot be invariant under (1) and (1'). This theorem would forbid unwanted processes such as $K^0 \to \mu+e$, $K \to \pi+\mu^\pm+e^\mp$, $\mu \to e+\gamma$, $\mu \to e+e+e$, $\mu+N \to N+e$, etc. (which are not forbidden by lepton conservation under the present assignment, according to which μ^-, e^-, ν are

leptons, and their charge conjugates antileptons). To prove such a theorem it is essential, however, to assume that the only sources of parity non-conservation are the couplings with the neutrino field. We do not see at present any reason for such a postulate.

5. Final Remarks

It was the purpose of this work to show how a relatively simple theory can be constructed such that:

(i) It is based on general theoretical assumptions rather than on phenomenological hypotheses. Parity non-conservation arises from a postulated invariance property for the charged leptonic fields. The theory can be interpreted in terms of two massless two-component neutrino fields, and parity non-conservation is simply a reflection of the different way in which the two fields are coupled.

(ii) It maintains all successful predictions of the simpler two-component theory with right-handed neutrinos. It leads, moreover, to more specific predictions in μ-decay. It does not provide an explanation of the absence of $\pi \to e+\nu$, but it strongly suggests that the derivative coupling is responsible for such decay, thus leading to a very small transition probability. The philosophy underlying the theory is that leptons appear in the interactions as particles with definite longitudinal polarizations. The deviations of ϱ from 3/4 in μ-decay would be due to effects that are neglected in the local approximation to the interaction Hamiltonian.

(iii) It allows for the possibility of having both S and V, and, if necessary, both T and A in β-decay without implying violation of time-reversal invariance. It leads, for any mixture of couplings, to the same values for the longitudinal polarizations of β-particles that are predicted by the two-component theory with right-handed neutrinos and with only S and T interactions. It is not consistent with all the β-decay experiments that have been reported in these last few months, but some of them appear in direct contradiction with each other †.

The theory discussed here is of course more complicated, and therefore less attractive, than a theory with one single two-component neutrino. We would conclude that a careful re-examination of the most relevant experimental results on β-decay has to be carried out before deciding on the two-component theory.

We may briefly examine two of the simplest possibilities. Suppose the conclusion from the He^6 experiment [7]) is not valid, and that A instead of T is the predominant G.T. interaction. Then, from the β-decay of the neutron [8]), one would conclude that V is the dominant Fermi type inter-

† For a review of recent β-decay experiments, see ref. [23]).

action. This result would be confirmed by the Ne^{19} experiments [6]), and a direct experimental test would be the A^{35} experiment [5]). The Co^{60} experiment [23]), all the experiments carried out on the longitudinal polarization of β-particles in G.T. transitions, and the Ga^{66} and Cl^{34} experiments [24]) would then indicate $C'_A = C_A$, $C'_V = C_V$. This theory would be a two-component theory with left-handed neutrinos †. The Co^{58} experiment [1, 2]) would still present a difficulty, unless time-reversal invariance is not valid.

If, on the other hand, the He^6 result is valid and T is the dominant G.T. interaction, then, from the β-decay of the neutron one would conclude that S is the dominant F interaction. This result would be confirmed by the Ne^{19} experiments, but the conclusion from the A^{35} experiment would be wrong. The Co^{60} experiment, the experiments on longitudinal polarization in G.T. transitions, and the Ga^{66} and Cl^{34} experiments would suggest $C'_T = -C_T$, $C'_S = -C_S$. This is the two-component theory with right-handed neutrinos. Again the Co^{58} experiment would constitute a difficulty if time reversal is valid.

The Rustad-Ruby experiment on He^6 is one of the most accurate experiments in β-decay. Its present role in deciding between the various theoretical possibilities is, however, so crucial, that we would strongly suggest a careful re-examination of the experimental conclusion in favor of tensor interaction in G.T. transitions. If, on the other hand, further experimental evidence substantiates the present indication that none of the single solutions with a single two-component neutrino (either right- or left-handed) is able to explain β-decay, we would consider the theory discussed in this paper as a most attractive possibility for the description of weak interactions.

The author is indebeted to Professors E. Segrè and R. Karplus for discussions and for information about the experimental results.

† *Note added in proof:* This solution has been recently advocated by Marshak and Sudarshan (reported at the Venice Conference) and by Feynman and Gell-Mann ("A theory of the Fermi interaction", preprint). It may be useful to examine the relation of the theory discussed here to the Feynman-Gell-Mann theory. It can be verified that the Feynman-Gell-Mann theory can be obtained from the theory presented here by a particular choice of the coupling constants. This choice is obtained by adding the following two postutates to our theory: 1) only μ_1 is coupled; 2) the Tiomno-Nishijima invariance is valid not only for leptons, as we have assumed, but also for baryons, as long as only their weak and electromagnetic interactions are considered. If 2) is found experimentally to be true, it would constitute the first example of an invariance property which holds for the weak but not for the strong interactions.

Appendix

Received 15 October 1957

A Modified Theory without Lepton Conservation

R. Davis, Jr. has recently performed an experiment to detect absorption according to

$$\nu + Cl^{37} \rightarrow A^{37} + e^- \tag{A1}$$

of neutrinos emitted from the pile (in the reaction $n \rightarrow p + e^- + \nu$) [29]). If leptons are conserved, it follows from neutron decay that e^- and ν have opposite leptonic number, and (A1) would be rigorously forbidden. Assuming that neutrinos and antineutrinos are identical, so that all neutrinos emitted from the neutron decay can be absorbed according to (A1), one can estimate for (A1) a cross section $\approx 2.6 \times 10^{-45}$ cm^2 from the inverse process (electron capture from A^{37}), neglecting any dependence on the neutrino energy in the nuclear matrix element [30]). If only one polarization state is allowed for neutrinos, the statistical weight for the inverse of (A1) becomes smaller by a factor two, which implies that the coupling constants must be taken larger by a factor $\sqrt{2}$, and the above estimate becomes 5.2×10^{-45} cm^2. Davis finds a cross section equal to or less than 1.1×10^{-45} cm^2, and he estimates as improbable that a large fraction of the observed A^{37} is produced by background reactions. However Alvarez has suggested that perhaps all A^{37} observed could be produced by cosmic ray μ-mesons [31]). Suppose we take the result of Davis' experiment literally. Then lepton conservation is excluded and also complete identity between neutrino and antineutrino would be excluded by the small cross section. One would rather assume an intermediate description of the kind discussed by Pauli [23]). We shall briefly examine a modification of the theory discussed in this paper, which is obtained by giving up the lepton conservation hypothesis. In a similar way as in the Mayer-Telegdi theory [16]) one recognizes immediately that, if lepton conservation is not assumed, one can assume only one left-handed and one right-handed neutrino, each charge conjugate to the other, and thus adopt a two-component description of the neutrino field. For a two-component neutrino, the μ-decay interaction, without any hypothesis of lepton conservation, can be written in the general form

$$\begin{aligned} H' = &\sum_{V,A} a_j (\bar{e}\Gamma_j \mu)(\tilde{\nu}\Gamma_j(1-\gamma_5)\nu) + \sum_{S,P} b_j (\bar{e}\Gamma_j \mu)(\tilde{\nu}^c \Gamma_j(1-\gamma_5)\nu) \\ &+ \sum_{S,P} c_j (\bar{e}\Gamma_j \mu)(\tilde{\nu}\Gamma_j(1+\gamma_5)\nu^c), \end{aligned} \tag{A2}$$

where we are using a four-component formalism (assuming for definiteness the projection operator $\frac{1}{2}(1-\gamma_5)$ for the neutrino field) and are taking the definitions, $\nu^c = C^{-1}\tilde{\nu}$ and $\tilde{\nu}^c = -\nu C$, C being the charge conjugation matrix

satisfying $CC\dagger = 1$ and $C\gamma_\mu C^{-1} = -\gamma_\mu^{\mathrm{T}}$. In (A2) a_j, b_j and c_j are coupling constants, and the summations over the indices j are restricted to particular values by the requirements, (i), that the neutrino field always occurs in the form $(1-\gamma_5)\nu$, and (ii), that ν anticommutes with itself and similarly for $\bar{\nu}$ (the absence of T in the second and third term is due to (ii)). Four classes of Hamiltonians are invariant under the transformations (1) and (1'); they are specified by the following conditions on the coupling constants:

(I)	$a_{\mathrm{V}} = a_{\mathrm{A}}$	$b,\ c = 0$
(II)	$a_{\mathrm{V}} = -a_{\mathrm{A}}$	$b,\ c = 0$
(III)	$a\ = 0$	$b_{\mathrm{S}}\ = b_{\mathrm{P}},\ c_{\mathrm{S}} = -c_{\mathrm{P}}$
(IV)	$a\ = 0$	$b_{\mathrm{S}}\ = -b_{\mathrm{P}},\ c_{\mathrm{S}} = c_{\mathrm{P}}$.

The ϱ value excludes (III) and (IV) and therefore only (I) and (II) are possible. The result is the same as for the two-component theory *with* lepton conservation and with the axial coupling constant equal or opposite to the vector coupling constant. In β-decay two classes of Hamiltonians are invariant:

$$\text{(I)} \qquad \sum_{\mathrm{S,T,P}} a_j(\bar{\mathrm{p}}\Gamma_j\mathrm{n})(\bar{\mathrm{e}}\Gamma_j(1-\gamma_5)\nu) + \sum_{\mathrm{V,A}} b_j(\bar{\mathrm{p}}\Gamma_j\mathrm{n})(\bar{\mathrm{e}}\Gamma_j(1+\gamma_5)\nu^{\mathrm{c}}),$$

$$\text{(II)} \qquad \sum_{\mathrm{V,A}} a_j(\bar{\mathrm{p}}\Gamma_j\mathrm{n})(\bar{\mathrm{e}}\Gamma_j(1-\gamma_5)\nu) + \sum_{\mathrm{S,T,P}} b_j(\bar{\mathrm{p}}\Gamma_j\mathrm{n})(\bar{\mathrm{e}}\Gamma_j(1+\gamma_5)\nu^{\mathrm{c}}).$$

Both classes lead to states containing both neutrinos and antineutrinos. The Fierz terms are naturally zero in this theory because of the absence of interference between the neutrino amplitudes and the antineutrino amplitudes. The discussion given before on β-decay experiments can easily be extended to the lepton non-conserving Hamiltonians (I) and (II) by making use of Pauli's transformations [23]), and it can be seen that all previous conclusions apply to the present case. The correct Hamiltonian is then found to be (I). Also for π and K decays the conclusions are exactly the same as for the four-component theory discussed in the text. As for the neutrino absorption experiment, $\nu + \mathrm{p} \to \mathrm{n} + \mathrm{e}^+$ [32]), we recall that in the two-component theory with lepton conservation only $\bar{\nu}$'s are emitted from the pile in the neutron decay, and they can all be absorbed by p to give e^+. From the inverse process, the expected cross section would be $13 \times 10^{-44}\ \mathrm{cm}^2$, while the observed cross section is $(4.0 \pm 1.5) \times 10^{-44}\ \mathrm{cm}^2$ [33]). In the present theory both ν and $\bar{\nu}$ are emitted from the pile and both can be absorbed by the protons. However $\bar{\nu}$ (emitted through S, T, P) is only absorbed through S, T, P; ν (emitted through V, A) is only absorbed through V, A. Therefore the cross section would be expected to be smaller than that predicted by the two-component theory — the same holds in the Mayer-Telegdi theory. In the $\nu + \mathrm{Cl}^{37} \to \mathrm{A}^{37} + \mathrm{e}^-$ experiment [29]) both ν and $\bar{\nu}$ are emitted from the pile (ν via V, A; $\bar{\nu}$ via S, T, P) and both are absorbed

(ν via S, T, P; $\bar{\nu}$ via V, A). However, as Mayer and Telegdi remark, Cl^{37} and A^{37} are not mirror nuclei, so there should be very little Fermi transition. Roughly, one can assume that only ν is absorbed (assuming no A) and thus only a fraction of the neutrinos emitted (those emitted through V) can be absorbed. A reduction of the cross section from 5.2×10^{-45} cm^2 to 1.1×10^{-45} cm^2 or less is perhaps acceptable. In double β-decay, $n+n\rightarrow p+p+e^-+e^-$, the virtual neutrino would be emitted according to

$$\nu \text{ via V, A;} \qquad \bar{\nu} \text{ via S, T, P;}$$

and absorbed according to

$$\nu \text{ via S, T, P;} \qquad \bar{\nu} \text{ via V, A.}$$

Unfortunately the mechanism proposed by Mayer and Telegdi to show the absence of double β-decay does not work in this case. The argument was based on the remark that double β-decay could possibly be observed between even nuclei for which the transition between the ground states is $0^+\rightarrow0^+$. In our case, with a virtual ν, starting from 0^+ the intermediate state is again 0^+ (V transition), from which the final 0^+ state can be reached through S (but not via T); with a virtual $\bar{\nu}$, the intermediate state can be reached only through S, from which the final state is reached through V. Therefore a general argument, similar to that of Mayer and Telegdi, could be given only if S were practically absent. However, the starting point of our discussion was the possibility of allowing for the simultaneous presence of S and V without violating time-reversal invariance. We would conclude that the absence of double β-decay is a difficulty for the modified theory discussed here — the simplest explanation is provided by the hypothesis of conservation of leptons.

References

1) Ambler, Hayward, Hoppes, Hudson and Wu, Phys. Rev. **106** (1957) 1361
2) Postma, Hiskamp, Miedma, Steenland, Tolhoek and Gorter, Physica **23** (1957) 259
3) D. F. Griffing and J. C. Wheatley, Phys. Rev. **104** (1956) 389
4) Kistner, Schwarzschild and Rustad, Phys. Rev. **104** (1956) 154
5) Herrmannsfeldt, Maxson, Stahelin and Allen (to be published)
6) Maxson, Allen and Jentschke, Phys. Rev. **97** (1955) 109;
   M. L. Good and E. J. Laner, Phys. Rev. **105** (1957) 213;
   W. P. Alford and D. R. Hamilton, Phys. Rev. **105** (1957) 673
7) B. M. Rustad and S. L. Ruby, Phys. Rev. **97** (1955) 991
8) J. M. Robson, Phys. Rev. **100** (1955) 933
9) A. Salam, Nuovo Cimento **5** (1957) 299; L. D. Landau, Nuclear Physics **3** (1957) 127;
   T. D. Lee and C. N. Yang, Phys. Rev. **105** (1957) 1671
10) R. Gatto, Phys. Rev. **106** (1957) 168
11) Lee, Oehme and Yang, Phys. Rev. **106** (1957) 340
12) T. D. Lee, Proc. of the VII Rochester Conference, 1957 (to be published)
13) Jackson, Treiman and Wyld, Phys. Rev. **106** (1957) 517;
   M. Morita and R. S. Morita, Phys. Rev. **107** (1957) 139
14) R. Gatto, Invariants in $K_{\mu3}$ and K_{e3} decays, UCRL 3949

15) K. Nishijima, Nuovo Cimento **5** (1957) 1349
16) M. Goeppert Mayer and V. L. Telegdi (to be published)
17) See K. Crowe, Bull. Am. Phys. Soc. **2** (1957) 206
18) Garwin, Lederman and Weinrich, Phys. Rev. **105** (1957) 1415;
J. Friedman and V. L. Telegdi, Phys. Rev. **105** (1957) 1681;
D. H. Wilkinson (to be published)
19) T. D. Lee and C. N. Yang (to be published)
20) W. Pauli, Nuovo Cimento **6** (1957) 204
21) D. L. Pursey (to be published)
22) R. Gatto and G. Lüders, Invariants in μ-decay, UCRL 3935
23) Wu, Ambler, Hayward, Hoppes and Hudson, Phys. Rev. **105** (1957) 413
24) Deutsch, Gittelman, Bauer, Grodzins and Sunyar (to be published)
25) Frauenfelder, Hanson, Levine, Rossi and DePasquali (to be published)
26) Frauenfelder, Bobone, von Goeler, Levine, Lewis, Peacock, Rossi and DePasquali (to be published)
27) S. Lokanathan and J. Steinberger, Phys. Rev. **98** (1955) 240
28) T. Kotani, Brief Review of Allowed β-Transitions, UCRL-3798 (May 1957)
29) R. Davis Jr., An attempt to observe the capture of reactor neutrinos in Cl^{37} (preprint)
30) L. W. Alvarez, University of California Radiation Laboratory Report UCRL-328 (1949) (unpublished)
31) L. W. Alvarez, private communication
32) F. Reines and C. L. Cowan, Phys. Rev. **92** (1953) 830

Nuclear Physics **5** (1958) 544—556; © *North-Holland Publishing Co., Amsterdam*
Not to be reproduced by photoprint or microfilm without written permission from the publisher

FINITE SIZE EFFECTS ON M1 CONVERSION COEFFICIENTS

A. S. REINER
Instituut voor Theoretische Physica, Amsterdam, Nederland †

Received 5 September

Abstract: Finite size effects in M1 conversion coefficients are calculated using the collective model. For transitions within one rotational band corrections relative to Sliv's conversion coefficient can be as large as 50 % in favourable cases. As an example of transitions between different rotational bands the 482 keV transition in ^{181}Ta is discussed. The theory predicts a value of β(theoretical)/β(point-nucleus) $\approx$ 20, whereas the observed value is 5 ± 2. Corrections on static magnetic moments, as discussed by Bohr and Weisskopf, are estimated for elements in the same region.

1. Introduction

Recent measurements of electron conversion coefficients [1]) have revealed appreciable deviations from the theoretical values as given by Rose *et al.* In these calculations the basic assumption has been made that the nucleus can be considered as a point-nucleus. This picture has the attractive feature in that the transition probabilities for an excited nucleus to reach a lower state by either photon emission or electron conversion are exactly proportional to each other. It is then understood that one compares processes in which the emitted photons (real in the case of γ emission and virtual in the case of electron conversion) carry the same angular momentum and parity. The ratio of the two probabilities, i.e. the electron conversion coefficient for the transition is in this approximation determined solely by electron mechanics.

It has been realized before that the interaction of an electron with a nucleus of finite dimensions would spoil this simple picture [2]). To be more specific one has to consider the possibility of the converting electron to be inside as well as outside the nucleus. These two possibilities necessitate different multipole expansions of the Green's function, which describes the retarded interaction between the electron and the nucleus for the two cases $r_e > r_N$ and $r_e < r_N$. The matrix element responsible for electron conversion with a specific polarity is in general a sum of products of separated nuclear and electron matrix elements. If the nucleus can be considered as a point nucleus only one product occurs. The nuclear part is exactly equal to the nuclear matrix element that describes γ emission and the conversion

† Work performed at CERN, Theoretical Study Division, Copenhagen.

coefficient has the property mentioned above. In general additional nuclear matrix elements will occur and the correct expression for the conversion coefficient will contain nuclear properties through ratios of these matrix elements.

A second modification regards the electron wave functions. As the electron experiences through the finite size of the nucleus a smeared-out nuclear charge distribution, the wave functions of s-electrons in particular will undergo changes compared to the wave functions appropriate to a point-nucleus. Both the multipole potentials in the electron matrix element and the s-electron wave functions are irregular at the origin for a point-nucleus, and their precise form matters much for processes, which take place in the neighbourhood of the nucleus. M1 conversion is just such a process.

Even before the first discrepancies between experimental and theoretical conversion coefficients came into evidence, calculations of finite size effects were performed by Sliv [3]). He used a model in which the currents in the nucleus were limited to the surface. For the nuclear charge distribution that determines the electron wave functions a homogeneous distribution was chosen. The calculations yielded the then unexpected result that M1 conversion coefficients for K conversion are much smaller than Rose's values. The reduction factor increases with Z and attains for energies of, say, 0.5 mc^2 a value ≈ 0.5 for the heaviest elements.

Church and Weneser finally shaped the general expression of Tralli and Goertzel [2]) for the M1 conversion coefficient in an amenable form, which clearly displays the role of a general current distribution [4]). They find for the coefficient of M1 conversion for K electrons the following expression:

$$\beta_1^{\mathrm{K}} = \beta_1^{0\mathrm{K}}(\mathrm{s}_{\frac{1}{2}})\left[1+\lambda\frac{3}{10\pi}\frac{R}{k}\,(f_{\mathrm{i}}^{0}g_{\mathrm{f}}^{0}+f_{\mathrm{f}}^{0}g_{\mathrm{i}}^{0})\left(\frac{2\pi^3 e^2}{k}\right)^{\frac{1}{2}}(\beta_1^{0\mathrm{K}}(\mathrm{s}_{\frac{1}{2}}))^{-\frac{1}{2}}\right]^2+\beta_1^{0\mathrm{K}}(\mathrm{d}_{3/2}). \tag{1}$$

Here $\beta_1^{0\mathrm{K}}(\mathrm{s}_{\frac{1}{2}})$ and $\beta_1^{0\mathrm{K}}(\mathrm{d}_{3/2})$ are the partial conversion coefficients for a point-nucleus, where the K electron is excited into a $\mathrm{s}_{\frac{1}{2}}$ and a $\mathrm{d}_{3/2}$ continuum state respectively; $(r/R)f^0$ and g^0 are the dominant terms in a series expansion of the radial Dirac wave functions in powers of (r/R), while the subscripts $_{\mathrm{i}}$ and $_{\mathrm{f}}$ refer to initial and final state; R is the nuclear radius and k the transition energy in units mc^2. Finally λ is defined as

$$\lambda \equiv \frac{M_e}{M_\gamma} = \frac{\int_0^\infty \mathrm{d}\tau_{\mathrm{N}}\,\mathbf{j}_{\mathrm{N}}\cdot\mathbf{A}_{1\mathrm{M}}^{*}(kr_{\mathrm{N}})(r_{\mathrm{N}}/R)^2}{\int_0^\infty \mathrm{d}\tau_{\mathrm{N}}\,\mathbf{j}_{\mathrm{N}}\cdot\mathbf{A}_{1\mathrm{M}}^{*}(kr_{\mathrm{N}})}, \tag{2}$$

where $\mathbf{j}_{\mathrm{N}}$ is the transition matrix element of the nuclear current density operator and $\mathbf{A}_{1\mathrm{M}}(kr_{\mathrm{N}})$ is the M1 standing wave vector potential. The nuclear properties enter into (1) through λ, which is the relative second moment of $\mathbf{j}_{\mathrm{N}}\cdot\mathbf{A}_{1\mathrm{M}}^{*}(kr_{\mathrm{N}})$.

As $\beta_1^0(d_{3/2}) \ll \beta_1^0(s_{\frac{1}{2}})$, formula (1) can be written approximately in the form

$$\beta_1^K(\lambda) \approx [1-(\lambda-1)\, C^K(Z,\, k)]^2\, \beta_1^K(1). \qquad (3)$$

The function $C(Z, k)$ has been tabulated for K conversion [4])† and was calculated for L_I conversion (see appendix B). In the form (3) $\beta_1(\lambda)$ is not expressed in the point-nucleus conversion coefficient β_1^0, but in $\beta_1(\lambda = 1)$. As can be seen from (2), $\beta_1(1)$ is the conversion coefficient, obtained for Sliv's model in which the current density lies on the nuclear surface [5]). The values of $C(Z, k)$ are small of the order of 1—2 %, and only fairly large deviations of λ from 1 will give significant modifications of Sliv's result. As λ is inversely proportional to M_γ (the matrix element for M1 γ-emission) large λ values can if at all only be expected for forbidden or inhibited M1 transitions, provided M_e in (2) is not subject to the same selection rule which forbids the γ transition.

Three classes of more or less forbidden M1 transitions were mentioned by Church and Weneser, viz. the l-forbidden single particle transitions [6]), the M1 transitions between the two lowest 2^+ states in so-called vibrational spectra [7]) and M1 transitions in some odd mass nuclei, which show rotational spectra. In what follows we shall limit ourselves to a calculation of λ and $\beta(\lambda)/\beta(1)$ for nuclei from the last group, because they have found perhaps the best theoretical description until now.

2. Application of the Collective Model to the Church and Weneser Theory

Low-lying states of an odd mass nucleus that shows a rotational spectrum are described by a wave function Ψ, which depends on the coordinates of the odd particle and collective coordinates [8]). For low excitations the collective rotations are most important. They are described by the wave functions of a symmetrical top, $D^I_{MK}(\theta_i)$, in terms of Eulerian angles θ_i and I, M and K which are the total angular momentum and the components of I on a space-fixed axis and on the nuclear symmetry axis respectively. Besides these collective motions the particle can occupy intrinsic states in a deformed spheroidal field, for instance in an anisotropic harmonic oscillator field. Particle states are then specified by an oscillator quantum number N, the component Ω of the particle angular momentum on the symmetry axis and the parity π. Due to the lack of spherical symmetry of the field the particle angular momentum j is not a good quantum number. Therefore, introducing particle states $\chi_{j\Omega}$ in a spherical field, any state

† *Note added in proof:* In the calculations of ref. [4]), a factor $\sqrt{(2/3)}$ has been omitted in the expression for $C(Z, k)$. This affects the numbers given in column 8 of table 1.

of the odd particle in the spheroidal field with given N, Ω, π is a linear combination of the $\chi_{j\Omega}$,

$$\chi_\Omega = \sum_j c_j \chi_{j\Omega}. \tag{4}$$

(It is usually assumed that only $\chi_{j\Omega}$ with the same N contribute significantly.)† The total nuclear wave function is

$$\Psi = \sqrt{\frac{2I+1}{16\pi^2}}\,\phi_{\text{vibr}}\,[\chi_\Omega D^I_{MK}(\theta_i)+(-)^{I-j}\chi_{-\Omega}D^I_{M-K}(\theta_i)] \tag{5}$$

where ϕ_{vibr} describes vibrations around the equilibrium shape, which do not matter here.

We now come back to our purpose, viz. to calculate structure dependent conversion coefficients, applying the collective model. The essential point in such a model is the description of the many body problem through a limited number of dynamical variables. This provides us with a simple expression for the nuclear current density operator, as needed in (2), viz.

$$\mathbf{j}_N(\mathbf{r}) = g_l \frac{e}{M}\{\mathbf{p},\, \delta(\mathbf{r}-\mathbf{r}_p)\}_+ + \frac{e}{M} g_s(\nabla\times\mathbf{s})\delta(\mathbf{r}-\mathbf{r}_p)+\varrho_p(\mathbf{r})\mathbf{v}(\mathbf{r}). \tag{6}$$

$\mathbf{j}_N$ is an operator in terms of the canonical variables of the system, namely the particle coordinates $\mathbf{r}_p$ and $\mathbf{p}$, and the collective coordinates α_μ and their canonical conjugates. The first two parts of (6) are the convection current and the spin current operators of the odd particle. The third term originates from the collective flow $\mathbf{v}$, which contains the collective variables α_μ and their conjugate momenta. The α_μ characterize the nuclear surface in a quadrupole deformation and are defined by the equation of the surface

$$r = R(1+\sum_\mu \alpha_\mu Y_{2\mu}(\vartheta,\,\phi)), \tag{7}$$

where R is the radius of the undeformed nucleus. $\varrho_p(\mathbf{r})$ in (6) represents the nuclear charge density; g_l and g_s are the gyromagnetic ratios for orbital and intrinsic spin respectively. Applying the long wave length limit $kR \ll 1$ for the multipole potential $\mathbf{A}_{1M}$ in (2), which reads ($\mathbf{e}_\mu$ being a unit-vector in the μ-direction)

$$\mathbf{A}_{1M} \approx \frac{k^2}{3\pi^{\frac{1}{2}}}\left(\frac{3}{4\pi}\right)^{\frac{1}{2}}\mathbf{r}\times\mathbf{e}_\mu, \tag{8}$$

and using (6), one can easily transform (2) into

† A different but equivalent representation was used by Nilsson [9]), in which χ_Ω is written as a linear combination of states labeled by $Nl\Lambda\Sigma$. Here l is the orbital angular momentum; Λ and Σ are the components of l and the intrinsic spin s on the nuclear symmetry axis respectively. Thus

$$\chi_\Omega = \sum_{l\Lambda} a_{l\Lambda}\,\chi_{Nl\Lambda\Sigma}. \tag{4a}$$

$$\lambda \equiv \frac{M_e}{M_\gamma}$$

$$= \frac{\sum_\mu \mathbf{e}_\mu \cdot \iint d\theta_i\, d\mathbf{r}\, \Psi_f^*(\mathbf{r},\ \theta_i)\left[\left\{g_l \mathbf{l} + g_s \mathbf{s} + g_s\left(\mathbf{s} - s_r \frac{\mathbf{r}}{r}\right)\right\}\left(\frac{r}{R}\right)^2 + g_R \int d\mathbf{r}'\, \mathbf{R}(\mathbf{r}')\left(\frac{r'}{R}\right)^2\right] \Psi_i(\mathbf{r}, \theta_i)}{\sum_\mu \mathbf{e}_\mu \cdot \iint d\theta_i\, d\mathbf{r}\, \Psi_f^*(\mathbf{r},\ \theta_i)[g_l \mathbf{l} + g_s \mathbf{s} + g_R \mathbf{R}]\, \Psi_i(\mathbf{r},\ \theta_i)} \quad (9$$

Here $s_r = \mathbf{s} \cdot \mathbf{r}/r$; g_R and $\mathbf{R}(\mathbf{r})$ are the gyromagnetic ratio and the angular momentum density of the collective motion respectively. They are defined through the introduction of a nuclear mass density, $\varrho_m(\mathbf{r}')$, by

$$\int \varrho_p(\mathbf{r}')\mathbf{r}' \times \mathbf{v}(\mathbf{r}')d\mathbf{r}' \equiv g_R \int \varrho_m(\mathbf{r}')\mathbf{r}' \times \mathbf{v}(\mathbf{r}')d\mathbf{r}' = g_R \int \mathbf{R}(\mathbf{r}')d\mathbf{r}' = g_R\, \mathbf{R}. \quad (10)$$

The numerator of (9) can in fact be treated in the same way as a matrix-element of a multipole operator, such as is for instance the denominator M_γ. One first transforms the operator to a coordinate frame fixed in the nucleus and performs then the integration over collective variables θ_i [9]). There remain then in (10) only integrals over the particle coordinate $\mathbf{r}$.

Whereas the denominator of (2) is simply the matrix element of the magnetic dipole operator, the numerator is not trivially the matrix element of the total magnetic dipole operator multiplied with $(r/R)^2$. As appears from (9) the spin part of the particle current and the two remaining orbital parts are affected differently. This point will turn out to be important.

The collective angular momentum density appears in (9) in the same form as the orbital part of the single particle. But whereas $g_l \mathbf{l}(r/R)^2$ is a simple operator, the corresponding result for the collective motion,

$$g_R \int d\mathbf{r}'\, \mathbf{R}(\mathbf{r}')(\mathbf{r}'/R)^2, \quad (11)$$

is usually a complicated operator in the α_μ and the $\dot{\alpha}_\mu$. The same is true for the actual expression for $\mathbf{R}$. Its effect on Ψ, however, can be found by replacing $\mathbf{R}$ by $\mathbf{I}-\mathbf{j}$. A version of the collective model is specified by giving both the type of flow and the density functions ϱ_p and ϱ_m. Whereas there are many arguments for more or less constant mass and charge densities, the type of flow $\mathbf{v}$ is subject to more speculation. In one method one correlates the velocity field $\mathbf{v}$ with the experimentally measurable moments of inertia. These quantities determine the absolute spacing of levels in one rotational band. They were found to deviate strongly from the values determined on the assumption of an incompressible flow inside the nucleus [10]). The data seem to point more into the direction of a flow intermediate between an irrotational flow (a) and one corresponding to a rotation of the nucleus as a rigid body (b). For these two cases the calculation of the angular momentum density, weighted by $(r/R)^2$, is quite simple.

a. *Incompressible flow*

The velocity field resulting from an incompressible flow inside the surface given by (7) is [11])

$$\mathbf{v} = -\nabla\Phi, \quad \Phi = \tfrac{1}{2}\sum_\mu \dot{\alpha}_\mu r^2 Y_{2\mu}(\vartheta, \phi). \tag{12}$$

Thus one finds for (11) by use of (10) and (12)

$$\int \varrho_p(\mathbf{r}')\mathbf{r}'\times\mathbf{v}(\mathbf{r}')(r'/R)^2$$

$$\approx g_R \cdot \tfrac{1}{2}\varrho_m R^5 \sum_{\mu\mu'} \alpha_\mu^* \dot{\alpha}_{\mu'} \int Y_{2\mu}^*(\vartheta, \phi)(\mathbf{r}\times\nabla)Y_{2\mu'}(\vartheta, \phi)\mathrm{d}\Omega = g_R \mathbf{R}, \tag{13a}$$

where we have only retained terms to the first order in α and $\dot{\alpha}$ [11]). Thus (13a) shows that the picture of an incompressible flow corresponds to a distribution of the angular momentum on the nuclear surface layer.

b. *Rigid body rotation*

The velocity field $\mathbf{v} = \boldsymbol{\omega}\times\mathbf{r}$, with $\boldsymbol{\omega}$ for the angular velocity, can be substituted in (11). One then finds

$$\int \varrho_p(\mathbf{r}')\mathbf{r}'\times\mathbf{v}(\mathbf{r}')(r'/R)^2\mathrm{d}\mathbf{r}' \approx \tfrac{5}{7} g_R \mathbf{R}. \tag{13b}$$

Eq. (13b) is of the same form as (13a) and differs only by a factor 5/7. Thus it appears reasonable to put the last term of the numerator in (8) in the form $\nu g_R \mathbf{R}$, where ν will be a number close to 1.

3. M1 Transitions within one Rotational Band

We shall calculate in this section λ values from (9) for the class of collective M1 transitions which take place within one rotational band. If we exclude nuclei with a ground state spin $I = \frac{1}{2}$, then M_γ, the matrix element of the γ transition, is $(g_\Omega - g_R)\Omega$, where g_Ω, the g-factor of the particle, is defined as

$$g_\Omega = \frac{1}{\Omega}\int \chi_\Omega^*(g_s s_3 + g_l l_3)\chi_\Omega \,\mathrm{d}\mathbf{r}. \tag{14}$$

If $(g_\Omega - g_R)\Omega$ is small as compared to the numerator M_e of (9) the ensuing λ will be large. Of course the forbiddenness of these transitions has only a relative meaning as there is no selection rule that makes M_γ vanish.

After performing in (9) the integration over collective variables as described in section 2, one is left with matrix elements of single particle operators only. A straightforward calculation of λ in terms of the component amplitudes c_j from (4) gives

$$\lambda = \frac{\sum_{jj'} c_j c_{j'} U_{jj'}(N;\ ll'\Omega)}{(g_\Omega - g_R)\Omega} \tag{15}$$

with

$$U_{jj'} \equiv \{\delta_{ll'} g_\Omega \Omega + g_s \sum_\Sigma (l\tfrac{1}{2}\Omega - \Sigma | l\tfrac{1}{2} j\Omega)(l\tfrac{1}{2}, \Omega - \Sigma, \Sigma | l\tfrac{1}{2} j\Omega)\Sigma\delta_{ll'}$$
$$-\tfrac{1}{2} g_s (l'100|l'1l0)(j1 - \Omega 0|j'1j' - \Omega) U(1lj'\tfrac{1}{2}; l'j)\}\langle Nl'|(r/R)^2 Nl'\rangle - \nu g_R \Omega. \quad (16)$$

Here $(j_1 j_2 m_1 m_2 | j_1 j_2 jm)$ and $U(j_1 j_2 J j_3;\ J_{12} J_{23})$ are Clebsch-Gordan and Racah coefficients, and $l = j \mp \frac{1}{2}$ if $l = j \pm \frac{1}{2}$. It turns out that usually one amplitude c_j dominates strongly in (4). If we then replace χ_Ω by $\chi_{j\Omega}$ eq. (14) simplifies to

$$\lambda - 1 = \frac{(\sigma - 1) g_\Omega - (\nu - 1) g_R \pm \dfrac{(2j+1)}{4j(j+1)} \sigma g_s}{g_\Omega - g_R}. \quad (17)$$

Here the sign occurring in the numerator corresponds to the sign in $j = l \pm \frac{1}{2}$; $\sigma = \langle r^2 \rangle_{Nl}/R^2$ will be taken as usually to be between 0.6 and 1. The coefficients in front of the g-factors in (17) show the result of the 'weighting' of the constituent parts of the total current. If not for the anomalous spin term in (9), one would have $\lambda - 1 \approx \sigma - 1 < 1$. The importance of the last term in the numerator of (17) depends on $g_s/g_\Omega - g_R$ and decreases with increasing j. To get quantitative results with (17) one needs explicit values for the g-factors. They are derived from two experimental data, viz. the static magnetic moment of the intrinsic state and the mixing ratio of a transition in a band, $\delta^2 = $ Intensity γ(E2)/Intensity γ(M1) [12]. These phenomenological g-values are in a sense effective gyromagnetic ratios that may account for possible contributions to the current density operator not contained in (6) (like exchange currents for instance).

In table 1 the relevant data and results are summarized. In the first six columns are listed the nucleus, the spin and parity of the intrinsic ground state, the dominant orbit l_j, the static magnetic moment μ and the two gyromagnetic ratios g_Ω and g_R. In columns 7 and 8 are given the calculated $\lambda - 1$ values and $[(\beta(\lambda)/\beta(1)] - 1$ for the σ values 1 and 0.6 (horizontally) and the ν values 1 and 0.7 (vertically). For the last numbers in the column we refer to the appendix A.

As can be seen from table 1, $|\lambda - 1|$ values are ≈ 1 in many cases, when the anomalous spin term in (14) does not contribute significantly. There are, however, a number of noteworthy exceptions, when larger values are found. It should be stressed that just in those cases where $|\lambda - 1|$ deviate considerably from 1, the precise value of $g_\Omega - g_R$ is crucial as $\lambda - 1 \propto 1/(g_\Omega - g_R)$. The values of $g_\Omega - g_R$ as given in table 1, are usually afflicted with experimental inaccuracy. As a consequence one should consider the $\lambda - 1$ values with reservation. A few remarks regarding special nuclei will be made.

In the case of ^{163}Dy ($I = 5/2^-$), $|g_\Omega - g_R|$ has been reported to be small, in fact < 0.2 [13]. From the static magnetic moment [14]) and the requirement that g_R will be as close to $+0.4$ as possible, the sign of the difference $g_\Omega - g_R$

TABLE 1

Summary of data and results.

	I^π	dominant orbit	μ	g_Ω	g_R	$\lambda-1$		$[\beta(\lambda)/\beta(1)]-1$ in %		ε in %	
$^{153}_{63}$Eu	5/2+	$g_{7/2}$	1.5	0.65	0.48	— 4.2	—4.0	14	13	—1.0	—0.7
						— 3.3	—3.2	11	11	—1.0	—0.6
$^{155}_{64}$Gd	3/2−	— [a]	—0.30	1.18	0.32	—	—	—	—	+5.9	+3.8
						—	—	—	—	+5.6	+3.6
$^{157}_{64}$Gd	3/2−	— [a]	—0.37	1.10	0.26	—	—	—	—	+4.3	+2.8
						—	—	—	—	+4.2	+2.6
$^{159}_{65}$Tb [b]	3/2+		1.58								
$^{163}_{66}$Dy [c]	5/2−	$h_{9/2}$—	0.53	0.18	0.28	— 3.9	—1.6	15	6	1.4	1.3
						— 4.7	—2.4	18	9	1.3	1.2
$^{165}_{67}$Ho	7/2−	$h_{11/2}$	3.3	1.12	0.34	—	—	—	—	—1.5	—0.9
						—	—	—	—	—1.4	—0.9
$^{175}_{71}$Lu	7/2+	$g_{7/2}$	2.6	0.90	0.38	— 1.4	—1.5	6	6	—1.7	—1.1
						— 1.1	—1.3	5	5	—1.6	—1.0
$^{177}_{72}$Hf	7/2−	$h_{9/2}$	0.61	0.17	0.20	—11.6	—4.9	55	22	—2.1	—1.5
						—13.4	—6.7	64	30	—2.0	—1.3
$^{179}_{72}$Hf	9/2+	$i_{13/2}$	—0.47	—0.17	0.21	—	—	—	—	—2.0	—1.0
						—	—	—	—	—2.2	—1.2
$^{181}_{73}$Ta	7/2+	$g_{7/2}$	2.1	0.72	0.19	— 1.3	—1.4	6	7	—1.6	—1.0
						— 1.2	—1.2	5	5	—1.5	—1.0
$^{185}_{75}$Re	5/2+	$d_{5/2}$	3.14	1.55	0.53	—	—	— 5	—	—2.0	—1.3
						—	—	— 6	—	—1.9	—1.2
$^{187}_{75}$Re	5/2+	$d_{5/2}$	3.18	1.58	0.47	—	—	— 4	—	—1.9	—1.3
						—	—	— 5	—	—1.9	—1.2
$^{233}_{92}$U	5/2+	$i_{11/2}$	0.8	0.46	0.38	4.0	—	—40	—	—5.0	—3.5
						5.4	1.5	—51	—16 [d]	—4.7	—3.1
$^{235}_{92}$U	7/2−	$j_{15/2}$	0.5	0.46	0.12	— 0.7	—1.0	+ 8	+12	+9.9	+6.2
						— 0.6	—0.8	+ 7	+10 [d]	+9.7	+6.0

In the columns are given the nucleus, the spin and parity of the intrinsic ground state, the dominant orbit, the static magnetic moment and the two gyromagnetic ratios. The columns 7 and 8 contain the $\lambda-1$ values for σ values 1 and 0.6 (horizontally) and ν values 1 and 0.7 (vertically). The corrections $[\beta(\lambda)/\beta(1)-1]$ have been calculated for the energy of the transitions $I+2 \to I$. In the last column are listed the structure dependent corrections to the static magnetic moments (see appendix A).

a) In the Gd isotopes there is appreciable mixing of orbits. The λ-values are < 1.

b) The uncertainties in the data do not permit a reliable estimate of g_Ω and g_R.

c) $g_\Omega - g_R$ was assumed to be —0.1 (see discussion in text).

d) $[\beta(\lambda)/\beta(1)-1]$ values for L_1 conversion.

can be found to be negative. We used the tentative value -0.1, but it is clear that $\lambda-1$ is very sensitive to changes in $g_\Omega - g_R$.

Care has to be taken too in the case of ^{177}Hf. Ofer deduced from angular correlation measurements a $g_\Omega - g_R$ value of $+0.03 \pm 0.01$[15]). So small a value implies a large $\lambda-1$ value, but there is, however, doubt as to the accuracy of the experiment [16]).

It is of interest to remark that isotopes with different intrinsic states can lead to widely different $[(\beta(\lambda)/\beta(1))]-1$ values. The examples of the Hf and U isotopes illustrate the influence of the anomalous spinterm in (7) for nuclei with different spin-orbit alignment and different total spins. (The gap in the $\lambda-1$ values in ^{233}U for the two σ values is due to an accidental almost complete cancellation in the numerator of (17) for $\sigma = 3/5$.) We shall come back to this isotope-effect in another context in appendix A.

4. M1-Transitions between Different Rotational Bands

In this section we consider M1 transitions between states belonging to two different rotational bands with $|\Delta K| = 1$. Then transitions may show such a degree of forbiddenness that large λ values are produced.

As an illustration we treat here the 482 keV transition in ^{181}Ta. It proceeds between the two rotational ground states built on the intrinsic states $5/2^+$ and $7/2^+$ respectively. Both the lifetime τ and the mixing ratio δ^2 have been determined experimentally, viz. $\tau \approx 10^{-8}$ sec [17]) and $\delta^2 > 20$, presumably 25 [18, 19]). The partial lifetimes, when compared to the single particle lifetimes, show a strong degree of forbiddenness, which can be understood as follows.

Collective E2 transitions between two states having $\Delta K = 1$ are rigorously forbidden [20]) †. Furthermore one can infer from Nilsson's tables [9]) that the dominant components of the two intrinsic states have opposite signs for Σ and have l values that differ by two units. These facts inhibit a single particle E2 transition and the M1 transition (l-forbiddenness). The observed partial E2 lifetime can, however, roughly be accounted for by a decoupling of the rotational bands through the perturbation [21]) ††

$$H' = -\frac{\hbar^2}{2\mathcal{I}}(j_+ I_- + j_- I_+). \tag{18}$$

In the case of ^{181}Ta (17) admixes the state $|IK\pi\rangle = |7/2,\ 5/2+\rangle$ in the $|5/2,\ 5/2+\rangle$ ground state with an amplitude a, which follows in absolute value from the partial E2 lifetime.

† This 'selection rule' results simply from the choice of the body-fixed coordinate system.

†† Stelson and McGowan [19]) give for the reduced E2 transition probability of the odd particle $e^2 \times 10^{-52}$ cm^4, which value would account for the observed lifetime. We believe, however, that their value is much too high in spite of some arbitrariness in the choice of constants that occur in the radial matrix element.

The result, $|a| = 1.2\ \%$, has to be compared with the amplitude that can be found from Nilsson's wave functions, which yield $a = -3.4\ \%$. The sign of a was assumed to be the same as found in the calculation of the mixing amplitude, in spite of the disagreement of the absolute values. For the calculation of λ one needs $M_\gamma(\mathrm{M1})$, which can be found in an indirect manner from the partial E2 lifetime δ and from a. The magnitude and the sign of δ follow both from angular correlation measurements [18, 19]. The numerator of (2) can be calculated in much the same way as set out in section 3. The resulting λ value is finally of the order of 250 and $\beta(\lambda)/\beta(1)$, from (3), consequently becomes ≈ 20. The observed value of $\beta(\lambda)/\beta(1)$ has been reported to be 5 ± 2 [18]). While the numerical agreement is bad, it should be stressed that small modifications in either the lifetime or the mixing ratio δ^2 could bring the theoretical value closer to the experimental one. In any case the example shows that very large departures from Sliv's conversion coefficients can indeed occur.

On the other hand a mere assignment of a transition as a l-forbidden transition in the sense sketched above, is *not* a guarantee that $\beta(\lambda)/\beta(1)$ values will be found as large as is obtained in the case of ^{181}Ta. Thus in ^{175}Lu for instance, one meets a transition between the same intrinsic states as in Ta and of comparable energy [22]). The observed δ^2 value, however, is ≈ 0.25 instead of ≈ 20 and the effect on the conversion coefficient is only of the order of $\approx 10\ \%$. This very different behaviour illustrates that small perturbations may effect apparently very similar 'l-forbidden' M1 transitions quite differently.

5. Conclusion

In the preceding sections it has been shown how the collective model through a known contribution to the nuclear current can be applied to a calculation of finite size corrections on M1 conversion coefficients. The corrections can be quite large in those nuclei, for which inhibited M1 transitions are observed.

As to conversion coefficients of transitions within one rotational band, the structure-dependent corrections depend on the gyromagnetic ratios g_Ω and g_R. They are in turn found by use of the mixing ratio δ^2. If δ^2 is determined from a K/L measurement, then the calculation of the correction is not self-consistent, and the discrepancy is the greater, the larger the correction. In these and more general cases a method to search for finite size effects is by measuring mixing ratios in two ways, viz. from K/L ratios and from angular correlation measurements. If on the other hand these two experimental data are not both available, a detection of real discrepancies in conversion coefficients may turn out to be quite hard.

Finally it follows from the λ values of table 1 that even a possible precision measurement of a conversion coefficient in one selected transition will not help to settle questions about the type of collective flow.

This work was performed at the Theoretical Study Division of CERN at the Institute of Theoretical Physics in Copenhagen. The hospitality extended by Prof. Niels Bohr in his Institute is gratefully acknowledged. The author is indebted to Dr. B. Mottelson for advice and criticism on the manuscript and to Dr. Bès, who provided him with most of the experimental data.

Appendix A

The corrections on M1 conversion coefficients as discussed in section 3 bear an analogy to the structure-dependent corrections on static magnetic moments [23, 24]). In the latter case it is the vector-potential of the electron-current instead of the radiation field that varies over the nuclear dimensions. The interaction of the electron current with a smeared-out magnetic dipole distribution results in a correction for the static magnetic moments as calculated for a point dipole. If W_0 and W are the magnetic h.f.s. splittings for a nucleus with a point-dipole and a smeared-out dipole respectively, then

$$\varepsilon = \frac{W_0 - W}{W} \tag{A1}$$

gives the relative change in the h.f.s. splitting due to the finite size of the nucleus. Under the same assumptions as in section 2 regarding the components of the nuclear current one finds for ε the following expression:

$$\varepsilon = -\frac{I}{(I+1)g_l(g_l-g_s)}\left[A_s g_s(g_l-g_\Omega)+A_l g_l(g_\Omega-g_s)+\frac{g_R}{I}A_R(g_l-g_s)\right]. \tag{A2}$$

The factors A are the results of the weighting of the different magnetic moments with r^2/R^2 and show the same difference of behaviour of spin and orbital parts as was found in the expression for λ. One finds

$$A_s = \{b_1+\zeta(b_1-b_2)\}\sigma, \qquad A_l = b_2\sigma, \qquad A_R = b_2\nu,$$

with

$$\zeta = \frac{(2j+1)\mp 2}{(4j+2)\pm 2} \text{ for } j = l\pm\tfrac{1}{2},$$

$$b_1 = \int_0^R fg\,dr \Big/ \int_0^\infty fg\,dr, \qquad b_2 = \int_0^R fg(1-r^3/R^3)dr \Big/ \int_0^\infty fg\,dr;$$

σ and ν have the same meaning as in section 2; f and g are the radial spinors for the s-electron, similar to those used in section 1, but now referring to the valence electron. The functions $b_{1,2}(Z)$, which are analogous to $C(Z,k)$ in the

preceding sections, have been tabulated for a nuclear radius $R = 1.5\times10^{-13}$ $A^{1/3}$ cm [23]). The given values are somewhat uncertain, due to both the change of R into the more correct value of $R = 1.2\times10^{-13}$ $A^{1/3}$ cm and the influence of screening effects. Eq. (A1) becomes identical to Bohr's formulae (15)—(19) [24]) in the case $\sigma = \nu$. The influence of the third term in (20) on ε is small in any case and the type of flow, characterized by ν, is correspondingly immaterial.

The approximate knowledge of the g_D and g_R values makes a calculation of ε possible for the nuclei listed in table 1. The results are shown in the last column of table 1 and show a general increase (1—2 %) of the magnetic moments compared to the point-dipole values. Substantial corrections are found for nuclei with small g_I values, in much the same way as large λ values occur for forbidden M1 transitions.

The nuclei of main practical interest, viz. ^{155}Gd and ^{157}Gd, show an ε value of 3 to 4 % depending on σ and ν. Speck [25]) instead corrected the magnetic moments as found in h.f.s. analysis by 1.6 %, which is apparently the smaller correction as calculated from a single particle model.

The U isotopes show a large difference in their ε values due to different intrinsic ground-states. It is not to be expected, however, that a real anomaly in the h.f.s. ratios will ever be measured. The numbers only show what corrections are to be applied to moments as found from hyperfine-structure patterns.

That a similar isotope effect is not met with in the Hf isotopes is purely accidental. One would also expect different ε values in the Eu nuclei, as indicated by the different g_I factors. Whereas ^{153}Eu shows all the characteristics of a nucleus with rotational spectra, ^{151}Eu does not [26]). There is up to now no model for ^{151}Eu that can describe the contribution to the current density of all nucleons except the odd one.

Appendix B

We have calculated some values of the function $C(Z, k)$, occurring in (3), for L_I conversion. The numbers are slightly higher than for K conversion.

TABLE 2

Values of $C(z, k)$ for L_1 conversion

	$Z = 55$	$Z = 75$	$Z = 92$
$k = 0.1$	1.2	2.5	5.4
0.2	1.2 (0.97)	2.5 (2.4)	5.6
0.4	1.2 (0.99)	2.6 (2.5)	5.8 (5.0)
0.6	1.2 (1.0)	2.7 (2.6)	6.1 (5.2)

The numbers in brackets are the corresponding values for K conversion and are either taken directly or interpolated from Church and Weneser's table. Screening has been neglected.

This result only means that $\beta(\lambda)/\beta(1)$, the correction relative to Sliv's conversion coefficients, is somewhat larger for L_I than for K conversion.

References

1) A. H. Wapstra and G. J. Nijgh, Nuclear Physics **1** (1956) 245
C. Nordling *et al.*, Nuclear Physics **1** (1956) 326
E. Sokolowski, K. Edvarson and K. Siegbahn, Nuclear Physics **1** (1956) 160
K. O. Nielsen, O. B. Nielsen and M. A. Waggoner, Nuclear Physics **2** (1956/1957) 476
F. K. McGowan and P. H. Stelson, Phys. Rev. **103** (1956) 1133
J. W. Michelich, T. J. Ward and K. P. Jacob, Phys. Rev. **103** (1956) 1285
J. J. Murray, F. Boehm, P. Marinier and J. W. M. Dumond, Phys. Rev. **97** (1955) 1007
2) N. Tralli and G. Goertzel, Phys. Rev. **83** (1951) 399
3) L. A. Sliv, JETP **21** (1951) 770
L. A. Sliv and M. Listengarten, JETP **22** (1952) 29
4) E. L. Church and J. Weneser, Phys. Rev. **104** (1956) 1382
5) L. A. Sliv and I. M. Band, Coefficients of internal conversion (Acad. of Sciences of the U.S.S.R., English edition by P. Axel)
6) L. Spruch and A. Rotenberg, Phys. Rev. **103** (1956) 365
7) G. Scharff-Goldhaber and J. Weneser, Phys. Rev. **98** (1955) 212
L. Wilets and M. Jean, Phys. Rev. **102** (1956) 788
8) A. Bohr and B. Mottelson, in Beta- and Gamma-Ray Spectroscopy, Ed. K. Siegbahn (North-Holland Publishing Company, Amsterdam)
9) S. G. Nilsson, Mat. Fys. Medd. Dan. Vid. Selsk. **29** (1955) no. 16
10) A. Bohr and B. Mottelson, Mat. Fys. Medd. Dan. Vid. Selsk. **30** (1956) no. 1
11) A. Bohr, Mat Fys. Medd. Dan. Vid. Selsk. **26** (1952) no. 14
12) K. Alder *et al.*, Revs. of Mod. Phys. **28** (1956) 432
N. P. Heydenburg and G. M. Temmer, Phys. Rev. **104** (1956) 981
13) G. M. Temmer and N. P. Heydenburg, to be published
Elbek *et al.*, to be published
14) A. H. Cooke and J. G. Park, Proc. Phys. Soc. A **69** (1956) 282
15) S. Ofer, Nuclear Physics **3** (1957) 479
16) Private communication from Dr. B. Mottelson
17) A. W. Sunyar, Phys. Rev. **98** (1955) 653
18) E. Snyder and S. Frankel, Phys. Rev. **106** (1957) 755
19) P. H. Stelson and F. K. McGowan, Phys. Rev. **105** (1957) 1347
20) G. Alaga *et al.*, Mat. Fys. Medd. Dan. Vid. Selsk. **29** (1955) no. 9
21) A. K. Kerman, Mat. Fys. Medd. Dan. Vid. Selsk. **30** (1955) no. 15
22) E. N. Hatch *et al.*, Phys. Rev. **104** (1956) 745
23) A. Bohr and V. Weisskopf, Phys. Rev. **77** (1950) 94
24) A. Bohr, Phys. Rev. **81** (1951) 331
25) J. Speck, Phys. Rev. **101** (1956) 1725
26) e.g. C. M. Class and U. Meyer-Berkhout, Nuclear Physics **3** (1957) 655

Nuclear Physics **5** (1958) 557—587; © *North-Holland Publishing Co., Amsterdam*

Not to be reproduced by photoprint or microfilm without written permission from the publisher

ON THE DETERMINATION OF THE NUCLEAR PAIR CORRELATION FUNCTION FROM THE HIGH ENERGY PHOTO-EFFECT

KURT GOTTFRIED

Society of Fellows, Harvard University†

Received 27 September 1957

Abstract: In accordance with Levinger's predictions, the absorption of a high energy photon frequently results in the simultaneous ejection of a neutron and proton. The present paper provides a theoretical analysis of this direct reaction which starts from first principles and is based on the following assumptions: (i) the impulse and closure approximations are valid, (ii) the photo-nuclear interaction is a sum of two-nucleon operators, and (iii) the pair correlation function is given by $\varrho_S(\mathbf{r}_1, \mathbf{r}_2)|g(\mathbf{r}_1-\mathbf{r}_2)|^2$ where ϱ_S is the shell model correlation function and $g(x)$ contains those correlations directly due to nuclear forces. The cross section is then shown to be proportional to the probability for finding two nucleons with a certain total momentum in a relative S-state, the contributions from P-states being demonstrably small. The further assumptions required to relate the nuclear cross section to the one for photodissociation of deuterium are examined, while final state interactions are treated with an optical model. The theory is compared with the present data and found to be in good agreement. The type of further information required for ascertaining the validity of assumptions (ii) and (iii) is discussed, and a method for acquiring it suggested.

1. Introduction

In virtue of their short wavelength, high energy particles are expected to be natural tools for probing the finer details of nuclear structure. The extraction of the desired information from the experimental data is complicated by two factors: (1) the interaction between the projectile and isolated individual constituents of the target is only imperfectly understood, (2) the interaction between probe and system leads to motions of a complicated character. This is to be contrasted with X-ray diffraction by atomic systems, where these complications either do not exist or can frequently be ignored, and the analysis can therefore be precise and highly informative.

Here we will illustrate the general problem by analyzing the photoproduction of high energy nucleons, a subject which has been intensively investigated at the MIT synchrotron laboratory [1–3]). In these experiments light nuclei are irradiated with a 340 MeV bremsstrahlung beam, ejected neutron-proton pairs are observed in coincidence, and their angular correlation is measured for fixed proton but undetermined neutron energies.

† Present address: CERN, Geneva 23, Switzerland.

Experiments in which the neutron energy is also determined are now planned, and so our analysis will, for the most part, assume that this information is available.

1.1. QUALITATIVE DISCUSSION

Before we enter into a more detailed discussion, we briefly review the significance of the qualitative factors which govern the process:

(1) A 300 MeV photon has a wavelength which will span the oxygen nucleus about ten times. This is taken to imply that the initial interaction *affects only a small part of the nucleus, not the system as a whole.*

(2) A 300 MeV photon possesses roughly the same momentum as a 50 MeV nucleon. This combination of high energy with relatively little momentum means that the energy must eventually be given to *at least* two nucleons. If the photo-nuclear interaction is of the classical type (i.e. the total electric current is the sum of the one-nucleon currents) the γ-ray will be absorbed by *one* nucleon, henceforth labelled by the index 1. Owing to the low photon momentum the subsequent intermediate state is very far off the energy-shell, and is correspondingly short-lived; in fact, the characteristic life time of this intermediate state only permits nucleon 1 to traverse a distance small compared to the average inter-nucleon spacing before it must collide and share its momentum with some other particle 2. If, as is commonly supposed, the probability of finding *two* particles much closer together than the average is large compared to that for finding *more* than two in such an configuration, nucleons 1 and 2 will leave the interaction region otherwise unmolested. As we shall see, this picture is oversimplified, because at our energy the photo-nuclear interaction is *not* simply the sum of one-body operators. Since, however, this mesic enhancement of the electromagnetic interaction is only important for nucleons closer together than the average, our previous conclusion is not altered in essence: the most important consequence of the low momentum but high energy of the photon is that the photo-nucleons are in very close proximity when the absorption takes place. It is this fact which makes the photo-effect a promising technique for investigating short-range pair correlations in nuclei.

(3) The pion-connected additions to the photo-nuclear interaction greatly enhance the cross-section above the value expected from conventional electrodynamic couplings.

(4) A 150 MeV nucleon sees the nucleus as a relatively transparent object [4]), and so there is a good chance that the two nucleons will traverse the space between the production point and the nuclear surface like free particles. Passage out of the nucleus can be accompanied by something akin to weak refraction.

Thus the qualitative features of the observations are reproduced: the

absorption of the photon of energy † ω, momentum $\boldsymbol{\omega}$ leads to the ejection of two nucleons whose energy is of order ω, and whose total momentum is $\mathbf{P}+\boldsymbol{\omega}$ where $\mathbf{P}$ is the total momentum of the photo-pair *before* absorption. The distribution of $\mathbf{P}$ in the target state is therefore of paramount importance in determining the angular correlation between the photo-nucleons.

Similar conclusions were reached by Levinger [5]) in his pioneering investigation of the high-energy photo-effect. Both our experimental knowledge of the photo-effect and our theoretical picture of nuclear structure have undergone far-reaching changes in the meantime, and it is the purpose of the present investigation to provide a more precise and detailed discussion of sufficient generality to incorporate important features unknown at the time of Levinger's work, in particular the more complex nature of the photo-nuclear interaction. Our analysis also differs from those of ref [1, 5]) in several other respects: a much more realistic target wavefunction is used, absorption of all multipole orders is included, effects due to final state interactions are estimated, and p-p production is considered.

1.2. ASSUMPTIONS UNDERLYING THE PRESENT ANALYSIS

The main objective of the present investigation is then to begin with first principles to determine the assumptions which must be made in order to arrive at the picture already outlined, and to see whether this constitutes a valid and tractable interpretation of the data. We now list these assumptions in the order of their appearance.

(i) *The photo-nuclear interaction*

At energies ω above 100 MeV the total cross-section for photo-dissociation of deuterium $\sigma_D(\omega)$ is far larger than one would expect from the conventional electromagnetic interaction [6, 7]). Since $\sigma_D(\omega)$ has a maximum at the same energy as the resonance in photo-meson production, it has been suggested [8]) that virtual pion emission and reabsorption is the predominant disintegration mechanism. Since a detailed and satisfactory theory of the electromagnetic properties of nuclear systems does not exist, we will make the following assumption: *the photo-nuclear interaction energy is the sum of two-body operators*. We justify our neglect of three nucleon effects with the observation that the distance within which the virtual pion mechanism appears to be important[8]) is sufficiently small ($\approx 1\times 10^{-13}$ cm) to render the probability for finding three nucleons within range of each other negligible.

(ii) *Closure*

The measured cross-section has contributions from a multitude of transitions wherein the residual nucleus is left in a variety of quantum states.

† We use units for which $\hbar = c = 1$.

We assume that the residual excitation energy is almost always very small compared with ω. The sum over final states can then be carried out. Experimental proof of the validity of the closure approximation is not available at present.

(iii) *Impulse approximation*

From our earlier discussion it is quite clear that the interaction between the photo-nucleons plays an essential role in the process, and so we shall treat it exactly. We shall, however, ignore the influence of the remaining nucleons during the absorption act, which approximation is closely related to the impulse approximation [9]). The multiple scattering pursuant to absorption is estimated with an optical analogue model [4]).

(iv) *Pair correlation function*

Although assumptions (i) to (iii) enable one to express the cross-section in a physically understandable form, some assumptions concerning the ground state Ψ_0 must be made if detailed predictions are desired. We shall assume that Ψ_0 leads to a pair correlation function of the form

$$\varrho(\mathbf{r}_1, \mathbf{r}_2) = \varrho_S(\mathbf{r}_1, \mathbf{r}_2)\,|g(|\mathbf{r}_1-\mathbf{r}_2|)|^2,$$

where ϱ_S is the pair correlation function of the shell model (i.e. of a Slater determinant), and g is a modification thereof at small inter-particle separations. Thus ϱ_S contains those correlations which arise from the Pauli principle and the finite size of the system, while the more violent correlations due to the forces reside in g.

Once the impulse and closure approximations are made, a reaction in which N nucleons are ejected will at best determine the N-body correlation function (or to be more precise, the N^{th} order density matrix). In particular, therefore, the present experiment will not distinguish between Ψ_0's which lead to the same $\varrho(\mathbf{r}_1, \mathbf{r}_2)$. Nevertheless, we may point out that the chosen form of ϱ follows from the popular [10, 11]) wavefunction Ψ_0 = (product of short-ranged pair correlation functions) $\times$ (Slater determinant of shell model states), and is probably a good approximation in the more sophisticated theory founded by Brueckner [12]).

If the enumerated assumptions are admitted, the cross section can be written as

$$\mathrm{d}\sigma = (2\pi)^{-4}\, F(P) S_{fi}\, \delta(E_f - E_i)\mathrm{d}^3 k_1\, \mathrm{d}^3 k_2, \qquad (1)$$

where $\mathbf{k}_1$ and $\mathbf{k}_2$ are the momenta of the ejected nucleons. The form factor $F(P)$ is proportional to the probability for finding two particles of zero separation and total momentum $P = |\mathbf{k}_1+\mathbf{k}_2-\boldsymbol{\omega}|$ in *the Slater determinant*. S_{fi} is the sum of squares of matrix elements in terms of states in the frame $\mathscr{Z}$ defined by $\mathbf{k}_1+\mathbf{k}_2 = 0$; the final state in these matrix elements is an exact two-body scattering state characterized by the relative momentum

$\mathbf{K} = \frac{1}{2}(\mathbf{k}_1 - \mathbf{k}_2)$, while the initial state is essentially the two-body correlation function g. This matrix element is a function of K, ω_0 (the photon energy in $\mathscr{Z}$) and $\mathbf{K} \cdot \boldsymbol{\omega}_0$, and is therefore a function of $\mathbf{P}$, since the Doppler shift $\omega \to \omega_0$ is determined by $\mathbf{P}$. The form factor $F(P)$ is a much more rapidly varying function of $\mathbf{P}$ than is S_{fi}, and so *the angular correlation yields far more information concerning the Slater determinant part of ϱ than about the more interesting short-range pair correlation function g.*

Nevertheless, there should be a detectable effect due to the variation of S_{fi}, and the observation of such an effect would lead to some insight into the fine grained structure of the nuclear ground-state Ψ_0. For example, if one assumes that for small separations g is well approximated by the deuteron ground state, S_{fi} can be deduced from the well-known [6, 7]) cross-section for photo-dissociation of deuterium. This then leads to an asymmetry in the angular correlation function which, if observed, would lend some measure of support for this particular hypothesis concerning $\varrho(\mathbf{r}_1, \mathbf{r}_2)$.

1.3. SUMMARY

In the following sections the matters briefly discussed here are treated in detail. In sect. 2. eq. (1) will be derived. Sect. 3 is devoted to a more complete discussion of the connection between the photo-effects in deuterium and complex nuclei; in particular, we deduce a formula — similar to one given by Levinger [5]) — which relates the two cross sections. In sect. 4 we present an optical model calculation of the final state interactions. The theory is compared with the present data in subsect. 5.1, where predictions for future experiments will also be found. Finally, the absence of p-p production [13]) is analyzed and interpreted in subsect. 5.2.

2. The Cross Section

Let Ψ_0 represent the ground state of the target, and $|0\rangle$ the initial state which also contains a photon of momentum $\boldsymbol{\omega}$, polarization λ $(=\pm 1)$. The final state selected by an idealized observer contains nucleons 1 and 2 with momenta $\mathbf{k}_1$, $\mathbf{k}_2$ (spin and charge labels are suppressed for the moment) in an anti-symmetric plane wave state Φ_f, a residual nucleus in the anti-symmetric $(A-2)$-body state Ξ_s, and no photons. Both Ψ_0 and Ξ_s are normalized to unity. The transition is due to the photo-nuclear interaction H_{int}, which we assume to be the sum of two-nucleon operators:

$$H_{\mathrm{int}} = \sum_{i<j=1}^{A} \mathscr{E}_\lambda^{ij}. \tag{2}$$

The transition amplitude, whose square is proportional to the required cross section, is given by †

† We have ignored the requirements of anti-symmetry between the photo-pair and the residual system. As in all high-energy processes, this is a good approximation provided the reaction products have momenta which are much larger than those present in the target.

$$T_{fs}^{\lambda}(\omega) = \sqrt{\tfrac{1}{2}A(A-1)}\,\langle \Psi_{fs}^{(-)} | \mathscr{E}_{\lambda}^{12} | 0 \rangle \tag{3}$$

to first order in H_{int} (i.e. to first order in the electromagnetic potential **A**). $\Psi_{fs}^{(-)}$ is an exact eigenstate of the nuclear Hamiltonian H, and is characterized by $\Phi_f \Xi_s$ as its incident "plane wave" part, and *in-coming* spherical waves for infinite separation between the photo-pair and the residual system. It satisfies [14])

$$|\Psi_{fs}^{(-)}\rangle = |\Phi_f \Xi_s\rangle + \frac{1}{E-K-U-i\eta}(W+V)\,|\Psi_{fs}^{(-)}\rangle. \tag{4}$$

Here H has been split into the total kinetic energy K, the potential energy of the residual system U, the interaction V between the photo-pair, and the interaction W between the photo-pair and the remaining $(A-2)$ nucleons. Thus

$$(K+U-E)|\Phi_f \Xi_s\rangle = 0,$$

where E is the common energy of $|0\rangle$ and $\Psi_{fs}^{(-)}$.

As previously stressed, the interaction between the photo-products during the absorption act is of crucial importance; on the other hand there is reason to believe that one can safely ignore the presence of the other particles as a first approximation. We must therefore treat V exactly, and in order to do so it will be necessary to rewrite eq. (3) in the following manner. Introduce the state vector

$$\begin{aligned} |\chi_f^{(-)} \Xi_s\rangle &= \left(1 + \frac{1}{E-K-U-V-i\eta} V\right) |\Phi_f \Xi_s\rangle \\ &= |\Phi_f \Xi_s\rangle + \frac{1}{E-K-U-i\eta} V\,|\chi_f^{(-)} \Xi_s\rangle. \end{aligned} \tag{5}$$

In contrast to $|\Phi_f \Xi_s\rangle$ this new state incorporates the interaction V between the photo-nucleons: $\chi_f^{(-)}$ is just the two-body scattering state corresponding to Φ_f as incident wave. By following a well trodden patn [14]) one arrives at

$$|\Psi_{fs}^{(-)}\rangle = (1+G_E^{\dagger} W)\,|\chi_f^{(-)} \Xi_s\rangle, \tag{6}$$

where $G_E = (E-H+i\eta)^{-1}$ is the propagation (Green's) function for the entire nuclear system.

The new expression for the transition amplitude is therefore

$$T_{fs}^{\lambda}(\omega) = \sqrt{\tfrac{1}{2}A(A-1)}\{\langle \Xi_s \chi_f^{(-)} | \mathscr{E}_{\lambda} | 0 \rangle + \langle \Xi_s \chi_f^{(-)} | W G_E \mathscr{E}_{\lambda} | 0 \rangle\}, \tag{7}$$

where we have dropped the now superfluous label from $\mathscr{E}_{\lambda}^{12}$. The second term of eq. (7) clearly represents the effects of the other particles on the photo-pair, both during and after the annihilation of the quantum. Putting $W = 0$ we arrive at a result which is in spirit (though not in detail) the same as the impulse approximation.

The cross section of interest is then

$$\mathrm{d}\sigma_{\mathrm{fs}}^{\lambda}(\omega) = 2\pi v\delta(E_{\mathrm{fs}}-E_0)|T_{\mathrm{fs}}^{\lambda}(\omega)|^2 \frac{v\mathrm{d}^3k_1}{(2\pi)^3}\frac{v\mathrm{d}^3k_2}{(2\pi)^3}\frac{v\mathrm{d}^3P_{\mathrm{r}}}{(2\pi)^3}, \tag{8}$$

where v is the quantization volume and $\mathbf{P}_{\mathrm{r}}$ is the recoil momentum of the residual nucleus.

The energies appearing in the δ-function are

$$E_0 = \omega - B_{\mathrm{t}}, \quad E_{\mathrm{fs}} = \varepsilon_1+\varepsilon_2+E_{\mathrm{s}}-B_{\mathrm{r}}+\varepsilon_{\mathrm{r}},$$

where B_{t}, B_{r} are the ground state binding energies of the target and residual nuclei respectively, ε_1, ε_2, and ε_{r} the kinetic energies of the two photonucleons and the residual system, respectively, and E_{s} the excitation energy of the state Ξ_{s}.

Our next task is to sum eq. (8) over all states of the residual system, and so we shall require

$$\sum_{\mathrm{s}}\int\frac{v\mathrm{d}^3P_{\mathrm{r}}}{(2\pi)^3}\delta(E_{\mathrm{fs}}-E_0)\,|T_{\mathrm{fs}}^{\lambda}|^2 = \tfrac{1}{2}A(A-1)\sum_{\mathrm{s}}\int\frac{v\mathrm{d}^3P_{\mathrm{r}}}{(2\pi)^3}$$
$$\cdot\,\delta(\varepsilon-E_{\mathrm{s}}-\varepsilon_{\mathrm{r}}-B_{\mathrm{t}}+B_{\mathrm{r}})\langle 0|Q_\lambda^{\dagger}|\chi_i^{(-)}\Xi_{\mathrm{s}}\rangle\langle\Xi_{\mathrm{s}}\chi_i^{(-)}|Q_\lambda|0\rangle, \tag{9}$$

where we have put $Q_\lambda \equiv (1+WG_E)\mathscr{O}_\lambda$, $\varepsilon = \omega-(\varepsilon_1+\varepsilon_2)$. We shall now assume † that the residual states which are populated come from a narrow band of the spectrum characterized by a well-defined average energy $\bar{\varepsilon} = \langle E_{\mathrm{s}}+\varepsilon_{\mathrm{r}}+B_{\mathrm{t}}-B_{\mathrm{r}}\rangle_{\mathrm{Av}} \ll \omega$. Upon inserting this average into the δ-function and using the completeness property of the set Ξ_{s} we can carry out the indicated summations. The right-hand member of eq. (9) then reads

$$\tfrac{1}{2}A(A-1)\delta(\varepsilon-\bar{\varepsilon})\langle Q_\lambda^{\dagger}\Lambda_i^{(-)}Q_\lambda\rangle_0, \tag{10}$$

where

$$\Lambda_i^{(-)} = |\chi_i^{(-)}\rangle\langle\chi_i^{(-)}| \tag{11}$$

is the projection operator onto the two-body state $\chi_i^{(-)}$, and $\langle\ \ \rangle_0$ designates an expectation value in the state $|0\rangle$.

The cross section now reads

$$\mathrm{d}\sigma_{\mathrm{f}} = (2\pi)^{-5}v^3k_1E_1k_2E_2\delta(\varepsilon-\bar{\varepsilon})\mathrm{d}\varepsilon_1\,\mathrm{d}\varepsilon_2\,\mathrm{d}\Omega_1\,\mathrm{d}\Omega_2$$
$$\cdot\,\tfrac{1}{2}A(A-1)\tfrac{1}{2}\sum_\lambda\langle Q_\lambda^{\dagger}\Lambda_i^{(-)}Q_\lambda\rangle_0, \tag{12}$$

where $E_i = \sqrt{k_i^2+M^2}$ (i.e. $\varepsilon_i = E_i-M$), M being the nucleon mass, $\mathrm{d}\Omega_i$ is the element of solid angle, and we have also averaged over the photon polarization directions.

In section 4 we shall investigate the effects of W, the (photo-pair)-

† A more detailed discussion of the closure approximation will be found in ref. [15]). A systematic expansion in which the closure approximation is the leading term can be made by using a technique well-known in the theory of neutron diffraction [16]). Since the ensuing corrections are very hard to evaluate, we shall not enter into this matter here.

(residual nucleus) potential, but now we shall make the so-called impulse approximation, $Q_\lambda \to \mathscr{E}_\lambda$. Introducing the coordinate representation, we have

$$u_\lambda \equiv v^3 \tfrac{1}{2}A(A-1)\langle \mathscr{E}_\lambda^\dagger \Lambda_f^{(-)} \mathscr{E}_\lambda \rangle_0$$

$$= v^3 \sum_{\substack{S'S'' \\ M'_S M''_S}} \sum_{\substack{T'T'' \\ M'_T M''_T}} \int (\mathrm{d}^3 r) \langle \mathbf{r}'''_1 \mathbf{r}'''_2 S'' M''_S T'' M''_T | \varrho | \mathbf{r}''_1 \mathbf{r}''_2 S' M'_S T' M'_T \rangle \tag{13}$$

$$\cdot \langle \mathbf{r}''_1 \mathbf{r}''_2 S' M'_S T' M'_T | \mathscr{E}_\lambda^\dagger | \mathbf{r}_1 \mathbf{r}_2 S M_S T M_T \rangle \langle \mathbf{r}_1 \mathbf{r}_2 S M_S T M_T | \chi_f^{(-)} \rangle$$

$$\cdot \langle \chi_f^{(-)} | \mathbf{r}'_1 \mathbf{r}'_2 S M_S T M_T \rangle \langle \mathbf{r}'_1 \mathbf{r}'_2 S M_S T M_T | \mathscr{E}_\lambda | \mathbf{r}'''_1 \mathbf{r}'''_2 S'' M''_S T'' M''_T \rangle,$$

where S, M_S, T, M_T, are the usual spin and isobaric spin quantum numbers for a pair of particles. The first factor in the integrand is the second order density matrix † for the state Ψ_0: its diagonal element equals the number of pairs times the probability for finding one particle at $\mathbf{r}_1$, another at $\mathbf{r}_2$, when they are in the spin-charge state (SM_S, TM_T). This diagonal element is just the pair correlation function.

Conservation of charge and momentum and linearity of $\mathscr{E}_\lambda$ in the electromagnetic field strengths imply that

$$\langle \mathbf{r}_1 \mathbf{r}_2 \zeta | \mathscr{E}_\lambda | \mathbf{r}'_1 \mathbf{r}'_2 \zeta' \rangle = \left(\frac{2\pi}{\omega v}\right)^{\frac{1}{2}} \delta(\mathbf{R}-\mathbf{R}') \delta_{M_T M'_T} \mathrm{e}^{i\boldsymbol{\omega}\cdot\mathbf{R}}$$

$$\cdot \langle \mathbf{x}\zeta | \mathscr{E}_\lambda(\boldsymbol{\omega}, -i\partial/\partial\mathbf{R}) | \mathbf{x}'\zeta' \rangle \tag{14}$$

with $\mathbf{R} = \frac{1}{2}(\mathbf{r}_1+\mathbf{r}_2)$, $\mathbf{x} = \mathbf{r}_1-\mathbf{r}_2$, etc. The notation $\mathscr{E}_\lambda(\boldsymbol{\omega}, -i\partial/\partial\mathbf{R})$ indicates *that the only permissible* $\mathbf{R}$*-dependence is through the differential operator* $\partial/\partial\mathbf{R}$. We have also introduced the symbol ζ to stand for the entire set of quantum numbers $(SM_S TM_T)$. Finally

$$\langle \mathbf{r}_1 \mathbf{r}_2 \zeta | \chi_f^{(-)} \rangle = v^{-1} \mathrm{e}^{i\mathbf{P}_f \cdot \mathbf{R}} \chi_f(\mathbf{x}\zeta_f), \tag{15}$$

with $\mathbf{P}_f = \mathbf{k}_1+\mathbf{k}_2$. Returning to eq. (13) we have

$$u_\lambda = \frac{(2\pi)^4}{\omega} \sum_{\zeta'\zeta''} \int \mathrm{d}^3 x_1 \ldots \mathrm{d}^3 x_4 \langle \mathbf{P}\mathbf{x}_1 \zeta' | \varrho | \mathbf{P}\mathbf{x}_2 \zeta'' \rangle$$

$$\cdot \langle \mathbf{x}_2 \zeta'' | \mathscr{E}_\lambda^\dagger(\boldsymbol{\omega}\mathbf{P}_f) | \mathbf{x}_3 \zeta_f \rangle \chi_f(\mathbf{x}_3 \zeta_f) \tag{16}$$

$$\cdot \chi_f^*(\mathbf{x}_4 \zeta_f) \langle \mathbf{x}_4 \zeta_f | \mathscr{E}_\lambda(\boldsymbol{\omega}\mathbf{P}_f) | \mathbf{x}_1 \zeta' \rangle,$$

where $\mathbf{P} = \mathbf{P}_f - \boldsymbol{\omega}$ is the total momentum of the photo-pair *before* absorption of the quantum. The density matrix appearing in eq. (16) is defined as

$$\langle \mathbf{P}\mathbf{x}_1 \zeta | \varrho | \mathbf{P}\mathbf{x}_2 \zeta' \rangle = (2\pi)^{-3} \int \mathrm{d}^3 R_1 \, \mathrm{d}^3 R_2 \, \mathrm{e}^{-i\mathbf{P}\cdot\mathbf{R}_1} \langle \mathbf{R}_1 \mathbf{x}_1 \zeta | \varrho | \mathbf{R}_2 \mathbf{x}_2 \zeta' \rangle \mathrm{e}^{i\mathbf{P}\cdot\mathbf{R}_2}; \tag{17}$$

for $\mathbf{x}_1 = \mathbf{x}_2$ it equals $\frac{1}{2}A(A-1) \times$ (probability for finding two particles of total momentum $\mathbf{P}$, separation $\mathbf{x}_1$, in Ψ_0).

Although one could draw some qualitative conclusions from eq. (16) as

† An exhaustive discussion of density matrices will be found in ref. [17]).

it stands, it will be easier to generalize our arguments once a particular model for Ψ_0 is analyzed. As mentioned in the introduction, we shall put

$$\langle \mathbf{r}_1 \mathbf{r}_2 \zeta | \varrho | \mathbf{r}'_1 \mathbf{r}'_2 \zeta' \rangle = g_\zeta(x) \langle \mathbf{r}_1 \mathbf{r}_2 \zeta | \varrho_S | \mathbf{r}'_1 \mathbf{r}'_2 \zeta' \rangle g_{\zeta'}^*(x'), \tag{18}$$

where $\langle \mathbf{r}_1 \mathbf{r}_2 \zeta | \varrho_S | \mathbf{r}'_1 \mathbf{r}'_2 \zeta' \rangle$ is the density matrix of a Slater determinant constructed from shell-model spin-orbitals, and $g_\zeta(x) \equiv g_{ST}(|\mathbf{r}_1 - \mathbf{r}_2|)$ describes the (presumably short-ranged) modifications due to the nuclear forces. The normalization of the wave function requires $g_\zeta \to 1$ for $x > d$, where d is a characteristic correlation length assumed to be small compared with the nuclear radius †.

According to Drell and Huang [10]), and to Jastrow [11]), this density matrix (18) follows from the wave function

$$\Psi_0(1 \ldots A) = \prod_{i>j=1}^{A} C_{ij} \Phi_S(1 \ldots A), \tag{19}$$

provided the range of the pair correlations due to C_{ij} is small compared to the average interparticle spacing † associated with the Slater determinant Φ_S. The connection between C_{ij} and our function g_ζ is provided by

$$C_{ij} = \sum_{ST} g_{ST}(x_{ij}) \Lambda^S_{\sigma_{ij}} \Lambda^T_{\tau_{ij}}, \tag{20}$$

where $x_{ij} = |\mathbf{r}_i - \mathbf{r}_j|$, and the Λ's are the usual projection operators onto singlet and triplet states; e.g.

$$\Lambda^0_{\sigma ij} = \tfrac{1}{4}(1 - \boldsymbol{\sigma}_i \cdot \boldsymbol{\sigma}_j), \quad \Lambda^1_{\tau ij} = \tfrac{1}{4}(3 + \boldsymbol{\tau}_i \cdot \boldsymbol{\tau}_j).$$

As we had stated earlier, there exist other wave functions than the one of eq. (19) which yield eq. (18). Our only purpose in bringing this Ψ_0 into the discussions is to give the reader some feeling for the type of wave functions implied by our assumption of eq. (18).

For the moment we wish to confine ourselves to the case of *completely* closed shells, i.e. where both j-shells belonging to a given orbital angular momentum l are filled, as in O^{16} and Ca^{40}. In this case eq. (18) reduces to

$$\delta_{\zeta\zeta'} g_\zeta(x) g_\zeta^*(x') \tfrac{1}{2}[\langle \mathbf{r}_1 | \mathcal{D} | \mathbf{r}'_1 \rangle \langle \mathbf{r}_2 | \mathcal{D} | \mathbf{r}'_2 \rangle - (-1)^{S+T} \langle \mathbf{r}_1 | \mathcal{D} | \mathbf{r}'_2 \rangle \langle \mathbf{r}_2 | \mathcal{D} | \mathbf{r}'_1 \rangle], \tag{21}$$

with

$$\langle \mathbf{r}_1 | \mathcal{D} | \mathbf{r}'_1 \rangle = \sum_{nlm} \varphi_{nlm}(\mathbf{r}_1) \varphi^*_{nlm}(\mathbf{r}'_1). \tag{22}$$

The φ's are the spatial parts of the one-body wave functions from which Φ_S is constructed, and n, l, m the usual quantum numbers in a central field.

We must now transform from the coordinate representation of eq. (21) to the mixed representation of eq. (17). A series of Fourier transformations yield the convenient integral representation

† Note the difference between these conditions.

$$\langle \mathbf{P}\mathbf{x}\zeta|\,\varrho\,|\mathbf{P}\mathbf{x}'\zeta\rangle = (2\pi)^{-3} g_\zeta(x) g_\zeta{}^*(x')\, e^{-\frac{1}{2}i\mathbf{P}\cdot(\mathbf{x}-\mathbf{x}')} \cdot \int d^3q d^3q'\, e^{i(\mathbf{q}\cdot\mathbf{x}-\mathbf{q}'\cdot\mathbf{x}')} \langle \mathbf{q},\ \mathbf{P}-\mathbf{q}|\,\mathscr{D}_{ST}\,|\mathbf{q}',\ \mathbf{P}-\mathbf{q}'\rangle, \tag{23}$$

where

$$\langle \mathbf{q}_1\mathbf{q}_2|\,\mathscr{D}_{ST}\,|\mathbf{q}'_1\mathbf{q}'_2\rangle = \tfrac{1}{2}[\langle \mathbf{q}_1|\,\mathscr{D}\,|\mathbf{q}'_1\rangle\langle \mathbf{q}_2|\,\mathscr{D}\,|\mathbf{q}'_2\rangle - (-1)^{S+T}\langle \mathbf{q}_1|\,\mathscr{D}\,|\mathbf{q}'_2\rangle\langle \mathbf{q}_2|\,\mathscr{D}\,|\mathbf{q}'_1\rangle], \tag{24}$$

and

$$\langle \mathbf{q}_1|\,\mathscr{D}\,|\mathbf{q}'_1\rangle = (2\pi)^{-3}\int d^3r_1 d^3r'_1\, e^{-i\mathbf{q}_1\cdot\mathbf{r}_1}\langle \mathbf{r}_1|\,\mathscr{D}\,|\mathbf{r}'_1\rangle e^{i\mathbf{q}'_1\cdot\mathbf{r}'_1}. \tag{25}$$

Returning to eq. (16), we have

$$u_\lambda = \frac{2\pi}{\omega}\sum_{\zeta'}\int d^3q d^3q'\, d^3x_1 \ldots d^3x_4 \langle \mathbf{q},\ \mathbf{P}-\mathbf{q}|\,\mathscr{D}_{S'T'}\,|\mathbf{q}',\ \mathbf{P}-\mathbf{q}'\rangle \cdot [\chi_t{}^*(\mathbf{x}_1\zeta_t)\langle \mathbf{x}_1\zeta_t|\,\mathscr{E}_\lambda\,|\mathbf{x}_2\zeta'\rangle g_{\zeta'}(x_2)\, e^{i(\mathbf{q}-\frac{1}{2}\mathbf{P})\cdot\mathbf{x}_2}] \cdot [\chi_t{}^*(\mathbf{x}_3\zeta_t)\langle \mathbf{x}_3\zeta_t|\,\mathscr{E}_\lambda\,|\mathbf{x}_4\zeta'\rangle g_{\zeta'}(x_4)\, e^{i(\mathbf{q}'-\frac{1}{2}\mathbf{P})\cdot\mathbf{x}_4}]^*. \tag{26}$$

In the introduction we presented several arguments which lead to the conclusion that the vast majority of transitions arise from photo-pairs which were in close proximity in the target. These arguments were based on wave kinematics and on the short-range nature of the pion-connected parts of the transition operator $\mathscr{E}_\lambda$. We therefore expect the integrand of eq. (26) to have a pronounced maximum for $|\mathbf{x}_i| \lesssim \lambda_F$, the inter-particle spacing. At this juncture it is also important to note that the momenta $\mathbf{q}$, $\mathbf{q}'$ appearing in eq. (26) arise from the Slater part of Ψ_0 solely; they *do not* contain the high momenta which are a necessary consequence of the pair-correlations. Hence an expansion of the exponential factors of eq. (26) into spherical harmonics suggests itself; the lowest term can be put into the form

$$u_\lambda{}^{(0)} = \frac{2\pi}{\omega}\sum_{\zeta'} F_{S'T'}(P)|\mathscr{M}_{\lambda t}(\zeta' \to \zeta_t)|^2. \tag{27}$$

Inspection of eq. (23) immediately reveals that the form factor

$$F_{ST}(P) = \int d^3q d^3q'\,\langle \mathbf{q},\ \mathbf{P}-\mathbf{q}|\,\mathscr{D}_{ST}\,|\mathbf{q}',\ \mathbf{P}-\mathbf{q}'\rangle \tag{28}$$

is proportional to the probability for finding two particles of total momentum $\mathbf{P}$ and *zero separation* in the Slater determinant. By truncating † this expansion we have tacitly assumed that most of the transitions originate in *relative* S-states, a fact which is reflected in the matrix element of eq. (27):

$$\mathscr{M}_{\lambda t}(\zeta' \to \zeta_t) = \int d^3x d^3x'\,\chi_t{}^*(\mathbf{x}\zeta_t)\langle \mathbf{x}\zeta_t|\,\mathscr{E}_\lambda\,|\mathbf{x}'\zeta'\rangle g_{\zeta'}(x'). \tag{29}$$

† It should be stressed that the removal of the exponentials in eq. (26) does *not* mean that we have restricted ourselves to dipole absorption: radiation of *all* multipole orders is taken into account. For a quantitative estimate of the error made in neglecting P-states, see last paragraph of Subsection 5.2.

Before discussing these results we want to show that eq. (28) reduces to quadratures. The first step is to reintroduce the coordinate representation; one finds

$$\begin{aligned} F_{ST}(P) &= 0 \quad \text{if } (S+T) \text{ is even,} \\ &= F(P) \text{ if } (S+T) \text{ is odd,} \end{aligned} \tag{30a}$$

where

$$F(P) = \int \mathrm{d}^3\boldsymbol{r}\mathrm{d}^3\boldsymbol{r}' \, \mathrm{e}^{-i\mathbf{P}\cdot(\mathbf{r}-\mathbf{r}')} [\langle \mathbf{r}| \mathscr{D} |\mathbf{r}'\rangle]^2. \tag{30b}$$

Next we use the explicit representation of eq. (22), expand $\exp[-i\mathbf{P}\cdot(\mathbf{r}-\mathbf{r}')]$ in terms of spherical harmonics and carry out the angular integrations. Since we are dealing with a closed shell nucleus the sums over magnetic quantum numbers are trivial, and the final result is

$$F(P) = \sum_{nn'll'} \sum_{\varrho=|l-l'|}^{l+l'} (2l+1)(2l'+1) |\langle ll'00|\varrho 0\rangle|^2 \cdot \left| \int_0^\infty R_{nl}(r) R_{n'l'}(r) j_\varrho(Pr) r^2 \mathrm{d}r \right|^2, \tag{31}$$

where $\langle ll'00|\varrho 0\rangle$ is a Clebsch-Gordan coefficient, $R_{nl}(r)$ is the radial part of the orbital $\varphi_{nlm}(\mathbf{r})$, and $j_\varrho(Pr)$ is the spherical Bessel function of order ϱ.

Our final result for the cross section is therefore

$$\mathrm{d}\sigma = (2\pi)^{-4} F(P) S_{fi} \delta(\varepsilon - \bar{\varepsilon}) \mathrm{d}^3 k_1 \mathrm{d}^3 k_2, \tag{32}$$

where

$$S_{fi} = \omega^{-1} \tfrac{1}{2} \sum_\lambda \sum_{\substack{\zeta_f \zeta' \\ (S' \neq T')}} |\mathscr{M}_{\lambda f}(\zeta' \to \zeta_f)|^2. \tag{33}$$

This is the more precise form of the result promised in the introduction. As we have already stated there, the cross-section is given by the product of three factors: (1) the available phase space, (2) the probability for finding two particles with total momentum $\mathbf{P}$, zero separation in the Slater determinant, and (3) the probability that two particles in a state of relative motion given by the short-range correlation function $g(x)$ perform a transition to the state χ_f.

We might point out that this result differs from that of other authors [1, 5]) in that we have not assumed independent probability distributions for total momentum and inter-particle separation. Such an assumption is only valid for an infinite nucleus, and is quite poor for the small systems we are considering.

It should be stressed that eq. (32) only holds for a particular set of nuclei, those having completely closed shells (e.g. O^{16}, Ca^{40}). For other targets a similar result can be derived, but two complications arise: (i) the form factor is no longer a function of $|\mathbf{P}|$ only, (ii) S_{fi} contains interference terms. The latter is a rather essential complication, since it eliminates the possibility of determining S_{fi} from the photo-effect in deuterium, as is done in sect. 3.

The function $F(P)$ is plotted in fig. 1 for O^{16} when the Slater determinant is constructed from the eigenfunction of the harmonic oscillator and the infinite square well. The radius of the square well and the oscillator's frequency are adjusted so that both yield the r.m.s. charge radius found in electron

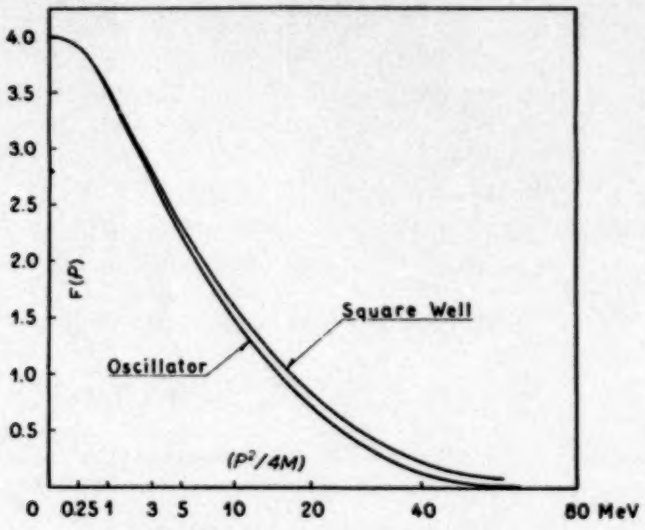

Fig. 1. The form factor $F(P)$ for O^{16}.

scattering [23]). The difference between the two form factors is seen to be quite small, and it is doubtful whether an experiment could differentiate them. Furthermore, we expect that more realistic Hartree fields would lead to $F(P)$'s lying between the two curves of fig. 1. In future we therefore use an average of these two as our $F(P)$.

3. Relationship between the Photo-Effect in Complex Nuclei and in Deuterium

3.1. THE SPIN OF THE INITIAL STATE

The possibility of relating n-p production in complex nuclei to the photodissociation of deuterium has been pointed out by a number of authors, especially Levinger [5]). His suggestion naturally leads to the following question: *Can transitions from states other than the* $^3S_1$ *be neglected*? In order to answer this query it is important to have at least a qualitative picture of the photo-nuclear interaction. The most convincing and successful scheme proposed to date is that of the isobar model [18]) which we now adopt for this purpose. The reader will recall that in this model the photon is absorbed by *one* nucleon which is thereby lifted into the quasi-stable $T = 3/2$, $J = 3/2$ (isobar) state. The subsequent decay of this intermediate state transforms the excitation energy of the isobar into the kinetic energy of the nucleons. Since this decay is due to a strong (i.e. T-conserving) interaction,

the final state must have $T = 1$ (i.e. ^{1}S, or ^{3}P, etc.). Therefore two nucleons in a relative ^{1}S state cannot absorb M1 radiation via the isobar, while E1 absorption would leave them in a $^3P_1$ state. Since E1 transitions with spin-flip can only arise from relativistic effects, or from non-adiabatic terms in the meson-nucleon coupling [19]), we can expect quanta of higher order than dipoles to play the major role. On the other hand, there is strong evidence [6, 20]) that the deuteron photo-effect proceeds mainly ($\approx 80\,\%$) via dipole absorption. Combining these observations with the trivial fact that there are three times as many pairs in triplet as in singlet states leads us to conclude that one may safely ignore the contributions of the $^1S_0$-state. As to transitions originating from states of higher orbital angular momentum, we have already argued (sect. 2) that they should have little likelihood of occurring. We therefore conclude that the question posed at the beginning of this paragraph is answered in the affirmative.

3.2. DETERMINATION OF S_{fi} FROM THE DEUTERIUM CROSS SECTION

We now address our attention to the quantity S_{fi} occurring in eq. (32). As we have already shown that the sums over spins and isobaric spins can be restricted to $S' = 1$, $T' = 0$, it would only be necessary to replace $g_{10}(x)$ by $\phi_0(x)$, the deuteron's ground state, in order to relate S_{fi} to the cross section for $\gamma + d \to p + n$. Since $\phi_0(x)$ tends to zero and $g_{10}(x)$ tends to one asymptotically, one certainly cannot identify these functions. However, for our purposes it would be sufficient [8]) if $[\phi_0(x)/g_{10}(x)]$ were a constant for $x \lesssim 10^{-13}$ cm. Whether these functions are so simply related or not could only be answered by a detailed theory of nuclear structure [12]). We shall simply *assume* that such a relationship holds, examine the consequences, and see whether they can be supported by empirical evidence.

Let us therefore put

$$|g_{10}(x)|^2 = \gamma^3 \, |\phi_0(x)|^2 \quad \text{for} \quad x \lesssim 10^{-13} \text{ cm}; \tag{34}$$

γ is a constant having the dimension of length. We then have

$$S_{fi} = \frac{\gamma^3}{2\omega} \sum_{\lambda \zeta_f \zeta_D} \left| \int \mathrm{d}^3x \mathrm{d}^3x' \, \chi_f^*(\mathbf{x}\zeta_f) \langle \mathbf{x}\zeta_f | \, \mathscr{E}_\lambda \, | \mathbf{x}' \zeta_D \rangle \phi_0(x') \right|^2$$
$$\equiv 3\gamma^3 D_{fi},$$

with ζ_D designating the spin-charge quantum numbers of the deuteron.

On the other hand, the cross section for photo-disintegration of the deuteron is

$$\frac{\mathrm{d}\sigma_D}{\mathrm{d}\Omega_{p0}} = \frac{k_{p0} E_{p0}}{4\pi} D_{fi} \tag{35}$$

in the centre-of-momentum frame (henceforth called $\mathscr{Z}$). In eq. 35 k_{p0}, E_{p0} and Ω_{p0} are the momentum, energy, and direction of the proton in $\mathscr{Z}$.

The explicit relationship between the photo-effects in complex nuclei and deuterium is then expressed by

$$\frac{\mathrm{d}\sigma/\mathrm{d}\Omega_{\mathrm{p}}}{[\mathrm{d}\sigma_{\mathrm{D}}/\mathrm{d}\Omega_{\mathrm{p}}]_0} = \frac{3\gamma^3}{4\pi^3} F(P) \frac{k_{\mathrm{p}} E_{\mathrm{p}}}{[k_{\mathrm{p}} E_{\mathrm{p}}]_0} \delta(\varepsilon - \bar{\varepsilon}) \mathrm{d}\varepsilon_{\mathrm{p}} \mathrm{d}^3 k_{\mathrm{n}}, \tag{36}$$

where $[\ \ ]_0$ indicates that the enclosed quantity is to be evaluated in the frame $\mathscr{Z}$ defined by $\mathbf{k}_{\mathrm{p}} + \mathbf{k}_{\mathrm{n}} = 0$.

There is one fundamental qualification to the relationship (36) which must be mentioned. The quantity D_{fi} is a function of ω_0, $k_{\mathrm{p}0}$ and $(\mathbf{k}_{\mathrm{p}0} \cdot \boldsymbol{\omega}_0)$, where $(\boldsymbol{\omega}_0, \omega_0)$ is the photon's 4-momentum in $\mathscr{Z}$. Owing to the requirement of energy conservation ω_0 and $k_{\mathrm{p}0}$ are not independent variables, and more important for us, their relationship is *not* the same in the deuteron and nuclear photo-effects. To put it more succinctly, the second process is not on the first's energy shell. We therefore have some leeway in evaluating eq. (36): we could choose $[\mathrm{d}\sigma_{\mathrm{D}}/\mathrm{d}\Omega_{\mathrm{p}}]_0$ at either the value of ω_0 *or* of $k_{\mathrm{p}0}$ appropriate to the actual event in question (other possibilities also exist). The best choice is clearly the one which makes the difference between the off- and on- energy shell D_{fi} as smalll as possible.

Since the slow energy-variation of the n-p scattering cross section could be taken to imply that χ_{f} is a slowly varying function of $k_{\mathrm{p}0}$, while $\sigma_{\mathrm{D}}(\omega_0)$ does change rapidly, we will always choose the value of $[\mathrm{d}\sigma_{\mathrm{D}}/\mathrm{d}\Omega_{\mathrm{p}}]_0$ appropriate to the frequency ω_0.

4. Final State Interactions

4.1. INTRODUCTION OF THE OPTICAL POTENTIAL

Before we can compare the formulae derived so far with the data, an understanding of the importance of final state interactions must be acquired.

Our task is then to generalize the formalism of section 2 so that W, the (photo-pair)-(residual nucleus) interaction can be taken into account. Instead of u_λ (see eq. 13)) we now consider the quantity

$$U_\lambda = v^3 \tfrac{1}{2} A(A-1) \langle Q_\lambda^\dagger \Lambda_{\mathrm{f}}^{(-)} Q_\lambda \rangle_0, \tag{37}$$

where

$$Q_\lambda = \left(1 + W \frac{1}{E - H + i\eta}\right) \mathscr{E}_\lambda. \tag{38}$$

Q_λ is seen to be an A-body operator, and therefore some further simplification is necessary if progress is to be made. As is well-known, the scattering of high-energy nucleons by complex nuclei is successfully described by the optical model [4, 21]) which we now adopt for the purpose of simplifying eqs. (37) and (38). Instead of treating the scattering of the photo-pair as a many-body problem, we assume that the remaining $(A-2)$ nucleons serve to define the static (optical) potential well $\mathscr{W}$ seen by the photo-

nucleons. Since inelastic and elastic scattering are of importance, $\mathscr{W}$ will be complex.

The transition from the exact treatment to the optical model is effected by the substitution †

$$\left(1+\frac{1}{E-H-i\eta}W\right)\chi_t^{(-)}\rightarrow\left(1+\frac{1}{\varepsilon_t-\mathscr{K}-V-\mathscr{W}^\dagger-i\eta}\mathscr{W}^\dagger\right)\chi_t^{(-)} \equiv \Omega_t\chi_t^{(-)}, \tag{39}$$

where $\varepsilon_t=\varepsilon_n+\varepsilon_p$ is the total energy of the photo-pair, and $\mathscr{K}$ their kinetic-energy operator. Thus U_λ becomes

$$U_\lambda = v^3\tfrac{1}{2}A(A-1)\langle\mathscr{E}_\lambda^\dagger\Omega_t\Lambda_t^{(-)}\Omega_t^\dagger\mathscr{E}_\lambda\rangle. \tag{40}$$

Introduction of a complete †† set of incoming wave two-body states $\chi_\alpha^{(-)}$ in eq. (40) results in

$$U_\lambda = v^3\tfrac{1}{2}A(A-1)\sum_{\alpha\beta}O_{t\alpha}O_{t\beta}^*\langle\mathscr{E}_\lambda^\dagger\Lambda_{\beta\alpha}^{(-)}\mathscr{E}_\lambda\rangle_0, \tag{41}$$

where

$$\Lambda_{\beta\alpha}^{(-)} = |\chi_\beta^{(-)}\rangle\langle\chi_\alpha^{(-)}|, \tag{42}$$

$$O_{t\alpha} = \langle\chi_t^{(-)}|\Omega_t^\dagger|\chi_\alpha^{(-)}\rangle, \tag{43}$$

$$(\mathscr{K}+V-\varepsilon_\alpha)\chi_\alpha^{(-)}=0.$$

Since the photo-nucleons tend to move in opposite directions, their mutual interactions V can be ignored during the multiple scattering. If we can also delete $\mathscr{W}$ during the absorption (i.e. the impulse approximation), we can put $V=0$ throughout eq. (43). Thus we treat V exactly while ignoring $\mathscr{W}$ during the absorption, and vice versa in the final state interaction. If we now define the two-body state

$$\psi_t^{(-)} = \Phi_t+\frac{1}{\varepsilon_t-\mathscr{K}-i\eta}\mathscr{W}^\dagger\psi_t^{(-)}, \tag{44}$$

eq. (43) becomes

$$O_{t\alpha}\underset{V\rightarrow 0}{\rightarrow}\delta_{t\alpha}+\frac{\langle\psi_t^{(-)}|\mathscr{W}|\Phi_\alpha\rangle}{\varepsilon_t-\varepsilon_\alpha+i\eta}, \tag{45}$$

Φ_α being the plane wave part of $\chi_\alpha^{(-)}$.

The expectation value appearing in eq. (41) can be evaluated by the methods of section 2, provided the various assumptions discussed there are made again. The result is

† If $\mathscr{W}$ is the potential in common usage [4, 21]), we must use $\mathscr{W}^\dagger$ in this equation since we have incoming waves at infinity.

†† We shall ignore the presence of a bound state (i.e. the deuteron) in this complete set. This is an excellent approximation at high energies.

$$v^3 \tfrac{1}{2}A(A-1)\langle \mathscr{E}_\lambda^\dagger \Lambda_{\beta\alpha}^{(-)} \mathscr{E}_\lambda \rangle_0 = \frac{2\pi}{\omega} \sum_{\zeta'} F_{\zeta'}(\mathbf{P}_\alpha|\mathbf{P}_\beta) \cdot \mathscr{M}_{\lambda\alpha}(\zeta' \to \zeta_\alpha)\mathscr{M}^*_{\lambda\beta}(\zeta' \to \zeta_\beta), \qquad (46)$$

where $\mathbf{P}_\alpha+\boldsymbol{\omega}$, $\mathbf{P}_\beta+\boldsymbol{\omega}$ are the total momenta of $\chi_\alpha^{(-)}$, $\chi_\beta^{(-)}$ respectively, while

$$\mathscr{M}_{\lambda\alpha}(\zeta' \to \zeta_\alpha) = \int \mathrm{d}^3x \mathrm{d}^3x' \, \chi_\alpha^*(\mathbf{x}\zeta_\alpha)\langle \mathbf{x}\zeta_\alpha|\mathscr{E}_\lambda|\mathbf{x}'\zeta'\rangle g_{\zeta'}(x') \qquad (47)$$

is defined as in eq. (29). The form factor is a slight generalization of the one employed previously (compare with eqs. (30) and (31)):

$$\begin{aligned} F_\zeta(\mathbf{P}_\alpha|\mathbf{P}_\beta) &= o_\zeta \int \mathrm{d}^3r \mathrm{d}^3r' \, \mathrm{e}^{-i(\mathbf{P}_\alpha\cdot\mathbf{r}-\mathbf{P}_\beta\cdot\mathbf{r}')}[\langle \mathbf{r}|\mathscr{D}|\mathbf{r}'\rangle]^2 \\ &= o_\zeta \sum_{\rho\mu\nu} f_{\rho\nu}(P_\alpha) f_{\rho\nu}(P_\beta) Y_{\rho\mu}(\mathbf{P}_\alpha) Y^*_{\rho\mu}(\mathbf{P}_\beta), \end{aligned} \qquad (48)$$

where o_ζ is zero or one according to whether $(S+T)$ is even or odd, and

$$f_{\rho\nu}(P) = [4\pi(2l+1)(2l'+1)(2\varrho+1)^{-1}]^{\frac{1}{2}}\langle l'00|\varrho 0\rangle \cdot \int_0^\infty R_{nl}(r)R_{n'l'}(r) j_\rho(Pr) r^2 \mathrm{d}r; \qquad (49)$$

thus $\sum_\nu$ stands for summation over the set of quantum numbers $(nln'l')$.

Eqs. (45), (46) and (48) allow us to re-express U_λ in a form reminiscent of eq. (27):

$$U_\lambda = \frac{2\pi}{\omega} \sum_{\rho\mu\nu} \sum_{\zeta'} o_{\zeta'} |\mathscr{T}^{\rho\mu\nu}_{\lambda\zeta'}|^2$$

with

$$\begin{aligned} \mathscr{T}^{\rho\mu\nu}_{\lambda\zeta'} &= f_{\rho\nu}(P) Y_{\rho\mu}(\mathbf{P}) \mathscr{M}_{\lambda t}(\zeta' \to \zeta_t) \\ &\quad + \sum_\alpha \langle \psi_t^{(-)}|\mathscr{W}|\Phi_\alpha\rangle (\varepsilon_t - \varepsilon_\alpha + i\eta)^{-1} \mathscr{M}_{\lambda\alpha}(\zeta' \to \zeta_\alpha) \\ &\qquad \cdot f_{\rho\nu}(P_\alpha) Y_{\rho\mu}(\mathbf{P}_\alpha). \end{aligned} \qquad (51)$$

The first term of eq. (51) is just the transition amplitude evaluated in section 2, with $\mathbf{P}$ retaining its former meaning. The second term incorporates the final state interactions. The physical significance of the various quantities is very apparent: reading from right to left the successive factors are the probability amplitude for finding a pair with total momentum $\mathbf{P}_\alpha$; the matrix element for absorption into the intermediate state $\chi_\alpha^{(-)}$, the propagator of this state, and the *exact* scattering amplitude due to the potential $\mathscr{W}$.

4.2. QUALITATIVE DISCUSSION

The evaluation of the second member of eq. (51) is beset by many difficulties. Foremost among them is our ignorance of the magnitude and phase of the off-energy shell matrix element $\mathscr{M}_{\lambda\alpha}$ — the connection with the reaction $\gamma+\mathrm{d} \to \mathrm{n}+\mathrm{p}$ being no longer valid, while interference terms are now unavoidable. The scattering amplitude $\langle \psi_t^{(-)}|\mathscr{W}|\Phi_\alpha\rangle$ can, in principle,

be computed. In practice, however, an analytic expression for it is necessary if the summation over α is to be carried out.

In view of these complications, we will have to make some drastic simplifications, and satisfy ourselves with rough estimates of the final state interaction. With this end in view we recall that there are two rather distinct processes which distort the simplified picture of a direct reaction: (1) absorption of the reaction products inside the nucleus, and (2) refraction of the outgoing wave at the nuclear surface. Absorption reduces the cross section by a roughly isotropic factor which is considerably less than unity for all but the very lightest nuclei. It therefore follows that the entire optical potential $\mathscr{W}$ cannot be treated in Born approximation. On the other hand, the real part of the potential becomes quite shallow (≈ 11 MeV) for high energy ($\gtrapprox 150$ MeV) nucleons [22]), and so the refraction is rather small in magnitude, though angle-dependent. This suggest an approximation wherein the surface refraction due to Re $\mathscr{W}$ is computed in Born approximation via eq. (51), while the attenuation (resulting from Im $\mathscr{W}$) is estimated by a mean-free-path calculation, as in the work of Serber *et al.* [15, 21]).

As for the variation of $\mathscr{M}_{\lambda\alpha}$ with the index α, we shall simply ignore it and put $\mathscr{M}_{\lambda\alpha} \approx \mathscr{M}_{\lambda f}$. This assumption has one important consequence whose virtue should not be belittled: it permits an analytic evaluation of the correction due to refraction, whereas a calculation in which $\mathscr{M}_{\lambda\alpha}$ is allowed to vary would entail very extensive computations and require a far better theory of the photo-nuclear interaction than is available at present. In any case, the calculation based on $\mathscr{M}_{\lambda\alpha} \approx \mathscr{M}_{\lambda f}$ will be useful in that we shall learn how the angular distribution is changed by refraction even when the basic matrix element is a constant.

4.3. REFRACTION AT THE NUCLEAR SURFACE

We now turn to the Born approximation of eq. (51). According to the foregoing discussion, we shall put $\mathscr{M}_{\lambda\alpha} = \mathscr{M}_{\lambda f}$, $\mathscr{W}^{\dagger} = \mathscr{W}$. Then

$$\mathscr{T}^{\rho\mu\nu}_{\lambda\zeta'} = \mathscr{M}_{\lambda f}(\zeta' \to \zeta_f)\left\{ f_{\rho\nu}(P) Y_{\rho\mu}(\mathbf{P}) + \frac{2Mv}{(2\pi)^3}\int \mathrm{d}^3 q_n \frac{\langle \mathbf{k}_n|\mathscr{W}|\mathbf{q}_n\rangle}{k_n^2 - q_n^2 + i\eta} f_{\rho\nu}(|\mathbf{P}+\mathbf{q}_n-\mathbf{k}_n|) Y_{\rho\mu}(\mathbf{P}+\mathbf{q}_n-\mathbf{k}_n) + [\mathrm{n} \longleftrightarrow \mathrm{p}]\right\} \tag{52}$$

where $\mathbf{q}$ is the momentum in the intermediate state (previously labelled by α), and n, p label the neutron and proton respectively.

Defining the coordinate representation of $\mathscr{W}$ by

$$\langle \mathbf{k}|\mathscr{W}|\mathbf{q}\rangle = v^{-1}\int \mathrm{d}^3 r e^{i(\mathbf{q}-\mathbf{k})\cdot\mathbf{r}} \mathscr{W}(r) \tag{53}$$

and letting

$$f_{\rho\nu}(P)Y_{\rho\mu}(\mathbf{P}) = (2\pi)^{-3/2}\int \mathrm{d}^3R\, e^{-i\mathbf{P}\cdot\mathbf{R}} h_{\rho\mu\nu}(\mathbf{R}) \tag{54}$$

we obtain

$$-\mathscr{M}_{\lambda f}\frac{M}{(2\pi)^{3/2}}\int\left\{\frac{e^{ik_n|\mathbf{r}-\mathbf{R}|}}{|\mathbf{r}-\mathbf{R}|}e^{-i\mathbf{k}_n\cdot\mathbf{r}}e^{-i(\mathbf{P}-\mathbf{k}_n)\cdot\mathbf{R}}+[\mathrm{n}\longleftrightarrow\mathrm{p}]\right\}$$
$$\cdot\mathscr{W}(r)h_{\rho\mu\nu}(\mathbf{R})\mathrm{d}^3r\mathrm{d}^3R \tag{55}$$

for the second member of eq. (52).

We now assume that all the nucleons are in the lowest state of a harmonic oscillator with spatial wave function proportional to exp $[-\frac{1}{2}(r/D)^2]$, and that the optical potential is a Gaussian

$$\mathscr{W}(r) = \mathscr{W}_0 e^{-(r/D)^2}. \tag{56}$$

Upon introducing new variables into eq. (55), we find that

$$\mathscr{T} = \text{const}\cdot\left[e^{-P^2D^2/4} - \frac{1}{\sqrt{8}}MD^2 e^{-P^2D^2/8}\mathscr{W}_0\mathscr{F}\right], \tag{57}$$

where

$$\mathscr{F} = (2/D^2)\int_0^\infty\{e^{ik_n x}j_0(\varkappa_n x)e^{-\frac{1}{4}(x/D)^2}+[\mathrm{n}\longleftrightarrow\mathrm{p}]\}x\mathrm{d}x;$$
$$\varkappa_n = |\tfrac{1}{2}\mathbf{P}-\mathbf{k}_n|,\quad \varkappa_p = |\tfrac{1}{2}\mathbf{P}-\mathbf{k}_p|. \tag{58}$$

As we need only retain the leading and interference terms of eq. (57) when forming $|\mathscr{T}|^2$, we only require the real part of $\mathscr{W}_0\mathscr{F}$. Since $\mathscr{W}_0$ itself is real, we can confine our attention to

$$\mathrm{Re}\,\mathscr{F} = \left\{\frac{1}{\varkappa_n D}[J(\varkappa_n+k_n)+J(\varkappa_n-k_n)]+(\mathrm{n}\longleftrightarrow\mathrm{p})\right\}, \tag{59}$$

where

$$J(s) = D^{-1}\int_0^\infty \sin sx\, e^{-\frac{1}{4}(x/D)^2}\mathrm{d}x$$
$$= Ds\, e^{-\frac{1}{4}D^2s^2}\,{}_1F_1(\tfrac{1}{2},\ \tfrac{3}{2};\ \tfrac{1}{2}D^2s^2) \tag{60a}$$
$$= Ds\sum_{n=0}^{\infty}\frac{(-1)^n(Ds)^n}{1\cdot 3\cdot\ldots\cdot(2n+1)}$$
$$\underset{s\to\infty}{\sim}\frac{1}{Ds}\left[1+\frac{1}{D^2s^2}+\frac{1\cdot 3}{D^4s^4}+\ldots\right], \tag{60b}$$

${}_1F_1(a, c; z)$ being the confluent hypergeometric function. For our purpose the two expansions of eq. (60) will suffice.

The cross section will then be proportional to

$$|\mathscr{T}|^2 = \text{const}\cdot e^{-\frac{1}{2}P^2D^2}\left[1-\frac{1}{\sqrt{2}}\mathscr{W}_0 MD^2 e^{P^2D^2/8}\,\mathrm{Re}\,\mathscr{F}\right] \tag{61}$$
$$\equiv |\mathscr{T}_0|^2\,\Gamma(\varepsilon_p\theta_p\phi_p;\ \ \varepsilon_n\theta_n\phi_n),$$

$\mathcal{T}_0$ being the amplitude in the absence of final state interactions, and $\Gamma(\mathbf{k}_p, \mathbf{k}_n)$ the correction factor due to refraction at the nuclear surface. (The angles between $\mathbf{k}_p$, $\mathbf{k}_n$ and the photon's momentum $\boldsymbol{\omega}$ have been designated by $\theta_p\phi_p$, $\theta_n\phi_n$, respectively.)

In fig. 2 we plot Γ as a function of θ_p for $\phi_p = \phi_n$, $\varepsilon_p = \varepsilon_n = 130$ MeV, $\theta_n = 75°$. The parameter D was chosen so that the r.m.s. radius of the charge

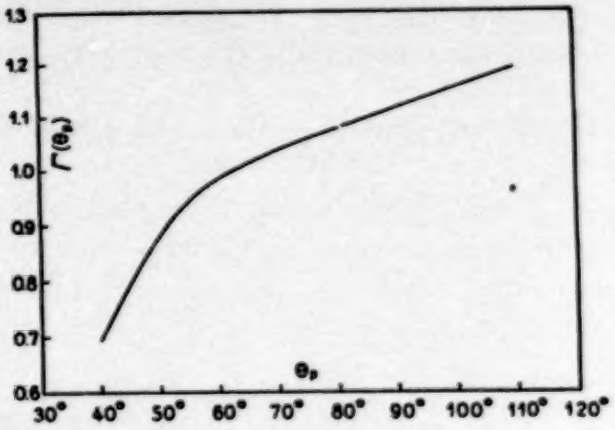

Fig. 2. The "surface refraction" correction factor Γ for $\varepsilon_n = \varepsilon_p = 130$ MeV, $\theta_n = 75°$.

distribution produced by the wave function $R(r) = \text{const} \cdot \exp[-\frac{1}{2}(r/D)^2]$ equalled the measured [23]) one for O^{16} †. The depth of the potential was taken to be 12 MeV [4, 22]).

4.4. ATTENUATION

Following Serber *et al.* [15, 21]) we shall say that the cross section is depleted by a factor

$$f_a = \frac{1}{V_0}\int dV_0\, e^{-X/\lambda_a}, \tag{62}$$

where X is the distance traversed by the photo-nucleons between the point of production and the points of emergence, and λ_a the mean-free-path for absorption. It is assumed that the nucleus has constant density inside a sphere of volume $V_0 = 4\pi R_0^3/3$. If we consider the situation where the nucleons are emitted in opposite directions, one can carry out the integration indicated by eq. (62). The result is

$$f_a = 6\xi^{-3}[1-e^{-\xi}(1+\xi+\tfrac{1}{2}\xi^2)], \tag{63}$$

with $\xi = 2R_0/\lambda_a$. For $R_0 = 1.33(16)^{1/3}\times 10^{-13}$ cm, and $\lambda_a = 4.0\times 10^{-13}$ cm, one has $f_a = 0.30$.

† In deriving eq. (61) we have assumed that all the nucleons are in s-orbits, although in O^{16} the p-shell is also occupied. In view of all our other approximations, it is doubtful whether the inclusion of states with both angular momenta would lead to a *significant* improvement in the value of Γ.

For events where the particles are not produced in opposite directions, we shall assume that f_a is still given by eq. (62). This approximation is based on the fact that the average distance traversed by the pair is independent of the angles of $\mathbf{k}_p$ and $\mathbf{k}_n$. Another supporting argument is that a Born approximation calculation with a very weak $\mathrm{Im}\mathscr{W}$ leads to a far more isotropic correction than the corresponding Γ.

To summarize, we have and will continue to incorporate the effects of final state interactions by multiplying the cross section computed with the impulse approximation by the factor $f_a\Gamma(\mathbf{k}_p, \mathbf{k}_n)$.

5. Evaluation of the Cross Section and Comparison with Experiment

In the first part of this section we shall evaluate the cross section for n-p production in O^{16}, assuming the connection with the photo-effect in deuterium. Secondly, the observed absence of p-p coincidences [13]) is considered in more detail than heretofore.

5.1. NEUTRON-PROTON PRODUCTION

The cross section formulae derived above are valid for monochromatic incident beams. In practice the target is irradiated with a continuous spectrum, and one frequently measures all counting rates relative to deuterium as target. We shall therefore introduce the a quantity $d\mathscr{R}$ defined by the ratio

$$\frac{[\text{coincidences per sec falling between } (\mathbf{k}_p, \mathbf{k}_n) \text{ and } (\mathbf{k}_p+d\mathbf{k}_p, \mathbf{k}_n+d\mathbf{k}_n)]_{\text{nucleus}}}{[\text{counts per sec falling between } \mathbf{k}_p \text{ and } \mathbf{k}_p+d\mathbf{k}_p]_{\text{deuterium}}}$$

or

$$d\mathscr{R} = \frac{\Sigma(\mathbf{k}_p, \mathbf{k}_n, \bar{\omega})}{d\sigma_D(\mathbf{k}_p)/d\Omega_p} \cdot \frac{I(\bar{\omega})}{I(\omega_D)} \cdot \left(\frac{\partial\omega_D}{\partial\varepsilon_p}\right)^{-1} d^3k_n. \tag{64}$$

Here Σ is determined from

$$d\sigma = \Sigma(\mathbf{k}_p, \mathbf{k}_n, \omega)\delta(\varepsilon-\bar{\varepsilon})d\varepsilon_p\, d\Omega_p\, d^3k_n; \tag{65}$$

$I(\omega)d\omega$ is the number of photons incident per sec per cm^2 in the interval $(\omega, \omega+d\omega)$; $d\sigma_D(\mathbf{k}_p)/d\Omega_p$ is the deuterium cross section in the laboratory system when the ejected proton has momentum $\mathbf{k}_p$; $\bar{\omega} = \varepsilon_n+\varepsilon_p+\bar{\varepsilon}$, and ω_D is the photon energy corresponding to $\mathbf{k}_p$ in the deuterium reaction.

On comparing eqs. (36) and (65), we arrive at

$$d\mathscr{R} = \frac{\gamma^3}{2\pi} W(\mathbf{k}_p, \mathbf{k}_n) \left(\frac{\partial\omega_D}{\partial\varepsilon_p}\right)^{-1} \frac{I(\bar{\omega})}{I(\omega_D)} d^3k_n, \tag{66}$$

with

$$W(\mathbf{k}_p, \mathbf{k}_n) = \frac{3}{2\pi^2} F(P) \frac{k_p E_p}{[k_p E_p]_0} \frac{[d\sigma_D/d\Omega_p]_0}{d\sigma_D(\mathbf{k}_p)/d\Omega_p}. \tag{67}$$

Final state interactions are to be corrected for by multiplication with $f_n\Gamma(\mathbf{k}_p, \mathbf{k}_n)$.

An estimate of the energy $\bar{\varepsilon}$ must now be made. It will be recalled (section 2) that $\bar{\varepsilon}$ is the average difference between the energy of the photo-pair and the photon; this difference is due to recoil, binding energy difference, and residual excitation. The difference in binding between O^{16} and N^{14} is 23 MeV, while the recoil energy varies between zero and about 15 MeV, depending on the angle of observation. Even if the average excitation energy is angle-independent, the quantity $\bar{\varepsilon}$ will therefore depend on $\mathbf{k}_p$, $\mathbf{k}_n$. These variations are all small compared to the energies ε_n, ε_p and ω, and if the closure approximation is valid, the final results should not be sensitive to them. In all our subsequent discussion, we have fixed $\bar{\varepsilon}$ at 40 MeV. One may easily verify that changes in $\bar{\varepsilon}$ of order 10 MeV are indeed indiscernible †.

All our calculations assume that $\mathbf{k}_p$ and $\mathbf{k}_n$ are coplanar, and $\varepsilon_p = 130$ MeV, $\theta_p = 75°$, as in the MIT experiments [1]). The angular correlation function $W(\mathbf{k}_p, \mathbf{k}_n)$ is evaluated for a variety of neutron energies and angles,

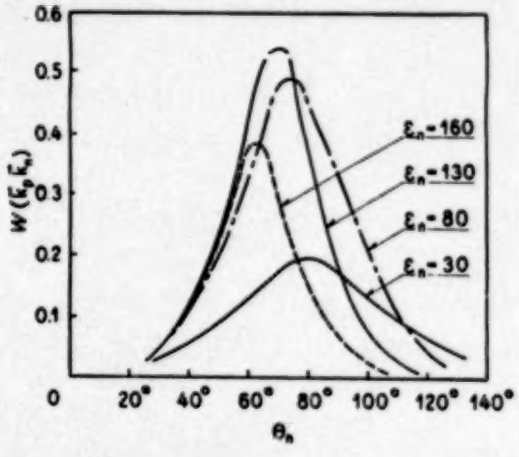

Fig. 3. The angular correlation function $W(\mathbf{k}_p, \mathbf{k}_n)$ when $\mathbf{k}_p$ and $\mathbf{k}_n$ are coplanar, $\varepsilon_p = 130$ MeV and $\theta_p = 75°$.

and plotted in fig. 3. For $\varepsilon_n = 130$ MeV some of the more interesting quantities are quoted in table 1.

A noteworthy feature (see table 1) which emerges from the calculation is that the deuteron cross section which is to be inserted into eq. (67) is a rather rapidly varying function of θ_n for *fixed* ε_n and ε_p. This is due to the Doppler shift $\omega \to \omega_0$, where, as before, ω_0 is the photon's energy in the frame $\mathscr{Y}$. A more detailed discussion of this point will be given below.

Table 1 also lists Δ, the "distance off the energy shell" discussed in the

† There is one obvious qualification: the maximum ε_n for fixed ε_p is sensitive to the choice of $\bar{\varepsilon}$ and offers a means of measuring it.

last paragraph of subsection 3.2. It is defined as $\Delta = 2(\varepsilon_{pD} - \varepsilon_{p_0})$, where ε_{pD} and ε_{p_0} are the proton's energy in $\mathscr{Z}$ in the deuteron photo-effect and

TABLE 1

θ_n	$P^2/4M$	$F(P)$	ω_0	ϑ	$[d\sigma_D/d\Omega_p]_0$	Δ
117	40	0.17	312	66	2.3	90
102	20	0.79	297	85	3.1	70
93	10	1.54	285	79	3.6	50
86	5	2.26	276	83	4.2	40
79	1.25	3.40	270	88	4.4	40
71	0	4.00	261	90	4.8	38
64	1.25	3.40	251	96	5.0	41
56	5	2.26	248	101	5.0	42
49	10	1.54	239	105	5.1	50
41	20	0.79	235	109	5.0	60
26	40	0.17	228	115	5.0	80

Here ϑ is the angle between $\mathbf{k}_{p_0}$ and $\boldsymbol{\omega}_0$, the proton and photon momenta in $\mathscr{Z}$, respectively. All energies are in MeV, angles in degrees, and cross sections in microbarns.

the present reaction, respectively. We note that Δ becomes quite large for the larger values of $P^2/4M$. The question of whether $[d\sigma_D/d\Omega_p]_0$ may be used for these values of Δ will have to go unanswered until a satisfactory theory of nuclear forces and electromagnetic interactions is developed.

The experiments which have already been carried out[1-3]) do not determine the neutron energy, and so an integration over ε_n must be carried out. As the neutron energy distribution will probably be measured in future experiments, and since we should like the reader to be aware of the importance of transitions with small ε_n in the final result, we plot the spectral function

$$Y(\mathbf{k}_p, \mathbf{k}_n) = \frac{1}{8.71} W(\mathbf{k}_p, \mathbf{k}_n) \frac{I(\bar{\omega})}{I(\omega_0)} \left(\frac{\partial \omega_D}{\partial \varepsilon_p}\right)^{-1} \frac{k_n E_n}{M^2} \tag{68}$$

in fig. 4. In terms of Y eq. (66) reads

$$\frac{d^2\mathscr{R}}{d\varepsilon_n d\Omega_n} = \frac{\gamma^3}{2\pi} Y(\mathbf{k}_p, \mathbf{k}_n), \tag{69}$$

where $d\varepsilon_n$ is in units of MeV, and γ in units of 10^{-13} cm.

Our simple-minded picture of the photo-effect is essentially based on the impulse approximation which is expected to break down for low neutron energies. According to fig. 4, however, reactions resulting in low energy neutrons contribute quite substantially to the integration over ε_n. Consequently we do not consider the ensuing comparison with experiment as very significant; a more meaningful test of the theory will have to await the promised experiments [24]) wherein ε_n is also fixed.

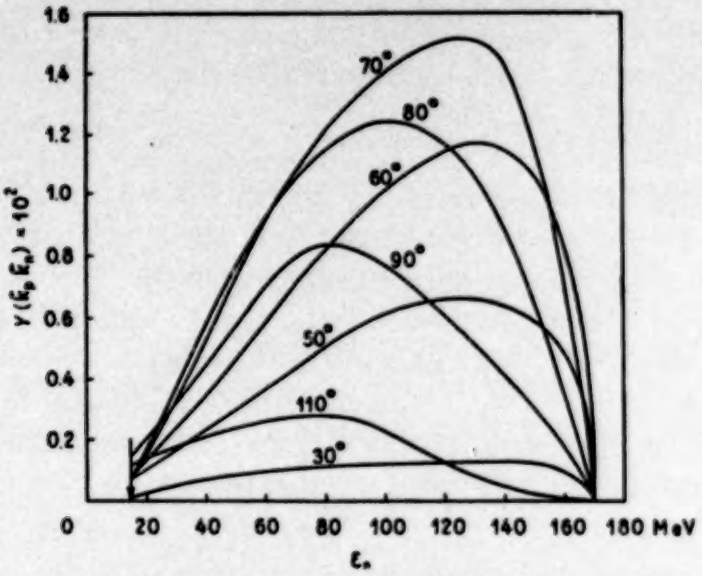

Fig. 4. The spectral function $Y(\mathbf{k}_p, \mathbf{k}_n)$ when $\mathbf{k}_p$ and $\mathbf{k}_n$ are coplanar, $\varepsilon_p = 130$ MeV, $\theta_p = 75°$; the curves are labelled by the angle θ_n.

Nevertheless some comparison with empirical data should be attempted at this juncture. In fig. 5 we therefore plot the angular correlation function † for undetermined ε_n,

$$Z(\mathbf{k}_p|\Omega_n) = \int_{\varepsilon_n \geq \varepsilon_{min}} Y(\mathbf{k}_p, \mathbf{k}_n) d\varepsilon_n ; \tag{70}$$

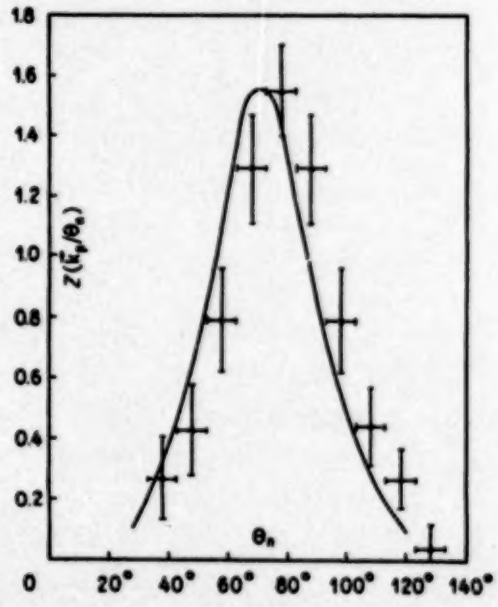

Fig. 5. The angular correlation function $Z(\mathbf{k}_p|\Omega_n)$ when ε_n is not determined, and $\mathbf{k}_p$ is as in figs. 3 and 4. The experimental points are for C^{12} and are taken from Wattenberg *et al.* [1]).

† Since the effect of surface refraction is probably smaller than the other errors made in the integration of eq. (70), we have not included the correction factor Γ in these calculations. When we come to consider experiments with determined ε_n, Γ will make its appearance. The much more important attenuation correction will be made presently.

ε_{min} is the bias of the neutron counter, which in the experiment of Wattenberg *et al.* [1]) was set at 15 MeV. On the same graph we plot the experimental counting rate [1]) for C^{12}, normalized so that it has the same maximum value as the theoretical one.

It is somewhat unfortunate that a theory for O^{16} must be confronted with data for C^{12}. This is due to two circumstances: in the first instance the theory for C^{12} would be greatly complicated by the presence of interference terms (see discussion in section 2), and secondly the present data [1]) for O^{16} has rather large uncertainties. On the other hand, by the time the integration over the neutron energy is carried out with the neglect of final state interactions, we should expect that the comparison forces upon us is almost as valid as one with O^{16} as the actual target.

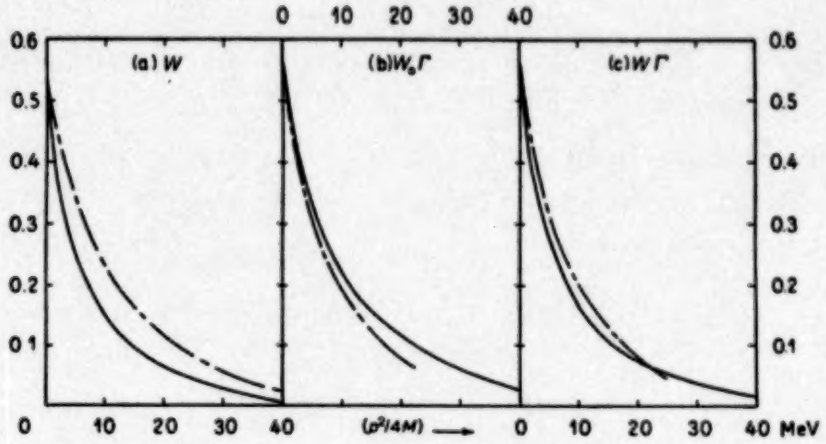

Fig. 6. The angular correlation function when $\varepsilon_n = \varepsilon_p = 130$ MeV, $\theta_p = 75^0$ plotted against $P^2/4M$. The broken curves correspond to $\theta_n \leqq 70^0$, and the solid ones to $\theta_n \geqq 70^0$. The connection between θ_n and $P^2/4M$ will be found in table 1. In (a) the function W of fig. 3 is shown; (c) shows the modification due to surface refraction; (b) gives the angular correlation when the basic matrix element $\mathcal{M}_{\lambda t}$ is a constant.

We note that the agreement between theory and experiment is very good. The small (7°) shift to smaller angles which would bring the data into complete coincidence with the theory could be justified in a number of ways [24]), such as degradation of the protons in the sample or a small error in the calibration of the proton counter. At the same time we must point out that a similar shift of the theoretical curve to larger angles would be hard to justify. It is therefore important to locate the absolute angular position of the experimental curve as accurately as possible.

The absolute value of the experimental counting ratio, as determined by Odian *et al.* (fig. 6 of ref. [2])), is

$$\int d\varepsilon_n \, d\Omega_n \left(\frac{d^2 \mathscr{R}}{d\varepsilon_n \, d\Omega_n} \right)_{k_p} = 5.6 \pm 0.5. \tag{71}$$

If we integrate $Z(\mathbf{k}_p|\Omega_n)$ over all neutron angles †, and multiply by the attenuation factor $f_a = 0.30$, we find that the value of γ required to secure agreement with experiment is

$$\gamma \approx 5.1 \times 10^{-13} \text{ cm}. \tag{72}$$

By applying the same f_a to the transitions in which low and high energy neutrons are ejected, we have overestimated the cross section. Due to the fact that γ^3 appears in $d\mathscr{R}$, such uncertainties are not of great consequence, however; indeed γ would only be raised to 5.6×10^{-13} cm even if a 50 % overestimate of the theoretical cross section is admitted. We reserve a discussion of the significance of this value of γ for the concluding section.

At this point a remark about the A-dependence of the cross section is in order. This dependence has two sources in the present theory: the form factor $F(P)$ and the attenuation factor f_a. Inspection of eq. (31) reveals that $F(0) = \frac{1}{4}A$. Thus the maximum value of the cross section (i.e. where $\varepsilon_n = \varepsilon_p$, $\mathbf{P} = 0$) varies like $A f_a$, and this dependence probably holds for measurements wherein $\mathbf{k}_n$ is not determined. If we keep λ_a independent of A we would therefore expect the cross section ratio $[d\sigma(\text{Li})/d\sigma(O^{16})] = 0.71$, while the experimental ratio [2]) at $\varepsilon_p = 130$ MeV, $\theta_p = 75°$ is 0.81 ± 0.12.

We now turn to the envisaged experiments in which ε_n will also be measured, and which will therefore obviate the integration over the bremsstrahlung spectrum. Such an experiment would shed light on several facets of this problem, but we shall confine our attention to the one expressed by the question: can the basic matrix element $\mathscr{M}_{\lambda f}$ be computed from the deuterium cross section? This question is most easily discussed in terms of a graph of the angular correlation function $W(\mathbf{k}_p, \mathbf{k}_n)$ versus $P^2/4M$, and not versus θ_n, as in fig. 3. According to our theory, the Doppler shift raises the curves where $\mathbf{P}$ is in the forward hemisphere, above those for $\mathbf{P}$'s in the opposite hemisphere. This is illustrated in fig. 6(a). The surface refraction correction factor Γ brings the curves closer together, as shown in fig. 6(c). If, on the other hand, $\mathscr{M}_{\lambda f}$ were not to depend on the Doppler shift, the situation would be reversed, as in fig. 6(b). The most accurate experiment of this type would then compare coincidence rates at the two values of θ_n which correspond to same $|\mathbf{P}|$.

The drawback of measurements such as these is that one is trying to extract the slowly varying function $|\mathscr{M}_{\lambda f}|^2\Gamma$ from the very rapidly varying angular correlation function. Moreover (see fig. 6) the most significant measurements occur at angles where the counting rate is low. If neutron and proton counters with variable energy acceptance are available, one can

† In carrying out this integration we have assumed that the dependence of Z on the azimuthal angle ϕ_n can be obtained by rotating the distribution shown in fig. 5 about the axis $\theta_n = 70°$, $\phi_n = 0°$.

overcome both of these difficulties in one stroke. For it is a simple matter (see fig. 7) to vary both $\mathbf{k}_p$ and $\mathbf{k}_n$ while keeping $\mathbf{P}$ and $(\varepsilon_p+\varepsilon_n)$ fixed, and if $\mathbf{P}$ is put equal to zero the counting rate will remain appreciable throughout. The cross section as a function of the angle Θ (fig. 7) should then show the same variation as the one in deuterium (but modified by the

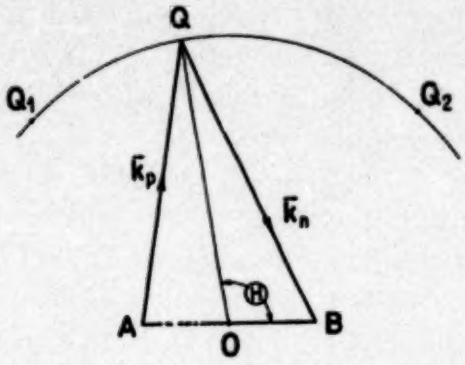

Fig. 7. Kinematics of the photo-effect when $\mathbf{P} = 0$. Here the photon momentum ω is represented by the directed segment AB. If Q lies on a circle centered at 0, the point which bisects AB, the energy $(\varepsilon_n+\varepsilon_p)$ remains constant to within a small relativistic correction. In this drawing $\omega = 300$ MeV, $\varepsilon_n+\varepsilon_p = 260$ MeV. If we desire $\varepsilon_n, \varepsilon_p \geqq 80$ MeV, Q must lie on the arc Q_1QQ_2. Except for a negligible relativistic correction, Θ is just the angle between the proton and photon momenta in the zero-momentum frame $\mathcal{Z}$.

surface refraction factor Γ). In the case illustrated by fig. 7 we would then expect † a variation of counting rate by a factor of about two as Θ ranges between its limiting values.

5.2. PROTON-PROTON PRODUCTION

Weinstein *et al.* [13]) †† have searched for p-p coincidences in various nuclei. In the case of O^{16}, and $\varepsilon_p = \varepsilon_{p'} \approx 110$ MeV, $\theta_p = -\theta_{p'} \approx 76°$, they report that the p-p cross section is approximately 2 % of the n-p cross section at the same angles and energy. In the following paragraphs we shall attempt to interpret this fact on the basis of the present theory.

Since we are now dealing with the $T = 1$ system, only ^1S, ^3P, ^1D etc. states arise. The expansion of the exponentials in eq. (26) therefore confines the initial state to $^1S_0$. Transitions from this state to $^3P_1$ would require an electromagnetic interaction operator antisymmetric in the two proton spin vectors, an object which does not arise in most meson theories under present consideration. The transition to the $^3P_2$ state also involves a spin-flip. Thus the $^1S_0$ state probably absorbs E2 quanta and uses $^1D_2$ as the final state. Due to the angles chosen by W, electric quadrupole absorption could not be observed, and so the probability for $^1S_0 \rightarrow {}^1D_2$ transitions is unknown.

† See the curve marked $K_L = 255$ in fig. 9 of ref. [6]).
†† Referred to by W henceforth.

When we consider ^{3}P as the initial state, a host of dipole transitions of the more conventional variety become possible, and the angular distribution of the photo-protons would not preclude their observation by W. We therefore address ourselves to the question of whether the virtual absence of p-p coincidences is compatible with the probability of finding two protons in a relative P state and at small separation.

Since we are looking for the maximum effect, we restrict ourselves to the case $\mathbf{P} = 0$. Returning to eq. (26), we have

$$u_\lambda = \frac{2\pi}{\omega} \sum_{\zeta'} \int \mathrm{d}^3q \mathrm{d}^3q' \mathrm{d}^3x_1 \ldots \mathrm{d}^3x_4 \langle \mathbf{q}-\mathbf{q}|\mathscr{D}_{S'T'}|\mathbf{q}'-\mathbf{q}'\rangle$$
$$\cdot [\chi_t(\mathbf{x}_1\zeta_t)^* \langle \mathbf{x}_1\zeta_t|\, \mathscr{E}_\lambda\, |\mathbf{x}_2\zeta'\rangle g_{\zeta'}(x_2) \mathrm{e}^{i\mathbf{q}\cdot\mathbf{x}_2}]$$
$$\cdot [\chi_t(\mathbf{x}_3\zeta_t)^* \langle \mathbf{x}_3\zeta_t|\, \mathscr{E}_\lambda\, |\mathbf{x}_4\zeta'\rangle g_{\zeta'}(x_4) \mathrm{e}^{i\mathbf{q}'\cdot\mathbf{x}_4}]^*.$$

We now expand the plane waves into spherical harmonics, and find that there is no interference between transitions arising from harmonics of different parity (this is only true when $\mathbf{P} = 0$). If we retain only the P-wave part of the plane waves, put $S = T = 1$, and use the first term in the power series for the spherical Bessel functions, we find that

$$u_\lambda \to u_\lambda^{(1)} = \frac{2\pi}{\omega} \sum_{\zeta'} \int \mathrm{d}^3x_1 \ldots \mathrm{d}^3x_4\, \varrho_{\mathrm{P}}(\mathbf{x}_2|\mathbf{x}_4)$$
$$\cdot [\chi_t^*(\mathbf{x}_1\zeta_t) \langle \mathbf{x}_1\zeta_t|\, \mathscr{E}_\lambda |\mathbf{x}_2\zeta'\rangle g_{\zeta'}(x_2)] \tag{73}$$
$$\cdot [\chi_t^*(\mathbf{x}_3\zeta_t) \langle \mathbf{x}_3\zeta_t|\, \mathscr{E}_\lambda |\mathbf{x}_4\zeta'\rangle g_{\zeta'}(x_4)]^*,$$

where

$$\varrho_{\mathrm{P}}(\mathbf{x}_2|\mathbf{x}_4) = \left(\frac{4\pi}{27}\right) \cdot x_2 x_4 \sum_\mu Y_{1\mu}(\mathbf{x}_2) Y_{1\mu}^*(\mathbf{x}_4)$$
$$\cdot \sum_{nn'll'} (2l+1)(2l'+1) |\langle ll'\, 00|10\rangle|^2 \left| \int_0^\infty K_{nl}(q) K_{n'l'}(q) q^3\, \mathrm{d}q \right|^2, \tag{74}$$

$K_{nl}(q)$ being the radial function in momentum space (i.e. the Fourier transform of the function $R_{nl}(q)$ appearing in eq. (31)). $\varrho_{\mathrm{P}}(\mathbf{x}|\mathbf{x})$ is essentially the probability for finding two protons with zero total momentum and separation $\mathbf{x}$ in a relative P-state.

Let us assume the existence of a characteristic separation $r_{\mathrm{pp}}(r_{\mathrm{np}})$ within which two protons (a neutron and proton) must be if they are to absorb the photon with appreciable probability. We would then expect the significant number for determining the (p-p) : (n-p) production-rate ratio to be the probability $\varrho_{\mathrm{P}}(\mathbf{x}|\mathbf{x})$ integrated over a sphere of radius r_{pp}, divided by the corresponding quantity for (n-p)-production. Calling this number $\bar{\varrho}$ (pp : np), we have

$$\bar{\varrho}(\mathrm{pp}:\mathrm{np}) = [\tfrac{4}{3}\pi r_{\mathrm{np}}^3 F(0)]^{-1} \int_{x \leq r_{\mathrm{pp}}} \varrho_{\mathrm{P}}(\mathbf{x}|\mathbf{x}) \mathrm{d}^3 x$$

$$= \frac{4}{15\mathrm{A}} \left(\frac{r_{\mathrm{pp}}}{r_{\mathrm{np}}}\right)^3 \sum_{nn'll'} (2l+1)(2l'+1) |\langle ll'\, 00|10\rangle|^2 \qquad (76)$$

$$\cdot \left| \int_0^\infty (r_{\mathrm{pp}} q) K_{nl}(q) K_{n'l'}(q) q^2 \mathrm{d}q \right|^2 .$$

According to Wilson's analysis of the photo-effect in deuterium [8]), $r_{\mathrm{np}} \approx 1.0 \times 10^{-13}$ cm. In O^{16} we would therefore expect

$$\bar{\varrho}(\mathrm{pp}:\mathrm{np}) \approx 0.051 (r_{\mathrm{pp}} \times 10^{13}\ \mathrm{cm}^{-1})^2, \qquad (77)$$

which implies that $r_{\mathrm{pp}} \approx 0.7 \times 10^{-13}$ cm. The fact that r_{pp} is smaller than r_{np} could be attributed to (1) a shorter range for the non-classical part of the electromagnetic interaction operator $\mathscr{E}_\lambda^{\mathrm{pp}}$ belonging to a p-p pair, and/or (2) that this meson-connected part of $\mathscr{E}_\lambda^{\mathrm{pp}}$ is smaller than $\mathscr{E}_\lambda^{\mathrm{np}}$ when the separation is about r_{np}. The latter explanation would follow from a treatment of the π-γ-nucleon system by perturbation theory.

A by-product of the calculation culminating in eq. (76) is a quantitative estimate of the error made in neglecting initial relative P-states in n-p production (see eq. (29) and preceding remarks). If we accept Wilson's value of r_{np} for P- as well as S-states, we need only put $r_{\mathrm{pp}} = r_{\mathrm{np}} \approx 1.0 \times 10^{-13}$ cm in eq. (77), and multiply by $\frac{4}{3}$ so as to account for both ^{3}P and ^{1}P states. We then find that the error made in ignoring the P-states is approximately 7 %.

6. Conclusions

The are two rather distinct levels at which one can examine a direct reaction. The first, which we call the kinematic level, is mainly concerned with the question of how many particles are ejected per event, and a qualitative understanding of their distribution in energy and angle. At this level one therefore determines various momentum distributions in the target, and the depletion of the cross section due to final state interactions.

The second, more inextricably buried level we shall call the dynamic one. Here one is concerned with processes which are not on the same energy shell as their isolated counterparts, many-body effects come into play, and certain fine details of the nuclear ground state are of significance. Obviously a thorough understanding of the kinematic level is a prerequisite to a serious attack on the deeper dynamic level.

In the case of the photo-effect, we can feel quite confident that the reaction is fairly well understood at the kinematic level. Levinger's prediction [5]) that neutrons and protons are emitted in coincidence has been confirmed repeatedly. The angular correlation between the photo-pair is

quite probably in agreement (see fig. 5) with the momentum distribution $F(P)$ as computed from almost *any* set of shell-model wave functions which have the correct r.m.s. radius. The (p-p) : (n-p) cross section ratio is of the expected order of magnitude, and the A-dependence of the cross section appears to be reproduced by the optical model.

As we descend to the dynamic level, our ignorance deepens rapidly. We cannot confirm or withdraw our basic assertion that the photo-nuclear interaction is the sum of two-body operators. Nor can we pass judgement on the validity of our assumptions concerning the pair correlation function and the associated determination of the basic matrix element $\mathscr{M}_{\lambda t}$ from the deuterium cross section. At this time we have to content ourselves with

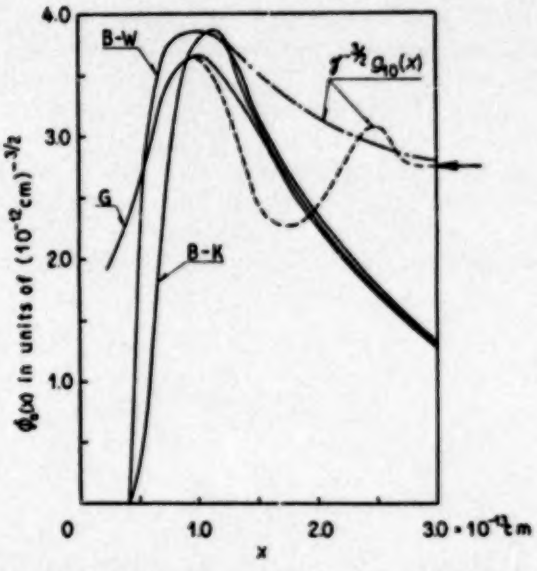

Fig. 8. The solid curves are three different deuteron wave functions proposed by Gartenhaus, Blatt and Kalos, and Brueckner and Watson (see fig. 3 of ref. [25]) for references, etc.). The large arrow indicates the value of $\gamma^{-3/2}$ as deduced in subsection 5.1 (see eq. (72)); this is the *asymptotic* value of the short range correlation function $g_{10}(x)$. If $g_{10}(x)$ is proportional to $\phi_0(x)$ for $x \lesssim 1.0 \times 10^{-13}$ cm, then the two broken curves are possible forms of $g_{10}(x)$. It should be stressed that these broken curves are not the result of any calculation, but are merely guessed.

a single fact concerning the short range modulation function $g_{ST}(x)$ in the $S = 1$, $T = 0$ state: an evaluation (see eq. (72)) of the constant γ defined by eq. (34). This value of γ is quite compatible with one's intuitive picture of pair correlations (see fig. 8). This lone fact will not suffice, however, and some further experimental information will have to be acquired if we are to increase our understanding of the photo-nuclear interaction and short-range pair correlations in nuclei. The procedure for taking measurements described by fig. 7 and the associated discussion probably provides the most convenient way of acquiring this missing information.

It is a pleasure to acknowledge a number of helpful discussions with B. T. Feld, H. Feshbach, and A. Wattenberg. This manuscript was prepared while the author was a visitor at the Institute for Theoretical Physics in Copenhagen; he should like to thank Prof. N. Bohr, Prof. A. Bohr and the members of the Institute for the very kind hospitality extended to him.

Notes added in proof: (1) As Dr. B. R. Mottelson has kindly pointed out, there is no *a priori* justification for neglecting *real* photo-pion production and reabsorption by two nucleons. Because it is coherent with the process treated in the text, elastic π^0-production and subsequent absorption by the "photo"-nucleons is the largest effect of this type. One can compute the size of the interference term since one knows [24]) the photoproduction amplitude, the cross section for $p+p \to d+\pi^+$ [27]) and the mean-free-path for pions in nuclear matter [28]). For $\omega = 300$ MeV we estimate that the interference term is $\lesssim 15$ % of the direct production term; whether this interference is constructive or destructive is not known, of course. (2) A paper by K. A. Brueckner, R. J. Eden and N. C. Francis (Phys. Rev. **98** (1955) 1445) which discusses high-energy reactions, including the photo-effect, has recently come to the author's attention. Brueckner *et al.*'s treatment of the photo-effect is also based on the impulse and closure approximations, a pair-correlation function similar to ours is introduced, and the data are then related to the *one*-nucleon momentum distribution in the target state. This latter interpretation is based on three assumptions which we believe to be questionable: (1) the interaction between the photo pair can be neglected (i.e. $\chi_f^{(-)} \approx \Phi_f$ in our notation), (2) the photo-nuclear interaction is of the conventional electric dipole type, and (3) the impulse approximation is valid for reactions like (p, pp′) and (p, pπ) even when internal momenta high compared to the Fermi momentum are involved.

References

1) A. Wattenberg, A. C. Odian, P. C. Stein, H. A. Wilson and R. Weinstein, Phys. Rev. **104** (1956) 1710
2) A. C. Odian, P. C. Stein, A. Wattenberg, B. T. Feld and R. Weinstein, Phys. Rev. **102** (1956) 837
3) M. Q. Barton and J. H. Smith, Phys. Rev. **95** (1954) 573
4) A. Wattenberg, Encyclopedia of Physics (Springer-Verlag, Berlin, 1957) vol. **40**
5) J. Levinger, Phys. Rev. **84** (1951) 43;
K. G. Dedrick, Phys. Rev. **100** (1955) 58
6) J. C. Keck and A. V. Tollestrup, Phys. Rev. **101** (1956) 360
7) E. A. Whalin, B. D. Schriever and A. O. Hanson, Phys. Rev. **101** (1956) 377
8) R. R. Wilson, Phys. Rev. **86** (1952) 125; **104** (1956) 218
9) G. F. Chew and M. L. Goldberger, Phys. Rev. **87** (1952) 778
10) S. D. Drell and K. Huang, Phys. Rev. **91** (1953) 1527
11) R. Jastrow, Phys. Rev. **98** (1955) 1479;
F. Iwamoto and M. Yamada, Prog. Theor. Phys. **17** (1957) 543
12) K. A. Brueckner and W. Wada, Phys. Rev. **103** (1956) 1008
13) R. Weinstein, A. Odian, P. C. Stein and A. Wattenberg, Phys. Rev. **99** (1955) 1621
14) M. Gell-Mann and M. L. Goldberger, Phys. Rev. **91** (1953) 398
15) K. A. Brueckner, R. Serber and K. M. Watson, Phys. Rev. **84** (1951) 258
16) A. C. Zemach and R. J. Glauber, Phys. Rev. **101** (1956) 118
17) P. O. Löwdin, Phys. Rev. **97** (1955) 1474
18) N. Austern, Phys. Rev. **100** (1955) 1522;
B. T. Feld, Nuovo Cimento **2** (1955) Suppl. 1, 145
19) R. G. Sachs, Nuclear Theory (Addison-Wesley, Cambridge, Mass., 1953) especially pp. 241-245
20) B. T. Feld, private communication

21) S. Fernbach, R. Serber and T. B. Taylor, Phys. Rev. **75** (1949) 1352
22) F. Mandl and T. H. R. Skyrme, Phil. Mag. **44** (1953) 1028
23) J. H. Fregeau, Phys. Rev. **104** (1956) 249
24) A. Wattenberg and R. Weinstein, private communication
25) J. Bernstein, Phys. Rev. **104** (1956) 225
26) Y. Yamaguchi, Prog. Theor. Phys. **13** (1955) 459;
G. Chew and F. Low, Phys. Rev. **101** (1956) 1579.
27) Meshcheryakov *et al.*, Doklady Akad. Nauk. SSSR **100** (1955) 677;
A. H. Rosenfeld, Phys. Rev. **96** (1954) 130
28) R. M. Sternheimer, Phys. Rev. **101** (1956) 384

Nuclear Physics **5** (1958) 588—594; © *North-Holland Publishing Co., Amsterdam*
Not to be reproduced by photoprint or microfilm without written permission from the publisher

POLARIZATION OF ELECTRONS EMITTED IN β-DECAY

A. I. ALIKHANOV, G. P. ELISEIEV, V. A. LUBIMOV and B. V. ERSHLER
USSR Academy of Sciences, Moscow

Received 20 September 1957

Abstract: In connection with a reconsideration of the law of conservation of parity some experiments have been performed with the purpose of detecting longitudinal polarization of electrons emitted in β-decay. It was found that the spin of the emerging β-electrons is opposite to the direction of electron motion. The magnitude of the longitudinal polarization agrees with the theoretical value, v/c, v being the electron velocity.

In connection with a reconsideration of the law of conservation of parity for weak interactions [1, 2]) L. D. Landau has recently porposed the hypothesis of a two-component neutrino [2, 3]) possessing only longitudinal polarization.

Landau showed that in this case the electrons emitted in β-decay should be polarized along the direction of motion, the degree of polarization being equal to v/c.

We have attempted to detect experimentally this phenomenon predicted by Landau†. For the determination of the polarization of the β-decay electrons we made use of the effect of azimuthal asymmetry of singly scattered electrons polarized perpendicularly to the direction of motion, the electrons being scattered through a large angle by a thin foil of a heavy element.

In our experiments longitudinally polarized β-electrons were passed into crossed magnetic and electric fields. The electron spins rotated through an angle φ defined by

$$\sin\varphi = \frac{\sin\varphi_0}{\sqrt{\dfrac{\left[\dfrac{v}{v_0} - 1 + \left(1 - \dfrac{vv_0}{c^2}\right)\cos\varphi_0\right]^2}{\left(1 - \dfrac{v^2}{c^2}\right)\left(1 - \dfrac{v_0^2}{c^2}\right)} + \sin^2\varphi_0}}$$

where

$$\varphi_0 = \frac{300Hl\sqrt{1-(v_0/c)^2}}{p_0 \cdot c},$$

l being the path length of the electron in the magnetic field (in cm), H the magnetic field strength in oersteds and p_0 the momentum in eV/c

† Preliminary results of this work were reported at the Rochester Conference in April 1957.

corresponding to the velocity v_0 defined by the relation $v_0/c = E/H$. The electric field E was so chosen as to compensate the trajectory deflection produced by the magnetic field. The trajectories of particles moving with a velocity v_0 were rectilinear. The electrons thus acquired a transverse polarization in the crossed fields.

The method described above is known as the Wien velocity selector method and was chosen for the following reasons:

1. The instrument possesses a simple geometry with axial symmetry and this reduces the probability of appearance of asymmetry effects due to the apparatus. It was confirmed by controlling experiments with aluminium scatterer.

2. The electron spin can be rotated through an arbitrary angle and the measurements can thus be performed within a broad velocity range.

3. Reversal of the electric and magnetic fields does not affect the geometry of the apparatus whereas the sign of the azimuthal asymmetry effect is reversed. This circumstance enables one to differentiate between this type of asymmetry and asymmetry of an instrumental origin.

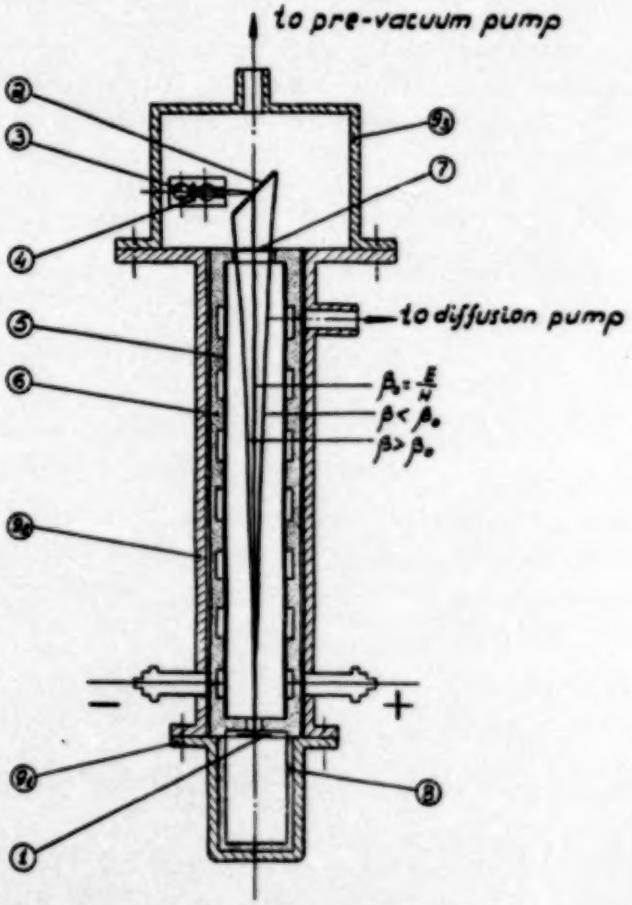

Fig. 1. Cross-section of instrument in a plane perpendicular to the magnetic field. 1 - source, 2 - scatterer, 3 - Geiger counters, 4 - filter, 5 - aluminium foil electrodes (10 μ), 6 - plexiglass, 7 - film (celluloid 0.3 mg/cm²), 8 - plexiglass, $9_{1,2,3}$ - brass body.

4. The energy resolution of the instrument can readily be changed by varying E and H while the ratio $E/H = v_0/c$ may remain constant. As in the region about 300 keV the effect is not sensitive to the energy (it is proportional to v/c) a decrease in the resolving power does not appreciably influence the effect but strongly increases the efficiency of the apparatus.

The effective length of the electron path in the crossed fields was 27 cm. The gap between the condenser plates was 12 mm. On exit from the fields the electrons were scattered by a gold scatterer placed in the "transmission position" at an angle of 45° with respect to the beam axis. Electrons scattered through an angle $90\pm4°$ were recorded by two Geiger counters connected in coincidence. Without violating the vacuum the counters and scatterer could be simultaneously rotated about an axis passing through the centre of the beam in a plane perpendicular to the beam. A low energy electron absorber was placed between the counters.

The design of the instrument is schematically shown in fig. 1.

A strontium-yttrium source corresponding to the transitions

$$_{38}Sr^{90}(0^+) \xrightarrow[540\,keV]{\beta^-\,28y} {}_{39}Y^{90}(2^-) \xrightarrow[2260\,keV]{\beta^-\,64h} {}_{40}Zr^{90}(0^+),\ {}_{38}Sr^{89}(\tfrac{5}{2}+) \xrightarrow[1463\,keV]{\beta^-\,53d} {}_{39}Y^{89}(\tfrac{1}{2}-)$$

of 4 mg/cm² thickness and activity $\approx 4 \times 10^8$ c/s was employed.

The measurements were conducted at an energy of about 300 keV.

In a plane perpendicular to the spin the expected azimuthal asymmetry is †

$$\delta_{expect} = 21.8\,\%.$$

Results of the measurements are given in table 1.

The following is evident from the table:

1. In the plane of rotation of the spin 0°—180° (fig. 2), the asymmetry was zero.

2. Asymmetry was observed in the 90°—270° plane, the sign being reversed when the field direction was reversed.

3. The asymmetry sign is just what one would expect for β-decay electrons possessing spins whose direction is opposite to that of the electron motion; this fact agrees with the experimental results obtained by Wu and coworkers [4]).

The measured magnitude of the asymmetry is

$$\delta_{measur.} = (17.4\pm4.3)\,\%.$$

Thus the degree of polarization of β-decay electrons is

$$\frac{v}{c}\cdot\frac{17.4\pm4.3}{21.8} = (0.80\pm0.20)\frac{v}{c}.$$

† The expected value was calculated supposing that for ($\Delta J = 2$, yes) transition the polarization equals to v/c (B. Ioffe and A. Rudik, in press).

TABLE 1

	0	180	90	270
Counting rate per min fields ⊖	129.7±5.7	132.7±5.8	150.1±3.9	125.2±4.0
Background in absence of scatterer	31.2±2.5	31.0±2.5	31.3±1.2	24.2±1.0
Effect	98.5±6.2	101.7±6.3	118.8±4.0	101.0±4.1
Counting rate per min fields ⊕	128.6±4.0	142.7±3.8	136.5±1.8	145.9±2.4
Background in absence of scatterer	29.8±2.2	34.2±2.4	37.4±1.1	27.5±1.1
Effect	98.6±4.8	108.5±4.2	99.1±2.0	118.4±2.4
Integral effect for fields ⊕ and ⊖	200.3±7.8 207.8±7.3		199.0±3.6 237.2±4.2	

The measurements were performed with a gold scatterer of 0.537 mg/cm² thickness.

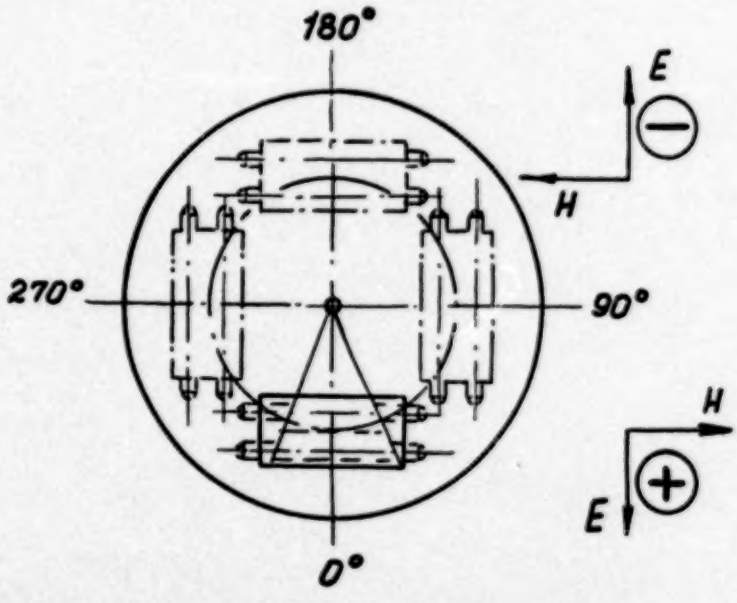

Fig. 2. Diagram of counter arrangement in the experiment. Electrons move towards the reader. Field combinations are denoted by (+) and (−).

Since the azimuthal asymmetry A strongly depends on the scattering angle and sharply drops at angles smaller than 90°, the asymmetry effect was small for electrons which suffered multiple scattering. The measured

asymmetry value should thus be increased by 13 %. The multiple scattering in all sources does not produce appreciable depolarization of electrons of a given energy.

In order to reduce the background and thus be able to employ a sufficiently "thin scatterer" we carried out polarization measurements on electrons possessing an energy of about 750 keV. Electrons in this energy range were emitted in the decay of $_{39}Y^{90}$ and $_{38}Sr^{89}$.

A filter was interposed between the two counters connected in coincidence; the filter absorbed all electrons with energies below 500 keV. The electrons were scattered by a 1.9 mg/cm² gold foil.

The expected magnitude of the azimuthal asymmetry is

$$\delta_{\text{expect.}} = 6.8\ \%.$$

Results of the measurements are given in table 2.

	0	180	90	270
Counts per min fields ⊖	31.7±0.7	32.8±0.7	33.2±0.4	30.7±0.4
Background in absence of scatterer	2.2±0.3	3.0±0.4	1.88±0.2	1.98±0.2
Effect	29.5±0.7	29.8±0.8	31.3±0.4	28.7±0.5
Count per min fields ⊕	31.6±0.9	31.1±0.9	30.6±0.4	31.9±0.4
Background in absence of scatterer	2.2±0.4	2.2±0.4	2.96±0.26	2.37±0.23
Effect	29.4±1.0	28.9±1.0	27.6±0.5	29.6±0.5
Integral effect for fields ⊕ and ⊖	58.4±1.3 59.2±1.3		60.9±0.6 56.3±0.6	
Counts per min fields turned off	31.6±0.9	32.6±0.6	32.6±0.7	32.0±0.7
Background in absence of scatterer	2.7±0.4	2.7±0.3	2.9±0.4	2.8±0.3
Effect	28.9±1.0	29.9±0.9	29.7±0.8	29.2±0.8

At about 750 keV the energy resolution of the instrument was poor. The number of scattered particles entering the counter therefore did not

depend on the applied fields but depended on the shape of the energy spectrum of the source, on the transmission of the filter interposed between the counters and also on the probability of scattering. This permitted us to carry out a control experiment with electrons of the same energy but with the electric and magnetic fields turned off. In this case the electrons should remain polarized longitudinally and no scattering azimuthal asymmetry should be expected.

From the date presented in the table 2 it can be seen that in fact no azimuthal asymmetry could be observed in the absence of the fields.

In a plane perpendicular to the plane of rotation of the spins the magnitude of azimuthal asymmetry in this experiment was

$$\delta_{\text{meas.}} = (7.8 \pm 2.5)\%.$$

Thus for the degree of polarization of ≈ 750 keV electrons we get

$$(1.15 \pm 0.4)\, v/c.$$

Finally, the experiment was repeated at an energy ≈ 300 keV in slightly different conditions ($E = 20$ keV/cm, $H = 86$ Oe and scattering angle 105°) with the 0.17 mg/cm^2 scatterer and with a thinner source (≈ 1.5 mg/cm^2).

The value of the azimuthal asymmetry was corrected for the multiple scattering in the scatterer. It was found to equal 35.5 % and the electron polarization is equal to

$$(1.10 \pm 0.19)\, v/c.$$

The control experiments were performed with aluminium scatterer and the asymmetry appearing in this experiment, equal to ≈ 7 %, was subtracted.

The mean value of the polarization for electrons with energy about 300 keV obtained in both experiments equals to

$$(1.02 \pm 0.15)\, v/c.$$

Thus, along with the experiments of Wu *et al.* [4]), Garwin, Lederman and Weinrich [5]) and Weissenberg and Smirnitsky [6]) experiments involving measurement of the polarization of electrons emitted in β-decay support the view that parity is not conserved in weak interactions. Our results furthermore support Landau's theory of the two-component neutrino, which yields the best agreement with experiment.

The authors wish to express their appreciation to L. Ya. Suvorov, M. P. Anikina and V. D. Laptyev for performing the complicated and tedious work of preparing the sources, to A. S. Kronrod for evaluating the efficiency of the instrument and to M. E. Vishnevsky for giving us the values of corrections for multiple scattering which we used.

Recently analogous data have been obtained by S. Ya. Nikitin of our Laboratory and his co-workers. These data confirm the longitudinal polarization of β-electrons. They used a curved electrically charged condenser of 108° angle to rotate the electron spin. The source was Cu^{64} (allowed transition).

As these experiments were finished we learned from L. D. Landau about the results of N. Frauenfelder and co-workers which, as the authors themselves say, are only of a qualitative nature. Their experiments were performed by a method resembling that of S. Ya. Nikitin *et al.*

References

1) T. D. Lee and C. N. Yang, Phys. Rev **104** (1956) 254
2) L. D. Landau, Nuclear Physics **3** (1957) 127
3) L. D. Landau, JETP **32** (1957) 405
4) C. S. Wu *et al.*, Phys. Rev. **105** (1957) 1413
5) R. L. Garwin, L. M. Lederman and M. Weinrich, Phys. Rev. **105** (1957) 1415
6) A. Weisenberg and V. Smirnitsky, JETP **32** (1957) 1340

Nuclear Physics **5** (1958) 595—602; © *North-Holland Publishing Co., Amsterdam*

Not to be reproduced by photoprint or microfilm without written permission from the publisher

X-RAY PHOTOEXCITATION OF Li^7

OLOF BECKMAN and ROLAND SANDSTRÖM

Institute of Physics, Uppsala, Sweden

Received 1 October 1957

Abstract: The level width and lifetime of the 477-keV level in Li^7 have been measured by photoexcitation using the continuous radiation from an X-ray tube. The level width has been calculated from an absolute measurement of the scattered radiation in an angle of 120 degrees and from a self-absorption experiment. The measured level width is $\Gamma = 6.2 \times 10^{-3}$ eV giving the lifetime $\tau = (1.1 \pm 0.3) \times 10^{-13}$ sec. The result is in agreement with earlier measurements by means of the Doppler-broadening of the gamma-line following the reaction B^{10} $(n\alpha)Li^7$.

1. Introduction

The study of nuclear resonance scattering gives valuable information of nuclear level widths and lifetimes in a region where the measurements by delayed coincidences fail. As the source of the exciting radiation the gamma-rays from nuclei of the same kind as the scattering nuclei have hitherto been used. In this case the energy loss due to the recoil of both the emitting and scattering nuclei has to be compensated for in some way, since the energy loss is much larger than the level width. Several methods for restoring the resonance condition have been successfully applied. The width of low-energy levels in heavy nuclei has been measured in experiments where the recoil energy loss was balanced by mechanical motion (rotation of the radioactive sample) or by thermal motion (heating of the sample) [1]). The recoil energy from the radioactive decay immediately preceeding the emission of the gamma radiation under study has been utilized by F. Metzger in an investigation of the 1.33 MeV level of Ni^{60} and other levels [2]).

The problem of the recoil energy loss can be eliminated by using a continuous X- or gamma-ray source for the excitation. This introduces other great difficulties, however. The background due to competing scattering processes will be severe and therefore causes great experimental troubles. Schiff [3]) has discussed this method using the continuous spectrum from a betatron, but several experiments with this method have given no positive results.

Since the completion of the present investigation a successful measurement of the width of the 15.1 MeV level in C^{12} has been published by E. Hayward and E. G. Fuller [4]), however. They have used the continuous

radiation from a betatron for the excitation of the carbon level. By studying the resonantly scattered radiation and the influence upon this radiation by carbon absorbers in the primary beam, they were able to give the total width of the 15.1 MeV level as well as the partial width for radiation to the ground state.

In the present investigation we have used the continuous X-radiation from the 800 kV van de Graaff-generator of the institute for excitation of the 477 keV level in Li^7. In experiments of this kind the scattered radiation contains besides the weak resonant radiation, an immense background resulting from competing scattering processes. Among these the inelastic Compton radiation can be eliminated by choosing a large scattering angle. Elastically scattered Rayleigh and Thomson radiations are not so intense at light nuclei, since they are proportional to Z^3 and Z^4 respectively.

2. Experimental Arrangement

The experimental arrangement is shown in fig. 1. The focal spot is surrounded by a heavy lead shield with a 2 × 2 cm channel for the primary beam. At the exit hole it was possible to insert a Li-absorber in the beam. The scattered radiation was studied at an angle of 120 degrees by means of a scintillation counter using a 25 mm ⌀ × 25 mm NaI-crystal in connection with an EMI 6260 photomultiplier. At the large scattering angle used the Compton radiation was cut off at 250 keV with the electrostatic generator running at 640 keV. Larger scattering angles could not conveniently be used because the NaI-crystal had to be effectively shielded from direct radiation and an increase of the distance focal spot-lithium sample would decrease the intensity too much.

The scintillation spectrum was recorded by a hundred-channel pulse-height analyzer. In order to prevent pile-up in the linear amplifier the low energy part of the spectrum due to the intense Compton radiation was reduced by a 2 mm lead absorber in front of the NaI-crystal. Nevertheless the counting rate in this part of the spectrum was too high for proper registering in the pulse analyzer. For that reason the low energy part was eliminated by a coincidence method. The pulses from the amplifier were carried via a discriminator to a coincidence stage, which only transmitted pulses higher than the discriminator value. This level corresponded to about 350 keV.

The scintillation spectra were measured with reference to a constant electric charge falling on the target in the accelerating tube.

A scintillation spectrum of the scattered radiation is shown in fig. 2. The small peak due to resonance scattering from the Li-level rises over the background resulting from other scattered radiation. The lower curve

(crosses) relates to a measurement where a 10 mm Li-absorber was placed in the primary beam. In this case the 477 keV energy is decreased in the continuous spectrum, which strongly influences the resonance peak.

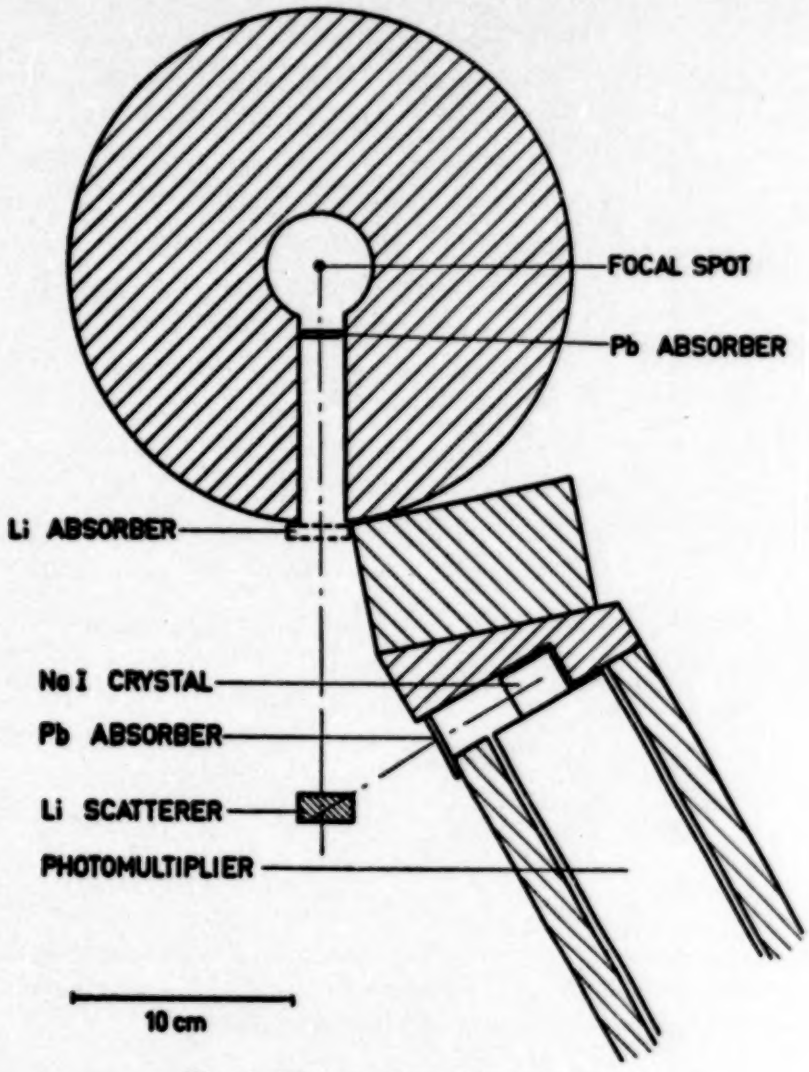

Fig. 1. The experimental arrangement.

The primary beam intensity was measured by the same scintillation counter as was used in the main experiment. Because of the great intensity the counter had to be placed at a distance of 4 metres from the target and supplied with a lead collimator 1.2 mm in diameter (fig. 3). In this way only the central part of the NaI-crystal was used. In the main experiment the whole crystal was utilized, however. As the crystal efficiency is not constant over the whole volume a special investigation had to be made in order to determine the effective solid angle taken up by the whole crystal as seen from the Li-scatterer.

For this purpose a point source (Hf^{181}, 482 keV line) was placed at the position of the Li-scatterer. A collimator limiting the solid angle to 4.16×10^{-3}

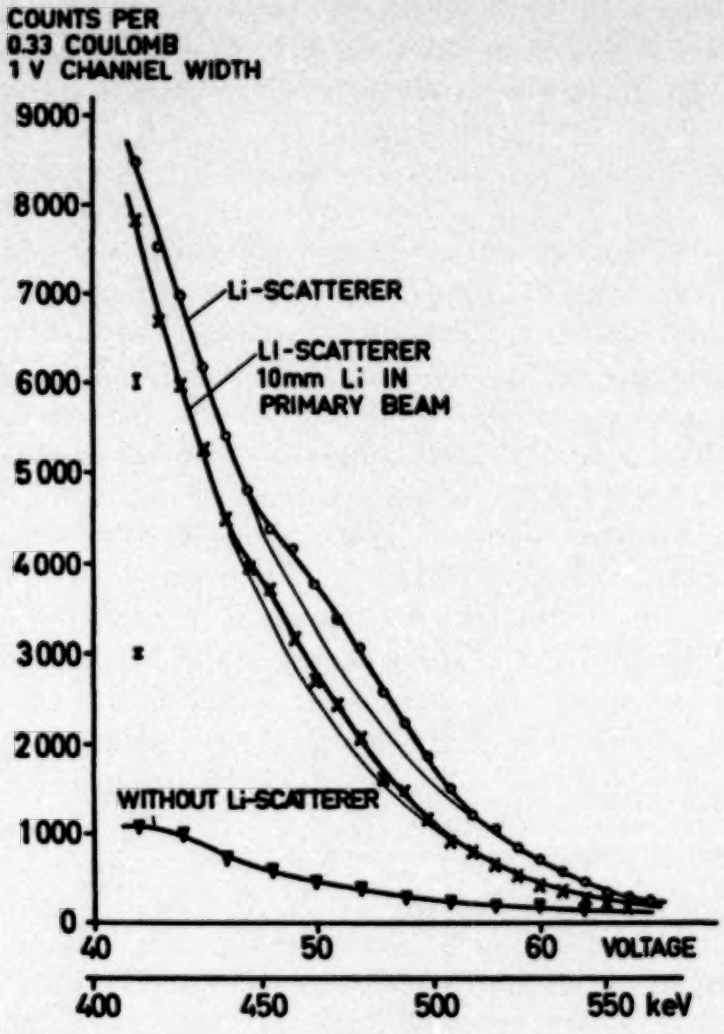

Fig. 2. Scintillation spectrum of the scattered radiation from a Li-sample showing the resonance peak due to nuclear fluorescence. The resonance radiation is decreased when a 10 mm Li absorber is inserted in the primary beam (lower curve, crosses).

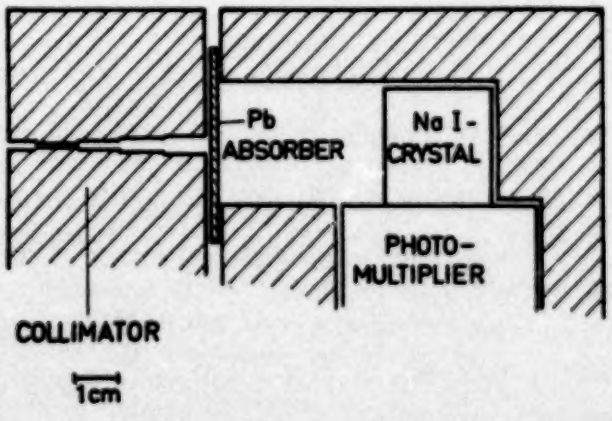

Fig. 3. Experimental arrangement for measurement of the primary beam intensity.

could be put in between source and detector. The 482 keV-line was registered with and without collimator. The intensity of the photopeak in the two cases was 650 and 3980 counts/min resp. The effective solid angle of the NaI-crystal at this energy is therefore $\Omega_{eff} = 2.54 \times 10^{-2}$. The solid angle as calculated from the geometry was 5.16×10^{-2}. As the same scintillation counter and crystal were used both for the primary beam measurements and for the scattering experiments further corrections due to the NaI-crystal efficiency and geometry are superfluous. The primary beam intensity in the 480 keV region at an accelerating voltage of 640 kV was $N_0(E) = 5.19 \times 10^8$ counts/sterad, Coulomb and eV energy-intervals.

3. Calculation of the Resonantly Scattered Radiation

Referring to fig. 4 we first calculate the scattering from an element dx in the Li-sample. The intensity of the beam hitting this element is

$$N_0(E)\Omega' \exp\left[-x(\mu_r+\mu_e)\right]; \tag{1}$$

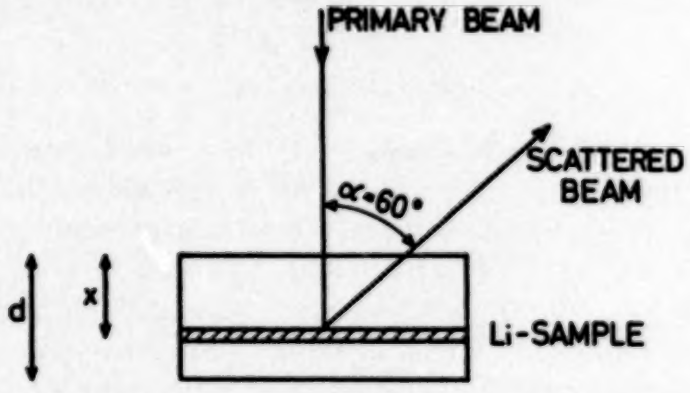

Fig. 4. The geometry of the Li-sample.

$N_0(E)$ is the intensity of the incoming beam, Ω' the solid angle of the sample seen from the target and μ_r, μ_e the absorption coefficients due to nuclear resonance and ordinary electronic absorption, respectively. The element dx emits a fraction $\mu_r dx$ of the radiation. On its way out from the sample the fluorescent radiation suffers electronic absorption only, since it is off resonance by an amount corresponding to the double recoil energy. The radiation registered by the NaI-crystal may be calculated through integration over the whole sample:

$$N_0(E)\Omega' \mu_r \frac{\Omega_{eff}}{4\pi} \int_0^d \exp\left[-x(\mu_r+\mu_e+(\mu_e/\cos\alpha))\right] dx \tag{2}$$

or

$$N_0(E)\,\frac{\Omega'\,\Omega_{eff}}{4\pi}\,\frac{\mu_r}{\mu_r+k\mu_e}\left\{1-\exp\left[-d(\mu_r+k\mu_e)\right]\right\}; \tag{3}$$

Ω_{eff} is the effective solid angle of the NaI-crystal as explained above and k stands for the factor $[1+(1/\cos\alpha)]$. Because of edge effects in the Li-sample the factor k will be somewhat too high, but this has a negligible influence since μ_e in itself is small compared to μ_r.

The fluorescent radiation is assumed to be isotropic, which is justified by the fact that the ground state of Li^7 has spin $J_0 = 3/2^-$ and the 477 keV level spin $J = 1/2^-$ [5]). This corresponds to two successive magnetic dipole transitions $J_0 \to J \to J_0$, showing an isotropic angular distribution.

The absorption coefficient μ_r resulting from the nuclear resonance is highly influenced by the thermal motion of the nuclei in the sample. The pure resonance peak is very sharp with a width of about 10^{-2} eV, but since the recoil energy loss at the excitation is highly dependent on the velocity of the nucleus, the resonance will be broadened and show a resulting width of about 1 eV.

The cross-section for nuclear resonance is determined by the Breit-Wigner expression

$$\sigma = g\frac{\lambda^2}{8\pi}\frac{\Gamma^2}{(E_1-E_0)^2+\frac{1}{4}\Gamma^2}, \tag{4}$$

where g is the ratio between the statistical weights of the excited and ground states ($g = \frac{1}{2}$ in this case). E_0 and E_1 are the resonance energy and available excitation energy, respectively, and Γ the level width.

A gamma-quantum of energy E gives off the energy E_1, where

$$E_1 = E-\tfrac{1}{2}\frac{E^2}{Mc^2}-\frac{u}{c}E; \tag{5}$$

M is the mass of the nucleus and u the thermal velocity of the nucleus in the direction of the incoming quantum. With the Maxwellian distribution of velocity

$$P(u)\mathrm{d}u = \left(\frac{M}{2\pi kT}\right)^{\frac{1}{2}}\cdot\exp\left(-\frac{Mu^2}{2kT}\right)\mathrm{d}u \tag{6}$$

we get for the resulting cross-section

$$\sigma_r = g\frac{\lambda^2}{8\pi}\int_{-\infty}^{+\infty}\frac{P(u)\Gamma^2}{\left(E-E_r-\frac{u}{c}E\right)^2+\frac{1}{4}\Gamma^2}\mathrm{d}u, \tag{7}$$

where E_r stands for $E_0+\frac{1}{2}E^2/Mc^2$. Because of the small width of the resonance level $P(u)$ is a slowly varying function and can be taken as a constant at the integration. We get

$$\sigma_r = g\frac{\lambda^2\Gamma c}{4E}\left(\frac{M}{2\pi kT}\right)^{\frac{1}{2}}\exp\left[-\left(\frac{E-E_r}{\Delta}\right)^2\right]; \tag{8}$$

Δ is the "thermal width" of the resonance:

$$\Delta = \frac{E}{c}\left(\frac{2kT}{M}\right)^{\frac{1}{2}}. \tag{9}$$

The Maxwellian distribution applies to free molecules in a gas. The above discussion is still valid, however, if the binding energy of the atoms in the solid state is taken into consideration. This is accomplished in this case by inserting an effective temperature, which can be calculated from the Debye-temperature of the sample [2, 6]). With the Debye-temperature of Li $\theta = 360°$ K we get the effective temperature $T_{eff} = 350°$ K at the temperature 303° K of the sample. For the thermal width of the resonance curve we get $\Delta = 1.44$ eV, which is great compared to the true resonance width Γ.

Integrating eq. (3) with respect to E gives the total amount of scattered radiation registered by the scintillation counter. The absorption coefficient μ_r corresponds to σ_r [eq. (8)]; the isotopic abundance of Li^7 (92.5 %) must here be taken into account.

The scattered radiation as calculated by integration of eq. (3) is plotted against the level width in fig. 5.

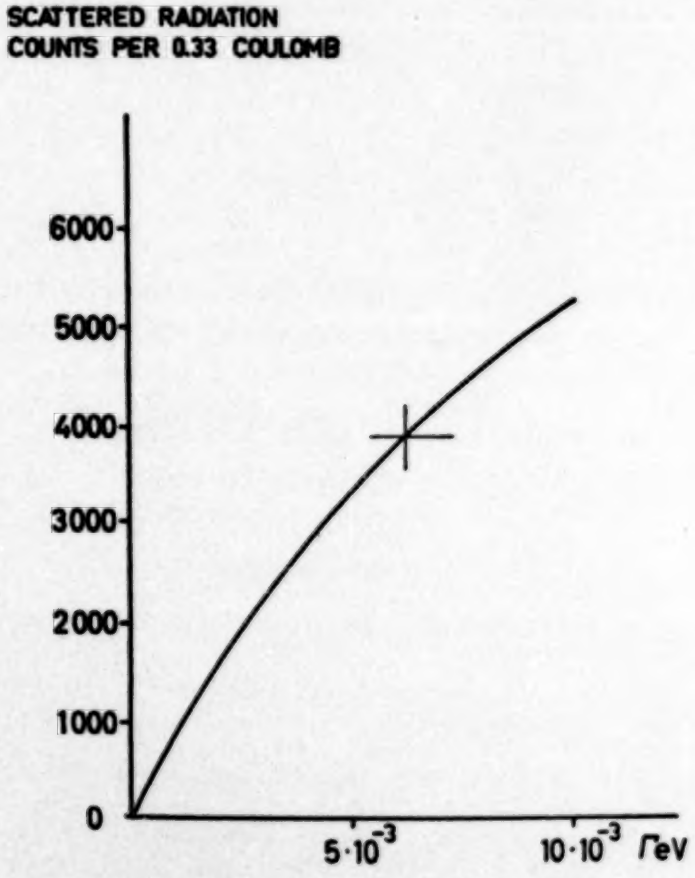

Fig. 5. The scattered intensity as function of the level width as calculated from eq. (3). The experimentally determined intensity is indicated by a cross.

The drawing of the background curve in fig. 2 will highly affect the area below the resonance peak and cause great uncertainty as to the value of Γ. This difficulty was avoided by the absorption experiment, where a 10 mm thick Li-absorber was put in the primary beam. The expression for the scattered radiation must in this case be multiplied by $\exp(-\mu_t d')$, where $d' = 10$ mm.

Obviously the two background curves of fig. 2 must have the same shape. With this criterion we get the proper drawing of the background curve, giving the same value of Γ as determined by the absorption experiment and by the absolute determination of the scattered radiation. The scattered radiation of 3 900 counts per 0.33 Coulomb and the attenuation of 0.59 in the Li-absorber corresponds to a level width of 6.2×10^{-3} eV. From this we obtain for the lifetime $\tau_\gamma = \hbar/\Gamma = (1.1 \pm 0.3) 10^{-13}$ sec.

The width of the 477-keV level has been determined earlier in experiments of other kinds. The reaction B^{10} (n, α) Li^7 leaves the Li-nucleus in the 477-keV level. On account of the short lifetime of the level the gamma-quantum is emitted before the recoiling Li-nucleus is slowed down. This causes a Doppler-broadening of the gamma-line. From measurements of this Doppler-broadening, using various boron compounds in the target, Elliott and Bell [7]) calculated the lifetime $\tau = (0.75 \pm 0.25) \times 10^{-13}$ sec.

Ajzenberg and Lauritsen [5]) give the value $\tau = 1.0 \times 10^{-13}$ sec in their review article on energy levels.

The ground state of Li^7 has the configuration $(\nu 1p_{3/2})^2$ $(\pi 1p_{3/2})$ and the spin $3/2^-$. If the 477-keV level is caused by single particle excitation of the proton to a $p_{\frac{1}{2}}$ level, the lifetime of the M1 transition to the ground state can be calculated by the Weisskopf formula [8]). This gives the value $\tau = 3.0 \times 10^{-13}$ sec in reasonable agreement with the experiments. However, the single particle excitation of the level is doubtful.

The authors are much indebted to Professor Per Ohlin and Professor Kai Siegbahn for their great interest in this work.

References

1) K. Siegbahn, Beta- and Gamma-Ray Spectroscopy (Amsterdam, 1955) K. G. Malmfors p. 521
2) F. Metzger, Phys. Rev. **101** (1956) 286; **103** (1956) 983
3) L. I. Schiff, Phys. Rev. **70** (1946) 761
4) E. Hayward and E. G. Fuller, Phys. Rev. **106** (1957) 991
5) F. Ajzenberg and T. Lauritsen, Revs. Mod. Phys. **27** (1955) 77
6) W. E. Lamb, Phys. Rev. **55** (1939) 190
7) L. G. Elliott and R. E. Bell, Phys. Rev. **76** (1949) 168
8) V. F. Weisskopf, Phys. Rev. **83** (1951) 1073

Nuclear Physics **5** (1958) 603—614; © *North-Holland Publishing Co., Amsterdam*
Not to be reproduced by photoprint or microfilm without written permission from the publisher

THE 2.85 keV NEUTRON RESONANCE OF SODIUM

J. E. LYNN, F. W. K. FIRK and M. C. MOXON
Atomic Energy Research Establishment, Harwell, Didcot, Berks

Received 11 October 1957

Abstract: The measurement of the total neutron cross-section of sodium in the region 600 eV to 15 keV using the Harwell 15 MeV linear electron accelerator is described. Analysis of the results in conjunction with the known values of the low energy elastic and radiative capture cross-sections leads to the following conclusions. The cross-section up to 15 keV may be described in terms of a potential scattering cross-section of 2.4 barn and two s-wave resonances, one at 2.85 ± 0.04 keV neutron energy and the other at negative energy. The 2.85 keV resonance has parameters $\sigma_0 = 370\pm5$ barn, $\Gamma_n = 405\pm12$ eV, $\Gamma_\gamma \leqq 0.34\pm0.01$ eV and spin $J = 1+$. The negative energy resonance has a ratio of reduced width to resonance energy of $\gamma_n^2/E_R = -0.5$ while $|E_R| \gg 1$ keV. The spin of this resonance is $J = 2+$.

1. Introduction

There has been, until recently, a region in the neutron energy range which was inaccessible with good resolution to any technique of neutron cross-section measurement. It extended from about 1 keV neutron energy to about 10 keV. It has been possible recently to examine this energy range with good resolution by improving the performance of time-of-flight spectrometers. Such improved measurements on sodium are described in section 2 of this paper.

The neutron cross-section of sodium is of some interest. Earlier measurements [1]) showed the presence of a large resonance at about 3 keV. There was, however, no sign of an interference minimum in the cross-section below the resonance and this has led to the suggestion [2]) that the potential scattering cross-section in sodium is spin-dependent. An alternative suggestion [3]) is that this resonance is due to p-wave neutrons. In section 3, below, the available low energy cross-section information is analysed and interpreted as being due to two s-wave resonances, one at 2.85 keV and the other at a negative energy.

2. Experimental

A general description of the use of the Harwell 15 MeV linear electron accelerator has been given by Wiblin [4]). The machine delivers pulses of photoneutrons at a rate of 400 pulses per sec and of about 1 μsec duration. In the

transmission measurements reported here the flight path length was 55.7 metres. The neutron detector consisted of a slab of B^{10} element surrounded by sodium iodide scintillation counters [5]). The output pulses from the

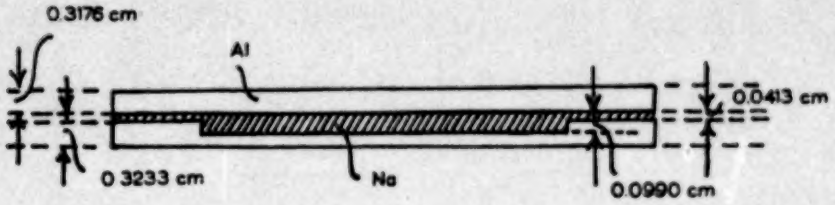

Fig. 1. Section through centre of thin sodium sample ($n = 0.00356 \times 10^{24}$ atoms per cm^3).

detector were fed into a set of 100 timing channels each of 1 μsec duration. The machine output was monitored with $B^{10}F_3$ proportional counters. A boron filter in the beam removed neutrons with flight times greater than the interval between consecutive neutron pulses.

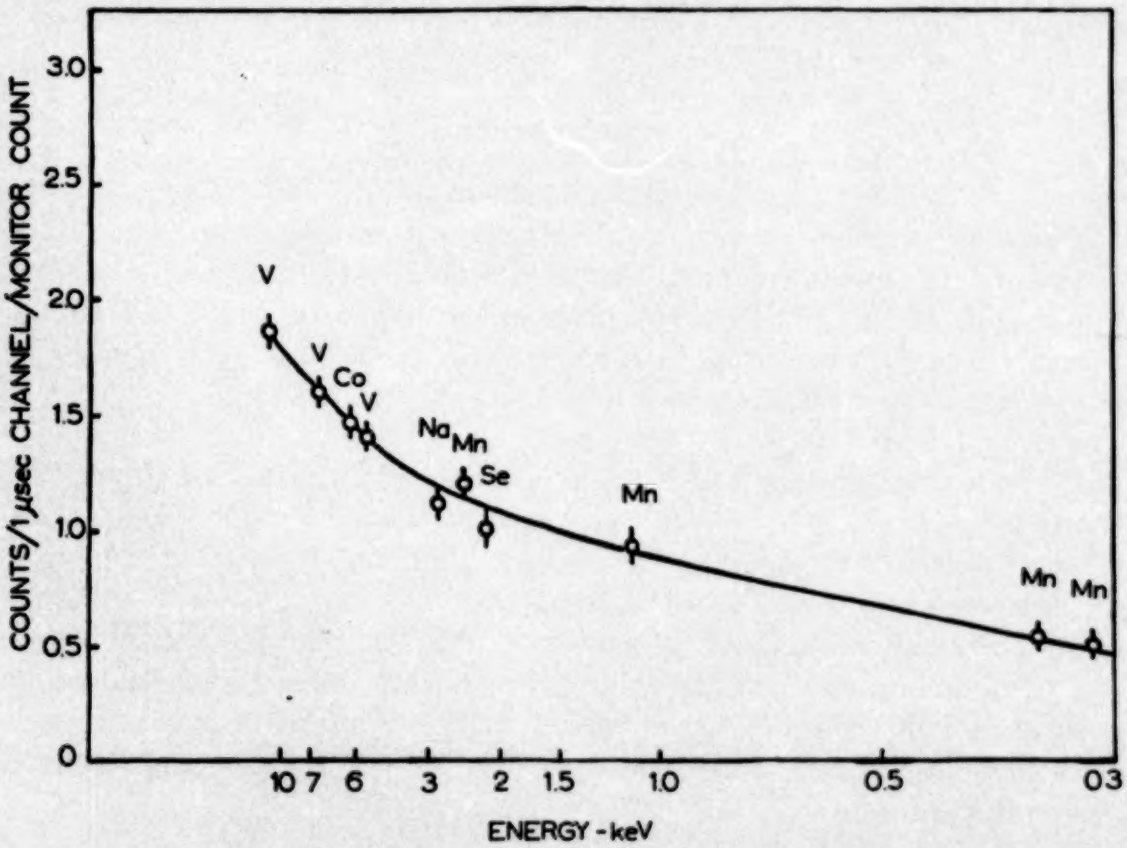

Fig. 2. Machine dependent background, as a function of neutron energy, with 55.7 m flight path. The symbol above each experimental point refers to the element used to measure the background at that energy.

The thicknesses of the three samples of distilled sodium used are given in the caption to fig. 4. A difficult problem was to prepare a thin uniform sample of accurately known thickness (approximately 1 mm). A 200 ton

press was used to clamp distilled sodium between two plane aluminium plates each 15 cm in diameter and having accurately known thicknesses. One of the plates was counterbored to a depth of 0.0990 cm (fig. 1). An X-ray examination of the sample showed no defects in the sodium. This was confirmed on dismantling the sample at the end of the experiment.

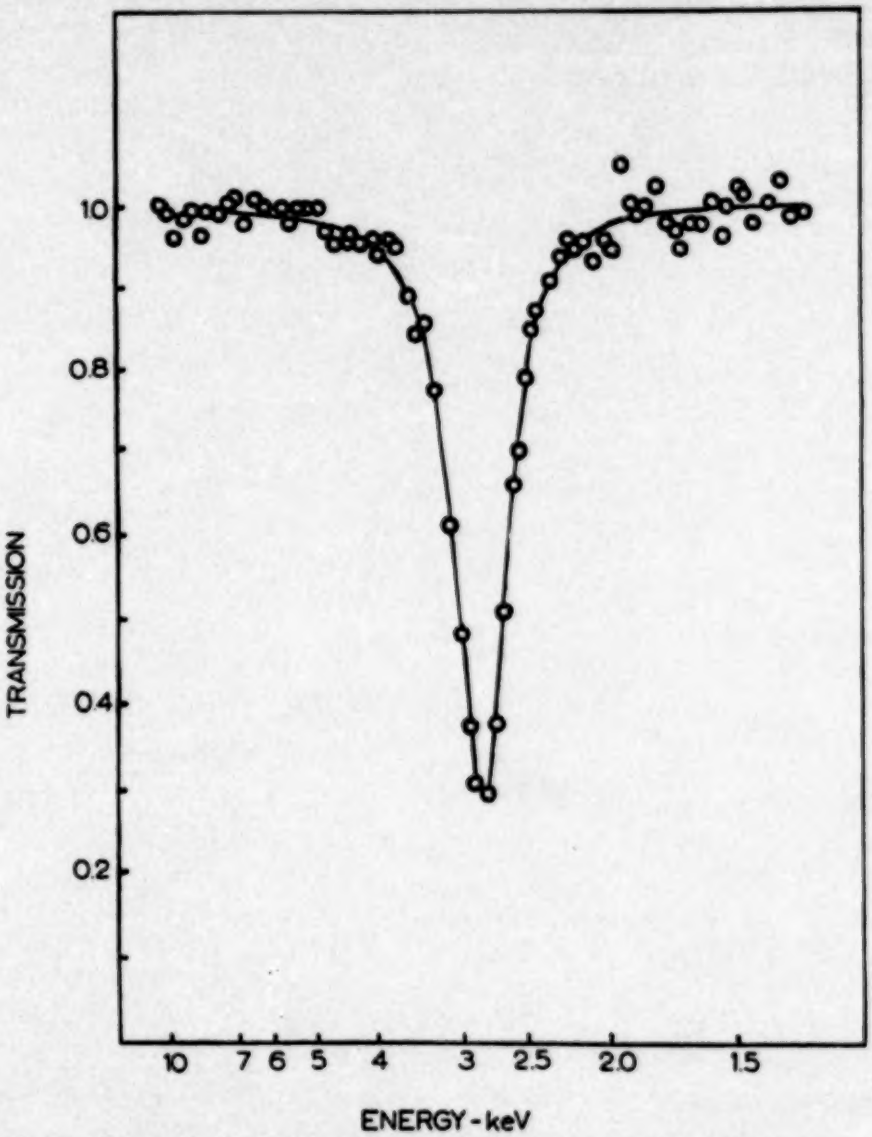

Fig. 3. Transmission of the thin sodium sample ($n = 0.00356 \times 10^{24}$ atoms per cm^2).

Two kinds of background were present in these measurements. The first was not correlated with the pulse repetition frequency of the machine; the other was due to the machine itself and was a function of the time delay following the neutron burst.

The uncorrelated background was measured by means of a timing channel of 100 μsec duration which opened 2 300 μsec after the appearance of the burst of neutrons at the machine target.

The machine-dependent background was determined by placing, in the beam, samples whose cross-sections contained strong resonances. The thickness of each sample was such that more than 3 of the 1 μsec timing channels registered zero transmission at the resonance energy. After the uncorrelated background rate was subtracted from the counting rate in these channels the remainder was the machine-dependent background rate at the time-of-flight corresponding to the resonance energy. The machine-dependent background rate as a function of time delay is shown in fig. 2.

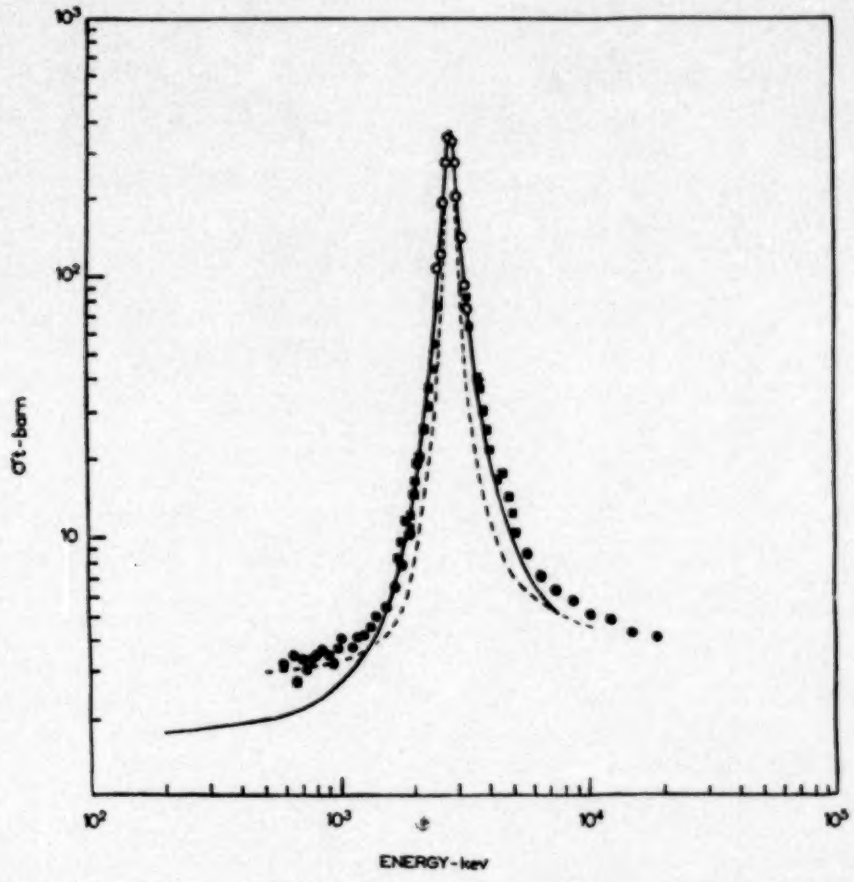

Fig. 4. The neutron cross-section of sodium from 600 eV to 15 keV.

- o Measurements made with a sample containing 0.00356×10^{24} atoms per cm^2.
- ■ Measurements made with a sample containing 0.0329×10^{24} atoms per cm^2.
- ● Measurements made with a sample containing 0.243×10^{24} atoms per cm^2.

The full curve is a single-level Breit-Wigner formula for the cross-section computed using the parameters $E_R = 2.85$ keV, $\sigma_0 = 370$, barn, $\Gamma = 405$ eV, $\sigma_p = 2.75$ barn. The dashed curve assumes $l = 1$, $J = 1$, $\Sigma_j \gamma^2{}_{nj} = .100$ MeV, $\sigma_p = 3$ barn.

Fig. 3 shows the transmission of the thinnest sodium sample ($n = 0.00356 \times 10^{24}$ atoms per cm^2) near the resonance. Fig. 4 shows the observed cross-section of sodium in the energy range 600 eV to 15 keV.

3. Analysis of the Cross-Section Data

3.1. ANALYSIS OF RESONANCE SHAPE

The observed transmission, T_{obs}, in the region of a resonance is not, in general, the true transmission of monochromatic neutrons at that energy but is given by

$$T_{obs}(E) = \int_0^\infty f(E'-E)T(E')\mathrm{d}E',$$

where $f(E'-E)$ is the resolution function [6]) at the nominal energy E. The observed cross-section, σ_{obs}, as given by the formula

$$\sigma_{obs} = -\frac{1}{n}\ln T_{obs}, \tag{1}$$

(where n is the number of atoms per cm^2 of the sample), is, therefore, not in general the true cross-section.

If the resolution function is Gaussian in form,

$$f(E'-E) = \frac{1}{R}\sqrt{\frac{2}{\pi}}\exp\left\{-\tfrac{1}{2}\left(\frac{E'-E}{\frac{1}{2}R}\right)^2\right\},$$

the observed transmission at the resonance energy is [6])

$$T_{obs}(E_R) = T(E_R)\left\{1+n\sigma_0\phi^2+\tfrac{3}{2}n\sigma_0(n\sigma_0-2)\phi^4+\ldots\right\}. \tag{2}$$

In equation (2) $\phi = R/\Gamma''$, Γ'' is the full natural width of the resonance at $\frac{1}{2}\sigma_0$ and σ_0 is the peak cross-section of the resonance. Eq. (2) holds if the Doppler broadening of the resonance due to the thermal motion of the atoms [7, 8]) is small compared with the natural width, Γ''. This holds for the 2.85 keV resonance in the sodium cross-section.

Let Γ_{obs} be the full width at half maximum of the resonance in the observed cross-section curve, then [6])

$$\frac{\Gamma_{obs}}{\Gamma''} = 1+\left(\frac{6-n\sigma_0}{4}\right)\phi^2\mp\ldots, \tag{3}$$

provided that $\phi < 0.2$ and $n\sigma_0 < 1$, approximately.

If R is known, equations (2) and (3) give corrections to apply to the observed resonance transmission $T_{obs}(E_R)$ and true width Γ''. The correction terms are evaluated by successive approximations.

Using $R = 61$ eV at 2.85 keV (see appendix), $E_R = 2.85$ keV, $\Gamma_{obs} = 440\pm20$ eV, $T_{obs}(E_R) = 0.294\pm0.012$ and $(n\sigma_0)_{obs} = 1.22\pm0.04$ we obtain, with the help of equations (2) and (3), $\Gamma'' = 430\pm20$ eV and $\sigma_0 = 350\pm12$ barn.

It may be seen from the transmission curve (fig. 1) that the lowest experimental values of the transmission must be somewhat greater than the transmission at the resonance energy; thus the result for σ_0 given above

will be low. To allow for this the mean of the transmission of the two lowest points is taken. This is the transmission at resonance as seen with a resolution function corresponding to a 2 μsec timing channel. This resolution function is approximately a triangle of full width at half maximum ot 150 eV. An equation analogous to (2) for a triangular resolution function has also been given [6]). This leads to $\sigma_0 = 360 \pm 12$ barn, $\Gamma' = 420 \pm 20$ eV.

3.2. THE RESONANCE SPIN

The peak cross-section, σ_0, of a resonance of spin, J, is

$$\sigma_0 = \frac{2J+1}{2(2I+1)} \cdot 4\pi\lambda^2 \frac{\Gamma_n}{\Gamma}, \qquad (4)$$

where I is the spin of the target nucleus ($I = 3/2$ for Na^{23}) Γ is the total width and Γ_n is the neutron width of the resonance. Hibden *et al.* [1]) showed from resonance integral measurements that $\Gamma_n/\Gamma > 0.99$. From this and the value ot the resonance energy (laboratory energy $E_R = 2.85 \pm 0.04$ keV) eq. (4) gives the possibilities in table 1. This shows clearly, from the measured value of σ_0, that this resonance has a total spin $J = 1$. This differs from the result of Hibden *et al.* [1]) who found $J = 2$.

TABLE 1

Possible spins, J, and peak cross-sections, σ_0, of the 2.85 keV resonance in the neutron cross-section of Na^{23}

Orbital angular momentum l of incoming neutron wave	Total spin J of compound nucleus	σ_0 (barn)
0	1	372 ± 5
	2	620 ± 8
1	0	124 ± 2
	1	372 ± 5
	2	620 ± 8
	3	866 ± 12

Using $J = 1$ a more accurate value of σ_0 is obtained from the resonance energy

$$\sigma_0 = 372 \pm 5 \text{ barn}$$

where the error is derived from the uncertainty in the resonance energy.

3.3 THE RESONANCE WIDTH FROM AREA ANALYSIS

The area, A_E, of the transmission dip of the sample containing $n = 0.00356 \times 10^{24}$ atoms per cm^2 was determined in the usual manner [9]) and is $A_E = 0.623$ keV. From curves of $A_E/(\Gamma' \sqrt{\pi})$ as a function of $n\sigma_0$ [10]), and using $\sigma_0 = 372$ barn,

$$\Gamma' = 405 \pm 12 \text{ eV},$$

in agreement with the more direct measurement of the width.

3.4. ANGULAR MOMENTUM OF RESONANCE NEUTRONS

From the natural width Γ' of a pure elastic scattering resonance the reduced neutron width may be obtained provided that the angular momentum l, of the resonance neutrons is known. Conversely, the values of the reduced widths obtained using different hypotheses about l may be used to limit the possible values of l, for the reduced neutron width should not exceed the Wigner single-particle limit which, for sodium, is of the order of a few MeV.

The resonance term of the single-level Breit-Wigner formula is (for pure elastic scattering)

$$\sigma(E) = \pi\lambda^2 \frac{(2J+1)}{2(2I+1)} \frac{\Gamma_n^2}{(E_R+\Delta-E)^2+(\frac{1}{2}\Gamma_n)^2}. \tag{5}$$

The neutron width, Γ_n, of an l-wave resonance is defined in terms of the sum of the reduced neutron widths for the two contributing channel spins, $\sum_j \gamma_{nj}^2$ by

$$\Gamma_n = \frac{2P_l}{|1-(S_l+iP_l)R^\infty|^2} \cdot \sum_j \gamma_{nj}^2$$

where P_l is the penetration for l-wave neutrons, S_l is the shift factor for l-wave neutrons and R^∞ is the residual effect of far-away levels (see, for example, Thomas [11]) or Lane and Thomas [12]) for the mathematical formulation of these quantities). The level shift Δ is defined as

$$\Delta = \frac{-S_l+R^\infty(S_l^2+P_l^2)}{|1-(S_l+iP_l)R^\infty|^2} \sum_j \gamma_{nj}^2.$$

It may be shown from (5) and the definitions of Γ_n and Δ that

$$\sum_j \gamma_{nj}^2 = \frac{\Gamma'}{\left(2P_l-\Gamma' \cdot \frac{dS_l}{dE}\right)(1+2S_l R^\infty)}, \tag{6}$$

$|R^\infty|$ is expected to be of the order of unity for p-waves and $S_l \ll 1$ at 3 keV neutron energy. Consequently the effect of other levels may be ignored in using (6). On substituting the relevant values for p-waves in (6) the result is that $\sum_j \gamma_{nj}^2$ is negative. This is impossible since the reduced width amplitudes are real quantities. It thus appears difficult to accept the suggestion of Stelson and Preston [3]) and Toller, Newson and Merzbacher [13]) that this may be a p-wave resonance.

The dashed curve in fig. 4 has been calculated from (5) using the quantities $l = 1$, $J = 1$, $E_R = 223.6$ keV, $\sum_j \gamma_{nj}^2 = 100$ MeV (this is about 25 times greater than the Wigner upper limit on reduced neutron widths) plus a potential scattering term of 3 barn. There is a marked discrepancy between the calculated curve and the experimental points even using this im-

plausibly high value for the reduced widths. It is concluded that the 2.85 keV resonance is an s-wave resonance.

3.5. POTENTIAL SCATTERING CROSS SECTION

Halpern and Johnson [14]) have shown that the coherent scattering cross section σ_{cs} and the total scattering cross section σ_s at very low energies may be expressed in terms of the nuclear scattering lengths a_+ and a_- for the two spin orientations of (s-wave) neutron and target nucleus by

$$\sigma_s = 4\pi\left(\frac{A+1}{A}\right)^2 (g_+ a_+^2 + g_- a_-^2), \tag{7}$$

$$\sigma_{cs} = 4\pi\left(\frac{A+1}{A}\right)^2 (g_+ a_+ + g_- a_-)^2, \tag{8}$$

where g_+ and g_- are the spin weighting factors (5/8 and 3/8 for Na^{23}). On substituting the values $\sigma_s = 3.5$ barn, $\sigma_{cs} = 1.5$ barn (Shull and Wollan [15])) into (7) and (8) the following four pairs of values (in units of 10^{-13} cm) are obtained:

$$\begin{aligned} a_+ &= \pm 6.36, \quad a_- = \mp 1.63, \\ a_+ &= \pm 0.34, \quad a_- = \pm 8.25. \end{aligned} \tag{9}$$

For a given spin orientation the single-level Breit-Wigner formula for s-waves is

$$\sigma_s = \pi\lambda^2 g \left| \frac{i\Gamma_n}{E - E_R + i\frac{1}{2}\Gamma} + 2ikR' \right|^2. \tag{10}$$

The quantity within the modulus signs multiplied by $\frac{1}{2}\lambda$ is the scattering length a, while R' determines the potential scattering cross section $4\pi R'^2$. At very low energy where $E \approx 0$, and provided that $E_R \gg \frac{1}{2}\Gamma$, a may be approximated by

$$a \approx R' - \frac{\Gamma_n}{2kE_R}. \tag{11}$$

A theoretical prediction of the value of R' is obtained from the complex potential model [16]). Using the parameters of the complex square well deduced from the neutron total cross sections of many elements [16]) it is calculated that $R' = 4.4 \times 10^{-13}$ cm. An experimental confirmation of this value is derived from (9) and (11) and the measured parameters of the 2.85 keV resonance: $J = 1$ and $\Gamma_n = \Gamma' = 405$ eV. The only pair of values in (9) which gives the correct order of magnitude of R' is $a_+ = 6.36 \times 10^{-13}$ cm and $a_- = -1.63 \times 10^{-13}$ cm, from which $R' = 4.4 \times 10^{-13}$ cm †.

The potential scattering cross section is thus 2.4 barn. The very reasonable

† Since no error in σ_{cs} is quoted by Shull and Wollan [15]) it is not possible to attach an error to R'. The uncertainties in the resonance parameters presented here alone give rise to approximately 5 % error in R'.

nature of this result is further evidence of the correctness of the view that the resonance is s-wave.

3.6. PROPERTIES OF A POSSIBLE NEGATIVE ENERGY LEVEL

Equation (10) has been computed using the parameters determined for the 2.85 keV resonance together with a contribution $4\pi g_+ R'^2$ to take into account the potential scattering cross-section from the other spin orientation. This computation is the full curve of fig. 4. The discrepancy of about one barn between the computed and experimental cross-sections is not unexpected since $a_+ = 6.36\times10^{-13}$ cm and not R' as the computed curve implies.

If the reduced width of the presumed $J = 2$ resonance which contributes to a_+, is $(\gamma_n^2)'$, and its resonance energy, E'_R, then, using $a_+ = 6.36\times10^{-13}$ cm and $R' + 4.4\times10^{-13}$ cm,

$$(\gamma_n^2)'/E'_R = -0.5;$$

E'_R must, therefore, be negative. From the observed persistence of the discrepancy in the computed and experimental cross-section curves at energies about 10 keV it is deduced that $|E'_R| \gg 1$ keV.

3.8. UPPER LIMIT TO THE RADIATIVE CAPTURE WIDTH

If $E_R \gg \Gamma$ the absorption cross-section, σ_γ, at very low energy, E, is easily deduced from the single-level Breit-Wigner formula to be

$$\sigma_\gamma = \frac{\sigma_0 \Gamma\Gamma_\gamma}{4E_R^{3/2}} \cdot \frac{1}{\sqrt{E}} \qquad (12)$$

(providing that only one resonance contributes appreciably). The value of σ_γ at 0.025 eV is 0.536 ± 0.006 barn [17]). If this value is substituted in (12) together with the resonance parameters of the 2.85 keV resonance it is found that

$$\Gamma_\gamma = 0.34\pm0.01 \text{ eV}.$$

Since some contribution to σ_γ is expected from the negative energy level this value of Γ_γ must be regarded as an upper estimate although probably a close one.

We are grateful to Dr. E. Bretscher, Dr. B. B. Kinsey, Dr. E. R. Rae and Mr. E. R. Wiblin for their interest in the work and advice on the manuscript. We also wish to acknowledge discussions with Dr. A. M. Lane concerning the parity of this resonance and the assistance of Mr. G. W. Horsley in the preparation of the thin sodium sample.

Appendix

THE RESOLUTION FUNCTION

The factors affecting the shape of the resolution function are a) the shape of the neutron pulse, in time, as it leaves the machine target, b) the fluctuations in time ("jitter") of the neutron pulse, measured with respect

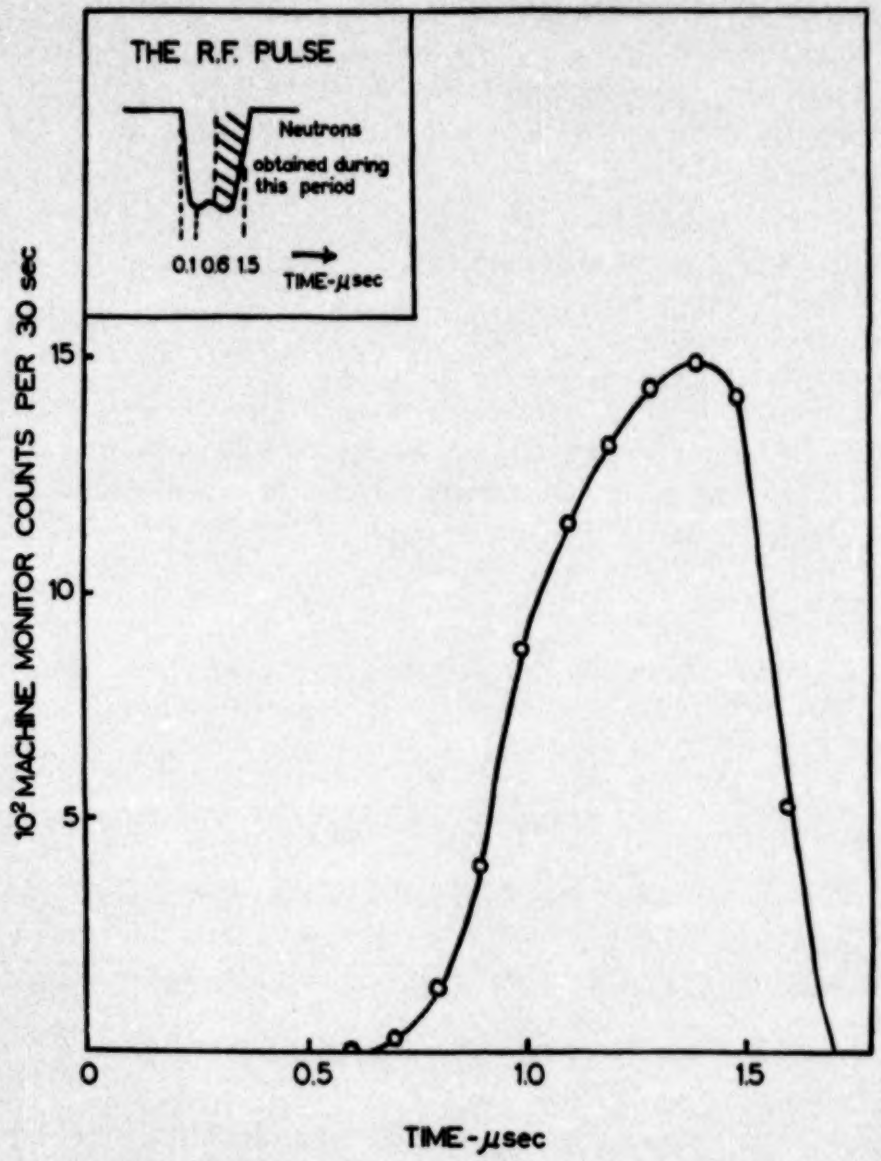

Fig. 5. The neutron pulse shape from the 15 MeV linear accelerator. The inset shows the shape of the RF pulse and the period during which neutrons are produced.

to the marker pulses which open the neutron timing channel, c) spread in detector response time, d) the duration of the neutron timing channels.

The shape of the neutron pulse was measured by substituting for the normal injection electron pulses (nearly 2 μsec in duration) an injection pulse of 0.25 μsec duration, produced from a separate modulator. This

pulse could be "scanned" through the RF pulse when the machine was running in a steady condition and the neutron output in a given time interval was obtained as a function of the time delay with respect to a marker pulse.

Measurements of jitter have been described elsewhere [18]). The shape of the neutron pulse after modification by jitter is shown in fig. 5. Spread in

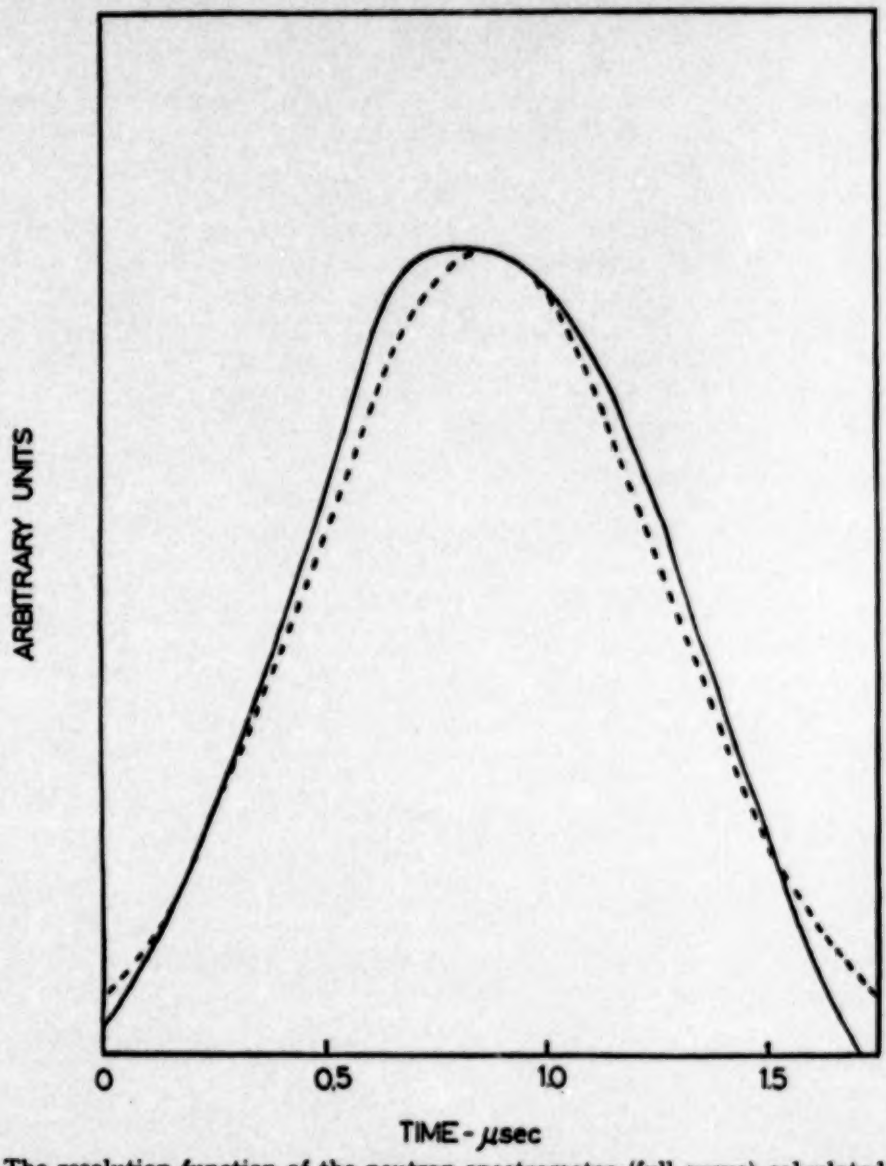

Fig. 6. The resolution function of the neutron spectrometer (full curve) calculated from the shape of the neutron pulse (fig. 5) when observed with 1 μsec timing channels. The dashed curve is a Gaussian function of full width 0.8 μsec at $1/\sqrt{e}$ of maximum which was used as an approximation to the resolution function in the analysis.

detector response time was calculated to be very small. The timing channels were of 1 μsec duration. The resolution function calculated from these factors is shown in fig. 6 as a full curve. The dashed curve is a Gaussian function of full width, R, at $1/\sqrt{e}$ of maximum, given by $R = 0.8$ μsec. At an energy of 2 850 eV this corresponds to 61 eV.

References

1) C. T. Hibdon, C. O. Muehlhause, W. Selove and W. Woolf, Phys. Rev. **77** (1950) 730
2) W. Selove, Phys. Rev. **80** (1950) 290
3) P. H. Stelson and W. M. Preston, Phys. Rev. **88** (1952) 1354
4) E. R. Wiblin, Proceedings of the International Conference on the Peaceful Uses of Atomic Energy **4** (United Nations, New York, 1956) 35
5) E. R. Rae and E. M. Bowey, Proc. Phys. Soc. A **56** (1953) 1073
6) J. E. Lynn and E. R. Rae, J. Nuclear Energy **4** (1957) 418
7) H. A. Bethe, Revs. Mod. Phys. **9** (1937) 140
8) W. E. Lamb, Phys. Rev. **55** (1939) 190
9) E. Melkonian, W. W. Havens, Jr. and L. J. Rainwater, Phys. Rev. **92** (1953) 702
10) F. G. P. Seidl, D. J. Hughes, H. Palevsky, J. S. Levin, W. Y. Kato and N. G. Sjostrand, Phys. Rev. **95** (1954) 476
11) R. G. Thomas, Phys. Rev. **97** (1955) 224
12) A. M. Lane and R. G. Thomas, Revs. Mod. Phys. (in press)
13) A. L. Toller, H. W. Newson and E. Merzbacher, Phys. Rev. **99** (1955) 1625(A)
14) O. Halpern and M. H. Johnson, Phys. Rev. **55** (1939) 898
15) C. G. Shull and E. O. Wollan, Phys. Rev. **81** (1951) 527
16) H. Feshbach, C. E. Porter and V. F. Weisskopf, Phys. Rev. **96** (1954) 448
17) S. J. Cocking and J. F. Raffle, J. Nuclear Energy **3** (1956) 70
18) F. W. K. Firk, A.E.R.E. Report NP/R 2043 (1956)

Nuclear Physics **5** (1958) 615—616; © *North-Holland Publishing Co., Amsterdam*
Not to be reproduced by photoprint or microfilm without written permission from the publisher

NOTE ON COULOMB WAVE FUNCTIONS

A. S. MELIGY
Faculty of Science, University of Alexandria, Egypt

Received 3 October 1957

In a previous paper on Coulomb wave functions [1]) the expansions (19) and (21) of the radial wave functions $J_{k,\,m}(\zeta)$ and $Y_{k,\,m}(\zeta)$ were reported. This note aims at making those expansions more useful in quantitative problems of nuclear collisions with positively charged particles by specifying the normalizing factors of these functions and relating them to the standard notations.

The regular and irregular Coulomb wave functions F and G are usually [2]) normalized so that when $\zeta \to \infty$, $F \sim \sin\theta$ and $G \sim \cos\theta$, where

$$\theta = \tfrac{1}{2}\zeta - \frac{\pi}{2}(m-\tfrac{1}{2}) - k\log\zeta + \arg\,\Gamma(\tfrac{1}{2}+m+ik).$$

The asymptotic forms, for large ζ, of the functions $J_{k,\,m}(\zeta)$ and $Y_{k,\,m}(\zeta)$ may be brought out by using Whittaker's function [3]) $W_{k,\,m}(z)$. In terms of this function one can find the following expressions:

$$J_{k,\,m}(\zeta) = \frac{e^{\frac{1}{2}i\pi(m+\frac{1}{2})+\pi k}}{\Gamma(\frac{1}{2}+m+ik)} W_{ik,\,m}(i\zeta) + \frac{e^{-\frac{1}{2}i\pi(m+\frac{1}{2})+\pi k}}{\Gamma(\frac{1}{2}+m-ik)} W_{-ik,\,m}(-i\zeta),$$

$$Y_{k,\,m}(\zeta) = -\frac{1}{2\pi}\Gamma(\tfrac{1}{2}+m-ik)\, e^{\frac{1}{2}i\pi(m-\frac{1}{2})} W_{ik,\,m}(i\zeta)$$

$$-\frac{1}{2\pi}\Gamma(\tfrac{1}{2}+m+ik) e^{-\frac{1}{2}i\pi(m-\frac{1}{2})} W_{-ik,\,m}(-i\zeta).$$

As $\zeta \to \infty$,

$$W_{ik,\,m}(i\zeta) \sim (i\zeta)^{ik} \exp(-\tfrac{1}{2}i\zeta),$$

and hence

$$J_{k,\,m}(\zeta) \sim 2|\Gamma(\tfrac{1}{2}+m+ik)|^{-1} e^{\frac{1}{2}\pi k} \sin\theta,$$

$$Y_{k,\,m}(\zeta) \sim -\frac{1}{\pi}|\Gamma(\tfrac{1}{2}+m+ik)| e^{-\frac{1}{2}\pi k} \cos\theta.$$

It follows that the normalizing factors of the functions $J_{k,\,m}(\zeta)$ and $Y_{k,\,m}(\zeta)$ are

$\frac{1}{2}|\Gamma(\frac{1}{2}+m+ik)|e^{-\frac{1}{2}\pi k}$ and $-\pi|\Gamma(\frac{1}{2}+m+ik)|^{-1}\, e^{\frac{1}{2}\pi k}$

respectively.

The normalized Coulomb wave functions may be written in accordance with the standard notations [4]) as follows:

$$F_L(\eta,\ \varrho) = \tfrac{1}{2}A_L(\eta)J_{\eta,\,L+\frac{1}{2}}(2\varrho),$$

$$G_L(\eta,\ \varrho) = -\frac{\pi}{A_L(\eta)}Y_{\eta,\,L+\frac{1}{2}}(2\varrho),$$

where

$$A_L(\eta) = |\Gamma(L+1+i\eta)|e^{-\frac{1}{2}\pi\eta}$$

$$= \left\{(1^2+\eta^2)(2^2+\eta^2)(3^2+\eta^2)\ldots(L^2+\eta^2)\frac{2\pi\eta}{e^{2\pi\eta}-1}\right\}^{\frac{1}{2}}.$$

The parameters η, ϱ and L are related to k, ζ and m, respectively, by the equations

$$\eta = k,\ \varrho = \zeta/2 \text{ and } L = m-\tfrac{1}{2}.$$

References

1) A. S. Meligy, Nuclear Physics **1** (1956) 610
2) Yost, Wheeler and Breit, Phys. Rev. **49** (1936) 174
3) Whittaker and Watson, Modern Analysis (Cambridge University Press, 1927)
4) M. Abramowitz, Tables of Coulomb Wave Functions, N. B. S. Applied Mathematics Series No. 17 (U. S. Government Printing Office, Washington, D. C., 1952)

Nuclear Physics **5** (1958) 617—646; © *North-Holland Publishing Co., Amsterdam*
Not to be reproduced by photoprint or microfilm without written permission from the publisher

ON ANOMALOUS CONVERSION COEFFICIENTS OF DIPOLE TRANSITIONS

SVEN GÖSTA NILSSON † and JOHN O. RASMUSSEN

Radiation Laboratory and Department of Chemistry, University of California, Berkeley, California ††

Received 12 September 1957

Abstract: General aspects of the problem of anomalous nuclear-structure-dependent contributions to the internal-conversion process are considered in conjunction with highly retarded electric or magnetic dipole transitions. Formulas for an elementary theory of anomalous internal conversion for E1 transitions are given. Selection rules for the relevant nuclear matrix elements are given in the quantum numbers appropriate to spheroidally deformed nuclei (K, N, n_z, Λ, Σ). Similar selection rules for M1 transitions are given on the basis of the anomalous operators previously derived by Church and Weneser.

The experimental data on dipole conversion coefficients of retarded transitions for odd-mass spheroidal nuclei are surveyed. It is noted that where retardation is ascribable to K-forbiddenness (up to retardation from the single-proton rate by a factor of 10^9) no detectable anomalies are found, but where transitions are allowed by K-selection rules detectable conversion-coefficient anomalies may generally be found at retardations greater than 10^5 to 10^6 and are not found at lesser retardation. There are some exceptions to this general rule, though. From the present meager data the utility of selection rules in the asymptotic quantum numbers, N, n_z, Λ and Σ, for anomalous-conversion matrix elements may be open to question, although their utility in qualitatively explaining retardation of the radiative transitions is very evident.

The simple E1 theory is applied in an attempt to explain quantitatively the very anomalous 85-keV transition in Pa^{231}. Values of the two parameters in the simple theoretical expressions can be found to explain all three L- subshell conversion coefficients. The magnitude of one parameter, the nuclear matrix element $\langle r^3 Y_1 \rangle$, is consistent with estimates from the single-particle model. However, the magnitude required of the other parameter is such as to suggest that in the intranuclear process terms of higher order in the electromagnetic field than treated here may be of importance.

1. Introduction

The internal conversion process whereby a bound orbital electron is ejected during a nuclear electromagnetic transition generally occurs in parallel with photon emission. The ratio of conversion-electron ejection to photon emission is defined as the conversion coefficient, α, with α_K, α_{L_I}, etc., referring to conversion of K, L_I, or other electrons alone. Comparison of experimental absolute conversion coefficients or relative conversion

† On leave from University of Lund, Lund, Sweden.

†† This work was done under the auspices of the U. S. Atomic Energy Commission.

coefficients (K/L ratios, L- or M-subshell ratios) with theoretical values constitutes the most generally useful means of determining gamma-transition gamma-transition multipolarities.

The overwhelming contribution to the normal internal-conversion process comes from regions outside the nuclear volume. The original calculations by Rose *et al.* [1]) assuming a point nucleus represent therefore a good approximation in most cases, as the probability of the electrons penetrating the nucleus is small even for the heaviest nuclei. However, later calculations, by Sliv and Band [2]), show some conversion coefficients (particularly M1) to be quite seriously affected when, instead of the point-nucleus model, they assume a nucleus of finite size but with all nuclear currents restricted to the surface. This correction is essentially a correction corresponding to improved electron wave functions. The intranuclear effects of the electron penetrating the nucleus are accounted for only in an average way by the model of Sliv *et al.* [2]) restricting the currents to the surface of the nucleus. The correction introduced by Sliv is, however, of real importance, and recent experimental evidence on M1 conversion coefficients agrees better with the latter theoretical values [3]).

Church and Weneser [4]) have further suggested that anomalous, model-dependent conversion coefficients may occur for retarded M1 transitions if one takes into account the distribution of currents throughout the nuclear volume. They have considered contributions to the internal conversion arising from integrals over the electron density within the nuclear volume, and they have shown that terms of this intranuclear contribution may obey certain selection rules in various approximate nuclear quantum numbers, which selection rules may be different or less restrictive than the selection rules governing both photon emission and the ordinary (electron outside the nucleus) internal-conversion contributions. Thus, if a transition is forbidden by the ordinary selection rules and correspondingly is highly retarded but an intranuclear contribution to internal conversion is allowed, the conversion coefficient may be anomalous. There is an experimental case of an anomalous M1 conversion coefficient in Ta^{181}, which we shall refer to later.

It has been known for some time that L-subshell conversion ratios for the 60-keV transition to ground in Np^{237} were not in agreement with theoretical values [5]). More recently, evidence has been collected for other E1 transitions in the heavy region (cf. Asaro, Stephens, Hollander and Perlman [6]). Some transitions exhibit $L_{I,\,II,\,III}$ conversion coefficients in agreement with the theoretical values of Rose, while others (notably the 85-keV transition to ground in Pa^{231}) exhibit anomalously large L_I and L_{II} conversion coefficients. Many of the low-energy E1 transitions of odd-A spheroidal nuclei have rates measurable by fast coincidence techniques

($\tau \gtrsim 10^{-9}$ sec), and are thus greatly retarded from single-proton lifetime formula estimates.

Comparing transitions of the same multipole order, one may expect anomalous contributions to the internal conversion to be competitive for initial and final states that both correspond to j-values as low as possible, since a smaller j-value in general implies a larger amplitude of the electron wave function inside the nucleus. The same rule that applies to the j-values in general also applies to the radial quantum numbers of the electron wave function.

Table 1 lists the continuum states available for internal conversion from various bound states for different multipolarities.

TABLE 1

Allowed continuum states for internal conversion

Bound state \ Multipolarity	E1	M1	E2	M2
$s_{1/2}$	$p_{1/2}$, $p_{3/2}$	$s_{1/2}$, $d_{3/2}$	$d_{3/2}$, $d_{5/2}$	$p_{3/2}$, $f_{5/2}$
$p_{1/2}$	$s_{1/2}$, $d_{3/2}$	$p_{1/2}$, $p_{3/2}$	$p_{3/2}$, $f_{5/2}$	$d_{3/2}$, $d_{5/2}$
$p_{3/2}$	$s_{1/2}$, $d_{3/2}$, $d_{5/2}$	$p_{1/2}$, $p_{3/2}$, $f_{5/2}$	$p_{1/2}$, $p_{3/2}$, $f_{5/2}$, $f_{7/2}$	$s_{1/2}$, $d_{3/2}$, $d_{5/2}$, $g_{7/2}$

The combinations in which anomalous intranuclear terms might have the best chance of being significant for dipole transitions are those with $j_1 = j_f = \frac{1}{2}$, namely, E1 and M1 conversion of $s_{\frac{1}{2}}(K, L_I)$ and $p_{\frac{1}{2}}(L_{II})$ electrons †.

In the following sections we give an elementary theory of the anomalous electric dipole conversion coefficients and examine its implications. Comparison with experimental data is made, and the strong points and shortcomings of the theory discussed.

2. Theory of the Anomalous Terms in the E1 Conversion Process

The probability for the ejection of an electron by the process of internal conversion is proportional to the matrix element $|U_{fi}|^2$ (in a perturbation approximation). We limit ourselves here to internal conversion accompanying E1 gamma radiation and write [7, 8]), in direct analogy with the treatment given for M1 internal conversion coefficients (hereafter referred to as ICC) in ref. [4]),

$$U_{fi}(\mathrm{E1}) \approx \sum_M (-)^M \Big[\int_0^\infty d\tau_e\, \psi_f^*\, O_e(h_1) \psi_i \int_0^{r_e} d\tau_n\, \phi_f^*\, O_n(j_1) \phi_i + \int_0^\infty d\tau_n\, \phi_f^*\, O_n(h_1) \phi_i \int_0^{r_n} d\tau_e\, \psi_f^*\, O_e(j_1) \psi_i \Big]. \quad (1)$$

† One cannot at this stage conclude that anomalous contributions to transitions involving higher multipoles than $L = 1$ are less important solely from the fact that the electron states involved are faster vanishing at small distances, as this effect is somewhat compensated for by the higher order singularities in the interaction terms for these higher multipoles.

Here ψ and ϕ, respectively, are the electron and nucleon wave functions. The integration over the nucleon coordinates $\int_0^{r_e} d\tau_n$ implies a complete angular integration over the angles of the nucleon position but an integration in the radial coordinates r_n only out to the radius of the electron r_e. The first term thus accounts for the case when the electron is outside the nucleon. The second term represents the reversed situation in which the electron is inside the nucleon radius vector.

The nuclear operator is

$$O_n(j_1) = iW \frac{\partial}{\partial r} [r j_1(Wr)] Y_{1-M}, \tag{2}$$

where $j_1(Wr)$ is the regular spherical Bessel function and W the energy of the gamma ray (for a more complete account of the derivations leading up to eq. (13) see ref. [8])). The quantity $O_n(j_1)$ is rather independent [9]) of the assumed interaction of the nucleon with the transverse photon field provided (a) that the assumed interaction is linear in the electromagnetic field, (b) that it is gauge-invariant, (c) that the long-wavelength limit is approached (i.e., $Wr_n \ll 1$), (d) that the nucleons are assumed to be point particles.

The electron operator is

$$O_e(j_1) = \left[-iW \frac{\partial}{\partial r} (r j_1) + \alpha_r W^2 r j_1 \right] Y_{1M}, \tag{3}$$

where j_1 as before is a function of Wr. The matrix α_r is defined as

$$\alpha_r = \begin{pmatrix} 0 & 1 \\ 1 & 0 \end{pmatrix} \frac{\boldsymbol{\sigma} \cdot \mathbf{r}}{r}.$$

This expression (3) is derived on the basis that the interaction of the electron with the transverse photon field is

$$H_e = -e\boldsymbol{\alpha}_e \cdot \mathbf{A}(\mathbf{r}_e), \tag{4}$$

where the matrix $\boldsymbol{\alpha} = \left(\begin{smallmatrix} 0 & 1 \\ 1 & 0 \end{smallmatrix}\right) \boldsymbol{\sigma}$.

The quantities $O_n(h_1)$ and $O_e(h_1)$ are obtained from eqs. (2) and (3) by replacing everywhere j_1 by h_1, the Hankel function of the first kind, corresponding to an outgoing wave.

Equation (1) may be conveniently rewritten as

$$\begin{aligned} U_{fi}(\mathrm{E1}) \approx \sum_M (-)^M \Big\{ & \int_0^\infty d\tau_e \psi_f^* O_e(h_1) \psi_i \int_0^\infty d\tau_n \phi_f^* O_n(j_1) \phi_i \\ & + \int_0^\infty d\tau_n \phi_f^* O_n(h_1) \phi_i \int_0^{r_n} d\tau_e \psi_f^* O_e(j_1) \psi_i \\ & - \int_0^\infty d\tau_n \phi_f^* O_n(j_1) \phi_i \int_0^{r_n} d\tau_e \psi_f^* O_e(h_1) \psi_i \Big\}. \end{aligned} \tag{5}$$

The first term in eq. (5) now corresponds to the "point nucleus" case, i.e., it is the only surviving term if we let the nucleus shrink to a point.

The other two terms represent "finite size" corrections to this limiting situation.

As the angular functions are identical in the corresponding operators for all three terms, it is easily shown that the "partial" conversion coefficient corresponding to ejection of a bound electron in state $\varkappa'$ into the free state $\varkappa$ is

$$\alpha_{\varkappa\varkappa'}(\mathrm{E1}) = \mathring{\alpha}_{\varkappa\varkappa'}|1+\lambda|^2, \tag{6}$$

where $\mathring{\alpha}_{\varkappa\varkappa'}$ is the partial conversion coefficient corresponding to a point nucleus, as far as nuclear matrix elements are concerned (and thus corresponds to the case in which only the first term in (5) is retained). Calculating $\mathring{\alpha}_{\varkappa\varkappa'}$ one should, strictly speaking, use electron wave functions adjusted for the finite extension of the central charge. In the qualitative considerations employed in the following, values of either Sliv or Rose are sufficiently accurate, even though neither strictly corresponds to our definition of $\mathring{\alpha}_{\varkappa\varkappa'}$. The term λ of eq. (6) is defined as

$$\lambda = \frac{\langle I||\mathrm{O}_n(h_1)S(r,\ j_1)-\mathrm{O}_n(j_1)S(r,\ h_1)||I'\rangle}{\langle I||\mathrm{O}_n(j_1)||I'\rangle S(\infty,\ h_1)}\ , \tag{7}$$

where

$$S(r,\ j_1) = \int_0^r r^2\,\mathrm{d}r\left\{Wrj_1(f_\varkappa g_{\varkappa'}-g_\varkappa f_{\varkappa'})+\left[\frac{\partial}{\partial r}(rj_1)\right](f_\varkappa f_{\varkappa'}+g_\varkappa g_{\varkappa'})\right\}. \tag{8}$$

In eq. (8) it is assumed that the expansion of $j_1(Wr)$ is employed, with only the leading term retained. Under this condition, $Wr \ll 1$, the second of the terms in eq. (8) appears to be dominant. In eq. (7) the "double-bar" matrix element (reduced matrix element) is employed in the usual definition. (The quantities I' and I in the bra- and ket-vectors of eq. (7) really denote all quantum numbers necessary to represent initial and final state, apart from the spacial projection m_I of the total angular momentum.)

The expression $S(r,\ h_1)$ is obtained from eq. (8) by employing h_1 instead of j_1. Furthermore $S(\infty,\ h_1)$ corresponds to $S(r,\ h_1)_{r\to\infty}$.

Finally the total conversion coefficients $\alpha_{\varkappa'}$ (i.e., respectively α_{K}, $\alpha_{\mathrm{L_I}}$, $\alpha_{\mathrm{L_{II}}}$, etc.) is defined as

$$\alpha_{\varkappa'} = \sum_{\varkappa}\alpha_{\varkappa\varkappa'}. \tag{9}$$

The electron wave functions $f_\varkappa$ and $g_\varkappa$ ("small" and "large" components of the Dirac electron wave functions) have now to be estimated.

In the interior of the nucleus one may assume an electrostatic potential corresponding to a homogeneous charge distribution [10, 11],

$$v(r) = -\frac{e^2Z}{2R}\left[3-\left(\frac{r}{R}\right)^2\right], \tag{10}$$

where R is the nuclear radius. In this potential, which is finite at the origin, one may find series expansions in r of f_κ and g_κ. The amplitude of the leading term is determined by matching at the nuclear boundary with the external solution. The leading terms are only weakly dependent on the particular shape of the interior potential assumed.

For L_I and L_{II} conversion one would expect the main contribution to the structure-dependent terms to originate from transitions $\varkappa' = -1$ to $\varkappa = 1$ (i.e., $s_{\frac{1}{2}} \to p_{\frac{1}{2}}$) and $\varkappa' = 1$ to $\varkappa = -1$ (i.e., $p_{\frac{1}{2}} \to s_{\frac{1}{2}}$), respectively. (The wave functions corresponding to these states have the largest amplitudes at the nuclear surface.) Indeed, these are the leading contributions, although they are considerably weakened owing to a particular cancellation, discussed in the following paragraphs.

We employ the following internal expansions, treating as an example the case $s_{\frac{1}{2}} \to p_{\frac{1}{2}}$.

$$(\varkappa' = -1;\ s_{\frac{1}{2}}) \begin{cases} f_{\kappa'} = \mathring{f}_{\kappa'}\left(\frac{r}{R}\right) + \ldots = -\frac{1}{3}[E - v'(0) - 1]\mathring{g}_{\kappa'} r + \ldots, & \text{(11a)} \\ g_{\kappa'} = \mathring{g}_{\kappa'} + \ldots, & \text{(11b)} \end{cases}$$

$$(\varkappa = +1;\ p_{\frac{1}{2}}) \begin{cases} f_\kappa = \mathring{f}_\kappa + \ldots, & \text{(11c)} \\ g_\kappa = \mathring{g}_\kappa\left(\frac{r}{R}\right) + \ldots = \frac{1}{3}[E - v(0) + 1]\mathring{f}_\kappa r + \ldots, & \text{(11d)} \end{cases}$$

where use has been made of the Dirac equation to determine the relation between $\mathring{f}_\kappa$ and $\mathring{g}_\kappa$.

A more detailed study shows that the first term in (8) is smaller than the second by a factor W/mc^2 only and not as expected by a factor WR. Provided that $W \ll mc^2$ we may still neglect the first term. $S(r, j_1)$ is then proportional to

$$f_\kappa f_{\kappa'} + g_\kappa g_{\kappa'} \approx r\,\mathring{f}_\kappa \mathring{g}_{\kappa'} \frac{2}{3}\left[1 + \frac{v'(0) - v(0)}{2}\right] + \ldots, \qquad (12)$$

where units $m = \hbar = c = 1$ are assumed throughout. Thus R is the nuclear radius in units of the electron Compton wave length, and $v'(0)$ and $v(0)$ are the initial and final values in units of mc^2 of the electrostatic potential at the origin.

The two terms on the left side of eq. (12) are opposite in sign and very nearly of equal magnitude. The sum $f_\kappa f_{\kappa'} + g_\kappa g_{\kappa'}$ is thus smaller by a factor of order $R(\approx 10^{-2})$ than the magnitude of either of its two constituent terms. This cancellation occurring for the case $\varkappa = -\varkappa'$ is dependent on the fact that the electron wave function is highly relativistic inside the nucleus, or more specifically on the fulfilment of the condition $|E - v| \gg 1$, as is seen from eqs. (11a, d).

In view of this underlying condition it is apparent that the cancellation will more affect the anomalous internal conversion (taking place within

the nucleus where the electrostatic potential is deep) than the normal conversion with its main contribution originating some distance outside the nuclear surface.

As pointed out the occurring cancellation represents a weakening of the transition amplitude by nearly a factor e^2 (i.e. 1/137). This may indicate the possibility that for anomalous E1 conversion higher order radiative effects may be of importance. Such more complicated effects have, however, not been included in this preliminary treatment.

As is indicated from eq. (12) the cancellation may be somewhat counteracted, for instance by a large change in the depth of the electrostatic potential during the transition, i.e. $v'(0)$ being very different from $v(0)$. Assuming, e.g., a homogeneous charge distribution over a spheroid of constant volume but varying eccentricity, the potential at the origin depends on the eccentricity parameter δ (excess of major axis over minor axis) as

$$v(0) = \mathring{v}(0)(1-\tfrac{4}{9}\delta^2). \tag{13}$$

If thus the nucleonic transition associated with the conversion process changes the equilibrium deformation from $\delta = 0.3$ to $\delta = 0.2$, $v(0)$ changes by approximately 2 %, i.e., by ≈ 1 MeV in the heavy-element region. It is quite possible that other effects may also tend to lift this cancellation.

Employing the expansions of eqs. (11a—d) one arrives at the following simplified expression for the corrected conversion coefficient:

$$\alpha_{\kappa\kappa'} = \mathring{\alpha}_{\kappa\kappa'} \left| 1-i\,\frac{M_{\kappa\kappa'} C_{\kappa\kappa'} x}{W^{3/2} \mathring{\alpha}_{\kappa\kappa'}^{1/2} e^{i\delta}} \right|^2 . \tag{14}$$

Here $\mathring{\alpha}_{\kappa\kappa'}$ is the normal "point nucleus" partial-conversion coefficient defined previously; $\exp i\delta$ is the phase of the integral $S(\infty, h_1)$, which enters into the expression for $\mathring{\alpha}_{\kappa\kappa'}$ as the absolute value squared. These phases have not been published, but we estimate, for low-energy transitions, $\delta \approx \pm\pi/2$ (i.e., $S(\infty, h_1)$ almost purely imaginary) for E1 as well as for M1 conversion. The phase problem for the M1 case has been previously discussed by Church and Weneser [4]). Further, W is the transition energy in units of mc^2; $C_{\kappa\kappa'}$ is a factor depending on the change of electrostatic potential at the origin brought about during the transition; x is a real quantity, the ratio of two nuclear matrix elements,

$$x = \frac{\langle I||r^3 Y_1||I'\rangle}{\langle I||r Y_1||I'\rangle}, \tag{15}$$

where r is expressed in units of $\sqrt{(\hbar/M\omega_0)}$ appropriate to the nucleon wave functions of Nilsson [12]), where the basic energy $\hbar\omega_0$ of the nuclear oscillator potentials employed in ref. [12]) is given as $\approx 80\, A^{-1/3}$ in units of mc^2. The correction term in eq. (14) can thus be expected to be almost purely real

for low-energy transitions. Furthermore, for nuclei in the heavy-element region and for gamma-ray energies less than ≈ 100 keV the estimates of $M_{\kappa\kappa'}$ of table 2 may be employed. The accuracy of the values of $M_{\kappa\kappa'}$ depend on the accuracy with which $\mathring{f}_\kappa$ and $\mathring{g}_\kappa$ may be estimated.

Values of the latter quantities have been obtained for bound states from the diagrams of Brysk and Rose [13]) based on calculations that allow for screening and the finite size extension of the central nuclear charge. The tables of Reitz [14]) have supplied values of the free-electron wave functions. A more detailed discussion of this point is found in ref. [8]).

It is clear that the calculated $M_{\kappa\kappa'}$ of table 2 are not very exact but should be sufficiently accurate for semi-quantitative estimates of the conversion anomalies.

TABLE 2

Values of $M_{\kappa\kappa'}$ and $C_{\kappa\kappa'}$ for $Z = 91$ and low energies

Shell	Initial	Final	$M_{\kappa\kappa'} \times 10^6$	$C_{\kappa\kappa'}$
K	$1s_{1/2}$	$p_{1/2}$	—5.3	$1+\frac{1}{2}(v'(0)-v(0))$
		$p_{3/2}$	3.9	1
L_I	$2s_{1/2}$	$p_{1/2}$	—2.1	$1+\frac{1}{2}(v'(0)-v(0))$
		$p_{3/2}$	1.6	1
L_{II}	$2p_{1/2}$	$s_{1/2}$	—1.9	$1+\frac{1}{2}(v(0)-v'(0))$
		$d_{3/2}$	0.1	1
L_{III}	$2p_{3/2}$	$s_{1/2}$	1.4	1
		$d_{3/2}$ †	—	—
		$d_{5/2}$ †	—	—

† In these cases the leading anomalous conversion operator is of the type $r^5 Y_1$; the coefficient corresponding to $M_{\kappa\kappa'}$ is, however, so small that the anomalous contributions to these terms may be safely neglected.

Let us examine the implications of the simple theory, as expressed in eqs. (14) and (15) and in table 2. The conversion coefficients for K, L_I, and L_{II} (i.e., $s_{\frac{1}{2}}$ and $p_{\frac{1}{2}}$) electrons in this formulation are functions of two parameters — the matrix element ratio x, defined in eq. (15), and the correction factor $C_{\kappa\kappa'}$, which depend on the electrostatic potential change. However, the L_{III} conversion coefficient is essentially a function of x only. For a typical heavy-element case ($Z = 91$, $W = 0.17$) an x value of about 400 to 600 should give rise to a second term in eq. (13) of order 0.1, causing the partial-conversion coefficient for $p_{3/2} \rightarrow s_{\frac{1}{2}}$ transitions to increase or decrease by 20 %, depending on the relative signs of x and $\exp i\delta$. For $v'(0) = v(0)$ the theory predicts anomalies in the L_I and L_{II} subshells only slightly greater than that in the L_{III} subshell.

The correction factor $C_{\kappa\kappa'}$ theoretically will usually differ for $s_{\frac{1}{2}}$ and $p_{\frac{1}{2}}$ electrons. As $v'(0)-v(0)$ is increased from zero, $C_{\kappa\kappa'}$ increases from unity for $s_{\frac{1}{2}}$ and decreases from unity for $p_{\frac{1}{2}}$, and in the limit of very large potential

change $C_{\kappa\kappa'}$ will be nearly of equal magnitude but of opposite sign for $s_{\frac{1}{2}}$ and $p_{\frac{1}{2}}$ electrons. In the next section we attempt some comparison with experiment.

The nuclei in which the anomalous cases occur lie in the region of spheroidal nuclei. Thus, one may expect selection rules in K and to a lesser extent in N, n_z, Λ and Σ to be applicable to transition matrix elements. The K-selection rules as applied to beta and gamma transitions have been frequently discussed elsewhere. The N, n_z, Λ, Σ selection rules have also been applied successfully to beta [15, 16]) and gamma [16, 17, 18, 19]) transitions previously, although they are not generally as restrictive as the K-selection rules.

As has been pointed out, the N quantum number should properly not be called an asymptotic quantum number as it is not dependent on the assumption of a very large deformation [20]). The evidence from ref. [20]) and from the studies by Hoffman and Dropesky [21]) on the K-capture of Pu^{237} to Np^{237} may suggest that a breaking of the selection rule in N is associated with a quantitatively somewhat greater hindrance than in n_z and Λ.

Let us now consider the selection rules in K and in N, n_z, Λ, and Σ

TABLE 3

Selection rules for radiative E1 transitions ($\Sigma_m rY_{1m}$)

ΔK	Operator	ΔN	Δn_z	$\Delta\Lambda$	$\Delta\Sigma$
1	$x+iy$	± 1	0	1	0
0	z	$+1$ -1	$+1$ -1	0	0

TABLE 4

Selection rules for anomalous E1 conversion ($\Sigma_m r^3 Y_{1m}$)

ΔK	Operator	ΔN	Δn_z	$\Delta\Lambda$	$\Delta\Sigma$
1	$(x+iy)(x^2+y^2)$	$\pm 1, \pm 3$	0	1	0
	$(x+iy)\cdot z^2$	± 1 $+1, +3$ $-1, +3$	0 $+2$ -2		
0	$z(x^2+y^2)$	$\pm 1, +3$ $\pm 1, -3$	$+1$ -1	0	0
	z^3	$+1$ $+3$ -1 -3	$+1$ $+3$ -1 -3		

for the matrix elements $\langle r^3 Y_1 \rangle$ giving rise to anomalous E1 conversion contributions.

If the matrix element of rY_1 is weakened by K-forbiddenness ($\Delta K > 1$), then this is also the case for $r^3 Y_1$, which has the same K-selection rule. However, the severe nucleonic selection rules that hinder E1 transitions, to some extent accounted for by the asymptotic selection rules in N, n_z, Λ and Σ, are relaxed for $r^3 Y_1$.

Tables 3 and 4 list the appropriate selection rules. For $\Delta K = -1$ the selection rules are obtained by changing signs in the $\Delta\Lambda$ and $\Delta\Sigma$ columns.

3. Nuclear-Structure Corrections for M1 Conversion Coefficients

The case of magnetic dipole K-shell ICC is treated in ref. [4]) by Church and Weneser. For the purpose of the survey of empirical data below we rewrite the final formulae of that paper. To preserve the analogy with the E1 case, eq. (14), we express r in the units of nuclear dimensions $\sqrt{(\hbar/M\omega_0)}$ employed in eq. (14). We obtain for the K-shell partial ICC (denoted $\beta_{\kappa\kappa'}$, and leading to the free $s_{\frac{1}{2}}$ state, i.e., $\kappa' = -1$, $\kappa = -1$) [4])

$$\beta_{-1-1} = \mathring{\beta}_{-1-1} |1 + x N_{-1-1}|^2, \tag{16}$$

where

$$x = \frac{\langle\!|| r^2(\mathbf{L} + 2\mu\boldsymbol{\sigma}) - \mu \mathbf{r}(\boldsymbol{\sigma}\cdot\mathbf{r}) ||\!\rangle}{\langle\!|| \mathbf{L} + \mu\boldsymbol{\sigma} ||\!\rangle}, \tag{17}$$

and where the value of the constant N_{-1-1} may be obtained from eq. (6) of ref. [4]). Furthermore, Church and Weneser, on the basis of available M1 partial ICC's $\mathring{\beta}_{\kappa\kappa'}$, rewrite the correction in terms of the total ICC. In the notation of the present paper (adopted for the use of the nucleonic wave functions of ref. [12]) their result may be rewritten

$$\beta_K \approx \mathring{\beta}_K [1 + x N_K]^2. \tag{18}$$

The step between eqs. (16) and (18) (or eqs. (6) and (7) in ref. [4]) appears to invoke the approximating assumption of $x N_K \ll 1$.

The constant N_K in eq. (18) is given as

$$N_K = C(Z, W) \cdot R^{-2}. \tag{19}$$

The energy involved in the transition is denoted W as before (k in ref. [4])). Values of the constant $C(Z, W)$ are tabulated in ref. [4]). The nuclear radius R is to be expressed in the above units (for $A \approx 230$, $R \approx 3$). For $W \leqq mc^2$ the factors N_K take on the values listed in table 5; for more accuracy table 1 of ref. [4]) should be used for $C(Z, W)$. It should be noted that if Sliv's values are used for $\mathring{\beta}_K$ and $\mathring{\beta}_{-1-1}$ it is appropriate to replace x by $(x - R^2)$, as pointed out in ref. [4]). The same holds true for the E1 case.

As large values of x are required for the transition to be detected as anomalous, this correction term to x is negligible, however.

TABLE 5

Values of N_K for K-conversion and $W < mc^2$.
(The numbers in parentheses denote powers of 10)

Z	70	85	100
N_K	2 to 3(—3)	4(—3)	7 to 8(—3)

It is thus found that the quantity N_K, characterizing the anomalous corrections to the M1 ICC, is in general much larger than the corresponding quantity for E1 transitions $M_{\kappa\kappa'} W^{-2/3} \overset{\circ}{\alpha}{}^{\frac{1}{2}}_{\kappa\kappa'}$ (see eq. (14); the correction there is, however, expressed in terms of the partial ICC). For example, in the experimentally interesting case of the 84-keV E1 transition in Pa^{231}, the latter quantity corresponding to the partial ICC α_{1-1} of L_I conversion (connecting the bound electron state $2s_{\frac{1}{2}}$ with the free state $p_{\frac{1}{2}}$) equals $\approx 2\times 10^{-4}$. (For the purely hypothetical case of K-conversion of the same energy we would have twice this value.) If the theoretically undetermined factor $C_{\kappa\kappa'}$ were of the order 1, the nuclear-structure deviations in ICC would be expected to be observed in E1 first for transitions that were 100 to 1000 times as hindered as M1 transitions showing anomalous conversion. However, there seems to be some experimental indication (interpreted in terms of this scheme) that $C_{\kappa\kappa'}$ indeed is of order 10, in which case the difference between E1 and M1 in this respect is less important.

Church and Weneser [4]) gave three categories of hindered M1 transitions in which anomalies might be observable, and to them may be added the fourth category of transitions in strongly deformed nuclei, transitions for which there is hindrance in N, n_z, Λ, or Σ.

In table 6 we give the "asymptotic" selection rules for M1 radiation and in table 7 the selection rules for the anomalous M1 conversion operator. As with tables 3 and 4, the selection rules are listed only for $\Delta K = +1$ and 0, and the corresponding rules for $\Delta K = -1$ are obtained by changing signs in the $\Delta\Lambda$ and $\Delta\Sigma$ columns.

TABLE 6

Selection rules for radiative M1 transitions
$[\Sigma_m \hat{\mathbf{e}}_m \cdot (\mathbf{L}+\mu\boldsymbol{\sigma})]$

ΔK	Operator	ΔN	Δn_z	$\Delta\Lambda$	$\Delta\Sigma$
1	σ_+	0	0	0	1
	L_+	0	± 1	1	0
0	σ_z	0	0	0	0
	L_z	0	0	0	0

TABLE 7

Selection rules for anomalous M1 conversion contribution
$\Sigma_m \hat{\mathbf{e}}_m \cdot [(\mathbf{L}+2\mu\boldsymbol{\sigma})r^2 - \mu\mathbf{r}(\boldsymbol{\sigma}\cdot\mathbf{r})]$

ΔK	Operator	ΔN	Δn_z	$\Delta\Lambda$	$\Delta\Sigma$
1	$z^2\sigma_+$	+2 0 −2	+2 0 −2	0	1
	$(x^2+y^2)\sigma_+$	0, ±2	0	0	1
	$z^2 L_+$	+2 0 −2	+1, +3 ±1 −1, −3	1	0
	$(x^2+y^2)L_+$	0, ±2	±1	1	0
	$(x+iy)^2\sigma_-$	0, ±2	0	2	−1
	$(x+iy)z\sigma_z$	0, +2 0, −2	+1 −1	1	0
0	$z^2 L_z$ or $z^2\sigma_z$	+2 0 −2	+2 0 −2	0	0
	$(x^2+y^2)L_z$ or $(x^2+y^2)\sigma_z$	0, ±2	0	0	0
	$(x+iy)z\sigma_-$	0, +2 0, −2	+1 −1	1	−1
0	$(x-iy)z\sigma_+$	0, ±2 0, −2	+1 −1	−1	1
	$z^2\sigma_z$	+2 0 −2	+2 0 −2	0	0

4. Qualitative Systematization of Conversion-Coefficient Anomalies

The occurrence in the 60-keV E1 transition of Np^{237} of L-subshell ICC's in disagreement with Rose's theoretical values has been pointed out by Hollander *et al.* [5]). L-subshell conversion coefficients have been studied for E1 transitions in neighbouring isotopes, and some are found to be anomalous (notably 85-keV E1 in Pa^{231}), whereas others are normal. The experimental evidence in the heavy region is detailed in a forthcoming paper by Asaro, Stephens, Hollander and Perlman [6]). Vartapetian [22, 23]) has reviewed lifetime and conversion-coefficient data for M1 and E1 transitions and has made the general observation for the heavy element E1's that the more delayed transitions usually exhibit conversion coefficients higher than theoretical

for E1 and requiring more M2 admixture than is reasonable for explanation in many cases. Vartapetian suggests that the anomalies may be due to nuclear-structure effects not treated by the Rose or Sliv theoretical calculations.

We now wish to make a brief survey of experimental conversion-coefficient data for E1 and M1 transitions in the principal two regions of spheroidal nuclear deformation. It is beyond the scope of this paper to analyze exhaustively the experimental evidence. We confine our cases to those in which a lifetime or limit is known and exclude from consideration those cases for which only a single conversion coefficient is known and in which there is no independent evidence bearing on possible quadrupole admixture.

The simple theoretical treatment exhibited in the first section of this paper predicts (a) that significant anomalies should appear only in transitions highly hindered from the single-particle transition value, (b) that when such hindrance is attributable to violation of the K-selection rule, anomalies should not be appreciable, and (c) that anomalies should be favoured for transitions in which the anomalous operator is allowed by "asymptotic" selection rules. The relevant experimental cases are summarized briefly in tables 8 to 11 in inverse order of retardation from the single-particle transition rate. The cases are discussed individually in the appendix. Separate tables are given for K-forbidden and K-allowed cases. Altogether there are four certain and four probable anomalous E1 cases and one certain M1 case.

Concerning the first of the three general theoretical predictions enumerated above we see, indeed, that all the clear cases of anomalies occur for transitions retarded from single-particle rates by factors of 1.5×10^4 or more.

Concerning the second, we see that except for the exceedingly retarded Hf^{180m} case, normal conversion coefficients are found in K-forbidden cases even though the retardation may be as large as 10^9 or more.

Concerning the third theoretical prediction, that asymptotic quantum-number selection rules for the anomalous operator are valid, there is some uncertainty. At the outset it should be borne in mind that violation of selection rules in n_z, Λ, or Σ is found to result, on the average, in retardation of only one order of magnitude in beta decay [15]). It has been suggested that cases such as those in tables 8 and 10 owe their retardation to violation of these selection rules, although the especially high retardation of E1 transitions associated with the removal of almost all the oscillator strength to the giant-resonance region of excitations seems to indicate some higher-order cancellation of matrix elements, in addition.

(Violation of the selection rules in Σ and Λ in E1 transitions is, for the normal cases $\Delta N = 1$, also associated with a violation n_z. One may possibly make the distinction, however, as to the *order* of forbiddenness in n_z alone.)

TABLE 8

Survey of E1 transitions not K-forbidden

Nucleus	Gamma energy (keV)	Retardation factor	Probable state assignments	Asymptotic classification for: Radiative trans. op. $\langle rY_1\rangle$	Asymptotic classification for: Anomalous ICC op. $\langle r^3 Y_1\rangle$	Conversion-coefficient observations
			$I\ K\Pi[Nn_z\Lambda]$			
Np^{237}	267	5.5×10^{8}	$\frac{3}{2}\frac{3}{2}$—[521] → $\frac{5}{2}\frac{5}{2}$+[642]	h†	u††	α_K probably high by factor of 10
Pa^{231} †††	84	3×10^{6}	$\frac{5}{2}\frac{5}{2}$+[642] → $\frac{3}{2}\frac{3}{2}$—[521](?)	h(?)	u(?)	α_{L_I} high by 20 $\alpha_{L_{II}}$ high by 20 $\alpha_{L_{III}}$ high by 1.3±0.4
Lu^{177}	146	5×10^{6}	$\frac{9}{2}\frac{9}{2}$—[514] → $\frac{7}{2}\frac{7}{2}$+[404]	h	h	α_K probably normal but uncertain
Lu^{175}	282	1.4×10^{6}	$\frac{9}{2}\frac{9}{2}$—[514] → $\frac{7}{2}\frac{7}{2}$+[404]	h	h	α_K normal
Pu^{239}	106	5×10^{5}	$\frac{7}{2}\frac{7}{2}$—[743] → $\frac{5}{2}\frac{5}{2}$+[622]	h	u	α_{L_I} high by 1.6±0.2 $\alpha_{L_{II}}$ high by 2.7±0.3 $\alpha_{L_{III}}$ not measurable
Np^{237}	60	2.8×10^{5}	$\frac{5}{2}\frac{5}{2}$—[523] → $\frac{5}{2}\frac{5}{2}$+[642]	h	h	α_{L_I} high by 1.7 $\alpha_{L_{II}}$ high by 3.8 $\alpha_{L_{III}}$ normal M-subshell pattern abnormal
Np^{237}	26	3×10^{5}	$\frac{5}{2}\frac{5}{2}$—[523] → $\frac{7}{2}\frac{5}{2}$+[642]	h	h	α_L high by 2
Tm^{169}	63	8×10^{4}	$\frac{7}{2}\frac{7}{2}$—[523] → $\frac{7}{2}\frac{7}{2}$+[404]	h	h	α_L normal
Ac^{227}	27	6×10^{4}	State assignments unknown			$\alpha_L \approx$ normal but $\alpha_{M_{II}}$ low
Pa^{231}	26	$\approx 5\times10^{4}$	$\frac{5}{2}\frac{5}{2}$+[642] → $\frac{5}{2}\frac{3}{2}$—[521](?)	h(?)	u(?)	α_M-subshell ratios normal
Pa^{234m}	29	1.5×10^{4}	† Note: odd-odd nucleus			α_L probably high (?)
Hf^{177}	208	$< 3\times10^{4}$	$\frac{9}{2}\frac{9}{2}$+[624] → $\frac{9}{2}\frac{7}{2}$—[514]	h	h	α_K normal
Am^{243}	85	$< 2\times10^{4}$	$\frac{5}{2}\frac{5}{2}$+[642] → $\frac{5}{2}\frac{5}{2}$—[523]	h	h	L-subshell ratio and α_{total} normal
Eu^{153}	98	$< 9\times10^{3}$	$\frac{5}{2}\frac{5}{2}$—[532] → $\frac{5}{2}\frac{5}{2}$+[413]	h	h	α_K normal
W^{182}	152	?	? Note: even-even nucleus			α_K low, α_{L_I} high

† h = hindered. †† u = unhindered.

††† Question marks indicate that the orbital assignments seem somewhat less certain then in the other cases listed.

Table 9

Survey of *K*-forbidden E1 transitions

Nucleus	Gamma energy (keV)	Retardation factor	$\lvert\Delta K\rvert$	Conversion-coefficient observations
Hf^{180m}	57.6	10^{15}	8 or 9	L-subshell pattern anomalous with L_I too high
Hf^{178m}	88.8	2×10^{14}	8 or 9	Total conversion coeff. normal for E1 within 20 %
Pu^{239}	316	9.4×10^{8}	3	α_K normal
	334	8.4×10^{8}	3	α_K normal
Re^{183}	382	2×10^{3}	2	α_K normal

Table 10

Survey of M1 transitions not *K*-forbidden

Nucleus	Gamma energy (keV)	Retardation factor	Probable state assignments	Asymptotic classification for		Conversion coefficient observations
				rad. trans. $\langle \mathbf{L}+\mu\boldsymbol{\sigma}\rangle$	anomalous ICC op. $\langle \mathbf{r}(\boldsymbol{\sigma}\cdot\mathbf{r})\rangle$	
Ta^{181}	482	2.6×10^{6}	$\frac{5}{2}\frac{5}{2}+[402]\rightarrow\frac{7}{2}\frac{7}{2}+[404]$	h	u	α_K high by factor of 2 to 10
Np^{237}	208	1.3×10^{4}	$\frac{3}{2}\frac{3}{2}-[521]\rightarrow\frac{5}{2}\frac{5}{2}-[523]$	h	u	α_K normal (95±10 % of Sliv theo.)
Eu^{153}	102	5×10^{2}	$\frac{3}{2}\frac{3}{2}+[411]\rightarrow\frac{5}{2}\frac{5}{2}+[413]$	h	u	α_K normal (82±10 % of Sliv theo.)

TABLE 11

Survey of K-forbidden M1 transitions

Nucleus	Gamma energy (keV)	Retardation factor	ΔK	Conversion-coefficient observations
Tm^{169}	178	5×10^5	3	α_K normal (or slightly high)
	199	5×10^5	3	α_K normal
Pu^{239}	277.9	6.0×10^4	2	α_K noraml
	228.2	4.7×10^4	2	α_K normal
	209.7	9×10^3	2	α_K normal (or low)

What the theory of anomalous ICC would lead us to seek is separate "threshold" values of retardation above which transitions would show anomalies (of greater than, say, 50 %): one threshold for transitions with unhindered anomalous operators and another higher threshold for transitions hindered in this operator. There is also a theoretical dependence of the anomalous ICC on atomic number. Numerical values exhibiting this dependence for M1 have been given by Church and Weneser [4]), and a similar dependence is expected for E1. (Our table 2 gives only values of $M_{\kappa\kappa'}$ for $Z = 91$.)

Among the E1 cases in table 8 all examples of transitions unhindered in r^3Y_1 are anomalous with the probable exception of the 26-keV in Pa^{231}, so we may presume the threshold retardation is about 10^5. It is somewhat surprising that the factor by which these examples are anomalous does not vary more, in view of the variation in retardation factor from 5×10^5 to 6×10^8. Perhaps in some cases of high retardation there is a change of configuration involving nucleons other than the odd one, and such rearrangement would decrease the anomalous-conversion matrix element classed as unhindered. Of the table 8 heavy-element cases hindered in r^3Y_1, the 60- and 26-keV Np^{237} transitions at 3×10^5 retardation show anomalies while in Am^{243} at a retardation $< 2\times10^4$ (with presumably the same proton states as the Np^{237} 60-keV) the ICC's are normal. In the rare earth region the E1 cases of table 8 are all hindered in r^3Y_1, and just one of them, Lu^{177} at 5×10^6 retardation, shows a possible anomaly. The other four cases with retardation ranging down from 1.4×10^6 to $< 9\times10^3$ are all normal. The threshold for anomalies in these 'h' cases seems around 10^5 in the heavy region and 10^6 in the rare earth region. There is no evident difference in threshhold for the cases hindered in r^3Y_1 and the unhindered cases. Probably the scatter in magnitudes of matrix elements is greater than the average separation of the 'h' and 'u' groups, but more experimental cases will be needed to establish the point.

All three M1 isomers of table 10 are unhindered in the anomalous operator, and they indicate a threshold retardation somewhere between 2×10^4

and 10^6. The cases designated "normal" show α_K values somewhat lower than the Sliv theoretical values, but the unretarded M1 transitions probably generally exhibit such slightly lower values according to the analysis of Wapstra and Nijgh [3]).

5. More Detailed Comparisons of Theory and Experiment

The simple theory of Church and Weneser [4]) for anomalous M1 conversion and the corresponding theory for E1 given in this paper, together with considerations of selection rules in the quantum numbers of deformed nuclei, have provided a basis for some systematization of the occurrence of anomalous conversion coefficients. It is next of interest to see if the simple theories are also capable of quantitative explanation of the anomalies.

In order to make really quantitative comparisons for E1 conversion it would be necessary to have theoretical partial-conversion coefficients (i.e., how much of E1 conversion of $s_{\frac{1}{2}}$ goes to $p_{\frac{1}{2}}$ and how much to $p_{3/2}$) and phases for the normal-conversion matrix elements, and these quantities have not been published. Nevertheless, in a particular case of exceedingly large deviations from the normal values of the ICC's we are relatively independent of a knowledge of these partial values. The experimental L_I, L_{II}, and L_{III} coefficients for the 85-keV transition in Pa^{231} are 1.32, 0.84, and 0.047, respectively, and Rose's theoretical values are 0.063, 0.042, and 0.037.

As is readily evident, the experimental ratios cannot be explained solely by M2 admixture † ($\alpha_{M2\ theor.} = 96$, 8,5, 29.2) but some M2 admixture cannot at present be excluded.

One might attempt to test the theory (cf. eqs. (14) and (15) and table 2) by examining first any anomaly of the L_{III} subshell conversion, which should depend only on x, the ratio of nuclear matrix elements. This procedure involves several difficulties: first, there is experimental uncertainty of at least 50 % in the value; second, the relative partial conversion coefficients to $s_{\frac{1}{2}}$, $d_{3/2}$, and $d_{5/2}$ final states are not known to us; third, it cannot be excluded that the entire small increase of experimental L_{III}-conversion coefficient over theory could be due to a small M2 admixture (0.03 %). This admixture corresponds to an M2 half life of 4×10^{-4} sec which is 10 times as long as the single-proton estimate, but still probably not long enough to be consistent with the fact that the M2 transition between the single-particle states assigned is classified as hindered. Depending upon which fraction of the total normal L_{III} internal conversion goes to final state $s_{\frac{1}{2}}$ (with which latter transition almost all the anomalous conversion is associated), the upper limit on x may be put between 5×10^3 (0 %) and 2×10^4 (100 %). (If we assume the fraction to be, e.g., 1/2, the upper limit on x from the experimental

† Provided that M2 is not anomalous.

L_{III} ICC may be put at 1.5×10^4.) This upper limit corresponds to the hypothetical case (somewhat improbable in view of other empirical L_{III} cases) that the correction term is almost twice as large as the normal term but enters with opposite sign.

The experimental L_I and L_{II} ICC's depend both on the structure parameter x and on $C_{\kappa\kappa'}$. Because they are an order of magnitude (≈ 20) larger than the normal values, the analysis is rather independent of a knowledge of the partial ICC's, $\mathring{\alpha}_{\kappa\kappa'}$. We may rewrite eq. (14) in the form

$$\alpha_{\kappa'} = \sum_{\kappa} |\sqrt{\mathring{\alpha}_{\kappa\kappa'}} - ie^{-i\delta} W^{-3/2} M_{\kappa\kappa'} C_{\kappa\kappa'} x|^2. \tag{20}$$

It is then apparent that in these particular cases $\mathring{\alpha}_{\kappa\kappa'}$ may be neglected, and from the empirical values of α_{L_I} and $\alpha_{L_{II}}$ for the Pa^{231} case considered, we obtain the relations

$$|x|^2\,(0.37+0.63\,C_{1-1}^2) \approx 8.2\times10^8, \tag{21}$$

$$|x|^2\,C_{-11}^2 \approx 10\times10^8. \tag{22}$$

From the analysis of the L_{III} conversion we had

$$|x|^2 < 4.0\times10^8. \tag{23}$$

In the most elementary form of the theory (eq. (14) and table 2) $C_{\kappa\kappa'}$ would be unity, corresponding to no change in electrostatic potential at the center of the nucleus and to a correspondingly high degree of cancellation of the two terms on the left of eq. (12). With the uncertainty of our values of $M_{\kappa\kappa'}$ and, in addition, the uncertainty introduced by neglecting the contribution from the normal terms in eq. (20), we cannot entirely exclude a solution $x \approx 3\times10^4$ and both $C_{\kappa\kappa'} = 1$ to eqs. (21) and (22). This x is somewhat larger than what is allowed by the inequality (23). The upper limit of this inequality corresponds in turn to a somewhat improbable case that the anomalous amplitude for L_{III} conversion enters with twice the size of the normal contribution, and with the opposite sign. The limit is furthermore lowered if part of the L_{III} conversion is due to M2 radiation.

Furthermore, we have calculated the single-particle value of the matrix element $\langle r^3 Y_1\rangle$ for the state assignments of table 8, using the wave functions of ref. [12]) in the so-called asymptotic approximation representing an approximate solution to the potential of ref. [12]) in the limit of large deformations. Using the empirical value on $|\langle rY_1\rangle|$ from the gamma lifetime, we obtain $|x| \approx 1100$. The asymptotic approximation in particular and any single-particle wave function in general obtained from a simple model is more likely to overestimate than underestimate the value of $\langle r^3 Y_1\rangle$. However, a possible enhancement of x might result from a collective octupole deformation of the nucleus. An enhancement by a factor of 20 seems, however, excessive.

It seems more probable that the true physical situation is more nearly represented by a solution of relations (21)—(23) with an x of the order of the estimated single-particle value and large factors $C_{\kappa\kappa'}$. On a naive basis one may insert the expressions of table 2 for $C_{\kappa\kappa'}$ and solve eqs. (21) and (22) in terms of x and the quantity $[v'(0)-v(0)]$, i.e., the change of depth of the electrostatic potential. (One may notice that this quantity enters with a different sign in C_{1-1} and C_{-11}.) The quantity $[v'(0)-v(0)]$ is then given by the ratio between eqs. (21) and (22), i.e., $[v'(0)-v(0)]$ is related essentially to the ratio L_I/L_{II}. Of the two solutions to the new relation so obtained, one corresponds to a very small value of $[v'(0)-v(0)]$ and requires the large x value already discussed and deemed improbable for other reasons. The other solution corresponding to a large value of $|v'(0)-v(0)|$, of the order of 10 MeV or more, is very sensitive to the exact ratio of the right sides of eqs. (21) and (22). In view of the fact that the normal conversion amplitudes are neglected in comparison with the anomalous ones (the latter being only five times as large) and furthermore in view of the uncertainty of the estimate of $M_{\kappa\kappa'}$, the numbers on the right-hand sides of eqs. (21) and (22) cannot be considered very accurate. We can then mainly conclude that $C_{\kappa\kappa'}$ seems to be of order 10, and x of the order of the single-particle estimate or somewhat larger.

In summary, we can assign values to the two parameters $\langle r^3 Y_1\rangle$ and $v'(0)-v(0)$ to give a consistent explanation of the three L-subshell coefficients in the Pa^{231} case, and such that the actual value of the matrix element $\langle r^3 Y_1\rangle$ is not inconsistent with reasonable single-particle values. However, the magnitude of $|(v'0)-v(0)|$ required seems quite excessive. This shortcoming of the elementary theory clearly calls for refinements and consideration of effects in addition to the change in the electrostatic potential, which would tend to lift the cancellation in eq. (12). The anomalous internal-conversion interaction takes place wholly within the nuclear volume (i.e., at short distances), and it would not be surprising if vacuum polarization or higher-order radiative corrections were significant. It is believed, for example, that such corrections are significant in calculation of X-ray fine-structure energy levels [24]).

The probably anomalously converted 29-keV transition in Pa^{234} discussed by Vartapetian [22]) (in which possibly the same orbitals are involved as in Pa^{231}) presents a difficulty of a quantitative kind for this elementary theory, as this transition is only 1/100 as hindered as the 84-keV transition in Pa^{231}. In view of possible experimental difficulties in conversion coefficient measurements at such low energies, further work on the ICC and subshell ratios is important.

It is interesting to note the pattern of L-subshell anomalies for the E1 cases of table 8 where such information is known (the 85-keV transition

of Pa^{231}, the 60-keV and 26-keV transitions of Np^{237}, and the 106-keV of Pu^{239}). In no case is the L_{III} subshell anomalous, although it may be about 30 % too high in Pa^{231}. (This may be interpreted as strong support for the argument of $C_{\kappa\kappa'} \gg 1$.) In Pa^{231}, the most striking case, the L_I and L_{II} subshells are equally enhanced by a factor of 20. In Np^{237} and Pu^{239} the enhancement is more modest, and is greater in the L_{II} subshell than in the L_I.

One may speculate on a possible effect on the K/L_I ratio associated with the existence of large anomalous matrix elements but more directly dependent on the phase of the normal-conversion amplitude. The K-as well as the L_I-conversion involves initial $s_{\frac{1}{2}}$ states; the initial states, however, are characterized by different radial quantum numbers. The sign of $S(\infty, h_1)$ (cf. eq. (8)) determines the phase of the "point charge" amplitude $\sqrt{\mathring{\alpha}_{\kappa\kappa'}}$. As we have not performed the calculation of $S(\infty, h_1)$ we have no way of estimating the effect quantitatively; it seems, however, conceivable that the phase of this quantity may be greatly different for the K-conversion and the L_I-conversion. It is thus possible that in anomalous conversion the K and L_I ICC's could deviate in different directions. This effect may be thought of as a possible explanation of the anomalous K/L_I ratio reported for an E1 transition in W^{182} (see discussion in the appendix).

One might attempt a quantitative comparison also for some of the M1 transitions. The case that lends itself most readily for such a comparison is the 480-keV M1 transition in Ta^{181}. The M1 K-conversion coefficient obtained on the basis of the measured total ICC and angular correlation data, as discussed in the appendix, is ≈ 0.5 as compared with Sliv's value $\alpha_K(M1) = 0.06$. Using eq. (18) to fit the observed ICC, one may roughly estimate

$$|x|^{\text{exp.}} = 1000-2000.$$

Actually the approximation involved in the step between eqs. (16) and (18) (i.e., between eqs. (6) and (7) of ref. [4])) seems to require that x (or λ) be not too large. This introduces an additional error in the estimate of the order

$$\sqrt{\frac{\mathring{\beta}_{-1-1}+\mathring{\beta}_{2-1}}{\mathring{\beta}_{-1-1}}}$$

for large x values. Equation (18) thus underestimates x.

A semi-theoretical estimate of x is obtained by using the observed partial M1 lifetime to determine the absolute value of the normal M1 matrix element and the wave functions of ref. [12]) in the "asymptotic approximation" to determine the anomalous internal-conversion matrix element. This estimate of x gives

$$|x|^{\text{theor.}} \approx 5000.$$

It is not disturbing to find the theoretical anomalous conversion matrix element as much as a factor of five too large. Indeed, most single particle theoretical matrix elements for gamma or beta transitions overestimate the experimental transition rates unless collective effects are important.

It is interesting to compare the Ta^{181} 480-keV case just treated with the case of the 208-keV M1 transition in Np^{237}. Both transitions are hindered for the radiative operator in the "asymptotic" selection rules and unhindered in the same rules for the anomalous internal-conversion operator, but they differ in their experimental hindrance factors. This latter transition is hindered by a factor $\approx 10^4$, compared with $\approx 10^6$ for the Ta^{181} transition considered.

The experimental value of α_K is 2.3, compared to Sliv's theoretical value of 2.4. This may be used to put a limit on $x^{\text{exp.}}$. With a deviation between theoretical and experimental α_K of, say, 10 %, we have

$$|x|^{\text{exp.}} < 10$$

(excluding the unlikely case that the anomalous contribution is of twice the magnitude but opposite in sign to the normal term). The semi-theoretical value of x obtained by taking the absolute value of the "normal" matrix element from the gamma lifetime and calculating the anomalous matrix element from the wave function of ref. [12]) in the "asymptotic approximation" is

$$|x|^{\text{theor.}} \approx 50.$$

Again the single-particle estimate of x seems too high, but as discussed with the Ta^{181} case, this overestimation is not particularly disturbing.

As a summary of the E1 and M1 cases treated quantitatively one may state that the anomalous terms introduced by Church and Weneser seem to account semi-quantitatively for the anomalous M1 case encountered and on the whole to be consistent with the cases of hindered M1 transitions in which no anomaly is found. As for the quantitative comparison of the anomalous E1 internal-conversion operator, the experimental effect seems somewhat greater than theoretically expected, and the large values of the correction factor $C_{\kappa\kappa'}$ obtained by the attempted fitting of experimental data may probably more appropriately be considered an indication of higher-order effects, neglected in the treatment presented here.

6. Effects on Angular Distribution

A few words may be added regarding the effects of ICC anomalies on angular-distribution experiments involving conversion electrons. Church and Weneser have already discussed the M1 transitions. For E1 transitions the $s_{\frac{1}{2}}$ electrons (K, L_1) convert into $p_{\frac{1}{2}}$ and $p_{3/2}$ continuum states, and

contributions to anisotropy arise from the $p_{3/2}$ part and—more importantly—from a $p_{\frac{1}{2}}-p_{3/2}$ interference. In the normal case $p_{\frac{1}{2}}$ and $p_{3/2}$ occur in comparable amounts, whereas it is clear empirically from anomalous subshell ratios that the $p_{\frac{1}{2}}$ final state is generally most affected and $p_{3/2}$ very little. In a greatly enhanced K-conversion, as is likely for the 267-keV transition in Np^{237}, the anisotropy in a conversion-line angular correlation would be depressed from normal, and the sign of the anisotropy might or might not be reversed from normal, depending on the relative phases of the normal and anomalous conversion to $p_{\frac{1}{2}}$ states. Angular-correlation experiments on conversion electrons could thus yield unique information on these relative phases.

We are grateful to Prof. I. Perlman for his encouragement and to Drs. A. Bohr and B. Mottelson as well as Drs. K. Alder, B. Stech, and A Winther for discussing with us certain aspects of the work. We wish also to thank Drs. F. Asaro, J. M. Hollander, and F. S. Stephens, Jr., and also Drs. G. T. Ewans, T. W. Knowles and G. Scharff-Goldhaber for supplying us with experimental data in advance of publication. We have furthermore profited from correspondence with Dr. G. Källen and Dr. P. O. Olsson.

Appendix

The cases in table 8 in the heavy-element region are thoroughly discussed in the paper of Asaro *et al.* [6]), but other cases in tables 8—9 that need special discussion are covered briefly here.

TABLE 8 CASES (*K*-ALLOWED E1)

Lu^{177}, 146 keV

The decay scheme of Yb^{177} to Lu^{177} has been studied by several groups in recent years [25, 26, 27, 28]). A prominent feature of the photon spectrum is the 146-keV gamma ray depopulating a state measured as having 1.2×10^{-7} sec half life [25, 26]). The conversion coefficient was reported by de Waard as $\alpha_K = 0.63\pm0.08$ and $K/LM \approx 3.5$ [26]). On this basis he designated the transition as 10 % M2—90 % E1, and Vartapetian [22]) points out that this admixture requires M2 radiation of 1.3 times the single-particle rate. From this observation one might suspect the ICC for E1 to be slightly high. However, Mize *et al.* [28]) remeasured α_K for the 146-keV gamma and set an upper limit $\alpha_K < 0.4$ and, using de Waard's K/LM ratio, they set a limit $M2/E1 < 0.04$. With this limit the M2 comparative lifetime is quite similar to that in the analogous transitions of 396 keV and 282 keV in neighbouring Lu^{175}. For the 282-keV transition the angular correlation measurements fix the M2/E1 ratio and lead to the conclusion that α_K for the E1 is probably

normal [28]). We must conclude from the present uncertain data that the 146-keV transition in Lu^{177} probably has a normal E1 conversion coefficient. Experimental work to resolve the disagreement on α_K and to establish L-subshell conversion ratios would be valuable.

Lu^{175}, 282 keV

Vartapetian [22, 23]) has measured the lifetime of the 396-keV level from which this E1 transition originates as $(3.4\pm0.3)\times10^{-9}$ sec. Several studies [29–34]) on Yb^{175} have helped to establish the decay scheme, and a theoretical interpretation of some features has been given by Chase and Wilets [35]).

From the angular correlation work of Åkerlind *et al.* [33]) on the 282-113 cascade it is possible to determine the E1/M2 ratio of the 282-keV independently of its conversion coefficient. Assuming de Waard's value of E2/M1 = 0.3 for the 113-keV gamma (recent work of Hatch *et al.* [34]) gives E2/M1 = 0.25, in reasonable agreement), one finds that the anisotropy measured by Åkerlind *et al.* supports 2 % M2—98 % E1 for the 282-keV transition. With this mixing ratio and Sliv's theoretical K-conversion coefficients (for E1, 0.0205, and for M2, 0.67) we calculate a theoretical normal ICC of 0.0334. Hatch *et al.* give an experimental α_K of 0.030 and Mize *et al.* [28]) give 0.038, so we conclude that the E1 ICC here is normal. Vartapetian [22]) has pointed out that the 2 % M2 admixture requires an M2 transition rate half that of the single particle formula.

Tm^{169}, 63 keV

The Yb^{169} electron capture decay has been studied in several recent investigations [27, 34, 36, 37]). Some features of the decay have been discussed also by Mottelson and Nilsson [38]).

The 63-keV transition proceeds from a level at 380 keV according to the decay scheme of Mihelich *et al.* [37]), and they measured a lifetime of 4.5×10^{-8} sec for the state. They determined an L-conversion coefficient of 0.19 ± 0.04 and Hatch *et al.* [34]) give 0.15 from the same quantity. The corresponding Rose theoretical value for E1 is 0.15. Mihelich *et al.* measure relative L subshell ratios of 2.3/0.8/1.0, consistent with the theoretical ratios 2.2/0.8/1.0. We conclude that this transition has normal conversion coefficients.

Hf^{177}, 208 keV

The beta decay of Lu^{177} to Hf^{177} has received considerable study in recent years [22, 39–41]), and the ground state spin of Hf^{177} has been determined as 7/2 by Speck and Jenkins [42]). Some information has also come from study of electron capture of Ta^{177} [43, 44]) and from Coulomb excitation [45]).

There appears to be a level at 321 keV populated both in beta decay and in electron capture. It decays by 321-keV and 208-keV gamma rays. For our

study of the ICC problem the latter transition is of the greater interest, since there is information on the E1—M2 mixing from angular-correlation data [22, 40]). The interpretation of the angular correlation requires independent knowledge of the M1—E2 ratio in the 113-keV cascade transition. From L-subshell ratios [39, 43]) one would calculate a small M1 admixture of 2 to 3 %. The experimental anisotropy is consistent with $M1/E2 = 0.03 \pm 0.005$ and a pure E1 transition; this interpretation is proposed by Ofer [41]). However the angular-correlation experiment does not fix the limit on M2 admixture in the 208-keV very well. Two percent M2 in the 208-keV is consistent with 2.8 % or 3.2 % M1/E2 possibilities in the 113-keV.

The experimental α_K of the 208-keV is 0.044 [39]), to be compared with Sliv's theoretical α_K (E1) = 0.0446 and $\alpha_K(M2) = 2.05$. We conclude in table 8 that α_K is normal, although we cannot exclude the remote possibility that $\alpha_K(E1)$ is anomalously small and that there is M2 admixture.

A limit on the 321-keV state lifetime was set by Vartapetian [22, 23]) as $t_{\frac{1}{2}} < 4 \times 10^{-10}$ sec.

Eu^{153}, 98 keV

The level system of Eu^{153} has been studied by Coulomb excitation [46]) and by beta decay [47–52]) of Sm^{153} and electron capture [53–58]) of Gd^{153}. Among the transitions is a 98-keV E1 transition to ground with a lifetime of $< 10^{-9}$ sec. Marty and Vergnes [56]) report $\alpha_K = 0.3 \pm 0.1$, and Church [59]) has given the α_K relative to that of the 103-keV M1 transition discussed later in this appendix. From his ratio we calculate $\alpha_K \approx 0.17$. The Sliv and Band theoretical α_K is 0.23. Hence, we conclude that α_K is normal within experimental uncertainty.

The initial and final state assignments are 5/2, 5/2—[532] and 5/2, 5/2+[413], respectively [19]).

W^{182}, 152 keV

Wapstra and Nijgh [3]) have recently renormalized and discussed conversion coefficients in W^{182} and W^{183} from measurements by Murray *et al.* [60]), and they list conversion-coefficient comparisons for a few E1 transitions in W^{182}. The α_K of the 152-keV transition from 3, 2— (*I*, *K II*) to 2, 2+ † is less than half the Rose theoretical value (which differs very little from Sliv and Band value, in this case). The 222-keV transition from 4, 4— to 3, 2+ exhibits a normal α_K for E1. It is interesting to note that the anomalous case is not *K*-forbidden, while the normal case if *K*-forbidden. With only one determination of these conversion coefficients we might maintain some reservation about labelling the 152-keV transition as anoma-

† For state assignments see ref. [61]). (Note their different convention, *KII*, in state designation.)

lous. However, recent work of Gallagher on Re^{182} decay to W^{182} has clearly shown that there is an anomaly in the K/L_I ratio [62]), the experimental value being 2.8 and Rose's theoretical being 8.3. This K/L_I measurement and the α_K measurement together indicate an α_{L_I} higher than normal. In the main text of this paper we have discussed the possibility that the E1 anomaly might give a constructive contribution to L_I (or K) conversion and a destructive contribution to K (or L_I). Gallagher also finds probable L_I/K anomalies in other E1 transitions of W^{182}, but there is considerably more experimental uncertainty with them than with the 152-keV transition.

We do not have a lifetime determination for the 152-keV transition, but we may estimate the order of its retardation from that of the analogous 67-keV transition (2,2−→2, 2+). The 2, 2− state has a half life of 1.03×10^{-9} sec according to measurements of Sunyar [63]). From this measurement and relative gamma intensity measurements [60]) we calculate a retardation factor of 4.5×10^3 for the 67-keV E1.

It seems surprising that E1 anomalies should set in at such low retardation, but W^{182} is an even nucleus and is not really to be compared closely with odd-mass nuclei. Further experimental studies in this and similar even nuclei are certainly desirable.

TABLE 9 CASES (*K*-FORBIDDEN E1)

Hf^{180m}, 57.6 keV

This unusual 5.5-h E1 isomeric transition [64, 65]) is the slowest E1 transition known; it is slower by a factor of 10^{15} than the single-particle formula predicts. The values $L_I : L_{II} : L_{III} \approx 5 : 0.5 : 1$ and $\alpha_L \approx 0.4$ have been reported [65, 66]), from which one determines approximately that α_{L_I}, $\alpha_{L_{II}}$, and $\alpha_{L_{III}}$ are 0.31, 0.03, and 0.06 compared with theoretical values of 0.11, 0.051, and 0.058 for the three L subshells for E1. (Corresponding values for M2 are 67, 6.1, and 21.) Clearly it is not proper to invoke M2 admixture, since $\alpha_{L_{III}}$ agrees for E1. The threefold enhancement of α_{L_I} and possible decrease of $\alpha_{L_{II}}$ is to be ascribed to anomalous E1 conversion contributions. The great retardation has been attributed to a high order of *K*-forbiddenness, $\Delta K = 8$ or 9. The appearance of anomalous internal conversion according to this interpretation indicates, however, that for the small components of the wave function by which the transition may proceed the anomalous matrix elements may greatly exceed those for the radiative transition †.

Hf^{178m}, 88.8 keV

This E1 transition [43, 67, 68]) seems analogous to the case of Hf^{180m} just discussed. With a lifetime of 3 sec, the retardation factor is 2×10^{14}. It is reported that the total conversion coefficient is 0.5 [43]) compared to the

† Part of the hindrance factor of 10^{15} is thus considered as a hindrance due to intrinsic structure.

theoretical value of 0.46. Here again the retardation is presumably due mainly to K-forbiddenness, $\Delta K = 8$ or 9.

Pu^{239}, 316 keV and 334 keV

These weak E1 transitions have been seen arising from the 1.93×10^{-7} sec level at 391.8 keV [69, 70]. From the branching ratios for transitions from this level we calculate that the 316-keV transition is retarded by a factor of 9.4×10^{8} and the 334 by 8.4×10^{8}.

Ewan and Knowles [70] measured the K-conversion coefficients of these gammas and found them in agreement with theoretical E1 values of Sliv or Rose, which are not very different from each other in this case.

The great slowness of these transitions is largely to be attributed to K-forbiddenness, since K_i is 7/2 (or possibly 5/2) and K_f is 1/2 [69, 19].

Re^{183}, 382 keV

Newton and Shirley [71] have found a 382-keV E1 transition in Re^{183} following the decay of Os^{183}. The state at 496 keV from which this transition originates was measured to have a half life of 8×10^{-9} sec. According to Newton's interpretation the initial state is $9/2-(K = 9/2)$ and the final state is $7/2+(K = 5/2)$, being the first excited state of the ground rotational band. Thus, the transition is K-forbidden. The experimental K-conversion coefficient is $(1.0\pm0.1)\times10^{-2}$, to be compared with Sliv's theoretical value of 1.12×10^{-2}, and thus seems normal.

TABLE 10 CASES (K-ALLOWED M1)

Ta^{181}, 482 keV

The levels and transitions of Ta^{181} have received much study through Coulomb excitation and beta decay of Hf^{181}. We shall not attempt to list references or give a detailed discussion, since the data have been thoroughly reviewed recently by Debrunner *et al.* [72]. Suffice it to say here that the M1—E2 mixing ratio of the 482-keV transition has been carefully determined by gamma-gamma and electron-gamma angular correlations as 98 % E2+2 % M1. Its half life is 1.06×10^{-8} sec. Several determinations of α_K are listed by Debrunner *et al.*, and they choose $\alpha_K = 0.026$ as the best value. Using Sliv's theoretical conversion coefficients one finds a significant discrepancy, which we choose to interpret as the M1 conversion coefficient being a factor of about 10 larger than normal and the unhindered E2 ICC's being normal. The experimental uncertainty on this enhancement factor is considerable, but there is clearly some enhancement outside limits of experimental error.

The initial and final state assignments 5/2, 5/2+[402] → 7/2, 7/2+[404] are supported by spin determinations as discussed by Debrunner *et al.* [72], and the orbital assignments are based on a variety of evidence to be reviewed

in a forthcoming publication [19]). The radiative M1 transition is allowed by K-selection rules but hindered in "asymptotic" quantum-number rules (see table 6), probably explaining at least partially its great retardation (2.6×10^6). The anomalous M1 conversion operator is unhindered ($\Delta n_z = 0$, $\Delta\Lambda = 2$, $\Delta\Sigma = -1$) (see table 7), a favourable situation for appearance of the ICC anomaly.

Np^{237}, 208 keV

The 208-keV M1 transition is a prominent feature of the beta decay of U^{237} (cf. Rasmussen, Canavan and Hollander [73]) and references listed therein). By L-subshell conversion ratios the E2/M1 mixing ratio is 0.5 % or less. Within experimental error the α_K of 2.3 agrees with the Sliv theoretical M1 value of 2.4. The half life of the state at 267 keV from which the 208-keV transition originates was measured by Bunker, Mize and Starner[74]) as 5.4×10^{-9} sec.

The reasons supporting the state assignments associated with this transition exhibited in table 10 are detailed in ref. [73]). With respect to the asymptotic quantum-number selection rules, the situation is the same as in Ta^{181} just discussed: $\Delta n_z = 0$, $\Delta\Lambda = 2$, $\Delta\Sigma = -1$. Hence, the radiative operator is hindered and the anomalous operator is unhindered.

Eu^{153}, 103 keV

The reader is referred to the paragraph on the 98-keV E1 transition in Eu^{153} for references on the Eu^{153} decay scheme. The 103-keV M1 transition is thought to proceed to ground from a state with half life 4×10^{-9} sec, as measured by McGowan [48]), by Graham and Walker [49]) and by Vergnes and Marty [51]). Its K-conversion coefficient has been variously measured as 1.19 (Dubey *et al.* [52]), 1.2 (Marty [51])), 1.1 (McGowan [48])), and 1.2 (Cohen *et al.* [54])). Bhattacherjee and Raman [57]) reported $\alpha_K = 0.67$, and Bisi *et al.* [58]) reported 0.68, but these two last-mentioned studies apparently failed to take into account the presence of the 98-keV E1 transition, which would not have been resolved from the 102-keV in the photon spectrum. From the L-subshell conversion ratios of the 102-keV transition it is established [75]) that there is less than 5 % E2 admixture. Sliv's theoretical K-conversion coefficients for this case are 1.48 for M1 and 1.10 for E2. The experimental ICC seems significantly lower than the theoretical by about 20 %. However, we have classified the conversion coefficient as normal in table 10, since the analysis by Wapstra and Nijgh [3]) on a number of M1 transitions, most of which were not of the retarded nature considered here, showed their conversion coefficients to be systematically still somewhat lower than the Sliv theoretical values.

TABLE 11 CASES (*K*-FORBIDDEN M1)

Tm^{169}, 178 and 199 keV

In the first section of this appendix, where the 63-keV E1 transition in Tm^{169} was discussed, we listed the references to experimental work elucidating the Tm^{169} level system. In Tm^{169} there is a level at 316.2 keV with a half life of 6.4×10^{-7} sec. The level is assigned 7/2, 7/2+[404] [19]) and it decays by *K*-forbidden ($\Delta K = -3$) transitions to states of the ground rotational band, 7/2+and 5/2+, $K = 1/2$ [411]. The analysis by Mihelich *et al.* [37]) determines the M1—E2 mixing ratios of the 178- and 199-keV transitions on the basis of L-subshell conversion coefficients, and they give the value 5×10^5 as factors of retardation for the M1 components of both transitions.

Using the Mihelich *et al.* mixing ratios and Sliv ICC values, we obtain the theoretical α_K for the 178-keV transition of 0.49, while Milelich *et al.* find experimentally 0.49 ± 0.10 and Hatch *et al.* [34]) find 0.51. For the 199-keV transition, the corresponding theoretical value is 0.35 and the experimental values 0.45 ± 0.09 [37]) and 0.40 [34]). Thus, we conclude that the ICC's are normal.

Pu^{239}, 277.9, 228.2, and 209.7 keV

There are three prominent M1 transitions seen following beta decay of Np^{239} or Am^{239} and following alpha decay of Cm^{243}. These transitions of 277.9, 228.2, and 209.7 keV arise from a level at 285.8 keV with half life 1.1×10^{-9} sec. The experimental work relevant to this level scheme has been reviewed by Perlman and Rasmussen [76]) and we refer to this review work for the original references. The level at 285.8 keV has been assigned 5/2, 5/2+[622], and the three M1 transitions go to excited states of the ground rotational band of spins 3/2, 5/2, and 7/2. The ground state of this latter band has been assigned $K = 1/2+$ and the orbital [631]. Hence, the retardation of the M1's may be largely ascribed to *K*-forbiddenness ($\Delta K = 2$).

TABLE 12

K-forbidden M1 transitions in Pu^{239}

Gamma energy (keV)	α_K			Retardation factor
	Exp.	Theoretical		
		Pure M1	90 % M1—10 % E2	
278	1.16 ± 0.12	1.18	1.07	6.0×10^4
228	1.60 ± 0.16	2.04	1.85	4.7×10^4
210	1.76 ± 0.30	2.58	2.33	9.0×10^3

The best determinations of conversion coefficients of these three transitions are probably those of Ewan and Knowles [70]). Limits of < 10 % E2 admixture

were set on the basis of L-subshell conversion coefficients, and table 12 lists their experimental α_K values and Sliv theoretical values for pure M1 and for the upper limit of 10 % E2 admixture. We conclude that these α_K values are probably normal although the 210-keV conversion coefficient shows a discrepancy with the theoretical values by twice the probable error.

References

1) Rose, Goertzel, Spinrad, Harr and Strong, Phys. Rev. **83** (1951) 79; M. E. Rose, Tables in Beta and Gamma Ray Spectroscopy, Editor Kai Siegbahn (North Holland Publishing Co., Amsterdam, 1955)
2) L. A. Sliv and I. M. Band, Coefficients of Internal Conversion of Gamma Radiation (Acad. of Sciences, USSR, 1956); Translation issued in U.S.A. as Report 57, ICCK1 (Phys. Dept., Univ. of Ill., Urbana, Ill, 1956); cf. also L. A. Sliv, J. Expt. Theoret. Phys. **22** (1952) 29; and L. A. Sliv and M. A. Listengarten, J. Expt. Theoret. Phys. **21** (1951) 770
3) A. W. Wapstra and G. J. Nijgh, Nuclear Physics **1** (1956) 245
4) E. L. Church and J. Weneser, Phys. Rev. **104** (1956) 1382
5) Hollander, Smith and Rasmussen, Phys. Rev. **105** (1956) 1514
6) Asaro, Stephens, Hollander and Perlman, Nuclear Physics (to be published)
7) G. Kramer, Z. Physik **146** (1956) 187; **147** (1957) 628
8) S. G. Nilsson, Nuclear-Structure Dependence of Conversion Coefficients in Electric Multipole Conversion, UCRL-3803 (June 1957)
9) R. G. Sachs and N. Austern, Phys. Rev. **81** (1951) 705
10) A. Bohr and V. F. Weisskopf, Phys. Rev. **77** (1950) 94
11) L. A. Sliv, J. Expt. Theoret. Phys. **21** (1951) 770
12) S. G. Nilsson, Mat. Fys. Medd. Dan. Vid. Selsk. **29** (1955) no. 16
13) H. Brysk and M. E. Rose, Theoretical Results on Orbital Capture, ORNL-1830 (Jan. (1955)
14) J. R. Reitz, Relativistic Wave Functions for a Fermi-Thomas-Dirac Statistical Atom (University of Chicago, 1949) unpublished
15) G. Alaga, Phys. Rev. **100** (1955) 732
16) G. Alaga, Nuclear Physics **4** (1957) 625
17) S. G. Nilsson, dissertation (Berlingska Boktr., Lund, 1955)
18) D. Chasman and J. O. Rasmussen, in University of California Radiation Laboratory Chemistry Division Quarterly Report, UCRL-3629 (Sept.-Nov. 1956) p. 77
19) B. R. Mottelson and S. G. Nilsson, Mat. Fys. Medd. Dan. Vid. Selsk. (to be published)
20) J. M. Hollander, Phys. Rev. **105** (1956) 1518
21) C. Hoffman and B. Dropesky (1957), private communication from C. Hoffman (Los Alamos Scientific Laboratory)
22) H. Vartapetian, dissertation (Univ. of Paris, 1957) unpublished
23) H. Vartapetian, Compt. Rend. **244** (1957) 65
24) E. H. Wichmann and N. M. Kroll, Phys. Rev. **101** (1956) 843
25) F. R. McGowan, Short-lived Isomeric States of Nuclei, ORNL-952 (Mar. 1951) unpublished
26) H. de Waard, Phil. Mag. **46** (1955) 445
27) Cork, Brice, Martin, Schmid and Helmer, Phys. Rev. **101** (1956) 1042
28) Mize, Bunker and Starner, Phys. Rev. **103** (1956) 182
29) Cork, Brice, Martin, Schmid and Helmer, Phys. Rev. **100** (1955) 1237A
30) Mize, Bunker, and Starner, Phys. Rev. **100** (1955) 1390
31) N. Marty, Compt. Rend. **240** (1955) 963
32) H. de Waard, Phil. Mag **46** (1955) 445

33) Åkerlind, Hartmann and Wiedling, Phil. Mag. **46** (1955) 448
34) Hatch, Boehm, Marmier and duMond, Phys. Rev. **104** (1956) 745
35) D. M. Chase and L. Wilets, Phys. Rev. **101** (1956) 1038
36) S. A. E. Johansson, Phys. Rev. **100** (1955) 835
37) Mihelich, Ward and Jacob, Phys. Rev. **103** (1956) 1285
38) B. R. Mottelson and S. G. Nilsson, Z. Physik **141** (1955) 217
39) P. Marmier and F. Boehm, Phys. Rev. **97** (1955) 103
40) B. Hartmann and T. Wiedling, Phil. Mag. **46** (1955) 1139
41) S. Ofer, Nuclear Physics **3** (1957) 479
42) D. R. Speck and F. A. Jenkins, Phys. Rev. **101** (1956) 1831
43) F. F. Felber, Jr., Nuclear Decay Schemes of Some of the Isotopes of Tantalum (M. S. Thesis), UCRL-3618 (Jan. 1957) unpublished
44) Mann, Nagle and West, Bull. Am. Phys. Soc. **2** (1957) 231; also private communication
45) N. P. Heydenburg and G. M. Temmer, Phys. Rev. **100** (1955) 150
46) Alder, Bohr, Huus, Mottelson and Winther, Revs. Modern Phys. **28** (1956) 432
47) M. R. Lee and R. Katz, Phys. Rev. **93** (1954) 155
48) F. K. McGowan, Phys. Rev. **93** (1954) 163
49) R. L. Graham and J. Walker, Phys. Rev. **94** (1954) 194A
50) N. Marty, J. Phys. Radium **15** (1954) 794A; **16** (1955) 458; Compt. Rend. **238** (1954) 2516
51) M. Vergnes and N. Marty, J. Phys. Radium **17** (1956) 908
52) Dubey, Mandeville and Rothman, Phys. Rev. **103** (1956) 1430
53) E. L. Church and M. Goldhaber, Phys. Rev. **95** (1954) 626A
54) Cohen, Burde and Ofer, Bull. Res. Council Israel **5A** (1955) 87A
55) M. Vergnes and N. Marty, J. Phys. Radium **17** (1956) 908
56) N. Marty and M. Vergnes, Compt. Rend. **242** (1956) 1438
57) S. K. Bhattercherjee and S. Raman, Nuclear Physics **1** (1956) 486
58) Bisi, Germagnoli and Zappa, Nuclear Physics **1** (1956) 593
59) E. L. Church (Brookhaven National Laboratory) private communication to B. R. Mottelson (1956)
60) Murray, Boehm, Marmier and duMond, Phys. Rev. **97** (1955) 1007
61) Alaga, Alder, Bohr and Mottelson, Mat. Fys. Medd. Dan. Vid. Selsk. **29** (1955) no. 9
62) C. J. Gallagher, Jr., unpublished results (1957)
63) A. W. Sunyar, Phys. Rev. **93** (1954) 1122; see also J. W. Mihelich, Phys. Rev. **95** (1954) 626A
64) Mihelich, Scharff, Goldhaber and McKeown, Phys. Rev. **94** (1954) 794A
65. Scharff-Goldhaber, McKeown and Mihelich, Bull. Am. Phys. Soc. **1** (1956) 206 (Cf. NBS data card 54-5-130)
66) G. Scharff-Goldhaber, private communication (1957)
67) Felber, Stephens and Asaro, Phys. Rev. (to be published)
68) Cochran, Mize and Bunker (Los Alamos National Laboratory) private communication from M. E. Bunker (1957)
69) Hollander, Smith and Mihelich, Phys. Rev. **102** (1956) 740
70) G. T. Ewan and J. W. Knowles in Physics Division Progress Report, Chalk River Lab. Report PR-P-31 (1957), 13 and 54; also private communication
71) J. O. Newton and V. S. Shirley, unpublished results (1957)
72) Debrunner, Heer, Kündig and Rüetschi, Helv. Physica Acta **29** (1956) 463
73) Rasmussen, Canavan and Hollander, Phys. Rev. **107** (1957) 141
74) Bunker, Mize and Starner, Bull. Am. Phys. Soc. **2** (1957) 104
75) V. S. Shirley and J. O. Rasmussen, unpublished results (1957)
76) I. Perlman and J. O. Rasmussen, Chapter on Alpha Radioactivity in Handbuch der Physik, Vol. **42** (Springer Verlag, Berlin)

Nuclear Physics **5** (1958) 647—652; © *North-Holland Publishing Co., Amsterdam*
Not to be reproduced by photoprint or microfilm without written permission from the publisher

ELASTIC SCATTERING OF GAMMA-RAYS

N. CINDRO and K. ILAKOVAC
Institute "Rudjer Bošković", Zagreb

Received 21 October 1957

Abstract: Measurements of elastic scattering of 0.66, 1.12 and 1.33 MeV gamma-rays from medium and heavy nuclei, designed to investigate energy and Z dependence, are described and their results presented.

1. Introduction

The elastic scattering of gamma rays by heavy and medium weight elements has recently been studied by many investigators [1–11]) mainly with the aim to separate the different processes by which a gamma-quantum can be scattered by electrons or by nuclear charge.

Except for the nuclear resonance scattering, — and there is only a slight probability for its occurrence — there are three different mechanisms which contribute to the cross section ot the elastic scattering:

(i) the Thomson scattering by the nuclear charge as a whole,
(ii) the Rayleigh scattering by bound electrons,
(iii) the Delbrück scattering by the Coulomb field of the nucleus.

While the Thomson scattering is well known, the problem of determining the angular distribution and the energy and Z dependence of the Rayleigh scattering, which constitutes the principal part of the elastically scattered gamma rays, is not yet completely solved. The first theoretical results were obtained as early as 1935 by Franz [12]), who followed the non-relativistic method of Debye. Using the form factor method, Bethe, Levinger and other authors [13, 14]) extended the calculations to the near-relativistic case and obtained considerably lower figures. Later work has been done by Brown, Woodward and other members of the Birmingham theoretical group [15–18]): with the assumption that in the intermediate state the scattering electron is bound, they obtained the cross sections for the Rayleigh scattering at large angles for heavy elements and for energies up to 1.33 MeV.

The above-mentioned investigations were concerned with a comparison between theoretical (Rayleigh scattering) and experimental angular distributions. We have tried to establish the Z and energy dependence at a fixed angle. In either case experiment is compared with theory. Because of a well known geometry, ratios of cross sections can be determined in our case to a much greater accuracy. It is hoped that this method could be

used to separate the Rayleigh scattering from other processes of elastic scattering.

2. The Experimental Arrangement

The scattering apparatus was as shown schematically on fig. 1. The source of about 100 mC was placed on the top of a lead cone, covered with

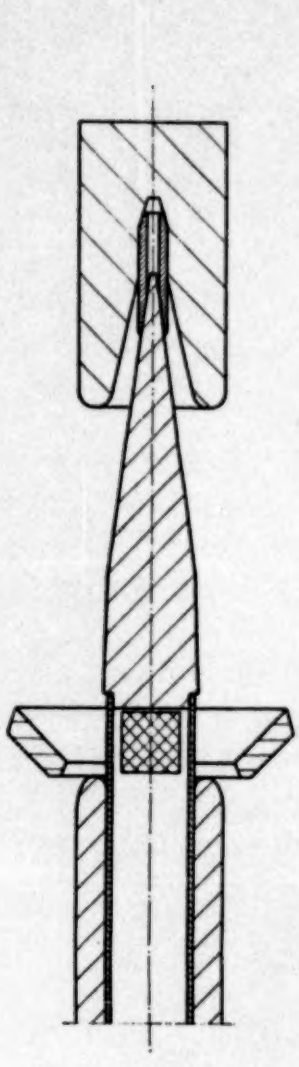

Fig. 1. The scattering apparatus. The lead cone was about 30 cm high.

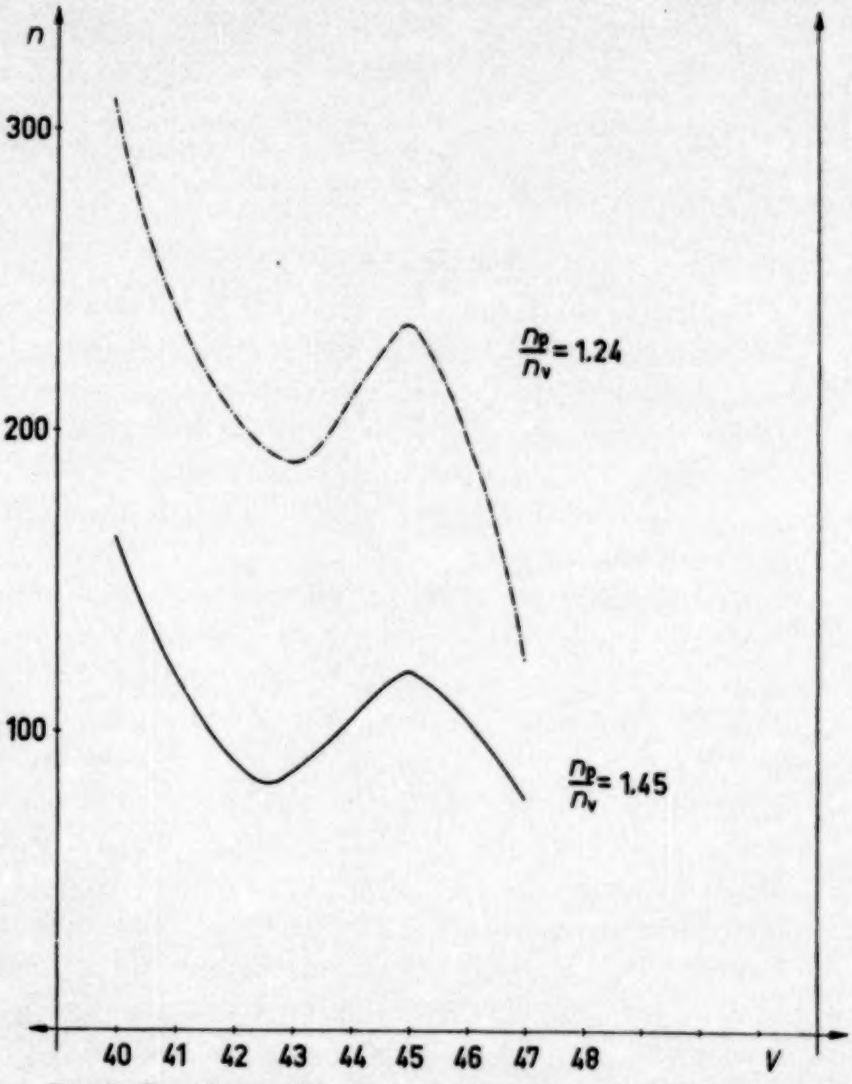

Fig. 2. The photopeaks of elastically scattered 0.66 MeV gamma rays by lead. The peak-to-valley ratio (n_p/n_v) is larger for the "sandwich" scatterer (solid curve) than for the thick scatterer (dotted curve).

a lead shield, such that the gamma rays originating from the source were collimated towards the scatterer. The scattered rays were recorded with a Harshaw $1\frac{1}{2}''$ dia $\times$ $1\frac{1}{2}''$ high NaI(Tl) crystal, mounted on a 6292 Du Mont PMP. Care was taken to protect the crystal from randomly scattered gamma rays from nearby standing objects. The pulses were analysed by a

single channel Ge-diode analyser. The resolving power of the whole system was about 6—7 %, varying with the energy of the gamma rays. The high voltage supply was stable to better than $1 : 5 \times 10^3$ over a period of 10 hours and a temperature variation of 5° C.

The scatterers were made in the form of conical rings. Some of them were of a "sandwich" type, made of thin layers of e.g. lead (0.1—0.2 mm) separated by 1 mm thick layers of paraffine. The probability that a photoelectron gives off a large part of its energy in the form of a gamma quantum in the layer itself is rather small. As, on the other hand, the probability of bremsstrahlung in paraffine is very small, the electron loses its energy mainly by ionisation. The peaks of elastically scattered rays from "sandwich" scatterers were more pronounced than those obtained with thick ones (fig. 2). But even with such scatterers it was not possible to eliminate completely the hard components of the inelastically scattered gamma rays. The elastic peaks obtained were not very sharp, especially for 1.33 MeV gamma rays.

3. Results and Discussion

The measurements were performed with different scatterers and for different gamma ray energies. Al, Fe, Cu, Sn, I, Ba, Hg and Pb were used as scatterers, and the gamma ray sources were Co^{60} (1.33 MeV), Sc^{46} (1.12 MeV) and Cs^{137} (0.66 MeV). The results are listed in table 1 and shown in fig. 3.

TABLE 1

The measured differential cross sections $\bar{\sigma}'(105°)$ in 10^{-29} cm²/sterad for various scatterers

γ-ray energy	Pb	Hg	Ba	I	Sn	Cu	Fe
0.66 MeV	160 ±16	130±14	12 ±2.6	13 ±2.6	10 ±2	1.5±0.5	1.2±0.4
1.12 MeV	12.6±2.5	11±2.2	2.2±0.7	1.1±0.3	1.1±0.3	0.21	0.14
1.33 MeV	11±2	9±2					

The errors given in table 1 and shown in the diagram are standard deviations of results. The values for Fe and Cu are only tentative. It is difficult to compare our results with those of other investigators, owing to the different angles at which the measurements were made, but, if one extrapolates their results it seems that ours are either in agreement or slightly lower [10, 11]).

The angle of scattering was 105°±10°, i.e., the results were averaged from 95° to 115°, with the assumption that the angular distribution is that of Franz, $(1+\cos^2\theta)/\sin^3\frac{1}{2}\theta$. This averaging reduced the measured cross sections by less than 3 % as compared to the medium scattering angle (115°). All corrections due to conical ring shape of the scatterers as well

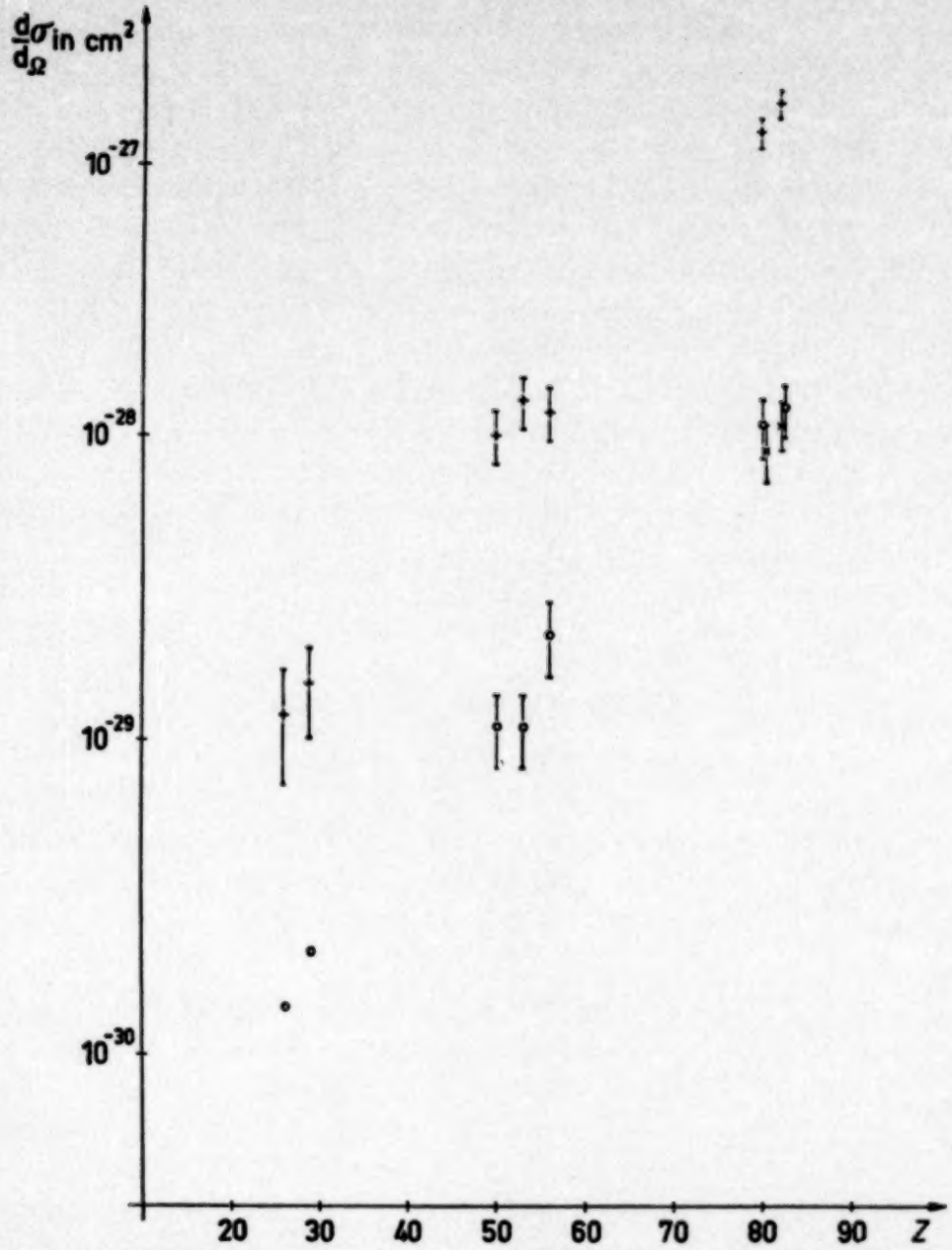

Fig. 3. The measured differential cross sections in cm²/sterad as functions of the atomic number Z. + : 0.66 MeV; ○ : 1.12 MeV; × : 1.33 MeV.

TABLE 2

The differential cross section $\bar{\sigma}'(105°)$ for lead and mercury, divided by the differential cross section for baryum, iodine and tin at the same angle, at energies of 0.66 and 1.12 MeV

X =	Ba	I	Sn
		0.66 MeV	
σ'_{Pb}/σ'_X	12.73±1.3	12.08±1.2	14.2±1.4
σ'_{Hg}/σ'_X	10.75±1.1	10.14±1.1	11.92±1.2
		1.12 MeV	
σ'_{Pb}/σ'_X	6.13±0.6	12.69±1.3	10.93±1.1
σ'_{Hg}/σ'_X	5.20±0.5	10.72±1.1	9.32±0.9

as the absorption of the gamma rays in the scatterers were taken into account.

The measurement of the absolute effectiveness of the detector was avoided by the well known method of comparing two sources of different intensities [10]).

The principal difficulty in estimating the cross sections was to separate the rays scattered elastically from those inelastically scattered, counted in the channel. Although the channel was rather narrow (140 keV for Co^{60} 1.33 MeV gamma rays and proportionally narrower for other gamma rays); a relatively great number of inelastically scattered gamma rays was recorded. The estimation of their amount was the principal source of error. This was done in three different ways:

(i) comparing the scattering by different scatterers with that of an Al scatterer which gave about the same number of Compton scattered rays (total count);

(ii) subtracting the obtained peak from a polynomial curve of best fit;

(iii) using the results given by Storruste [11]).

By all these methods the contribution of the inelastically scattered rays was estimated to be from 15 to 35 %, depending on the material and the thickness of the scatterer.

The results given in table 1 and fig. 3 are those obtained for elastic scattering. The values for Pb and Hg at 0.66 MeV are in agreement with the calculations of the Birmingham group, but those at 1.12 and 1.33 MeV are considerably higher. As one can neglect the Thomson scattering, the values are a measure of the Rayleigh scattering and, perhaps, of its interference with the Delbrück scattering. From these experiments no definite conclusions can be drawn about the Delbrück scattering.

The ratios of elastic scattering of Co^{60}, Sc^{46} and Cs^{137} gamma rays from various elements are presented in table 2. These values are more accurate than those of cross sections because simple comparisons of scattering with the same geometry were made. The main source of inaccuracy was again estimating the percentage due to elastic scattering in the total count of the detector.

These results are still not of such an accuracy that reliable conclusions about the Rayleigh and other scattering processes could be drawn. However, this method seems to be a promising way to investigate the elastic scattering of gamma rays, and further experiments in this direction are in progress.

References

1) P. B. Moon, Proc. Phys. Soc. **63** (1950) 1189
2) R. R. Wilson, Phys. Rev. **82** (1951) 295
3) W. G. Dawey, Proc. Phys. Soc. **66** (1953) 1059

4) R. R. Wilson, Phys. Rev. **90** (1953) 720
5) L. Goldzahl et P. Eberhard, Comp. Rend. **240** (1955) 965
6) K. Mann, Phys. Rev. **98** (1955) 234
7) J. R. Cook, Proc. Phys. Soc. **68** (1955) 1171
8) A. K. Mann, Phys. Rev. **101** (1956) 4
9) H. Shopper, Z. für Phys. **147** (1957) 257
10) L. Goldzahl et P. Eberhard, Journ. de Physique **18** (1957) 33
11) S. Messelt and A. Storruste, Proc. Phys. Soc. **70** (1957)
12) W. Franz, Z. für Phys. **98** (1936) 314
13) J. S. Levinger, Phys. Rev. **87** (1952) 656
14) J. S. Levinger, Phys. Rev. **101** (1956) 1020
15) G. E. Brown and J. B. Woodward, Proc. Phys. Soc. **65** (1952) 977
16) G. E. Brown, R. E. Peierls and J. B. Woodward, Proc. Roy. Soc. A **227** (1954) 51
17) G. E. Brown and D. F. Mayers, Proc. Roy. Soc. A **234** (1956) 387
18) G. E. Brown and D. F. Mayers, private communication

Nuclear Physics **5** (1958) 653—668; © *North-Holland Publishing Co., Amsterdam*
Not to be reproduced by photoprint or microfilm without written permission from the publisher

ANGULAR DISTRIBUTION IN REACTIONS INVOLVING THE FORMATION OF THREE LOW ENERGY PARTICLES, WITH APPLICATION TO τ^+ MESON DECAY

V. N. GRIBOV

Physico-Technical Institute of the USSR Academy of Sciences, Leningrad

Received 18 June 1957

Abstract: The effect of interaction in the final state on the angular distribution in reactions involving the formation of three low energy particles is considered. In the case of non-resonance interaction the angular distribution can be expressed in terms of scattering amplitudes of pairs of particles. It is shown how the meson-meson scattering amplitudes can be deduced from the angular distribution of the decay products of the $\tau^+ \to 2\pi^+ + \pi^-$, $\tau^+ \to 2\pi^0 + \pi^+$ reactions. Experimental data presently available are insufficient for determining these amplitudes.

1. Statement of Problem

The angular distribution in reactions involving the formation of three low energy particles can be studied in the same way as the angular distributions of two particles processes are investigated, that is, by means of angular momentum expansions. However, even when the particle energy is not large, the energy and momentum dependence of the matrix elements determining the angular distribution is not a very simple one. In the case of two particles this dependence is mainly determined by the coefficient of transmission through the centrifugal barrier, whereas for three particles it significantly depends on the scattering amplitude of a pair of particles in the final state. The purpose of the present paper is a study of the angular distribution in three-particle low energy reactions and elucidation of the possibility of determining the scattering amplitudes from this distribution. The state of three particles in the c.m.s. is specified by two momenta: by the momentum of relative motion of two particles $\mathbf{k}_{12}$ and the momentum of the third particle $\mathbf{p}_3$. This corresponds to introduction of Jacobi variables

$$R = \frac{m_1\mathbf{r}_1 + m_2\mathbf{r}_2 + m_3\mathbf{r}_3}{m_1+m_2+m_3}; \quad \boldsymbol{\rho}_3 = \mathbf{r}_3 - \frac{m_1\mathbf{r}_1 + m_2\mathbf{r}_2}{m_1+m_2}; \quad \boldsymbol{\rho}_{12} = \mathbf{r}_1 - \mathbf{r}_2,$$

and similarly for $\boldsymbol{\rho}_2$, $\boldsymbol{\rho}_{13}$; $\boldsymbol{\rho}_1$, $\boldsymbol{\rho}_{23}$:

$$\begin{aligned} \boldsymbol{\rho}_2 &= -\frac{m_3}{m_1+m_3}\boldsymbol{\rho}_3 - \frac{m_1(m_1+m_2+m_3)}{(m_1+m_3)(m_1+m_2)}\boldsymbol{\rho}_{12}, \\ \boldsymbol{\rho}_{13} &= -\boldsymbol{\rho}_3 - \frac{m_2}{m_1+m_2}\boldsymbol{\rho}_{12}. \end{aligned} \tag{1}$$

The amplitude of the reaction $\langle \mathbf{p}_3, \mathbf{k}_{12} | S | \Phi_1 \rangle$ (Φ_1 is the initial state, S is the S-matrix) can be expanded in a series of spherical functions of the angles of vectors $\mathbf{p}_3$ and $\mathbf{k}_{12}$:

$$\langle \mathbf{p}_3, \mathbf{k}_{12} | S | \Phi_1 \rangle = \sum_{LM\Lambda\mu} Y_{LM}(\Omega_{\mathbf{p}_3}) Y_{\Lambda\mu}(\Omega_{\mathbf{k}_{12}}) \langle \Phi_{LMp_3, \Lambda\mu k_{12}} | S | \Phi_1 \rangle; \qquad (2)$$

Λ has the meaning of angular momentum of particles 1 and 2; L is the angular momentum of the third particle relative to the centre of mass of the first two particles; μ and M are their respective projections.

For simplicity we shall consider spinless particles.

If interaction in the final state is neglected and it be assumed that the three particles are created in a finite volume of radius r_0, the matrix elements in the right hand part will be proportional to $p_3{}^L\, k_{12}{}^\Lambda$ at low energies, since the matrix elements can always be represented as integrals over the region $\varrho_3\ \varrho_{12} < r_0$ and in this region

$$\Phi_{LMp_3, \Lambda\mu k_{12}} \approx \frac{(p_3\varrho_3)^L (k_{12}\varrho_{12})^\Lambda}{(2L-1)!!(2\Lambda-1)!!}$$

if $p_3 r_0 \ll L$, $k_{12} r_0 \ll \Lambda$. However, this will not be true if interaction in the final state is taken into account since in this case the integration should not only be performed over the region in which the particles are created but also over the region in which they interact, such as over the region

$$\varrho_{13} = \left| \boldsymbol{\rho}_3 - \frac{m_1}{m_1+m_2} \boldsymbol{\rho}_{12} \right| < r_0$$

in which $\Phi_{LMp_3, \Lambda\mu k_{12}}$ does not have such a simple form.

In order to find the energy dependence of the matrix elements in this case it will be convenient to consider the interaction in the final state separately. This can be done if the interaction energy operator U can be represented as a sum $V+W$ in which W refers only to creation of the particles and V to their interaction. In such reactions as

$$\tau^+ \to 2\pi^+ + \pi^0, \qquad \gamma + \mathrm{p} \to \mathrm{p} + \pi^+ + \pi^-$$

this is just the usual type of division into weak and strong interactions. Instead of (2) we may write

$$\langle \mathbf{p}_3, \mathbf{k}_{12} | S | \Phi_1 \rangle = \sum_{j\mu L\Lambda\nu} C^{j\mu}_{LM, \Lambda\nu} Y_{LM}(\Omega_{\mathbf{p}_3}) Y_{\Lambda\nu}(\Omega_{\mathbf{k}_{12}}) \langle \Psi_{j\mu Lp_3 \Lambda k_{12}} | W | \Psi_1{}^{j\mu} \rangle; \quad (3)$$

$\Psi_{j\mu Lp_3 \Lambda k_{12}}$ is the wave function for three interacting particles with a total angular momentum j and its projection μ; at infinity this function changes into the wave function of three particles with definite L and Λ.

$\Psi_1{}^{j\mu}$ is the exact wave function of the system and $C^{j\mu}_{LM, \Lambda\nu}$ are Clebsch-Gordan coefficients.

In the matrix elements of eq. (3) the integration is carried out only over

the region ϱ_3, $\varrho_{12} < r_0$. However, the dependence of $\Psi_{j\mu L p_3 \Lambda k_{12}}$ on $\mathbf{p}_3$ and $\mathbf{k}_{12}$ is now more complex. At low energies and $L = \Lambda = 0$ this wave function is still independent of p_3 and k_{12}. For other values of L, Λ the change is very significant. The appearance of the factors $p_3{}^L$ and $k_{12}{}^\Lambda$ in the wave function for small values of ϱ_3 and ϱ_{12} is due to the presence of the coefficients of transmission through the centrifugal barrier which must be surmounted before the particles can enter the region of small ϱ_3 and ϱ_{12}. In the presence of an interaction the particles may pass around the barrier instead of passing under it. Two of three particles, such as 1 and 3, may approach each other if they are located in the region of large ϱ_3 and ϱ_{12}. In order to approach each other it is not necessary for the particles to surmount the centrifugal barrier because the angular momentum of relative motion of particles 1 and 3 is indefinite. Upon close approach particles 1 and 3 may interact in such a way that the whole system will go over to a state with $L = \Lambda = 0$ (if $j = 0$) inasmuch as the total angular momentum j is the only conservative quantity. In the new state the centrifugal barrier is no longer effective and all three particles may gather together. Thus for small ϱ_{12}, ϱ_3 the wave function will not be proportional to the barrier transmission coefficient but to the transition amplitude from a state with L, $\Lambda \neq 0$ to a state with $\Lambda = L = 0$ (if $j = 0$) under the condition, of course, that this amplitude is larger than the transmission coefficient. It will be shown that for any L, Λ this amplitude is proportional to the first power of k_{12} or p_3 and therefore for small k_{12} and p_3 and sufficiently large L and Λ it is larger than the transmission coefficient. Under this condition it may be expected that for ϱ_3, $\varrho_{12} \approx r_0$,

$$\Psi_{j=0,\, L p_3,\, \Lambda k_{12}} = C_L \Psi_{j=0,\, 0 p_3,\, 0 k_{12}}, \tag{4}$$

where C_L depends only on p_3, k_{12} and on the scattering amplitudes of pairs of mutually scattered particles. If the angular momentum of the initial state is zero we find, by inserting (4) into (3), that the angular distribution is defined by the sum

$$\sum_{LM} C^{00}_{LM,\, L-M}\, Y_{LM}(\Omega_{\mathbf{p}_3}) Y_{L-M}(\Omega_{\mathbf{k}_{12}}) C_L \tag{5}$$

and is independent of the form of the interaction $\hat{W}$. Coefficients C_L can be found by examining the wave function of the three interacting particles. An example of a reaction with such properties is the τ-meson decay, which is considered in detail in section 3. In this case [1, 2]) $j = 0$, $L = \Lambda = 0, 2, 4 \ldots$ that is, for all values of L the examined transition to a state with $L = 0$ is more important than direct penetration through the centrifugal barrier. A relation similar to (5), but only for the imaginary part of the amplitude, was obtained for this reaction in ref. [3]) by considering the general properties of the S-matrix.

A proof of relation (4) is presented in the present paper and coefficients C_L are expressed in terms of the scattering amplitudes for a pair of particles in the case when the interaction is not of a resonance type at zero energy, i.e., when the scattering amplitude at zero energy is of the order of the range of the forces.

This condition is satisfied in interactions of π-mesons with nucleons and, possibly, in the interaction between two π-mesons. Assuming the latter to be true it is shown how the pion-pion scattering amplitude can be approximately determined from the angular distribution in τ-meson decay. We shall confine our attention in this paper to states with $j = 0$.

2. Wave Functions of Three Particle System

2.1. THE WAVE EQUATION

Considering the particles to be non-relativistic we shall consider the Schroedinger equation

$$\left\{-\frac{\hbar^2}{2\mu_{12}}\nabla^2_{\rho_{12}}-\frac{\hbar^2}{2\mu_3}\nabla^2_{\rho_3}+V\right\}\Psi = E\Psi,$$
$$\frac{1}{\mu_{12}}=\frac{1}{m_1}+\frac{1}{m_2};\quad \frac{1}{\mu_3}=\frac{1}{m_3}+\frac{1}{m_1+m_2}. \tag{6}$$

The potential V can be represented in the form

$$V = V_{12}(\varrho_{12})+V_{13}(\varrho_{13})+V_{23}(\varrho_{23})+V_{123}(\varrho_{12},\ \varrho_3). \tag{7}$$

It will be assumed that a certain r_0 exists for which $V_{ik}(\varrho_{ik}) = 0$ if $\varrho_{ik} > r_0$ and $V_{123}(\varrho_{12}, \varrho_3) = 0$ if either ϱ_3 or ϱ_{12} is larger than r_0. As wave functions with various boundary conditions at infinity will interest us, it will be convenient to take these conditions into account immediately by changing to an integral equation with the help of the Green's function. The latter satisfies the equation

$$\left\{-\frac{\hbar^2}{2\mu_{12}}\nabla^2_{\rho_{12}}-\frac{\hbar^2}{2\mu_3}\nabla^2_{\rho_3}-E\right\}G(\boldsymbol{\rho}_{12},\ \boldsymbol{\rho}_3) = \delta(\boldsymbol{\rho}_{12})\delta(\boldsymbol{\rho}_3). \tag{8}$$

Since we are interested in a solution which is the sum of a plane and incoming waves we find from here

$$G(\boldsymbol{\rho}_{12},\ \boldsymbol{\rho}_3) = \frac{1}{(2\pi)^6}\int \mathrm{d}^3p\,\mathrm{d}^3k\,\frac{\mathrm{e}^{i\mathbf{p}\cdot\boldsymbol{\rho}_3}\cdot\mathrm{e}^{i\mathbf{k}\cdot\boldsymbol{\rho}_{12}}}{\dfrac{\hbar^2p^2}{2\mu_3}+\dfrac{\hbar^2k^2}{2\mu_{12}}-E-i\varepsilon}. \tag{9}$$

It will also be useful to have the explicit expression

$$G(\boldsymbol{\rho}_{12},\ \boldsymbol{\rho}_3) = -\frac{i}{8\pi^2\hbar^2}(\mu_{12}\mu_3)^{\frac{1}{2}}\cdot\frac{\varkappa^2 H_2^{(2)}(\varkappa\sqrt{\gamma_{12}\varrho_{12}^2+\gamma_3\varrho_3^2})}{\gamma_{12}\varrho_{12}^2+\gamma_3\varrho_3^2}$$
$$\varkappa = \frac{1}{\hbar}\sqrt{2E(\mu_{12}\mu_3)^{\frac{1}{2}}};\quad \gamma_{12}=\frac{1}{\gamma_3}=\left(\frac{\mu_{12}}{\mu_3}\right)^{\frac{1}{2}}. \tag{10}$$

The integral equation has the form

$$\Psi(\boldsymbol{\rho}_{12},\boldsymbol{\rho}_3)=\Phi(\boldsymbol{\rho}_{12},\boldsymbol{\rho}_3)-\int G(\boldsymbol{\rho}_{12}-\boldsymbol{\rho}'_{12},\boldsymbol{\rho}_3-\boldsymbol{\rho}'_3)V_{12}(\varrho'_{12})\Psi(\boldsymbol{\rho}'_{12},\boldsymbol{\rho}'_3)\mathrm{d}^3\varrho'_{12}\,\mathrm{d}^3\varrho'_3$$
$$-\int G(\boldsymbol{\rho}_{13}-\boldsymbol{\rho}'_{13},\ \boldsymbol{\rho}_2-\boldsymbol{\rho}'_2)V_{13}(\boldsymbol{\rho}'_{13})\Psi(\boldsymbol{\rho}'_{13}\,\boldsymbol{\rho}'_2)\mathrm{d}^3\varrho'_{13}\,\mathrm{d}^3\varrho'_2-(1\to 2)\quad(11)$$
$$-\int G(\boldsymbol{\rho}_{12}-\boldsymbol{\rho}'_{12},\ \boldsymbol{\rho}_3-\boldsymbol{\rho}'_3)V_{123}(\boldsymbol{\rho}'_{12}\,\boldsymbol{\rho}'_3)\Psi(\boldsymbol{\rho}'_{12},\ \boldsymbol{\rho}'_3)\mathrm{d}^3\varrho'_{12}\,\mathrm{d}^3\varrho'_3.$$

$\Phi(\boldsymbol{\rho}_{12},\ \boldsymbol{\rho}_3)$ is the wave function in the absence of interaction. For a state with $j=0$, $L=\Lambda=l$ we choose $\Phi(\boldsymbol{\rho}_{12},\ \boldsymbol{\rho}_3)$ in the form

$$\Phi(\boldsymbol{\rho}_{12},\ \boldsymbol{\rho}_3)=\Phi_l=f_l(p_3\varrho_3)f_l(k_{12}\varrho_{12})P_l(\cos\vartheta),$$
$$f_l(x)=\sqrt{\frac{\pi}{2x}}J_{l+\frac{1}{2}}(x);\qquad(12)$$

ϑ is the angle between $\boldsymbol{\rho}_3$ and $\boldsymbol{\rho}_{12}$.

In order to prove the statement made in section 1 (eq. (4)) it is not necessary to consider equation (11) in the region $\varrho_{12},\ \varrho_3\approx r_0$, that is, in the region in which three-particle forces are effective. It should be sufficient to know the wave functions, say, in the region $\varrho_{12}\approx r_0, \varrho_3\gg r_0, \varrho_{12},\varrho_3\ll 1/\varkappa$. Evidently this region exists only if $\varkappa r_0\ll 1$ and in the following exposition this will be assumed to be the case. At zero energy ($\varkappa\to 0$) this signifies that it should be sufficient to know the functions for arbitrary ϱ_{12} and $\varrho_3\to\infty$. Indeed, since $\Psi_{j=0,\,lp_3\,lk_{12}}$ and $\Psi_{j=0,\,0p_3,\,0k_{12}}$ satisfy the same equation and finiteness conditions at $\varrho_{12},\ \varrho_3\to 0$, then, if they are identical within a factor for arbitrary ϱ_{12} and $\varrho_3\to\infty$, they should coincide within the same accuracy at any other point. It will be seen later on that the zero energy solution will be sufficient for us. Taking into account the foregoing we shall not consider the solution of equation (11) for $\varrho_{12},\ \varrho_3\approx r_0$, but only for those values which lie in the regions

$$\varrho_{12}\approx r_0\qquad \varrho_3\gg r_0\qquad \varrho_{12},\ \varrho_3\lesssim 1/\varkappa\qquad(13a)$$
$$\varrho_{13}\approx r_0\qquad \varrho_2\gg r_0\qquad \varrho_{13},\ \varrho_2\lesssim 1/\varkappa\qquad(13b)$$
$$\varrho_{23}\approx r_0\qquad \varrho_1\gg r_0\qquad \varrho_{23},\ \varrho_1\lesssim 1/\varkappa.\qquad(13c)$$

2.2. STATES WITH $l=0$

It will be shown that in the zero approximation with respect to r_0/ϱ_3 and $\varkappa r_0$ the wave function, say in region (13a), will be determined only by the interaction between particles 1 and 2 and has the following form for $\Phi=\Phi_0$:

$$\Psi_0=\frac{\sin p_3\varrho_3}{p_3\varrho_3}\varphi_{12}(\varrho_{12})\qquad(14a)$$

where $\varphi_{12}(\varrho_{12})$ is the wave function of particles 1 and 2 at zero energy. This expression can be obtained from (12) by substituting $\varphi_{12}(\varrho_{12})$ for

$\sin k_{12}\varrho_{12}/k_{12}\varrho_{12}$. In order to obtain the solution in regions (13b) and (13c) for the same value of Φ_l, $\Phi_l(\varrho_{12}, \varrho_3)$ should first be expressed in terms of such variables as ϱ_2 and ϱ_{13}. It is shown in appendix 1 that

$$\begin{aligned}\Phi_l &= f_l(p_3\varrho_3)f_l(k_{12}\varrho_{12})P_l(\cos\vartheta)\\ &= \tfrac{1}{2}\sum_{l'}\int \mathrm{d}\cos\vartheta_{\mathbf{p}_3\mathbf{k}_{12}} P_l(\cos\vartheta_{\mathbf{p}_3\mathbf{k}_{12}})P_{l'}(\cos\vartheta_{\mathbf{p}_3\mathbf{k}_{12}})(2l'+1)\\ &\times f_{l'}(p_2\varrho_2)f_{l'}(k_{13}\varrho_{13})P_{l'}(\cos\vartheta_{\boldsymbol{\varrho}_{13}\boldsymbol{\varrho}_2}),\end{aligned} \tag{15}$$

with

$$\begin{aligned}\mathbf{p}_2 &= -\frac{m_3}{m_1+m_2}\mathbf{p}_3+\mathbf{k}_{12},\\ \mathbf{k}_{13} &= -\frac{m_3}{m_1+m_3}\mathbf{k}_{12}-\frac{m_2(m_1+m_2+m_3)}{(m_1+m_3)(m_1+m_2)}\mathbf{p}_3.\end{aligned} \tag{16}$$

On the right hand side of (15) the quantities p_2, k_{13} and $\cos\vartheta_{\mathbf{p}_3\mathbf{k}_{13}}$ should be expressed in terms of p_3, k_{12} and $\cos\vartheta_{\mathbf{p}_3\mathbf{k}_{12}}$ and the integration carried out over $\cos\vartheta_{\mathbf{p}_3\mathbf{k}_{12}}$. If only interaction between particles 1 and 2 is taken into account we obtain in region (13b)

$$\Psi_0 = \tfrac{1}{2}\int \mathrm{d}\cos\vartheta_{\mathbf{p}_3\mathbf{k}_{12}}\frac{\sin p_2\varrho_2}{p_2\varrho_2}\varphi_{13}(\varrho_{13}) \tag{14b}$$

and a similar expression for $\varphi_{13}(\varrho_{13})$. Analogously, in region (13c)

$$\Psi_0 = \tfrac{1}{2}\int \mathrm{d}\cos\vartheta_{\mathbf{p}_3\mathbf{k}_{12}}\frac{\sin p_1\varrho_1}{p_1\varrho_1}\varphi_{23}(\varrho_{23}) \tag{14c}$$

the meaning of the notations being evident.

In order to prove formulae (14a, b, c) we shall ascertain just what regions of the variables are important in the integrals entering (11). Consider the first of the integrals in region (13a). Condition (13a) and the presence of $V_{12}(\varrho'_{12})$ in the integrand imply that $\varrho_{12}, \varrho'_{12} \approx r_0$. Under these conditions $G(\boldsymbol{\rho}_{12}-\boldsymbol{\rho}'_{12}, \boldsymbol{\rho}_3-\boldsymbol{\rho}'_3)$ considered as a function of $\boldsymbol{\rho}'_3-\boldsymbol{\rho}_3$ has a sharp maximum at $\boldsymbol{\rho}'_3 = \boldsymbol{\rho}_3$, the width being of the order of $|\boldsymbol{\rho}_{12}-\boldsymbol{\rho}'_{12}|$. In the vicinity of the maximum

$$G(\boldsymbol{\rho}_{12}-\boldsymbol{\rho}'_{12}, \boldsymbol{\rho}_3-\boldsymbol{\rho}'_3) \approx \frac{(\mu_{12}\mu_3)^{\frac{1}{2}}}{2\pi^2\hbar^2}\cdot\frac{1}{(\gamma_{12}|\boldsymbol{\rho}_{12}-\boldsymbol{\rho}'_{12}|^2+\gamma_3|\boldsymbol{\rho}_3-\boldsymbol{\rho}'_3|^2)^2}. \tag{17}$$

If $\Psi(\boldsymbol{\rho}'_{12}, \boldsymbol{\rho}'_3)$ as a function of $\boldsymbol{\rho}'_3$ appreciably varies over distances of the order of $1/\varkappa$ it will be possible in the zero approximation with respect to r_0/ϱ_3 and $\varkappa r_0$ to write it before the integral with respect to ϱ'_3, that is, to replace $\Psi(\boldsymbol{\rho}'_{12}, \boldsymbol{\rho}'_3)$ by $\Psi(\boldsymbol{\rho}'_{12}, \boldsymbol{\rho}_3)$. Performing after this the integration over ϱ'_3 we find that the term under consideration equals

$$-\frac{1}{4\pi}\frac{2\mu_{12}}{\hbar^2}\int\frac{1}{|\boldsymbol{\rho}_{12}-\boldsymbol{\rho}'_{12}|}V(\varrho'_{12})\Psi(\boldsymbol{\rho}'_{12}, \boldsymbol{\rho}_3)\mathrm{d}^3\varrho'_{12}. \tag{18}$$

In the third and fourth terms of equation (11) the functions do not have such a pronounced maximum because, for example, although $\varrho'_{13} \approx r_0$, ϱ_{13} is nevertheless large. Those values of the variables which coincide respectively with (13b) and (13c) are important in the integrals. The integration region in the last term of equation (11) is restricted by the condition $\varrho'_{12}, \varrho'_3 < r_0$ and this term is therefore approximately equal to

$$-\frac{i\mu_{12}}{8\pi^2\hbar^2}\left(\frac{\mu_{12}}{\mu_3}\right)^{\frac{1}{2}}\frac{\varkappa^2}{\varrho_3^2}H_2^{(2)}(\varkappa\varrho_3)\int V_{123}(\boldsymbol{\rho}'_{12},\ \boldsymbol{\rho}'_3)\Psi(\boldsymbol{\rho}'_{12},\ \boldsymbol{\rho}'_3)\mathrm{d}^3\varrho'_{12}\,\mathrm{d}^3\varrho'_3.$$

The latter integral is of the order of $\bar{V}r_0^6$ and if, as usual, $(\mu_{12}/\hbar)\bar{V}r_0^2 \lesssim 1$, one may neglect with a high degree of accuracy the last term in (11). This term will be dropped in all subsequent formulae.

It follows from the foregoing that in order to prove formulae (14a, b, c) it is necessary, for example in region (13a), to insert (14a, b, c) respectively in the second, third and fourth terms of (11). This substitution yields

$$\begin{aligned}\frac{\sin p_3\varrho_3}{p_3\varrho_3}\varphi_{12}(\varrho_{12}) &= \frac{\sin p_3\varrho_3}{p_3\varrho_3} - \frac{\mu_{12}}{2\pi\hbar^2}\int\frac{V_{12}(\varrho'_{12})}{|\boldsymbol{\rho}_{12}-\boldsymbol{\rho}'_{12}|}\varphi(\varrho'_{12})\mathrm{d}^3\varrho'_{12}\frac{\sin p_3\varrho_3}{p_3\varrho_3}\\ &+\tfrac{1}{2}\int\mathrm{d}\cos\vartheta_{\mathbf{p}_3\mathbf{k}_{12}}\left[\frac{\sin p_2\varrho_3}{p_2\varrho_2}\frac{\mathrm{e}^{-ik_{13}\rho_{13}}}{\varrho_{13}}a_{13}+\frac{\sin p_1\varrho_1}{p_1\varrho_1}\frac{\mathrm{e}^{ik_{23}\rho_{23}}}{\varrho_{23}}a_{23}\right].\end{aligned} \tag{19}$$

The integration which leads to this expression can be easily performed by using representation (9) for the Green's function;

$$a_{13} = -\frac{\mu_{13}}{2\pi\hbar^2}\int V_{13}(\varrho'_3)\varphi_{13}(\varrho'_{13})\mathrm{d}^3\varrho'_{13}$$

is the zero energy scattering amplitude for particles 1 and 3. A similar formula holds for a_{23}. If $a_{13}, a_{23} \approx r_0$ that is, no resonance scattering is observed at zero energy, the last term in (19) can be neglected in the zero approximation in r_0/ϱ_3. Neglecting this term we obtain

$$\varphi_{12}(\varrho_{12}) = 1 - \frac{\mu_{12}}{2\pi\hbar^2}\int\frac{V_{12}(\varrho'_{12})}{|\boldsymbol{\rho}_{12}-\boldsymbol{\rho}'_{12}|}\varphi_{12}(\varrho'_{12})\mathrm{d}^3\varrho'_{12} \tag{20}$$

which is identical with the equation for the zero energy wave function for particles 1 and 2. In conjunction with analogous considerations for regions (13b) and (13c) this proves formulae (14a, b, c). In the regions which are of interest for us we have thus found the zero approximation wave function. In order to determine it in the first approximation we write

$$\Psi_0 = \Psi_0^{(0)} + \Psi_0^{(1)}. \tag{21}$$

Inserting in eq. (11) for the region (13a) and carrying out the integration with account of the previous considerations we obtain

$$\Psi^{(1)} = \frac{\sin p_3\varrho_3}{p_3\varrho_3} ik_{12}a_{12} + \tfrac{1}{2}\int \mathrm{d}\cos\vartheta_{\mathbf{p}_3\mathbf{k}_{12}}\left[\frac{\sin p_2\varrho_2}{p_2\varrho_2}\cdot\frac{\mathrm{e}^{-ik_{13}\rho_{13}}}{p_{13}}a_{13}\right.$$
$$\left. + \frac{\sin p_1\varrho_1}{p_1\varrho_1}\frac{\mathrm{e}^{-ik_{23}\rho_{23}}}{\varrho_{23}}a_{23}\right] - \frac{\mu_{12}}{2\pi\hbar^2}\int\frac{V_{12}(\varrho'_{12})}{|\varrho_{12}-\varrho'_{12}|}\Psi_0^{(1)}(\varrho'_{12},\ \varrho_3)\mathrm{d}^3\varrho'_{12}. \tag{22}$$

Substituting in the second term from the right ϱ_3 for ϱ_{13} and ϱ_{23} and $-(m_3/(m_1+m_3))\varrho_3$ and $-(m_3/(m_2+m_3))\varrho_3$ respectively for ϱ_2 and ϱ_1 in accord with (1), we find for Ψ_0 in region (13a) in a first approximation

$$\Psi_0 = \left\{\frac{\sin p_3\varrho_3}{p_3\varrho_3} + \tfrac{1}{2}\int \mathrm{d}\cos\vartheta_{\mathbf{p}_3\mathbf{k}_{12}}\left[\frac{\sin\frac{\mu_{13}}{m_1}p_2\varrho_3}{\frac{\mu_{13}}{m_1}p_2\varrho_3}\cdot\frac{\mathrm{e}^{-ik_{13}\rho_3}}{\varrho_3}a_{13}\right.\right.$$
$$\left.\left. + \frac{\sin\frac{\mu_{23}}{m_2}p_1\varrho_3}{\frac{\mu_{23}}{m_2}p_1\varrho_3}\cdot\frac{\mathrm{e}^{-ik_{23}\rho_3}}{\varrho_3}a_{23}\right]\right\}\varphi_{12}(\varrho_{12}) \tag{23}$$

and similar expressions for the other two regions.

Up to the present no restrictions were imposed on the product $\varkappa\varrho_3$. Consider now the wave function in the region $\varrho_{12}\approx r_0 \ll \varrho_3 \ll 1/\varkappa$ mentioned at the beginning of this section. In this region

$$\Psi_0 = \left[1 + \frac{a_{13}}{\varrho_3} + \frac{a_{23}}{\varrho_3} - i(k_{12}a_{12}+k_{13}a_{13}+k_{23}a_{23})\right]\varphi_{12}(\varrho_{12})$$
$$+ \text{ terms of the order of } \varkappa^2\varrho_3^2,\ r_0^2/\varrho_3^2,\ \varkappa r_0^2/\varrho_3;$$
$$k_{13} = \tfrac{1}{2}\int \mathrm{d}\cos\vartheta_{\mathbf{p}_3\mathbf{k}_{12}}k_{13};$$

or within the same accuracy

$$\Psi_0 = [1-i(k_{12}a_{12}+k_{13}a_{13}+k_{23}a_{23})]\left(1+\frac{a_{13}}{\varrho_3}+\frac{a_{23}}{\varrho_3}\right)\varphi_{12}(\varrho_{12}). \tag{24}$$

On the other hand, any solution of the Schroedinger equation for ϱ_{12}, $\varrho_3 \ll 1/\varkappa$ can be written in the form

$$C(k_{12},\ p_3)f(\rho_{12},\ \rho_3)\ [1 + \text{terms of the order of } \varkappa^2\varrho_{12}^2,\ \varkappa^2\varrho_3^2] \tag{25}$$

where $f(\varrho_{12},\ \varrho_3)$ is the zero energy solution.

Comparing (29) and (25) we conclude that for $\varrho_{12},\ \varrho_3 \approx r_0 \ll 1/\varkappa$

$$\Psi_0(\rho_{12},\ \rho_3) = (1-ik_{12}a_{12}-ik_{13}a_{13}-ik_{23}a_{23})f(\rho_{12},\ \rho_3)$$
$$+ \text{ terms of the order of } \varkappa^2 r_0^2; \tag{26}$$

$f(\varrho_{12},\ \varrho_3)$ is the zero energy solution normalized so that for $\varrho_3 \to \infty$ it equals $\varphi_{12}(\varrho_{12})$.

2.3. STATES WITH $L = \Lambda = l \geqq 2$

Consider now a state with $l \neq 0$. Our aim is to obtain formulae similar to (26). In this case using (12), (15) and repeating the reasoning applied in the previous subsection we find that in regions (13b, c) the zero energy wave functions are respectively

$$\Psi_l^{(0)} = \tfrac{1}{2}\int \mathrm{d}\cos\vartheta_{\mathbf{p}_3\mathbf{k}_{12}} P_l(\cos\vartheta_{\mathbf{p}_3\mathbf{k}_{12}}) \frac{\sin p_2\varrho_2}{p_2\varrho_2}\varphi_{13}(\varrho_{13}), \tag{27b}$$

$$\Psi_l^{(0)} = \tfrac{1}{2}\int \mathrm{d}\cos\vartheta_{\mathbf{p}_3\mathbf{k}_{12}} P_l(\cos\vartheta_{\mathbf{p}_3\mathbf{k}_{12}}) \frac{\sin p_1\varrho_1}{p_1\varrho_1}\varphi_2(\varrho_{23}). \tag{27c}$$

In region (13a) we find that in this case $\Psi_l = 0$ in the zero approximation. As in the foregoing we find in a first approximation that in region (13a)

$$\Psi_l^{(1)} = \tfrac{1}{2}\int \mathrm{d}\cos\vartheta_{\mathbf{p}_3\mathbf{k}_{12}} P_l(\cos\vartheta_{\mathbf{p}_3\mathbf{k}_{12}}) \left[\frac{\sin p_2\varrho_2}{p_2\varrho_2}\frac{\mathrm{e}^{-ik_{13}\rho_{13}}}{\varrho_{13}} a_{13} + \frac{\sin p_1\varrho_1}{p_1\varrho_1}\frac{\mathrm{e}^{-ik_{23}\rho_{23}}}{\varrho_{23}} a_{23}\right]\varphi_{12}(\varrho_{12}) \tag{28a}$$

and in region (13b), for example,

$$\Psi_l^{(0)}+\Psi_l^{(1)} = \tfrac{1}{2}\int \mathrm{d}\cos\vartheta_{\mathbf{p}_3\mathbf{k}_{12}} P_l(\cos\vartheta_{\mathbf{p}_3\mathbf{k}_{12}}) \left[\frac{\sin p_2\varrho_2}{p_2\varrho_2}(1-ik_{13}a_{13}) + \frac{\sin p_1\varrho_1}{p_1\varrho_1}\frac{\mathrm{e}^{-ik_{23}\rho_{23}}}{\varrho_{23}} a_{23}\right]\varphi_{13}(\varrho_{13}). \tag{28b}$$

Going over to region $\varrho_{12} \approx r_0 \ll \varrho_3 \ll 1/\varkappa$ we find from (28a)

$$\Psi_l^{(1)} = -\tfrac{1}{2}\int \mathrm{d}\cos\vartheta_{\mathbf{p}_3\mathbf{k}_{12}} P_l(\cos\vartheta_{\mathbf{p}_3\mathbf{k}_{12}})(ik_{13}a_{13}+ik_{23}a_{23})\varphi_{12}(\varrho_{12}). \tag{28}$$

In distinction to the previous subsection, in which we restricted our consideration to the first approximation, we shall now consider also the second approximation, inasmuch as the zero approximation vanishes in the region of interest. However, we shall exclude the case $l = 1$, in which the barrier transmission coefficient is likewise of the order of k^2.

Writing Ψ_l as $\Psi_l^{(0)}+\Psi_l^{(1)}+\Psi_l^{(2)}$ and inserting (28a, b, c) in (11) we obtain in region (13a)

$$\Psi_l^{(2)} = -\tfrac{1}{2}\int \mathrm{d}\cos\vartheta_{\mathbf{p}_3\mathbf{k}_{12}} P_l(\cos\vartheta_{\mathbf{p}_3\mathbf{k}_{12}}) \left\{\int \mathrm{d}^3\varrho'_3\,\mathrm{d}^3\varrho'_{12}\left[G(\boldsymbol{\rho}_{12}-\boldsymbol{\rho}'_{12},\ \boldsymbol{\rho}_3-\boldsymbol{\rho}'_3) - \frac{\mu_{12}}{2\pi\hbar^2}\frac{\delta(\boldsymbol{\rho}_3-\boldsymbol{\rho}'_3)}{|\boldsymbol{\rho}_{12}-\boldsymbol{\rho}'_{12}|}\right] V_{12}(\varrho'_{12})\varphi_{12}(\varrho'_{12})\left[\frac{\sin\frac{\mu_{13}}{m_1}p_2\varrho'_3}{\frac{\mu_{13}}{m_1}p_2\varrho'_3}\frac{\mathrm{e}^{-ik_{13}\rho'_3}}{\varrho'_3} a_{13}\right.\right. \tag{29}$$

$$+\frac{\sin\frac{\mu_{23}}{m_2}p_1\varrho'_3}{\frac{\mu_{23}}{m_2}p_1\varrho'_3}\frac{e^{-ik_{23}\rho'_3}}{\varrho'_3}a_{23}\Bigg]+\int d^3\varrho'_{13}d^3\varrho'_2 G(\rho_{13}-\rho'_{13},\ \rho_2-\rho'_2)$$

$$\times V_{13}(\varrho'_{13})\varphi_{13}(\varrho'_{13})\frac{\sin\frac{\mu_{23}}{m_2}p_1\varrho'_3}{\frac{\mu_{23}}{m_2}p_1\varrho'_3}\frac{e^{-ik_{23}\rho'_3}}{\varrho'_3}a_{23}+(1\to 2)\Bigg\} \tag{29}$$

$$-\frac{\mu_{12}}{2\pi\hbar^2}\int\frac{V_{12}(\varrho'_{12})}{|\rho_{12}-\rho'_{12}|}\Psi_l^{(2)}(\rho'_{12},\ \rho_3)d^3\varrho'_{12}.$$

In order to determine the free term in this equation one must evaluate the integrals

$$I_{13}=-\tfrac{1}{2}\int d\cos\vartheta_{p_3k_{12}}P_l(\cos\vartheta_{p_3k_{12}})\int G(\rho_{12}-\rho'_{12},\ \rho_3-\rho'_3)$$

$$\times\frac{\sin\frac{\mu_{23}}{m_2}p_1\varrho'_3}{\frac{\mu_{23}}{m_2}p_1\varrho'_3}\frac{e^{-ik_{23}\rho'_3}}{\varrho'_3}d^3\varrho'_3 \tag{30}$$

and the others obtained by changing the subscripts in I_{13}.

In appendix 2 these integrals are computed by assuming $\varkappa|\rho_{12}-\rho'_{12}|\ll 1$, $\varkappa\varrho_3\ll 1$. According to eq. (B2),

$$I_{13}=-\tfrac{1}{2}\int d\cos\vartheta_{p_3k_{12}}P_l(\cos\vartheta_{p_3k_{12}})\cdot\frac{\mu_{12}}{2\pi\hbar^2}\left[\frac{-ik_{23}}{|\rho_{12}-\rho'_{12}|}+\mathcal{I}_{13}\right],$$

$$\mathcal{I}_{13}=-\frac{1}{3\pi}\frac{m_2\varkappa}{\mu_{23}p_1}[(1-\alpha^2)^{3/2}\arccos\alpha-(1-\beta^2)^{3/2}\arccos\beta], \tag{31}$$

$$\alpha=\frac{1}{\varkappa\gamma_3^{\frac{1}{2}}}\left(k_{23}-\frac{\mu_{23}}{m_2}p_1\right);\quad\beta=\frac{1}{\varkappa\gamma_3^{\frac{1}{2}}}\left(k_{23}+\frac{\mu_{23}}{m_2}p_1\right).$$

Inserting these results in (29) we obtain the following expression for $\Psi_l(\varrho_{12},\ \varrho_3)$ in the region $\varrho_{12}\ll\varrho_3\ll 1/\varkappa$:

$$\Psi_l=\tfrac{1}{2}\int d\cos\vartheta_{p_3k_{12}}P_l(\cos\vartheta_{p_3k_{12}})[-ik_{13}a_{13}-ik_{23}a_{23}+\mathcal{I}_{13}a_{12}a_{23}$$

$$+\mathcal{I}_{23}a_{12}a_{13}+\mathcal{I}_{12}a_{13}a_{23}+\mathcal{I}_{21}a_{23}a_{13}]\varphi_{12}(\varrho_{12})\left(1+\frac{a_{13}}{\varrho_3}+\frac{a_{23}}{\varrho_3}\right).$$

By repeating the procedure which yielded (26) we arrive at a similar formula:

$$\Psi_l(\rho_{12}\rho_3) = \tfrac{1}{2}\int \mathrm{d}\cos\vartheta_{\mathbf{p}_3\mathbf{k}_{12}} P_l(\cos\vartheta_{\mathbf{p}_3\mathbf{k}_{12}})[-ik_{13}a_{13}-ik_{23}a_{23}+\mathscr{I}_{13}a_{12}a_{23} \\ +\mathscr{I}_{23}a_{12}a_{13}+\mathscr{I}_{12}a_{13}a_{23}+\mathscr{I}_{21}a_{13}a_{23}]\, f\,(\rho_{12},\ \rho_3) \tag{32}$$

for $\varrho_{12},\ \varrho_3 \approx r_0$ with the same value of $f(\varrho_{12},\ \varrho_3)$.

Formulae (26) and (32) solve the problem stated above and define the angular distribution at low energies. The only quantities which have not been determined are the quadratic terms in k for $l = 1$. Further details pertaining to application of formulae (26) and (32) will be illustrated by considering τ^+ meson decay.

3. Angular Distribution in τ^+ Meson Decay

We shall examine the reactions

$$\tau^+ \to 2\pi^+ + \pi^-, \tag{33}$$

$$\tau^+ \to 2\pi^0 + \pi^+. \tag{34}$$

It should be noted that the energy of relative motion in these reactions is not very small. Thus, comparison of formulae derived in this section with the experimental data can yield only approximate results.

In both cases identical charged particles will be chosen as particles 1 and 2. Then, assuming the τ^+ meson spin to be zero, we obtain

$$L = \Lambda = l = 0,\ 2,\ 4\ldots.$$

In order to apply the results of the previous section it will be necessary to take into account the isobaric variables of the π-mesons. It will suffice for this purpose to supply the function f with isobaric indices and instead of the scattering amplitudes a_{ik} to introduce scattering amplitudes a_0, a_2 in states with an isobaric spin of $T = 0,2$ (states with $T = 1$ are not possible at zero energy). Amplitude a_{12}, for example, will be replaced by

$$\sum_{T_{12}} C^{T_{12}T'_{12}}_{1\tau_1,\,1\tau_2} C^{T_{12}T'_{12}}_{1\tau'_1,1\tau'_2}\,\delta_{\tau_3\tau'_3}\,a_{T_{12}}$$

where $C^{TT'}_{1\tau_1 1\tau_2}$ is a Clebsch-Gordan coefficient, $\tau_1\tau_2\tau_3$, $\tau'_1\tau'_2\tau'_3$ are projections of the isobaric spins of the particles before and after scattering. Thus instead of (26) and (32) we obtain the following equations:

$$\Psi_{0,\,\tau_1\tau_2\tau_3} = \sum_{\tau'_1\tau'_2\tau'_3}\{\delta_{\tau_1\tau'_1}\delta_{\tau_2\tau'_2}\delta_{\tau_3\tau'_3} - ik_{12}\sum_{T_{12}} C^{T_{12}T'_{12}}_{1\tau_1,1\tau_2}\, C^{T_{12}T'_{12}}_{1\tau'_1,1\tau'_2}\,\delta_{\tau_3\tau'_3}\,a_{T_{12}} \\ -i(k_{13}+k_{23})\sum_{T_{13}} C^{T_{13}T'_{13}}_{1\tau_1,1\tau_3} C^{T_{13}T'_{13}}_{1\tau'_1,1\tau'_3}\,\delta_{\tau_2\tau'_2}\,a_{T_{13}}\}\, f_{\tau'_1\tau'_2\tau'_3} \tag{35}$$

$$\Psi_{l,\,\tau_1\tau_2\tau_3} \\ = \sum_{\tau'_1\tau'_2\tau'_3}\tfrac{1}{2}\int \mathrm{d}\cos\vartheta_{\mathbf{p}_3\mathbf{k}_{12}}\, P_l(\cos\vartheta_{\mathbf{p}_3\mathbf{k}_{12}})\{-i(k_{13}+k_{23})\sum_{T_{13}} C^{T_{13}T'_{13}}_{1\tau_1,1\tau_3} C^{T_{13}T'_{13}}_{1\tau'_1,1\tau'_3}\,\delta_{\tau_2\tau'_2}\,a_{T_{13}} \\ +(\mathscr{I}_1+\mathscr{I}_2)[\sum_{T_{13},\,T_{23},\,\tau''_2} C^{T_{13}T'_{13}}_{1\tau_1,1\tau_2} C^{T_{13}T'_{13}}_{1\tau'_1,1\tau''_2}\cdot C^{T_{23}T'_{23}}_{1\tau''_2,1\tau_3} C^{T_{23}T'_{23}}_{1\tau'_2,1\tau'_3}\,a_{T_{12}}a_{T_{23}} \\ +\sum_{T_{13},\,T_{23},\,\tau''_3} C^{T_{13}T'_{13}}_{1\tau_1,1\tau_3} C^{T_{13}T'_{13}}_{1\tau'_1,1\tau''_3} C^{T_{23}T'_{23}}_{1\tau''_3,1\tau_2} C^{T_{23}T'_{23}}_{1\tau'_3,1\tau'_2}\,a_{T_{13}}a_{T_{23}}]\}\, f_{\tau'_1\tau'_2\tau'_3}. \tag{36}$$

It was taken into account in deriving this equation that $\tau_1 = \tau_2$ and that $f_{\tau_1\tau_2\tau_3}$ is a symmetric function of $\tau_1\tau_2\tau_3$; $\mathcal{I}_{13}=\mathcal{I}_{12}=\mathcal{I}_1$ and $\mathcal{I}_{23}=\mathcal{I}_{21}=\mathcal{I}_2$. Corresponding to the two modes of decay only two different functions exist, $f^{(-)} = f_{1,1,-1}$, $f^{(+)} = f_{0,0,1}$. Collecting the coefficients before $f^{(-)}$ and $f^{(+)}$ and using the numerical values of the Clebsch-Gordan coefficients we obtain

$$\Psi_{0,11-1} = [+1-ik_{12}a_2-i(k_{13}+k_{23})\tfrac{1}{3}(a_2+2a_0)]f^{(-)}-i(k_{13}+k_{23})\tfrac{1}{3}(a_2-a_3)f^{(+)},$$

$$\begin{aligned}\Psi_{l,11-1} = {} & \tfrac{1}{2}\int \mathrm{d}\cos\vartheta_{\mathbf{p}_3\mathbf{k}_{12}} P_l(\cos\vartheta_{\mathbf{p}_3\mathbf{k}_{12}}) \\ & \times\{[-i(k_{13}+k_{23})\tfrac{1}{3}(a_2+2a_0)+(\mathcal{I}_1+\mathcal{I}_2)\tfrac{1}{9}(2a_0^2+11a_2a_0+5a_2^2)]\,f^{(-)} \\ & +[-i(k_{13}+k_{23})\tfrac{1}{3}(a_2-a_0)+(\mathcal{I}_1+\mathcal{I}_2)\tfrac{1}{9}(13a_2^2-11a_2a_0-2a_0^2)]\,f^{(+)}\},\end{aligned} \tag{37}$$

$$\Psi_{0,001} = [1-ik_{12}\tfrac{1}{3}(2a_2+a_0)-i(k_{13}+k_{23})a_2]f^{(+)}-\tfrac{2}{3}(a_2-a_0)ik_{12}f^{(-)},$$

$$\begin{aligned}\Psi_{l,001} = {} & \tfrac{1}{2}\int \mathrm{d}\cos_{\mathbf{p}_3\mathbf{k}_{12}} P_l(\cos\vartheta_{\mathbf{p}_3\mathbf{k}_{12}}) \\ & \times\{[-i(k_{13}+k_{23})a_2+(\mathcal{I}_1+\mathcal{I}_2)\tfrac{1}{18}(29a_2^2+5a_0a_2+2a_2^2)]\,f^{(+)} \\ & +(\mathcal{I}_1+\mathcal{I}_2)\tfrac{1}{9}(7a_2^2-9a_2a_0+2a_0^2)\,f^{(-)}\}.\end{aligned}$$

We may now proceed to compute the decay amplitude. Applying (3) we may write

$$\langle \mathbf{p}_3\mathbf{k}_{12}\tau_1\tau_2\tau_3\,|S|\,\tau^+\rangle = \sum_{l=0,2\ldots}^{\infty}(2l+1)P_l(\cos\vartheta_{\mathbf{p}_3\mathbf{k}_{12}})\,\langle\Psi_{l,\tau_1\tau_2\tau_3}|\hat{W}|\Psi_{\tau^+}\rangle. \tag{38}$$

Substituting (37) in (38) and making use of the fact that the set of Legendre polynomials is a complete one we obtain

$$\begin{aligned}&\langle \mathbf{p}_3 k_{12}\,11-1\,|S|\,\tau^+\rangle = [1+ik_{12}+i(k_{13}+k_{23})\tfrac{1}{3}(a_2+2a_0) \\ &+(\mathcal{I}_1+\mathcal{I}_2)\tfrac{1}{9}(5a_2^2+11a_2a_0+2a_0^2)]\langle f^{(-)}|\hat{W}|\Psi_{\tau^+}\rangle \\ &+[i(k_{13}+k_{23})\tfrac{1}{3}(a_2-a_0)+(\mathcal{I}_1+\mathcal{I}_2)\tfrac{1}{9}(13a_2^2-11a_2a_0-2a_0^2)]\langle f^{(+)}|\hat{W}|\Psi_{\tau^+}\rangle \\ &+O(\varkappa^2)+O(\varkappa^3);\end{aligned} \tag{39}$$

$$\begin{aligned}&\langle \mathbf{p}_3 k_{12}\,00+1\,|S|\,\tau^+\rangle = [1+ik_{12}\tfrac{1}{3}(2a_2+a_0) \\ &\quad +i(k_{13}+k_{23})a_2+(\mathcal{I}_1+\mathcal{I}_2)\tfrac{1}{18}(29a_2^2+5a_2a_0+2a_0^2)]\langle f^{+}|\hat{W}|\Psi_{\tau^+}\rangle \\ &\quad +[\tfrac{2}{3}(a_2-a_0)ik_{12}+(\mathcal{I}_1+\mathcal{I}_2)(7a_2^2-9a_2a_0+2a_0^2)]\langle f^{(-)}|\hat{W}|\Psi_{\tau^+}\rangle \\ &\quad +O(\varkappa^2)+O(\varkappa^3).\end{aligned} \tag{40}$$

Since in (38) $\Psi_{0,\tau_1\tau_2\tau_3}$ is known only up to terms which are linear with respect to $\varkappa$ and $\Psi_{l,\tau_1\tau_2\tau_3}$ for $l \geqq 2$ up to quadratic terms, $O(\varkappa^2)$ in (39) and (40) should be independent of the angle between $\mathbf{p}_3$ and $\mathbf{k}_{12}$. Part of the terms of order of $\varkappa$ which are independent of $\vartheta_{\mathbf{p}_3\mathbf{k}_{12}}$ were retained in (39), (40) for convenience of notation and will be dropped in the following.

If the interaction $\hat{W}$ is invariant under time reversal, the quantities $\langle f^{(-)}|\hat{W}|\Psi_{\tau^+}\rangle$, $\langle f^{(+)}|\hat{W}|\Psi_{\tau^+}\rangle$ will be real. In this case the probabilities for both types of decay per unit time will be proportional to

$$W^{(-)}(p_3, \vartheta_{\mathbf{p}_3\mathbf{k}_{12}}) = |\langle f^{(-)}|\hat{W}|\Psi_{\tau^+}\rangle|^2\{1+\tfrac{2}{9}(\mathcal{I}_1+\mathcal{I}_2)$$
$$\times [5a_2^2+11a_2a_0+2a_0^2+(13a_2^2-11a_2a_0-2a_0^2)\varrho] \qquad (41)$$
$$+[k_{12}a_2+(k_{13}+k_{23})\tfrac{1}{3}(a_2+2a_0)+\tfrac{1}{3}(k_{13}+k_{23})(a_2-a_0)\varrho]^2;$$

$$W^{(+)}(p_3, \vartheta_{\mathbf{p}_3\mathbf{k}_{12}}) = |\langle f^{(+)}|\hat{W}|\Psi_{\tau^+}\rangle|^2\{1+\tfrac{1}{9}(\mathcal{I}_1+\mathcal{I}_2)$$
$$\times [29a_2^2+5a_2a_0+2a_0^2+2(7a_2^2-9a_2a_0+2a_0^2)\varrho^{-1}] \qquad (42)$$
$$+(k_{13}+k_{23})a_2[\tfrac{2}{3}k_{12}(2a_2+a_0)+(k_{13}+k_{23})a_2+\tfrac{4}{3}(a_2-a_0)k_{12}\varrho^{-1}];$$

$\varrho^2 = |\langle f^{(-)}|\hat{W}|\Psi_{\tau+}\rangle/\langle f^{(+)}|\hat{W}|\Psi_{\tau+}|^2$ is the ratio of the probabilities for the two types of decay. It can be seen from these formulae that the first and second order terms in Ψ_i yield equal contributions to the decay probability. This is due to the fact that the first order terms are imaginary. If the interaction $\hat{W}$ is not invariant under time reversal the following terms will correspondingly appear in the expressions between brackets in (41) and (42):

$$-2\varrho(k_{13}+k_{23})\tfrac{1}{3}(a_2-a_0)\sin\varphi+2\varrho(\cos\varphi-1)$$
$$\times\{(\mathcal{I}_1+\mathcal{I}_2)\tfrac{1}{9}(13a_2^2-11a_2a_0-2a_0^2)+\tfrac{1}{3}(a_2-a_0)(k_{13}+k_{23}) \qquad (41')$$
$$\times [k_{12}a_2+(k_{13}+k_{23})\tfrac{1}{3}(a_2+2a_0)]\};$$

$$-2\varrho^{-1}k_{12}(a_2-a_0)\sin\varphi+2\varrho^{-1}(\cos\varphi-1)\{(\mathcal{I}_1+\mathcal{I}_2)\tfrac{1}{9}(7a_2^2-9a_2a_0+2a_0^2)$$
$$+\tfrac{2}{3}k_{12}(k_{13}+k_{23})(a_2-a_0)a_2\}; \qquad (42')$$

$$\varphi = \varphi_+-\varphi_-; \quad \langle f^{(+)}|\hat{W}|\Psi_{\tau+}\rangle/\langle f^{(-)}|\hat{W}|\Psi_{\tau+}\rangle = \varrho e^{i\varphi}.$$

In this case π-meson interaction is manifested already in the first approximation in $\varkappa$. In reaction (33) it affects the angular as well as the energy distribution and in reaction (34) only the energy distribution. These terms can consequently be separated from the previous ones and in principle the set of formulae (41, 42, 41′, 42′) permits one to determine a_2, a_0 and φ from the angular and energy distributions of the decay products.

If the interaction $\hat{W}$ is invariant under time reversal ($\varphi = 0$) it should be sufficient to know the angular distribution in order to determine a_2 and a_0. To obtain this distribution formulae (41) and (42) should be integrated over the energy of the third particle. To perform the integration we replace $\mathcal{I}_1$ and $\mathcal{I}_2$ by their approximate values

$$\mathcal{I}_1 = -\sqrt{\frac{mE}{\hbar^2}}k_{23}; \quad \mathcal{I}_2 = -\sqrt{\frac{mE}{\hbar^2}}k_{13},$$

which are obtained from (31) by expanding $(1-\alpha^2)^{3/2}$ and arc cos α in a series and retaining only the first terms. If k_{13}, k_{23} are simultaneously

expanded in a power series in $\cos\vartheta_{\mathbf{p}_3\mathbf{k}_{12}}$ and all powers above the second are neglected we obtain the following expression for the differential probabilities $dW^{(-)}(\vartheta)$ and $dW^{(+)}(\vartheta)$:

$$dW^{(-)}(\vartheta) = W^{(-)}\left\{1+\cos^2\vartheta\frac{mE}{\hbar^2}\left[0.07\,a_2^2+0.1\,a_2a_0-0.07\,a_0^2\right.\right.$$
$$\left.\left.+\varrho(0.25\,a_2^2-0.32\,a_2a_0+0.07\,a_0^2)+0.03(a_2-a_0)^2\varrho^2\right]\right\}d\cos\vartheta; \quad (43)$$

$$dW^{(+)}(\vartheta) = W^{(+)}\left\{1+\cos^2\vartheta\frac{mE}{\hbar^2}\left[0.1\,a_2^2+0.03\,a_2a_0+0.03\,a_0^2\right.\right.$$
$$\left.\left.+\varrho^{-1}(0.12\,a_2^2-0.17\,a_2a_0+0.05a_0^2)\right]\right\}d\cos\vartheta. \quad (44)$$

If the interaction range r_0 is $\approx 1/m$, corrections to the angular distribution arise as a result of relativistic effects which are of the same order of magnitude as those considered above.

These corrections can be taken into account, for example, by studying the dependence of the decay product distribution not on $\vartheta_{\mathbf{p}_3\mathbf{k}_{12}}$ but on the angle $\vartheta_{\mathbf{p}_3\mathbf{k}'_{12}}$ between $\mathbf{p}_3$ and the momentum $\mathbf{k}'_{12}$ of one of two identical π-mesons in their c.m.s.

Since the energy of the three particles

$$W = c^2\sqrt{m^2+\frac{\mathbf{p}_3^2}{c^2}}+c^2\sqrt{M^2+\frac{\mathbf{p}_3^2}{c^2}}; \quad M = 2\sqrt{m^2+\frac{\mathbf{k}_{12}^2}{c^2}}$$

is independent of $\vartheta_{\mathbf{p}_3\mathbf{k}'_{12}}$, expansion (38) will remain valid in the relativistic case as well. The usual method of estimating the matrix elements in the absence of interaction will also be applicable. Thus up to terms of the order of $(\varkappa r_0)^4$, the decay amplitude (without account of interaction) will be independent of $\vartheta_{\mathbf{p}_3\mathbf{k}'_{12}}$. Since the order of magnitude of the relativistic corrections to the term due to interaction is the same as that of the neglected terms, formulae (43), (44) will remain valid if $\vartheta_{\mathbf{p}_3\mathbf{k}_{12}}$ is replaced by $\vartheta_{\mathbf{p}_3\mathbf{k}'_{12}}$.

Since (43) and (44) have the form

$$dW(x) = (1+\alpha x^2)dx; \quad x = \cos\vartheta_{\mathbf{p}_3\mathbf{k}_{12}}$$

it will be sufficient for experimental determination of α to compute the ratio of the difference of the number of decays with $x > \frac{1}{2}$ and $x < \frac{1}{2}-\Delta N$ to the total number of observed decays N, that is $\Delta N/N = \frac{1}{4}\alpha$.

Presently available experimental data do not permit one to determine α, since $\Delta N/N$ does not exceed the statistical spread.

Appendix 1

The simplest way of obtaining formula (15) is the following. The product of two plane waves exp $(i\mathbf{p}_3\boldsymbol{\rho}_3+i\mathbf{k}_{12}\boldsymbol{\rho}_{12})$ is expanded into states with definite total momenta values in the following two ways:

$$e^{i(\mathbf{p}_3\boldsymbol{\rho}_3+\mathbf{k}_{12}\boldsymbol{\rho}_{12})} = \sum_{j\mu LM\Lambda\nu} C^{j\mu}_{LM,\Lambda\nu}\, Y_{LM}(\Omega_{\mathbf{p}_3}) Y_{\Lambda\nu}(\Omega_{\mathbf{k}_{12}}) \Psi^{j\mu}_{L\Lambda}(\boldsymbol{\rho}_{12}, \boldsymbol{\rho}_3),$$

$$e^{i(\mathbf{p}_1\boldsymbol{\rho}_1+\mathbf{k}_{23}\boldsymbol{\rho}_{23})} = \sum_{j\mu LM\Lambda\nu} C^{j\mu}_{LM,\Lambda\nu}\, Y_{LM}(\Omega_{\mathbf{p}_1}) Y_{\Lambda\nu}(\Omega_{\mathbf{k}_{23}}) \Psi^{j\mu}_{L\Lambda}(\boldsymbol{\rho}_{23}, \boldsymbol{\rho}_1).$$

Since $\mathbf{p}_3\boldsymbol{\rho}_3+\mathbf{k}_{12}\boldsymbol{\rho}_{12} = \mathbf{p}_1\boldsymbol{\rho}_1+\mathbf{k}_{23}\boldsymbol{\rho}_{23}$ we obtain, after multiplying both equations by

$$\sum_{M\nu} C^{j\mu}_{LM,\Lambda\nu}\, Y^*_{LM}(\Omega_{\mathbf{p}_3}) Y^*_{\Lambda\nu}(\Omega_{\mathbf{k}_{12}})$$

and integrating over $\Omega_{\mathbf{p}_3}$, $\Omega_{\mathbf{k}_{12}}$,

$$\Psi^{j\mu}_{L,\Lambda}(\boldsymbol{\rho}_{12}, \boldsymbol{\rho}_3)$$

$$= \sum\int d\theta_{\mathbf{p}_3} d\cos\vartheta_{\mathbf{p}_3\mathbf{k}_{12}}\, C^{j\mu}_{LM,\Lambda\nu}\, Y^*_{LM}(\Omega_{\mathbf{p}_3}) \mathscr{D}^{\Lambda*}_{\nu\rho}(\theta_{\mathbf{p}_3}) Y^*_{\Lambda\rho}(\vartheta_{\mathbf{p}_3\mathbf{k}_{12}}, 0) C^{j\mu'}_{L'M',\Lambda'\nu'} \mathscr{D}^{L'}_{M'\rho_1}(\theta$$

$$\times Y_{L'\rho_1}(\vartheta_{\mathbf{p}_3\mathbf{p}_1}, 0)\, \mathscr{D}^{\Lambda'}_{\nu'\rho_2}(\theta_{\mathbf{p}_3}) Y_{\Lambda'\rho_2}(\vartheta_{\mathbf{p}_3\mathbf{k}_{23}}, 0) \Psi^{j\mu}_{L',\Lambda'}(\varrho_{23}, \varrho_1).$$

Here the variables $\Omega_{\mathbf{p}_3}$, $\Omega_{\mathbf{k}_{12}}$ have been replaced by Euler angles $\theta_{\mathbf{p}_3}$ in a coordinate system with the z axis directed along vector $\mathbf{p}_3$ and the x axis lying in the plane of vectors $\mathbf{p}_3$ and $\mathbf{k}_{12}$, and also by the angle $\vartheta_{\mathbf{p}_3\mathbf{k}_{12}}$ between $\mathbf{p}_3$ and $\mathbf{k}_{12}$. The transformation formulae for spherical functions under rotation of the coordinate system have been applied:

$$Y_{\Lambda\nu}(\Omega_{\mathbf{k}_{12}}) = \sum_{\rho} \mathscr{D}^{\Lambda}_{\nu\rho}(\theta_{\mathbf{p}_3}) Y_{\Lambda\rho}(\vartheta_{\mathbf{p}_3\mathbf{k}_{12}}, 0).$$

Integrating over $\theta_{\mathbf{p}_3}$ we get

$$\Psi^{j\mu}_{L\Lambda}(\boldsymbol{\rho}_{12}, \boldsymbol{\rho}_3) = \sum_{L'\Lambda'} \tfrac{1}{2}\int d\cos\vartheta_{\mathbf{p}_3\mathbf{k}_{12}}\, f^j(L\Lambda, L'\Lambda';\, \vartheta_{\mathbf{p}_3\mathbf{k}_{12}}) \Psi^{j\mu}_{L'\Lambda'}(\boldsymbol{\rho}_{23}, \boldsymbol{\rho}_1),$$

$$f^j(L\Lambda, L'\Lambda';\, \vartheta_{\mathbf{p}_3\mathbf{k}_{12}}) = \sum_{\rho\rho_1\rho_2} C^{j\rho}_{L0,\Lambda\rho} C^{j\rho}_{L\rho,\Lambda\rho_2} \frac{\sqrt{(2L+1)(2\Lambda+1)(2L'+1)(2\Lambda'+1)}}{2j+1}$$

$$\times P_{\Lambda\rho}(\cos\vartheta_{\mathbf{p}_3\mathbf{k}_{12}}) P_{L'\rho_1}(\cos\vartheta_{\mathbf{p}_3\mathbf{p}_2})\, P_{\Lambda'\rho_2}(\cos\vartheta_{\mathbf{p}_3\mathbf{k}_{23}}). \quad \text{(A1)}$$

For $j = 0$ (A1) reduces in a simple fashion to (15).

Appendix 2

Integral (30) can conveniently be evaluated by using representation (9) for the Green's function. Integrating (9) over $\mathbf{k}_{12}$ we obtain

$$G(\rho_{12}-\rho'_{12},\ \rho_3-\rho'_3) = \frac{\mu_{12}}{2\pi\hbar^2}\int \frac{d^3p}{(2\pi)^3}\, e^{ip\cdot(\rho_3-\rho'_3)}\, \frac{e^{-ik|\rho_{12}-\rho'_{12}|}}{|\rho_{12}-\rho'_{12}|}$$

$$= \frac{\mu_{12}}{2\pi\hbar^2}\,\delta(\rho_3-\rho'_3)\,\frac{1}{|\rho_{12}-\rho'_{12}|} + \frac{\mu_{12}}{2\pi\hbar^2}\int \frac{d^3p}{(2\pi)^3}\, e^{ip\cdot(\rho_3-\rho'_3)}\, \frac{e^{ik|\rho_{12}-\rho'_{12}|}-1}{|\rho_{12}-\rho_{12}'|}\,; \qquad \text{(B1)}$$

$$k = \frac{1}{\hbar}\sqrt{2\mu_{12}\left(E-\frac{\hbar^2p^2}{2\mu_3}\right)}.$$

The last term in this expression has no singularity at $|\rho_{12}-\rho'_{12}| = 0$, $\varrho_3 = 0$. Therefore, by putting $|\rho_{12}-\rho'_{12}| = 0$ and $\varrho_3 = 0$ we introduce an error of the order of $\varkappa|\rho_{12}-\rho'_{12}|$ and $\varkappa\varrho_3$. Neglecting terms of this order we get

$$G(\rho_{12}-\rho_{12},\ \rho_3-\rho'_3) = \frac{\mu_{12}}{2\pi\hbar^2}\,\frac{\delta(\rho_3-\rho'_3)}{|\rho_{12}-\rho'_{12}|} + \frac{\mu_{12}}{2\pi\hbar^2}\int \frac{d^3p}{(2\pi)^3}\,(-ik)\, e^{ip\cdot\rho'_3}. \qquad \text{(B2)}$$

Inserting this expression in (30) and integrating over ϱ'_3 we obtain

$$I_{13} = -\tfrac{1}{2}\int d\cos\vartheta_{p_3k_{12}}\, P_l(\cos\vartheta_{p_3k_{12}})\,\frac{\mu_{12}}{2\pi\hbar^2}\left[\frac{-ik_{23}}{|\rho_{12}-\rho'_{12}|}+\mathcal{J}_{13}\right],$$

$$\mathcal{J}_{13} = -i\int_0^\infty \frac{p\,dp\cdot k}{2\pi\dfrac{\mu_{23}}{m_2}p_1}\ln\frac{\left(p+\dfrac{\mu_{23}}{m_2}p_1\right)^2-k_{23}^2}{\left(p-\dfrac{\mu_{23}}{m_2}p_1\right)^2-k_{23}^2}.$$

Integration with respect to p leads to the result presented in the text. One must take into account that from 0 to $\sqrt{2\mu_3 E/\hbar^2}$ the imaginary part of k_{23} is negative, and that from $\sqrt{2\mu_3 E/\hbar^2}$ to ∞,

$$k = -\frac{i}{\hbar}\sqrt{2\mu_{12}\left(\frac{p^2\hbar^2}{2\mu_3}-E\right)}.$$

References

1) R. Dalitz, Phil. Mag. **44** (1953) 1068; Phys. Rev. **94** (1954) 1046
2) E. Fabri, Nuovo Cimento **11** (1954) 479
3) V. N. Gribov, JETP (in print)

Nuclear Physics **5** (1958) 669—676; © *North-Holland Publishing Co., Amsterdam*
Not to be reproduced by photoprint or microfilm without written permission from the publisher

THREE BODY BREAK UP

T. H. BERLIN and GEORGE E. OWEN
Department of Physics, The Johns Hopkins University
Baltimore 18, *Maryland*

Received 3 September 1957

Abstract: The continuous phase space distribution function is evaluated for (n, 2n) processes. The constraints of energy and momentum conservation are imposed in the form of delta functions. To facilitate transformation of the distribution function from the center of mass coordinates to the laboratory coordinates, a general form of the Jacobian is developed.

The Be^9(n, 2n)Be^8 reaction is considered as an example.

1. Kinematics

In the following discussion, capital letters will be used to designate laboratory variables, and small letters to designate centre of mass variables.

A. Assume that P_0 and T_0 are the laboratory momentum and kinetic energy respectively of a neutron incident upon a target nucleus T. The laboratory momentum diagram is shown in fig. 1.

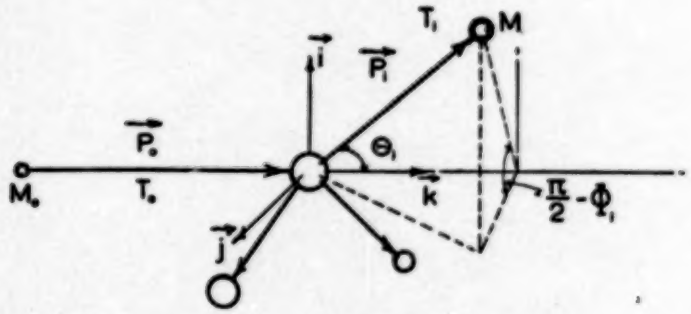

Fig. 1

Let $\mathbf{P_1}$ = momentum (lab) of the 1st neutron
$\mathbf{P_2}$ = ,, ,, ,, ,, 2nd neutron
$\mathbf{P_3}$ = ,, ,, ,, ,, recoil nucleus.

Conservation of energy and momentum gives

$$T_0+Q=\sum_{j=1}^{3} T_j, \tag{1}$$

$$\sum_{j=1}^{3} P_j \zeta_j \cos \Phi_j = 0, \tag{2}$$

$$\sum_{j=1}^{3} P_j \zeta_j \sin \Phi_j = 0, \tag{3}$$

$$\sum_{j=1}^{3} P_j \mu_j = P_0, \tag{4}$$

where

$$\zeta_j = \sin \Theta_j, \qquad \mu_j = \cos \Theta_j$$

and Q is the Q value of the reaction.

Orient the kinematics in the xz plane by letting $\Phi_1 = 0$; $\Phi_2 = \pi$; and $\sin \Phi_3 = 0$. Eliminating $\mathbf{P}_3$ and Θ_3 we obtain $P_2(P_0, P_1, \Theta_1, \Theta_2)$, and

$$\left\{1+\frac{M_3}{M_2}\right\} R_2^2 + \left\{1+\frac{M_3}{M_1}\right\} R^2{}_1 + 2\mu_{12} R_1 R_2 - 2\mu_2 R_2 - 2\mu_1 R_1 + \left\{1-\frac{M_3}{M_0}\right\} - \sigma^2 = 0,$$

where

$$R_i = P_i/P_0, \quad \mu_{12} = \cos(\Theta_1+\Theta_2) = \mu_1\mu_2 - \zeta_1\zeta_2, \quad \sigma^2 = (2M_3/P_0^2)Q.$$

If

$$a(R_1) = \frac{2M_2}{M_2+M_3}(\mu_{12} R_1 - \mu_2),$$

and

$$b(R_1) = \frac{M_2}{M_2+M_3}\left[\left(1+\frac{M_3}{M_1}\right) R_1^2 - 2\mu_1 R_1 - \left(\frac{M_3}{M_0}-1\right) - \sigma^2\right],$$

then

$$R_2 = -\frac{a(R_1)}{2} + \sqrt{\frac{a^2(R_1)}{4} - b}. \tag{5}$$

The minimum value of R_2 occurs when

$$R_{2(\min)} = \frac{M_2}{M_2+M_3}(\mu_2 - \mu_{12} R_{1(\max)}). \tag{6}$$

In this case R_1 is a maximum (i.e. when $(a^2/4)-b = 0$):

$$R_{1(\max)} = C + \sqrt{C^2+d}$$

where

$$C = \frac{\mu_1 - \dfrac{M_2}{M_2+M_3}\mu_{12}\mu_2}{\dfrac{M_1+M_3}{M_1} - \mu_{12}^2 \dfrac{M_2}{M_2+M_3}}$$

and

$$d = \frac{\dfrac{M_2}{M_2+M_3}\mu_2^2 + \dfrac{M_3-M_0}{M_0} + \sigma^2}{\dfrac{M_1+M_3}{M_1} - \mu_{12}^2 \dfrac{M_2}{M_2+M_3}}.$$

Interchanging the indices 1 and 2 gives $R_{1(\min)}$ and $R_{2(\max)}$. Finally, let

$$\varepsilon_i = \frac{T_i}{T_0} = \frac{M_0}{M_i} R_i^2. \tag{7}$$

B. In a given experiment the laboratory angles of the neutrons are fixed by the neutron detection system. For this reason it is advantageous to express the centre of mass momenta in terms of the laboratory angles. Fig. 2 illustrates the relation between the laboratory variables and the centre of mass variables:

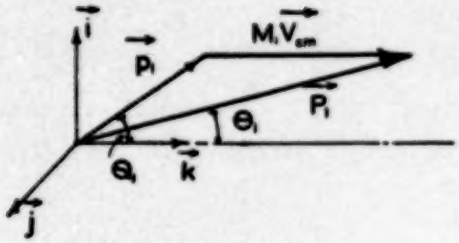

Fig. 2

$$r_i^2 = R_i^2 - 2\frac{M_i}{M_\tau}\mu_i R_i + \left(\frac{M_i}{M_\tau}\right)^2, \tag{8}$$

$$\xi_i = \frac{t_i}{T_0} = \frac{M_0}{M_i} r_i^2 = \text{CM energy of the } i\text{-th particle}/T_0, \tag{9}$$

where

$$r_i = p_i/P_0, \qquad M_\tau = M_0 + M_T = M_1 + M_2 + M_3.$$

Also,

$$\zeta'_i = \sin\vartheta_i = \frac{R_i}{r_i}\zeta_i, \qquad \mu'_i = \cos\vartheta_i = \frac{R_i}{r_i}\left\{\mu_i - \frac{M_i}{M_\tau R_i}\right\}.$$

2. The Centre of Mass Distribution Function

The problem to be treated is the following: What is the probability of finding neutron "1" with momentum between $\mathbf{p}_1$ and $\mathbf{p}_1 + \mathrm{d}\mathbf{p}_1$, when neutron "2" has emerged in the given solid angle Ω'_2? In other words, we wish to compute the distribution function $N(r_1 \cos\vartheta_1, \cos\vartheta_2)$ with $\Phi_1 = 0$, $\Phi_2 = \pi$.

The number of cells $\mathrm{d}Z$ in phase space for the three particles in the final state is

$$\mathrm{d}Z = \frac{\mathrm{d}\mathbf{p}_1 V}{(2\pi\hbar)^3}\frac{\mathrm{d}\mathbf{p}_2 V}{(2\pi\hbar)^3}\frac{\mathrm{d}\mathbf{p}_3 V}{(2\pi\hbar)^3}\,\delta(t - \sum_{i=1}^{3} p_i^2/2M_i)\,\delta(\mathbf{p}_1 + \mathbf{p}_2 + \mathbf{p}_3). \tag{10}$$

The delta functions provide the conservation of energy and momentum.

2.1. NORMALIZATION

Define

$$Z^{(0)}=\frac{V^3}{(2\pi\hbar)^9}\int\int d\mathbf{p}_1 d\mathbf{p}_2 \delta\left[t-\tfrac{1}{2}p_1^2\left(\frac{1}{M_1}+\frac{1}{M_3}\right)-\tfrac{1}{2}p_2^2\left(\frac{1}{M_2}+\frac{1}{M_3}\right)-\frac{1}{M_3}\mathbf{p}_1\cdot\mathbf{p}_2\right] \quad (11)$$

where the integration over $\mathbf{p}_3$ has been carried out.

Let

$$\delta(x)=\frac{1}{2\pi i}\int_{c-i\infty}^{c+i\infty} dw e^{wx}$$

where

$$x=t-\tfrac{1}{2}p_1^2\left(\frac{1}{M_1}+\frac{1}{M_3}\right)-\tfrac{1}{2}p_2^2\left(\frac{1}{M_2}+\frac{1}{M_3}\right)-\frac{1}{M_3}\mathbf{p}_1\cdot\mathbf{p}_2$$

and c is real. On replacing the delta function by its Fourier transform, and assuming that interchange of the order of integrations is permissible, we find on integrating over $\mathbf{p}_2$ that

$$Z^{(0)}=\frac{V^3}{(2\pi\hbar)^9}\frac{\pi^{\frac{1}{2}}}{2\pi i}\int_{c-i\infty}^{c+i\infty} dw e^{wt}\int d\mathbf{p}_1 e^{-\alpha p_1^2}\prod_{j=1}^{3}\frac{e^{wp_{1j}^2/4\alpha M_3^2}}{\alpha^{\frac{1}{2}}}$$

where

$$\alpha=\frac{w}{2}\left(\frac{1}{M_1}+\frac{1}{M_3}\right)=\frac{w}{2}\left(\frac{1}{M_2}+\frac{1}{M_3}\right)$$

for the (n, 2n) process, and p_{1j} denotes the j-th component of $\mathbf{p}_1$.

Consider the argument of the exponential functions

$$\beta(w)=\alpha-\frac{w^2}{4\alpha M_3^2}=\frac{w}{2M_1}\frac{M_3+2M_1}{M_3+M_1}.$$

If the integral over $\mathbf{p}_1$ is to converge, we require $\beta(w)>0$ or the real part of $w>0$. Under this condition

$$Z^{(0)}=\frac{V^3}{(2\pi\hbar)^9}\frac{1}{2\pi i}\int_{c-i\infty}^{c+i\infty} dw e^{wt}\left(\frac{2\pi M_1}{w}\right)^3\left(\frac{M_3}{M_3+2M_1}\right)^{3/2}$$

and the interchange of order of integration is permissible if $c>0$. In order for the integral not to vanish, t must be positive (see fig. 3).

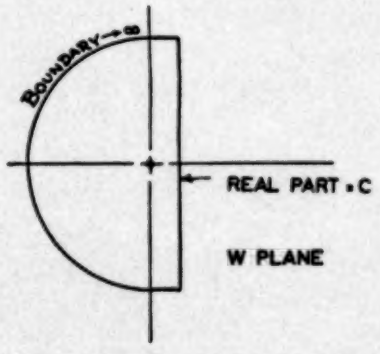

Fig. 3

Integrating over w,

$$Z^{(0)} = \frac{V^3}{(2\pi\hbar)^9}(2\pi M_1)^3 \frac{M_3}{M_3+2M_1}\frac{t^2}{2}. \tag{12}$$

2.2. THE DISTRIBUTION FUNCTION FOR THE VARIABLES p_1, ϑ_1, AND ϑ_2

Set

$$N(p_1, \mu'_1, \mu'_2) = \frac{\mathrm{d}Z^{(1)}}{Z^{(0)}} \tag{13}$$

where

$$\mathrm{d}Z_1^{(1)} = \frac{V^3}{(2\pi\hbar)^9}\mathrm{d}\mathbf{p}_1\,\mathrm{d}\Omega'_2 I, \tag{14}$$

and

$$I = \int_0^\infty \mathrm{d}p_2 (p_2)^2 \delta\left[t - \tfrac{1}{2}p_1^2\left(\frac{1}{M_1}+\frac{1}{M_3}\right) - \tfrac{1}{2}p_2^2\left(\frac{1}{M_2}+\frac{1}{M_3}\right) - \frac{\mu'_{12}}{M_3}p_1p_2\right], \tag{15}$$

$$\mu'_{12} = \mu'_1\mu'_2 - \zeta'_1\zeta'_2,$$

and where the integration over p_3 has been carried out. The primes indicate centre of mass angles.

In order to obtain the integral I, we set

$$t - s = ap_1^2 + ap_2^2 + (p_1p_2\mu'_{12}/M_3)$$

where

$$a = \tfrac{1}{2}\left(\frac{1}{M_1}+\frac{1}{M_3}\right) = \tfrac{1}{2}\left(\frac{1}{M_2}+\frac{1}{M_3}\right).$$

$$I = \int_0^\infty \mathrm{d}p_2 (p_2)^2 \delta(s) = \int_{s(p_2=0)=s_0}^{s(p_2\to\infty)\to\infty} \mathrm{d}s \cdot \frac{\mathrm{d}p_2}{\mathrm{d}s}(p_2(s))^2\delta(s)$$

with

$$s_0 = s(p_2 = 0) = t - ap_1^2.$$

Then

$$I = \left\{\frac{\mathrm{d}p_2}{\mathrm{d}s}\cdot p_2^2\right\}_{\substack{s=0\\ s_0>0}} = -\frac{p_2^2}{2ap_2 + \mu'_{12}(p_1/M_3)}.$$

Writing $N(p_1, \Omega'_1, \Omega'_2)$ as $N(r_1, \mu'_1, \mu'_2)$, we get

$$N(r_1, \mu'_1, \mu'_2) = \frac{1}{\pi^3}\left[\frac{M_3+2M_1}{M_3}\right]^{3/2}\frac{M_3}{M_1}\left(\frac{T_0}{t}\right)^2 \frac{\xi_1\xi_2}{2a\xi_2^{\frac{1}{2}} + (\mu'_{12}\xi_1^{\frac{1}{2}}/M_3)}. \tag{16}$$

Now

$$t/T_0 = \xi_1+\xi_2+\xi_3 = \frac{M_1}{M_3+2M_1} + \frac{Q}{T_0},$$

$$\xi_i = \frac{M_0}{M_i}r_i^2.$$

$\xi_1 = r_1^2$ and $\xi_2 = r_2^2$ for the (n, 2n) reaction.

3. The Laboratory Functions

3.1. THE JACOBIAN AND $N(R_1, \mu_1, \mu_2)$

The laboratory distribution function can be generated from the centre of mass function:

$$N(R_1, \mu_1, \mu_2) = N(r_1, \mu'_1, \mu'_2) J \left(\frac{r_1, \mu'_1, \mu'_2}{R_1, \mu_1, \mu_2} \right) \tag{17}$$

where J is the Jacobian for the coordinate transformation. Since

$$\partial \mu'_1 / \partial \mu_2 = 0 \text{ and } \partial r_1 / \partial \mu_2 = 0,$$

$$J = \left\{ \frac{\partial \mu_1'}{\partial \mu_1} \cdot \frac{\partial r_1}{\partial R_1} - \frac{\partial \mu'_1}{\partial R_1} \cdot \frac{\partial r_1}{\partial \mu_1} \right\} \frac{\partial \mu'_2}{\partial \mu_2}. \tag{18}$$

The partial derivatives of the coordinates are

$$\frac{\partial \mu'_1}{\partial \mu_1} = \frac{R_1^2}{r_1^3} \left(R_1 - \mu_1 \cdot \frac{M_1}{M_\tau} \right), \qquad \frac{\partial \mu'_1}{\partial R_1} = \frac{M_1}{M_\tau} \left(\frac{R_1}{r_1^2} \right) \zeta_1^2,$$

$$\frac{\partial r_1}{\partial R_1} = \frac{1}{r_1} \left(R_1 - \mu_1 \cdot \frac{M_1}{M_\tau} \right), \qquad \frac{\partial r_1}{\partial \mu_1} = - \frac{M^1}{M_\tau} \frac{R_1}{r_1},$$

$$\frac{\partial \mu'_2}{\partial \mu_2} = \frac{M_2}{M_2 + M_3} \frac{R_2^2}{r_2^3} \left\{ \frac{M_2 + M_3}{M_2} R_2 - \mu_2 + \frac{\zeta_2 (\zeta_2 - R_1 \zeta_{12})}{[R_2 + \frac{1}{2} a_2]} \right\}$$

where

$$\zeta_{12} = \mu_1 \zeta_2 + \zeta_1 \mu_2, \qquad M_\tau = M_1 + M_2 + M_3,$$

$$\frac{a_2}{2} = \frac{M_2}{M_2 + M_3} (\mu_{12} R_1 - \mu_2).$$

Usually $a_2/2 \ll R_2$.

Now

$$J = \frac{R_1^2}{r_1^2} \frac{\partial \mu'_2}{\partial \mu_2} = \frac{\varepsilon_1}{\xi_1'} \frac{\partial \mu'_2}{\partial \mu_2}. \tag{19}$$

Combining equations (16) and (19), we obtain

$$N(R_1, \mu_1, \mu_2) = \pi^{-3} \left(\frac{M_\tau}{M_3} \right)^{3/2} \frac{M_3}{M} \left(\frac{T_0}{t} \right)^2 \frac{\varepsilon_1 \cdot \xi_2 \cdot (\partial \mu'_2 / \partial \mu_2)}{2a \xi_2^{\frac{1}{2}} + (\mu_{12} \xi_1^{\frac{1}{2}} / M_3)} \tag{20}$$

where

$$\frac{t}{T_0} = \frac{M_1}{M_\tau} + \frac{Q}{T_0}.$$

3.2. THE ENERGY DISTRIBUTION FUNCTION IN THE LABORATORY COORDINATES

$$N(\varepsilon_1, \mu_1, \mu_2) = N(R_1, \mu_1, \mu_2)\frac{dR_1}{d\varepsilon_1} = \varepsilon_1^{-\frac{1}{2}} N(R_1, \mu_1, \mu_2).$$

Thus

$$N(\varepsilon_1, \mu_1, \mu_2) = \pi^{-3}\left(\frac{M_\tau}{M_3}\right)^{3/2}\frac{M_3}{M_1}\left(\frac{T_0}{l}\right)^2 \frac{\varepsilon_1^{\frac{1}{2}}\xi_2\dfrac{\partial \mu'_2}{\partial \mu_2}}{2a\xi_2^{\frac{1}{2}} + \dfrac{1}{M_3}\mu'_{12}\xi_1^{\frac{1}{2}}}. \tag{21}$$

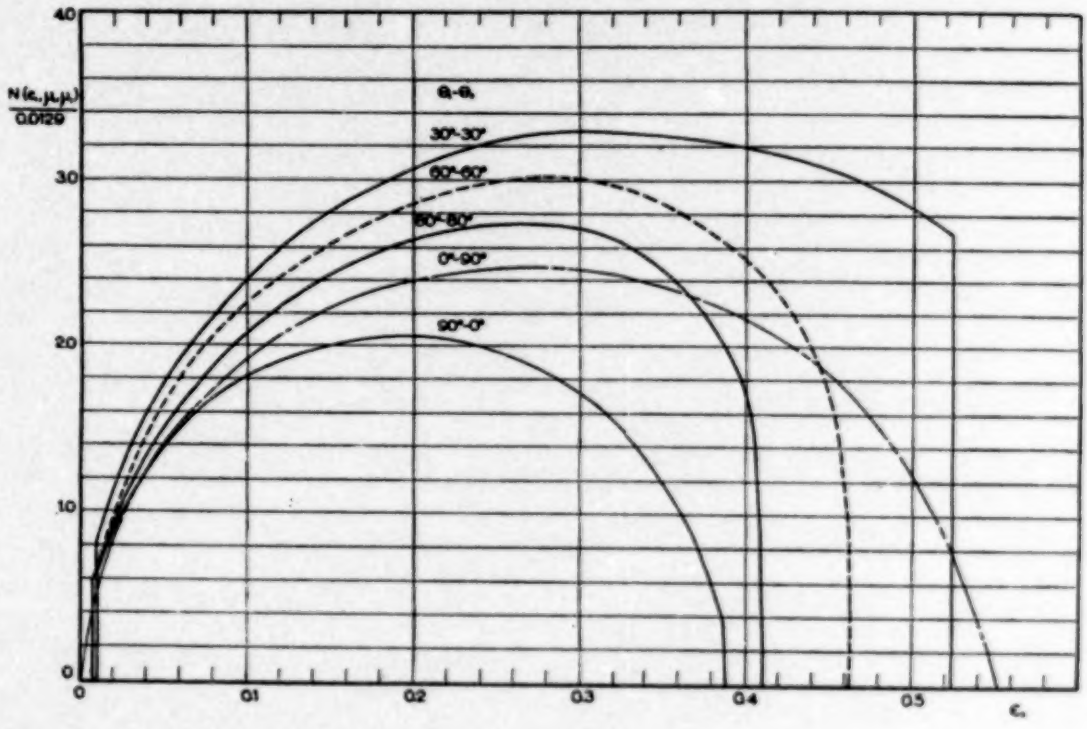

Fig. 4

4. Application to the Kinematic Problem $Be^9(n, 2n)Be^8$

We take the reaction $Be^9(n, 2n)Be^8$ as an example to illustrate the shapes of the energy distribution function of one neutron when the angles of emission of 1 and 2 are fixed. In this case,

$$N(\varepsilon_1, \mu_1, \mu_2) = \frac{8}{90\pi^3}\left(\frac{9}{10}\right)^{3/2}\left(\frac{T_0}{l}\right)^2 \frac{\varepsilon_1^{\frac{1}{2}}\varepsilon_2^{\frac{1}{2}}[\zeta_2(\zeta_2 - \zeta_{12}R_1) + 9R_2(10R_2 - \mu_2)]}{9\xi_2^{\frac{1}{2}} + \varepsilon_1^{\frac{1}{2}}\varepsilon_2^{\frac{1}{2}}\left(\mu_{12} - 2 + \dfrac{\xi_1}{\varepsilon_1} + \dfrac{\xi_2}{\varepsilon_2}\right)}. \tag{22}$$

Fig. 4 shows the distribution functions for the cases

θ_1	30°	60°	80°	0°	90°
θ_2	30°	60°	80°	90°	0°

The parameters used in these curves are $T_0 = 3.77$ MeV and $\sigma^2 = 3.53$. It should be emphasized that the curves of fig. 4 are presented as an example. It has been established in this laboratory that the reaction $Be^9(n, 2n)Be^8$ goes by a two step break up through an excited state of Be^9.

The authors wish to thank Miss B. Wertz for aid in the computation of the curves in fig. 4.

Nuclear Physics **5** (1958) 677—683; © *North-Holland Publishing Co., Amsterdam*

Not to be reproduced by photoprint or microfilm without written permission from the publisher

FOURTH ORDER MAGNETIC MOMENT OF THE ELECTRON

A. PETERMANN

CERN, *Theoretical Study Division at the Institute for Theoretical Physics, University of Copenhagen*

Received 3 August 1957

Abstract: A more complete account is given of an estimation, by rigourous upper and lower bounds, of the fourth order magnetic moment of the electron which has already been published by the author. The method is illustrated for one typical term. Then the results of a more elaborate estimation are given. In the terminology used by Karplus and Kroll, the term symbolized by the diagram IIc is found to satisfy

$$\mu(\text{IIc}) = (-0.60 \pm 0.11)\frac{\alpha^2}{\pi^2} - \tfrac{1}{2}\frac{\alpha^2}{\pi^2}\log\frac{\lambda^2}{m^2},$$

in contradiction with the value

$$-3.18\frac{\alpha^2}{\pi^2} - \tfrac{1}{2}\frac{\alpha^2}{\pi^2}\log\frac{\lambda^2}{m^2}$$

given by the previous authors. It has been found that the other terms are not in disagreement with Karplus and Kroll values. If one accepts them, then the total fourth order moment amounts to $\mu^{(4)} = (-0.39 \pm 0.11)(\alpha^2/\pi^2)$. One notes finally that this new value increases the Lamb shift by (0.82 ± 0.03) Mc/s and brings the fine structure constant to $1/\alpha = 137.0384$.

1. Introduction

The new experimental determination of the electron g-factor done by Franken and Liebes [1]) has been the real starting point of a doubt concerning the exactness of the theoretical calculations performed some years ago by R. Karplus and N. Kroll [2]) †. However, such a feeling was already expressed by W. E. Lamb in 1953 [3]) in connection with a slight disagreement between the observed and the calculated $2^2S_{\frac{1}{2}} - 2^2P_{\frac{1}{2}}$ shift in hydrogen and deuterium, which clearly exceeded both the experimental and the theoretical uncertainties. Immediately a check was undertaken by the author. To be as fast as possible, the term by term check has been performed by using a method of rigorous and lower upper bounds. To obtain the safest results the inequalities for the lower bounds were derived for the integrals involving many auxiliary variables. This, of course, gave the simplest integrals, consequently the safest, but did not provide very narrow bounds. Nevertheless, whereas for diagrams I, IIa, IId, and IIe (in the KK terminology) the bounds agreed with the values given in their paper, the inequality $\mu(\text{IIc}) \geqq -1.55\ (\alpha^2/\pi^2)$ (infra-red term disregarded) was obtained for the diagram IIc. A slackening of this lower bound was allowed to make obvious the contradiction with $-3.18\ (\alpha^2/\pi^2)$ quoted by KK. This result has been published [4]). Then, deriving for this term more involved inequalities on the

† Denoted in the following by KK.

many-variable integrals, better bounds have been found to yield, without the infra-red term, $-0.49\ (\alpha^2/\pi^2) \geqq \mu(\mathrm{IIc}) \geqq -0.71\ (\alpha^2/\pi^2)$. In the present paper, section 2 will give, for the diagram IIc only, the detailed auxiliary-variable integrals. Then, in section 3, a typical term will be examined in detail as an example of the inequality technique for the many-variable integrals, illustrating its simplicity. Finally, in section 4, numerical results will be quoted concerning the diagram IIc, the total moment, and other observable electro-dynamical quantities such as the Lamb-shift, the moment of the mu-meson and the fine structure constant, taking into account the new value of the theoretical electron moment.

2. Auxiliary-Variable Integrals

No mention will be made here of the diagrams I, IIa, IId, and IIe, these not being in disagreement with the bounds calculated. It is of course not claimed that these four terms are correct, but simply that they are not in contradiction with the checking bounds†. For IIc, details are given. First of all, this term is expressed as follows:

$$\mathrm{IIc} = \frac{ie\alpha^2}{4\pi^4\hbar c}\,\frac{1}{(2\pi)^4}\int \mathrm{d}^4p_1\,\mathrm{d}^4p_2 \int \mathrm{d}^4k\,\bar{\psi}(p_1)k^{-2}\int_0^1 u\,\mathrm{d}u\int_0^1 \mathrm{d}v$$
$$\times\gamma_\nu(i\gamma p_1 - i\gamma k + m)^{-1}\gamma_\mu(i\gamma p_2 - i\gamma k + m)^{-1}[A_1+A_2+A_3+B+C \qquad (2.1)$$
$$+D+E+F+H+J]\psi(p_2),$$

with the definitions

$$\begin{aligned}
A_1 &= -m(1-u^2)(i\gamma p_2 - i\gamma k + m)\gamma_\nu \Lambda'^{-2}(p_2-k,\ p_2),\\
A_2 &= -i(2p_{2\nu}-k_\nu)(1-u)(1-uv)(i\gamma p_2 - i\gamma k + m)\Lambda'^{-2},\\
A_3 &= -ik_\nu(1-u+2uv)(1-uv)(i\gamma p_2 - i\gamma k + m)\Lambda'^{-2},\\
B &= -(1-u)\gamma_\nu(1-uv)[(p_2-k)^2+m^2]\Lambda'^{-2},\\
C &= ik_\nu mu(1+u)(1-2v)\Lambda'^{-2},\\
D &= k^2\gamma_\nu(1-u+u^2v(1-v))\Lambda'^{-2},\\
E &= -k_\alpha\sigma_{\nu\alpha}mu(1-u)\Lambda'^{-2}, \qquad (2.2)\\
F &= \int_0^1 \mathrm{d}z\gamma_\nu\frac{\Lambda'^2-\Lambda_0^2}{\Lambda_0^2+(\Lambda'^2-\Lambda_0^2)z},\\
H &= -2m^2\left(1-u-\frac{u^2}{2}\right)\gamma_\nu\Lambda_0^{-2},\\
J &= 2m^2\left(1-u-\frac{u^2}{2}\right)\gamma_\nu\Lambda'^{-2},\\
\Lambda'^2(p_2-k,\ p_2) &= u^2m^2+k^2u^2v(1-v)+u(1-u)v[(p_2-k)^2+m^2],\\
\Lambda_0^2 &= u^2m^2.
\end{aligned}$$

† *Note added in proof:* A further analytic evaluation performed in the meantime by the author [7]) shows that in fact $\mu(\mathrm{I})$ does not check with the value of Karplus and Kroll. The discrepancy amounts to $+0.031\ \alpha^2/\pi^2$.

Furthermore, after combination of the denominators and integration over k, the contributions to the fourth order magnetic moment from the terms A_1-J of (22) are given, in units of α^2/π^2, by

$$\begin{aligned}
\mu(A_1) &= (1-u^2)(1-w\beta\alpha^{-1})T,\\
\mu(A_2) &= -(1-u)(1-t)w(1-u+uv)T,\\
\mu(A_3) &= 0,\\
\mu(B) &= (1-u)(1-u+uv)w\beta\alpha^{-1}(1-w\beta\alpha^{-1})T,\\
\mu(C) &= 0,\\
\mu(D) &= -(1-u+u^2v(1-v))w(1-\beta\alpha^{-1})[1-w(1-\beta\alpha^{-1})]T',\\
\mu(E) &= -u(1-u)(1-w\beta\alpha^{-1})T \qquad (2.3)\\
&\quad +2u(1-u)x(1-w(1-\beta\alpha^{-1}))[1-x(1-w(1-\beta\alpha^{-1}))]T_j+u(u-1)T'_j,\\
\mu(F) &= -u^2v(1-v)[w(1-\beta\alpha^{-1})(1-w(1-\beta\alpha^{-1}))]T'_z\\
&\quad -u(1-u)(1-v)w\beta\alpha^{-1}(1-w\beta\alpha^{-1})T_z,\\
\mu(H) &= -\tfrac{5}{4}-\tfrac{1}{2}\log\frac{\lambda^2}{m^2},\\
\mu(J) &= 2\left(1-u-\frac{u^2}{2}\right)x(1-w(1-\beta\alpha^{-1}))[1-x(1-w(1-\beta\alpha^{-1}))]T_j,
\end{aligned}$$

with the abbreviations (integrations over u, v, t, w, z and x from 0 to 1 understood)

$$\begin{aligned}
\beta &= u(1-v)[1-u+uv(1-t)],\\
\alpha &= u(1-v)(1-u+uv),\\
T &= (1-u+uv)\{ut(1-u+uv)+w(1-v)[1-u+uv(1-t)]^2\}^{-1},\\
T' &= w(1-u+uv)\{utw(1-u+uv)+(1-v)[1-u+uv(1-wt)]^2\}^{-1},\\
T_z &= (1-u+uv)\{ut(1-u+uv)+zw(1-v)[1-u+uv(1-t)]^2\}^{-1},\\
T'_z &= w(1-u+uv)\{utw(1-u+uv)+z(1-v)[1-u+uv(1-wt)]^2\}^{-1}, \qquad (2.4)\\
T_j &= w(1-v)(1-u+uv)^3\\
&\quad \times\{utw(1-u+uv)+x(1-v)[1-u+uv(1-wt)]^2\}^{-2},\\
T'_j &= wx(1-u+uv)\{utw(1-u+uv)+x(1-v)[1-u+uv(1-wt)]^2\}^{-1}.
\end{aligned}$$

As shown in (2.3), the infra-red cut-off λ^2 appears only in H. In the following, it will be dropped, being understood that it has been taken into account to compensate the same term with opposite sign occurring in IId. Once (2.3) and (2.4) are obtained by means of well-known Dirac algebra tricks and particular combinations of the denominators by means of Feyn-

man variables †, the next problem is to get estimates for the different contributions. First, special attention has been given to the lower bound in order to put in evidence, in the simplest way, the fact that μ(IIc) could not reach the value $-3.18\ (\alpha^2/\pi^2)$ Bohr magnetons. The next section will show how the inequality technique for the original many-auxiliary-variable integrals has been applied. An illustration of it will be performed on $\mu(A_1)$.

3. Inequality on a Four-Variable Integral

According to (2.3) and (2.4), the contribution of the A_1 term in (2.1) to the fourth order magnetic moment is given, in units of α^2/π^2, by

$$\mu(A_1) = \int_0^1\int_0^1\int_0^1\int_0^1 (1-u^2)[1-w(1-u+uv(1-t))(1-u+uv)^{-1}] \times (1-u+uv)\times\{ut(1-u+uv)+w(1-v)[1-u+uv(1-t)]^2\}^{-1}\mathrm{d}u\mathrm{d}v\mathrm{d}w\mathrm{d}t. \tag{3.1}$$

It is first noticed that $\mu(A_1)$ is positive definite. Every factor is indeed positive definite, as is trivially seen for $(1-u^2)$; for $(1-w(1-u+uv(1-t)))$ $(1-u+uv)^{-1}$ the same is true since the coefficient of w is always contained between 0 and 1. Finally, the last term in the integrand is obviously positive as $1-u+uv$ is. To get a lower bound, we then look for an inequality of the form

$$\mu(A_1) \geqq L. \tag{3.2}$$

One increases the denominator of the last term, thus decreasing the corresponding integral, by replacing $[1-u+uv(1-t)]^2$ by $1-u+uv$ and then dividing numerator and denominator by $1-u+uv$. Moreover, $[1-u+uv(1-t)](1-u+uv)^{-1}$ being always positive and less than 1, one decreases the integral by replacing this factor by 1 in the second term, i.e. writing $(1-w)$ instead of $1-w[1-u+uv(1-t)](1-u+uv)^{-1}$. Then one gets

$$\mu(A_1) \geqq \int_0^1\int_0^1\int_0^1\int_0^1 (1-u^2)(1-w)[ut+wv]^{-1}\mathrm{d}u\mathrm{d}v\mathrm{d}w\mathrm{d}t, \tag{3.3}$$

the integral over v being unchanged when $1-v$ is replaced by v. Displaying the first two factors:

$$(1-u^2)(1-w) = 1-w-u^2+wu^2, \tag{3.4}$$

four integrals, corresponding to each of the separate terms in (3.4) are to be computed.

The term proportional to 1, $\int_0^1 \ldots \int_0^1 [ut+wv)^{-1}\mathrm{d}u\mathrm{d}v\mathrm{d}w\mathrm{d}t$, is first integrated over t, giving

† The way of combining denominators used here has been found to be very suitable to get easy bounds owing to the positive definiteness of special combinations of Feynman variables. Different ways may exist, having the same properties, but many others have been experimented and found more complicated than the present ones.

$$\int_0^1 \cdots \int_0^1 \frac{1}{u} [\log (u+wv) - \log wv] du dv dw. \tag{3.5}$$

Then, an integration over w leads to

$$\int_0^1 \int_0^1 \left\{ \left(\frac{1}{u} + \frac{1}{v} \right) \log (u+v) - \frac{1}{v} \log u - \frac{1}{u} \log v \right\} du dv. \tag{3.6}$$

The expression (3.6) is integrated first over u or v, depending on the terms, to give

$$\begin{aligned} &\int_0^1 \frac{1}{u} \log (1+u) du + \int_0^1 \frac{1}{v} \log (1+v) dv + \int_0^1 \log (1+u) du \\ &+ \int_0^1 \log (1+v) dv - \int_0^1 \log u \, du - \int_0^1 \log dv = 4.42. \end{aligned} \tag{3.7}$$

For the term proportional to w, after an integration over t, one is led to compute

$$\int_0^1 \int_0^1 \int_0^1 \frac{w}{u} \log \frac{u+wv}{wv} du dv dw. \tag{3.8}$$

The integral is first performed over v, then over w, then over u. It is expressed in terms of elementary functions and $\int_0^1 u^{-1} \log (1+u) du$. It yields

$$\int_0^1 \int_0^1 \int_0^1 du dw dv \frac{w}{u} \log \frac{u+wv}{wv} = 1.56. \tag{3.9}$$

For the term proportional to u^2, one integrates in the order t, w, u, v to get, always in terms of the same functions,

$$\int_0^1 \cdots \int_0^1 u^2 [ut+wv]^{-1} dv du dw dt = 0.92. \tag{3.10}$$

The term proportional to wu^2 is integrated in the order t, v, u, w to yield

$$\int_0^1 \cdots \int_0^1 wu^2 [ut+wv]^{-1} dw du dv dt = 0.36. \tag{3.11}$$

The value L of (3.2) is now obtained by collecting, according to (3.4), (3.7), (3.9), (3.10) and (3.11) with the result†

$$\mu(A_1) \geqq 2.30. \tag{3.12}$$

Similar techniques can be applied as simply to the other terms in (2.3), taken separately or in special combinations, grouping for instance the first and second term of E with A_1, A_2, B and J respectively. It will be observed that the most cumbersome bound was that of the J kind. Here the technique outlined for A_1 was used in the interval $0 \leqq u \leqq 0.1$. For $0.1 \leqq u \leqq 1$, the first mean value theorem was applied.

The results for these elementary lower bounds are

† *Note added in proof:* The analytic value for $\mu(A_1)$ has been found to be 2.60.

$$\mu(A_1+A_2+B+\text{ first term of } E) \geqq +1.45\frac{\alpha^2}{\pi^2}$$

$$\mu(D) \geqq -0.11\frac{\alpha^2}{\pi^2}$$

$$\mu(\text{third term of } E) \geqq -0.23\frac{\alpha^2}{\pi^2}$$

$$\mu(F) \geqq -0.15\frac{\alpha^2}{\pi^2} \tag{3.13}$$

$$\mu(H) = -1.25\frac{\alpha^2}{\pi^2}$$

$$\mu(J+\text{ seond term of } E) \geqq -1.26\frac{\alpha^2}{\pi^2}$$

and

$$\mu(\text{IIc}) \geqq -1.55\frac{\alpha^2}{\pi^2}.$$

After this result has been obtained, it becomes clear that the value $-3.18\,(\alpha^2/\pi^2)$, reported in KK, is erroneous and it is then worthwhile to compute more elaborate bounds in order to determine more precisely the value of IIc and, consequently, that of the total fourth order moment. These bounds will be quoted in the following section together with the new values of some physical quantities affected by the change of the magnetic moment.

4. Numerical Values

Deriving the auxiliary integrals, sometimes with a combination of the denominators different from those used for the elemnatry bounds, and then deriving more involved inequalities for these, one gets much better bounds. However, the calculations are much more involved too, without presenting special interest. In this way, $\mu(\text{IIc})$ has been shown to satisfy †

$$-0.49\frac{\alpha^2}{\pi^2} \geqq \mu(\text{IIc}) \geqq -0.71\frac{\alpha^2}{\pi^2}. \tag{4.1}$$

Accepting now the numerical results reported by Karplus and Kroll for $\mu(\text{I})$, $\mu(\text{IIa})$, $\mu(\text{IId})$ and $\mu(\text{IIe})$, the total fourth order moment would turn out to satisfy ††

† The upper bound in (4.1) had already been obtained when ref. [4]) was published. The improvement of the present work on the latter has been a tightening of the lower bound which was previously kept intentionally very broad so as to provide the simplest proof that $\mu(\text{IIc})$ was inexact in ref. [3]).

†† This is in good agreement with a calculation done by C. Sommerfield [6]) who finds, by a quite different method, $\mu^{(4)} = -0.33(\alpha^2/\pi^2)$.

$$-0.28\frac{\alpha^2}{\pi^2} \geqq \mu^{(4)} \geqq -0.50\frac{\alpha^2}{\pi^2}. \tag{4.2}$$

This is to be compared with the recent experimental value [1])

$$\mu^{(4)}_{\text{exp}} = (+0.7 \pm 2.0)\frac{\alpha^2}{\pi^2}$$

expressed in the same units.

Taking for $\mu^{(4)}$ the average value $(-0.39 \pm 0.11)\,\alpha^2/\pi^2$ increases the Lamb shifts for hydrogen and deuterium to

$$\text{(H)} \quad 2^2S_{\frac{1}{2}} - 2^2P_{\frac{1}{2}} = (1057.92 \pm 0.21)\text{Mc/s} \tag{4.3}$$

$$\text{(D)} \quad 2^2S_{\frac{1}{2}} - 2^2P_{\frac{1}{2}} = (1059.26 \pm 0.21)\text{Mc/s}, \tag{4.4}$$

respectively, in excellent agreement with observation.

The electromagnetic fourth order magnetic moment of the μ-meson taking into account the vacuum polarization by electrons [5]), amounts to

$$\mu'^{(4)} = (+0.69 \pm 0.11)\frac{\alpha^2}{\pi^2}\frac{e\hbar}{2M_\mu c}, \tag{4.5}$$

M_μ being the mass of the μ-meson.

Finally, the fine structure constant is slightly modified; it becomes

$$1/\alpha = 137.0384 \tag{4.6}$$

compared to the previous value 137.0365.

The author is grateful to Drs. S. Deser and G. Källén for many interesting discussions. He wishes to thank Prof. Niels Bohr for the hospitality at the Institute.

References

1) P. Franken and S. Liebes Jr., Phys. Rev. **104** (1956) 1197
2) R. Karplus and N. M. Kroll, Phys. Rev. **77** (1950) 536
3) W. E. Lamb Jr., Physica **19** (1953) 832
4) A. Petermann, Nuclear Physics **3** (1957) 683
5) Suura and Wichman, Phys. Rev. **105** (1957) 1930;
A. Petermann, Phys. Rev. **105** (1957) 1931
6) C. Sommerfield, Phys. Rev. (in the press)
7) A. Petermann, Helv. Phys. Acta (in the press)

Nuclear Physics **5** (1958) 684—692; © *North-Holland Publishing Co., Amsterdam*
Not to be reproduced by photoprint or microfilm without written permission from the publisher

ON THE POSSIBILITY OF AN EXPERIMENTAL TEST OF DISPERSION RELATIONS FOR γ-PROTON SCATTERING

M. CINI
Istituto di Fisica dell'Università di Roma
and
R. STROFFOLINI
Istituto di Fisica dell'Università di Torino

Received 11 October 1957

Abstract: The possibility of arriving at an experimental test of the dispersion relations for γ-proton scattering in a sufficiently reliable way, such that any observed discrepancy would be considered a proof against dispersion relations, is investigated. It is found that immediately above the threshold for pion photoproduction the best conditions are found, because the forward cross section has a minimum, and its theoretical value is mainly determined by the dispersion integral containing the total photoproduction cross sections for unpolarized γ's.

1. Introduction

The problem of testing the validity of dispersion relations is of great importance for field theory, because any well established discrepancy between theory and experiment would force us to abandon some very general and fundamental concept. Recently Puppi and Stanghellini [1]) have shown that the experimental data thus far available on pion-nucleon scattering already cast some doubt on the validity of dispersion relations for this process.

The dispersion relations derived for the scattering of γ's on protons by Gell-Mann, Goldberger and Thirring [2]) have already been used to predict the scattering cross-sections at various energies [2, 3]). Nevertheless, comparison with experiment is not up to now very meaningful, not only because the experimental results are still affected by large errors, but also because the theoretical predictions involve, besides the dispersion relations, many assumptions about the phase shifts.

We will discuss briefly the possibility of arriving at a test of the dispersion relations for γ-proton scattering sufficiently reliable to warrant that any discrepancy which might be observed in future should be considered meaningful.

For this purpose the first remark we want to make is that as the expe-

rience with meson scattering shows, one has to avoid the use of a phase shift analysis, if a reliable test is wanted. This means that, rather than deriving from the theory an angular distribution and comparing it with experiment, one should extrapolate in the forward direction the experimental angular distribution and compare it with the theoretical forward cross-section. This is in fact the procedure followed by Puppi and Stanghellini for meson scattering.

It is generally believed that, once allowance is made for the transformation factor

$$\frac{1+2\gamma}{[1+\gamma(1-\cos\vartheta_L)]^2} \quad \left(\gamma = \frac{\nu_L}{M}\right)$$

from the laboratory to the centre of mass frame, the c.m. angular distribution up to, say, 200 MeV, can be well described, for Compton scattering on protons, in terms of three coefficients:

$$\frac{d\sigma(\vartheta)}{d\Omega} = a+b\cos\vartheta+c\cos^2\vartheta. \tag{1}$$

The Klein-Nishina formula departs from (1) only by a few percent up to the energy stated above, and the structure-dependent terms should not include angular momenta higher than one. Strictly speaking, some speculation has been done about the possibility [4]) that the direct interaction of the photon with a meson in the proton's cloud might be of long range, and therefore include many partial waves of high angular momentum. This happens in the photoproduction of charged mesons above 300 MeV, where the angular distribution starts to be strongly peaked forward at small angles [5]). Nevertheless, if this is the case, the forward cross section predicted by large angle scattering through formula (1) will be lower than the actual value. Since, as we shall see later, in the region where the best conditions are found, the theoretical forward cross section has a minimum, the presence of a forward peak in the cross section due to long range interaction does not prevent, in our opinion, a reliable comparison between theory and experiment, provided that fairly accurate angular distributions from, say, 45° upwards are measured, and that the forward cross section is known theoretically. The main part of our consideration will be devoted to a discussion of this last point.

2. Dispersion Relations for γ-Scattering by Protons

In the case of meson scattering it was easy to obtain the forward cross section directly from dispersion relations in terms of the total cross sections at all energies, because the meson has spin zero and the modulus squared

of the forward scattering amplitude gives directly the forward cross section. In the case of γ scattering the forward cross section for unpolarized γ's is given by the sum of the moduli squared of the forward amplitudes for polarized γ's:

$$\frac{d\sigma(0^0)}{d\Omega} = \tfrac{1}{2}(|f_p|^2+|f_a|^2) \tag{2}$$

where the scattering amplitudes for γ's polarized parallel and antiparallel to the proton's spin, f_p and f_a respectively, are given, as is well known, by

$$f_p = f_1+f_2, \qquad f_a = f_1-f_2, \tag{3}$$

in terms of f_1 and f_2, the coherent and spin flip forward amplitudes respectively. Now the dispersion relation for f_1:

$$d_1(\nu) = d_1(0)+D_1(\nu),$$

$$d_1(\nu) = \mathrm{Re}\, f_1(\nu), \quad d_1(0) = -e^2/M, \quad D_1(\nu) = \frac{\nu^2}{4\pi^2}\int_0^\infty d\nu' \frac{\sigma_p(\nu')+\sigma_a(\nu')}{\nu'^2-\nu^2}, \tag{4}$$

contains the measured total cross section $\frac{1}{2}(\sigma_p+\sigma_a)$ for unpolarized γ's, but the dispersion relation for f_2:

$$d_2(\nu) = \nu d'_2(0)+D_2(\nu),$$

$$d_2(\nu) = \mathrm{Re}\, f_2(\nu), \quad d'_2(0) = -e^2\lambda^2/2M^2, \quad D_2(\nu) = \frac{\nu^3}{4\pi^2}\int_0^\infty d\nu' \frac{\sigma_p(\nu')-\sigma_a(\nu')}{\nu'(\nu'^2-\nu^2)} \tag{5}$$

(λ = anomalous part of proton's magnetic moment), contains the difference between the total cross sections for polarized photons, a quantity which is not easy to measure.

We think it is useful to discuss in detail what assumptions are necessary, to obtain from eqs. (3), (4), (5) the forward cross section through (2), and how they affect the result.

Before going into details some remarks about eq. (5) are useful. Because of the factor ν^3 in front of the integral, and of the extra factor ν' in the denominator of the integrand, one can expect that below the threshold for photoproduction ($\nu < 150$ MeV) the contribution from $D_2(\nu)$ should be small in comparison with the contribution from the term $D_1(\nu)$ in eq. (4). This expectation is confirmed by the numerical results, as we shall see, to such an extent, that we can safely say that below threshold the knowledge of experimental total cross sections for unpolarized γ's is sufficient to predict completely reliable values of the forward cross section.

Immediately above threshold ($\nu < 180$ MeV) the main contribution to the forward cross section still comes from the real parts of the scattering amplitudes, d_p and d_a, because the imaginary parts

$$a_{p,a} = \frac{\nu}{4\pi}\sigma_{p,a} \tag{6}$$

are small. At this energy $D_2(\nu)$ is no longer negligible, but it is still much smaller than $D_1(\nu)$. It turns out that a 100 % error in the value of the integral produces at most only a 10 % error in the forward cross section.

Finally at higher energies ($\nu > 180$ MeV), the forward cross section depends mainly on the absorptive parts of the amplitudes, and the effect of D_2 becomes again negligible.

3. Assumptions on Total Cross Sections

The total cross sections σ_p and σ_a are, in the energy region of interest, given completely by the single photoproduction cross sections on protons by polarized γ's. (The omission of the electron pair creation cross section is balanced by the omission of the Delbrück scattering amplitude.) Because of the ν' in the denominator in D_2 it turns out that contributions of the integrand for $\nu' > 300$ MeV are completely negligible. We feel therefore that a good justification exists for the following

Assumption I: The photoproduction matrix elements contain only the amplitudes

$$E_d^{+,0},\ M_d^{+,0}(\tfrac{1}{2}),\ M_d^{+,0}(\tfrac{3}{2}),\ E_q^{+,0}.$$

If this is the case, it is easy to obtain (appendix 1)

$$\sigma_p = \frac{16\pi}{3}\,[|X^+|^2+|X^0|^2] \tag{7}$$

$$\sigma_a = 8\pi[|E_d^+|^2+\tfrac{1}{3}|K^+|^2+\tfrac{2}{3}|Y^+|^2+|E_d^0|^2+\tfrac{1}{3}|K^0|^2+\tfrac{2}{3}|Y^0|^2] \tag{8}$$

where the well known quantities introduced by Fermi,

$$\begin{aligned} X^{+,0} &= \tfrac{3}{2}M_d^{+,0}(\tfrac{3}{2})+\tfrac{1}{4}E_q^{+,0},\\ Y^{+,0} &= \tfrac{1}{2}M_d^{+,0}(\tfrac{3}{2})-\tfrac{1}{4}E_q^{+,0}+M_d^{+,0}(\tfrac{1}{2}),\\ K^{+,0} &= M_d^{+,0}(\tfrac{3}{2})-\tfrac{1}{2}E_q^{+,0}-M_d^{+,0}(\tfrac{1}{2}), \end{aligned} \tag{9}$$

have been used. Experimental angular distributions can give directly, without further assumptions, the quantities $|E_d|^2$, $|K|^2$, $|X|^2+|Y|^2$, but cannot give separately the two terms $|X|^2$ and $|Y|^2$. It is therefore necessary, in order to make use of available experimental results, to introduce further well known assumptions:

Assumption II: The eight complex multipole amplitudes of assumption I are expressed by means of charge independence and time reversal in terms of twelve real quantities:

$$E_1,\ E_3,\ M_{11},\ M_{13},\ M_{31},\ M_{33},\ E_{13},\ E_{33},\ \delta E_1,\ \delta E_{13},\ \delta M_{11},\ \delta M_{13},$$

and the scattering phase shifts [7]).

Assumption III: Squares of matrix elements of the type

$$\mathfrak{M} = \mathfrak{M}_{33}\, e^{i\alpha_{33}} + \mathfrak{M}' \tag{10}$$

can be approximated by [6])

$$|\mathfrak{M}|^2 = \mathfrak{M}_{33}{}^2 + 2\cos\alpha_{33}\,\mathfrak{M}_{33}\,\mathfrak{M}'. \tag{11}$$

This is permissible if the resonant pion-nucleon state $(\frac{3}{2}, \frac{3}{2})$ is assumed to dominate the dispersion integral.

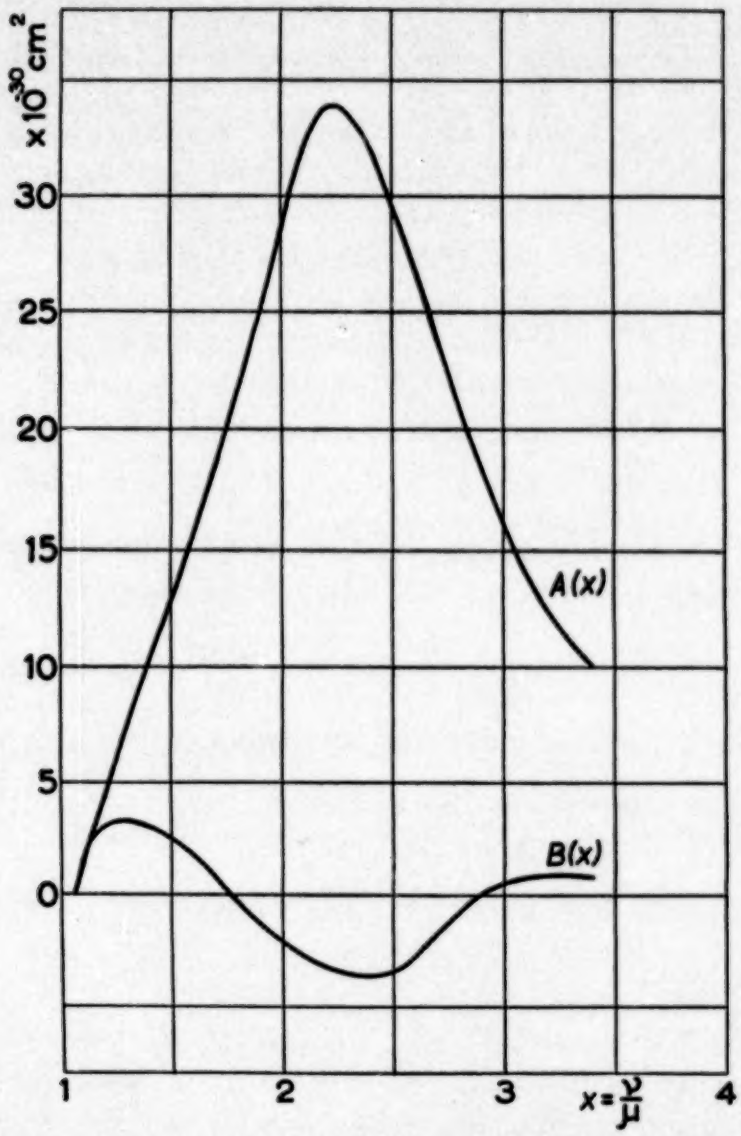

Fig. 1. $A(x) = \frac{1}{8\pi}(\sigma_p + \sigma_a)$, $\quad B(x) = \frac{1}{8\pi}\frac{\mu}{\nu}(\sigma_p - \sigma_a)$.

With these assumptions it turns out that σ_p and σ_a can be expressed in terms of quantities readily derived from experiments, namely the coefficients of the angular distributions. $A^{+,0}$ and $C^{+,0}$ for the charged and neutral photoproduction, together with the spin flip p-wave part A_{K_0} of the charged photoproduction, which experimentally turns out to be negligible [6, 7]) (appendix 2):

$$\sigma_a = 8\pi(A^+ + C^+ + \tfrac{1}{2}A_{K_0}),$$
$$\sigma_p = 8\pi(A^0 + \tfrac{1}{3}C^0 - \tfrac{2}{3}C^+ - \tfrac{1}{2}A_{K_0}). \quad (12)$$

It must be stressed that, although eqs. (12) involve only quantities directly obtained from the angular distributions of photoproduction from unpolarized γ's, nevertheless assumptions II and III are needed, as well as assumption I, for their derivation.

From eqs. (12) the contribution D_2 to eq. (5) is readily evaluated by making use of available experimental data [6, 7]†. In fig. 1 the quantities

$$A(x) = A^+ + A^0 + \tfrac{1}{3}(C^+ + C^0) = \frac{1}{8\pi}(\sigma_p + \sigma_a) \quad (13)$$

$$B(x) = \frac{1}{x}[A^0 + \tfrac{1}{3}C^0 - A^+ - \tfrac{5}{3}C^+ - A_{K_0}] = \frac{\mu}{8\pi\nu}(\sigma_p - \sigma_a) \quad (14)$$

(where $x = \nu/\mu$, with μ = meson mass) which appear in the integrands of D_1 and D_2 are plotted. We obtain at different energies the following values for these quantities:

TABLE 1

ν (MeV)	65	100	140	160	180	190	210
$D_1/\frac{e^2}{M}$	0.07	0.17	0.44	0.75	0.96	1.02	0.80
$D_2/\frac{e^2}{M}$	0	0	−0.02	−0.14	+0.02	+0.07	+0.20

Above threshold the knowledge of a_p and a_a is necessary in order to obtain from eq. (2) the forward cross section.

Eqs. (6), (12), together with the values of D_1 and D_2 of table 1, give immediately the forward scattering amplitudes reported in table 2.

TABLE 2

ν (MeV)	65	100	140	160	180	190	210
$d_p/\frac{e^2}{M}$	−1.04	−1.0	−0.82	−0.66	−0.31	−0.24	−0.36
$d_a/\frac{e^2}{M}$	−0.82	−0.64	−0.30	+0.16	+0.25	+0.28	−0.04
$a_p/\frac{e^2}{M}$	0	0	0	0.03	0.21	0.33	0.58
$a_a/\frac{e^2}{M}$	0	0	0	0.38	0.72	0.85	1.13

† The experimental data on π^+ photoproduction from ref. [6]) have been used at energies below 200 MeV, while the data on π^+ at energies above 200 MeV and the data on π^0 photoproduction have been taken from ref. [7]).

The anticipations stated above about the relative importance of the various terms follow easily by examination of tables 1 and 2: one sees that

a) up to threshold (140 MeV) the forward cross section depends only on experimental total cross sections for unpolarized γ's.

b) In the range 140—180 MeV a relative error $\Delta D_2/D_2 \approx 100\,\%$ produces at most a relative error in $d\sigma(0^0)/d\Omega$ of $\approx 10\,\%$.

c) Above 180 MeV the forward cross section depends mainly on a_p and a_s.

The forward cross section calculated from the data of table 2 is plotted in

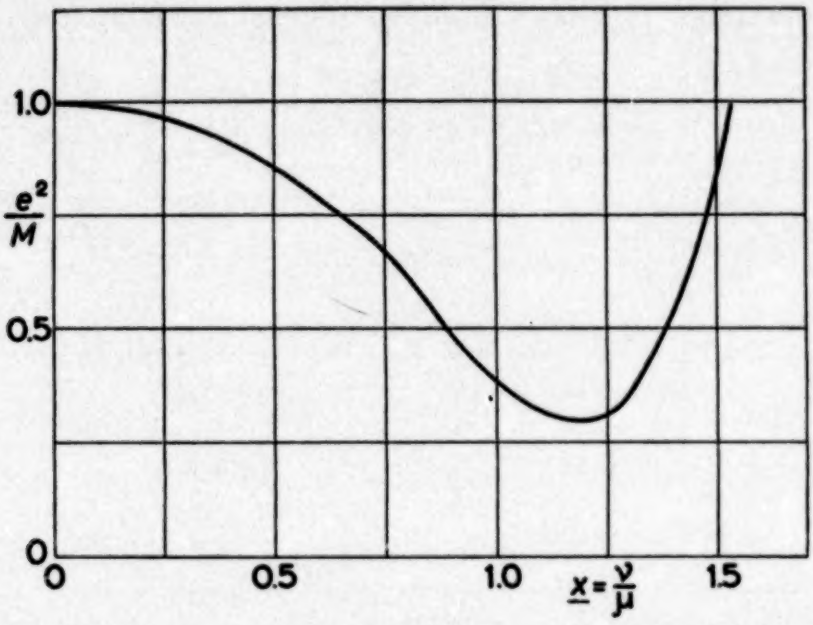

Fig. 2. Forward cross section for γ-proton scattering in laboratory system in units e^2/M.

fig. 2. One sees that the forward cross section, as already noticed by other authors, attains a minimum. The minimum is about 0.30 times the Thomson cross section at about 170 MeV.

We therefore conclude that a reliable experimental test of dispersion relations for γ-proton scattering is possible in the region around the minimum, for the following reasons:

1) at energies above 200 MeV the forward cross section is practically determined completely by the optical theorem: no violation of dispersion relations could be detected because the real parts of the scattering amplitudes are negligible;

2) at energies immediately above threshold the forward cross section is almost stationary and uncertainties in energy do not produce appreciable errors;

3) at energies immediately above threshold the theoretical predictions are not strongly dependent on assumptions II and III, because a variation in D_2 produces a much smaller change in the forward cross section.

An interesting discussion with Professor G. Bernardini is gratefully acknowledged.

Appendix 1

The matrix element for photoproduction of a pion of momentum $\mathbf{q}$, by a photon of polarization vector $\mathbf{e}$ and momentum $\mathbf{K}$ is [8])

$$\begin{aligned} T_e = {} & iE_d\,\boldsymbol{\sigma}\cdot\mathbf{e} - M_d(\tfrac{1}{2})[\mathbf{K}\times\mathbf{e}\cdot\mathbf{q} - i\boldsymbol{\sigma}\cdot(\mathbf{K}\times\mathbf{e})\times\mathbf{q}]K^{-1}q^{-1} \\ & - M_d(\tfrac{3}{2})[2\mathbf{K}\times\mathbf{e}\cdot\mathbf{q} + i\boldsymbol{\sigma}\cdot(\mathbf{K}\times\mathbf{e})\times\mathbf{q}]K^{-1}q^{-1} \\ & + \frac{i}{2}E_q[\boldsymbol{\sigma}\cdot\mathbf{K}\,\mathbf{e}\cdot\mathbf{q} + \boldsymbol{\sigma}\cdot\mathbf{e}\,\mathbf{K}\cdot\mathbf{q}]K^{-1}q^{-1}. \end{aligned} \tag{A1}$$

If we take the direction of $\mathbf{K}$ along the z-axis, which is also the axis of quantization of the proton's spin, then the polarization vector of a photon circularly polarized parallel to the proton's spin will be $1/\sqrt{2}\,(e_x+ie_y)$ and the polarization vector of a photon polarized antiparallel will be $1/\sqrt{2}\,(e_x-ie_y)$. If we denote, as usual, with ϑ and φ the polar angles of the momentum $\mathbf{q}$, then

$$\frac{1}{\sqrt{2}}(T_{e_x}+iT_{e_y})|\uparrow\rangle = T_p|\uparrow\rangle = \frac{i}{\sqrt{2}}\sin\vartheta\,e^{i\varphi}(3M_d(\tfrac{3}{2})+\tfrac{1}{2}E_q)|\uparrow\rangle, \tag{A2}$$

$$\begin{aligned} \frac{1}{\sqrt{2}}(T_{e_x}-iT_{e_y})|\uparrow\rangle = T_n|\uparrow\rangle = \frac{i}{\sqrt{2}}\{ & 2[E_d+\cos\vartheta(M_d(\tfrac{1}{2})-M_d(\tfrac{3}{2})+\tfrac{1}{2}E_q)]|\uparrow\rangle \\ & +\sin\vartheta\,e^{i\varphi}[2M_d(\tfrac{1}{2})+M_d(\tfrac{3}{2})-\tfrac{1}{2}E_q]|\downarrow\rangle\}, \end{aligned} \tag{A3}$$

where $|\uparrow\rangle$ and $|\downarrow\rangle$ are the eigenstates of σ_z. Eqs. (A2), (A3) give immediately

$$\frac{d\sigma_p}{d\Omega} = \langle\uparrow|T_p^+T_p|\uparrow\rangle = 2\sin^2\vartheta\,|X|^2, \tag{A4}$$

$$\begin{aligned} \frac{d\sigma_n}{d\Omega} = \tfrac{1}{2}\langle\uparrow|T_n^+T_n|\uparrow\rangle = {} & 2|E_d|^2 - 4\,\mathrm{Re}\,(E_d^*K)\cos\vartheta + 2|K^2|\cos^2\vartheta \\ & + 2|Y|^2\sin^2\vartheta. \end{aligned} \tag{A5}$$

Integrating on angles one obtains immediately eqs. (7), (8).

Appendix 2

Watson *et al.* [7]) have shown that, under assumptions I, II, III, the coefficients of the angular distributions of charged and neutral photoproduction can be expressed by

$$\begin{aligned} A^+ &= A_S + A_{X_0} + \tfrac{1}{4}A_{K_0} + A_{\Delta_1}\cos\alpha_{33} \\ C^+ &= \tfrac{3}{4}A_{K_0} - A_{X_0} - A_{\Delta_1}\cos\alpha_{33} \\ A^0 &= 2A_{X_0} + \tfrac{1}{2}A_{K_0} - A_{\Delta_1}\cos\alpha_{33} \\ C^0 &= 3A_{K_0} - 2A_{X_0} + A_{\Delta_1}\cos\alpha_{33} \end{aligned} \tag{A6}$$

where the quantities A_S, A_{X_0}, A_{K_0}, A_{Δ_1} can be determined from experimental angular distributions. In terms of the same quantities it turns out that

$$|X^+|^2 = \left|\left[\frac{3}{\sqrt{2}} M_{33} + \frac{1}{2\sqrt{2}} E_{33}\right] e^{i\alpha_{33}} + \frac{1}{2\sqrt{2}} [3(M_{13}-\delta M_{13}) + \tfrac{1}{2}(E_{13}-\delta E_{13})]\right|^2$$
$$\approx A_{X_0} + A_{\Delta_1} \cos \alpha_{33}, \tag{A7}$$
$$|X^0|^2 = |[3M_{33} + \tfrac{1}{2}E_{33}] e^{i\alpha_{33}} - \tfrac{1}{4}[3(M_{13}-\delta M_{13}) + \tfrac{1}{2}(E_{13}-\delta E_{13})]|^2$$
$$\approx 2A_{X_0} - A_{\Delta_1} \cos \alpha_{33}.$$

Therefore

$$\sigma_p = 16\pi A_{X_0}, \tag{A8}$$
$$\sigma_a = 8\pi[A^+ + A^0 + \tfrac{1}{3}(C^+ + C^0) - 2A_{X_0}]. \tag{A9}$$

The last expression becomes immediately, by using eqs. (A6)

$$= 8\pi[A_S + \tfrac{3}{2} A_{K_0}]. \tag{A10}$$

Instead of eqs. (A8), (A9) which involve A_{X_0}, one can use the equivalent eqs. (12), obtained from eqs. (A8), (A9), (A10) and

$$\sigma_p + \sigma_a = 8\pi[A^+ + A^0 + \tfrac{1}{3}(C^+ + C^0)], \tag{A11}$$

together with the relation

$$A_S + A_{K_0} = A^+ + C^+. \tag{A12}$$

References

1) G. Puppi and A. Stanghellini, Nuovo Cimento **5** (1957) 1305
2) M. Gell-Mann, M. L. Goldberger and W. Thirring, Phys. Rev. **95** (1954) 1612
3) R. H. Capps, Phys. Rev. **106** (1957)
4) S. Fubini, private communication
5) G. Bernardini, private communication
6) Beneventano, Bernardini, Carlson-Lee, Stoppini and Tau, Nuovo Cimento **4** (1956) 323
7) Watson, Keck, Tollestrup and Walker, Phys. Rev. **101** (1955) 1159
8) M. Gell-Mann and K. Watson, Ann. Rev. Nucl. Sci. **4** (1954) 219

Nuclear Physics **5** (1958) 693; © *North-Holland Publishing Co., Amsterdam*

BOOK REVIEW

D. HALLIDAY, *Introduction à la Physique Nucléaire*, translated from the English (John Wiley and Sons, 1955) by R. Barjon (Paris, Dunod, 1957. xv-486 pages. 4700 fr. fr.)

The author starts this introductory course with a concise review of historically important experiments and discoveries and a brief and elementary résumé of wave mechanics.

He assumes a working knowledge of the theory of atomic spectra when in the next few chapters he describes and discusses radioactive emissions and internal conversions. At this stage several chapters follow, devoted to the neutron, charged particles and gamma rays, with particular stress on the techniques and apparatus needed to measure their presence and their properties; this practical aspect is indeed noticeable all through the book. Then come chapters on nuclear structure, nuclear reactions and fission, and two concluding chapters on nuclear spin and magnetism, and on cosmic rays.

Several features of the book serve to commend it particularly to the student. Firstly, the style is lucid, and ideas are expressed in a language easily understood, important points being emphasized by examples worked out in the text. Mathematical developments, however, are not allowed to obscure the physical arguments; instead, thirteen appendices, referred to at the appropriate places in the text, take care of most of the mathematics. Secondly, groups of problems follow each chapter, allowing the student to check his progress. (It is, however, left to his supervisor to check the correctness of his solutions; no answers being provided to the problems.)

In the French edition further interesting snippets include a list of experimental apparatus located in France, and an English-French vocabulary of technical words.

The translation is faithful and only a handful of printing errors spoil the otherwise excellent production. Numerous graphs and several photographs illustrate the text.

This book would therefore serve an undergraduate studying physics as a first introduction to this specialized branch, and contains as much as a student of nuclear chemistry usefully requires to know of the subject.

J. R.

AUTHOR INDEX

ALIKHANOV, A. I., G. P. ELISEIEV, V. A. LUBIMOV and B. V. ERSHLER, Polarization of electrons emitted in β-decay 588
BADRINATHAN, C., *see* Kondaiah
BARASHENKOV, V. S., B. M. BARBASHEV, E. G. BUBELOV and V. M. MAKSIMENKO, Multiple production of heavy particles in two nucleon collisions 17
BARBASHEV, B. M., *see* Barashenkov
BARNEVELD, H. H. VAN, *see* Sikkema
BECKMAN, O. and R. SANDSTRÖM, X-ray photoexcitation of Li^7 595
BELL, J. S., Many body effects in beta-decay 167
BERESTETSKY, V. B., B. L. IOFFE, A. P. RUDIK and K. A. TER-MARTIROSYAN, β-decay and non-conservation of parity 464
BERLIN, T. H. and G. E. OWEN, Three body break up 669
BILENKY, S. M., *see* Bogolubov
BIRD, J. R., *see* Bowey
BISHOP, G. R., A contribution to the establishment of the level scheme of radium C′ 358
BOGOLUBOV, N. N., S. M. BILENKY and A. A. LOGUNOV, Dispersion relations for weak interactions 383
BOUCHIAT, C. et L. MICHEL, Mesure de la polarisation des électrons relativistes 416
BOWEY, ELEANOR M. and J. R. BIRD, A note on the isotopic assignment of slow neutron resonances in samarium, iridium and gadolinium 294
BREDIN, D., *see* Burcham
BUBELOV, E. G. *see* Barashenkov
BURCHAM, W. E., G. P. MCCAULEY, D. BREDIN, W. M. GIBSON, D. J. PROWSE and J. ROTBLAT, The reaction He^4 (α, p) Li^7 141
CAVANAGH, P. E., C. F. COLEMAN, B. W. RIDLEY and J. F. TURNER, A four-state theory of the neutrino 11
CINDRO, N. and K. ILAKOVAC, Elastic scattering of gamma-rays . 647
CINI, M. and R. STROFFOLINI, On the possibility of an experimental test of dispersion relations for γ-proton scattering 684
COLEMAN, C. F., The analysis of angular and direction-polarization correlation measurements on mixed transitions 495
COLEMAN, C. F., *see* Cavanagh
COLLINS, E. R., *see* Rae

DANOS, M., On the long-range correlation model of the photonuclear effect 23
D'ESPAGNAT, B. J., PRENTKI and A. SALAM, On symmetries of weak interactions 447
DIDDENS, A. N., W. J. HUISKAMP, J. C. SEVERIENS, A. R. MIEDEMA and M. J. STEENLAND, Angular distribution and linear polarization of the gamma rays from oriented ^{56}Co nuclei 58
DOLGINOV, A. Z., Beta-gamma correlation and polarization of particles in the beta decay of oriented nuclei in connection with parity non-conservation 512
DZHELEPOV, B., S. SHESTOPALOVA and I. UCHEVATKIN, On the 2450—3400 keV region of the RaC gamma spectrum 413
ELISEIEV, G. P. *see* Alikhanov
ELTON, L. R. B., A semi-empirical formula for the nuclear radius 173
ERSHLER, B. V., *see* Alikhanov
FERGUSON, A. T. G. and G. C. MORRISON, The spectrum of neutrons from the reaction p+d → p+p+n 41
FIRK, F. W. K., *see* Lynn
FREEMAN, JOAN M., R. C. HANNA and J. H. MONTAGUE, The reaction Li^7 (p, α) He^4. 148
GATTO, R., Possible experiments on the behaviour of the weak hyperon decay interactions under P, C, and T 183
GATTO, R., Parity non-conservation in neutrino interactions and the τ—θ problem. 235
GATTO, R., A possible theory of weak interactions 530
GIBSON, W. M., *see* Burcham
GIRGIS, R. K., *see* Polak
GOLDSTEIN, S., *see* Lipkin
GOTTFRIED, K., On the determination of the nuclear pair correlation function from the high energy photo-effect 557
GREEN, A. E. S., *see* Sood
GRIBOV, V. N., Angular distribution in reactions involving the formation of three low energy particles with τ^+meson decay 653
GUSEINOV, I. I., *see* Sokolov
GYÖRGYI, G. and H. ÜBERALL, Parity non-conservation and transverse polarization of β-particles 405
HANNA, R. C., *see* Freeman
HEISENBERG, W., Application of the Tamm-Dancoff-method to the Lee-model 195
HUISKAMP, W. J., *see* Diddens
ILAKOVAC, K., *see* Cindro
IOFFE, B. L., *see* Berestetsky
IYENGAR, K. V. K., *see* Kondaiah

KAMEFUCHI, S., *see* Oneda
KERIMOV, B. K., *see* Sokolov
KINSEY, B. B., *see* Rae
KIRK, F. W. K., *see* Lynn
KONDAIAH, E., K. V. K. IYENGAR and C. BADRINATHAN, (n, α) and (n, p) reactions in fluorine 346
KONUMA, M., On the conservation of the lepton number. 504
LEACHMAN, R. B., *see* Nobles
LIESHOUT, R. VAN, *see* Polak
LINDQVIST, T., B. G. PETTERSSON and K. SIEGBAHN, The internal Compton effect. A determination of cross section and angular correlation 47
LIPKIN, H. J. and S. GOLDSTEIN, Rotational properties of the two-dimensional anisotropic harmonic oscillator. I. Expectation values 202
LOGUNOV, A. A., *see* Bogolubov
LUBIMOV, V. A., *see* Alikhanov
LYNN, J. E., F. W. K. FIRK and M. C. MOXON, The 2.85 keV neutron resonance of sodium 603
LYNN, J. E., *see* Rae
MAKSIMENKO, V. M., *see* Barashenkov
MCCAULEY, G. P., *see* Burcham
MCCUTCHEN, C. W., Excited states of Eu^{153} 187
MELIGY, A. S., Note on Coulomb wave functions 615
MESSELT, S., K-shell ionization by protons 435
MICHEL, L., *see* Bouchiat
MIEDEMA, A. R., *see* Diddens
MONTAGUE, J. H., *see* Freeman
MORRISON, G. C., *see* Ferguson
MOXON, M. C., *see* Lynn
NATHAN, O., Lifetime of the first rotational state of Gd^{156} 401
NEWTON, J. O., The Coulomb excitation of U^{233} and Np^{237} and a discussion of the energy levels of U^{233} 218
NIELSEN, K. O. and O. B. NIELSEN, Measurements on isotope separated β-ray sources of Re^{186} and Re^{188}. 319
NIELSEN, O. B., *see* K. O. Nielsen
NILSSON, S. G. and J. O. RASMUSSEN, On anomalous conversion coefficients of dipole transitions 617
NING HU, Scattering functions with crossing symmetry and their applications to the problems of meson-nucleon scattering. 1
NOBLES, R. A. and R. B. LEACHMAN, Neutron-induced fission of Ra^{226} 211
OFER, S., The energy levels of Dy^{160}. 331
OKUN, L., On the polarization of μ-mesons in $K_{\mu 3}$-decays 455

ONEDA, S. and S. KAMEFUCHI, Some remarks on K-meson decays 301
OWEN, G. E., *see* Berlin
PAIS, A., The scientific work of T. D. Lee and C. N. Yang . . . 297
PASMA, P. J., *see* Sikkema
PETERMANN, A., Fourth order magnetic moment of the electron 677
PETTERSSON, B. G., *see* Lindqvist
POLAK, H. L., W. SCHOO, B. L. SCHRAM, R. K. GIRGIS and R. VAN LIESHOUT, Gamma radiation from ^{141}Nd 271
POLKINGHORNE, J. C., A theoretical basis for a possible theory of β-decay 288
PRENTKI, J., *see* D'Espagnat
PROWSE, D. J., *see* Burcham
RAE, E. R., E. R. COLLINS, B. B. KINSEY, J. E. LYNN and E. R. WIBLIN, An analysis of slow neutron resonances in silver . . . 89
RASMUSSEN, J. O., *see* Nilsson
REINER, A. S., Finite size effects on M1 conversion coefficients . . 544
RIDLEY, B. W., *see* Cavanagh
ROTBLAT, J., *see* Burcham
RUDIK, A. P., *see* Berestetsky
SALAM, A., *see* D'Espagnat
SANDSTRÖM, R., *see* Beckman
SCHOO, W., *see* Polak
SCHRAM, B. L., *see* Polak
SEVERIENS, J. C., *see* Diddens
SHESTOPALOVA, S., *see* Dzhelepov
SIEGBAHN, K., *see* Lindqvist
SIKKEMA, C. P., P. J. PASMA and H. H. VAN BARNEVELD, Scattering of fast neutrons by neon-22 351
SMIRNITSKY, V. A., *see* Weissenberg
SOKOLOV, A. A., B. K. KERIMOV and I. I. GUSEINOV, Damping theory study of elastic scattering of Dirac particles with account of polarization effects 390
SOLOVYOV, L. D., Photoproduction of mesons on nucleons: phase shift analysis and dispersion relations 256
SOOD, P. C. and A. E. S. GREEN, Proton potential anomaly and nuclear radius constant for mirror nuclei 274
STEENLAND, M. J., *see* Diddens
STROFFOLINI, R., *see* Cini
TER-MARTIROSYAN, K. A., *see* Berestetsky
TURNER, J. F., *see* Cavanagh
ÜBERALL, H., *see* Györgyi
UCHEVATKIN, I., *see* Dzhelepov

VAIDYA, S. M., The two-body spin-orbit interaction 179
WEISSENBERG, A. O. and V. A. SMIRNITSKY, Investigation of asymmetry of $\pi^+ \to \mu^+ \to e^+$ decays in photographic emulsions . . . 33
WIBLIN, E. R. *see* (Rae)
YOSHIZAWA, Y., Beta and gamma ray spectroscopy of Cs^{137} . . . 122
YVON, J., La diffusion d'un projectile par un système complexe lié 150

BOOK REVIEWS

Atom 411
Atomo e Industria 411
The Index of technical Articles 411
BENEDICT, M. and T. H. PIGFORD, Nuclear Chemical engineering (H. R. C. Pratt) 411
FERMI, L., Atoms for the world (J. R.) 411
HAISSINSKY, M., La chimie nucléaire et ses applications (D. G. Tuck) 410

SUBJECT INDEX

Beta and Gamma Spectroscopy

The internal Compton effect. A determination of cross section and angular correlation, T. Lindqvist, B. G. Petterson and K. Siegbahn 47
Beta and gamma ray spectroscopy of Cs^{137}, Y. Yoshizawa. 122
Gamma radiation from ^{141}Nd, H. L. Polak, W. Schoo, B. L. Schram, R. K. Girgis and R. van Lieshout 271
Measurements on isotope separated β-ray sources of Re^{186} and Re^{188}, K. O. Nielsen and O. B. Nielsen 319
The energy levels of Dy^{160}, S. Ofer 331
A contribution to the establishment of the level scheme of radium C′, G. R. Bishop 358
Lifetime of the first rotational state of Gd^{156}, Ove Nathan 401
On the 2450—3400 keV region of the RaC gamma spectrum, B. Dzhelepov, S. Shestopalova and I. Uchevatkin 413
Finite size effects on M1 conversion coefficients, A. S. Reiner 544
X-ray photoexcitation of Li^7, O. Beckman and R. Sandström 595
On anomalous conversion coefficients of dipole transitions, S. G. Nilsson and J. O. Rasmussen 617

Elementary Particles

A four-state theory of the neutrino, P. E. Cavanagh, C. F. Coleman, B. W. Ridley and J. F. Turner 11
Multiple production of heavy particles in two nucleon collisions, V. S. Barashenkov, B. M. Barbashev, E. G. Bubelov and V. M. Maksimenko 17
Investigation of asymmetry of $\pi^+ \to \mu^+ \to e^+$ decays in photographic emulsions, A. O. Weissenberg and V. A. Smirnitsky 33
Angular distribution and linear polarization of the gamma rays from oriented ^{58}Co nuclei, A. N. Diddens, W. J. Huiskamp, J. C. Severiens, A. R. Miedema and M. J. Steenland 58

Possible experiments on the behaviour of the weak hyperon decay interactions under P, C, and T, R. Gatto 183
Parity non-conservation in neutrino interactions and the τ—θ problem, R. Gatto 235
A theoretical basis for a possible theory of β-decay, J. C. Polkinghorne 288
Some remarks on K-meson decays, S. Oneda and S. Kamefuchi 301
Parity non-conservation and transverse polarization of β-particles, G. Györgyi and H. Überall 405
Mesure de la polarisation des électrons relativistes, C. Bouchiat et L. Michel . . 416
On symmetries of weak interactions, B. D'Espagnat, J. Prentki and A. Salam . 447
On the polarization of μ-mesons in $K_{\mu 3}$-decays, L. Okun. 455
β-decay and non-conservation of parity, V. B. Berestetsky, B. L. Ioffe, A. P. Rudik and K. A. Ter-Martirosyan 464
The analysis of angular and direction-polarization correlation measurements on mixed transitions, C. F. Coleman 495
On the conservation of the lepton number, M. Konuma. 504
Beta-gamma correlation and polarization of particles in the beta decay of oriented nuclei in connection with parity non-conservation, A. Z. Dolginov 512
A possible theory of weak interactions, R. Gatto 530
Polarization of electrons emitted in β-decay, A. I. Alikhanov, G. P. Eliseiev, V. A. Lubimov and B. V. Ershler. 588
Angular distribution in reactions involving the formation of three low energy particles with τ^+ meson decay, V. N. Gribov 653

Field Theory

Scattering functions with crossing symmetry and their applications to the problems of meson-nucleon scattering, Ning Hu 1
Application of the Tamm-Dancoff-method to the Lee-model, W. Heisenberg . . . 195
Photoproduction of mesons on nucleons: phase shift analysis and dispersion relations, L. D. Solovyov 256
Dispersion relations for weak interactions, N. N. Bogolubov, S. M. Bilenky and A. A. Logunov 383
Fourth order magnetic moment of the electron, A. Petermann 677
On the possibility of an experimental test of dispersion relations for γ-proton scattering, M. Cini and R. Stroffolini 684

News Items

The scientific work of T. D. Lee and C. N. Yang, A. Pais 297
International conference on mesons and recently discovered particles (Padua and Venice, 22—28 September 1957). 409

Nuclear States

Excited states of Eu^{153}, C. W. McCutchen 187

Photonuclear Reactions

On the long-range correlation model of the photonuclear effect, M. Danos 23
On the determination of the nuclear pair correlation function from the high energy photo-effect, K. Gottfried. 557

Reactions Induced by Particles

The spectrum of neutrons from the reaction p+d → p+p+n, A. T. G. Ferguson and G. C. Morrison. 41
An analysis of slow neutron resonances in silver, E. R. Rae, E. R. Collins, B. B. Kinsey, J. E. Lynn and E. R. Wiblin 89
The reaction He^4 (α, p) Li^7, W. E. Burcham, G. P. McCauley, D. Bredin, W. M. Gibson, D. J. Prowse and J. Rotblat 141

The reaction Li^7 (p, α) He^4, Joan M. Freeman, R. C. Hanna and J. H. Montague 148
Neutron-induced fission of Ra^{226}, R. A. Nobles and R. B. Leachman. 211
The Coulomb excitation of U^{233} and Np^{237} and a discussion of the energy levels of U^{233}, J. O. Newton 218
A note on the isotopic assignment of slow neutron resonances in samarium, iridium and gadolinium, Eleanor M. Bowey and R. J. Bird. 294
(n, α) and (n, p) reactions in fluorine, E. Kondaiah, K. V. K. Iyengar and C. Badrinathan 346
K-shell ionization by protons, S. Messelt 435
The 2.85 keV neutron resonance of sodium, J. E. Lynn, F. W. K. Firk and M. C. Moxon 603
Three body break up, T. H. Berlin and G. E. Owen 669

Scattering

La diffusion d'un projectile par un système complexe lié, J. Yvon. 150
Scattering of fast neutrons by neon-22, C. P. Sikkema, P. J. Pasma and H. H. van Barneveld 351
Damping theory study of elastic scattering of Dirac particles with account of polarization effects, A. A. Sokolov, B. K. Kerimov and I. I. Guseinov 390
Note on Coulomb wave functions, A. S. Meligy. 615
Elastic scattering of gamma-rays, N. Cindro and K. Ilakovac 647

Structure of Nuclei

Many body effects in beta-decay, J. S. Bell 167
A semi-empirical formula for the nuclear radius, L. R. B. Elton. 173
The two-body spin-orbit interaction, S. M. Vaidya 179
Rotational properties of the two-dimensional anisotropic harmonic oscillator. I. Expectation values. H. J. Lipkin and S. Goldstein 202
Proton potential anomaly and nuclear radius constant for mirror nuclei, P. C. Sood and A. E. S. Green 274